# Q-Chem 5.0 User’s Manual

# Version 5.0

May, 2017

## Q-CHEM User's Manual

**Version 5.0 was edited by:**
Dr Andrew Gilbert

**Version 4 editors:**
Prof. John Herbert
Prof. Anna Krylov
Prof. Martin Head-Gordon
Dr Emil Proynov
Dr Andrew Gilbert
Dr Jing Kong.

**Other editors:**
Dr. Yihan Shao
Dr. Jeremy Dombroski

**The contributions of individual developers to each version are highlighted in "New Features", Section 1.3**

**Published by:**
Q-Chem, Inc.
6601 Owens Dr.
Suite 105
Pleasanton, CA 94588

**Customer Support:**

| | |
|---|---|
| Telephone: | (412) 687-0695 |
| Facsimile: | (412) 687-0698 |
| email: | `support@q-chem.com` |
| website: | `www.q-chem.com` |

The information in this document applies to version 5.0 of Q-CHEM.
This document version generated on August 18, 2017.

# Contents

# Chapter 1

# Introduction

## 1.1 About This Manual

### 1.1.1 Overview

This manual is intended as a general-purpose user's guide for Q-CHEM, a modern electronic structure program. The manual contains background information that describes Q-CHEM methods and user-selected parameters. It is assumed that the user has some familiarity with the Unix/Linux environment, an ASCII file editor, and a basic understanding of quantum chemistry.

After installing Q-CHEM and making necessary adjustments to your user account, it is recommended that particular attention be given to Chapters 3 and 4. The latter, which describes Q-CHEM's self-consistent field capabilities, has been formatted so that advanced users can quickly find the information they require while supplying new users with a moderate level of important background information. This format has been maintained throughout the manual, and every attempt has been made to guide the user forward and backward to other relevant information so that a logical progression through this manual is not necessary.

Documentation for IQMOL, a graphical user interface designed for use with Q-CHEM, can be found on the `www.iqmol.org`. IQMOL functions as a molecular structure builder, as an interface for local or remote submission of Q-CHEM jobs, and as a post-calculation visualization program for densities and molecular orbitals.

### 1.1.2 Chapter Summaries

**Ch. 1:** General overview of Q-CHEM's features, contributors, and contact information.

**Ch. 2:** Procedures to install, test, and run Q-CHEM on your machine.

**Ch. 3:** Overview of the Q-CHEM command-line input.

**Ch. 4:** Running ground-state self-consistent field calculations.

**Ch. 5:** Running post-Hartree-Fock correlated wave function calculations for ground states.

**Ch. 6:** Running calculations for excited states and open-shell species.

**Ch. 7:** Using Q-CHEM's built-in basis sets, or specifying a user-defined basis set.

**Ch. 8:** Using Q-CHEM's effective core potential capabilities.

**Ch. 9:** Options available for exploring potential energy surfaces, such as determining critical points (transition states and local minima on a single surface, or minimum-energy crossing points between surfaces) as well as *ab initio* molecular dynamics.

**Ch. 10:** Molecular properties and *a posteriori* wave function analysis.

**Ch. 11:** Methods for molecules in complex environments, including implicit solvation models, QM/MM models, the Effective Fragment Potential, and density embedding.

**Ch. 12:** Fragment-based approaches for efficient calculations on large systems, calculation of non-covalent interactions, and energy decomposition analysis.

**App. A:** Overview of the OPTIMIZE package used for determining molecular geometry critical points.

**App. B:** Overview of the AOINTS library, which contains some of the fastest two-electron integral code currently available.

**App. C:** Quick-reference section containing an alphabetized list of job control variables.

## 1.2 Q-CHEM, Inc.

### 1.2.1 Contact Information and Customer Support

For general information regarding Q-CHEM program, visit `www.q-chem.com`. Full customer support is promptly provided via telephone or email (`support@q-chem.com`) for those customers who have purchased Q-CHEM's "QMP" maintenance contract. In addition to free customer support, this contract provides discounts on future updates and releases of Q-CHEM. For details of the maintenance contract please see `www.q-chem.com`.

### 1.2.2 About the Company

Q-CHEM, Inc. was founded in 1993 and was based in Pittsburgh, PA until 2013, when it relocated to Pleasanton, CA. Q-CHEM's scientific contributors include leading quantum chemists around the world. The company is governed by the Board of Directors which currently consists of Peter Gill (Canberra), Anna Krylov (USC), John Herbert (Ohio State), and Hilary Pople. Fritz Schaefer (Georgia) is a Board Member Emeritus. Martin Head-Gordon is a Scientific Advisor to the Board. The close coupling between leading university research groups and Q-CHEM Inc. ensures that the methods and algorithms available in Q-CHEM are state-of-the-art.

In order to create this technology, the founders of Q-CHEM, Inc. built entirely new methodologies from the ground up, using the latest algorithms and modern programming techniques. Since 1993, well over 300 person-years have been devoted to the development of the Q-CHEM program. The author list of the program shows the full list of contributors to the current version, and the journal citations for Q-CHEM versions 2, 3, and 4[1–3] illustrate the breadth of the Q-CHEM developer community. The current group of developers consist of more than 100 people in 9 countries. A brief history of Q-CHEM is given in the recent article *Q-Chem: An Engine for Innovation*[4].

### 1.2.3 Company Mission

The mission of Q-CHEM, Inc. is to develop, distribute, and support innovative and *sustainable* quantum chemistry software for industrial, government and academic researchers in the chemical, petrochemical, biochemical, pharmaceutical and material sciences.

## 1.3 Q-CHEM Features

Quantum chemistry methods have proven invaluable for studying chemical and physical properties of molecules. The Q-CHEM system brings together a variety of advanced computational methods and tools in an integrated *ab initio* software package, greatly improving the speed and accuracy of calculations being performed. In addition, Q-CHEM will accommodate larger molecular structures than previously possible, with no loss in accuracy, thereby bringing the power of quantum chemistry to critical research projects for which this tool was previously unavailable. Below is a reverse-chronological listing of new features added to Q-CHEM.

### 1.3.1 New Features in Q-CHEM 5.0

- Enhancements to the coupled-cluster package:
  - Analytic gradients for Cholesky-decomposed CCSD and EOM-CCSD; efficiency improvement for canonical CCSD and EOM-CCSD gradients (X. Feng, E. Epifanovsky).
  - CAP-EOM-CCSD analytic gradients (Z. Benda and T.-C. Jagau) and Dyson orbitals for metastable states (T.-C. Jagau, A.I. Krylov), Section 6.7.5).
  - CAP-EOM-MP2 method (A. Kunitsa, K. Bravaya).
  - Evaluation of polarizabilities using CCSD and EOM-CCSD (EE and SF) wave functions using full derivative formulation (K. Nanda and A. Krylov, Section 6.7.15.4).
  - Evaluation of $\langle S^2 \rangle$ for EOM-CCSD wave functions (X. Feng).
  - Evaluation of NACs for EOM-CCSD wave functions (S. Faraji, A. Krylov, E. Epifanovski, X. Feng, Section 6.7.15.3).
  - Efficiency improvement and new multicore-parallel code for (T) correction (I. Kaliman).
  - New coupled-cluster based methods for core states (A. Krylov).
- New capabilities for implicit solvation modeling:
  - PCM capabilities for computing vertical excitation, ionization, and electron attachment energies at EOM-CC and MP2 levels (Section 6.7.10).
  - State-specific equilibrium and non-equilibrium solvation for all orders and variants of ADC (J. M. Mewes and A. Dreuw; Section 6.8.7).
  - Poisson equation boundary conditions allowing use of an arbitrary, anisotropic dielectric function $\epsilon(\mathbf{r})$, with full treatment of volume polarization (M. P. Coons and J. M. Herbert; Section 11.2.10).
  - Composite Model for Implicit Representation of Solvent (CMIRS), an accurate model for free energies of solvation (Section 11.2.6)

- New density functionals (N. Mardirossian and M. Head-Gordon; Section 4.4.3):
  - GGA functionals: BEEF-vdW, HLE16, KT1, KT2, KT3, rVV10
  - Meta-GGA functionals: B97M-rV, BLOC, mBEEF, oTPSS, TM
  - Hybrids: CAM-QTP(00), CAM-QTP(01), HSE-HJS, LC-$\omega$PBE08, MN15, rCAM-B3LYP, WC04, WP04
  - Double hybrids: B2GP-PLYP, DSD-PBEB95-D3, DSD-PBEP86-D3, DSD-PBEPBE-D3, LS1DH-PBE, PBE-QIDH, PTPSS-D3, PWPB95-D3
  - Grimme's PBEh-3c "low-cost" composite method
  - rVV10 non-local correlation functional
- Additional DFT developments:
  - New forms of DFT-D3 (J. Witte; Section 4.4.7.2).
  - New standard integration grids, SG-2 and SG-3 (S. Dasgupta and J. M. Herbert; Section 4.4.5.2).
  - More efficient propagator algorithms for real-time TDDFT (Y. Zhu and J. M. Herbert; Section 6.11).
- New integral package for for computing effective core potential (ECP) integrals (S. C. McKenzie, E. Epifanovsky; Chapter 8).
  - More efficient analytic algorithms for energies and first derivatives.
  - Support for arbitrary projector angular momentum.
  - Support up to $h$ angular momentum in the basis set.
- Analytic derivative couplings for the *ab initio* Frenkel-Davydov exciton model (A. F. Morrison and J. M. Herbert; Section 12.14.3).
- Wave function correlation capabilities:
  - Coupled cluster valence bond (CCVB) method for describing open-shell molecules with strong spin correlations (D. W. Small and M. Head-Gordon; Section 5.15.2).
  - Implementation of coupled-cluster valence bond with singles and doubles (CCVB-SD) for closed-shell species (J. Lee, D. W. Small and M. Head-Gordon; Section 5.10.4).

**Note:** Several important changes in Q-CHEM's default settings have occurred since version 4.4.

- Core electrons are now frozen by default in most post-Hartree-Fock calculations; see Section 5.2.
- The keywords for calculation of SOCs and NACs were renamed for consistency between different methods.
- Some newer density functionals now use either the SG-2 or SG-3 quadrature grid by default, whereas all functionals used SG-1 by default in v. 4.4. Table 4.4 lists the default grid for various classes of functionals.

### 1.3.2 New Features in Q-CHEM 4.4

- occ-RI-K algorithm for the evaluation of exact exchange in energy and force calculations (S. Manzer, F. Rob and M. Head-Gordon; Section 4.8.11)
- Combinatorially-optimized exchange-correlation functionals (N. Mardirossian and M. Head-Gordon; Section 4.4.3):
    - $\omega$B97M-V (range-separated hybrid, meta-GGA functional with VV10 non-local correlation)
    - B97M-V (meta-GGA functional with VV10 non-local correlation)
    - $\omega$B97X-V (range-separated hybrid functional with VV10 non-local correlation)
- Implementation of new exchange-correlation functionals from the literature (N. Mardirossian and M. Head-Gordon; Section 4.4.3). These include:
    - MGGA_MS0, MGGA_MS1, MGGA_MS2, MGGA_MS2h, MGGA_MVS, MGGA_MVSh, PKZB, revTPSS, revTPSSh, SCAN, SCAN0, PBEsol, revPBE, revPBE0
    - N12, N12-SX, GAM, MN12-L, MN12-SX, MN15-L, dlDF
    - VV10, LC-VV10
    - B97-K, B97-D3(0), B97-3, $\tau$-HCTH, $\tau$-HCTHh
    - SRC1-R1, SRC1-R2, SRC2-R1, SRC2-R2
    - B1LYP, B1PW91, MPW1K, LRC-BOP, BHH, BB1K, PW6B95, PWB6K, B2PLYP
- Hessian-free minimum point verification (S. M. Sharada and M. Head-Gordon; Section 9.2.2)
- Exciton-based excited-state models:
    - *Ab initio* Frenkel-Davydov model for coupled excitations in multi-chromophore systems (A. F. Morrison and J. M. Herbert; Section 12.14).
    - TDDFT for molecular interactions [TDDFT(MI)], a set of local excitation approximations for efficient TDDFT calculations in multi-chromophore systems and for single chromophores in the presence of explicit solvent molecules (J. Liu and J. M. Herbert; Section 12.15).
- Improvements to many-body and XSAPT methods (K. U. Lao and J. M. Herbert)
    - MPI-parallelized many-body expansion with analytic gradient (Section 12.13).
    - Efficient atomic orbital implementation of XSAPT for both closed- and open-shell systems (Section 12.11.2).
- Thermostats for *ab initio* molecular dynamics (R. P. Steele and J. M. Herbert).
- Analytic energy gradient for the Ewald summation in QM/MM calculations (Z. C. Holden and J. M. Herbert)
- Zeolite QM/MM methods (J. Gomes and M. Head-Gordon).
- EOM-MP2 methods for excitation, ionization and electron attachment energies (A. Kunitsa and K. Bravaya; Section 6.7.8).
- Evaluation of polarizabilities using CCSD and EOM-CCSD wave functions (Section 6.7.15.4, K. Nanda and A. I. Krylov)

- Distributed-memory parallel implementation of CC and EOM-CC methods and performance improvements in disk-based algorithms (E. Epifanovsky, I. Kaliman, and A. I. Krylov)
- Improvements to the maximum overlap method (MOM) for SCF calculations (A. T. B. Gilbert; Section 6.4).
- Non-equilibrium PCM method to describe solvent effects in ADC excited-state calculations (J.-M. Mewes and A. Dreuw; Section 6.8.7).
- Spin-flip ADC method (D. Lefrancois and A. Dreuw; Section 6.8.5).

### 1.3.3 New Features in Q-CHEM 4.3

- Analytic derivative couplings (*i.e.*, non-adiabatic couplings) between electronic states computed at the CIS, spin-flip CIS, TDDFT, and spin-flip TDDFT levels (S. Fatehi, Q. Ou, J. E. Subotnik, X. Zhang, and J. M. Herbert; Section 9.6).
- A third-generation ("+D3") dispersion potential for XSAPT (K. U. Lao and J. M. Herbert; Section 12.11).
- Non-equilibrium PCM for computing vertical excitation energies (at the TDDFT level) and ionization energies in solution (Z.-Q. You and J. M. Herbert; Section 11.2.2.3).
- Spin-orbit couplings between electronic states for CC and EOM-CC wave functions (E. Epifanovsky, J. Gauss, and A. I. Krylov; Section 6.7.15.2).
- PARI-K method for evaluation of exact exchange, which affords dramatic speed-ups for triple-$\zeta$ and larger basis sets in hybrid DFT calculations (S. Manzer and M. Head-Gordon).
- Transition moments and cross sections for two-photon absorption using EOM-CC wave functions (K. Nanda and A. I. Krylov; Section 6.7.15.1).
- New excited-state analysis for ADC and CC/EOM-CC methods (M. Wormit; Section 10.2.7).
- New Dyson orbital code for EOM-IP-CCSD and EOM-EA-CCSD (A. Gunina and A. I. Krylov; Section 6.7.26).
- Transition moments, state dipole moments, and Dyson orbitals for CAP-EOM-CCSD (T.-C. Jagau and A. I. Krylov; Sections 6.7.5 and 6.7.26).
- TAO-DFT: Thermally-assisted-occupation density functional theory (J.-D. Chai; Section 4.4.12).
- MP2[V], a dual basis method that approximates the MP2 energy (J. Deng and A. Gilbert).
- Iterative Hirshfeld population analysis for charged systems, and CM5 semi-empirical charge scheme (K. U. Lao and J. M. Herbert; Section 10.2.1).
- New DFT functionals: (Section 4.4.3):
  - Long-range corrected functionals with empirical dispersion-: $\omega$M05-D, $\omega$B97X-D3 and $\omega$M06-D3 (Y.-S. Lin, K. Hui, and J.-D. Chai.
  - PBE0_DH and PBE0_2 double-hybrid functionals (K. Hui and J.-D. Chai; Section 4.4.9).
  - AK13 (K. Hui and J.-D. Chai).

  - LFAs asymptotic correction scheme (P.-T. Fang and J.-D. Chai).
- LDA/GGA fundamental gap using a frozen-orbital approximation (K. Hui and J.-D. Chai; Section 4.4.11).

### 1.3.4 New Features in Q-CHEM 4.2

- Input file changes:
  - New keyword METHOD simplifies input in most cases by replacing the pair of keywords EXCHANGE and CORRELATION (see Chapter 4).
  - Keywords for requesting excited-state calculations have been modified and simplified (see Chapter 6 for details).
  - Keywords for solvation models have been modified and simplified (see Section 11.2 for details).
- New features for NMR calculations including spin-spin couplings (J. Kussmann, A. Luenser, and C. Ochsenfeld; Section 10.15).
- New built-in basis sets (see Chapter 7).
- New features and performance improvements in EOM-CC:
  - EOM-CC methods extended to treat meta-stable electronic states (resonances) via complex scaling and complex absorbing potentials (D. Zuev, T.-C. Jagau, Y. Shao, and A. I. Krylov; Section 6.7.5).
  - New features added to EOM-CC iterative solvers, such as methods for interior eigenvalues and user-specified guesses (D. Zuev; Section 6.7.11).
  - Multi-threaded parallel code for (EOM-)CC gradients and improved CCSD(T) performance.
- New features and performance improvements in ADC methods (M. Wormit, A. Dreuw):
  - RI-ADC can tackle much larger systems at reduced cost (Section 6.8.2).
  - SOS-ADC methods (Section 6.8.3).
  - State-to-state properties for ADC (Section 6.8.6).
- SM12 implicit solvation model (A. V. Marenich, D. G. Truhlar, and Y. Shao; Section 11.2.8.1).
- Interface to NBO v. 6 (Section 10.3).
- Optimization of MECPs between electronic states at the SOS-CIS(D) and TDDFT levels (X. Zhang and J. M. Herbert; Section 9.6.3).
- ROKS method for $\Delta$SCF calculations of excited states (T. Kowalczyk and T. Van Voorhis; Section 6.5).
- Fragment-based initial guess for SCF methods (Section 12.3).
- Pseudo-fractional occupation number method for improved SCF convergence in small-gap systems (D. S. Lambrecht; Section 4.6.8).
- Density embedding scheme (B. J. Albrecht, E. Berquist, and D. S. Lambrecht; Section 11.6).

- New features and enhancements in fragment-based many-body expansion methods (K. U. Lao and J. M. Herbert):
  - XSAPT(KS)+D: A dispersion corrected version of symmetry-adapted perturbation theory for fast and accurate calculation of interaction energies in non-covalent clusters (Section 12.11).
  - Many-body expansion and fragment molecular orbital (FMO) methods for clusters (Section 12.13).
- Periodic boundary conditions with proper Ewald summation, for energies only (Z. C. Holden and J. M. Herbert; Section 11.3).

### 1.3.5 New Features in Q-CHEM 4.1

- Fundamental algorithms:
  - Improved parallel performance at all levels including new OpenMP capabilities for Hartree-Fock, DFT, MP2, and coupled cluster theory (Z. Gan, E. Epifanovsky, M. Goldey, and Y. Shao; Section 2.8).
  - Significantly enhanced ECP capabilities, including gradients and frequencies in all basis sets for which the energy can be evaluated (Y. Shao and M. Head-Gordon; Chap. 8).
- SCF and DFT capabilities:
  - TDDFT energy with the M06, M08, and M11 series of functionals.
  - XYGJ-OS analytical energy gradient.
  - TDDFT/C-PCM excitation energies, gradient, and Hessian (J. Liu and W. Liang; Section 6.3.4).
  - Additional features in the maximum overlap method (MOM) approach for converging difficult SCF calculations (N. A. Besley; Section 4.6.6).
- Wave function correlation capabilities:
  - RI and Cholesky decomposition implementation of all CC and EOM-CC methods enabling applications to larger systems with reduced disk and memory requirements and improved performance (E. Epifanovsky, X. Feng, D. Zuev, Y. Shao, and A. I. Krylov; Sections 5.8.5 and 5.8.6).
  - Attenuated MP2 theory in the aug-cc-pVDZ and aug-cc-pVTZ basis sets, which truncates two-electron integrals to cancel basis set superposition error, yielding results for intermolecular interactions that are much more accurate than standard MP2 in the same basis set (M. Goldey and M. Head-Gordon; Section 5.7).
  - Extended RAS-$n$SF methodology for ground and excited states involving strong non-dynamical correlation (P. M. Zimmerman, D. Casanova, and M. Head-Gordon; Section 6.9).
  - Coupled cluster valence bond (CCVB) method for describing molecules with strong spin correlations (D. W. Small and M. Head-Gordon; Section 5.15.2).
- Searching and scanning potential energy surfaces:
  - Potential energy surface scans (Y. Shao; Section 9.4).
  - Improvements in automatic transition structure searching via the "freezing string" method, including the ability to perform such calculations without a Hessian calculation (S. M. Sharada and M. Head-Gordon; Section 9.2.2).

  - Enhancements to partial Hessian vibrational analysis (N. A. Besley; Section 10.11.3).

- Calculating and characterizing inter- and intramolecular interactions

  - Extension of EFP to macromolecules: fEFP approach (A. Laurent, D. Ghosh, A. I. Krylov, and L. V. Slipchenko; Section 11.5.3).
  - Symmetry-adapted perturbation theory level at the "SAPT0" level, for intermolecular interaction energy decomposition analysis into physically-meaningful components such as electrostatics, induction, dispersion, and exchange. An RI version is also available (L. D. Jacobson, J. M. Herbert; Section 12.10).
  - The "explicit polarization" (XPol) monomer-based SCF calculations to compute many-body polarization effects in linear-scaling time via charge embedding (Section 12.9), which can be combined either with empirical potentials (*e.g.*, Lennard-Jones) for the non-polarization parts of the intermolecular interactions, or better yet, with SAPT for an *ab initio* approach called XSAPT that extends SAPT to systems containing more that two monomers (L. D. Jacobson and J. M. Herbert; Section 12.11).
  - Extension of the absolutely-localized molecular orbital (ALMO)-based energy decomposition analysis to unrestricted cases (P. R. Horn and M. Head-Gordon; Section 12.5).
  - Calculation of the populations of "effectively unpaired electrons" in low-spin state using DFT, a new method of evaluating localized atomic magnetic moments within Kohn-Sham without symmetry breaking, and Mayer-type bond order analysis with inclusion of static correlation effects (E. I. Proynov; Section 10.18).

- Quantum transport calculations including electron transmission functions and electron tunneling currents under applied bias voltage (B. D. Dunietz and N. Sergueev; Section 10.19).

- Searchable online version of the Q-CHEM PDF manual (J. M. Herbert and E. Epifanovsky).

### 1.3.6 New Features in Q-CHEM 4.0.1

- Remote submission capability in IQMOL (A. T. B. Gilbert).

- Scaled nuclear charge and charge-cage stabilization capabilities (T. Kús and A. I. Krylov; Section 6.7.6).

- Calculations of excited state properties including transition dipole moments between different excited states in CIS and TDDFT as well as couplings for electron and energy transfer (Z.-Q. You and C.-P. Hsu; Section 10.17).

### 1.3.7 New Features in Q-CHEM 4.0

- New exchange-correlation functionals (Section 4.4.3):

  - Density-functional dispersion using Becke and Johnson's XDM model in an efficient, analytic form (Z. Gan, E. I. Proynov, and J. Kong; Section 4.4.7.3).
  - Van der Waals density functionals vdW-DF-04 and vdW-DF-10 of Langreth and co-workers (O. Vydrov; Section 4.4.7.1).
  - VV09 and VV10, new analytic dispersion functionals (O. Vydrov, T. Van Voorhis; Section 4.4.7.1)

  - DFT-D3 empirical dispersion methods for non-covalent interactions (S.-P. Mao and J.-D. Chai; Section 4.4.7.2).
  - $\omega$B97X-2, a double-hybrid functional based on the long-range corrected B97 functional, with improved accounting for medium- and long-range interactions (J.-D. Chai and M. Head-Gordon; Section 4.4.9).
  - XYGJ-OS, a double-hybrid functional for predictions of non-bonded interactions and thermochemistry at nearly chemical accuracy (X. Xu, W. A. Goddard, and Y. Jung; Section 4.4.9).
  - Short-range corrected functional for calculation of near-edge X-ray absorption spectra (N. A. Besley; Section 6.10.1).
  - LB94 asymptotically-corrected exchange-correlation functional for TDDFT (Y.-C. Su and J.-D. Chai; Section 4.4.10.1).
  - Non-dynamical correlation in DFT with an efficient RI implementation of the Becke05 model in a fully analytic formulation (E. I. Proynov, Y. Shao, F. Liu, and J. Kong; Section 4.4.3).
  - TPSS and its hybrid version TPSSh, and rPW86 (F. Liu and O. Vydrov).
  - Double-hybrid functional B2PLYP-D (J.-D. Chai).
  - Hyper-GGA functional MCY2 from Mori-Sánchez, Cohen, and Yang (F. Liu).
  - SOGGA, SOGGA11 and SOGGA11-X family of GGA functionals (R. Peverati, Y. Zhao, and D. G. Truhlar).
  - M08-HX and M08-SO suites of high HF exchange meta-GGA functionals (Y. Zhao and D. G. Truhlar).
  - M11-L and M11 suites of meta-GGA functionals (R. Peverati, Y. Zhao, D. G. Truhlar).

- Improved DFT algorithms:

  - Multi-resolution exchange-correlation (mrXC) for fast calculation of grid-based XC quadrature (S. T. Brown, C.-M. Chang, and J. Kong; Section 4.8.7).
  - Efficient computation of the XC part of the dual basis DFT (Z. Gan and J. Kong; Section 4.5.5).
  - Fast DFT calculation with "triple jumps" between different sizes of basis set and grid, and different levels of functional (J. Deng, A. T. B. Gilbert, and P. M. W. Gill; Section 4.10).
  - Faster DFT and HF calculation with an atomic resolution-of-identity algorithm (A. Sodt and M. Head-Gordon; Section 4.8.8).

- Post-Hartree–Fock methods:

  - Significantly enhanced coupled-cluster code rewritten for better performance on multi-core architectures, including energy and gradient calculations with CCSD and energy calculations with EOM-EE/SF/IP/EA-CCSD, and CCSD(T) energy calculations (E. Epifanovsky, M. Wormit, T. Kús, A. Landau, D. Zuev, K. Khistyaev, I. Kaliman, A. I. Krylov, and A. Dreuw; Chaps. 5 and 6).
  - Fast and accurate coupled-cluster calculations with frozen natural orbitals (A. Landau, D. Zuev, and A. I. Krylov; Section 5.11).
  - Correlated excited states with the perturbation-theory based, size-consistent ADC scheme (M. Wormit and A. Dreuw; Section 6.8).
  - Restricted active space, spin-flip method for multi-configurational ground states and multi-electron excited states (P. M. Zimmerman, F. Bell, D. Casanova, and M. Head-Gordon; Section 6.2.4).

- Post-Hartree–Fock methods for describing strong correlation:
  - "Perfect quadruples" and "perfect hextuples" methods for strong correlation problems (J. A. Parkhill and M. Head-Gordon; Section 5.10.5).
  - Coupled-cluster valence bond (CCVB) methods for multiple-bond breaking (D. W. Small, K. V. Lawler, and M. Head-Gordon; Section 5.15).
- TDDFT for excited states:
  - Nuclear gradients for TDDFT (Z. Gan, C.-P. Hsu, A. Dreuw, M. Head-Gordon, and J. Kong; Section 6.3.1).
  - Direct coupling of charged states for study of charge transfer reactions (Z.-Q. You and C.-P. Hsu; Section 10.17.2).
  - Analytical excited-state Hessian for TDDFT within the Tamm-Dancoff approximation (J. Liu and W. Liang; Section 6.3.5).
  - Self-consistent excited-states with the maximum overlap method (A. T. B. Gilbert, N. A. Besley, and P. M. W. Gill; Section 6.4).
  - Calculation of reactions via configuration interactions of charge-constrained states computed with constrained DFT (Q. Wu, B. Kaduk and T. Van Voorhis; Section 4.11).
  - Overlap analysis of the charge transfer in a TDDFT excited state (N. A. Besley; Section 6.3.2).
  - Localizing diabatic states with Boys or Edmiston-Ruedenberg localization, for charge or energy transfer (J. E Subotnik, R. P. Steele, N. Shenvi, and A. Sodt; Section 10.17.1.2).
  - Non-collinear formalism for spin-flip TDDFT (Y. Shao, Y. A. Bernard, and A. I. Krylov; Section 6.3)
- Solvation and condensed-phase modeling
  - Smooth free energy surface for solvated molecules via SWIG-PCMs, for QM and QM/MM calculations, including a linear-scaling QM/MM/PCM algorithm (A. W. Lange and J. M. Herbert; Sections 11.2.2 and 11.2.4).
  - Klamt's COSMO solvation model with DFT energy and gradient (Y. Shao; Section 11.2.7).
  - Polarizable explicit solvent via EFP, for ground- and excited-state calculations at the DFT/ TDDFT and CCSD/EOM-CCSD levels, as well as CIS and CIS(D). A library of effective fragments for common solvents is also available, along with energy and gradient for EFP–EFP calculations (V. Vanovschi, D. Ghosh, I. Kaliman, D. Kosenkov, C. F. Williams, J. M. Herbert, M. S. Gordon, M. W. Schmidt, Y. Shao, L. V. Slipchenko, and A. I. Krylov; Section 11.5).
- Optimizations, vibrations, and dynamics:
  - "Freezing" and "growing" string methods for efficient automated reaction-path finding (A. Behn, P. M. Zimmerman, A. T. Bell, and M. Head-Gordon; Section 9.2.1).
  - Improved robustness of the intrinsic reaction coordinate (IRC)-following code (M. Head-Gordon).
  - Quantum-mechanical treatment of nuclear motion at equilibrium via path integrals (R. P. Steele; Section 9.8).
  - Calculation of local vibrational modes of interest with partial Hessian vibrational analysis (N. A. Besley; Section 10.11.3).

  - Accelerated *ab initio* molecular dynamics MP2 and/or dual-basis methods, based on $Z$-vector extrapolation (R. P. Steele; Section 4.9.2).
  - Quasi-classical *ab initio* molecular dynamics (D. S. Lambrecht and M. Head-Gordon; Section 9.7.5).

- Fragment-based methods:
  - Symmetry-adapted perturbation theory (SAPT) for computing and analyzing dimer interaction energies (L. D. Jacobson, M. A. Rohrdanz, and J. M. Herbert; Section 12.10).
  - Many-body generalization of SAPT ("XSAPT"), with empirical dispersion corrections for high accuracy and low cost in large clusters (L. D. Jacobson, K. U. Lao, and J. M. Herbert; Section 12.11).
  - Methods based on a truncated many-body expansion, including the fragment molecular orbital (FMO) method (K. U. Lao and J. M. Herbert; Section 12.13).

- Properties and wave function analysis:
  - Analysis of metal oxidation states via localized orbital bonding analysis (A. J. W. Thom, E. J. Sundstrom, and M. Head-Gordon; Section 10.2.5).
  - Hirshfeld population analysis (S. Yeganeh; Section 10.2.1).
  - Visualization of non-covalent bonding using Johnson and Yang's NCI algorithm (Y. Shao; Section 10.5.5).
  - Electrostatic potential on a grid for transition densities (Y. Shao; Section 10.6).

- Support for modern computing platforms
  - Efficient multi-threaded parallel performance for CC, EOM, and ADC methods.
  - Better performance for multi-core systems with shared-memory parallel DFT and Hartree-Fock (Z. Gan, Y. Shao, and J. Kong) and RI-MP2 (M. Goldey and M. Head-Gordon; Section 5.14).
  - Accelerated RI-MP2 calculation on GPUs (R. Olivares-Amaya, M. Watson, R. Edgar, L. Vogt, Y. Shao, and A. Aspuru-Guzik; Section 5.6.4).

- Graphical user interfaces:
  - Input file generation, Q-CHEM job submission, and visualization is supported by IQMOL, a fully integrated GUI developed by Andrew Gilbert. IQMOL is a free software and does not require purchasing a Q-CHEM license. See `www.iqmol.org` for details and installation instructions.
  - Other graphical interfaces are also available, including MOLDEN, MACMOLPLT, and AVOGADRO (Chapter 10 and elsewhere).

### 1.3.8 Summary of Features in Q-CHEM versions 3.*x*

- DFT functionals and algorithms:
  - Long-ranged corrected (LRC) functionals, also known as range-separated hybrid functionals (M. A. Rohrdanz and J. M. Herbert)
  - Constrained DFT (Q. Wu and T. Van Voorhis)

  - Grimme's "DFT-D" empirical dispersion corrections (C.-D. Sherrill)
  - "Incremental" DFT method that significantly accelerates exchange-correlation quadrature in later SCF cycles (S. T. Brown)
  - Efficient SG-0 quadrature grid with approximately half the number of grid points relative to SG-1 (S.-H. Chien)

- Solvation models:
  - SM8 model (A. V. Marenich, R. M. Olson, C. P. Kelly, C. J. Cramer, and D. G. Truhlar)
  - Onsager reaction-field model (C.-L. Cheng, T. Van Voorhis, K. Thanthiriwatte, and S. R. Gwaltney)
  - Chipman's SS(V)PE model (S. T. Brown)

- Second-order perturbation theory algorithms for ground and excited states:
  - Dual-basis RIMP2 energy and analytical gradient (R. P. Steele, R. A. DiStasio Jr., and M. Head-Gordon)
  - O2 energy and gradient (R. C. Lochan and M. Head-Gordon)
  - SOS-CIS(D), SOS-CIS($D_0$), and RI-CIS(D) for excited states (D. Casanova, Y. M. Rhee, and M. Head-Gordon)
  - Efficient resolution-of-identity (RI) implementations of MP2 and SOS-MP2 (including both energies and gradients), and of RI-TRIM and RI-CIS(D) energies (Y. Jung, R. A. DiStasio, Jr., R. C. Lochan, and Y. M. Rhee)

- Coupled-cluster methods (P. A. Pieniazek, E. Epifanovsky, A. I. Krylov):
  - IP-CISD and EOM-IP-CCSD energy and gradient
  - Multi-threaded (OpenMP) parallel coupled-cluster calculations
  - Potential energy surface crossing minimization with CCSD and EOM-CCSD methods (E. Epifanovsky)
  - Dyson orbitals for ionization from the ground and excited states within CCSD and EOM-CCSD methods (M. Oana)

- QM/MM methods (H. L. Woodcock, A. Ghysels, Y. Shao, J. Kong, and H. B. Brooks)
  - Q-CHEM/CHARMM interface (H. L. Woodcock)
  - Full QM/MM Hessian evaluation and approximate mobile-block-Hessian evaluation
  - Two-layer ONIOM model (Y. Shao).
  - Integration with the MOLARIS simulation package (E. Rosta).

- Improved two-electron integrals package
  - Rewrite of the Head-Gordon–Pople algorithm for modern computer architectures (Y. Shao)
  - Fourier Transform Coulomb method for linear-scaling construction of the Coulomb matrix, even for basis sets with high angular moment and diffuse functions (L. Fusti-Molnar)

- Dual basis self-consistent field calculations, offering an order-of-magnitude reduction in the cost of large-basis DFT calculations (J. Kong and R. P. Steele)

- Enhancements to the correlation package including:
  - Most extensive range of EOM-CCSD methods available including EOM-SF-CCSD, EOM-EE-CCSD, EOM-DIP-CCSD, EOM-IP/EA-CCSD (A. I. Krylov).
  - Available for RHF, UHF, and ROHF references.
  - Analytic gradients and properties calculations (permanent and transition dipoles *etc.*.).
  - Full use of Abelian point-group symmetry.
- Coupled-cluster perfect-paring methods applicable to systems with $>$ 100 active electrons (M. Head-Gordon)
- Transition structure search using the "growing string" algorithm (A. Heyden and B. Peters):
- *Ab initio* molecular dynamics (J. M. Herbert)
- Linear scaling properties for large systems (J. Kussmann, C. Ochsenfeld):
  - NMR chemical shifts
  - Static and dynamic polarizabilities
  - Static hyper-polarizabilities, optical rectification, and electro-optical Pockels effect
- Anharmonic frequencies (C. Y. Lin)
- Wave function analysis tools:
  - Analysis of intermolecular interactions with ALMO-EDA (R. Z. Khaliullin and M. Head-Gordon)
  - Electron transfer analysis (Z.-Q. You and C.-P. Hsu)
  - Spin densities at the nuclei (V. A. Rassolov)
  - Position, momentum, and Wigner intracules (N. A. Besley and D. P. O'Neill)
- Graphical user interface options:
  - IQmol, a fully integrated GUI. IQmol includes input file generator and contextual help, molecular builder, job submission tool, and visualization kit (molecular orbital and density viewer, frequencies, etc). For the latest version and download/installation instructions, please see the IQmol homepage (`www.iqmol.org`).
  - Seamless integration with the Spartan package (see `www.wavefun.com`).
  - Support for several other public-domain visualization programs:
    - WebMO  
      `www.webmo.net`
    - Avogadro  
      `www.avogadro.openmolecules.net/wiki/Get_Avogadro`
    - MolDen  
      `www.cmbi.ru.nl/molden`
    - MacMolPlt (via a MolDen-formatted input file)  
      `wiki.wxmacmolplt.googlecode.com/git/MacMolPlt_Manual.html`
    - JMol  
      `www.sourceforge.net/project/showfiles.php?group_id= 23629&release_id=6689`

### 1.3.9 Summary of Features Prior to Q-CHEM 3.0

- Efficient algorithms for large-molecule density functional calculations:
  - CFMM for linear scaling Coulomb interactions (energies and gradients) (C. A. White).
  - Second-generation J-engine and J-force engine (Y. Shao).
  - LinK for exchange energies and forces (C. Ochsenfeld and C. A. White).
  - Linear scaling DFT exchange-correlation quadrature.
- Local, gradient-corrected, and hybrid DFT functionals:
  - Slater, Becke, GGA91 and Gill '96 exchange functionals.
  - VWN, PZ81, Wigner, Perdew86, LYP and GGA91 correlation functionals.
  - EDF1 exchange-correlation functional (R. Adamson).
  - B3LYP, B3P and user-definable hybrid functionals.
  - Analytical gradients and analytical frequencies.
  - SG-0 standard quadrature grid (S.-H. Chien).
  - Lebedev grids up to 5294 points (S. T. Brown).
- High level wave function-based electron correlation methods
  - Efficient semi-direct MP2 energies and gradients.
  - MP3, MP4, QCISD, CCSD energies.
  - OD and QCCD energies and analytical gradients.
  - Triples corrections (QCISD(T), CCSD(T) and OD(T) energies).
  - CCSD(2) and OD(2) energies.
  - Active space coupled cluster methods: VOD, VQCCD, VOD(2).
  - Local second order Møller-Plesset (MP2) methods (DIM and TRIM).
  - Improved definitions of core electrons for post-HF correlation (V. A. Rassolov).
- Extensive excited state capabilities:
  - CIS energies, analytical gradients and analytical frequencies.
  - CIS(D) energies.
  - Time-dependent density functional theory energies (TDDFT).
  - Coupled cluster excited state energies, OD and VOD (A. I. Krylov).
  - Coupled-cluster excited-state geometry optimizations.
  - Coupled-cluster property calculations (dipoles, transition dipoles).
  - Spin-flip calculations for CCSD and TDDFT excited states (A. I. Krylov and Y. Shao).
- High performance geometry and transition structure optimization (J. Baker):
  - Optimizes in Cartesian, *Z*-matrix or delocalized internal coordinates.
  - Impose bond angle, dihedral angle (torsion) or out-of-plane bend constraints.
  - Freezes atoms in Cartesian coordinates.

  - Constraints do not need to be satisfied in the starting structure.
  - Geometry optimization in the presence of fixed point charges.
  - Intrinsic reaction coordinate (IRC) following code.

- Evaluation and visualization of molecular properties
  - Onsager, SS(V)PE and Langevin dipoles solvation models.
  - Evaluate densities, electrostatic potentials, orbitals over cubes for plotting.
  - Natural Bond Orbital (NBO) analysis.
  - Attachment/detachment densities for excited states via CIS, TDDFT.
  - Vibrational analysis after evaluation of the nuclear coordinate Hessian.
  - Isotopic substitution for frequency calculations (R. Doerksen).
  - NMR chemical shifts (J. Kussmann).
  - Atoms in Molecules (AIMPAC) support (J. Ritchie).
  - Stability analysis of SCF wave functions (Y. Shao).
  - Calculation of position and momentum molecular intracules A. Lee, N. A. Besley, and D. P. O'Neill).

- Flexible basis set and effective core potential (ECP) functionality: (Ross Adamson and Peter Gill)
  - Wide range of built-in basis sets and ECPs.
  - Basis set superposition error correction.
  - Support for mixed and user-defined basis sets.
  - Effective core potentials for energies and gradients.
  - Highly efficient PRISM-based algorithms to evaluate ECP matrix elements.
  - Faster and more accurate ECP second derivatives for frequencies.

## 1.4 Citing Q-Chem

Users who publish papers based on Q-Chem calculations are asked to cite the official peer-reviewed literature citation for the software. For versions corresponding to 4.0 and later, this is:

> Y. Shao, Z. Gan, E. Epifanovsky, A. T. B. Gilbert, M. Wormit, J. Kussmann, A. W. Lange, A. Behn, J. Deng, X. Feng, D. Ghosh, M. Goldey P. R. Horn, L. D. Jacobson, I. Kaliman, R. Z. Khaliullin, T. Kús, A. Landau, J. Liu, E. I. Proynov, Y. M. Rhee, R. M. Richard, M. A. Rohrdanz, R. P. Steele, E. J. Sundstrom, H. L. Woodcock III, P. M. Zimmerman, D. Zuev, B. Albrecht, E. Alguire, B. Austin, G. J. O. Beran, Y. A. Bernard, E. Berquist, K. Brandhorst, K. B. Bravaya, S. T. Brown, D. Casanova, C.-M. Chang, Y. Chen, S. H. Chien, K. D. Closser, D. L. Crittenden, M. Diedenhofen, R. A. DiStasio Jr., H. Dop, A. D. Dutoi, R. G. Edgar, S. Fatehi, L. Fusti-Molnar, A. Ghysels, A. Golubeva-Zadorozhnaya, J. Gomes, M. W. D. Hanson-Heine, P. H. P. Harbach, A. W. Hauser, E. G. Hohenstein, Z. C. Holden, T.-C. Jagau, H. Ji, B. Kaduk, K. Khistyaev, J. Kim, J. Kim, R. A. King, P. Klunzinger, D. Kosenkov, T. Kowalczyk, C. M. Krauter, K. U. Lao, A. Laurent, K. V. Lawler, S. V. Levchenko, C. Y. Lin, F. Liu, E. Livshits, R. C. Lochan, A. Luenser, P. Manohar, S. F. Manzer, S.-P. Mao, N. Mardirossian, A. V. Marenich, S. A. Maurer, N. J. Mayhall, C. M. Oana, R. Olivares-Amaya,

D. P. O'Neill, J. A. Parkhill, T. M. Perrine, R. Peverati, P. A. Pieniazek, A. Prociuk, D. R. Rehn, E. Rosta, N. J. Russ, N. Sergueev, S. M. Sharada, S. Sharmaa, D. W. Small, A. Sodt, T. Stein, D. Stück, Y.-C. Su, A. J. W. Thom, T. Tsuchimochi, L. Vogt, O. Vydrov, T. Wang, M. A. Watson, J. Wenzel, A. White, C. F. Williams, V. Vanovschi, S. Yeganeh, S. R. Yost, Z.-Q. You, I. Y. Zhang, X. Zhang, Y. Zhou, B. R. Brooks, G. K. L. Chan, D. M. Chipman, C. J. Cramer, W. A. Goddard III, M. S. Gordon, W. J. Hehre, A. Klamt, H. F. Schaefer III, M. W. Schmidt, C. D. Sherrill, D. G. Truhlar, A. Warshel, X. Xua, A. Aspuru-Guzik, R. Baer, A. T. Bell, N. A. Besley, J.-D. Chai, A. Dreuw, B. D. Dunietz, T. R. Furlani, S. R. Gwaltney, C.-P. Hsu, Y. Jung, J. Kong, D. S. Lambrecht, W. Liang, C. Ochsenfeld, V. A. Rassolov, L. V. Slipchenko, J. E. Subotnik, T. Van Voorhis, J. M. Herbert, A. I. Krylov, P. M. W. Gill, and M. Head-Gordon. *Advances in molecular quantum chemistry contained in the Q-Chem 4 program package.* [*Mol. Phys.* **113**, 184–215 (2015)]

Literature citations for Q-CHEM v. 2.0[1] and v. 3.0[2] are also available, and the most current list of Q-CHEM authors can always be found on the website, `www.q-chem.com`. The primary literature is extensively referenced throughout this manual, and users are urged to cite the original literature for particular theoretical methods. This is how our large community of academic developers gets credit for its effort.

## References and Further Reading

[1] J. Kong et al., *J. Comput. Chem.* **21**, 1532 (2000).

[2] Y. Shao et al., *Phys. Chem. Chem. Phys.* **8**, 3172 (2006).

[3] Y. Shao et al., *Mol. Phys.* **113**, 184 (2015).

[4] A. I. Krylov and P. M. W. Gill, *Wiley Interdiscip. Rev.: Comput. Mol. Sci.* **3**, 317 (2013).

# Chapter 2

# Installation, Customization, and Execution

## 2.1 Installation Requirements

### 2.1.1 Execution Environment

Q-CHEM is shipped as a single executable along with several scripts. No compilation is required. Once the package is installed it is ready to run. Please refer to the installation notes for your particular platform, which are distributed with the software. The system software required to run Q-CHEM on your platform is minimal, and includes:

- A suitable operating system.
- Run-time libraries (usually provided with your operating system).
- Perl, version 5 or greater.
- Vendor implementation of MPI or MPICH libraries (for the MPI-based parallel version only).

Please check the Q-CHEM web site (`www.q-chem.com`), or contact Q-CHEM support (`support@q-chem.com`) if further details are required.

### 2.1.2 Hardware Platforms and Operating Systems

Q-CHEM runs on a wide varieties of computer systems, ranging from Intel and AMD microprocessor-based PCs and workstations, to high-performance server nodes used in clusters and supercomputers. Q-CHEM supports the Linux, Mac, and Windows operating systems. To determine the availability of a specific platform or operating system, please contact `support@q-chem.com`.

### 2.1.3 Memory and Disk Requirements

***Memory***

Q-CHEM, Inc. has endeavored to minimize memory requirements and maximize the efficiency of its use. Still, the larger the structure or the higher the level of theory, the more memory is needed. Although Q-CHEM can be run successfully in very small-memory environments, this is seldom an issue nowadays and we recommend 1 Gb as a minimum. Q-CHEM also offers the ability for user control of important, memory-intensive aspects of the program. In general, the more memory your system has, the larger the calculation you will be able to perform.

Q-CHEM uses two types of memory: a chunk of static memory that is used by multiple data sets and managed by the code, and dynamic memory which is allocated using system calls. The size of the static memory is specified by the user through the *$rem* variable MEM_STATIC and has a default value of 64 Mb.

The *$rem* word MEM_TOTAL specifies the limit of the total memory the user's job can use. The default value is sufficiently large that on most machines it will allow Q-CHEM to use all the available memory. This value should be reduced on machines where this is undesirable (for example if the machine is used by multiple users). The limit for the dynamic memory allocation is given by (MEM_TOTAL − MEM_STATIC). The amount of MEM_STATIC needed depends on the size of the user's particular job. Please note that one should not specify an excessively large value for MEM_STATIC, otherwise it will reduce the available memory for dynamic allocation. Memory settings in CC, EOM, and ADC calculations are described in Section 5.14. The use of *$rem* variables will be discussed in the next Chapter.

***Disk***

The Q-CHEM executables, shell scripts, auxiliary files, samples and documentation require between 360–400 Mb of disk space, depending on the platform. The default Q-CHEM output, which is printed to the designated output file, is usually only a few kilobytes. This will be exceeded, of course, in difficult geometry optimizations, QM/MM and QM/EFP jobs, as well as in cases where users invoke non-default print options. In order to maximize the capabilities of your copy of Q-CHEM, additional disk space is required for scratch files created during execution, and these are automatically deleted on normal termination of a job. The amount of disk space required for scratch files depends critically on the type of job, the size of the molecule and the basis set chosen.

Q-CHEM uses direct methods for Hartree-Fock and density functional theory calculations, which do not require large amount of scratch disk space. Wave function-based correlation methods, such as MP2 and coupled-cluster theory require substantial amounts of temporary (scratch) disk storage, and the faster the access speeds, the better these jobs will perform. With the low cost of disk drives, it is feasible to have between 100 and 1000 Gb of scratch space available as a dedicated file system for these large temporary job files. The more you have available, the larger the jobs that will be feasible and in the case of some jobs, like MP2, the jobs will also run faster as two-electron integrals are computed less often.

Although the size of any one of the Q-CHEM temporary files will not exceed 2 Gb, a user's job will not be limited by this. Q-CHEM writes large temporary data sets to multiple files so that it is not bounded by the 2 Gb file size limitation on some operating systems.

## 2.2 Installing Q-CHEM

Users are referred to the detailed installation instructions distributed with your copy of Q-CHEM.

An encrypted license file, *qchem.license.dat*, must be obtained from your vendor before you will be able to use Q-Chem. This file should be placed in the directory *$QCAUX/license* and must be able to be read by all users of the software. This file is node-locked, *i.e.*, it will only operate correctly on the machine for which it was generated. Further details about obtaining this file, can be found in the installation instructions.

**Do not alter the license file unless directed by Q-Chem, Inc.**

## 2.3 Q-Chem Auxiliary files (*$QCAUX*)

The *$QCAUX* environment variable determines the directory where Q-Chem searches for auxiliary files and the machine license. If not set explicitly, it defaults to *$QC/qcaux*.

The *$QCAUX* directory contains files required to run Q-Chem calculations, including basis set and ECP specifications, SAD guesses (see Chapter 4), library of standard effective fragments (see Section 11.5), and instructions for the AOInts package for generating two-electron integrals efficiently.

## 2.4 Q-Chem Run-time Environment Variables

Q-Chem requires the following shell environment variables setup prior to running any calculations:

QC Defines the location of the Q-Chem directory structure. The *qchem.install* shell script determines this automatically.

QCAUX Defines the location of the auxiliary information required by Q-Chem, which includes the license required to run Q-Chem. If not explicitly set by the user, this defaults to *$QC/qcaux*.

QCSCRATCH Defines the directory in which Q-Chem will store temporary files. Q-Chem will usually remove these files on successful completion of the job, but they can be saved, if so wished. Therefore, *$QCSCRATCH* should not reside in a directory that will be automatically removed at the end of a job, if the files are to be kept for further calculations.

Note that many of these files can be very large, and it should be ensured that the volume that contains this directory has sufficient disk space available. The *$QCSCRATCH* directory should be periodically checked for scratch files remaining from abnormally terminated jobs. *$QCSCRATCH* defaults to the working directory if not explicitly set. Please see section 2.7 for details on saving temporary files and consult your systems administrator.

QCLOCALSCR On certain platforms, such as Linux clusters, it is sometimes preferable to write the temporary files to a disk local to the node. *$QCLOCALSCR* specifies this directory. The temporary files will be copied to *$QCSCRATCH* at the end of the job, unless the job is terminated abnormally. In such cases Q-Chem will attempt to remove the files in *$QCLOCALSCR*, but may not be able to due to access restrictions. Please specify this variable only if required.

## 2.5 User Account Adjustments

In order for individual users to run Q-CHEM, User file access permissions must be set correctly so that the user can read, write and execute the necessary Q-CHEM files. It may be advantageous to create a *qchem* user group on your machine and recursively change the group ownership of the Q-CHEM directory to *qchem* group.

The Q-CHEM run-time environment need to be initiated prior to running any Q-CHEM calculations, which is done by sourcing the environment setup script qcenv.sh (for bash) or qcenv.csh (for csh and tcsh) placed in your Q-CHEM top directory after a successful installation. It might be more convenient for user to include the Q-CHEM environment setup in their shell startup script, *e.g.*, *.cshrc/.tcshrc* for csh/tcsh or *.bashrc* for bash.

If using the csh or tcsh shell, add the following lines to the *.cshrc* file in the user's home directory:

```
#
setenv  QC         qchem_root_directory_name
setenv  QCSCRATCH  scratch_directory_name
source  $QC/qcenv.csh
#
```

If using the Bourne-again shell (bash), add the following lines to the *.bashrc* file in the user's home directory:

```
#
export QC=qchem_root_directory_name
export QCSCRATCH=scratch_directory_name
. $QC/qcenv.sh
#
```

## 2.6 Further Customization: *.qchemrc* and *preferences* Files

Q-CHEM has developed a simple mechanism for users to set user-defined long-term defaults to override the built-in program defaults. Such defaults may be most suited to machine specific features such as memory allocation, as the total available memory will vary from machine to machine depending on specific hardware and accounting configurations. However, users may identify other important uses for this customization feature. Q-CHEM obtains input initialization variables from four sources:

1. User input file
2. *$HOME/.qchemrc* file
3. *$QC/config/preferences* file
4. "Factory installed" program defaults

Input mechanisms higher in this list override those that are lower. Mechanisms #2 and #3 allow the user to specify alternative default settings for certain variables that will override the Q-CHEM "factory-installed" defaults. This can be done by a system administrator via a *preferences* file added to the *$QC/config* directory, or by an individual user by means of a *.qchemrc* file in her home directory.

**Note:** The *.qchemrc* and *preferences* files are not requisites for running Q-CHEM and currently only support keywords in the *$rem* input section.

The format of the *.qchemrc* and *preferences* files consists of a *$rem* keyword section, as in the Q-CHEM input file, terminated with the usual *$end* keyword. Any other *$whatever* section will be ignored. To aid in reproducibility, a copy of the *.qchemrc* file (if present) is included near the top of the job's output file. (The *.qchemrc* and *preferences* files must have file permissions such that they are readable by the user invoking Q-CHEM.) The format of both of these files is as follows:

```
$rem
   rem_variable   option   comment
   rem_variable   option   comment
   ...
$end
```

**Example 2.1** An example of a *.qchemrc* file to override default *$rem* settings for all of the user's Q-CHEM jobs.

```
$rem
   INCORE_INTS_BUFFER   4000000   More integrals in memory
   DIIS_SUBSPACE_SIZE   5         Modify max DIIS subspace size
   THRESH               10        10**(-10) threshold
   MAX_SCF_CYCLES       100       More than the default of 50
$end
```

The following *$rem* variables are specifically recommended as those that a user might want to customize:

- AO2MO_DISK
- INCORE_INTS_BUFFER
- MEM_STATIC
- SCF_CONVERGENCE
- THRESH
- MAX_SCF_CYCLES
- GEOM_OPT_MAX_CYCLES

## 2.7 Running Q-CHEM

Once installation is complete, and any necessary adjustments are made to the user account, the user is now able to run Q-CHEM. There are several ways to invoke Q-CHEM:

1. IQMOL offers a fully integrated graphical interface for the Q-CHEM package and includes a sophisticated input generator with contextual help which is able to guide you through the many Q-CHEM options available. It also provides a molecular builder, job submission and monitoring tools, and is able to visualize molecular orbitals, densities and vibrational frequencies. For the latest version and download/installation instructions, please see the IQMOL homepage (`www.iqmol.org`).

2. *qchem* command line shell script. The simple format for command line execution is given below. The remainder of this manual covers the creation of input files in detail.

3. Via a third-party GUI. The two most popular ones are:

   - A general web-based interface for electronic structure software, WEBMO (`www.webmo.net`).
   - Wavefunction's SPARTAN user interface on some platforms. Contact Wavefunction, Inc. (`www.wavefun.com`) or Q-CHEM for full details of current availability.

Using the Q-CHEM command line shell script (*qchem*) is straightforward provided Q-CHEM has been correctly installed on your machine and the necessary environment variables have been set in your *.cshrc*, *.profile*, or equivalent login file. If done correctly, the necessary changes will have been made to the *$PATH* variable automatically on login so that Q-CHEM can be invoked from your working directory.

The *qchem* shell script can be used in either of the following ways:

```
qchem infile outfile
qchem infile outfile savename
qchem -save infile outfile savename
```

where *infile* is the name of a suitably formatted Q-CHEM input file (detailed in Chapter 3, and the remainder of this manual), and the *outfile* is the name of the file to which Q-CHEM will place the job output information.

**Note:** If the *outfile* already exists in the working directory, it will be overwritten.

The use of the *savename* command line variable allows the saving of a few key scratch files between runs, and is necessary when instructing Q-CHEM to read information from previous jobs. If the *savename* argument is not given, Q-CHEM deletes all temporary scratch files at the end of a run. The saved files are in *$QCSCRATCH/savename/*, and include files with the current molecular geometry, the current molecular orbitals and density matrix and the current force constants (if available). The *–save* option in conjunction with *savename* means that all temporary files are saved, rather than just the few essential files described above. Normally this is not required. When *$QCLOCALSCR* has been specified, the temporary files will be stored there and copied to *$QCSCRATCH/savename/* at the end of normal termination.

The name of the input parameters *infile*, *outfile* and *save* can be chosen at the discretion of the user (usual UNIX file and directory name restrictions apply). It maybe helpful to use the same job name for *infile* and *outfile*, but with varying suffixes. For example:

```
localhost-1> qchem water.in water.out &
```

invokes Q-CHEM where the input is taken from *water.in* and the output is placed into *water.out*. The `&` places the job into the background so that you may continue to work in the current shell.

```
localhost-2> qchem water.com water.log water &
```

invokes Q-CHEM where the input is assumed to reside in *water.com*, the output is placed into *water.log* and the key scratch files are saved in a directory *$QCSCRATCH/water/.*

**Note:** A checkpoint file can be requested by setting GUI = 2 in the *$rem* section of the input. The checkpoint file name is determined by the *$GUIFILE* environment variable which by default is set to *${input}.fchk*

## 2.8 Parallel Q-CHEM Jobs

Parallel execution of Q-CHEM can be threaded across multiple processors on a single node, using the OpenMP protocol, or using the message-passing interface (MPI) protocol to parallelize over multiple processor cores and/or multiple compute nodes. A hybrid MPI + OpenMP scheme is also available for certain calculations, in which each MPI process spawns several OpenMP threads. In this hybrid scheme, cross-node communication is handled by the MPI protocol and intra-node communication is done implicitly using OpenMP threading for efficient utilization of shared-memory parallel (SMP) systems. This parallelization strategy reflects current trends towards multi-core architectures in cluster computing.

As of the v. 4.2 release, the OpenMP parallelization is fully supported by HF/DFT, RIMP2, CC, EOM-CC, and ADC methods. The MPI parallel capability is available for SCF, DFT, CIS, and TDDFT methods. The hybrid MPI+OpenMP parallelization is introduced in v. 4.2 for HF/DFT energy and gradient calculations only. Distributed memory MPI+OpenMP parallelization of CC and EOM-CC methods was added in Q-CHEM v. 4.3. Table 2.1 summarizes the parallel capabilities of Q-CHEM v. 4.4.

| **Method** | OpenMP | MPI | MPI+OpenMP |
|---|---|---|---|
| HF energy & gradient | yes | yes | yes |
| DFT energy & gradient | yes | yes | yes |
| CDFT/CDFT-CI | no | no | no |
| RI-MP2 energy | yes | no | no |
| Attenuated RI-MP2 energy | yes | no | no |
| Integral transformation | yes | no | no |
| CCMAN & CCMAN2 methods | yes | yes | yes |
| ADC methods | yes | no | no |
| CIS energy & gradient | no | yes | no |
| TDDFT energy & gradient | no | yes | no |
| HF & DFT analytical Hessian | no | yes | no |

Table 2.1: Parallel capabilities of Q-CHEM v. 4.4

To run Q-CHEM calculation with OpenMP threads specify the number of threads (*nthreads*) using *qchem* command option *-nt*. Since each thread uses one CPU core, you should not specify more threads than the total number of available CPU cores for performance reason. When unspecified, the number of threads defaults to 1 (serial calculation).

```
qchem -nt nthreads infile outfile
qchem -nt nthreads infile outfile save
qchem -save -nt nthreads infile outfile save
```

Similarly, to run parallel calculations with MPI use the option *-np* to specify the number of MPI processes to be spawned.

```
qchem -np n infile outfile
qchem -np n infile outfile savename
qchem -save -np n infile outfile savename
```

where $n$ is the number of processors to use. If the *-np* switch is not given, Q-CHEM will default to running locally on a single node.

To run hybrid MPI+OpenMP HF/DFT calculations use combined options *-np* and *-nt* together, where *-np* followed by the number of MPI processes to be spawned and *-nt* followed by the number of OpenMP threads used in each MPI process.

```
qchem -np n -nt nthreads infile outfile
qchem -np n -nt nthreads infile outfile savename
qchem -save -np n -nt nthreads infile outfile savename
```

When the additional argument *savename* is specified, the temporary files for MPI-parallel Q-CHEM are stored in *$QCSCRATCH/savename.0* At the start of a job, any existing files will be copied into this directory, and on successful completion of the job, be copied to *$QCSCRATCH/savename/* for future use. If the job terminates abnormally, the files will not be copied.

To run parallel Q-CHEM using a batch scheduler such as PBS, users may need to set QCMPIRUN environment variable to point to the *mpirun* command used in the system. For further details users should read the *$QC/README.Parallel* file, and contact Q-CHEM if any problems are encountered (`support@q-chem.com`).

## 2.9 IQMOL Installation Requirements

IQMOL provides a fully integrated molecular builder and viewer for the Q-CHEM package. It is available for the Windows, Linux, and Mac OS X platforms and instructions for downloading and installing the latest version can be found at `www.iqmol.org/downloads.html`.

IQMOL can be run as a stand-alone package which is able to open existing Q-CHEM input/output files, but it can also be used as a fully functional front end which is able to submit and monitor Q-CHEM jobs, and to analyze the resulting output. By default, IQMOL submits Q-CHEM jobs to a server that is owned by Q-CHEM, Inc., which provides prospective users with the opportunity to run short Q-CHEM demonstration jobs for free simply by downloading IQMOL, without the need to install Q-CHEM.

For customers who own Q-CHEM, it is necessary to configure IQMOL to submit jobs to an appropriate server. To do this, first ensure Q-CHEM has been correctly installed on the target machine and can be run from the command line. Second, open IQMOL and carry out the following steps:

1. Select the Calculation→Edit Servers menu option. A dialog will appear with a list of configured servers (which will initially be empty).
2. Click the Add New Server button with the '+' icon. This opens a dialog which allows the new server to be configured. The server is the machine which has your Q-CHEM installation.

3. Give the server a name (this is simply used to identify the current server configuration and does not have to match the actual machine name) and select if the machine is local (*i.e.* the same machine as IQMOL is running on) or remote.

4. If there is PBS software running on the server, select the PBS 'Type' option, otherwise in most cases the Basic option should be sufficient. Please note that the server must be Linux based and cannot be a Windows server.

5. If required, the server can be further configured using the Configure button. Details on this can be found in the embedded IQMOL help which can be accessed via the Help→Show Help menu option.

6. For non-PBS servers the number of concurrent Q-CHEM jobs can be limited using a simple inbuilt queuing system. The maximum number of jobs is set by the Job Limit control. If the Job Limit is set to zero the queue is disabled and any number of jobs can be run concurrently. Please note that this limit applies to the current IQMOL session and does not account for jobs submitted by other users or by other IQMOL sessions.

7. The $QC environment variable should be entered in the given box.

8. For remote servers the address of the machine and your user name are also required. IQMOL uses SSH2 to connect to remote machines and the most convenient way to set this up is by using authorized keys (`www.debian.org/devel/passwordlessssh`) for details on how these can be set up). IQMOL can then connect via the SSH Agent and will not have to prompt you for your password. If you are not able to use an SSH Agent, several other authentication methods are offered:

   - **Public Key** This requires you to enter your SSH passphrase (if any) to unlock your private key file. The passphrase is stored in memory, not disk, so you will need to re-enter this each time IQMOL is run.
   - **Password Vault** This allows a single password (the vault key) to be used to unlock the passwords for all the configured servers. The server passwords are salted with 64 random bits and encrypted using the AES algorithm before being stored on disk. The vault key is not stored permanently and must be re-entered each time IQMOL is run.
   - **Password Prompt** This requires each server password to be entered each time IQMOL is run. Once the connection has been established the memory used to hold the password is overwritten to reduce the risk of recovery from a core dump.

   Further configuration of SSH options should not be required unless your public/private keys are stored in a non-standard location.

It is recommended that you test the server configuration to ensure everything is working before attempting to submit a job. Multiple servers can be configured if you have access to more than one copy of Q-CHEM or have different account configurations. In this case the default server is the first on the list and if you want to change this you should use the arrow buttons in the Server List dialog. The list of configured servers will be displayed when submitting Q-CHEM jobs and you will be able to select the desired server for each job.

Please note that while Q-CHEM is file-based, as of version 2.1 IQMOL uses a directory to keep the various files from a calculation. More details can be found in the IQMOL `user manual`.

## 2.10 Testing and Exploring Q-CHEM

Q-CHEM is shipped with a small number of test jobs which are located in the *$QC/samples* directory. If you wish to test your version of Q-CHEM, run the test jobs in the samples directory and compare the output files with the reference files (suffixed *.out*) of the same name.

These test jobs are not an exhaustive quality control test (a small subset of the test suite used at Q-CHEM, Inc.), but they should all run correctly on your platform. If any fault is identified in these, or any output files created by your version, do not hesitate to contact customer service immediately.

These jobs are also an excellent way to begin learning about Q-CHEM's text-based input and output formats in detail. In many cases you can use these inputs as starting points for building your own input files, if you wish to avoid reading the rest of this manual!

Please check the Q-CHEM web page (`www.q-chem.com`) and the README files in the *$QC/bin* directory for updated information.

I

# Chapter 3

# Q-CHEM Inputs

## 3.1 IQMOL

The easiest way to run Q-CHEM is by using the IQMOL interface which can be downloaded for free from `www.iqmol.org`. Before submitting a Q-CHEM job from you will need to configure a Q-CHEM server and details on how to do this are given in Section 2.9 of this manual.

IQMOL provides a free-form molecular builder and a comprehensive interface for setting up the input for Q-CHEM jobs. Additionally calculations can be submitted to either the local or a remote machine and monitored using the built in job monitor. The output can also be analyzed allowing visualization of molecular orbitals and densities, and animation of vibrational modes and reaction pathways. A more complete list of features can be found at `www.iqmol.org/features.html`.

The IQMOL program comes with a built-in help system that details how to set up and submit Q-CHEM calculations. This help can be accessed via the Help→Show Help menu option.

## 3.2 General Form

IQMOL (or another graphical interface) is the simplest way to control Q-CHEM. However, the low level command line interface is available to enable maximum customization and allow the user to exploit all Q-CHEM's features. The command line interface requires a Q-CHEM input file which is simply an ASCII text file. This input file can be created using your favorite editor (*e.g.*, vi, emacs, jot, *etc.*) following the basic steps outlined in the next few chapters.

Q-CHEM's input mechanism uses a series of **keywords** to signal user input sections of the input file. As required, the Q-CHEM program searches the input file for supported keywords. When Q-CHEM finds a keyword, it then reads the section of the input file beginning at the keyword until that keyword section is terminated the *$end* keyword. A short description of all Q-CHEM keywords is provided in Table 3.1 and the following sections. The user **must** understand the function and format of the *$molecule* (Section 3.3) and *$rem* (Section 3.4) keywords, as these keyword sections are where the user places the molecular geometry information and job specification details.

| **Section Name** | **Description** |
|---|---|
| *$molecule* | Contains the molecular coordinate input (input file requisite). |
| *$rem* | Job specification and customization parameters (input file requisite). |
| *$basis* | User-defined basis set information (Chapter 7). |
| *$cdft* | Options for the constrained DFT method (Section 4.11). |
| *$chem_sol* | Job control for the Q-CHEM/CHEMSOL interface (Langevin dipoles model; Section 11.2.9). |
| *$comment* | User comments for inclusion into output file. |
| *$complex_ccman* | Contains parameters for complex-scaled and CAP-augmented EOM-CC calculations (Chapter 6.7). |
| *$ecp* | User-defined effective core potentials (Chapter 8). |
| *$efei* | Application of external forces in a geometry optimization (Section 9.3.6). |
| *$efp_fragments* | Specifies labels and positions of EFP fragments (Section 11.5). |
| *$efp_params* | Contains user-defined parameters for effective fragments (Section 11.5). |
| *$empirical_dispersion* | User-defined van der Waals parameters for DFT dispersion correction (Section 4.4.7.2). |
| *$eom_user_guess* | User-defined guess for EOM-CC calculations (Chapter 6.7). |
| *$external_charges* | Specifies external point charges and their positions. |
| *$force_field_params* | Force-field parameters for QM/MM calculations (Section 11.3). |
| *$intracule* | Intracule parameters (Section 10.10). |
| *$isotopes* | Isotopic substitutions for vibrational calculations (Section 10.11.2). |
| *$localized_diabatization* | Information for mixing together multiple adiabatic states into diabatic states (Chapter 10). |
| *$multipole_field* | Details of an external multipole field (Section 3.5.7). |
| *$nbo* | Options for the Natural Bond Orbital package (Section 10.3). |
| *$occupied* | Guess orbitals to be occupied (Section 4.5.4). |
| *$opt* | Constraint definitions for geometry optimizations (Section 9.3). |
| *$pcm* | Job control for polarizable continuum models (Section 11.2.3). |
| *$plots* | Generate plotting information over a grid of points (Section 10.5). |
| *$qct_active_modes* | Information for quasi-classical trajectory calculations (Section 9.7.5). |
| *$qct_vib_distribution* | |
| *$qct_vib_phase* | |
| *$qm_atoms* | Specify the QM region for QM/MM calculations (Section 11.3). |
| *$solvent* | Additional parameters and variables for implicit solvent models (Section 11.2). |
| *$smx* | Job control for SM$x$ implicit solvent models (Section 11.2.8). |
| *$swap_occupied_virtual* | Guess orbitals to be swapped (Section 4.5.4). |
| *$svp* | Special parameters for the iso-density SS(V)PE module (Section 11.2.5). |
| *$svpirf* | Initial guess for the iso-density SS(V)PE module (Section 11.2.5). |
| *$2pa* | Additional parameters for two-photon absorption calculations (Section 6.7.15.1). |
| *$van_der_waals* | User-defined atomic radii for Langevin dipoles solvation (Section 11.2.9) and PCMs (Section 11.2.2). |
| *$xc_functional* | User-defined DFT exchange-correlation functional (Section 4.4.3.6). |

Table 3.1: A list of Q-CHEM input sections; the first two (*$molecule* and *$rem*) are required for all jobs, whereas the rest are required only for certain job types, or else are optional places to specify additional job-control variables. Each input section ("*$section*") should be terminated with *$end*. See the *$QC/samples* directory that is included with your release for specific examples of Q-CHEM input files using these keywords.

**The keywords *$rem* and *$molecule* are required in any Q-CHEM input file**

As each keyword has a different function, the format required for specific keywords varies somewhat, to account for these differences (format requirements are summarized in Appendix C). However, because each keyword in the input file is sought out independently by the program, the overall format requirements of Q-CHEM input files are much less stringent. For example, the *$molecule* section does not have to occur at the very beginning of the input file.

**Note:** (1) Users are able to enter keyword sections in any order.
(2) Each keyword section must be terminated with the *$end* keyword.
(3) The *$rem* and *$molecule* sections must be included.
(4) It is not necessary to have all keywords in an input file.
(5) Each keyword section is described in Appendix C.
(6) The entire Q-CHEM input is case-insensitive.

The second general aspect of Q-CHEM input is that there are effectively four input sources:

- User input file (required)
- *.qchemrc* file in *$HOME* (optional)
- *preferences* file in *$QC/config* (optional)
- Internal program defaults and calculation results (built-in)

The order of preference is as shown, *i.e.*, the input mechanism offers a program default override for *all* users, default override for *individual* users and, of course, the input file provided by the user overrides all defaults. Refer to Section 2.6 for details of *.qchemrc* and *preferences*. Currently, Q-CHEM only supports the *$rem* keyword in *.qchemrc* and *preferences* files.

In general, users will need to enter variables for the *$molecule* and *$rem* keyword section and are encouraged to add a *$comment* for future reference. The necessity of other keyword input will become apparent throughout the manual.

## 3.3 Molecular Coordinate Input (*$molecule*)

The *$molecule* section communicates to the program the charge, spin multiplicity, and geometry of the molecule being considered. The molecular coordinates input begins with two integers: the net charge and the spin multiplicity of the molecule. The net charge must be between $-50$ and 50, inclusive (0 for neutral molecules, 1 for cations, $-1$ for anions, *etc.*.). The multiplicity must be between 1 and 10, inclusive (1 for a singlet, 2 for a doublet, 3 for a triplet, *etc.*.). Each subsequent line of the molecular coordinate input corresponds to a single atom in the molecule (or dummy atom), regardless of whether using *Z*-matrix internal coordinates or Cartesian coordinates.

**Note:** The coordinate system used for declaring an initial molecular geometry by default does not affect that used in a geometry optimization procedure. See Appendix A which discusses the OPTIMIZE package in further detail.

Q-CHEM begins all calculations by rotating and translating the user-defined molecular geometry into a Standard Nuclear Orientation whereby the center of nuclear charge is placed at the origin. This is a standard feature of most quantum chemistry programs. This action can be turned off by using SYM_IGNORE TRUE.

**Note:** SYM_IGNORE = TRUE will also turn off determining and using of the point group symmetry.

**Note:** Q-CHEM ignores commas and equal signs, and requires all distances, positions and angles to be entered as Ångstroms and degrees unless the INPUT_BOHR *$rem* variable is set to TRUE, in which case all lengths are assumed to be in bohr.

## 3.3.1 Specifying the Molecular Coordinates Manually

### 3.3.1.1 Cartesian Coordinates

Q-CHEM can accept a list of $N$ atoms and their $3N$ Cartesian coordinates. The atoms can be entered either as atomic numbers or atomic symbols where each line corresponds to a single atom. The Q-CHEM format for declaring a molecular geometry using Cartesian coordinates (in Ångstroms) is:

```
atom  x-coordinate  y-coordinate  z-coordinate
```

**Note:** The geometry can by specified in bohr by setting the *$rem* variable INPUT_BOHR equal to TRUE.

**Example 3.1** Atomic number Cartesian coordinate input for $H_2O$. The first line species the molecular charge and multiplicity, respectively.

```
$molecule
   0 1
   8   0.000000   0.000000  -0.212195
   1   1.370265   0.000000   0.848778
   1  -1.370265   0.000000   0.848778
$end
```

**Example 3.2** Atomic symbol Cartesian coordinate input for $H_2O$.

```
$molecule
   0 1
   O   0.000000   0.000000  -0.212195
   H   1.370265   0.000000   0.848778
   H  -1.370265   0.000000   0.848778
$end
```

**Note:** (1) Atoms can be declared by either atomic number or symbol.
(2) Coordinates can be entered either as variables/parameters or real numbers.
(3) Variables/parameters can be declared in any order.
(4) A single blank line separates parameters from the atom declaration.

Once all the molecular Cartesian coordinates have been entered, terminate the molecular coordinate input with the *$end* keyword.

#### 3.3.1.2 *Z*-matrix Coordinates

For small molecules, *Z*-matrix notation is a common input format. The *Z*-matrix defines the positions of atoms relative to previously defined atoms using a length, an angle and a dihedral angle. Again, note that all bond lengths and angles must be in Ångstroms and degrees, unless INPUT_BOHR is set to TRUE, in which case bond lengths are specified in bohr.

**Note:** As with the Cartesian coordinate input method, Q-CHEM begins a calculation by taking the user-defined coordinates and translating and rotating them into a Standard Nuclear Orientation.

The first three atom entries of a *Z*-matrix are different from the subsequent entries. The first *Z*-matrix line declares a single atom. The second line of the *Z*-matrix input declares a second atom, refers to the first atom and gives the distance between them. The third line declares the third atom, refers to either the first or second atom, gives the distance between them, refers to the remaining atom and gives the angle between them. All subsequent entries begin with an atom declaration, a reference atom and a distance, a second reference atom and an angle, a third reference atom and a dihedral angle. This can be summarized as:

1. First atom.
2. Second atom, reference atom, distance.
3. Third atom, reference atom A, distance between A and the third atom, reference atom B, angle defined by atoms A, B and the third atom.
4. Fourth atom, reference atom A, distance, reference atom B, angle, reference atom C, dihedral angle (A, B, C and the fourth atom).
5. All subsequent atoms follow the same basic form as (4)

**Example 3.3** *Z*-matrix for hydrogen peroxide

```
O1
O2   O1   oo
H1   O1   ho   O2   hoo
H2   O2   ho   O1   hoo   H1   hooh
```

Line 1 declares an oxygen atom (O1). Line 2 declares the second oxygen atom (O2), followed by a reference to the first atom (O1) and a distance between them denoted `oo`. Line 3 declares the first hydrogen atom (H1), indicates it is separated from the first oxygen atom (O1) by a distance HO and makes an angle with the second oxygen atom (O2) of `hoo`. Line 4 declares the fourth atom and the second hydrogen atom (H2), indicates it is separated from the second oxygen atom (O2) by a distance HO and makes an angle with the first oxygen atom (O1) of `hoo` and makes a dihedral angle with the first hydrogen atom (H1) of `hooh`.

Some further points to note are:

- Atoms can be declared by either atomic number or symbol.
  - If declared by atomic number, connectivity needs to be indicated by *Z*-matrix line number.
  - If declared by atomic symbol either number similar atoms (*e.g.*, H1, H2, O1, O2 *etc.*) and refer connectivity using this symbol, or indicate connectivity by the line number of the referred atom.

- Bond lengths and angles can be entered either as variables/parameters or real numbers.
    - Variables/parameters can be declared in any order.
    - A single blank line separates parameters from the *Z*-matrix.

All the following examples are equivalent in the information forwarded to the Q-CHEM program.

**Example 3.4** Using parameters to define bond lengths and angles, and using numbered symbols to define atoms and indicate connectivity.

```
$molecule
   0 1
   O1
   O2  O1  oo
   H1  O1  ho  O2  hoo
   H2  O2  ho  O1  hoo  H1  hooh

   oo   =   1.5
   oh   =   1.0
   hoo  = 120.0
   hooh = 180.0
$end
```

**Example 3.5** Not using parameters to define bond lengths and angles, and using numbered symbols to define atoms and indicate connectivity.

```
$molecule
   0 1
   O1
   O2  O1  1.5
   H1  O1  1.0  O2  120.0
   H2  O2  1.0  O1  120.0  H1  180.0
$end
```

**Example 3.6** Using parameters to define bond lengths and angles, and referring to atom connectivities by line number.

```
$molecule
   0 1
   8
   8  1  oo
   1  1  ho  2  hoo
   1  2  ho  1  hoo  3  hooh

   oo   =   1.5
   oh   =   1.0
   hoo  = 120.0
   hooh = 180.0
$end
```

**Example 3.7** Referring to atom connectivities by line number, and entering bond length and angles directly.

```
$molecule
  0 1
  8
```

```
   8  1  1.5
   1  1  1.0  2  120.0
   1  2  1.0  1  120.0  3  180.0
$end
```

Obviously, a number of the formats outlined above are less appealing to the eye and more difficult for us to interpret than the others, but each communicates *exactly* the same *Z*-matrix to the Q-CHEM program.

#### 3.3.1.3 Dummy Atoms

Dummy atoms are indicated by the identifier $X$ and followed, if necessary, by an integer. (*e.g.*, $X1$, $X2$. Dummy atoms are often useful for molecules where symmetry axes and planes are not centered on a real atom, and have also been useful in the past for choosing variables for structure optimization and introducing symmetry constraints.

**Note:** Dummy atoms play no role in the quantum mechanical calculation, and are used merely for convenience in specifying other atomic positions or geometric variables.

### 3.3.2 Reading Molecular Coordinates from a Previous Job or File

Often users wish to perform several calculations in sequence, where the later calculations rely on results obtained from the previous ones. For example, a geometry optimization at a low level of theory, followed by a vibrational analysis and then, perhaps, single-point energy at a higher level. Rather than having the user manually transfer the coordinates from the output of the optimization to the input file of a vibrational analysis or single point energy calculation, Q-CHEM can transfer them directly from job to job.

To achieve this requires that:

- The *READ* variable is entered into the molecular coordinate input
- Scratch files from a previous calculation have been saved. These may be obtained *explicitly* by using the save option across multiple job runs as described below and in Chapter 2, or *implicitly* when running multiple calculations in one input file, as described in Section 3.6.

**Example 3.8** Reading a geometry from a prior calculation.

```
$molecule
   READ
$end
```

```
localhost-1> qchem job1.in job1.out job1
localhost-2> qchem job2.in job2.out job1
```

In this example, the *job1* scratch files are saved in a directory *$QCSCRATCH/job1* and are then made available to the *job2* calculation.

**Note:** The program must be instructed to read specific scratch files by the input of *job2*.

The *READ* function can also be used to read molecular coordinates from a second input file. The format for the coordinates in the second file follows that for standard Q-CHEM input, and must be delimited with the *$molecule* and *$end* keywords.

**Example 3.9** Reading molecular coordinates from another file. *filename* may be given either as the full file path, or path relative to the working directory.

```
$molecule
   READ filename
$end
```

## 3.4 Job Specification: The *$rem* Input Section

The *$rem* section in the input file is the means by which users specify the type of calculation that they wish to perform (*i.e.*, level of theory, basis set, convergence criteria, additional special features, *etc.*.). The keyword *$rem* signals the beginning of the overall job specification. Within the *$rem* section the user inserts ***$rem* variables** (one per line) which define the essential details of the calculation. The allowed format is either

```
REM_VARIABLE      VALUE     [ comment ]
```

or alternatively

```
REM_VARIABLE    =  VALUE    [ comment ]
```

The "=" sign is automatically discarded and only the first two remaining arguments are read, so that all remaining text is ignored and can be used to place comments in the input file. Thus the *$rem* section that provides Q-CHEM job control takes the form shown in the following example.

**Example 3.10** General format of the *$rem* section of the text input file.

```
$rem
  REM_VARIABLE  value  [ comment ]
  REM_VARIABLE  value  [ comment ]
   ...
$end
```

**Note:** (1) Tab stops can be used to format input.
(2) A line prefixed with an exclamation mark '!' is treated as a comment and will be ignored by the program.
(3) *$rem* variables are case-insensitive (as is the whole Q-CHEM input file).
(4) Depending on the particular *$rem* variable, "`value`" may be a keyword (string), an integer, or a logical value (true or false).
(5) A complete list of *$rem* variables can be found in Appendix C.

In this manual, *$rem* variables will be described using the following format:

**REM_VARIABLE_NAME**

A short description of what the variable controls.

TYPE:

The type of variable (INTEGER, LOGICAL or STRING)

DEFAULT:

The default value, if any.

OPTIONS:

A list of the options available to the user.

RECOMMENDATION:

A brief recommendation, where appropriate.

If a default setting is indicated for a particular *$rem* variable, then it is not necessary to declare that variable in order for the default setting to be used. For example, the default value for the variable JOBTYPE is SP, indicating a single-point energy calculation, so to perform such a calculation the user does **not** need to set the JOBTYPE variable. To perform a geometry optimization, however, it is necessary to override this default by setting JOBTYPE = OPT. System administrator preferences for default *$rem* settings can be specified in the *$QC/config/preferences* file, and user preferences in a *$HOME/.qchemrc* file, both of which are described in Section 2.6.

Q-CHEM provides defaults for most *$rem* variables, but the user will always have to stipulate a few others. In a single point energy calculation, for example, the minimum requirements will be BASIS (defining the basis set) and METHOD (defining the level of theory for correlation and exchange). For example, METHOD = HF invokes a Hartree-Fock calculation, whereas METHOD = CIS specifies a CIS excited-state calculation.

**Example 3.11** Example of minimal *$rem* requirements to run an MP2/6-31G* single-point energy calculation.

```
$rem
   BASIS         6-31G*    Just a small basis set
   METHOD        mp2       MP2
$end
```

The level of theory can alternatively be specified by setting values for two other *$rem* variables, EXCHANGE (defining the level of theory to treat exchange) and CORRELATION (defining the level of theory to treat electron correlation, if required). For excited states computed using equation-of-motion (EOM) methods (Chapter 6), there is a third *$rem* variable, EOM_CORR, which specifies the level of correlation for the target states.

For DFT calculations, METHOD specifies an exchange-correlation functional; see Section 4.4.4 for a list of supported functionals. For wave function approaches, supported values of METHOD can be found in Section 5.1 for ground-state methods and in Section 6.1 for excited-state methods. If a wave function-based correlation treatment such as MP2 or CC is requested using the CORRELATION keyword, then HF is taken as the default for EXCHANGE.

## 3.5 Additional Input Sections

The *$molecule* and *$rem* sections are required for all Q-CHEM jobs, but depending on the details of the job a number of other input sections may be required. These are summarized briefly below, with references to more detailed descriptions to be found later in this manual.

### 3.5.1 Comments (*$comment*)

Users are able to add comments to the input file outside keyword input sections, which will be ignored by the program. This can be useful as reminders to the user, or perhaps, when teaching another user to set up inputs. Comments can also be provided in a *$comment* block, which is actually redundant given that the entire input deck is copied to the output file.

### 3.5.2 User-Defined Basis Sets (*$basis* and *$aux_basis*)

By setting the *$rem* keyword BASIS = GEN, the user indicates that the basis set will be user defined. In that case, the *$basis* input section is used to specify the basis set. Similarly, if AUX_BASIS = GEN then the *$aux_basis* input section is used to specify the auxiliary basis set. See Chapter 7 for details on how to input a user-defined basis set.

### 3.5.3 User-Defined Effective Core Potential (*$ecp*)

By setting ECP = GEN, the user indicates that the effective core potentials (pseudopotentials, which replace explicit core electrons) to be used will be defined by the user. In that case, the *$ecp* section is used to specify these pseudopotentials. See Chapter 8 for further details.

### 3.5.4 User-Defined Exchange-Correlation Density Functionals (*$xc_functional*)

If the keyword EXCHANGE = GEN then a DFT calculation will be performed using a user-specified combination of exchange and correlation functional(s), as described in Chapter 4. Custom functionals of this sort can be constructed as any linear combination of exchange and/or correlation functionals that are supported by Q-CHEM; see Section 4.4.4 for a list of supported functionals. The format for the *$xc_functional* input section is the following:

```
$xc_functional
   X  exchange_symbol  coefficient
   X  exchange_symbol  coefficient
   ...
   C  correlation_symbol  coefficient
   C  correlation_symbol  coefficient
   ...
   K  coefficient
$end
```

**Note:** The coefficients must be real numbers.

### 3.5.5 User-defined Parameters for DFT Dispersion Correction (*$empirical_dispersion*)

If a user wants to change from the default values recommended by Grimme, then user-defined parameters can be specified using the *$empirical_dispersion* input section. See Section 4.4.7.2 for details.

### 3.5.6 Addition of External Point Charges (*$external_charges*)

If the *$external_charges* keyword is present, Q-CHEM scans for a set of external charges to be incorporated into a calculation. The format is shown below and consists of Cartesian coordinates and the value of the point charge, with one charge per line. The charge is in atomic units and the coordinates are in Ångstroms, unless bohrs are selected by setting the *$rem* keyword INPUT_BOHR to TRUE. The external charges are rotated with the molecule into the standard nuclear orientation.

**Example 3.12** General format for incorporating a set of external charges.

```
$external_charges
   x-coord1  y-coord1  z-coord1  charge1
   x-coord2  y-coord2  z-coord2  charge2
   x-coord3  y-coord3  z-coord3  charge3
$end
```

In addition, the user can request to add a charged cage around the molecule (for so-called "charge stabilization" calculations) using the keyword ADD_CHARGED_CAGE. See Section 6.7.6 for details.

### 3.5.7 Applying a Multipole Field (*$multipole_field*)

A multipole field can be applied to the molecule under investigation by specifying the *$multipole_field* input section. Each line in this section consists of a single component of the applied field, in the following format.

**Example 3.13** General format for imposing a multipole field.

```
$multipole_field
   field_component_1   value_1
   field_component_2   value_2
$end
```

Each *field_component* is stipulated using the Cartesian representation *e.g.*, X, Y, and/or Z, (dipole field components); XX, XY, and/or YY (quadrupole field components); XXX, XXY, *etc.*. The value (magnitude) of each field component should be provided in atomic units.

### 3.5.8 User-Defined Occupied Guess Orbitals (*$occupied* and *$swap_occupied_virtual*)

It is sometimes useful for the occupied guess orbitals to be different from the lowest $N_\alpha$ (or $N_\alpha + N_\beta$) orbitals. Q-CHEM allows the occupied guess orbitals to be defined using the *$occupied* keyword. Using the *$occupied* input section, the user can choose which orbitals (by number) to occupy by specifying the

$\alpha$-spin orbitals on the first line of the *$occupied* section and the $\beta$-spin orbitals on the second line. For large molecules where only a few occupied $\rightarrow$ virtual promotions are desired, it is simpler to use the *$swap_occupied_virtual* input section. Details can be found in Section 4.5.4.

### 3.5.9 Polarizable Continuum Solvation Models (*$pcm*)

The *$pcm* section provides fine-tuning of the job control for polarizable continuum models (PCMs), which are requested by setting the *$rem* keyword SOLVENT_METHOD equal to PCM. Supported PCMs include C-PCM, IEF-PCM, and SS(V)PE, which share a common set of job-control variables. Details are provided in Section 11.2.2.

### 3.5.10 SS(V)PE Solvation Modeling (*$svp* and *$svpirf*)

The *$svp* section is available to specify special parameters to the solvation module such as cavity grid parameters and modifications to the numerical integration procedure. The *$svpirf* section allows the user to specify an initial guess for the solution of the cavity charges. As discussed in section 11.2.5, the *$svp* and *$svpirf* input sections are used to specify parameters for the iso-density implementation of SS(V)PE. An alternative implementation of the SS(V)PE mode, based on a more empirical definition of the solute cavity, is available in the PCM (see Section 11.2.2) and controlled from within the *$pcm* input section.

### 3.5.11 User-Defined van der Waals Radii (*$van_der_waals*)

The *$van_der_waals* section of the input enables the user to customize the van der Waals radii that are important parameters in the Langevin dipoles solvation model; see Section 11.2.

### 3.5.12 Effective Fragment Potential Calculations (*$efp_fragments* and *$efp_params*)

These keywords are used to specify positions and parameters for effective fragments in EFP calculations. Details are provided in Section 11.5.

### 3.5.13 Natural Bond Orbital Package (*$nbo*)

When NBO is set to TRUE in the *$rem* section, a natural bond orbital (NBO) calculation is performed, using the Q-Chem interface to the NBO 5.0 and NBO 6.0 packages. In such cases, the *$nbo* section may contain standard parameters and keywords for the NBO program.

### 3.5.14 Orbitals, Densities and Electrostatic Potentials on a Mesh (*$plots*)

The *$plots* part of the input permits the evaluation of molecular orbitals, densities, electrostatic potentials, transition densities, electron attachment and detachment densities on a user-defined mesh of points. Q-Chem will print out the raw data, but can also format these data into the form of a "cube" file that is a standard input format for volumetric data that can be read various visualization programs. See Section 10.5 for details.

### 3.5.15 Intracules (*$intracule*)

Setting the *$rem* keyword INTRACULE = TRUE requests a molecular intracule calculation, in which case additional customization is possible using the *$intracule* input section. See Section 10.10.

### 3.5.16 Geometry Optimization with Constraints (*$opt*)

For JOBTYPE = OPT, Q-CHEM scans the input file for the *$opt* section. Here, the user may specify distance, angle, dihedral and out-of-plane bend constraints to be imposed on the optimization procedure, as described in Chapter 9.

### 3.5.17 Isotopic Substitutions (*$isotopes*)

For vibrational frequency calculations (JOBTYPE = FREQ), nuclear masses are set by default to be those corresponding to the most abundant naturally-occurring isotopes. Alternative masses for one or more nuclei can be requested by setting ISOTOPES = TRUE in the *$rem* section, in which case the *$isotopes* section is used to specify the desired masses as described in Section 10.11.2. Isotopic substitutions incur negligible additional cost in a frequency calculation.

## 3.6 Multiple Jobs in a Single File: Q-CHEM Batch Jobs

It is sometimes useful to place a sequence of jobs into a single Q-CHEM input file, where the individual inputs should be separated from one another by a line consisting of the string `@@@`. The output from these jobs is then appended sequentially to a single output file. This is useful to ($i$) use information obtained in a prior job (*i.e.*, an optimized geometry) in a subsequent job; or ($ii$) keep related calculations together in a single output file.

Some limitations should be kept in mind:

- The first job will overwrite any existing output file of the same name in the working directory. Restarting the job will also overwrite any existing file.
- Q-CHEM reads all the jobs from the input file immediately and stores them. Therefore no changes can be made to the details of subsequent jobs following command-line initiation of Q-CHEM, even if these subsequent jobs have not yet run.
- If any single job fails, Q-CHEM proceeds to the next job in the batch file, for good or ill.
- No check is made to ensure that dependencies are satisfied, or that information is consistent. For example, in a geometry optimization followed by a frequency calculation, no attempt is made by the latter to check that the optimization was successful. When reading MO coefficients from a previous job, it is the user's responsibility to ensure that the basis set is the same in both calculations, as this is assumed by the program.
- Scratch files are saved from one job to the next in a batch job, so that information from previous jobs can be shared with subsequent ones, but are deleted upon completion of the entire batch job unless the *–save* command-line argument is supplied, as discussed in Chapter 2.

The following example requests a batch job consisting of $(i)$ a HF/6-31G* geometry optimization; followed by $(ii)$ a frequency calculation at the same level of theory that uses the previously-optimized geometry (and also reads in the final MOs from the optimization job); and finally $(iii)$ a single-point calculation at the same geometry but at a higher level of theory, MP2/6-311G(d,p).

**Example 3.14** Example of using information from previous jobs in a single input file.

```
$comment
   Optimize H-H at HF/6-31G*
$end

$molecule
   0 1
   H
   H  1  r

   r = 1.1
$end

$rem
   JOBTYPE       opt    Optimize the bond length
   METHOD        hf
   BASIS         6-31G*
$end

@@@

$comment
   Now calculate the frequency of H-H at the same level of theory.
$end

$molecule
   read
$end

$rem
   JOBTYPE       freq    Calculate vibrational frequency
   METHOD        hf
   BASIS         6-31G*
   SCF_GUESS     read    Read the MOs from disk
$end

@@@

$comment
  Now a single point calculation at at MP2/6-311G(d,p)//HF/6-31G*
$end

$molecule
   read
$end

$rem
   METHOD        mp2
   BASIS         6-311G(d,p)
$end
```

## 3.7 Q-CHEM Output File

When Q-CHEM is invoked using

```
qchem infile outfile
```

the output file *outfile* contains a variety of information, depending on the type of job(s), but in general consists of the following.

- Q-CHEM citation
- User input (for record-keeping purposes)
- Molecular geometry in Cartesian coordinates
- Molecular point group, nuclear repulsion energy, number of $\alpha$- and $\beta$-spin electrons
- Basis set information (number of functions, shells and function pairs)
- SCF details (method, guess, and convergence procedure)
- Energy and DIIS error for each SCF iteration
- Results of any post-SCF calculation that is requested
- Results of any excited-state calculation that is requested
- Molecular orbital symmetries and energies
- Wave function analysis
- Message signaling successful job completion

**Note:** If *outfile* above already exists when the job is started, then the existing file is overwritten with the results of the new calculation.

# Chapter 4

# Self-Consistent-Field Ground-State Methods

## 4.1 Overview

Theoretical “model chemistries"[5] involve two principle approximations. One must specify, first of all, the type of atomic orbital (AO) basis set that will be used to construct molecular orbitals (MOs), via the “linear combination of atomic orbitals” (LCAO) *ansatz*, available options for which are discussed in Chapters 7 and 8. Second, one must specify the manner in which the instantaneous interactions between electrons (“electron correlation”) are to be treated. Self-consistent field (SCF) methods, in which electron correlation is described in a mean-field way, represent the simplest, most affordable, and most widely-used electronic structure methods. The SCF category of methods includes both Hartree-Fock (HF) theory as well as Kohn-Sham (KS) density functional theory (DFT). This chapter summarizes Q-CHEM’s SCF capabilities, whereas Chapter 5 describes the more sophisticated (but also more computationally expensive!) post-HF, wave function-based methods for describing electron correlation. If you are new to quantum chemistry, we recommend an introductory textbook such as Refs. 5, 6, or 7.

Section 4.2 provides the theoretical background behind SCF methods, including both HF and KS-DFT. In some sense, the former may be considered as a special case of the latter, and job-control *$rem* variables are much the same in both cases. Basic SCF job control is described in Section 4.3. Later sections introduce more specialized options that can be consulted as needed. Of particular note are the following:

- Initial guesses for SCF calculations (Section 4.5). Modification of the guess is recommended in cases where the SCF calculation fails to converge.
- Changing the SCF convergence algorithm (Section 4.6) is also a good strategy when the SCF calculation fails to converge.
- Linear-scaling [“$\mathcal{O}(N)$”] and other reduced-cost methods are available for large systems (see Section 4.8).
- Unconventional SCF calculations. Some non-standard SCF methods with novel physical and mathematical features are available. These include:

- Dual-basis SCF calculations (Section 4.9) and DFT perturbation theory (Section 4.10), which facilitate large-basis quality results but require self-consistent iterations only in a smaller basis set.
- Charge-constrained DFT (CDFT; Section 4.11), in the DFT calculation is subject to the constraint that certain fragments integrate to a pre-defined numbers of electrons. This can be used to circumvent some delocalization problems in conventional DFT.
- Configuration interaction (CI) with a CDFT reference state (CDFT-CI; Section 4.11.3)
- SCF meta-dynamics (Section 4.12.2), which can be used to locate multiple solutions to the SCF equations and to help check that the solution obtained is actually the lowest minimum.

Some of these unconventional SCF methods are available exclusively in Q-CHEM.

## 4.2 Theoretical Background

### 4.2.1 SCF and LCAO Approximations

The fundamental equation of non-relativistic quantum chemistry is the time-independent Schrödinger equation,

$$\hat{H}(\mathbf{R},\mathbf{r})\;\Psi(\mathbf{R},\mathbf{r}) = E(\mathbf{R})\;\Psi(\mathbf{R},\mathbf{r})\;. \tag{4.1}$$

In quantum chemistry, this equation is solved as a function of the electronic variables ($\mathbf{r}$), for fixed values of the nuclear coordinates ($\mathbf{R}$). The Hamiltonian operator in Eq. (4.1), in atomic units, is

$$\hat{H} = -\frac{1}{2}\sum_{i=1}^{N}\nabla_i^2 - \frac{1}{2}\sum_{A=1}^{M}\frac{1}{M_A}\nabla_A^2 - \sum_{i=1}^{N}\sum_{A=1}^{M}\frac{Z_A}{r_{iA}} + \sum_{i=1}^{N}\sum_{j>i}^{N}\frac{1}{r_{ij}} + \sum_{A=1}^{M}\sum_{B>A}^{M}\frac{Z_A Z_B}{R_{AB}} \tag{4.2}$$

where

$$\nabla^2 = \frac{\partial^2}{\partial x^2} + \frac{\partial^2}{\partial y^2} + \frac{\partial^2}{\partial z^2}\;. \tag{4.3}$$

In Eq. (4.2), $Z$ is the nuclear charge, $M_A$ is the ratio of the mass of nucleus $A$ to the mass of an electron, $R_{AB} = |\mathbf{R}_A - \mathbf{R}_B|$ is the distance between nuclei $A$ and $B$, $r_{ij} = |\mathbf{r}_i - \mathbf{r}_j|$ is the distance between the $i$th and $j$th electrons, $r_{iA} = |\mathbf{r}_i - \mathbf{R}_A|$ is the distance between the $i$th electron and the $A$th nucleus, $M$ is the number of nuclei and $N$ is the number of electrons. The total energy $E$ is an eigenvalue of $\hat{H}$, with a corresponding eigenfunction (wave function) $\Psi$.

Separating the motions of the electrons from that of the nuclei, an idea originally due to Born and Oppenheimer[8], yields the electronic Hamiltonian operator:

$$\hat{H}_{\text{elec}} = -\frac{1}{2}\sum_{i=1}^{N}\nabla_i^2 - \sum_{i=1}^{N}\sum_{A=1}^{M}\frac{Z_A}{r_{iA}} + \sum_{i=1}^{N}\sum_{j>i}^{N}\frac{1}{r_{ij}} \tag{4.4}$$

The solution of the corresponding electronic Schrödinger equation,

$$\hat{H}_{\text{elec}}\Psi_{\text{elec}} = E_{\text{elec}}\Psi_{\text{elec}}\;, \tag{4.5}$$

affords the total electronic energy, $E_{\text{elec}}$, and electronic wave function, $\Psi_{\text{elec}}$, which describes the distribution of the electrons for fixed nuclear positions. The total energy is obtained by simply adding the nuclear–nuclear repulsion energy [the fifth term in Eq. (4.2)] to the total electronic energy:

$$E_{\text{tot}} = E_{\text{elec}} + E_{\text{nuc}}\;. \tag{4.6}$$

Solving the eigenvalue problem in Eq. (4.5) yields a set of eigenfunctions ($\Psi_0$, $\Psi_1$, $\Psi_2 \ldots$) with corresponding eigenvalues $E_0 \leq E_1 \leq E_2 \leq \ldots$.

Our interest lies in determining the lowest eigenvalue and associated eigenfunction which correspond to the ground state energy and wave function of the molecule. However, solving Eq. (4.5) for other than the most trivial systems is extremely difficult and the best we can do in practice is to find approximate solutions.

The first approximation used to solve Eq. (4.5) is the independent-electron (mean-field) approximation, in which the wave function is approximated as an antisymmetrized product of one-electron functions, namely, the MOs. Each MO is determined by considering the electron as moving within an average field of all the other electrons. This affords the well-known Slater determinant wave function[9,10]

$$\Psi = \frac{1}{\sqrt{n!}} \begin{vmatrix} \chi_1(1) & \chi_2(1) & \cdots & \chi_n(1) \\ \chi_1(2) & \chi_2(2) & \cdots & \chi_n(2) \\ \vdots & \vdots & & \vdots \\ \chi_1(n) & \chi_2(n) & \cdots & \chi_n(n) \end{vmatrix} , \tag{4.7}$$

where $\chi_i$, a spin orbital, is the product of a molecular orbital $\psi_i$ and a spin function ($\alpha$ or $\beta$).

One obtains the optimum set of MOs by variationally minimizing the energy in what is called a "self-consistent field" or SCF approximation to the many-electron problem. The archetypal SCF method is the Hartree-Fock (HF) approximation, but these SCF methods also include KS-DFT (Section 4.4). All SCF methods lead to equations of the form

$$\hat{f}(i)\,\chi(\mathbf{x}_i) = \varepsilon\,\chi(\mathbf{x}_i) \ , \tag{4.8}$$

where the Fock operator $\hat{f}(i)$ for the $i$th electron is

$$\hat{f}(i) = -\frac{1}{2}\nabla_i^2 + \upsilon_{\text{eff}}(i) \ . \tag{4.9}$$

Here $\mathbf{x}_i$ are spin and spatial coordinates of the $i$th electron, the functions $\chi$ are spin orbitals and $\upsilon_{\text{eff}}$ is the effective potential "seen" by the $i$th electron, which depends on the spin orbitals of the other electrons. The nature of the effective potential $\upsilon_{\text{eff}}$ depends on the SCF methodology, *i.e.*, on the choice of density-functional approximation.

The second approximation usually introduced when solving Eq. (4.5) is the introduction of an AO basis $\{\phi_\mu\}$ linear combinations of which will then determine the MOs. There are many standardized, atom-centered Gaussian basis sets and details of these are discussed in Chapter 7.

After eliminating the spin components in Eq. (4.8) and introducing a finite basis,

$$\psi_i = \sum_\mu c_{\mu i}\phi_\mu \ , \tag{4.10}$$

Eq. (4.8) reduces to the Roothaan-Hall matrix equation

$$\mathbf{FC} = \varepsilon\mathbf{SC} \ . \tag{4.11}$$

Here, $\mathbf{F}$ is the Fock matrix, $\mathbf{C}$ is a square matrix of molecular orbital coefficients, $\mathbf{S}$ is the AO overlap matrix with elements

$$S_{\mu\nu} = \int \phi_\mu(\mathbf{r})\phi_\nu(\mathbf{r})d\mathbf{r} \tag{4.12}$$

and $\varepsilon$ is a diagonal matrix containing the orbital energies. Generalizing to an unrestricted formalism by introducing separate spatial orbitals for $\alpha$ and $\beta$ spin in Eq. (4.7) yields the Pople-Nesbet equations[11]

$$\begin{aligned} \mathbf{F}^\alpha\mathbf{C}^\alpha &= \varepsilon^\alpha\mathbf{S}\mathbf{C}^\alpha \\ \mathbf{F}^\beta\mathbf{C}^\beta &= \varepsilon^\beta\mathbf{S}\mathbf{C}^\beta \end{aligned} \tag{4.13}$$

| **Calculation** | ***$rem* Variable JOBTYPE** | |
|---|---|---|
| Single point energy (default) | SINGLE_POINT or SP | |
| Force (energy + gradient) | FORCE | |
| Equilibrium structure search | OPTIMIZATION or OPT | (Ch. 9) |
| Transition structure search | TS | (Ch. 9) |
| Intrinsic reaction pathway | RPATH | (Sect. 9.5) |
| Potential energy scan | PES_SCAN | (Sect. 9.4) |
| Vibrational frequency calculation | FREQUENCY or FREQ | (Sect. 10.11 and 10.12) |
| NMR chemical shift | NMR | (Sect. 10.13 |
| Indirect nuclear spin-spin coupling | ISSC | (Sect. 10.15 |
| *Ab initio* molecular dynamics | AIMD | (Sect. 9.7 |
| *Ab initio* path integrals | PIMD, PIMC | (Sect. 9.8) |
| BSSE (counterpoise) correction | BSSE | (Sect. 12.4.3) |
| Energy decomposition analysis | EDA | (Sect. 12.5) |

Table 4.1: The type of calculation to be run by Q-CHEM is controlled by the *$rem* variable JOBTYPE.

In SCF methods, an initial guess is for the MOs is first determined, and from this, an average field seen by each electron can be calculated. A new set of MOs can be obtained by solving the Roothaan-Hall or Pople-Nesbet eigenvalue equations, resulting in the restricted or unrestricted finite-basis SCF approximation. This procedure is repeated until the new MOs differ negligibly from those of the previous iteration. The Hartree-Fock approximation for the effective potential in Eq. (4.9) inherently neglects the instantaneous electron-electron correlations that are averaged out by the SCF procedure, and while the chemistry resulting from HF calculations often offers valuable qualitative insight, quantitative energetics are often poor. In principle, the DFT methodologies are able to capture all the correlation energy, *i.e.*, the difference in energy between the HF energy and the true energy. In practice, the best-available density functionals perform well but not perfectly, and conventional post-HF approaches to calculating the correlation energy (see Chapter 5) are often required.

That said, because SCF methods often yield acceptably accurate chemical predictions at low- to moderate computational cost, self-consistent field methods are the cornerstone of most quantum-chemical programs and calculations. The formal costs of many SCF algorithms is $\mathcal{O}(N^4)$, that is, they grow with the fourth power of system size, $N$. This is slower than the growth of the cheapest conventional correlated methods, which scale as $\mathcal{O}(N^5)$ or worse, algorithmic advances available in Q-CHEM can reduce the SCF cost to $\mathcal{O}(N)$ in favorable cases, an improvement that allows SCF methods to be applied to molecules previously considered beyond the scope of *ab initio* quantum chemistry.

In order to carry out an SCF calculation using Q-CHEM, two *$rem* variables need to be set:

| | |
|---|---|
| BASIS | to specify the basis set (see Chapter 7). |
| METHOD | SCF method: HF or a density functional (see Section 4.4). |

Types of ground-state energy calculations currently available in Q-CHEM are summarized in Table 4.1.

### 4.2.2 Hartree-Fock Theory

As with much of the theory underlying modern quantum chemistry, the HF approximation was developed shortly after publication of the Schrödinger equation, but remained a qualitative theory until the advent of the computer. Although the HF approximation tends to yield qualitative chemical accuracy, rather than quantitative information, and is generally inferior to many of the DFT approaches available, it remains as a useful tool in the quantum chemist's toolkit. In particular, for organic chemistry, HF predictions of molecular structure are very useful.

Consider once more the Roothaan-Hall equations, Eq. (4.11), or the Pople-Nesbet equations, Eq. (4.13), which can be traced back to Eq. (4.8), in which the effective potential $\upsilon_{\text{eff}}$ depends on the SCF methodology. In a restricted HF (RHF) formalism, the effective potential can be written as

$$\upsilon_{\text{eff}} = \sum_{a}^{N/2} \big[2\hat{J}_a(1) - \hat{K}_a(1)\big] - \sum_{A=1}^{M} \frac{Z_A}{r_{1A}} \tag{4.14}$$

where the Coulomb and exchange operators are defined as

$$\hat{J}_a(1) = \int \psi_a^*(2) \frac{1}{r_{12}} \psi_a(2)\, d\mathbf{r}_2 \tag{4.15}$$

and

$$\hat{K}_a(1)\psi_i(1) = \left[\int \psi_a^*(2) \frac{1}{r_{12}} \psi_i(2)\, d\mathbf{r}_2\right] \psi_a(1) \tag{4.16}$$

respectively. By introducing an atomic orbital basis, we obtain Fock matrix elements

$$F_{\mu\nu} = H_{\mu\nu}^{\text{core}} + J_{\mu\nu} - K_{\mu\nu} \tag{4.17}$$

where the core Hamiltonian matrix elements

$$H_{\mu\nu}^{\text{core}} = T_{\mu\nu} + V_{\mu\nu} \tag{4.18}$$

consist of kinetic energy elements

$$T_{\mu\nu} = \int \phi_\mu(\mathbf{r}) \left(-\frac{1}{2}\nabla^2\right) \phi_\nu(\mathbf{r})\, d\mathbf{r} \tag{4.19}$$

and nuclear attraction elements

$$V_{\mu\nu} = \int \phi_\mu(\mathbf{r}) \left(-\sum_A \frac{Z_A}{|\mathbf{R}_A - \mathbf{r}|}\right) \phi_\nu(\mathbf{r})\, d\mathbf{r} \tag{4.20}$$

The Coulomb and exchange elements are given by

$$J_{\mu\nu} = \sum_{\lambda\sigma} P_{\lambda\sigma}\, (\mu\nu|\lambda\sigma) \tag{4.21}$$

and

$$K_{\mu\nu} = \frac{1}{2} \sum_{\lambda\sigma} P_{\lambda\sigma}\, (\mu\lambda|\nu\sigma) \tag{4.22}$$

respectively, where the density matrix elements are

$$P_{\mu\nu} = 2 \sum_{a=1}^{N/2} C_{\mu a} C_{\nu a} \tag{4.23}$$

and the two electron integrals are

$$(\mu\nu|\lambda\sigma) = \int\int \phi_\mu(\mathbf{r}_1)\phi_\nu(\mathbf{r}_1) \left(\frac{1}{r_{12}}\right) \phi_\lambda(\mathbf{r_2})\phi_\sigma(\mathbf{r_2})\, d\mathbf{r}_1\, d\mathbf{r}_2\ . \tag{4.24}$$

**Note:** The formation and utilization of two-electron integrals is a topic central to the overall performance of SCF methodologies. The performance of the SCF methods in new quantum chemistry software programs can be quickly estimated simply by considering the quality of their atomic orbital integrals packages. See Appendix B for details of Q-CHEM's AOINTS package.

Substituting the matrix element in Eq. (4.17) back into the Roothaan-Hall equations, Eq. (4.11), and iterating until self-consistency is achieved will yield the RHF energy and wave function. Alternatively, one could have adopted the unrestricted form of the wave function by defining separate $\alpha$ and $\beta$ density matrices:

$$\begin{aligned} P^{\alpha}_{\mu\nu} &= \sum_{a=1}^{n_\alpha} C^{\alpha}_{\mu a} C^{\alpha}_{\nu a} \\ P^{\beta}_{\mu\nu} &= \sum_{a=1}^{n_\beta} C^{\beta}_{\mu a} C^{\beta}_{\nu a} \end{aligned} \tag{4.25}$$

The total electron density matrix $\mathbf{P} = \mathbf{P}^{\alpha} + \mathbf{P}^{\beta}$. The unrestricted $\alpha$ Fock matrix,

$$F^{\alpha}_{\mu\nu} = H^{\text{core}}_{\mu\nu} + J_{\mu\nu} - K^{\alpha}_{\mu\nu} \ , \tag{4.26}$$

differs from the restricted one only in the exchange contributions, where the $\alpha$ exchange matrix elements are given by

$$K^{\alpha}_{\mu\nu} = \sum_{\lambda}^{N} \sum_{\sigma}^{N} P^{\alpha}_{\lambda\sigma} \left(\mu\lambda|\nu\sigma\right) \tag{4.27}$$

### 4.2.3 Wave Function Stability Analysis

At convergence, the SCF energy will be at a stationary point with respect to changes in the MO coefficients. However, this stationary point is not guaranteed to be an energy minimum, and in cases where it is not, the wave function is said to be unstable. Even if the wave function is at a minimum, this minimum may be an artifact of the constraints placed on the form of the wave function. For example, an unrestricted calculation will usually give a lower energy than the corresponding restricted calculation, and this can give rise to a RHF $\rightarrow$ UHF instability.

To understand what instabilities can occur, it is useful to consider the most general form possible for the spin orbitals:

$$\chi_i(\mathbf{r}, \zeta) = \psi^{\alpha}_i(\mathbf{r})\alpha(\zeta) + \psi^{\beta}_i(\mathbf{r})\beta(\zeta) \ . \tag{4.28}$$

Here, $\psi^{\alpha}_i$ and $\psi^{\beta}_i$ are complex-valued functions of the Cartesian coordinates $\mathbf{r}$, and $\alpha$ and $\beta$ are spin eigenfunctions of the spin-variable $\zeta$. The first constraint that is almost universally applied is to assume the spin orbitals depend only on one or other of the spin-functions $\alpha$ or $\beta$. Thus, the spin-functions take the form

$$\chi_i(\mathbf{r}, \zeta) = \psi^{\alpha}_i(\mathbf{r})\alpha(\zeta) \quad \text{or} \quad \chi_i(\mathbf{r}, \zeta) = \psi^{\beta}_i(\mathbf{r})\beta(\zeta) \ . \tag{4.29}$$

In addition, most SCF programs, including Q-CHEM's, deal only with real functions, and this places an additional constraint on the form of the wave function. If there exists a complex solution to the SCF equations that has a lower energy, the wave function exhibits a real $\rightarrow$ complex instability. The final constraint that is commonly placed on the spin-functions is that $\psi^{\alpha}_i = \psi^{\beta}_i$, *i.e.*, that the spatial parts of the spin-up and spin-down orbitals are the same. This gives the familiar restricted formalism and can lead to a RHF $\rightarrow$ UHF instability as mentioned above. Further details about the possible instabilities can be found in Ref. 12.

Wave function instabilities can arise for several reasons, but frequently occur if

- There exists a singlet diradical at a lower energy then the closed-shell singlet state.
- There exists a triplet state at a lower energy than the lowest singlet state.
- There are multiple solutions to the SCF equations, and the calculation has not found the lowest energy solution.

If a wave function exhibits an instability, the seriousness of it can be judged from the magnitude of the negative eigenvalues of the stability matrices. These matrices and eigenvalues are computed by Q-CHEM's Stability Analysis package, which was implemented by Dr Yihan Shao. The package is invoked by setting the STABILITY_ANALYSIS *$rem* variable equal to TRUE. In order to compute these stability matrices Q-CHEM must first perform a CIS calculation. This will be performed automatically, and does not require any further input from the user. By default Q-CHEM computes only the lowest eigenvalue of the stability matrix, which is usually sufficient to determine if there is a negative eigenvalue and thus an instability. To compute additional eigenvalues, set CIS_N_ROOTS *$rem* to a number larger than 1.

Q-CHEM's Stability Analysis package also seeks to correct internal instabilities (RHF → RHF or UHF → UHF). Then, if such an instability is detected, Q-CHEM automatically performs a unitary transformation of the molecular orbitals following the directions of the lowest eigenvector, and writes a new set of MOs to disk. One can read in these MOs as an initial guess in a second SCF calculation (set the SCF_GUESS *$rem* variable to READ), it might also be desirable to set the SCF_ALGORITHM to GDM. In cases where the lowest-energy SCF solution breaks the molecular point-group symmetry, the SYM_IGNORE *$rem* should be set to TRUE.

**Note:** The stability analysis package can be used to analyze both DFT and HF wave functions.

## 4.3 Basic SCF Job Control

### 4.3.1 Basic Options

In brief, Q-CHEM supports the three main variants of the HF method. They are:

- Restricted Hartree-Fock (RHF) for closed-shell molecules. It is typically appropriate for closed shell molecules at their equilibrium geometry, where electrons occupy orbitals in pairs.
- Unrestricted Hartree-Fock (UHF) for open-shell molecules. Appropriate for radicals with an odd number of electrons, and also for molecules with even numbers of electrons where not all electrons are paired, *e.g.*, stretched bonds and diradicals.
- Restricted open-shell Hartree-Fock (ROHF) for open-shell molecules, where the $\alpha$ and $\beta$ orbitals are constrained to be identical.

Only two *$rem* variables are required in order to run HF calculations:

| | |
|---|---|
| BASIS | to specify the basis set (see Chapter 7). |
| METHOD | SCF method: HF or a density functional (see Section 4.4). |

In slightly more detail, here is a list of basic *$rem* variables associated with running SCF calculations. See Chapter 7 for further detail on basis sets available and Chapter 8 for specifying effective core potentials.

**JOBTYPE**

Specifies the type of calculation.

TYPE:

STRING

DEFAULT:

SP

OPTIONS:

| | |
|---|---|
| SP | Single point energy. |
| OPT | Geometry minimization. |
| TS | Transition structure search. |
| FREQ | Frequency calculation. |
| FORCE | Analytical force calculation. |
| RPATH | Intrinsic reaction coordinate calculation. |
| NMR | NMR chemical shift calculation. |
| ISSC | Indirect nuclear spin-spin coupling calculation. |
| BSSE | Basis-set superposition error (counterpoise) correction. |
| EDA | Energy decomposition analysis. |

RECOMMENDATION:

None

**METHOD**

Specifies the exchange-correlation functional.

TYPE:

STRING

DEFAULT:

No default

OPTIONS:

| | |
|---|---|
| *NAME* | Use METHOD = *NAME*, where *NAME* is either HF for Hartree-Fock theory or else one of the DFT methods listed in Section 4.4.3.4. |

RECOMMENDATION:

In general, consult the literature to guide your selection. Our recommendations for DFT are indicated in bold in Section 4.4.3.4.

**BASIS**

Specifies the basis sets to be used.

TYPE:

STRING

DEFAULT:

No default basis set

OPTIONS:

| | |
|---|---|
| General, Gen | User defined (*$basis* keyword required). |
| Symbol | Use standard basis sets as per Chapter 7. |
| Mixed | Use a mixture of basis sets (see Chapter 7). |

RECOMMENDATION:

Consult literature and reviews to aid your selection.

**PRINT_ORBITALS**

Prints orbital coefficients with atom labels in analysis part of output.

TYPE:

INTEGER/LOGICAL

DEFAULT:

FALSE

OPTIONS:

| | |
|---|---|
| FALSE | Do not print any orbitals. |
| TRUE | Prints occupied orbitals plus 5 virtual orbitals. |
| NVIRT | Number of virtual orbitals to print. |

RECOMMENDATION:

Use true unless more virtual orbitals are desired.

**THRESH**

Cutoff for neglect of two electron integrals. $10^{-\text{THRESH}}$ (THRESH $\leq 14$).

TYPE:

INTEGER

DEFAULT:

| | |
|---|---|
| 8 | For single point energies. |
| 10 | For optimizations and frequency calculations. |
| 14 | For coupled-cluster calculations. |

OPTIONS:

$n$ for a threshold of $10^{-n}$.

RECOMMENDATION:

Should be at least three greater than SCF_CONVERGENCE. Increase for more significant figures, at greater computational cost.

**SCF_CONVERGENCE**

SCF is considered converged when the wave function error is less that $10^{-\text{SCF\_CONVERGENCE}}$. Adjust the value of THRESH at the same time. (Starting with Q-CHEM 3.0, the DIIS error is measured by the maximum error rather than the RMS error as in earlier versions.)

TYPE:

INTEGER

DEFAULT:

| | |
|---|---|
| 5 | For single point energy calculations. |
| 8 | For geometry optimizations and vibrational analysis. |
| 8 | For SSG calculations, see Chapter 5. |

OPTIONS:

User-defined

RECOMMENDATION:

Tighter criteria for geometry optimization and vibration analysis. Larger values provide more significant figures, at greater computational cost.

**UNRESTRICTED**

Controls the use of restricted or unrestricted orbitals.

TYPE:

LOGICAL

DEFAULT:

| | |
|---|---|
| FALSE | Closed-shell systems. |
| TRUE | Open-shell systems. |

OPTIONS:

| | |
|---|---|
| FALSE | Constrain the spatial part of the alpha and beta orbitals to be the same. |
| TRUE | Do not Constrain the spatial part of the alpha and beta orbitals. |

RECOMMENDATION:

Use the default unless ROHF is desired. Note that for unrestricted calculations on systems with an even number of electrons it is usually necessary to break $\alpha/\beta$ symmetry in the initial guess, by using SCF_GUESS_MIX or providing *$occupied* information (see Section 4.5 on initial guesses).

### 4.3.2 Additional Options

Listed below are a number of useful options to customize an SCF calculation. This is only a short summary of the function of these *$rem* variables. A full list of all SCF-related variables is provided in Appendix C. Several important sub-topics are discussed separately, including $\mathcal{O}(N)$ methods for large molecules (Section 4.8), customizing the initial guess (Section 4.5), and converging the SCF calculation (Section 4.6).

**INTEGRALS_BUFFER**

Controls the size of in-core integral storage buffer.

TYPE:

INTEGER

DEFAULT:

| | |
|---|---|
| 15 | 15 Megabytes. |

OPTIONS:

User defined size.

RECOMMENDATION:

Use the default, or consult your systems administrator for hardware limits.

**DIRECT_SCF**

Controls direct SCF.

TYPE:

LOGICAL

DEFAULT:

Determined by program.

OPTIONS:

| | |
|---|---|
| TRUE | Forces direct SCF. |
| FALSE | Do not use direct SCF. |

RECOMMENDATION:

Use the default; direct SCF switches off in-core integrals.

**METECO**

Sets the threshold criteria for discarding shell-pairs.

TYPE:

INTEGER

DEFAULT:

2 Discard shell-pairs below $10^{-\mathrm{THRESH}}$.

OPTIONS:

1 Discard shell-pairs four orders of magnitude below machine precision.

2 Discard shell-pairs below $10^{-\mathrm{THRESH}}$.

RECOMMENDATION:

Use the default.

**STABILITY_ANALYSIS**

Performs stability analysis for a HF or DFT solution.

TYPE:

LOGICAL

DEFAULT:

FALSE

OPTIONS:

TRUE Perform stability analysis.

FALSE Do not perform stability analysis.

RECOMMENDATION:

Set to TRUE when a HF or DFT solution is suspected to be unstable.

**SCF_PRINT**

Controls level of output from SCF procedure to Q-CHEM output file.

TYPE:

INTEGER

DEFAULT:

0 Minimal, concise, useful and necessary output.

OPTIONS:

0 Minimal, concise, useful and necessary output.

1 Level 0 plus component breakdown of SCF electronic energy.

2 Level 1 plus density, Fock and MO matrices on each cycle.

3 Level 2 plus two-electron Fock matrix components (Coulomb, HF exchange and DFT exchange-correlation matrices) on each cycle.

RECOMMENDATION:

Proceed with care; can result in *extremely* large output files at level 2 or higher. These levels are primarily for program debugging.

**SCF_FINAL_PRINT**

Controls level of output from SCF procedure to Q-CHEM output file at the end of the SCF.

TYPE:

INTEGER

DEFAULT:

| | |
|---|---|
| 0 | No extra print out. |

OPTIONS:

| | |
|---|---|
| 0 | No extra print out. |
| 1 | Orbital energies and break-down of SCF energy. |
| 2 | Level 1 plus MOs and density matrices. |
| 3 | Level 2 plus Fock and density matrices. |

RECOMMENDATION:

The break-down of energies is often useful (level 1).

**KS_GAP_PRINT**

Control printing of (generalized Kohn-Sham) HOMO-LUMO gap information.

TYPE:

Boolean

DEFAULT:

false

OPTIONS:

| | |
|---|---|
| false | (default) do not print gap information |
| true | print gap information |

RECOMMENDATION:

Use in conjunction with KS_GAP_UNIT if true.

**KS_GAP_UNIT**

Unit for KS_GAP_PRINT and FOA_FUNDGAP (see Section 4.4.11)

TYPE:

INTEGER

DEFAULT:

0

OPTIONS:

| | |
|---|---|
| 0 | (default) hartrees |
| 1 | eV |

RECOMMENDATION:

none

**DIIS_SEPARATE_ERRVEC**

Control optimization of DIIS error vector in unrestricted calculations.

TYPE:

LOGICAL

DEFAULT:

FALSE Use a combined $\alpha$ and $\beta$ error vector.

OPTIONS:

FALSE Use a combined $\alpha$ and $\beta$ error vector.

TRUE Use separate error vectors for the $\alpha$ and $\beta$ spaces.

RECOMMENDATION:

When using DIIS in Q-CHEM a convenient optimization for unrestricted calculations is to sum the $\alpha$ and $\beta$ error vectors into a single vector which is used for extrapolation. This is often extremely effective, but in some pathological systems with symmetry breaking, can lead to false solutions being detected, where the $\alpha$ and $\beta$ components of the error vector cancel exactly giving a zero DIIS error. While an extremely uncommon occurrence, if it is suspected, set DIIS_SEPARATE_ERRVEC = TRUE to check.

### 4.3.3 Examples

Provided below are examples of Q-CHEM input files to run ground state, HF single point energy calculations.

**Example 4.1** Example Q-CHEM input for a single point energy calculation on water. Note that the declaration of the single point *$rem* variable and level of theory to treat correlation are redundant because they are the same as the Q-CHEM defaults.

```
$molecule
   0  1
   O
   H1  O  oh
   H2  O  oh  H1  hoh

   oh  =   1.2
   hoh = 120.0
$end

$rem
   JOBTYPE       sp       Single Point energy
   METHOD        hf       Hartree-Fock
   BASIS         sto-3g   Basis set
$end

$comment
HF/STO-3G water single point calculation
$end
```

**Example 4.2** UHF/6-311G calculation on the Li atom. Note that correlation and the job type were not indicated because Q-CHEM defaults automatically to no correlation and single point energies. Note also that, since the number of $\alpha$ and $\beta$ electron differ, MOs default to an unrestricted formalism.

```
$molecule
   0,2
   3
$end

$rem
   METHOD      HF       Hartree-Fock
   BASIS       6-311G   Basis set
$end
```

**Example 4.3** ROHF/6-311G calculation on the Lithium atom. Note again that correlation and the job type need not be indicated.

```
$molecule
   0,2
   3
$end

$rem
   METHOD         hf       Hartree-Fock
   UNRESTRICTED   false    Restricted MOs
   BASIS          6-311G   Basis set
$end
```

**Example 4.4** RHF/6-31G stability analysis calculation on the singlet state of the oxygen molecule. The wave function is RHF → UHF unstable.

```
$molecule
   0 1
   O
   O  1  1.165
$end

$rem
   METHOD               hf         Hartree-Fock
   UNRESTRICTED         false      Restricted MOs
   BASIS                6-31G(d)   Basis set
   STABILITY_ANALYSIS   true       Perform a stability analysis
$end
```

### 4.3.4 Symmetry

Symmetry is a powerful branch of mathematics and is often exploited in quantum chemistry, both to reduce the computational workload and to classify the final results obtained[13–15]. Q-CHEM is able to determine the point group symmetry of the molecular nuclei and, on completion of the SCF procedure, classify the symmetry of molecular orbitals, and provide symmetry decomposition of kinetic and nuclear attraction energy (see Chapter 10).

Molecular systems possessing point group symmetry offer the possibility of large savings of computational time, by avoiding calculations of integrals which are equivalent *i.e.*, those integrals which can be mapped on to one another under one of the symmetry operations of the molecular point group. The Q-CHEM default is to use symmetry to reduce computational time, when possible.

There are several keywords that are related to symmetry, which causes frequent confusion. SYM_IGNORE controls symmetry throughout all modules. The default is FALSE. In some cases it may be desirable to turn off symmetry altogether, for example if you do not want Q-CHEM to reorient the molecule into the standard nuclear orientation, or if you want to turn it off for finite difference calculations. If the SYM_IGNORE keyword is set to TRUE then the coordinates will not be altered from the input, and the point group will be set to $C_1$.

The SYMMETRY keyword controls symmetry in some integral routines. It is set to FALSE by default. Note that setting it to FALSE does not turn point group symmetry off, and does not disable symmetry in the coupled-cluster suite (CCMAN and CCMAN2), which is controlled by CC_SYMMETRY (see Chapters 5 and 6), although we noticed that sometimes it may interfere with the determination of orbital symmetries, possibly due to numerical noise. In some cases, SYMMETRY = TRUE can cause problems (poor convergence and wildly incorrect SCF energies) and turning it off can avoid these problems.

**Note:** The user should be aware about different conventions for defining symmetry elements. The arbitrariness affects, for example, $C_{2v}$ point group. The specific choice affects how the irreps in the affected groups are labeled. For example, $b_1$ and $b_2$ irreps in $C_{2v}$ are flipped when using different conventions. Q-CHEM uses non-Mulliken symmetry convention. See http://iopenshell.usc.edu/howto/symmetry for detailed explanations.

**SYMMETRY**

Controls the efficiency through the use of point group symmetry for calculating integrals.

TYPE:

LOGICAL

DEFAULT:

TRUE Use symmetry for computing integrals.

OPTIONS:

TRUE Use symmetry when available.

FALSE Do not use symmetry. This is always the case for RIMP2 jobs

RECOMMENDATION:

Use the default unless benchmarking. Note that symmetry usage is disabled for RIMP2, FFT, and QM/MM jobs.

**SYM_IGNORE**

Controls whether or not Q-CHEM determines the point group of the molecule and reorients the molecule to the standard orientation.

TYPE:

LOGICAL

DEFAULT:

FALSE Do determine the point group (disabled for RIMP2 jobs).

OPTIONS:

TRUE/FALSE

RECOMMENDATION:

Use the default unless you do not want the molecule to be reoriented. Note that symmetry usage is disabled for RIMP2 jobs.

**SYM_TOL**

Controls the tolerance for determining point group symmetry. Differences in atom locations less than $10^{-\mathrm{SYM\_TOL}}$ are treated as zero.

TYPE:

INTEGER

DEFAULT:

5 Corresponding to $10^{-5}$.

OPTIONS:

User defined.

RECOMMENDATION:

Use the default unless the molecule has high symmetry which is not being correctly identified. Note that relaxing this tolerance too much may introduce errors into the calculation.

## 4.4 Density Functional Theory

### 4.4.1 Introduction

DFT[16–19] has emerged as an accurate, alternative first-principles approach to quantum mechanical molecular investigations. DFT calculations account for the overwhelming majority of all quantum chemistry calculations, not only because of its proven chemical accuracy, but also because of its relatively low computational expense, comparable to Hartree-Fock theory but with treatment of electron correlation that is neglected in a HF calculation. These two features suggest that DFT is likely to remain a leading method in the quantum chemist's toolkit well into the future. Q-CHEM contains fast, efficient and accurate algorithms for all popular density functionals, making calculations on large molecules possible and practical.

DFT is primarily a theory of electronic ground state structures based on the electron density, $\rho(\mathbf{r})$, as opposed to the many-electron wave function, $\Psi(\mathbf{r}_1, \ldots, \mathbf{r}_N)$. (It's excited-state extension, time-dependent DFT, is discussed in Section 6.3.) There are a number of distinct similarities and differences between traditional wave function approaches and modern DFT methodologies. First, the essential building blocks of the many-electron wave function $\Psi$ are single-electron orbitals, which are directly analogous to the Kohn-Sham orbitals in the DFT framework. Second, both the electron density and the many-electron wave function tend to be constructed via a SCF approach that requires the construction of matrix elements that are conveniently very similar.

However, traditional *ab initio* approaches using the many-electron wave function as a foundation must resort to a post-SCF calculation (Chapter 5) to incorporate correlation effects, whereas DFT approaches incorporate correlation at the SCF level. Post-SCF methods, such as perturbation theory or coupled-cluster theory are extremely expensive relative to the SCF procedure. On the other hand, while the DFT approach is exact in principle, in practice it relies on modeling an unknown exchange-correlation energy functional. While more accurate forms of such functionals are constantly being developed, there is no systematic way to improve the functional to achieve an arbitrary level of accuracy. Thus, the traditional approaches offer the possibility of achieving a systematically-improvable level of accuracy, but can be computationally demanding, whereas DFT approaches offer a practical route, but the theory is currently incomplete.

### 4.4.2 Kohn-Sham Density Functional Theory

The density functional theory by Hohenberg, Kohn, and Sham[20,21] stems from the original work of Dirac[22], who found that the exchange energy of a uniform electron gas may be calculated exactly, knowing only the charge density. However, while the more traditional DFT constitutes a direct approach where the necessary equations contain only the electron density, difficulties associated with the kinetic energy functional obstructed the extension of DFT to anything more than a crude level of approximation. Kohn and Sham developed an indirect approach to the kinetic energy functional, which transformed DFT into a practical tool for quantum-chemical calculations.

Within the Kohn-Sham formalism[21], the ground state electronic energy, $E$, can be written as

$$E = E_{\mathrm{T}} + E_{\mathrm{V}} + E_{\mathrm{J}} + E_{\mathrm{XC}} \tag{4.30}$$

where $E_{\mathrm{T}}$ is the kinetic energy, $E_{\mathrm{V}}$ is the electron–nuclear interaction energy, $E_{\mathrm{J}}$ is the Coulomb self-interaction of the electron density, $\rho(\mathbf{r})$ and $E_{\mathrm{XC}}$ is the exchange-correlation energy. Adopting an unrestricted format, the $\alpha$ and $\beta$ total electron densities can be written as

$$\begin{aligned} \rho_\alpha(\mathbf{r}) &= \sum_{i=1}^{n_\alpha} |\psi_i^\alpha|^2 \\ \rho_\beta(\mathbf{r}) &= \sum_{i=1}^{n_\beta} |\psi_i^\beta|^2 \end{aligned} \tag{4.31}$$

where $n_\alpha$ and $n_\beta$ are the number of alpha and beta electron respectively, and $\psi_i$ are the Kohn-Sham orbitals. Thus, the total electron density is

$$\rho(\mathbf{r}) = \rho_\alpha(\mathbf{r}) + \rho_\beta(\mathbf{r}) \tag{4.32}$$

Within a finite basis set[23], the density is represented by

$$\rho(\mathbf{r}) = \sum_{\mu\nu} P_{\mu\nu} \phi_\mu(\mathbf{r}) \phi_\nu(\mathbf{r}) \ , \tag{4.33}$$

where the $P_{\mu\nu}$ are the elements of the one-electron density matrix; see Eq. (4.23) in the discussion of Hartree-Fock theory. The various energy components in Eq. (4.30) can now be written

$$\begin{aligned} E_{\mathrm{T}} &= \sum_{i=1}^{n_\alpha} \left\langle \psi_i^\alpha \left| -\frac{1}{2}\nabla^2 \right| \psi_i^\alpha \right\rangle + \sum_{i=1}^{n_\beta} \left\langle \psi_i^\beta \left| -\frac{1}{2}\nabla^2 \right| \psi_i^\beta \right\rangle \\ &= \sum_{\mu\nu} P_{\mu\nu} \left\langle \phi_\mu(\mathbf{r}) \left| -\frac{1}{2}\nabla^2 \right| \phi_\nu(\mathbf{r}) \right\rangle \end{aligned} \tag{4.34}$$

$$\begin{aligned} E_{\mathrm{V}} &= -\sum_{A=1}^{M} Z_A \int \frac{\rho(\mathbf{r})}{|\mathbf{r}-\mathbf{R}_A|} d\mathbf{r} \\ &= -\sum_{\mu\nu} P_{\mu\nu} \sum_A \left\langle \phi_\mu(\mathbf{r}) \left| \frac{Z_A}{|\mathbf{r}-\mathbf{R}_A|} \right| \phi_\nu(\mathbf{r}) \right\rangle \end{aligned} \tag{4.35}$$

$$\begin{aligned} E_{\mathrm{J}} &= \frac{1}{2} \left\langle \rho(\mathbf{r}_1) \left| \frac{1}{|\mathbf{r}_1-\mathbf{r}_2|} \right| \rho(\mathbf{r}_2) \right\rangle \\ &= \frac{1}{2} \sum_{\mu\nu} \sum_{\lambda\sigma} P_{\mu\nu} P_{\lambda\sigma} \, (\mu\nu|\lambda\sigma) \end{aligned} \tag{4.36}$$

$$E_{\mathrm{XC}} = \int f\left[\rho(\mathbf{r}), \nabla\rho(\mathbf{r}), \ldots\right] d\mathbf{r} \tag{4.37}$$

Minimizing $E$ with respect to the unknown Kohn-Sham orbital coefficients yields a set of matrix equations exactly analogous to Pople-Nesbet equations of the UHF case, Eq. (4.13), but with modified Fock matrix elements [*cf.* Eq. (4.26)]

$$\begin{aligned} F^{\alpha}_{\mu\nu} &= H^{\mathrm{core}}_{\mu\nu} + J_{\mu\nu} - F^{\mathrm{XC}\alpha}_{\mu\nu} \\ F^{\beta}_{\mu\nu} &= H^{\mathrm{core}}_{\mu\nu} + J_{\mu\nu} - F^{\mathrm{XC}\beta}_{\mu\nu} \ . \end{aligned} \tag{4.38}$$

Here, $\mathbf{F}^{\mathrm{XC}\alpha}$ and $\mathbf{F}^{\mathrm{XC}\beta}$ are the exchange-correlation parts of the Fock matrices and depend on the exchange-correlation functional used. UHF theory is recovered as a special case simply by taking $F^{\mathrm{XC}\alpha}_{\mu\nu} = K^{\alpha}_{\mu\nu}$, and similarly for $\beta$. Thus, the density and energy are obtained in a manner analogous to that for the HF method. Initial guesses are made for the MO coefficients and an iterative process is applied until self-consistency is achieved.

### 4.4.3 Overview of Available Functionals

Q-CHEM currently has more than 30 exchange functionals as well as more than 30 correlation functionals, and in addition over 150 exchange-correlation (XC) functionals, which refer to functionals that are not separated into exchange and correlation parts, either because the way in which they were parameterized renders such a separation meaningless (*e.g.*, B97-D[24] or $\omega$B97X[25]) or because they are a standard linear combination of exchange and correlation (*e.g.*, PBE[26] or B3LYP[27,28]). User-defined XC functionals can be created as specified linear combinations of any of the 30+ exchange functionals and/or the 30+ correlation functionals.

KS-DFT functionals can be organized onto a ladder with five rungs, in a classification scheme ("Jacob's Ladder") proposed by John Perdew[29] in 2001. The first rung contains a functional that only depends on the (spin-)density $\rho_\sigma$, namely, the local spin-density approximation (LSDA). These functionals are exact for the infinite uniform electron gas (UEG), but are highly inaccurate for molecular properties whose densities exhibit significant inhomogeneity. To improve upon the weaknesses of the LSDA, it is necessary to introduce an ingredient that can account for inhomogeneities in the density: the density gradient, $\nabla\rho_\sigma$. These generalized gradient approximation (GGA) functionals define the second rung of Jacob's Ladder and tend to improve significantly upon the LSDA. Two additional ingredients that can be used to further improve the performance of GGA functionals are either the Laplacian of the density $\nabla^2\rho_\sigma$, and/or the kinetic energy density,

$$\tau_\sigma = \sum_i^{n_\sigma} |\nabla\psi_{i,\sigma}|^2 \ . \tag{4.39}$$

While functionals that employ both of these options are available in Q-CHEM, the kinetic energy density is by far the more popular ingredient and has been used in many modern functionals to add flexibility to the functional form with respect to both constraint satisfaction (non-empirical functionals) and least-squares fitting (semi-empirical parameterization). Functionals that depend on either of these two ingredients belong to the third rung of the Jacob's Ladder and are called meta-GGAs. These meta-GGAs often further improve upon GGAs in areas such as thermochemistry, kinetics (reaction barrier heights), and even non-covalent interactions.

Functionals on the fourth rung of Jacob's Ladder are called hybrid density functionals. This rung contains arguably the most popular density functional of our time, B3LYP, the first functional to see widespread application in chemistry. "Global" hybrid (GH) functionals such as B3LYP (as distinguished from the "range-separated hybrids" introduced below) add a constant fraction of "exact" (Hartree-Fock) exchange to any of the functionals from the first three rungs. Thus, hybrid LSDA, hybrid GGA, and hybrid meta-GGA functionals can be constructed, although the latter two types are much more common. As an example, the formula for the B3LYP functional, as implemented in Q-CHEM, is

$$E_{xc}^{\text{B3LYP}} = c_x E_x^{\text{HF}} + (1 - c_x - a_x)\, E_x^{\text{Slater}} + a_x E_x^{\text{B88}} + (1 - a_c)\, E_c^{\text{VWN1RPA}} + a_c E_c^{\text{LYP}} \tag{4.40}$$

where $c_x = 0.20$, $a_x = 0.72$, and $a_c = 0.81$.

A more recent approach to introducing exact exchange into the functional form is via range separation. Range-separated hybrid (RSH) functionals split the exact exchange contribution into a short-range (SR) component and a long-range (LR) component, often by means of the error function (erf) and complementary error function ($\text{erfc} \equiv 1 - \text{erf}$):

$$\frac{1}{r_{12}} = \frac{\text{erfc}(\omega r_{12})}{r_{12}} + \frac{\text{erf}(\omega r_{12})}{r_{12}} \tag{4.41}$$

The first term on the right in Eq. (4.41) is singular but short-range, and decays to zero on a length scale of $\sim 1/\omega$, while the second term constitutes a non-singular, long-range background. An RSH XC functional can be expressed generically as

$$E_{xc}^{\text{RSH}} = c_{x,\text{SR}} E_{x,\text{SR}}^{\text{HF}} + c_{x,\text{LR}} E_{x,\text{LR}}^{\text{HF}} + (1 - c_{x,\text{SR}}) E_{x,\text{SR}}^{\text{DFT}} + (1 - c_{x,\text{LR}}) E_{x,\text{LR}}^{\text{DFT}} + E_c^{\text{DFT}} \ , \tag{4.42}$$

where the SR and LR parts of the Coulomb operator are used, respectively, to evaluate the HF exchange energies $E_{x,\text{SR}}^{\text{HF}}$ and $E_{x,\text{LR}}^{\text{HF}}$. The corresponding DFT exchange functional is partitioned in the same manner, but the correlation energy $E_c^{\text{DFT}}$ is evaluated using the full Coulomb operator, $r_{12}^{-1}$. Of the two linear parameters in Eq. (4.42), $c_{x,\text{LR}}$ is usually either set to 1 to define long-range corrected (LRC) RSH functionals (see Section 4.4.6) or else set to 0, which defines screened-exchange (SE) RSH functionals. On the other hand, the fraction of short-range exact exchange ($c_{x,\text{SR}}$) can either be determined via least-squares fitting, theoretically justified using the adiabatic connection, or simply set to zero. As with the global hybrids, RSH functionals can be fashioned using all of the ingredients from the lower three rungs. The rate at which the local DFT exchange is turned off and the non-local exact exchange is turned on is controlled by the parameter $\omega$. Large values of $\omega$ tend to lead to attenuators that are less smooth (unless the fraction of short-range exact exchange is very large), while small values of (*e.g.*, $\omega$ =0.2–0.3 bohr$^{-1}$) are the most common in semi-empirical RSH functionals.

The final rung on Jacob's Ladder contains functionals that utilize not only occupied orbitals (via exact exchange), but virtual orbitals as well (via methods such as MP2 or the random phase approximation, RPA). These double hybrids (DH) are the most expensive density functionals available in Q-CHEM, but can also be very accurate. The most basic form of a DH functional is

$$E_{xc}^{\text{DH}} = c_x E_x^{\text{HF}} + (1 - c_x)\, E_x^{\text{DFT}} + c_c E_x^{\text{MP2}} + (1 - c_c)\, E_c^{\text{DFT}} \ . \tag{4.43}$$

As with hybrids, the coefficients can either be theoretically motivated or empirically determined. In addition, double hybrids can utilize exact exchange both globally or via range-separation, and their components can be as primitive as LSDA or as advanced as in meta-GGA functionals. More information on double hybrids can be found in Section 4.4.9.

Finally, the last major advance in KS-DFT in recent years has been the development of methods that are capable of accurately describing non-covalent interactions, particularly dispersion. All of the functionals from Jacob's Ladder can technically be combined with these dispersion corrections, although in some cases the combination is detrimental, particularly for semi-empirical functionals that were parameterized in part using data sets of non-covalent interactions, and already tend to overestimate non-covalent interaction energies. The most popular such methods available in Q-CHEM are:

- Non-local correlation (NLC) functionals (Section 4.4.7.1), including those of Vydrov and Van Voorhis[30,31] (VV09 and VV10) and of Lundqvist and Langreth[32,33] (vdW-DF-04 and vdW-DF-10). The revised VV10 NLC functional of Sabatini and coworkers (rVV10) is also available[34].

| | **Single-Point** | **Optimization** | **Frequency** |
|---|---|---|---|
| **Ground State** | LSDA$^{\dagger\star}$ | LSDA$^{\dagger\star}$ | LSDA$^{\star}$ |
| | GGA$^{\dagger\star}$ | GGA$^{\dagger\star}$ | GGA$^{\star}$ |
| | meta-GGA$^{\dagger\star}$ | meta-GGA$^{\dagger}$ | — |
| | GH$^{\dagger\star}$ | GH$^{\dagger\star}$ | GH$^{\star}$ |
| | RSH$^{\dagger\star}$ | RSH$^{\dagger\star}$ | RSH$^{\star}$ |
| | NLC$^{\dagger\star}$ | NLC$^{\dagger\star}$ | — |
| | DFT-D | DFT-D | DFT-D |
| | XDM | — | — |
| **TDDFT** | LSDA$^{\dagger\star}$ | LSDA$^{\dagger\star}$ | LSDA |
| | GGA$^{\dagger\star}$ | GGA$^{\dagger\star}$ | GGA |
| | meta-GGA$^{\dagger\star}$ | — | — |
| | GH$^{\dagger\star}$ | GH$^{\dagger\star}$ | GH |
| | RSH$^{\dagger\star}$ | RSH$^{\dagger\star}$ | — |
| | — | — | — |
| | DFT-D | DFT-D | DFT-D |
| | — | — | — |

$^{\dagger}$OpenMP parallelization available

$^{\star}$MPI parallelization available

Table 4.2: Available analytic properties and parallelization for SCF calculations.

- Damped, atom–atom pairwise empirical dispersion potentials from Grimme and others[24,35–39] [DFT-D2, DFT-CHG, DFT-D3(0), DFT-D3(BJ), DFT-D3(CSO), DFT-D3M(0), DFT-D3M(BJ), and DFT-D3(op)]; see Section 4.4.7.2.
- The exchange-dipole models (XDM) of Johnson and Becke (XDM6 and XDM10); see Section 4.4.7.3.

Below, we categorize the functionals that are available in Q-CHEM, including exchange functionals (Section 4.4.3.2), correlation functionals (Section 4.4.3.3), and exchange-correlation functionals (Section 4.4.3.4). Within each category the functionals will be categorized according to Jacob's Ladder. Exchange and correlation functionals can be invoked using the *$rem* variables EXCHANGE and CORRELATION, while the exchange-correlation functionals can be invoked either by setting the *$rem* variable METHOD or alternatively (in most cases, and for backwards compatibility with earlier versions of Q-CHEM) by using the *$rem* variable EXCHANGE. Some caution is warranted here. While setting METHOD to PBE, for example, requests the Perdew-Burke-Ernzerhof (PBE) exchange-correlation functional,[26] which includes both PBE exchange and PBE correlation, setting EXCHANGE = PBE requests only the exchange component and setting CORRELATION = PBE requests only the correlation component. Setting both of these values is equivalent to specifying METHOD = PBE.

Finally, Table 4.2 provides a summary, arranged according to Jacob's Ladder, of which categories of functionals are available with analytic first derivatives (for geometry optimizations) or second derivatives (for vibrational frequency calculations). If analytic derivatives are not available for the requested job type, Q-CHEM will automatically generate them via finite difference. Tests of the finite-difference procedure, in cases where analytic second derivatives *are* available, suggest that finite-difference frequencies are accurate to $< 1$ cm$^{-1}$, except for very low-frequency, non-bonded modes[40]. Also listed in Table 4.2 are which functionals are available for excited-state time-dependent DFT (TDDFT) calculations, as described in Section 6.3. Lastly, Table 4.2 describes which functionals have been parallelized with OpenMP and/or

MPI.

#### 4.4.3.1 Suggested Density Functionals

Q-CHEM contains over 150 exchange-correlation functionals, not counting those that can be straightforwardly appended with a dispersion correction (such as B3LYP-D3). Therefore, we suggest a few functionals from the second through fourth rungs of Jacob's Ladder in order to guide functional selection. Most of these suggestions come from a benchmark of over 200 density functionals on a vast database of nearly 5000 data points, covering non-covalent interactions, isomerization energies, thermochemistry, and barrier heights. **The single recommended method from each category is indicated in bold.**

From the GGAs on Rung 2, we recommend:

- **B97-D3(BJ)** – METHOD B97-D3 and DFT_D D3_BJ
- revPBE-D3(BJ) – METHOD revPBE and DFT_D D3_BJ
- BLYP-D3(BJ) – METHOD BLYP and DFT_D D3_BJ
- PBE – METHOD PBE

From the meta-GGAs on Rung 3, we recommend:

- **B97M-rV** – METHOD B97M-rV
- MS1-D3(0) – METHOD MS1 and DFT_D D3_ZERO
- MS2-D3(0) – METHOD MS2 and DFT_D D3_ZERO
- M06-L-D3(0) – METHOD M06-L and DFT_D D3_ZERO
- TPSS-D3(BJ) – METHOD TPSS and DFT_D D3_BJ

From the hybrid GGAs on Rung 4, we recommend:

- $\omega$**B97X-V** – METHOD wB97X-V
- $\omega$B97X-D3 – METHOD wB97X-D3
- $\omega$B97X-D – METHOD wB97X-D
- B3LYP-D3(BJ) – METHOD B3LYP and DFT_D D3_BJ
- revPBE0-D3(BJ) – METHOD revPBE0 and DFT_D D3_BJ

From the hybrid meta-GGAs on Rung 4, we recommend:

- $\omega$**B97M-V** – METHOD wB97M-V
- $\omega$M05-D – METHOD wM05-D
- M06-2X-D3(0) – METHOD M06-2X and DFT_D D3_ZERO
- TPSSh-D3(BJ) – METHOD TPSSh and DFT_D D3_BJ

#### 4.4.3.2 Exchange Functionals

**Note:** All exchange functionals in this section can be invoked using the *$rem* variable EXCHANGE. Popular and/or recommended functionals within each class are listed first and indicated in bold. The rest are in alphabetical order.

Local Spin-Density Approximation (LSDA)

- **Slater** – Slater-Dirac exchange functional (X$\alpha$ method with $\alpha = 2/3$)[22]
- SR_LSDA (BNL) – Short-range version of the Slater-Dirac exchange functional[41]

Generalized Gradient Approximation (GGA)

- **PBE** – Perdew, Burke, and Ernzerhof exchange functional[26]
- **B88** – Becke exchange functional from 1988[42]
- **revPBE** – Zhang and Yang one-parameter modification of the PBE exchange functional[43]
- AK13 – Armiento-Kümmel exchange functional from 2013[44]
- B86 – Becke exchange functional (X$\alpha\beta\gamma$) from 1986[45]
- G96 – Gill exchange functional from 1996[46]
- mB86 – Becke "modified gradient correction" exchange functional from 1986[47]
- mPW91 – modified version (Adamo and Barone) of the 1991 Perdew-Wang exchange functional[48]
- muB88 ($\mu$B88) – Short-range version of the B88 exchange functional by Hirao and coworkers[49]
- muPBE ($\mu$PBE) – Short-range version of the PBE exchange functional by Hirao and coworkers[49]
- optB88 – Refit version of the original B88 exchange functional (for use with vdW-DF-04) by Michaelides and coworkers[50]
- OPTX – Two-parameter exchange functional by Handy and Cohen[51]
- PBEsol – PBE exchange functional modified for solids[52]
- PW86 – Perdew-Wang exchange functional from 1986[53]
- PW91 – Perdew-Wang exchange functional from 1991[54]
- RPBE – Hammer, Hansen, and Norskov exchange functional (modification of PBE)[55]
- rPW86 – Revised version (Murray *et al.*) of the 1986 Perdew-Wang exchange functional[56]
- SOGGA – Second-order GGA functional by Zhao and Truhlar[57]
- wPBE ($\omega$PBE) – Henderson *et al.* model for the PBE GGA short-range exchange hole[58]

Meta-Generalized Gradient Approximation (meta-GGA)

- **TPSS** – Tao, Perdew, Staroverov, and Scuseria exchange functional[59]
- **revTPSS** – Revised version of the TPSS exchange functional[60]
- BLOC – Minor modification of the TPSS exchange functional that works best with TPSSloc correlation (both by Della Sala and coworkers)[61]
- modTPSS – One-parameter version of the TPSS exchange functional[62]
- oTPSS – TPSS exchange functional with 5 refit parameters (for use with oTPSS correlation) by Grimme and coworkers[63]
- PBE-GX – First exchange functional based on a finite uniform electron gas (rather than an infinite UEG) by Pierre-François Loos[64]
- PKZB – Perdew, Kurth, Zupan, and Blaha exchange functional[65]
- regTPSS – Regularized (fixed order of limits issue) version of the TPSS exchange functional[66]
- SCAN – Strongly Constrained and Appropriately Normed exchange functional[67]
- TM – Tao-Mo exchange functional derived via an accurate modeling of the conventional exchange hole[68]

#### 4.4.3.3 Correlation Functionals

**Note:** All correlation functionals in this section can be invoked using the *$rem* variable CORRELATION. Popular and/or recommended functionals within each class are listed first and indicated in bold. The rest are in alphabetical order.

Local Spin-Density Approximation (LSDA)

- **PW92** – Perdew-Wang parameterization of the LSDA correlation energy from 1992[69]
- **VWN5** (VWN) – Vosko-Wilk-Nusair parameterization of the LSDA correlation energy #5[70]
- Liu-Parr – Liu-Parr $\rho^{1/3}$ model from the functional expansion formulation[71]
- PK09 – Proynov-Kong parameterization of the LSDA correlation energy from 2009[72]
- PW92RPA – Perdew-Wang parameterization of the LSDA correlation energy from 1992 with RPA values[69]
- PZ81 – Perdew-Zunger parameterization of the LSDA correlation energy from 1981[73]
- VWN1 – Vosko-Wilk-Nusair parameterization of the LSDA correlation energy #1[70]
- VWN1RPA – Vosko-Wilk-Nusair parameterization of the LSDA correlation energy #1 with RPA values[70]
- VWN2 – Vosko-Wilk-Nusair parameterization of the LSDA correlation energy #2[70]
- VWN3 – Vosko-Wilk-Nusair parameterization of the LSDA correlation energy #3[70]
- VWN4 – Vosko-Wilk-Nusair parameterization of the LSDA correlation energy #4[70]

- Wigner – Wigner correlation functional (simplification of LYP)[74,75]

Generalized Gradient Approximation (GGA)

- **PBE** – Perdew, Burke, and Ernzerhof correlation functional[26]
- **LYP** – Lee-Yang-Parr opposite-spin correlation functional[76]
- P86 – Perdew-Wang correlation functional from 1986 based on the PZ81 LSDA functional[77]
- P86VWN5 – Perdew-Wang correlation functional from 1986 based on the VWN5 LSDA functional[77]
- PBEloc – PBE correlation functional with a modified beta term by Della Sala and coworkers[78]
- PBEsol – PBE correlation functional modified for solids[52]
- PW91 – Perdew-Wang correlation functional from 1991[54]
- regTPSS – Slight modification of the PBE correlation functional (also called vPBEc)[66]

Meta-Generalized Gradient Approximation (meta-GGA)

- **TPSS** – Tao, Perdew, Staroverov, and Scuseria correlation functional[59]
- **revTPSS** – Revised version of the TPSS correlation functional[60]
- B95 – Becke's two-parameter correlation functional from 1995[79]
- oTPSS – TPSS correlation functional with 2 refit parameters (for use with oTPSS exchange) by Grimme and coworkers[63]
- PK06 – Proynov-Kong "tLap" functional with $\tau$ and Laplacian dependence[80]
- PKZB – Perdew, Kurth, Zupan, and Blaha correlation functional[65]
- SCAN – Strongly Constrained and Appropriately Normed correlation functional[67]
- TM – Tao-Mo correlation functional, representing a minor modification to the TPSS correlation functional[68]
- TPSSloc – The TPSS correlation functional with the PBE component replaced by the PBEloc correlation functional[78]

#### 4.4.3.4 Exchange-Correlation Functionals

**Note:** All exchange-correlation functionals in this section can be invoked using the *$rem* variable METHOD. For backwards compatibility, all of the exchange-correlation functionals *except* for the ones marked with an asterisk can be utilized with the *$rem* variable EXCHANGE. Popular and/or recommended functionals within each class are listed first and indicated in bold. The rest are in alphabetical order.

Local Spin-Density Approximation (LSDA)

- **SPW92*** – Slater LSDA exchange + PW92 LSDA correlation
- LDA – Slater LSDA exchange + VWN5 LSDA correlation
- SVWN5* – Slater LSDA exchange + VWN5 LSDA correlation

Generalized Gradient Approximation (GGA)

- **B97-D3(0)** – B97-D with a fitted DFT-D3(0) tail instead of the original DFT-D2 tail[36]
- **B97-D** – 9-parameter dispersion-corrected (DFT-D2) functional by Grimme[24]
- **PBE*** – PBE GGA exchange + PBE GGA correlation
- **BLYP*** – B88 GGA exchange + LYP GGA correlation
- **revPBE*** – revPBE GGA exchange + PBE GGA correlation
- BEEF-vdW – 31-parameter semi-empirical exchange functional developed via a Bayesian error estimation framework paired with PBE correlation and vdW-DF-10 NLC[81]
- BOP – B88 GGA exchange + BOP "one-parameter progressive" GGA correlation[82]
- BP86* – B88 GGA exchange + P86 GGA correlation
- BP86VWN* – B88 GGA exchange + P86VWN5 GGA correlation
- BPBE* – B88 GGA exchange + PBE GGA correlation
- EDF1 – Modification of BLYP to give good performance in the 6-31+G* basis set[83]
- EDF2 – Modification of B3LYP to give good performance in the cc-pVTZ basis set for frequencies[84]
- GAM – 21-parameter non-separable gradient approximation functional by Truhlar and coworkers[85]
- HCTH93 (HCTH/93) – 15-parameter functional trained on 93 systems by Handy and coworkers[86]
- HCTH120 (HCTH/120) – 15-parameter functional trained on 120 systems by Boese *et al.*[87]
- HCTH147 (HCTH/147) – 15-parameter functional trained on 147 systems by Boese *et al.*[87]
- HCTH407 (HCTH/407) – 15-parameter functional trained on 407 systems by Boese and Handy[88]
- HLE16 – HCTH/407 exchange functional enhanced by a factor of 1.25 + HCTH/407 correlation functional enhanced by a factor of 0.5[89]
- KT1 – GGA functional designed specifically for shielding constant calculations[90]
- KT2 – GGA functional designed specifically for shielding constant calculations[90]
- KT3 – GGA functional with improved results for main-group nuclear magnetic resonance shielding constants[91]
- mPW91* – mPW91 GGA exchange + PW91 GGA correlation
- N12 – 21-parameter non-separable gradient approximation functional by Peverati and Truhlar[92]
- OLYP* – OPTX GGA exchange + LYP GGA correlation

- PBEOP – PBE GGA exchange + PBEOP "one-parameter progressive" GGA correlation[82]
- PBEsol* – PBEsol GGA exchange + PBEsol GGA correlation
- PW91* – PW91 GGA exchange + PW91 GGA correlation
- RPBE* – RPBE GGA exchange + PBE GGA correlation
- rVV10* – rPW86 GGA exchange + PBE GGA correlation + rVV10 non-local correlation[34]
- SOGGA* – SOGGA GGA exchange + PBE GGA correlation
- SOGGA11 – 20-parameter functional by Peverati, Zhao, and Truhlar[93]
- VV10 – rPW86 GGA exchange + PBE GGA correlation + VV10 non-local correlation[31]

Meta-Generalized Gradient Approximation (meta-GGA)

- **B97M-V** – 12-parameter combinatorially-optimized, dispersion-corrected (VV10) functional by Mardirossian and Head-Gordon[94]
- **B97M-rV*** – B97M-V density functional with the VV10 NLC functional replaced by the rVV10 NLC functional[95]
- **M06-L** – 34-parameter functional by Zhao and Truhlar[96]
- **TPSS*** – TPSS meta-GGA exchange + TPSS meta-GGA correlation
- **revTPSS*** – revTPSS meta-GGA exchange + revTPSS meta-GGA correlation
- BLOC* – BLOC meta-GGA exchange + TPSSloc meta-GGA correlation
- M11-L – 44-parameter dual-range functional by Peverati and Truhlar[97]
- mBEEF – 64-parameter exchange functional paired with the PBEsol correlation functional[98]
- MGGA_MS0 – MGGA_MS0 meta-GGA exchange + regTPSS GGA correlation[99]
- MGGA_MS1 – MGGA_MS1 meta-GGA exchange + regTPSS GGA correlation[100]
- MGGA_MS2 – MGGA_MS2 meta-GGA exchange + regTPSS GGA correlation[100]
- MGGA_MVS – MGGA_MVS meta-GGA exchange + regTPSS GGA correlation[101]
- MN12-L – 58-parameter meta-nonseparable gradient approximation functional by Peverati and Truhlar[102]
- MN15-L – 58-parameter meta-nonseparable gradient approximation functional by Yu, He, and Truhlar[103]
- oTPSS* – oTPSS meta-GGA exchange + oTPSS meta-GGA correlation
- PKZB* – PKZB meta-GGA exchange + PKZB meta-GGA correlation
- SCAN* – SCAN meta-GGA exchange + SCAN meta-GGA correlation
- t-HCTH ($\tau$-HCTH) – 16-parameter functional by Boese and Handy[104]

- TM* – TM meta-GGA exchange + TM meta-GGA correlation[68]
- VSXC – 21-parameter functional by Voorhis and Scuseria[105]

Global Hybrid Generalized Gradient Approximation (GH GGA)

- **B3LYP** – 20% HF exchange + 8% Slater LSDA exchange + 72% B88 GGA exchange + 19% VWN1RPA LSDA correlation + 81% LYP GGA correlation[27,28]
- **PBE0** – 25% HF exchange + 75% PBE GGA exchange + PBE GGA correlation[106]
- **revPBE0** – 25% HF exchange + 75% revPBE GGA exchange + PBE GGA correlation
- **B97** – Becke's original 10-parameter density functional with 19.43% HF exchange[107]
- B1LYP – 25% HF exchange + 75% B88 GGA exchange + LYP GGA correlation[108]
- B1PW91 – 25% HF exchange + 75% B88 GGA exchange + PW91 GGA correlation[108]
- B3LYP5 – 20% HF exchange + 8% Slater LSDA exchange + 72% B88 GGA exchange + 19% VWN5 LSDA correlation + 81% LYP GGA correlation[27,28]
- B3P86 – 20% HF exchange + 8% Slater LSDA exchange + 72% B88 GGA exchange+ 19% VWN1RPA LSDA correlation + 81% P86 GGA correlation
- B1LYP – 25% HF exchange + 75% B88 GGA exchange + LYP GGA correlation[108]
- B1PW91 – 25% HF exchange + 75% B88 GGA exchange + PW91 GGA correlation[108]
- B3LYP5 – 20% HF exchange + 8% Slater LSDA exchange + 72% B88 GGA exchange + 19% VWN5 LSDA correlation + 81% LYP GGA correlation[27,28]
- B3P86 – 20% HF exchange + 8% Slater LSDA exchange + 72% B88 GGA exchange+ 19% VWN1RPA LSDA correlation + 81% P86 GGA correlation
- B3PW91 – 20% HF exchange + 8% Slater LSDA exchange + 72% B88 GGA exchange+ 19% PW92 LSDA correlation + 81% PW91 GGA correlation[27]
- B5050LYP – 50% HF exchange + 8% Slater LSDA exchange + 42% B88 GGA exchange + 19% VWN5 LSDA correlation + 81% LYP GGA correlation[109]
- B97-1 – Self-consistent parameterization of Becke's B97 density functional with 21% HF exchange[86]
- B97-2 – Re-parameterization of B97 by Tozer and coworkers with 21% HF exchange[110]
- B97-3 – 16-parameter version of B97 by Keal and Tozer with $\approx$ 26.93% HF exchange[111]
- B97-K – Re-parameterization of B97 for kinetics by Boese and Martin with 42% HF exchange[112]
- BHHLYP – 50% HF exchange + 50% B88 GGA exchange + LYP GGA correlation
- HFLYP* – 100% HF exchange + LYP GGA correlation
- MPW1K – 42.8% HF exchange + 57.2% mPW91 GGA exchange + PW91 GGA correlation[113]
- MPW1LYP – 25% HF exchange + 75% mPW91 GGA exchange + LYP GGA correlation[48]
- MPW1PBE – 25% HF exchange + 75% mPW91 GGA exchange + PBE GGA correlation[48]

- MPW1PW91 – 25% HF exchange + 75% mPW91 GGA exchange + PW91 GGA correlation[48]
- O3LYP – 11.61% HF exchange + ≈ 7.1% Slater LSDA exchange + 81.33% OPTX GGA exchange + 19% VWN5 LSDA correlation + 81% LYP GGA correlation[114]
- PBEh-3c – Low-cost composite scheme of Grimme and coworkers for use with the def2-mSVP basis set only[115]
- PBE50 – 50% HF exchange + 50% PBE GGA exchange + PBE GGA correlation[116]
- SOGGA11-X – 21-parameter functional with 40.15% HF exchange by Peverati and Truhlar[117]
- WC04 – Hybrid density functional optimized for the computation of $^{13}$C chemical shifts[118]
- WP04 – Hybrid density functional optimized for the computation of $^{1}$H chemical shifts[118]
- X3LYP – 21.8% HF exchange + 7.3% Slater LSDA exchange + ≈ 54.24% B88 GGA exchange + ≈ 16.66% PW91 GGA exchange + 12.9% VWN1RPA LSDA correlation + 87.1% LYP GGA correlation[119]

Global Hybrid Meta-Generalized Gradient Approximation (GH meta-GGA)

- **M06-2X** – 29-parameter functional with 54% HF exchange by Zhao and Truhlar[120]
- **M08-HX** – 47-parameter functional with 52.23% HF exchange by Zhao and Truhlar[121]
- **TPSSh** – 10% HF exchange + 90% TPSS meta-GGA exchange + TPSS meta-GGA correlation[122]
- **revTPSSh** – 10% HF exchange + 90% revTPSS meta-GGA exchange + revTPSS meta-GGA correlation[123]
- B1B95 – 28% HF exchange + 72% B88 GGA exchange + B95 meta-GGA correlation[79]
- B3TLAP – 17.13% HF exchange + 9.66% Slater LSDA exchange + 72.6% B88 GGA exchange + PK06 meta-GGA correlation[80,124]
- BB1K – 42% HF exchange + 58% B88 GGA exchange + B95 meta-GGA correlation[125]
- BMK – Boese-Martin functional for kinetics with 42% HF exchange[112]
- dlDF – Dispersion-less density functional (based on the M05-2X functional form) by Szalewicz and coworkers[126]
- M05 – 22-parameter functional with 28% HF exchange by Zhao, Schultz, and Truhlar[127]
- M05-2X – 19-parameter functional with 56% HF exchange by Zhao, Schultz, and Truhlar[128]
- M06 – 33-parameter functional with 27% HF exchange by Zhao and Truhlar[120]
- M06-HF – 32-parameter functional with 100% HF exchange by Zhao and Truhlar[129]
- M08-SO – 44-parameter functional with 56.79% HF exchange by Zhao and Truhlar[121]
- MGGA_MS2h – 9% HF exchange + 91 % MGGA_MS2 meta-GGA exchange + regTPSS GGA correlation[100]

- MGGA_MVSh – 25% HF exchange + 75 % MGGA_MVS meta-GGA exchange + regTPSS GGA correlation[101]
- MN15 – 59-parameter functional with 44% HF exchange by Truhlar and coworkers[130]
- MPW1B95 – 31% HF exchange + 69% mPW91 GGA exchange + B95 meta-GGA correlation[131]
- MPWB1K – 44% HF exchange + 56% mPW91 GGA exchange + B95 meta-GGA correlation[131]
- PW6B95 – 6-parameter combination of 28 % HF exchange, 72 % optimized PW91 GGA exchange, and re-optimized B95 meta-GGA correlation by Zhao and Truhlar[132]
- PWB6K – 6-parameter combination of 46 % HF exchange, 54 % optimized PW91 GGA exchange, and re-optimized B95 meta-GGA correlation by Zhao and Truhlar[132]
- SCAN0 – 25% HF exchange + 75% SCAN meta-GGA exchange + SCAN meta-GGA correlation[133]
- t-HCTHh ($\tau$-HCTHh) – 17-parameter functional with 15% HF exchange by Boese and Handy[104]
- TPSS0 – 25% HF exchange + 75% TPSS meta-GGA exchange + TPSS meta-GGA correlation[134]

Range-Separated Hybrid Generalized Gradient Approximation (RSH GGA)

- **wB97X-V** ($\omega$B97X-V) – 10-parameter combinatorially-optimized, dispersion-corrected (VV10) functional with 16.7% SR HF exchange, 100% LR HF exchange, and $\omega = 0.3$[135]
- **wB97X-D3** ($\omega$B97X-D3) – 16-parameter dispersion-corrected (DFT-D3(0)) functional with ≈ 19.57% SR HF exchange, 100% LR HF exchange, and $\omega = 0.25$[136]
- **wB97X-D** ($\omega$B97X-D) – 15-parameter dispersion-corrected (DFT-CHG) functional with ≈ 22.2% SR HF exchange, 100% LR HF exchange, and $\omega = 0.2$[35]
- CAM-B3LYP – Coulomb-attenuating method functional by Handy and coworkers[137]
- CAM-QTP00 – Re-parameterized CAM-B3LYP designed to satisfy the IP-theorem for all occupied orbitals of the water molecule[138]
- CAM-QTP01 – Re-parameterized CAM-B3LYP optimized to satisfy the valence IPs of the water molecule, 34 excitation states, and G2-1 atomization energies[139]
- HSE-HJS – Screened-exchange "HSE06" functional with 25% SR HF exchange, 0% LR HF exchange, and $\omega$=0.11, using the updated HJS PBE exchange hole model[58,140]
- LC-rVV10* – LC-VV10 density functional with the VV10 NLC functional replaced by the rVV10 NLC functional[95]
- LC-VV10 – 0% SR HF exchange + 100% LR HF exchange + $\omega$PBE GGA exchange + PBE GGA correlation + VV10 non-local correlation ($\omega$=0.45)[31]
- LC-wPBE08 (LC-$\omega$PBE08) – 0% SR HF exchange + 100% LR HF exchange + $\omega$PBE GGA exchange + PBE GGA correlation ($\omega$=0.45)[141]
- LRC-BOP (LRC-$\mu$BOP)– 0% SR HF exchange + 100% LR HF exchange + muB88 GGA exchange + BOP GGA correlation ($\omega$=0.47)[142]

- LRC-wPBE (LRC-$\omega$PBE) – 0% SR HF exchange + 100% LR HF exchange + $\omega$PBE GGA exchange + PBE GGA correlation ($\omega$=0.3)[143]
- LRC-wPBEh (LRC-$\omega$PBEh) – 20% SR HF exchange + 100% LR HF exchange + 80% $\omega$PBE GGA exchange + PBE GGA correlation ($\omega$=0.2)[144]
- N12-SX – 26-parameter non-separable GGA with 25% SR HF exchange, 0% LR HF exchange, and $\omega = 0.11$[145]
- rCAM-B3LYP – Re-fit CAM-B3LYP with the goal of minimizing many-electron self-interaction error[146]
- wB97 ($\omega$B97) – 13-parameter functional with 0% SR HF exchange, 100% LR HF exchange, and $\omega = 0.4$[25]
- wB97X ($\omega$B97X) – 14-parameter functional with $\approx$ 15.77% SR HF exchange, 100% LR HF exchange, and $\omega = 0.3$[25]
- wB97X-rV* ($\omega$B97X-rV) – $\omega$B97X-V density functional with the VV10 NLC functional replaced by the rVV10 NLC functional[95]

Range-Separated Hybrid Meta-Generalized Gradient Approximation (RSH meta-GGA)

- **wB97M-V** ($\omega$B97M-V) – 12-parameter combinatorially-optimized, dispersion-corrected (VV10) functional with 15% SR HF exchange, 100% LR HF exchange, and $\omega = 0.3$[147]
- M11 – 40-parameter functional with 42.8% SR HF exchange, 100% LR HF exchange, and $\omega = 0.25$[148]
- MN12-SX – 58-parameter non-separable meta-GGA with 25% SR HF exchange, 0% LR HF exchange, and $\omega = 0.11$[145]
- wB97M-rV* ($\omega$B97X-rV) – $\omega$B97M-V density functional with the VV10 NLC functional replaced by the rVV10 NLC functional[95]
- wM05-D ($\omega$M05-D) – 21-parameter dispersion-corrected (DFT-CHG) functional with $\approx$ 36.96% SR HF exchange, 100% LR HF exchange, and $\omega = 0.2$[149]
- wM06-D3 ($\omega$M06-D3) – 25-parameter dispersion-corrected [DFT-D3(0)] functional with $\approx$ 27.15% SR HF exchange, 100% LR HF exchange, and $\omega = 0.3$[136]

Double Hybrid Generalized Gradient Approximation (DH GGA)

**Note:** In order to use the resolution-of-the-identity approximation for the MP2 component, specify an auxiliary basis set with the *$rem* variable AUX_BASIS

- **DSD-PBEPBE-D3** – 68% HF exchange + 32% PBE GGA exchange + 49% PBE GGA correlation + 13% SS MP2 correlation + 55% OS MP2 correlation with DFT-D3(BJ) tail[150]
- **wB97X-2(LP)** ($\omega$B97X-2(LP)) – 13-parameter functional with $\approx$ 67.88% SR HF exchange, 100% LR HF exchange, $\approx$ 58.16% SS MP2 correlation, $\approx$ 47.80% OS MP2 correlation, and $\omega = 0.3$[151]
- **wB97X-2(TQZ)** ($\omega$B97X-2(TQZ)) – 13-parameter functional with $\approx$ 63.62% SR HF exchange, 100% LR HF exchange, $\approx$ 52.93% SS MP2 correlation, $\approx$ 44.71% OS MP2 correlation, and $\omega = 0.3$[151]

- **XYG3** – 80.33% HF exchange - 1.4% Slater LSDA exchange + 21.07% B88 GGA exchange + 67.89% LYP GGA correlation + 32.11% MP2 correlation (evaluated with B3LYP orbitals)[152]
- **XYGJ-OS** – 77.31% HF exchange + 22.69% Slater LSDA exchange + 23.09% VWN1RPA LSDA correlation + 27.54% LYP GGA correlation + 43.64% OS MP2 correlation (evaluated with B3LYP orbitals)[153]
- B2PLYP – 53% HF exchange + 47% B88 GGA exchange + 73% LYP GGA correlation + 27% MP2 correlation[154]
- B2GPPLYP – 65% HF exchange + 35% B88 GGA exchange + 64% LYP GGA correlation + 36% MP2 correlation[155]
- DSD-PBEP86-D3 – 69% HF exchange + 31% PBE GGA exchange + 44% P86 GGA correlation + 22% SS MP2 correlation + 52% OS MP2 correlation with DFT-D3(BJ) tail[150]
- LS1DH-PBE – 75% HF exchange + 25% PBE GGA exchange + 57.8125% PBE GGA correlation + 42.1875% MP2 correlation[156]
- PBE-QIDH – 69.3361% HF exchange + 30.6639% PBE GGA exchange + 66.6667% PBE GGA correlation + 33.3333% MP2 correlation[157]
- PBE0-2 – $\approx$ 79.37% HF exchange + $\approx$ 20.63% PBE GGA exchange + 50% PBE GGA correlation + 50% MP2 correlation[158]
- PBE0-DH – 50% HF exchange + 50% PBE GGA exchange + 87.5% PBE GGA correlation + 12.5% MP2 correlation[159]

Double Hybrid Meta-Generalized Gradient Approximation (DH MGGA)

- **PTPSS-D3** – 50% HF exchange + 50% Re-Fit TPSS meta-GGA exchange + 62.5% Re-Fit TPSS meta-GGA correlation + 37.5% OS MP2 correlation with DFT-D3(0) tail[160]
- DSD-PBEB95-D3 – 66% HF exchange + 34% PBE GGA exchange + 55% B95 GGA correlation + 9% SS MP2 correlation + 46% OS MP2 correlation with DFT-D3(BJ) tail[150]
- PWPB95-D3 – 50% HF exchange + 50% Re-Fit PW91 GGA exchange + 73.1% Re-Fit B95 meta-GGA correlation + 26.9% OS MP2 correlation with DFT-D3(0) tail[160]

#### 4.4.3.5 Specialized Functionals

- SRC1-R1 – TDDFT short-range corrected functional (Equation 1 in Ref. 161, 1st row atoms)
- SRC1-R2 – TDDFT short-range corrected functional (Equation 1 in Ref. 161, 2nd row atoms)
- SRC2-R1 – TDDFT short-range corrected functional (Equation 2 in Ref. 161, 1st row atoms)
- SRC2-R2 – TDDFT short-range corrected functional (Equation 2 in Ref. 161, 2nd row atoms)
- BR89 – Becke-Roussel meta-GGA exchange functional modeled after the hydrogen atom[162]
- B94 – meta-GGA correlation functional by Becke that utilizes the BR89 exchange functional to compute the Coulomb potential[163]

- B94hyb – modified version of the B94 correlation functional for use with the BR89B94hyb exchange-correlation functional[163]
- BR89B94h – 15.4% HF exchange + 84.6% BR89 meta-GGA exchange + BR89hyb meta-GGA correlation[163]
- BRSC – Exchange component of the original B05 exchange-correlation functional[164]
- MB05 – Exchange component of the modified B05 (BM05) exchange-correlation functional[165]
- B05 – A full exact-exchange Kohn-Sham scheme of Becke that uses the exact-exchange energy density (RI) and accounts for static correlation[164,166,167]
- BM05 (XC) – Modified B05 hyper-GGA scheme that uses MB05 instead of BRSC as the exchange functional[165]
- PSTS – Hyper-GGA (100% HF exchange) exchange-correlation functional of Perdew, Staroverov, Tao, and Scuseria[168]
- MCY2 – Mori-Sánchez-Cohen-Yang adiabatic connection-based hyper-GGA exchange-correlation functional[169–171]

#### 4.4.3.6 User-Defined Density Functionals

Users can also request a customized density functional consisting of any linear combination of exchange and/or correlation functionals available in Q-CHEM. A "general" density functional of this sort is requested by setting EXCHANGE = GEN and then specifying the functional by means of an *$xc_functional* input section consisting of one line for each desired exchange (X) or correlation (C) component of the functional, and having the format shown below.

```
$xc_functional
   X   exchange_symbol   coefficient
   X   exchange_symbol   coefficient
   ...
   C   correlation_symbol   coefficient
   C   correlation_symbol   coefficient
   ...
   K   coefficient
$end
```

Each line requires three variables: X or C to designate whether this is an exchange or correlation component; the symbolic representation of the functional, as would be used for the EXCHANGE or CORRELATION keywords variables as described above; and a real number coefficient for each component. Note that Hartree-Fock exchange can be designated either as "X" or as "K". Examples are shown below.

**Example 4.5** Q-CHEM input for $H_2O$ with the B3tLap functional.

```
$molecule
  0  1
  O
  H1  O  oh
  H2  O  oh  H1  hoh
  oh  =   0.97
  hoh = 120.0
$end

$rem
   EXCHANGE     gen
   CORRELATION  none
   BASIS        g3large   ! recommended for high accuracy
   THRESH       14        ! and better convergence
$end

$xc_functional
X    Becke     0.726
X    S         0.0966
C    PK06      1.0
K    0.1713
$end
```

**Example 4.6** Q-CHEM input for $H_2O$ with the BR89B94hyb functional.

```
$molecule
   0  1
   O
   H1  O  oh
   H2  O  oh  H1  hoh
   oh  =   0.97
   hoh = 120.0
$end

$rem
   EXCHANGE     gen
   CORRELATION  none
   BASIS        g3large   ! recommended for high accuracy
   THRESH       14        ! and better convergence
$end

$xc_functional
   X    BR89      0.846
   C    B94hyb    1.0
   K              0.154
$end
```

The next two examples illustrate the use of the RI-B05 and RI-PSTS functionals. These are presently available only for single-point calculations, and convergence is greatly facilitated by obtaining converged SCF orbitals from, *e.g.*, an LDA or HF calculation first. (LDA is used in the example below but HF can be substituted.) Use of the RI approximation (Section 5.6) requires specification of an auxiliary basis set.

**Example 4.7** Q-CHEM input of $H_2$ using RI-B05.

```
$comment
   H2, example of SP RI-B05.  First do a well-converged LSD, G3LARGE is the
   basis of choice for good accuracy. The input lines
   PURECART    2222
   SCF_GUESS   CORE
   are obligatory for the time being here.
$end
```

```
$molecule
0 1
H   0.  0.   0.0
H   0.  0.   0.7414
$end

$rem
   SCF_GUESS        core
   METHOD           lda
   BASIS            g3large
   PURECART         2222
   THRESH           14
   MAX_SCF_CYCLES   80
   PRINT_INPUT      true
   INCDFT           false
   SYM_IGNORE       true
   SYMMETRY         false
   SCF_CONVERGENCE  9
$end

@@@@

$comment
   For the time being the following input lines are obligatory:
   PURECART        2222
   AUX_BASIS       riB05-cc-pvtz
   DFT_CUTOFFS     0
   MAX_SCF_CYCLES  0
$end

$molecule
   read
$end

$rem
   SCF_GUESS       read
   EXCHANGE        b05   ! or set to psts for ri-psts
   PURECART        2222
   BASIS           g3large
   AUX_BASIS       rib05-cc-pvtz  ! the aux basis for both RI-B05 and RI-PSTS
   THRESH          4
   PRINT_INPUT     true
   INCDFT          false
   SYM_IGNORE      true
   SYMMETRY           false
   MAX_SCF_CYCLES  0
   DFT_CUTOFFS     0
$end
```

### 4.4.4 Basic DFT Job Control

Basic SCF job control was described in Section 4.3 in the context of Hartree-Fock theory and is largely the same for DFT. The keywords METHOD and BASIS are required, although for DFT the former could be substituted by specifying EXCHANGE and CORRELATION instead.

**METHOD**

Specifies the exchange-correlation functional.

TYPE:

STRING

DEFAULT:

No default

OPTIONS:

*NAME* Use METHOD = *NAME*, where *NAME* is either HF for Hartree-Fock theory or else one of the DFT methods listed in Section 4.4.3.4.

RECOMMENDATION:

In general, consult the literature to guide your selection. Our recommendations for DFT are indicated in bold in Section 4.4.3.4.

**EXCHANGE**

Specifies the exchange functional (or most exchange-correlation functionals for backwards compatibility).

TYPE:

STRING

DEFAULT:

No default

OPTIONS:

*NAME* Use EXCHANGE = *NAME*, where *NAME* is either:

1) One of the exchange functionals listed in Section 4.4.3.2

2) One of the XC functionals listed in Section 4.4.3.4 that is not marked with an asterisk.

3) GEN, for a user-defined functional (see Section 4.4.3.6).

RECOMMENDATION:

In general, consult the literature to guide your selection. Our recommendations are indicated in bold in Sections 4.4.3.4 and 4.4.3.2.

**CORRELATION**

Specifies the correlation functional.

TYPE:

STRING

DEFAULT:

NONE

OPTIONS:

*NAME* Use CORRELATION = *NAME*, where *NAME* is one of the correlation functionals listed in Section 4.4.3.3.

RECOMMENDATION:

In general, consult the literature to guide your selection. Our recommendations are indicated in bold in Section 4.4.3.3.

The following *$rem* variables are related to the choice of the quadrature grid required to integrate the XC part of the functional, which does not appear in Hartree-Fock theory. DFT quadrature grids are described in Section 4.4.5.

**FAST_XC**

Controls direct variable thresholds to accelerate exchange-correlation (XC) in DFT.

TYPE:

LOGICAL

DEFAULT:

FALSE

OPTIONS:

| | |
|---|---|
| TRUE | Turn FAST_XC on. |
| FALSE | Do not use FAST_XC. |

RECOMMENDATION:

Caution: FAST_XC improves the speed of a DFT calculation, but may occasionally cause the SCF calculation to diverge.

**XC_GRID**

Specifies the type of grid to use for DFT calculations.

TYPE:

INTEGER

DEFAULT:

Functional-dependent; see Table 4.4.

OPTIONS:

| | |
|---|---|
| 0 | Use SG-0 for H, C, N, and O; SG-1 for all other atoms. |
| $n$ | Use SG-$n$ for all atoms, $n = 1, 2$, or 3 |
| $XY$ | A string of two six-digit integers $X$ and $Y$, where $X$ is the number of radial points and $Y$ is the number of angular points where possible numbers of Lebedev angular points, which must be an allowed value from Table 4.3 in Section 4.4.5. |
| $-XY$ | Similar format for Gauss-Legendre grids, with the six-digit integer $X$ corresponding to the number of radial points and the six-digit integer $Y$ providing the number of Gauss-Legendre angular points, $Y = 2N^2$. |

RECOMMENDATION:

Use the default unless numerical integration problems arise. Larger grids may be required for optimization and frequency calculations.

**NL_GRID**

Specifies the grid to use for non-local correlation.

TYPE:

INTEGER

DEFAULT:

1

OPTIONS:

Same as for XC_GRID

RECOMMENDATION:

Use the default unless computational cost becomes prohibitive, in which case SG-0 may be used. XC_GRID should generally be finer than NL_GRID.

**XC_SMART_GRID**

Uses SG-0 (where available) for early SCF cycles, and switches to the (larger) target grid specified by XC_GRID for final cycles of the SCF.

TYPE:

LOGICAL

DEFAULT:

FALSE

OPTIONS:

| | |
|---|---|
| TRUE (or 1) | Use the smaller grid for the initial cycles. |
| FALSE (or 0) | Use the target grid for all SCF cycles. |

RECOMMENDATION:

The use of the smart grid can save some time on initial SCF cycles.

### 4.4.5 DFT Numerical Quadrature

In practical DFT calculations, the forms of the approximate exchange-correlation functionals used are quite complicated, such that the required integrals involving the functionals generally cannot be evaluated analytically. Q-CHEM evaluates these integrals through numerical quadrature directly applied to the exchange-correlation integrand. Several standard quadrature grids are available ("SG-$n$", $n = 0, 1, 2, 3$), with a default value that is automatically set according to the complexity of the functional in question.

The quadrature approach in Q-CHEM is generally similar to that found in many DFT programs. The multi-center XC integrals are first partitioned into "atomic" contributions using a nuclear weight function. Q-CHEM uses the nuclear partitioning of Becke[172], though without the "atomic size adjustments" of Ref. 172. The atomic integrals are then evaluated through standard one-center numerical techniques. Thus, the exchange-correlation energy is obtained as

$$E_{\rm XC} = \sum_{A}^{\rm atoms} \sum_{i\in A}^{\rm points} w_{Ai} f(\mathbf{r}_{Ai}) \; , \tag{4.44}$$

where the function $f$ is the aforementioned XC integrand and the quantities $w_{Ai}$ are the quadrature weights. The sum over $i$ runs over grid points belonging to atom $A$, which are located at positions $\mathbf{r}_{Ai} = \mathbf{R}_A + \mathbf{r}_i$, so this approach requires only the choice of a suitable one-center integration grid (to define the $\mathbf{r}_i$), which is independent of nuclear configuration. These grids are implemented in Q-CHEM in a way that ensures that the $E_{\rm XC}$ is rotationally-invariant, *i.e.*, that is does not change when the molecule undergoes rigid rotation in space[173].

Quadrature grids are further separated into radial and angular parts. Within Q-CHEM, the radial part is usually treated by the Euler-Maclaurin scheme proposed by Murray *et al.*[174], which maps the semi-infinite domain $[0,\infty)$ onto $[0,1)$ and applies the extended trapezoid rule to the transformed integrand. Alternatively, Gill and Chien[175] proposed a radial scheme based on a Gaussian quadrature on the interval $[0,1]$ with a different weight function. This "MultiExp" radial quadrature is exact for integrands that are a linear combination of a geometric sequence of exponential functions, and is therefore well suited to evaluating atomic integrals. However, the task of generating the MultiExp quadrature points becomes increasingly ill-conditioned as the number of radial points increases, so that a "double exponential" radial quadrature[176,177] is used for the largest standard grids in Q-CHEM, namely SG-2 and SG-3[178]. (See Section 4.4.5.2.)

| No. Points | Degree ($\ell_{\max}$) | No. Points | Degree ($\ell_{\max}$) | No. Points | Degree ($\ell_{\max}$) |
|---|---|---|---|---|---|
| 6 | 3 | 230 | 25 | 1730 | 71 |
| 14 | 5 | 266 | 27 | 2030 | 77 |
| 26 | 7 | 302 | 29 | 2354 | 83 |
| 38 | 9 | 350 | 31 | 2702 | 89 |
| 50 | 11 | 434 | 35 | 3074 | 95 |
| 74 | 13 | 590 | 41 | 3470 | 101 |
| 86 | 15 | 770 | 47 | 3890 | 107 |
| 110 | 17 | 974 | 53 | 4334 | 113 |
| 146 | 19 | 1202 | 59 | 4802 | 119 |
| 170 | 21 | 1454 | 65 | 5294 | 125 |
| 194 | 23 | | | | |

Table 4.3: Lebedev angular quadrature grids available in Q-CHEM.

#### 4.4.5.1 Angular Grids

For a fixed value of the radial spherical-polar coordinate $r$, a function $f(\mathbf{r}) \equiv f(r,\theta,\phi)$ has an exact expansion in spherical harmonic functions,

$$f(r,\theta,\phi) = \sum_{\ell=0}^{\infty} \sum_{m=-\ell}^{\ell} c_{\ell m} \mathrm{Y}_{\ell m}(\theta,\phi) \ . \tag{4.45}$$

Angular quadrature grids are designed to integrate $f(r,\theta,\phi)$ for fixed $r$, and are often characterized by their degree, meaning the maximum value of $\ell$ for which the quadrature is exact, as well as by their efficiency, meaning the number of spherical harmonics exactly integrated per degree of freedom in the formula. Q-CHEM supports the following two types of angular grids.

- **Lebedev grids.** These are specially-constructed grids for quadrature on the surface of a sphere[179–182], based on the octahedral point group. Lebedev grids available in Q-CHEM are listed in Table 4.3. These grids typically have near-unit efficiencies, with efficiencies exceeding unity in some cases. A Lebedev grid is selected by specifying the number of grid points (from Table 4.3) using the *$rem* keyword XC_GRID, as discussed below.
- **Gauss-Legendre grids.** These are spherical direct-product grids in the two spherical-polar angles, $\theta$ and $\phi$. Integration in over $\theta$ is performed using a Gaussian quadrature derived from the Legendre polynomials, while integration over $\phi$ is performed using equally-spaced points. A Gauss-Legendre grid is selected by specifying the total number of points, $2N^2$, to be used for the integration, which specifies a grid consisting of $2N_\phi$ points in $\phi$ and $N_\theta$ in $\theta$, for a degree of $2N-1$. Gauss-Legendre grids exhibit efficiencies of only 2/3, and are thus lower in quality than Lebedev grids for the same number of grid points, but have the advantage that they are defined for arbitrary (and arbitrarily-large) numbers of grid points. This offers a mechanism to achieve arbitrary accuracy in the angular integration, if desired.

Combining these radial and angular schemes yields an intimidating selection of quadratures, so it is useful to standardize the grids. This is done for the convenience of the user, to facilitate comparisons in the literature, and also for developers wishing to compared detailed results between different software programs,

| Pruned Grid | Ref. | Parent Grid $(N_r, N_\Omega)$ | No. Grid Points (C atom)[a] | Default Grid for Which Functionals?[b] |
|---|---|---|---|---|
| SG-0 | 184 | (23, 170) | 1,390 (36%) | None |
| SG-1 | 183 | (50, 194) | 3,816 (39%) | LDA, most GGAs and hybrids |
| SG-2 | 178 | (75, 302) | 7,790 (34%) | Meta-GGAs; B95- and B97-based functionals |
| SG-3 | 178 | (99, 590) | 17,674 (30%) | Minnesota functionals |

[a] Number in parenthesis is the fraction of points retained from the parent grid

[b] Reflects Q-CHEM versions since v. 4.4.2

Table 4.4: Standard quadrature grids available in Q-CHEM, along with the number of grid points for a carbon atom, showing the reduction in grid points due to pruning.

because the total electronic energy is sensitive to the details of the grid, just as it is sensitive to details of the basis set. Standard quadrature grids are discussed next.

#### 4.4.5.2 Standard Quadrature Grids, SG-$n$

Four different "standard grids" are available in Q-CHEM, designated SG-$n$, for $n = 0, 1, 2$, or 3; both quality and the computational cost of these grids increases with $n$. These grids are constructed starting from a "parent" grid $(N_r,\ N_\Omega)$ consisting of $N_r$ radial spheres with $N_\Omega$ angular (Lebedev) grid points on each, then systematically pruning the number of angular points in regions where sophisticated angular quadrature is not necessary, such as near the nuclei where the charge density is nearly spherically symmetric and at long distance from the nuclei where it varies slowly. A large number of points is retained in the valence region where angular accuracy is critical. The SG-$n$ grids are summarized in Table 4.4. While many electronic structure programs use some kind of procedure to delete unnecessary grid points in the interest of computational efficiency, Q-CHEM's SG-$n$ grids are notable in that the complete grid specifications are available in the peer-reviewed literature[178,183,184], to facilitate reproduction of Q-CHEM DFT calculations using other electronic structure programs. Just as computed energies may vary quite strongly with the choice of basis set, so too in DFT may they vary strongly with the choice of quadrature grid. In publications, users should always specify the grid that is used, and it is suggested to cite the appropriate literature reference from Table 4.4.

The SG-0 and SG-1 grids are designed for calculations on large molecules using GGA functionals. SG-1 affords integration errors on the order of ~0.2 kcal/mol for medium-sized molecules and GGA functionals, including for demanding test cases such as reaction enthalpies for isomerizations. (Integration errors in total energies are no more than a few $\mu$hartree, or ~0.01 kcal/mol.) The SG-0 grid was derived in similar fashion, and affords a root-mean-square error in atomization energies of 72 $\mu$hartree with respect to SG-1, while relative energies are reproduced well[184]. In either case, errors of this magnitude are typically considerably smaller than the intrinsic errors in GGA energies, and hence acceptable. As seen in Table 4.4, SG-1 retains $< 40\%$ of the grid points of its parent grid, which translates directly into cost savings.

Both SG-0 and SG-1 were optimized so that the integration error in the energy falls below a target threshold, but derivatives of the energy (including such properties as (hyper)polarizabilities[185]) are often more sensitive to the quality of the integration grid. Special care is required, for example, when imaginary vibrational frequencies are encountered, as low-frequency (but real) vibrational frequencies can manifest as imaginary if the grid is sparse. If imaginary frequencies are found, or if there is some doubt about the frequencies reported by Q-CHEM, the recommended procedure is to perform the geometry optimization and vibrational frequency calculations again using a higher-quality grid. (The optimization should converge quite quickly if the previously-optimized geometry is used as an initial guess.)

SG-1 was the default DFT integration grid for all density functionals for Q-CHEM versions 3.2–4.4. (Note that SG-0 was re-optimized for Q-CHEM v. 3.0, so results may differ slightly as compared to older versions of the program.) Beginning with Q-CHEM v. 4.4.2, however, the default grid is functional-dependent, as summarized in Table 4.4. This is a reflection of the fact that although SG-1 is adequate for energy calculations using most GGA and hybrid functionals (although care must be taken for some other properties, as discussed below), it is *not* adequate to integrate many functionals developed since $\sim$2005. These include meta-GGAs, which are more complicated due to their dependence on the kinetic energy density ($\tau_\sigma$ in Eq. (4.39)) and/or the Laplacian of the density ($\nabla^2\rho_\sigma$). Functionals based on B97, along with the Minnesota suite of functionals [120,186], contain relatively complicated expressions for the exchange inhomogeneity factor, and are therefore also more sensitive to the quality of the integration grid [135,178,187]. To integrate these modern density functionals, the SG-2 and SG-3 grids were developed [178], which are pruned versions of the medium-quality (75, 302) and high-quality (99, 590) integration grids, respectively. Tests of properties known to be highly sensitive to the quality of the integration grid, such as vibrational frequencies, hyper-polarizabilities, and potential energy curves for non-bonded interactions, demonstrate that SG-2 is usually adequate for meta-GGAs and B97-based functionals, and in many cases is essentially converged with respect to an unpruned (250, 974) grid [178]. The Minnesota functionals are more sensitive to the grid, and while SG-3 is often adequate, it is not completely converged in the case of non-bonded interactions. [178].

#### 4.4.5.3 Consistency Check and Cutoffs

Whenever Q-CHEM calculates numerical density functional integrals, the electron density itself is also integrated numerically as a test of the quality of the numerical quadrature. The extent to which this numerical result differs from the number of electrons is an indication of the accuracy of the other numerical integrals. A warning message is printed whenever the relative error in the numerical electron count reaches 0.01%, indicating that the numerical XC results may not be reliable. If the warning appears on the first SCF cycle it is probably not serious, because the initial-guess density matrix is sometimes not idempotent. This is the case with the SAD guess discussed in Section 4.5, and also with a density matrix that is taken from a previous geometry optimization cycle, and in such cases the problem will likely correct itself in subsequent SCF iterations. If the warning persists, however, then one should consider either using a finer grid or else selecting an alternative initial guess.

By default, Q-CHEM will estimate the magnitude of various XC contributions on the grid and eliminate those determined to be numerically insignificant. Q-CHEM uses specially-developed cutoff procedures which permits evaluation of the XC energy and potential in only $\mathcal{O}(N)$ work for large molecules. This is a significant improvement over the formal $\mathcal{O}(N^3)$ scaling of the XC cost, and is critical in enabling DFT calculations to be carried out on very large systems. In rare cases, however, the default cutoff scheme can be too aggressive, eliminating contributions that should be retained; this is almost always signaled by an inaccurate numerical density integral. An example of when this could occur is in calculating anions with multiple sets of diffuse functions in the basis. A remedy may be to increase the size of the quadrature grid.

### 4.4.6 Range-Separated Hybrid Density Functionals

Whereas RSH functionals such as LRC-$\omega$PBE are attempts to add 100% LR Hartree-Fock exchange with minimal perturbation to the original functional (PBE, in this example), other RSH functionals are of a more empirical nature and their range-separation parameters have been carefully parameterized along with all of the other parameters in the functional. These cases are functionals are discussed first, in Section 4.4.6.1, because their range-separation parameters should be taken as fixed. User-defined values of the range-separation parameter are discussed in Section 4.4.6.2, and Section 4.4.6.3 discusses a procedure for which an optimal, system-specific value of this parameter ($\omega$ or $\mu$) can be chosen for functionals such as LRC-$\omega$PBE or LRC-$\mu$PBE.

#### 4.4.6.1 Semi-Empirical RSH Functionals

Semi-empirical RSH functionals for which the range-separation parameter should be considered fixed include the $\omega$B97, $\omega$B97X, and $\omega$B97X-D functionals developed by Chai and Head-Gordon[25,35]; $\omega$B97X-V and $\omega$B97M-V from Mardirossian and Head-Gordon[135,147]; M11 from Peverati and Truhlar[148]; $\omega$B97X-D3, $\omega$M05-D, and $\omega$M06-D3 from Chai and coworkers[136,149]; and the screened exchange functionals N12-SX and MN12-SX from Truhlar and co-workers[145]. More recently, Mardirossian and Head-Gordon developed two RSH functionals, $\omega$B97X-V and $\omega$B97M-V, via a combinatorial approach by screening over 100,000 possible functionals in the first case and over 10 billion possible functionals in the second case. Both of the latter functionals use the VV10 non-local correlation functional in order to improve the description of non-covalent interactions and isomerization energies. $\omega$B97M-V is a 12-parameter meta-GGA with 15% short-range exact exchange and 100% long-range exact exchange and is one of the most accurate functionals available through rung 4 of Jacob's Ladder, across a wide variety of applications. This has been verified by benchmarking the functional on nearly 5000 data points against over 200 alternative functionals available in Q-CHEM[147].

#### 4.4.6.2 User-Defined RSH Functionals

As pointed out in Ref. 188 and elsewhere, the description of charge-transfer excited states within density functional theory (or more precisely, time-dependent DFT, which is discussed in Section 6.3) requires full (100%) non-local HF exchange, at least in the limit of large donor–acceptor distance. Hybrid functionals such as B3LYP[27,28] and PBE0[189] that are well-established and in widespread use, however, employ only 20% and 25% HF exchange, respectively. While these functionals provide excellent results for many ground-state properties, they cannot correctly describe the distance dependence of charge-transfer excitation energies, which are enormously underestimated by most common density functionals. This is a serious problem in any case, but it is a *catastrophic* problem in large molecules and in non-covalent clusters, where TDDFT often predicts a near-continuum of spurious, low-lying charge transfer states[190,191]. The problems with TDDFT's description of charge transfer are not limited to large donor–acceptor distances, but have been observed at ~2 Å separation, in systems as small as uracil–$(H_2O)_4$[190]. Rydberg excitation energies also tend to be substantially underestimated by standard TDDFT.

One possible avenue by which to correct such problems is to parameterize functionals that contain 100% HF exchange, though few such functionals exist to date. An alternative option is to attempt to preserve the form of common GGAs and hybrid functionals at short range (*i.e.*, keep the 25% HF exchange in PBE0) while incorporating 100% HF exchange at long range, which provides a rigorously correct description of the long-range distance dependence of charge-transfer excitation energies, but aims to avoid contaminating short-range exchange-correlation effects with additional HF exchange. The separation is accomplished using the range-separation *ansatz* that was introduced in Section 4.4.3. In particular, functionals that use 100% HF exchange at long range ($c_{x,\mathrm{LR}} = 1$ in Eq. (4.42)) are known as "long-range-corrected" (LRC) functionals. An LRC version of PBE0 would, for example, have $c_{x,\mathrm{SR}} = 0.25$.

To fully specify an LRC functional, one must choose a value for the range separation parameter $\omega$ in

Eq. (4.41). In the limit $\omega \to 0$, the LRC functional in Eq. (4.42) reduces to a non-RSH functional where there is no "SR" or "LR", because all exchange and correlation energies are evaluated using the full Coulomb operator, $r_{12}^{-1}$. Meanwhile the $\omega \to \infty$ limit corresponds to a new functional, $E_{xc}^{\mathrm{RSH}} = E_c + E_x^{\mathrm{HF}}$. Full HF exchange is inappropriate for use with most contemporary GGA correlation functionals, so the latter limit is expected to perform quite poorly. Values of $\omega > 1.0$ bohr$^{-1}$ are likely not worth considering, according to benchmark tests[143,192].

Evaluation of the short- and long-range HF exchange energies is straightforward[193], so the crux of any RSH functional is the form of the short-range GGA exchange functional, and several such functionals are available in Q-CHEM. These include short-range variants of the B88 and PBE exchange described by Hirao and co-workers[49,142], called $\mu$B88 and $\mu$PBE in Q-CHEM[194], and an alternative formulation of short-range PBE exchange proposed by Scuseria and co-workers[58], which is known as $\omega$PBE. These functionals are available in Q-CHEM thanks to the efforts of the Herbert group[143,144]. By way of notation, the terms "$\mu$PBE", "$\omega$PBE", *etc.*, refer only to the short-range exchange functional, $E_{x,\mathrm{SR}}^{\mathrm{DFT}}$ in Eq. (4.42). These functionals could be used in "screened exchange" mode, as described in Section 4.4.3, as for example in the HSE03 functional[195], therefore the designation "LRC-$\omega$PBE", for example, should only be used when the short-range exchange functional $\omega$PBE is combined with 100% Hartree-Fock exchange in the long range.

In general, LRC-DFT functionals have been shown to remove the near-continuum of spurious charge-transfer excited states that appear in large-scale TDDFT calculations[192]. However, certain results depend sensitively upon the value of the range-separation parameter $\omega$[143,144,191,192,196], especially in TDDFT calculations (Section 6.3) and therefore the results of LRC-DFT calculations must therefore be interpreted with caution, and probably for a range of $\omega$ values. This can be accomplished by requesting a functional that contains some short-range GGA exchange functional ($\omega$PBE or $\mu$PBE, in the examples mentioned above), in combination with setting the *$rem* variable LRC_DFT = TRUE, which requests the addition of 100% Hartree-Fock exchange in the long-range. Basic job-control variables and an example can be found below. The value of the range-separation parameter is then controlled by the variable OMEGA, as shown in the examples below.

**LRC_DFT**

Controls the application of long-range-corrected DFT

TYPE:

LOGICAL

DEFAULT:

FALSE

OPTIONS:

| | |
|---|---|
| FALSE (or 0) | Do not apply long-range correction. |
| TRUE (or 1) | Add 100% long-range Hartree-Fock exchange to the requested functional. |

RECOMMENDATION:

The *$rem* variable OMEGA must also be specified, in order to set the range-separation parameter.

**OMEGA**

Sets the range-separation parameter, $\omega$, also known as $\mu$, in functionals based on Hirao's RSH scheme.

TYPE:

INTEGER

DEFAULT:

No default

OPTIONS:

$n$ Corresponding to $\omega = n/1000$, in units of bohr$^{-1}$

RECOMMENDATION:

None

**COMBINE_K**

Controls separate or combined builds for short-range and long-range K

TYPE:

LOGICAL

DEFAULT:

FALSE

OPTIONS:

FALSE (or 0) Build short-range and long-range K separately (twice as expensive as a global hybrid)

TRUE (or 1) Build short-range and long-range K together ($\approx$ as expensive as a global hybrid)

RECOMMENDATION:

Most pre-defined range-separated hybrid functionals in Q-CHEM use this feature by default. However, if a user-specified RSH is desired, it is necessary to manually turn this feature on.

**Example 4.8** Application of LRC-BOP to $(\mathrm{H_2O})_2^-$.

```
$comment
The value of omega is 0.47 by default but can
be overwritten by specifying OMEGA.
$end

$molecule
-1 2
O           1.347338    -0.017773    -0.071860
H           1.824285     0.813088     0.117645
H           1.805176    -0.695567     0.461913
O          -1.523051    -0.002159    -0.090765
H          -0.544777    -0.024370    -0.165445
H          -1.682218     0.174228     0.849364
$end

$rem
   EXCHANGE       LRC-BOP
   BASIS          6-31(1+,3+)G*
   LRC_DFT        TRUE
   OMEGA          300       ! = 0.300 bohr**(-1)
$end
```

Recently, Rohrdanz *et al.*[144] have published a thorough benchmark study of both ground- and excited-state properties, using the "LRC-$\omega$PBEh" functional, in which the "h" indicates a short-range hybrid (*i.e.*, the presence of some short-range HF exchange). Empirically-optimized parameters of $c_{x,\mathrm{SR}} = 0.2$ (see Eq. (4.42)) and $\omega = 0.2$ bohr$^{-1}$ were obtained[144], and these parameters are taken as the defaults for LRC-$\omega$PBEh. Caution is warranted, however, especially in TDDFT calculations for large systems, as excitation energies for states that exhibit charge-transfer character can be rather sensitive to the precise value of $\omega$.[144,191] In such cases (and maybe in general), the "tuning" procedure described in Section 4.4.6.3 is recommended.

**Example 4.9** Application of LRC-$\omega$PBEh to the $C_2H_4$–$C_2F_4$ dimer at 5 Å separation.

```
$comment
    This example uses the "optimal" parameter set discussed above.
    It can also be run by setting METHOD = LRC-wPBEh.
$end

$molecule
0 1
C          0.670604    0.000000    0.000000
C         -0.670604    0.000000    0.000000
H          1.249222    0.929447    0.000000
H          1.249222   -0.929447    0.000000
H         -1.249222    0.929447    0.000000
H         -1.249222   -0.929447    0.000000
C          0.669726    0.000000    5.000000
C         -0.669726    0.000000    5.000000
F          1.401152    1.122634    5.000000
F          1.401152   -1.122634    5.000000
F         -1.401152   -1.122634    5.000000
F         -1.401152    1.122634    5.000000
$end

$rem
   EXCHANGE       GEN
   BASIS          6-31+G*
   LRC_DFT        TRUE
   OMEGA          200       ! = 0.2 a.u.
   CIS_N_ROOTS    4
   CIS_TRIPLETS   FALSE
$end

$xc_functional
   C  PBE   1.00
   X  wPBE  0.80
   X  HF    0.20
$end
```

Both LRC functionals and also the asymptotic corrections that will be discussed in Section 4.4.10.1 are thought to reduce self-interaction error in approximate DFT. A convenient way to quantify—or at least depict—this error is by plotting the DFT energy as a function of the (fractional) number of electrons, $N$, because $E(N)$ should in principle consist of a sequence of line segments with abrupt changes in slope (the so-called derivative discontinuity[197,198]) at integer values of $N$, but in practice these $E(N)$ plots bow away from straight-line segments[197]. Examination of such plots has been suggested as a means to adjust the fraction of short-range exchange in an LRC functional[199], while the range-separation parameter is tuned as described in Section 4.4.6.3.

**Example 4.10** Example of a DFT job with a fractional number of electrons. Here, we make the $-1.x$

anion of fluoride by subtracting a fraction of an electron from the HOMO of $F^{2-}$.

```
$comment
   Subtracting a whole electron recovers the energy of F-.
   Adding electrons to the LUMO is possible as well.
$end

$rem
   EXCHANGE             b3lyp
   BASIS                6-31+G*
   FRACTIONAL_ELECTRON  -500   ! divide by 1000 to get the fraction, -0.5 here.
$end

$molecule
-2 2
F
$end
```

#### 4.4.6.3 Tuned RSH Functionals

Whereas the range-separation parameters for the functionals described in Section 4.4.6.1 are wholly empirical in nature and should not be adjusted, for the functionals described in Section 4.4.6.2 some adjustment *was* suggested, especially for TDDFT calculations and for any properties that require interpretation of orbital energies, *e.g.*, HOMO/LUMO gaps. This adjustment can be performed in a non-empirical, albeit system-specific way, by “tuning” the value of $\omega$ in order to satisfy certain criteria that ought rigorously to be satisfied by an exact density functional.

System-specific optimization of $\omega$ is based on the Koopmans condition that would be satisfied for the exact density functional, namely, that for an $N$-electron molecule[200]

$$-\,\varepsilon_{\mathrm{HOMO}}(N) = \mathrm{IE}(N) \equiv E(N-1) - E(N)\ . \tag{4.46}$$

In other words, the HOMO eigenvalue should be equal to minus the ionization energy (IE), where the latter is defined by a $\Delta$SCF procedure[201,202]. When an RSH functional is used, all of the quantities in Eq. (4.46) are $\omega$-dependent, so this parameter is adjusted until the condition in Eq. (4.46) is met, which requires a sequence of SCF calculations on both the neutral and ionized species, using different values of $\omega$. For proper description of charge-transfer states, Baer and co-workers[200] suggest finding the value of $\omega$ that (to the extent possible) satisfies both Eq. (4.46) for the neutral donor molecule and its analogue for the *anion* of the acceptor species. Note that for a given approximate density functional, there is no guarantee that the IE condition can actually be satisfied for *any* value of $\omega$, but in practice it usually can be, and published benchmarks suggest that this system-specific approach affords the most accurate values of IEs and TDDFT excitation energies[200,203,204]. It should be noted, however, that the optimal value of $\omega$ can very dramatically with system size, *e.g.*, it is very different for the cluster anion $(H_2O)_6^-$ than it is for cluster $(H_2O)_{70}^-$ [196].

A script that optimizes $\omega$, called `OptOmegaIPEA.pl`, is located in the *$QC/bin* directory. The script scans $\omega$ over the range 0.1–0.8 bohr$^{-1}$, corresponding to values of the *$rem* variable OMEGA in the range 100–800. See the script for the instructions how to modify the script to scan over a wider range. To execute the script, you need to create three inputs for a BNL job using the same geometry and basis set, for a neutral molecule (`N.in`), its anion (`M.in`), and its cation (`P.in`), and then run the command

```
OptOmegaIPEA.pl >& optomega
```

which both generates the input files (`N_*`, `P_*`, `M_*`) and runs Q-CHEM on them, writing the optimization output into `optomega`. This script applies the IE condition to both the neutral molecule and its anion, minimizing the sum of $(\text{IE} + \varepsilon_{\text{HOMO}})^2$ for these two species. A similar script, `OptOmegaIP.pl`, uses Eq. (4.46) for the neutral molecule only.

**Note:** (i) If the system does not have positive EA, then the tuning should be done according to the IP condition only. The IP/EA script will yield an incorrect value of $\omega$ in such cases.
(ii) In order for the scripts to work, one must specify SCF_FINAL_PRINT = 1 in the inputs. The scripts look for specific regular expressions and will not work correctly without this keyword.

Although the tuning procedure was originally developed by Baer and co-workers using the BNL functional[200,203,204], it has more recently been applied using functionals such as LRC-$\omega$PBE (see, *e.g.*, Ref. 196), and the scripts will work with functionals other than BNL.

#### 4.4.6.4 Tuned RSH Functionals Based on the Global Density-Dependent Condition

The value of range-separation parameter based on IP tuning procedure ($\omega_{\text{IP}}$) exhibits a troublesome dependence on system size[196,205–208]. An alternative method to select $\omega$ is the global density-dependent (GDD) tuning procedure[209], in which the optimal value

$$\omega_{\text{GDD}} = C\langle d_{\text{x}}^2\rangle^{-1/2} \tag{4.47}$$

is related to the average distance $d_{\text{x}}$ between an electron in the outer regions of a molecule and the exchange hole in the region of localized orbitals. The quantity $C$ is an empirical constant for a given LRC functional, which was determined in Ref. 209 for LRC-$\omega$PBE ($C = 0.90$) and LRC-$\omega$PBEh ($C = 0.75$), using the def2-TZVPP basis set. Since LRC-$\omega$PBE($\omega_{\text{GDD}}$) provides a better description of polarizabilities in polyacetylene as compared to $\omega_{\text{IP}}$[210], it is anticipated that using $\omega_{\text{GDD}}$ in place of $\omega_{\text{IP}}$ may afford more accurate molecular properties, especially in conjugated systems. The $\omega$ value based on the GDD tuning procedure for RSH functionals can be invoked by setting the *$rem* variable OMEGA_GDD = TRUE. Basic job-control variables and an example can be found below. Since $\omega_{\text{GDD}}$ depends on the electron density, the converged density obtained by RSH functionals is used to compute $\omega_{\text{GDD}}$. The range-separation parameter for RSH functionals is still necessary to set by the variable OMEGA, for example, OMEGA = 300 for LRC-$\omega$PBE and OMEGA = 200 for LRC-$\omega$PBEh although the final $\omega_{\text{GDD}}$ value is not very sensitive to the initial OMEGA input.

**OMEGA_GDD**
Controls the application of $\omega_{\text{GDD}}$ tuning for long-range-corrected DFT
TYPE:
LOGICAL
DEFAULT:
FALSE
OPTIONS:

| | |
|---|---|
| FALSE (or 0) | Do not apply $\omega_{\text{GDD}}$ tuning. |
| TRUE (or 1) | Use $\omega_{\text{GDD}}$ tuning. |

RECOMMENDATION:
The *$rem* variable OMEGA must also be specified, in order to set the initial range-separation parameter.

**OMEGA_GDD_SCALING**

Sets the empirical constant $C$ in $\omega_{\text{GDD}}$ tuning procedure.

TYPE:

INTEGER

DEFAULT:

885

OPTIONS:

$n$ Corresponding to $C = n/1000$.

RECOMMENDATION:

The quantity $n$ = 885 was determined by Lao and Herbert in Ref. 211 using LRC-$\omega$PBE and def2-TZVPP augmented with diffuse functions on non-hydrogen atoms that are taken from Dunning's aug-cc-pVTZ basis set.

**Example 4.11** Sample input illustrating a calculation to determine the $\omega$ value for LRC-$\omega$PBE based on the $\omega_{\text{GDD}}$ tuning procedure.

```
$comment
    The initial omega value has to set.
$end

$rem
exchange          gen
basis             aug-cc-pvdz
lrc_dft           true
omega             300
omega_gdd         true
$end

$xc_functional
x   wPBE   1.0
c    PBE   1.0
$end

$molecule
0 1
O -0.042500 0.091700 0.110000
H  0.749000 0.556800 0.438700
H -0.825800 0.574700 0.432500
$end
```

## 4.4.7 DFT Methods for van der Waals Interactions

This section describes three different procedures for obtaining a better description of dispersion (*i.e.*, van der Waals) interactions DFT calculations: non-local correlation functionals (Section 4.4.7.1), empirical atom–atom dispersion potentials ("DFT-D", Section 4.4.7.2), and finally the Becke-Johnson exchange-dipole model (XDM, Section 4.4.7.3).

### 4.4.7.1 Non-Local Correlation (NLC) Functionals

Q-CHEM includes four non-local correlation functionals that describe long-range dispersion:

- vdW-DF-04, developed by Langreth, Lundqvist, and coworkers[32,33], implemented as described in Ref. 212.
- vdW-DF-10 (also known as vdW-DF2), which is a re-parameterization[213] of vdW-DF-04, implemented in the same way as its precursor.
- VV09, developed[30] and implemented[214] by Vydrov and Van Voorhis.
- VV10 by Vydrov and Van Voorhis[31].
- rVV10 by Sabatini and coworkers[34].

All of these functionals are implemented self-consistently and analytic gradients with respect to nuclear displacements are available[31,212,214]. The non-local correlation is governed by the *$rem* variable NL_CORRELATION, which can be set to one of the four values: vdW-DF-04, vdW-DF-10, VV09, or VV10. Note that the vdW-DF-04, vdW-DF-10, and VV09 functionals are used in combination with LSDA correlation, which must be specified explicitly. For instance, vdW-DF-10 is invoked by the following keyword combination:

```
CORRELATION         PW92
NL_CORRELATION      vdW-DF-10
```

VV10 is used in combination with PBE correlation, which must be added explicitly. In addition, the values of two parameters, $C$ and $b$ must be specified for VV10. These parameters are controlled by the *$rem* variables NL_VV_C and NL_VV_B, respectively. For instance, to invoke VV10 with $C = 0.0093$ and $b = 5.9$, the following input is used:

```
CORRELATION         PBE
NL_CORRELATION      VV10
NL_VV_C             93
NL_VV_B             590
```

The variable NL_VV_C may also be specified for VV09, where it has the same meaning. By default, $C = 0.0089$ is used in VV09 (i.e. NL_VV_C is set to 89). However, in VV10 neither $C$ nor $b$ are assigned a default value and must always be provided in the input.

Unlike local (LSDA) and semi-local (GGA and meta-GGA) functionals, for non-local functionals evaluation of the correlation energy requires a double integral over the spatial variables [*cf.* Eq. (4.37)]:

$$E_{\mathrm{c}}^{\mathrm{nl}} = \int f(\mathbf{r}, \mathbf{r}')\, d\mathbf{r}\; d\mathbf{r}'. \tag{4.48}$$

In practice, this double integration is performed numerically on a quadrature grid[31,212,214]. By default, the SG-1 quadrature (described in Section 4.4.5.2 below) is used to evaluate $E_{\mathrm{c}}^{\mathrm{nl}}$, but a different grid can be requested via the *$rem* variable NL_GRID. The non-local energy is rather insensitive to the fineness of the grid, so that SG-1 or even SG-0 grids can be used in most cases. However, a finer grid may be required to integrate other components of the functional, as controlled by the XC_GRID variable (see Section 4.4.5.2).

Several exchange-correlation functionals in Q-CHEM are pre-defined to use the VV10 non-local correlation functional. The two functionals from the original paper[31] can be used by specifying METHOD = VV10 or METHOD LC-VV10. In addition, the combinatorially-optimized functionals of Mardirossian and Head-Gordon ($\omega$B97X-V, B97M-V, and $\omega$B97M-V) use non-local correlation and can be invoked by setting METHOD to wB97X-V, B97M-V, or wB97M-V.

**Example 4.12** Geometry optimization of the methane dimer using VV10 with rPW86 exchange.

```
$molecule
   0 1
   C   0.000000  -0.000140   1.859161
   H  -0.888551   0.513060   1.494685
   H   0.888551   0.513060   1.494685
   H   0.000000  -1.026339   1.494868
   H   0.000000   0.000089   2.948284
   C   0.000000   0.000140  -1.859161
   H   0.000000  -0.000089  -2.948284
   H  -0.888551  -0.513060  -1.494685
   H   0.888551  -0.513060  -1.494685
   H   0.000000   1.026339  -1.494868
$end

$rem
   JOBTYPE             opt
   BASIS               aug-cc-pVTZ
   EXCHANGE            rPW86
   CORRELATION         PBE
   XC_GRID             2
   NL_CORRELATION      VV10
   NL_GRID             1
   NL_VV_C             93
   NL_VV_B             590
$end
```

In the above example, the SG-2 grid is used to evaluate the rPW86 exchange and PBE correlation, but a coarser SG-1 grid is used for the non-local part of VV10. Furthermore, the above example is identical to specifying METHOD = VV10.

**NL_CORRELATION**

Specifies a non-local correlation functional that includes non-empirical dispersion.

TYPE:

STRING

DEFAULT:

None No non-local correlation.

OPTIONS:

| | |
|---|---|
| None | No non-local correlation |
| vdW-DF-04 | the non-local part of vdW-DF-04 |
| vdW-DF-10 | the non-local part of vdW-DF-10 (also known as vdW-DF2) |
| VV09 | the non-local part of VV09 |
| VV10 | the non-local part of VV10 |

RECOMMENDATION:

Do not forget to add the LSDA correlation (PW92 is recommended) when using vdW-DF-04, vdW-DF-10, or VV09. VV10 should be used with PBE correlation. Choose exchange functionals carefully: HF, rPW86, revPBE, and some of the LRC exchange functionals are among the recommended choices.

**NL_VV_C**

Sets the parameter $C$ in VV09 and VV10. This parameter is fitted to asymptotic van der Waals $C_6$ coefficients.

TYPE:

INTEGER

DEFAULT:

| | |
|---|---|
| 89 | for VV09 |
| No default | for VV10 |

OPTIONS:

$n$ Corresponding to $C = n/10000$

RECOMMENDATION:

$C = 0.0093$ is recommended when a semi-local exchange functional is used. $C = 0.0089$ is recommended when a long-range corrected (LRC) hybrid functional is used. For further details see Ref. 31.

**NL_VV_B**

Sets the parameter $b$ in VV10. This parameter controls the short range behavior of the non-local correlation energy.

TYPE:

INTEGER

DEFAULT:

No default

OPTIONS:

$n$ Corresponding to $b = n/100$

RECOMMENDATION:

The optimal value depends strongly on the exchange functional used. $b = 5.9$ is recommended for rPW86. For further details see Ref. 31.

**USE_RVV10**

Used to turn on the rVV10 NLC functional

TYPE:

LOGICAL

DEFAULT:

FALSE

OPTIONS:

| | |
|---|---|
| FALSE | VV10 NLC is utilized (the default for NL_CORRELATION) |
| TRUE | rVV10 NLC is utilized |

RECOMMENDATION:

Set to TRUE if the rVV10 NLC is desired.

#### 4.4.7.2 Empirical Dispersion Corrections: DFT-D

There are currently three unique DFT-D methods in Q-CHEM, which are requested via the *$rem* variable DFT_D, and which are discussed below.

**DFT_D**

Controls the empirical dispersion correction to be added to a DFT calculation.

TYPE:

LOGICAL

DEFAULT:

None

OPTIONS:

| | |
|---|---|
| FALSE | (or 0) Do not apply the DFT-D2, DFT-CHG, or DFT-D3 scheme |
| EMPIRICAL_GRIMME | DFT-D2 dispersion correction from Grimme |
| EMPIRICAL_CHG | DFT-CHG dispersion correction from Chai and Head-Gordon |
| EMPIRICAL_GRIMME3 | DFT-D3(0) dispersion correction from Grimme (deprecated as of Q-CHEM 5.0) |
| D3_ZERO | DFT-D3(0) dispersion correction from Grimme *et al.* |
| D3_BJ | DFT-D3(BJ) dispersion correction from Grimme *et al.* |
| D3_CSO | DFT-D3(CSO) dispersion correction from Schröder *et al.* |
| D3_ZEROM | DFT-D3M(0) dispersion correction from Smith *et al.* |
| D3_BJM | DFT-D3M(BJ) dispersion correction from Smith *et al.* |
| D3_OP | DFT-D3(op) dispersion correction from Witte *et al.* |
| D3 | Recommended; chooses the "best" available D3 dispersion correction |

RECOMMENDATION:

NONE

Thanks to the efforts of the Sherrill group, Grimm's popular DFT-D2 empirical dispersion correction[24] is available in Q-CHEM, along with analytic gradients and frequencies. This correction can be added to any density functional that is available in Q-CHEM, although its use with the non-local correlation functionals discussed in Section 4.4.7.1 is obviously not recommended.

DFT-D2 adds an extra term,

$$E_{\text{disp}} = -s_6 \sum_A \sum_{B<A} \frac{C_6^{AB}}{R_{AB}^6} f_{\text{damp}}(R_{AB}) \tag{4.49}$$

$$C_6^{AB} = \left(C_6^A C_6^B\right)^{1/2} \tag{4.50}$$

$$f_{\text{damp}}(R_{AB}) = \left[1 + e^{-d(R_{AB}/R_{AB}^0 - 1)}\right]^{-1} \tag{4.51}$$

where $s_6$ is a global scaling parameter (near unity) and $f_{\text{damp}}$ is a damping function meant to help avoid double-counting correlation effects at short range (and to prevent the divergence of $R_{AB}^{-6}$), which depends on another parameter, $d$. The quantity $R_{AB}^0$ is the sum of the van der Waals radii of atoms A and B. Grimme has suggested using $s_6 = 0.75$ for PBE, $s_6 = 1.2$ for BLYP, $s_6 = 1.05$ for BP86, and $s_6 = 1.05$ for B3LYP, and these are the default values when those functionals are used. Otherwise, the default value is $s_6 = 1$.

DFT-D2 parameters, including the atomic van der Waals radii, can be altered using a *$empirical_dispersion* input section. For example:

```
$empirical_dispersion
S6 1.1
D 10.0
C6 Ar 4.60 Ne 0.60
VDW_RADII Ar 1.60 Ne 1.20
$end
```

Any values not specified explicitly will default to the values optimized by Grimme.

**Note:** (i) DFT-D2 is only defined for elements up to Xe.
(ii) B97-D is an exchange-correlation functional that automatically employs the DFT-D2 dispersion correction when used via METHOD B97-D.

An alternative to Grimme's DFT-D2 is the empirical dispersion correction of Chai and Head-Gordon[35], which employs a slightly different damping function

$$f_{\text{damp}}(R_{AB}) = \left[1 + a(R_{AB}/R^0_{AB})^{-12}\right]^{-1} \tag{4.52}$$

The Chai–Head-Gordon dispersion correction is activated by setting DFT_D = EMPIRICAL_CHG, and the damping parameter $a$ is controlled by the keyword DFT_D_A.

**DFT_D_A**
Controls the strength of dispersion corrections in the Chai–Head-Gordon DFT-D scheme, Eq. (4.52).
TYPE:
INTEGER
DEFAULT:
600
OPTIONS:
$n$ Corresponding to $a = n/100$.
RECOMMENDATION:
Use the default.

**Note:** (i) DFT-CHG is only defined for elements up to Xe.
(ii) The $\omega$B97X-D and $\omega$M05-D functionals automatically employ the DFT-CHG dispersion correction when used via METHOD = wB97X-D or wM05-D.

Finally, Grimme's more recent DFT-D3 method[36], and improvement on his DFT-D2 approach,[24] is available along with analytic first and second derivatives, and can be combined with any of the density functionals available in Q-CHEM. The total DFT-D3 energy is given by $E_{\text{DFT-D3}} = E_{\text{KS-DFT}} + E_{\text{disp}}$, where $E_{\text{KS-DFT}}$ is the total energy from KS-DFT and the dispersion correction $E_{\text{disp}} = E^{(2)} + E^{(3)}$ is a sum of two- and three-body energies. As of Q-CHEM 5.0, several versions of DFT-D3 are implemented.

All versions of DFT-D3 are based on the addition of an empirical dispersion term to the energy. This term is given by

$$E_{\text{D3}} = -\sum_{i<j}\sum_{n=6,8} s_n \frac{C_{n,ij}}{r_{ij}^n} f_{\text{damp},n}(r_{ij}), \tag{4.53}$$

where the sum runs over all unique pairs of atoms $i$ and $j$; the $C_{n,ij}$ are $n$th-order isotropic dispersion coefficients for atom pair $ij$; $r_{ij}$ is the distance between atoms $i$ and $j$; $s_n$ are global, functional-dependent scaling parameters; and $f_{\text{damp},n}$ are damping functions. The original zero-damping formulation, DFT-D3(0), of Grimme *et al.*[36] utilizes a damping function of the form

$$f^{\text{D3(0)}}_{\text{damp},n}(r_{ij}) = \left[1 + 6\left(\frac{r_{ij}}{s_{r,n} r_{0,ij}}\right)^{-\beta_n}\right]^{-1}, \tag{4.54}$$

where $r_{0,ij}$ are pre-tabulated van der Waals radii, $s_{r,6}$ is a functional-dependent parameter, $s_{r,8} = 1$, $\beta_6 = 12$, and $\beta_8 = 14$. In this approach, $s_6$ is generally fixed to unity, and $s_8$ is optimized for each density functional.

The more recent BJ-damping model,[37] DFT-D3(BJ), adds in some finite amount of correlation even at short distances. Its damping function is given by

$$f^{\text{D3(BJ)}}_{\text{damp},n}(r_{ij}) = \frac{r_{ij}^n}{r_{ij}^n + (\alpha_1 r_{0,ij} + \alpha_2)^n}, \tag{4.55}$$

where $\alpha_1$ and $\alpha_2$ are adjustable nonlinear parameters fit to each density functional. As in DFT-D3(0), $s_6$ is generally fixed to unity and $s_8$ is optimized for each functional. The DFT-D3(BJ) approach generally outperforms the original DFT-D3(0) formulation.[37]

The C-six-only (CSO) approach of Schröder *et al.*[38] utilizes a damping function with one nonlinear parameter, $\alpha_1$:

$$f^{\text{D3(CSO)}}_{\text{damp},6}(r_{ij}) = \frac{r_{ij}^6}{r_{ij}^6 + (2.5)^6}\left[1 + \frac{\alpha_1}{s_6\left[1 + \exp\left(r_{ij} - 2.5 r_{0,ij}\right)\right]}\right]. \tag{4.56}$$

The DFT-D3(BJ) approach was re-parameterized by Smith *et al.*[39] to yield the DFT-D3M(BJ) approach. This approach was parameterized heavily on non-equilibrium systems. Those same authors altered and modified the original DFT-D3(0) to obtain DFT-D3M(0), which has one additional parameter on top of the original DFT-D3(0) set, $\alpha_1$:

$$f^{\text{D3(0)}}_{\text{damp},n}(r_{ij}) = \left[1 + 6\left(\frac{r_{ij}}{s_{r,n} r_{0,ij}} + \alpha_1 r_{0,ij}\right)^{-\beta_n}\right]^{-1}. \tag{4.57}$$

The optimized power approach of Witte *et al.*[215] treats the exponent, $\beta_6$, as an optimizable parameter (Note: $\beta_8 = \beta_6 + 2$), and is given by

$$f^{\text{D3(op)}}_{\text{damp},n}(r_{ij}) = \frac{r_{ij}^{\beta_n}}{r_{ij}^{\beta_n} + (\alpha_1 r_{0,ij} + \alpha_2)^{\beta_n}}. \tag{4.58}$$

DFT-D3(0) is requested by setting DFT_D = D3_ZERO. The model depends on four scaling factors [$s_6$, $s_{r,6}$, $s_8$, and $s_{r,8}$, as defined in eq. (4.54), which can be adjusted using the *$rem* variables described below.

DFT-D3(BJ) is requested by setting DFT_D = D3_BJ. The model depends on four scaling factors [$s_6$, $s_8$, $\alpha_1$, and $\alpha_2$, as defined in eq. (4.55), which can be adjusted using the *$rem* variables described below.

DFT-D3(CSO) is requested by setting DFT_D = D3_CSO. The model depends on two scaling factors [$s_6$ and $\alpha_1$, as defined in eq. (4.56), which can be adjusted using the *$rem* variables described below.

DFT-D3M(0) is requested by setting DFT_D = D3_ZEROM. The model depends on five scaling factors [$s_6$, $s_8$, $s_{r,6}$, $s_{r,8}$, and $\alpha_1$, as defined in eq. (4.57), which can be adjusted using the *$rem* variables described below.

DFT-D3M(BJ) is requested by setting DFT_D = D3_BJM. The model depends on four scaling factors [$s_6$, $s_8$, $\alpha_1$, and $\alpha_2$, as defined in eq. (4.55), which can be adjusted using the *$rem* variables described below.

DFT-D3(op) is requested by setting DFT_D = D3_OP. The model depends on four scaling factors [$s_6$, $s_8$, $\alpha_1$, $\alpha_2$, and $\beta_6$ as defined in eq. (4.55), which can be adjusted using the *$rem* variables described below.

Or, one may simply set DFT_D = D3, and a D3 tail will be chosen automatically, if one is available for the selected functional.

**Note:** (i) DFT-D3(0) is defined for elements up to Pu ($Z = 94$).

(ii) The B97-D3(0), $\omega$B97X-D3, $\omega$M06-D3 functionals automatically employ the DFT-D3(0) dispersion correction when invoked by setting METHOD equal to B97-D3, wB97X-D3, or wM06-D3.

(iii) The old way of invoking DFT-D3, namely through the use of EMPIRICAL_GRIMME3, is still supported, though its use is discouraged, since D3_ZERO accomplishes the same thing, but with additional precision for the relevant parameters.

(iv) When DFT_D = D3, parameters may not be overwritten, with the exception of DFT_D3_3BODY; this is intended as a user-friendly option. This is also the case when EMPIRICAL_GRIMME3 is employed for a functional parameterized in Q-CHEM. When any of D3_ZERO, D3_BJ, etc. are chosen, Q-CHEM will automatically populate the parameters with values if available for the given functional, but will still allow these defaults to be overwritten.

**DFT_D3_S6**

The linear parameter $s_6$ in eq. (4.53). Utilized in all forms of DFT-D3.

TYPE:

INTEGER

DEFAULT:

100000

OPTIONS:

$n$ Corresponding to $s_6 = n/100000$.

RECOMMENDATION:

NONE

**DFT_D3_RS6**

The nonlinear parameter $s_{r,6}$ in eqs. (4.54) and (4.57). Utilized in DFT-D3(0) and DFT-D3M(0).

TYPE:

INTEGER

DEFAULT:

100000

OPTIONS:

$n$ Corresponding to $s_{r,6} = n/100000$.

RECOMMENDATION:

NONE

**DFT_D3_S8**

The linear parameter $s_8$ in eq. (4.53). Utilized in DFT-D3(0), DFT-D3(BJ), DFT-D3M(0), DFT-D3M(BJ), and DFT-D3(op).

TYPE:

INTEGER

DEFAULT:

100000

OPTIONS:

$n$ Corresponding to $s_8 = n/100000$.

RECOMMENDATION:

NONE

**DFT_D3_RS8**

The nonlinear parameter $s_{r,8}$ in eqs. (4.54) and (4.57). Utilized in DFT-D3(0) and DFT-D3M(0).

TYPE:

INTEGER

DEFAULT:

100000

OPTIONS:

$n$ Corresponding to $s_{r,8} = n/100000$.

RECOMMENDATION:

NONE

**DFT_D3_A1**

The nonlinear parameter $\alpha_1$ in eqs. (4.55), (4.56), (4.57), and (4.58). Utilized in DFT-D3(BJ), DFT-D3(CSO), DFT-D3M(0), DFT-D3M(BJ), and DFT-D3(op).

TYPE:

INTEGER

DEFAULT:

100000

OPTIONS:

$n$ Corresponding to $\alpha_1 = n/100000$.

RECOMMENDATION:

NONE

**DFT_D3_A2**

The nonlinear parameter $\alpha_2$ in eqs. (4.55) and (4.58). Utilized in DFT-D3(BJ), DFT-D3M(BJ), and DFT-D3(op).

TYPE:

INTEGER

DEFAULT:

100000

OPTIONS:

$n$ Corresponding to $\alpha_2 = n/100000$.

RECOMMENDATION:

NONE

**DFT_D3_POWER**

The nonlinear parameter $\beta_6$ in eq. (4.58). Utilized in DFT-D3(op). Must be greater than or equal to 6 to avoid divergence.

TYPE:

INTEGER

DEFAULT:

600000

OPTIONS:

$n$ Corresponding to $\beta_6 = n/100000$.

RECOMMENDATION:

NONE

The three-body interaction term[36], $E^{(3)}$, must be explicitly turned on, if desired.

**DFT_D3_3BODY**

Controls whether the three-body interaction in Grimme's DFT-D3 method should be applied (see Eq. (14) in Ref. 36).

TYPE:

LOGICAL

DEFAULT:

FALSE

OPTIONS:

FALSE (or 0) Do not apply the three-body interaction term

TRUE Apply the three-body interaction term

RECOMMENDATION:

NONE

**Example 4.13** Applications of B3LYP-D3(0) with custom parameters to a methane dimer.

```
$comment
   Geometry optimization, followed by single-point calculations using a larger
   basis set.
$end

$molecule
   0 1
   C       0.000000    -0.000323     1.755803
   H      -0.887097     0.510784     1.390695
   H       0.887097     0.510784     1.390695
   H       0.000000    -1.024959     1.393014
   H       0.000000     0.001084     2.842908
   C       0.000000     0.000323    -1.755803
   H       0.000000    -0.001084    -2.842908
   H      -0.887097    -0.510784    -1.390695
   H       0.887097    -0.510784    -1.390695
   H       0.000000     1.024959    -1.393014
$end

$rem
   JOBTYPE         opt
   EXCHANGE        B3LYP
   BASIS           6-31G*
   DFT_D           D3_ZERO
   DFT_D3_S6       100000
   DFT_D3_RS6      126100
   DFT_D3_S8       170300
   DFT_D3_3BODY    FALSE
$end

@@@

$molecule
   read
$end

$rem
```

```
   JOBTYPE         sp
   EXCHANGE        B3LYP
   BASIS           6-311++G**
   DFT_D           D3_ZERO
   DFT_D3_S6       100000
   DFT_D3_RS6      126100
   DFT_D3_S8       170300
   DFT_D3_3BODY    FALSE
$end
```

#### 4.4.7.3 Exchange-Dipole Model (XDM)

Becke and Johnson have proposed a conceptually simple yet accurate dispersion model called the exchange-dipole model (XDM)[164,216]. In this model the dispersion attraction emerges from the interaction between the instantaneous dipole moment of the exchange hole in one molecule and the induced dipole moment in another. It is a conceptually simple but powerful approach that has been shown to yield very accurate dispersion coefficients without fitting parameters. This allows the calculation of both intermolecular and intramolecular dispersion interactions within a single DFT framework. The implementation and validation of this method in the Q-CHEM code is described in Ref. 217.

Fundamental to the XDM model is the calculation of the norm of the dipole moment of the exchange hole at a given point:

$$d_\sigma(\mathbf{r}) = -\int h_\sigma(\mathbf{r},\mathbf{r}')\;\mathbf{r}'\;d\mathbf{r}' - \mathbf{r} \tag{4.59}$$

where $\sigma$ labels the spin and $h_\sigma(\mathbf{r},\mathbf{r}')$ is the exchange-hole function. The XDM version that is implemented in Q-CHEM employs the Becke-Roussel (BR) model exchange-hole function. In previous work on the BR model, $h_\sigma$ was not available in analytical form and one had to determine its value numerically at each grid point. Q-CHEM has developed for the first time an analytical expression for this function based on non-linear interpolation and spline techniques, which greatly improves efficiency as well as the numerical stability[217].

There are two different damping functions used in the XDM model of Becke and Johnson. One of them uses only the intermolecular $C_6$ dispersion coefficient, and its implementation in Q-CHEM is denoted as "XDM6". In this version the dispersion energy is computed as

$$E_{\mathrm{vdW}} = \sum_{i>j} E_{\mathrm{vdW},ij} = -\sum_{i>j} \frac{C_{6,ij}}{R_{ij}^6 + kC_{6,ij}(E_i^C + E_j^C)^{-1}} \tag{4.60}$$

where $k$ is a universal parameter, $R_{ij}$ is the distance between atoms $i$ and $j$, and $E_{ij}^C$ is the sum of the absolute values of the correlation energies of the free atoms $i$ and $j$. The dispersion coefficients $C_{6,ij}$ is computed as

$$C_{6,ij} = \frac{\langle d_{\mathrm{X}}^2\rangle_i \langle d_{\mathrm{X}}^2\rangle_j\;\alpha_i\,\alpha_j}{\langle d_{\mathrm{X}}^2\rangle_i \alpha_j + \langle d_{\mathrm{X}}^2\rangle_j \alpha_i} \tag{4.61}$$

where $\langle d_{\mathrm{X}}^2\rangle_i$ is the exchange-hole dipole moment of the atom, and $\alpha_i$ is the effective polarizability of the atom $i$ in the molecule.

The XDM6 scheme can be further generalized to include higher-order dispersion coefficients, which leads to the "XDM10" model in Q-CHEM, whose dispersion energy is

$$E_{\mathrm{vdW}} = -\sum_{i>j}\left(\frac{C_{6,ij}}{R_{\mathrm{vdW},ij}^6 + R_{ij}^6} + \frac{C_{8,ij}}{R_{\mathrm{vdW},ij}^8 + R_{ij}^8} + \frac{C_{10,ij}}{R_{\mathrm{vdW},ij}^{10} + R_{ij}^{10}}\right) \tag{4.62}$$

where $C_{6,ij}$, $C_{8,ij}$ and $C_{10,ij}$ are dispersion coefficients computed using higher-order multipole moments of the exchange hole, including dipole, quadrupole and octupole)[218]. The quantity $R_{\text{vdW},ij}$ is the sum of the effective vdW radii of atoms $i$ and $j$, which is a linear function

$$R_{\text{vdW},ij} = a_1 R_{\text{C},ij} + a_2 \tag{4.63}$$

of the so called critical distance $R_{\text{C},ij}$ between atoms $i$ and $j$, computed according to

$$R_{\text{C},ij} = \frac{1}{3}\left[\left(\frac{C_{8,ij}}{C_{6,ij}}\right)^{1/2} + \left(\frac{C_{10,ij}}{C_{6,ij}}\right)^{1/4} + \left(\frac{C_{10,ij}}{C_{8,ij}}\right)^{1/2}\right] . \tag{4.64}$$

In the XDM10 scheme there are two universal parameters, $a_1$ and $a_2$. Their default values of 0.83 and 1.35, respectively, are due to Johnson and Becke[216], determined by least-squares fitting to the binding energies of a set of intermolecular complexes. These values are not the only possible optimal set to use with XDM. Becke's group later suggested several other XC functional combinations with XDM that employ different values of $a_1$ and $a_2$. The user is advised to consult the recent literature for details[219,220].

The computed vdW energy $E_{\text{vdW}}$ is added as a post-SCF correction. Analytic gradients and Hessians are available for both XDM6 and XDM10. Additional job control and customization options are listed below.

**DFTVDW_JOBNUMBER**

Basic vdW job control

TYPE:

INTEGER

DEFAULT:

0

OPTIONS:

0 Do not apply the XDM scheme.

1 Add vdW as energy/gradient correction to SCF.

2 Add vDW as a DFT functional and do full SCF (this option only works with XDM6).

RECOMMENDATION:

None

**DFTVDW_METHOD**

Choose the damping function used in XDM

TYPE:

INTEGER

DEFAULT:

1

OPTIONS:

1 Use Becke's damping function including $C_6$ term only.

2 Use Becke's damping function with higher-order ($C_8$ and $C_{10}$) terms.

RECOMMENDATION:

None

**DFTVDW_MOL1NATOMS**

The number of atoms in the first monomer in dimer calculation

TYPE:

INTEGER

DEFAULT:

0

OPTIONS:

0–$N_{\mathrm{atoms}}$

RECOMMENDATION:

None

**DFTVDW_KAI**

Damping factor $k$ for $C_6$-only damping function

TYPE:

INTEGER

DEFAULT:

800

OPTIONS:

10–1000

RECOMMENDATION:

None

**DFTVDW_ALPHA1**

Parameter in XDM calculation with higher-order terms

TYPE:

INTEGER

DEFAULT:

83

OPTIONS:

10-1000

RECOMMENDATION:

None

**DFTVDW_ALPHA2**

Parameter in XDM calculation with higher-order terms.

TYPE:

INTEGER

DEFAULT:

155

OPTIONS:

10-1000

RECOMMENDATION:

None

**DFTVDW_USE_ELE_DRV**

Specify whether to add the gradient correction to the XDM energy. only valid with Becke's $C_6$ damping function using the interpolated BR89 model.

TYPE:

LOGICAL

DEFAULT:

1

OPTIONS:

1 Use density correction when applicable.

0 Do not use this correction (for debugging purposes).

RECOMMENDATION:

None

**DFTVDW_PRINT**

Printing control for VDW code

TYPE:

INTEGER

DEFAULT:

1

OPTIONS:

0 No printing.

1 Minimum printing (default)

2 Debug printing

RECOMMENDATION:

None

**Example 4.14** Sample input illustrating a frequency calculation of a vdW complex consisted of He atom and $N_2$ molecule.

```
$molecule
   0 1
   He 0.000000  0.00000   3.800000
   N  0.000000  0.000000  0.546986
   N  0.000000  0.000000 -0.546986
$end

$rem
   JOBTYPE            FREQ
   IDERIV             2
   EXCHANGE           B3LYP
   INCDFT             0
   SCF_CONVERGENCE    8
   BASIS              6-31G*
   !vdw parameters settings
   DFTVDW_JOBNUMBER   1
   DFTVDW_METHOD      1
   DFTVDW_PRINT       0
   DFTVDW_KAI         800
   DFTVDW_USE_ELE_DRV 0
$end
```

XDM can be used in conjunction with different GGA, meta-GGA pure or hybrid functionals, even though the original implementation of Becke and Johnson was in combination with HF exchange, or with a specific meta-GGA exchange and correlation (the BR89 exchange and BR94 correlation functionals). For example, encouraging results have been obtained using XDM with B3LYP[217]. Becke has found more recently that this model can be efficiently combined with the P86 exchange functional, with the hyper-GGA functional B05. Using XDM together with PBE exchange plus LYP correlation, or PBE exchange plus BR94 correlation, has been also found fruitful.

### 4.4.8 DFT Methods for Empirical BSSE Correction

This section describes one low-cost procedure – DFT-C – for estimating basis set suporposition error (BSSE) in DFT calculations. Unlike the traditional counterpoise correction, DFT-C can be easily applied to estimate both intra- and intermolecular BSSE.

#### 4.4.8.1 DFT-C

The DFT-C empirical correction for BSSE[221] has been implemented in Q-CHEM. This correction is strictly geometry-based, and as such is essentially free on the scale of an electronic structure calculation. It is given by

$$E_{\text{DFT-C}} = \sigma \sum_{A} c_A \sum_{B \neq A} g^{\text{DFT-C}}_{AB^*}(r_{AB}) h_{AB^*}\left(\{A, B, ...\}\right), \tag{4.65}$$

where $g^{\text{DFT-C}}_{AB^*}(r_{AB})$ is a damped atomic pairwise BSSE, given by

$$g^{\text{DFT-C}}_{AB^*}(r_{AB}) = d(r_{AB}) f^{\text{DFT-C}}_{AB^*}(r_{AB}) + \left(1 - d(r_{AB})\right) f^{\text{DFT-C}}_{AB^*}(r_{\text{cov},AB}), \tag{4.66}$$

with undamped pairwise BSSE

$$f^{\text{DFT-C}}_{AB^*}(r_{AB}) = c_{AB} \exp\left(-\alpha_{AB} r^2_{AB} + \beta_{AB} r_{AB}\right) \tag{4.67}$$

and damping function

$$d(r_{AB}) = \frac{1}{1 + k_{1,AB}\left(r_{AB}/r_{0,AB}\right)^{-k_{2,AB}}}; \tag{4.68}$$

and $h_{AB^*}(\{A, B, ...\})$ is a many-body correction to the two-body BSSE, given by

$$h_{AB^*}(\{A, B, ...\}) = \left[1 + \sum_{C \neq A,B} \frac{N^{\text{virt}}_C}{N^{\text{virt}}_B} \operatorname{terfc}\left(r_{AC}, r_{AB}\right) \operatorname{terfc}\left(r_{BC}, r_{AB}\right)\right]^{-1}, \tag{4.69}$$

where

$$\operatorname{terfc}(x, y) = 1 - \frac{1}{2}\left[\operatorname{erf}(x + y) + \operatorname{erf}(x - y)\right]. \tag{4.70}$$

The coefficients $c_A$ and $c_{AB}$ and decay rates $\alpha_{AB}$ and $\beta_{AB}$ are basis-set-dependent, and the overall scaling parameter $\sigma$ is loosely method-dependent. All of these parameters are set internally based on the method and basis *$rem* specifications. Currently, the following basis sets are supported for use with DFT-C:

- def2-SVPD[221]

The DFT-C correction is governed by the *$rem* variable DFT_C; to invoke the DFT-C method, simply add this to your input:

```
DFT_C    TRUE
```

The DFT-C method can be applied to any local, GGA, or meta-GGA density functional, as in the following example.

**Example 4.15** Geometry optimization of the methane dimer using B97M-V-C/def2-SVPD, i.e. the B97M-V functional with the DFT-C BSSE correction in the def2-SVPD basis set.

```
$molecule
   0 1
   C   0.000000  -0.000140   1.859161
   H  -0.888551   0.513060   1.494685
   H   0.888551   0.513060   1.494685
   H   0.000000  -1.026339   1.494868
   H   0.000000   0.000089   2.948284
   C   0.000000   0.000140  -1.859161
   H   0.000000  -0.000089  -2.948284
   H  -0.888551  -0.513060  -1.494685
   H   0.888551  -0.513060  -1.494685
   H   0.000000   1.026339  -1.494868
$end

$rem
   JOBTYPE            opt
   BASIS              def2-SVPD
   METHOD             b97m-v
   DFT_C              true
$end
```

**DFT_C**
Controls whether the DFT-C empirical BSSE correction should be added.
TYPE:
LOGICAL
DEFAULT:
FALSE
OPTIONS:
FALSE (or 0) Do not apply the DFT-C correction
TRUE (or 1) Apply the DFT-C correction
RECOMMENDATION:
NONE

### 4.4.9 Double-Hybrid Density Functional Theory

The recent advance in double-hybrid density functional theory (DH-DFT)[152,154,222–224], has demonstrated its great potential for approaching the chemical accuracy with a computational cost comparable to the second-order Møller-Plesset perturbation theory (MP2). In a DH-DFT, a Kohn-Sham (KS) DFT calculation is performed first, followed by a treatment of non-local orbital correlation energy at the level of second-order Møller-Plesset perturbation theory (MP2)[225]. This MP2 correlation correction includes a a same-spin (ss) component, $E_c^{\text{ss}}$, as well as an opposite-spin (os) component, $E_c^{\text{os}}$, which are added to the total energy obtained from the KS-DFT calculation. Two scaling parameters, $c_{\text{ss}}$ and $c_{\text{os}}$, are introduced in order to avoid double-counting correlation:

$$E_{\text{DH-DFT}} = E_{\text{KS-DFT}} + c_{\text{ss}} E_c^{\text{ss}} + c_{\text{os}} E_c^{\text{os}} \tag{4.71}$$

A starting point for understanding where a functional form like Eq. (4.71) might come from is the adiabatic connection formula that provides a rigorous way to define double-hybrid functionals. One considers an adiabatic path between the fictitious non-interacting Kohn-Sham reference system ($\lambda = 0$) and the real physical system ($\lambda = 1$), while holding the electron density fixed at its value for the real system, for all $\lambda$. Then

$$E_{\text{XC}}[\rho] = \int_0^1 U_{\text{XC},\lambda}[\rho]\, d\lambda\,, \tag{4.72}$$

where $U_{\text{XC},\lambda}$ is the exchange-correlation energy at a coupling strength $\lambda$, meaning that the exchange-correlation energy if the electron–electron terms in the Hamiltonian had the form $\lambda/r_{ij}$ rather than $1/r_{ij}$. Using a linear model of this quantity,

$$U_{\text{XC},\lambda} = a + b\lambda\;, \tag{4.73}$$

one obtains the popular hybrid functional that includes the HF exchange (or occupied orbitals) such as B3LYP[27,28]. If one further uses the Gorling-Levy's perturbation theory (GL2) to define the initial slope at $\lambda$= 0, one obtains the doubly hybrid functional form in Eq. (4.71) that includes MP2 type perturbative terms (PT2) involving virtual Kohn-Sham orbitals[226]:

$$U_{\text{XC},\lambda} = \left.\frac{\partial U_{\text{XC},\lambda}}{\lambda}\right|_{\lambda=0} = 2E_{\text{C}}^{\text{GL2}}\,. \tag{4.74}$$

The adiabatic connection formula has been used to develop double hybrid functionals such as XYG3[152]. Note that XYG3, as implemented in Q-CHEM, uses B3LYP orbitals to generate the density and evaluate the PT2 terms. This is different from B2PLYP, an earlier doubly hybrid functional from Grimme[154]. The latter uses truncated Kohn-Sham orbitals while XYG3 uses converged KS orbitals to evaluate the PT2 terms. The performance of XYG3 is not only comparable to that of the G2 or G3 theory for thermochemistry, but barrier heights and non-covalent interactions, including stacking interactions, are also very well described by XYG3[152]. The recommended basis set for XYG3 is 6-311+G(3df,2p).

Due to the inclusion of PT2 terms, the cost of double-hybrid calculations is formally $\mathcal{O}(N^5)$, as in conventional MP2, thereby not applicable to large systems and partly losing DFT's cost advantages. However, the highly successful SOS-MP2 and local SOS-MP2 algorithms in Q-CHEM can be leveraged to develop double-hybrid functionals based on these $\mathcal{O}(N^4)$ methods. A version of XYG3 that uses SOS-MP2 is the XYGJ-OS functional[153]. This functional has 4 parameters that are optimized using thermochemical data. It is not only faster than XYG3, but comparable to XYG3 (or perhaps slightly better) in accuracy. If the local SOS-MP2 algorithm is applied, the scaling of XYGJ-OS is further reduced to $\mathcal{O}(N^3)$. Recently, XYGJ-OS became the first double-hybrid functional whose analytic energy gradient has been derived and implemented[227].

Other more empirical double-hybrid functionals have been implemented in Q-CHEM. Among the $\omega$B97 series of functionals, $\omega$B97X-2[151] is a long-range corrected double hybrid that can greatly reduce the self-interaction errors (due to its high fraction of HF exchange), and has been shown significantly superior to other functionals for systems with both bonded and non-bonded interactions. Due to the sensitivity of PT2 correlation energy with respect to the choices of basis sets, $\omega$B97X-2 was parameterized with two different basis sets: the $\omega$B97X-2(LP) was parameterized for use with 6-311++G(3df,3pd), while $\omega$B97X-2(TQZ) was parameterized with the T/Q (triple-$\zeta$/quadruple-$\zeta$) extrapolation to the basis set limit. A careful reading of Ref. 151 is highly advised before using either of these two functionals.

Job control variables for double-hybrid DFT are described below. Note that the PT2 correlation energy can also be computed with the efficient resolution-of-identity (RI) methods; see Section 5.6.

**DH**

Controls the application of DH-DFT scheme.

TYPE:

LOGICAL

DEFAULT:

FALSE

OPTIONS:

| | |
|---|---|
| FALSE (or 0) | Do not apply the DH-DFT scheme |
| TRUE (or 1) | Apply DH-DFT scheme |

RECOMMENDATION:

NONE

The following to *$rem* variables pertain to the $\omega$B97X-2(LP) and $\omega$B97X-2(TQZ) functionals.

**SSS_FACTOR**

Controls the strength of the same-spin component of PT2 correlation energy.

TYPE:

INTEGER

DEFAULT:

0

OPTIONS:

$n$ Corresponding to $c_{\text{ss}} = n/10^6$ in Eq. (4.71).

RECOMMENDATION:

NONE

**SOS_FACTOR**

Controls the strength of the opposite-spin component of PT2 correlation energy.

TYPE:

INTEGER

DEFAULT:

0

OPTIONS:

$n$ Corresponding to $c_{\text{os}} = n/10^6$ in Eq. (4.71).

RECOMMENDATION:

NONE

**Example 4.16** Applications of B2PLYP functional to LiH.

```
$comment
   Single-point calculation on LiH without RI, followed by a single-point
   calculation with RI.
$end

$molecule
   0 1
   H
   Li H 1.6
$end

$rem
   JOBTYPE     sp
   EXCHANGE    B2PLYP
   BASIS       cc-pvtz
$end

@@@

$molecule
   read
$end

$rem
   JOBTYPE     sp
   EXCHANGE    B2PLYP
   BASIS       cc-pvtz
   AUX_BASIS   rimp2-cc-pvtz
$end
```

**Example 4.17** Application of $\omega$B97X-2(TQZ) functional (with and without RI) to LiH molecules.

```
$comment
   Single-point calculation on LiH (with RI).
$end

$molecule
   0 1
   H
   Li H 1.6
$end

$rem
   JOBTYPE     sp
   EXCHANGE    omegaB97X-2(TQZ)
   BASIS       cc-pvqz
   AUX_BASIS   rimp2-cc-pvqz
$end

@@@

$comment
   Single-point calculation on LiH (without RI).
```

```
$end

$molecule
   read
$end

$rem
   JOBTYPE      sp
   EXCHANGE      omegaB97X-2(TQZ)
   BASIS      cc-pvqz
$end
```

In the following example of XYG3, Q-Chem automatically performs a B3LYP calculation first, then uses the resulting orbitals to evaluate the PT2 correlation terms. Once can also use XYG3 combined with the RI approximation; use EXCHANGE = XYG3RI to do so, along with an appropriate choice of auxiliary basis set.

**Example 4.18** XYG3 calculation of N$_2$

```
$molecule
   0 1
   N      0.000000   0.000000   0.547775
   N      0.000000   0.000000  -0.547775
$end

$rem
   EXCHANGE  xyg3
   BASIS     6-311+G(3df,2p)
$end
```

The next example illustrates XYGJ-OS. This functional uses the RI approximation by default, so it is necessary to specify an auxiliary basis set.

**Example 4.19** XYGJ-OS calculation of N$_2$

```
$molecule
  0 1
  N      0.000000   0.000000   0.547775
  N      0.000000   0.000000  -0.547775
$end

$rem
   EXCHANGE    xygjos
   BASIS       6-311+G(3df,2p)
   AUX_BASIS   rimp2-cc-pVtZ
   PURECART    1111
   TIME_MP2    true
$end
```

The final example uses the local version of XYGJ-OS, which is the same as the original XYGJ-OS but with the use of the attenuated Coulomb metric to solve the RI coefficients. Here, the keyword omega determines the locality of the metric.

**Example 4.20** Local XYGJ-OS calculation of N$_2$

```
$molecule
   0 1
   N    0.000    0.000   0.54777500
   N    0.000    0.000  -0.54777500
$end

$rem
   EXCHANGE   lxygjos
   OMEGA      200
   BASIS      6-311+G(3df,2p)
   AUX_BASIS  rimp2-cc-pVtZ
   PURECART   1111
$end
```

### 4.4.10 Asymptotically Corrected Exchange-Correlation Potentials

No GGA exchange functional can simultaneously produce the correct contribution to the exchange energy density and exchange potential in the asymptotic region of molecular systems[228], and existing GGA exchange-correlation (XC) potentials decay much faster than the correct $-1/r$ XC potential in the asymptotic region[229]. High-lying occupied orbitals and low-lying virtual orbitals are therefore too loosely bound, and $-\varepsilon_{\rm HOMO}$ becomes far smaller than the ionization energy, despite the exact condition that these should be the same for the exact functional[201,202]. Moreover, response properties may be poorly predicted from TDDFT calculations with GGA functionals[201]. Long-range corrected hybrid DFT (LRC-DFT), described in Section 4.4.6, has greatly remedied this situation, but is more expensive that KS-DFT with GGA functionals due to the use of Hatree-Fock exchange. The asymptotic corrections described in this section are designed to remedy the same problems but within the GGA framework.

#### 4.4.10.1 LB94 Scheme

An asymptotically corrected (AC) exchange potential proposed by van Leeuwen and Baerends is[228]

$$v_x^{\rm LB} = -\beta\left(\frac{x^2}{1+3\beta{\rm sinh}^{-1}(x)}\right) \tag{4.75}$$

where $x = \frac{|\nabla\rho|}{\rho^{4/3}}$ is the reduced density gradient. For an exponentially-decaying density, this potential reduces to $-1/r$ in the asymptotic region of molecular systems. The LB94 xc potential is formed by a linear combination of LDA XC potential and the LB exchange potential[228]:

$$v_{xc}^{\rm LB94} = v_{xc}^{\rm LDA} + v_x^{\rm LB}\ . \tag{4.76}$$

The parameter $\beta$ in Eq. (4.75) was determined by fitting to the exact XC potential for Be atom. As mentioned in Refs. 230 and 231, for TDDFT calculations, it is sufficient to include the AC XC potential for ground-state calculations followed by TDDFT calculations with an adiabatic LDA XC kernel. The implementation of the LB94 XC potential in Q-CHEM takes this approach, using the LB94 XC potential for the ground state calculations, followed by a TDDFT calculation with an adiabatic LDA XC kernel. This TDLDA/LB94 approach has been widely applied to study excited-state properties of large molecules.

Since the LB exchange potential in Eq. (4.75) does not come from the functional derivative of an exchange energy functional, the Levy-Perdew virial relation[232] is used instead to obtain the exchange energy:

$$E_x^{\rm LB} = -\int v_x^{\rm LB}([\rho],\mathbf{r})[3\rho(\mathbf{r})+\mathbf{r}\nabla\rho(\mathbf{r})]d\mathbf{r} \tag{4.77}$$

An LB94 calculation is requested by setting EXCHANGE = LB94 in the *$rem* section. Additional job control and examples appear below.

**LB94_BETA**
Sets the $\beta$ parameter for the LB94 XC potential
TYPE:
INTEGER
DEFAULT:
500
OPTIONS:
$n$ Corresponding to $\beta = n/10000$.
RECOMMENDATION:
Use the default.

**Example 4.21** Applications of LB94 XC potential to $N_2$ molecule.

```
$comment
   TDLDA/LB94 calculation is performed for excitation energies.
$end

$molecule
   0 1
   N    0.0000    0.0000    0.0000
   N    1.0977    0.0000    0.0000
$end

$rem
   JOBTYPE     = sp
   EXCHANGE    = lb94
   BASIS       = 6-311(2+,2+)G**
   CIS_N_ROOTS = 30
   RPA         = true
$end
```

#### 4.4.10.2 Localized Fermi-Amaldi (LFA) Schemes

Another alternative, proposed by Pan, Fang and Chai[233], is to use a *localized* version of Fermi-Amaldi exchange-correlation functional. The resulting exchange density functional, whose functional derivative has the correct $-1/r$ asymptotic behavior, can be directly added to any semi-local density functional. Three variants of this method were proposed in Ref. 233. The simplest of these, the strictly-localized Fermi-Amaldi (LFAs) scheme, is implemented in Q-CHEM, for molecules consisting of atoms with $Z \leq 55$.

**Example 4.22** LFAs-PBE single-point TD-DFT calculation with water molecule

```
$comment
   Use LFAs-PBE potential for ground-state calculations, followed by
   TDDFT calculations with an adiabatic PBE XC kernel.
$end

$molecule
   0  1
   O
   H1  O  oh
   H2  O  oh  H1  hoh

   oh  =   1.0
   hoh = 110.0
$end.

$rem
   JOBTYPE       sp
   EXCHANGE      gen
   BASIS         6-311(2+,2+)G**
   CIS_N_ROOTS   30
   RPA           true
$end

$xc_functional
   X   PBE   1.0
   C   PBE   1.0
   X   LFAs  1.0
$end
```

### 4.4.11 Derivative Discontinuity Restoration

From the perspective of perturbation theory, Chai and Chen[234] proposed a systematic procedure for the evaluation of the derivative discontinuity of the exchange-correlation energy functional in KS-DFT, wherein the exact derivative discontinuity can in principle be obtained by summing up all the perturbation corrections to infinite order. Truncation of the perturbation series at low order yields an efficient scheme for obtaining the approximate derivative discontinuity. In particular, the first-order correction term is equivalent to the frozen-orbital approximation method. Its implementation in Q-CHEM supports only local and GGA functionals at present, not meta-GGA, hybrid, or non-local functionals. Job control variables and examples appear below.

**FOA_FUNDGAP**

Compute the frozen-orbital approximation of the fundamental gap.

TYPE:

Boolean

DEFAULT:

FALSE

OPTIONS:

FALSE Do not compute FOA derivative discontinuity and fundamental gap.

TRUE Compute and print FOA fundamental gap information. Implies KS_GAP_PRINT.

RECOMMENDATION:

Use in conjunction with KS_GAP_UNIT if true.

**Example 4.23** frozen-orbital approximation of derivative discontinuity with PBE and LFAs-PBE functionals on carbon atom

```
$comment
    Frozen-orbital derivative discontinuity, C atom, PBE
$end
```

```
$molecule
   0 3
   C
$end

$rem
   JOBTYPE       sp
   BASIS         6-31G*
   METHOD        PBE
   FOA_FUNDGAP   true
   KS_GAP_UNIT   1    ! print gap info in eV
$end

@@@

$comment
   with LFAs-PBE functional instead
$end

$molecule
   READ
$end

$rem
   JOBTYPE       sp
   BASIS         6-31G*
   SCF_GUESS     READ
   EXCHANGE      gen
   FOA_FUNDGAP   true
   KS_GAP_UNIT   1
$end

$xc_functional
   X   PBE    1.0
   X   LFAs   1.0
   C   PBE    1.0
$end
```

### 4.4.12 Thermally-Assisted-Occupation Density Functional Theory (TAO-DFT)

Aiming to study the ground-state properties of large, strongly correlated systems with minimum computational complexity, Prof. Jeng-Da Chai recently developed thermally-assisted-occupation density functional theory (TAO-DFT)[235]. Unlike conventional multi-reference methods, the computational complexity of TAO-DFT increases very insignificantly with the size of the active space (*i.e.*, an active space restriction is not needed for TAO-DFT calculations), and TAO-DFT appears to be very promising for the study of large poly-radical systems. TAO-DFT is a DFT scheme with fractional orbital occupations produced by the Fermi-Dirac distribution, controlled by a fictitious temperature $\theta$, and existing XC functionals (*e.g.*, LDA or GGAs) can be used in TAO-DFT[236]. The computational cost of the method is similar to that of KS-DFT for single-point energy calculations and analytical nuclear gradients, and reduces to the cost of KS-DFT in the absence of strong static correlation effects.

There are several *$rem* variables that are used for TAO-DFT.

**TAO_DFT**

Controls whether to use TAO-DFT.

TYPE:

Boolean

DEFAULT:

false

OPTIONS:

false Do not use TAO-DFT

true Use TAO-DFT

RECOMMENDATION:

NONE

**TAO_DFT_THETA**

Controls the value of the fictitious temperature $\theta$ in TAO-DFT.

TYPE:

INTEGER

DEFAULT:

7

OPTIONS:

$m$ $\theta = m \times 10^{-n}$ (hartrees), where $n$ is the value of TAO_DFT_THETA_NDP

RECOMMENDATION:

NONE

**TAO_DFT_THETA_NDP**

Controls the value of the fictitious temperature $\theta$ in TAO-DFT.

TYPE:

INTEGER

DEFAULT:

3

OPTIONS:

$n$ $\theta = m \times 10^{-n}$ (hartrees), where $m$ is the value of TAO_DFT_THETA

RECOMMENDATION:

NONE

Note that setting TAO_DFT_THETA = 0 recovers ordinary KS-DFT[235]. In addition to the XC functional, a functional $E_\theta[\rho]$ is needed in TAO-DFT. Currently available in Q-CHEM are an LDA version[235] (the ETheta_LDA functional) as well as a version based on the gradient expansion approximation (GEA)[236] (ETheta_GEA functional), and the latter may be substituted for the former in the sample jobs below.

**Example 4.24** TAO-LDA calculation on Be atom

```
$molecule
   0 1
   Be
$end

$rem
   JOBTYPE             sp
   BASIS               6-31G*
   EXCHANGE            gen
   TAO_DFT             true
   TAO_DFT_THETA       7    ! default, theta=7 mhartree
   TAO_DFT_THETA_NDP   3    ! default
$end

$xc_functional
   X   S            1.0
   C   PW92         1.0
   X   ETheta_LDA   1.0
$end
```

**Example 4.25** TAO-PBE, spin-restricted calculation on stretched $N_2$

```
$molecule
   0 1
   N1
   N2 N1 5
$end

$rem
   JOBTYPE             sp
   BASIS               6-31G*
   EXCHANGE            gen
   TAO_DFT             true
   TAO_DFT_THETA       40  ! theta = 40 mhartree
   TAO_DFT_THETA_NDP   3
$end

$xc_functional
   X PBE         1.0
   C PBE         1.0
   X ETheta_LDA  1.0
$end
```

**Example 4.26** TAO-PBE, spin-unrestricted calculation on stretched $N_2$

```
$molecule
   0 1
   N1
   N2 N1 5
$end

$rem
   JOBTYPE             opt
   UNRESTRICTED        true
   BASIS               6-31G*
   EXCHANGE            gen
   TAO_DFT             true
   TAO_DFT_THETA       40  ! theta = 40 mhartrees
   TAO_DFT_THETA_NDP   3   ! can omit this line
   SCF_GUESS           gwh
   SCF_GUESS_MIX       3   ! mix in 30% LUMO in alpha to break symmetry
$end

$xc_functional
   X PBE         1.0
   C PBE         1.0
   X ETheta_LDA  1.0
$end
```

## 4.5 SCF Initial Guess

### 4.5.1 Introduction

The Roothaan-Hall and Pople-Nesbet equations of SCF theory are non-linear in the molecular orbital coefficients. Like many mathematical problems involving non-linear equations, prior to the application of a technique to search for a numerical solution, an initial guess for the solution must be generated. If the guess is poor, the iterative procedure applied to determine the numerical solutions may converge very slowly, requiring a large number of iterations, or at worst, the procedure may diverge.

Thus, in an *ab initio* SCF procedure, the quality of the initial guess is of utmost importance for (at least) two main reasons:

- To ensure that the SCF converges to an appropriate ground state. Often SCF calculations can converge to different local minima in wave function space, depending upon which part of "LCAO space" in which the initial guess lands.
- When considering jobs with many basis functions requiring the recalculation of ERIs at each iteration, using a good initial guess that is close to the final solution can reduce the total job time significantly by decreasing the number of SCF iterations.

For these reasons, sooner or later most users will find it helpful to have some understanding of the different options available for customizing the initial guess. Q-CHEM currently offers six options for the initial guess:

- Superposition of Atomic Density (SAD)
- Purified SAD guess (provides molecular orbitals; SADMO)
- Core Hamiltonian (CORE)
- Generalized Wolfsberg-Helmholtz (GWH)
- Reading previously obtained MOs from disk. (READ)
- Basis set projection (BASIS2)

The first four of these guesses are built-in, and are briefly described in Section 4.5.2. The option of reading MOs from disk is described in Section 4.5.3. The initial guess MOs can be modified, either by mixing, or altering the order of occupation. These options are discussed in Section 4.5.4. Finally, Q-CHEM's novel basis set projection method is discussed in Section 4.5.5.

### 4.5.2 Simple Initial Guesses

There are four simple initial guesses available in Q-CHEM. While they are all simple, they are by no means equal in quality, as we discuss below.

1. **Superposition of Atomic Densities (SAD):** The SAD guess is almost trivially constructed by summing together atomic densities that have been spherically averaged to yield a trial density matrix. The SAD guess is far superior to the other two options below, particularly when large basis sets and/or large molecules are employed. There are three issues associated with the SAD guess to be aware of:

   (a) No molecular orbitals are obtained, which means that SCF algorithms requiring orbitals (the direct minimization methods discussed in Section 4.6) cannot directly use the SAD guess, and,

   (b) The SAD guess is not available for general (read-in) basis sets. All internal basis sets support the SAD guess.

   (c) The SAD guess is not idempotent and thus requires *at least* two SCF iterations to ensure proper SCF convergence (idempotency of the density).

2. **Purified Superposition of Atomic Densities (SADMO):** This guess is similar to the SAD guess, with two critical differences, namely, the removal of issues 1a and 1c above. The functional difference to the SAD guess is that the density matrix obtained from the superposition is diagonalized to obtain natural molecular orbitals, after which an idempotent density matrix is created by aufbau occupation of the natural orbitals. Since the initial density matrix is created with the SAD guess, the SADMO guess is not available either for a general (read-in) basis set.

3. **Generalized Wolfsberg-Helmholtz (GWH):** The GWH guess procedure[237] uses a combination of the overlap matrix elements in Eq. (4.12), and the diagonal elements of the Core Hamiltonian matrix in Eq. (4.18). This initial guess is most satisfactory in small basis sets for small molecules. It is constructed according to the relation given below, where $c_x$ is a constant typically chosen as $c_x = 1.75$.

$$H_{\mu v} = c_x S_{\mu v}(H_{\mu\mu} + H_{vv})/2. \tag{4.78}$$

4. **Core Hamiltonian:** The core Hamiltonian guess simply obtains the guess MO coefficients by diagonalizing the core Hamiltonian matrix in Eq. (4.18). This approach works best with small basis sets, and degrades as both the molecule size and the basis set size are increased.

The selection of these choices (or whether to read in the orbitals) is controlled by the following *$rem* variables:

**SCF_GUESS**

Specifies the initial guess procedure to use for the SCF.

TYPE:

STRING

DEFAULT:

| | |
|---|---|
| SAD | Superposition of atomic densities (available only with standard basis sets) |
| GWH | For ROHF where a set of orbitals are required. |
| FRAGMO | For a fragment MO calculation |

OPTIONS:

| | |
|---|---|
| CORE | Diagonalize core Hamiltonian |
| SAD | Superposition of atomic density |
| SADMO | Purified superposition of atomic densities (available only with standard basis sets) |
| GWH | Apply generalized Wolfsberg-Helmholtz approximation |
| READ | Read previous MOs from disk |
| FRAGMO | Superimposing converged fragment MOs |

RECOMMENDATION:

SAD or SADMO guess for standard basis sets. For general basis sets, it is best to use the BASIS2 *$rem*. Alternatively, try the GWH or core Hamiltonian guess. For ROHF it can be useful to READ guesses from an SCF calculation on the corresponding cation or anion. Note that because the density is made spherical, this may favor an undesired state for atomic systems, especially transition metals. Use FRAGMO in a fragment MO calculation.

**SCF_GUESS_ALWAYS**

Switch to force the regeneration of a new initial guess for each series of SCF iterations (for use in geometry optimization).

TYPE:

LOGICAL

DEFAULT:

False

OPTIONS:

| | |
|---|---|
| False | Do not generate a new guess for each series of SCF iterations in an optimization; use MOs from the previous SCF calculation for the guess, if available. |
| True | Generate a new guess for each series of SCF iterations in a geometry optimization. |

RECOMMENDATION:

Use the default unless SCF convergence issues arise

### 4.5.3 Reading MOs from Disk

There are two methods by which MO coefficients can be used from a previous job by reading them from disk:

1. Running two independent jobs sequentially invoking *qchem* with three command line variables:.

```
localhost-1> qchem job1.in job1.out save
localhost-2> qchem job2.in job2.out save
```

**Note:** (1) The *$rem* variable SCF_GUESS must be set to READ in *job2.in.*
(2) Scratch files remain in *$QCSCRATCH/save* on exit.

2. Running a batch job where two jobs are placed into a single input file separated by the string `@@@` on a single line.
   **Note:** (1) SCF_GUESS must be set to READ in the second job of the batch file.
   (2) A third qchem command line variable is not necessary.
   (3) As for the SAD guess, Q-CHEM requires at least two SCF cycles to ensure proper SCF convergence (idempotency of the density).

**Note:** It is up to the user to make sure that the basis sets match between the two jobs. There is no internal checking for this, although the occupied orbitals are re-orthogonalized in the current basis after being read in. If you want to project from a smaller basis into a larger basis, consult section 4.5.5.

### 4.5.4 Modifying the Occupied Molecular Orbitals

It is sometimes useful for the occupied guess orbitals to be other than the lowest $N_\alpha$ (or $N_\beta$) orbitals. Reasons why one may need to do this include:

- To converge to a state of different symmetry or orbital occupation.
- To break spatial symmetry.
- To break spin symmetry, as in unrestricted calculations on molecules with an even number of electrons.

There are two mechanisms for modifying a set of guess orbitals: either by SCF_GUESS_MIX, or by specifying the orbitals to occupy. Q-CHEM users may define the occupied guess orbitals using the *$occupied* or *$swap_occupied_virtual* keywords. In the former, occupied guess orbitals are defined by listing the alpha orbitals to be occupied on the first line and beta on the second. In the former, only pair of orbitals that needs to be swapped is specified.

**Note:** To prevent Q-CHEM to change orbital occupation during SCF procedure, MOM_START option is often used in combination with *$occupied* or *$swap_occupied_virtual* keywords.

**Note:** The need for orbitals renders these options incompatible with the SAD guess. Most often, they are used with SCF_GUESS = READ.

**Example 4.27** Format for modifying occupied guess orbitals.

```
$occupied
   1  2  3  4 ...  nalpha
   1  2  3  4 ...  nbeta
$end
```

**Example 4.28** Alternative format for modifying occupied guess orbitals.

```
$swap_occupied_virtual
   <spin> <io1> <iv1>
   <spin> <io2> <iv2>
$end
```

**Example 4.29** Example of swapping guess orbitals.

```
$swap_occupied_virtual
   alpha  5  6
   beta   6  7
$end
```

This is identical to: **Example 4.30** Example of specifying occupied guess orbitals.

```
$occupied
   1  2  3  4  6  5  7
   1  2  3  4  5  7  6
$end
```

or **Example 4.31** Example of specifying occupied guess orbitals.

```
$occupied
   1:4  6  5  7
   1:5  7  6
$end
```

The other *$rem* variables related to altering the orbital occupancies are:

**SCF_GUESS_PRINT**

Controls printing of guess MOs, Fock and density matrices.

TYPE:

INTEGER

DEFAULT:

0

OPTIONS:

| | |
|---|---|
| 0 | Do not print guesses. |
| SAD | |
| 1 | Atomic density matrices and molecular matrix. |
| 2 | Level 1 plus density matrices. |
| CORE and GWH | |
| 1 | No extra output. |
| 2 | Level 1 plus Fock and density matrices and, MO coefficients and eigenvalues. |
| READ | |
| 1 | No extra output |
| 2 | Level 1 plus density matrices, MO coefficients and eigenvalues. |

RECOMMENDATION:

None

**SCF_GUESS_MIX**

Controls mixing of LUMO and HOMO to break symmetry in the initial guess. For unrestricted jobs, the mixing is performed only for the alpha orbitals.

TYPE:

INTEGER

DEFAULT:

| | |
|---|---|
| 0 (FALSE) | Do not mix HOMO and LUMO in SCF guess. |

OPTIONS:

| | |
|---|---|
| 0 (FALSE) | Do not mix HOMO and LUMO in SCF guess. |
| 1 (TRUE) | Add 10% of LUMO to HOMO to break symmetry. |
| $n$ | Add $n \times 10\%$ of LUMO to HOMO ($0 < n < 10$). |

RECOMMENDATION:

When performing unrestricted calculations on molecules with an even number of electrons, it is often necessary to break alpha/beta symmetry in the initial guess with this option, or by specifying input for *$occupied*.

### 4.5.5 Basis Set Projection

Q-CHEM also includes a novel basis set projection method developed by Dr Jing Kong of Q-CHEM Inc. It permits a calculation in a large basis set to bootstrap itself up *via* a calculation in a small basis set that is automatically spawned when the user requests this option. When basis set projection is requested (by providing a valid small basis for BASIS2), the program executes the following steps:

- A simple DFT calculation is performed in the small basis, BASIS2, yielding a converged density matrix in this basis.
- The large basis set SCF calculation (with different values of EXCHANGE and CORRELATION set by the input) begins by constructing the DFT Fock operator in the large basis but with the density matrix obtained from the small basis set.
- By diagonalizing this matrix, an accurate initial guess for the density matrix in the large basis is obtained, and the target SCF calculation commences.

Two different methods of projection are available and can be set using the BASISPROJTYPE *$rem*. The OVPROJECTION option expands the MOs from the BASIS2 calculation in the larger basis, while the FOPPROJECTION option constructs the Fock matrix in the larger basis using the density matrix from the initial, smaller basis set calculation. Basis set projection is a very effective option for general basis sets, where the SAD guess is not available. In detail, this initial guess is controlled by the following *$rem* variables:

**BASIS2**

Sets the small basis set to use in basis set projection.

TYPE:

STRING

DEFAULT:

No second basis set default.

OPTIONS:

Symbol. Use standard basis sets as per Chapter 7.

| | |
|---|---|
| BASIS2_GEN | General BASIS2 |
| BASIS2_MIXED | Mixed BASIS2 |

RECOMMENDATION:

BASIS2 should be smaller than BASIS. There is little advantage to using a basis larger than a minimal basis when BASIS2 is used for initial guess purposes. Larger, standardized BASIS2 options are available for dual-basis calculations (see Section 4.9).

**BASISPROJTYPE**

Determines which method to use when projecting the density matrix of BASIS2

TYPE:

STRING

DEFAULT:

FOPPROJECTION (when DUAL_BASIS_ENERGY=false)
OVPROJECTION (when DUAL_BASIS_ENERGY=true)

OPTIONS:

| | |
|---|---|
| FOPPROJECTION | Construct the Fock matrix in the second basis |
| OVPROJECTION | Projects MOs from BASIS2 to BASIS. |

RECOMMENDATION:

None

**Note:** BASIS2 sometimes affects post-Hartree-Fock calculations. It is recommended to split such jobs into two subsequent one, such that in the first job a desired Hartree-Fock solution is found using BASIS2, and in the second job, which performs a post-HF calculation, SCF_GUESS=READ is invoked.

### 4.5.6 Examples

**Example 4.32** Input where basis set projection is used to generate a good initial guess for a calculation employing a general basis set, for which the default initial guess is not available.

```
$molecule
   0  1
   O
   H  1  r
   H  1  r  2  a

   r    0.9
   a  104.0
$end

$rem
```

```
   METHOD        mp2
   BASIS         general
   BASIS2        sto-3g
$end

$basis
   O   0
   S   3   1.000000
           3.22037000E+02   5.92394000E-02
           4.84308000E+01   3.51500000E-01
           1.04206000E+01   7.07658000E-01
   SP  2   1.000000
           7.40294000E+00  -4.04453000E-01   2.44586000E-01
           1.57620000E+00   1.22156000E+00   8.53955000E-01
   SP  1   1.000000
           3.73684000E-01   1.00000000E+00   1.00000000E+00
   SP  1   1.000000
           8.45000000E-02   1.00000000E+00   1.00000000E+00
****
   H   0
   S   2   1.000000
           5.44717800E+00   1.56285000E-01
           8.24547000E-01   9.04691000E-01
   S   1   1.000000
           1.83192000E-01   1.00000000E+00
****
$end
```

**Example 4.33** Input for an ROHF calculation on the OH radical. One SCF cycle is initially performed on the cation, to get reasonably good initial guess orbitals, which are then read in as the guess for the radical. This avoids the use of Q-CHEM's default GWH guess for ROHF, which is often poor.

```
$comment
   OH radical, part 1. Do 1 iteration of cation orbitals.
$end

$molecule
   1  1
   O  0.000   0.000   0.000
   H  0.000   0.000   1.000
$end

$rem
   BASIS            =  6-311++G(2df)
   METHOD           =  hf
   MAX_SCF_CYCLES   =  1
   THRESH           =  10
$end

@@@

$comment
   OH radical, part 2. Read cation orbitals, do the radical
$end

$molecule
   0  2
   O  0.000   0.000   0.000
   H  0.000   0.000   1.000
$end

$rem
   BASIS             =  6-311++G(2df)
   METHOD            =  hf
   UNRESTRICTED      =  false
   SCF_ALGORITHM     =  dm
   SCF_CONVERGENCE   =  7
   SCF_GUESS         =  read
   THRESH            =  10
$end
```

**Example 4.34** Input for an unrestricted HF calculation on $H_2$ in the dissociation limit, showing the use of SCF_GUESS_MIX = 2 (corresponding to 20% of the alpha LUMO mixed with the alpha HOMO). Geometric direct minimization with DIIS is used to converge the SCF, together with MAX_DIIS_CYCLES = 1 (using the default value for MAX_DIIS_CYCLES, the DIIS procedure just oscillates).

```
$molecule
   0  1
   H  0.000   0.000   0.0
   H  0.000   0.000 -10.0
$end

$rem
   UNRESTRICTED      =  true
   METHOD            =  hf
   BASIS             =  6-31g**
   SCF_ALGORITHM     =  diis_gdm
   MAX_DIIS_CYCLES   =  1
   SCF_GUESS         =  gwh
   SCF_GUESS_MIX     =  2
$end
```

## 4.6 Converging SCF Calculations

### 4.6.1 Introduction

As for any numerical optimization procedure, the rate of convergence of the SCF procedure is dependent on the initial guess and on the algorithm used to step towards the stationary point. Q-CHEM features a number of alternative SCF optimization algorithms, which are discussed in the following sections, along with the *$rem* variables that are used to control the calculations. The main options are discussed in sections which follow and are, in brief:

- The highly successful DIIS procedures, which are the default, except for restricted open-shell SCF calculations.
- The new geometric direct minimization (GDM) method, which is highly robust, and the recommended fall-back when DIIS fails. It can also be invoked after a few initial iterations with DIIS to improve the initial guess. GDM is the default algorithm for restricted open-shell SCF calculations.

- The older and less robust direct minimization method (DM). As for GDM, it can also be invoked after a few DIIS iterations (except for RO jobs).
- The maximum overlap method (MOM) which ensures that DIIS always occupies a continuous set of orbitals and does not oscillate between different occupancies.
- The relaxed constraint algorithm (RCA) which guarantees that the energy goes down at every step.

### 4.6.2 Basic Convergence Control Options

See also more detailed options in the following sections, and note that the SCF convergence criterion and the integral threshold must be set in a compatible manner, (this usually means THRESH should be set to at least 3 higher than SCF_CONVERGENCE).

**MAX_SCF_CYCLES**
Controls the maximum number of SCF iterations permitted.
TYPE:
INTEGER
DEFAULT:
50
OPTIONS:
$n$ $n > 0$ User-selected.
RECOMMENDATION:
Increase for slowly converging systems such as those containing transition metals.

**SCF_ALGORITHM**
Algorithm used for converging the SCF.
TYPE:
STRING
DEFAULT:
DIIS Pulay DIIS.
OPTIONS:

| | |
|---|---|
| DIIS | Pulay DIIS. |
| DM | Direct minimizer. |
| DIIS_DM | Uses DIIS initially, switching to direct minimizer for later iterations (See THRESH_DIIS_SWITCH, MAX_DIIS_CYCLES). |
| DIIS_GDM | Use DIIS and then later switch to geometric direct minimization (See THRESH_DIIS_SWITCH, MAX_DIIS_CYCLES). |
| GDM | Geometric Direct Minimization. |
| RCA | Relaxed constraint algorithm |
| RCA_DIIS | Use RCA initially, switching to DIIS for later iterations (see THRESH_RCA_SWITCH and MAX_RCA_CYCLES described later in this chapter) |
| ROOTHAAN | Roothaan repeated diagonalization. |

RECOMMENDATION:
Use DIIS unless performing a restricted open-shell calculation, in which case GDM is recommended. If DIIS fails to find a reasonable approximate solution in the initial iterations, RCA_DIIS is the recommended fallback option. If DIIS approaches the correct solution but fails to finally converge, DIIS_GDM is the recommended fallback.

**SCF_CONVERGENCE**

SCF is considered converged when the wave function error is less that $10^{-\text{SCF\_CONVERGENCE}}$. Adjust the value of THRESH at the same time. Note that in Q-CHEM 3.0 the DIIS error is measured by the maximum error rather than the RMS error.

TYPE:

INTEGER

DEFAULT:

5 For single point energy calculations.

7 For geometry optimizations and vibrational analysis.

8 For SSG calculations, see Chapter 5.

OPTIONS:

$n$ Corresponding to $10^{-n}$

RECOMMENDATION:

Tighter criteria for geometry optimization and vibration analysis. Larger values provide more significant figures, at greater computational cost.

In some cases besides the total SCF energy, one needs its separate energy components, like kinetic energy, exchange energy, correlation energy, *etc.* The values of these components are printed at each SCF cycle if one specifies SCF_PRINT = 1 in the input.

### 4.6.3 Direct Inversion in the Iterative Subspace (DIIS)

The SCF implementation of the Direct Inversion in the Iterative Subspace (DIIS) method[238,239] uses the property of an SCF solution that requires the density matrix to commute with the Fock matrix:

$$\mathbf{SPF} - \mathbf{FPS} = \mathbf{0} \tag{4.79}$$

During the SCF cycles, prior to achieving self-consistency, it is therefore possible to define an error vector $\mathbf{e}_i$, which is non-zero except at convergence:

$$\mathbf{S}\mathbf{P}_i\mathbf{F}_i - \mathbf{F}_i\mathbf{P}_i\mathbf{S} = \mathbf{e}_i \tag{4.80}$$

Here $\mathbf{P}_i$ is obtained by diagonalizing $\mathbf{F}_i$, and

$$\mathbf{F}_k = \sum_{j=1}^{k-1} c_j \mathbf{F}_j \tag{4.81}$$

The DIIS coefficients $c_k$, are obtained by a least-squares constrained minimization of the error vectors, *viz*

$$Z = \left(\sum_k c_k \mathbf{e}_k\right) \cdot \left(\sum_k c_k \mathbf{e}_k\right) \tag{4.82}$$

where the constraint $\sum_k c_k = 1$ is imposed to yield a set of linear equations, of dimension $N+1$:

$$\begin{pmatrix} \mathbf{e}_1 \cdot \mathbf{e}_1 & \cdots & \mathbf{e}_1 \cdot \mathbf{e}_N & 1 \\ \vdots & \ddots & \vdots & \vdots \\ \mathbf{e}_N \cdot \mathbf{e}_1 & \cdots & \mathbf{e}_N \cdot \mathbf{e}_N & 1 \\ 1 & \cdots & 1 & 0 \end{pmatrix} \begin{pmatrix} c_1 \\ \vdots \\ c_N \\ \lambda \end{pmatrix} = \begin{pmatrix} 0 \\ \vdots \\ 0 \\ 1 \end{pmatrix} . \tag{4.83}$$

Convergence criteria require the largest element of the $N$th error vector to be below a cutoff threshold, usually $10^{-5}$ a.u. for single point energies, but often increased to $10^{-8}$ a.u. for optimizations and frequency calculations.

The rate of convergence may be improved by restricting the number of previous Fock matrices (size of the DIIS subspace, *$rem* variable DIIS_SUBSPACE_SIZE) used for determining the DIIS coefficients:

$$\mathbf{F}_k = \sum_{j=k-(L+1)}^{k-1} c_j \mathbf{F}_j \tag{4.84}$$

where $L$ is the size of the DIIS subspace. As the Fock matrix nears self-consistency, the linear matrix equations in Eq. (4.83) tend to become severely ill-conditioned and it is often necessary to reset the DIIS subspace (this is automatically carried out by the program).

Finally, on a practical note, we observe that DIIS has a tendency to converge to global minima rather than local minima when employed for SCF calculations. This seems to be because only at convergence is the density matrix in the DIIS iterations idempotent. On the way to convergence, one is not on the true energy surface, and this seems to permit DIIS to "tunnel" through barriers in wave function space. This is usually a desirable property, and is the motivation for the options that permit initial DIIS iterations before switching to direct minimization to converge to the minimum in difficult cases.

The following *$rem* variables permit some customization of the DIIS iterations:

**DIIS_SUBSPACE_SIZE**
  Controls the size of the DIIS and/or RCA subspace during the SCF.
TYPE:
  INTEGER
DEFAULT:
  15
OPTIONS:
  User-defined
RECOMMENDATION:
  None

**DIIS_PRINT**
  Controls the output from DIIS SCF optimization.
TYPE:
  INTEGER
DEFAULT:
  0
OPTIONS:
  0 Minimal print out.
  1 Chosen method and DIIS coefficients and solutions.
  2 Level 1 plus changes in multipole moments.
  3 Level 2 plus Multipole moments.
  4 Level 3 plus extrapolated Fock matrices.
RECOMMENDATION:
  Use the default

**Note:** In Q-CHEM 3.0 the DIIS error is determined by the maximum error rather than the RMS error. For backward compatibility the RMS error can be forced by using the following *$rem*

**DIIS_ERR_RMS**

Changes the DIIS convergence metric from the maximum to the RMS error.

TYPE:

LOGICAL

DEFAULT:

FALSE

OPTIONS:

TRUE, FALSE

RECOMMENDATION:

Use the default, the maximum error provides a more reliable criterion.

### 4.6.4 Geometric Direct Minimization (GDM)

Troy Van Voorhis, working at Berkeley with Martin Head-Gordon, has developed a novel direct minimization method that is extremely robust, and at the same time is only slightly less efficient than DIIS. This method is called geometric direct minimization (GDM) because it takes steps in an orbital rotation space that correspond properly to the hyper-spherical geometry of that space. In other words, rotations are variables that describe a space which is curved like a many-dimensional sphere. Just like the optimum flight paths for airplanes are not straight lines but great circles, so too are the optimum steps in orbital rotation space. GDM takes this correctly into account, which is the origin of its efficiency and its robustness. For full details, we refer the reader to Ref. 240. GDM is a good alternative to DIIS for SCF jobs that exhibit convergence difficulties with DIIS.

Recently, Barry Dunietz, also working at Berkeley with Martin Head-Gordon, has extended the GDM approach to restricted open-shell SCF calculations. Their results indicate that GDM is much more efficient than the older direct minimization method (DM).

In section 4.6.3, we discussed the fact that DIIS can efficiently head towards the global SCF minimum in the early iterations. This can be true even if DIIS fails to converge in later iterations. For this reason, a hybrid scheme has been implemented which uses the DIIS minimization procedure to achieve convergence to an intermediate cutoff threshold. Thereafter, the geometric direct minimization algorithm is used. This scheme combines the strengths of the two methods quite nicely: the ability of DIIS to recover from initial guesses that may not be close to the global minimum, and the ability of GDM to robustly converge to a local minimum, even when the local surface topology is challenging for DIIS. This is the recommended procedure with which to invoke GDM (*i.e.*, setting SCF_ALGORITHM = DIIS_GDM). This hybrid procedure is also compatible with the SAD guess, while GDM itself is not, because it requires an initial guess set of orbitals. If one wishes to disturb the initial guess as little as possible before switching on GDM, one should additionally specify MAX_DIIS_CYCLES = 1 to obtain only a single Roothaan step (which also serves up a properly orthogonalized set of orbitals).

*$rem* options relevant to GDM are SCF_ALGORITHM which should be set to either GDM or DIIS_GDM and the following:

**MAX_DIIS_CYCLES**

The maximum number of DIIS iterations before switching to (geometric) direct minimization when SCF_ALGORITHM is DIIS_GDM or DIIS_DM. See also THRESH_DIIS_SWITCH.

TYPE:

INTEGER

DEFAULT:

50

OPTIONS:

1 Only a single Roothaan step before switching to (G)DM

$n$ $n$ DIIS iterations before switching to (G)DM.

RECOMMENDATION:

None

**THRESH_DIIS_SWITCH**

The threshold for switching between DIIS extrapolation and direct minimization of the SCF energy is $10^{-\text{THRESH\_DIIS\_SWITCH}}$ when SCF_ALGORITHM is DIIS_GDM or DIIS_DM. See also MAX_DIIS_CYCLES

TYPE:

INTEGER

DEFAULT:

2

OPTIONS:

User-defined.

RECOMMENDATION:

None

### 4.6.5 Direct Minimization (DM)

Direct minimization (DM) is a less sophisticated forerunner of the geometric direct minimization (GDM) method discussed in the previous section. DM does not properly step along great circles in the hyperspherical space of orbital rotations, and therefore converges less rapidly and less robustly than GDM, in general. It is retained for legacy purposes, and because it is at present the only method available for restricted open shell (RO) SCF calculations in Q-CHEM. In general, the input options are the same as for GDM, with the exception of the specification of SCF_ALGORITHM, which can be either DIIS_DM (recommended) or DM.

**PSEUDO_CANONICAL**

When SCF_ALGORITHM = DM, this controls the way the initial step, and steps after subspace resets are taken.

TYPE:

LOGICAL

DEFAULT:

FALSE

OPTIONS:

| | |
|---|---|
| FALSE | Use Roothaan steps when (re)initializing |
| TRUE | Use a steepest descent step when (re)initializing |

RECOMMENDATION:

The default is usually more efficient, but choosing TRUE sometimes avoids problems with orbital reordering.

### 4.6.6 Maximum Overlap Method (MOM)

In general, the DIIS procedure is remarkably successful. One difficulty that is occasionally encountered is the problem of an SCF that occupies two different sets of orbitals on alternating iterations, and therefore oscillates and fails to converge. This can be overcome by choosing orbital occupancies that maximize the overlap of the new occupied orbitals with the set previously occupied. Q-CHEM contains the maximum overlap method (MOM)[241], developed by Andrew Gilbert and Peter Gill.

MOM is therefore is a useful adjunct to DIIS in convergence problems involving flipping of orbital occupancies. It is controlled by the *$rem* variable MOM_START, which specifies the SCF iteration on which the MOM procedure is first enabled. There are two strategies that are useful in setting a value for MOM_START. To help maintain an initial configuration it should be set to start on the first cycle. On the other hand, to assist convergence it should come on later to avoid holding on to an initial configuration that may be far from the converged one.

The MOM-related *$rem* variables in full are the following:.

**MOM_PRINT**

Switches printing on within the MOM procedure.

TYPE:

LOGICAL

DEFAULT:

FALSE

OPTIONS:

| | |
|---|---|
| FALSE | Printing is turned off |
| TRUE | Printing is turned on. |

RECOMMENDATION:

None

**MOM_START**

Determines when MOM is switched on to stabilize DIIS iterations.

TYPE:

INTEGER

DEFAULT:

0 (FALSE)

OPTIONS:

| | |
|---|---|
| 0 (FALSE) | MOM is not used |
| $n$ | MOM begins on cycle $n$. |

RECOMMENDATION:

Set to 1 if preservation of initial orbitals is desired. If MOM is to be used to aid convergence, an SCF without MOM should be run to determine when the SCF starts oscillating. MOM should be set to start just before the oscillations.

**MOM_METHOD**

Determines the target orbitals with which to maximize the overlap on each SCF cycle.

TYPE:

INTEGER

DEFAULT:

3

OPTIONS:

| | |
|---|---|
| 3 | Maximize overlap with the orbitals from the previous SCF cycle. |
| 13 | Maximize overlap with the initial guess orbitals. |

RECOMMENDATION:

If appropriate guess orbitals can be obtained, then MOM_METHOD = 13 can provide more reliable convergence to the desired solution.

### 4.6.7 Relaxed Constraint Algorithm (RCA)

The relaxed constraint algorithm (RCA) is an ingenious and simple means of minimizing the SCF energy that is particularly effective in cases where the initial guess is poor. The latter is true, for example, when employing a user-specified basis (when the "core" or GWH guess must be employed) or when near-degeneracy effects imply that the initial guess will likely occupy the wrong orbitals relative to the desired converged solution.

Briefly, RCA begins with the SCF problem as a constrained minimization of the energy as a function of the density matrix, $E(\mathbf{P})$[242,243]. The constraint is that the density matrix be idempotent, $\mathbf{P} \cdot \mathbf{P} = \mathbf{P}$, which basically forces the occupation numbers to be either zero or one. The fundamental realization of RCA is that this constraint can be relaxed to allow sub-idempotent density matrices, $\mathbf{P} \cdot \mathbf{P} \leq \mathbf{P}$. This condition forces the occupation numbers to be between zero and one. Physically, we expect that any state with fractional occupations can lower its energy by moving electrons from higher energy orbitals to lower ones. Thus, if we solve for the minimum of $E(\mathbf{P})$ subject to the relaxed sub-idempotent constraint, we expect that the ultimate solution will nonetheless be idempotent. In fact, for Hartree-Fock this can be rigorously proven. For density functional theory, it is possible that the minimum will have fractional occupation numbers but these occupations have a physical interpretation in terms of ensemble DFT. The reason the relaxed constraint is easier to deal with is that it is easy to prove that a linear combination of sub-idempotent matrices is also sub-idempotent as long as the linear coefficients are between zero and one. By exploiting this property, convergence can be accelerated in a way that guarantees the energy will go down at every step.

The implementation of RCA in Q-CHEM closely follows the "Energy DIIS" implementation of the RCA algorithm[244]. Here, the current density matrix is written as a linear combination of the previous density matrices:

$$\mathbf{P}(x) = \sum_i x_i \mathbf{P}_i \tag{4.85}$$

To a very good approximation (exact for Hartree-Fock) the energy for $\mathbf{P}(x)$ can be written as a quadratic function of x:

$$\mathbf{E}(x) = \sum_i E_i x_i + \frac{1}{2} \sum_i x_i (\mathbf{P}_i - \mathbf{P}_j) \cdot (\mathbf{F}_i - \mathbf{F}_j) x_j \tag{4.86}$$

At each iteration, $x$ is chosen to minimize $\mathbf{E}(x)$ subject to the constraint that all of the $x_i$ are between zero and one. The Fock matrix for $\mathbf{P}(x)$ is further written as a linear combination of the previous Fock matrices,

$$\mathbf{F}(x) = \sum_i x_i \mathbf{F}_i + \delta \mathbf{F}_{xc}(x) \tag{4.87}$$

where $\delta \mathbf{F}_{xc}(x)$ denotes a (usually quite small) change in the exchange-correlation part that is computed once $x$ has been determined. We note that this extrapolation is very similar to that used by DIIS. However, this procedure is guaranteed to reduce the energy $\mathbf{E}(x)$ at every iteration, unlike DIIS.

In practice, the RCA approach is ideally suited to difficult convergence situations because it is immune to the erratic orbital swapping that can occur in DIIS. On the other hand, RCA appears to perform relatively poorly near convergence, requiring a relatively large number of steps to improve the precision of a good approximate solution. It is thus advantageous in many cases to run RCA for the initial steps and then switch to DIIS either after some specified number of iterations or after some target convergence threshold has been reached. Finally, note that by its nature RCA considers the energy as a function of the density matrix. As a result, it cannot be applied to restricted open shell calculations which are explicitly orbital-based. Note: RCA interacts poorly with INCDFT, so INCDFT is disabled by default when an RCA or RCA_DIIS calculation is requested. To enable INCDFT with such a calculation, set INCDFT = 2 in the *$rem* section. RCA may also have poor interactions with incremental Fock builds; if RCA fails to converge, setting INCFOCK = FALSE may improve convergence in some cases.

Job-control variables for RCA are listed below, and an example input can be found in Section 4.6.9.

**RCA_PRINT**

Controls the output from RCA SCF optimizations.

TYPE:

INTEGER

DEFAULT:

0

OPTIONS:

| | |
|---|---|
| 0 | No print out |
| 1 | RCA summary information |
| 2 | Level 1 plus RCA coefficients |
| 3 | Level 2 plus RCA iteration details |

RECOMMENDATION:

None

**MAX_RCA_CYCLES**

The maximum number of RCA iterations before switching to DIIS when SCF_ALGORITHM is RCA_DIIS.

TYPE:

INTEGER

DEFAULT:

50

OPTIONS:

N N RCA iterations before switching to DIIS

RECOMMENDATION:

None

**THRESH_RCA_SWITCH**

The threshold for switching between RCA and DIIS when SCF_ALGORITHM is RCA_DIIS.

TYPE:

INTEGER

DEFAULT:

3

OPTIONS:

N Algorithm changes from RCA to DIIS when Error is less than $10^{-N}$.

RECOMMENDATION:

None

### 4.6.8 Small-Gap Systems

SCF calculations for systems with zero or small HOMO-LUMO gap (such as metals) can exhibit very slow convergence or may even fail to converge. This problem arises because the energetic ordering of orbitals and states can switch during the SCF optimization leading to discontinuities in the optimization. Using fractional MO occupation numbers can improve the convergence for small-gap systems. In this approach, the occupation numbers of MOs around the Fermi level are allowed to assume non-integer values. This "occupation smearing" allows one to include multiple electron configurations in the same optimization, which improves the stability of the optimization.

We follow the pseudo-Fractional Occupation Number (pFON) method of Rabuck and Scuseria[245] that scales the MO occupation used to construct the AO density:

$$P_{\mu\nu} = \sum_{p=1}^{N} n_p C_{\mu p} C_{\nu p}. \tag{4.88}$$

For a conventional (integer occupation number) SCF run, the occupation number $n_p$ is either one (occupied) or zero (virtual). In pFON, the occupation numbers are following a Fermi-Dirac distribution,

$$n_p = \left(1 + e^{(\epsilon_p - \epsilon_{\mathrm{F}})/kT}\right)^{-1}, \tag{4.89}$$

where $\epsilon_p$ is the respective orbital energy and $kT$ the Boltzmann constant and temperature, respectively. The Fermi energy $\epsilon_{\mathrm{F}}$ is set to $(\epsilon_{\mathrm{HOMO}} + \epsilon_{\mathrm{LUMO}})/2$ in our implementation. To ensure conservation of the total number of electrons, the pFON approach re-scales the occupation numbers so that $\sum_p n_p = N_{\mathrm{el}}$.

There are several parameters to control the electronic temperature $T$ throughout a pFON SCF run. The temperature can either be held constant at finite temperature ($T_{\mathrm{init}}$ = $T_{\mathrm{final}}$), or the system can be cooled from a higher temperature down to the final temperature. So far, no zero-temperature extrapolation has been implemented.

**OCCUPATIONS**

Activates pFON calculation.

TYPE:

INTEGER

DEFAULT:

0

OPTIONS:

| | |
|---|---|
| 0 | Integer occupation numbers |
| 1 | Not yet implemented |
| 2 | Pseudo-fractional occupation numbers (pFON) |

RECOMMENDATION:

Use pFON to improve convergence for small-gap systems.

**FON_T_START**

Initial electronic temperature (in K) for FON calculation.

TYPE:

INTEGER

DEFAULT:

1000

OPTIONS:

Any desired initial temperature.

RECOMMENDATION:

Pick the temperature to either reproduce experimental conditions (*e.g.* room temperature) or as low as possible to approach zero-temperature.

**FON_T_END**

Final electronic temperature for FON calculation.

TYPE:

INTEGER

DEFAULT:

0

OPTIONS:

Any desired final temperature.

RECOMMENDATION:

Pick the temperature to either reproduce experimental conditions (*e.g.* room temperature) or as low as possible to approach zero-temperature.

**FON_NORB**

Number of orbitals above and below the Fermi level that are allowed to have fractional occupancies.

TYPE:

INTEGER

DEFAULT:

4

OPTIONS:

n number of active orbitals

RECOMMENDATION:

The number of valence orbitals is a reasonable choice.

**FON_T_SCALE**

Determines the step size for the cooling.

TYPE:

INTEGER

DEFAULT:

90

OPTIONS:

n temperature is scaled by $0.01 \cdot n$ in each cycle (cooling method 1)

n temperature is decreased by n K in each cycle (cooling method 2)

RECOMMENDATION:

The cooling rate should be neither too slow nor too fast. Too slow may lead to final energies that are at undesirably high temperatures. Too fast may lead to convergence issues. Reasonable choices for methods 1 and 2 are 98 and 50, respectively. When in doubt, use constant temperature.

**FON_E_THRESH**

DIIS error below which occupations will be kept constant.

TYPE:

INTEGER

DEFAULT:

4

OPTIONS:

n freeze occupations below DIIS error of $10^{-n}$

RECOMMENDATION:

This should be one or two numbers bigger than the desired SCF convergence threshold.

**FON_T_METHOD**

Selects cooling algorithm.

TYPE:

INTEGER

DEFAULT:

1

OPTIONS:

1 temperature is scaled by a factor in each cycle

2 temperature is decreased by a constant number in each cycle

RECOMMENDATION:

We have made slightly better experience with a constant cooling rate. However, choose constant temperature when in doubt.

### 4.6.9 Examples

**Example 4.35** Input for a UHF calculation using geometric direct minimization (GDM) on the phenyl radical, after initial iterations with DIIS. This example fails to converge if DIIS is employed directly.

```
$molecule
   0   2
   c1
   x1  c1  1.0
   c2  c1  rc2  x1  90.0
   x2  c2  1.0  c1  90.0  x1    0.0
   c3  c1  rc3  x1  90.0  c2    tc3
   c4  c1  rc3  x1  90.0  c2   -tc3
   c5  c3  rc5  c1   ac5  x1  -90.0
   c6  c4  rc5  c1   ac5  x1   90.0
   h1  c2  rh1  x2  90.0  c1  180.0
   h2  c3  rh2  c1   ah2  x1   90.0
   h3  c4  rh2  c1   ah2  x1  -90.0
   h4  c5  rh4  c3   ah4  c1  180.0
   h5  c6  rh4  c4   ah4  c1  180.0

   rc2 =   2.672986
   rc3 =   1.354498
   tc3 =  62.851505
   rc5 =   1.372904
   ac5 = 116.454370
   rh1 =   1.085735
   rh2 =   1.085342
   ah2 = 122.157328
   rh4 =   1.087216
   ah4 = 119.523496
$end

$rem
   BASIS           = 6-31G*
   METHOD          = hf
   INTSBUFFERSIZE  = 15000000
   SCF_ALGORITHM   = diis_gdm
   SCF_CONVERGENCE = 7
   THRESH          = 10
$end
```

**Example 4.36** An example showing how to converge a ROHF calculation on the $^3A_2$ state of DMX. Note the use of reading in orbitals from a previous closed-shell calculation and the use of MOM to maintain the orbital occupancies. The $^3B_1$ is obtained if MOM is not used.

```
$molecule
  +1 1
   C       0.000000     0.000000     0.990770
   H       0.000000     0.000000     2.081970
   C      -1.233954     0.000000     0.290926
   C      -2.444677     0.000000     1.001437
   H      -2.464545     0.000000     2.089088
   H      -3.400657     0.000000     0.486785
   C      -1.175344     0.000000    -1.151599
   H      -2.151707     0.000000    -1.649364
   C       0.000000     0.000000    -1.928130
   C       1.175344     0.000000    -1.151599
   H       2.151707     0.000000    -1.649364
   C       1.233954     0.000000     0.290926
   C       2.444677     0.000000     1.001437
   H       2.464545     0.000000     2.089088
   H       3.400657     0.000000     0.486785
$end

$rem
   UNRESTRICTED      false
   METHOD            hf
   BASIS             6-31+G*
   SCF_GUESS         core
$end

@@@

$molecule
   read
$end

$rem
   UNRESTRICTED      false
   METHOD            hf
   BASIS             6-31+G*
   SCF_GUESS         read
   MOM_START         1
$end

$occupied
   1:26 28
   1:26 28
$end

@@@

$molecule
   -1 3
   read
$end
```

```
$rem
   UNRESTRICTED      false
   METHOD            hf
   BASIS             6-31+G*
   SCF_GUESS         read
$end
```

**Example 4.37** RCA_DIIS algorithm applied a radical

```
$molecule
0 2
   H    1.004123   -0.180454    0.000000
   O   -0.246002    0.596152    0.000000
   O   -1.312366   -0.230256    0.000000
$end

$rem
   UNRESTRICTED         true
   METHOD               hf
   BASIS                cc-pVDZ
   SCF_GUESS            gwh
   SCF_ALGORITHM        RCA_DIIS
   DIIS_SUBSPACE_SIZE   15
   THRESH               9
$end
```

**Example 4.38** pFON calculation of a metal cluster.

```
$molecule
   0 1
   Pt        -0.20408        1.19210        0.54029
   Pt         2.61132        1.04687        0.66196
   Pt         0.83227        0.03296       -1.49084
   Pt         0.95832       -1.05360        0.92253
   Pt        -1.66760       -1.07875       -1.02416
$end

$rem
   METHOD           pbe
   ECP              lanl2dz
   MAX_SCF_CYCLES   2000
   SYMMETRY         false
   OCCUPATIONS      2   ! pseudo-fractional occupation numbers
   FON_NORB         10
   FON_T_START      300 ! electronic temperature: 300 K
   FON_T_END        300
   FON_E_THRESH     5   ! freeze occupation numbers once DIIS error is 10^-5
$end
```

# 4.7 SCF Calculations Based on GEN_SCFMAN

## 4.7.1 Overview

GEN_SCFMAN is an object-oriented SCF job manager in Q-CHEM developed by E. J. Sundstrom, P. R. Horn and many other co-workers. Up till now, it has been able to support most of the basic features of the old SCF routines (*e.g.* restricted, unrestricted and restricted open-shell Hartree-Fock/KS-DFT calculations). Besides that, many absent features in the old SCF code are available in GEN_SCFMAN, mainly including

- Addition of several useful SCF algorithms and support of user-specified hybrid algorithm.
- More general and user-friendly internal stability analysis and automatic correction for the energy minimum.
- Support of several unconventional orbital types.

A full list of orbital types supported in GEN_SCFMAN:

- The basic ones that are supported in the old SCF code: restricted (R), unrestricted (U), restricted open-shell (RO).
- Open-shell singlet ROSCF (OS_RO, see the “ROKS" method documented in Section 6.5).
- Generalized Hartree-Fock method (G), *i.e.*, each MO is associated with both $\alpha$ and $\beta$ spin components.
- The use of complex orbitals (with Hartree-Fock only): restricted (CR), unrestricted (CU), and generalized (CG).

A list of useful SCF algorithms available in GEN_SCFMAN (each entry stands for a method that the *$rem* variable SCF_ALGORITHM can be set to):

Methods that are based on extrapolation/interpolation:

- DIIS (see Section 4.6.3, available for all orbital types).
- ADIIS (the Accelerated DIIS algorithm developed by Hu *et al.*[246], available for R and U only).

Methods that make use of orbital gradient:

- DM (re-implemented as simple steepest descent with line search, available for all orbital types).
- GDM (see Section 4.6.4, available for all orbital types).
- GDM_LS (it is essentially a preconditioned (using orbital energy differences as the preconditioner) L-BFGS algorithm with line search, available for R, U, RO and OS_RO).

Methods that require orbital Hessian:

- NEWTON_CG/NEWTON_MINRES (solve $\mathbf{Hd} = -\mathbf{g}$ for the update direction with CG/MINRES solvers).
- SF_NEWTON_CG (the “saddle-free" version of NEWTON_CG).

The analytical orbital Hessian is available for R/U/RO/G/CR unless special density functionals (*e.g.* those containing VV10) are used, while the use of finite-difference Hessian is available for all orbital types by setting FD_MAT_VEC_PROD = TRUE.

Besides these, the Maximum-Overlap Method (MOM) for excited states is also available. We note that the RCA algorithm is not available in GEN_SCFMAN yet. Nevertheless, the performance of the ADIIS algorithm should be similar to it.

Since the code in GEN_SCFMAN is highly modular, the availability of different SCF algorithms to different SCF (orbital) types is largely extended in general. For example, the old ROSCF implementation requires the use of the GWH guess and the GDM algorithm exclusively. Such a limitation has been eliminated in GEN_SCFMAN based RO calculations.

The other aspects of an SCF calculation, such as the SCF guess, the use of efficient algorithms to construct the Fock matrix like occ-RI-K (see Section 4.8.11), would not be affected by the use of GEN_SCFMAN. Also, using GEN_SCFMAN would not make any difference to the post-SCF procedures such as correlated methods, excited state calculations and evaluation of molecular properties.

It should be noted that many special features (*e.g.* dual-basis SCF, CDFT, *etc.*) based on Q-CHEM's old SCF code are not supported in GEN_SCFMAN yet. They will gradually become available in the future.

### 4.7.2 Basic GEN_SCFMAN Job Control

For standard R/U/RO calculations using GEN_SCFMAN, the setup of the input is basically identical to whatever the old SCF code requires, except that we need to set GEN_SCFMAN = TRUE.

**GEN_SCFMAN**
 Use GEN_SCFMAN for the present SCF calculation.
TYPE:
 BOOLEAN
DEFAULT:
 FALSE
OPTIONS:
 FALSE Use the old SCF code.
 TRUE Use GEN_SCFMAN.
RECOMMENDATION:
 Setting to TRUE when features in GEN_SCFMAN are needed.

**Example 4.39** Restricted SCF calculation using GEN_SCFMAN

```
molecule
   0 1
   O  -1.551007  -0.114520   0.000000
   H  -1.934259   0.762503   0.000000
   H  -0.599677   0.040712   0.000000
$end

$rem
   JOBTYPE          sp
   METHOD           wB97X-V
   BASIS            def2-tzvpd
   GEN_SCFMAN        true
   UNRESTRICTED      false
   SCF_ALGORITHM     diis
   SCF_CONVERGENCE   8
   THRESH            14
   SYMMETRY          false
   SYM_IGNORE        true
   SCF_FINAL_PRINT   1
$end
```

In the up-to-date GEN_SCFMAN, RO calculations are triggered in the same way as in the old SCF routines (when UNRESTRICTED = FALSE and the multiplicity of the system is greater than 1). Also, setting *$rem* variable ROSCF = TRUE forces GEN_SCFMAN to run an RO calculation.

**ROSCF**
Run an ROSCF calculation with GEN_SCFMAN.
TYPE:
BOOLEAN
DEFAULT:
FALSE
OPTIONS:
FALSE Let Q-CHEM automatically decide if RO is needed.
TRUE Run an ROSCF calculation forcefully.
RECOMMENDATION:
No need to set this rem for standard calculations.

**Example 4.40** Restricted open-shell SCF calculation using GEN_SCFMAN. The DIIS algorithm is employed.

```
$molecule
   0 2
   C1
   H1  C1  1.09267
   H2  C1  1.09267  H1  107.60335
   H3  C1  1.09267  H2  107.60335  H1  115.692
$end

$rem
   JOBTYPE           sp
   METHOD            wB97X-D
   BASIS             6-31+G*
   GEN_SCFMAN        true
   UNRESTRICTED      false  !this triggers the RO calculation
   MAX_SCF_CYCLES    100
   SCF_ALGORITHM     diis
   SCF_CONVERGENCE   8
   THRESH            14
   SYMMETRY          false
   SYM_IGNORE        true
   SCF_FINAL_PRINT   1
$end
```

The calculations using other more special orbital types are controlled by the following *$rem* variables (they are not effective unless GEN_SCFMAN = TRUE):

**OS_ROSCF**

Run an open-shell singlet ROSCF calculation with GEN_SCFMAN.

TYPE:

BOOLEAN

DEFAULT:

FALSE

OPTIONS:

| | |
|---|---|
| TRUE | OS_ROSCF calculation is performed. |
| FALSE | Do not run OS_ROSCF (it will run a close-shell RSCF calculation instead). |

RECOMMENDATION:

Set to TRUE if desired.

**GHF**

Run a generalized Hartree-Fock calculation with GEN_SCFMAN.

TYPE:

BOOLEAN

DEFAULT:

FALSE

OPTIONS:

| | |
|---|---|
| TRUE | Run a GHF calculation. |
| FALSE | Do not use GHF. |

RECOMMENDATION:

Set to TRUE if desired.

**COMPLEX**

Run an SCF calculation with complex MOs using GEN_SCFMAN.

TYPE:

BOOLEAN

DEFAULT:

FALSE

OPTIONS:

| | |
|---|---|
| TRUE | Use complex orbitals. |
| FALSE | Use real orbitals. |

RECOMMENDATION:

Set to TRUE if desired.

**COMPLEX_MIX**

Mix a certain percentage of the real part of the HOMO to the imaginary part of the LUMO.

TYPE:

INTEGER

DEFAULT:

0

OPTIONS:

| | |
|---|---|
| 0–100 | The mix angle = $\pi \cdot$COMPLEX_MIX/100. |

RECOMMENDATION:

It may help find the stable complex solution (similar idea as SCF_GUESS_MIX).

**Example 4.41** Restricted open-shell singlet ROSCF calculation for the first excited state of formaldehyde using GEN_SCFMAN. The first job provides the guess orbitals through a restricted SCF calculation.

```
$molecule
   0 1
   H -0.940372  0.000000  1.268098
   H  0.940372  0.000000  1.268098
   C  0.000000  0.000000  0.682557
   O  0.000000  0.000000 -0.518752
$end

$rem
   GEN_SCFMAN         true
   METHOD             wb97x-d
   BASIS              def2-svpd
   THRESH             14
   SCF_CONVERGENCE    9
   SYM_IGNORE         true
$end

@@@

$molecule
   read
$end

$rem
   JOBTYPE            sp
   METHOD             wb97x-d
   BASIS              def2-svpd
   GEN_SCFMAN         true
   OS_ROSCF           true
   THRESH             14
   SCF_CONVERGENCE    9
   SCF_ALGORITHM      diis
   SYM_IGNORE         true
   SCF_GUESS          read
$end
```

### 4.7.3 User-Customized Hybrid SCF Algorithm

It is often the case that a single algorithm is not able to guarantee SCF convergence. Meanwhile, some SCF algorithms (*e.g.* ADIIS) can accelerate convergence at the beginning of an SCF calculation but becomes less efficient near the convergence. While a few hybrid algorithms (DIIS_GDM, RCA_DIIS) have been enabled in Q-CHEM's original SCF implementation, in GEN_SCFMAN, we seek for a more flexible setup for the use of multiple SCF algorithms so that users can have a more precise control on the SCF procedure. With the current implementation, at most four distinct algorithms (usually more than enough) can be employed in one single SCF calculation based on GEN_SCFMAN, and the basic job control is as follows:

**GEN_SCFMAN_HYBRID_ALGO**

Use multiple algorithms in an SCF calculation based on GEN_SCFMAN.

TYPE:

BOOLEAN

DEFAULT:

FALSE

OPTIONS:

| | |
|---|---|
| FALSE | Use a single SCF algorithm (given by SCF_ALGORITHM). |
| TRUE | Use multiple SCF algorithms (to be specified). |

RECOMMENDATION:

Set it to TRUE when the use of more than one algorithm is desired.

**GEN_SCFMAN_ALGO_1**

The first algorithm to be used in a hybrid-algorithm calculation.

TYPE:

STRING

DEFAULT:

0

OPTIONS:

All the available SCF_ALGORITHM options, including the GEN_SCFMAN additions (Section 4.7.1).

RECOMMENDATION:

None

**GEN_SCFMAN_ITER_1**

Maximum number of iterations given to the first algorithm. If used up, switch to the next algorithm.

TYPE:

INTEGER

DEFAULT:

50

OPTIONS:

User-defined

RECOMMENDATION:

None

**GEN_SCFMAN_CONV_1**

The convergence criterion given to the first algorithm. If reached, switch to the next algorithm.

TYPE:

INTEGER

DEFAULT:

0

OPTIONS:

| | |
|---|---|
| $n$ | $10^{-n}$ |

RECOMMENDATION:

None

**Note:** *$rem* variables GEN_SCFMAN_ALGO_X, GEN_SCFMAN_ITER_X, GEN_SCFMAN_CONV_X (X = 2, 3, 4) are defined and used in a similar way.

**Example 4.42** B3LYP/3-21G calculation for a cadmium-imidazole complex using the ADIIS-DIIS algorithm (an example from Ref. 246). Due to the poor quality of the CORE guess, using a single algorithm such as DIIS or GDM fails to converge.

```
$molecule
   2 1
   Cd     0.000000     0.000000     0.000000
   N      0.000000     0.000000    -2.260001
   N     -0.685444     0.000000    -4.348035
   C      0.676053     0.000000    -4.385069
   C      1.085240     0.000000    -3.091231
   C     -1.044752     0.000000    -3.060220
   H      1.231530     0.000000    -5.300759
   H      2.088641     0.000000    -2.711077
   H     -2.068750     0.000000    -2.726515
   H     -1.313170     0.000000    -5.174718
$end

$rem
   JOBTYPE                  SP
   EXCHANGE                 B3LYP
   BASIS                    3-21g
   UNRESTRICTED             FALSE
   SYMMETRY                 FALSE
   SYM_IGNORE               TRUE
   THRESH                   14
   SCF_GUESS                CORE
   GEN_SCFMAN               TRUE
   GEN_SCFMAN_HYBRID_ALGO   TRUE
   GEN_SCFMAN_ALGO_1        ADIIS
   GEN_SCFMAN_CONV_1        3  !switch to DIIS when error < 1E-3
   GEN_SCFMAN_ITER_1        50
   GEN_SCFMAN_ALGO_2        DIIS
   GEN_SCFMAN_CONV_2        8
   GEN_SCFMAN_ITER_2        50
$end
```

### 4.7.4 Internal Stability Analysis and Automated Correction for Energy Minima

Since an SCF algorithm searches for stationary points where $\partial E/\partial\theta_{ai} = 0$, chances always exist that an unstable solution is found, for which the orbital Hessian is not positive-definite. Based on our experience, even for very simple data set such as the G2 atomization energies,[247] using the default algorithm (DIIS) produces unstable solutions for quite a few species (even for single atoms with some density functionals). In such scenarios, failure to check the internal stability of SCF solutions can result in flawed benchmark results. Although in general the use of gradient-based algorithms such as GDM is more likely to locate the true minimum, it still cannot entirely eliminate the possibility for an unstable solution to appear.

The original STABILITY_ANALYSIS method for calculations using the old SCF code has the following limitations:

- It is only available for restricted (close-shell) and unrestricted SCF calculations.

- It requires the analytical orbital Hessian of the wave function energy.
- The calculation terminates after the corrected MOs are generated, and a second job is needed to read in these orbitals and run another SCF calculation.

The implementation of internal stability analysis in GEN_SCFMAN overcomes almost all these shortcomings. Its availability has been extended to all the implemented orbital types. As in the old code, when the analytical Hessian of the given orbital type and theory (*e.g.* RO/B3LYP) is available, it computes matrix-vector products requested by the Davidson algorithm[248] analytically. If the analytical Hessian is not available, user can still run stability analysis by using the finite-difference matrix-vector product technique developed by Sharada *et al.*[249] which requires the gradient (related to the Fock matrix) only:

$$\mathbf{H}\mathbf{b}_1 = \frac{\nabla E(\mathbf{X}_0 + \xi\mathbf{b}_1) - \nabla E(\mathbf{X}_0 - \xi\mathbf{b}_1)}{2\xi} \tag{4.90}$$

where $\mathbf{H}$ is the Hessian matrix, $\mathbf{b}_1$ is a trial vector, $\mathbf{X}_0$ stands for the current stationary point, and $\xi$ is the finite step size. With this method, internal stability analysis is available for all the implemented orbital types in GEN_SCFMAN. It should be noted that since the second derivative of NLC functionals such as VV10 is not available in Q-CHEM, this finite-difference method will be used by default for the evaluation of Hessian-vector products, while the old STABILITY_ANALYSIS method is not capable of handling functionals that contain NLC.

Meanwhile, GEN_SCFMAN allows multiple SCF calculations + stability analyses to be performed in a single job so that it can make use of the corrected MOs and locate the true minimum automatically. As in the old implementation, the MOs are displaced along the direction of the lowest-energy eigenvector (with line search) if an SCF solution is found to be unstable. A new SCF calculation that reads in these corrected MOs as initial guess will be launched automatically if INTERNAL_STABILITY_ITER > 0. Such macro-loops will keep going until a stable solution is reached.

**INTERNAL_STABILITY**
Perform internal stability analysis in GEN_SCFMAN.
TYPE:
BOOLEAN
DEFAULT:
FALSE
OPTIONS:
FALSE Do not perform internal stability analysis after convergence.
TRUE Perform internal stability analysis and generate the corrected MOs.
RECOMMENDATION:
Turn it on when the SCF solution is prone to unstable solutions, especially for open-shell species.

**FD_MAT_VEC_PROD**

Compute Hessian-vector product using the finite difference technique.

TYPE:

BOOLEAN

DEFAULT:

FALSE (TRUE when the employed functional contains NLC)

OPTIONS:

| | |
|---|---|
| FALSE | Compute Hessian-vector product analytically. |
| TRUE | Use finite difference to compute Hessian-vector product. |

RECOMMENDATION:

Set it to TRUE when analytical Hessian is not available.

**Note:** For simple R and U calculations, it can always be set to FALSE, which indicates that only the NLC part will be computed with finite difference.

**INTERNAL_STABILITY_ITER**

Maximum number of new SCF calculations permitted after the first stability analysis is performed.

TYPE:

INTEGER

DEFAULT:

0 (automatically set to 1 if INTERNAL_STABILITY = TRUE)

OPTIONS:

| | |
|---|---|
| $n$ | $n$ new SCF calculations permitted. |

RECOMMENDATION:

Give a larger number if 1 is not enough (still unstable).

**INTERNAL_STABILITY_DAVIDSON_ITER**

Maximum number of Davidson iterations allowed in one stability analysis.

TYPE:

INTEGER

DEFAULT:

50

OPTIONS:

| | |
|---|---|
| $n$ | Perform up to $n$ Davidson iterations. |

RECOMMENDATION:

Use the default.

**INTERNAL_STABILITY_CONV**

Convergence criterion for the Davidson solver (for the lowest eigenvalues).

TYPE:

INTEGER

DEFAULT:

4 (3 when FD_MAT_ON_VECS = TRUE)

OPTIONS:

| | |
|---|---|
| $n$ | Terminate Davidson iterations when the norm of the residual vector is below $10^{-n}$. |

RECOMMENDATION:

Use the default.

**INTERNAL_STABILITY_ROOTS**

Number of lowest Hessian eigenvalues to solve for.

TYPE:

INTEGER

DEFAULT:

2

OPTIONS:

$n$ Solve for $n$ lowest eigenvalues.

RECOMMENDATION:

Use the default.

**Example 4.43** Unrestricted SCF calculation of triplet $B_2$ using B97M-V/6-31g with the GDM algorithm. A displacement is performed when the first solution is characterized as a saddle point, and the second SCF gives a stable solution.

```
$molecule
   0 3
   b
   b 1 R

   R = 1.587553
$end

$rem
   JOBTYPE             sp
   METHOD              b97m-v
   BASIS               6-31g
   GEN_SCFMAN          true
   UNRESTRICTED        true
   THRESH              14
   SYMMETRY            false
   SYM_IGNORE          true
   SCF_FINAL_PRINT     1
   SCF_ALGORITHM       gdm
   SCF_CONVERGENCE     9
   INTERNAL_STABILITY  true  !turn on internal stability analysis
   FD_MAT_VEC_PROD     false !use finite-diff for the vv10 part only
$end
```

## 4.8 Large Molecules and Linear Scaling Methods

### 4.8.1 Introduction

Construction of the effective Hamiltonian, or Fock matrix, has traditionally been the rate-determining step in self-consistent field calculations, due primarily to the cost of two-electron integral evaluation, even with the efficient methods available in Q-CHEM (see Appendix B). However, for large enough molecules, significant speedups are possible by employing linear-scaling methods for each of the nonlinear terms that can arise. Linear scaling means that if the molecule size is doubled, then the computational effort likewise only doubles. There are three computationally significant terms:

- Electron-electron Coulomb interactions, for which Q-CHEM incorporates the Continuous Fast Multipole Method (CFMM) discussed in section 4.8.2
- Exact exchange interactions, which arise in hybrid DFT calculations and Hartree-Fock calculations, for which Q-CHEM incorporates the LinK method discussed in section 4.8.3 below.
- Numerical integration of the exchange and correlation functionals in DFT calculations, which we have already discussed in section 4.4.5.

Q-CHEM supports energies and efficient analytical gradients for all three of these high performance methods to permit structure optimization of large molecules, as well as relative energy evaluation. Note that analytical second derivatives of SCF energies do not exploit these methods at present.

For the most part, these methods are switched on automatically by the program based on whether they offer a significant speedup for the job at hand. Nevertheless it is useful to have a general idea of the key concepts behind each of these algorithms, and what input options are necessary to control them. That is the primary purpose of this section, in addition to briefly describing two more conventional methods for reducing computer time in large calculations in Section 4.8.4.

There is one other computationally significant step in SCF calculations, and that is diagonalization of the Fock matrix, once it has been constructed. This step scales with the cube of molecular size (or basis set size), with a small pre-factor. So, for large enough SCF calculations (very roughly in the vicinity of 2000 basis functions and larger), diagonalization becomes the rate-determining step. The cost of cubic scaling with a small pre-factor at this point exceeds the cost of the linear scaling Fock build, which has a very large pre-factor, and the gap rapidly widens thereafter. This sets an effective upper limit on the size of SCF calculation for which Q-CHEM is useful at several thousand basis functions.

### 4.8.2 Continuous Fast Multipole Method (CFMM)

The quantum chemical Coulomb problem, perhaps better known as the DFT bottleneck, has been at the forefront of many research efforts throughout the 1990s. The quadratic computational scaling behavior conventionally seen in the construction of the Coulomb matrix in DFT or HF calculations has prevented the application of *ab initio* methods to molecules containing many hundreds of atoms. Q-CHEM, Inc., in collaboration with White and Head-Gordon at the University of California at Berkeley, and Gill now at the Australian National University, were the first to develop the generalization of Greengard's Fast Multipole Method (FMM)[250] to Continuous charged matter distributions in the form of the CFMM, which is the first linear scaling algorithm for DFT calculations. This initial breakthrough has since lead to an increasing number of linear scaling alternatives and analogies, but for Coulomb interactions, the CFMM remains state of the art. There are two computationally intensive contributions to the Coulomb interactions which we discuss in turn:

- Long-range interactions, which are treated by the CFMM
- Short-range interactions, corresponding to overlapping charge distributions, which are treated by a specialized "J-matrix engine" together with Q-CHEM's state-of-the art two-electron integral methods.

The Continuous Fast Multipole Method was the first implemented linear scaling algorithm for the construction of the **J** matrix. In collaboration with Q-CHEM, Inc., Dr. Chris White began the development of the CFMM by more efficiently deriving[251] the original Fast Multipole Method before generalizing it to the CFMM[252]. The generalization applied by White *et al.* allowed the principles underlying the success of the FMM to be applied to *arbitrary* (subject to constraints in evaluating the related integrals) continuous, but localized, matter distributions. White and co-workers further improved the underlying CFMM algorithm[253,254] then implemented it efficiently[255], achieving performance that is an order of magnitude faster than some competing implementations.

The success of the CFMM follows similarly with that of the FMM, in that the charge system is subdivided into a hierarchy of boxes. Local charge distributions are then systematically organized into multipole representations so that each distribution interacts with local expansions of the potential due to all distant charge distributions. Local and distant distributions are distinguished by a well-separated (WS) index, which is the number of boxes that must separate two collections of charges before they may be considered distant and can interact through multipole expansions; near-field interactions must be calculated directly. In the CFMM each distribution is given its own WS index and is sorted on the basis of the WS index, and the position of their space centers. The implementation in Q-CHEM has allowed the efficiency gains of contracted basis functions to be maintained.

The CFMM algorithm can be summarized in five steps:

1. Form and translate multipoles.
2. Convert multipoles to local Taylor expansions.
3. Translate Taylor information to the lowest level.
4. Evaluate Taylor expansions to obtain the far-field potential.
5. Perform direct interactions between overlapping distributions.

Accuracy can be carefully controlled by due consideration of tree depth, truncation of the multipole expansion and the definition of the extent of charge distributions in accordance with a rigorous mathematical error bound. As a rough guide, 10 poles are adequate for single point energy calculations, while 25 poles yield sufficient accuracy for gradient calculations. Subdivision of boxes to yield a one-dimensional length of about 8 boxes works quite well for systems of up to about one hundred atoms. Larger molecular systems, or ones which are extended along one dimension, will benefit from an increase in this number. The program automatically selects an appropriate number of boxes by default.

For the evaluation of the remaining short-range interactions, Q-CHEM incorporates efficient J-matrix engines, originated by White and Head-Gordon[256]. These are analytically exact methods that are based on standard two-electron integral methods, but with an interesting twist. If one knows that the two-electron integrals are going to be summed into a Coulomb matrix, one can ask whether they are in fact the most efficient intermediates for this specific task. Or, can one instead find a more compact and computationally efficient set of intermediates by folding the density matrix into the recurrence relations for the two-electron integrals. For integrals that are not highly contracted (*i.e.*, are not linear combinations of more than a few Gaussians), the answer is a dramatic yes. This is the basis of the J-matrix approach, and Q-CHEM includes the latest algorithm developed by Yihan Shao working with Martin Head-Gordon at Berkeley for this purpose. Shao's J-engine is employed for both energies[257] and forces[258] and gives substantial speedups relative to the use of two-electron integrals without any approximation (roughly a factor of 10 (energies) and 30 (forces) at the level of an uncontracted *dddd* shell quartet, and increasing with angular momentum). Its use is automatically selected for integrals with low degrees of contraction, while regular integrals are employed when the degree of contraction is high, following the state of the art PRISM approach of Gill and co-workers[259].

The CFMM is controlled by the following input parameters:

**CFMM_ORDER**

Controls the order of the multipole expansions in CFMM calculation.

TYPE:

INTEGER

DEFAULT:

| | |
|---|---|
| 15 | For single point SCF accuracy |
| 25 | For tighter convergence (optimizations) |

OPTIONS:

| | |
|---|---|
| $n$ | Use multipole expansions of order $n$ |

RECOMMENDATION:

Use the default.

**GRAIN**

Controls the number of lowest-level boxes in one dimension for CFMM.

TYPE:

INTEGER

DEFAULT:

| | |
|---|---|
| -1 | Program decides best value, turning on CFMM when useful |

OPTIONS:

| | |
|---|---|
| -1 | Program decides best value, turning on CFMM when useful |
| 1 | Do not use CFMM |
| $n \geq 8$ | Use CFMM with $n$ lowest-level boxes in one dimension |

RECOMMENDATION:

This is an expert option; either use the default, or use a value of 1 if CFMM is not desired.

### 4.8.3 Linear Scaling Exchange (LinK) Matrix Evaluation

Hartree-Fock calculations and the popular hybrid density functionals such as B3LYP also require two-electron integrals to evaluate the exchange energy associated with a single determinant. There is no useful multipole expansion for the exchange energy, because the bra and ket of the two-electron integral are coupled by the density matrix, which carries the effect of exchange. Fortunately, density matrix elements decay exponentially with distance for systems that have a HOMO-LUMO gap[260]. The better the insulator, the more localized the electronic structure, and the faster the rate of exponential decay. Therefore, for insulators, there are only a linear number of numerically significant contributions to the exchange energy. With intelligent numerical thresholding, it is possible to rigorously evaluate the exchange matrix in linear scaling effort. For this purpose, Q-CHEM contains the linear scaling K (LinK) method[261] to evaluate both exchange energies and their gradients[262] in linear scaling effort (provided the density matrix is highly sparse). The LinK method essentially reduces to the conventional direct SCF method for exchange in the small molecule limit (by adding no significant overhead), while yielding large speedups for (very) large systems where the density matrix is indeed highly sparse. For full details, we refer the reader to the original papers[261,262]. LinK can be explicitly requested by the following option (although Q-CHEM automatically switches it on when the program believes it is the preferable algorithm).

**LIN_K**

Controls whether linear scaling evaluation of exact exchange (LinK) is used.

TYPE:

LOGICAL

DEFAULT:

Program chooses, switching on LinK whenever CFMM is used.

OPTIONS:

| | |
|---|---|
| TRUE | Use LinK |
| FALSE | Do not use LinK |

RECOMMENDATION:

Use for HF and hybrid DFT calculations with large numbers of atoms.

### 4.8.4 Incremental and Variable Thresh Fock Matrix Building

The use of a variable integral threshold, operating for the first few cycles of an SCF, is justifiable on the basis that the MO coefficients are usually of poor quality in these cycles. In Q-CHEM, the integrals in the first iteration are calculated at a threshold of $10^{-6}$ (for an anticipated final integral threshold greater than, or equal to $10^{-6}$) to ensure the error in the first iteration is solely sourced from the poor MO guess. Following this, the integral threshold used is computed as

$$tmp\_thresh = varthresh \times DIIS\_error \tag{4.91}$$

where the $DIIS\_error$ is that calculated from the previous cycle, $varthresh$ is the variable threshold set by the program (by default) and $tmp\_thresh$ is the temporary threshold used for integral evaluation. Each cycle requires recalculation of all integrals. The variable integral threshold procedure has the greatest impact in early SCF cycles.

In an incremental Fock matrix build[263], $\mathbf{F}$ is computed recursively as

$$\mathbf{F^m} = \mathbf{F^{m-1}} + \Delta\mathbf{J^{m-1}} - \frac{1}{2}\Delta\mathbf{K^{m-1}} \tag{4.92}$$

where $m$ is the SCF cycle, and $\Delta\mathbf{J}^m$ and $\Delta\mathbf{K}^m$ are computed using the difference density

$$\Delta\mathbf{P^m} = \mathbf{P^m} - \mathbf{P^{m-1}} \tag{4.93}$$

Using Schwartz integrals and elements of the difference density, Q-CHEM is able to determine at each iteration which ERIs are required, and if necessary, recalculated. As the SCF nears convergence, $\Delta\mathbf{P}^m$ becomes sparse and the number of ERIs that need to be recalculated declines dramatically, saving the user large amounts of computational time.

Incremental Fock matrix builds and variable thresholds are only used when the SCF is carried out using the direct SCF algorithm and are clearly complementary algorithms. These options are controlled by the following input parameters, which are only used with direct SCF calculations.

**INCFOCK**

Iteration number after which the incremental Fock matrix algorithm is initiated

TYPE:

INTEGER

DEFAULT:

1 Start INCFOCK after iteration number 1

OPTIONS:

User-defined (0 switches INCFOCK off)

RECOMMENDATION:

May be necessary to allow several iterations before switching on INCFOCK.

**VARTHRESH**

Controls the temporary integral cut-off threshold. $tmp\_thresh = 10^{-\text{VARTHRESH}} \times DIIS\_error$

TYPE:

INTEGER

DEFAULT:

0 Turns VARTHRESH off

OPTIONS:

$n$ User-defined threshold

RECOMMENDATION:

3 has been found to be a practical level, and can slightly speed up SCF evaluation.

### 4.8.5 Incremental DFT

Incremental DFT (IncDFT) uses the difference density and functional values to improve the performance of the DFT quadrature procedure by providing a better screening of negligible values. Using this option will yield improved efficiency at each successive iteration due to more effective screening.

**INCDFT**

Toggles the use of the IncDFT procedure for DFT energy calculations.

TYPE:

LOGICAL

DEFAULT:

TRUE

OPTIONS:

FALSE Do not use IncDFT

TRUE Use IncDFT

RECOMMENDATION:

Turning this option on can lead to faster SCF calculations, particularly towards the end of the SCF. Please note that for some systems use of this option may lead to convergence problems.

**INCDFT_DENDIFF_THRESH**

Sets the threshold for screening density matrix values in the IncDFT procedure.

TYPE:

INTEGER

DEFAULT:

SCF_CONVERGENCE + 3

OPTIONS:

$n$ Corresponding to a threshold of $10^{-n}$.

RECOMMENDATION:

If the default value causes convergence problems, set this value higher to tighten the threshold.

**INCDFT_GRIDDIFF_THRESH**

Sets the threshold for screening functional values in the IncDFT procedure

TYPE:

INTEGER

DEFAULT:

SCF_CONVERGENCE + 3

OPTIONS:

$n$ Corresponding to a threshold of $10^{-n}$.

RECOMMENDATION:

If the default value causes convergence problems, set this value higher to tighten the threshold.

**INCDFT_DENDIFF_VARTHRESH**

Sets the lower bound for the variable threshold for screening density matrix values in the IncDFT procedure. The threshold will begin at this value and then vary depending on the error in the current SCF iteration until the value specified by INCDFT_DENDIFF_THRESH is reached. This means this value must be set lower than INCDFT_DENDIFF_THRESH.

TYPE:

INTEGER

DEFAULT:

0 Variable threshold is not used.

OPTIONS:

$n$ Corresponding to a threshold of $10^{-n}$.

RECOMMENDATION:

If the default value causes convergence problems, set this value higher to tighten accuracy. If this fails, set to 0 and use a static threshold.

**INCDFT_GRIDDIFF_VARTHRESH**

Sets the lower bound for the variable threshold for screening the functional values in the IncDFT procedure. The threshold will begin at this value and then vary depending on the error in the current SCF iteration until the value specified by INCDFT_GRIDDIFF_THRESH is reached. This means that this value must be set lower than INCDFT_GRIDDIFF_THRESH.

TYPE:

INTEGER

DEFAULT:

0 Variable threshold is not used.

OPTIONS:

$n$ Corresponding to a threshold of $10^{-n}$.

RECOMMENDATION:

If the default value causes convergence problems, set this value higher to tighten accuracy. If this fails, set to 0 and use a static threshold.

### 4.8.6 Fourier Transform Coulomb Method

The Coulomb part of the DFT calculations using ordinary Gaussian representations can be sped up dramatically using plane waves as a secondary basis set by replacing the most costly analytical electron repulsion integrals with numerical integration techniques. The main advantages to keeping the Gaussians as the primary basis set is that the diagonalization step is much faster than using plane waves as the primary basis set, and all electron calculations can be performed analytically.

The Fourier Transform Coulomb (FTC) technique[264,265] is precise and tunable and all results are practically identical with the traditional analytical integral calculations. The FTC technique is at least 2–3 orders of magnitude more accurate then other popular plane wave based methods using the same energy cutoff. It is also at least 2–3 orders of magnitude more accurate than the density fitting (resolution-of-identity) technique. Recently, an efficient way to implement the forces of the Coulomb energy was introduced[266], and a new technique to localize filtered core functions. Both of these features have been implemented within Q-CHEM and contribute to the efficiency of the method.

The FTC method achieves these spectacular results by replacing the analytical integral calculations, whose computational costs scales as $\mathcal{O}(N^4)$ (where $N$ is the number of basis function) with procedures that scale as only $\mathcal{O}(N^2)$. The asymptotic scaling of computational costs with system size is linear versus the analytical integral evaluation which is quadratic. Research at Q-CHEM Inc. has yielded a new, general, and very efficient implementation of the FTC method which work in tandem with the J-engine and the CFMM (Continuous Fast Multipole Method) techniques[267].

In the current implementation the speed-ups arising from the FTC technique are moderate when small or medium Pople basis sets are used. The reason is that the J-matrix engine and CFMM techniques provide an already highly efficient solution to the Coulomb problem. However, increasing the number of polarization functions and, particularly, the number of diffuse functions allows the FTC to come into its own and gives the most significant improvements. For instance, using the 6-311G+(df,pd) basis set for a medium-to-large size molecule is more affordable today then before. We found also significant speed ups when non–Pople basis sets are used such as cc-pvTZ. The FTC energy and gradients calculations are implemented to use up to $f$-type basis functions.

**FTC**

Controls the overall use of the FTC.

TYPE:

INTEGER

DEFAULT:

0

OPTIONS:

0 Do not use FTC in the Coulomb part

1 Use FTC in the Coulomb part

RECOMMENDATION:

Use FTC when bigger and/or diffuse basis sets are used.

**FTC_SMALLMOL**

Controls whether or not the operator is evaluated on a large grid and stored in memory to speed up the calculation.

TYPE:

INTEGER

DEFAULT:

1

OPTIONS:

1 Use a big pre-calculated array to speed up the FTC calculations

0 Use this option to save some memory

RECOMMENDATION:

Use the default if possible and use 0 (or buy some more memory) when needed.

**FTC_CLASS_THRESH_ORDER**

Together with FTC_CLASS_THRESH_MULT, determines the cutoff threshold for included a shell-pair in the $dd$ class, *i.e.*, the class that is expanded in terms of plane waves.

TYPE:

INTEGER

DEFAULT:

5 Logarithmic part of the FTC classification threshold. Corresponds to $10^{-5}$

OPTIONS:

$n$ User specified

RECOMMENDATION:

Use the default.

**FTC_CLASS_THRESH_MULT**

Together with FTC_CLASS_THRESH_ORDER, determines the cutoff threshold for included a shell-pair in the $dd$ class, *i.e.*, the class that is expanded in terms of plane waves.

TYPE:

INTEGER

DEFAULT:

5 Multiplicative part of the FTC classification threshold. Together with the default value of the FTC_CLASS_THRESH_ORDER this leads to the $5 \times 10^{-5}$ threshold value.

OPTIONS:

$n$ User specified.

RECOMMENDATION:

Use the default. If diffuse basis sets are used and the molecule is relatively big then tighter FTC classification threshold has to be used. According to our experiments using Pople-type diffuse basis sets, the default $5 \times 10^{-5}$ value provides accurate result for an alanine5 molecule while $1 \times 10^{-5}$ threshold value for alanine10 and $5 \times 10^{-6}$ value for alanine15 has to be used.

### 4.8.7 Multi-resolution Exchange-Correlation (MRXC) Method

MRXC (multi-resolution exchange-correlation)[268–270] is a new method developed by the Q-CHEM development team for the accelerating the computation of exchange-correlation (XC) energy and matrix originated from the XC functional. As explained in 4.8.6, the XC functional is so complicated that the integration of it is usually done on a numerical quadrature. There are two basic types of quadrature. One is the atom-centered grid (ACG), a superposition of atomic quadrature described in 4.8.6. The ACG has high density of points near the nucleus to handle the compact core density and low density of points in the valence and non-bonding region where the electron density is smooth. The other type is even-spaced cubic grid (ESCG), which is typically used together with pseudopotentials and plane-wave basis functions where only the valence and non-bonded electron density is assumed smooth. In quantum chemistry, an ACG is more often used as it can handle accurately all-electron calculations of molecules. MRXC combines those two integration schemes seamlessly to achieve an optimal computational efficiency by placing the calculation of the smooth part of the density and XC matrix onto the ESCG. The computation associated with the smooth fraction of the electron density is the major bottleneck of the XC part of a DFT calculation and can be done at a much faster rate on the ESCG due to its low resolution. Fast Fourier transform and B-spline interpolation are employed for the accurate transformation between the two types of grids such that the final results remain the same as they would be on the ACG alone. Yet, a speed-up of several times for the calculations of electron-density and XC matrix is achieved. The smooth part of the calculation with MRXC can also be combined with FTC (see section 4.8.6) to achieve further gain of efficiency.

**MRXC**

Controls the use of MRXC.

TYPE:

INTEGER

DEFAULT:

0

OPTIONS:

0 Do not use MRXC

1 Use MRXC in the evaluation of the XC part

RECOMMENDATION:

MRXC is very efficient for medium and large molecules, especially when medium and large basis sets are used.

The following two keywords control the smoothness precision. The default value is carefully selected to maintain high accuracy.

**MRXC_CLASS_THRESH_MULT**

Controls the of smoothness precision

TYPE:

INTEGER

DEFAULT:

1

OPTIONS:

$im$ An integer

RECOMMENDATION:

A prefactor in the threshold for MRXC error control: $im \times 10^{-io}$

**MRXC_CLASS_THRESH_ORDER**

Controls the of smoothness precision

TYPE:

INTEGER

DEFAULT:

6

OPTIONS:

$io$ An integer

RECOMMENDATION:

The exponent in the threshold of the MRXC error control: $im \times 10^{-io}$

The next keyword controls the order of the B-spline interpolation:

**LOCAL_INTERP_ORDER**
Controls the order of the B-spline
TYPE:
INTEGER
DEFAULT:
6
OPTIONS:
$n$ An integer
RECOMMENDATION:
The default value is sufficiently accurate

### 4.8.8 Resolution of the Identity Fock Matrix Methods

Evaluation of the Fock matrix (both Coulomb, J, and exchange, K, pieces) can be sped up by an approximation known as the resolution-of-the-identity approximation (RI-JK). Essentially, the full complexity in common basis sets required to describe chemical bonding is not necessary to describe the mean-field Coulomb and exchange interactions between electrons. That is, $\rho$ in the left side of

$$(\mu\nu|\rho) = \sum_{\lambda\sigma}(\mu\nu|\lambda\sigma)\mathbf{P}_{\lambda\sigma} \tag{4.94}$$

is much less complicated than an individual $\lambda\sigma$ function pair. The same principle applies to the FTC method in subsection 4.8.6, in which case the slowly varying piece of the electron density is replaced with a plane-wave expansion.

With the RI-JK approximation, the Coulomb interactions of the function pair $\rho(r) = \lambda\sigma(r)P_{\lambda\sigma}$ are fit by a smaller set of atom-centered basis functions. In terms of J:

$$\sum_{\lambda\sigma}\int \mathrm{d}^3\mathbf{r}_1 P_{\lambda\sigma}\lambda\sigma(\mathbf{r}_1)\frac{1}{|\mathbf{r}_1-\mathbf{r}|} \approx \sum_{K}\int \mathrm{d}^3\mathbf{r}_1 P_K K(\mathbf{r}_1)\frac{1}{|\mathbf{r}_1-\mathbf{r}|} \tag{4.95}$$

The coefficients $P_K$ must be determined to accurately represent the potential. This is done by performing a least-squared minimization of the difference between $P_{\lambda\sigma}\lambda\sigma(\mathbf{r}_1)$ and $P_K K(\mathbf{r}_1)$, *with differences measured by the Coulomb metric*. This requires a matrix inversion over the space of auxiliary basis functions, which may be done rapidly by Cholesky decomposition.

The RI method applied to the Fock matrix may be further enhanced by performing *local* fitting of a density or function pair element. This is the basis of the atomic-RI method (ARI), which has been developed for both Coulomb (J) matrix[271] and exchange (K) matrix evaluation[272]. In ARI, only nearby auxiliary functions $K(\mathbf{r})$ are employed to fit the target function. This reduces the asymptotic scaling of the matrix-inversion step as well as that of many intermediate steps in the digestion of RI integrals. Briefly, atom-centered auxiliary functions on nearby atoms are only used if they are within the "outer" radius ($R_1$) of the fitting region. Between $R_1$ and the "inner" radius ($R_0$), the amplitude of interacting auxiliary functions is smoothed by a function that goes from zero to one and has continuous derivatives. To optimize efficiency, the van der Waals radius of the atom is included in the cutoff so that smaller atoms are dropped from the fitting radius sooner. The values of $R_0$ and $R_1$ are specified as REM variables as described below.

**RI_J**

Toggles the use of the RI algorithm to compute J.

TYPE:

LOGICAL

DEFAULT:

FALSE RI will not be used to compute J.

OPTIONS:

TRUE Turn on RI for J.

RECOMMENDATION:

For large (especially 1D and 2D) molecules the approximation may yield significant improvements in Fock evaluation time when used with ARI.

**RI_K**

Toggles the use of the RI algorithm to compute K.

TYPE:

LOGICAL

DEFAULT:

FALSE RI will not be used to compute K.

OPTIONS:

TRUE Turn on RI for K.

RECOMMENDATION:

For large (especially 1D and 2D) molecules the approximation may yield significant improvements in Fock evaluation time when used with ARI.

**ARI**

Toggles the use of the atomic resolution-of-the-identity (ARI) approximation.

TYPE:

LOGICAL

DEFAULT:

FALSE ARI will not be used by default for an RI-JK calculation.

OPTIONS:

TRUE Turn on ARI.

RECOMMENDATION:

For large (especially 1D and 2D) molecules the approximation may yield significant improvements in Fock evaluation time.

**ARI_R0**

Determines the value of the inner fitting radius (in Ångstroms)

TYPE:

INTEGER

DEFAULT:

4 A value of 4 Å will be added to the atomic van der Waals radius.

OPTIONS:

$n$ User defined radius.

RECOMMENDATION:

For some systems the default value may be too small and the calculation will become unstable.

**ARI_R1**

Determines the value of the outer fitting radius (in Ångstroms)

TYPE:

INTEGER

DEFAULT:

5 A value of 5 Å will be added to the atomic van der Waals radius.

OPTIONS:

$n$ User defined radius.

RECOMMENDATION:

For some systems the default value may be too small and the calculation will become unstable. This value also determines, in part, the smoothness of the potential energy surface.

### 4.8.9 PARI-K Fast Exchange Algorithm

PARI-K[273] is an algorithm that significantly accelerates the construction of the exchange matrix in Hartree-Fock and hybrid density functional theory calculations with large basis sets. The speedup is made possible by fitting products of atomic orbitals using only auxiliary basis functions found on their respective atoms. The PARI-K implementation in Q-CHEM is an efficient MO-basis formulation similar to the AO-basis formulation of Merlot *et al.*[274]. PARI-K is highly recommended for calculations using basis sets of size augmented triple-zeta or larger, and should be used in conjunction with the standard RI-J algorithm[275] for constructing the Coulomb matrix. The exchange fitting basis sets of Weigend (cc-pVTZ-JK and cc-pVQZ-JK)[275] are recommended for use in conjunction with PARI-K. The errors associated with the PARI-K approximation appear to be only slightly worse than standard RI-HF[274].

**PARI_K**

Controls the use of the PARI-K approximation in the construction of the exchange matrix

TYPE:

LOGICAL

DEFAULT:

FALSE Do not use PARI-K.

OPTIONS:

TRUE Use PARI-K.

RECOMMENDATION:

Use for basis sets aug-cc-pVTZ and larger.

### 4.8.10 CASE Approximation

The Coulomb Attenuated Schrödinger Equation (CASE)[276] approximation follows from the KWIK[277] algorithm in which the Coulomb operator is separated into two pieces using the error function, Eq. (4.41). Whereas in Section 4.4.6 this partition of the Coulomb operator was used to incorporate long-range Hartree-Fock exchange into DFT, within the CASE approximation it is used to attenuate all occurrences of the Coulomb operator in Eq. (4.2), by neglecting the long-range portion of the identity in Eq. (4.41). The parameter $\omega$ in Eq. (4.41) is used to tune the level of attenuation. Although the total energies from Coulomb attenuated calculations are significantly different from non-attenuated energies, it is found that relative energies, correlation energies and, in particular, wave functions, are not, provided a reasonable value of $\omega$ is chosen.

By virtue of the exponential decay of the attenuated operator, ERIs can be neglected on a proximity basis yielding a rigorous $\mathcal{O}(N)$ algorithm for single point energies. CASE may also be applied in geometry optimizations and frequency calculations.

**OMEGA**
Controls the degree of attenuation of the Coulomb operator.
TYPE:
INTEGER
DEFAULT:
No default
OPTIONS:
$n$ Corresponding to $\omega = n/1000$, in units of bohr$^{-1}$
RECOMMENDATION:
None

**INTEGRAL_2E_OPR**
Determines the two-electron operator.
TYPE:
INTEGER
DEFAULT:
-2 Coulomb Operator.
OPTIONS:
-1 Apply the CASE approximation.
-2 Coulomb Operator.
RECOMMENDATION:
Use the default unless the CASE operator is desired.

### 4.8.11 occ-RI-K Exchange Algorithm

The occupied orbital RI-K (occ-RI-K)[278] is a new scheme for building the exchange matrix (K) partially in the MO basis using the RI approximation. occ-RI-K typically matches current alternatives in terms of both the accuracy (energetics identical to standard RI-K) and convergence (essentially unchanged relative to conventional methods). On the other hand, this algorithm exhibits significant speedups over conventional integral evaluation (14x) and standard RI-K (3.3x) for a test system, a graphene fragment ($C_{68}H_{22}$) using cc-pVQZ basis set (4400 basis functions), whereas the speedup increases with the size of the AO basis set. Thus occ-RI-K helps to make larger basis set hybrid DFT calculations more feasible, which is quite desirable for achieving improved accuracy in DFT calculations with modern functionals.

The idea of the occ-RI-K formalism comes from a simple observation that the exchange energy $E_K$ and its gradient can be evaluated from the diagonal elements of the exchange matrix in the occupied-occupied block $K_{ii}$, and occupied-virtual block $K_{ia}$, respectively, rather than the full matrix in the AO representation, $K_{\mu\nu}$. Mathematically,

$$E_K = -\sum_{\mu\nu} P_{\mu\nu} K_{\mu\nu} = -\sum_{\mu\nu} c_{\mu i} K_{\mu\nu} c_{\nu i} = -\sum_i K_{ii} \tag{4.96}$$

and

$$\frac{\partial E_K}{\partial \Delta_{ai}} = 2K_{ai} \tag{4.97}$$

where $\Delta$ is a skew-symmetric matrix used to parameterize the unitary transformation $U$, which represents the variations of the MO coefficients as follows:

$$U = e^{(\Delta - \Delta^T)}. \tag{4.98}$$

From Eq. 4.96 and 4.97 it is evident that the exchange energy and gradient need just $K_{i\nu}$ rather than $K_{\mu\nu}$.

In regular RI-K[275] one has to compute two quartic terms, whereas there are three quartic terms for the occ-RI-K algorithm. The speedup of the latter with respect to former can be explained from the following ratio of operations (refer to[278] for detail),

$$\frac{\text{\# of RI-K quartic operations}}{\text{\# of occ-RI-K quartic operations}} = \frac{oNX^2 + oN^2X}{o^2X^2 + o^2NX + o^2NX} = \frac{N(X+N)}{o(X+2N)} \tag{4.99}$$

With a conservative approximation of $X \approx 2N$, the speedup is $\frac{3}{4}(N/o)$. The occ-RI-K algorithm also involves some cubic steps which should be negligible in the very large molecule limit. Tests in the Ref. 278 suggest that occ-RI-K for small systems with large basis will gain less speed than a large system with small basis, because the cubic terms will be more dominant for the former than the latter case.

In the course of SCF iteration, the occ-RI-K method does not require us to construct the exact Fock matrix explicitly. Rather, $k_{i\nu}$ contributes to the Fock matrix in the mixed MO and AO representations ($F_{i\nu}$) and yields orbital gradient and DIIS error vectors for converging SCF. On the other hand, since occ-RI-K does not provide exactly the same unoccupied eigenvalues, the diagonalization updates can differ from the conventional SCF procedure. In Ref. 278, occ-RI-K was found to require, on average, the same number of SCF iterations to converge and to yield accurate energies.

**OCC_RI_K**

Controls the use of the occ-RI-K approximation for constructing the exchange matrix

TYPE:

LOGICAL

DEFAULT:

False Do not use occ-RI-K.

OPTIONS:

True Use occ-RI-K.

RECOMMENDATION:

Larger the system, better the performance

#### 4.8.11.1 occ-RI-K for exchange energy gradient evaluation

A very attractive feature of occ-RI-K framework is that one can compute the exchange energy gradient with respect to nuclear coordinates with the same leading quartic-scaling operations as the energy calculation.

The occ-RI-K formulation yields the following formula for the gradient of exchange energy in global Coulomb-metric RI:

$$\begin{aligned} E_K^x &= (ij|ij)^x \\ &= \sum_{\mu\nu P}\sum_{ij} c_{\mu i} c_{\nu j} C_{ij}^P (\mu\nu|P)^x - \sum_{RS}\sum_{ij} C_{ij}^R C_{ij}^S (R|S)^x. \end{aligned} \tag{4.100}$$

The superscript $x$ represents the derivative with respect to a nuclear coordinate. Note that the derivatives of the MO coefficients $c_{\mu i}$ are not included here, because they are already included in the total energy derivative calculation by Q-CHEM via the derivative of the overlap matrix.

In Eq. 4.100, the construction of the density fitting coefficients ($C^P_{\mu\nu}$) has the worst scaling of $\mathcal{O}(M^4)$ because it involves MO to AO back transformations:

$$C^P_{\mu\nu} = \sum_{ij} c_{\mu i} c_{\nu j} C^P_{ij} \tag{4.101}$$

where the operation cost is $o^2NX + o$[NB2]$X$.

**RI_K_GRAD**
Turn on the nuclear gradient calculations
TYPE:
LOGICAL
DEFAULT:
FALSE Do not invoke occ-RI-K based gradient
OPTIONS:
TRUE Use occ-RI-K based gradient
RECOMMENDATION:
Use "RI_J false"

### 4.8.12 Examples

**Example 4.44** Q-CHEM input for a large single point energy calculation. The CFMM is switched on automatically when LinK is requested.

```
$comment
   HF/3-21G single point calculation on a large molecule
   read in the molecular coordinates from file
$end

$molecule
   read dna.inp
$end

$rem
   METHOD     HF      Hartree-Fock
   BASIS      3-21G   Basis set
   LIN_K      TRUE    Calculate K using LinK
$end
```

**Example 4.45** Q-CHEM input for a large single point energy calculation. This would be appropriate for a medium-sized molecule, but for truly large calculations, the CFMM and LinK algorithms are far more efficient.

```
$comment
   HF/3-21G single point calculation on a large molecule
   read in the molecular coordinates from file
$end
```

```
$molecule
   read dna.inp
$end

$rem
   METHOD      HF      Hartree-Fock
   BASIS       3-21G   Basis set
   INCFOCK     5       Incremental Fock after 5 cycles
   VARTHRESH   3       1.0d-03 variable threshold
$end
```

**Example 4.46** Q-CHEM input for a energy and gradient calculations with occ-RI-K method.

```
$molecule
   read  C30H62.inp
$end

$rem
   JOBTYPE          force
   EXCHANGE         HF
   BASIS            cc-pVTZ
   AUX_BASIS        cc-pVTZ-JK
   OCC_RI_K         1
   RI_K_GRAD        1
   INCFOCK          0
   PURECART         1111
$end
```

## 4.9 Dual-Basis Self-Consistent Field Calculations

The dual-basis approximation[279–284] to self-consistent field (HF or DFT) energies provides an efficient means for obtaining large basis set effects at vastly less cost than a full SCF calculation in a large basis set. First, a full SCF calculation is performed in a chosen small basis (specified by BASIS2). Second, a single SCF-like step in the larger, target basis (specified, as usual, by BASIS) is used to perturbatively approximate the large basis energy. This correction amounts to a first-order approximation in the change in density matrix, after the single large-basis step:

$$E_{\text{total}} = E_{\text{small basis}} + \text{Tr}[(\Delta\mathbf{P})\cdot\mathbf{F}]_{\text{large basis}} \tag{4.102}$$

where $\mathbf{F}$ (in the large basis) is built from the converged (small basis) density matrix. Thus, only a single Fock build is required in the large basis set. Currently, HF and DFT energies (SP) as well as analytic first derivatives (FORCE or OPT) are available.

**Note:** As of version 4.0, first derivatives of unrestricted dual-basis DFT energies—though correct—require a code-efficiency fix. We do not recommend use of these derivatives until this improvement has been made.

Across the G3 set[285–287] of 223 molecules, using cc-pVQZ, dual-basis errors for B3LYP are 0.04 kcal/mol (energy) and 0.03 kcal/mol (atomization energy per bond) and are at least an order of magnitude less than using a smaller basis set alone. These errors are obtained at roughly an order of magnitude savings in cost, relative to the full, target-basis calculation.

### 4.9.1 Dual-Basis MP2

The dual-basis approximation can also be used for the reference energy of a correlated second-order Møller-Plesset (MP2) calculation[280,284]. When activated, the dual-basis HF energy is first calculated as described above; subsequently, the MO coefficients and orbital energies are used to calculate the correlation energy in the large basis. This technique is particularly effective for RI-MP2 calculations (see Section 5.6), in which the cost of the underlying SCF calculation often dominates.

Furthermore, efficient analytic gradients of the DB-RI-MP2 energy have been developed[282] and added to Q-CHEM. These gradients allow for the optimization of molecular structures with RI-MP2 near the basis set limit. Typical computational savings are on the order of 50% (aug-cc-pVDZ) to 71% (aug-cc-pVTZ). Resulting dual-basis errors are only 0.001 Å in molecular structures and are, again, significantly less than use of a smaller basis set alone.

### 4.9.2 Dual-Basis Dynamics

The ability to compute SCF and MP2 energies and forces at reduced cost makes dual-basis calculations attractive for *ab initio* molecular dynamics simulations, which are described in Section 9.7. Dual-basis BOMD has demonstrated[288] savings of 58%, even relative to state-of-the-art, Fock-extrapolated BOMD. Savings are further increased to 71% for dual-basis RI-MP2 dynamics. Notably, these timings outperform estimates of extended Lagrangian ("Car-Parrinello") dynamics, without detrimental energy conservation artifacts that are sometimes observed in the latter[289].

Two algorithm improvements make modest but worthwhile improvements to dual-basis dynamics. First, the iterative, small-basis calculation can benefit from Fock matrix extrapolation[289]. Second, extrapolation of the response equations ("$Z$-vector" equations) for nuclear forces further increases efficiency[290]. (See Section 9.7.) Q-CHEM automatically adjusts to extrapolate in the proper basis set when DUAL_BASIS_ENERGY is activated.

### 4.9.3 Basis-Set Pairings

We recommend using basis pairings in which the small basis set is a proper subset of the target basis (6-31G into 6-31G*, for example). They not only produce more accurate results; they also lead to more efficient integral screening in both energies and gradients. Subsets for many standard basis sets (including Dunning-style cc-pV$XZ$ basis sets and their augmented analogs) have been developed and thoroughly tested for these purposes. A summary of the pairings is provided in Table 4.9.3; details of these truncations are provided in Figure 4.1.

A new pairing for 6-31G*-type calculations is also available. The 6-4G subset (named r64G in Q-CHEM) is a subset by *primitive* functions and provides a smaller, faster alternative for this basis set regime[283]. A case-dependent switch in the projection code (still OVPROJECTION) properly handles 6-4G. For DB-HF, the calculations proceed as described above. For DB-DFT, empirical scaling factors (see Ref. 283 for details) are applied to the dual-basis correction. This scaling is handled automatically by the code and prints accordingly.

As of Q-CHEM version 3.2, the basis set projection code has also been adapted to properly account for linear dependence[284], which can often be problematic for large, augmented (aug-cc-pVTZ, *etc.*) basis set calculations. The same standard keyword (LIN_DEP_THRESH) is utilized for linear dependence in the projection code. Because of the scheme utilized to account for linear dependence, only proper-subset pairings are now allowed.

Like single-basis calculations, user-specified general or mixed basis sets may be employed (see Chapter 7) with dual-basis calculations. The target basis specification occurs in the standard *$basis* section. The smaller, secondary basis is placed in a similar *$basis*2 section; the syntax within this section is the same as the syntax for *$basis*. General and mixed small basis sets are activated by BASIS2 = BASIS2_GEN and BASIS2 = BASIS2_MIXED, respectively.

| **BASIS** | **BASIS2** |
|---|---|
| cc-pVTZ | rcc-pVTZ |
| cc-pVQZ | rcc-pVQZ |
| aug-cc-pVDZ | racc-pVDZ |
| aug-cc-pVTZ | racc-pVTZ |
| aug-cc-pVQZ | racc-pVQZ |
| 6-31G* | r64G, 6-31G |
| 6-31G** | r64G, 6-31G |
| 6-31++G** | 6-31G* |
| 6-311++G(3df,3pd) | 6-311G*, 6-311+G* |

Table 4.5: Summary and nomenclature of recommended dual-basis pairings

### 4.9.4 Job Control

Dual-Basis calculations are controlled with the following *$rem*. DUAL_BASIS_ENERGY turns on the Dual-Basis approximation. Note that use of BASIS2 without DUAL_BASIS_ENERGY *only* uses basis set projection to generate the initial guess and does not invoke the Dual-Basis approximation (see Section 4.5.5). OVPROJECTION is used as the default projection mechanism for Dual-Basis calculations; it is not recommended that this be changed. Specification of SCF variables (*e.g.*, THRESH) will apply to calculations in both basis sets.

**DUAL_BASIS_ENERGY**

Activates dual-basis SCF (HF or DFT) energy correction.

TYPE:

LOGICAL

DEFAULT:

FALSE

OPTIONS:

Analytic first derivative available for HF and DFT (see JOBTYPE)

Can be used in conjunction with MP2 or RI-MP2

See BASIS, BASIS2, BASISPROJTYPE

RECOMMENDATION:

Use Dual-Basis to capture large-basis effects at smaller basis cost. Particularly useful with RI-MP2, in which HF often dominates. Use only proper subsets for small-basis calculation.

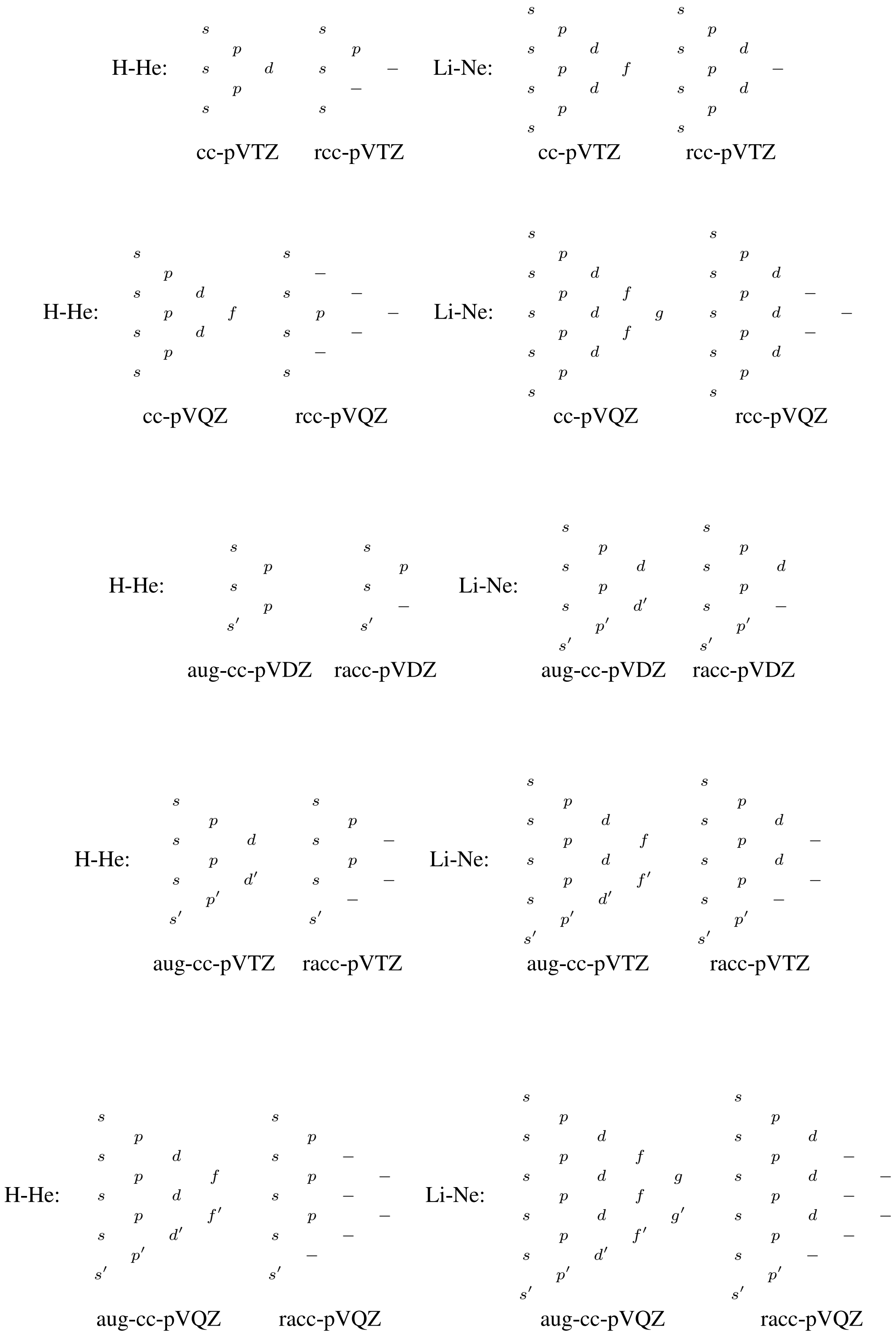

Figure 4.1: Structure of the truncated basis set pairings for cc-pV(T,Q)Z and aug-cc-pV(D,T,Q)Z. The most compact functions are listed at the top. Primed functions depict *aug* (diffuse) functions. Dashes indicate eliminated functions, relative to the paired standard basis set. In each case, the truncations for hydrogen and heavy atoms are shown, along with the nomenclature used in Q-Chem.

### 4.9.5 Examples

**Example 4.47** Input for a Dual-Basis B3LYP single-point calculation.

```
$molecule
   0 1
   H
   H   1   0.75
$end

$rem
   JOBTYPE             sp
   METHOD              b3lyp
   BASIS               6-311++G(3df,3pd)
   BASIS2              6-311G*
   DUAL_BASIS_ENERGY   true
$end
```

**Example 4.48** Input for a Dual-Basis B3LYP single-point calculation with a minimal 6-4G small basis.

```
$molecule
   0 1
   H
   H   1   0.75
$end

$rem
   JOBTYPE             sp
   METHOD              b3lyp
   BASIS               6-31G*
   BASIS2              r64G
   DUAL_BASIS_ENERGY   true
$end
```

**Example 4.49** Input for a Dual-Basis RI-MP2 single-point calculation.

```
$molecule
   0 1
   H
   H   1   0.75
$end

$rem
   JOBTYPE             sp
   METHOD              rimp2
   AUX_BASIS           rimp2-cc-pVQZ
   BASIS               cc-pVQZ
   BASIS2              rcc-pVQZ
   DUAL_BASIS_ENERGY   true
$end
```

**Example 4.50** Input for a Dual-Basis RI-MP2 geometry optimization.

```
$molecule
   0 1
   H
   H   1   0.75
$end

$rem
   JOBTYPE             opt
   METHOD              rimp2
   AUX_BASIS           rimp2-aug-cc-pVDZ
   BASIS               aug-cc-pVDZ
   BASIS2              racc-pVDZ
   DUAL_BASIS_ENERGY   true
$end
```

**Example 4.51** Input for a Dual-Basis RI-MP2 single-point calculation with mixed basis sets.

```
$molecule
   0 1
   H
   O   1   1.1
   H   2   1.1  1  104.5
$end

$rem
   JOBTYPE             opt
   METHOD              rimp2
   AUX_BASIS           aux_mixed
   BASIS               mixed
   BASIS2              basis2_mixed
   DUAL_BASIS_ENERGY   true
$end

$basis
 H 1
 cc-pVTZ
 ****
 O 2
 aug-cc-pVTZ
 ****
 H 3
 cc-pVTZ
 ****
$end

$basis2
 H 1
 rcc-pVTZ
 ****
 O 2
 racc-pVTZ
 ****
 H 3
 rcc-pVTZ
 ****
$end

$aux_basis
 H 1
 rimp2-cc-pVTZ
```

```
  ****
  O 2
  rimp2-aug-cc-pVTZ
  ****
  H 3
  rimp2-cc-pVTZ
  ****
$end
```

# 4.10 Hartree-Fock and Density-Functional Perturbative Corrections

## 4.10.1 Theory

Closely related to the dual-basis approach of Section 4.9, but somewhat more general, is the Hartree-Fock perturbative correction (HFPC) developed by Deng *et al.*[291,292]. An HFPC calculation consists of an iterative HF calculation in a small primary basis followed by a single Fock matrix formation, diagonalization, and energy evaluation in a larger, secondary basis. In the following, we denote a conventional HF calculation by HF/basis, and a HFPC calculation by HFPC/primary/secondary. Using a primary basis of $n$ functions, the restricted HF matrix elements for a $2m$-electron system are

$$F_{\mu\nu} = h_{\mu\nu} + \sum_{\lambda\sigma}^{n} P_{\lambda\sigma}\left[(\mu\nu|\lambda\sigma) - \frac{1}{2}(\mu\lambda|\nu\sigma)\right] \tag{4.103}$$

Solving the Roothaan-Hall equation in the primary basis results in molecular orbitals and an associated density matrix, $\mathbf{P}$. In an HFPC calculation, $\mathbf{P}$ is subsequently used to build a new Fock matrix, $\mathbf{F}^{[1]}$, in a larger secondary basis of $N$ functions

$$F_{ab}^{[1]} = h_{ab} + \sum_{\lambda\sigma}^{n} P_{\lambda\sigma}\left[(ab|\lambda\sigma) - \frac{1}{2}(a\lambda|b\sigma)\right] \tag{4.104}$$

where $\lambda$, $\sigma$ indicate primary basis functions and $a$, $b$ represent secondary basis functions. Diagonalization of $\mathbf{F}^{[1]}$ affords improved molecular orbitals and an associated density matrix $\mathbf{P}^{[1]}$. The HFPC energy is given by

$$E^{\text{HFPC}} = \sum_{ab}^{N} P_{ab}^{[1]} h_{ab} + \frac{1}{2}\sum_{abcd}^{N} P_{ab}^{[1]} P_{cd}^{[1]}\left[2(ab|cd) - (ac|bd)\right] \tag{4.105}$$

where $a$, $b$, $c$ and $d$ represent secondary basis functions. This differs from the DBHF energy evaluation where $\mathbf{P}\mathbf{P}^{[1]}$, rather than $\mathbf{P}^{[1]}\mathbf{P}^{[1]}$, is used. The inclusion of contributions that are quadratic in $\mathbf{P}\mathbf{P}^{[1]}$ is the key reason for the fact that HFPC is more accurate than DBHF.

Unlike dual-basis HF, HFPC does not require that the small basis be a proper subset of the large basis, and is therefore able to jump between any two basis sets. Benchmark study of HFPC on a large and diverse data set of total and reaction energies demonstrate that, for a range of primary/secondary basis set combinations, the HFPC scheme can reduce the error of the primary calculation by around two orders of magnitude at a cost of about one third that of the full secondary calculation[291,292].

A density-functional version of HFPC ("DFPC")[293] seeks to combine the low cost of pure DFT calculations using small bases and grids, with the high accuracy of hybrid calculations using large bases and grids. The DFPC approach is motivated by the dual-functional method of Nakajima and Hirao[294] and the dual-grid scheme of Tozer *et al.*[295] Combining these features affords a triple perturbation: to the functional, to the grid, and to the basis set. We call this approach density-functional "triple jumping".

### 4.10.2 Job Control

HFPC/DFPC calculations are controlled with the following *$rem*. HFPT turns on the HFPC/DFPC approximation. Note that HFPT_BASIS specifies the secondary basis set.

**HFPT**

Activates HFPC/DFPC calculation.

TYPE:

LOGICAL

DEFAULT:

FALSE

OPTIONS:

Single-point energy only

RECOMMENDATION:

Use Dual-Basis to capture large-basis effects at smaller basis cost. See reference for recommended basis set, functional, and grid pairings.

**HFPT_BASIS**

Specifies the secondary basis in a HFPC/DFPC calculation.

TYPE:

STRING

DEFAULT:

None

OPTIONS:

None

RECOMMENDATION:

See reference for recommended basis set, functional, and grid pairings.

**DFPT_XC_GRID**

Specifies the secondary grid in a HFPC/DFPC calculation.

TYPE:

STRING

DEFAULT:

None

OPTIONS:

None

RECOMMENDATION:

See reference for recommended basis set, functional, and grid pairings.

**DFPT_EXCHANGE**

Specifies the secondary functional in a HFPC/DFPC calculation.

TYPE:

STRING

DEFAULT:

None

OPTIONS:

None

RECOMMENDATION:

See reference for recommended basis set, functional, and grid pairings.

### 4.10.3 Examples

**Example 4.52** Input for a HFPC single-point calculation.

```
$molecule
   0 1
   H
   H   1   0.75
$end

$rem
   JOBTYPE      sp
   EXCHANGE     hf
   BASIS        cc-pVDZ  ! primary basis
   HFPT_BASIS   cc-pVQZ  ! secondary basis
   PURECART     1111     ! set to purecart of the target basis
   HFPT         true
$end
```

**Example 4.53** Input for a DFPC single-point calculation.

```
$molecule
   0 1
   H
   H   1   0.75
$end

$rem
   JOBTYPE          sp
   EXCHANGE         blyp                ! primary functional
   DFPT_EXCHANGE    b3lyp               ! secondary functional
   DFPT_XC_GRID     00075000302         ! secondary grid
   XC_GRID          0                   ! primary grid
   HFPT_BASIS       6-311++G(3df,3pd)   ! secondary basis
   BASIS            6-311G*             ! primary basis
   PURECART         1111
   HFPT             true
$end
```

## 4.11 Methods Based on "Constrained" DFT

### 4.11.1 Theory

Under certain circumstances it is desirable to apply constraints to the electron density during an SCF calculation. For example, in a transition metal complex it may be desirable to constrain the net spin density on a particular metal atom to integrate to a value consistent with the $M_S$ value expected from ligand field theory. Similarly, in a donor–acceptor complex one might be interested in constraining the total density on the acceptor group so that the formal charge on the acceptor is either neutral or negatively charged, depending as the molecule is in its neutral or its charge-transfer state. In these situations, one is interested in controlling the average value of some observable, $O(\mathbf{r})$, to take on a given value, $N$:

$$\int \rho(\mathbf{r})\, O(\mathbf{r})\; d\mathbf{r} = N \tag{4.106}$$

There are of course many states that satisfy such a constraint, but in practice one is usually looking for the lowest energy such state. To solve the resulting constrained minimization problem, one introduces a Lagrange multiplier, $V$, and solves for the stationary point of

$$V[\rho, V] = E[\rho] - V\left(\int \rho(\mathbf{r})\, O(\mathbf{r})\; d\mathbf{r} - N\right) \tag{4.107}$$

where $E[\rho]$ is the energy of the system described using density functional theory (DFT). At convergence, the functional $W$ gives the density, $\rho$, that satisfies the constraint exactly (*i.e.*, it has exactly the prescribed number of electrons on the acceptor or spins on the metal center) but has the lowest energy possible. The resulting self-consistent procedure can be efficiently solved by ensuring at every SCF step the constraint is satisfied exactly. The Q-CHEM implementation of these equations closely parallels those in Ref. 296.

The first step in any constrained DFT calculation is the specification of the constraint operator, $O(\mathbf{r})$. Within Q-CHEM, the user is free to specify any constraint operator that consists of a linear combination of the Becke's atomic partitioning functions[172]:

$$O(\mathbf{r}) = \sum_{A}^{\text{atoms}} \sum_{\sigma=\alpha,\beta} C_A^\sigma\, w_A(\mathbf{r}) \tag{4.108}$$

Here the summation runs over the atoms in the system and over electron spins. The weight function $w_A$ is designed to be $\approx 1$ near the nucleus of atom $A$ and rapidly fall to zero near the nucleus of any other atom in the system[172]. The user-specified coefficients $C_A^\sigma$ are input using a *$cdft* input section having the following format.

```
$cdft
   CONSTRAINT_VALUE_X
   COEFFICIENT1_X        FIRST_ATOM1_X        LAST_ATOM1_X     TYPE1_X
   COEFFICIENT2_X        FIRST_ATOM2_X        LAST_ATOM2_X     TYPE2_X
   ...
   CONSTRAINT_VALUE_Y
   COEFFICIENT1_Y        FIRST_ATOM1_Y        LAST_ATOM1_Y     TYPE1_Y
   COEFFICIENT2_Y        FIRST_ATOM2_Y        LAST_ATOM2_Y     TYPE2_Y
   ...
$end
```

Here, each CONSTRAINT_VALUE is a real number that specifies the desired average value ($N$) of the ensuing linear combination of atomic partition functions. Each COEFFICIENT specifies the coefficient of a partition function or group of partition functions in the constraint operator $O$. For each coefficient, all the atoms between the integers FIRST_ATOM and LAST_ATOM contribute with the specified weight in the constraint operator. Finally, TYPE specifies the type of constraint being applied—either "CHARGE" or "SPIN". For a CHARGE constraint the spin up and spin down densities contribute equally ($C_A^\alpha = C_A^\beta = C_A$) yielding the total number of electrons on the atom A. For a SPIN constraint, the spin up and spin down densities contribute with opposite sign ($C_A^\alpha - C_A^\beta = C_A$) resulting in a measure of the net spin on the atom A. Each separate CONSTRAINT_VALUE creates a new operator whose average is to be constrained—for instance, the example above includes several independent constraints: $\mathrm{X}, \mathrm{Y}, \ldots$. Q-CHEM can handle an arbitrary number of constraints and will minimize the energy subject to all of these constraints simultaneously.

If an atom is not included in a particular operator, then the coefficient of that atoms partition function is set to zero for that operator. The TYPE specification is optional, and the default is to perform a charge constraint. Further, note that any charge constraint is on the *net* atomic charge. That is, the constraint is on the difference between the average number of electrons on the atom and the nuclear charge. Thus, to constrain CO to be negative, the constraint value would be 1 and not 15.

**Note:** Charge constraint in *$cdft* specifies the number of excess electrons on a fragment, not the total charge, *i.e.*, the value 1.0 means charge $= -1$, whereas charge constraint of $-1.0$ corresponds to the total $+1$ charge.

The choice of which atoms to include in different constraint regions is left entirely to the user and in practice must be based somewhat on chemical intuition. Thus, for example, in an electron transfer reaction the user must specify which atoms are in the "donor" and which are in the "acceptor". In practice, the most stable choice is typically to make the constrained region as large as physically possible. Thus, for the example of electron transfer again, it is best to assign *every* atom in the molecule to one or the other group (donor or acceptor), recognizing that it makes no sense to assign any atoms to both groups. On the other end of the spectrum, constraining the formal charge on a single atom is highly discouraged. The problem is that while our chemical intuition tells us that the lithium atom in LiF should have a formal charge of +1, in practice the quantum mechanical charge is much closer to +0.5 than +1. Only when the fragments are far enough apart do our intuitive pictures of formal charge actually become quantitative.

Note that the atomic populations that Q-CHEM prints out are Mulliken populations, not the Becke weight populations. As a result, the printed populations will not generally add up to the specified constrained values, even though the constraint is exactly satisfied. You can print Becke populations to confirm that the computed states have the desired charge/spin character.

Finally, we note that SCF convergence is typically more challenging in constrained DFT calculations as compared to their unconstrained counterparts. This effect arises because applying the constraint typically leads to a broken symmetry, diradical-like state. As SCF convergence for these cases is known to be difficult even for unconstrained states, it is perhaps not surprising that there are additional convergence difficulties in this case. See Section 4.6 on SCF convergence algorithms for ideas on how to improve convergence for constrained calculations. Also, CDFT is more sensitive to grid size than ground-state DFT, so sometimes increasing the integration grid to (50,194) or (75, 302), instead of the default SG-1 grid, improves the convergence.

**Note:** (i) To improve convergence, use the fewest possible constraints. For example, if your system consists of two fragments, specify the constrains for one of them only. The overall charge and multiplicity will force the "unconstrained" fragment to attain the right charge and multiplicity.
(ii) The direct minimization methods are not available for constrained calculations. Hence, some combination of DIIS and RCA must be used to obtain convergence. Further, it is often necessary to break symmetry in the initial guess (using SCF_GUESS_MIX) to ensure that the lowest energy solution is obtained.

Analytic gradients are available for constrained DFT calculations[297]. Second derivatives are only available by finite difference of analytic gradients. For details on how to apply constrained DFT to compute magnetic exchange couplings, see Ref. 298. For details on using constrained DFT to compute electron transfer parameters, see Ref. 299.

### 4.11.2 CDFT Job Control and Examples

A CDFT calculation is requested by setting CDFT = TRUE in the *$rem* section, as as by specifying a *$cdft* input section as described above. Additional job control variables are described below.

**CDFT**
Initiates a constrained DFT calculation
TYPE:
LOGICAL
DEFAULT:
FALSE
OPTIONS:

| | |
|---|---|
| TRUE | Perform a Constrained DFT Calculation |
| FALSE | No Density Constraint |

RECOMMENDATION:
Set to TRUE if a Constrained DFT calculation is desired.

**CDFT_POSTDIIS**
Controls whether the constraint is enforced after DIIS extrapolation.
TYPE:
LOGICAL
DEFAULT:
TRUE
OPTIONS:

| | |
|---|---|
| TRUE | Enforce constraint after DIIS |
| FALSE | Do not enforce constraint after DIIS |

RECOMMENDATION:
Use the default unless convergence problems arise, in which case it may be beneficial to experiment with setting CDFT_POSTDIIS to FALSE. With this option set to TRUE, energies should be variational after the first iteration.

**CDFT_PREDIIS**

Controls whether the constraint is enforced before DIIS extrapolation.

TYPE:

LOGICAL

DEFAULT:

FALSE

OPTIONS:

| | |
|---|---|
| TRUE | Enforce constraint before DIIS |
| FALSE | Do not enforce constraint before DIIS |

RECOMMENDATION:

Use the default unless convergence problems arise, in which case it may be beneficial to experiment with setting CDFT_PREDIIS to TRUE. Note that it is possible to enforce the constraint both before and after DIIS by setting both CDFT_PREDIIS and CDFT_POSTDIIS to TRUE.

**CDFT_THRESH**

Threshold that determines how tightly the constraint must be satisfied.

TYPE:

INTEGER

DEFAULT:

5

OPTIONS:

N Constraint is satisfied to within $10^{-N}$.

RECOMMENDATION:

Use the default unless problems occur.

**CDFT_CRASHONFAIL**

Whether the calculation should crash or not if the constraint iterations do not converge.

TYPE:

LOGICAL

DEFAULT:

TRUE

OPTIONS:

| | |
|---|---|
| TRUE | Crash if constraint iterations do not converge. |
| FALSE | Do not crash. |

RECOMMENDATION:

Use the default.

**CDFT_BECKE_POP**

Whether the calculation should print the Becke atomic charges at convergence

TYPE:

LOGICAL

DEFAULT:

TRUE

OPTIONS:

TRUE Print Populations

FALSE Do not print them

RECOMMENDATION:

Use the default. Note that the Mulliken populations printed at the end of an SCF run will not typically add up to the prescribed constraint value. Only the Becke populations are guaranteed to satisfy the user-specified constraints.

**Example 4.54** Charge separation on FAAQ

```
$molecule
   0 1
   C     -0.64570736     1.37641945    -0.59867467
   C      0.64047568     1.86965826    -0.50242683
   C      1.73542663     1.01169939    -0.26307089
   C      1.48977850    -0.39245666    -0.15200261
   C      0.17444585    -0.86520769    -0.27283957
   C     -0.91002699    -0.02021483    -0.46970395
   C      3.07770780     1.57576311    -0.14660056
   C      2.57383948    -1.35303134     0.09158744
   C      3.93006075    -0.78485926     0.20164558
   C      4.16915637     0.61104948     0.08827557
   C      5.48914671     1.09087541     0.20409492
   H      5.64130588     2.16192921     0.11315072
   C      6.54456054     0.22164774     0.42486947
   C      6.30689287    -1.16262761     0.53756193
   C      5.01647654    -1.65329553     0.42726664
   H     -1.45105590     2.07404495    -0.83914389
   H      0.85607395     2.92830339    -0.61585218
   H      0.02533661    -1.93964850    -0.19096085
   H      7.55839768     0.60647405     0.51134530
   H      7.13705743    -1.84392666     0.71043613
   H      4.80090178    -2.71421422     0.50926027
   O      2.35714021    -2.57891545     0.20103599
   O      3.29128460     2.80678842    -0.23826460
   C     -2.29106231    -0.63197545    -0.53957285
   O     -2.55084900    -1.72562847    -0.95628300
   N     -3.24209015     0.26680616     0.03199109
   H     -2.81592456     1.08883943     0.45966550
   C     -4.58411403     0.11982669     0.15424004
   C     -5.28753695     1.14948617     0.86238753
   C     -5.30144592    -0.99369577    -0.39253179
   C     -6.65078185     1.06387425     1.01814801
   H     -4.73058059     1.98862544     1.26980479
   C     -6.66791492    -1.05241167    -0.21955088
   H     -4.76132422    -1.76584307    -0.92242502
   C     -7.35245187    -0.03698606     0.47966072
   H     -7.18656323     1.84034269     1.55377875
   H     -7.22179827    -1.89092743    -0.62856041
   H     -8.42896369    -0.10082875     0.60432214
$end

$rem
   JOBTYPE         FORCE
   METHOD          B3LYP
   BASIS           6-31G*
   SCF_PRINT       TRUE
   CDFT            TRUE
$end

$cdft
   2
   1   1  25
  -1  26  38
$end
```

**Example 4.55** Cu2-Ox High Spin

```
$molecule
   2 3
   Cu      1.4674     1.6370     1.5762
   O       1.7093     0.0850     0.3825
   O      -0.5891     1.3402     0.9352
   C       0.6487    -0.3651    -0.1716
   N       1.2005     3.2680     2.7240
   N       3.0386     2.6879     0.6981
   N       1.3597     0.4651     3.4308
   H       2.1491    -0.1464     3.4851
   H       0.5184    -0.0755     3.4352
   H       1.3626     1.0836     4.2166
   H       1.9316     3.3202     3.4043
   H       0.3168     3.2079     3.1883
   H       1.2204     4.0865     2.1499
   H       3.8375     2.6565     1.2987
   H       3.2668     2.2722    -0.1823
   H       2.7652     3.6394     0.5565
   Cu     -1.4674    -1.6370    -1.5762
   O      -1.7093    -0.0850    -0.3825
   O       0.5891    -1.3402    -0.9352
   C      -0.6487     0.3651     0.1716
   N      -1.2005    -3.2680    -2.7240
   N        -3.0386    -2.6879    -0.6981
   N      -1.3597    -0.4651    -3.4308
   H      -2.6704    -3.4097    -0.1120
   H      -3.6070    -3.0961    -1.4124
   H      -3.5921    -2.0622    -0.1485
   H      -0.3622    -3.1653    -3.2595
   H      -1.9799    -3.3721    -3.3417
   H      -1.1266    -4.0773    -2.1412
   H      -0.5359     0.1017    -3.4196
   H      -2.1667     0.1211    -3.5020
   H      -1.3275    -1.0845    -4.2152
$end

$rem
   JOBTYPE         SP
   METHOD          B3LYP
   BASIS           6-31G*
   SCF_PRINT       TRUE
   CDFT            TRUE
$end

$cdft
   2
   1   1   3  s
  -1  17  19  s
$end
```

### 4.11.3 Configuration Interaction with Constrained DFT (CDFT-CI)

There are some situations in which a system is not well-described by a DFT calculation on a single configuration. For example, transition states are known to be poorly described by most functionals, with the computed barrier being too low. We can, in particular, identify homolytic dissociation of diatomic species as situations where static correlation becomes extremely important. Existing DFT functionals have proved to be very effective in capturing dynamic correlation, but frequently exhibit difficulties in the presence of strong static correlation. Configuration Interaction, well known in wave function methods, is a multi-reference method that is quite well-suited for capturing static correlation; the CDFT-CI technique allows for CI calculations on top of DFT calculations, harnessing both static and dynamic correlation methods.

Constrained DFT is used to compute densities (and Kohn-Sham wave functions) for two or more diabatic-like states; these states are then used to build a CI matrix. Diagonalizing this matrix yields energies for the ground *and excited* states within the configuration space. The coefficients of the initial diabatic states are printed, to show the characteristics of the resultant states.

Since DFT only gives converged densities, not actual wave functions, computing the off-diagonal coupling elements $H_{12}$ is not completely straightforward, as the physical meaning of the Kohn-Sham wave function is not entirely clear. We can, however, perform the following manipulation[300]:

$$\begin{aligned} H_{12} &= \frac{1}{2}\Big[\langle 1|H + V_{C_1}\omega_{C_1} - V_{C1}\omega_{C_1}|2\rangle + \langle 1|H + V_{C_2}\omega_{C_2} - V_{C_2}\omega_{C_2}|2\rangle\Big] \\ &= \frac{1}{2}\Big[(E_1 + V_{C_1}N_{C_1} + E_2 + V_{C_2}N_{C_2})\,\langle 1|2\rangle - V_{C_1}\langle 1|\omega_{C_1}|2\rangle - V_{C_2}\langle 1|\omega_{C_2}|2\rangle\Big] \end{aligned} \tag{4.109}$$

where the converged states $|i\rangle$ are assumed to be the ground state of $H + V_{C_i}\omega_{C_i}$ with eigenvalue $E_i + V_{C_i}N_{C_i}$). This manipulation eliminates the two-electron integrals from the expression, and experience has shown that the use of Slater determinants of Kohn-Sham orbitals is a reasonable approximation for the quantities $\langle 1|2\rangle$ and $\langle 1|\omega_{C_i}|2\rangle$.

Note that since these constrained states are eigenfunctions of different Hamiltonians (due to different constraining potentials), they are *not* orthogonal states, and we must set up our CI matrix as a generalized eigenvalue problem. Symmetric orthogonalization is used by default, though the overlap matrix and Hamiltonian in non-orthogonal basis are also printed at higher print levels so that other orthogonalization schemes can be used after-the-fact. In a limited number of cases, it is possible to find an orthogonal basis for the CDFT-CI Hamiltonian, where a physical interpretation can be assigned to the orthogonal states. In such cases, the matrix representation of the Becke weight operator is diagonalized, and the (orthogonal) eigenstates can be characterized[301]. This matrix is printed as the “CDFT-CI Population Matrix” at increased print levels.

In order to perform a CDFT-CI calculation, the $N$ interacting states must be defined, which is accomplished using a *$cdft* input section in a fashion similar to the specification of CDFT states:

```
$cdft
STATE_1_CONSTRAINT_VALUE_X
COEFFICIENT1_X       FIRST_ATOM1_X       LAST_ATOM1_X    TYPE1_X
COEFFICIENT2_X       FIRST_ATOM2_X       LAST_ATOM2_X    TYPE2_X
...
STATE_1_CONSTRAINT_VALUE_Y
COEFFICIENT1_Y       FIRST_ATOM1_Y       LAST_ATOM1_Y    TYPE1_Y
COEFFICIENT2_Y       FIRST_ATOM2_Y       LAST_ATOM2_Y    TYPE2_Y
...
---
STATE_2_CONSTRAINT_VALUE_X
COEFFICIENT1_X       FIRST_ATOM1_X       LAST_ATOM1_X    TYPE1_X
COEFFICIENT2_X       FIRST_ATOM2_X       LAST_ATOM2_X    TYPE2_X
...
STATE_2_CONSTRAINT_VALUE_Y
COEFFICIENT1_Y       FIRST_ATOM1_Y       LAST_ATOM1_Y    TYPE1_Y
COEFFICIENT2_Y       FIRST_ATOM2_Y       LAST_ATOM2_Y    TYPE2_Y
...
$end
```

Each state is specified with the CONSTRAINT_VALUE and the corresponding weights on sets of atoms whose average value should be the constraint value. Different states are separated by a single line containing three or more dash characters.

If it is desired to use an unconstrained state as one of the interacting configurations, charge and spin constraints of zero may be applied to the atom range from 0 to 0.

**Note:** It is mandatory to specify a spin constraint corresponding to every charge constraint (and it must be immediately following that charge constraint in the input deck), for reasons described below.

In addition to the *$cdft* input section of the input file, a CDFT-CI calculation must also set the CDFTCI flag to TRUE for the calculation to run. Note, however, that the CDFT flag is used internally by CDFT-CI, and should *not* be set in the input deck. The variable CDFTCI_PRINT may also be set manually to control the level of output. The default is 0, which will print the energies and weights (in the diabatic basis) of the $N$ CDFT-CI states. Setting it to 1 or above will also print the CDFT-CI overlap matrix, the CDFT-CI Hamiltonian matrix before the change of basis, and the CDFT-CI Population matrix. Setting it to 2 or above will also print the eigenvectors and eigenvalues of the CDFT-CI Population matrix. Setting it to 3 will produce more output that is only useful during application debugging.
For convenience, if CDFTCI_PRINT is not set in the input file, it will be set to the value of SCF_PRINT.

As mentioned in the previous section, there is a disparity between our chemical intuition of what charges should be and the actual quantum-mechanical charge. The example was given of LiF, where our intuition gives the lithium atom a formal charge of $+1$; we might similarly imagine performing a CDFT-CI calculation on $H_2$, with two ionic states and two spin-constrained states. However, this would result in attempting to force both electrons of $H_2$ onto the same nucleus, and this calculation is impossible to converge (since by the nature of the Becke weight operators, there will be some non-zero amount of the density that gets proportioned onto the other atom, at moderate internuclear separations). To remedy problems such as this, we have adopted a mechanism by which to convert the formal charges of our chemical intuition into reasonable quantum-mechanical charge constraints. We use the formalism of "promolecule" densities, wherein the molecule is divided into fragments (based on the partitioning of constraint operators), and a DFT calculation is performed on these fragments, completely isolated from each other[301]. (This step is why both spin and charge constraints are required, so that the correct partitioning of electrons for each fragment may be made.) The resulting promolecule densities, converged for the separate fragments, are then added together, and the value of the various weight operators as applied to this new density, is used as a constraint for the actual CDFT calculations on the interacting states. The promolecule density method compensates for the effect of nearby atoms on the actual density that will be constrained.

The comments about SCF convergence for CDFT calculations also apply to the calculations used for CDFT-CI, with the addition that if the SCF converges but CDFT does not, it may be necessary to use a denser integration grid or reduce the value of CDFT_THRESH.

Analytic gradients are not available. For details on using CDFT-CI to calculate reaction barrier heights, see Ref. 302.

### 4.11.4 CDFT-CI Job Control and Examples

**CDFTCI**

Initiates a constrained DFT-configuration interaction calculation

TYPE:

LOGICAL

DEFAULT:

FALSE

OPTIONS:

| | |
|---|---|
| TRUE | Perform a CDFT-CI Calculation |
| FALSE | No CDFT-CI |

RECOMMENDATION:

Set to TRUE if a CDFT-CI calculation is desired.

**CDFTCI_PRINT**

Controls level of output from CDFT-CI procedure to Q-CHEM output file.

TYPE:

INTEGER

DEFAULT:

0

OPTIONS:

| | |
|---|---|
| 0 | Only print energies and coefficients of CDFT-CI final states |
| 1 | Level 0 plus CDFT-CI overlap, Hamiltonian, and population matrices |
| 2 | Level 1 plus eigenvectors and eigenvalues of the CDFT-CI population matrix |
| 3 | Level 2 plus promolecule orbital coefficients and energies |

RECOMMENDATION:

Level 3 is primarily for program debugging; levels 1 and 2 may be useful for analyzing the coupling elements

**CDFT_LAMBDA_MODE**

Allows CDFT potentials to be specified directly, instead of being determined as Lagrange multipliers.

TYPE:

BOOLEAN

DEFAULT:

FALSE

OPTIONS:

FALSE Standard CDFT calculations are used.

TRUE Instead of specifying target charge and spin constraints, use the values from the input deck as the value of the Becke weight potential

RECOMMENDATION:

Should usually be set to FALSE. Setting to TRUE can be useful to scan over different strengths of charge or spin localization, as convergence properties are improved compared to regular CDFT(-CI) calculations.

**CDFTCI_SKIP_PROMOLECULES**

Skips promolecule calculations and allows fractional charge and spin constraints to be specified directly.

TYPE:

BOOLEAN

DEFAULT:

FALSE

OPTIONS:

FALSE Standard CDFT-CI calculation is performed.

TRUE Use the given charge/spin constraints directly, with no promolecule calculations.

RECOMMENDATION:

Setting to TRUE can be useful for scanning over constraint values.

**Note:** CDFT_LAMBDA_MODE and CDFTCI_SKIP_PROMOLECULES are mutually incompatible.

**CDFTCI_SVD_THRESH**

By default, a symmetric orthogonalization is performed on the CDFT-CI matrix before diagonalization. If the CDFT-CI overlap matrix is nearly singular (*i.e.*, some of the diabatic states are nearly degenerate), then this orthogonalization can lead to numerical instability. When computing $\mathbf{S}^{-1/2}$, eigenvalues smaller than $10^{-\mathrm{CDFTCI\_SVD\_THRESH}}$ are discarded.

TYPE:

INTEGER

DEFAULT:

4

OPTIONS:

$n$ for a threshold of $10^{-n}$.

RECOMMENDATION:

Can be decreased if numerical instabilities are encountered in the final diagonalization.

**CDFTCI_STOP**

The CDFT-CI procedure involves performing independent SCF calculations on distinct constrained states. It sometimes occurs that the same convergence parameters are not successful for all of the states of interest, so that a CDFT-CI calculation might converge one of these diabatic states but not the next. This variable allows a user to stop a CDFT-CI calculation after a certain number of states have been converged, with the ability to restart later on the next state, with different convergence options.

TYPE:

INTEGER

DEFAULT:

0

OPTIONS:

$n$ Stop after converging state $n$ (the first state is state 1)

0 Do not stop early

RECOMMENDATION:

Use this setting if some diabatic states converge but others do not.

**CDFTCI_RESTART**

To be used in conjunction with CDFTCI_STOP, this variable causes CDFT-CI to read already-converged states from disk and begin SCF convergence on later states. Note that the same *$cdft* section must be used for the stopped calculation and the restarted calculation.

TYPE:

INTEGER

DEFAULT:

0

OPTIONS:

$n$ Start calculations on state $n + 1$

RECOMMENDATION:

Use this setting in conjunction with CDFTCI_STOP.

Many of the CDFT-related rem variables are also applicable to CDFT-CI calculations.

**Example 4.56** CDFT-CI calculation of couplings between the anionic GFP chromophore (CHR:1-27) and a tyrosine (TYR:28-43) residue. The two diabatic states are Chro-($M_S = 0$)...Tyr($M_S = 0$) and Chro($M_S = 1/2$)...Tyr-($M_S = 1/2$).

```
$molecule
  -1 1
  C        -1.453000       -1.953000       -0.264000
  N        -0.278000       -1.402000       -0.440000
  N        -1.804000       -2.052000        1.091000
  C        -0.687000       -1.548000        1.806000
  O        -0.688000       -1.514000        3.031000
  C         0.291000       -1.140000        0.799000
  C         1.500000       -0.563000        1.254000
  H         1.585000       -0.660000        2.346000
  C         2.608000        0.030000        0.605000
  C         2.763000        0.182000       -0.865000
  H         1.926000       -0.073000       -1.543000
  C         3.733000        0.548000        1.313000
```

```
   H         3.682000        0.571000        2.326000
   C         3.821000        0.875000       -1.473000
   H         3.844000        1.102000       -2.575000
   C         4.938000        1.111000        0.700000
   H         5.734000        1.441000        1.308000
   C         5.037000        1.228000       -0.739000
   O         6.011000        1.818000       -1.261000
   C        -3.000000       -2.533000        1.832000
   H        -2.859000       -2.250000        2.892000
   H        -3.829000       -2.121000        1.354000
   C        -2.373000       -2.282000       -1.448000
   H        -1.790000       -3.026000       -2.045000
   H        -2.626000       -1.300000       -1.865000
   H        -3.054000       -3.631000        1.855000
   H        -3.308000       -2.854000       -1.357000
   C         7.648000       -5.429000        0.303000
   H         8.028000       -4.514000        0.845000
   H         7.274000       -5.098000       -0.671000
   C         6.499001       -5.986000        1.016000
   C         6.462999       -6.032001        2.390000
   H         7.284000       -5.579000        2.957000
   C         5.243000       -6.435000        3.018000
   H         5.190001       -6.315001        4.035000
   C         4.242001       -7.048000        2.189000
   O         3.095000       -7.615000        2.715000
   H         2.500999       -7.869000        1.979000
   C         5.454000       -6.469000        0.200000
   H         5.565001       -6.363000       -0.835000
   C         4.294001       -7.003000        0.803000
   H         3.469000       -7.324000        0.139000
   H         8.511000       -6.108000        0.245000
$end

$rem
   SYMMETRY          = off
   SYM_IGNORE        = true
   METHOD            = b3lyp
   BASIS             = cc-pvdz
   UNRESTRICTED      = true
   SCF_CONVERGENCE   =  8
   MAX_SCF_CYCLES    = 200
   CDFTCI            = true
   CDFTCI_PRINT      = 2
   CDFT_THRESH       = 7
$end

$cdft
   1.0
   1.0   1   27
   0.0
   1.0   1   27  S
--------------
   0.0
   1.0   1   27
  -1.0
   1.0   1   27  S
$END
```

# 4.12 Unconventional SCF Calculations

## 4.12.1 Polarized Atomic Orbital (PAO) Calculations

Polarized atomic orbital (PAO) calculations are an interesting unconventional SCF method, in which the molecular orbitals and the density matrix are not expanded directly in terms of the basis of atomic orbitals. Instead, an intermediate molecule-optimized minimal basis of polarized atomic orbitals (PAOs) is used[303]. The polarized atomic orbitals are defined by an atom-blocked linear transformation from the fixed atomic orbital basis, where the coefficients of the transformation are optimized to minimize the energy, at the same time as the density matrix is obtained in the PAO representation. Thus a PAO-SCF calculation is a constrained variational method, whose energy is above that of a full SCF calculation in the same basis. However, a molecule optimized minimal basis is a very compact and useful representation for purposes of chemical analysis, and it also has potential computational advantages in the context of MP2 or local MP2 calculations, as can be done after a PAO-HF calculation is complete to obtain the PAO-MP2 energy.

PAO-SCF calculations tend to systematically underestimate binding energies (since by definition the exact result is obtained for atoms, but not for molecules). In tests on the G2 database, PAO-B3LYP/6-311+G(2df,p) atomization energies deviated from full B3LYP/6-311+G(2df,p) atomization energies by roughly 20 kcal/mol, with the error being essentially extensive with the number of bonds. This deviation can be reduced to only 0.5 kcal/mol with the use of a simple non-iterative second order correction for "beyond-minimal basis" effects[304]. The second order correction is evaluated at the end of each PAO-SCF calculation, as it involves negligible computational cost. Analytical gradients are available using PAOs, to permit structure optimization. For additional discussion of the PAO-SCF method and its uses, see the references cited above.

Calculations with PAOs are determined controlled by the following *$rem* variables. PAO_METHOD = PAO invokes PAO-SCF calculations, while the algorithm used to iterate the PAOs can be controlled with PAO_ALGORITHM.

**PAO_ALGORITHM**
Algorithm used to optimize polarized atomic orbitals (see PAO_METHOD)
TYPE:
INTEGER
DEFAULT:
0
OPTIONS:
0 Use efficient (and riskier) strategy to converge PAOs.
1 Use conservative (and slower) strategy to converge PAOs.
RECOMMENDATION:
None

**PAO_METHOD**

Controls evaluation of polarized atomic orbitals (PAOs).

TYPE:

STRING

DEFAULT:

EPAO For local MP2 calculations Otherwise no default.

OPTIONS:

PAO Perform PAO-SCF instead of conventional SCF.

EPAO Obtain EPAOs after a conventional SCF.

RECOMMENDATION:

None

### 4.12.2 SCF Meta-Dynamics

As the SCF equations are non-linear in the electron density, there are in theory very many solutions (*i.e.*, sets of orbitals where the energy is stationary with respect to changes in the orbital subset). Most often sought is the solution with globally minimal energy as this is a variational upper bound to the true eigenfunction in this basis. The SCF methods available in Q-CHEM allow the user to converge upon an SCF solution, and (using STABILITY_ANALYSIS) ensure it is a minimum, but there is no known method of ensuring that the found solution is a global minimum; indeed in systems with many low-lying energy levels the solution converged upon may vary considerably with initial guess.

SCF meta-dynamics[305] is a technique which can be used to locate multiple SCF solutions, and thus gain some confidence that the calculation has converged upon the global minimum. It works by searching out a solution to the SCF equations. Once found, the solution is stored, and a biasing potential added so as to avoid re-converging to the same solution. More formally, the distance between two solutions, $w$ and $x$, can be expressed as $d_{wx}^2 = \langle {}^w\Psi | {}^w\hat{\rho} - {}^x\hat{\rho} | {}^w\Psi \rangle$, where ${}^w\Psi$ is a Slater determinant formed from the orthonormal orbitals, ${}^w\phi_i$, of solution $w$, and ${}^w\hat{\rho}$ is the one-particle density operator for ${}^w\Psi$. This definition is equivalent to $d_{wx}^2 = N - {}^wP^{\mu\nu}S_{\nu\sigma} \cdot {}^xP^{\sigma\tau}S_{\tau\mu}$. and is easily calculated.

$d_{wx}^2$ is bounded by 0 and the number of electrons, and can be taken as the distance between two solutions. As an example, any singly excited determinant from an SCF determinant (which will not in general be another SCF solution), would be a distance 1 away from it.

In a manner analogous to classical meta-dynamics, to bias against the set of previously located solutions, $x$, we create a new Lagrangian,

$$\tilde{E} = E + \sum_x N_x e^{-\lambda_x d_{0x}^2} \tag{4.110}$$

where 0 represents the present density. From this we may derive a new effective Fock matrix,

$$\tilde{F}_{\mu\nu} = F_{\mu\nu} + \sum_x^x P_{\mu\nu} N_x \lambda_x e^{-\lambda_x d_{0x}^2} \tag{4.111}$$

This may be used with very little modification within a standard DIIS procedure to locate multiple solutions. When close to a new solution, the biasing potential is removed so the location of that solution is not affected by it. If the calculation ends up re-converging to the same solution, $N_x$ and $\lambda_x$ can be modified to avert this. Once a solution is found it is added to the list of solutions, and the orbitals mixed to provide a new guess for locating a different solution.

This process can be customized by the REM variables below. Both DIIS and GDM methods can be used, but it is advisable to turn on MOM when using DIIS to maintain the orbital ordering. Post-HF correlation methods can also be applied. By default they will operate for the last solution located, but this can be changed with the SCF_MINFIND_RUNCORR variable.

The solutions found through meta-dynamics also appear to be good approximations to diabatic surfaces where the electronic structure does not significantly change with geometry. In situations where there are such multiple electronic states close in energy, an adiabatic state may be produced by diagonalizing a matrix of these states - Configuration Interaction. As they are distinct solutions of the SCF equations, these states are non-orthogonal (one cannot be constructed as a single determinant made out of the orbitals of another), and so the CI is a little more complicated and is a non-orthogonal CI (NOCI). More information on NOCI can be found in Section 6.2.7.

**SCF_SAVEMINIMA**

Turn on SCF meta-dynamics and specify how many solutions to locate.

TYPE:

INTEGER

DEFAULT:

0

OPTIONS:

0 Do not use SCF meta-dynamics

$n$ Attempt to find $n$ distinct SCF solutions.

RECOMMENDATION:

Perform SCF Orbital meta-dynamics and attempt to locate $n$ different SCF solutions. Note that these may not all be minima. Many saddle points are often located. The last one located will be the one used in any post-SCF treatments. In systems where there are infinite point groups, this procedure cannot currently distinguish between spatial rotations of different densities, so will likely converge on these multiply.

**SCF_READMINIMA**

Read in solutions from a previous SCF meta-dynamics calculation

TYPE:

INTEGER

DEFAULT:

0

OPTIONS:

$n$ Read in $n$ previous solutions and attempt to locate them all.

$-n$ Read in $n$ previous solutions, but only attempt to locate solution $n$.

RECOMMENDATION:

This may not actually locate all solutions required and will probably locate others too. The SCF will also stop when the number of solutions specified in SCF_SAVEMINIMA are found. Solutions from other geometries may also be read in and used as starting orbitals. If a solution is found and matches one that is read in within SCF_MINFIND_READDISTTHRESH, its orbitals are saved in that position for any future calculations. The algorithm works by restarting from the orbitals and density of a the minimum it is attempting to find. After 10 failed restarts (defined by SCF_MINFIND_RESTARTSTEPS), it moves to another previous minimum and attempts to locate that instead. If there are no minima to find, the restart does random mixing (with 10 times the normal random mixing parameter).

**SCF_MINFIND_WELLTHRESH**

Specify what SCF_MINFIND believes is the basin of a solution

TYPE:

INTEGER

DEFAULT:

5

OPTIONS:

$n$ for a threshold of $10^{-n}$

RECOMMENDATION:

When the DIIS error is less than $10^{-n}$, penalties are switched off to see whether it has converged to a new solution.

**SCF_MINFIND_RESTARTSTEPS**

Restart with new orbitals if no minima have been found within this many steps

TYPE:

INTEGER

DEFAULT:

300

OPTIONS:

$n$ Restart after $n$ steps.

RECOMMENDATION:

If the SCF calculation spends many steps not finding a solution, lowering this number may speed up solution-finding. If the system converges to solutions very slowly, then this number may need to be raised.

**SCF_MINFIND_INCREASEFACTOR**

Controls how the height of the penalty function changes when repeatedly trapped at the same solution

TYPE:

INTEGER

DEFAULT:

10100 meaning 1.01

OPTIONS:

$abcde$ corresponding to $a.bcde$

RECOMMENDATION:

If the algorithm converges to a solution which corresponds to a previously located solution, increase both the normalization N and the width lambda of the penalty function there. Then do a restart.

**SCF_MINFIND_INITLAMBDA**

Control the initial width of the penalty function.

TYPE:

INTEGER

DEFAULT:

02000 meaning 2.000

OPTIONS:

$abcde$ corresponding to $ab.cde$

RECOMMENDATION:

The initial inverse-width (*i.e.*, the inverse-variance) of the Gaussian to place to fill solution's well. Measured in electrons$^( - 1)$. Increasing this will repeatedly converging on the same solution.

**SCF_MINFIND_INITNORM**

Control the initial height of the penalty function.

TYPE:

INTEGER

DEFAULT:

01000 meaning 1.000

OPTIONS:

$abcde$ corresponding to $ab.cde$

RECOMMENDATION:

The initial normalization of the Gaussian to place to fill a well. Measured in hartrees.

**SCF_MINFIND_RANDOMMIXING**

Control how to choose new orbitals after locating a solution

TYPE:

INTEGER

DEFAULT:

00200 meaning .02 radians

OPTIONS:

$abcde$ corresponding to $a.bcde$ radians

RECOMMENDATION:

After locating an SCF solution, the orbitals are mixed randomly to move to a new position in orbital space. For each occupied and virtual orbital pair picked at random and rotate between them by a random angle between 0 and this. If this is negative then use exactly this number, *e.g.*, $-15708$ will almost exactly swap orbitals. Any number$< -15708$ will cause the orbitals to be swapped exactly.

**SCF_MINFIND_NRANDOMMIXES**

Control how many random mixes to do to generate new orbitals

TYPE:

INTEGER

DEFAULT:

10

OPTIONS:

$n$ Perform $n$ random mixes.

RECOMMENDATION:

This is the number of occupied/virtual pairs to attempt to mix, per separate density (*i.e.*, for unrestricted calculations both alpha and beta space will get this many rotations). If this is negative then only mix the highest 25% occupied and lowest 25% virtuals.

**SCF_MINFIND_READDISTTHRESH**

The distance threshold at which to consider two solutions the same

TYPE:

INTEGER

DEFAULT:

00100 meaning 0.1

OPTIONS:

$abcde$ corresponding to $ab.cde$

RECOMMENDATION:

The threshold to regard a minimum as the same as a read in minimum. Measured in electrons. If two minima are closer together than this, reduce the threshold to distinguish them.

**SCF_MINFIND_MIXMETHOD**

Specify how to select orbitals for random mixing

TYPE:

INTEGER

DEFAULT:

0

OPTIONS:

0 Random mixing: select from any orbital to any orbital.

1 Active mixing: select based on energy, decaying with distance from the Fermi level.

2 Active Alpha space mixing: select based on energy, decaying with distance from the Fermi level only in the alpha space.

RECOMMENDATION:

Random mixing will often find very high energy solutions. If lower energy solutions are desired, use 1 or 2.

**SCF_MINFIND_MIXENERGY**

Specify the active energy range when doing Active mixing

TYPE:

INTEGER

DEFAULT:

00200 meaning 00.200

OPTIONS:

$abcde$ corresponding to $ab.cde$

RECOMMENDATION:

The standard deviation of the Gaussian distribution used to select the orbitals for mixing (centered on the Fermi level). Measured in Hartree. To find less-excited solutions, decrease this value

**SCF_MINFIND_RUNCORR**

Run post-SCF correlated methods on multiple SCF solutions

TYPE:

INTEGER

DEFAULT:

0

OPTIONS:

If this is set $> 0$, then run correlation methods for all found SCF solutions.

RECOMMENDATION:

Post-HF correlation methods should function correctly with excited SCF solutions, but their convergence is often much more difficult owing to intruder states.

## 4.13 Ground State Method Summary

To summarize the main features of Q-CHEM's ground state self-consistent field capabilities, the user needs to consider:

- Input a molecular geometry (*$molecule* keyword)
  - Cartesian
  - *Z*-matrix
  - Read from prior calculations
- Declare the job specification (*$rem* keyword)
  - JOBTYPE
    - Single point
    - Optimization
    - Frequency
    - See Table 4.1 for further options
  - BASIS
    - Refer to Chapter 7 (note: *$basis* keyword for user defined basis sets)
    - Effective core potentials (if desired); refer to Chapter 8

- METHOD
    - Single method specification for exchange and correlation. Alternatively these can be specified separately.
- EXCHANGE
    - Linear scaling algorithms for all methods
    - Arsenal of exchange density functionals
    - User definable functionals and hybrids
- CORRELATION
    - DFT or wave function-based methods
    - Linear scaling (CPU and memory) incorporation of correlation with DFT
    - Arsenal of correlation density functionals
    - User definable functionals and hybrids
    - See Chapter 5 for wave function-based correlation methods.

- Exploit Q-CHEM's special features
    - CFMM, LinK large molecule options
    - SCF rate of convergence increased through improved guesses and alternative minimization algorithms
    - Explore novel methods if desired: CASE approximation, PAOs.

# References and Further Reading

[1] Basis Sets (Chapter 7) and Effective Core Potentials (Chapter 8).

[2] Molecular Geometry and Critical Points (Chapter 9).

[3] Molecular Properties Analysis (Chapter 10).

[4] AOINTS (Appendix B).

[5] W. J. Hehre, L. Radom, P. v. R. Schleyer, and J. A. Pople, *Ab Initio Molecular Orbital Theory*, Wiley, New York, 1986.

[6] A. Szabo and N. S. Ostlund, *Modern Quantum Chemistry*, Dover, 1996.

[7] F. Jensen, *Introduction to Computational Chemistry*, Wiley, New York, 1994.

[8] M. Born and J. R. Oppenheimer, *Ann. Phys.* **84**, 457 (1927).

[9] J. C. Slater, *Phys. Rev.* **34**, 1293 (1929).

[10] J. C. Slater, *Phys. Rev.* **35**, 509 (1930).

[11] J. A. Pople and R. K. Nesbet, *J. Chem. Phys.* **22**, 571 (1954).

[12] R. Seeger and J. A. Pople, *J. Chem. Phys.* **66**, 3045 (1977).

[13] T. Takada, M. Dupuis, and H. F. King, *J. Chem. Phys.* **75**, 332 (1981).

[14] M. Dupuis and H. F. King, *Int. J. Quantum Chem.* **11**, 613 (1977).

[15] M. Dupuis and H. F. King, *J. Chem. Phys.* **68**, 3998 (1978).

[16] R. G. Parr and W. Yang, *Density-Functional Theory of Atoms and Molecules*, Oxford University Press, New York, 1989.

[17] W. Kohn, A. D. Becke, and R. G. Parr, *J. Phys. Chem.* **100**, 12974 (1996).

[18] B. B. Laird, R. B. Ross, and T. Ziegler, editors, volume 629 of *ACS Symposium Series*, American Chemical Society, Washington, D.C., 1996.

[19] T. Ziegler, *Chem. Rev.* **91**, 651 (1991).

[20] P. Hohenberg and W. Kohn, *Phys. Rev. B* **136**, 864 (1964).

[21] W. Kohn and L. J. Sham, *Phys. Rev. A* **140**, 1133 (1965).

[22] P. A. M. Dirac, *P. Camb. Philos. Soc.* **26**, 376 (1930).

[23] J. A. Pople, P. M. W. Gill, and B. G. Johnson, *Chem. Phys. Lett.* **199**, 557 (1992).

[24] S. Grimme, *J. Comput. Chem.* **27**, 1787 (2006).

[25] J.-D. Chai and M. Head-Gordon, *J. Chem. Phys.* **128**, 084106 (2008).

[26] J. P. Perdew, K. Burke, and M. Ernzerhof, *Phys. Rev. Lett.* **77**, 3865 (1996).

[27] A. D. Becke, *J. Chem. Phys.* **98**, 5648 (1993).

[28] P. J. Stephens, F. J. Devlin, C. F. Chabolowski, and M. J. Frisch, *J. Phys. Chem.* **98**, 11623 (1994).

[29] J. P. Perdew et al., *J. Chem. Phys.* **123**, 062201 (2005).

[30] O. A. Vydrov and T. Van Voorhis, *Phys. Rev. Lett.* **103**, 063004 (2009).

[31] O. A. Vydrov and T. Van Voorhis, *J. Chem. Phys.* **133**, 244103 (2010).

[32] M. Dion, H. Rydberg, E. Schröder, D. C. Langreth, and B. I. Lundqvist, *Phys. Rev. Lett.* **92**, 246401 (2004).

[33] M. Dion, H. Rydberg, E. Schröder, D. C. Langreth, and B. I. Lundqvist, *Phys. Rev. Lett.* **95**, 109902 (2005).

[34] R. Sabatini, T. Gorni, and S. de Gironcoli, *Phys. Rev. B* **87**, 041108 (2013).

[35] J.-D. Chai and M. Head-Gordon, *Phys. Chem. Chem. Phys.* **10**, 6615 (2008).

[36] S. Grimme, J. Antony, S. Ehrlich, and H. Krieg, *J. Chem. Phys.* **132**, 154104 (2010).

[37] S. Grimme, S. Ehrlich, and L. Goerigk, *J. Chem. Theory Comput.* **32**, 1456 (2011).

[38] H. Schröder, A. Creon, and T. Schwabe, *J. Chem. Theory Comput.* **11**, 3163 (2015).

[39] D. G. A. Smith, L. A. Burns, K. Patkowski, and C. D. Sherrill, *J. Phys. Chem. Lett.* **7**, 2197 (2016).

[40] K.-Y. Liu, J. Liu, and J. M. Herbert, 2017.

[41] P. M. W. Gill, R. D. Adamson, and J. A. Pople, *Mol. Phys.* **88**, 1005 (1996).

[42] A. D. Becke, *Phys. Rev. A* **38**, 3098 (1988).

[43] Y. Zhang and W. Yang, *Phys. Rev. Lett.* **80**, 890 (1998).

[44] R. Armiento and S. Kümmel, *Phys. Rev. Lett.* **111**, 036402 (2013).

[45] A. D. Becke, *J. Chem. Phys.* **84**, 4524 (1986).

[46] P. M. W. Gill, *Mol. Phys.* **89**, 433 (1996).

[47] A. D. Becke, *J. Chem. Phys.* **85**, 7184 (1986).

[48] C. Adamo and V. Barone, *J. Chem. Phys.* **108**, 664 (1998).

[49] H. Iikura, T. Tsuneda, T. Yanai, and K. Hirao, *J. Chem. Phys.* **115**, 3540 (2001).

[50] J. Klimeš, D. R. Bowler, and A. Michaelides, *J. Phys. Condens. Matter* **22**, 022201 (2010).

[51] N. C. Handy and A. J. Cohen, *Mol. Phys.* **99**, 403 (2001).

[52] J. P. Perdew et al., *Phys. Rev. Lett.* **100**, 136406 (2008).

[53] J. P. Perdew and Y. Wang, *Phys. Rev. B* **33**, 8800 (1986).

[54] J. P. Perdew et al., *Phys. Rev. B* **46**, 6671 (1992).

[55] B. Hammer, L. B. Hansen, and J. K. Nørskov, *Phys. Rev. B* **59**, 7413 (1999).

[56] E. D. Murray, K. Lee, and D. C. Langreth, *J. Chem. Theory Comput.* **5**, 2754 (2009).

[57] Y. Zhao and D. G. Truhlar, *J. Chem. Phys.* **128**, 184109 (2006).

[58] T. M. Henderson, B. G. Janesko, and G. E. Scuseria, *J. Chem. Phys.* **128**, 194105 (2008).

[59] J. Tao, J. P. Perdew, V. N. Staroverov, and G. E. Scuseria, *Phys. Rev. Lett.* **91**, 146401 (2003).

[60] J. P. Perdew, A. Ruzsinszky, G. I. Csonka, L. A. Constantin, and J. Sun, *Phys. Rev. Lett.* **103**, 026403 (2009).

[61] L. A. Constantin, E. Fabiano, and F. D. Sala, *J. Chem. Theory Comput.* **9**, 2256 (2013).

[62] J. P. Perdew, A. Ruzsinszky, J. Tao, G. I. Csonka, and G. E. Scuseria, *Phys. Rev. A* **76**, 042506 (2007).

[63] L. Goerigk and S. Grimme, *J. Chem. Theory Comput.* **6**, 107 (2010).

[64] P.-F. Loos, *J. Chem. Phys.* **146**, 114108 (2017).

[65] J. P. Perdew, S. Kurth, A. Zupan, and P. Blaha, *Phys. Rev. Lett.* **82**, 2544 (1999).

[66] A. Ruzsinszky, J. Sun, B. Xiao, and G. Csonka, *J. Chem. Theory Comput.* **8**, 2078 (2012).

[67] J. Sun, A. Ruzsinszky, and J. P. Perdew, *Phys. Rev. Lett.* **115**, 036402 (2015).

[68] J. Tao and Y. Mo, *Phys. Rev. Lett.* **117**, 073001 (2016).

[69] J. P. Perdew and Y. Wang, *Phys. Rev. B* **45**, 13244 (1992).

[70] S. H. Vosko, L. Wilk, and M. Nusair, *Can. J. Phys.* **58**, 1200 (1980).

[71] S. Liu and R. G. Parr, *J. Mol. Struct. (Theochem)* **501**, 29 (2000).

[72] E. Proynov and J. Kong, *Phys. Rev. A* **79**, 014103 (2009).

[73] J. P. Perdew and A. Zunger, *Phys. Rev. B* **23**, 5048 (1981).

[74] E. P. Wigner, *Trans. Faraday Soc.* **34**, 678 (1938).

[75] P. A. Stewart and P. M. W. Gill, *J. Chem. Soc. Faraday Trans.* **91**, 4337 (1995).

[76] C. Lee, W. Yang, and R. G. Parr, *Phys. Rev. B* **37**, 785 (1988).

[77] J. P. Perdew, *Phys. Rev. B* **33**, 8822 (1986).

[78] L. A. Constantin, E. Fabiano, and F. D. Sala, *Phys. Rev. B* **86**, 035130 (2012).

[79] A. D. Becke, *J. Chem. Phys.* **104**, 1040 (1996).

[80] E. Proynov and J. Kong, *J. Chem. Theory Comput.* **3**, 746 (2007).

[81] J. Wellendorff et al., *Phys. Rev. B* **85**, 235149 (2012).

[82] T. Tsuneda, T. Suzumura, and K. Hirao, *J. Chem. Phys.* **110**, 10664 (1999).

[83] R. D. Adamson, P. M. W. Gill, and J. A. Pople, *Chem. Phys. Lett.* **284**, 6 (1998).

[84] C. Y. Lin, M. W. George, and P. M. W. Gill, *Aust. J. Chem.* **57**, 365 (2004).

[85] H. S. Yu, W. Zhang, P. Verma, X. He, and D. G. Truhlar, *Phys. Chem. Chem. Phys.* **17**, 12146 (2015).

[86] F. A. Hamprecht, A. J. Cohen, D. J. Tozer, and N. C. Handy, *J. Chem. Phys.* **109**, 6264 (1998).

[87] A. D. Boese, N. L. Doltsinis, N. C. Handy, and M. Sprik, *J. Chem. Phys.* **112**, 1670 (2000).

[88] A. D. Boese and N. C. Handy, *J. Chem. Phys.* **114**, 5497 (2001).

[89] P. Verma and D. G. Truhlar, *J. Phys. Chem. Lett.* **8**, 380 (2017).

[90] T. W. Keal and D. J. Tozer, *J. Chem. Phys.* **119**, 3015 (2003).

[91] T. W. Keal and D. J. Tozer, *J. Chem. Phys.* **121**, 5654 (2004).

[92] R. Peverati and D. G. Truhlar, *J. Chem. Theory Comput.* **8**, 2310 (2012).

[93] R. Peverati, Y. Zhao, and D. G. Truhlar, *J. Phys. Chem. Lett.* **2**, 1991 (2011).

[94] N. Mardirossian and M. Head-Gordon, *J. Chem. Phys.* **142**, 074111 (2015).

[95] N. Mardirossian et al., *J. Phys. Chem. Lett.* **8**, 35 (2017).

[96] Y. Zhao and D. G. Truhlar, *J. Chem. Phys.* **125**, 194101 (2006).

[97] R. Peverati and D. G. Truhlar, *J. Phys. Chem. Lett.* **3**, 117 (2012).

[98] J. Wellendorff, K. T. Lundgaard, K. W. Jacobsen, and T. Bligaard, *J. Chem. Phys.* **140**, 144107 (2014).

[99] J. Sun, B. Xiao, and A. Ruzsinszky, *J. Chem. Phys.* **137**, 051101 (2012).

[100] J. Sun et al., *J. Chem. Phys.* **138**, 044113 (2013).

[101] J. Sun, J. P. Perdew, and A. Ruzsinszky, *Proc. Natl. Acad. Sci. USA* **112**, 685 (2015).

[102] R. Peverati and D. G. Truhlar, *Phys. Chem. Chem. Phys.* **14**, 13171 (2012).

[103] H. S. Yu, X. He, and D. G. Truhlar, *J. Chem. Theory Comput.* **12**, 1280 (2016).

[104] A. D. Boese and N. C. Handy, *J. Chem. Phys.* **116**, 9559 (2002).

[105] T. Van Voorhis and G. E. Scuseria, *J. Chem. Phys.* **109**, 400 (1998).

[106] C. Adamo and V. Barone, *J. Chem. Phys.* **110**, 6158 (1999).

[107] A. D. Becke, *J. Chem. Phys.* **107**, 8554 (1997).

[108] C. Adamo and V. Barone, *Chem. Phys. Lett.* **274**, 242 (1997).

[109] Y. Shao, M. Head-Gordon, and A. I. Krylov, *J. Chem. Phys.* **118**, 4807 (2003).

[110] P. J. Wilson, T. J. Bradley, and D. J. Tozer, *J. Chem. Phys.* **115**, 9233 (2001).

[111] T. W. Keal and D. J. Tozer, *J. Chem. Phys.* **123**, 121103 (2005).

[112] A. D. Boese and J. M. L. Martin, *J. Chem. Phys.* **121**, 3405 (2004).

[113] B. J. Lynch, P. L. Fast, M. Harris, and D. G. Truhlar, *J. Phys. Chem. A* **104**, 4811 (2000).

[114] W.-M. Hoe, A. J. Cohen, and N. H. Handy, *Chem. Phys. Lett.* **341**, 319 (2001).

[115] S. Grimme, J. G. Brandenburg, C. Bannwarth, and A. Hansen, *J. Chem. Phys.* **143**, 054107 (2015).

[116] Y. A. Bernard, Y. Shao, and A. I. Krylov, *J. Chem. Phys.* **136**, 204103 (2012).

[117] R. Peverati and D. G. Truhlar, *J. Chem. Phys.* **135**, 191102 (2011).

[118] K. W. Wiitala, T. R. Hoye, and C. J. Cramer, *J. Chem. Theory Comput.* **2**, 1085 (2006).

[119] X. Xu and W. A. Goddard III, *Proc. Natl. Acad. Sci. USA* **101**, 2673 (2004).

[120] Y. Zhao and D. G. Truhlar, *Theor. Chem. Acc.* **120**, 215 (2008).

[121] Y. Zhao and D. G. Truhlar, *J. Chem. Theory Comput.* **4**, 1849 (2007).

[122] V. N. Staroverov, G. E. Scuseria, J. Tao, and J. P. Perdew, *J. Chem. Phys.* **119**, 12129 (2003).

[123] G. I. Csonka, J. P. Perdew, and A. Ruzsinszky, *J. Chem. Theory Comput.* **6**, 3688 (2010).

[124] E. Proynov and J. Kong, in *Theoretical Aspects of Catalysis*, edited by G. Vaysilov and T. Mineva, Heron Press, Birmingham, UK, 2008.

[125] Y. Zhao, B. J. Lynch, and D. G. Truhlar, *J. Phys. Chem. A* **108**, 2715 (2004).

[126] K. Pernal, R. Podeszwa, K. Patkowski, and K. Szalewicz, *Phys. Rev. Lett.* **103**, 263201 (2009).

[127] Y. Zhao, N. E. Schultz, and D. G. Truhlar, *J. Chem. Phys.* **123**, 161103 (2005).

[128] Y. Zhao, N. E. Schultz, and D. G. Truhlar, *J. Chem. Theory Comput.* **2**, 364 (2006).

[129] Y. Zhao and D. G. Truhlar, *J. Phys. Chem. A* **110**, 13126 (2006).

[130] H. S. Yu, X. He, S. L. Li, and D. G. Truhlar, *Chem. Sci.* **7**, 5032 (2016).

[131] Y. Zhao and D. G. Truhlar, *J. Phys. Chem. A* **108**, 6908 (2004).

[132] Y. Zhao and D. G. Truhlar, *J. Phys. Chem. A* **109**, 5656 (2005).

[133] K. Hui and J.-D. Chai, *J. Chem. Phys.* **144**, 044114 (2016).

[134] S. Grimme, *J. Phys. Chem. A* **109**, 3067 (2005).

[135] N. Mardirossian and M. Head-Gordon, *Phys. Chem. Chem. Phys.* **16**, 9904 (2014).

[136] Y.-S. Lin, G.-D. Li, S.-P. Mao, and J.-D. Chai, *J. Chem. Theory Comput.* **9**, 263 (2013).

[137] T. Yanai, D. Tew, and N. Handy, *Chem. Phys. Lett.* **393**, 51 (2004).

[138] P. Verma and R. J. Bartlett, *J. Chem. Phys.* **140**, 18A534 (2014).

[139] Y. Jin and R. J. Bartlett, *J. Chem. Phys.* **145**, 034107 (2016).

[140] A. V. Krukau, O. A. Vydrov, A. F. Izmaylov, and G. E. Scuseria, *J. Chem. Phys.* **125**, 224106 (2006).

[141] E. Weintraub, T. M. Henderson, and G. E. Scuseria, *J. Chem. Theory Comput.* **5**, 754 (2009).

[142] J. W. Song, T. Hirosawa, T. Tsuneda, and K. Hirao, *J. Chem. Phys.* **126**, 154105 (2007).

[143] M. A. Rohrdanz and J. M. Herbert, *J. Chem. Phys.* **129**, 034107 (2008).

[144] M. A. Rohrdanz, K. M. Martins, and J. M. Herbert, *J. Chem. Phys.* **130**, 054112 (2009).

[145] R. Peverati and D. G. Truhlar, *Phys. Chem. Chem. Phys.* **14**, 16187 (2012).

[146] A. J. Cohen, P. Mori-Sánchez, and W. Yang, *J. Chem. Phys.* **126**, 191109 (2007).

[147] N. Mardirossian and M. Head-Gordon, *J. Chem. Phys.* **144**, 214110 (2016).

[148] R. Peverati and D. G. Truhlar, *J. Phys. Chem. Lett.* **2**, 2810 (2011).

[149] Y.-S. Lin, C.-W. Tsai, G.-D. Li, and J.-D. Chai, *J. Chem. Phys.* **136**, 154109 (2012).

[150] S. Kozuch and J. M. L. Martin, *J. Comput. Chem.* **34**, 2327 (2013).

[151] J.-D. Chai and M. Head-Gordon, *J. Chem. Phys.* **131**, 174105 (2009).

[152] Y. Zhang, X. Xu, and W. A. Goddard III, *Proc. Natl. Acad. Sci. USA* **106**, 4963 (2009).

[153] I. Y. Zhang, X. Xin, Y. Jung, and W. A. Goddard III, *Proc. Natl. Acad. Sci. USA* **108**, 19896 (2011).

[154] S. Grimme, *J. Chem. Phys.* **124**, 034108 (2006).

[155] A. Karton, A. Tarnopolsky, J.-F. Lamère, G. C. Schatz, and J. M. L. Martin, *J. Phys. Chem. A* **112**, 12868 (2008).

[156] J. Toulouse, K. Sharkas., E. Brémond, and C. Adamo, *J. Chem. Phys.* **135**, 101102 (2011).

[157] E. Brémond, J. C. Sancho-García, A. J. Pérez-Jiménez, and C. Adamo, *J. Chem. Phys.* **141**, 031101 (2014).

[158] J.-D. Chai and S.-P. Mao, *Chem. Phys. Lett.* **538**, 121 (2012).

[159] E. Brémond and C. Adamo, *J. Chem. Phys.* **135**, 024106 (2011).

[160] L. Goerigk and S. Grimme, *J. Chem. Theory Comput.* **7**, 291 (2011).

[161] N. A. Besley, M. J. G. Peach, and D. J. Tozer, *Phys. Chem. Chem. Phys.* **11**, 10350 (2009).

[162] A. D. Becke and M. R. Roussel, *Phys. Rev. A* **39**, 3761 (1989).

[163] A. D. Becke, *Int. J. Quantum Chem. Symp.* **28**, 625 (1994).

[164] A. D. Becke and E. R. Johnson, *J. Chem. Phys.* **122**, 154104 (2005).

[165] E. Proynov, F. Liu, and J. Kong, *Chem. Phys. Lett.* **525**, 150 (2012).

[166] E. Proynov, Y. Shao, and J. Kong, *Chem. Phys. Lett.* **493**, 381 (2010).

[167] E. Proynov, F. Liu, Y. Shao, and J. Kong, *J. Chem. Phys.* **136**, 034102 (2012).

[168] J. P. Perdew, V. N. Staroverov, J. Tao, and G. E. Scuseria, *Phys. Rev. A* **78**, 052513 (2008).

[169] P. Mori-Sánchez, A. J. Cohen, and W. Yang, *J. Chem. Phys.* **124**, 091102 (2006).

[170] A. J. Cohen, P. Mori-Sánchez, and W. Yang, *J. Chem. Phys.* **127**, 034101 (2007).

[171] F. Liu, E. Proynov, J.-G. Yu, T. R. Furlani, and J. Kong, *J. Chem. Phys.* **137**, 114104 (2012).

[172] A. D. Becke, *J. Chem. Phys.* **88**, 2547 (1988).

[173] B. G. Johnson, P. M. W. Gill, and J. A. Pople, *Chem. Phys. Lett.* **220**, 377 (1994).

[174] C. W. Murray, N. C. Handy, and G. J. Laming, *Mol. Phys.* **78**, 997 (1993).

[175] S.-H. Chien and P. M. W. Gill, *J. Comput. Chem.* **24**, 732 (2003).

[176] M. Mitani, *Theor. Chem. Acc.* **130**, 645 (2011).

[177] M. Mitani and Y. Yoshioka, *Theor. Chem. Acc.* **131**, 1169 (2012).

[178] S. Dasgupta and J. M. Herbert, *J. Comput. Chem.* **38**, 869 (2017).

[179] V. I. Lebedev, *Sibirsk. Mat. Zh.* **18**, 132 (1977).

[180] V. I. Lebedev, *Zh. Vychisl. Mat. Mat. Fix.* **15**, 48 (1975).

[181] V. I. Lebedev, *Zh. Vychisl. Mat. Mat. Fix.* **16**, 293 (1976).

[182] V. I. Lebedev and D. N. Laikov, *Dokl. Math.* **366**, 741 (1999).

[183] P. M. W. Gill, B. G. Johnson, and J. A. Pople, *Chem. Phys. Lett.* **209**, 506 (1993).

[184] S.-H. Chien and P. M. W. Gill, *J. Comput. Chem.* **27**, 730 (2006).

[185] F. Castet and B. Champagne, *J. Chem. Theory Comput.* **8**, 2044 (2012).

[186] Y. Zhao and D. G. Truhlar, *Chem. Phys. Lett.* **502**, 1 (2011).

[187] S. E. Wheeler and K. N. Houk, *J. Chem. Theory Comput.* **6**, 395 (2010).

[188] A. Dreuw, J. L. Weisman, and M. Head-Gordon, *J. Chem. Phys.* **119**, 2943 (2003).

[189] C. Adamo, G. E. Scuseria, and V. Barone, *J. Chem. Phys.* **111**, 2889 (1999).

[190] A. Lange and J. M. Herbert, *J. Chem. Theory Comput.* **3**, 1680 (2007).

[191] A. W. Lange and J. M. Herbert, *J. Am. Chem. Soc.* **131**, 124115 (2009).

[192] A. W. Lange, M. A. Rohrdanz, and J. M. Herbert, *J. Phys. Chem. B* **112**, 6304 (2008).

[193] R. D. Adamson, J. P. Dombroski, and P. M. W. Gill, *J. Comput. Chem.* **20**, 921 (1999).

[194] R. M. Richard and J. M. Herbert, *J. Chem. Theory Comput.* **7**, 1296 (2011).

[195] J. Heyd, G. E. Scuseria, and M. Ernzerhof, *J. Chem. Phys.* **118**, 8207 (2003).

[196] F. Uhlig, J. M. Herbert, M. P. Coons, and P. Jungwirth, *J. Phys. Chem. A* **118**, 7507 (2014).

[197] A. J. Cohen, P. Mori-Sánchez, and W. Yang, *Science* **321**, 792 (2008).

[198] P. Mori-Sánchez and A. J. Cohen, *Phys. Chem. Chem. Phys.* **16**, 14378 (2014).

[199] J. Autschbach and M. Srebro, *Acc. Chem. Res.* **47**, 2592 (2014).

[200] R. Baer, E. Livshits, and U. Salzner, *Annu. Rev. Phys. Chem.* **61**, 85 (2010).

[201] S. J. A. van Gisbergen et al., *J. Chem. Phys.* **105**, 3142 (1996).

[202] Q. Wu, P. W. Ayers, and W. Yang, *J. Chem. Phys.* **119**, 2978 (2003).

[203] E. Livshits and R. Baer, *Phys. Chem. Chem. Phys.* **9**, 2932 (2007).

[204] U. Salzner and R. Baer, *J. Chem. Phys.* **131**, 231101 (2009).

[205] K. Garrett et al., *J. Chem. Theory Comput.* **10**, 3821 (2014).

[206] X. A. S. Vazquez and C. M. Isborn, *J. Chem. Phys.* **143**, 244105 (2015).

[207] M. P. Coons, Z. You, and J. M. Herbert, *J. Am. Chem. Soc.* **138**, 10879 (2016).

[208] M. B. Oviedo, N. V. Ilawe, and B. M. Wong, *J. Chem. Theory Comput.* **12**, 3593 (2016).

[209] M. Modrzejewski, L. Rajchel, G. Chalasinski, and M. M. Szczesniak, *J. Phys. Chem. A* **117**, 11580 (2013).

[210] M. Hapka, L. Rajchel, M. Modrzejewski, G. Chałasiǹski, and M. M. Szczęśniak, *J. Chem. Phys.* **141**, 134120:1 (2014).

[211] K. U. Lao and J. M. Herbert, Implementation of restricted and unrestricted versions of extended symmetry-adapted perturbation theory (XSAPT) in the atomic orbital basis, and benchmark calculations for large supramolecular complexes, (in preparation).

[212] O. A. Vydrov, Q. Wu, and T. Van Voorhis, *J. Chem. Phys.* **129**, 014106 (2008).

[213] K. Lee, É. D. Murray, L. Kong, B. I. Lundqvist, and D. C. Langreth, *Phys. Rev. B* **82**, 081101(R) (2010).

[214] O. A. Vydrov and T. Van Voorhis, *J. Chem. Phys.* **132**, 164113 (2010).

[215] J. Witte, N. Mardirossian, J. B. Neaton, and M. Head-Gordon, *J. Chem. Theory Comput.* **13**, 2043 (2017).

[216] E. R. Johnson and A. D. Becke, *J. Chem. Phys.* **123**, 024101 (2005).

[217] J. Kong, Z. Gan, E. Proynov, M. Freindorf, and T. Furlani, *Phys. Rev. A* **79**, 042510 (2009).

[218] E. R. Johnson and A. D. Becke, *J. Chem. Phys.* **124**, 174104 (2006).

[219] A. D. Becke and F. O. Kannemann, *Can. J. Chem.* **88**, 1057 (2010).

[220] F. O. Kannemann and A. D. Becke, *J. Chem. Theory Comput.* **6**, 1081 (2010).

[221] J. Witte, J. B. Neaton, and M. Head-Gordon, *J. Chem. Phys.* **146**, 234105 (2017).

[222] T. Schwabe and S. Grimme, *Phys. Chem. Chem. Phys.* **9**, 3397 (2007).

[223] A. Tarnopolsky, A. Karton, R. Sertchook, D. Vuzman, and J. M. L. Martin, *J. Phys. Chem. A* **112**, 3 (2008).

[224] T. Benighaus, R. A. DiStasio, Jr., R. C. Lochan, J.-D. Chai, and M. Head-Gordon, *J. Phys. Chem. A* **112**, 2702 (2008).

[225] C. Møller and M. S. Plesset, *Phys. Rev.* **46**, 618 (1934).

[226] J. Kim and Y. Jung, *J. Chem. Theory Comput.* **11**, 45 (2015).

[227] H. Ji, Y. Shao, W. A. Goddard, and Y. Jung, *J. Chem. Theory Comput.* **9**, 1971 (2013).

[228] R. van Leeuwen and E. J. Baerends, *Phys. Rev. A* **49**, 2421 (1994).

[229] M. E. Casida and D. R. Salahub, *J. Chem. Phys.* **113**, 8918 (2000).

[230] M. E. Casida, C. Jamorski, K. C. Casida, and D. R. Salahub, *J. Chem. Phys.* **108**, 4439 (1998).

[231] S. Hirata and M. Head-Gordon, *Chem. Phys. Lett.* **314**, 291 (1999).

[232] M. Levy and J. P. Perdew, *Phys. Rev. A* **32**, 2010 (1985).

[233] C.-R. Pan, P.-T. Fang, and J.-D. Chai, *Phys. Rev. A* **87**, 052510 (2013).

[234] J.-D. Chai and P.-T. Chen, *Phys. Rev. Lett.* **110**, 033002 (2013).

[235] J.-D. Chai, *J. Chem. Phys.* **136**, 154104 (2012).

[236] J.-D. Chai, *J. Chem. Phys.* **140**, 18A521 (2014).

[237] M. Wolfsberg and L. Helmholtz, *J. Chem. Phys.* **20**, 837 (1952).

[238] P. Pulay, *Chem. Phys. Lett.* **73**, 393 (1980).

[239] P. Pulay, *J. Comput. Chem.* **3**, 556 (1982).

[240] T. Van Voorhis and M. Head-Gordon, *Mol. Phys.* **100**, 1713 (2002).

[241] A. T. B. Gilbert, N. A. Besley, and P. M. W. Gill, *J. Phys. Chem. A* **112**, 13164 (2008).

[242] E. Cancès and C. Le Bris, *Int. J. Quantum Chem.* **79**, 82 (2000).

[243] E. Cancès, *J. Chem. Phys.* **114**, 10616 (2001).

[244] K. N. Kudin, G. E. Scuseria, and E. Cancès, *J. Chem. Phys.* **116**, 8255 (2002).

[245] A. D. Rabuck and G. E. Scuseria, *J. Chem. Phys.* **110**, 695 (1999).

[246] X. Hu and W. Yang, *J. Chem. Phys.* **132**, 054109 (2010).

[247] L. A. Curtiss, K. Raghavachari, P. C. Redfern, and J. A. Pople, *J. Chem. Phys.* **106**, 1063 (1997).

[248] E. R. Davidson, *J. Chem. Phys.* **17**, 87 (1975).

[249] S. M. Sharada, D. Stück, E. J. Sundstrom, A. T. Bell, and M. Head-Gordon, *Mol. Phys.* **113**, 1802 (2015).

[250] L. Greengard, *The Rapid Evaluation of Potential Fields in Particle Systems*, MIT Press, London, 1987.

[251] C. A. White and M. Head-Gordon, *J. Chem. Phys.* **101**, 6593 (1994).

[252] C. A. White, B. G. Johnson, P. M. W. Gill, and M. Head-Gordon, *Chem. Phys. Lett.* **230**, 8 (1994).

[253] C. A. White and M. Head-Gordon, *J. Chem. Phys.* **105**, 5061 (1996).

[254] C. A. White and M. Head-Gordon, *Chem. Phys. Lett.* **257**, 647 (1996).

[255] C. A. White, B. G. Johnson, P. M. W. Gill, and M. Head-Gordon, *Chem. Phys. Lett.* **253**, 268 (1996).

[256] C. A. White and M. Head-Gordon, *J. Chem. Phys.* **104**, 2620 (1996).

[257] Y. Shao and M. Head-Gordon, *Chem. Phys. Lett.* **323**, 425 (2000).

[258] Y. Shao and M. Head-Gordon, *J. Chem. Phys.* **114**, 6572 (2001).

[259] T. R. Adams, R. D. Adamson, and P. M. W. Gill, *J. Chem. Phys.* **107**, 124 (1997).

[260] E. Schwegler, M. Challacombe, and M. Head-Gordon, *J. Chem. Phys.* **106**, 9708 (1997).

[261] C. Ochsenfeld, C. A. White, and M. Head-Gordon, *J. Chem. Phys.* **109**, 1663 (1998).

[262] C. Ochsenfeld, *Chem. Phys. Lett.* **327**, 216 (2000).

[263] E. Schwegler and M. Challacombe, *J. Chem. Phys.* **106**, 9708 (1996).

[264] L. Fusti-Molnar and P. Pulay, *J. Chem. Phys.* **116**, 7795 (2002).

[265] L. Fusti-Molnar and P. Pulay, *J. Chem. Phys.* **117**, 7827 (2002).

[266] L. Fusti-Molnar, *J. Chem. Phys.* **119**, 11080 (2003).

[267] L. Fusti-Molnar and J. Kong, *J. Chem. Phys.* **122**, 074108 (2005).

[268] J. Kong, S. T. Brown, and L. Fusti-Molnar, *J. Chem. Phys.* **124**, 094109 (2006).

[269] N. J. Russ, C.-M. Chang, and J. Kong, *Can. J. Chem.* **89**, 657 (2011).

[270] C.-M. Chang, N. J. Russ, and J. Kong, *Phys. Rev. A* **84**, 022504 (2011).

[271] A. Sodt and M. Head-Gordon, *J. Chem. Phys.* **125**, 074116 (2006).

[272] A. Sodt and M. Head-Gordon, *J. Chem. Phys.* **128**, 104106 (2008).

[273] S. F. Manzer, E. Epifanovsky, and M. Head-Gordon, *J. Chem. Theory Comput.* **11**, 518 (2015).

[274] P. Merlot et al., *J. Comput. Chem.* **34**, 1486 (2013).

[275] F. Weigend, *Phys. Chem. Chem. Phys.* **4**, 4285 (2002).

[276] R. D. Adamson, J. P. Dombroski, and P. M. W. Gill, *Chem. Phys. Lett.* **254**, 329 (1996).

[277] J. P. Dombroski, S. W. Taylor, and P. M. W. Gill, *J. Phys. Chem.* **100**, 6272 (1996).

[278] S. F. Manzer, P. R. Horn, N. Mardirossian, and M. Head-Gordon, *J. Chem. Phys.* **143**, 024113 (2015).

[279] W. Z. Liang and M. Head-Gordon, *J. Phys. Chem. A* **108**, 3206 (2004).

[280] R. P. Steele, R. A. DiStasio, Jr., Y. Shao, J. Kong, and M. Head-Gordon, *J. Chem. Phys.* **125**, 074108 (2006).

[281] R. P. Steele, Y. Shao, R. A. DiStasio, Jr., and M. Head-Gordon, *J. Phys. Chem. A* **110**, 13915 (2006).

[282] R. A. DiStasio, Jr., R. P. Steele, and M. Head-Gordon, *Mol. Phys.* **105**, 27331 (2007).

[283] R. P. Steele and M. Head-Gordon, *Mol. Phys.* **105**, 2455 (2007).

[284] R. P. Steele, R. A. DiStasio, Jr., and M. Head-Gordon, *J. Chem. Theory Comput.* **5**, 1560 (2009).

[285] L. A. Curtiss, K. Raghavachari, G. W. Trucks, and J. A. Pople, *J. Chem. Phys.* **94**, 7221 (1991).

[286] L. A. Curtiss, K. Raghavachari, P. C. Redfern, V. Rassolov, and J. A. Pople, *J. Chem. Phys.* **109**, 7764 (1998).

[287] L. A. Curtiss, K. Raghavachari, P. C. Redfern, and J. A. Pople, *J. Chem. Phys.* **112**, 7374 (2000).

[288] R. P. Steele, M. Head-Gordon, and J. C. Tully, *J. Phys. Chem. A* **114**, 11853 (2010).

[289] J. M. Herbert and M. Head-Gordon, *J. Chem. Phys.* **121**, 11542 (2004).

[290] R. P. Steele and J. C. Tully, *Chem. Phys. Lett.* **500**, 167 (2010).

[291] J. Deng, A. T. B. Gilbert, and P. M. W. Gill, *J. Chem. Phys.* **130**, 231101 (2009).

[292] J. Deng, A. T. B. Gilbert, and P. M. W. Gill, *J. Chem. Phys.* **133**, 044116 (2009).

[293] J. Deng, A. T. B. Gilbert, and P. M. W. Gill, *Phys. Chem. Chem. Phys.* **12**, 10759 (2010).

[294] T. Nakajima and K. Hirao, *J. Chem. Phys.* **124**, 184108 (2006).

[295] D. J. Tozer, M. E. Mura, R. D. Amos, and N. C. Handy, in *Computational Chemistry*, AIP Conference Proceedings, page 3, 1994.

[296] Q. Wu and T. Van Voorhis, *Phys. Rev. A* **72**, 024502 (2005).

[297] Q. Wu and T. Van Voorhis, *J. Phys. Chem. A* **110**, 9212 (2006).

[298] Q. Wu and T. Van Voorhis, *J. Chem. Theory Comput.* **2**, 765 (2006).

[299] Q. Wu and T. Van Voorhis, *J. Chem. Phys.* **125**, 164105 (2006).

[300] Q. Wu and T. Van Voorhis, *J. Chem. Phys.* **125**, 164105 (2006).

[301] Q. Wu, C. L. Cheng, and T. Van Voorhis, *J. Chem. Phys.* **127**, 164119 (2007).

[302] Q. Wu, B. Kaduk, and T. Van Voorhis, *J. Chem. Phys.* **130**, 034109 (2009).

[303] M. S. Lee and M. Head-Gordon, *J. Chem. Phys.* **107**, 9085 (1997).

[304] M. S. Lee and M. Head-Gordon, *Comp. Chem.* **24**, 295 (2000).

[305] A. J. W. Thom and M. Head-Gordon, *Phys. Rev. Lett.* **101**, 193001 (2008).

# Chapter 5

# Wave Function-Based Correlation Methods

## 5.1 Introduction

The Hartree-Fock procedure, while often qualitatively correct, is frequently quantitatively deficient. The deficiency is due to the underlying assumption of the Hartree-Fock approximation: that electrons move *independently* within molecular orbitals subject to an averaged field imposed by the remaining electrons. The error that this introduces is called the correlation energy and a wide variety of procedures exist for estimating its magnitude. The purpose of this Chapter is to introduce the main wave function-based methods available in Q-CHEM to describe electron correlation.

Wave function-based electron correlation methods concentrate on the design of corrections to the wave function beyond the mean-field Hartree-Fock description. This is to be contrasted with the density functional theory methods discussed in the previous Chapter. While density functional methods yield a description of electronic structure that accounts for electron correlation subject only to the limitations of present-day functionals (which, for example, omit dispersion interactions), DFT cannot be systematically improved if the results are deficient. Wave function-based approaches for describing electron correlation[4,5] offer this main advantage. Their main disadvantage is relatively high computational cost, particularly for the higher-level theories.

There are four broad classes of models for describing electron correlation that are supported within Q-CHEM. The first three directly approximate the full time-independent Schrödinger equation. In order of increasing accuracy, and also increasing cost, they are:

1. Perturbative treatment of pair correlations between electrons, typically capable of recovering 80% or so of the correlation energy in stable molecules.

2. Self-consistent treatment of pair correlations between electrons (most often based on coupled-cluster theory), capable of recovering on the order of 95% or so of the correlation energy.

3. Non-iterative corrections for higher than double substitutions, which can account for more than 99% of the correlation energy. They are the basis of many modern methods that are capable of yielding chemical accuracy for ground state reaction energies, as exemplified by the G2[6] and G3 methods[7].

These methods are discussed in the following subsections.

There is also a fourth class of methods supported in Q-CHEM, which have a different objective. These active space methods aim to obtain a balanced description of electron correlation in highly correlated systems, such as diradicals, or along bond-breaking coordinates. Active space methods are discussed in Section 5.10. Finally, equation-of-motion (EOM) methods provide tools for describing open-shell and electronically excited species. Selected configuration interaction (CI) models are also available.

In order to carry out a wave function-based electron correlation calculation using Q-CHEM, three *$rem* variables need to be set:

- BASIS to specify the basis set (see Chapter 7)
- METHOD for treating correlation
- N_FROZEN_CORE frozen core electrons (FC default, optionally FC, or $n$)

For wave function-based correlation methods, the default option for exchange is Hartree-Fock. If desired, correlated calculations can employ DFT orbitals, which should be set up using a pair of EXCHANGE and CORRELATION keywords. EXCHANGE should be set to a specific DFT method (see Section 5.12).

Additionally, for EOM or CI calculations the number of target states of each type (excited, spin-flipped, ionized, attached, *etc.*) in each irreducible representation (irrep) should be specified (see Section 6.7.12). The level of correlation of the target EOM states may be different from that used for the reference, and can be specified by EOM_CORR keyword.

The full range of ground and excited state wave function-based correlation methods available (*i.e.* the recognized options to the METHOD keyword) are as follows. Ground-state methods are also a valid option for the CORRELATION keyword.

**METHOD**

Specifies the level of theory, either DFT or wave function-based.

TYPE:

STRING

DEFAULT:

HF No correlation, Hartree-Fock exchange

OPTIONS:

| | |
|---|---|
| MP2 | Sections 5.3 and 5.4 |
| RI-MP2 | Section 5.6 |
| Local_MP2 | Section 5.5 |
| RILMP2 | Section 5.6.1 |
| ATTMP2 | Section 5.7 |
| ATTRIMP2 | Section 5.7 |
| ZAPT2 | A more efficient restricted open-shell MP2 method[8]. |
| MP3 | Section 5.3 |
| MP4SDQ | Section 5.3 |
| MP4 | Section 5.3 |
| CCD | Section 5.8 |
| CCD(2) | Section 5.9 |
| CCSD | Section 5.8 |
| CCSD(T) | Section 5.9 |
| CCSD(2) | Section 5.9 |
| CCSD(fT) | Section 5.9.3 |
| CCSD(dT) | Section 5.9.3 |
| QCISD | Section 5.8 |
| QCISD(T) | Section 5.9 |
| OD | Section 5.8 |
| OD(T) | Section 5.9 |
| OD(2) | Section 5.9 |
| VOD | Section 5.10 |
| VOD(2) | Section 5.10 |
| QCCD | Section 5.8 |
| QCCD(T) | |
| QCCD(2) | |
| VQCCD | Section 5.10 |

RECOMMENDATION:

Consult the literature for guidance.

## 5.2 Treatment and the Definition of Core Electrons

Treatment of core electrons is controlled by N_FROZEN_CORE. Starting from version Q-Chem 5.0, the core electrons are frozen by default in most post-Hartree–Fock calculations. Selected virtual orbitals can also be frozen by using N_FROZEN_VIRTUAL keyword (the default for this is zero).

The number of core electrons in an atom is relatively well-defined, and consists of certain atomic shells. (Note that ECPs are available in both "small-core" and "large-core" varieties; see Chapter 8.) For example, in phosphorus the core consists of $1s$, $2s$, and $2p$ shells, for a total of ten electrons. In molecular systems, the core electrons are usually chosen as those occupying the $n/2$ lowest energy orbitals, where $n$ is the number of core electrons in the constituent atoms. In some cases, particularly in the lower parts of the periodic table, this definition is inappropriate and can lead to significant errors in the correlation energy. Vitaly Rassolov has implemented an alternative definition of core electrons within Q-CHEM which is based on a Mulliken population analysis, and which addresses this problem[9].

The current implementation is restricted to *n-kl* type basis sets such as 3-21 or 6-31, and related bases such as 6-31+G(d). There are essentially two cases to consider, the outermost 6G functions (or 3G in the case of the 3-21G basis set) for Na, Mg, K and Ca, and the 3d functions for the elements Ga—Kr. Whether or not these are treated as core or valence is determined by the CORE_CHARACTER *$rem*, as summarized in Table 5.2.

| **CORE_CHARACTER** | **Outermost 6G (3G)**<br>**for Na, Mg, K, Ca** | **3d (Ga–Kr)** |
|---|---|---|
| 1 | valence | valence |
| 2 | valence | core |
| 3 | core | core |
| 4 | core | valence |

Table 5.1: A summary of the effects of different core definitions

**N_FROZEN_CORE**

Sets the number of frozen core orbitals in a post-Hartree–Fock calculation.

TYPE:

INTEGER

DEFAULT:

FC

OPTIONS:

FC Frozen Core approximation (all core orbitals frozen).

$n$ Freeze $n$ core orbitals (if set to 0, all electrons will be active).

RECOMMENDATION:

Correlated calculations calculations are more efficient with frozen core orbitals. Use default if possible.

**N_FROZEN_VIRTUAL**

Sets the number of frozen virtual orbitals in a post-Hartree–Fock calculation.

TYPE:

INTEGER

DEFAULT:

0

OPTIONS:

$n$ Freeze $n$ virtual orbitals.

RECOMMENDATION:

None

**CORE_CHARACTER**

Selects how the core orbitals are determined in the frozen-core approximation.

TYPE:

INTEGER

DEFAULT:

0

OPTIONS:

0 Use energy-based definition.

1-4 Use Mulliken-based definition (see Table 5.2 for details).

RECOMMENDATION:

Use the default, unless performing calculations on molecules with heavy elements.

**PRINT_CORE_CHARACTER**

Determines the print level for the CORE_CHARACTER option.

TYPE:

INTEGER

DEFAULT:

0

OPTIONS:

0 No additional output is printed.

1 Prints core characters of occupied MOs.

2 Print level 1, plus prints the core character of AOs.

RECOMMENDATION:

Use the default, unless you are uncertain about what the core character is.

## 5.3 Møller-Plesset Perturbation Theory

### 5.3.1 Introduction

Møller-Plesset Perturbation Theory [10] is a widely used method for approximating the correlation energy of molecules. In particular, second-order Møller-Plesset perturbation theory (MP2) is one of the simplest and most useful levels of theory beyond the Hartree-Fock approximation. Conventional and local MP2 methods available in Q-CHEM are discussed in detail in Sections 5.4 and 5.5 respectively. The MP3 method is still occasionally used, while MP4 calculations are quite commonly employed as part of the G2 and G3 thermochemical methods [6,7]. In the remainder of this section, the theoretical basis of Møller-Plesset theory is reviewed.

### 5.3.2 Theoretical Background

The Hartree-Fock wave function $\Psi_0$ and energy $E_0$ are *approximate* solutions (eigenfunction and eigenvalue) to the exact Hamiltonian eigenvalue problem or Schrödinger's electronic wave equation, Eq. (4.5). The HF wave function and energy are, however, exact solutions for the Hartree-Fock Hamiltonian $H_0$ eigenvalue problem. If we assume that the Hartree-Fock wave function $\Psi_0$ and energy $E_0$ lie near the exact wave function $\Psi$ and energy $E$, we can now write the exact Hamiltonian operator as

$$H = H_0 + \lambda V \tag{5.1}$$

where $V$ is the small perturbation and $\lambda$ is a dimensionless parameter. Expanding the exact wave function and energy in terms of the HF wave function and energy yields

$$E = E^{(0)} + \lambda E^{(1)} + \lambda^2 E^{(2)} + \lambda^3 E^{(3)} + \ldots \tag{5.2}$$

and

$$\Psi = \Psi_0 + \lambda \Psi^{(1)} + \lambda^2 \Psi^{(2)} + \lambda^3 \Psi^{(3)} + \ldots \tag{5.3}$$

Substituting these expansions into the Schrödinger equation and collecting terms according to powers of $\lambda$ yields

$$H_0 \Psi_0 = E^{(0)} \Psi_0 \tag{5.4}$$

$$H_0 \Psi^{(1)} + V \Psi_0 = E^{(0)} \Psi^{(1)} + E^{(1)} \Psi_0 \tag{5.5}$$

$$H_0 \Psi^{(2)} + V \Psi^{(1)} = E^{(0)} \Psi^{(2)} + E^{(1)} \Psi^{(1)} + E^{(2)} \Psi_0 \tag{5.6}$$

and so forth. Multiplying each of the above equations by $\Psi_0$ and integrating over all space yields the following expression for the $n$th-order (MP$n$) energy:

$$E^{(0)} = \langle \Psi_0 | H_0 | \Psi_0 \rangle \tag{5.7}$$

$$E^{(1)} = \langle \Psi_0 | V | \Psi_0 \rangle \tag{5.8}$$

$$E^{(2)} = \left\langle \Psi_0 | V | \Psi^{(1)} \right\rangle \tag{5.9}$$

Thus, the Hartree-Fock energy

$$E_0 = \langle \Psi_0 | \, H_0 + V \, | \Psi_0 \rangle \tag{5.10}$$

is simply the sum of the zeroth- and first- order energies

$$E_0 = E^{(0)} + E^{(1)} \tag{5.11}$$

The correlation energy can then be written

$$E_{\text{corr}} = E_0^{(2)} + E_0^{(3)} + E_0^{(4)} + \ldots \tag{5.12}$$

of which the first term is the MP2 energy.

It can be shown that the MP2 energy can be written (in terms of spin-orbitals) as

$$E_0^{(2)} = -\frac{1}{4} \sum_{ab}^{\text{virt}} \sum_{ij}^{\text{occ}} \frac{|\langle ab| \, |ij\rangle|^2}{\varepsilon_a + \varepsilon_b - \varepsilon_i - \varepsilon_j} \tag{5.13}$$

where

$$\langle ab \, || ij \, \rangle = \langle ab | abijij \rangle - \langle ab | abjiji \rangle \tag{5.14}$$

and

$$\langle ab | abcdcd \rangle = \int \psi_a(\mathbf{r}_1) \psi_c(\mathbf{r}_1) \left[ \frac{1}{r_{12}} \right] \psi_b(\mathbf{r}_2) \psi_d(\mathbf{r}_2) d\mathbf{r}_1 d\mathbf{r}_2 \tag{5.15}$$

which can be written in terms of the two-electron repulsion integrals

$$\langle ab | abcdcd \rangle = \sum_\mu \sum_\nu \sum_\lambda \sum_\sigma C_{\mu a} C_{\nu c} C_{\lambda b} C_{\sigma d} \, (\mu\nu | \lambda\sigma) \tag{5.16}$$

Expressions for higher order terms follow similarly, although with much greater algebraic and computational complexity. MP3 and particularly MP4 (the third and fourth order contributions to the correlation energy) are both occasionally used, although they are increasingly supplanted by the coupled-cluster methods described in the following sections. The disk and memory requirements for MP3 are similar to the self-consistent pair correlation methods discussed in Section 5.8 while the computational cost of MP4 is similar to the (T) corrections discussed in Section 5.9.

## 5.4 Exact MP2 Methods

### 5.4.1 Algorithm

Second-order Møller-Plesset theory (MP2)[10] probably the simplest useful wave function-based electron correlation method. Revived in the mid-1970s, it remains highly popular today, because it offers systematic improvement in optimized geometries and other molecular properties relative to Hartree-Fock (HF) theory[11]. Indeed, in a recent comparative study of small closed-shell molecules[12], MP2 outperformed much more expensive singles and doubles coupled-cluster theory for such properties! Relative to state-of-the-art Kohn-Sham density functional theory (DFT) methods, which are the most economical methods to account for electron correlation effects, MP2 has the advantage of properly incorporating long-range dispersion forces. The principal weaknesses of MP2 theory are for open shell systems, and other cases where the HF determinant is a poor starting point.

Q-CHEM contains an efficient conventional semi-direct method to evaluate the MP2 energy and gradient[13]. These methods require $OVN$ memory ($O$, $V$, $N$ are the numbers of occupied, virtual and total orbitals, respectively), and disk space which is bounded from above by $OVN^2/2$. The latter can be reduced to $IVN^2/2$ by treating the occupied orbitals in batches of size $I$, and re-evaluating the two-electron integrals $O/I$ times. This approach is tractable on modern workstations for energy and gradient calculations of at least 500 basis functions or so, or molecules of between 15 and 30 first row atoms, depending on the basis set size. The computational cost increases between the 3rd and 5th power of the size of the molecule, depending on which part of the calculation is time-dominant.

The algorithm and implementation in Q-CHEM is improved over earlier methods[14,15], particularly in the following areas:

- Uses pure functions, as opposed to Cartesians, for all fifth-order steps. This leads to large computational savings for basis sets containing pure functions.
- Customized loop unrolling for improved efficiency.
- The sort-less semi-direct method avoids a read and write operation resulting in a large I/O savings.
- Reduction in disk and memory usage.
- No extra integral evaluation for gradient calculations.
- Full exploitation of frozen core approximation.

The implementation offers the user the following alternatives:

- Direct algorithm (energies only).
- Disk-based sort-less semi-direct algorithm (energies and gradients).
- Local occupied orbital method (energies only).

The semi-direct algorithm is the only choice for gradient calculations. It is also normally the most efficient choice for energy calculations. There are two classes of exceptions:

- If the amount of disk space available is not significantly larger than the amount of memory available, then the direct algorithm is preferred.

- If the calculation involves a very large basis set, then the local orbital method may be faster, because it performs the transformation in a different order. It does not have the large memory requirement (no $OVN$ array needed), and always evaluates the integrals four times. The AO2MO_DISK option is also ignored in this algorithm, which requires up to $O^2VN$ megabytes of disk space.

There are three important options that should be wisely chosen by the user in order to exploit the full efficiency of Q-CHEM's direct and semi-direct MP2 methods (as discussed above, the LOCAL_OCCUPIED method has different requirements).

- MEM_STATIC: The value specified for this *$rem* variable must be sufficient to permit efficient integral evaluation (10-80Mb) and to hold a large temporary array whose size is $OVN$, the product of the number of occupied, virtual and total numbers of orbitals.
- AO2MO_DISK: The value specified for this *$rem* variable should be as large as possible (*i.e.*, perhaps 80% of the free space on your *$QCSCRATCH* partition where temporary job files are held). The value of this variable will determine how many times the two-electron integrals in the atomic orbital basis must be re-evaluated, which is a major computational step in MP2 calculations.
- N_FROZEN_CORE: The computational requirements for MP2 are proportional to the number of occupied orbitals for some steps, and the square of that number for other steps. Therefore the CPU time can be significantly reduced if your job employs the frozen core approximation. Additionally the memory and disk requirements are reduced when the frozen core approximation is employed.

### 5.4.2 Algorithm Control and Customization

The direct and semi-direct integral transformation algorithms used by Q-CHEM (*e.g.*, MP2, CIS(D)) are limited by available disk space, $D$, and memory, $C$, the number of basis functions, $N$, the number of virtual orbitals, $V$ and the number of occupied orbitals, $O$, as discussed above. The generic description of the key *$rem* variables are:

**MEM_STATIC**
Sets the memory for Fortran AO integral calculation and transformation modules.
TYPE:
INTEGER
DEFAULT:
64 corresponding to 64 Mb.
OPTIONS:
$n$ User-defined number of megabytes.
RECOMMENDATION:
For direct and semi-direct MP2 calculations, this must exceed OVN + requirements for AO integral evaluation (32–160 Mb), as discussed above.

**MEM_TOTAL**

Sets the total memory available to Q-CHEM, in megabytes.

TYPE:

INTEGER

DEFAULT:

2000 Corresponding to 2000 Mb.

OPTIONS:

$n$ User-defined number of megabytes.

RECOMMENDATION:

Use the default, or set equal to the physical memory of your machine. Note that if the memory allocation total more than 1 Gb for a CCMAN job, the memory is allocated as follows

| | |
|---|---|
| 12% | MEM_STATIC |
| 50% | CC_MEMORY |
| 35% | Other memory requirements: |

**AO2MO_DISK**

Sets the amount of disk space (in megabytes) available for MP2 calculations.

TYPE:

INTEGER

DEFAULT:

2000 Corresponding to 2000 Mb.

OPTIONS:

$n$ User-defined number of megabytes.

RECOMMENDATION:

Should be set as large as possible, discussed in Section 5.4.1.

**CD_ALGORITHM**

Determines the algorithm for MP2 integral transformations.

TYPE:

STRING

DEFAULT:

Program determined.

OPTIONS:

| | |
|---|---|
| DIRECT | Uses fully direct algorithm (energies only). |
| SEMI_DIRECT | Uses disk-based semi-direct algorithm. |
| LOCAL_OCCUPIED | Alternative energy algorithm (see 5.4.1). |

RECOMMENDATION:

Semi-direct is usually most efficient, and will normally be chosen by default.

### 5.4.3 Example

**Example 5.1** Example of an MP2/6-31G* calculation employing the frozen core approximation. Note that the EXCHANGE *$rem* variable will default to HF

```
$molecule
   0 1
   O
   H1  O  oh
   H2  O  oh  H1  hoh

   oh  = 1.01
   hoh = 105
$end

$rem
   METHOD          mp2
   BASIS           6-31g*
   N_FROZEN_CORE   fc
$end
```

# 5.5 Local MP2 Methods

## 5.5.1 Local Triatomics in Molecules (TRIM) Model

The development of what may be called "fast methods" for evaluating electron correlation is a problem of both fundamental and practical importance, because of the unphysical increases in computational complexity with molecular size which afflict "exact" implementations of electron correlation methods. Ideally, the development of fast methods for treating electron correlation should not impact either model errors or numerical errors associated with the original electron correlation models. Unfortunately this is not possible at present, as may be appreciated from the following rough argument. *Spatial locality* is what permits reformulations of electronic structure methods that yield the same answer as traditional methods, but faster. The one-particle density matrix decays exponentially with a rate that relates to the HOMO-LUMO gap in periodic systems. When length scales longer than this characteristic decay length are examined, sparsity will emerge in both the one-particle density matrix and also pair correlation amplitudes expressed in terms of localized functions. Very roughly, such a length scale is about 5 to 10 atoms in a line, for good insulators such as alkanes. Hence sparsity emerges beyond this number of atoms in 1-D, beyond this number of atoms squared in 2-D, and this number of atoms cubed in 3-D. Thus for three-dimensional systems, locality only begins to emerge for systems of between hundreds and thousands of atoms.

If we wish to accelerate calculations on systems below this size regime, we must therefore introduce additional errors into the calculation, either as numerical noise through looser tolerances, or by modifying the theoretical model, or perhaps both. Q-CHEM's approach to local electron correlation is based on modifying the theoretical models describing correlation with an additional well-defined local approximation. We do not attempt to accelerate the calculations by introducing more numerical error because of the difficulties of controlling the error as a function of molecule size, and the difficulty of achieving reproducible significant results. From this perspective, local correlation becomes an integral part of specifying the electron correlation treatment. This means that the considerations necessary for a correlation treatment to qualify as a well-defined theoretical model chemistry apply equally to local correlation modeling. The local approximations should be

- *Size-consistent:* meaning that the energy of a super-system of two non-interacting molecules should be the sum of the energy obtained from individual calculations on each molecule.
- *Uniquely defined:* Require no input beyond nuclei, electrons, and an atomic orbital basis set. In other words, the model should be uniquely specified without customization for each molecule.

- *Yield continuous potential energy surfaces:* The model approximations should be smooth, and not yield energies that exhibit jumps as nuclear geometries are varied.

To ensure that these model chemistry criteria are met, Q-CHEM's local MP2 methods [16,17] express the double substitutions (*i.e.*, the pair correlations) in a redundant basis of atom-labeled functions. The advantage of doing this is that local models satisfying model chemistry criteria can be defined by performing an *atomic truncation* of the double substitutions. A general substitution in this representation will then involve the replacement of occupied functions associated with two given atoms by empty (or virtual) functions on two other atoms, coupling together four different atoms. We can force one occupied to virtual substitution (of the two that comprise a double substitution) to occur only between functions on the same atom, so that only three different atoms are involved in the double substitution. This defines the *triatomics in molecules* (TRIM) local model for double substitutions. The TRIM model offers the potential for reducing the computational requirements of exact MP2 theory by a factor proportional to the number of atoms. We could also force each occupied to virtual substitution to be on a given atom, thereby defining a more drastic *diatomics in molecules* (DIM) local correlation model.

The simplest atom-centered basis that is capable of spanning the occupied space is a *minimal basis* of core and valence atomic orbitals on each atom. Such a basis is necessarily redundant because it also contains sufficient flexibility to describe the empty valence anti-bonding orbitals necessary to correctly account for non-dynamical electron correlation effects such as bond-breaking. This redundancy is actually important for the success of the atomic truncations because occupied functions on adjacent atoms to some extent describe the same part of the occupied space. The minimal functions we use to span the occupied space are obtained at the end of a large basis set calculation, and are called *extracted polarized atomic orbitals* (EPAOs) [18]. We discuss them briefly below. It is even possible to explicitly perform an SCF calculation in terms of a molecule-optimized minimal basis of *polarized atomic orbitals* (PAOs) (see Chapter 4). To span the virtual space, we use the full set of atomic orbitals, appropriately projected into the virtual space.

We summarize the situation. The number of functions spanning the occupied subspace will be the minimal basis set dimension, $M$, which is greater than the number of occupied orbitals, $O$, by a factor of up to about two. The virtual space is spanned by the set of projected atomic orbitals whose number is the atomic orbital basis set size $N$, which is fractionally greater than the number of virtuals $VNO$. The number of double substitutions in such a redundant representation will be typically three to five times larger than the usual total. This will be more than compensated by reducing the number of retained substitutions by a factor of the number of atoms, $A$, in the local triatomics in molecules model, or a factor of $A^2$ in the diatomics in molecules model.

The local MP2 energy in the TRIM and DIM models are given by the following expressions, which can be compared against the full MP2 expression given earlier in Eq. (5.13). First, for the DIM model:

$$E_{\mathrm{DIM\,MP2}} = -\frac{1}{2}\sum_{\bar{P},\bar{Q}} \frac{(\bar{P}|\bar{Q})(\bar{P}||\bar{Q})}{\Delta_{\bar{P}} + \Delta_{\bar{Q}}} \tag{5.17}$$

The sums run over the linear number of atomic single excitations after they have been canonicalized. Each term in the denominator is thus an energy difference between occupied and virtual levels in this local basis. Similarly, the TRIM model corresponds to the following local MP2 energy:

$$E_{\mathrm{TRIM\,MP2}} = -\sum_{\bar{P},jb} \frac{(\bar{P}|jb)(\bar{P}||jb)}{\Delta_{\bar{P}} + \varepsilon_b - \varepsilon_j} - E_{\mathrm{DIM\,MP2}} \tag{5.18}$$

where the sum is now mixed between atomic substitutions $\bar{P}$, and non-local occupied $j$ to virtual $b$ substitutions. See Refs. 16,17 for a full derivation and discussion.

The accuracy of the local TRIM and DIM models has been tested in a series of calculations[16,17]. In particular, the TRIM model has been shown to be quite faithful to full MP2 theory via the following tests:

- The TRIM model recovers around 99.7% of the MP2 correlation energy for covalent bonding. This is significantly higher than the roughly 98–99% correlation energy recovery typically exhibited by the Saebo-Pulay local correlation method[19]. The DIM model recovers around 95% of the correlation energy.
- The performance of the TRIM model for relative energies is very robust, as shown in Ref. 16 for the challenging case of torsional barriers in conjugated molecules. The RMS error in these relative energies is only 0.031 kcal/mol, as compared to around 1 kcal/mol when electron correlation effects are completely neglected.
- For the water dimer with the aug-cc-pVTZ basis, 96% of the MP2 contribution to the binding energy is recovered with the TRIM model, as compared to 62% with the Saebo-Pulay local correlation method.
- For calculations of the MP2 contribution to the G3 and G3(MP2) energies with the larger molecules in the G3-99 database[20], introduction of the TRIM approximation results in an RMS error relative to full MP2 theory of only 0.3 kcal/mol, even though the absolute magnitude of these quantities is on the order of tens of kcal/mol.

### 5.5.2 EPAO Evaluation Options

When a local MP2 job (requested by the LOCAL_MP2 option for CORRELATION) is performed, the first new step after the SCF calculation is converged is to extract a minimal basis of polarized atomic orbitals (EPAOs) that spans the occupied space. There are three valid choices for this basis, controlled by the PAO_METHOD and EPAO_ITERATE keywords described below.

- *Non-iterated EPAOs:* The initial guess EPAOs are the default for local MP2 calculations, and are defined as follows. For each atom, the covariant density matrix (SPS) is diagonalized, giving eigenvalues which are approximate natural orbital occupancies, and eigenvectors which are corresponding atomic orbitals. The $m$ eigenvectors with largest populations are retained (where $m$ is the minimal basis dimension for the current atom). This non-orthogonal minimal basis is symmetrically orthogonalized, and then modified as discussed in Ref. 18 to ensure that these functions rigorously span the occupied space of the full SCF calculation that has just been performed. These orbitals may be denoted as EPAO(0) to indicate that no iterations have been performed after the guess. In general, the quality of the local MP2 results obtained with this option is very similar to the EPAO option below, but it is much faster and fully robust. For the example of the torsional barrier calculations discussed above[16], the TRIM RMS deviations of 0.03 kcal/mol from full MP2 calculations are increased to only 0.04 kcal/mol when EPAO(0) orbitals are employed rather than EPAOs.
- *EPAOs:* EPAOs are defined by minimizing a localization functional as described in Ref. 18. These functions were designed to be suitable for local MP2 calculations, and have yielded excellent results in all tests performed so far. Unfortunately the functional is difficult to converge for large molecules, at least with the algorithms that have been developed to this stage. Therefore it is not the default, but is switched on by specifying a (large) value for EPAO_ITERATE, as discussed below.

- *PAO:* If the SCF calculation is performed in terms of a molecule-optimized minimal basis, as described in Chapter 4, then the resulting PAO-SCF calculation can be corrected with either conventional or local MP2 for electron correlation. PAO-SCF calculations alter the SCF energy, and are therefore not the default. This can be enabled by specifying PAO_METHOD as PAO, in a job which also requests CORRELATION as LOCAL_MP2.

**PAO_METHOD**

Controls the type of PAO calculations requested.

TYPE:

STRING

DEFAULT:

EPAO For local MP2, EPAOs are chosen by default.

OPTIONS:

EPAO Find EPAOs by minimizing delocalization function.

PAO Do SCF in a molecule-optimized minimal basis.

RECOMMENDATION:

None

**EPAO_ITERATE**

Controls iterations for EPAO calculations (see PAO_METHOD).

TYPE:

INTEGER

DEFAULT:

0 Use non-iterated EPAOs based on atomic blocks of SPS.

OPTIONS:

$n$ Optimize the EPAOs for up to $n$ iterations.

RECOMMENDATION:

Use the default. For molecules that are not too large, one can test the sensitivity of the results to the type of minimal functions by the use of optimized EPAOs in which case a value of $n = 500$ is reasonable.

**EPAO_WEIGHTS**

Controls algorithm and weights for EPAO calculations (see PAO_METHOD).

TYPE:

INTEGER

DEFAULT:

115 Standard weights, use $1^{\text{st}}$ and $2^{\text{nd}}$ order optimization

OPTIONS:

15 Standard weights, with $1^{\text{st}}$ order optimization only.

RECOMMENDATION:

Use the default, unless convergence failure is encountered.

### 5.5.3 Algorithm Control and Customization

A local MP2 calculation (requested by the LOCAL_MP2 option for CORRELATION) consists of the following steps:

- After the SCF is converged, a minimal basis of EPAOs are obtained.

- The TRIM (and DIM) local MP2 energies are then evaluated (gradients are not yet available).

Details of the efficient implementation of the local MP2 method described above are reported in the recent thesis of Dr. Michael Lee[21]. Here we simply summarize the capabilities of the program. The computational advantage associated with these local MP2 methods varies depending upon the size of molecule and the basis set. As a rough general estimate, TRIM MP2 calculations are feasible on molecule sizes about twice as large as those for which conventional MP2 calculations are feasible on a given computer, and this is their primary advantage. Our implementation is well suited for large basis set calculations. The AO basis two-electron integrals are evaluated four times. DIM MP2 calculations are performed as a by-product of TRIM MP2 but no separately optimized DIM algorithm has been implemented.

The resource requirements for local MP2 calculations are as follows:

- *Memory:* The memory requirement for the integral transformation does not exceed $OON$, and is thresholded so that it asymptotically grows linearly with molecule size. Additional memory of approximately $32N^2$ is required to complete the local MP2 energy evaluation.
- *Disk:* The disk space requirement is only about $8OVN$, but is not governed by a threshold. This is a very large reduction from the case of a full MP2 calculation, where, in the case of four integral evaluations, $OVN^2/4$ disk space is required. As the local MP2 disk space requirement is not adjustable, the AO2MO_DISK keyword is ignored for LOCAL_MP2 calculations.

The evaluation of the local MP2 energy does not require any further customization. An adequate amount of MEM_STATIC (80 to 160 Mb) should be specified to permit efficient AO basis two-electron integral evaluation, but all large scratch arrays are allocated from MEM_TOTAL.

### 5.5.4 Examples

**Example 5.2** A relative energy evaluation using the local TRIM model for MP2 with the 6-311G** basis set. The energy difference is the internal rotation barrier in propenal, with the first geometry being planar trans, and the second the transition structure.

```
$molecule
   0 1
   C
   C  1  1.32095
   C  2  1.47845  1  121.19
   O  3  1.18974  2  123.83  1   180.00
   H  1  1.07686  2  121.50  3     0.00
   H  1  1.07450  2  122.09  3   180.00
   H  2  1.07549  1  122.34  3   180.00
   H  3  1.09486  2  115.27  4   180.00
$end

$rem
   METHOD        local_mp2
   BASIS         6-311g**
$end

@@@

$molecule
```

```
   0 1
   C
   C  1  1.31656
   C  2  1.49838  1  123.44
   O  3  1.18747  2  123.81  1   92.28
   H  1  1.07631  2  122.03  3   -0.31
   H  1  1.07484  2  121.43  3  180.28
   H  2  1.07813  1  120.96  3  180.34
   H  3  1.09387  2  115.87  4  179.07
$end

$rem
   CORRELATION   local_mp2
   BASIS         6-311g**
$end
```

## 5.6 Auxiliary Basis (Resolution of the Identity) MP2 Methods

For a molecule of fixed size, increasing the number of basis functions *per atom*, $n$, leads to $\mathcal{O}(n^4)$ growth in the number of significant four-center two-electron integrals, since the number of non-negligible product charge distributions, $|\mu\nu\rangle$, grows as $\mathcal{O}(n^2)$. As a result, the use of large (high-quality) basis expansions is computationally costly. Perhaps the most practical way around this "basis set quality" bottleneck is the use of auxiliary basis expansions[22–24]. The ability to use auxiliary basis sets to accelerate a variety of electron correlation methods, including both energies and analytical gradients, is a major feature of Q-CHEM.

The auxiliary basis $\{|K\rangle\}$ is used to approximate products of Gaussian basis functions:

$$|\mu\nu\rangle \approx |\widetilde{\mu\nu}\rangle = \sum_K |K\rangle C_{\mu\nu}^K \tag{5.19}$$

Auxiliary basis expansions were introduced long ago, and are now widely recognized as an effective and powerful approach, which is sometimes synonymously called resolution of the identity (RI) or density fitting (DF). When using auxiliary basis expansions, the rate of growth of computational cost of large-scale electronic structure calculations with $n$ is reduced to approximately $n^3$.

If $n$ is fixed and molecule size increases, auxiliary basis expansions reduce the pre-factor associated with the computation, while not altering the scaling. The important point is that the pre-factor can be reduced by 5 or 10 times or more. Such large speedups are possible because the number of auxiliary functions required to obtain reasonable accuracy, $X$, has been shown to be only about 3 or 4 times larger than $N$.

The auxiliary basis expansion coefficients, **C**, are determined by minimizing the deviation between the fitted distribution and the actual distribution, $\langle\mu\nu - \widetilde{\mu\nu}|\mu\nu - \widetilde{\mu\nu}\rangle$, which leads to the following set of linear equations:

$$\sum_L \langle K\,|L\rangle C_{\mu\nu}^L = \langle K\,|\mu\nu\rangle \tag{5.20}$$

Evidently solution of the fit equations requires only two- and three-center integrals, and as a result the (four-center) two-electron integrals can be approximated as the following optimal expression for a given choice of auxiliary basis set:

$$\langle\mu\nu|\lambda\sigma\rangle \approx \langle\widetilde{\mu\nu}|\widetilde{\lambda\sigma}\rangle = \sum_{K,L} C_{\mu\nu}^L \langle L|K\rangle C_{\lambda\sigma}^K \tag{5.21}$$

In the limit where the auxiliary basis is complete (*i.e.* all products of AOs are included), the fitting procedure described above will be exact. However, the auxiliary basis is invariably incomplete (as mentioned above, $X \approx 3N$) because this is essential for obtaining increased computational efficiency.

Standardized auxiliary basis sets have been developed by the Karlsruhe group for second-order perturbation (MP2) calculations[25,26] of the correlation energy. With these basis sets, small absolute errors (*e.g.*, below 60 $\mu$Hartree per atom in MP2) and even smaller relative errors in computed energies are found, while the speed-up can be 3–30 fold. This development has made the routine use of auxiliary basis sets for electron correlation calculations possible.

Correlation calculations that can take advantage of auxiliary basis expansions are described in the remainder of this section (MP2, and MP2-like methods) and in Section 5.15 (simplified active space coupled cluster methods such as PP, PP(2), IP, RP). These methods automatically employ auxiliary basis expansions when a valid choice of auxiliary basis set is supplied using the AUX_BASIS keyword which is used in the same way as the BASIS keyword. The PURECART *$rem* is no longer needed here, even if using a auxiliary basis that does not have a predefined value. There is a built-in automatic procedure that provides the effect of the PURECART *$rem* in these cases by default.

### 5.6.1 RI-MP2 Energies and Gradients.

Following common convention, the MP2 energy evaluated approximately using an auxiliary basis is referred to as "resolution of the identity" MP2, or RI-MP2 for short. RI-MP2 energy and gradient calculations are enabled simply by specifying the AUX_BASIS keyword discussed above. As discussed above, RI-MP2 energies[22] and gradients[27,28] are significantly faster than the best conventional MP2 energies and gradients, and cause negligible loss of accuracy, when an appropriate standardized auxiliary basis set is employed. Therefore they are recommended for jobs where turnaround time is an issue. Disk requirements are very modest; one merely needs to hold various 3-index arrays. Memory requirements grow more slowly than our conventional MP2 algorithms—only quadratically with molecular size. The minimum memory requirement is approximately $3X^2$, where $X$ is the number of auxiliary basis functions, for both energy and analytical gradient evaluations, with some additional memory being necessary for integral evaluation and other small arrays.

In fact, for molecules that are not too large (perhaps no more than 20 or 30 heavy atoms) the RI-MP2 treatment of electron correlation is so efficient that the computation is dominated by the initial Hartree-Fock calculation. This is despite the fact that as a function of molecule size, the cost of the RI-MP2 treatment still scales more steeply with molecule size (it is just that the pre-factor is so much smaller with the RI approach). Its scaling remains 5th order with the size of the molecule, which only dominates the initial SCF calculation for larger molecules. Thus, for RI-MP2 energy evaluation on moderate size molecules (particularly in large basis sets), it is desirable to use the dual basis HF method to further improve execution times (see Section 4.9).

### 5.6.2 Example

**Example 5.3** Q-CHEM input for an RI-MP2 geometry optimization.

```
$molecule
   0 1
   O
   H  1  0.9
   F  1  1.4  2  100.
$end

$rem
   JOBTYPE       opt
   METHOD        rimp2
   BASIS         cc-pvtz
   AUX_BASIS     rimp2-cc-pvtz
   SYMMETRY      false
$end
```

For the size of required memory, the followings need to be considered.

**MEM_STATIC**

Sets the memory for AO-integral evaluations and their transformations.

TYPE:

INTEGER

DEFAULT:

64 corresponding to 64 Mb.

OPTIONS:

$n$ User-defined number of megabytes.

RECOMMENDATION:

For RI-MP2 calculations, $150(ON+V)$ of MEM_STATIC is required. Because a number of matrices with $N^2$ size also need to be stored, 32–160 Mb of additional MEM_STATIC is needed.

**MEM_TOTAL**

Sets the total memory available to Q-CHEM, in megabytes.

TYPE:

INTEGER

DEFAULT:

2000 2 Gb

OPTIONS:

$n$ User-defined number of megabytes.

RECOMMENDATION:

Use the default, or set to the physical memory of your machine. The minimum requirement is $3X^2$.

### 5.6.3 OpenMP Implementation of RI-MP2

An OpenMP RI-MP2 energy algorithm is used by default in Q-CHEM 4.1 onward. This can be invoked by using CORR=primp2 for older versions, but note that in 4.01 and below, only RHF/RI-MP2 was supported. Now UHF/RI-MP2 is supported, and the formation of the 'B' matrices as well as three center integrals are parallelized. This algorithm uses the remaining memory from the MEM_TOTAL allocation for all computation, which can drastically reduce hard drive reads in the formation of t-amplitudes.

**Example 5.4** Example of OpenMP-parallel RI-MP2 job.

```
$molecule
   0 1
   C1
   H1  C1    1.077260
   H2  C1    1.077260  H1  131.608240
$end

$rem
   JOBTYPE            SP
   EXCHANGE           HF
   CORRELATION        pRIMP2
   BASIS              cc-pVTZ
   AUX_BASIS          rimp2-cc-pVTZ
   PURECART           11111
   SYMMETRY           false
   THRESH             12
   SCF_CONVERGENCE    8
   MAX_SUB_FILE_NUM   128
   !TIME_MP2          true
$end
```

### 5.6.4 GPU Implementation of RI-MP2

#### 5.6.4.1 Requirements

Q-CHEM currently offers the possibility of accelerating RI-MP2 calculations using graphics processing units (GPUs). Currently, this is implemented for CUDA-enabled NVIDIA graphics cards only, such as (in historical order from 2008) the GeForce, Quadro, Tesla and Fermi cards. More information about CUDA-enabled cards is available at

`http://www.nvidia.com/object/cuda_gpus.html`

It should be noted that these GPUs have specific power and motherboard requirements.

Software requirements include the installation of the appropriate NVIDIA CUDA driver (at least version 1.0, currently 3.2) and linear algebra library, CUBLAS (at least version 1.0, currently 2.0). These can be downloaded jointly in NVIDIA's developer website:

`http://developer.nvidia.com/object/cuda_3_2_downloads.html`

We have implemented a mixed-precision algorithm in order to get *better than* single precision when users only have single-precision GPUs. This is accomplished by noting that RI-MP2 matrices have a *large* fraction of numerically "small" elements and a *small* fraction of numerically "large" ones. The latter can greatly affect the accuracy of the calculation in single-precision only calculations, but calculation involves a relatively small number of compute cycles. So, given a threshold value $\delta$, we perform a separation between "small" and "large" elements and accelerate the former compute-intensive operations using the GPU (in single-precision) and compute the latter on the CPU (using double-precision). We are thus able to determine how much double-precision we desire by tuning the $\delta$ parameter, and tailoring the balance between computational speed and accuracy.

#### 5.6.4.2 Options

**CUDA_RI-MP2**

Enables GPU implementation of RI-MP2

TYPE:

LOGICAL

DEFAULT:

FALSE

OPTIONS:

| | |
|---|---|
| FALSE | GPU-enabled MGEMM off |
| TRUE | GPU-enabled MGEMM on |

RECOMMENDATION:

Necessary to set to 1 in order to run GPU-enabled RI-MP2

**USECUBLAS_THRESH**

Sets threshold of matrix size sent to GPU (smaller size not worth sending to GPU).

TYPE:

INTEGER

DEFAULT:

250

OPTIONS:

| | |
|---|---|
| n | user-defined threshold |

RECOMMENDATION:

Use the default value. Anything less can seriously hinder the GPU acceleration

**USE_MGEMM**

Use the mixed-precision matrix scheme (MGEMM) if you want to make calculations in your card in single-precision (or if you have a single-precision-only GPU), but leave some parts of the RI-MP2 calculation in double precision)

TYPE:

LOGICAL

DEFAULT:

FALSE

OPTIONS:

| | |
|---|---|
| FALSE | MGEMM disabled |
| TRUE | MGEMM enabled |

RECOMMENDATION:

Use when having single-precision cards

**MGEMM_THRESH**

Sets MGEMM threshold to determine the separation between "large" and "small" matrix elements. A larger threshold value will result in a value closer to the single-precision result. Note that the desired factor should be multiplied by 10000 to ensure an integer value.

TYPE:

INTEGER

DEFAULT:

10000 (corresponds to 1)

OPTIONS:

$n$ User-specified threshold

RECOMMENDATION:

For small molecules and basis sets up to triple-$\zeta$, the default value suffices to not deviate too much from the double-precision values. Care should be taken to reduce this number for larger molecules and also larger basis-sets.

#### 5.6.4.3 Input examples

**Example 5.5** RI-MP2 double-precision calculation

```
$molecule
   0 1
   c
   h1  c  1.089665
   h2  c  1.089665  h1  109.47122063
   h3  c  1.089665  h1  109.47122063  h2   120.
   h4  c  1.089665  h1  109.47122063  h2  -120.
$end

$rem
   JOBTYPE      sp
   EXCHANGE     hf
   METHOD       rimp2
   BASIS        cc-pvdz
   AUX_BASIS    rimp2-cc-pvdz
   CUDA_RIMP2   1
$end
```

**Example 5.6** RI-MP2 calculation with MGEMM

```
$molecule
   0 1
   c
   h1  c  1.089665
   h2  c  1.089665  h1  109.47122063
   h3  c  1.089665  h1  109.47122063  h2   120.
   h4  c  1.089665  h1  109.47122063  h2  -120.
$end

$rem
   JOBTYPE        sp
   EXCHANGE       hf
   METHOD         rimp2
   BASIS          cc-pvdz
   AUX_BASIS      rimp2-cc-pvdz
   CUDA_RIMP2     1
   USE_MGEMM      1
   MGEMM_THRESH   10000
$end
```

### 5.6.5 Spin-Biased MP2 Methods (SCS-MP2, SOS-MP2, MOS-MP2, and O2)

The accuracy of MP2 calculations can be significantly improved by semi-empirically scaling the opposite-spin (OS) and same-spin (SS) correlation components with separate scaling factors, as shown by Grimme[29]. Scaling with 1.2 and 0.33 (or OS and SS components) defines the SCS-MP2 method, but other parameterizations are desirable for systems involving intermolecular interactions, as in the SCS-MI-MP2 method, which uses 0.40 and 1.29 (for OS and SS components)[30].

Results of similar quality for thermochemistry can be obtained by only retaining and scaling the opposite spin correlation (by 1.3), as was recently demonstrated[31]. Furthermore, the SOS-MP2 energy can be evaluated using the RI approximation together with a Laplace transform technique, in effort that scales only with the 4th power of molecular size. Efficient algorithms for the energy[31] and the analytical gradient[32] of this method are available in Q-CHEM 3.0, and offer advantages in speed over MP2 for larger molecules, as well as statistically significant improvements in accuracy.

However, we note that the SOS-MP2 method does systematically underestimate long-range dispersion (for which the appropriate scaling factor is 2 rather than 1.3) but this can be accounted for by making the scaling factor distance-dependent, which is done in the modified opposite spin variant (MOS-MP2) that has recently been proposed and tested[33]. The MOS-MP2 energy and analytical gradient are also available in Q-CHEM 3.0 at a cost that is essentially identical with SOS-MP2. Timings show that the 4th-order implementation of SOS-MP2 and MOS-MP2 yields substantial speedups over RI-MP2 for molecules in the 40 heavy atom regime and larger. It is also possible to customize the scale factors for particular applications, such as weak interactions, if required.

A fourth order scaling SOS-MP2/MOS-MP2 energy calculation can be invoked by setting the CORRELATION keyword to either SOSMP2 or MOSMP2. MOS-MP2 further requires the specification of the *$rem* variable OMEGA, which tunes the level of attenuation of the MOS operator[33]:

$$g_\omega(r_{12}) = \frac{1}{r_{12}} + c_{\mathrm{MOS}} \frac{\mathrm{erf}\,(\omega r_{12})}{r_{12}} \tag{5.22}$$

The recommended OMEGA value is $\omega = 0.6$ bohr$^{-1}$[33]. The fast algorithm makes use of auxiliary basis expansions and therefore, the keyword AUX_BASIS should be set consistently with the user's choice of BASIS. Fourth-order scaling analytical gradient for both SOS-MP2 and MOS-MP2 are also available and is automatically invoked when JOBTYPE is set to OPT or FORCE. The minimum memory requirement is $3X^2$, where $X$ = the number of auxiliary basis functions, for both energy and analytical gradient evaluations. Disk space requirement for closed shell calculations is $\sim 2OVX$ for energy evaluation and $\sim 4OVX$ for analytical gradient evaluation.

More recently, Brueckner orbitals (BO) are introduced into SOSMP2 and MOSMP2 methods to resolve the problems of symmetry breaking and spin contamination that are often associated with Hartree-Fock orbitals. So the molecular orbitals are optimized with the mean-field energy plus a correlation energy taken as the opposite-spin component of the second-order many-body correlation energy, scaled by an empirically chosen parameter. This "optimized second-order opposite-spin" abbreviated as O2 method[34] requires fourth-order computation on each orbital iteration. O2 is shown to yield predictions of structure and frequencies for closed-shell molecules that are very similar to scaled MP2 methods. However, it yields substantial improvements for open-shell molecules, where problems with spin contamination and symmetry breaking are shown to be greatly reduced.

Summary of key *$rem* variables to be specified:

| | |
|---|---|
| CORRELATION | RIMP2<br>SOSMP2<br>MOSMP2 |
| JOBTYPE | sp (default) single point energy evaluation<br>opt geometry optimization with analytical gradient<br>force evaluation with analytical gradient |
| BASIS | user's choice (standard or user-defined: GENERAL or MIXED) |
| AUX_BASIS | corresponding auxiliary basis (standard or user-defined: AUX_GENERAL or AUX_MIXED |
| OMEGA | no default $n$; use $\omega = n/1000$. The recommended value is $n = 600$ ($\omega = 0.6$ bohr$^{-1}$) |
| N_FROZEN_CORE | Optional |
| N_FROZEN_VIRTUAL | Optional |
| SCS | Turns on spin-component scaling with SCS-MP2(1), SOS-MP2(2), and arbitrary SCS-MP2(3) |

### 5.6.6 Examples

**Example 5.7** Example of SCS-MP2 geometry optimization

```
$molecule
   0 1
   C
   H  1  1.0986
   H  1  1.0986  2  109.5
   H  1  1.0986  2  109.5  3   120.0 0
   H  1  1.0986  2  109.5  3  -120.0 0
$end

$rem
   JOBTYPE             opt
   EXCHANGE            hf
   CORRELATION         rimp2
   BASIS               aug-cc-pvdz
   AUX_BASIS           rimp2-aug-cc-pvdz
   BASIS2              racc-pvdz            Optional Secondary basis
   THRESH              12
   SCF_CONVERGENCE     8
   MAX_SUB_FILE_NUM    128
   SCS                 1                    Turn on spin-component scaling
   DUAL_BASIS_ENERGY   true                 Optional dual-basis approximation
   N_FROZEN_CORE       fc
   SYMMETRY            false
   SYM_IGNORE          true
$end
```

**Example 5.8** Example of SCS-MI-MP2 energy calculation

```
$molecule
   0 1
   C       0.000000     -0.000140      1.859161
   H      -0.888551      0.513060      1.494685
   H       0.888551      0.513060      1.494685
   H       0.000000     -1.026339      1.494868
   H       0.000000      0.000089      2.948284
   C       0.000000      0.000140     -1.859161
   H       0.000000     -0.000089     -2.948284
   H      -0.888551     -0.513060     -1.494685
   H       0.888551     -0.513060     -1.494685
   H       0.000000      1.026339     -1.494868
$end

$rem
   JOBTYPE             sp
   EXCHANGE            hf
   CORRELATION         rimp2
   BASIS               aug-cc-pvtz
   AUX_BASIS           rimp2-aug-cc-pvtz
   BASIS2              racc-pvtz    Optional Secondary basis
   THRESH              12
   SCF_CONVERGENCE     8
   MAX_SUB_FILE_NUM    128
   SCS                 3            Spin-component scale arbitrarily
   SOS_FACTOR          0400000      Specify OS parameter
   SSS_FACTOR          1290000      Specify SS parameter
   DUAL_BASIS_ENERGY   true         Optional dual-basis approximation
   N_FROZEN_CORE       fc
   SYMMETRY            false
   SYM_IGNORE          true
$end
```

**Example 5.9** Example of SOS-MP2 geometry optimization

```
$molecule
   0 3
   C1
   H1   C1   1.07726
   H2   C1   1.07726   H1  131.60824
$end

$rem
   JOBTYPE        opt
   METHOD         sosmp2
   BASIS          cc-pvdz
   AUX_BASIS      rimp2-cc-pvdz
   UNRESTRICTED   true
   SYMMETRY       false
$end
```

**Example 5.10** Example of MOS-MP2 energy evaluation with frozen core approximation

```
$molecule
   0 1
   Cl
   Cl 1 2.05
```

```
$end

$rem
   JOBTYPE            sp
   METHOD             mosmp2
   OMEGA              600
   BASIS              cc-pVTZ
   AUX_BASIS          rimp2-cc-pVTZ
   N_FROZEN_CORE      fc
   THRESH             12
   SCF_CONVERGENCE    8
$end
```

**Example 5.11** Example of O2 methodology applied to $\mathcal{O}(N^4)$ SOSMP2

```
$molecule
   1 2
   F
   H 1 1.001
$end

$rem
   UNRESTRICTED       TRUE
   JOBTYPE            FORCE                Options are SP/FORCE/OPT
   EXCHANGE           HF
   DO_O2              1                    O2 with O(N^4) SOS-MP2 algorithm
   SOS_FACTOR         1000000              Opposite Spin scaling factor = 1.0
   SCF_ALGORITHM      DIIS_GDM
   SCF_GUESS          GWH
   BASIS              sto-3g
   AUX_BASIS          rimp2-vdz
   SCF_CONVERGENCE    8
   THRESH             14
   SYMMETRY           FALSE
   PURECART           1111
$end
```

**Example 5.12** Example of O2 methodology applied to $\mathcal{O}(N^4)$ MOSMP2

```
$molecule
   1 2
   F
   H 1 1.001
$end

$rem
   UNRESTRICTED       TRUE
   JOBTYPE            FORCE                Options are SP/FORCE/OPT
   EXCHANGE           HF
   DO_O2              2                    O2 with O(N^4) MOS-MP2 algorithm
   OMEGA              600                  Omega = 600/1000 = 0.6 a.u.
   SCF_ALGORITHM      DIIS_GDM
   SCF_GUESS          GWH
   BASIS              sto-3g
   AUX_BASIS          rimp2-vdz
   SCF_CONVERGENCE    8
   THRESH             14
   SYMMETRY          FALSE
   PURECART          1111
$end
```

### 5.6.7 RI-TRIM MP2 Energies

The triatomics in molecules (TRIM) local correlation approximation to MP2 theory[16] was described in detail in Section 5.5.1 which also discussed our implementation of this approach based on conventional four-center two-electron integrals. Q-CHEM 3.0 also includes an auxiliary basis implementation of the TRIM model. The new RI-TRIM MP2 energy algorithm[35] greatly accelerates these local correlation calculations (often by an order of magnitude or more for the correlation part), which scale with the 4th power of molecule size. The electron correlation part of the calculation is speeded up over normal RI-MP2 by a factor proportional to the number of atoms in the molecule. For a hexadecapeptide, for instance, the speedup is approximately a factor of 4[35]. The TRIM model can also be applied to the scaled opposite spin models discussed above. As for the other RI-based models discussed in this section, we recommend using RI-TRIM MP2 instead of the conventional TRIM MP2 code whenever run-time of the job is a significant issue. As for RI-MP2 itself, TRIM MP2 is invoked by adding AUX_BASIS *$rem*s to the input deck, in addition to requesting CORRELATION = RILMP2.

**Example 5.13** Example of RI-TRIM MP2 energy evaluation

```
$molecule
   0 3
   C1
   H1   C1   1.07726
   H2   C1   1.07726   H1   131.60824
$end

$rem
   METHOD         rilmp2
   BASIS          cc-pVDZ
   AUX_BASIS      rimp2-cc-pVDZ
   PURECART       1111
   UNRESTRICTED   true
   SYMMETRY       false
$end
```

### 5.6.8 Dual-Basis MP2

The successful computational cost speedups of the previous sections often leave the cost of the underlying SCF calculation dominant. The dual-basis method provides a means of accelerating the SCF by roughly an order of magnitude, with minimal associated error (see Section 4.9). This dual-basis reference energy may be combined with RI-MP2 calculations for both energies[36,37] and analytic first derivatives[38]. In the latter case, further savings (beyond the SCF alone) are demonstrated in the gradient due to the ability to solve the response ($Z$-vector) equations in the smaller basis set. Refer to Section 4.9 for details and job control options.

## 5.7 Attenuated MP2

MP2(attenuator, basis) approximates MP2 by splitting the Coulomb operator in two pieces and preserving only short-range two-electron interactions, akin to the CASE approximation[39,40], but without modification of the underlying SCF calculation. While MP2 is a comparatively efficient method for estimating the correlation energy, it converges slowly with basis set size — and, even in the complete basis limit, contains fundamentally inaccurate physics for long-range interactions. Basis set superposition error and the MP2-level treatment of long-range interactions both typically artificially increase correlation energies for non-covalent interactions. Attenuated MP2 improves upon MP2 for inter- and intramolecular interactions, with significantly better performance for relative and binding energies of non-covalent complexes, frequently outperforming complete basis set estimates of MP2[41,42].

Attenuated MP2, denoted MP2(attenuator, basis) is implemented in Q-CHEM based on the complementary terf function, below:

$$\mathrm{s(r) = terfc(r, r_0) = \frac{1}{2}\left\{erfc\left[\omega(r - r_0)\right] + erfc\left[\omega(r + r_0)\right]\right\}} \tag{5.23}$$

By choosing the terfc short-range operator, we optimally preserve the short-range behavior of the Coulomb operator while smoothly and rapidly switching off around the distance $r_0$. Since this directly addresses basis set superposition error, parameterization must be done for specific basis sets. This has been performed for the basis sets, aug-cc-pVDZ[41] and aug-cc-pVTZ[42]. Other basis sets are not recommended for general use until further testing has been done.

Energies and gradients are functional with and without the resolution of the identity approximation using correlation keywords ATTMP2 and ATTRIMP2.

**Example 5.14** Example of RI-MP2(terfc, aug-cc-pVDZ) energy evaluation

```
$molecule
   0 1
   O    -1.551007   -0.114520    0.000000
   H    -1.934259    0.762503    0.000000
   H    -0.599677    0.040712    0.000000
$end

$rem
   JOBTYPE          sp
   METHOD           attrimp2
   BASIS            aug-cc-pvdz
   AUX_BASIS        rimp2-aug-cc-pvdz
   N_FROZEN_CORE    fc
$end
```

**Example 5.15** Example of MP2(terfc, aug-cc-pVTZ) geometry optimization

```
$molecule
   0 1
   H    0.0   0.0   0.0
   H    0.0   0.0   0.9
$end

$rem
   JOBTYPE          opt
   METHOD           attmp2
   BASIS           aug-cc-pvtz
   N_FROZEN_CORE   fc
$end
```

## 5.8 Coupled-Cluster Methods

The following sections give short summaries of the various coupled-cluster based methods available in Q-CHEM, most of which are variants of coupled-cluster theory. The basic object-oriented tools necessary to permit the implementation of these methods in Q-CHEM was accomplished by Profs. Anna Krylov and David Sherrill, working at Berkeley with Martin Head-Gordon, and then continuing independently at the University of Southern California and Georgia Tech, respectively. While at Berkeley, Krylov and Sherrill also developed the optimized orbital coupled-cluster method, with additional assistance from Ed Byrd. The extension of this code to MP3, MP4, CCSD and QCISD is the work of Prof. Steve Gwaltney at Berkeley, while the extensions to QCCD were implemented by Ed Byrd at Berkeley. The original tensor library and CC/EOM suite of methods are handled by the CCMAN module of Q-CHEM. Recently, a new code (termed CCMAN2) has been developed in Krylov group by Evgeny Epifanovsky and others, and a gradual transition from CCMAN to CCMAN2 has began. During the transition time, both codes will be available for users via the CCMAN2 keyword.

**CORRELATION**

Specifies the correlation level of theory handled by CCMAN/CCMAN2.

TYPE:

STRING

DEFAULT:

None No Correlation

OPTIONS:

| | |
|---|---|
| CCMP2 | Regular MP2 handled by CCMAN/CCMAN2 |
| MP3 | CCMAN and CCMAN2 |
| MP4SDQ | CCMAN |
| MP4 | CCMAN |
| CCD | CCMAN and CCMAN2 |
| CCD(2) | CCMAN |
| CCSD | CCMAN and CCMAN2 |
| CCSD(T) | CCMAN and CCMAN2 |
| CCSD(2) | CCMAN |
| CCSD(fT) | CCMAN and CCMAN2 |
| CCSD(dT) | CCMAN |
| CCVB-SD | CCMAN2 |
| QCISD | CCMAN and CCMAN2 |
| QCISD(T) | CCMAN and CCMAN2 |
| OD | CCMAN |
| OD(T) | CCMAN |
| OD(2) | CCMAN |
| VOD | CCMAN |
| VOD(2) | CCMAN |
| QCCD | CCMAN |
| QCCD(T) | CCMAN |
| QCCD(2) | CCMAN |
| VQCCD | CCMAN |
| VQCCD(T) | CCMAN |
| VQCCD(2) | CCMAN |

RECOMMENDATION:

Consult the literature for guidance.

**Note:** All methods implemented in CCMAN2 can be executed in combination with the C-PCM implicit solvent model (section 6.7.10) and with the EFP method (section 11.5). Only energies and unrelaxed properties are available (no gradient).

### 5.8.1 Coupled Cluster Singles and Doubles (CCSD)

The standard approach for treating pair correlations self-consistently are coupled-cluster methods where the cluster operator contains all single and double substitutions[43], abbreviated as CCSD. CCSD yields results that are only slightly superior to MP2 for structures and frequencies of stable closed-shell molecules. However, it is far superior for reactive species, such as transition structures and radicals, for which the performance of MP2 is quite erratic.

A full textbook presentation of CCSD is beyond the scope of this manual, and several comprehensive references are available. However, it may be useful to briefly summarize the main equations. The CCSD wave function is:

$$|\Psi_{\mathrm{CCSD}}\rangle = \exp\left(\hat{T}_1 + \hat{T}_2\right)|\Phi_0\rangle \tag{5.24}$$

where the single and double excitation operators may be defined by their actions on the reference single determinant (which is normally taken as the Hartree-Fock determinant in CCSD):

$$\hat{T}_1|\Phi_0\rangle = \sum_i^{\mathrm{occ}}\sum_a^{\mathrm{virt}} t_i^a|\Phi_i^a\rangle \tag{5.25}$$

$$\hat{T}_2|\Phi_0\rangle = \frac{1}{4}\sum_{ij}^{\mathrm{occ}}\sum_{ab}^{\mathrm{virt}} t_{ij}^{ab}|\Phi_{ij}^{ab}\rangle \tag{5.26}$$

It is not feasible to determine the CCSD energy by variational minimization of $\langle E\rangle_{\mathrm{CCSD}}$ with respect to the singles and doubles amplitudes because the expressions terminate at the same level of complexity as full configuration interaction (!). So, instead, the Schrödinger equation is satisfied in the subspace spanned by the reference determinant, all single substitutions, and all double substitutions. Projection with these functions and integration over all space provides sufficient equations to determine the energy, the singles and doubles amplitudes as the solutions of sets of nonlinear equations. These equations may be symbolically written as follows:

$$\begin{aligned}
E_{\mathrm{CCSD}} &= \langle\Phi_0|\hat{H}|\Psi_{\mathrm{CCSD}}\rangle \\
&= \left\langle\Phi_0\left|\hat{H}\right|\left(1+\hat{T}_1+\frac{1}{2}\hat{T}_1^2+\hat{T}_2\right)\Phi_0\right\rangle_C &\quad(5.27)\\
0 &= \left\langle\Phi_i^a\left|\hat{H}-E_{\mathrm{CCSD}}\right|\Psi_{\mathrm{CCSD}}\right\rangle \\
&= \left\langle\Phi_i^a\left|\hat{H}\right|\left(1+\hat{T}_1+\frac{1}{2}\hat{T}_1^2+\hat{T}_2+\hat{T}_1\hat{T}_2+\frac{1}{3!}\hat{T}_1^3\right)\Phi_0\right\rangle_C &\quad(5.28)\\
0 &= \left\langle\Phi_{ij}^{ab}\left|\hat{H}-E_{\mathrm{CCSD}}\right|\Psi_{\mathrm{CCSD}}\right\rangle \\
&= \left\langle\Phi_{ij}^{ab}\left|\hat{H}\right|\left(1+\hat{T}_1+\frac{1}{2}\hat{T}_1^2+\hat{T}_2+\hat{T}_1\hat{T}_2+\frac{1}{3!}\hat{T}_1^3\right.\right. \\
&\qquad\left.\left.+\frac{1}{2}\hat{T}_2^2+\frac{1}{2}\hat{T}_1^2\hat{T}_2+\frac{1}{4!}\hat{T}_1^4\right)\Phi_0\right\rangle_C &\quad(5.29)
\end{aligned}$$

The result is a set of equations which yield an energy that is not necessarily variational (*i.e.*, may not be above the true energy), although it is strictly size-consistent. The equations are also exact for a pair of electrons, and, to the extent that molecules are a collection of interacting electron pairs, this is the basis for expecting that CCSD results will be of useful accuracy.

The computational effort necessary to solve the CCSD equations can be shown to scale with the 6th power of the molecular size, for fixed choice of basis set. Disk storage scales with the 4th power of molecular size, and involves a number of sets of doubles amplitudes, as well as two-electron integrals in the molecular orbital basis. Therefore the improved accuracy relative to MP2 theory comes at a steep computational cost. Given these scalings it is relatively straightforward to estimate the feasibility (or non feasibility) of a CCSD calculation on a larger molecule (or with a larger basis set) given that a smaller trial calculation is first performed. Q-CHEM supports both energies and analytic gradients for CCSD for RHF and UHF references (including frozen-core). For ROHF, only energies and unrelaxed properties are available.

### 5.8.2 Quadratic Configuration Interaction (QCISD)

Quadratic configuration interaction with singles and doubles (QCISD)[44] is a widely used alternative to CCSD, that shares its main desirable properties of being size-consistent, exact for pairs of electrons, as well as being also non variational. Its computational cost also scales in the same way with molecule size and basis set as CCSD, although with slightly smaller constants. While originally proposed independently of CCSD based on correcting configuration interaction equations to be size-consistent, QCISD is probably best viewed as approximation to CCSD. The defining equations are given below (under the assumption of Hartree-Fock orbitals, which should always be used in QCISD). The QCISD equations can clearly be viewed as the CCSD equations with a large number of terms omitted, which are evidently not very numerically significant:

$$E_{QCISD} = \left\langle \Phi_0 \left| \hat{H} \right| \left( 1 + \hat{T}_2 \right) \Phi_0 \right\rangle_C \tag{5.30}$$

$$0 = \left\langle \Phi_i^a \left| \hat{H} \right| \left( \hat{T}_1 + \hat{T}_2 + \hat{T}_1 \hat{T}_2 \right) \Phi_0 \right\rangle_C \tag{5.31}$$

$$0 = \left\langle \Phi_{ij}^{ab} \left| \hat{H} \right| \left( 1 + \hat{T}_1 + \hat{T}_2 + \frac{1}{2}\hat{T}_2^2 \right) \Phi_0 \right\rangle_C \tag{5.32}$$

QCISD energies are available in Q-CHEM, and are requested with the QCISD keyword. As discussed in Section 5.9, the non iterative QCISD(T) correction to the QCISD solution is also available to approximately incorporate the effect of higher substitutions.

### 5.8.3 Optimized Orbital Coupled Cluster Doubles (OD)

It is possible to greatly simplify the CCSD equations by omitting the single substitutions (*i.e.*, setting the $T_1$ operator to zero). If the same single determinant reference is used (specifically the Hartree-Fock determinant), then this defines the coupled-cluster doubles (CCD) method, by the following equations:

$$E_{\mathrm{CCD}} = \left\langle \Phi_0 \left| \hat{H} \right| \left( 1 + \hat{T}_2 \right) \Phi_0 \right\rangle_C \tag{5.33}$$

$$0 = \left\langle \Phi_{ij}^{ab} \left| \hat{H} \right| \left( 1 + \hat{T}_2 + \frac{1}{2}\hat{T}_2^2 \right) \Phi_0 \right\rangle_C \tag{5.34}$$

The CCD method cannot itself usually be recommended because while pair correlations are all correctly included, the neglect of single substitutions causes calculated energies and properties to be significantly less reliable than for CCSD. Single substitutions play a role very similar to orbital optimization, in that they effectively alter the reference determinant to be more appropriate for the description of electron correlation (the Hartree-Fock determinant is optimized in the absence of electron correlation).

This suggests an alternative to CCSD and QCISD that has some additional advantages. This is the optimized orbital CCD method (OO-CCD), which we normally refer to as simply optimized doubles (OD)[45]. The OD method is defined by the CCD equations above, plus the additional set of conditions that the cluster energy is minimized with respect to orbital variations. This may be mathematically expressed by

$$\frac{\partial E_{\mathrm{CCD}}}{\partial \theta_i^a} = 0 \tag{5.35}$$

where the rotation angle $\theta_i^a$ mixes the $i$th occupied orbital with the $a$th virtual (empty) orbital. Thus the orbitals that define the single determinant reference are optimized to minimize the coupled-cluster energy, and are variationally best for this purpose. The resulting orbitals are approximate Brueckner orbitals.

The OD method has the advantage of formal simplicity (orbital variations and single substitutions are essentially redundant variables). In cases where Hartree-Fock theory performs poorly (for example artificial symmetry breaking, or non-convergence), it is also practically advantageous to use the OD method, where the HF orbitals are not required, rather than CCSD or QCISD. Q-CHEM supports both energies and analytical gradients using the OD method. The computational cost for the OD energy is more than twice that of the CCSD or QCISD method, but the total cost of energy plus gradient is roughly similar, although OD remains more expensive. An additional advantage of the OD method is that it can be performed in an active space, as discussed later, in Section 5.10.

### 5.8.4 Quadratic Coupled Cluster Doubles (QCCD)

The non variational determination of the energy in the CCSD, QCISD, and OD methods discussed in the above subsections is not normally a practical problem. However, there are some cases where these methods perform poorly. One such example are potential curves for homolytic bond dissociation, using closed shell orbitals, where the calculated energies near dissociation go significantly below the true energies, giving potential curves with unphysical barriers to formation of the molecule from the separated fragments[46]. The Quadratic Coupled Cluster Doubles (QCCD) method[47] recently proposed by Troy Van Voorhis at Berkeley uses a different energy functional to yield improved behavior in problem cases of this type. Specifically, the QCCD energy functional is defined as

$$E_{\mathrm{QCCD}} = \left\langle \Phi_0 \left(1 + \hat{\Lambda}_2 + \frac{1}{2}\hat{\Lambda}_2^2\right) \left|\hat{H}\right| \exp\left(\hat{T}_2\right) \Phi_0 \right\rangle_C \tag{5.36}$$

where the amplitudes of both the $\hat{T}_2$ and $\hat{\Lambda}_2$ operators are determined by minimizing the QCCD energy functional. Additionally, the optimal orbitals are determined by minimizing the QCCD energy functional with respect to orbital rotations mixing occupied and virtual orbitals.

To see why the QCCD energy should be an improvement on the OD energy, we first write the latter in a different way than before. Namely, we can write a CCD energy functional which when minimized with respect to the $\hat{T}_2$ and $\hat{\Lambda}_2$ operators, gives back the same CCD equations defined earlier. This energy functional is

$$E_{\mathrm{CCD}} = \left\langle \Phi_0 \left(1 + \hat{\Lambda}_2\right) \left|\hat{H}\right| \exp\left(\hat{T}_2\right) \Phi_0 \right\rangle_C \tag{5.37}$$

Minimization with respect to the $\hat{\Lambda}_2$ operator gives the equations for the $\hat{T}_2$ operator presented previously, and, if those equations are satisfied then it is clear that we do not require knowledge of the $\hat{\Lambda}_2$ operator itself to evaluate the energy.

Comparing the two energy functionals, Eqs. (5.36) and (5.37), we see that the QCCD functional includes up through quadratic terms of the Maclaurin expansion of $\exp(\hat{\Lambda}_2)$ while the conventional CCD functional includes only linear terms. Thus the bra wave function and the ket wave function in the energy expression are treated more equivalently in QCCD than in CCD. This makes QCCD closer to a true variational treatment[46] where the bra and ket wave functions are treated precisely equivalently, but without the exponential cost of the variational method.

In practice QCCD is a dramatic improvement relative to any of the conventional pair correlation methods for processes involving more than two active electrons (*i.e.*, the breaking of at least a double bond, or, two spatially close single bonds). For example calculations, we refer to the original paper[47], and the follow-up paper describing the full implementation[48]. We note that these improvements carry a computational price. While QCCD scales formally with the 6th power of molecule size like CCSD, QCISD, and OD, the coefficient is substantially larger. For this reason, QCCD calculations are by default performed as OD calculations until they are partly converged. Q-CHEM also contains some configuration interaction models (CISD and CISDT). The CI methods are inferior to CC due to size-consistency issues, however, these models may be useful for benchmarking and development purposes.

### 5.8.5 Resolution of the Identity with CC (RI-CC)

The RI approximation (see Section 5.6) can be used in coupled-cluster calculations, which substantially reduces the cost of integral transformation and disk storage requirements. The RI approximations may be used for integrals only such that integrals are generated in conventional MO form and canonical CC/EOM calculations are performed, or in a more complete version when modified CC/EOM equations are used such that the integrals are used in their RI representation. The latter version allows for more substantial savings in storage and in computational speed-up.

The RI for integrals is invoked when AUX_BASIS is specified. All two-electron integrals are used in RI decomposed form in CC when AUX_BASIS is specified.

By default, the integrals will be stored in the RI form and special CC/EOM code will be invoked. Keyword CC_DIRECT_RI allows one to use RI generated integrals in conventional form (by transforming RI integrals back to the standard format) invoking conventional CC procedures.

**Note:** RI for integrals is available for all CCMAN/CCMAN2 methods. CCMAN requires that the unrestricted reference be used, CCMAN2 does not have this limitation. In addition, while RI is available for jobs that need analytical gradients, only energies and properties are computed using RI. Energy derivatives are calculated using regular electron repulsion integral derivatives. Full RI implementation (with integrals used in decomposed form) is only available for CCMAN2. For maximum computational efficiency, combine with FNO (see Sections 5.11 and 6.7.7) when appropriate.

### 5.8.6 Cholesky decomposition with CC (CD-CC)

Two-electron integrals can be decomposed using Cholesky decomposition[49] giving rise to the same representation as in RI and substantially reducing the cost of integral transformation, disk storage requirements, and improving parallel performance:

$$(\mu\nu|\lambda\sigma) \approx \sum_{P=1}^{M} B_{\mu\nu}^{P} B_{\lambda\sigma}^{P}, \tag{5.38}$$

The rank of Cholesky decomposition, $M$, is typically 3-10 times larger than the number of basis functions $N$ (Ref. 50); it depends on the decomposition threshold $\delta$ and is considerably smaller than the full rank of the matrix, $N(N+1)/2$ (Refs. 50–52). Cholesky decomposition removes linear dependencies in product densities[50] $(\mu\nu|$ allowing one to obtain compact approximation to the original matrix with accuracy, in principle, up to machine precision.

Decomposition threshold $\delta$ is the only parameter that controls accuracy and the rank of the decomposition. Cholesky decomposition is invoked by specifying CHOLESKY_TOL that defines the accuracy with which decomposition should be performed. For most calculations tolerance of $\delta = 10^{-3}$ gives a good balance between accuracy and compactness of the rank. Tolerance of $\delta = 10^{-2}$ can be used for exploratory calculations and $\delta = 10^{-4}$ for high-accuracy calculations. Similar to RI, Cholesky-decomposed integrals can be transformed back, into the canonical MO form, using CC_DIRECT_RI keyword.

**Note:** Cholesky decomposition is available for all CCMAN2 methods. Analytic gradients are not yet available; only energies and properties are computed using CD. For maximum computational efficiency, combine with FNO (see Sections 5.11 and 6.7.7) when appropriate.

### 5.8.7 Job Control Options

There are a large number of options for the coupled-cluster singles and doubles methods. They are documented in Appendix C, and, as the reader will find upon following this link, it is an extensive list indeed. Fortunately, many of them are not necessary for routine jobs. Most of the options for non-routine jobs concern altering the default iterative procedure, which is most often necessary for optimized orbital calculations (OD, QCCD), as well as the active space and EOM methods discussed later in Section 5.10. The more common options relating to convergence control are discussed there, in Section 5.10.6. Below we list the options that one should be aware of for routine calculations.

For memory options and parallel execution, see Section 5.14.

**CC_CONVERGENCE**

Overall convergence criterion for the coupled-cluster codes. This is designed to ensure at least $n$ significant digits in the calculated energy, and automatically sets the other convergence-related variables (CC_E_CONV, CC_T_CONV, CC_THETA_CONV, CC_THETA_GRAD_CONV) [$10^{-n}$].

TYPE:

INTEGER

DEFAULT:

6 Energies.

7 Gradients.

OPTIONS:

$n$ Corresponding to $10^{-n}$ convergence criterion. Amplitude convergence is set automatically to match energy convergence.

RECOMMENDATION:

Use the default

**Note:** For single point calculations, CC_E_CONV=6 and CC_T_CONV=4. Tighter amplitude convergence (CC_T_CONV=5) is used for gradients and EOM calculations.

**CC_DOV_THRESH**

Specifies minimum allowed values for the coupled-cluster energy denominators. Smaller values are replaced by this constant during early iterations only, so the final results are unaffected, but initial convergence is improved when the HOMO-LUMO gap is small or when non-conventional references are used.

TYPE:

INTEGER

DEFAULT:

0

OPTIONS:

$abcde$ Integer code is mapped to $abc \times 10^{-de}$, *e.g.*, 2502 corresponds to 0.25

RECOMMENDATION:

Increase to 0.25, 0.5 or 0.75 for non convergent coupled-cluster calculations.

**CC_SCALE_AMP**

If not 0, scales down the step for updating coupled-cluster amplitudes in cases of problematic convergence.

TYPE:

INTEGER

DEFAULT:

0 no scaling

OPTIONS:

$abcd$ Integer code is mapped to $abcd \times 10^{-2}$, *e.g.*, 90 corresponds to 0.9

RECOMMENDATION:

Use 0.9 or 0.8 for non convergent coupled-cluster calculations.

**CC_MAX_ITER**

Maximum number of iterations to optimize the coupled-cluster energy.

TYPE:

INTEGER

DEFAULT:

200

OPTIONS:

$n$ up to $n$ iterations to achieve convergence.

RECOMMENDATION:

None

**CC_PRINT**

Controls the output from post-MP2 coupled-cluster module of Q-CHEM

TYPE:

INTEGER

DEFAULT:

1

OPTIONS:

$0 - 7$ higher values can lead to deforestation…

RECOMMENDATION:

Increase if you need more output and don't like trees

**CHOLESKY_TOL**

Tolerance of Cholesky decomposition of two-electron integrals

TYPE:

INTEGER

DEFAULT:

3

OPTIONS:

$n$ Corresponds to a tolerance of $10^{-n}$

RECOMMENDATION:

2 - qualitative calculations, 3 - appropriate for most cases, 4 - quantitative (error in total energy typically less than 1 $\mu$hartree)

**CC_DIRECT_RI**

Controls use of RI and Cholesky integrals in conventional (undecomposed) form

TYPE:

LOGICAL

DEFAULT:

FALSE

OPTIONS:

FALSE use all integrals in decomposed format

TRUE transform all RI or Cholesky integral back to conventional format

RECOMMENDATION:

By default all integrals are used in decomposed format allowing significant reduction of memory use. If all integrals are transformed back (TRUE option) no memory reduction is achieved and decomposition error is introduced, however, the integral transformation is performed significantly faster and conventional CC/EOM algorithms are used.

### 5.8.8 Examples

**Example 5.16** A series of jobs evaluating the correlation energy (with core orbitals frozen) of the ground state of the $NH_2$ radical with three methods of coupled-cluster singles and doubles type: CCSD itself, OD, and QCCD.

```
$molecule
   0  2
   N
   H1  N  1.02805
   H2  N  1.02805  H1  103.34
$end

$rem
   METHOD          ccsd
   BASIS           6-31g*
   N_FROZEN_CORE   fc
$end

@@@

$molecule
   read
$end
```

```
$rem
   METHOD          od
   BASIS           6-31g*
   N_FROZEN_CORE   fc
$end

@@@

$molecule
   read
$end

$rem
   METHOD          qccd
   BASIS           6-31g*
   N_FROZEN_CORE   fc
$end
```

**Example 5.17** A job evaluating CCSD energy of water using RI-CCSD

```
$molecule
  0 1
  O
  H1 O OH
  H2 O OH H1 HOH

  OH  = 0.947
  HOH = 105.5
$end

$rem
   METHOD          ccsd
   BASIS           aug-cc-pvdz
   AUX_BASIS       rimp2-aug-cc-pvdz
$end
```

**Example 5.18** A job evaluating CCSD energy of water using CD-CCSD (tolerance = $10^{-3}$)

```
$molecule
  0 1
  O
  H1 O OH
  H2 O OH H1 HOH

  OH  = 0.947
  HOH = 105.5
$end

$rem
   METHOD          ccsd
   BASIS           aug-cc-pvdz
   CHOLESKY_TOL    3
$end
```

**Example 5.19** A job evaluating CCSD energy of water using CD-CCSD (tolerance = $10^{-3}$) with FNO

```
$molecule
   0 1
   O
   H1 O OH
   H2 O OH H1 HOH

   OH  = 0.947
   HOH = 105.5
$end

$rem
   METHOD          ccsd
   BASIS           aug-cc-pvdz
   CHOLESKY_TOL    3
   CC_FNO_THRESH   9950
$end
```

## 5.9 Non-iterative Corrections to Coupled Cluster Energies

### 5.9.1 (T) Triples Corrections

To approach chemical accuracy in reaction energies and related properties, it is necessary to account for electron correlation effects that involve three electrons simultaneously, as represented by triple substitutions relative to the mean field single determinant reference, which arise in MP4. The best standard methods for including triple substitutions are the CCSD(T)[53] and QCISD(T) methods[44] The accuracy of these methods is well-documented for many cases[54], and in general is a very significant improvement relative to the starting point (either CCSD or QCISD). The cost of these corrections scales with the 7th power of molecule size (or the 4th power of the number of basis functions, for a fixed molecule size), although no additional disk resources are required relative to the starting coupled-cluster calculation. Q-CHEM supports the evaluation of CCSD(T) and QCISD(T) energies, as well as the corresponding OD(T) correction to the optimized doubles method discussed in the previous subsection. Gradients and properties are not yet available for any of these (T) corrections.

### 5.9.2 (2) Triples and Quadruples Corrections

While the (T) corrections discussed above have been extraordinarily successful, there is nonetheless still room for further improvements in accuracy, for at least some important classes of problems. They contain judiciously chosen terms from 4th- and 5th-order Møller-Plesset perturbation theory, as well as higher order terms that result from the fact that the converged cluster amplitudes are employed to evaluate the 4th- and 5th-order order terms. The (T) correction therefore depends upon the bare reference orbitals and orbital energies, and in this way its effectiveness still depends on the quality of the reference determinant. Since we are correcting a coupled-cluster solution rather than a single determinant, this is an aspect of the (T) corrections that can be improved. Deficiencies of the (T) corrections show up computationally in cases where there are near-degeneracies between orbitals, such as stretched bonds, some transition states, open shell radicals, and diradicals.

Prof. Steve Gwaltney, while working at Berkeley with Martin Head-Gordon, has suggested a new class of non iterative correction that offers the prospect of improved accuracy in problem cases of the types identified above[55]. Q-CHEM contains Gwaltney's implementation of this new method, for energies only.

The new correction is a true second-order correction to a coupled-cluster starting point, and is therefore denoted as (2). It is available for two of the cluster methods discussed above, as OD(2) and CCSD(2)[55,56]. Only energies are available at present.

The basis of the (2) method is to partition not the regular Hamiltonian into perturbed and unperturbed parts, but rather to partition a similarity-transformed Hamiltonian, defined as $\tilde{H} = e^{-\hat{T}}\hat{H}e^{\hat{T}}$. In the truncated space (call it the $p$-space) within which the cluster problem is solved (*e.g.*, singles and doubles for CCSD), the coupled-cluster wave function is a true eigenvalue of $\tilde{H}$. Therefore we take the zero order Hamiltonian, $\tilde{H}^{(0)}$, to be the full $\tilde{H}$ in the p-space, while in the space of excluded substitutions (the q-space) we take only the one-body part of $\tilde{H}$ (which can be made diagonal). The fluctuation potential describing electron correlations in the $q$-space is $\tilde{H} - \tilde{H}^{(0)}$, and the (2) correction then follows from second-order perturbation theory.

The new partitioning of terms between the perturbed and unperturbed Hamiltonians inherent in the (2) correction leads to a correction that shows both similarities and differences relative to the existing (T) corrections. There are two types of higher correlations that enter at second-order: not only triple substitutions, but also quadruple substitutions. The quadruples are treated with a factorization ansatz, that is exact in 5th order Møller-Plesset theory[57], to reduce their computational cost from $N^9$ to $N^6$. For large basis sets this can still be larger than the cost of the triples terms, which scale as the 7th power of molecule size, with a factor twice as large as the usual (T) corrections.

These corrections are feasible for molecules containing between four and ten first row atoms, depending on computer resources, and the size of the basis set chosen. There is early evidence that the (2) corrections are superior to the (T) corrections for highly correlated systems[55]. This shows up in improved potential curves, particularly at long range and may also extend to improved energetic and structural properties at equilibrium in problematical cases. It will be some time before sufficient testing on the new (2) corrections has been done to permit a general assessment of the performance of these methods. However, they are clearly very promising, and for this reason they are available in Q-CHEM.

### 5.9.3 (dT) and (fT) corrections

Alternative inclusion of non-iterative $N^7$ triples corrections is described in Section 6.7.22. These methods called (dT) and (fT) are of similar accuracy to other triples corrections. CCSD(dT) and CCSD(fT) are equivalent to the CR-CCSD(T)$_L$ and CR-CCSD(T)$_2$ methods of Piecuch and co-workers[58]

### 5.9.4 Job Control Options

The evaluation of a non-iterative (T) or (2) correction after a coupled-cluster singles and doubles level calculation (either CCSD, QCISD or OD) is controlled by the correlation keyword, and the specification of any frozen orbitals via N_FROZEN_CORE (and possibly N_FROZEN_VIRTUAL).

For the (2) correction, it is possible to apply the frozen core approximation in the reference coupled cluster calculation, and then correlate all orbitals in the (2) correction. This is controlled by CC_INCL_CORE_CORR, described below.

The default is to include core and core-valence correlation automatically in the CCSD(2) or OD(2) correction, if the reference CCSD or OD calculation was performed with frozen core orbitals. The reason for this choice is that core correlation is economical to include via this method (the main cost increase is only linear in the number of core orbitals), and such effects are important to account for in accurate calculations.

This option should be made false if a job with explicitly frozen core orbitals is desired. One good reason for freezing core orbitals in the correction is if the basis set is physically inappropriate for describing core correlation (*e.g.*, standard Pople basis sets, and Dunning cc-pV$x$Z basis sets are designed to describe valence-only correlation effects). Another good reason is if a direct comparison is desired against another method such as CCSD(T) which is always used in the same orbital window as the CCSD reference.

There are several implementations of non-iterative triples available in Q-CHEM. In the original CCMAN suite, (T), (2), and (dT)/(fT) corrections can be computed. The parallel scaling of this code is very modest (4 cores max). CCMAN2 currently allows only the calculation of (T) correction for CCSD wave fucntions. By default, the CCMAN2 code is used for (T). The CCMAN code CCMAN2 is set to false. There are two versions of (T) in CCMAN2: The default version (native CCMAN2) and a new version using *libpt*. The implementation based on *libpt* is in-core MPI/OpenMP distributed-parallel. It is significantly faster in most realistic calculations (but it does not use point group symmetry, so it might show slower performance for small jobs with high symmetry). The *libpt* code is enabled by setting USE_LIBPT to true.

**Note:** For the best performance of *libpt* (T) code, parallel execution should be requested, see Section 2.8.

**USE_LIBPT**
Enable libpt for CCSD(T) calculations in CCMAN2.
TYPE:
LOGICAL
DEFAULT:
FALSE
OPTIONS:
TRUE FALSE
RECOMMENDATION:

**CC_INCL_CORE_CORR**
Whether to include the correlation contribution from frozen core orbitals in non iterative (2) corrections, such as OD(2) and CCSD(2).
TYPE:
LOGICAL
DEFAULT:
TRUE
OPTIONS:
TRUE FALSE
RECOMMENDATION:
Use the default unless no core-valence or core correlation is desired (*e.g.*, for comparison with other methods or because the basis used cannot describe core correlation).

### 5.9.5 Examples

**Example 5.20** Two jobs that compare the correlation energy calculated via the standard CCSD(T) method with the new CCSD(2) approximation, both using the frozen core approximation. This requires that CC_INCL_CORE_CORR must be specified as FALSE in the CCSD(2) input.

```
$molecule
   0  2
   O
   H  O  0.97907
$end

$rem
   METHOD          ccsd(t)
   BASIS           cc-pvtz
   N_FROZEN_CORE   fc
$end

@@@

$molecule
   read
$end

$rem
   METHOD              ccsd(2)
   BASIS               cc-pvtz
   N_FROZEN_CORE       fc
   CC_INCL_CORE_CORR   false
$end
```

**Example 5.21** Using *libpt* for a standard CCSD(T) calculation

```
$molecule
   0  2
   O
   H  O  0.97907
$end

$rem
   METHOD          ccsd(t)
   BASIS           cc-pvtz
   N_FROZEN_CORE   fc
   USE_LIBPT       true
$end
```

**Example 5.22** Water: Ground state CCSD(dT) calculation using RI

```
$molecule
   0 1
   O
   H1  O  OH
   H2  O  OH  H1  HOH

   OH  = 0.957
   HOH = 104.5
$end

$rem
   JOBTYPE     SP
   BASIS       cc-pvtz
   AUX_BASIS   rimp2-cc-pvtz
   METHOD      CCSD(dT)
$end
```

# 5.10 Coupled Cluster Active Space Methods

## 5.10.1 Introduction

Electron correlation effects can be qualitatively divided into two classes. The first class is static or non-dynamical correlation: long wavelength low-energy correlations associated with other electron configurations that are nearly as low in energy as the lowest energy configuration. These correlation effects are important for problems such as homolytic bond breaking, and are the hardest to describe because by definition the single configuration Hartree-Fock description is not a good starting point. The second class is dynamical correlation: short wavelength high-energy correlations associated with atomic-like effects. Dynamical correlation is essential for *quantitative* accuracy, but a reasonable description of static correlation is a prerequisite for a calculation being *qualitatively* correct.

In the methods discussed in the previous several subsections, the objective was to approximate the total correlation energy. However, in some cases, it is useful to model directly the non-dynamical and dynamical correlation energies separately. The reasons for this are pragmatic: with approximate methods, such a separation can give a more balanced treatment of electron correlation along bond-breaking coordinates, or reaction coordinates that involve diradicaloid intermediates. The non-dynamical correlation energy is conveniently defined as the solution of the Schrödinger equation within a small basis set composed of valence bonding, anti-bonding and lone pair orbitals: the so-called full valence active space. Solved exactly, this is the so-called full valence complete active space SCF (CASSCF)[59], or equivalently, the fully optimized reaction space (FORS) method[60].

Full valence CASSCF and FORS involve computational complexity which increases exponentially with the number of atoms, and is thus unfeasible beyond systems of only a few atoms, unless the active space is further restricted on a case-by-case basis. Q-CHEM includes two relatively economical methods that directly approximate these theories using a truncated coupled-cluster doubles wave function with optimized orbitals[61]. They are active space generalizations of the OD and QCCD methods discussed previously in Sections 5.8.3 and 5.8.4, and are discussed in the following two subsections. By contrast with the exponential growth of computational cost with problem size associated with exact solution of the full valence CASSCF problem, these cluster approximations have only 6th-order growth of computational cost with problem size, while often providing useful accuracy.

The full valence space is a well-defined theoretical chemical model. For these active space coupled-cluster doubles methods, it consists of the union of *valence* levels that are occupied in the single determinant reference, and those that are empty. The occupied levels that are to be replaced can only be the occupied valence and lone pair orbitals, whose number is defined by the sum of the valence electron counts for each atom (*i.e.*, 1 for H, 2 for He, 1 for Li, *etc.*.). At the same time, the empty virtual orbitals to which the double substitutions occur are restricted to be empty (usually anti-bonding) valence orbitals. Their number is the difference between the number of valence atomic orbitals, and the number of occupied valence orbitals given above. This definition (the full valence space) is the default when either of the “valence” active space methods are invoked (VOD or VQCCD)

There is also a second useful definition of a valence active space, which we shall call the 1:1 or perfect pairing active space. In this definition, the number of occupied valence orbitals remains the same as above. The number of empty correlating orbitals in the active space is defined as being exactly the same number, so that each occupied orbital may be regarded as being associated 1:1 with a correlating virtual orbital. In the water molecule, for example, this means that the lone pair electrons as well as the bond-orbitals are correlated. Generally the 1:1 active space recovers more correlation for molecules dominated by elements on the right of the periodic table, while the full valence active space recovers more correlation for molecules dominated by atoms to the left of the periodic table.

If you wish to specify either the 1:1 active space as described above, or some other choice of active space based on your particular chemical problem, then you must specify the numbers of active occupied and virtual orbitals. This is done via the standard "window options", documented earlier in this Chapter.

Finally we note that the entire discussion of active spaces here leads only to specific numbers of active occupied and virtual orbitals. The orbitals that are contained within these spaces are optimized by minimizing the trial energy with respect to all the degrees of freedom previously discussed: the substitution amplitudes, and the orbital rotation angles mixing occupied and virtual levels. In addition, there are new orbital degrees of freedom to be optimized to obtain the best active space of the chosen size, in the sense of yielding the lowest coupled-cluster energy. Thus rotation angles mixing active and inactive occupied orbitals must be varied until the energy is stationary. Denoting inactive orbitals by primes and active orbitals without primes, this corresponds to satisfying

$$\frac{\partial E_{\text{CCD}}}{\partial \theta_i^{j'}} = 0 \tag{5.39}$$

Likewise, the rotation angles mixing active and inactive virtual orbitals must also be varied until the coupled-cluster energy is minimized with respect to these degrees of freedom:

$$\frac{\partial E_{\text{CCD}}}{\partial \theta_a^{b'}} = 0 \tag{5.40}$$

### 5.10.2 VOD and VOD(2) Methods

The VOD method is the active space version of the OD method described earlier in Section 5.8.3. Both energies and gradients are available for VOD, so structure optimization is possible. There are a few important comments to make about the usefulness of VOD. First, it is a method that is capable of accurately treating problems that fundamentally involve 2 active electrons in a given local region of the molecule. It is therefore a good alternative for describing single bond-breaking, or torsion around a double bond, or some classes of diradicals. However it often performs poorly for problems where there is more than one bond being broken in a local region, with the non variational solutions being quite possible. For such problems the newer VQCCD method is substantially more reliable.

Assuming that VOD is a valid zero order description for the electronic structure, then a second-order correction, VOD(2), is available for energies only. VOD(2) is a version of OD(2) generalized to valence active spaces. It permits more accurate calculations of relative energies by accounting for dynamical correlation.

### 5.10.3 VQCCD

The VQCCD method is the active space version of the QCCD method described earlier in Section 5.8.3. Both energies and gradients are available for VQCCD, so that structure optimization is possible. VQCCD is applicable to a substantially wider range of problems than the VOD method, because the modified energy functional is not vulnerable to non variational collapse. Testing to date suggests that it is capable of describing double bond breaking to similar accuracy as full valence CASSCF, and that potential curves for triple bond-breaking are qualitatively correct, although quantitatively in error by a few tens of kcal/mol. The computational cost scales in the same manner with system size as the VOD method, albeit with a significantly larger prefactor.

### 5.10.4 CCVB-SD

Working with Prof. Head-Gordon at Berkeley, Dr. D. W. Small and Joonho Lee have developed and implemented a novel single-reference coupled-cluster method with singles and doubles, called CCVB-SD.[62,63] CCVB-SD improves upon a more crude model CCVB (5.15.2) and can be considered a simple modification to restricted CCSD (RCCSD). CCVB-SD inherits good properties from CCVB and RCCSD; it is spin-pure, size-extensive, and capable of breaking multiple bonds as long as only the valence space is correlated. It is a full doubles model and thus scales $\mathcal{O}(N^6)$. However, its energy is invariant under rotations in occupied space and virtual space, which makes it much more black-box than CCVB. Its energy function follows

$$E_{\text{CCVB-SD}} = \left\langle \Phi_0 \left(1 + \hat{\Lambda}\right) \left|\hat{H}\right| \left(\exp\left(\hat{T}\right) - \hat{\text{I}}_{\text{S}} \frac{\hat{Q}^2}{2}\right) \Phi_0 \right\rangle_C \tag{5.41}$$

where $\hat{\text{I}}_{\text{S}}$ is a singlet projection operator and $\hat{Q}$ is a quintet doubles operator. Unlike QCCD, CCVB-SD improves the right eigenfunction while leaving the left eigenfunction unchanged. The quintet term in Eq. (5.41) represents approximate connected quadruples which are responsible for describing strong correlation. The cost of CCVB-SD is only twice as expensive as RCCSD, and it is better suited for strong correlation than QCCD/VQCCD in the sense that the method becomes exact at the dissociation limits of most multiple bond breaking whereas QCCD does not except special cases.

Although CCVB-SD can be used without the active space constraints, we recommend that users use it with the valence active space in general. For benchmarking purposes, using a minimal basis will automatically provide the valence space correctly with frozen cores. Both the energy and nuclear gradients of CCVB-SD are available through CCMAN2.

It should be noted that there is no orbital optimization implemented for CCVB-SD at the moment. This means that using basis sets larger than minimal basis requires choosing right valence orbitals to use. Therefore, we recommend that users run GVB-PP (or CCVB) to obtain orbitals to begin with. Orbital optimization (i.e. CCVB-OD) will soon be implemented and running CCVB-OD will be much more black-box than CCVB-SD as it does not require selecting proper valence space orbitals.

Furthermore, CCVB-SD can be applied to only closed-shell molecules at the moment. The extension to open-shell molecules is under development.

**Example 5.23** A CCVB-SD force calculation of benzene in a minimal basis.

```
$comment
CCVB-SD job for benzene
It will compute energy+gradients.
It will also print out natural orbital occupation numbers (NOONs)
$end

$molecule
   0 1
   C    0.000000    0.698200    0.000000
   C    0.000000   -0.698200    0.000000
   C    1.209318    1.396400    0.000000
   C    1.209318   -1.396400    0.000000
   C    2.418636    0.698200    0.000000
   C    2.418636   -0.698200    0.000000
   H   -0.931410    1.235950    0.000000
   H   -0.931410   -1.235950    0.000000
   H    1.209318    2.471900    0.000000
   H    1.209318   -2.471900    0.000000
   H    3.350046    1.235950    0.000000
   H    3.350046   -1.235950    0.000000
$end

$rem
   JOBTYPE         = force
   BASIS           = sto-3g
   METHOD          = ccvbsd
   THRESH          = 14
   SCF_ALGORITHM   = gdm
   SCF_CONVERGENCE = 10
   CC_REF_PROP     = true
   SYMMETRY        = false
   SYM_IGNORE      = true
$end
```

### 5.10.5 Local Pair Models for Valence Correlations Beyond Doubles

Working with Prof. Head-Gordon at Berkeley, John Parkhill has developed implementations for pair models which couple 4 and 6 electrons together quantitatively. Because these truncate the coupled cluster equations at quadruples and hextuples respectively they have been termed the "Perfect Quadruples" and "Perfect Hextuples" models. These can be viewed as local approximations to CASSCF. The PQ and PH models are executed through an extension of Q-CHEM's coupled cluster code, and several options defined for those models will have the same effects although the mechanism may be different (CC_DIIS_START, CC_DIIS_SIZE, CC_DOV_THRESH, CC_CONV, *etc.*).

In the course of implementation, the non-local coupled cluster models were also implemented up to $\hat{T}_6$. Because the algorithms are explicitly sparse their costs relative to the existing implementations of CCSD are much higher (and should never be used in lieu of an existing CCMAN code), but this capability may be useful for development purposes, and when computable, models above CCSDTQ are highly accurate. To use PQ, PH, their dynamically correlated "+SD" versions or this machine generated cluster code set: METHOD = MGC.

**MGC_AMODEL**
Choice of approximate cluster model.
TYPE:
INTEGER
DEFAULT:
Determines how the CC equations are approximated:
OPTIONS:
0 Local Active-Space Amplitude iterations (pre-calculate GVB orbitals with your method of choice (RPP is good)).
7 Optimize-Orbitals using the VOD 2-step solver.
(Experimental-only use with MGC_AMPS = 2, 24 ,246)

8 Traditional Coupled Cluster up to CCSDTQPH.
9 MR-CC version of the Pair-Models. (Experimental)
RECOMMENDATION:
None

**MGC_NLPAIRS**

Number of local pairs on an amplitude.

TYPE:

INTEGER

DEFAULT:

None

OPTIONS:

Must be greater than 1, which corresponds to the PP model. 2 for PQ, and 3 for PH.

RECOMMENDATION:

None

**MGC_AMPS**

Choice of Amplitude Truncation

TYPE:

INTEGER

DEFAULT:

None

OPTIONS:

$2 \leq$ n $\leq$ 123456, a sorted list of integers for every amplitude
which will be iterated. Choose 1234 for PQ and 123456 for PH

RECOMMENDATION:

None

**MGC_LOCALINTS**

Pair filter on an integrals.

TYPE:

LOGICAL

DEFAULT:

FALSE

OPTIONS:

Enforces a pair filter on the 2-electron integrals, significantly
reducing computational cost. Generally useful. for more than 1 pair locality.

RECOMMENDATION:

None

**MGC_LOCALINTER**

Pair filter on an intermediate.

TYPE:

LOGICAL

DEFAULT:

FALSE

OPTIONS:

Any nonzero value enforces the pair constraint on intermediates,
significantly reducing computational cost. Not recommended for $\leq$ 2 pair locality

RECOMMENDATION:

None

### 5.10.6 Convergence Strategies and More Advanced Options

These optimized orbital coupled-cluster active space methods enable the use of the full valence space for larger systems than is possible with conventional complete active space codes. However, we should note at the outset that often there are substantial challenges in converging valence active space calculations (and even sometimes optimized orbital coupled cluster calculations without an active space). Active space calculations cannot be regarded as "routine" calculations in the same way as SCF calculations, and often require a considerable amount of computational trial and error to persuade them to converge. These difficulties are largely because of strong coupling between the orbital degrees of freedom and the amplitude degrees of freedom, as well as the fact that the energy surface is often quite flat with respect to the orbital variations defining the active space.

Being aware of this at the outset, and realizing that the program has nothing against you personally is useful information for the uninitiated user of these methods. What the program does have, to assist in the struggle to achieve a converged solution, are accordingly many convergence options, fully documented in Appendix C. In this section, we describe the basic options and the ideas behind using them as a starting point. Experience plays a critical role, however, and so we encourage you to experiment with toy jobs that give rapid feedback in order to become proficient at diagnosing problems.

If the default procedure fails to converge, the first useful option to employ is CC_PRECONV_T2Z, with a value of between 10 and 50. This is useful for jobs in which the MP2 amplitudes are very poor guesses for the converged cluster amplitudes, and therefore initial iterations varying only the amplitudes will be beneficial:

**CC_PRECONV_T2Z**
Whether to pre-converge the cluster amplitudes before beginning orbital optimization in optimized orbital cluster methods.
TYPE:
INTEGER
DEFAULT:
0 (FALSE)
10 If CC_RESTART, CC_RESTART_NO_SCF or CC_MP2NO_GUESS are TRUE
OPTIONS:
0 No pre-convergence before orbital optimization.
$n$ Up to $n$ iterations in this pre-convergence procedure.
RECOMMENDATION:
Experiment with this option in cases of convergence failure.

Other options that are useful include those that permit some damping of step sizes, and modify or disable the standard DIIS procedure. The main choices are as follows.

**CC_DIIS**

Specify the version of Pulay's Direct Inversion of the Iterative Subspace (DIIS) convergence accelerator to be used in the coupled-cluster code.

TYPE:

INTEGER

DEFAULT:

0

OPTIONS:

0 Activates procedure 2 initially, and procedure 1 when gradients are smaller than DIIS12_SWITCH.

1 Uses error vectors defined as differences between parameter vectors from successive iterations. Most efficient near convergence.

2 Error vectors are defined as gradients scaled by square root of the approximate diagonal Hessian. Most efficient far from convergence.

RECOMMENDATION:

DIIS1 can be more stable. If DIIS problems are encountered in the early stages of a calculation (when gradients are large) try DIIS1.

**CC_DIIS_START**

Iteration number when DIIS is turned on. Set to a large number to disable DIIS.

TYPE:

INTEGER

DEFAULT:

3

OPTIONS:

$n$ User-defined

RECOMMENDATION:

Occasionally DIIS can cause optimized orbital coupled-cluster calculations to diverge through large orbital changes. If this is seen, DIIS should be disabled.

**CC_DOV_THRESH**

Specifies minimum allowed values for the coupled-cluster energy denominators. Smaller values are replaced by this constant during early iterations only, so the final results are unaffected, but initial convergence is improved when the guess is poor.

TYPE:

INTEGER

DEFAULT:

2502 Corresponding to 0.25

OPTIONS:

$abcde$ Integer code is mapped to $abc \times 10^{-de}$

RECOMMENDATION:

Increase to 0.5 or 0.75 for non convergent coupled-cluster calculations.

**CC_THETA_STEPSIZE**

Scale factor for the orbital rotation step size. The optimal rotation steps should be approximately equal to the gradient vector.

TYPE:

INTEGER

DEFAULT:

100 Corresponding to 1.0

OPTIONS:

$abcde$ Integer code is mapped to $abc \times 10^{-de}$
If the initial step is smaller than 0.5, the program will increase step
when gradients are smaller than the value of THETA_GRAD_THRESH,
up to a limit of 0.5.

RECOMMENDATION:

Try a smaller value in cases of poor convergence and very large orbital gradients. For example, a value of 01001 translates to 0.1

An even stronger—and more-or-less last resort—option permits iteration of the cluster amplitudes without changing the orbitals:

**CC_PRECONV_T2Z_EACH**

Whether to pre-converge the cluster amplitudes before each change of the orbitals in optimized orbital coupled-cluster methods. The maximum number of iterations in this pre-convergence procedure is given by the value of this parameter.

TYPE:

INTEGER

DEFAULT:

0 (FALSE)

OPTIONS:

0 No pre-convergence before orbital optimization.

$n$ Up to $n$ iterations in this pre-convergence procedure.

RECOMMENDATION:

A very slow last resort option for jobs that do not converge.

### 5.10.7 Examples

**Example 5.24** Two jobs that compare the correlation energy of the water molecule with partially stretched bonds, calculated via the two coupled-cluster active space methods, VOD, and VQCCD. These are relatively “easy” jobs to converge, and may be contrasted with the next example, which is not easy to converge. The orbitals are restricted.

```
$molecule
   0  1
   O
   H  1  r
   H  1  r  a

   r =   1.5
   a = 104.5
$end
```

```
$rem
   METHOD        vod
   BASIS         6-31G
$end

@@@

$molecule
  read
$end

$rem
   METHOD        vqccd
   BASIS         6-31G
$end
```

**Example 5.25** The water molecule with highly stretched bonds, calculated via the two coupled-cluster active space methods, VOD, and VQCCD. These are "difficult" jobs to converge. The convergence options shown permitted the job to converge after some experimentation (thanks due to Ed Byrd for this!). The difficulty of converging this job should be contrasted with the previous example where the bonds were less stretched. In this case, the VQCCD method yields far better results than VOD!.

```
$molecule
   0  1
   O
   H  1  r
   H  1  r  a

   r =   3.0
   a = 104.5
$end

$rem
   METHOD                vod
   BASIS                 6-31G
   SCF_CONVERGENCE       9
   THRESH                12
   CC_PRECONV_T2Z        50
   CC_PRECONV_T2Z_EACH   50
   CC_DOV_THRESH         7500
   CC_THETA_STEPSIZE     3200
   CC_DIIS_START         75
$end

@@@

$molecule
   read
$end

$rem
   METHOD                vqccd
   BASIS                 6-31G
   SCF_CONVERGENCE       9
   THRESH                12
   CC_PRECONV_T2Z        50
   CC_PRECONV_T2Z_EACH   50
   CC_DOV_THRESH         7500
   CC_THETA_STEPSIZE     3200
   CC_DIIS_START         75
$end
```

## 5.11 Frozen Natural Orbitals in CCD, CCSD, OD, QCCD, and QCISD Calculations

Large computational savings are possible if the virtual space is truncated using the frozen natural orbital (FNO) approach. For example, using a fraction $f$ of the full virtual space results in a $1/(1-f)^4$-fold speed up for each CCSD iteration (CCSD scales with the forth power of the virtual space size). FNO-based truncation for ground-states CC methods was introduced by Bartlett and co-workers[64–66]. Extension of the FNO approach to ionized states within EOM-CC formalism was recently introduced and benchmarked[67] (see Section 6.7.7).

The FNOs are computed as the eigenstates of the virtual-virtual block of the MP2 density matrix [$\mathcal{O}(N^5)$ scaling], and the eigenvalues are the occupation numbers associated with the respective FNOs. By using a user-specified threshold, the FNOs with the smallest occupations are frozen in CC calculations. This could be done in CCSD, CCSD(T), CCSD(2), CCSD(dT), CCSD(fT) as well as CCD, OD,QCCD, VQCCD, and all possible triples corrections for these wave functions.

The truncation can be performed using two different schemes. The first approach is to simply specify the total number of virtual orbitals to retain, *e.g.*, as the percentage of total virtual orbitals, as was done in Refs. 65,66. The second approach is to specify the percentage of total natural occupation (in the virtual space) that needs to be recovered in the truncated space. These two criteria are referred to as the POVO (percentage of virtual orbitals) and OCCT (occupation threshold) cutoffs, respectively[67].

Since the OCCT criterion is based on the correlation in a specific molecule, it yields more consistent results than POVO. For ionization energy calculations employing 99–99.5% natural occupation threshold should yields errors (relative to the full virtual space values) below 1 kcal/mol[67]. The errors decrease linearly as a function of the total natural occupation recovered, which can be exploited by extrapolating truncated calculations to the full virtual space values. This extrapolation scheme is called the extrapolated FNO (XFNO) procedure[67]. The linear behavior is exhibited by the total energies of the ground and the ionized states as a function of OCCT. Therefore, the XFNO scheme can be employed even when the two states are not calculated on the same level, *e.g.*, in adiabatic energy differences and EOM-IP-CC(2,3) calculations (more on this in Ref. 67).

The FNO truncation often causes slower convergence of the CCSD and EOM procedures. Nevertheless, despite larger number of iterations, the FNO-based truncation of orbital space reduces computational cost considerably, with a negligible decline in accuracy[67].

### 5.11.1 Job Control Options

**CC_FNO_THRESH**

Initialize the FNO truncation and sets the threshold to be used for both cutoffs (OCCT and POVO)

TYPE:

INTEGER

DEFAULT:

None

OPTIONS:

| | |
|---|---|
| range | 0000-10000 |
| *abcd* | Corresponding to *ab.cd%* |

RECOMMENDATION:

None

**CC_FNO_USEPOP**

Selection of the truncation scheme

TYPE:

INTEGER

DEFAULT:

1 OCCT

OPTIONS:

0 POVO

RECOMMENDATION:

None

### 5.11.2 Example

**Example 5.26** CCSD(T) calculation using FNO with POVO=65%

```
$molecule
   0 1
   O
   H 1 1.0
   H 1 1.0 2 100.
$end

$rem
   METHOD        = CCSD(T)
   BASIS         = 6-311+G(2df,2pd)
   CC_FNO_THRESH = 6500   65% of the virtual space
   CC_FNO_USEPOP = 0
$end
```

## 5.12 Non-Hartree-Fock Orbitals in Correlated Calculations

In cases of problematic open-shell references, *e.g.*, strongly spin-contaminated doublet radicals, one may choose to use DFT orbitals, which can yield significantly improved results[68]. This can be achieved by first doing DFT calculation and then reading the orbitals and turning the Hartree-Fock procedure off. A more convenient way is just to specify EXCHANGE, *e.g.*, EXCHANGE = B3LYP means that B3LYP orbitals will be computed and used in the CCMAN/CCMAN2 module, as in the following example.

**Example 5.27** CCSD calculation of triplet methylene using B3LYP orbitals

```
$molecule
   0 3
   C
   H  1  CH
   H  1  CH  2  HCH

   CH  = 1.07
   HCH = 111.0
$end

$rem
   JOBTYPE         sp      single point
   EXCHANGE        b3lyp
   CORRELATION     ccsd
   BASIS           cc-pvdz
   N_FROZEN_CORE   1
$end
```

## 5.13 Analytic Gradients and Properties for Coupled-Cluster Methods

Analytic gradients are available for CCSD, OO-CCD/VOD, CCD, and QCCD/VQCCD methods for both closed- and open-shell references (UHF and RHF only), including frozen core and/or virtual functionality. Analytic gradients are available for CCVB-SD for only closed-shell references (RHF). In addition, gradients for selected GVB models are available.

For the CCSD and OO-CCD wave functions, Q-CHEM can also calculate dipole moments, $\langle R^2 \rangle$ (as well as XX, YY and ZZ components separately, which is useful for assigning different Rydberg states, *e.g.*, $3p_x$ vs. $3s$, *etc.*), and the $\langle S^2 \rangle$ values. Interface of the CCSD and (V)OO-CCD codes with the NBO 5.0 package is also available. This code is closely related to EOM-CCSD properties/gradient calculations (Section 6.7.15). Solvent models available for CCSD are described in Chapter 11.2.

Limitations: Gradients and fully relaxed properties for ROHF and non-HF (*e.g.*, B3LYP) orbitals as well as RI approximation are not yet available.

**Note:** If gradients or properties are computed with frozen core/virtual, the algorithm will replace frozen orbitals to restricted. This will not affect the energies, but will change the orbital numbering in the CCMAN printout.

### 5.13.1 Job Control Options

**CC_REF_PROP**

Whether or not the non-relaxed (expectation value) or full response (including orbital relaxation terms) one-particle CCSD properties will be calculated. The properties currently include permanent dipole moment, the second moments $\langle X^2\rangle$, $\langle Y^2\rangle$, and $\langle Z^2\rangle$ of electron density, and the total $\langle R^2\rangle = \langle X^2\rangle + \langle Y^2\rangle + \langle Z^2\rangle$ (in atomic units). Incompatible with JOBTYPE=FORCE, OPT, FREQ.

TYPE:

LOGICAL

DEFAULT:

FALSE (no one-particle properties will be calculated)

OPTIONS:

FALSE, TRUE

RECOMMENDATION:

Additional equations need to be solved (lambda CCSD equations) for properties with the cost approximately the same as CCSD equations. Use the default if you do not need properties. The cost of the properties calculation itself is low. The CCSD one-particle density can be analyzed with NBO package by specifying NBO=TRUE, CC_REF_PROP=TRUE and JOBTYPE=FORCE.

**CC_REF_PROP_TE**

Request for calculation of non-relaxed two-particle CCSD properties. The two-particle properties currently include $\langle S^2\rangle$. The one-particle properties also will be calculated, since the additional cost of the one-particle properties calculation is inferior compared to the cost of $\langle S^2\rangle$. The variable CC_REF_PROP must be also set to TRUE.

TYPE:

LOGICAL

DEFAULT:

FALSE (no two-particle properties will be calculated)

OPTIONS:

FALSE, TRUE

RECOMMENDATION:

The two-particle properties are computationally expensive, since they require calculation and use of the two-particle density matrix (the cost is approximately the same as the cost of an analytic gradient calculation). Do not request the two-particle properties unless you really need them.

**CC_FULLRESPONSE**

Fully relaxed properties (including orbital relaxation terms) will be computed. The variable CC_REF_PROP must be also set to TRUE.

TYPE:

LOGICAL

DEFAULT:

FALSE (no orbital response will be calculated)

OPTIONS:

FALSE, TRUE

RECOMMENDATION:

Not available for non UHF/RHF references and for the methods that do not have analytic gradients (*e.g.*, QCISD).

### 5.13.2 Examples

**Example 5.28** CCSD geometry optimization of HHeF followed up by properties calculations

```
$molecule
   0 1
   H    0.000000    0.000000   -1.886789
   He   0.000000    0.000000   -1.093834
   F    0.000000    0.000000    0.333122
$end

$rem
   JOBTYPE                      OPT
   METHOD                       CCSD
   BASIS                        aug-cc-pVDZ
   GEOM_OPT_TOL_GRADIENT        1
   GEOM_OPT_TOL_DISPLACEMENT    1
   GEOM_OPT_TOL_ENERGY          1
$end

@@@

$molecule
   read
$end

$rem
   JOBTYPE           SP
   METHOD            CCSD
   BASIS             aug-cc-pVDZ
   SCF_GUESS         READ
   CC_REF_PROP       1
   CC_FULLRESPONSE   1
$end
```

**Example 5.29** CCSD on 1,2-dichloroethane gauche conformation using SCRF solvent model

```
$molecule
   0 1
   C     0.654133   -0.381705    0.880884
   C    -0.654133    0.381705    0.880884
   Cl    1.732259    0.087759   -0.463055
   H     1.186245   -0.166574    1.796075
   H     0.488935   -1.444440    0.805846
   Cl   -1.732259   -0.087759   -0.463055
   H    -1.186245    0.166574    1.796075
   H    -0.488935    1.444440    0.805846
$end

$rem
   METHOD              CCSD
   BASIS               6-31g**
   N_FROZEN_CORE       FC
   CC_SAVEAMPL         1         Save CC amplitudes on disk
   SOLVENT_METHOD      SCRF
   SOL_ORDER           15        L=15 Multipole moment order
   SOLUTE_RADIUS       36500     3.65 Angstrom Solute Radius
```

```
      SOLVENT_DIELECTRIC   89300     8.93 Dielectric (Methylene Chloride)
      CCMAN2               false               Only works with CCMAN1
   $end
```

## 5.14 Memory Options and Parallelization of Coupled-Cluster Calculations

The coupled-cluster suite of methods, which includes ground-state methods mentioned earlier in this Chapter and excited-state methods in the next Chapter, has been parallelized to take advantage of distributed memory and multi-core architectures. The code is parallelized at the level of the underlying tensor algebra library[69].

### 5.14.1 Serial and Shared Memory Parallel Jobs

Parallelization on multiple CPUs or CPU cores is achieved by breaking down tensor operations into batches and running each batch in a separate thread. Because each thread occupies one CPU core entirely, the maximum number of threads must not exceed the total available number of CPU cores. If multiple computations are performed simultaneously, they together should not run more threads than available cores. For example, an eight-core node can accommodate one eight-thread calculation, two four-thread calculations, and so on.

The number of threads to be used in a calculation is specified as a command line option (*-nt nthreads*). Here *nthreads* should be given a positive integer value. If this option is not specified, the job will run in the serial mode.

Both CCMAN (old version of the couple-cluster codes) and CCMAN2 (default) have shared-memory parallel capabilities. However, they have different memory requirements as described below.

Setting the memory limit correctly is very important for attaining high performance when running large jobs. To roughly estimate the amount of memory required for a coupled-cluster calculation use the following formula:

$$\text{Memory} = \frac{(\text{Number of basis set functions})^4}{131072}\ \text{Mb} \tag{5.42}$$

If CCMAN2 is used and the calculation is based on a RHF reference, the amount of memory needed is a half of that given by the formula. If forces or excited states are calculated, the amount should be multiplied by a factor of two. Because the size of data increases steeply with the size of the molecule computed, both CCMAN and CCMAN2 are able to use disk space to supplement physical RAM if so required. The strategies of memory management in CCMAN and CCMAN2 slightly differ, and that should be taken into account when specifying memory-related keywords in the input file.

The MEM_STATIC keyword specifies the amount of memory in megabytes to be made available to routines that run prior to coupled-clusters calculations: Hartree-Fock and electronic repulsion integrals evaluation. A safe recommended value is 500 Mb. The value of MEM_STATIC should not exceed 2000 Mb even for very large jobs.

The memory limit for coupled-clusters calculations is set by CC_MEMORY. When running CCMAN, CC_MEMORY value is used as the recommended amount of memory, and the calculation can in fact use less or run over the limit. If the job is to run exclusively on a node, CC_MEMORY should be given 50% of all RAM. If the calculation runs out of memory, the amount of CC_MEMORY should be *reduced* forcing CCMAN to use memory-saving algorithms.

CCMAN2 uses a different strategy. It allocates the entire amount of RAM given by CC_MEMORY before the calculation and treats that as a strict memory limit. While that significantly improves the stability of larger jobs, it also requires the user to set the correct value of CC_MEMORY to ensure high performance. The default value is computed automatically based on the job size, but may not always be appropriate for large calculations, especially if the node has more resources available. When running CCMAN2 exclusively on a node, CC_MEMORY should be set to 75–80% of the total available RAM.

**Note:** When running small jobs, using too large CC_MEMORY in CCMAN2 is not recommended because Q-CHEM will allocate more resources than needed for the calculation, which may affect other jobs that you may wish to run on the same node.

For large disk-based coupled cluster calculations it is recommended to use a new tensor contraction code available in CCMAN2 via *libxm*, which can significantly speed up calculations on Linux nodes. Use the CC_BACKEND variable to switch on *libxm*. The new algorithm represents tensor contractions as multiplications of large matrices, which are performed using efficient *BLAS* routines. Tensor data is stored on disk and is asynchronously prefetched to fast memory before evaluating contractions. The performance of the code is not affected by the amount of RAM after about 128 GB if fast disks (such as SAS array in RAID0) are available on the system.

### 5.14.2 Distributed Memory Parallel Jobs

CCMAN2 has capabilities to run ground and excited state energy and property calculations on computer clusters and supercomputers using the Cyclops Tensor Framework (CTF)[70] as a computational back-end. To switch on the use of CTF, use the CC_BACKEND keyword. In addition, Q-CHEM should be invoked with the *-np nproc* command line option to specify the number of processors for a distributed calculation as *nproc*. Consult Section 2.8 for more details about running Q-CHEM in parallel.

### 5.14.3 Summary of Keywords

**MEM_STATIC**

Sets the memory for individual Fortran program modules

TYPE:

INTEGER

DEFAULT:

240 corresponding to 240 Mb or 12% of MEM_TOTAL

OPTIONS:

$n$ User-defined number of megabytes.

RECOMMENDATION:

For direct and semi-direct MP2 calculations, this must exceed OVN + requirements for AO integral evaluation (32–160 Mb). Up to 2000 Mb for large coupled-clusters calculations.

**CC_MEMORY**

Specifies the maximum size, in Mb, of the buffers for in-core storage of block-tensors in CCMAN and CCMAN2.

TYPE:

INTEGER

DEFAULT:

50% of MEM_TOTAL. If MEM_TOTAL is not set, use 1.5 Gb. A minimum of 192 Mb is hard-coded.

OPTIONS:

$n$ Integer number of Mb

RECOMMENDATION:

Larger values can give better I/O performance and are recommended for systems with large memory (add to your *.qchemrc* file. When running CCMAN2 exclusively on a node, CC_MEMORY should be set to 75–80% of the total available RAM. )

**CC_BACKEND**

Used to specify the computational back-end of CCMAN2.

TYPE:

STRING

DEFAULT:

VM Default shared-memory disk-based back-end

OPTIONS:

XM *libxm* shared-memory disk-based back-end

CTF Distributed-memory back-end for MPI jobs

RECOMMENDATION:

Use XM for large jobs with limited memory or when the performance of the default disk-based back-end is not satisfactory, CTF for MPI jobs

## 5.15 Simplified Coupled-Cluster Methods Based on a Perfect-Pairing Active Space

The methods described below are related to valence bond theory and are handled by the GVBMAN module. The following models are available:

**CORRELATION**

Specifies the correlation level in GVB models handled by GVBMAN.

TYPE:

STRING

DEFAULT:

None No Correlation

OPTIONS:

PP

CCVB

GVB_IP

GVB_SIP

GVB_DIP

OP

NP

2P

RECOMMENDATION:

As a rough guide, use PP for biradicaloids, and CCVB for polyradicaloids involving strong spin correlations. Consult the literature for further guidance.

Molecules where electron correlation is strong are characterized by small energy gaps between the nominally occupied orbitals (that would comprise the Hartree-Fock wave function, for example) and nominally empty orbitals. Examples include so-called diradicaloid molecules[71], or molecules with partly broken chemical bonds (as in some transition-state structures). Because the energy gap is small, electron configurations other than the reference determinant contribute to the molecular wave function with considerable amplitude, and omitting them leads to a significant error.

Including all possible configurations however, is a vast overkill. It is common to restrict the configurations that one generates to be constructed not from all molecular orbitals, but just from orbitals that are either "core" or "active". In this section, we consider just one type of active space, which is composed of two orbitals to represent each electron pair: one nominally occupied (bonding or lone pair in character) and the other nominally empty, or correlating (it is typically anti-bonding in character). This is usually called the perfect pairing active space, and it clearly is well-suited to represent the bonding/anti-bonding correlations that are associated with bond-breaking.

The quantum chemistry within this (or any other) active space is given by a Complete Active Space SCF (CASSCF) calculation, whose exponential cost growth with molecule size makes it prohibitive for systems with more than about 14 active orbitals. One well-defined coupled cluster (CC) approximation based on CASSCF is to include only double substitutions in the valence space whose orbitals are then optimized. In the framework of conventional CC theory, this defines the valence optimized doubles (VOD) model[61], which scales as $\mathcal{O}(N^6)$ (see Section 5.10.2). This is still too expensive to be readily applied to large molecules.

The methods described in this section bridge the gap between sophisticated but expensive coupled cluster methods and inexpensive methods such as DFT, HF and MP2 theory that may be (and indeed often are) inadequate for describing molecules that exhibit strong electron correlations such as diradicals. The coupled cluster perfect pairing (PP)[72,73], imperfect pairing (IP)[74] and restricted coupled cluster (RCC)[75] models are local approximations to VOD that include only a linear and quadratic number of double substitution amplitudes respectively. They are close in spirit to generalized valence bond (GVB)-type wave functions[76], because in fact they are all coupled cluster models for GVB that share the same perfect pairing active space. The most powerful method in the family, the Coupled Cluster Valence Bond (CCVB) method[62,77,78], is a valence bond approach that goes well beyond the power of GVB-PP and related methods, as discussed below in Sec. 5.15.2.

### 5.15.1 Perfect pairing (PP)

To be more specific, the coupled cluster PP wave function is written as

$$|\Psi\rangle = \exp\left(\sum_{i=1}^{n_{\text{active}}} t_i \hat{a}^{\dagger}_{i*} \hat{a}^{\dagger}_{\bar{i}*} \hat{a}_{\bar{i}} \hat{a}_i\right) |\Phi\rangle \tag{5.43}$$

where $n_{\text{active}}$ is the number of active electrons, and the $t_i$ are the linear number of unknown cluster amplitudes, corresponding to exciting the two electrons in the $i$th electron pair from their bonding orbital pair to their anti-bonding orbital pair. In addition to $t_i$, the core and the active orbitals are optimized as well to minimize the PP energy. The algorithm used for this is a slight modification of the GDM method, described for SCF calculations in Section 4.6.4. Despite the simplicity of the PP wave function, with only a linear number of correlation amplitudes, it is still a useful theoretical model chemistry for exploring strongly correlated systems. This is because it is exact for a single electron pair in the PP active space, and it is also exact for a collection of non-interacting electron pairs in this active space. Molecules, after all, are in a sense a collection of interacting electron pairs! In practice, PP on molecules recovers between 60% and 80% of the correlation energy in its active space.

If the calculation is perfect pairing (CORRELATION = PP), it is possible to look for unrestricted solutions in addition to restricted ones. Unrestricted orbitals are the default for molecules with odd numbers of electrons, but can also be specified for molecules with even numbers of electrons. This is accomplished by setting GVB_UNRESTRICTED = TRUE. Given a restricted guess, this will, however usually converge to a restricted solution anyway, so additional REM variables should be specified to ensure an initial guess that has broken spin symmetry. This can be accomplished by using an unrestricted SCF solution as the initial guess, using the techniques described in Chapter 4. Alternatively a restricted set of guess orbitals can be explicitly symmetry broken just before the calculation starts by using GVB_GUESS_MIX, which is described below. There is also the implementation of Unrestricted-in-Active Pairs (UAP)[79] which is the default unrestricted implementation for GVB methods. This method simplifies the process of unrestriction by optimizing only one set of ROHF MO coefficients and a single rotation angle for each occupied-virtual pair. These angles are used to construct a series of 2x2 Given's rotation matrices which are applied to the ROHF coefficients to determine the $\alpha$ spin MO coefficients and their transpose is applied to the ROHF coefficients to determine the $\beta$ spin MO coefficients. This algorithm is fast and eliminates many of the pathologies of the unrestricted GVB methods near the dissociation limit. To generate a full potential curve we find it is best to start at the desired UHF dissociation solution as a guess for GVB and follow it inwards to the equilibrium bond distance.

**GVB_UNRESTRICTED**

Controls restricted versus unrestricted PP jobs. Usually handled automatically.

TYPE:

LOGICAL

DEFAULT:

same value as UNRESTRICTED

OPTIONS:

TRUE/FALSE

RECOMMENDATION:

Set this variable explicitly only to do a UPP job from an RHF or ROHF initial guess. Leave this variable alone and specify UNRESTRICTED = TRUE to access the new Unrestricted-in-Active-Pairs GVB code which can return an RHF or ROHF solution if used with GVB_DO_ROHF

**GVB_DO_ROHF**

Sets the number of Unrestricted-in-Active Pairs to be kept restricted.

TYPE:

INTEGER

DEFAULT:

0

OPTIONS:

$n$ User-Defined

RECOMMENDATION:

If $n$ is the same value as GVB_N_PAIRS returns the ROHF solution for GVB, only works with the UNRESTRICTED = TRUE implementation of GVB with GVB_OLD_UPP = 0 (its default value)

**GVB_OLD_UPP**

Which unrestricted algorithm to use for GVB.

TYPE:

INTEGER

DEFAULT:

0

OPTIONS:

0 Use Unrestricted-in-Active Pairs described in Ref. 79

1 Use Unrestricted Implementation described in Ref. 73

RECOMMENDATION:

Only works for Unrestricted PP and no other GVB model.

**GVB_GUESS_MIX**

Similar to SCF_GUESS_MIX, it breaks alpha/beta symmetry for UPP by mixing the alpha HOMO and LUMO orbitals according to the user-defined fraction of LUMO to add the HOMO. 100 corresponds to a 1:1 ratio of HOMO and LUMO in the mixed orbitals.

TYPE:

INTEGER

DEFAULT:

0

OPTIONS:

$n$ User-defined, $0 \leq n \leq 100$

RECOMMENDATION:

25 often works well to break symmetry without overly impeding convergence.

Whilst all of the description in this section refers to PP solved via projection, it is also possible, as described in Sec. 5.15.2 below, to solve variationally for the PP energy. This variational PP solution is the reference wave function for the CCVB method. In most cases use of spin-pure CCVB is preferable to attempting to improve restricted PP by permitting the orbitals to spin polarize.

### 5.15.2 Coupled Cluster Valence Bond (CCVB)

Cases where PP needs improvement include molecules with several strongly correlated electron pairs that are all localized in the same region of space, and therefore involve significant inter-pair, as well as intra-pair correlations. For some systems of this type, Coupled Cluster Valence Bond (CCVB)[77,78] is an appropriate method. CCVB is designed to qualitatively treat the breaking of covalent bonds. At the most basic theoretical level, as a molecular system dissociates into a collection of open-shell fragments, the energy should approach the sum of the ROHF energies of the fragments. CCVB is able to reproduce this for a wide class of problems, while maintaining proper spin symmetry. Along with this, CCVB's main strength, come many of the spatial symmetry breaking issues common to the GVB-CC methods.

Like the other methods discussed in this section, the leading contribution to the CCVB wave function is the perfect pairing wave function, which is shown in eqn. (5.43). One important difference is that CCVB uses the PP wave function as a reference in the same way that other GVBMAN methods use a reference determinant.

The PP wave function is a product of simple, strongly orthogonal singlet geminals. Ignoring normalization, two equivalent ways of displaying these geminals are

$$\begin{aligned} (\phi_i\phi_i + t_i\phi_i^*\phi_i^*)(\alpha\beta - \beta\alpha) &\quad \text{(Natural-orbital form)} \\ \chi_i\chi_i'(\alpha\beta - \beta\alpha) &\quad \text{(Valence-bond form)}, \end{aligned} \tag{5.44}$$

where on the left and right we have the spatial part (involving $\phi$ and $\chi$ orbitals) and the spin coupling, respectively. The VB-form orbitals are non-orthogonal within a pair and are generally AO-like. The VB form is used in CCVB and the NO form is used in the other GVBMAN methods. It turns out that occupied UHF orbitals can also be rotated (without affecting the energy) into the VB form (here the spin part would be just $\alpha\beta$), and as such we store the CCVB orbital coefficients in the same way as is done in UHF (even though no one spin is assigned to an orbital in CCVB).

These geminals are uncorrelated in the same way that molecular orbitals are uncorrelated in a HF calculation. Hence, they are able to describe uncoupled, or independent, single-bond-breaking processes, like that found in $C_2H_6 \rightarrow 2\ CH_3$, but not coupled multiple-bond-breaking processes, such as the dissociation of $N_2$. In the latter system the three bonds may be described by three singlet geminals, but this picture must somehow translate into the coupling of two spin-quartet N atoms into an overall singlet, as found at dissociation. To achieve this sort of thing in a GVB context, it is necessary to correlate the geminals. The part of this correlation that is essential to bond breaking is obtained by replacing clusters of singlet geminals with triplet geminals, and re-coupling the triplets to an overall singlet. A triplet geminal is obtained from a singlet by simply modifying the spin component accordingly. We thus obtain the CCVB wave function:

$$\begin{aligned} |\Psi\rangle = |\Phi_0\rangle + \sum_{k<l} t_{kl} |\Phi_{(kl)}\rangle + \sum_{k<l<m<n} \Big[ & t_{kl} t_{mn} |\Phi_{(kl)(mn)}\rangle \\ & + t_{km} t_{ln} |\Phi_{(km)(ln)}\rangle + t_{kn} t_{lm} |\Phi_{(kn)(lm)}\rangle \Big] + \cdots . \end{aligned} \tag{5.45}$$

In this expansion, the summations go over the active singlet pairs, and the indices shown in the labellings of the kets correspond to pairs that are being coupled as described just above. We see that this wave function couples clusters composed of even numbers of geminals. In addition, we see that the amplitudes for clusters containing more than 2 geminals are parameterized by the amplitudes for the 2-pair clusters. This approximation is important for computational tractability, but actually is just one in a family of CCVB methods: it is possible to include coupled clusters of odd numbers of pairs, and also to introduce independent parameters for the higher-order amplitudes. At present, only the simplest level is included in Q-CHEM.

Older methods which attempt to describe substantially the same electron correlation effects as CCVB are the IP[74] and RCC[75] wave functions. In general CCVB should be used preferentially. It turns out that CCVB relates to the GVB-IP model. In fact, if we were to expand the CCVB wave function relative to a set of determinants, we would see that for each pair of singlet pairs, CCVB contains only one of the two pertinent GVB-IP doubles amplitudes. Hence, for CCVB the various computational requirements and timings are very similar to those for GVB-IP. The main difference between the two models lies in how the doubles amplitudes are used to parameterize the quadruples, sextuples, etc., and this is what allows CCVB to give correct energies at full bond dissociation.

A CCVB calculation is invoked by setting CORRELATION = CCVB. The number of active singlet geminals must be specified by GVB_N_PAIRS. After this, an initial guess is chosen. There are three main options for this, specified by the following keyword

**CCVB_GUESS**

Specifies the initial guess for CCVB calculations

TYPE:

INTEGER

DEFAULT:

NONE

OPTIONS:

1 Standard GVBMAN guess (orbital localization via GVB_LOCAL + Sano procedure).

2 Use orbitals from previous GVBMAN calculation, along with SCF_GUESS = read.

3 Convert UHF orbitals into pairing VB form.

RECOMMENDATION:

Option 1 is the most useful overall. The success of GVBMAN methods is often dependent on localized orbitals, and this guess shoots for these. Option 2 is useful for comparing results to other GVBMAN methods, or if other GVBMAN methods are able to obtain a desired result more efficiently. Option 3 can be useful for bond-breaking situations when a pertinent UHF solution has been found. It works best for small systems, or if the unrestriction is a local phenomenon within a larger molecule. If the unrestriction is non-local and the system is large, this guess will often produce a solution that is not the global minimum. Any UHF solution has a certain number of pairs that are unrestricted, and this will be output by the program. If GVB_N_PAIRS exceeds this number, the standard GVBMAN initial-guess procedure will be used to obtain a guess for the excess pairs

For potential energy surfaces, restarting from a previously computed CCVB solution is recommended. This is invoked by GVB_RESTART = TRUE. Whenever this is used, or any time orbitals are being read directly into CCVB from another calculation, it is important to also set:

- SCF_GUESS = READ
- MP2_RESTART_NO_SCF = TRUE
- SCF_ALGORITHM = DIIS

This bypasses orthogonalization schemes used elsewhere within Q-CHEM that are likely to jumble the CCVB guess.

In addition to the parent CCVB method as discussed up until now, we have included two related schemes for energy optimization, whose operation is controlled by the following keyword:

**CCVB_METHOD**

Optionally modifies the basic CCVB method

TYPE:

INTEGER

DEFAULT:

1

OPTIONS:

1 Standard CCVB model

3 Independent electron pair approximation (IEPA) to CCVB

4 Variational PP (the CCVB reference energy)

RECOMMENDATION:

Option 1 is generally recommended. Option 4 is useful for preconditioning, and for obtaining localized-orbital solutions, which may be used in subsequent calculations. It is also useful for cases in which the regular GVBMAN PP code becomes variationally unstable. Option 3 is a simple independent-amplitude approximation to CCVB. It avoids the cubic-scaling amplitude equations of CCVB, and also is able to reach the correct dissociation energy for any molecular system (unlike regular CCVB which does so only for cases in which UHF can reach a correct dissociate limit). However the IEPA approximation to CCVB is sometimes variationally unstable, which we have yet to observe in regular CCVB.

**Example 5.30** $N_2$ molecule in the intermediately dissociated region. In this case, SCF_ALGORITHM DIIS is necessary to obtain the symmetry unbroken RHF solution, which itself is necessary to obtain the proper CCVB solution. Note that many keywords general to GVBMAN are also used in CCVB.

```
$molecule
   0 1
   N  0  0  0
   N  0  0  2.0
$end

$rem
   JOBTYPE            = sp
   UNRESTRICTED       = false
   BASIS              = 6-31g*
   EXCHANGE           = hf
   CORRELATION        = ccvb
   GVB_N_PAIRS        = 3
   CCVB_METHOD        = 1
   CCVB_GUESS         = 1
   GVB_LOCAL          = 2
   GVB_ORB_MAX_ITER   = 100000
   GVB_ORB_CONV       = 7
   GVB_RESTART        = false
   SCF_CONVERGENCE    = 10
   THRESH             = 14
   SCF_GUESS          = sad
   MP2_RESTART_NO_SCF = false
   SCF_ALGORITHM      = diis
   MAX_SCF_CYCLES     = 2000
   SYMMETRY           = false
   SYM_IGNORE         = true
   PRINT_ORBITALS     = true
$end
```

### 5.15.3 Second-order Correction to Perfect Pairing: PP(2)

The PP and CCVB models are potential replacements for HF theory as a zero order description of electronic structure and can be used as a starting point for perturbation theory. They neglect all correlations that involve electron configurations with one or more orbitals that are outside the active space. Physically this means that the so-called "dynamic correlations", which correspond to atomic-like correlations involving high angular momentum virtual levels are neglected. Therefore, the GVB models may not be very accurate for describing energy differences that are sensitive to this neglected correlation energy, *e.g.*, atomization energies. It is desirable to correct them for this neglected correlation in a way that is similar to how the HF reference is corrected via MP2 perturbation theory.

For this purpose, the leading (second-order) correction to the PP model, termed PP(2)[80], has been formulated and efficiently implemented for restricted and unrestricted orbitals (energy only). PP(2) improves upon many of the worst failures of MP2 theory (to which it is analogous), such as for open shell radicals. PP(2) also greatly improves relative energies relative to PP itself. PP(2) is implemented using a resolution of the identity (RI) approach to keep the computational cost manageable. This cost scales in the same 5th-order way with molecular size as RI-MP2, but with a pre-factor that is about 5 times larger. It is therefore vastly cheaper than CCSD or CCSD(T) calculations which scale with the 6th and 7th powers of system size respectively. PP(2) calculations are requested with CORRELATION = PP(2). Since the only available algorithm uses auxiliary basis sets, it is essential to also provide a valid value for AUX_BASIS to have a complete input file.

The example below shows a PP(2) input file for the challenging case of the N2 molecule with a stretched bond. For this reason a number of the non-standard options discussed in Sec. 5.15.1 and Sec. 5.15.4 for orbital convergence are enabled here. First, this case is an unrestricted calculation on a molecule with an even number of electrons, and so it is essential to break the alpha/beta spin symmetry in order to find an unrestricted solution. Second, we have chosen to leave the lone pairs uncorrelated, which is accomplished by specifying GVB_N_PAIRS.

**Example 5.31** A non-standard PP(2) calculation. UPP(2) for stretched N2 with only 3 correlating pairs Try Boys localization scheme for initial guess.

```
$molecule
   0 1
   N
   N   1   1.65
$end

$rem
   UNRESTRICTED    true
   CORRELATION     pp(2)
   EXCHANGE        hf
   BASIS           cc-pvdz
   AUX_BASIS       rimp2-cc-pvdz   must use RI with PP(2)
   SCF_GUESS_MIX   10              mix SCF guess 100{\%}
   GVB_GUESS_MIX   25              mix GVB guess 25{\%} also!
   GVB_N_PAIRS     3               correlate only 3 pairs
   GVB_ORB_CONV    6               tighter convergence
   GVB_LOCAL       1               use Boys initial guess
$end
```

### 5.15.4 Other GVBMAN Methods and Options

In Q-CHEM, the unrestricted and restricted GVB methods are implemented with a resolution of the identity (RI) algorithm that makes them computationally very efficient[81,82]. They can be applied to systems with more than 100 active electrons, and both energies and analytical gradients are available. These methods are requested via the standard CORRELATION keyword. If AUX_BASIS is not specified, the calculation uses four-center two-electron integrals by default. Much faster auxiliary basis algorithms (see 5.6 for an introduction), which are used for the correlation energy (not the reference SCF energy), can be enabled by specifying a valid string for AUX_BASIS. The example below illustrates a simple IP calculation.

**Example 5.32** Imperfect pairing with auxiliary basis set for geometry optimization.

```
$molecule
   0 1
   H
   F   1   1.0
$end

$rem
   JOBTYPE        opt
   CORRELATION    gvb_ip
   BASIS          cc-pVDZ
   AUX_BASIS      rimp2-cc-pVDZ
$end
```

If further improvement in the orbitals are needed, the GVB_SIP, GVB_DIP, OP, NP and 2P models are also included[79]. The GVB_SIP model includes all the amplitudes of GVB_IP plus a set of quadratic amplitudes the represent the single ionization of a pair. The GVB_DIP model includes the GVB_SIP models amplitudes and the doubly ionized pairing amplitudes which are analogous to the correlation of the occupied electrons of the $i$th pair exciting into the virtual orbitals of the $j$th pair. These two models have the implementation limit of no analytic orbital gradient, meaning that a slow finite differences calculation must be performed to optimize their orbitals, or they must be computed using orbitals from a different method. The 2P model is the same as the GVB_DIP model, except it only allows the amplitudes to couple via integrals that span only two pairs. This allows for a fast implementation of it's analytic orbital gradient and enables the optimization of it's own orbitals. The OP method is like the 2P method except it removes the "direct"-like IP amplitudes and all of the same-spin amplitudes. The NP model is the GVB_IP model with the DIP amplitudes. This model is the one that works best with the symmetry breaking corrections that will be discussed later. All GVB methods except GVB_SIP and GVB_DIP have an analytic nuclear gradient implemented for both regular and RI four-center two-electron integrals.

There are often considerable challenges in converging the orbital optimization associated with these GVB-type calculations. The situation is somewhat analogous to SCF calculations but more severe because there are more orbital degrees of freedom that affect the energy (for instance, mixing occupied active orbitals amongst each other, mixing active virtual orbitals with each other, mixing core and active occupied, mixing active virtual and inactive virtual). Furthermore, the energy changes associated with many of these new orbital degrees of freedom are rather small and delicate. As a consequence, in cases where the correlations are strong, these GVB-type jobs often require many more iterations than the corresponding GDM calculations at the SCF level. This is a reflection of the correlation model itself. To deal with convergence issues, a number of REM values are available to customize the calculations, as listed below.

**GVB_ORB_MAX_ITER**

Controls the number of orbital iterations allowed in GVB-CC calculations. Some jobs, particularly unrestricted PP jobs can require 500–1000 iterations.

TYPE:

INTEGER

DEFAULT:

256

OPTIONS:

User-defined number of iterations.

RECOMMENDATION:

Default is typically adequate, but some jobs, particularly UPP jobs, can require 500–1000 iterations if converged tightly.

**GVB_ORB_CONV**

The GVB-CC wave function is considered converged when the root-mean-square orbital gradient and orbital step sizes are less than $10^{-\text{GVB\_ORB\_CONV}}$. Adjust THRESH simultaneously.

TYPE:

INTEGER

DEFAULT:

5

OPTIONS:

$n$ User-defined

RECOMMENDATION:

Use 6 for PP(2) jobs or geometry optimizations. Tighter convergence (*i.e.* 7 or higher) cannot always be reliably achieved.

**GVB_ORB_SCALE**

Scales the default orbital step size by $n$/1000.

TYPE:

INTEGER

DEFAULT:

1000 Corresponding to 100%

OPTIONS:

$n$ User-defined, 0–1000

RECOMMENDATION:

Default is usually fine, but for some stretched geometries it can help with convergence to use smaller values.

**GVB_AMP_SCALE**

Scales the default orbital amplitude iteration step size by $n$/1000 for IP/RCC. PP amplitude equations are solved analytically, so this parameter does not affect PP.

TYPE:

INTEGER

DEFAULT:

1000 Corresponding to 100%

OPTIONS:

$n$ User-defined, 0–1000

RECOMMENDATION:

Default is usually fine, but in some highly-correlated systems it can help with convergence to use smaller values.

**GVB_RESTART**

Restart a job from previously-converged GVB-CC orbitals.

TYPE:

LOGICAL

DEFAULT:

FALSE

OPTIONS:

TRUE/FALSE

RECOMMENDATION:

Useful when trying to converge to the same GVB solution at slightly different geometries, for example.

**GVB_REGULARIZE**

Coefficient for GVB_IP exchange type amplitude regularization to improve the convergence of the amplitude equations especially for spin-unrestricted amplitudes near dissociation. This is the leading coefficient for an amplitude dampening term $-(c/10000)(e^{t^p_{ij}} - 1)/(e^1 - 1)$

TYPE:

INTEGER

DEFAULT:

0 For restricted

1 For unrestricted

OPTIONS:

$c$ User-defined

RECOMMENDATION:

Should be increased if unrestricted amplitudes do not converge or converge slowly at dissociation. Set this to zero to remove all dynamically-valued amplitude regularization.

**GVB_POWER**

Coefficient for GVB_IP exchange type amplitude regularization to improve the convergence of the amplitude equations especially for spin-unrestricted amplitudes near dissociation. This is the leading coefficient for an amplitude dampening term included in the energy denominator: -($c$/10000)$(e^{t^p_{ij}} - 1)/(e^1 - 1)$

TYPE:

INTEGER

DEFAULT:

6

OPTIONS:

$p$ User-defined

RECOMMENDATION:

Should be decreased if unrestricted amplitudes do not converge or converge slowly at dissociation, and should be kept even valued.

**GVB_SHIFT**

Value for a statically valued energy shift in the energy denominator used to solve the coupled cluster amplitude equations, $n$/10000.

TYPE:

INTEGER

DEFAULT:

0

OPTIONS:

$n$ User-defined

RECOMMENDATION:

Default is fine, can be used in lieu of the dynamically valued amplitude regularization if it does not aid convergence.

Another issue that a user of these methods should be aware of is the fact that there is a multiple minimum challenge associated with GVB calculations. In SCF calculations it is sometimes possible to converge to more than one set of orbitals that satisfy the SCF equations at a given geometry. The same problem can arise in GVB calculations, and based on our experience to date, the problem in fact is more commonly encountered in GVB calculations than in SCF calculations. A user may therefore want to (or have to!) tinker with the initial guess used for the calculations. One way is to set GVB_RESTART = TRUE (see above), to replace the default initial guess (the converged SCF orbitals which are then localized). Another way is to change the localized orbitals that are used in the initial guess, which is controlled by the GVB_LOCAL variable, described below. Sometimes different localization criteria, and thus different initial guesses, lead to different converged solutions. Using the new amplitude regularization keywords enables some control over the solution GVB optimizes[83]. A calculation can be performed with amplitude regularization to find a desired solution, and then the calculation can be rerun with GVB_RESTART = TRUE and the regularization turned off to remove the energy penalty of regularization.

**GVB_LOCAL**

Sets the localization scheme used in the initial guess wave function.

TYPE:

INTEGER

DEFAULT:

2 Pipek-Mezey orbitals

OPTIONS:

0 No Localization

1 Boys localized orbitals

2 Pipek-Mezey orbitals

RECOMMENDATION:

Different initial guesses can sometimes lead to different solutions. It can be helpful to try both to ensure the global minimum has been found.

**GVB_DO_SANO**

Sets the scheme used in determining the active virtual orbitals in a Unrestricted-in-Active Pairs GVB calculation.

TYPE:

INTEGER

DEFAULT:

2

OPTIONS:

0 No localization or Sano procedure

1 Only localizes the active virtual orbitals

2 Uses the Sano procedure

RECOMMENDATION:

Different initial guesses can sometimes lead to different solutions. Disabling sometimes can aid in finding more non-local solutions for the orbitals.

Other *$rem* variables relevant to GVB calculations are given below. It is possible to explicitly set the number of active electron pairs using the GVB_N_PAIRS variable. The default is to make all valence electrons active. Other reasonable choices are certainly possible. For instance all electron pairs could be active ($n_{\text{active}} = n_\beta$). Or alternatively one could make only formal bonding electron pairs active ($n_{\text{active}} = N_{\text{STO-3G}} - n_\alpha$). Or in some cases, one might want only the most reactive electron pair to be active ($n_{\text{active}}$ =1). Clearly making physically appropriate choices for this variable is essential for obtaining physically appropriate results!

**GVB_N_PAIRS**

Alternative to CC_REST_OCC and CC_REST_VIR for setting active space size in GVB and valence coupled cluster methods.

TYPE:

INTEGER

DEFAULT:

PP active space (1 occ and 1 virt for each valence electron pair)

OPTIONS:

$n$ user-defined

RECOMMENDATION:

Use the default unless one wants to study a special active space. When using small active spaces, it is important to ensure that the proper orbitals are incorporated in the active space. If not, use the *$reorder_mo* feature to adjust the SCF orbitals appropriately.

**GVB_PRINT**

Controls the amount of information printed during a GVB-CC job.

TYPE:

INTEGER

DEFAULT:

0

OPTIONS:

$n$ User-defined

RECOMMENDATION:

Should never need to go above 0 or 1.

**GVB_TRUNC_OCC**

Controls how many pairs' occupied orbitals are truncated from the GVB active space.

TYPE:

INTEGER

DEFAULT:

0

OPTIONS:

$n$ User-defined

RECOMMENDATION:

This allows for asymmetric GVB active spaces removing the $n$ lowest energy occupied orbitals from the GVB active space while leaving their paired virtual orbitals in the active space. Only the models including the SIP and DIP amplitudes (ie NP and 2P) benefit from this all other models this equivalent to just reducing the total number of pairs.

**GVB_TRUNC_VIR**

Controls how many pairs' virtual orbitals are truncated from the GVB active space.

TYPE:

INTEGER

DEFAULT:

0

OPTIONS:

$n$ User-defined

RECOMMENDATION:

This allows for asymmetric GVB active spaces removing the $n$ highest energy occupied orbitals from the GVB active space while leaving their paired virtual orbitals in the active space. Only the models including the SIP and DIP amplitudes (ie NP and 2P) benefit from this all other models this equivalent to just reducing the total number of pairs.

**GVB_REORDER_PAIRS**

Tells the code how many GVB pairs to switch around.

TYPE:

INTEGER

DEFAULT:

0

OPTIONS:

$n$ $0 \leq n \leq 5$

RECOMMENDATION:

This allows for the user to change the order the active pairs are placed in after the orbitals are read in or are guessed using localization and the Sano procedure. Up to 5 sequential pair swaps can be made, but it is best to leave this alone.

**GVB_REORDER_1**

Tells the code which two pairs to swap first.

TYPE:

INTEGER

DEFAULT:

0

OPTIONS:

$n$ User-defined XXXYYY

RECOMMENDATION:

This is in the format of two 3-digit pair indices that tell the code to swap pair XXX with YYY, for example swapping pair 1 and 2 would get the input 001002. Must be specified in GVB_REORDER_PAIRS $\geq$ 1.

**GVB_REORDER_2**

Tells the code which two pairs to swap second.

TYPE:

INTEGER

DEFAULT:

0

OPTIONS:

$n$ User-defined XXXYYY

RECOMMENDATION:

This is in the format of two 3-digit pair indices that tell the code to swap pair XXX with YYY, for example swapping pair 1 and 2 would get the input 001002. Must be specified in GVB_REORDER_PAIRS $\geq$ 2.

**GVB_REORDER_3**

Tells the code which two pairs to swap third.

TYPE:

INTEGER

DEFAULT:

0

OPTIONS:

$n$ User-defined XXXYYY

RECOMMENDATION:

This is in the format of two 3-digit pair indices that tell the code to swap pair XXX with YYY, for example swapping pair 1 and 2 would get the input 001002. Must be specified in GVB_REORDER_PAIRS $\geq 3$.

**GVB_REORDER_4**

Tells the code which two pairs to swap fourth.

TYPE:

INTEGER

DEFAULT:

0

OPTIONS:

$n$ User-defined XXXYYY

RECOMMENDATION:

This is in the format of two 3-digit pair indices that tell the code to swap pair XXX with YYY, for example swapping pair 1 and 2 would get the input 001002. Must be specified in GVB_REORDER_PAIRS $\geq 4$.

**GVB_REORDER_5**

Tells the code which two pairs to swap fifth.

TYPE:

INTEGER

DEFAULT:

0

OPTIONS:

$n$ User-defined XXXYYY

RECOMMENDATION:

This is in the format of two 3-digit pair indices that tell the code to swap pair XXX with YYY, for example swapping pair 1 and 2 would get the input 001002. Must be specified in GVB_REORDER_PAIRS $\geq 5$.

It is known that symmetry breaking of the orbitals to favor localized solutions over non-local solutions is an issue with GVB methods in general. A combined coupled-cluster perturbation theory approach to solving symmetry breaking (SB) using perturbation theory level double amplitudes that connect up to three pairs has been examined in the literature[84,85], and it seems to alleviate the SB problem to a large extent. It works in conjunction with the GVB_IP, NP, and 2P levels of correlation for both restricted and unrestricted wave functions (barring that there is no restricted implementation of the 2P model, but setting GVB_DO_ROHF to the same number as the number of pairs in the system is equivalent).

**GVB_SYMFIX**

Should GVB use a symmetry breaking fix.

TYPE:

INTEGER

DEFAULT:

0

OPTIONS:

0 no symmetry breaking fix

1 symmetry breaking fix with virtual orbitals spanning the active space

2 symmetry breaking fix with virtual orbitals spanning the whole virtual space

RECOMMENDATION:

It is best to stick with type 1 to get a symmetry breaking correction with the best results coming from CORRELATION=NP and GVB_SYMFIX = 1.

**GVB_SYMPEN**

Sets the pre-factor for the amplitude regularization term for the SB amplitudes.

TYPE:

INTEGER

DEFAULT:

160

OPTIONS:

$\gamma$ User-defined

RECOMMENDATION:

Sets the pre-factor for the amplitude regularization term for the SB amplitudes: $-(\gamma/1000)(e^{(c*100)*t^2}-1)$.

**GVB_SYMSCA**

Sets the weight for the amplitude regularization term for the SB amplitudes.

TYPE:

INTEGER

DEFAULT:

125

OPTIONS:

$c$ User-defined

RECOMMENDATION:

Sets the weight for the amplitude regularization term for the SB amplitudes: $-(\gamma/1000)(e^{(c*100)*t^2}-1)$.

We have already mentioned a few issues associated with the GVB calculations: the neglect of dynamic correlation [which can be remedied with PP(2)], the convergence challenges and the multiple minimum issues. Another weakness of these GVB methods is the occasional symmetry-breaking artifacts that are a consequence of the limited number of retained pair correlation amplitudes. For example, benzene in the PP approximation prefers $D_{3h}$ symmetry over $D_{6h}$ by 3 kcal/mol (with a 2° distortion), while in IP, this difference is reduced to 0.5 kcal/mol and less than 1°[74]. Likewise the allyl radical breaks symmetry in the unrestricted PP model[73], although to a lesser extent than in restricted open shell HF. Another occasional weakness is the limitation to the perfect pairing active space, which is not necessarily appropriate for molecules with expanded valence shells, such as in some transition metal compounds (*e.g.* expansion from $4s3d$ into $4s4p3d$) or possibly hyper-valent molecules (expansion from $3s3p$ into $3s3p3d$). The singlet strongly orthogonal geminal method (see the next section) is capable of dealing with expanded valence shells and could be used for such cases. The perfect pairing active space is satisfactory for most organic and first row inorganic molecules.

To summarize, while these GVB methods are powerful and can yield much insight when used properly, they do have enough pitfalls for not to be considered true "black box" methods.

## 5.16 Geminal Models

### 5.16.1 Reference Wave Function

Computational models that use single reference wave function describe molecules in terms of independent electrons interacting via mean Coulomb and exchange fields. It is natural to improve this description by using correlated electron pairs, or *geminals*, as building blocks for molecular wave functions. Requirements of computational efficiency and size consistency constrain geminals to have $S_z = 0$[86], with each geminal spanning its own subspace of molecular orbitals[87]. Geminal wave functions were introduced into computational chemistry by Hurley, Lennard-Jones, and Pople[88]. An excellent review of the history and properties of geminal wave functions is given by Surjan[89].

We implemented a size consistent model chemistry based on Singlet type Strongly orthogonal Geminals (SSG). In SSG, the number of molecular orbitals in each singlet electron pair is an adjustable parameter chosen to minimize total energy. Open-shell orbitals remain uncorrelated. The SSG wave function is computed by setting SSG *$rem* variable to 1. Both spin-restricted (RSSG) and spin-unrestricted (USSG) versions are available, chosen by the UNRESTRICTED *$rem* variable.

The wave function has the form

$$\begin{aligned}
\Psi_{\mathrm{SSG}} &= \hat{A}\left[\psi_1(\mathbf{r}_1,\mathbf{r}_2)\ldots\psi_{n_\beta}(\mathbf{r}_{2n_\beta-1},\mathbf{r}_{2n_\beta})\phi_i(\mathbf{r}_{2n_\beta+1})\ldots\phi_j(\mathbf{r}_{n_\beta+n_\alpha})\right] \\
\psi_a(\mathbf{r}_1,\mathbf{r}_2) &= \sum_{k\in A}\frac{D_i^A}{\sqrt{2}}[\phi_k(\mathbf{r}_1)\bar{\phi_k}(\mathbf{r}_2)-\phi_k(\mathbf{r}_2)\bar{\phi_k}(\mathbf{r}_1)] \\
\phi_k(\mathbf{r}_1) &= \sum_\lambda C_\lambda^k\chi_\lambda(\mathbf{r}_1) \\
\bar{\phi_k}(\mathbf{r}_1) &= \sum_\lambda \bar{C}_\lambda^k\chi_\lambda(\mathbf{r}_1)
\end{aligned} \tag{5.46}$$

with the coefficients $C$, $D$, and subspaces $A$ chosen to minimize the energy

$$E_{\mathrm{SSG}} = \frac{\langle\Psi_{\mathrm{SSG}}|\hat{H}|\Psi_{\mathrm{SSG}}\rangle}{\langle\Psi_{\mathrm{SSG}}|\Psi_{\mathrm{SSG}}\rangle} \tag{5.47}$$

evaluated with the exact Hamiltonian $\hat{H}$. A constraint $\bar{C}_\lambda^k = C_\lambda^k$ for all MO coefficients yields a spin-restricted version of SSG.

SSG model can use any orbital-based initial guess. It is often advantageous to compute Hartree-Fock orbitals and then read them as initial guess for SSG. The program distinguishes Hartree-Fock and SSG initial guess wave functions, and in former case makes preliminary assignment of individual orbital pairs into geminals. The verification of orbital assignments is performed every ten wave function optimization steps, and the orbital pair is reassigned if total energy is lowered.

The convergence algorithm consists of combination of three types of minimization steps. The direct minimization steps[90] seeks a minimum along the gradient direction, rescaled by the quantity analogous to the orbital energy differences in SCF theory[86]. If the orbitals are nearly degenerate or inverted, a perturbative re-optimization of single geminal is performed. Finally, new set of the coefficients $C$ and $D$ is formed from a linear combination of previous iterations, in a manner similar to DIIS algorithm[91,92]. The size of iterative subspace is controlled by the DIIS_SUBSPACE_SIZE keyword.

After convergence is achieved, SSG reorders geminals based on geminal energy. The energy, along with geminal expansion coefficients, is printed for each geminal. Presence of any but the leading coefficient with large absolute value (value of 0.1 is often used for the definition of "large") indicates the importance of electron correlation in the system. The Mulliken population analysis is also performed for each geminal, which enables easy assignment of geminals into such chemical objects as core electron pairs, chemical bonds, and lone electron pairs.

As an example, consider the sample calculation of ScH molecule with 6-31G basis set at the experimental bond distance of 1.776 Å. In its singlet ground state the molecule has 11 geminals. Nine of them form core electrons on Sc. Two remaining geminals are:

*Geminal 10 E = -1.342609*
0.99128 -0.12578 -0.03563 -0.01149 -0.01133 -0.00398

*Geminal 11 E = -0.757086*
0.96142 -0.17446 -0.16872 -0.12414 -0.03187 -0.01227 -0.01204 -0.00435 -0.00416 -0.00098

Mulliken population analysis shows that geminal 10 is delocalized between Sc and H, indicating a bond. It is moderately correlated, with second expansion coefficient of a magnitude 0.126. The geminal of highest energy is localized on Sc. It represents $4s^2$ electrons and describes their excitation into $3d$ orbitals. Presence of three large expansion coefficients show that this effect cannot be described within GVB framework[93].

### 5.16.2 Perturbative Corrections

The SSG description of molecular electronic structure can be improved by perturbative description of missing inter-geminal correlation effects. We have implemented Epstein-Nesbet form of perturbation theory[94,95] that permits a balanced description of one- and two-electron contributions to excited states' energies in SSG model. This form of perturbation theory is especially accurate for calculation of weak intermolecular forces. Also, two-electron $[i\bar{j}, j\bar{i}]$ integrals are included in the reference Hamiltonian in addition to intra-geminal $[i\bar{j}, i\bar{j}]$ integrals that are needed for reference wave function to be an eigenfunction of the reference Hamiltonian[96].

All perturbative contributions to the SSG(EN2) energy (second-order Epstein-Nesbet perturbation theory of SSG wave function) are analyzed in terms of largest numerators, smallest denominators, and total energy contributions by the type of excitation. All excited states are subdivided into dispersion-like with correlated excitation within one geminal coupled to the excitation within another geminal, single, and double electron charge transfer. This analysis permits careful assessment of the quality of SSG reference wave function. Formally, the SSG(EN2) correction can be applied both to RSSG and USSG wave functions. Experience shows that molecules with broken or nearly broken bonds may have divergent RSSG(EN2) corrections. USSG(EN2) theory is balanced, with largest perturbative corrections to the wave function rarely exceeding 0.1 in magnitude.

**SSG**

Controls the calculation of the SSG wave function.

TYPE:

INTEGER

DEFAULT:

0

OPTIONS:

0 Do not compute the SSG wave function

1 Do compute the SSG wave function

RECOMMENDATION:

See also the UNRESTRICTED and DIIS_SUBSPACE_SIZE *$rem* variables.

# References and Further Reading

[1] Self-Consistent Field Methods (Chapter 4).

[2] Excited-State Calculations (Chapter 6).

[3] Basis Sets (Chapter 7) and Effective Core Potentials (Chapter 8).

[4] For a tutorial introduction to electron correlation methods based on wavefunctions, see Ref. 97.

[5] For a general textbook introduction to electron correlation methods and their respective strengths and weaknesses, see Ref. 98.

[6] L. A. Curtiss, K. Raghavachari, G. W. Trucks, and J. A. Pople, *J. Chem. Phys.* **94**, 7221 (1991).

[7] L. A. Curtiss, K. Raghavachari, P. C. Redfern, V. Rassolov, and J. A. Pople, *J. Chem. Phys.* **109**, 7764 (1998).

[8] D. Jayatilaka and T. J. Lee, *Chem. Phys. Lett.* **199**, 211 (1992).

[9] V. A. Rassolov, J. A. Pople, P. C. Redfern, and L. A. Curtiss, *Chem. Phys. Lett.* **350**, 573 (2001).

[10] C. Møller and M. S. Plesset, *Phys. Rev.* **46**, 618 (1934).

[11] W. J. Hehre, L. Radom, P. v. R. Schleyer, and J. A. Pople, *Ab Initio Molecular Orbital Theory*, Wiley, New York, 1986.

[12] T. Helgaker, J. Gauss, P. Jorgensen, and J. Olsen, *J. Chem. Phys.* **106**, 6430 (1997).

[13] M. Head-Gordon, *Mol. Phys.* **96**, 673 (1999).

[14] M. Head-Gordon, J. A. Pople, and M. J. Frisch, *Chem. Phys. Lett.* **153**, 503 (1988).

[15] M. J. Frisch, M. Head-Gordon, and J. A. Pople, *Chem. Phys. Lett.* **166**, 275 (1990).

[16] M. S. Lee, P. E. Maslen, and M. Head-Gordon, *J. Chem. Phys.* **112**, 3592 (2000).

[17] M. Head-Gordon, M. S. Lee, and P. E. Maslen, in *Simulation and Theory of Electrostatic Interactions in Solution*, edited by L. R. Pratt and G. Hummer, volume 492 of *AIP Conference Proceedings*, page 301, American Institute of Physics, New York, 1999.

[18] M. S. Lee and M. Head-Gordon, *Int. J. Quantum Chem.* **76**, 169 (2000).

[19] S. Saebo and P. Pulay, *Annu. Rev. Phys. Chem.* **44**, 213 (1993).

[20] L. A. Curtiss, K. Raghavachari, P. C. Redfern, and J. A. Pople, *J. Chem. Phys.* **112**, 7374 (2000).

[21] M. S. Lee, PhD thesis, University of California, Berkeley, CA, 2000.

[22] M. Feyereisen, G. Fitzgerald, and A. Komornicki, *Chem. Phys. Lett.* **208**, 359 (1993).

[23] B. I. Dunlap, *Phys. Chem. Chem. Phys.* **2**, 2113 (2000).

[24] Y. Jung, A. Sodt, P. M. W. Gill, and M. Head-Gordon, *Proc. Natl. Acad. Sci. USA* **102**, 6692 (2005).

[25] F. Weigend, M. Haser, H. Patzelt, and R. Ahlrichs, *Chem. Phys. Lett.* **294**, 143 (1998).

[26] F. Weigend, A. Kohn, and C. Hättig, *J. Chem. Phys.* **116**, 3175 (2002).

[27] F. Weigend and M. Haser, *Theor. Chem. Acc.* **97**, 331 (1997).

[28] R. A. DiStasio, Jr., R. P. Steele, Y. M. Rhee, Y. Shao, and M. Head-Gordon, *J. Comput. Chem.* **28**, 839 (2007).

[29] S. Grimme, *J. Chem. Phys.* **118**, 9095 (2003).

[30] R. A. DiStasio, Jr. and M. Head-Gordon, *Mol. Phys.* **105**, 1073 (2007).

[31] Y. Jung, R. C. Lochan, A. D. Dutoi, and M. Head-Gordon, *J. Chem. Phys.* **121**, 9793 (2004).

[32] R. C. Lochan, Y. Shao, and M. Head-Gordon, *J. Chem. Theory Comput.* **3**, 988 (2007).

[33] R. C. Lochan, Y. Jung, and M. Head-Gordon, *J. Phys. Chem. A* **109**, 7598 (2005).

[34] R. C. Lochan and M. Head-Gordon, *J. Chem. Phys.* **126**, 164101 (2007).

[35] R. A. DiStasio, Jr., Y. Jung, and M. Head-Gordon, *J. Chem. Theory Comput.* **1**, 862 (2005).

[36] R. P. Steele, R. A. DiStasio, Jr., Y. Shao, J. Kong, and M. Head-Gordon, *J. Chem. Phys.* **125**, 074108 (2006).

[37] R. P. Steele, R. A. DiStasio, Jr., and M. Head-Gordon, *J. Chem. Theory Comput.* **5**, 1560 (2009).

[38] R. A. DiStasio, Jr., R. P. Steele, and M. Head-Gordon, *Mol. Phys.* **105**, 27331 (2007).

[39] J. P. Dombroski, S. W. Taylor, and P. M. W. Gill, *J. Phys. Chem.* **100**, 6272 (1996).

[40] R. D. Adamson, J. P. Dombroski, and P. M. W. Gill, *Chem. Phys. Lett.* **254**, 329 (1996).

[41] M. Goldey and M. Head-Gordon, *J. Phys. Chem. Lett.* **3**, 3592 (2012).

[42] M. Goldey, A. Dutoi, and M. Head-Gordon, *Phys. Chem. Chem. Phys.* **15**, 15869 (2013).

[43] G. D. Purvis and R. J. Bartlett, *J. Chem. Phys.* **76**, 1910 (1982).

[44] J. A. Pople, M. Head-Gordon, and K. Raghavachari, *J. Chem. Phys.* **87**, 5968 (1987).

[45] C. D. Sherrill, A. I. Krylov, E. F. C. Byrd, and M. Head-Gordon, *J. Chem. Phys.* **109**, 4171 (1998).

[46] T. Van Voorhis and M. Head-Gordon, *J. Chem. Phys.* **113**, 8873 (2000).

[47] T. Van Voorhis and M. Head-Gordon, *Chem. Phys. Lett.* **330**, 585 (2000).

[48] E. F. C. Byrd, T. Van Voorhis, and M. Head-Gordon, *J. Phys. Chem. B* **106**, 8070 (2002).

[49] E. Epifanovsky et al., *J. Chem. Phys.* **139**, 134105 (2013).

[50] F. Aquilante, T. B. Pedersen, and R. Lindh, *Theor. Chem. Acc.* **124**, 1 (2009).

[51] N. H. F. Beebe and J. Linderberg, *Int. J. Quantum Chem.* **12**, 683 (1977).

[52] S. Wilson, *Comput. Phys. Commun.* **58**, 71 (1990).

[53] K. Raghavachari, G. W. Trucks, J. A. Pople, and M. Head-Gordon, *Chem. Phys. Lett.* **157**, 479 (1989).

[54] T. J. Lee and G. E. Scuseria, in *Quantum Mechanical Calculations with Chemical Accuracy*, edited by S. R. Langhoff, page 47, Kluwer, Dordrecht, 1995.

[55] S. R. Gwaltney and M. Head-Gordon, *Chem. Phys. Lett.* **323**, 21 (2000).

[56] S. R. Gwaltney and M. Head-Gordon, *J. Chem. Phys.* **115**, 5033 (2001).

[57] S. A. Kucharski and R. J. Bartlett, *J. Chem. Phys.* **108**, 5243 (1998).

[58] P. Piecuch and M. Włoch, *J. Chem. Phys.* **123**, 224105 (2005).

[59] B. O. Roos, *Adv. Chem. Phys.* **69**, 399 (1987).

[60] K. Ruedenberg, M. W. Schmidt, M. M. Gilbert, and S. T. Elbert, *Chem. Phys.* **71**, 49 (1982).

[61] A. I. Krylov, C. D. Sherrill, E. F. C. Byrd, and M. Head-Gordon, *J. Chem. Phys.* **109**, 10669 (1998).

[62] D. W. Small and M. Head-Gordon, *J. Chem. Phys.* **137**, 114103 (2012).

[63] E. E. J. Lee, D. W. Small and M. Head-Gordon, *J. Chem. Theory Comput.* **13**, 602 (2017).

[64] C. Sosa, J. Geertsen, G. W. Trucks, and R. J. Bartlett, *Chem. Phys. Lett.* **159**, 148 (1989).

[65] A. G. Taube and R. J. Bartlett, *Collect. Czech. Chem. Commun.* **70**, 837 (2005).

[66] A. G. Taube and R. J. Bartlett, *J. Chem. Phys.* **128**, 164101 (2008).

[67] A. Landau, K. Khistyaev, S. Dolgikh, and A. I. Krylov, *J. Chem. Phys.* **132**, 014109 (2010).

[68] G. J. O. Beran, S. R. Gwaltney, and M. Head-Gordon, *Phys. Chem. Chem. Phys.* **5**, 2488 (2003).

[69] E. Epifanovsky et al., *J. Comput. Chem.* **34**, 2293 (2013).

[70] E. Solomonik, D. Matthews, J. R. Hammond, J. F. Stanton, and J. Demmel, *J. Parallel Dist. Comp.* **74**, 3176 (2014).

[71] Y. Jung and M. Head-Gordon, *ChemPhysChem* **4**, 522 (2003).

[72] J. Cullen, *Chem. Phys.* **202**, 217 (1996).

[73] G. J. O. Beran, B. Austin, A. Sodt, and M. Head-Gordon, *J. Phys. Chem. A* **109**, 9183 (2005).

[74] T. Van Voorhis and M. Head-Gordon, *Chem. Phys. Lett.* **317**, 575 (2000).

[75] T. Van Voorhis and M. Head-Gordon, *J. Chem. Phys.* **115**, 7814 (2001).

[76] W. A. Goddard III and L. B. Harding, *Annu. Rev. Phys. Chem.* **29**, 363 (1978).

[77] D. W. Small and M. Head-Gordon, *J. Chem. Phys.* **130**, 084103 (2009).

[78] D. W. Small and M. Head-Gordon, *Phys. Chem. Chem. Phys.* **13**, 19285 (2011).

[79] K. V. Lawler, D. W. Small, and M. Head-Gordon, *J. Phys. Chem. A* **114**, 2930 (2010).

[80] G. J. O. Beran, M. Head-Gordon, and S. R. Gwaltney, *J. Chem. Phys.* **124**, 114107 (2006).

[81] T. Van Voorhis and M. Head-Gordon, *J. Chem. Phys.* **117**, 9190 (2002).

[82] A. Sodt, G. J. O. Beran, Y. Jung, B. Austin, and M. Head-Gordon, *J. Chem. Theory Comput.* **2**, 300 (2006).

[83] K. V. Lawler, J. A. Parkhill, and M. Head-Gordon, *J. Chem. Phys.* **130**, 184113 (2009).

[84] K. V. Lawler, G. J. O. Beran, and M. Head-Gordon, *J. Chem. Phys.* **128**, 024107 (2008).

[85] K. V. Lawler, J. A. Parkhill, and M. Head-Gordon, *Mol. Phys.* **106**, 2309 (2008).

[86] V. A. Rassolov, *J. Chem. Phys.* **117**, 5978 (2002).

[87] T. Arai, *J. Chem. Phys.* **33**, 95 (1960).

[88] A. C. Hurley, J. E. Lennard-Jones, and J. A. Pople, *Proc. Roy. Soc. London A* **220**, 446 (1953).

[89] P. R. Surján, *Topics Curr. Chem.* **203**, 63 (1999).

[90] R. Seeger and J. A. Pople, *J. Chem. Phys.* **65**, 265 (1976).

[91] P. Pulay, *Chem. Phys. Lett.* **73**, 393 (1980).

[92] P. Pulay, *J. Comput. Chem.* **3**, 556 (1982).

[93] F. W. Bobrowicz and W. A. Goddard III, in *Methods of Electronic Structure Theory*, edited by H. F. Schaefer III, volume 3, page 79, Plenum, New York, 1977.

[94] P. S. Epstein, *Phys. Rev.* **28**, 695 (1926).

[95] R. K. Nesbet, *Proc. Roy. Soc. Ser. A* **230**, 312 (1955).

[96] V. A. Rassolov, F. Xu, and S. Garaschchuk, *J. Chem. Phys.* **120**, 10385 (2004).

[97] R. J. Bartlett and J. F. Stanton, in *Reviews in Computational Chemistry*, edited by K. B. Lipkowitz and D. B. Boyd, volume 5, chapter 2, page 65, Wiley-VCH, New York, 1994.

[98] F. Jensen, *Introduction to Computational Chemistry*, Wiley, New York, 1994.

# Chapter 6

# Open-Shell and Excited-State Methods

## 6.1 General Excited-State Features

As for ground state calculations, performing an adequate excited-state calculation involves making an appropriate choice of method and basis set. The development of effective approaches to modeling electronic excited states has historically lagged behind advances in treating the ground state. In part this is because of the much greater diversity in the character of the wave functions for excited states, making it more difficult to develop broadly applicable methods without molecule-specific or even state-specific specification of the form of the wave function. Recently, however, a hierarchy of single-reference *ab initio* methods has begun to emerge for the treatment of excited states. Broadly speaking, Q-CHEM contains methods that are capable of giving qualitative agreement, and in many cases quantitative agreement with experiment for lower optically allowed states. The situation is less satisfactory for states that involve two-electron excitations, although even here reasonable results can sometimes be obtained. Moreover, some of the excited state methods can treat open-shell wave functions, *e.g.* diradicals, ionized and electron attachment states and more[3].

In excited-state calculations, as for ground state calculations, the user must strike a compromise between cost and accuracy. This chapter summarizes Q-CHEM's capabilities in four general classes of excited state methods:

- Single-electron wave function-based methods (Section 6.2). These are excited state treatments of roughly the same level of sophistication as the Hartree-Fock ground state method, in the sense that electron correlation is essentially ignored. Single excitation configuration interaction (CIS) is the workhorse method of this type. The spin-flip variant of CIS extends it to diradicals.
- Time-dependent density functional theory (TDDFT, Section 6.3). TDDFT is a widely used extension of DFT to excited states. For a cost that is only a little larger than that of a CIS calculation, TDDFT typically affords significantly greater accuracy due to a treatment of electron correlation. It, too, has a spin-flip variant that can be used to study di- and tri-radicals as well as bond breaking.
- The Maximum Overlap Method (MOM) for excited SCF states (Section 6.4). This method overcomes some of the deficiencies of TDDFT and, in particular, can be used for modeling charge-transfer and Rydberg transitions as well as core-excited states.

- Restricted open-shell Kohn-Sham (ROKS) method is another Δ-SCF approach for excited states (Section 6.5).
- Wave function-based electron correlation treatments (Sections 6.6, 6.8, 6.9 and 6.7). Roughly speaking, these are excited state analogues of the ground state wave function-based electron correlation methods discussed in Chapter 5. They are more accurate than the methods of Section 6.2, but also significantly more computationally expensive. These methods can also describe certain multi-configurational wave functions, for example, problematic doublet radicals, diradicals, triradicals, and more.

**Note:** Core electrons are frozen by default in most correlated excited-state calculations (see Section 5.2).

In general, a basis set appropriate for a ground state density functional theory or a Hartree-Fock calculation will be appropriate for describing valence excited states. However, many excited states involve significant contributions from diffuse Rydberg orbitals, and, therefore, it is often advisable to use basis sets that include additional diffuse functions. The 6-31+G* basis set is a reasonable compromise for the low-lying valence excited states of many organic molecules. To describe true Rydberg excited states, Q-CHEM allows the user to add two or more sets of diffuse functions (see Chapter 7). For example the 6-311(2+)G* basis includes two sets of diffuse functions on heavy atoms and is generally adequate for description of both valence and Rydberg excited states.

Q-CHEM supports four main types of excited state calculation:

- **Vertical absorption spectrum**
  This is the calculation of the excited states of the molecule at the ground state geometry, as appropriate for absorption spectroscopy. The methods supported for performing a vertical absorption calculation are: CIS, RPA, XCIS, SF-XCIS, CIS(D), ADC(2)-s, ADC(2)-x, ADC(3), RAS-SF, EOM-CCSD and EOM-OD, each of which will be discussed in turn. The calculation of core-excited states for the simulation of X-ray absorption spectra can be performed with the CVS-ADC(2)-s, CVS-ADC(2)-x and CVS-ADC(3) methods. All ADC-based methods can be combined with the polarizable continuum model (PCM) to model the absorption spectrum in solution following state-specific non-equilibrium approach.
- **Visualization**
  It is possible to visualize the excited states either by attachment/detachment density analysis (available for CIS, RPA, TDDFT, ADC, EOM-CC) or by plotting the transition density (see *$plots* descriptions in Chapters 3 and 10). Transition densities can be calculated for CIS, EOM-CCSD, and ADC methods. The theoretical basis of the attachment/detachment density analysis is discussed in Section 6.12.1 of this Chapter (more details are given in Section 10.2.7. In addition Dyson orbitals can be calculated and plotted for ionization from the ground and electronically excited states or detachment from electron-attached states for CCSD and EOM-CCSD wave functions. For the RAS-SF method (Section 6.9), one can plot the natural orbitals of a computed electronic state.
- **Excited-state optimization**
  Optimization of the geometry of stationary points on excited state potential energy surfaces is valuable for understanding the geometric relaxation that occurs between the ground and excited state. Analytic first derivatives are available for UCIS, RCIS, TDDFT and EOM-CCSD. Excited state optimizations may also be performed using finite difference methods, however, these can be very time-consuming to perform.

- **Optimization of the crossings between potential energy surfaces**
  Seams between potential energy surfaces can be located and optimized by using analytic gradients within EOM-CCSD, CIS, and TD-DFT formalisms.

- **Properties**
  Properties such as dipole moments, spatial extent of electron densities and $\langle S^2 \rangle$ values can be computed for ADC, EOM-CCSD, EOM-MP2, EOM-OD, RAS-SF and CIS wave functions. Static polarizabilities are available for CCSD, EOM-EE-CCSD, and EOM-SF-CCSD methods.

- **Transition properties and state interactions**
  Transition dipole moments and oscillator strengths can be computed with practically all excited-state methods. Matrix elements and cross-sections for two-photon absorption are available for EOM-EE-CCSD and ADC methods. Spin-orbit couplings can be computed for EOM-CCSD, CIS, and TDDFT wave functions. Dyson orbitals are available for EOM-CC wave functions. Transition properties can be computed between the reference and target states (*e.g.*, HF-CIS) or between different target states (*e.g.*, CIS-CIS).

- **Excited-state vibrational analysis**
  Given an optimized excited state geometry, Q-CHEM can calculate the force constants at the stationary point to predict excited state vibrational frequencies. Stationary points can also be characterized as minima, transition structures or $n$th-order saddle points. Analytic excited state vibrational analysis can only be performed using the UCIS, RCIS, and TDDFT methods, for which efficient analytical second derivatives are available. EOM-CCSD frequencies are also available using analytic first derivatives and second derivatives obtained from finite difference methods. EOM-OD frequencies are only available through finite difference calculations.

**Note:** EOM-CC and most of the CI codes are part of CCMAN and CCMAN2. CCMAN is a legacy code which is being phased out. All new developments and performance-enhancing features are implemented in CCMAN2.

**METHOD**

Specifies the level of theory.

TYPE:

STRING

DEFAULT:

None No Correlation

OPTIONS:

| | |
|---|---|
| CIS | Section 6.2.1 |
| CIS(D) | Section 6.6.1 |
| RI-CIS(D) | Section 6.6.2 |
| SOS-CIS(D) | Section 6.6.3 |
| SOS-CIS(D0) | Section 6.6.4 |
| CISD | Section 6.7.2 |
| CISDT | Section 6.7.2 |
| EOM-OD | Section 6.7.2 |
| EOM-CCSD | Section 6.7.2 |
| EOM-MP2 | Section 6.7.8 |
| EOM-MP2T | Section 6.7.8 |
| EOM-CCSD-S(D) | Section 6.7.9 |
| EOM-MP2-S(D) | Section 6.7.9 |
| EOM-CCSD(dT) | Section 6.7.22 |
| EOM-CCSD(fT) | Section 6.7.22 |
| EOM-CC(2,3) | Section 6.7.18 |
| ADC(0) | Section 6.8 |
| ADC(1) | Section 6.8 |
| ADC(2) | Section 6.8 |
| ADC(2)-X | Section 6.8 |
| ADC(3) | Section 6.8 |
| SOS-ADC(2) | Section 6.8 |
| SOS-ADC(2)-X | Section 6.8 |
| CVS-ADC(1) | Section 6.8 |
| CVS-ADC(2) | Section 6.8 |
| CVS-ADC(2)-X | Section 6.8 |
| CVS-ADC(3) | Section 6.8 |
| RAS-CI | Section 6.9 |
| RAS-CI-2 | Section 6.9 |

RECOMMENDATION:

Consult the literature for guidance.

## 6.2 Uncorrelated Wave Function Methods

Q-Chem includes several excited state methods which do not incorporate correlation: CIS, XCIS and RPA. These methods are sufficiently inexpensive that calculations on large molecules are possible, and are roughly comparable to the HF treatment of the ground state in terms of performance. They tend to yield qualitative rather than quantitative insight. Excitation energies tend to exhibit errors on the order of an electron volt, consistent with the neglect of electron correlation effects, which are generally different in the ground state and the excited state.

### 6.2.1 Single Excitation Configuration Interaction (CIS)

The derivation of the CI-singles[4,5] energy and wave function begins by selecting the HF single-determinant wave function as reference for the ground state of the system:

$$\Psi_{\mathrm{HF}} = \frac{1}{\sqrt{n!}} \det \{\chi_1 \chi_2 \cdots \chi_i \chi_j \cdots \chi_n\} \tag{6.1}$$

where $n$ is the number of electrons, and the spin orbitals

$$\chi_i = \sum_{\mu}^{N} c_{\mu i} \phi_\mu \tag{6.2}$$

are expanded in a finite basis of $N$ atomic orbital basis functions. Molecular orbital coefficients $\{c_{\mu i}\}$ are usually found by SCF procedures which solve the Hartree-Fock equations

$$\mathbf{FC} = \varepsilon \mathbf{SC} \;, \tag{6.3}$$

where **S** is the overlap matrix, **C** is the matrix of molecular orbital coefficients, $\varepsilon$ is a diagonal matrix of orbital eigenvalues and **F** is the Fock matrix with elements

$$F_{\mu \upsilon} = H_{\mu \upsilon} + \sum_{\lambda \sigma} \sum_{i} c_{\mu i} c_{\upsilon i} \left(\mu \lambda \mid\mid \upsilon \sigma\right) \tag{6.4}$$

involving the core Hamiltonian and the anti-symmetrized two-electron integrals

$$(\mu\mu || \lambda\sigma) = \int \int \phi_\mu(\mathbf{r}_1) \phi_\nu(\mathbf{r}_2) \left(\frac{1}{r_{12}}\right) \left[\phi_\lambda(\mathbf{r}_1)\phi_\sigma(\mathbf{r}_2) - \phi_\sigma(\mathbf{r}_1)\phi_\lambda(\mathbf{r}_2)\right] d\mathbf{r}_1 \, d\mathbf{r}_2 \tag{6.5}$$

On solving Eq. (6.3), the total energy of the ground state single determinant can be expressed as

$$E_{\mathrm{HF}} = \sum_{\mu \upsilon} P_{\mu \upsilon}^{\mathrm{HF}} H_{\mu \upsilon} + \frac{1}{2} \sum_{\mu \upsilon \lambda \sigma} P_{\mu \upsilon}^{\mathrm{HF}} P_{\lambda \sigma}^{\mathrm{HF}} \left(\mu \lambda \mid\mid \upsilon \sigma\right) + V_{\mathrm{nuc}} \tag{6.6}$$

where $P^{\mathrm{HF}}$ is the HF density matrix and $V_{\mathrm{nuc}}$ is the nuclear repulsion energy.

Equation (6.1) represents only one of many possible determinants made from orbitals of the system; there are in fact $n(N-n)$ possible singly substituted determinants constructed by replacing an orbital occupied in the ground state ($i$, $j$, $k, \ldots$) with an orbital unoccupied in the ground state ($a$, $b$, $c, \ldots$). Such wave functions and energies can be written

$$\Psi_i^a = \frac{1}{\sqrt{n!}} \det \{\chi_1 \chi_2 \cdots \chi_a \chi_j \cdots \chi_n\} \tag{6.7}$$

$$E_{ia} = E_{\mathrm{HF}} + \varepsilon_a - \varepsilon_i - (ia \mid\mid ia) \tag{6.8}$$

where we have introduced the anti-symmetrized two-electron integrals in the molecular orbital basis

$$(pq \mid\mid rs) = \sum_{\mu \upsilon \lambda \sigma} c_{\mu p} c_{\upsilon q} c_{\lambda r} c_{\sigma s} \left(\mu \lambda \mid\mid \upsilon \sigma\right) \tag{6.9}$$

These singly excited wave functions and energies could be considered crude approximations to the excited states of the system. However, determinants of the form Eq. (6.7) are deficient in that they:

- do not yield pure spin states
- resemble more closely ionization rather than excitation
- are not appropriate for excitation into degenerate states

These deficiencies can be partially overcome by representing the excited state wave function as a linear combination of *all* possible singly excited determinants,

$$\Psi_{\text{CIS}} = \sum_{ia} a_i^a \Psi_i^a \tag{6.10}$$

where the coefficients $\{a_{ia}\}$ can be obtained by diagonalizing the many-electron Hamiltonian, **A**, in the space of all single substitutions. The appropriate matrix elements are:

$$A_{ia,jb} = \langle \Psi_i^a | \, H \left| \Psi_j^b \right\rangle = (\varepsilon_a - \varepsilon_j)\delta_{ij}\delta_{ab} - (ja \, || \, ib) \tag{6.11}$$

According to Brillouin's, theorem single substitutions do not interact directly with a reference HF determinant, so the resulting eigenvectors from the CIS excited state represent a treatment roughly comparable to that of the HF ground state. The excitation energy is simply the difference between HF ground state energy and CIS excited state energies, and the eigenvectors of **A** correspond to the amplitudes of the single-electron promotions.

CIS calculations can be performed in Q-CHEM using restricted (RCIS)[4,5], unrestricted (UCIS), or restricted open shell (ROCIS)[6] spin orbitals.

### 6.2.2 Random Phase Approximation (RPA)

The Random Phase Approximation (RPA)[7,8], also known as time-dependent Hartree-Fock (TD-HF) theory, is an alternative to CIS for uncorrelated calculations of excited states. It offers some advantages for computing oscillator strengths, *e.g.*, exact satisfaction of the Thomas-Reike-Kuhn sum rule[9], and is roughly comparable in accuracy to CIS for singlet excitation energies, but is inferior for triplet states. RPA energies are non-variational, and in moving around on excited-state potential energy surfaces, this method can occasionally encounter singularities that prevent numerical solution of the underlying equations[10], whereas such singularities are mathematically impossible in CIS calculations.

### 6.2.3 Extended CIS (XCIS)

The motivation for the extended CIS procedure (XCIS)[11] stems from the fact that ROCIS and UCIS are less effective for radicals that CIS is for closed shell molecules. Using the attachment/detachment density analysis procedure[12], the failing of ROCIS and UCIS methodologies for the nitromethyl radical was traced to the neglect of a particular class of double substitution which involves the simultaneous promotion of an $\alpha$ spin electron from the singly occupied orbital and the promotion of a $\beta$ spin electron into the singly occupied orbital. The spin-adapted configurations

$$\left| \tilde{\Psi}_i^a(1) \right\rangle = \frac{1}{\sqrt{6}} \left( |\Psi_{\bar{i}}^{\bar{a}}\rangle - |\Psi_i^a\rangle \right) + \frac{2}{\sqrt{6}} |\Psi_{p\bar{i}}^{a\bar{p}}\rangle \tag{6.12}$$

are of crucial importance. (Here, $a, b, c, \ldots$ are virtual orbitals; $i, j, k, \ldots$ are occupied orbitals; and $p, q, r, \ldots$ are singly-occupied orbitals.) It is quite likely that similar excitations are also very significant in other radicals of interest.

The XCIS proposal, a more satisfactory generalization of CIS to open shell molecules, is to simultaneously include a restricted class of double substitutions similar to those in Eq. (6.12). To illustrate this, consider the resulting orbital spaces of an ROHF calculation: doubly occupied ($d$), singly occupied ($s$) and virtual ($v$). From this starting point we can distinguish three types of single excitations of the same multiplicity as the ground state: $d \rightarrow s$, $s \rightarrow v$ and $d \rightarrow v$. Thus, the spin-adapted ROCIS wave function is

$$|\Psi_{\text{ROCIS}}\rangle = \frac{1}{\sqrt{2}}\sum_{ia}^{dv} a_i^a \left(|\Psi_i^a\rangle + |\Psi_{\bar{i}}^{\bar{a}}\rangle\right) + \sum_{pa}^{sv} a_p^a|\Psi_p^a\rangle + \sum_{ip}^{ds} a_{\bar{i}}^{\bar{p}}|\Psi_{\bar{i}}^{\bar{p}}\rangle \tag{6.13}$$

The extension of CIS theory to incorporate higher excitations maintains the ROHF as the ground state reference and adds terms to the ROCIS wave function similar to that of Eq. (6.13), as well as those where the double excitation occurs through different orbitals in the $\alpha$ and $\beta$ space:

$$\begin{aligned} |\Psi_{\text{XCIS}}\rangle = \tfrac{1}{\sqrt{2}}\sum_{ia}^{dv} a_i^a \left(|\Psi_i^a\rangle + |\Psi_{\bar{i}}^{\bar{a}}\rangle\right) + \sum_{pa}^{sv} a_p^a|\Psi_p^a\rangle + \sum_{ip}^{ds} a_{\bar{i}}^{\bar{p}}|\Psi_{\bar{i}}^{\bar{p}}\rangle \\ + \sum_{iap}^{dvs} \tilde{a}_i^a(p)|\tilde{\Psi}_i^a(p)\rangle + \sum_{ia,p\neq q}^{dv,ss} a_{p\bar{i}}^{a\bar{q}}|\Psi_{p\bar{i}}^{a\bar{q}}\rangle \end{aligned} \tag{6.14}$$

XCIS is defined only from a restricted open shell Hartree-Fock ground state reference, as it would be difficult to uniquely define singly occupied orbitals in a UHF wave function. In addition, $\beta$ unoccupied orbitals, through which the spin-flip double excitation proceeds, may not match the half-occupied $\alpha$ orbitals in either character or even symmetry.

For molecules with closed shell ground states, both the HF ground and CIS excited states emerge from diagonalization of the Hamiltonian in the space of the HF reference and singly excited substituted configuration state functions. The XCIS case is different because the restricted class of double excitations included could mix with the ground state and lower its energy. This mixing is avoided to maintain the size consistency of the ground state energy.

With the inclusion of the restricted set of doubles excitations in the excited states, but not in the ground state, it could be expected that some fraction of the correlation energy be recovered, resulting in anomalously low excited state energies. However, the fraction of the total number of doubles excitations included in the XCIS wave function is very small and those introduced cannot account for the pair correlation of any pair of electrons. Thus, the XCIS procedure can be considered one that neglects electron correlation.

The computational cost of XCIS is approximately four times greater than CIS and ROCIS, and its accuracy for open shell molecules is generally comparable to that of the CIS method for closed shell molecules. In general, it achieves qualitative agreement with experiment. XCIS is available for doublet and quartet excited states beginning from a doublet ROHF treatment of the ground state, for excitation energies only.

### 6.2.4 Spin-Flip Extended CIS (SF-XCIS)

Spin-flip extended CIS (SF-XCIS)[13] is a spin-complete extension of the spin-flip single excitation configuration interaction (SF-CIS) method[14]. The method includes all configurations in which no more than one virtual level of the high spin triplet reference becomes occupied and no more than one doubly occupied level becomes vacant.

SF-XCIS is defined only from a restricted open shell Hartree-Fock triplet ground state reference. The final SF-XCIS wave functions correspond to spin-pure $M_S = 0$ (singlet or triplet) states. The fully balanced treatment of the half-occupied reference orbitals makes it very suitable for applications with two strongly correlated electrons, such as single bond dissociation, systems with important diradical character or the study of excited states with significant double excitation character.

The computational cost of SF-XCIS scales in the same way with molecule size as CIS itself, with a prefactor 13 times larger.

### 6.2.5 Spin-Adapted Spin-Flip CIS

Spin-Adapted Spin-Flip CIS (SA-SF-CIS)[15] is a spin-complete extension of the spin-flip single excitation configuration interaction (SF-CIS) method.[14] Unlike SF-XCIS, SA-SF-CIS only includes the minimal set of necessary electronic configurations to remove the spin contamination in the conventional SF-CIS method. The target SA-SF-CIS states have spin eigenvalues one less than the reference ROHF state. Based on a tensor equation-of-motion formalism,[15] the dimension of the CI vectors in SA-SF-CIS remains exactly the same as that in conventional SF-CIS. Currently, the DFT correction to SA-SF-CIS is added in an *ad-hoc* way.[15]

### 6.2.6 CIS Analytical Derivatives

While CIS excitation energies are relatively inaccurate, with errors of the order of 1 eV, CIS excited state properties, such as structures and frequencies, are much more useful. This is very similar to the manner in which ground state Hartree-Fock (HF) structures and frequencies are much more accurate than HF relative energies. Generally speaking, for low-lying excited states, it is expected that CIS vibrational frequencies will be systematically 10% higher or so relative to experiment[16–18]. If the excited states are of pure valence character, then basis set requirements are generally similar to the ground state. Excited states with partial Rydberg character require the addition of one or preferably two sets of diffuse functions.

Q-CHEM includes efficient analytical first and second derivatives of the CIS energy[19,20], to yield analytical gradients, excited state vibrational frequencies, force constants, polarizabilities, and infrared intensities. Analytical gradients can be evaluated for any job where the CIS excitation energy calculation itself is feasible, so that efficient excited-state geometry optimizations and vibrational frequency calculations are possible at the CIS level. In such cases, it is necessary to specify on which Born-Oppenheimer potential energy surface the optimization should proceed, and care must be taken to ensure that the optimization remains on the excited state of interest, as state crossings may occur. (A "state-tracking" algorithm, as discussed in Section 9.6.5, can aid with this.)

Sometimes it is precisely the crossings between Born-Oppenheimer potential energy surfaces (*i.e.*, conical intersections) that are of interest, as these intersections provide pathways for non-adiabatic transitions between electronic states[21,22]. A feature of Q-CHEM that is not otherwise widely available in an analytic implementation[23–26] (for both CIS and TDDFT) of the non-adiabatic couplings that define the topology around conical intersections. Due to the analytic implementation, these couplings can be evaluated at a cost that is not significantly greater than the cost of a CIS or TDDFT analytic gradient calculation, and the availability of these couplings allows for much more efficient optimization of minimum-energy crossing points along seams of conical intersection, as compared to when only analytic gradients are available[24]. These features, including a brief overview of the theory of conical intersections, can be found in Section 9.6.1.

For CIS vibrational frequencies, a semi-direct algorithm similar to that used for ground-state Hartree-Fock frequencies is available, whose computer time scales as approximately $\mathcal{O}(N^3)$ for large molecules[11]. The main complication associated with analytical CIS frequency calculations is ensuring that Q-CHEM has sufficient memory to perform the calculations. Default settings are adequate for many purposes but if a large calculation fails due to a memory limitation, then the following additional information may be useful.

The memory requirements for CIS (and HF) analytic frequencies primarily come from dynamic memory, defined as

$$\text{dynamic memory} = \text{MEM\_TOTAL} - \text{MEM\_STATIC} \quad .$$

This quantity must be large enough to contain several arrays whose size is $3N_{\rm atoms}N_{\rm basis}^2$. Meanwhile the value of the *$rem* variable MEM_STATIC, which obviously reduces the available dynamic memory, must be sufficiently large to permit integral evaluation, else the job may fail. For most purposes, setting MEM_STATIC to about 80 Mb is sufficient, and by default MEM_TOTAL is set to a larger value that what is available on most computers, so that the user need not guess or experiment about an appropriate value of MEM_TOTAL for low-memory jobs. However, a memory allocation error will occur if the calculation demands more memory than available.

**Note:** Unlike Q-CHEM's MP2 frequency code, the analytic CIS second derivative code currently does not support frozen core or virtual orbitals. These approximations do not lead to large savings at the CIS level, as all computationally-expensive steps are performed in the atomic orbital basis.

### 6.2.7 Non-Orthogonal Configuration Interaction

Systems such as transition metals, open-shell species, and molecules with highly-stretched bonds often exhibit multiple, near-degenerate solutions to the SCF equations. Multiple solutions can be located using SCF meta-dynamics (Section 4.12.2), but given the approximate nature of the SCF calculation in the first place, there is in such cases no clear reason to choose one of these solutions over another. These SCF solutions are not subject to any non-crossing rule, and often do cross (*i.e.*, switch energetic order) as the geometry is changed, so the lowest energy state may switch abruptly with consequent discontinuities in the energy gradients. It is therefore desirable to have a method that treats all of these near-degenerate SCF solutions on an equal footing an might yield a smoother, qualitatively correct potential energy surface. This can be achieved by using multiple SCF solutions (obtained, *e.g.*, via SCF meta-dynamics) as a basis for a configuration interaction (CI) calculation. Since the various SCF solutions are not orthogonal to one another—meaning that one solution cannot be constructed as a single determinant composed of orbitals from another solution—this CI is a bit more complicated and is denoted as a non-orthogonal CI (NOCI)[27].

NOCI can be viewed as an alternative to CASSCF within an "active space" consisting of the SCF states of interest, and has the advantage that the SCF states, and thus the NOCI wave functions, are size-consistent. In common with CASSCF, it is able to describe complicated phenomena such as avoided crossings (where states mix instead of passing through each other) as well as conical intersections (whereby via symmetry or else accidental reasons, there is no coupling between the states, and they pass cleanly through each other at a degeneracy).

Another use for a NOCI calculation is that of symmetry restoration. At some geometries, the SCF states break spatial or spin symmetry to achieve a lower energy single determinant than if these symmetries were conserved. As these symmetries still exist within the proper electron Hamiltonian, its exact eigenfunctions should preserve them. In the case of spin this manifests as spin contamination and for spatial symmetries it usually manifests as artefactual localization. To recover a (yet lower energy) wave function retaining the correct symmetries, one can include these broken-symmetry states (with all relevant symmetry permutations) in a NOCI calculation; the resultant eigenfunction will have the true symmetries restored, as a linear combination of the broken-symmetry states.

A common example occurs in the case of a spin-contaminated UHF reference state. Performing a NOCI calculation in a basis consisting of this state, plus a second state in which all $\alpha$ and $\beta$ orbitals have been switched, often reduces spin contamination in the same way as the half-projected Hartree-Fock method[28], although there is no guarantee that the resulting wave function is an eigenfunction of $\hat{S}^2$. Another example consists in using a UHF wave function with $M_S = 0$ along with its spin-exchanged version (wherein all $\alpha \leftrightarrow \beta$ orbitals are switched), which two new NOCI eigenfunctions, one with even $S$ (a mixture of $S = 0, 2, \ldots$), and one with odd $S$ (mixing $S = 1, 3, \ldots$). These may be used to approximate singlet and triplet wave functions.

NOCI can be enabled by specifying CORRELATION_NOCI, and will automatically use all of the states located with SCF meta-dynamics. Two spin-exchanged versions of a UHF wave function can be requested simply by *not* turning on meta-dynamics. For more customization, a *$noci* input section can be included having, *e.g.*, the following format:

```
$noci
   1 2 -2 4
   2
$end
```

In this particular case, the first line specifies that states 1, 2, and 4 are to be included in the NOCI calculation, along with state "$-2$", which indicates the spin-exchanged version of state 2. The second (optional) line indicates which eigenvalue is to be returned to Q-CHEM, with the convention that 0 indicates the lowest state so the *$noci* input section above is requesting the third state.

Analytic gradients are not available for NOCI but geometry optimizations can be performed automatically using finite-difference gradients.

**NOCI_PRINT**
Specify the debug print level of NOCI.
TYPE:
INTEGER
DEFAULT:
1
OPTIONS:
$n$ Positive integer
RECOMMENDATION:
Increase this for additional debug information.

### 6.2.8 Basic CIS Job Control Options

CIS-type jobs are requested by setting the *$rem* variable EXCHANGE = HF and CORRELATION = NONE, as in a ground-state Hartree-Fock calculation, but then also specifying a number of excited-state roots using the *$rem* keyword CIS_N_ROOTS.

**Note:** For RHF case, $n$ singlets and $n$ triplets will be computed, unless specified otherwise by using CIS_TRIPLETS and CIS_SINGLETS.

**CIS_N_ROOTS**

Sets the number of CI-Singles (CIS) excited state roots to find.

TYPE:

INTEGER

DEFAULT:

0 Do not look for any excited states.

OPTIONS:

$n$ $n > 0$ Looks for $n$ CIS excited states.

RECOMMENDATION:

None

**CIS_SINGLETS**

Solve for singlet excited states in RCIS calculations (ignored for UCIS).

TYPE:

LOGICAL

DEFAULT:

TRUE

OPTIONS:

TRUE Solve for singlet states.

FALSE Do not solve for singlet states.

RECOMMENDATION:

None

**CIS_TRIPLETS**

Solve for triplet excited states in RCIS calculations (ignored for UCIS).

TYPE:

LOGICAL

DEFAULT:

TRUE

OPTIONS:

TRUE Solve for triplet states.

FALSE Do not solve for triplet states.

RECOMMENDATION:

None

**RPA**

Do an RPA calculation in addition to a CIS or TDDFT/TDA calculation.

TYPE:

LOGICAL/INTEGER

DEFAULT:

FALSE

OPTIONS:

FALSE Do not do an RPA calculation.

TRUE Do an RPA calculation.

2 Do an RPA calculation without running CIS or TDDFT/TDA first.

RECOMMENDATION:

None

**CIS_STATE_DERIV**

Sets CIS state for excited state optimizations and vibrational analysis.

TYPE:

INTEGER

DEFAULT:

0 Does not select any of the excited states.

OPTIONS:

$n$ Select the $n$th state.

RECOMMENDATION:

Check to see that the states do not change order during an optimization, due to state crossings.

**SPIN_FLIP**

Selects whether to perform a standard excited state calculation, or a spin-flip calculation. Spin multiplicity should be set to 3 for systems with an even number of electrons, and 4 for systems with an odd number of electrons.

TYPE:

LOGICAL

DEFAULT:

FALSE

OPTIONS:

TRUE/FALSE

RECOMMENDATION:

None

**SPIN_FLIP_XCIS**

Do a SF-XCIS calculation.

TYPE:

LOGICAL

DEFAULT:

FALSE

OPTIONS:

FALSE Do not do an SF-XCIS calculation.

TRUE Do an SF-XCIS calculation (requires ROHF triplet ground state).

RECOMMENDATION:

None

**SFX_AMP_OCC_A**

Defines a customer amplitude guess vector in SF-XCIS method.

TYPE:

INTEGER

DEFAULT:

0

OPTIONS:

$n$ builds a guess amplitude with an $\alpha$-hole in the $n$th orbital (requires SFX_AMP_VIR_B).

RECOMMENDATION:

Only use when default guess is not satisfactory.

**SFX_AMP_VIR_B**

Defines a user-specified amplitude guess vector in SF-XCIS method.

TYPE:

INTEGER

DEFAULT:

0

OPTIONS:

$n$ builds a guess amplitude with a $\beta$-particle in the $n$th orbital (requires SFX_AMP_OCC_A).

RECOMMENDATION:

Only use when default guess is not satisfactory.

**XCIS**

Do an XCIS calculation in addition to a CIS calculation.

TYPE:

LOGICAL

DEFAULT:

FALSE

OPTIONS:

FALSE Do not do an XCIS calculation.

TRUE Do an XCIS calculation (requires ROHF ground state).

RECOMMENDATION:

None

**SASF_RPA**

Do an SA-SF-CIS/DFT calculation.

TYPE:

LOGICAL

DEFAULT:

FALSE

OPTIONS:

FALSE Do not do an SA-SF-CIS/DFT calculation.

TRUE Do an SA-SF-CIS/DFT calculation (requires ROHF ground state).

RECOMMENDATION:

None

### 6.2.9 CIS Job Customization

**N_FROZEN_CORE**

Controls the number of frozen core orbitals.

TYPE:

INTEGER/STRING

DEFAULT:

0 No frozen core orbitals.

OPTIONS:

FC Frozen core approximation.

$n$ Freeze $n$ core orbitals.

RECOMMENDATION:

There is no computational advantage to using frozen core for CIS, and analytical derivatives are only available when no orbitals are frozen. It is helpful when calculating CIS(D) corrections (see Sec. 6.6).

**N_FROZEN_VIRTUAL**

Controls the number of frozen virtual orbitals.

TYPE:

INTEGER

DEFAULT:

0 No frozen virtual orbitals.

OPTIONS:

$n$ Freeze $n$ virtual orbitals.

RECOMMENDATION:

There is no computational advantage to using frozen virtuals for CIS, and analytical derivatives are only available when no orbitals are frozen.

**MAX_CIS_CYCLES**

Maximum number of CIS iterative cycles allowed.

TYPE:

INTEGER

DEFAULT:

30

OPTIONS:

$n$ User-defined number of cycles.

RECOMMENDATION:

Default is usually sufficient.

**MAX_CIS_SUBSPACE**

Maximum number of subspace vectors allowed in the CIS iterations

TYPE:

INTEGER

DEFAULT:

As many as required to converge all roots

OPTIONS:

$n$ User-defined number of subspace vectors

RECOMMENDATION:

The default is usually appropriate, unless a large number of states are requested for a large molecule. The total memory required to store the subspace vectors is bounded above by $2nOV$, where $O$ and $V$ represent the number of occupied and virtual orbitals, respectively. $n$ can be reduced to save memory, at the cost of a larger number of CIS iterations. Convergence may be impaired if $n$ is not much larger than CIS_N_ROOTS.

**CIS_CONVERGENCE**

CIS is considered converged when error is less than $10^{-\mathrm{CIS\_CONVERGENCE}}$

TYPE:

INTEGER

DEFAULT:

6 CIS convergence threshold $10^{-6}$

OPTIONS:

$n$ Corresponding to $10^{-n}$

RECOMMENDATION:

None

**CIS_DYNAMIC_MEM**

Controls whether to use static or dynamic memory in CIS and TDDFT calculations.

TYPE:

LOGICAL

DEFAULT:

FALSE

OPTIONS:

FALSE Partly use static memory

TRUE Fully use dynamic memory

RECOMMENDATION:

The default control requires static memory (MEM_STATIC) to hold a temporary array whose minimum size is $OV \times$ CIS_N_ROOTS. For a large calculation, one has to specify a large value for MEM_STATIC, which is not recommended (see Chapter 2). Therefore, it is recommended to use dynamic memory for large calculations.

**CIS_RELAXED_DENSITY**

Use the relaxed CIS density for attachment/detachment density analysis.

TYPE:

LOGICAL

DEFAULT:

FALSE

OPTIONS:

| | |
|---|---|
| FALSE | Do not use the relaxed CIS density in analysis. |
| TRUE | Use the relaxed CIS density in analysis. |

RECOMMENDATION:

None

**CIS_GUESS_DISK**

Read the CIS guess from disk (previous calculation).

TYPE:

LOGICAL

DEFAULT:

FALSE

OPTIONS:

| | |
|---|---|
| FALSE | Create a new guess. |
| TRUE | Read the guess from disk. |

RECOMMENDATION:

Requires a guess from previous calculation.

**CIS_GUESS_DISK_TYPE**

Determines the type of guesses to be read from disk

TYPE:

INTEGER

DEFAULT:

Nil

OPTIONS:

| | |
|---|---|
| 0 | Read triplets only |
| 1 | Read triplets and singlets |
| 2 | Read singlets only |

RECOMMENDATION:

Must be specified if CIS_GUESS_DISK is TRUE.

**STS_MOM**

Control calculation of the transition moments between excited states in the CIS and TDDFT calculations (including SF-CIS and SF-DFT).

TYPE:

LOGICAL

DEFAULT:

FALSE

OPTIONS:

FALSE Do not calculate state-to-state transition moments.

TRUE Do calculate state-to-state transition moments.

RECOMMENDATION:

When set to true requests the state-to-state dipole transition moments for all pairs of excited states and for each excited state with the ground state.

**Note:** This option is not available for SF-XCIS.

**CIS_MOMENTS**

Controls calculation of excited-state (CIS or TDDFT) multipole moments.

TYPE:

LOGICAL

DEFAULT:

FALSE

OPTIONS:

FALSE Do not calculate excited-state moments.

TRUE Calculate moments for each excited state.

RECOMMENDATION:

Set to TRUE if excited-state moments are desired. (This is a trivial additional calculation.) The MULTIPOLE_ORDER controls how many multipole moments are printed.

### 6.2.10 Examples

**Example 6.1** A basic CIS excitation energy calculation on formaldehyde at the HF/6-31G* optimized ground state geometry, which is obtained in the first part of the job. Above the first singlet excited state, the states have Rydberg character, and therefore a basis with two sets of diffuse functions is used.

```
$molecule
   0  1
   C
   O  1  CO
   H  1  CH  2  A
   H  1  CH  2  A  3  D

   CO =   1.2
   CH =   1.0
   A  = 120.0
   D  = 180.0
$end

$rem
```

```
   JOBTYPE   =  opt
   EXCHANGE  =  hf
   BASIS     =  6-31G*
$end

@@@

$molecule
   read
$end

$rem
   EXCHANGE      =  hf
   BASIS         =  6-311(2+)G*
   CIS_N_ROOTS   =  15           Do 15 states
   CIS_SINGLETS  =  true         Do do singlets
   CIS_TRIPLETS  =  false        Don’t do Triplets
$end
```

**Example 6.2** An XCIS calculation of excited states of an unsaturated radical, the phenyl radical, for which double substitutions make considerable contributions to low-lying excited states.

```
$comment
   C6H5 phenyl radical C2v symmetry MP2(full)/6-31G* = -230.7777459
$end

$molecule
   0  2
   c1
   x1  c1  1.0
   c2  c1  rc2  x1  90.0
   x2  c2  1.0  c1  90.0  x1    0.0
   c3  c1  rc3  x1  90.0  c2    tc3
   c4  c1  rc3  x1  90.0  c2   -tc3
   c5  c3  rc5  c1   ac5  x1  -90.0
   c6  c4  rc5  c1   ac5  x1   90.0
   h1  c2  rh1  x2  90.0  c1  180.0
   h2  c3  rh2  c1   ah2  x1   90.0
   h3  c4  rh2  c1   ah2  x1  -90.0
   h4  c5  rh4  c3   ah4  c1  180.0
   h5  c6  rh4  c4   ah4  c1  180.0

   rh1  =    1.08574
   rh2  =    1.08534
   rc2  =    2.67299
   rc3  =    1.35450
   rh4  =    1.08722
   rc5  =    1.37290
   tc3  =   62.85
   ah2  =  122.16
   ah4  =  119.52
   ac5  =  116.45
$end

$rem
   BASIS             =  6-31+G*
   EXCHANGE          =  hf
   MEM_STATIC        =  80
   INTSBUFFERSIZE    =  15000000
   SCF_CONVERGENCE   =  8
   CIS_N_ROOTS       =  5
   XCIS              =  true
$end
```

**Example 6.3** A SF-XCIS calculation of ground and excited states of trimethylenemethane (TMM) diradical, for which double substitutions make considerable contributions to low-lying excited states.

```
$molecule
   0 3
   C
   C  1  CC1
   C  1  CC2    2  A2
   C  1  CC2    2  A2     3  180.0
   H  2  C2H    1  C2CH   3  0.0
   H  2  C2H    1  C2CH   4  0.0
   H  3  C3Hu   1  C3CHu  2  0.0
   H  3  C3Hd   1  C3CHd  4  0.0
   H  4  C3Hu   1  C3CHu  2  0.0
   H  4  C3Hd   1  C3CHd  3  0.0

   CC1     = 1.35
   CC2     = 1.47
   C2H     = 1.083
   C3Hu    = 1.08
   C3Hd    = 1.08
   C2CH    = 121.2
   C3CHu   = 120.3
   C3CHd   = 121.3
   A2      = 121.0
$end

$rem
  UNRESTRICTED     = false   SF-XCIS runs from ROHF triplet reference
  EXCHANGE         = HF
  BASIS            = 6-31G*
  SCF_CONVERGENCE  = 10
  SCF_ALGORITHM    = DM
  MAX_SCF_CYCLES   = 100
  SPIN_FLIP_XCIS   = true    Do SF-XCIS
  CIS_N_ROOTS      = 3
  CIS_SINGLETS     = true    Do singlets
  CIS_TRIPLETS     = true    Do triplets
$end
```

**Example 6.4** An SA-SF-DFT calculation of singlet ground and excited states of ethylene.

```
$molecule
0 3
 C
 C                  1             B1
 H                  1             B2    2             A1
 H                  1             B3    2             A2    3             D1
 H                  2             B4    1             A3    3             D2
 H                  2             B5    1             A4    3             D3
```

```
   B1            1.32808942
   B2            1.08687297
   B3            1.08687297
   B4            1.08687297
   B5            1.08687297
   A1          121.62604150
   A2          121.62604150
   A3          121.62604150
   A4          121.62604150
   D1          180.00000000
   D2            0.00000000
   D3          180.00000000
$end

$rem
unrestricted 0
jobtype sp
basis   cc-pvtz
basis2 sto-3g
exchange bhhlyp
cis_n_roots 5
sasf_rpa 1
cis_triplets false
$end
```

**Example 6.5** This example illustrates a CIS geometry optimization followed by a vibrational frequency analysis on the lowest singlet excited state of formaldehyde. This $n \to \pi^*$ excited state is non-planar, unlike the ground state. The optimization converges to a non-planar structure with zero forces, and all frequencies real.

```
$molecule
   0 1
   C
   O  1  CO
   H  1  CH  2  A
   H  1  CH  2  A  3  D

   CO  =    1.2
   CH  =    1.0
   A   =  120.0
   D   =  150.0
$end

$rem
   JOBTYPE          =  opt
   EXCHANGE         =  hf
   BASIS            =  6-31+G*
   CIS_STATE_DERIV  =  1         Optimize state 1
   CIS_N_ROOTS      =  3         Do 3 states
   CIS_SINGLETS     =  true      Do do singlets
   CIS_TRIPLETS     =  false     Don't do Triplets
$end

@@@

$molecule
```

```
  read
$end

$rem
   JOBTYPE          =  freq
   EXCHANGE         =  hf
   BASIS            =  6-31+G*
   CIS_STATE_DERIV  =  1         Focus on state 1
   CIS_N_ROOTS      =  3         Do 3 states
   CIS_SINGLETS     =  true      Do do singlets
   CIS_TRIPLETS     =  false     Don't do Triplets
$end
```

# 6.3 Time-Dependent Density Functional Theory (TDDFT)

## 6.3.1 Brief Introduction to TDDFT

Excited states may be obtained from density functional theory by time-dependent density functional theory[29,30], which calculates poles in the response of the ground state density to a time-varying applied electric field. These poles are Bohr frequencies, or in other words the excitation energies. Operationally, this involves solution of an eigenvalue equation

$$\begin{pmatrix} \mathbf{A} & \mathbf{B} \\ \mathbf{B}^\dagger & \mathbf{A}^\dagger \end{pmatrix} \begin{pmatrix} \mathbf{x} \\ \mathbf{y} \end{pmatrix} = \omega \begin{pmatrix} -\mathbf{1} & \mathbf{0} \\ \mathbf{0} & \mathbf{1} \end{pmatrix} \begin{pmatrix} \mathbf{x} \\ \mathbf{y} \end{pmatrix} \tag{6.15}$$

where the elements of the matrix $\mathbf{A}$ similar to those used at the CIS level (Eq. (6.11)), but with an exchange-correlation correction[31]. Elements of $\mathbf{B}$ are similar. Equation (6.15) is solved iteratively for the lowest few excitation energies, $\omega$. Alternatively, one can make a CIS-like Tamm-Dancoff approximation (TDA)[32], in which the "de-excitation" amplitudes $\mathbf{Y}$ are neglected, the $\mathbf{B}$ matrix is not required, and Eq. (6.15) reduces to $\mathbf{Ax} = \omega\mathbf{x}$.

TDDFT is popular because its computational cost is roughly similar to that of the simple CIS method, but a description of differential electron correlation effects is implicit in the method. It is advisable to only employ TDDFT for low-lying valence excited states that are below the first ionization potential of the molecule[29], or more conservatively, below the first Rydberg state, and in such cases the valence excitation energies are often remarkably improved relative to CIS, with an accuracy of $\sim$0.3 eV for many functionals[33]. The calculation of the nuclear gradients of full TDDFT and within the TDA is implemented[34].

On the other hand, standard density functionals do not yield a potential with the correct long-range Coulomb tail, owing to the so-called self-interaction problem, and therefore excitation energies corresponding to states that sample this tail (*e.g.*, diffuse Rydberg states and some charge transfer excited states) are not given accurately[35–37]. The extent to which a particular excited state is characterized by charge transfer can be assessed using an a spatial overlap metric proposed by Peach, Benfield, Helgaker, and Tozer (PBHT)[38]. (However, see Ref. 39 for a cautionary note regarding this metric.)

Standard TDDFT also does not yield a good description of static correlation effects (see Section 5.10), because it is based on a single reference configuration of Kohn-Sham orbitals. Recently, a new variation of TDDFT called spin-flip (SF) DFT was developed by Yihan Shao, Martin Head-Gordon and Anna Krylov to address this issue[40]. SF-DFT is different from standard TDDFT in two ways:

- The reference is a high-spin triplet (quartet) for a system with an even (odd) number of electrons;

- One electron is spin-flipped from an alpha Kohn-Sham orbital to a beta orbital during the excitation.

SF-DFT can describe the ground state as well as a few low-lying excited states, and has been applied to bond-breaking processes, and di- and tri-radicals with degenerate or near-degenerate frontier orbitals. Recently, we also implemented[41] a SF-DFT method with a non-collinear exchange-correlation potential from Tom Ziegler *et al.*[42,43], which is in many case an improvement over collinear SF-DFT[40]. Recommended functionals for SF-DFT calculations are 5050 and PBE50 (see Ref. 41 for extensive benchmarks). See also Section 6.7.3 for details on wave function-based spin-flip models.

### 6.3.2 TDDFT within a Reduced Single-Excitation Space

Much of chemistry and biology occurs in solution or on surfaces. The molecular environment can have a large effect on electronic structure and may change chemical behavior. Q-CHEM is able to compute excited states within a local region of a system through performing the TDDFT (or CIS) calculation with a reduced single excitation subspace[44], in which some of the amplitudes $\mathbf{x}$ in Eq. (6.15) are excluded. (This is implemented within the TDA, so $\mathbf{y} \equiv \mathbf{0}$.) This allows the excited states of a solute molecule to be studied with a large number of solvent molecules reducing the rapid rise in computational cost. The success of this approach relies on there being only weak mixing between the electronic excitations of interest and those omitted from the single excitation space. For systems in which there are strong hydrogen bonds between solute and solvent, it is advisable to include excitations associated with the neighboring solvent molecule(s) within the reduced excitation space.

The reduced single excitation space is constructed from excitations between a subset of occupied and virtual orbitals. These can be selected from an analysis based on Mulliken populations and molecular orbital coefficients. For this approach the atoms that constitute the solvent needs to be defined. Alternatively, the orbitals can be defined directly. The atoms or orbitals are specified within a *$solute* block. These approach is implemented within the TDA and has been used to study the excited states of formamide in solution[45], CO on the Pt(111) surface[46], and the tryptophan chromophore within proteins[47].

### 6.3.3 Job Control for TDDFT

Input for time-dependent density functional theory calculations follows very closely the input already described for the uncorrelated excited state methods described in the previous section (in particular, see Section 6.2.8). There are several points to be aware of:

- The exchange and correlation functionals are specified exactly as for a ground state DFT calculation, through EXCHANGE and CORRELATION.
- If RPA is set to TRUE, a “full” TDDFT calculation will be performed, however the default value is RPA = FALSE, which invokes the TDA[32], in which the de-excitation amplitudes $\mathbf{Y}$ in Eq. (6.15) are neglected, which is usually a good approximation for excitation energies, although oscillator strengths within the TDA no longer formally satisfy the Thomas-Reiche-Kuhn sum rule[29]. For RPA = TRUE, a TDA calculation is performed first and used as the initial guess for the full TDDFT calculation. The TDA calculation can be skipped altogether using RPA = 2
- If SPIN_FLIP is set to TRUE when performing a TDDFT calculation, a SF-DFT calculation will also be performed. At present, SF-DFT is only implemented within TDDFT/TDA so RPA must be set to FALSE. Remember to set the spin multiplicity to 3 for systems with an even-number of electrons (*e.g.*, diradicals), and 4 for odd-number electron systems (*e.g.*, triradicals).

**TRNSS**

Controls whether reduced single excitation space is used.

TYPE:

LOGICAL

DEFAULT:

FALSE Use full excitation space.

OPTIONS:

TRUE Use reduced excitation space.

RECOMMENDATION:

None

**TRTYPE**

Controls how reduced subspace is specified.

TYPE:

INTEGER

DEFAULT:

1

OPTIONS:

1 Select orbitals localized on a set of atoms.

2 Specify a set of orbitals.

3 Specify a set of occupied orbitals, include excitations to all virtual orbitals.

RECOMMENDATION:

None

**N_SOL**

Specifies number of atoms or orbitals in the *$solute* section.

TYPE:

INTEGER

DEFAULT:

No default.

OPTIONS:

User defined.

RECOMMENDATION:

None

**CISTR_PRINT**

Controls level of output.

TYPE:

LOGICAL

DEFAULT:

FALSE Minimal output.

OPTIONS:

TRUE Increase output level.

RECOMMENDATION:

None

**CUTOCC**

Specifies occupied orbital cutoff.

TYPE:

INTEGER

DEFAULT:

50

OPTIONS:

0-200 CUTOFF = CUTOCC/100

RECOMMENDATION:

None

**CUTVIR**

Specifies virtual orbital cutoff.

TYPE:

INTEGER

DEFAULT:

0 No truncation

OPTIONS:

0-100 CUTOFF = CUTVIR/100

RECOMMENDATION:

None

**PBHT_ANALYSIS**

Controls whether overlap analysis of electronic excitations is performed.

TYPE:

LOGICAL

DEFAULT:

FALSE

OPTIONS:

FALSE Do not perform overlap analysis.

TRUE Perform overlap analysis.

RECOMMENDATION:

None

**PBHT_FINE**

Increases accuracy of overlap analysis.

TYPE:

LOGICAL

DEFAULT:

FALSE

OPTIONS:

FALSE

TRUE Increase accuracy of overlap analysis.

RECOMMENDATION:

None

**SRC_DFT**

Selects form of the short-range corrected functional.

TYPE:

INTEGER

DEFAULT:

No default

OPTIONS:

1 SRC1 functional.

2 SRC2 functional.

RECOMMENDATION:

None

**OMEGA**

Sets the Coulomb attenuation parameter for the short-range component.

TYPE:

INTEGER

DEFAULT:

No default

OPTIONS:

$n$ Corresponding to $\omega = n/1000$, in units of bohr$^{-1}$

RECOMMENDATION:

None

**OMEGA2**

Sets the Coulomb attenuation parameter for the long-range component.

TYPE:

INTEGER

DEFAULT:

No default

OPTIONS:

$n$ Corresponding to $\omega 2 = n/1000$, in units of bohr$^{-1}$

RECOMMENDATION:

None

**HF_SR**

Sets the fraction of Hartree-Fock exchange at $r_{12} = 0$.

TYPE:

INTEGER

DEFAULT:

No default

OPTIONS:

$n$ Corresponding to HF_SR = $n/1000$

RECOMMENDATION:

None

**HF_LR**

Sets the fraction of Hartree-Fock exchange at $r_{12} = \infty$.

TYPE:

INTEGER

DEFAULT:

No default

OPTIONS:

$n$ Corresponding to HF_LR = $n/1000$

RECOMMENDATION:

None

**WANG_ZIEGLER_KERNEL**

Controls whether to use the Wang-Ziegler non-collinear exchange-correlation kernel in a SF-DFT calculation.

TYPE:

LOGICAL

DEFAULT:

FALSE

OPTIONS:

FALSE Do not use non-collinear kernel.

TRUE Use non-collinear kernel.

RECOMMENDATION:

None

### 6.3.4 TDDFT Coupled with C-PCM for Excitation Energies and Properties Calculations

As described in Section 11.2 (and especially Section 11.2.2), continuum solvent models such as C-PCM allow one to include solvent effect in the calculations. TDDFT/C-PCM allows excited-state modeling in solution. Q-CHEM also features TDDFT coupled with C-PCM which extends TDDFT to calculations of properties of electronically-excited molecules in solution. In particular, TDDFT/C-PCM allows one to perform geometry optimization and vibrational analysis[48].

When TDDFT/C-PCM is applied to calculate vertical excitation energies, the solvent around vertically excited solute is out of equilibrium. While the solvent electron density equilibrates fast to the density of the solute (electronic response), the relaxation of nuclear degrees of freedom (*e.g.*, orientational polarization) takes place on a slower timescale. To describe this situation, an optical dielectric constant is employed. To distinguish between equilibrium and non-equilibrium calculations, two dielectric constants are used in these calculations: a static constant ($\varepsilon_0$), equal to the equilibrium bulk value, and a fast constant ($\varepsilon_{fast}$) related to the response of the medium to high frequency perturbations. For vertical excitation energy calculations (corresponding to the unrelaxed solvent nuclear degrees of freedom), it is recommended to use the optical dielectric constant for $\varepsilon_{fast}$), whereas for the geometry optimization and vibrational frequency calculations, the static dielectric constant should be used[48].

The example below illustrates TDDFT/C-PCM calculations of vertical excitation energies. More information concerning the C-PCM and the various PCM job control options can be found in Section 11.2.

**Example 6.6** TDDFT/C-PCM low-lying vertical excitation energy

```
$molecule
   0 1
   C    0.0   0.0   0.0
   O    0.0   0.0   1.21
$end

$rem
   EXCHANGE         B3lyp
   CIS_N_ROOTS      10
   CIS_SINGLETS     true
   CIS_TRIPLETS     true
   RPA              TRUE
   BASIS            6-31+G*
   XC_GRID          1
   SOLVENT_METHOD   pcm
$end

$pcm
   Theory   CPCM
   Method   SWIG
   Solver   Inversion
   Radii    Bondi
$end

$solvent
   Dielectric         78.39
   OpticalDielectric  1.777849
$end
```

### 6.3.5 Analytical Excited-State Hessian in TDDFT

To carry out vibrational frequency analysis of an excited state with TDDFT[49,50], an optimization of the excited-state geometry is always necessary. Like the vibrational frequency analysis of the ground state, the frequency analysis of the excited state should be also performed at a stationary point on the excited state potential surface. The *$rem* variable CIS_STATE_DERIV should be set to the excited state for which an optimization and frequency analysis is needed, in addition to the *$rem* keywords used for an excitation energy calculation.

Compared to the numerical differentiation method, the analytical calculation of geometrical second derivatives of the excitation energy needs much less time but much more memory. The computational cost is mainly consumed by the steps to solve both the CPSCF equations for the derivatives of molecular orbital coefficients $C^x$ and the CP-TDDFT equations for the derivatives of the transition vectors, as well as to build the Hessian matrix. The memory usages for these steps scale as $\mathcal{O}(3mN^2)$, where $N$ is the number of basis functions and m is the number of atoms. For large systems, it is thus essential to solve all the coupled-perturbed equations in segments. In this case, the *$rem* variable CPSCF_NSEG is always needed.

In the calculation of the analytical TDDFT excited-state Hessian, one has to evaluate a large number of energy-functional derivatives: the first-order to fourth-order functional derivatives with respect to the density variables as well as their derivatives with respect to the nuclear coordinates. Therefore, a very fine integration grid for DFT calculation should be adapted to guarantee the accuracy of the results.

Analytical TDDFT/C-PCM Hessian has been implemented in Q-CHEM. Normal mode analysis for a system in solution can be performed with the frequency calculation by TDDFT/C-PCM method. The *$rem* and *$pcm* variables for the excited state calculation with TDDFT/C-PCM included in the vertical excitation energy example above are needed. When the properties of large systems are calculated, you must pay attention to the memory limit. At present, only a few exchange correlation functionals, including Slater+VWN, BLYP, B3LYP, are available for the analytical Hessian calculation.

**Example 6.7** A B3LYP/6-31G* optimization in gas phase, followed by a frequency analysis for the first excited state of the peroxy radical

```
$molecule
   0 2
   C  1.004123  -0.180454   0.000000
   O -0.246002   0.596152   0.000000
   O -1.312366  -0.230256   0.000000
   H  1.810765   0.567203   0.000000
   H  1.036648  -0.805445  -0.904798
   H  1.036648  -0.805445   0.904798
$end

$rem
   JOBTYPE           opt
   EXCHANGE          b3lyp
   CIS_STATE_DERIV   1
   BASIS             6-31G*
   CIS_N_ROOTS       10
   CIS_SINGLETS      true
   CIS_TRIPLETS      false
   XC_GRID           000075000302
   RPA               0
$end

@@@

$molecule
   read
$end

$rem
   JOBTYPE           freq
   EXCHANGE          b3lyp
   CIS_STATE_DERIV   1
   BASIS             6-31G*
   CIS_N_ROOTS       10
   CIS_SINGLETS      true
   CIS_TRIPLETS      false
   XC_GRID           000075000302
   RPA               0
$end
```

**Example 6.8** The optimization and Hessian calculation for low-lying excited state with TDDFT/C-PCM

```
$comment
9-Fluorenone + 2 methanol in methanol solution
$end

$molecule
   0 1
   6   -1.987249    0.699711    0.080583
   6   -1.987187   -0.699537   -0.080519
   6   -0.598049   -1.148932   -0.131299
   6    0.282546    0.000160    0.000137
   6   -0.598139    1.149219    0.131479
   6   -0.319285   -2.505397   -0.285378
   6   -1.386049   -3.395376   -0.388447
   6   -2.743097   -2.962480   -0.339290
   6   -3.049918   -1.628487   -0.186285
   6   -3.050098    1.628566    0.186246
   6   -2.743409    2.962563    0.339341
   6   -1.386397    3.395575    0.388596
   6   -0.319531    2.505713    0.285633
   8    1.560568    0.000159    0.000209
   1    0.703016   -2.862338   -0.324093
   1   -1.184909   -4.453877   -0.510447
   1   -3.533126   -3.698795   -0.423022
   1   -4.079363   -1.292006   -0.147755
   1    0.702729    2.862769    0.324437
   1   -1.185378    4.454097    0.510608
   1   -3.533492    3.698831    0.422983
   1   -4.079503    1.291985    0.147594
   8    3.323150    2.119222    0.125454
   1    2.669309    1.389642    0.084386
   6    3.666902    2.489396   -1.208239
   1    4.397551    3.298444   -1.151310
   1    4.116282    1.654650   -1.759486
   1    2.795088    2.849337   -1.768206
   1    2.669205   -1.389382   -0.084343
   8    3.322989   -2.119006   -0.125620
   6    3.666412   -2.489898    1.207974
   1    4.396966   -3.299023    1.150789
   1    4.115800   -1.655485    1.759730
   1    2.794432   -2.850001    1.767593
$end

$rem
   JOBTYPE             OPT
   EXCHANGE            B3lyp
   CIS_N_ROOTS         10
   CIS_SINGLETS        true
   CIS_TRIPLETS        true
   CIS_STATE_DERIV     1   Lowest TDDFT state
   RPA                 TRUE
   BASIS               6-311G**
   XC_GRID             000075000302
   SOLVENT_METHOD      pcm
$end

$pcm
   Theory      CPCM
   Method      SWIG
   Solver      Inversion
   Radii       Bondi
$end

$solvent
   Dielectric 32.613
$end
```

```
@@@

$molecule
   read
$end

$rem
   JOBTYPE            freq
   EXCHANGE           B3lyp
   CIS_N_ROOTS        10
   CIS_SINGLETS       true
   CIS_TRIPLETS       true
   RPA                TRUE
   CIS_STATE_DERIV    1   Lowest TDDFT state
   BASIS              6-311G**
   XC_GRID            000075000302
   SOLVENT_METHOD     pcm
   MEM_STATIC         4000
   MEM_TOTAL          24000
   CPSCF_NSEG         3
$end

$pcm
   Theory       CPCM
   Method       SWIG
   Solver       Inversion
   Radii        Bondi
$end

$solvent
   Dielectric  32.613
$end
```

### 6.3.6 Calculations of Spin-Orbit Couplings Between TDDFT States

Calculations of spin-orbit couplings (SOCs) for TDDFT states within the Tamm-Dancoff approximation or RPA (including TDHF and CIS states) is available. We employ the one-electron Breit Pauli Hamiltonian to calculate the SOC constant between TDDFT states.

$$\hat{H}_{\text{SO}} = -\frac{\alpha_0^2}{2}\sum_{i,A}\frac{Z_A}{r_{iA}^3}(\mathbf{r}_{iA}\times\mathbf{p}_i)\cdot\mathbf{s}_i \tag{6.16}$$

where $i$ denotes electrons, $A$ denotes nuclei, $\alpha_0 = 137.037^{-1}$ is the fine structure constant. $Z_A$ is the bare positive charge on nucleus A. In the second quantization representation, the spin-orbit Hamiltonian in different directions can be expressed as

$$\hat{H}_{SO_x} = -\frac{\alpha_0^2}{2}\sum_{pq}\tilde{L}_{xpq}\cdot\frac{\hbar}{2}\left(a_p^\dagger a_{\bar{q}} + a_{\bar{p}}^\dagger a_q\right) \tag{6.17}$$

$$\hat{H}_{SO_y} = -\frac{\alpha_0^2}{2}\sum_{pq}\tilde{L}_{ypq}\cdot\frac{\hbar}{2i}\left(a_p^\dagger a_{\bar{q}} - a_{\bar{p}}^\dagger a_q\right) \tag{6.18}$$

$$\hat{H}_{SO_z} = -\frac{\alpha_0^2}{2}\sum_{pq}\tilde{L}_{zpq}\cdot\frac{\hbar}{2}\left(a_p^\dagger a_q - a_{\bar{p}}^\dagger a_{\bar{q}}\right) \tag{6.19}$$

where $\tilde{L_\alpha} = L_\alpha/r^3$ $(\alpha = x, y, z)$. The single-reference *ab initio* excited states (within the Tamm-Dancoff approximation) are given by

$$
\begin{aligned}
|\Phi^I_{\text{singlet}}\rangle &= \sum_{i,a} s_i^{Ia}\left(a_a^\dagger a_i + a_{\bar{a}}^\dagger a_{\bar{i}}\right)|\Phi_{\text{HF}}\rangle && (6.20)\\
|\Phi^{I,m_s=0}_{\text{triplet}}\rangle &= \sum_{i,a} t_i^{Ia}\left(a_a^\dagger a_i - a_{\bar{a}}^\dagger a_{\bar{i}}\right)|\Phi_{\text{HF}}\rangle && (6.21)\\
|\Phi^{I,m_s=1}_{\text{triplet}}\rangle &= \sum_{i,a} \sqrt{2}t_i^{Ia} a_a^\dagger a_{\bar{i}}|\Phi_{\text{HF}}\rangle && (6.22)\\
|\Phi^{I,m_s=-1}_{\text{triplet}}\rangle &= \sum_{i,a} \sqrt{2}t_i^{Ia} a_{\bar{a}}^\dagger a_i|\Phi_{\text{HF}}\rangle && (6.23)
\end{aligned}
$$

where $s_i^{Ia}$ and $t_i^{Ia}$ are singlet and triplet excitation coefficients of the $I^{th}$ singlet or triplet state respectively, with the normalization $\sum\limits_{ia} s_i^{Ia^2} = \sum\limits_{ia} t_i^{Ia^2} = \frac{1}{2}$; $|\Phi_{\text{HF}}\rangle$ refers to the Hartree-Fock ground state. Thus the SOC constant from the singlet state to different triplet manifolds can be obtained as follows,

$$
\begin{aligned}
\langle\Phi^I_{\text{singlet}}|\hat{H}_{\text{SO}}|\Phi^{J,m_s=0}_{\text{triplet}}\rangle &= \frac{\alpha_0^2\hbar}{2}\left(\sum_{i,a,b}\tilde{L}_{zab}s_i^{Ia}t_i^{Jb} - \sum_{i,j,a}\tilde{L}_{zij}s_i^{Ia}t_j^{Ja}\right) && (6.24)\\
\langle\Phi^I_{\text{singlet}}|\hat{H}_{\text{SO}}|\Phi^{J,m_s=\pm1}_{\text{triplet}}\rangle &= \mp\frac{\alpha_0^2\hbar}{2\sqrt{2}}\left(\sum_{i,a,b}\tilde{L}_{xab}s_i^{Ia}t_i^{Jb} - \sum_{i,j,a}\tilde{L}_{xij}s_i^{Ia}t_j^{Ja}\right)\\
&\quad+\frac{\alpha_0^2\hbar}{2\sqrt{2}i}\left(\sum_{i,a,b}\tilde{L}_{yab}s_i^{Ia}t_i^{Jb} - \sum_{i,j,a}\tilde{L}_{yij}s_i^{Ia}t_j^{Ja}\right) && (6.25)
\end{aligned}
$$

The SOC constant between different triplet manifolds can be obtained

$$
\begin{aligned}
\langle\Phi^{I,m_s=0}_{\text{triplet}}|\hat{H}_{\text{SO}}|\Phi^{J,m_s=\pm1}_{\text{triplet}}\rangle &= \mp\frac{\alpha_0^2\hbar}{2\sqrt{2}}\left(\sum_{i,a,b}\tilde{L}_{xab}t_i^{Ia}t_i^{Jb} + \sum_{i,j,a}\tilde{L}_{xij}t_i^{Ia}t_j^{Ja}\right)\\
&\quad+\frac{\alpha_0^2\hbar}{2\sqrt{2}i}\left(\sum_{i,a,b}\tilde{L}_{yab}t_i^{Ia}t_i^{Jb} + \sum_{i,j,a}\tilde{L}_{yij}t_i^{Ia}t_j^{Ja}\right) && (6.26)\\
\langle\Phi^{I,m_s=\pm1}_{\text{triplet}}|\hat{H}_{\text{SO}}|\Phi^{J,m_s=\pm1}_{\text{triplet}}\rangle &= \pm\frac{\alpha_0^2\hbar}{2}\left(\sum_{i,a,b}\tilde{L}_{zab}t_i^{Ia}t_i^{Jb} + \sum_{i,j,a}\tilde{L}_{zij}t_i^{Ia}t_j^{Ja}\right) && (6.27)
\end{aligned}
$$

Note that $\langle\Phi^{I,m_s=0}_{\text{triplet}}|\hat{H}_{\text{SO}}|\Phi^{J,m_s=0}_{\text{triplet}}\rangle = \langle\Phi^{I,m_s=\pm1}_{\text{triplet}}|\hat{H}_{\text{SO}}|\Phi^{J,m_s=\mp1}_{\text{triplet}}\rangle = 0$. The total (root-mean-square) spin-orbit coupling is given by

$$
\begin{aligned}
\langle\Phi^I_{\text{singlet}}|\hat{H}_{\text{SO}}|\Phi^J_{\text{triplet}}\rangle &= \sqrt{\sum_{m_s=0,\pm1}\|\langle\Phi^I_{\text{singlet}}|\hat{H}_{\text{SO}}|\Phi^{J,m_s}_{\text{triplet}}\rangle\|^2} && (6.28)\\
\langle\Phi^I_{\text{triplet}}|\hat{H}_{\text{SO}}|\Phi^J_{\text{triplet}}\rangle &= \sqrt{\sum_{m_s=0,\pm1}\|\langle\Phi^{I,m_s}_{\text{triplet}}|\hat{H}_{\text{SO}}|\Phi^{J,m_s}_{\text{triplet}}\rangle\|^2} && (6.29)
\end{aligned}
$$

For RPA states, the SOC constant can simply be obtained by replacing $s_i^{Ia}t_j^{Jb}$ $(t_i^{Ia}t_j^{Jb})$ with $X^{Ia}_{i,\text{singlet}}X^{Jb}_{j,\text{triplet}}+Y^{Ia}_{i,\text{singlet}}Y^{Jb}_{j,\text{triplet}}$ $(X^{Ia}_{i,\text{triplet}}X^{Jb}_{j,\text{triplet}}+Y^{Ia}_{i,\text{triplet}}Y^{Jb}_{j,\text{triplet}})$ Setting the *$rem* variable CALC_SOC = TRUE will enable the SOC calculation for all calculated TDDFT states.

**CALC_SOC**

Controls whether to calculate the SOC constants for EOM-CC, ADC, and TDDFT within the TDA.

TYPE:

LOGICAL

DEFAULT:

FALSE

OPTIONS:

FALSE Do not perform the SOC calculation.

TRUE Perform the SOC calculation.

RECOMMENDATION:

None

**Example 6.9** Calculation of SOCs for water molecule using TDDFT/B3LYP functional within the TDA.

```
$comment
   This sample input calculates the spin-orbit coupling constants for water
   between its ground state and its TDDFT/TDA excited triplets as well as the
   coupling between its TDDFT/TDA singlets and triplets.  Results are given in
   cm-1.
$end

$molecule
   0 1
   H       0.000000    -0.115747     1.133769
   H       0.000000     1.109931    -0.113383
   O       0.000000     0.005817    -0.020386
$end

$rem
   JOBTYPE              sp
   EXCHANGE             b3lyp
   BASIS                6-31G
   CIS_N_ROOTS          4
   CIS_CONVERGENCE      8
   CORRELATION          none
   MAX_SCF_CYCLES       600
   MAX_CIS_CYCLES       50
   SCF_ALGORITHM        diis
   MEM_STATIC           300
   MEM_TOTAL            2000
   SYMMETRY             false
   SYM_IGNORE           true
   UNRESTRICTED         false
   CIS_SINGLETS         true
   CIS_TRIPLETS         true
   CALC_SOC             true
   SET_ITER             300
$end
```

### 6.3.7 Various TDDFT-Based Examples

**Example 6.10** This example shows two jobs which request variants of time-dependent density functional theory calculations. The first job, using the default value of RPA = FALSE, performs TDDFT in the Tamm-Dancoff approximation (TDA). The second job, with RPA = TRUE performs a both TDA and full TDDFT calculations.

```
$comment
   methyl peroxy radical
   TDDFT/TDA and full TDDFT with 6-31+G*
$end

$molecule
   0  2
   C  1.00412  -0.18045    0.00000
   O -0.24600   0.59615    0.00000
   O -1.31237  -0.23026    0.00000
   H  1.81077   0.56720    0.00000
   H  1.03665  -0.80545   -0.90480
   H  1.03665  -0.80545    0.90480
$end

$rem
   EXCHANGE          b
   CORRELATION       lyp
   CIS_N_ROOTS       5
   BASIS             6-31+G*
   SCF_CONVERGENCE   7
$end

@@@

$molecule
   read
$end

$rem
   EXCHANGE          b
   CORRELATION       lyp
   CIS_N_ROOTS       5
   RPA               true
   BASIS             6-31+G*
   SCF_CONVERGENCE   7
$end
```

**Example 6.11** This example shows a calculation of the excited states of a formamide-water complex within a reduced excitation space of the orbitals located on formamide

```
$comment
   formamide-water TDDFT/TDA in reduced excitation space
$end

$molecule
   0 1
   H  1.13  0.49 -0.75
   C  0.31  0.50 -0.03
   N -0.28 -0.71  0.08
   H -1.09 -0.75  0.67
   H  0.23 -1.62 -0.22
   O -0.21  1.51  0.47
   O -2.69  1.94 -0.59
   H -2.59  2.08 -1.53
   H -1.83  1.63 -0.30
$end

$rem
   EXCHANGE          b3lyp
   CIS_N_ROOTS       10
   BASIS             6-31++G**
   TRNSS             TRUE
   TRTYPE            1
   CUTOCC            60
   CUTVIR            40
   CISTR_PRINT       TRUE
$end

$solute
1
2
3
4
5
6
$end
```

**Example 6.12** This example shows a calculation of the core-excited states at the oxygen $K$-edge of CO with a short-range corrected functional.

```
$comment
   TDDFT with short-range corrected (SRC1) functional for the
   oxygen K-edge of CO
$end

$molecule
   0 1
   C     0.000000    0.000000   -0.648906
   O     0.000000    0.000000    0.486357
$end

$rem
   EXCHANGE       SRC1-R1
   BASIS          6-311(2+,2+)G**
   CIS_N_ROOTS    6
   CIS_TRIPLETS   false
   TRNSS          true
   TRTYPE         3
   N_SOL          1
$end

$solute
   1
$end
```

**Example 6.13** This example shows a calculation of the core-excited states at the phosphorus $K$-edge with a short-range corrected functional.

```
$comment
   TDDFT with short-range corrected (SRC2) functional for the
   phosphorus K-edge of PH3
$end

$molecule
   0 1
   H     1.196206    0.000000   -0.469131
   P     0.000000    0.000000    0.303157
   H    -0.598103   -1.035945   -0.469131
   H    -0.598103    1.035945   -0.469131
$end

$rem
   EXCHANGE       SRC2-R2
   BASIS          6-311(2+,2+)G**
   CIS_N_ROOTS    6
   CIS_TRIPLETS   false
   TRNSS          true
   TRTYPE         3
   N_SOL          1
$end

$solute
   1
$end
```

**Example 6.14** SF-TDDFT SP calculation of the 6 lowest states of the TMM diradical using recommended 50-50 functional

```
$molecule
   0 3
   C
   C  1  CC1
   C  1  CC2   2  A2
   C  1  CC2   2  A2     3  180.0
   H  2  C2H   1  C2CH   3    0.0
   H  2  C2H   1  C2CH   4    0.0
   H  3  C3Hu  1  C3CHu  2    0.0
   H  3  C3Hd  1  C3CHd  4    0.0
   H  4  C3Hu  1  C3CHu  2    0.0
   H  4  C3Hd  1  C3CHd  3    0.0

   CC1    = 1.35
   CC2    = 1.47
   C2H    = 1.083
   C3Hu   = 1.08
   C3Hd   = 1.08
   C2CH   = 121.2
   C3CHu  = 120.3
   C3CHd  = 121.3
   A2    = 121.0
```

```
$end

$rem
   EXCHANGE          gen
   BASIS             6-31G*
   SCF_GUESS         core
   SCF_CONVERGENCE   10
   MAX_SCF_CYCLES    100
   SPIN_FLIP         1
   CIS_N_ROOTS       6
   CIS_CONVERGENCE   10
   MAX_CIS_CYCLES    100
$end

$xc_functional
   X  HF    0.50
   X  S     0.08
   X  B     0.42
   C  VWN   0.19
   C  LYP   0.81
$end
```

**Example 6.15** SF-DFT with non-collinear exchange-correlation functional for low-lying states of $CH_2$

```
$comment
  Non-collinear SF-DFT calculation for CH2 at 3B1 state geometry from
  EOM-CCSD(fT) calculation
$end

$molecule
   0 3
   C
   H  1 rCH
   H  1 rCH  2 HCH

   rCH = 1.0775
   HCH = 133.29
$end

$rem
   EXCHANGE             PBE0
   BASIS                cc-pVTZ
   SPIN_FLIP            1
   WANG_ZIEGLER_KERNEL  TRUE
   SCF_CONVERGENCE      10
   CIS_N_ROOTS          6
   CIS_CONVERGENCE      10
$end
```

## 6.4 Maximum Overlap Method (MOM) for SCF Excited States

The Maximum Overlap Method (MOM)[51] is a useful alternative to CIS and TDDFT for obtaining low-cost excited states. It works by modifying the orbital selection step in the SCF procedure. By choosing orbitals that most resemble those from the previous cycle, rather than those with the lowest eigenvalues, excited

SCF determinants are able to be obtained. The MOM has several advantages over existing low-cost excited state methods. Current implementations of TDDFT usually struggle to accurately model charge-transfer and Rydberg transitions, both of which can be well-modeled using the MOM. The MOM also allows the user to target very high energy states, such as those involving excitation of core electrons[52], which are hard to capture using other excited state methods.

In order to calculate an excited state using MOM, the user must correctly identify the orbitals involved in the transition. For example, in a $\pi \rightarrow \pi^*$ transition, the $\pi$ and $\pi^*$ orbitals must be identified and this usually requires a preliminary calculation. The user then manipulates the orbital occupancies using the *$occupied* section, removing an electron from the $\pi$ and placing it in the $\pi^*$. The MOM is then invoked to preserve this orbital occupancy. The success of the MOM relies on the quality of the initial guess for the calculation. If the virtual orbitals are of poor quality then the calculation may 'fall down' to a lower energy state of the same symmetry. Often the virtual orbitals of the corresponding cation are more appropriate for using as initial guess orbitals for the excited state.

Because the MOM states are single determinants, all of Q-CHEM's existing single determinant properties and derivatives are available. This allows, for example, analytic harmonic frequencies to be computed on excited states. The orbitals from a Hartree-Fock MOM calculation can also be used in an MP2 calculation. For all excited state calculations, it is important to add diffuse functions to the basis set. This is particularly true if Rydberg transitions are being sought. For DFT based methods, it is also advisable to increase the size of the quadrature grid so that the more diffuse densities are accurately integrated.

**Example 6.16** Calculation of the lowest singlet state of CO.

```
$comment
   CO spin-purified calculation
$end

$molecule
   0 1
   C
   O  C  1.05
$end

$rem
   METHOD            B3LYP
   BASIS             6-31G*
$end

@@@

$molecule
   read
$end

$rem
   METHOD            B3LYP
   BASIS             6-31G*
   SCF_GUESS           read
   MOM_START         1
   UNRESTRICTED      true
   OPSING            true
$end

$occupied
```

```
   1 2 3 4 5 6 7
   1 2 3 4 5 6 8
$end
```

The following *$rem* is used to invoke the MOM:

**MOM_START**

Determines when MOM is switched on to preserve orbital occupancies.

TYPE:

INTEGER

DEFAULT:

0 (FALSE)

OPTIONS:

| | |
|---|---|
| 0 (FALSE) | MOM is not used |
| $n$ | MOM begins on cycle $n$. |

RECOMMENDATION:

For calculations on excited states, an initial calculation without MOM is usually required to get satisfactory starting orbitals. These orbitals should be read in using SCF_GUESS = true and MOM_START = 1.

**Example 6.17** Input for obtaining the $^2$A$'$ excited state of formamide corresponding to the $\pi \rightarrow \pi^*$ transition. The $^1$A$'$ ground state is obtained if MOM is not used in the second calculation. Note the use of diffuse functions and a larger quadrature grid to accurately model the larger excited state.

```
$molecule
   1  2
   C
   H  1  1.091480
   O  1  1.214713  2  123.10
   N  1  1.359042  2  111.98  3  -180.00
   H  4  0.996369  1  121.06  2    -0.00
   H  4  0.998965  1  119.25  2  -180.00
$end

$rem
   METHOD         B3LYP
   BASIS          6-311(2+,2+)G(d,p)
   XC_GRID        000100000194
$end

@@@

$molecule
   0  1
   C
   H  1  1.091480
   O  1  1.214713  2  123.10
   N  1  1.359042  2  111.98  3  -180.00
   H  4  0.996369  1  121.06  2    -0.00
   H  4  0.998965  1  119.25  2  -180.00
$end

$rem
   METHOD         B3LYP
   BASIS          6-311(2+,2+)G(d,p)
   XC_GRID        000100000194
   MOM_START      1
   SCF_GUESS      read
   UNRESTRICTED   true
$end

$occupied
   1:12
   1:11 13
$end
```

Additionally, it is possible to perform a CIS/TDDFT calculation on top of the MOM excitation. This capability can be useful when modeling pump-probe spectra. In order to run MOM followed by CIS/TDDFT, the $rem variable cis_n_roots must be specified. Truncated subspaces may also be used, see Section 6.3.2.

**Example 6.18** MOM valence excitation followed by core-state TDDFT using a restricted subspace

```
$molecule
   0 1
   O    0.0000    0.0000    0.1168
   H    0.0000    0.7629   -0.4672
   H    0.0000   -0.7629   -0.4672
$end

$rem
   METHOD       B3LYP
   BASIS        aug-cc-pvdz
   SYMMETRY     false
   SYM_IGNORE   true
$end

@@@

$molecule
read
$end

$rem
   METHOD         B3LYP
   BASIS          aug-cc-pvdz
   SCF_GUESS      read
   MOM_START      1
   UNRESTRICTED   true
   SYMMETRY       false
   SYM_IGNORE     true
   CIS_N_ROOTS    5
   TRNSS          true  ! use truncated subspace for TDDFT
   TRTYPE         3     ! specify occupied orbitals
   CUTVIR         15    ! truncate high energy virtual orbitals
   N_SOL          1     ! number core orbitals, specified in $solute section
$end

$solute
   1
$end

$occupied
```

```
   1 2 3 4 5
   1 2 3 4 6
$end
```

If the MOM excitation corresponds to a core hole, a reduced subspace must be used to avoid de-excitations to the core hole. The *$rem* variable CORE_IONIZE allows only the hole to be specified so that not all occupied orbitals need to be entered in the *$solute* section.

**CORE_IONIZE**

Indicates how orbitals are specified for reduced excitation spaces.

TYPE:

INTEGER

DEFAULT:

1

OPTIONS:

1 all valence orbitals are listed in *$solute* section

2 only hole(s) are specified all other occupations same as ground state

RECOMMENDATION:

For MOM + TDDFT this specifies the input form of the *$solute* section. If set to 1 all occupied orbitals must be specified, 2 only the empty orbitals to ignore must be specified.

**Example 6.19** O(1s) core excited state using MOM followed by excitations among valence orbitals. Note that a reduced excitation subspace must be used to avoid "excitations" into the empty core hole

```
$molecule
   0 1
   O   0.0000   0.0000   0.1168
   H   0.0000   0.7629  -0.4672
   H   0.0000  -0.7629  -0.4672
$end

$rem
   METHOD       B3LYP
   BASIS        aug-cc-pvdz
   SYMMETRY     false
   SYM_IGNORE   true
$end

@@@

$molecule
   read
$end

$rem
   METHOD             B3LYP
   BASIS              aug-cc-pvdz
   SCF_GUESS          read
   MOM_START          1
   UNRESTRICTED       true
   SYMMETRY           false
   SYMMETRY_IGNORE    true
   CIS_N_ROOTS        5
   TRNSS              true  ! use truncated subspace for TDDFT
   TRTYPE            3     ! specify occupied orbitals
   N_SOL             1     ! number core holes, specified in $solute section
   CORE_IONIZE       2     ! hole orbital specified
$end

$solute
   6
$end

$occupied
   1 2 3 4 5
   2 3 4 5 6
$end
```

## 6.5 Restricted Open-Shell Kohn-Sham Method for $\Delta$-SCF Calculations of Excited States

Q-CHEM provides access to certain singlet excited states – namely, those well-described by a single-electron HOMO-LUMO transition – via restricted open-shell Kohn-Sham (ROKS) theory. In contrast to the MOM approach (see Section 6.4), which requires separate SCF calculations of the non-aufbau and triplet energies, the ROKS approach attempts to combine the properties of both determinants at the level of the Fock matrix in one SCF calculation. ROKS thus presents as a single SCF loop, but the structure of the Fock matrix differs from the ground-state case. Note that this excited-state method is distinct from ROKS theory for open-shell ground states.

The implementation of ROKS excited states in Q-CHEM largely follows the theoretical framework established by Filatov and Shaik[53] and is described in detail in Ref. 54. Singlet excited state energies and gradients are available, enabling single-point, geometry optimization and molecular dynamics.

To perform an ROKS excited state calculation, simply set the keywords ROKS = TRUE and UNRESTRICTED = FALSE. An additional keyword ROKS_LEVEL_SHIFT is included to assist in cases of convergence difficulties with a standard level-shift technique. It is recommended to perform a preliminary ground-state calculation on the system first, and then use the ground-state orbitals to construct the initial guess using SCF_GUESS = READ.

**ROKS**
Controls whether ROKS calculation will be performed.
TYPE:
LOGICAL
DEFAULT:
FALSE
OPTIONS:
FALSE ROKS is not performed.
TRUE ROKS will be performed.
RECOMMENDATION:
Set to TRUE if ROKS calculation is desired. You should also set UNRESTRICTED = FALSE

**ROKS_LEVEL_SHIFT**

Introduce a level shift of N/100 hartree to aid convergence.

TYPE:

INTEGER

DEFAULT:

0

OPTIONS:

0 No shift

N level shift of N/100 hartree.

RECOMMENDATION:

Use in cases of problematic convergence.

**Example 6.20** RO-PBE0/6-311+G* excited state gradient of formaldehyde, using the ground state orbitals as an initial guess.

```
$comment
   ROKS excited state gradient of formaldehyde
   Use orbitals from ground state for initial guess
$end

$rem
   EXCHANGE          pbe0
   BASIS             6-311+G*
   SCF_CONVERGENCE   9
   SYM_IGNORE        true
$end

$molecule
   0 1
   H      -0.940372    0.000000    1.268098
   H       0.940372    0.000000    1.268098
   C       0.000000    0.000000    0.682557
   O       0.000000    0.000000   -0.518752
$end

@@@

$molecule
   read
$end

$rem
   ROKS              true
   UNRESTRICTED      false
   EXCHANGE          pbe0
   BASIS             6-311+G*
   JOBTYPE           force
   SCF_CONVERGENCE   9
   SYM_IGNORE        true
   SCF_GUESS         read
$end
```

# 6.6 Correlated Excited State Methods: The CIS(D) Family

CIS(D)[55,56] is a simple size-consistent doubles correction to CIS which has a computational cost scaling as the fifth power of the basis set for each excited state. In this sense, CIS(D) can be considered as an excited state analog of the ground state MP2 method. CIS(D) yields useful improvements in the accuracy of excitation energies relative to CIS, and yet can be applied to relatively large molecules using Q-CHEM's efficient integrals transformation package. In addition, as in the case of MP2 method, the efficiency can be significantly improved through the use of the auxiliary basis expansions (Section 5.6)[57].

## 6.6.1 CIS(D) Theory

The CIS(D) excited state procedure is a second-order perturbative approximation to the computationally expensive CCSD, based on a single excitation configuration interaction (CIS) reference. The coupled-cluster wave function, truncated at single and double excitations, is the exponential of the single and double substitution operators acting on the Hartree-Fock determinant:

$$|\Psi\rangle = \exp\left(T_1 + T_2\right)|\Psi_0\rangle \tag{6.30}$$

Determination of the singles and doubles amplitudes requires solving the two equations

$$\langle\Psi_i^a|\, H - E\left|\left(1 + T_1 + T_2 + \frac{1}{2}T_1^2 + T_1T_2 + \frac{1}{3!}T_1^3\right)\Psi_0\right\rangle = 0 \tag{6.31}$$

and

$$\left\langle\Psi_{ij}^{ab}\right|\, H - E\left|\left(1 + T_1 + T_2 + \frac{1}{2}T_1^2 + T_1T_2 + \frac{1}{3!}T_1^3 + \frac{1}{2}T_2^2 + \frac{1}{2}T_1^2T_2 + \frac{1}{4!}T_1^4\right)\Psi_0\right\rangle = 0 \tag{6.32}$$

which lead to the CCSD excited state equations. These can be written

$$\langle\Psi_i^a|\, H - E\left|\left(U_1 + U_2 + T_1U_1 + T_1U_2 + U_1T_2 + \frac{1}{2}T_1^2U_1\right)\Psi_0\right\rangle = \omega b_i^a \tag{6.33}$$

and

$$\begin{aligned}\langle\Psi_i^a|\, H - E\,\big|\big(U_1 + U_2 + T_1U_1 + T_1U_2 + U_1T_2 + \tfrac{1}{2}T_1^2U_1\ + T_2U_2 \\ +\tfrac{1}{2}T_1^2U_2 + T_1T_2U_1 + \tfrac{1}{3!}T_1^3U_1\big|\ \Psi_0\rangle = \omega b_{ij}^{ab}\end{aligned} \tag{6.34}$$

This is an eigenvalue equation $\mathbf{Ab} = \omega\mathbf{b}$ for the transition amplitudes ($\mathbf{b}$ vectors), which are also contained in the $U$ operators.

The second-order approximation to the CCSD eigenvalue equation yields a second-order contribution to the excitation energy which can be written in the form

$$\omega^{(2)} = \mathbf{b}^{(0)^{\mathbf{t}}}\mathbf{A}^{(1)}\mathbf{b}^{(1)} + \mathbf{b}^{(0)^{\mathbf{t}}}\mathbf{A}^{(2)}\mathbf{b}^{(0)} \tag{6.35}$$

or in the alternative form

$$\omega^{(2)} = \omega^{\mathrm{CIS(D)}} = E^{\mathrm{CIS(D)}} - E^{\mathrm{MP2}} \tag{6.36}$$

where

$$E^{\mathrm{CIS(D)}} = \left\langle\Psi^{\mathrm{CIS}}\right|V\left|U_2\Psi^{\mathrm{HF}}\right\rangle + \left\langle\Psi^{\mathrm{CIS}}\right|V\left|T_2U_1\Psi^{\mathrm{HF}}\right\rangle \tag{6.37}$$

and

$$E^{\mathrm{MP2}} = \left\langle\Psi^{\mathrm{HF}}\right|V\left|T_2\Psi^{\mathrm{HF}}\right\rangle \tag{6.38}$$

The output of a CIS(D) calculation contains useful information beyond the CIS(D) corrected excitation energies themselves. The stability of the CIS(D) energies is tested by evaluating a diagnostic, termed the "theta diagnostic"[58]. The theta diagnostic calculates a mixing angle that measures the extent to which electron correlation causes each pair of calculated CIS states to couple. Clearly the most extreme case would be a mixing angle of $45°$, which would indicate breakdown of the validity of the initial CIS states and any subsequent corrections. On the other hand, small mixing angles on the order of only a degree or so are an indication that the calculated results are reliable. The code can report the largest mixing angle for each state to all others that have been calculated.

### 6.6.2 Resolution of the Identity CIS(D) Methods

Because of algorithmic similarity with MP2 calculation, the "resolution of the identity" approximation can also be used in CIS(D). In fact, RI-CIS(D) is orders of magnitudes more efficient than previously explained CIS(D) algorithms for effectively all molecules with more than a few atoms. Like in MP2, this is achieved by reducing the prefactor of the computational load. In fact, the overall cost still scales with the fifth power of the system size.

Presently in Q-CHEM, RI approximation is supported for closed-shell restricted CIS(D) and open-shell unrestricted UCIS(D) energy calculations. The theta diagnostic is not implemented for RI-CIS(D).

### 6.6.3 SOS-CIS(D) Model

As in MP2 case, the accuracy of CIS(D) calculations can be improved by semi-empirically scaling the opposite-spin components of CIS(D) expression:

$$E^{\mathrm{SOS-CIS(D)}} = c_U \left\langle \Psi^{\mathrm{CIS}} \right| V \left| U_2^{\mathrm{OS}} \Psi^{\mathrm{HF}} \right\rangle + c_T \left\langle \Psi^{\mathrm{CIS}} \right| V \left| T_2^{\mathrm{OS}} U_1 \Psi^{\mathrm{HF}} \right\rangle \tag{6.39}$$

with the corresponding ground state energy

$$E^{\mathrm{SOS-MP2}} = c_T \left\langle \Psi^{\mathrm{HF}} \right| V \left| T_2^{\mathrm{OS}} \Psi^{\mathrm{HF}} \right\rangle \tag{6.40}$$

More importantly, this SOS-CIS(D) energy can be evaluated with the 4th power of the molecular size by adopting Laplace transform technique[57]. Accordingly, SOS-CIS(D) can be applied to the calculations of excitation energies for relatively large molecules.

### 6.6.4 SOS-CIS($\mathrm{D}_0$) Model

CIS(D) and its cousins explained in the above are all based on a second-order non-degenerate perturbative correction scheme on the CIS energy ("diagonalize-and-then-perturb" scheme). Therefore, they may fail when multiple excited states come close in terms of their energies. In this case, the system can be handled by applying quasi-degenerate perturbative correction scheme ("perturb-and-then-diagonalize" scheme). The working expression can be obtained by slightly modifying CIS(D) expression shown in Section 6.6.1[59].

First, starting from Eq. (6.35), one can be explicitly write the CIS(D) energy as[59,60]

$$\omega^{\mathrm{CIS}} + \omega^{(2)} = \mathbf{b}^{(\mathbf{0})^{\mathbf{t}}} \mathbf{A}_{\mathrm{SS}}^{(0)} \mathbf{b}^{(\mathbf{0})} + \mathbf{b}^{(\mathbf{0})^{\mathbf{t}}} \mathbf{A}_{\mathrm{SS}}^{(2)} \mathbf{b}^{(\mathbf{0})} - \mathbf{b}^{(\mathbf{0})^{\mathbf{t}}} \mathbf{A}_{\mathrm{SD}}^{(1)} \left( \mathbf{D}_{\mathrm{DD}}^{(0)} - \omega^{\mathrm{CIS}} \right)^{-1} \mathbf{A}_{\mathrm{DS}}^{(1)} \mathbf{b}^{(\mathbf{0})} \tag{6.41}$$

To avoid the failures of the perturbation theory near degeneracies, the entire single and double blocks of the response matrix should be diagonalized. Because such a diagonalization is a non-trivial non-linear problem, an additional approximation from the binomial expansion of the $\left(\mathbf{D}_{\mathrm{DD}}^{(0)} - \omega^{\mathrm{CIS}}\right)^{-1}$ is further applied[59]:

$$\left(\mathbf{D}_{\mathrm{DD}}^{(0)} - \omega^{\mathrm{CIS}}\right)^{-1} = \left(\mathbf{D}_{\mathrm{DD}}^{(0)}\right)^{-1} \left(1 + \omega \left(\mathbf{D}_{\mathrm{DD}}^{(0)}\right)^{-1} + \omega^2 \left(\mathbf{D}_{\mathrm{DD}}^{(0)}\right)^{-2} + ...\right) \tag{6.42}$$

The CIS($D_0$) energy $\omega$ is defined as the eigen-solution of the response matrix with the zero-th order expansion of this equation. Namely,

$$\left(\mathbf{A}_{\mathrm{SS}}^{(0)} + \mathbf{A}_{\mathrm{SS}}^{(2)} - \mathbf{A}_{\mathrm{SD}}^{(1)}(\mathbf{D}_{\mathrm{DD}}^{(0)})^{-1}\mathbf{A}_{\mathrm{DS}}^{(1)}\right)\mathbf{b} = \omega\mathbf{b} \tag{6.43}$$

Similar to SOS-CIS(D), SOS-CIS($D_0$) theory is defined by taking the opposite-spin portions of this equation and then scaling them with two semi-empirical parameters[60]:

$$\left(\mathbf{A}_{\mathrm{SS}}^{(0)} + c_T\mathbf{A}_{\mathrm{SS}}^{\mathrm{OS}(2)} - c_U\mathbf{A}_{\mathrm{SD}}^{\mathrm{OS}(1)}(\mathbf{D}_{\mathrm{DD}}^{(0)})^{-1}\mathbf{A}_{\mathrm{DS}}^{\mathrm{OS}(1)}\right)\mathbf{b} = \omega\mathbf{b} \tag{6.44}$$

Using the Laplace transform and the auxiliary basis expansion techniques, this can also be handled with a 4th-order scaling computational effort. In Q-CHEM, an efficient 4th-order scaling analytical gradient of SOS-CIS($D_0$) is also available. This can be used to perform excited state geometry optimizations on the electronically excited state surfaces.

### 6.6.5 CIS(D) Job Control and Examples

The legacy CIS(D) algorithm in Q-CHEM is handled by the CCMAN/CCMAN2 modules of Q-CHEM's and shares many of the *$rem* options. RI-CIS(D), SOS-CIS(D), and SOS-CIS($D_0$) do not depend on the coupled-cluster routines. Users who will not use this legacy CIS(D) method may skip to Section 6.6.6.

As with all post-HF calculations, it is important to ensure there are sufficient resources available for the necessary integral calculations and transformations. For CIS(D), these resources are controlled using the *$rem* variables CC_MEMORY, MEM_STATIC and MEM_TOTAL (see Section 5.8.7).

To request a CIS(D) calculation the METHOD *$rem* should be set to CIS(D) and the number of excited states to calculate should be specified by EE_STATES (or EE_SINGLETS and EE_TRIPLETS when appropriate). Alternatively, CIS(D) will be performed when EXCHANGE = HF, CORRELATION = CI and EOM_CORR = CIS(D). The SF-CIS(D) is invoked by using SF_STATES.

**EE_STATES**

Sets the number of excited state roots to find. For closed-shell reference, defaults into EE_SINGLETS. For open-shell references, specifies all low-lying states.

TYPE:

INTEGER/INTEGER ARRAY

DEFAULT:

0 Do not look for any excited states.

OPTIONS:

$[i, j, k \ldots]$ Find $i$ excited states in the first irrep, $j$ states in the second irrep *etc.*

RECOMMENDATION:

None

**EE_SINGLETS**

Sets the number of singlet excited state roots to find. Valid only for closed-shell references.

TYPE:

INTEGER/INTEGER ARRAY

DEFAULT:

0 Do not look for any excited states.

OPTIONS:

$[i, j, k \ldots]$ Find $i$ excited states in the first irrep, $j$ states in the second irrep *etc.*

RECOMMENDATION:

None

**EE_TRIPLETS**

Sets the number of triplet excited state roots to find. Valid only for closed-shell references.

TYPE:

INTEGER/INTEGER ARRAY

DEFAULT:

0 Do not look for any excited states.

OPTIONS:

$[i, j, k \ldots]$ Find $i$ excited states in the first irrep, $j$ states in the second irrep *etc.*

RECOMMENDATION:

None

**SF_STATES**

Sets the number of spin-flip target states roots to find.

TYPE:

INTEGER/INTEGER ARRAY

DEFAULT:

0 Do not look for any spin-flip states.

OPTIONS:

$[i, j, k \ldots]$ Find $i$ SF states in the first irrep, $j$ states in the second irrep *etc.*

RECOMMENDATION:

None

**Note:** It is a symmetry of a *transition* rather than that of a *target state* which is specified in excited state calculations. The symmetry of the target state is a product of the symmetry of the reference state and the transition. For closed-shell molecules, the former is fully symmetric and the symmetry of the target state is the same as that of transition, however, for open-shell references this is not so.

**CC_STATE_TO_OPT**

Specifies which state to optimize.

TYPE:

INTEGER ARRAY

DEFAULT:

None

OPTIONS:

$[i,j]$ optimize the $j$th state of the $i$th irrep.

RECOMMENDATION:

None

**Note:** Since there are no analytic gradients for CIS(D), the symmetry should be turned off for geometry optimization and frequency calculations, and CC_STATE_TO_OPT should be specified assuming $C_1$ symmetry, *i.e.*, as [1,N] where N is the number of state to optimize (the states are numbered from 1).

**Example 6.21** CIS(D) excitation energy calculation for ozone at the experimental ground state geometry $C_{2v}$

```
$molecule
   0 1
   O
   O  1  RE
   O  2  RE  1  A

   RE = 1.272
   A  = 116.8
$end

$rem
   JOBTYPE             SP
   METHOD              CIS(D)
   BASIS               6-31G*
   N_FROZEN_CORE       3            use frozen core
   EE_SINGLETS         [2,2,2,2]     find 2 lowest singlets in each irrep.
   EE_TRIPLETS         [2,2,2,2]     find two lowest triplets in each irrep.
$end
```

**Example 6.22** CIS(D) geometry optimization for the lowest triplet state of water. The symmetry is automatically turned off for finite difference calculations

```
$molecule
   0 1
   o
   h  1  r
   h  1  r  2  a

   r  0.95
   a  104.0
$end
```

```
$rem
   JOBTYPE            opt
   BASIS              3-21g
   METHOD             cis(d)
   EE_TRIPLETS        1  calculate one lowest triplet
   CC_STATE_TO_OPT    [1,1] optimize the lowest state (1st state in 1st irrep)
$end
```

**Example 6.23** CIS(D) excitation energy and transition property calculation (between all states) for ozone at the experimental ground state geometry $C_{2v}$

```
$molecule
   0 1
   O
   O  1  RE
   O  2  RE  1  A

   RE = 1.272
   A  = 116.8
$end

$rem
   JOBTYPE            SP
   BASIS              6-31G*
   PURCAR             2             Non-spherical (6D)
   METHOD             CIS(D)
   EE_SINGLETS        [2,2,2,2]
   EE_TRIPLETS        [2,2,2,2]
   CC_TRANS_PROP      1
$end
```

### 6.6.6 RI-CIS(D), SOS-CIS(D), and SOS-CIS($D_0$): Job Control

These methods are activated by setting the *$rem* keyword METHOD to RICIS(D), SOSCIS(D), and SOSCIS(D0), respectively. Other keywords are the same as in CIS method explained in Section 6.2.1. As these methods rely on the RI approximation, AUX_BASIS needs to be set by following the same guide as in RI-MP2 (Section 5.6).

**METHOD**
Excited state method of choice
TYPE:
STRING
DEFAULT:
None
OPTIONS:

| | |
|---|---|
| RICIS(D) | Activate RI-CIS(D) |
| SOSCIS(D) | Activate SOS-CIS(D) |
| SOSCIS(D0) | Activate SOS-CIS($D_0$) |

RECOMMENDATION:
None

**CIS_N_ROOTS**

Sets the number of excited state roots to find

TYPE:

INTEGER

DEFAULT:

0 Do not look for any excited states

OPTIONS:

$n$ $n > 0$ Looks for $n$ excited states

RECOMMENDATION:

None

**CIS_SINGLETS**

Solve for singlet excited states (ignored for spin unrestricted systems)

TYPE:

LOGICAL

DEFAULT:

TRUE

OPTIONS:

TRUE Solve for singlet states

FALSE Do not solve for singlet states.

RECOMMENDATION:

None

**CIS_TRIPLETS**

Solve for triplet excited states (ignored for spin unrestricted systems)

TYPE:

LOGICAL

DEFAULT:

TRUE

OPTIONS:

TRUE Solve for triplet states

FALSE Do not solve for triplet states.

RECOMMENDATION:

None

**SET_STATE_DERIV**

Sets the excited state index for analytical gradient calculation for geometry optimizations and vibrational analysis with SOS-CIS($D_0$)

TYPE:

INTEGER

DEFAULT:

0

OPTIONS:

$n$ Select the $n$th state.

RECOMMENDATION:

Check to see that the states do no change order during an optimization. For closed-shell systems, either CIS_SINGLETS or CIS_TRIPLETS must be set to false.

**MEM_STATIC**

Sets the memory for individual program modules

TYPE:

INTEGER

DEFAULT:

64 corresponding to 64 Mb

OPTIONS:

$n$ User-defined number of megabytes.

RECOMMENDATION:

At least $150(N^2 + N)D$ of MEM_STATIC is required ($N$: number of basis functions, $D$: size of a double precision storage, usually 8). Because a number of matrices with $N^2$ size also need to be stored, 32–160 Mb of additional MEM_STATIC is needed.

**MEM_TOTAL**

Sets the total memory available to Q-CHEM

TYPE:

INTEGER

DEFAULT:

2000 2 Gb

OPTIONS:

$n$ User-defined number of megabytes

RECOMMENDATION:

The minimum memory requirement of RI-CIS(D) is approximately MEM_STATIC + max$(3SVXD, 3X^2D)$ ($S$: number of excited states, $X$: number of auxiliary basis functions, $D$: size of a double precision storage, usually 8). However, because RI-CIS(D) uses a batching scheme for efficient evaluations of electron repulsion integrals, specifying more memory will significantly speed up the calculation. Put as much memory as possible if you are not sure what to use, but never put any more than what is available. The minimum memory requirement of SOS-CIS(D) and SOS-CIS($D_0$) is approximately MEM_STATIC + $20X^2D$. SOS-CIS($D_0$) gradient calculation becomes more efficient when $30X^2D$ more memory space is given. Like in RI-CIS(D), put as much memory as possible if you are not sure what to use. The actual memory size used in these calculations will be printed out in the output file to give a guide about the required memory.

**AO2MO_DISK**

Sets the scratch space size for individual program modules

TYPE:

INTEGER

DEFAULT:

2000 2 Gb

OPTIONS:

$n$ User-defined number of megabytes.

RECOMMENDATION:

The minimum disk requirement of RI-CIS(D) is approximately $3SOVXD$. Again, the batching scheme will become more efficient with more available disk space. There is no simple formula for SOS-CIS(D) and SOS-CIS($D_0$) disk requirement. However, because the disk space is abundant in modern computers, this should not pose any problem. Just put the available disk space size in this case. The actual disk usage information will also be printed in the output file.

**SOS_FACTOR**

Sets the scaling parameter $c_T$

TYPE:

INTEGER

DEFAULT:

1300000 corresponding to 1.30

OPTIONS:

$n$ $c_T = n/1000000$

RECOMMENDATION:

Use the default

**SOS_UFACTOR**

Sets the scaling parameter $c_U$

TYPE:

INTEGER

DEFAULT:

151 For SOS-CIS(D), corresponding to 1.51

140 For SOS-CIS($D_0$), corresponding to 1.40

OPTIONS:

$n$ $c_U = n/100$

RECOMMENDATION:

Use the default

### 6.6.7 Examples

**Example 6.24** Q-CHEM input for an RI-CIS(D) calculation.

```
$molecule
   0 1
   C     0.667472     0.000000     0.000000
   C    -0.667472     0.000000     0.000000
   H     1.237553     0.922911     0.000000
   H     1.237553    -0.922911     0.000000
   H    -1.237553     0.922911     0.000000
   H    -1.237553    -0.922911     0.000000
$end

$rem
   METHOD           ricis(d)
   BASIS            aug-cc-pVDZ
   MEM_TOTAL        1000
   MEM_STATIC       100
   AO2MO_DISK       1000
   AUX_BASIS        rimp2-aug-cc-pVDZ
   PURECART         1111
   CIS_N_ROOTS      10
   CIS_SINGLETS     true
   CIS_TRIPLETS     false
$end
```

**Example 6.25** Q-CHEM input for an SOS-CIS(D) calculation.

```
$molecule
   0 1
   C    -0.627782     0.141553     0.000000
   O     0.730618    -0.073475     0.000000
   H    -1.133677    -0.033018    -0.942848
   H    -1.133677    -0.033018     0.942848
$end

$rem
   METHOD          soscis(d)
   BASIS           aug-cc-pVDZ
   MEM_TOTAL       1000
   MEM_STATIC      100
   AO2MO_DISK      500000     ! 0.5 Terabyte of disk space available
   AUX_BASIS       rimp2-aug-cc-pVDZ
   PURECART        1111
   CIS_N_ROOTS     5
   CIS_SINGLETS    true
   CIS_TRIPLETS    true
$end
```

**Example 6.26** Q-CHEM input for an SOS-CIS($D_0$) geometry optimization on $S_2$ surface.

```
$molecule
   0 1
   o
   h  1  r
   h  1  r  2  a

   r  0.95
   a  104.0
$end

$rem
   JOBTYPE           = opt
   METHOD            = soscis(d0)
   BASIS             = 6-31G**
   AUX_BASIS         = rimp2-VDZ
   PURECART          = 1112
   SET_STATE_DERIV   = 2
   CIS_N_ROOTS       = 5
   CIS_SINGLETS      = true
   CIS_TRIPLETS      = false
$end
```

## 6.7 Coupled-Cluster Excited-State and Open-Shell Methods

EOM-CC and most of the CI codes are part of CCMAN and CCMAN2. CCMAN is a legacy code which is being phased out. All new developments and performance-enhancing features are implemented in CCMAN2. Some options behave differently in the two modules. Below we make an effort to mark which features are available in legacy code only.

### 6.7.1 Excited States via EOM-EE-CCSD

One can describe electronically excited states at a level of theory similar to that associated with coupled-cluster theory for the ground state by applying either linear response theory[61] or equation-of-motion methods[62]. A number of groups have demonstrated that excitation energies based on a coupled-cluster singles and doubles ground state are generally very accurate for states that are primarily single electron promotions. The error observed in calculated excitation energies to such states is typically 0.1–0.2 eV, with 0.3 eV as a conservative estimate, including both valence and Rydberg excited states. This, of course, assumes that a basis set large and flexible enough to describe the valence and Rydberg states is employed. The accuracy of excited state coupled-cluster methods is much lower for excited states that involve a substantial double excitation character, where errors may be 1 eV or even more. Such errors arise because the description of electron correlation of an excited state with substantial double excitation character requires higher truncation of the excitation operator. The description of these states can be improved by including triple excitations, as in EOM(2,3).

Q-CHEM includes coupled-cluster methods for excited states based on the coupled cluster singles and doubles (CCSD) method described earlier. CCMAN also includes the optimized orbital coupled-cluster doubles (OD) variant. OD excitation energies have been shown to be essentially identical in numerical performance to CCSD excited states[63].

These methods, while far more computationally expensive than TDDFT, are nevertheless useful as proven high accuracy methods for the study of excited states of small molecules. Moreover, they are capable of describing both valence and Rydberg excited states, as well as states of a charge-transfer character. Also, when studying a series of related molecules it can be very useful to compare the performance of TDDFT and coupled-cluster theory for at least a small example to understand its performance. Along similar lines, the CIS(D) method described earlier as an economical correlation energy correction to CIS excitation energies is in fact an approximation to EOM-CCSD. It is useful to assess the performance of CIS(D) for a class of problems by benchmarking against the full coupled-cluster treatment. Finally, Q-CHEM includes extensions of EOM methods to treat ionized or electron attachment systems, as well as di- and tri-radicals.

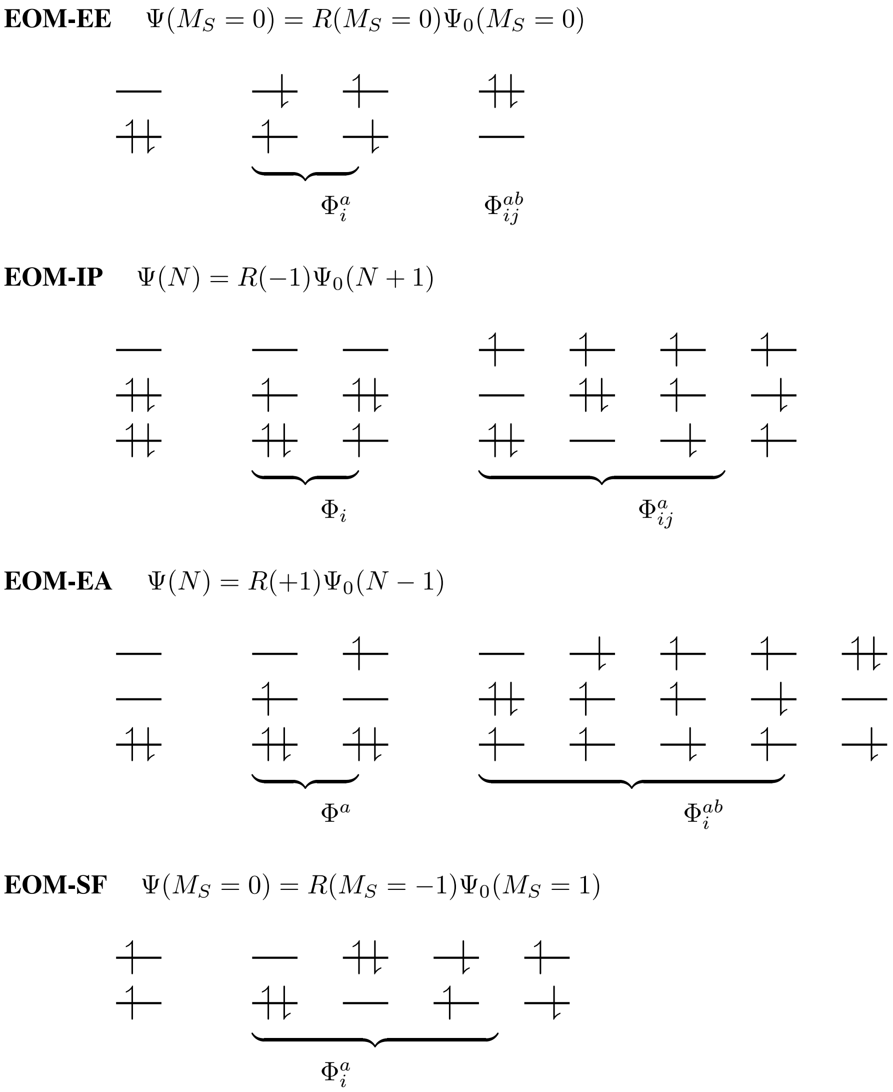
**EOM-EE** $\Psi(M_S = 0) = R(M_S = 0)\Psi_0(M_S = 0)$
$\Phi_i^a$
$\Phi_{ij}^{ab}$
**EOM-IP** $\Psi(N) = R(-1)\Psi_0(N + 1)$
$\Phi_i$
$\Phi_{ij}^a$
**EOM-EA** $\Psi(N) = R(+1)\Psi_0(N - 1)$
$\Phi^a$
$\Phi_i^{ab}$
**EOM-SF** $\Psi(M_S = 0) = R(M_S = -1)\Psi_0(M_S = 1)$
$\Phi_i^a$

Figure 6.1: In the EOM formalism, target states $\Psi$ are described as excitations from a reference state $\Psi_0$: $\Psi = R\Psi_0$, where $R$ is a general excitation operator. Different EOM models are defined by choosing the reference and the form of the operator $R$. In the EOM models for electronically excited states (EOM-EE, upper panel), the reference is the closed-shell ground state Hartree-Fock determinant, and the operator $R$ conserves the number of $\alpha$ and $\beta$ electrons. Note that two-configurational open-shell singlets can be correctly described by EOM-EE since both leading determinants appear as single electron excitations. The second and third panels present the EOM-IP/EA models. The reference states for EOM-IP/EA are determinants for $N+1/N-1$ electron states, and the excitation operator $R$ is ionizing or electron-attaching, respectively. Note that both the EOM-IP and EOM-EA sets of determinants are spin-complete and balanced with respect to the target multi-configurational ground and excited states of doublet radicals. Finally, the EOM-SF method (the lowest panel) employs the high-spin triplet state as a reference, and the operator $R$ includes spin-flip, *i.e.*, does not conserve the number of $\alpha$ and $\beta$ electrons. All the determinants present in the target low-spin states appear as single excitations, which ensures their balanced treatment both in the limit of large and small HOMO-LUMO gaps. Other EOM methods available in Q-CHEM are EOM-2SF and EOM-DIP.

### 6.7.2 EOM-XX-CCSD and CI Suite of Methods

Q-CHEM features the most complete set of EOM-CCSD models[64] that enables accurate, robust, and efficient calculations of electronically excited states (EOM-EE-CCSD or EOM-EE-OD)[62,63,65–67]; ground and excited states of diradicals and triradicals (EOM-SF-CCSD and EOM-SF-OD[67,68]); ionization potentials and electron attachment energies as well as problematic doublet radicals, cation or anion radicals, (EOM-IP/EA-CCSD)[69–71], as well as EOM-DIP-CCSD and EOM-2SF-CCSD. Conceptually, EOM is very similar to configuration interaction (CI): target EOM states are found by diagonalizing the similarity transformed Hamiltonian $\bar{H} = e^{-T}He^{T}$,

$$\bar{H}R = ER, \tag{6.45}$$

where $T$ and $R$ are general excitation operators with respect to the reference determinant $|\Phi_0\rangle$. In the EOM-CCSD models, $T$ and $R$ are truncated at single and double excitations, and the amplitudes $T$ satisfy the CC equations for the reference state $|\Phi_0\rangle$:

$$\langle\Phi_i^a|\bar{H}|\Phi_0\rangle = 0 \tag{6.46}$$

$$\langle\Phi_{ij}^{ab}|\bar{H}|\Phi_0\rangle = 0 \tag{6.47}$$

The computational scaling of EOM-CCSD and CISD methods is identical, *i.e.*, $\mathcal{O}(N^6)$, however EOM-CCSD is numerically superior to CISD because correlation effects are "folded in" in the transformed Hamiltonian, and because EOM-CCSD is rigorously size-intensive.

By combining different types of excitation operators and references $|\Phi_0\rangle$, different groups of target states can be accessed as explained in Fig. 6.1. For example, electronically excited states can be described when the reference $|\Phi_0\rangle$ corresponds to the ground state wave function, and operators $R$ conserve the number of electrons and a total spin[62]. In the ionized/electron attached EOM models[70,71], operators $R$ are not electron conserving (*i.e.*, include different number of creation and annihilation operators)—these models can accurately treat ground and excited states of doublet radicals and some other open-shell systems. For example, singly ionized EOM methods, *i.e.*, EOM-IP-CCSD and EOM-EA-CCSD, have proven very useful for doublet radicals whose theoretical treatment is often plagued by symmetry breaking. Finally, the EOM-SF method[67,68] in which the excitation operators include spin-flip allows one to access diradicals, triradicals, and bond-breaking[3].

Q-CHEM features EOM-EE/SF/IP/EA/DIP/DSF-CCSD methods for both closed and open-shell references (RHF/UHF/ROHF), including frozen core/virtual options. For EE, SF, IP, and EA, a more economical flavor of EOM-CCSD is available (EOM-MP2 family of methods). All EOM models take full advantage of molecular point group symmetry. Analytic gradients are available for RHF and UHF references, for the full orbital space, and with frozen core/virtual orbitals[72]. Properties calculations (permanent and transition dipole moments, $\langle S^2\rangle$, $\langle R^2\rangle$, *etc.*) are also available. The current implementation of the EOM-XX-CCSD methods enables calculations of medium-size molecules, *e.g.*, up to 15–20 heavy atoms. Using RI approximation 5.8.5 or Cholesky decomposition 5.8.6 helps to reduce integral transformation time and disk usage enabling calculations on much larger systems. EOM-MP2 and EOM-MP2t variants are also less computationally demanding. The computational cost of EOM-IP calculations can be considerably reduced (with negligible decline in accuracy) by truncating virtual orbital space using FNO scheme (see Section 6.7.7).

**Legacy features available in CCMAN.** The CCMAN module of Q-CHEM includes two implementations of EOM-IP-CCSD. The proper implementation[73] is used by default is more efficient and robust. The EOM_FAKE_IPEA keyword invokes is a pilot implementation in which EOM-IP-CCSD calculation is set up by adding a very diffuse orbital to a requested basis set, and by solving EOM-EE-CCSD equations for the target states that include excitations of an electron to this diffuse orbital. The implementation of EOM-EA-CCSD in CCMAN also uses this trick. Fake IP/EA calculations are only recommended for

Dyson orbital calculations and debug purposes. (CCMAN2 features proper implementations of EOM-IP and EOM-EA (including Dyson orbitals)).

A more economical CI variant of EOM-IP-CCSD, IP-CISD is also available in CCMAN. This is an $N^5$ approximation of IP-CCSD, and can be used for geometry optimizations of problematic doublet states[74].

### 6.7.3 Spin-Flip Methods for Di- and Triradicals

The spin-flip method[14,68,75] addresses the bond-breaking problem associated with a single-determinant description of the wave function. Both closed and open shell singlet states are described within a single reference as spin-flipping, (*e.g.*, $\alpha \to \beta$ excitations from the triplet reference state, for which both dynamical and non-dynamical correlation effects are smaller than for the corresponding singlet state. This is because the exchange hole, which arises from the Pauli exclusion between same-spin electrons, partially compensates for the poor description of the coulomb hole by the mean-field Hartree-Fock model. Furthermore, because two $\alpha$ electrons cannot form a bond, no bond breaking occurs as the internuclear distance is stretched, and the triplet wave function remains essentially single-reference in character. The spin-flip approach has also proved useful in the description of di- and tri-radicals as well as some problematic doublet states.

The spin-flip method is available for the CIS, CIS(D), CISD, CISDT, OD, CCSD, and EOM-(2,3) levels of theory and the spin complete SF-XCIS (see Section 6.2.4). An $N^7$ non-iterative triples corrections are also available. For the OD and CCSD models, the following non-relaxed properties are also available: dipoles, transition dipoles, eigenvalues of the spin-squared operator ($\langle S^2 \rangle$), and densities. Analytic gradients are also for SF-CIS and EOM-SF-CCSD methods. To invoke a spin-flip calculation the SF_STATES *$rem* should be used, along with the associated *$rem* settings for the chosen level of correlation by using METHOD (recommended) or using older keywords (CORRELATION, and, optionally, EOM_CORR). Note that the high multiplicity triplet or quartet reference states should be used.

Several double SF methods have also been implemented[76]. To invoke these methods, use DSF_STATES.

### 6.7.4 EOM-DIP-CCSD

Double-ionization potential (DIP) is another non-electron-conserving variant of EOM-CCSD[77–79]. In DIP, target states are reached by detaching two electrons from the reference state:

$$\Psi_k = R_{N-2}\Psi_0(N+2), \tag{6.48}$$

and the excitation operator $R$ has the following form:

$$\begin{aligned} R &= R_1 + R_2, && (6.49)\\ R_1 &= 1/2\sum_{ij} r_{ij} ji, && (6.50)\\ R_2 &= 1/6\sum_{ijka} r_{ijk}^{a} a^{\dagger} kji. && (6.51) \end{aligned}$$

As a reference state in the EOM-DIP calculations one usually takes a well-behaved closed-shell state. EOM-DIP is a useful tool for describing molecules with electronic degeneracies of the type "$2n-2$ electrons on $n$ degenerate orbitals". The simplest examples of such systems are diradicals with two-electrons-on-two-orbitals pattern. Moreover, DIP is a preferred method for four-electrons-on-three-orbitals wave functions.

Accuracy of the EOM-DIP-CCSD method is similar to accuracy of other EOM-CCSD models, *i.e.*, 0.1–0.3 eV. The scaling of EOM-DIP-CCSD is $\mathcal{O}(N^6)$, analogous to that of other EOM-CCSD methods. However, its computational cost is less compared to, *e.g.*, EOM-EE-CCSD, and it increases more slowly with the basis set size. An EOM-DIP calculation is invoked by using DIP_STATES, or DIP_SINGLETS and DIP_TRIPLETS.

### 6.7.5 EOM-CC Calculations of Meta-stable States: Super-Excited Electronic States, Temporary Anions, and Core-Ionized States

While conventional coupled-cluster and equation-of-motion methods allow one to tackle electronic structure ranging from well-behaved closed shell molecules to various open-shell and electronically excited species[64], meta-stable electronic states, so-called resonances, present a difficult case for theory. By using complex scaling and complex absorbing potential techniques, we extended these powerful methods to describe auto-ionizing states, such as transient anions, highly excited electronic states, and core-ionized species[80–82]. In addition, users can employ stabilization techniques using charged sphere and scaled atomic charges options[79]. These methods are only available within CCMAN2. The complex CC/EOM code is engaged by COMPLEX_CCMAN; the specific parameters should be specified in the *$complex_ccman* section.

**COMPLEX_CCMAN**
Requests complex-scaled or CAP-augmented CC/EOM calculations.
TYPE:
LOGICAL
DEFAULT:
FALSE
OPTIONS:
TRUE Engage complex CC/EOM code.
RECOMMENDATION:
Not available in CCMAN. Need to specify CAP strength or complex-scaling parameter in *$complex_ccman* section.

The *$complex_ccman* section is used to specify the details of the complex-scaled/CAP calculations, as illustrated below. If user specifies CS_THETA, complex scaling calculation is performed.

```
$complex_ccman
CS_THETA  10   Complex-scaling parameter theta=0.01, r->r exp(-i*theta)
CS_ALPHA  10   Real part of the scaling parameter alpha=0.01,
!              r->alpha r exp(-itheta)
$end
```

Alternatively, for CAP calculations, the CAP parameters need to be specified.

```
$complex_ccman
CAP_ETA 1000  CAP strength in 10-5 a.u. (0.01)
CAP_X 2760  CAP onset along X in 10^-3 bohr (2.76 bohr)
CAP_Y 2760  CAP onset along Y in 10^-3 bohr (2.76 bohr)
CAP_Z 4880  CAP onset along Z in 10^-3 bohr (4.88 bohr)
CAP_TYPE 1  Use cuboid cap (CAP_TYPE=0 will use spherical CAP)
$end
```

CS_THETA is specified in radian× $10^{-3}$. CS_ALPHA, CAP_X/Y/Z are specified in a.u.× $10^{-3}$, i.e., CS_THETA = 10 means $\theta$=0.01; CAP_ETA is specified in a.u.× $10^{-5}$. The CAP is calculated by numerical integration, the default grid is 000099000590. For testing the accuracy of numerical integration, the numerical overlap matrix is calculated and compared to the analytical one. If the performance of the default grid is poor, the grid type can be changed using the keyword XC_GRID (see Section 4.4.5 for further details). When CAP calculations are performed, CC_EOM_PROP=TRUE by default; this is necessary for calculating first-order perturbative correction.

Advanced users may find the following options useful. Several ways of conducing complex calculations are possible, *i.e.*, complex scaling/CAPs can be either engaged at all levels (HF, CCSD, EOM), or not. By default, if COMPLEX_CCMAN is specified, the EOM calculations are conducted using complex code. Other parameters are set up as follows:

```
$complex_ccman
CS_HF=true
CS_CCSD=true
$end
```

Alternatively, the user can disable complex HF. These options are experimental and should only be used by advanced users. For CAP-EOM-CC, only CS_HF = TRUE and CS_CCSD = TRUE is implemented.

Non-iterative triples corrections are available for all complex scaled and CAP-augmented CC/EOM-CC models and requested in analogy to regular CC/EOM-CC (see Section 6.7.22 for details).

Molecular properties and transition moments are requested for complex scaled or CAP-augmented CC/ EOM-CC calculations in analogy to regular CC/EOM-CC (see Section 6.7.15 for details). Analytic gradients are available for complex CC/EOM-CC only for cuboid CAPs ( CAP_TYPE = 1) introduced at the HF level (CS_HF = TRUE), as described in Ref. 83. The frozen core approximation is disabled for CAP-CC/ EOM-CC gradient calculations. Geometry optimization can be requested in analogy to regular CC/EOM-CC (see Section 6.7.15 for details).

### 6.7.6 Charge Stabilization for EOM-DIP and Other Methods

The performance of EOM-DIP deteriorates when the reference state is unstable with respect to electron-detachment[78,79], which is usually the case for dianion references employed to describe neutral diradicals by EOM-DIP. Similar problems are encountered by all excited-state methods when dealing with excited states lying above ionization or electron-detachment thresholds.

To remedy this problem, one can employ charge stabilization methods, as described in Refs. 78,79. In this approach (which can also be used with any other electronic structure method implemented in Q-CHEM), an additional Coulomb potential is introduced to stabilize unstable wave functions. The following keywords invoke stabilization potentials: SCALE_NUCLEAR_CHARGE and ADD_CHARGED_CAGE. In the former case, the potential is generated by increasing nuclear charges by a specified amount. In the latter, the potential is generated by a cage built out of point charges comprising the molecule. There are two cages available: dodecahedral and spherical. The shape, radius, number of points, and the total charge of the cage are set by the user.

**Note:** A perturbative correction estimating the effect of the external Coulomb potential on EOM energy will be computed when target state densities are calculated, *e.g.*, when CC_EOM_PROP = TRUE.

**Note:** Charge stabilization techniques can be used with other methods such as EOM-EE, CIS, and TDDFT to improve the description of resonances. It can also be employed to describe meta-stable ground states.

### 6.7.7 Frozen Natural Orbitals in CC and IP-CC Calculations

Large computational savings are possible if the virtual space is truncated using the frozen natural orbital (FNO) approach (see Section 5.11). Extension of the FNO approach to ionized states within EOM-CC formalism was recently introduced and benchmarked[84]. In addition to ground-state coupled-cluster calculations, FNOs can also be used in EOM-IP-CCSD, EOM-IP-CCSD(dT/fT) and EOM-IP-CC(2,3). In IP-CC the FNOs are computed for the reference (neutral) state and then are used to describe several target (ionized) states of interest. Different truncation scheme are described in Section 5.11.

### 6.7.8 Approximate EOM-CC Methods: EOM-MP2 and EOM-MP2T

Approximate EOM-CCSD models with $T$-amplitudes obtained at the MP2 level offer reduced computational cost compared to the full EOM-CCSD since the computationally demanding $\mathcal{O}(N^6)$ CCSD step is eliminated from the calculation. Two methods of this type are implemented in Q-CHEM. The first is invoked with the keyword METHOD = EOM-MP2. Its formulation and implementation follow the original EOM-CCSD(2) approach developed by Stanton and co-workers[85]. The second method can be requested with the METHOD = EOM-MP2T keyword and is similar to EOM-MP2, but it accounts for the additional terms in $\bar{H}$ that appear because the MP2 $T-$amplitudes do not satisfy the CCSD equations. EOM-MP2 ansatz is implemented for IP/EA/EE/SF energies, state properties, and interstate properties (EOM-EOM, but not REF-EOM). EOM-MP2t is available for the IP/EE/EA energy calculations only.

### 6.7.9 Approximate EOM-CC Methods: EOM-CCSD-S(D) and EOM-MP2-S(D)

These are very light-weight EOM methods in which the EOM problem is solved in the singles block and the effect of doubles is evaluated perturbatively. The $\bar{H}$ is evaluated by using either CCSD or MP2 amplitudes, just as in the regular EOM calculations. The EOM-MP2-S(D) method, which is similar in level of correlation treatment to SOS-CIS(D), is particularly fast. These methods are implemented for IP and EE states. For valence states, the errors for absolute ionization or excitation energies against regular EOM-CCSD are about 0.4 eV and appear to be systematically blue-shifted; the EOM-EOM energy gaps look better. The calculations are set as in regular EOM-EE/IP, but using method = EOM-CCSD-SD(D) or method = EOM-MP2-SD(D). State properties and EOM-EOM transition properties can be computed using these methods (reference-EOM properties are not yet implemented). These methods are designed for treating core-level states[86].

**Note:** These methods are still in the experimental stage.

### 6.7.10 Implicit solvent models in EOM-CC/MP2 calculations.

Vertical excitation/ionization/attachment energies can be computed for all EOM-CC/MP2 methods using a non-equilibrium C-PCM model. To perform a PCM-EOM calculation, one has to invoke the PCM

(SOLVENT_METHOD to PCM in the *$rem* block) and specify the solvent parameters, i.e. the dielectric constant $\epsilon$ and the squared refractive index $n^2$ (DIELECTRIC and DIELECTRIC_INFI in the *$solvent* block). If nothing is given, the parameters for water will be used by default. For EOM methods, only the simplest model, C-PCM, is implemented. More sophisticated flavors of PCM are available for ADC methods (see Section 6.8.7). For a detailed description of PCM theory, see Sections 6.8.7, 11.2.2 and 11.2.3.

**Note:** Only energies and unrelaxed properties can be computed (no gradient).

**Note:** Symmetry is turned off for C-CPM calculations.

### 6.7.11 EOM-CC Jobs: Controlling Guess Formation and Iterative Diagonalizers

An EOM-CC eigen-problem is solved by an iterative diagonalization procedure that avoids full diagonalization and only looks for several eigen-states, as specified by the XX_STATES keywords.

The default procedure is based on the modified Davidson diagonalization algorithm, as explained in Ref. 67. In addition to several keywords that control the convergence of algorithm, memory usage, and fine details of its execution, there are several important keywords that allow user to specify how the target state selection will be performed.

By default, the diagonalization looks for several lowest eigenstates, as specified by XX_STATES. The guess vectors are generated as singly excited determinants selected by using Koopmans' theorem; the number of guess vectors is equal to the number of target states. If necessary, the user can increase the number of singly excited guess vectors (EOM_NGUESS_SINGLES) and include doubly excited guess vectors (EOM_NGUESS_DOUBLES).

**Note:** In CCMAN2, if there is not enough singly excited guess vectors, the algorithm adds doubly excited guess vectors. In CCMAN, doubly excited guess vectors are generated only if EOM_NGUESS_DOUBLES is invoked.

The user can request to pre-converge singles (solve the equations in singles-only block of the Hamiltonian. This is done by using EOM_PRECONV_SINGLES.

**Note:** In CCMAN, the user can pre-converge both singles and doubles blocks (EOM_PRECONV_SINGLES. and EOM_PRECONV_DOUBLES)

If a state (or several states) of a particular character is desired (*e.g.*, HOMO→LUMO+10 excitation or HOMO-10 ionization), the user can specify this by using EOM_USER_GUESS keyword and *$eom_user_guess* section, as illustrated by an example below. The algorithm will attempt to find an eigenstate that has the maximum overlap with this guess vector. The multiplicity of the state is determined as in the regular calculations, by using the EOM_XX_SINGLETS and EOM_EE_TRIPLETS keywords. This option is useful for looking for high-lying states such as core-ionized or core-excited states. It is only available with CCMAN2.

The examples below illustrate how to use user-specified guess in EOM calculations:

```
$eom_user_guess
4  Calculate excited state corresponding to 4(OCC)->5(VIRT) transition.
5
$end
```

or

```
$eom_user_guess
1  1   Calculate excited states corresponding to 1(OCC)->5(VIRT) and 1(OCC)->6(VIRT)
5  6
$end
```

In IP/EA calculations, only one set of orbitals is specified:

```
$eom_user_guess
4 5 6
$end
```

If IP_STATES is specified, this will invoke calculation of the EOM-IP states corresponding to the ionization from 4th, 5th, and 6th occupied MOs. If EA_STATES is requested, then EOM-EA equations will be solved for a root corresponding to electron-attachment to the 4th, 5th, and 6th virtual MOs.

For these options to work correctly, user should make sure that XX_STATES requests a sufficient number of states. In case of symmetry, one can request several states in each irrep, but the algorithm will only compute those states which are consistent with the user guess orbitals.

Alternatively, the user can specify an energy shift by EOM_SHIFT. In this case, the solver looks for the XX_STATES eigenstates that are closest to this energy; the guess vectors are generated accordingly, using Koopmans' theorem. This option is useful when highly excited states (*i.e.*, interior eigenstates) are desired.

## 6.7.12 Equation-of-Motion Coupled-Cluster Job Control

It is important to ensure there are sufficient resources available for the necessary integral calculations and transformations. For CCMAN/CCMAN2 algorithms, these resources are controlled using the *$rem* variables CC_MEMORY, MEM_STATIC and MEM_TOTAL (see Section 5.14).

The exact flavor of correlation treatment within equation-of-motion methods is defined by METHOD (see Section 6.1). For EOM-CCSD, once should set METHOD to EOM-CCSD, for EOM-MP2, METHOD = EOM-CCSD, etc. In addition, a specification of the number of *target states* is required through XX_STATES (XX designates the type of the target states, *e.g.*, EE, SF, IP, EA, DIP, DSF, *etc.*). Users must be aware of the point group symmetry of the system being studied and also the symmetry of the initial and target states of interest, as well as symmetry of transition. It is possible to turn off the use of symmetry by CC_SYMMETRY. If set to FALSE the molecule will be treated as having $C_1$ symmetry and all states will be of $A$ symmetry.

**Note:** In finite-difference calculations, the symmetry is turned off automatically, and the user must ensure that XX_STATES is adjusted accordingly.

**Note:** In CCMAN, mixing different EOM models in a single calculation is only allowed in Dyson orbitals calculations. In CCMAN2, different types of target states can be requested in a single calculation.

### 6.7.12.1 Alternative way to set up EOM calculations

Below we describe alternative way to specify correlation treatment in EOM-CC/CI calculations. These keywords will be eventually phased out. By default, the level of correlation of the EOM part of the wave function (*i.e.*, maximum excitation level in the EOM operators $R$) is set to match CORRELATION, however, one can mix different correlation levels for the reference and EOM states by using EOM_CORR. To request

| CORRELATION | Default<br>EOM_CORR | Allowed<br>EOM_CORR | Target states | CCMAN /<br>CCMAN2 |
|---|---|---|---|---|
| CI | none | CIS, CIS(D) | EE, SF | y/n |
| | | CISD | EE, SF, IP | y/n |
| | | SDT, DT | EE, SF, DSF | y/n |
| CIS(D) | CIS(D) | N/A | EE, SF | y/n |
| CCSD, OD | CISD | | EE, SF, IP, EA, DIP | y/y |
| | | SD(fT) | EE, IP, EA | n/y |
| | | SD(dT), SD(fT) | EE, SF, fake IP/EA | y/n |
| | | SD(dT), SD(fT), SD(sT) | IP | y/n |
| | | SDT, DT | EE, SF, IP, EA, DIP, DSF | y/n |

Table 6.1: Default and allowed CORRELATION and EOM_CORR combinations as well as valid target state types. The last column shows if a method is available in CCMAN or CCMAN2.

a CI calculation, set CORRELATION = CI and select type of CI expansion by EOM_CORR. The table below shows default and allowed CORRELATION and EOM_CORR combinations.

Table 6.7.12.1 shows the correct combinations of CORRELATION and EOM_CORR for standard EOM and CI models.

The most relevant EOM-CC input options follow.

**EE_STATES**

Sets the number of excited state roots to find. For closed-shell reference, defaults into EE_SINGLETS. For open-shell references, specifies all low-lying states.

TYPE:

INTEGER/INTEGER ARRAY

DEFAULT:

0 Do not look for any excited states.

OPTIONS:

$[i, j, k \ldots]$ Find $i$ excited states in the first irrep, $j$ states in the second irrep *etc.*

RECOMMENDATION:

None

**EE_SINGLETS**

Sets the number of singlet excited state roots to find. Valid only for closed-shell references.

TYPE:

INTEGER/INTEGER ARRAY

DEFAULT:

0 Do not look for any excited states.

OPTIONS:

$[i, j, k \ldots]$ Find $i$ excited states in the first irrep, $j$ states in the second irrep *etc.*

RECOMMENDATION:

None

| Method | CORRELATION | EOM_CORR | Target states selection |
|---|---|---|---|
| CIS | CI | CIS | EE_STATES |
| | | | EE_SNGLETS, EE_TRIPLETS |
| SF-CIS | CI | CIS | SF_STATES |
| CIS(D) | CI | CIS(D) | EE_STATES |
| | | | EE_SNGLETS, EE_TRIPLETS |
| SF-CIS(D) | CI | CIS(D) | SF_STATES |
| CISD | CI | CISD | EE_STATES |
| | | | EE_SNGLETS, EE_TRIPLETS |
| SF-CISD | CI | CISD | SF_STATES |
| IP-CISD | CI | CISD | IP_STATES |
| CISDT | CI | SDT | EE_STATES |
| | | | EE_SNGLETS, EE_TRIPLETS |
| SF-CISDT | CI | SDT or DT | SF_STATES |
| EOM-EE-CCSD | CCSD | | EE_STATES |
| | | | EE_SNGLETS, EE_TRIPLETS |
| EOM-SF-CCSD | CCSD | | SF_STATES |
| EOM-IP-CCSD | CCSD | | IP_STATES |
| EOM-EA-CCSD | CCSD | | EA_STATES |
| EOM-DIP-CCSD | CCSD | | DIP_STATES |
| | | | DIP_SNGLETS, DIP_TRIPLETS |
| EOM-2SF-CCSD | CCSD | SDT or DT | DSF_STATES |
| EOM-EE-(2,3) | CCSD | SDT | EE_STATES |
| | | | EE_SNGLETS, EE_TRIPLETS |
| EOM-SF-(2,3) | CCSD | SDT | SF_STATES |
| EOM-IP-(2,3) | CCSD | SDT | IP_STATES |
| EOM-SF-CCSD(dT) | CCSD | SD(dT) | SF_STATES |
| EOM-SF-CCSD(fT) | CCSD | SD(fT) | SF_STATES |
| EOM-IP-CCSD(dT) | CCSD | SD(dT) | IP_STATES |
| EOM-IP-CCSD(fT) | CCSD | SD(fT) | IP_STATES |
| EOM-IP-CCSD(sT) | CCSD | SD(sT) | IP_STATES |

Table 6.2: Commonly used EOM and CI models. 'SINGLETS' and 'TRIPLETS' are only available for closed-shell references.

**EE_TRIPLETS**

Sets the number of triplet excited state roots to find. Valid only for closed-shell references.

TYPE:

INTEGER/INTEGER ARRAY

DEFAULT:

0 Do not look for any excited states.

OPTIONS:

$[i, j, k \ldots]$ Find $i$ excited states in the first irrep, $j$ states in the second irrep *etc.*

RECOMMENDATION:

None

**SF_STATES**

Sets the number of spin-flip target states roots to find.

TYPE:

INTEGER/INTEGER ARRAY

DEFAULT:

0 Do not look for any excited states.

OPTIONS:

$[i, j, k \ldots]$ Find $i$ SF states in the first irrep, $j$ states in the second irrep *etc.*

RECOMMENDATION:

None

**DSF_STATES**

Sets the number of doubly spin-flipped target states roots to find.

TYPE:

INTEGER/INTEGER ARRAY

DEFAULT:

0 Do not look for any DSF states.

OPTIONS:

$[i, j, k \ldots]$ Find $i$ doubly spin-flipped states in the first irrep, $j$ states in the second irrep *etc.*

RECOMMENDATION:

None

**IP_STATES**

Sets the number of ionized target states roots to find. By default, $\beta$ electron will be removed (see EOM_IP_BETA).

TYPE:

INTEGER/INTEGER ARRAY

DEFAULT:

0 Do not look for any IP states.

OPTIONS:

$[i, j, k \ldots]$ Find $i$ ionized states in the first irrep, $j$ states in the second irrep *etc.*

RECOMMENDATION:

None

**EOM_IP_ALPHA**

Sets the number of ionized target states derived by removing $\alpha$ electron (M$_s = -\frac{1}{2}$).

TYPE:

INTEGER/INTEGER ARRAY

DEFAULT:

0 Do not look for any IP/$\alpha$ states.

OPTIONS:

$[i, j, k \ldots]$ Find $i$ ionized states in the first irrep, $j$ states in the second irrep *etc.*

RECOMMENDATION:

None

**EOM_IP_BETA**

Sets the number of ionized target states derived by removing $\beta$ electron (M$_s$=$\frac{1}{2}$, default for EOM-IP).

TYPE:

INTEGER/INTEGER ARRAY

DEFAULT:

0 Do not look for any IP/$\beta$ states.

OPTIONS:

$[i, j, k \ldots]$ Find $i$ ionized states in the first irrep, $j$ states in the second irrep *etc.*

RECOMMENDATION:

None

**EA_STATES**

Sets the number of attached target states roots to find. By default, $\alpha$ electron will be attached (see EOM_EA_ALPHA).

TYPE:

INTEGER/INTEGER ARRAY

DEFAULT:

0 Do not look for any EA states.

OPTIONS:

$[i, j, k \ldots]$ Find $i$ EA states in the first irrep, $j$ states in the second irrep *etc.*

RECOMMENDATION:

None

**EOM_EA_ALPHA**

Sets the number of attached target states derived by attaching $\alpha$ electron (M$_s$=$\frac{1}{2}$, default in EOM-EA).

TYPE:

INTEGER/INTEGER ARRAY

DEFAULT:

0 Do not look for any EA states.

OPTIONS:

$[i, j, k \ldots]$ Find $i$ EA states in the first irrep, $j$ states in the second irrep *etc.*

RECOMMENDATION:

None

**EOM_EA_BETA**

Sets the number of attached target states derived by attaching $\beta$ electron (M$_s$=$-\frac{1}{2}$, EA-SF).

TYPE:

INTEGER/INTEGER ARRAY

DEFAULT:

0 Do not look for any EA states.

OPTIONS:

$[i, j, k \ldots]$ Find $i$ EA states in the first irrep, $j$ states in the second irrep *etc.*

RECOMMENDATION:

None

**DIP_STATES**

Sets the number of DIP roots to find. For closed-shell reference, defaults into DIP_SINGLETS. For open-shell references, specifies all low-lying states.

TYPE:

INTEGER/INTEGER ARRAY

DEFAULT:

0 Do not look for any DIP states.

OPTIONS:

$[i, j, k \ldots]$ Find $i$ DIP states in the first irrep, $j$ states in the second irrep *etc.*

RECOMMENDATION:

None

**DIP_SINGLETS**

Sets the number of singlet DIP roots to find. Valid only for closed-shell references.

TYPE:

INTEGER/INTEGER ARRAY

DEFAULT:

0 Do not look for any singlet DIP states.

OPTIONS:

$[i, j, k \ldots]$ Find $i$ DIP singlet states in the first irrep, $j$ states in the second irrep *etc.*

RECOMMENDATION:

None

**DIP_TRIPLETS**

Sets the number of triplet DIP roots to find. Valid only for closed-shell references.

TYPE:

INTEGER/INTEGER ARRAY

DEFAULT:

0 Do not look for any DIP triplet states.

OPTIONS:

$[i, j, k \ldots]$ Find $i$ DIP triplet states in the first irrep, $j$ states in the second irrep *etc.*

RECOMMENDATION:

None

**Note:** It is a symmetry of a *transition* rather than that of a *target state* which is specified in excited state calculations. The symmetry of the target state is a product of the symmetry of the reference state and the transition. For closed-shell molecules, the former is fully symmetric and the symmetry of the target state is the same as that of transition, however, for open-shell references this is not so.

**Note:** For the XX_STATES options, Q-CHEM will increase the number of roots if it suspects degeneracy, or change it to a smaller value, if it cannot generate enough guess vectors to start the calculations.

**EOM_FAKE_IPEA**

If TRUE, calculates fake EOM-IP or EOM-EA energies and properties using the diffuse orbital trick. Default for EOM-EA and Dyson orbital calculations in CCMAN.

TYPE:

LOGICAL

DEFAULT:

FALSE (use proper EOM-IP code)

OPTIONS:

FALSE, TRUE

RECOMMENDATION:

None. This feature only works for CCMAN.

**Note:** When EOM_FAKE_IPEA is set to TRUE, it can change the convergence of Hartree-Fock iterations compared to the same job without EOM_FAKE_IPEA, because a very diffuse basis function is added to a center of symmetry *before* the Hartree-Fock iterations start. For the same reason, BASIS2 keyword is incompatible with EOM_FAKE_IPEA. In order to read Hartree-Fock guess from a previous job, you must specify EOM_FAKE_IPEA (even if you do not request for any correlation or excited states) in that previous job. Currently, the second moments of electron density and Mulliken charges and spin densities are incorrect for the EOM-IP/EA-CCSD target states.

**EOM_USER_GUESS**

Specifies if user-defined guess will be used in EOM calculations.

TYPE:

LOGICAL

DEFAULT:

FALSE

OPTIONS:

TRUE Solve for a state that has maximum overlap with a trans-n specified in *$eom_user_guess*.

RECOMMENDATION:

The orbitals are ordered by energy, as printed in the beginning of the CCMAN2 output.
Not available in CCMAN.

**EOM_SHIFT**

Specifies energy shift in EOM calculations.

TYPE:

INTEGER

DEFAULT:

0

OPTIONS:

$n$ corresponds to $n \cdot 10^{-3}$ hartree shift (i.e., 11000 = 11 hartree); solve for eigenstates around this value.

RECOMMENDATION:

Not available in CCMAN.

**EOM_NGUESS_DOUBLES**

Specifies number of excited state guess vectors which are double excitations.

TYPE:

INTEGER

DEFAULT:

0

OPTIONS:

$n$ Include $n$ guess vectors that are double excitations

RECOMMENDATION:

This should be set to the expected number of doubly excited states, otherwise they may not be found.

**EOM_NGUESS_SINGLES**

Specifies number of excited state guess vectors that are single excitations.

TYPE:

INTEGER

DEFAULT:

Equal to the number of excited states requested

OPTIONS:

$n$ Include $n$ guess vectors that are single excitations

RECOMMENDATION:

Should be greater or equal than the number of excited states requested, unless .

**EOM_PRECONV_SINGLES**

When not zero, singly excited vectors are converged prior to a full excited states calculation. Sets the maximum number of iterations for pre-converging procedure.

TYPE:

INTEGER

DEFAULT:

0

OPTIONS:

0 do not pre-converge

1 pre-converge singles

RECOMMENDATION:

Sometimes helps with problematic convergence.

**Note:** In CCMAN, setting EOM_PRECONV_SINGLES = N would result in N Davidson iterations pre-converging singles.

**EOM_PRECONV_DOUBLES**

When not zero, doubly excited vectors are converged prior to a full excited states calculation. Sets the maximum number of iterations for pre-converging procedure

TYPE:

INTEGER

DEFAULT:

0

OPTIONS:

0 Do not pre-converge

N Perform N Davidson iterations pre-converging doubles.

RECOMMENDATION:

Occasionally necessary to ensure a doubly excited state is found. Also used in DSF calculations instead of EOM_PRECONV_SINGLES

**Note:** Not available in CCMAN2.

**EOM_PRECONV_SD**

When not zero, EOM vectors are pre-converged prior to a full excited states calculation. Sets the maximum number of iterations for pre-converging procedure.

TYPE:

INTEGER

DEFAULT:

0

OPTIONS:

0 do not pre-converge

N perform N Davidson iterations pre-converging singles and doubles.

RECOMMENDATION:

Occasionally necessary to ensure that all low-lying states are found. Also, very useful in EOM(2,3) calculations.

None

**Note:** Not available in CCMAN2.

**EOM_DAVIDSON_CONVERGENCE**

Convergence criterion for the RMS residuals of excited state vectors.

TYPE:

INTEGER

DEFAULT:

5 Corresponding to $10^{-5}$

OPTIONS:

$n$ Corresponding to $10^{-n}$ convergence criterion

RECOMMENDATION:

Use the default. Normally this value be the same as EOM_DAVIDSON_THRESHOLD.

**EOM_DAVIDSON_THRESHOLD**

Specifies threshold for including a new expansion vector in the iterative Davidson diagonalization. Their norm must be above this threshold.

TYPE:

INTEGER

DEFAULT:

00103 Corresponding to 0.00001

OPTIONS:

$abcde$ Integer code is mapped to $abc \times 10^{-(de+2)}$, i.e., 02505->2.5$\times 10^{-6}$

RECOMMENDATION:

Use the default unless converge problems are encountered. Should normally be set to the same values as EOM_DAVIDSON_CONVERGENCE, if convergence problems arise try setting to a value slightly larger than EOM_DAVIDSON_CONVERGENCE.

**EOM_DAVIDSON_MAXVECTORS**

Specifies maximum number of vectors in the subspace for the Davidson diagonalization.

TYPE:

INTEGER

DEFAULT:

60

OPTIONS:

$n$ Up to $n$ vectors per root before the subspace is reset

RECOMMENDATION:

Larger values increase disk storage but accelerate and stabilize convergence.

**EOM_DAVIDSON_MAX_ITER**

Maximum number of iteration allowed for Davidson diagonalization procedure.

TYPE:

INTEGER

DEFAULT:

30

OPTIONS:

$n$ User-defined number of iterations

RECOMMENDATION:

Default is usually sufficient

**EOM_IPEA_FILTER**

If TRUE, filters the EOM-IP/EA amplitudes obtained using the diffuse orbital implementation (see EOM_FAKE_IPEA). Helps with convergence.

TYPE:

LOGICAL

DEFAULT:

FALSE (EOM-IP or EOM-EA amplitudes will not be filtered)

OPTIONS:

FALSE, TRUE

RECOMMENDATION:

None

**Note:** Not available in CCMAN2.

**CC_FNO_THRESH**
Initialize the FNO truncation and sets the threshold to be used for both cutoffs (OCCT and POVO).
TYPE:
INTEGER
DEFAULT:
None
OPTIONS:

| | |
|---|---|
| range | 0000-10000 |
| $abcd$ | Corresponding to $ab.cd\%$ |

RECOMMENDATION:
None

**CC_FNO_USEPOP**
Selection of the truncation scheme.
TYPE:
INTEGER
DEFAULT:
1 OCCT
OPTIONS:
0 POVO
RECOMMENDATION:
None

**SCALE_NUCLEAR_CHARGE**
Scales charge of each nuclei by a certain value. The nuclear repulsion energy is calculated for the unscaled nuclear charges.
TYPE:
INTEGER
DEFAULT:
0 No scaling.
OPTIONS:
$n$ A total positive charge of (1+$n$/100)e is added to the molecule.
RECOMMENDATION:
NONE

**ADD_CHARGED_CAGE**

Add a point charge cage of a given radius and total charge.

TYPE:

INTEGER

DEFAULT:

0 No cage.

OPTIONS:

0 No cage.

1 Dodecahedral cage.

2 Spherical cage.

RECOMMENDATION:

Spherical cage is expected to yield more accurate results, especially for small radii.

**CAGE_RADIUS**

Defines radius of the charged cage.

TYPE:

INTEGER

DEFAULT:

225

OPTIONS:

$n$ radius is $n$/100 Å.

RECOMMENDATION:

None

**CAGE_POINTS**

Defines number of point charges for the spherical cage.

TYPE:

INTEGER

DEFAULT:

100

OPTIONS:

$n$ Number of point charges to use.

RECOMMENDATION:

None

**CAGE_CHARGE**

Defines the total charge of the cage.

TYPE:

INTEGER

DEFAULT:

400 Add a cage charged +4e.

OPTIONS:

$n$ Total charge of the cage is $n$/100 a.u.

RECOMMENDATION:

None

### 6.7.13 Examples

**Example 6.27** EOM-EE-OD and EOM-EE-CCSD calculations of the singlet excited states of formaldehyde

```
$molecule
   0 1
   O
   C  1  R1
   H  2  R2  1  A
   H  2  R2  1  A  3  180.

   R1  =  1.4
   R2  =  1.0
   A   =  120.
$end

$rem
   METHOD      eom-od
   BASIS       6-31+g
   EE_STATES   [2,2,2,2]
$end

@@@

$molecule
   read
$end

$rem
   METHOD        eom-ccsd
   BASIS         6-31+g
   EE_SINGLETS   [2,2,2,2]
   EE_TRIPLETS   [2,2,2,2]
$end
```

**Example 6.28** EOM-EE-CCSD calculations of the singlet excited states of PYP using Cholesky decomposition

```
$molecule
0 1
...too long to enter...
$end

$rem
   METHOD          eom-ccsd
   BASIS           aug-cc-pVDZ
   PURECART        1112
   N_FROZEN_CORE   fc
   CC_T_CONV       4
   CC_E_CONV       6
   CHOLESKY_TOL    2    using CD/1e-2 threshold
   EE_SINGLETS     [2,2]
$end
```

**Example 6.29** EOM-SF-CCSD calculations for methylene from high-spin $^3B_2$ reference

```
$molecule
   0 3
   C
   H  1 rCH
   H  1 rCH 2 aHCH

   rCH   = 1.1167
   aHCH  = 102.07
$end

$rem
   METHOD      eom-ccsd
   BASIS       6-31G*
   SCF_GUESS   core
   SF_STATES   [2,0,0,2]   Two singlet A1 states and singlet and triplet B2 states
$end
```

**Example 6.30** EOM-SF-MP2 calculations for $SiH_2$ from high-spin $^3B_2$ reference. Both energies and properties are computed.

```
$molecule
   0 3
   Si
   H  1 1.5145
   H  1 1.5145 2 92.68
$end

$rem
   BASIS             = cc-pVDZ
   UNRESTRICTED      = true
   SCF_CONVERGENCE   = 8
   METHOD            = eom-mp2
   SF_STATES         = [1,1,0,0]
   CC_EOM_PROP_TE    = true   ! Compute <S^2> of excited states
$end
```

**Example 6.31** EOM-IP-CCSD calculations for $NO_3$ using closed-shell anion reference

```
$molecule
   -1 1
   N
   O  1  r1
   O  1  r2   2 A2
   O  1  r2   2 A2    3 180.0

   r1    = 1.237
   r2    = 1.237
   A2    = 120.00
$end

$rem
   METHOD       eom-ccsd
   BASIS        6-31G*
   IP_STATES    [1,1,2,1]    ground and excited  states of the radical
$end
```

**Example 6.32** EOM-IP-CCSD calculation using FNO with OCCT=99%.

```
$molecule
   0 1
   O
   H  1  1.0
   H  1  1.0  2  100.
$end

$rem
   METHOD          eom-ccsd
   BASIS           6-311+G(2df,2pd)
   IP_STATES       [1,0,1,1]
   CC_FNO_THRESH   9900        99% of the total natural population recovered
$end
```

**Example 6.33** EOM-IP-MP2 calculation of the three low lying ionized states of the phenolate anion

```
$molecule
   0 1
   C   -0.189057  -1.215927  -0.000922
   H   -0.709319  -2.157526  -0.001587
   C    1.194584  -1.155381  -0.000067
   H    1.762373  -2.070036  -0.000230
   C    1.848872   0.069673   0.000936
   H    2.923593   0.111621   0.001593
   C    1.103041   1.238842   0.001235
   H    1.595604   2.196052   0.002078
   C   -0.283047   1.185547   0.000344
   H   -0.862269   2.095160   0.000376
   C   -0.929565  -0.042566  -0.000765
   O   -2.287040  -0.159171  -0.001759
   H   -2.663814   0.725029   0.001075
$end

$rem
   THRESH      16
   CC_MEMORY   30000
   BASIS       6-31+g(d)
   METHOD      eom-mp2
   IP_STATES   [3]
$end
```

**Example 6.34** EOM-EE-MP2T calculation of the $H_2$ excitation energies

```
$molecule
   0 1
   H   0.0000   0.0000   0.0000
   H   0.0000   0.0000   0.7414
$end

$rem
   THRESH     16
   BASIS      cc-pvdz
   METHOD     eom-mp2t
   EE_STATES  [3,0,0,0,0,0,0,0]
$end
```

**Example 6.35** EOM-EA-CCSD calculation of CN using user-specified guess

```
$molecule
   +1 1
   C
   N  1  1.1718
$end

$rem
   METHOD          = eom-ccsd
   BASIS          = 6-311+g*
   EA_STATES      = [1,1,1,1]
   CC_EOM_PROP    = true
   EOM_USER_GUESS = true   ! attach to HOMO, HOMO+1, and HOMO+3
$end

$eom_user_guess
   1  2  4
$end
```

**Example 6.36** DSF-CIDT calculation of methylene starting with quintet reference

```
$molecule
   0 5
   C
   H 1 CH
   H 1 CH 2 HCH

   CH  = 1.07
   HCH = 111.0
$end

$rem
   METHOD               cisdt
   BASIS                6-31G
   DSF_STATES           [0,2,2,0]
   EOM_NGUESS_SINGLES   0
   EOM_NGUESS_DOUBLES   2
$end
```

**Example 6.37** EOM-EA-CCSD job for cyano radical. We first do Hartree-Fock calculation for the cation in the basis set with one extremely diffuse orbital (EOM_FAKE_IPEA) and use these orbitals in the second job. We need make sure that the diffuse orbital is occupied using the OCCUPIED keyword. No SCF iterations are performed as the diffuse electron and the molecular core are uncoupled. The attached states show up as "excited" states in which electron is promoted from the diffuse orbital to the molecular ones.

```
$molecule
   +1 1
   C
   N 1 bond

   bond   1.1718
$end

$rem
   METHOD            hf
   BASIS             6-311+G*
   PURECART          111
   SCF_CONVERGENCE   8
   EOM_FAKE_IPEA     true
$end

@@@

$molecule
   0 2
   C
   N 1 bond

   bond   1.1718
$end

$rem
   BASIS            6-311+G*
   PURECART         111
   SCF_GUESS        read
   MAX_SCF_CYCLES   0
   METHOD           eom-ccsd
   CC_DOV_THRESH    2501   use thresh for CC iters with convergence problems
   EA_STATES        [2,0,0,0]
   EOM_FAKE_IPEA    true
$end

$occupied
   1 2 3 4 5 6 14
   1 2 3 4 5 6
$end
```

**Example 6.38** EOM-DIP-CCSD calculation of electronic states in methylene using charged cage stabilization method.

```
$molecule
   -2 1
   C   0.000000     0.000000     0.106788
   H  -0.989216     0.000000    -0.320363
   H   0.989216     0.000000    -0.320363
$end

$rem
   BASIS                     = 6-311g(d,p)
   SCF_ALGORITHM             = diis_gdm
   SYMMETRY                  = false
   METHOD                    = eom-ccsd
   CC_SYMMETRY               = false
   DIP_SINGLETS              = [1]  ! Compute one EOM-DIP singlet state
   DIP_TRIPLETS              = [1]  ! Compute one EOM-DIP triplet state
   EOM_DAVIDSON_CONVERGENCE = 5
   CC_EOM_PROP               = true ! Compute excited state properties
   ADD_CHARGED_CAGE          = 2    ! Install a charged sphere around the molecule
   CAGE_RADIUS               = 225  ! Radius = 2.25 A
   CAGE_CHARGE               = 500  ! Charge = +5 a.u.
   CAGE_POINTS               = 100  ! Place 100 point charges
   CC_MEMORY                 = 256  ! Use 256Mb of memory, increase for larger jobs
$end
```

**Example 6.39** EOM-EE-CCSD calculation of excited states in NO$^-$ using scaled nuclear charge stabilization method.

```
$molecule
   -1 1
    N  -1.08735    0.0000    0.0000
    O   1.08735    0.0000    0.0000
$end

$rem
   INPUT_BOHR           = true
   BASIS                = 6-31g
   SYMMETRY             = false
   CC_SYMMETRY          = false
   METHOD               = eom-ccsd
   EE_SINGLETS          = [2]  ! Compute two EOM-EE singlet excited states
   EE_TRIPLETS          = [2]  ! Compute two EOM-EE triplet excited states
   CC_REF_PROP          = true ! Compute ground state properties
   CC_EOM_PROP          = true ! Compute excited state properties
   CC_MEMORY            = 256  ! Use 256Mb of memory, increase for larger jobs
   SCALE_NUCLEAR_CHARGE = 180  ! Adds +1.80e charge to the molecule
$end
```

**Example 6.40** EOM-EE-CCSD calculation for phenol with user-specified guess requesting the EE transition from the occupied orbital number 24 (3 A") to the virtual orbital number 2 (23 A')

```
$molecule
   0 1
   C    0.935445   -0.023376    0.000000
   C    0.262495    1.197399    0.000000
   C   -1.130915    1.215736    0.000000
   C   -1.854154    0.026814    0.000000
   C   -1.168805   -1.188579    0.000000
   C    0.220600   -1.220808    0.000000
   O    2.298632   -0.108788    0.000000
   H    2.681798    0.773704    0.000000
   H    0.823779    2.130309    0.000000
   H   -1.650336    2.170478    0.000000
   H   -2.939976    0.044987    0.000000
   H   -1.722580   -2.123864    0.000000
   H    0.768011   -2.158602    0.000000
$end

$rem
   METHOD                     EOM-CCSD
   BASIS                      6-31+G(d,p)
   CC_MEMORY                  3000   ccman2 memory
   MEM_STATIC                 250
   CC_T_CONV                  4      T-amplitudes convergence threshold
   CC_E_CONV                  6      Energy convergence threshold
   EE_STATES                  [0,1]  Calculate 1 A" states
   EOM_DAVIDSON_CONVERGENCE   5      Convergence threshold for the Davidson procedure
   EOM_USER_GUESS             true   Use user guess from $eom_user_guess section
$end

$eom_user_guess
   24   Transition from the occupied orbital number 24(3 A")
   2    to the virtual orbital number 2 (23 A')
$end
```

**Example 6.41** Complex-scaled EOM-EE calculation for He. All roots of Ag symmetry are computed (full diagonalization)

```
$molecule
   0 1
   He  0    0  0.0
$end

$rem
   COMPLEX_CCMAN         1         engage complex_ccman
   METHOD                EOM-CCSD
   BASIS                 gen       use general basis
   PURECART              1111
   EE_SINGLETS           [2000,0,0,0,0,0,0,0]  compute all Ag excitations
   EOM_DAVIDSON_CONV     5
   EOM_DAVIDSON_THRESH   5
   EOM_NGUESS_SINGLES    2000      Number of guess singles
   EOM_NGUESS_DOUBLES    2000      Number of guess doubles
   CC_MEMORY             5000
   MEM_TOTAL             3000
$end

$complex_ccman
   CS_HF 1                         Use complex HF
   CS_ALPHA 1000                   Set alpha equal 1
   CS_THETA 300                    Set theta (angle) equals 0.3 (radian)
$end

$basis
He   0
S    4    1.000000
   2.34000000E+02    2.58700000E-03
   3.51600000E+01    1.95330000E-02
   7.98900000E+00    9.09980000E-02
   2.21200000E+00    2.72050000E-01
S    1    1.000000
   6.66900000E-01    1.00000000E+00
S    1    1.000000
   2.08900000E-01    1.00000000E+00
P    1    1.000000
   3.04400000E+00    1.00000000E+00
P    1    1.000000
   7.58000000E-01    1.00000000E+00
D    1    1.000000
   1.96500000E+00    1.00000000E+00
S    1    1.000000
   5.13800000E-02    1.00000000E+00
P    1    1.000000
   1.99300000E-01    1.00000000E+00
D    1    1.000000
   4.59200000E-01    1.00000000E+00
S    1    1.000000
   2.44564000E-02    1.00000000E+00
S    1    1.000000
   1.2282000E-02    1.00000000E+00
S    1    1.000000
```

```
   6.1141000E-03    1.00000000E+00
P   1   1.0
    8.130000e-02    1.0
P   1   1.0
    4.065000e-02    1.0
P   1   1.0
    2.032500e-02    1.0
D   1   1.0
    2.34375e-01    1.0
D   1   1.0
    1.17187e-01    1.0
D   1   1.0
    5.85937e-02    1.0
****
$end
```

**Example 6.42** CAP-augmented EOM-EA-CCSD calculation for N2-. aug-cc-pVTZ basis augmented by the 3s3p3d diffuse functions placed in the COM. 2 EA states are computed for CAP strength eta=0.002

```
$molecule
   0 1
   N   0.0  0.0 -0.54875676501
   N   0.0  0.0  0.54875676501
   Gh  0.0  0.0  0.0
$end

$rem
   COMPLEX_CCMAN   1             engage complex_ccman
   METHOD          EOM-CCSD
   BASIS           gen           use general basis
   EA_STATES       [0,0,2,0,0,0,0,0]  compute electron attachment energies
   CC_MEMORY       5000          ccman2 memory
   MEM_TOTAL       2000
   CC_EOM_PROP     true          compute excited state properties
$end

$complex_ccman
   CS_HF 1           Use complex HF
   CAP_ETA 200       Set strength of CAP potential 0.002
   CAP_X 2760        Set length of the box along x dimension
   CAP_Y 2760        Set length of the box along y dimension
   CAP_Z 4880        Set length of the box along z dimension
   CAP_TYPE 1        Use cuboid CAP
$end

$basis
N    0
aug-cc-pvtz
****
Gh   0
S    1    1.000000
   2.88000000E-02    1.00000000E+00
S    1    1.000000
   1.44000000E-02    1.00000000E+00
S    1    1.000000
   0.72000000E-02    1.00000000E+00
P    1    1.000000
```

```
   2.45000000E-02    1.00000000E+00
P    1    1.000000
   1.22000000E-02    1.00000000E+00
P    1    1.000000
   0.61000000E-02    1.00000000E+00
D    1    1.000000
   0.755000000E-01    1.00000000E+00
D    1    1.000000
   0.377500000E-01    1.00000000E+00
D    1    1.000000
   0.188750000E-01    1.00000000E+00
****
$end
```

**Example 6.43** Formaldehyde, calculating EOM-IP-CCSD-S(D) and EOM-IP-MP2-S(D) energies of 4 valence ionized states

```
$molecule
   0 1
   C
   H  1  1.096135
   H  1  1.096135  2  116.191164
   O  1  1.207459  2  121.904418  3  -180.000000 0
$end

$rem
   METHOD       eom-ccsd-s(d)
   BASIS        6-31G*
   IP_STATES    [1,1,1,1]
$end

@@@

$molecule
   read
$end

$rem
   METHOD       eom-mp2-s(d)
   BASIS        6-31G*
   IP_STATES    [1,1,1,1]
$end
```

**Example 6.44** Formaldehyde, calculating EOM-EE-CCSD states with C-PCM method.

```
$molecule
   0 1
   O
   C,1,R1
   H,2,R2,1,A
   H,2,R2,1,A,3,180.

   R1 = 1.4
   R2 = 1.0
   A  = 120.
$end
```

```
$rem
   METHOD            eom-ccsd
   BASIS             cc-pvdz
   EE_STATES         [4]
   SOLVENT_METHOD    pcm
$end

$pcm
   theory           cpcm
$end

$solvent
   dielectric       4.34
   dielectric_infi  1.829
$end
```

**Example 6.45** $NO_2^-$, calculating EOM-IP-CCSD states with C-PCM method.

```
$molecule
   -1 1
   N1
   O2 N1 RNO
   O3 N1 RNO O2 AONO

   RNO  = 1.305
   AONO = 106.7
$end

$rem
   METHOD            eom-ccsd
   BASIS             cc-pvdz
   IP_STATES         [2]
   SOLVENT_METHOD    pcm
$end

$pcm
   theory           cpcm
$end

$solvent
   dielectric       4.34
   dielectric_infi  1.829
$end
```

### 6.7.14 Non-Hartree-Fock Orbitals in EOM Calculations

In cases of problematic open-shell references, *e.g.*, strongly spin-contaminated doublet, triplet or quartet states, one may choose to use DFT orbitals. This can be achieved by first doing DFT calculation and then reading the orbitals and turning Hartree-Fock off (by setting SCF_GUESS = READ MAX_SCF_CYCLES = 0 in the CCMAN or CCMAN2 job). In CCMAN, a more convenient way is just to specify EXCHANGE, *e.g.*, if EXCHANGE = B3LYP, B3LYP orbitals will be computed and used.

**Note:** Using non-HF exchange in CCMAN2 is not possible.

## 6.7.15 Analytic Gradients and Properties for the CCSD and EOM-XX-CCSD Methods

The coupled-cluster package in Q-CHEM can calculate properties of target EOM states including permanent dipoles, static polarizabilities, $\langle S^2 \rangle$ and $\langle R^2 \rangle$ values, nuclear gradients (and geometry optimizations). The target state of interest is selected by CC_STATE_TO_OPT *$rem*, which specifies the symmetry and the number of the EOM state. In addition to state properties, calculations of various interstate properties are available (transition dipoles, two-photon absorption transition moments (and cross-sections), spin-orbit couplings).

Analytic gradients are available for the CCSD and all EOM-CCSD methods for both closed- and open-shell references (UHF and RHF only), including frozen core/virtual functionality[72] (see also Section 5.13). These calculations should be feasible whenever the corresponding single-point energy calculation is feasible.

**Note:** Gradients for ROHF and non-HF (*e.g.*, B3LYP) orbitals are not yet available.

For the CCSD and EOM-CCSD wave functions, Q-CHEM currently can calculate permanent and transition dipole moments, oscillator strengths, $\langle R^2 \rangle$ (as well as XX, YY and ZZ components separately, which is useful for assigning different Rydberg states, *e.g.*, $3p_x$ vs. $3s$, *etc.*), and the $\langle S^2 \rangle$ values. Interface of the CCSD and EOM-CCSD codes with the NBO 5.0 package is also available. Furthermore, excited state analyses can be requested for EOM-CCSD excited states. For EOM-MP2, only state properties (dipole moments, $\langle R^2 \rangle$, $\langle S^2 \rangle$ are available). Similar functionality is available for some EOM-OD and CI models (CCMAN only).

Analysis of the EOM-CC wave functions can also be performed; see Section 10.2.7.

Users must be aware of the point group symmetry of the system being studied and also the symmetry of the excited (target) state of interest. It is possible to turn off the use of symmetry using the CC_SYMMETRY. If set to FALSE the molecule will be treated as having $C_1$ symmetry and all states will be of $A$ symmetry.

#### 6.7.15.1 Transition moments and cross-sections for two-photon absorption within EOM-EE-CCSD

Calculation of transition moments and cross-sections for two-photon absorption for EOM-EE-CCSD wave functions is available in Q-CHEM (CCMAN2 only). Both CCSD-EOM and EOM-EOM transitions can be computed. The formalism is described in Ref. 87. This feature is available both for canonical and RI/CD implementations. Relevant keywords are CC_EOM_2PA (turns on the calculation), CC_STATE_TO_OPT (used for EOM-EOM transitions); additional customization can be performed using the *$2pa* section.

The *$2pa* section is used to specify the range of frequency-pairs satisfying the resonance condition. If *$2pa* section is absent in the input, the transition moments are computed for 2 degenerate photons with total energy matching the excitation energy of each target EOM state (for CCSD-EOM) or each EOM-EOM energy difference (for EOM-EOM transitions): $2h\nu = E_{ex}$

```
$2pa                 Non-degenerate resonant 2PA
N_2PA_POINTS 6       Number of frequency pairs
OMEGA_1 500000 10000 Scans 500 cm$^{-1}$ to 550 cm$^{-1}$
                     in steps of 10 cm$^{-1}$
$end
```

N_2PA_POINTS is the number of frequency pairs across the spectrum. The first value associated with OMEGA_1 is the frequency $\times 1000$ in $\mathrm{cm}^{-1}$ at the start of the spectrum and the second value is the step size $\times 1000$ in $\mathrm{cm}^{-1}$. The frequency of the second photon at each step is determined within the code as the excitation energy minus OMEGA_1.

#### 6.7.15.2 Calculations of Spin-Orbit Couplings Using EOM-CC Wave Functions

Calculations of spin-orbit couplings (SOCs) for EOM-CC wave functions is available in CCMAN2[88]. We employ a perturbative approach in which SOCs are computed as matrix elements of the respective part of the Breit-Pauli Hamiltonian using zero-order non-relativistic wave functions. Both the full two-electron treatment and the mean-field approximation (a partial account of the two-electron contributions) are available for the EOM-EE/SF/IP/EA wave functions, as well as between the CCSD reference and EOM-EE/SF. To enable SOC calculation, transition properties between EOM states must be enabled via CC_TRANS_PROP, and SOC requested using CALC_SOC. By default, one-electron and mean-field two-electron couplings will be computed. Full two-electron coupling calculation is activated by setting CC_EOM_PROP_TE.

As with other EOM transition properties, the initial EOM state is set by CC_STATE_TO_OPT, and couplings are computed between that state and all other EOM states. In the absence of CC_STATE_TO_OPT, SOCs are computed between the reference state and all EOM-EE or EOM-SF states.

**Note:** In a spin-restricted case, such as EOM-EE calculations using closed-shell reference state, SOCs between the singlet and triplet EOM manifolds cannot be computed (only SOCs between the reference state and EOM triplets can be calculated). To compute SOCs between EOM-EE singlets and EOM-EE triplets, run the same job with UNRESTRICTED=TRUE, such that triplets and singlets appear in the same manifold.

#### 6.7.15.3 Calculations of Non-Adiabatic Couplings Using EOM-CC Wave Functions

Calculations of non-adiabatic (derivative) couplings (NACs) for EOM-CC wave functions is available in CCMAN2. We employ Szalay's approach in which couplings are computed by a modified analytic gradient code, via "summed states"[89]

$$h^x_{IJ} \equiv \langle \Psi_I | H^x | \Psi_J \rangle = \frac{1}{2}\left(G_{(I+J)} - G_I - G_J\right), \tag{6.52}$$

where, $G_I$, $G_J$, and $G_{IJ}$ are analytic gradients for states $I$, $J$, and a ficticious summed state $|\Psi_{I+J}\rangle \equiv |\Psi_I\rangle + |\Psi_J\rangle$. Currenlty, NACs for EE/IP/EA are available[90]. NACs between all pairs of the traget EOM states (and the reference state, in the case of EOM-EE) are computed.

**Note:** Within this approach for NAC caculations, the symmetry should be turned off by using either CC_SYMMETRY = FALSE or SYM_IGNORE = TRUE (the latter will also disable molecular re-orientation). Note that the individual components of the NAC vector depend on the molecular orientation.

#### 6.7.15.4 Calculations of Static Polarizabilities for CCSD and EOM-CCSD Wave Functions

Calculation of the static dipole polarizability for the CCSD and EOM-EE/SF wave function is available in CCMAN2. CCSD polarizabilities are calculated as second derivatives of the CCSD energy[91]. Only the response of the cluster amplitudes is taken into the account; orbital relaxation is not included. Currently, this feature is available for canonical implementation only. Relevant keywords are CC_POL (turns on the calculation), EOM_POL (turns on the calculation for EOM states, otherwise, only polarizability of CCSD will be computed), and CC_FULLRESPONSE (must be set to TRUE).

**Note:** Only EOM-CCSD polarizabilities are available for EE and SF wave functions only.

### 6.7.16 EOM-CC Optimization and Properties Job Control

**CC_STATE_TO_OPT**

Specifies which state to optimize (or from which state compute EOM-EOM inter-state properties).

TYPE:

INTEGER ARRAY

DEFAULT:

None

OPTIONS:

$[i,j]$ optimize the $j$th state of the $i$th irrep.

RECOMMENDATION:

None

**Note:** The state number should be smaller or equal to the number of excited states calculated in the corresponding irrep.

**Note:** If analytic gradients are not available, the finite difference calculations will be performed and the symmetry will be turned off. In this case, CC_STATE_TO_OPT should be specified assuming $C_1$ symmetry, *i.e.*, as [1,N] where N is the number of state to optimize (the states are numbered from 1).

**CC_EOM_PROP**

Whether or not the non-relaxed (expectation value) one-particle EOM-CCSD target state properties will be calculated. The properties currently include permanent dipole moment, the second moments $\langle X^2 \rangle$, $\langle Y^2 \rangle$, and $\langle Z^2 \rangle$ of electron density, and the total $\langle R^2 \rangle = \langle X^2 \rangle + \langle Y^2 \rangle + \langle Z^2 \rangle$ (in atomic units). Incompatible with JOBTYPE=FORCE, OPT, FREQ.

TYPE:

LOGICAL

DEFAULT:

FALSE (no one-particle properties will be calculated)

OPTIONS:

FALSE, TRUE

RECOMMENDATION:

Additional equations (EOM-CCSD equations for the left eigenvectors) need to be solved for properties, approximately doubling the cost of calculation for each irrep. The cost of the one-particle properties calculation itself is low. The one-particle density of an EOM-CCSD target state can be analyzed with NBO or libwfa packages by specifying the state with CC_STATE_TO_OPT and requesting NBO = TRUE and CC_EOM_PROP = TRUE.

**CC_TRANS_PROP**

Whether or not the transition dipole moment (in atomic units) and oscillator strength for the EOM-CCSD target states will be calculated. By default, the transition dipole moment is calculated between the CCSD reference and the EOM-CCSD target states. In order to calculate transition dipole moment between a set of EOM-CCSD states and another EOM-CCSD state, the CC_STATE_TO_OPT must be specified for this state.

TYPE:

LOGICAL

DEFAULT:

FALSE (no transition dipole and oscillator strength will be calculated)

OPTIONS:

FALSE, TRUE

RECOMMENDATION:

Additional equations (for the left EOM-CCSD eigenvectors plus lambda CCSD equations in case if transition properties between the CCSD reference and EOM-CCSD target states are requested) need to be solved for transition properties, approximately doubling the computational cost. The cost of the transition properties calculation itself is low.

**CC_EOM_2PA**

Whether or not the transition moments and cross-sections for two-photon absorption will be calculated. By default, the transition moments are calculated between the CCSD reference and the EOM-CCSD target states. In order to calculate transition moments between a set of EOM-CCSD states and another EOM-CCSD state, the CC_STATE_TO_OPT must be specified for this state.

TYPE:

INTEGER

DEFAULT:

0 (do not compute 2PA transition moments)

OPTIONS:

1 Compute 2PA using the fastest algorithm (use $\tilde{\sigma}$-intermediates for canonical and $\sigma$-intermediates for RI/CD response calculations).

2 Use $\sigma$-intermediates for 2PA response equation calculations.

3 Use $\tilde{\sigma}$-intermediates for 2PA response equation calculations.

RECOMMENDATION:

Additional response equations (6 for each target state) will be solved, which increases the cost of calculations. The cost of 2PA moments is about 10 times that of energy calculation. Use the default algorithm. Setting CC_EOM_2PA $>$ 0 turns on CC_TRANS_PROP.

**CALC_SOC**

Whether or not the spin-orbit couplings between CC/EOM/ADC/CIS/TDDFT electronic states will be calculated. In the CC/EOM-CC suite, by default the couplings are calculated between the CCSD reference and the EOM-CCSD target states. In order to calculate couplings between EOM states, CC_STATE_TO_OPT must specify the initial EOM state.

TYPE:

LOGICAL

DEFAULT:

FALSE (no spin-orbit couplings will be calculated)

OPTIONS:

FALSE, TRUE

RECOMMENDATION:

One-electron and mean-field two-electron SOCs will be computed by default. To enable full two-electron SOCs, two-particle EOM properties must be turned on (see CC_EOM_PROP_TE).

**CALC_NAC**

Whether or not non-adiabatic couplings will be calculated for the EOM-CC, CIS, and TDDFT wave functions.

TYPE:

INTEGER

DEFAULT:

0 (do not compute NAC)

OPTIONS:

1 NYI for EOM-CC

2 Compute NACs using Szalay's approach (this what needs to be specified for EOM-CC).

RECOMMENDATION:

Additional response equations will be solved and gradients for all EOM states and for summed states will be computed, which increases the cost of calculations. Request only when needed and do not ask for too many EOM states.

**CC_POL**

Whether or not the static polarizability for the CCSD wave function will be calculated.

TYPE:

LOGICAL

DEFAULT:

FALSE (CCSD static polarizability will not be calculated)

OPTIONS:

FALSE, TRUE

RECOMMENDATION:

Static polarizabilities are expensive since they require solving three additional response equations. Do no request this property unless you need it.

**EOM_POL**

Whether or not the static polarizability for the EOM-CCSD wave function will be calculated.

TYPE:

LOGICAL

DEFAULT:

FALSE (EOM polarizability will not be calculated)

OPTIONS:

FALSE, TRUE

RECOMMENDATION:

Static polarizabilities are expensive since they require solving three additional response equations. Do no request this property unless you need it.

**EOM_REF_PROP_TE**

Request for calculation of non-relaxed two-particle EOM-CC properties. The two-particle properties currently include $\langle S^2 \rangle$. The one-particle properties also will be calculated, since the additional cost of the one-particle properties calculation is inferior compared to the cost of $\langle S^2 \rangle$. The variable CC_EOM_PROP must be also set to TRUE. Alternatively, CC_CALC_SSQ can be used to request $\langle S^2 \rangle$ calculation.

TYPE:

LOGICAL

DEFAULT:

FALSE (no two-particle properties will be calculated)

OPTIONS:

FALSE, TRUE

RECOMMENDATION:

The two-particle properties are computationally expensive since they require calculation and use of the two-particle density matrix (the cost is approximately the same as the cost of an analytic gradient calculation). Do not request the two-particle properties unless you really need them.

**CC_FULLRESPONSE**

Fully relaxed properties (including orbital relaxation terms) will be computed. The variable CC_EOM_PROP must be also set to TRUE.

TYPE:

LOGICAL

DEFAULT:

FALSE (no orbital response will be calculated)

OPTIONS:

FALSE, TRUE

RECOMMENDATION:

Not available for non-UHF/RHF references. Only available for EOM/CI methods for which analytic gradients are available.

**CC_SYMMETRY**

Controls the use of symmetry in coupled-cluster calculations

TYPE:

LOGICAL

DEFAULT:

TRUE

OPTIONS:

| | |
|---|---|
| TRUE | Use the point group symmetry of the molecule |
| FALSE | Do not use point group symmetry (all states will be of $A$ symmetry). |

RECOMMENDATION:

It is automatically turned off for any finite difference calculations, *e.g.* second derivatives.

**STATE_ANALYSIS**

Activates excited state analyses using libwfa.

TYPE:

LOGICAL

DEFAULT:

FALSE (no excited state analyses)

OPTIONS:

TRUE, FALSE

RECOMMENDATION:

Set to TRUE if excited state analysis is required, but also if plots of densities or orbitals are needed. For details see section 10.2.7.

### 6.7.17 Examples

**Example 6.46** Geometry optimization for the excited open-shell singlet state, $^1B_2$, of methylene followed by the calculations of the fully relaxed one-electron properties using EOM-EE-CCSD

```
$molecule
   0 1
   C
   H  1 rCH
   H  1 rCH 2 aHCH

   rCH    = 1.083
   aHCH   = 145.
$end

$rem
   JOBTYPE                    OPT
   METHOD                     EOM-CCSD
   BASIS                      cc-pVTZ
   SCF_GUESS                  CORE
   SCF_CONVERGENCE            9
   EE_SINGLETS                [0,0,0,1]
   EOM_NGUESS_SINGLES         2
   CC_STATE_TO_OPT            [4,1]
   EOM_DAVIDSON_CONVERGENCE   9    use tighter convergence for EOM amplitudes
$end
```

```
@@@

$molecule
   read
$end

$rem
   METHOD               EOM-CCSD
   BASIS                cc-pVTZ
   SCF_GUESS            READ
   EE_SINGLETS          [0,0,0,1]
   EOM_NGUESS_SINGLES   2
   CC_EOM_PROP          1  calculate properties for EOM states
   CC_FULLRESPONSE      1  use fully relaxed properties
$end
```

**Example 6.47** Property and transition property calculation on the lowest singlet state of $CH_2$ using EOM-SF-CCSD

```
$molecule
   0 3
   C
   H  1 rch
   H  1 rch 2 ahch

  rch  = 1.1167
  ahch = 102.07
$end

$rem
   METHOD             eom-ccsd
   BASIS              cc-pvtz
   SCF_GUESS          core
   SCF_CONVERGENCE    9
   SF_STATES          [2,0,0,3]   Get three 1^B2 and two 1^A1 SF states
   CC_EOM_PROP        1
   CC_TRANS_PROP      1
   CC_STATE_TO_OPT    [4,1] First EOM state in the 4th irrep
$end
```

**Example 6.48** Geometry optimization with tight convergence for the $^2A_1$ excited state of $CH_2Cl$, followed by calculation of non-relaxed and fully relaxed permanent dipole moment and $\langle S^2 \rangle$.

```
$molecule
   0 2
   H
   C   1  CH
   CL  2  CCL  1  CCLH
   H   2  CH   3  CCLH  1  DIH

   CH   = 1.096247
   CCL  = 2.158212
   CCLH = 122.0
   DIH  = 180.0
$end

$rem
```

```
   JOBTYPE                     OPT
   METHOD                      EOM-CCSD
   BASIS                       6-31G*  Basis Set
   SCF_GUESS                   SAD
   EOM_DAVIDSON_CONVERGENCE    9    EOM amplitude convergence
   CC_T_CONV                   9    CCSD amplitudes convergence
   EE_STATES                   [0,0,0,1]
   CC_STATE_TO_OPT             [4,1]
   EOM_NGUESS_SINGLES          2
   GEOM_OPT_TOL_GRADIENT       2
   GEOM_OPT_TOL_DISPLACEMENT   2
   GEOM_OPT_TOL_ENERGY         2
$end

@@@

$molecule
   read
$end

$rem
   METHOD             EOM-CCSD
   BASIS              6-31G*  Basis Set
   SCF_GUESS          READ
   EE_STATES          [0,0,0,1]
   CC_NGUESS_SINGLES  2
   CC_EOM_PROP        1   calculate one-electron properties
   CC_EOM_PROP_TE     1   and two-electron properties (S^2)
$end

@@@

$molecule
   read
$end

$rem
   METHOD              EOM-CCSD
   BASIS               6-31G*  Basis Set
   SCF_GUESS           READ
   EE_STATES           [0,0,0,1]
   EOM_NGUESS_SINGLES  2
   CC_EOM_PROP         1  calculate one-electron properties
   CC_EOM_PROP_TE      1  and two-electron properties (S^2)CC_EXSTATES_PROP 1
   CC_FULLRESPONSE     1  same as above, but do fully relaxed properties
$end
```

**Example 6.49** CCSD calculation on three $A_2$ and one $B_2$ state of formaldehyde. Transition properties will be calculated between the third $A_2$ state and all other EOM states

```
$molecule
   0  1
   O
   C  1  1.4
   H  2  1.0  1  120
   H  3  1.0  1  120
$end
```

```
$rem
   BASIS             6-31+G
   METHOD            EOM-CCSD
   EE_STATES         [0,3,0,1]
   CC_STATE_TO_OPT   [2,3]
   CC_TRANS_PROP     true
$end
```

**Example 6.50** EOM-IP-CCSD geometry optimization of X $^2B_2$ state of $H_2O^+$.

```
$molecule
   0 1
   H    0.774767     0.000000     0.458565
   O    0.000000     0.000000    -0.114641
   H   -0.774767     0.000000     0.458565
$end

$rem
   JOBTYPE           opt
   METHOD            eom-ccsd
   BASIS             6-311G
   IP_STATES         [0,0,0,1]
   CC_STATE_TO_OPT   [4,1]
$end
```

**Example 6.51** CAP-EOM-EA-CCSD geometry optimization of the $^2B_1$ anionic resonance state of formaldehyde. The applied basis is aug-cc-pVDZ augmented by 3s3p diffuse functions on heavy atoms.

```
$molecule
   0 1
   C       0.0000000000     0.0000000000     0.5721328608
   O       0.0000000000     0.0000000000    -0.7102635035
   H       0.9478180646     0.0000000000     1.1819748108
   H      -0.9478180646     0.0000000000     1.1819748108
$end

$rem
   JOBTYPE                    opt
   METHOD                     eom-ccsd
   BASIS                      gen
   SCF_CONVERGENCE            9
   CC_CONVERGENCE             9
   EOM_DAVIDSON_CONVERGENCE   9
   EA_STATES                  [0,0,0,2]
   CC_STATE_TO_OPT            [4,1]
   XC_GRID                    000250000974
   COMPLEX_CCMAN              1
$end

$complex_ccman
   CS_HF 1
   CAP_TYPE 1
   CAP_ETA 60
   CAP_X 3850
   CAP_Y 2950
   CAP_Z 6100
```

```
$end

$basis
 H   0
 S   3  1.00
       13.0100000          0.196850000E-01
       1.96200000          0.137977000
      0.444600000          0.478148000
 S   1  1.00
      0.122000000           1.00000000
 P   1  1.00
      0.727000000           1.00000000
 S   1  1.00
      0.297400000E-01       1.00000000
 P   1  1.00
      0.141000000           1.00000000
 ****
 C   0
 S   8  1.00
       6665.00000          0.692000000E-03
       1000.00000          0.532900000E-02
       228.000000          0.270770000E-01
       64.7100000          0.101718000
       21.0600000          0.274740000
       7.49500000          0.448564000
       2.79700000          0.285074000
      0.521500000          0.152040000E-01
 S   8  1.00
       6665.00000         -0.146000000E-03
       1000.00000         -0.115400000E-02
       228.000000         -0.572500000E-02
       64.7100000         -0.233120000E-01
       21.0600000         -0.639550000E-01
       7.49500000         -0.149981000
       2.79700000         -0.127262000
      0.521500000          0.544529000
 S   1  1.00
      0.159600000           1.00000000
 P   3  1.00
       9.43900000          0.381090000E-01
       2.00200000          0.209480000
      0.545600000          0.508557000
 P   1  1.00
      0.151700000           1.00000000
 D   1  1.00
      0.550000000           1.00000000
 S   1  1.00
      0.469000000E-01      1.00000000
 P   1  1.00
      0.404100000E-01      1.00000000
 D   1  1.00
      0.151000000          1.00000000
 S   1  1.00
      0.234500000E-01       1.00000000
 S   1  1.00
      0.117250000E-01       1.00000000
 S   1  1.00
      0.058625000E-01       1.00000000
 P   1  1.00
      0.202050000E-01      1.00000000
 P   1  1.00
      0.101025000E-01      1.00000000
 P   1  1.00
      0.050512500E-01      1.00000000
 ****
 O   0
 S   8  1.00
       11720.0000         0.710000000E-03
       1759.00000         0.547000000E-02
       400.800000         0.278370000E-01
       113.700000         0.104800000
       37.0300000         0.283062000
       13.2700000         0.448719000
       5.02500000         0.270952000
       1.01300000         0.154580000E-01
 S   8  1.00
       11720.0000        -0.160000000E-03
       1759.00000        -0.126300000E-02
       400.800000        -0.626700000E-02
       113.700000        -0.257160000E-01
       37.0300000        -0.709240000E-01
       13.2700000        -0.165411000
       5.02500000        -0.116955000
       1.01300000         0.557368000
 S   1  1.00
      0.302300000          1.00000000
 P   3  1.00
       17.7000000         0.430180000E-01
       3.85400000         0.228913000
       1.04600000         0.508728000
 P   1  1.00
      0.275300000          1.00000000
 D   1  1.00
       1.18500000          1.00000000
 S   1  1.00
      0.789600000E-01      1.00000000
 P   1  1.00
      0.685600000E-01      1.00000000
 D   1  1.00
      0.332000000          1.00000000
 S   1  1.00
      0.394800000E-01      1.00000000
 S   1  1.00
      0.197400000E-01      1.00000000
 S   1  1.00
      0.098700000E-01      1.00000000
 P   1  1.00
      0.342800000E-01      1.00000000
 P   1  1.00
      0.171400000E-01      1.00000000
 P   1  1.00
      0.085700000E-01      1.00000000
 ****
$end
```

**Example 6.52** Calculating resonant 2PA with degenerate photons.

```
$molecule
   0 1
   O
   H  1 0.959
   H  1 0.959 2 104.654
$end

$rem
   METHOD         eom-ccsd
   BASIS          aug-cc-pvtz
   EE_SINGLETS    [1,0,0,0]   1A_1 state
   CC_TRANS_PROP  1    Compute transition properties
   CC_EOM_2PA     1    Calculate 2PA cross-sections using the fastest algorithm
$end
```

**Example 6.53** Non-degenerate, resonant 2PA scan over a range of frequency pairs.

```
$molecule
   0 1
   O
   H  1 0.959
   H  1 0.959 2 104.654
$end

$rem
   METHOD         eom-ccsd
   BASIS          aug-cc-pvtz
   EE_SINGLETS    [2,0,0,0]  Two A_1 states
   CC_TRANS_PROP  1          Calculate transition properties
   CC_EOM_2PA     1          Calculate 2PA cross-sections using the fastest algorithm
$end

$2pa                Non-degenerate resonant 2PA
   n_2pa_points 11     Number of frequency pairs
   omega_1 500000 5000 Scans 500 cm$^{-1}$ to 550 cm$^{-1}$ in steps of 5 cm$^{-1}$
$end
```

**Example 6.54** Resonant 2PA with degenerate photons between two excited states.

```
$molecule
   0 1
   O
   H  1 0.959
   H  1 0.959 2 104.654
$end

$rem
   METHOD          eom-ccsd
   BASIS           aug-cc-pvtz
   EE_SINGLETS     [2,0,0,0] Two A_1 states
   STATE_TO_OPT    [1,1]     "Reference" state for transition properties is 1A_1 state
   CC_TRANS_PROP   1         Compute transition properties
   CC_EOM_2PA      1         Calculate 2PA cross-sections using the fastest algorithm
```

```
$end
```

**Example 6.55** Computation of spin-orbit couplings between closed-shell singlet and $M_S = 1$ triplet state in NH using EOM-SF-CCSD

```
$molecule
   0 3
   N
   H N 1.0450
$end

$rem
   METHOD          = eom-ccsd
   BASIS           = 6-31g
   SF_STATES       = [1,2,0,0]
   CC_TRANS_PROP   = true
   CALC_SOC        = true
   CC_STATE_TO_OPT = [1,1]
$end
```

**Example 6.56** Computation of non-adiabatic couplings between EOM-EE states within triplet (first job) and singlet (second job) manifolds

```
$molecule
+1 1
H          0.00000        0.00000        0.0
He         0.00000        0.00000        3.0
$end

$rem
JOBTYPE FORCE
BASIS cc-pVDZ
METHOD EOM-CCSD
INPUT_BOHR true
EE_TRIPLETS [2]
cc_eom_prop = true
SYM_IGNORE = TRUE   Do not reorient molecule and turn off symmetry
CALC_NAC = 2   Invoke Szalay NAC
eom_davidson_convergence = 9   ! tight davidson convergence
scf_convergence = 9            ! Hartree-Fock convergence threshold 1e-9
cc_convergence = 9
$end

@@@
$molecule
read
$end

$rem
JOBTYPE FORCE
BASIS cc-pVDZ
METHOD EOM-CCSD
INPUT_BOHR true
EE_STATES [2] singlets
SYM_IGNORE = TRUE   Do not reorient molecule and turn off symmetry
CALC_NAC = 2   Invoke Szalay NAC
eom_davidson_convergence = 9   ! tight davidson convergence
```

```
scf_convergence = 9            ! Hartree-Fock convergence threshold 1e-9
cc_convergence = 9
$end
```

**Example 6.57** Calculation of the static dipole polarizability of the CCSD wave function of Helium.

```
$molecule
   0 1
   He
$end

$rem
   METHOD            ccsd
   BASIS             cc-pvdz
   CC_REF_PROP       1
   CC_POL            2
   CC_DIIS_SIZE      15
   CC_FULLRESPONSE   1
$end
```

### 6.7.18 EOM(2,3) Methods for Higher-Accuracy and Problematic Situations (CC-MAN only)

In the EOM-CC(2,3) approach[92], the transformed Hamiltonian $\bar{H}$ is diagonalized in the basis of the reference, singly, doubly, and triply excited determinants, *i.e.*, the excitation operator $R$ is truncated at triple excitations. The excitation operator $T$, however, is truncated at double excitation level, and its amplitudes are found from the CCSD equations, just like for EOM-CCSD [or EOM-CC(2,2)] method.

The accuracy of the EOM-CC(2,3) method closely follows that of full EOM-CCSDT [which can be also called EOM-CC(3,3)], whereas computational cost of the former model is less.

The inclusion of triple excitations is necessary for achieving chemical accuracy (1 kcal/mol) for ground state properties. It is even more so for excited states. In particular, triple excitations are crucial for doubly excited states[92], excited states of some radicals and SF calculations (diradicals, triradicals, bond-breaking) when a reference open-shell state is heavily spin-contaminated. Accuracy of EOM-CCSD and EOM-CC(2,3) is compared in Table 6.7.18.

| **System** | **EOM-CCSD** | **EOM-CC(2,3)** |
|---|---:|---:|
| Singly-excited electronic states | 0.1–0.2 eV | 0.01 eV |
| Doubly-excited electronic states | $\geq$ 1 eV | 0.1–0.2 eV |
| Severe spin-contamination of the reference | $\sim$ 0.5 eV | $\leq$ 0.1 eV |
| Breaking single bond (EOM-SF) | 0.1–0.2 eV | 0.01 eV |
| Breaking double bond (EOM-2SF) | $\sim$ 1 eV | 0.1–0.2 eV |

Table 6.3: Performance of the EOM-CCSD and EOM-CC(2,3) methods

The applicability of the EOM-EE/SF-CC(2,3) models to larger systems can be extended by using their active-space variants, in which triple excitations are restricted to semi-internal ones.

Since the computational scaling of EOM-CC(2,3) method is $\mathcal{O}(N^8)$, these calculations can be performed only for relatively small systems. Moderate size molecules (10 heavy atoms) can be tackled by either using the active space implementation or tiny basis sets. To achieve high accuracy for these systems, energy additivity schemes can be used. For example, one can extrapolate EOM-CCSDT/large basis set values by combining large basis set EOM-CCSD calculations with small basis set EOM-CCSDT ones.

Running the full EOM-CC(2,3) calculations is straightforward, however, the calculations are expensive with the bottlenecks being storage of the data on a hard drive and the CPU time. Calculations with around 80 basis functions are possible for a molecule consisting of four first row atoms (NO dimer). The number of basis functions can be larger for smaller systems.

**Note:** In EE calculations, one needs to always solve for at least one low-spin root in the first symmetry irrep in order to obtain the correlated EOM energy of the reference. The triples correction to the total reference energy must be used to evaluate EOM-(2,3) excitation energies.

**Note:** EOM-CC(2,3) works for EOM-EE, EOM-SF, and EOM-IP/EA. In EOM-IP, “triples” correspond to $3h2p$ excitations, and the computational scaling of EOM-IP-CC(2,3) is less.

### 6.7.19 Active-Space EOM-CC(2,3): Tricks of the Trade (CCMAN only)

Active space calculations are less demanding with respect to the size of a hard drive. The main bottlenecks here are the memory usage and the CPU time. Both arise due to the increased number of orbital blocks in the active space calculations. In the current implementation, each block can contain from 0 up to 16 orbitals of the same symmetry irrep, occupancy, and spin-symmetry. For example, for a typical molecule of $C_{2v}$ symmetry, in a small/moderate basis set (*e.g.*, TMM in 6-31G*), the number of blocks for each index is:

occupied: $(\alpha + \beta) \times (a_1 + a_2 + b_1 + b_2) = 2 \times 4 = 8$
virtuals: $(\alpha + \beta) \times (2a_1 + a_2 + b_1 + 2b_2) = 2 \times 6 = 12$
(usually there are more than 16 $a_1$ and $b_2$ virtual orbitals).

In EOM-CCSD, the total number of blocks is $O^2V^2 = 8^2 \times 12^2 = 9216$. In EOM-CC(2,3) the number of blocks in the EOM part is $O^3V^3 = 8^3 \times 12^3 = 884736$. In active space EOM-CC(2,3), additional fragmentation of blocks occurs to distinguish between the restricted and active orbitals. For example, if the active space includes occupied and virtual orbitals of all symmetry irreps (this will be a very large active space), the number of occupied and virtual blocks for each index is 16 and 20, respectively, and the total number of blocks increases to $3.3 \times 10^7$. Not all of the blocks contain real information, some blocks are zero because of the spatial or spin-symmetry requirements. For the $C_{2v}$ symmetry group, the number of non-zero blocks is about 10–12 times less than the total number of blocks, *i.e.*, $3 \times 10^6$. This is the number of non-zero blocks in *one* vector. Davidson diagonalization procedure requires (2*MAX_VECTORS + 2*NROOTS) vectors, where MAX_VECTORS is the maximum number of vectors in the subspace, and NROOTS is the number of the roots to solve for. Taking NROOTS = 2 and MAX_VECTORS = 20, we obtain 44 vectors with the total number of non-zero blocks being $1.3 \times 10^8$.

In CCMAN implementation, each block is a logical unit of information. Along with real data, which are kept on a hard drive at all the times except of their direct usage, each non-zero block contains an auxiliary information about its size, structure, relative position with respect to other blocks, location on a hard drive, and so on. The auxiliary information about blocks is *always* kept in memory. Currently, the approximate size of this auxiliary information is about 400 bytes per block. It means, that in order to keep information about one vector ($3\times10^6$ blocks), 1.2 Gb of memory is required! The information about 44 vectors amounts 53 Gb. Moreover, the huge number of blocks significantly slows down the code.

To make the calculations of active space EOM-CC(2,3) feasible, we need to reduce the total number of blocks. One way to do this is to reduce the symmetry of the molecule to lower or $\mathrm{C}_1$ symmetry group (of course, this will result in more expensive calculation). For example, lowering the symmetry group from $\mathrm{C}_{2\mathrm{v}}$ to $\mathrm{C}_\mathrm{s}$ would results in reducing the total number of blocks in active space EOM-CC(2,3) calculations in about $2^6 = 64$ times, and the number of non-zero blocks in about 30 times (the relative portion of non-zero blocks in $\mathrm{C}_\mathrm{s}$ symmetry group is smaller compared to that in $\mathrm{C}_{2\mathrm{v}}$).

Alternatively, one may keep the MAX_VECTORS and NROOTS parameters of Davidson's diagonalization procedure as small as possible (this mainly concerns the MAX_VECTORS parameter). For example, specifying MAX_VECTORS = 12 instead of 20 would require 30% less memory.

One more trick concerns specifying the active space. In a desperate situation of a severe lack of memory, should the two previous options fail, one can try to modify (increase) the active space in such a way that the fragmentation of active and restricted orbitals would be less. For example, if there is one restricted occupied $b_1$ orbital and one active occupied $B_1$ orbital, adding the restricted $b_1$ to the active space will reduce the number of blocks, by the price of increasing the number of FLOPS. In principle, adding extra orbital to the active space should increase the accuracy of calculations, however, a special care should be taken about the (near) degenerate pairs of orbitals, which should be handled in the same way, *i.e.*, both active or both restricted.

### 6.7.20 Job Control for EOM-CC(2,3)

EOM-CC(2,3) is invoked by METHOD=EOM-CC(2,3). The following options are available:

**EOM_PRECONV_SD**
Solves the EOM-CCSD equations, prints energies, then uses EOM-CCSD vectors as initial vectors in EOM-CC(2,3). Very convenient for calculations using energy additivity schemes.
TYPE:
INTEGER
DEFAULT:
0
OPTIONS:
$n$ Do $n$ SD iterations
RECOMMENDATION:
Turning this option on is recommended

**CC_REST_AMPL**

Forces the integrals, $T$, and $R$ amplitudes to be determined in the full space even though the CC_REST_OCC and CC_REST_VIR keywords are used.

TYPE:

LOGICAL

DEFAULT:

TRUE

OPTIONS:

| | |
|---|---|
| FALSE | Do apply restrictions |
| TRUE | Do not apply restrictions |

RECOMMENDATION:

None

**CC_REST_TRIPLES**

Restricts $R_3$ amplitudes to the active space, *i.e.*, one electron should be removed from the active occupied orbital and one electron should be added to the active virtual orbital.

TYPE:

INTEGER

DEFAULT:

1

OPTIONS:

| | |
|---|---|
| 1 | Applies the restrictions |

RECOMMENDATION:

None

**CC_REST_OCC**

Sets the number of restricted occupied orbitals including frozen occupied orbitals.

TYPE:

INTEGER

DEFAULT:

0

OPTIONS:

| | |
|---|---|
| $n$ | Restrict $n$ occupied orbitals. |

RECOMMENDATION:

None

**CC_REST_VIR**

Sets the number of restricted virtual orbitals including frozen virtual orbitals.

TYPE:

INTEGER

DEFAULT:

0

OPTIONS:

| | |
|---|---|
| $n$ | Restrict $n$ virtual orbitals. |

RECOMMENDATION:

None

To select the active space, orbitals can be reordered by specifying the new order in the *$reorder_mo*section.

The section consists of two rows of numbers ($\alpha$ and $\beta$ sets), starting from 1, and ending with $n$, where $n$ is the number of the last orbital specified.

**Example 6.58** Example *$reorder_mo* section with orbitals 16 and 17 swapped for both $\alpha$ and $\beta$ electrons

```
$reorder_mo
1 2 3 4 5 6 7 8 9 10 11 12 13 14 15 17 16
1 2 3 4 5 6 7 8 9 10 11 12 13 14 15 17 16
$end
```

### 6.7.21 Examples

**Example 6.59** EOM-SF(2,3) calculations of methylene.

```
$molecule
   0 3
   C
   H 1 CH
   H 1 CH 2 HCH

   CH  = 1.07
   HCH = 111.0
$end

$rem
   METHOD             eom-cc(2,3)
   BASIS              6-31G
   SF_STATES          [2,0,0,2]
   N_FROZEN_CORE      1
   N_FROZEN_VIRTUAL   1
   EOM_PRECONV_SD      20 Get EOM-CCSD energies first (max_iter=20).
$end
```

**Example 6.60** This is active-space EOM-SF(2,3) calculations for methane with an elongated CC bond. HF MOs should be reordered as specified in the *$reorder_mo*section such that active space for triples consists of sigma and sigma* orbitals.

```
$molecule
   0 3
   C
   H  1  CH
   H  1  CHX  2  HCH
   H  1  CH   2  HCH  3  A120
   H  1  CH   2  HCH  4  A120

   CH   = 1.086
   HCH  = 109.4712206
   A120 = 120.
   CHX  = 1.8
$end

$rem
   METHOD            eom-cc(2,3)
   BASIS             6-31G*
   SF_STATES         [1,0]
   N_FROZEN_CORE     1
   EOM_PRECONV_SD    20    does eom-ccsd first, max_iter=20
   CC_REST_TRIPLES   1    triples are restricted to the active space only
   CC_REST_AMPL      0    ccsd and eom singles and doubles are full-space
   CC_REST_OCC       4    specifies active space
   CC_REST_VIR       17   specifies active space
   PRINT_ORBITALS    10   (number of virtuals to print)
$end

$reorder_mo
   1 2 5 4 3
   1 2 3 4 5
$end
```

**Example 6.61** EOM-IP-CC(2,3) calculation of three lowest electronic states of water cation.

```
$molecule
0 1
   H   0.774767     0.000000     0.458565
   O   0.000000     0.000000    -0.114641
   H  -0.774767     0.000000     0.458565
$end

$rem
   METHOD       eom-cc(2,3)
   BASIS        6-311G
   IP_STATES    [1,0,1,1]
$end
```

### 6.7.22 Non-Iterative Triples Corrections to EOM-CCSD and CCSD

The effect of triple excitations to EOM-CCSD energies can be included via perturbation theory in an economical $N^7$ computational scheme. Using EOM-CCSD wave functions as zero-order wave functions, the second order triples correction to the $\mu$th EOM-EE or SF state is:

$$\Delta E_\mu^{(2)} = -\frac{1}{36}\sum_{i,j,k}\sum_{a,b,c}\frac{\tilde{\sigma}_{ijk}^{abc}(\mu)\sigma_{ijk}^{abc}(\mu)}{D_{ijk}^{abc}-\omega_\mu} \tag{6.53}$$

where $i, j$ and $k$ denote occupied orbitals, and $a, b$ and $c$ are virtual orbital indices. $\omega_\mu$ is the EOM-CCSD excitation energy of the $\mu$th state. The quantities $\tilde{\sigma}$ and $\sigma$ are:

$$\begin{aligned}\tilde{\sigma}_{ijk}^{abc}(\mu) &= \langle\Phi_0|(L_{1\mu}+L_{2\mu})(He^{(T_1+T_2)})_c|\Phi_{ijk}^{abc}\rangle \\ \sigma_{ijk}^{abc}(\mu) &= \langle\Phi_{ijk}^{abc}|[He^{(T_1+T_2)}(R_{0\mu}+R_{1\mu}+R_{2\mu})]_c|\Phi_0\rangle\end{aligned} \tag{6.54}$$

where, the $L$ and $R$ are left and right eigen-vectors for $\mu$th state. Two different choices of the denominator, $D_{ijk}^{abc}$, define the (dT) and (fT) variants of the correction. In (fT), $D_{ijk}^{abc}$ is just Hartree-Fock orbital energy differences. A more accurate (but not fully orbital invariant) (dT) correction employs the complete three body diagonal of $\bar{H}$, $\langle\Phi_{ijk}^{abc}|(He^{(T_1+T_2)})_C|\Phi_{ijk}^{abc}\rangle$, $D_{ijk}^{abc}$as a denominator. For the reference (*e.g.*, a ground-state CCSD wave function), the (fT) and (dT) corrections are identical to the CCSD(2)$_T$ and CR-CCSD(T)$_L$ corrections of Piecuch and co-workers[93].

The EOM-SF-CCSD(dT) and EOM-SF-CCSD(fT) methods yield a systematic improvement over EOM-SF-CCSD bringing the errors below 1 kcal/mol. For theoretical background and detailed benchmarks, see Ref. 94.

Similar corrections are available for EOM-IP-CCSD[95], where triples correspond to $3h2p$ excitations and EOM-EA-CCSD, where triples correspond to $2h3p$ excitations.

### 6.7.23 Job Control for Non-Iterative Triples Corrections

Triples corrections are requested by using METHOD or EOM_CORR:

**METHOD**

Specifies the calculation method.

TYPE:

STRING

DEFAULT:

No default value

OPTIONS:

| | |
|---|---|
| EOM-CCSD(DT) | EOM-CCSD(dT), available for EE, SF, and IP |
| EOM-CCSD(FT) | EOM-CCSD(fT), available for EE, SF, IP, and EA |
| EOM-CCSD(ST) | EOM-CCSD(sT), available for IP |

RECOMMENDATION:

None

**EOM_CORR**

Specifies the correlation level.

TYPE:

STRING

DEFAULT:

| | |
|---|---|
| None | No correction will be computed |

OPTIONS:

| | |
|---|---|
| SD(DT) | EOM-CCSD(dT), available for EE, SF, and IP |
| SD(FT) | EOM-CCSD(fT), available for EE, SF, IP, and EA |
| SD(ST) | EOM-CCSD(sT), available for IP |

RECOMMENDATION:

None

### 6.7.24 Examples

**Example 6.62** EOM-EE-CCSD(fT) calculation of CH$^+$

```
$molecule
   1 1
   C
   H  C CH

   CH  = 2.137130
$end
```

```
$rem
   INPUT_BOHR              true
   METHOD                  eom-ccsd(ft)
   BASIS                   general
   EE_STATES               [1,0,1,1]
   EOM_DAVIDSON_MAX_ITER  60  increase number of Davidson iterations
$end

$basis
 H   0
 S   3  1.00
       19.24060000         0.3282800000E-01
       2.899200000         0.2312080000
      0.6534000000         0.8172380000
 S   1  1.00
      0.1776000000          1.000000000
 S   1  1.00
      0.0250000000          1.000000000
 P   1  1.00
       1.00000000          1.00000000
 ****
 C   0
 S   6  1.00
       4232.610000         0.2029000000E-02
       634.8820000         0.1553500000E-01
       146.0970000         0.7541100000E-01
       42.49740000         0.2571210000
       14.18920000         0.5965550000
       1.966600000         0.2425170000
 S   1  1.00
       5.147700000          1.000000000
 S   1  1.00
      0.4962000000          1.000000000
 S   1  1.00
      0.1533000000          1.000000000
 S   1  1.00
      0.0150000000          1.000000000
 P   4  1.00
       18.15570000         0.1853400000E-01
       3.986400000         0.1154420000
       1.142900000         0.3862060000
      0.3594000000         0.6400890000
 P   1  1.00
      0.1146000000          1.000000000
 P   1  1.00
      0.0110000000          1.000000000
 D   1  1.00
      0.750000000          1.00000000
 ****
$end
```

**Example 6.63** EOM-SF-CCSD(dT) calculations of methylene

```
$molecule
   0 3
   C
   H 1 CH
   H 1 CH 2 HCH

   CH  = 1.07
   HCH = 111.0
$end

$rem
   METHOD            eom-ccsd(dt)
   BASIS             6-31G
   SF_STATES         [2,0,0,2]
   N_FROZEN_CORE     1
   N_FROZEN_VIRTUAL  1
$end
```

**Example 6.64** EOM-IP-CCSD(dT) calculations of Mg

```
$molecule
   0 1
   Mg    0.000000     0.000000    0.000000
$end

$rem
   JOBTYPE      sp
   METHOD       eom-ccsd(dt)
   BASIS        6-31g
   IP_STATES    [1,0,0,0,0,1,1,1]
$end
```

### 6.7.25 Potential Energy Surface Crossing Minimization

Potential energy surface crossing optimization procedure finds energy minima on crossing seams. On the seam, the potential surfaces are degenerated in the subspace perpendicular to the plane defined by two vectors: the gradient difference

$$\mathbf{g} = \frac{\partial}{\partial \mathbf{q}}(E_1 - E_2) \tag{6.55}$$

and the derivative coupling

$$\mathbf{h} = \left\langle \Psi_1 \left| \frac{\partial \mathbf{H}}{\partial \mathbf{q}} \right| \Psi_2 \right\rangle \tag{6.56}$$

At this time Q-CHEM is unable to locate crossing minima for states which have non-zero derivative coupling. Fortunately, often this is not the case. Minima on the seams of conical intersections of states of different multiplicity can be found as their derivative coupling is zero. Minima on the seams of intersections of states of different point group symmetry can be located as well.

To run a PES crossing minimization, CCSD and EOM-CCSD methods must be employed for the ground and excited state calculations respectively.

**Note:** MECP optimization is only available for methods with analytic gradients. Finite-difference evaluation of two gradients is not possible.

#### 6.7.25.1 Job Control Options

**XOPT_STATE_1, XOPT_STATE_2**

Specify two electronic states the intersection of which will be searched.

TYPE:

[INTEGER, INTEGER, INTEGER]

DEFAULT:

No default value (the option must be specified to run this calculation)

OPTIONS:

[spin, irrep, state]

| | |
|---|---|
| spin = 0 | Addresses states with low spin,<br>see also EE_SINGLETS or IP_STATES,EA_STATES. |
| spin = 1 | Addresses states with high spin,<br>see also EE_TRIPLETS. |
| irrep | Specifies the irreducible representation to which the state belongs, for $C_{2v}$ point group symmetry irrep = 1 for $A_1$, irrep = 2 for $A_2$, irrep = 3 for $B_1$, irrep = 4 for $B_2$. |
| state | Specifies the state number within the irreducible representation, state = 1 means the lowest excited state, state = 2 is the second excited state, *etc.*. |
| 0, 0, -1 | Ground state. |

RECOMMENDATION:

Only intersections of states with different spin or symmetry can be calculated at this time.

**Note:** The spin can only be specified when using closed-shell RHF references. In the case of open-shell references all states are treated together, see also EE_STATES. E.g., in SF calculations use spin=0 regardless of what is the actual multiplicity of the target state.

**XOPT_SEAM_ONLY**

Orders an intersection seam search only, no minimization is to perform.

TYPE:

LOGICAL

DEFAULT:

FALSE

OPTIONS:

| | |
|---|---|
| TRUE | Find a point on the intersection seam and stop. |
| FALSE | Perform a minimization of the intersection seam. |

RECOMMENDATION:

In systems with a large number of degrees of freedom it might be useful to locate the seam first setting this option to TRUE and use that geometry as a starting point for the minimization.

#### 6.7.25.2 Examples

**Example 6.65** Minimize the intersection of $\tilde{A}^2A_1$ and $\tilde{B}^2B_1$ states of the $NO_2$ molecule using EOM-IP-CCSD method

```
$molecule
   -1  1
   N1
   O2  N1  rno
   O3  N1  rno  O2  aono

   rno  = 1.3040
   aono = 106.7
$end

$rem
   JOBTYPE                opt          Optimize the intersection seam
   UNRESTRICTED           true
   METHOD                 eom-ccsd
   BASIS                  6-31g
   IP_STATES              [1,0,1,0]    C2v point group symmetry
   EOM_FAKE_IPEA          1
   XOPT_STATE_1           [0,1,1]      1A1 low spin state
   XOPT_STATE_2           [0,3,1]      1B1 low spin state
   GEOM_OPT_TOL_GRADIENT  30           Tighten gradient tolerance
$END
```

**Example 6.66** Minimize the intersection of $\tilde{A}^1B_2$ and $\tilde{B}^1A_2$ states of the $N_3^+$ ion using EOM-CCSD method

```
$molecule
   1 1
   N1
   N2 N1 rnn
   N3 N2 rnn N1 annn

   rnn=1.46
   annn=70.0
$end

$rem
   JOBTYPE                opt
   METHOD                 eom-ccsd
   BASIS                  6-31g
   EE_SINGLES             [0,2,0,2]    C2v point group symmetry
   XOPT_STATE_1           [0,4,1]      1B2 low spin state
   XOPT_STATE_2           [0,2,2]      2A2 low spin state
   XOPT_SEAM_ONLY         true         Find the seam only
   GEOM_OPT_TOL_GRADIENT  100
$end

$opt
CONSTRAINT                Set constraints on the N-N bond lengths
   stre  1  2  1.46
   stre  2  3  1.46
ENDCONSTRAINT
$end

@@@

$molecule
   READ
```

```
$end

$rem
   JOBTYPE               opt        Optimize the intersection seam
   METHOD                eom-ccsd
   BASIS                 6-31g
   EE_SINGLETS           [0,2,0,2]
   XOPT_STATE_1          [0,4,1]
   XOPT_STATE_2          [0,2,2]
   GEOM_OPT_TOL_GRADIENT  30
$end
```

### 6.7.26 Dyson Orbitals for Ionization States within the EOM-CCSD Formalism

Dyson orbitals can be used to compute total photodetachment/photoionization cross-sections, as well as angular distribution of photoelectrons. A Dyson orbital is the overlap between the N-electron molecular wave function and the N-1/N+1 electron wave function of the corresponding cation/anion:

$$\phi^d(1) = \frac{1}{N-1}\int \Psi^N(1,\ldots,n)\Psi^{N-1}(2,\ldots,n)d2\ldots dn \tag{6.57}$$

$$\phi^d(1) = \frac{1}{N+1}\int \Psi^N(2,\ldots,n+1)\Psi^{N+1}(1,\ldots,n+1)d2\ldots d(n+1) \tag{6.58}$$

For the Hartree-Fock wave functions and within Koopmans' approximation, these are just the canonical HF orbitals. For correlated wave functions, Dyson orbitals are linear combinations of the reference molecular orbitals:

$$\phi^d = \sum_p \gamma_p \phi_p \tag{6.59}$$

$$\gamma_p = \langle \Psi^N | p^+ | \Psi^{N-1} \rangle \tag{6.60}$$

$$\gamma_p = \langle \Psi^N | p | \Psi^{N+1} \rangle \tag{6.61}$$

The calculation of Dyson orbitals is straightforward within the EOM-IP/EA-CCSD methods, where cation/ anion and initial molecule states are defined with respect to the same MO basis. Since the left and right CC vectors are not the same, one can define correspondingly two Dyson orbitals (left and right):

$$\gamma_p^R = \langle \Phi_0 e^{T_1+T_2} L^{EE} | p^+ | R^{IP} e^{T_1+T_2} \Phi_0 \rangle \tag{6.62}$$

$$\gamma_p^L = \langle \Phi_0 e^{T_1+T_2} L^{IP} | p | R^{EE} e^{T_1+T_2} \Phi_0 \rangle \tag{6.63}$$

The norm of these orbitals is proportional to the one-electron character of the transition.

Dyson orbitals also offer qualitative insight visualizing the difference between molecular and ionized/ attached states. In ionization/photodetachment processes, these orbitals can be also interpreted as the wave function of the leaving electron. For additional details, see Refs. 96,97.

#### 6.7.26.1 Dyson Orbitals Job Control

The calculation of Dyson orbitals is implemented for the ground (reference) and excited states ionization/ electron attachment. To obtain the ground state Dyson orbitals one needs to run an EOM-IP/EA-CCSD calculation, request transition properties calculation by setting CC_TRANS_PROP=TRUE and CC_DO_DYSON

= TRUE. The Dyson orbitals decomposition in the MO basis is printed in the output, for all transitions between the reference and all IP/EA states. At the end of the file, also the coefficients of the Dyson orbitals in the AO basis are available.

Two implementations of Dyson orbitals are currently available: (i) the original implementation in CCMAN; and (ii) new implementation in CCMAN2. The CCMAN implementation is using a diffuse orbital trick (*i.e.*, EOM_FAKE_IPEA will be automatically set to TRUE in these calculations). Note: this implementation has a bug affecting the values of norms of Dyson orbitals (the shapes are correct); thus, using this code is strongly discouraged. The CCMAN2 implementation has all types of initial states available: Dyson orbitals from ground CC, excited EOM-EE, and spin-flip EOM-SF states; it is fully compatible with all helper features for EOM calculations, like FNO, RI, Cholesky decomposition. The CCMAN2 implementation can utilize user-specified EOM guess (using EOM_USER_GUESS keyword and *$eom_user_guess* section), which is recommended for highly excited states (such as core-ionized states). In addition, CCMAN2 can calculate Dyson orbitals involving meta-stable states (see Section 6.7.5).

For calculating Dyson orbitals between excited or spin-flip states from the reference configuration and IP/ EA states, same CC_TRANS_PROP = TRUE and CC_DO_DYSON = TRUE keywords have to be added to the combination of usual EOM-IP/EA-CCSD and EOM-EE-CCSD or EOM-SF-CCSD calculations (however, note separate keyword CC_DO_DYSON_EE = TRUE for CCMAN). The IP_STATES keyword is used to specify the target ionized states. The attached states are specified by EA_STATES. The EA-SF states are specified by EOM_EA_BETA. The excited (or spin-flipped) states are specified by EE_STATES and SF_STATES. The Dyson orbital decomposition in MO and AO bases is printed for each EE/SF-IP/EA pair of states first for reference, then for all excited states in the order: CC - IP/EA1, CC - IP/EA2,. . ., EE/SF1 - IP/EA1, EE/SF1 - IP/EA2,. . ., EE/SF2 - IP/EA1, EE/SF2 - IP/EA2,. . ., and so on. CCMAN implementation keeps reference transitions separate, in accordance with separating keywords.

**CC_DO_DYSON**

CCMAN2: starts all types of Dyson orbitals calculations. Desired type is determined by requesting corresponding EOM-XX transitions CCMAN: whether the reference-state Dyson orbitals will be calculated for EOM-IP/EA-CCSD calculations.

TYPE:

LOGICAL

DEFAULT:

FALSE (the option must be specified to run this calculation)

OPTIONS:

TRUE/FALSE

RECOMMENDATION:

none

**CC_DO_DYSON_EE**

Whether excited-state or spin-flip state Dyson orbitals will be calculated for EOM-IP/EA-CCSD calculations with CCMAN.

TYPE:

LOGICAL

DEFAULT:

FALSE (the option must be specified to run this calculation)

OPTIONS:

TRUE/FALSE

RECOMMENDATION:

none

Dyson orbitals can be also plotted using IANLTY = 200 and the *$plots* utility. Only the sizes of the box need to be specified, followed by a line of zeros:

```
$plots
comment
   10   -2   2
   10   -2   2
   10   -2   2
   0     0   0    0
$plots
```

All Dyson orbitals on the Cartesian grid will be written in the resulting *plot.mo* file (only CCMAN). For RHF(UHF) reference, the columns order in *plot.mo* is: $\phi_1^{lr}\alpha$ ($\phi_1^{lr}\beta$) $\phi_1^{rl}\alpha$ ($\phi_1^{rl}\beta$) $\phi_2^{lr}\alpha$ ($\phi_2^{lr}\beta$) $\ldots$

In addition, setting the MAKE_CUBE_FILES keyword to TRUE will create cube files for Dyson orbitals which can be viewed with VMD or other programs (see Section 10.5.4 for details). This option is available for CCMAN and CCMAN2. The Dyson orbitals will be written to files mo.1.cube, mo.2.cube, . . . in the order $\phi_1^{lr}$ $\phi_1^{rl}$ $\phi_2^{lr}$ $\phi_2^{rl}$ . . .. For meta-stable states, the real and imaginary parts of the Dyson orbitals are written to separate files in the order Re($\phi_1^{lr}$) Re($\phi_1^{rl}$) Re($\phi_2^{lr}$) Re($\phi_2^{rl}$) . . . Im($\phi_1^{lr}$) Im($\phi_1^{rl}$) Im($\phi_2^{lr}$) Im($\phi_2^{rl}$) . . .

Other means of visualization (*e.g.*, with MOLDEN_FORMAT = TRUE or GUI = 2) are currently not available.

#### 6.7.26.2 Examples

**Example 6.67** Plotting grd-ex and ex-grd state Dyson orbitals for ionization of the oxygen molecule. The target states of the cation are $^2$A$_g$ and $^2$B$_{2u}$. Works for CCMAN only.

```
$molecule
   0 3
   O    0.000  0.000  0.000
   O    1.222  0.000  0.000
$end

$rem
   BASIS          6-31G*
   METHOD         eom-ccsd
   IP_STATES      [1,0,0,0,0,0,1,0] Target EOM-IP states
   CC_TRANS_PROP  true  request transition OPDMs to be calculated
   CC_DO_DYSON    true  calculate Dyson orbitals
   IANLTY         200
$end

$plots
plots excited states densities and trans densities
   10   -2   2
   10   -2   2
   10   -2   2
   0     0   0    0
$plots
```

**Example 6.68** Plotting ex-ex state Dyson orbitals between the 1st $^2A_1$ excited state of the HO radical and the the 1st $A_1$ and $A_2$ excited states of $HO^-$. Works for CCMAN only.

```
$molecule
   -1 1
   H    0.000   0.000  0.000
   O    1.000   0.000  0.000
$end

$rem
   METHOD              eom-ccsd
   BASIS               6-31G*
   IP_STATES           [1,0,0,0]  states of HO radical
   EE_STATES           [1,1,0,0]  excited states of HO-
   CC_TRANS_PROP       true       calculate transition properties
   CC_DO_DYSON_EE      true       calculate Dyson orbitals for ionization from ex. states
   IANLTY              200
$end

$plots
plot excited states densities and trans densities
   10   -2   2
   10   -2   2
   10   -2   2
   0     0   0    0
$plots
```

**Example 6.69** Dyson orbitals for ionization of CO molecule; $A_1$ and $B_1$ ionized states requested.

```
$molecule
   0 1
   O
   C  O  1.131
$end

$rem
   CORRELATION           CCSD
   BASIS                 cc-pVDZ
   PURECART              111        5d, will be required for ezDyson
   IP_STATES             [1,0,1,0]  (A1,A2,B1,B2)
   CCMAN2                true
   CC_DO_DYSON           true
   CC_TRANS_PROP         true       necessary for Dyson orbitals job
   PRINT_GENERAL_BASIS   true       will be required for ezDyson
```

```
$end
```

**Example 6.70** Dyson orbitals for ionization of $H_2O$; core ($A_1$) state requested — ionization from O(1s).

```
$molecule
   0 1
   O
   H1  O  0.955
   H2  O  0.955  H1  104.5
$end

$rem
   CORRELATION           CCSD
   BASIS                 cc-pVTZ
   PURECART              111        5d, will be required for ezDyson
   IP_STATES             [1,0,0,0]  (A1,A2,B1,B2)
   EOM_USER_GUESS        1          on, further defined in $eom_user_guess
   CCMAN2                true
   CC_DO_DYSON           true
   CC_TRANS_PROP         true       necessary for Dyson orbitals job
   PRINT_GENERAL_BASIS   true       will be required for ezDyson
$end

$eom_user_guess
   1
$end
```

**Example 6.71** Dyson orbitals for ionization of NO molecule using EOM-EA and a closed-shell cation reference; $A_1$ and $B_2$ states requested.

```
$molecule
   +1 1
   N   0.00000  0.00000  0.00000
   O   0.00000  0.00000  1.02286
$end

$rem
   CORRELATION            CCSD
   BASIS                  aug-cc-pVTZ
   PURECART               111       5d, will be required for ezDyson
   EA_STATES              [1,0,0,1] (A1,A2,B1,B2)
   CCMAN2                 true
   CC_DO_DYSON            true
   CC_TRANS_PROP          true      necessary for Dyson orbitals job
   PRINT_GENERAL_BASIS    true      will be required for ezDyson
$end
```

**Example 6.72** Dyson orbitals for ionization of triplet $O_2$ and $O_2^-$ at slightly stretched (relative to the equilibrium $O_2$ geometry); $B_{3g}$ states are requested.

```
$comment
   EOM-IP-CCSD/6-311+G* and EOM-EA-CCSD/6-311+G* levels of theory,
   UHF reference.  Start from O2:
    1) detach electron - ionization of neutral (alpha IP).
    2) attach electron, use EOM-EA w.f. as initial state
```

```
        - ionization of anion (beta EA).
$end

$molecule
   0 3
   O   0.00000  0.00000  0.00000
   O   0.00000  0.00000  1.30000
$end

$rem
   CORRELATION           CCSD
   BASIS                 6-311(3+)G*
   PURECART              2222          6d, will be required for ezDyson
   EOM_IP_ALPHA          [0,0,0,1,0,0,0,0]  (Ag,B1g,B2g,B3g,Au,B1u,B2u,B3u)
   EOM_EA_BETA           [0,0,0,1,0,0,0,0]  (Ag,B1g,B2g,B3g,Au,B1u,B2u,B3u)
   CCMAN2                true
   CC_DO_DYSON           true
   CC_TRANS_PROP         true          necessary for Dyson orbitals job
   PRINT_GENERAL_BASIS   true          will be required for ezDyson
$end
```

**Example 6.73** Dyson orbitals for detachment from the meta-stable $^2\Pi_g$ state of $N_2^-$.

```
$molecule
   0 1
   N   0.0   0.0    0.55
   N   0.0   0.0   -0.55
   GH  0.0   0.0    0.0
$end

$rem
   METHOD            EOM-CCSD
   EA_STATES         [0,0,2,0,0,0,0,0]
   CC_MEMORY         5000
   MEM_STATIC        1000
   BASIS             GEN
   COMPLEX_CCMAN     TRUE
   CC_TRANS_PROP     TRUE
   CC_DO_DYSON       TRUE
   MAKE_CUBE_FILES   TRUE
   IANLTY            200
$end

$complex_ccman
   CS_HF 1
   CAP_TYPE 1
   CAP_X 2760
   CAP_Y 2760
   CAP_Z 4880
   CAP_ETA 400
$end

$plots
plot Dyson orbitals
   50 -10.0 10.0
   50 -10.0 10.0
   50 -10.0 10.0
   0 0 0 0
```

```
$end

$basis
N    0
S    8    1.000000
   1.14200000E+04    5.23000000E-04
   1.71200000E+03    4.04500000E-03
   3.89300000E+02    2.07750000E-02
   1.10000000E+02    8.07270000E-02
   3.55700000E+01    2.33074000E-01
   1.25400000E+01    4.33501000E-01
   4.64400000E+00    3.47472000E-01
   5.11800000E-01   -8.50800000E-03
S    8    1.000000
   1.14200000E+04   -1.15000000E-04
   1.71200000E+03   -8.95000000E-04
   3.89300000E+02   -4.62400000E-03
   1.10000000E+02   -1.85280000E-02
   3.55700000E+01   -5.73390000E-02
   1.25400000E+01   -1.32076000E-01
   4.64400000E+00   -1.72510000E-01
   5.11800000E-01    5.99944000E-01
S    1    1.000000
   1.29300000E+00    1.00000000E+00
S    1    1.000000
   1.78700000E-01    1.00000000E+00
P    3    1.000000
   2.66300000E+01    1.46700000E-02
   5.94800000E+00    9.17640000E-02
   1.74200000E+00    2.98683000E-01
P    1    1.000000
   5.55000000E-01    1.00000000E+00
P    1    1.000000
   1.72500000E-01    1.00000000E+00
D    1    1.000000
   1.65400000E+00    1.00000000E+00
D    1    1.000000
   4.69000000E-01    1.00000000E+00
F    1    1.000000
   1.09300000E+00    1.00000000E+00
S    1    1.000000
   5.76000000E-02    1.00000000E+00
P    1    1.000000
   4.91000000E-02    1.00000000E+00
D    1    1.000000
   1.51000000E-01    1.00000000E+00
F    1    1.000000
   3.64000000E-01    1.00000000E+00
****
GH   0
S    1    1.000000
   2.88000000E-02    1.00000000E+00
S    1    1.000000
   1.44000000E-02    1.00000000E+00
S    1    1.000000
   0.72000000E-02    1.00000000E+00
S    1    1.000000
   0.36000000E-02    1.00000000E+00
```

```
S    1    1.000000
   0.18000000E-02    1.00000000E+00
S    1    1.000000
   0.09000000E-02    1.00000000E+00
P    1    1.000000
   2.45000000E-02    1.00000000E+00
P    1    1.000000
   1.22000000E-02    1.00000000E+00
P    1    1.000000
   0.61000000E-02    1.00000000E+00
P    1    1.000000
   0.305000000E-02    1.00000000E+00
P    1    1.000000
   0.152500000E-02    1.00000000E+00
P    1    1.000000
   0.076250000E-02    1.00000000E+00
D    1    1.000000
   0.755000000E-01    1.00000000E+00
D    1    1.000000
   0.377500000E-01    1.00000000E+00
D    1    1.000000
   0.188750000E-01    1.00000000E+00
D    1    1.000000
   0.094375000E-01    1.00000000E+00
D    1    1.000000
   0.047187500E-01    1.00000000E+00
D    1    1.000000
   0.023593750E-01    1.00000000E+00
****
$end
```

**Example 6.74** Dyson orbitals for ionization of formaldehyde from the first excited state AND from the ground state

```
$molecule
   0 1
   O     1.535338855      0.000000000     -0.438858006
   C     1.535331598     -0.000007025      0.767790994
   H     1.535342484      0.937663512      1.362651452
   H     1.535342484     -0.937656488      1.362672535
$end

$rem
   CORRELATION           CCSD
   BASIS                 6-31G*
   PURECART              2222    6d, will be required for ezDyson
   CCMAN2                true    new Dyson code
   EE_STATES             [1]
   EOM_IP_ALPHA          [1]
   EOM_IP_BETA           [1]
   CC_TRANS_PROP         true    necessary for Dyson orbitals job
   CC_DO_DYSON           true
   PRINT_GENERAL_BASIS   true    will be required for ezDyson
$end
```

**Example 6.75** Dyson orbitals for core ionization of Li atom use $Li^+$ as a reference, get neutral atom via EOM-EA get 1st excitation for the cation via EOM-EE totally: core ionization AND 1st ionization of Li atom

```
$molecule
   +1 1
   Li   0.00000  0.00000  0.00000
$end

$rem
   CORRELATION            CCSD
   BASIS                  6-311+G*
   PURECART               2222          6d, will be required for ezDyson
   CCMAN2                 true          new Dyson code
   EE_STATES              [1,0,0,0,0,0,0,0]
   EA_STATES              [1,0,0,0,0,0,0,0]
   EOM_NGUESS_SINGLES     5             to converge to the lowest EA state
   CC_TRANS_PROP          true          necessary for Dyson orbitals job
   CC_DO_DYSON            true
   PRINT_GENERAL_BASIS    true          will be required for ezDyson
$end
```

**Example 6.76** Dyson orbitals for ionization of CH2 from high-spin triplet reference and from the lowest SF state

```
$molecule
   0 3
   C
   H  1 rCH
   H  1 rCH 2 aHCH

   rCH    = 1.1167
   aHCH   = 102.07
$end

$rem
   CORRELATION           CCSD
   BASIS                 6-31G*
   PURECART              2222    6d, will be required for ezDyson
   SCF_GUESS             core
   CCMAN2                true    new Dyson code
   CC_SYMMETRY           false
   SF_STATES             [1]
   EOM_IP_ALPHA          [2]     one should be careful to request
   EOM_EA_BETA           [2]     meaningful spin for EA/IP state(s)
   CC_TRANS_PROP         true    necessary for Dyson orbitals job
   CC_DO_DYSON           true
   PRINT_GENERAL_BASIS   true    will be required for ezDyson
$end
```

### 6.7.27 Interpretation of EOM/CI Wave Functions and Orbital Numbering

Analysis of the leading wave function amplitudes is always necessary for determining the character of the state (*e.g.*, HOMO-LUMO excitation, open-shell diradical, *etc.*). The CCMAN module print out leading EOM/CI amplitudes using its internal orbital numbering scheme, which is printed in the beginning. The typical CCMAN EOM-CCSD output looks like:

```
Root 1 Conv-d yes Tot Ene= -113.722767530 hartree (Ex Ene 7.9548 eV),
U1^2=0.858795, U2^2=0.141205 ||Res||=4.4E-07
Right U1:
       Value                  i            ->    a
       0.5358                 7( B2  ) B   ->   17( B2  ) B
       0.5358                 7( B2  ) A   ->   17( B2  ) A
      -0.2278                 7( B2  ) B   ->   18( B2  ) B
      -0.2278                 7( B2  ) A   ->   18( B2  ) A
```

This means that this state is derived by excitation from occupied orbital #7 (which has $b_2$ symmetry) to virtual orbital #17 (which is also of $b_2$ symmetry). The two leading amplitudes correspond to $\beta \to \beta$ and $\alpha \to \alpha$ excitation (the spin part is denoted by $A$ or $B$). The orbital numbering for this job is defined by the following map:

```
The orbitals are ordered and numbered as follows:
Alpha orbitals:
Number  Energy    Type    Symmetry  ANLMAN number  Total number:
  0    -20.613     AOCC      A1        1A1      1
  1    -11.367     AOCC      A1        2A1      2
  2     -1.324     AOCC      A1        3A1      3
  3     -0.944     AOCC      A1        4A1      4
  4     -0.600     AOCC      A1        5A1      5
  5     -0.720     AOCC      B1        1B1      6
  6     -0.473     AOCC      B1        2B1      7
  7     -0.473     AOCC      B2        1B2      8

  0      0.071     AVIRT     A1        6A1      9
  1      0.100     AVIRT     A1        7A1      10
  2      0.290     AVIRT     A1        8A1      11
  3      0.327     AVIRT     A1        9A1      12
  4      0.367     AVIRT     A1       10A1      13
  5      0.454     AVIRT     A1       11A1      14
  6      0.808     AVIRT     A1       12A1      15
  7      1.196     AVIRT     A1       13A1      16
  8      1.295     AVIRT     A1       14A1      17
  9      1.562     AVIRT     A1       15A1      18
 10      2.003     AVIRT     A1       16A1      19
 11      0.100     AVIRT     B1        3B1      20
 12      0.319     AVIRT     B1        4B1      21
 13      0.395     AVIRT     B1        5B1      22
 14      0.881     AVIRT     B1        6B1      23
 15      1.291     AVIRT     B1        7B1      24
 16      1.550     AVIRT     B1        8B1      25
 17      0.040     AVIRT     B2        2B2      26
 18      0.137     AVIRT     B2        3B2      27
 19      0.330     AVIRT     B2        4B2      28
 20      0.853     AVIRT     B2        5B2      29
 21      1.491     AVIRT     B2        6B2      30
```

The first column is CCMAN's internal numbering (*e.g.*, 7 and 17 from the example above). This is followed by the orbital energy, orbital type (frozen, restricted, active, occupied, virtual), and orbital symmetry. Note that the orbitals are blocked by symmetries and then ordered by energy within each symmetry block, (*i.e.*, first all occupied $a_1$, then all $a_2$, *etc.*), and numbered starting from 0. The occupied and virtual orbitals are numbered separately, and frozen orbitals are excluded from CCMAN numbering. The two last columns give numbering in terms of the final ANLMAN printout (starting from 1), *e.g.*, our occupied orbital #7 will be numbered as $1B_2$ in the final printout. The last column gives the absolute orbital number (all occupied and all virtuals together, starting from 1), which is often used by external visualization routines.

CCMAN2 numbers orbitals by their energy within each irrep keeping the same numbering for occupied and virtual orbitals. This numbering is exactly the same as in the final printout of the SCF wave function analysis. Orbital energies are printed next to the respective amplitudes. For example, a typical CCMAN2 EOM-CCSD output will look like that:

```
EOMEE-CCSD transition 2/A1
Total energy = -75.87450159 a.u.  Excitation energy = 11.2971 eV.
R1^2 = 0.9396  R2^2 = 0.0604  Res^2 = 9.51e-08

Amplitude    Orbitals with energies
 0.6486       1 (B2) A                 ->    2 (B2) A
             -0.5101                         0.1729
 0.6486       1 (B2) B                 ->    2 (B2) B
             -0.5101                         0.1729
-0.1268       3 (A1) A                 ->    4 (A1) A
             -0.5863                         0.0404
-0.1268       3 (A1) B                 ->    4 (A1) B
             -0.5863                         0.0404
```

which means that for this state, the leading EOM amplitude corresponds to the transition from the first $b_2$ orbital (orbital energy $-0.5101$) to the second $b_2$ orbital (orbital energy 0.1729).

## 6.8 Correlated Excited State Methods: The ADC($n$) Family

The ADC($n$) family of correlated excited state methods is a series of size-extensive excited state methods based on perturbation theory. Each order $n$ of ADC presents the excited state equivalent to the well-known $n$th order Møller-Plesset perturbation theory for the ground state. Currently, the ADC variants ADC(0), ADC(1), ADC(2)-s, ADC(2)-x and ADC(3) are implemented into Q-CHEM.[98,99] The "resolution-of-the-identity" approximation can be used with any ADC variant. Additionally, there are spin-opposite scaling versions of both ADC(2) variants available.[98,100] Core-excited states for the simulation of X-ray absorption spectra can be computed exploiting the core-valence separation (CVS) approximation. Currently, the CVS-ADC(1), CVS-ADC(2)-s, CVS-ADC(2)-x and CVS-ADC(3) methods are available.[98,101–103]

### 6.8.1 The Algebraic Diagrammatic Construction (ADC) Scheme

The Algebraic Diagrammatic Construction (ADC) scheme of the polarization propagator is an excited state method originating from Green's function theory. It has first been derived employing the diagrammatic perturbation expansion of the polarization propagator using the Møller-Plesset partition of the Hamiltonian[104].

An alternative derivation is available in terms of the intermediate state representation (ISR)[105] which will be presented in the following.

As starting point for the derivation of ADC equations via ISR serves the exact N electron ground state $\left|\Psi_0^N\right\rangle$. From $\left|\Psi_0^N\right\rangle$ a complete set of correlated excited states is obtained by applying physical excitation operators $\hat{C}_J$.

$$\left|\bar{\Psi}_J^N\right\rangle = \hat{C}_J \left|\Psi_0^N\right\rangle \tag{6.64}$$

with

$$\left\{\hat{C}_J\right\} = \left\{c_a^\dagger c_i; c_a^\dagger c_b^\dagger c_i c_j, i < j, a < b; \ldots\right\} \tag{6.65}$$

Yet, the resulting excited states do not form an orthonormal basis. To construct an orthonormal basis out of the $|\bar{\Psi}_J^N\rangle$ the Gram-Schmidt orthogonalization scheme is employed successively on the excited states in the various excitation classes starting from the exact ground state, the singly excited states, the doubly excited states *etc.*. This procedure eventually yields the basis of intermediate states $\{|\tilde{\Psi}_J^N\rangle\}$ in which the Hamiltonian of the system can be represented forming the Hermitian ADC matrix

$$M_{IJ} = \left\langle \tilde{\Psi}_I^N \right| \hat{H} - E_0^N \left| \tilde{\Psi}_J^N \right\rangle \tag{6.66}$$

Here, the Hamiltonian of the system is shifted by the exact ground state energy $E_0^N$. The solution of the secular ISR equation

$$\mathbf{MX} = \mathbf{X\Omega}, \quad \text{with} \quad \mathbf{X}^\dagger\mathbf{X} = \mathbf{1} \tag{6.67}$$

yields the exact excitation energies $\Omega_n$ as eigenvalues. From the eigenvectors the exact excited states in terms of the intermediate states can be constructed as

$$\left|\Psi_n^N\right\rangle = \sum_J X_{nJ} \left|\tilde{\Psi}_J^N\right\rangle \tag{6.68}$$

This also allows for the calculation of dipole transition moments via

$$T_n = \left\langle \Psi_n^N \right| \hat{\mu} \left|\Psi_0^N\right\rangle = \sum_J X_{nJ}^\dagger \left\langle \tilde{\Psi}_J^N \right| \hat{\mu} \left|\Psi_0^N\right\rangle, \tag{6.69}$$

as well as excited state properties via

$$O_n = \left\langle \Psi_n^N \right| \hat{o} \left|\Psi_n^N\right\rangle = \sum_{I,J} X_{nI}^\dagger X_{nJ} \left\langle \tilde{\Psi}_I^N \right| \hat{o} \left|\Psi_J^N\right\rangle, \tag{6.70}$$

where $O_n$ is the property associated with operator $\hat{o}$.

Up to now, the exact $N$-electron ground state has been employed in the derivation of the ADC scheme, thereby resulting in exact excitation energies and exact excited state wave functions. Since the exact ground state is usually not known, a suitable approximation must be used in the derivation of the ISR equations. An obvious choice is the $n$th order Møller-Plesset ground state yielding the $n$th order approximation of the ADC scheme. The appropriate ADC equations have been derived in detail up to third order in Refs. 106–108. Due to the dependency on the Møller-Plesset ground state the $n$th order ADC scheme should only be applied to molecular systems whose ground state is well described by the respective MP($n$) method.

As in Møller-Plesset perturbation theory, the first ADC scheme which goes beyond the non-correlated wave function methods in Section 6.2 is ADC(2). ADC(2) is available in a *strict* and an *extended* variant which are usually referred to as ADC(2)-s and ADC(2)-x, respectively. The strict variant ADC(2)-s scales with the 5th power of the basis set. The quality of ADC(2)-s excitation energies and corresponding excited states is comparable to the quality of those obtained with CIS(D) (Section 6.6) or CC2. More precisely, excited states with mostly single excitation character are well-described by ADC(2)-s, while excited states with double excitation character are usually found to be too high in energy. The ADC(2)-x variant which scales as the sixth power of the basis set improves the treatment of doubly excited states, but at the cost of introducing an imbalance between singly and doubly excited states. As result, the excitation energies of doubly excited states are substantially decreased in ADC(2)-x relative to the states possessing mostly single excitation character with the excitation energies of both types of states exhibiting relatively large errors. Still, ADC(2)-x calculations can be used as a diagnostic tool for the importance doubly excited states in the low-energy region of the spectrum by comparing to ADC(2)-s results. A significantly better description of both singly and doubly excited states is provided by the third order ADC scheme ADC(3). The accuracy of excitation energies obtained with ADC(3) is almost comparable to CC3, but at computational costs that scale with the sixth power of the basis set only[99].

### 6.8.2 Resolution of the Identity ADC Methods

Similar to MP2 and CIS(D), the ADC equations can be reformulated using the resolution-of-the-identity (RI) approximation. This significantly reduces the cost of the integral transformation and the storage requirements. Although it does not change the overall computational scaling of $O(N^5)$ for ADC(2)-s or $O(N^6)$ for ADC(2)-x with the system size, employing the RI approximation will result in computational speed-up of calculations of larger systems.

The RI approximation can be used with all available ADC methods. It is invoked as soon as an auxiliary basis set is specified using AUX_BASIS.

### 6.8.3 Spin Opposite Scaling ADC(2) Models

The spin-opposite scaling (SOS) approach originates from MP2 where it was realized that the same spin contributions can be completely neglected, if the opposite spin components are scaled appropriately. In a similar way it is possible to simplify the second order ADC equations by neglecting the same spin contributions in the ADC matrix, while the opposite-spin contributions are scaled with appropriate semi-empirical parameters.[100,109,110]

Starting from the SOS-MP2 ground state the same scaling parameter $c_T = 1.3$ is introduced into the ADC equations to scale the $t_2$ amplitudes. This alone, however, does not result in any computational savings or substantial improvements of the ADC(2) results. In addition, the opposite spin components in the ph/2p2h and 2p2h/ph coupling blocks have to be scaled using a second parameter $c_c$ to obtain a useful SOS-ADC(2)-s model. With this model the optimal value of the parameter $c_c$ has been found to be 1.17 for the calculation of singlet excited states.[110]

To extend the SOS approximation to the ADC(2)-x method yet another scaling parameter $c_x$ for the opposite spin components of the off-diagonal elements in the 2p2h/2p2h block has to be introduced. Here, the optimal values of the scaling parameters have been determined as $c_c = 1.0$ and $c_x = 0.9$ keeping $c_T$ unchanged.[100]

The spin-opposite scaling models can be invoked by setting METHOD to either SOSADC(2) or SOSADC(2)-x. By default, the scaling parameters are chosen as the optimal values reported above, i.e. $c_T = 1.3$ and $c_c = 1.17$ for ADC(2)-s and $c_T = 1.3$, $c_c = 1.0$, and $c_x = 0.9$ for ADC(2)-x. However, it is possible to adjust any of the three parameters by setting ADC_C_T, ADC_C_C, or ADC_C_X, respectively.

### 6.8.4 Core-Excitation ADC Methods

Core-excited electronic states are located in the high energy X-ray region of the spectrum. Thus, to compute core-excited states using standard diagonalization procedures, which usually solve for the energetically lowest-lying excited states first, requires the calculation of a multitude of excited states. This is computationally very expensive and only feasible for calculations on very small molecules and small basis sets.

The core-valence separation (CVS) approximation solves the problem by neglecting the couplings between core and valence excited states *a priori*.[111,112] Thereby, the ADC matrix acquires a certain block structure which allows to solve only for core-excited states. The application of the CVS approximation is justified, since core and valence excited states are energetically well separated and the coupling between both types of states is very small. To achieve the separation of core and valence excited states the CVS approximation forces the following types of two-electron integrals to zero

$$\begin{aligned} \langle Ip|qr\rangle = \langle pI|qr\rangle = \langle pq|Ir\rangle = \langle pq|rI\rangle &= 0 \\ \langle IJ|pq\rangle = \langle pq|IJ\rangle &= 0 \\ \langle IJ|Kp\rangle = \langle IJ|pK\rangle = \langle Ip|JK\rangle = \langle pI|JK\rangle &= 0, \end{aligned} \tag{6.71}$$

where capital letters $I, J, K$ refer to core orbitals while lower-case letters $p, q, r$ denote non-core occupied or virtual orbitals.

The core-valence approximation is currently available of ADC models up to third order (including the extended variant).[101–103] It can be invoked by setting METHOD to the respective ADC model prefixed by CVS. Besides the general ADC related keywords, two additional keywords in the *$rem* block are necessary to control CVS-ADC calculations:

- ADC_CVS = TRUE switches on the CVS-ADC calculation
- CC_REST_OCC = n controls the number of core orbitals included in the excitation space. The integer n corresponds to the n energetically lowest core orbitals.

*Example:* cytosine with the molecular formula $C_4H_5N_3O$ includes one oxygen atom. To calculate O 1s core-excited states, CC_REST_OCC has to be set to 1, because the 1s orbital of oxygen is the energetically lowest. To obtain the N 1s core excitations, the integer has to be set to 4, because the 1s orbital of the oxygen atom is included as well, since it is energetically below the three 1s orbitals of the nitrogen atoms. Accordingly, to simulate the C 1s XAS spectrum of cytosine, CC_REST_OCC must be set to 8.

To obtain the best agreement with experimental data, one should use the CVS-ADC(2)-x method in combination with at least a diffuse triple-$\zeta$ basis set.[101–103]

### 6.8.5 Spin-Flip ADC Methods

The spin-flip (SF) method[14,68,75,113] is used for molecular systems with few-reference wave functions like diradicals, bond-breaking, rotations around single bonds, and conical intersections. Starting from a triplet ($m_s = 1$) ground state reference a spin-flip excitation operator $\{\hat{C}_J\} = \{c^\dagger_{a\beta}c_{i\alpha};\ c^\dagger_{a\beta}c^\dagger_{b\sigma}c_{i\alpha}c_{j\sigma}$, a < b, i < j} is introduced, which flipped the spin of one electron while singlet and ($m_s = 0$) triplet excited target states are yielded. The spin-flip method is implemented for the ADC(2) (strict and extended) and the ADC(3) methods.[113] Note that high-spin ($m_s = 1$) triplet states can be calculated with the SF-ADC method as well using a closed-shell singlet reference state. The number of spin-flip states that shall be calculated is controlled with the *$rem* variable SF_STATES.

### 6.8.6 Properties and Visualization

The calculation of excited states using the ADCMAN module yields by default the usual excitation energies and the excitation amplitudes, as well as the transition dipole moments, oscillator strengths, and the norm of the doubles part of the amplitudes (if applicable). In addition, the calculation of excited state properties, like dipole moments, and transition properties between excited states can be requested by setting the *$rem* variables ADC_PROP_ES and ADC_PROP_ES2ES, respectively. Resonant two-photon absorption cross-sections of the excited states can be computed as well, using either sum-over-states expressions or the matrix inversion technique. The calculation via sum-over-state expressions is automatically activated, if ADC_PROP_ES2ES is set. The accuracy of the results, however, strongly depends on the number of states which are included in the summation, *i.e.* the number of states computed. At least, 20-30 excited states (per irreducible representation) are required to yield useful results for the two-photon absorption cross-sections. Alternatively, the resonant two-photon absorption cross-sections can be calculated by setting ADC_PROP_TPA to TRUE. In this case, the computation of a large number of excited states is avoided and there is no dependence on the number of excited states. Instead, an additional linear matrix equation has to be solved for every excited state for which the two-photon absorption cross-section is computed. Thus, the obtained resonant two-photon absorption cross-sections are usually more reliable.

Furthermore, the ADCMAN module allows for the detailed analysis of the excited states and export of various types of excited state related orbitals and densities. This can be activated by setting the keyword STATE_ANALYSIS. Details on the available analyses and export options can be found in section 10.2.7.

### 6.8.7 Excited States in Solution with ADC/SS-PCM

ADCMAN is interfaced to the versatile polarizable-continuum model (PCM) implemented in Q-CHEM (Section 11.2.2) and may thus be employed for the calculation and analysis of excited-state wave functions and transitions in solution, or more general in dielectric environments. The interface follows the state-specific approach, and supports a self-consistent equilibration of the solvent field for long-lived excited states commonly referred to as *equilibrium solvation*, as well as the calculation of perturbative corrections for vertical transitions, known as *non-equilibrium solvation* (see also section 11.2.2.3). Combining both approaches, virtually all photochemically relevant processes can be modeled, including ground- and excited-state absorption, fluorescence, phosphorescence, as well as photochemical reactivity. Requiring only the electron-densities of ground- and excited states of the solute as well as and the dielectric constant and refractive index of the solvent, ADC/SS-PCM is straightforward to set up and supports all orders and variants of ADC for which densities are available via the ISR. This includes all levels of canonical ADC, SOS-ADC, SF-ADC for electronically complicated situations, as well as CVS-ADC for the description of core-excited states with and without the resolution of the identity and frozen-core approximation, restricted closed-shell references as well unrestricted open-shell. The computed solvent-relaxed wave functions can be visualized and analyzed using the interface to libwfa.

Although we give a short introduction to the theory in this section, it is limited to a brief, qualitative overview with only the most important equations, leaving out major aspects such as the polarization work. For a comprehensive, formal introduction to the theory please be referred to Refs. 114 and 115 as well as sections 11.2.2 and11.2.2.3.

#### 6.8.7.1 Modeling the Absorption Spectrum in Solution

**(A) Theory**

Let us begin with a brief review of the theoretical and technical aspects of the calculation of absorption spectra in solution. For this purpose, one would typically employ the perturbative, state-specific approach in combination with an ADC of second or third order. The first step is a self-consistent reaction field calculation [SCRF, Hartree-Fock with a PCM, Eq. (6.72)].

$$E_0 = \langle 0|\hat{H}^{\text{vac}} + \hat{R}(0)|0\rangle \tag{6.72}$$

The PCM is formally represented by the reaction- or solvent-field operator $\hat{R}$. In practice, $\hat{R}$ is a set of point charges placed on the molecular surface, which are optimized together with the orbitals during the SCF procedure. Note that since $\hat{R}$ accounts for the self-induced polarization of the solute, it depends on solute's wave function (here the ground state), which will in the following be indicated in the subscript $\hat{R}_0$.

After the SCRF is converged, the final surface charges and the respective operator can, according to the Franck-Condon principle, be separated into a "slow" solvent-nuclei related ($\epsilon - n^2$) and "fast", solvent-electron related ($n^2$) component (using Marcus partitioning, eq. (6.73)), and are stored on disk.

$$\hat{R}(0) \equiv \hat{R}_0^{\text{tot}} = \hat{R}_0^{\text{f}} + \hat{R}_0^{\text{s}} \tag{6.73}$$

$$q^f = \frac{n^2-1}{\epsilon-1} q^{total} \quad q^s = \frac{\epsilon - n^2}{\epsilon - 1} q^{total} = q - q^f \tag{6.74}$$

The "polarized" MOs resulting from the SCRF step are subjected to ordinary MP/ADC calculations, which yield the correlation energy for the ground and excitation energies for the excited states. However, since the MOs contain the interaction with the complete "frozen" solvent-polarization of the SCF ground-state density ($\hat{R}^{\text{tot}}$, i.e., *both* components), the resulting excitation energies violate the Franck-Condon principle, which requires the solvents electronic degrees of freedom (fast component of the polarization) to be relaxed. Furthermore, the solvent field has been obtained for the SCF density, which more often than not provides a poor description of the electrostatic nature of the solute and may in turn lead to systematic errors in the excitation energies.

To account for the relaxation of the solvent electrons and bring the excitation energies in accordance with Franck-Condon, we employ the perturbative ansatz shown in eq. (6.75), in which the fast component of the ground-state solvent field $\hat{R}_0^{\text{f}}$ is replaced by the respective quantity computed for the excited-state density $\hat{R}_{\text{i}}^{\text{f}}$. In this framework, the excitation energy of an excited state $i$ computed with the polarized MOs can be identified as the zeroth-order energy (eq. (6.77)), while the first-order term becomes the difference between the interaction of the zeroth-order excited-state density with the fast component of the ground- and excited-state solvent fields given in eq. (6.78).

$$E_{\text{i}}^{\text{NEq}} = \langle i|\hat{H}^{\text{vac}} + \hat{R}_0^{\text{tot}} + \lambda(\hat{R}_{\text{i}}^{\text{f}} - \hat{R}_0^{\text{f}})|i\rangle \tag{6.75}$$

$$E_i^{\text{NEq}(0)} = \quad E_i^{(0)} + \lambda E_i^{(1)} + \ ... \tag{6.76}$$

$$E_i^{(0)} = \quad \langle i^{(0)}|\hat{H}^{\text{vac}} + \hat{R}_0^{\text{tot}}|i^{(0)}\rangle \tag{6.77}$$

$$E_i^{(1)} = \quad \langle i^{(0)}|\hat{R}_{\text{i}}^{\text{f}} - \hat{R}_0^{\text{f}}|i^{(0)}\rangle \tag{6.78}$$

After the ADC iterations have converged, $\hat{R}_{\text{i}}^{\text{f}}$ is computed from the respective excited-state density and $\hat{R}_0^{\text{f}}$ read from disk to form the first-order correction. Adding this so-called ptSS-term to the zeroth order energy, one arrives at the vertical excitation energy in the non-equilibrium limit $E_{\text{i}}^{\text{NEq}}$. Since the ptSS-term accounts for the response of the electron density of the implicit solvent molecules to excitation of the solute, its always a negative and lowers the excitation energy.

To eliminate problems resulting from the poor description of the ground-state solvent field at the SCF/HF level of theory, we use an additive correction that is based on the MP2 ground-state density. In a nutshell, it replaces the interaction between the potential of the difference density of the excited state $\hat{V}_{i^{(0)}} - \hat{V}_{0^{MP}}$ with the SCF solvent field $\hat{Q}_{0^{HF}}$ by the respective interaction with the MP solvent field $\hat{Q}_{0^{MP}}$:

$$E_{PTD} = (\hat{V}_{i^{(0)}} - \hat{V}_{0^{MP}}) \cdot \hat{Q}_{0^{MP}} \tag{6.79}$$

$$- (\hat{V}_{i^{(0)}} - \hat{V}_{0^{MP}}) \cdot \hat{Q}_{0^{HF}} \tag{6.80}$$

We will in the following refer to this as "perturbative, density-based" (PTD) correction and denote the respective approach as ptSS(PTD). Accordingly, the non-PTD corrected results will be denoted ptSS(PTE).

In addition to the ptSS-PCM discussed above, a perturbative variant of the so-called linear response corrections (termed ptLR presented in Ref. 114) is also available. In contrast to the ptSS approach, the ptLR corrections depend on the transition rather than the state (difference) densities. Although the ptLR corrections are always computed and printed, we discourage their use with the correlated ADC variants (2 and higher), for which the ptSS approach is better suited. The ptSS and ptLR approaches are also available for TDDFT as described in Section 11.2.2.3.

A detailed, comprehensive introduction to the theory and implementation, as well as extensive benchmark data for the non-equilibrium formalism in combination with all orders of ADC can be found in Ref. 114.

**(B) Usage**

The calculation of vertical transition energies with the ptSS-PCM approach is fairly straightforward. One just needs to activate the PCM (set SOLVENT_METHOD in the *$rem* block to PCM), enable the non-equilibrium functionality (set NONEQUILIBRIUM in the *$pcm* block to TRUE), and specify the solvent parameters, i.e., dielectric constant $\epsilon$ (DIELECTRIC) and squared refractive index $n^2$ (DIELECTRIC_INFI) in the *$solvent* block.

**Note:** Symmetry will be disabled for all calculations with a PCM.

In the output of a ptSS-PCM calculation with any correlated ADC variant, multiple values are given for the total and transition energies depending in the level of theory. For the correlated ADC variants these include:

- *Zeroth-order results*, direct outcome of the ADC calculation with solvated orbitals, excited states are ordered according to this value.
- *First-order results*, incl. only ptSS non-equilibrium corrections, termed ptSS(PTE).
- *Corrected first-order results*, incl. also the correlation correction, termed ptSS(PTD).
- *Scaled and corrected first-order results*, incl. an empirical scaling of the correlation correction, termed ptSS(PTD*).

We recommend to use the corrected first-order results since the PTD correction generally yields the most accurate results. The ptSS(PTD) approach is typically a very good approximation to the fully consistent, but more expensive PTED scheme, in which the solvent field is made self-consistent with the MP2 density (see next section for the PTED scheme and sample-jobs for a comparison of the two). Oscillator strengths are computed using the ptSS(PTD) energies. The PTD* approach includes an empirical scaling of the PTD correction that was developed to improve the solvatochromic-shifts of a series of nitro-aromatics with a cc-pVDZ basis.[114] However, we later found that for most other systems, the scaling slightly worsens the agreement with the fully consistent PTED scheme. In addition to the compiled total and transition energies, all contributing terms (ptSS, PTD etc.) are given separately. An even more verbose output detailing all the integrals contributing to the 1st order corrections can be obtained by increasing PCM_PRINT to 1.

**Note:** The zeroth-order results are by no means identical to the gas-phase excitation energies, and in turn the ptSS-term is not the solvatochromic shift.

**(C) Tips and Tricks**
To model the absorption spectrum in polar solvents, it is advisable to use a structure optimized in the presence of a PCM since the influence can be quite significant.

It should also be taken into account that a PCM, being a purely electrostatic model, lacks at the description of explicit interactions like e.g. hydrogen bonds. If fairly strong h-bond donors/acceptors are present and a protic/Lewis-basic solvent is to be modeled, consider adding a few (one or maximum two per donor/acceptor site) explicit solvent molecules (and optimize them together with the molecule in the presence of a PCM). A systematic investigation of this aspect for two representative examples can be found in Ref. 114.

If large differences between the HF and MP description of the molecule exist (PTD terms $> 0.2$ eV), it is advisable to employ the iterative ptSS(PTED) scheme described in the next section. Due to the inverse nature of the systematic errors of ADC(2) and ADC(3), the best guess for the excitation energy in solution is usually the average of both values.

For the PCM, we recommend the formally exact and slightly more expensive integral-equation formalism (IEF)-PCM variant (THEORY to IEFPCM in the *$pcm* block) in place of the approximate C-PCM, and otherwise default parameters.

#### 6.8.7.2 Modeling Emission, Excited-State Absorption and Photochemical Reactivity

**(A) Theory**
To model emission/absorption of solvent-equilibrated excited states and/or to investigate their photochemical reactivity, both components of the polarization have to be relaxed with respect to the desired state. This becomes evident considering that a full solvent-field equilibration (including the nuclear component) is essentially a geometry optimization for the implicit solvent, and should thus be employed whenever the geometry of the solute is optimized for the desired excited state. The Hamiltonian for a solvent-equilibrated state $|k\rangle$ simply reads

$$E_{\mathrm{k}}^{\mathrm{EqS}} = \langle k|\hat{H}^{\mathrm{vac}} + \hat{R}_{\mathrm{k}}|k\rangle \,. \tag{6.81}$$

Since the interaction with solvent field of any state has to be introduced to the MOs in the SCF step of a calculation, a solvent-field equilibration for excited states (and correlated ground states) is an iterative procedure requiring multiple SCF+ADC calculations until convergence is achieved. This also means that a guess (typically from a ptSS calculation) for the solvent field has to generated and used in the first SCF step. The MOs resulting from this first SCF are subjected to an ADC calculation, providing a first excited-state density, for which a new solvent field is computed and employed in the SCF step of the second iteration. This procedure is repeated until the solvent field (charges) and energies are converged and ultimately provides the total energy and wave function of the solvent-equilibrated excited state $|k\rangle$, as well as the out-of-equilibrium wave functions of other states. However, as the name already suggest, this state-specific approach yields a meaningful energy only for the solvent-equilibrated reference state $|k\rangle$. All other states have to be treated in the non-equilibrium limit and subjected to the formalism presented in the previous section to be consistent with the Franck-Condon principle. The respective generalization of the perturbative ansatz for the Hamiltonian for the $i^{\mathrm{th}}$ out-of-equilibrium state (*e.g.* the ground or any other excited state) in the field of the equilibrated state $|k\rangle$ reads as

$$E_{\rm i}^{\rm NEq(k)} = \langle i|\hat{H}^{\rm vac} + \hat{R}_{\rm k}^{\rm tot} + \lambda(\hat{R}_{\rm i}^{\rm f} - \hat{R}_{\rm k}^{\rm f})|i\rangle \ , \tag{6.82}$$

which can be solved using the procedure introduced in the previous section.

While most of the technical aspects concerning the application of the model will be covered in the following, we highly recommend to read at least the formalism and implementation section of Ref. 115 before using the model.

**(B) Usage**

The main switch for the state-specific equilibrium solvation (SS-PCM) is the variable EQSOLV in the *$pcm* block. Setting it to TRUE will cause the SCF+ADC calculation to be carried out using the solvent field of the first excited state (if that is found on disk), while any integer $> 1$ triggers the automatic solvent-field optimization and is interpreted as the maximum number of steps. We recommend to use EQSOLV = 15. Note that to use the SS-PCM, the PCM (SOLVENT_METHOD = PCM in *$rem*) and its non-equilibrium functionalities (NONEQUILIBRIUM = TRUE in *$pcm* ) have to be activated as well. Since the solvent-field iterations require an initial guess, a SS-PCM calculation is always the second (or third...) step of a multi-step job.

**Note:** Any SS-PCM calculation requires a preceding converged ptSS-PCM calculation (*i.e.*, EQSOLV = FALSE) for the desired state to provide a guess for the initial solvent field, or it will crash during the SCF.

To create the input-file for a multi step job, add "@@@" at the end of the input for the first job and append the input for the second job. See also section 3.6. Note that the solvent field used in the subsequent step is stored in the basis of the molecular-surface elements and thus, the geometry of the molecule as well as parameters that affect construction and discretization of the molecular cavity must not be changed between the jobs/steps. This, however, is not enforced.

The state for which the solvent field is to be optimized is specified using the variable EQSTATE in the *$pcm* block. A value of 0 refers to the MP ground-state (for PTED calculations), 1 selects the energetically lowest excited state (default), 2 the second lowest, and so on. The solvent field can be optimized for any singlet, triplet or spin-flip excited state. However, *only the desired class of states should be requested*, *i.e.*, either EE_SINGLETS or EE_TRIPLETS for singlet references, and either EE_STATES or SF_STATES for triplet references. To compute, *e.g.*, the phosphorescence energy, only triplet states should be requested and EQSTATE would typically be set to 1.

**Note:** Computing multiple classes of excited states during the solvent-field iterations will confuse the state-ordering logic of the program and yield the wrong results.

Convergence is controlled by EQS_CONV. Criteria are the SCF energy as well as the RMSD, MAD and largest single difference of the surface-charges. The convergence should not need to be modified. It is per default derived from the SCF convergence parameter (SCF_CONVERGENCE$-4$). The default value of 4 (since SCF_CONVERGENCE is 8 for ADC calculations) corresponds to an maximum energy change of 2.72 meV and will yield converged total energies for all states. Excitation energies and in particular the total energy of the reference state converge somewhat faster than the SCF energy, and a value of 3 may save some time for the computation e.g. the emission energy of large solutes.

A typical ADC/SS-PCM calculation consists of three steps/subsequent jobs:

1. Generation of an initial guess for the solvent field using a non-equilibrium calculation (EQSTATE = FALSE). To save time, this would typically be done with a smaller basis set and lower convergence criteria (e.g. ADC_DAVIDSON_CONVERGENCE 4).

2. Converging the solvent field for the desired state. In this step it is advisable to compute as few states as possible (maybe one more than EQSTATE to be aware of looming state crossings), and more importantly, only the desired class of excited states.

3. Computing all excited states of interest and their properties in the previously converged solvent field. If the reference state of the solvent-field equilibration is a singlet state, this is straightforward and any number of singlet/triplet states can be computed in this final step without further input. *If singlet states are to be computed in the solvent field of a triplet state*, the additional variable EQS_REF in *$pcm* has to be set to tell the program which state is to be treated as the reference state in this last step. For this purpose, EQS_REF is set to the desired triplet state plus the number of *converged* singlet states. Hence, assuming 2 singlet states are to be calculated along with the triplets in previously converged solvent field of $T_1$, and furthermore that both singlets converge, EQS_REF needs to be set to 3 (this can not be realized using the variable EQSTATE, because we still want to use the solvent field of the lowest triplet state stored in the previous step).

The self-consistent SS-PCM can also be used to compute a fully consistent solvent field for the MP2 ground state by setting EQSTATE to 0. This is known as ptSS(PTED) approach and can improve vertical excitation energies if there are large differences between the electrostatic properties of the SCF and MP ground states (large PTD corrections). In most cases, however, the non-iterative PTD approach is a very good approximation to the PTED approach (see the sample jobs below). The output of a PTED calculation is essentially identical to that of a ptSS calculation.

The program possesses limited intelligence in detecting the type of the calculation (PTED or EQS/SS-PCM) as well as the target state of the solvent-field equilibration and will assemble and designate the ptSS corrections, total energies and transition energies accordingly. This logic will be confused if multiple classes of states (*e.g.* singlet and triplets) are computed simultaneously during the iterations, and/or if the ordering of the states changes. Nevertheless, in a final job for a previously converged solvent field *of a singlet reference* singlet and triplet states can be computed together yielding the correct output. However, if singlet states are computed in the converged solvent field of *a triplet reference* the additional variable EQS_REF has to be set (and only then, see above).

In the “HF/MP2/MP3 Summary” section, zeroth (without ptSS) and first (with ptSS) order total energies of the respective ground state in the solvent field of the target state are given along with the ptSS term for a vertical transition from the equilibrated state (emission). Note that to obtain the MP3 ground state energy during an ADC(3)/EQS calculation, the ptSS term has to be added manually (it is printed in the MP2 Summary since we use the MP2 density for this purpose).

In the “Excited-State Summary” section the reference state is distinguished from the out-of-equilibrium states. Respective total and transition energies are given along with the non-equilibrium corrections, transition moments and some remarks. Note that for emission, in contrast to absorption, the ptSS term increases the transition energy as it lowers the energy of the out-of-equilibrium ground state. The so-called "self-ptSS term" is a perturbative estimate of how much the solvent field of this state is off from its equilibrium. Although the line in the output changes depending on the value (from "not converged" to "reasonably converged" to "converged") it is not used in the actual convergence check. Note that the self-ptSS term is computed with $n^2$ (dielectric_infi) and not $\epsilon$, as it probably should be. The self-ptSS term may be used to judge how well a solvent field computed with a different methodology (basis, ADC order/variant) fits. In such a case, values $< 0.01$ eV signal a reasonable agreement.

To calculate inter-state transition moments for excited-state absorption, the variable ADC_PROP_ES2ES has to be set to TRUE. Unfortunately, transition energies have to be computed manually from the (first-order) total energies given in the excited-state summary, since the transition energies given along with the state-to-state transition moments following the excite-state summary are incorrect (missing non-equilibrium terms).

The progress of the solvent-field iteration and their convergence is reported following the "Excited-State Summary".

**(C) Tips and Tricks**

To compute fluorescence and phosphorescence energies, solute geometry AND solvent field should both be optimized for the suspected emitting state. Since hardly any programs can perform excited-state optimizations with the SS-PCM solvent models, you will probably have to use gas-phase geometries. In our experience, the errors introduced by this approximation are small to negligible (typically $< 0.1$ eV) in non-polar solvents, but can become significant in polar solvents, in particular for polar charge-transfer states.

Concerning the predicted emission energies, we found that ADC(2)/SS-PCM typically over-stabilizes CT states, yielding emission energies that are too low. SOS-ADC(2) can improve this error, but does not eliminate it. In general, while emission energies are more accurate with (SOS-)ADC(2)/SS-PCM than with ADC(3)/SS-PCM, the latter affords better relative state energies (see Ref. 115).

Keep in mind that the solute-solvent interaction of polar solvents with polar (e.g. charge-transfer) states can become quite large (multiple eV), and may thus affect the ordering and nature of the excited states. This is quite typical for charge-transfer states even in remotely polar solvents. If they are not the lowest state in the non-equilibrium calculation, but say $S_2$, it is typically necessary to do one solvent-field iteration for the CT state (EQSOLV = 1 and EQSTATE = 2), which brings the CT down to become $S_1$, and then continue the iterations with EQSOLV = 15 and EQSTATE = 1. It is in general advisable to carefully check if the character and/or energetic ordering of the states changes during the procedure, in particular for any equilibration of the solvent field for all but the lowest excited state (*e.g.* $S_2$ or $S_3$). But even the solvent-field equilibration for a weakly polar $S_1$ in a polar solvent can cause a more polar state with the same dipole-vector to become the lowest state.

If the excited-states swap during the procedure, find out in which step the swap occurred and do only so many iterations (*i.e.*, set EQSOLV accordingly). In a following job, adjust the variable EQSTATE and continue the iterations. If states start to mix when they get close, it might help to first set an artificially large dielectric constant to induce the change in ordering, and then continue with the desired dielectric constant in a following job.

If performance is critical, the calculations may be accelerated by lowering the ADC convergence during the solvent-field iterations (set ADC_DAVIDSON_CONVERGENCE = 5). The number of iterations may be reduced by first converging the solvent field with a smaller basis/at a lower level of ADC followed by another job with the full basis/level of ADC. However, in our experience ADC(2) and ADC(3) solvent fields for the same state differ quite significantly and the approach probably does not help much. In contrast, the solvent field computed with a smaller basis (*e.g.* 3-21G, SVP) is often a good approximation for that computed with a larger basis (*e.g.* def2-TZVP, see examples), such this may actually help. It is in general advisable to compute just as many states as is necessary during the solvent-field iterations and include higher lying excited states and triplets in the final job. In ADC(2) calculations for large systems, one should always employ the resolution-of-the-identity approximation.

To save time in PTED jobs, it is suggested to disable the computation of excited states during the solvent-field iterations of a PTED job by setting EE_SINGLETS (and/or EE_TRIPLETS/ EE_STATES) to 0 and compute the excited-states in a final job once the reaction field is converged.

For more tips and examples see the sample jobs.

### 6.8.8 Frozen-Density Embedding: FDE-ADC methods

FDE-ADC[116] represents a method to include interactions between an embedded species and its environment into an ADC($n$) calculation based on Frozen Density Embedding Theory (FDET)[117,118]. FDE-ADC supports ADC and CVS-ADC methods of orders 2s,2x and 3 and regular ADC job control keywords also apply.

The FDE-ADC method starts with generating an embedding potential using a MP($n$) density for the embedded system (A) and a DFT or HF density for the environment (B). A Hartree-Fock calculation is then carried out during which the embedding potential is added to the Fock operator. The embedded Hartree-Fock orbitals act as an input for the subsequent ADC calculation which yields the embedded properties (vertical excitation energies, oscillator strengths, etc.). Further information on the FDE-ADC method and FDE-ADC job control are described in Section 11.7.1.

### 6.8.9 ADC Job Control

For an ADC calculation it is important to ensure that there are sufficient resources available for the necessary integral calculations and transformations. These resources are controlled using the *$rem* variables MEM_STATIC and MEM_TOTAL. The memory used by ADC is currently 95% of the difference MEM_TOTAL - MEM_STATIC.

An ADC calculation is requested by setting the *$rem* variable METHOD to the respective ADC variant. Furthermore, the number of excited states to be calculated has to be specified using one of the *$rem* variables EE_STATES, EE_SINGLETS, or EE_TRIPLETS. The former variable should be used for open-shell or unrestricted closed-shell calculations, while the latter two variables are intended for restricted closed-shell calculations. Even though not recommended, it is possible to use EE_STATES in a restricted calculation which translates into EE_SINGLETS, if neither EE_SINGLETS nor EE_TRIPLETS is set. Similarly, the use EE_SINGLETS in an unrestricted calculation will translate into EE_STATES, if the latter is not set as well.

All *$rem* variables to set the number of excited states accept either an integer number or a vector of integer numbers. A single number specifies that the same number of excited states are calculated for every irreducible representation the point group of the molecular system possesses (molecules without symmetry are treated as $C_1$ symmetric). In contrast, a vector of numbers determines the number of states for each irreducible representation explicitly. Thus, the length of the vector always has to match the number of irreducible representations. Hereby, the excited states are labeled according to the irreducible representation of the electronic transition which might be different from the irreducible representation of the excited state wave function. Users can choose to calculate any molecule as $C_1$ symmetric by setting CC_SYMMETRY = FALSE.

**METHOD**

Controls the order in perturbation theory of ADC.

TYPE:

STRING

DEFAULT:

None

OPTIONS:

| | |
|---|---|
| ADC(1) | Perform ADC(1) calculation. |
| ADC(2) | Perform ADC(2)-s calculation. |
| ADC(2)-x | Perform ADC(2)-x calculation. |
| ADC(3) | Perform ADC(3) calculation. |
| SOS-ADC(2) | Perform spin-opposite scaled ADC(2)-s calculation. |
| SOS-ADC(2)-x | Perform spin-opposite scaled ADC(2)-x calculation. |
| CVS-ADC(1) | Perform ADC(1) calculation of core excitations. |
| CVS-ADC(2) | Perform ADC(2)-s calculation of core excitations. |
| CVS-ADC(2)-x | Perform ADC(2)-x calculation of core excitations. |

RECOMMENDATION:

None

**EE_STATES**

Controls the number of excited states to calculate.

TYPE:

INTEGER/ARRAY

DEFAULT:

0 Do not perform an ADC calculation

OPTIONS:

| | |
|---|---|
| $n > 0$ | Number of states to calculate for each irrep or |
| $[n_1, n_2, ...]$ | Compute $n_1$ states for the first irrep, $n_2$ states for the second irrep, ... |

RECOMMENDATION:

Use this variable to define the number of excited states in case of unrestricted or open-shell calculations. In restricted calculations it can also be used, if neither EE_SINGLETS nor EE_TRIPLETS is given. Then, it has the same effect as setting EE_SINGLETS.

**EE_SINGLETS**

Controls the number of singlet excited states to calculate.

TYPE:

INTEGER/ARRAY

DEFAULT:

0 Do not perform an ADC calculation of singlet excited states

OPTIONS:

| | |
|---|---|
| $n > 0$ | Number of singlet states to calculate for each irrep or |
| $[n_1, n_2, ...]$ | Compute $n_1$ states for the first irrep, $n_2$ states for the second irrep, ... |

RECOMMENDATION:

Use this variable to define the number of excited states in case of restricted calculations of singlet states. In unrestricted calculations it can also be used, if EE_STATES not set. Then, it has the same effect as setting EE_STATES.

**EE_TRIPLETS**

Controls the number of triplet excited states to calculate.

TYPE:

INTEGER/INTEGER ARRAY

DEFAULT:

0 Do not perform an ADC calculation of triplet excited states

OPTIONS:

| | |
|---|---|
| $n > 0$ | Number of triplet states to calculate for each irrep or |
| $[n_1, n_2, ...]$ | Compute $n_1$ states for the first irrep, $n_2$ states for the second irrep, ... |

RECOMMENDATION:

Use this variable to define the number of excited states in case of restricted calculations of triplet states.

**CC_SYMMETRY**

Activates point-group symmetry in the ADC calculation.

TYPE:

LOGICAL

DEFAULT:

TRUE If the system possesses any point-group symmetry.

OPTIONS:

| | |
|---|---|
| TRUE | Employ point-group symmetry |
| FALSE | Do not use point-group symmetry |

RECOMMENDATION:

None

**ADC_PROP_ES**

Controls the calculation of excited state properties (currently only dipole moments).

TYPE:

LOGICAL

DEFAULT:

FALSE

OPTIONS:

| | |
|---|---|
| TRUE | Calculate excited state properties. |
| FALSE | Do not compute state properties. |

RECOMMENDATION:

Set to TRUE, if properties are required.

**ADC_PROP_ES2ES**

Controls the calculation of transition properties between excited states (currently only transition dipole moments and oscillator strengths), as well as the computation of two-photon absorption cross-sections of excited states using the sum-over-states expression.

TYPE:

LOGICAL

DEFAULT:

FALSE

OPTIONS:

| | |
|---|---|
| TRUE | Calculate state-to-state transition properties. |
| FALSE | Do not compute transition properties between excited states. |

RECOMMENDATION:

Set to TRUE, if state-to-state properties or sum-over-states two-photon absorption cross-sections are required.

**ADC_PROP_TPA**

Controls the calculation of two-photon absorption cross-sections of excited states using matrix inversion techniques.

TYPE:

LOGICAL

DEFAULT:

FALSE

OPTIONS:

| | |
|---|---|
| TRUE | Calculate two-photon absorption cross-sections. |
| FALSE | Do not compute two-photon absorption cross-sections. |

RECOMMENDATION:

Set to TRUE, if to obtain two-photon absorption cross-sections.

**STATE_ANALYSIS**

Controls the analysis and export of excited state densities and orbitals (see 10.2.7 for details).

TYPE:

LOGICAL

DEFAULT:

FALSE

OPTIONS:

| | |
|---|---|
| TRUE | Perform excited state analyses. |
| FALSE | No excited state analyses or export will be performed. |

RECOMMENDATION:

Set to TRUE, if detailed analysis of the excited states is required or if density or orbital plots are needed.

**ADC_C_T**

Set the spin-opposite scaling parameter $c_T$ for an SOS-ADC(2) calculation. The parameter value is obtained by multiplying the given integer by $10^{-3}$.

TYPE:

INTEGER

DEFAULT:

1300 Optimized value $c_T = 1.3$.

OPTIONS:

$n$ Corresponding to $n \cdot 10^{-3}$

RECOMMENDATION:

Use the default.

**ADC_C_C**

Set the spin-opposite scaling parameter $c_c$ for the ADC(2) calculation. The parameter value is obtained by multiplying the given integer by $10^{-3}$.

TYPE:

INTEGER

DEFAULT:

1170 Optimized value $c_c = 1.17$ for ADC(2)-s or

1000 $c_c = 1.0$ for ADC(2)-x

OPTIONS:

$n$ Corresponding to $n \cdot 10^{-3}$

RECOMMENDATION:

Use the default.

**ADC_C_X**

Set the spin-opposite scaling parameter $c_x$ for the ADC(2)-x calculation. The parameter value is obtained by multiplying the given integer by $10^{-3}$.

TYPE:

INTEGER

DEFAULT:

1300 Optimized value $c_x = 0.9$ for ADC(2)-x.

OPTIONS:

$n$ Corresponding to $n \cdot 10^{-3}$

RECOMMENDATION:

Use the default.

**ADC_NGUESS_SINGLES**

Controls the number of excited state guess vectors which are single excitations. If the number of requested excited states exceeds the total number of guess vectors (singles and doubles), this parameter is automatically adjusted, so that the number of guess vectors matches the number of requested excited states.

TYPE:

INTEGER

DEFAULT:

Equals to the number of excited states requested.

OPTIONS:

$n$ User-defined integer.

RECOMMENDATION:

**ADC_NGUESS_DOUBLES**

Controls the number of excited state guess vectors which are double excitations.

TYPE:

INTEGER

DEFAULT:

0

OPTIONS:

$n$ User-defined integer.

RECOMMENDATION:

**ADC_DO_DIIS**

Activates the use of the DIIS algorithm for the calculation of ADC(2) excited states.

TYPE:

LOGICAL

DEFAULT:

FALSE

OPTIONS:

| | |
|---|---|
| TRUE | Use DIIS algorithm. |
| FALSE | Do diagonalization using Davidson algorithm. |

RECOMMENDATION:

None.

**ADC_DIIS_START**

Controls the iteration step at which DIIS is turned on.

TYPE:

INTEGER

DEFAULT:

1

OPTIONS:

$n$ User-defined integer.

RECOMMENDATION:

Set to a large number to switch off DIIS steps.

**ADC_DIIS_SIZE**

Controls the size of the DIIS subspace.

TYPE:

INTEGER

DEFAULT:

7

OPTIONS:

$n$ User-defined integer

RECOMMENDATION:

None

**ADC_DIIS_MAXITER**

Controls the maximum number of DIIS iterations.

TYPE:

INTEGER

DEFAULT:

50

OPTIONS:

$n$ User-defined integer.

RECOMMENDATION:

Increase in case of slow convergence.

**ADC_DIIS_ECONV**

Controls the convergence criterion for the excited state energy during DIIS.

TYPE:

INTEGER

DEFAULT:

6 Corresponding to $10^{-6}$

OPTIONS:

$n$ Corresponding to $10^{-n}$

RECOMMENDATION:

None

**ADC_DIIS_RCONV**

Convergence criterion for the residual vector norm of the excited state during DIIS.

TYPE:

INTEGER

DEFAULT:

6 Corresponding to $10^{-6}$

OPTIONS:

$n$ Corresponding to $10^{-n}$

RECOMMENDATION:

None

**ADC_DAVIDSON_MAXSUBSPACE**

Controls the maximum subspace size for the Davidson procedure.

TYPE:

INTEGER

DEFAULT:

$5\times$ the number of excited states to be calculated.

OPTIONS:

$n$ User-defined integer.

RECOMMENDATION:

Should be at least $2-4\times$ the number of excited states to calculate. The larger the value the more disk space is required.

**ADC_DAVIDSON_MAXITER**

Controls the maximum number of iterations of the Davidson procedure.

TYPE:

INTEGER

DEFAULT:

60

OPTIONS:

$n$ Number of iterations

RECOMMENDATION:

Use the default unless convergence problems are encountered.

**ADC_DAVIDSON_CONV**

Controls the convergence criterion of the Davidson procedure.

TYPE:

INTEGER

DEFAULT:

$6$ Corresponding to $10^{-6}$

OPTIONS:

$n\leq 12$ Corresponding to $10^{-n}$.

RECOMMENDATION:

Use the default unless higher accuracy is required or convergence problems are encountered.

**ADC_DAVIDSON_THRESH**

Controls the threshold for the norm of expansion vectors to be added during the Davidson procedure.

TYPE:

INTEGER

DEFAULT:

Twice the value of ADC_DAVIDSON_CONV, but at maximum $10^{-14}$.

OPTIONS:

$n\leq 14$ Corresponding to $10^{-n}$

RECOMMENDATION:

Use the default unless convergence problems are encountered. The threshold value $10^{-n}$ should always be smaller than the convergence criterion ADC_DAVIDSON_CONV.

**ADC_PRINT**

Controls the amount of printing during an ADC calculation.

TYPE:

INTEGER

DEFAULT:

1 Basic status information and results are printed.

OPTIONS:

0 Quiet: almost only results are printed.

1 Normal: basic status information and results are printed.

2 Debug: more status information, extended information on timings.

...

RECOMMENDATION:

Use the default.

**ADC_CVS**

Activates the use of the CVS approximation for the calculation of CVS-ADC core-excited states.

TYPE:

LOGICAL

DEFAULT:

FALSE

OPTIONS:

TRUE Activates the CVS approximation.

FALSE Do not compute core-excited states using the CVS approximation.

RECOMMENDATION:

Set to TRUE, if to obtain core-excited states for the simulation of X-ray absorption spectra. In the case of TRUE, the *$rem* variable CC_REST_OCC has to be defined as well.

**CC_REST_OCC**

Sets the number of restricted occupied orbitals including active core occupied orbitals.

TYPE:

INTEGER

DEFAULT:

0

OPTIONS:

$n$ Restrict $n$ energetically lowest occupied orbitals to correspond to the active core space.

RECOMMENDATION:

*Example:* cytosine with the molecular formula $C_4H_5N_3O$ includes one oxygen atom. To calculate O 1s core-excited states, $n$ has to be set to 1, because the 1s orbital of oxygen is the energetically lowest. To obtain the N 1s core excitations, the integer $n$ has to be set to 4, because the 1s orbital of the oxygen atom is included as well, since it is energetically below the three 1s orbitals of the nitrogen atoms. Accordingly, to simulate the C 1s spectrum of cytosine, $n$ must be set to 8.

**SF_STATES**

Controls the number of excited spin-flip states to calculate.

TYPE:

INTEGER

DEFAULT:

0 Do not perform a SF-ADC calculation

OPTIONS:

| | |
|---|---|
| $n > 0$ | Number of states to calculate for each irrep or |
| $[n_1, n_2, ...]$ | Compute $n_1$ states for the first irrep, $n_2$ states for the second irrep, ... |

RECOMMENDATION:

Use this variable to define the number of excited states in the case of a spin-flip calculation. SF-ADC is available for ADC(2)-s, ADC(2)-x and ADC(3).

**Keywords for SS-PCM control in *$pcm*:**

**EQSOLV**

Main switch of the self-consistent SS-PCM procedure.

INPUT SECTION: *$pcm*

TYPE:

INTEGER

DEFAULT:

0

OPTIONS:

| | |
|---|---|
| 0 | No self-consistent SS-PCM. |
| 1 | Single SS-PCM calculation (SCF+ADC) with the solvent field found on disk. |
| $n$ >1 | Do a maximum of $n$ automatic solvent-field iterations. |

RECOMMENDATION:

We recommend to use 15 steps max. Typical convergence is 3-5 steps. In difficult cases 6-12. If the solvent-field iteration do not converge in 15 steps, something is wrong. *Also make sure that a solvent field has been stored on disk by a previous job.*

**EQSTATE**

Specifies the state for which the solvent field is to be optimized.

INPUT SECTION: *$pcm*

TYPE:

INTEGER

DEFAULT:

0

OPTIONS:

| | |
|---|---|
| 0 | MP2 ground state (for PTED approach) |
| 1 | energetically lowest excited state |
| 2 | 2nd lowest excited state |
| ... | |

RECOMMENDATION:

Given that only one class of excited states is calculated, the state will be selected according to its energetic position shown in the "Exited-State Summary" of the output file. A maximum of 99 states is stored and can be selected.

**EQS_CONV**

Controls the convergence of the solvent-field iterations by setting the convergence criteria (a mixture of SCF energy and charge-vector). SCF energy criterion computes as $10^{-\text{value}}$ eH

INPUT SECTION: *$pcm*

TYPE:

INTEGER

DEFAULT:

SCF_CONVERGENCE$-4 = 4$

OPTIONS:

3 May be sufficient for emission energies
4 Assured converged total energies (2.7 meV)
5 Really tight

RECOMMENDATION:

Use the default.

**EQS_REF**

Allows to specify which state is to be treated as the reference state in the ADC part of the calculation. Does in contrast to EQSTATE not affect which solvent field is loaded in the SCF step. Only has to be used when singlets are computed in the solvent field of a triplet reference. Note that (converged) singlets states are always counted before triplets, and thus to select $T_1$ in a calculation with EE_SINGLETS = 2 this has to be set to 3.

INPUT SECTION: *$pcm*

TYPE:

INTEGER

DEFAULT:

Same as EQSTATE

OPTIONS:

1 First excited state
2 Second excited state
...

RECOMMENDATION:

Only needed when computing singlet states in the solvent field of a triplet reference.

### 6.8.10 Examples

**Example 6.77** Q-CHEM input for an ADC(2)-s calculation of singlet exited states of methane with D2 symmetry. In total six excited states are requested corresponding to four (two) electronic transitions with irreducible representation $B_1$ ($B_2$).

```
$molecule
   0 1
   C
   H   1 r0
   H   1 r0   2  d0
   H   1 r0   2  d0   3  d1
   H   1 r0   2  d0   4  d1

   r0 = 1.085
   d0 = 109.4712206
   d1 = 120.0
$end

$rem
   METHOD              adc(2)
   BASIS               6-31g(d,p)
   MEM_TOTAL           4000
   MEM_STATIC          100
   EE_SINGLETS         [0,4,2,0]
$end
```

**Example 6.78** Q-CHEM input for an unrestricted RI-ADC(2)-s calculation with $C_1$ symmetry using DIIS. In addition, excited state properties and state-to-state properties are computed.

```
$molecule
   0 2
   C    0.0    0.0   -0.630969
   N    0.0    0.0    0.540831
$end

$rem
   METHOD           adc(2)
   BASIS            aug-cc-pVDZ
   AUX_BASIS        rimp2-aug-cc-pVDZ
   MEM_TOTAL        4000
   MEM_STATIC       100
   CC_SYMMETRY      false
   EE_STATES        6
   ADC_DO_DIIS      true
   ADC_PROP_ES      true
   ADC_PROP_ES2ES   true
   ADC_PROP_TPA     true
$end
```

**Example 6.79** Q-CHEM input for a restricted CVS-ADC(2)-x calculation with $C_1$ symmetry using 4 parallel CPU cores. In this case, the 10 lowest nitrogen K-shell singlet excitations are computed.

```
$molecule
   0 1
   C    -5.17920    2.21618    0.01098
   C    -3.85603    2.79078    0.05749
   N    -2.74877    2.08372    0.05569
   C    -5.23385    0.85443   -0.04040
   C    -2.78766    0.70838    0.01226
   N    -4.08565    0.13372   -0.03930
   N    -3.73433    4.14564    0.16144
   O    -1.81716   -0.02560    0.00909
   H    -4.50497    4.74117   -0.12037
   H    -2.79158    4.50980    0.04490
   H    -4.10443   -0.88340   -0.07575
   H    -6.08637    2.82445    0.02474
   H    -6.17341    0.29221   -0.07941
$end

$rem
   METHOD                      cvs-adc(2)-x
   EE_SINGLETS                10
   ADC_DAVIDSON_MAXSUBSPACE   60
   MEM_TOTAL                  10000
   MEM_STATIC                 1000
   THREADS                    4
   CC_SYMMETRY                false
   BASIS                      6-31G*
   ADC_DAVIDSON_THRESH        8
   SYMMETRY                   false
   ADC_DAVIDSON_MAXITER       900
   ADC_CVS                    true
   CC_REST_OCC                4
$end
```

**Example 6.80** Q-CHEM input for a restricted SF-ADC(2)-s calculation of the first three spin-flip target states of cyclobutadiene without point group symmetry.

```
$molecule
   0 3
   C     0.000000     0.000000     0.000000
   C     1.439000     0.000000     0.000000
   C     1.439000     0.000000     1.439000
   C     0.000000     0.000000     1.439000
   H    -0.758726     0.000000    -0.758726
   H     2.197726     0.000000    -0.758726
   H     2.197726     0.000000     2.197726
   H    -0.758726     0.000000     2.197726
$end

$rem
   METHOD          adc(2)
   MEM_TOTAL       15000
   MEM_STATIC      1000
   CC_SYMMETRY     false
   BASIS           3-21G
   SF_STATES       3
$end
```

**Example 6.81** Q-CHEM input for a restricted ADC(2)-x calculation of water with $C_s$ symmetry. Four singlet A" excited states and two triplet A' excited states are requested. For the first two states ($1^1$A" and $1^3$A') the transition densities as well as the attachment and detachment densities are exported into cube files.

```
$molecule
   0 1
   O   0.000   0.000   0.000
   H   0.000   0.000   0.950
   H   0.896   0.000  -0.317
$end

$rem
   METHOD            adc(2)-x
   BASIS             6-31g(d,p)
   THREADS           2
   MEM_TOTAL         3000
   MEM_STATIC        100
   EE_SINGLETS       [0,4]
   EE_TRIPLETS       [2,0]
   ADC_PROP_ES       true
   MAKE_CUBE_FILES   true
$end

$plots
Plot transition and a/d densities
   40 -3.0 3.0
   40 -3.0 3.0
   40 -3.0 3.0
   0 0 2 2
   1 2
   1 2
$end
```

**Example 6.82** Q-CHEM input for a ADC(2)-s/ptSS-PCM calculation of the five lowest singlet-excited states of N,N-dimethylnitroaniline in diethylether. PCM settings are all default values except THEORY, which is set to IEFPCM instead of the default CPCM.

```
$rem
   THREADS                4
   METHOD                 adc(2)
   BASIS                  3-21G
   MEM_TOTAL              32000
   MEM_STATIC             2000
   ADC_PROP_ES            true
   ADC_PRINT              1
   EE_SINGLETS            5
   ADC_DAVIDSON_MAXITER   100
   PCM_PRINT              1        !increase print level
   SOLVENT_METHOD         pcm      !invokes PCM solvent model
$end

$pcm
   nonequilibrium    true
   theory                 IEFPCM  !default is CPCM, IEFPCM is more accurate
   Solver                 Inversion
   vdwScale               1.20
$end

$solvent
   dielectric             4.34  !epsilon of Et2O
   dielectric_infi        1.829 !n_square of Et2O
$end

$molecule
   0 1
   C   -4.263068      2.512843      0.025391
   C   -5.030982      1.361365      0.007383
   C   -4.428196      0.076338     -0.021323
   C   -3.009941      0.019036     -0.030206
   C   -2.243560      1.171441     -0.011984
   C   -2.871710      2.416638      0.015684
   H   -4.740854      3.480454      0.047090
   H   -2.502361     -0.932570     -0.052168
   H   -1.166655      1.104642     -0.020011
   H   -6.104933      1.461766      0.015870
   N   -5.178541     -1.053870     -0.039597
   C   -6.632186     -0.969550     -0.034925
   H   -6.998203     -0.462970      0.860349
   H   -7.038179     -1.975370     -0.051945
   H   -7.001616     -0.431420     -0.910237
   C   -4.531894     -2.358860     -0.066222
   H   -3.912683     -2.476270     -0.957890
   H   -5.298508     -3.126680     -0.075403
   H   -3.902757     -2.507480      0.813678
   N   -2.070815      3.621238      0.033076
   O   -0.842606      3.510489      0.025476
   O   -2.648404      4.710370      0.054545
$end
```

**Example 6.83** Q-CHEM input for a ADC/SS-PCM EQS solvent-field equilibration for the first excited singlet state of peroxinitrite in water, which provides e.g. the fluorescence energy. After generating a starting point in the first job (using a smaller basis and lower adc convergence criteria), the solvent-field iterations are carried out until convergence in the second job. In the third job, ADC(2) excited states are computed in the converged solvent field that was left on disk by the second Job. In the fourth job, we additionally compute ADC(3) excited states. This mixed approach should in general be used with great caution. If the self-ptSS term of the reference state becomes too large (>0.01 eV) like it is the case here, the fully consistent approach should be used (i.e. also the solvent-field computed at the ADC(3) level). PCM settings are all default values except THEORY, which is set to IEFPCM instead of the default CPCM.

```
$comment
   ADC(2)/ptSS-PCM to generate starting point for the EqS
   Step in the next Job
$end

$rem
   THREADS             2
   METHOD              adc(2)
   BASIS               3-21G !using a small basis to speed up this step
   MEM_TOTAL           6000
   MEM_STATIC          1000
   EE_SINGLETS         1
   ADC_PROP_ES         true
   ADC_DAVIDSON_CONV   4
   SOLVENT_METHOD      pcm
$end

$pcm
   nonequilibrium true
$end

$solvent !Water
   dielectric       78.4
   dielectric_infi   1.76
$end

$molecule
   -1 1
   N    -0.068642000000     -0.600693000000     -0.723424000000
   O     0.349666000000      0.711166000000      1.187490000000
   O    -0.948593000000      0.200668000000     -0.956940000000
   O     0.659040000000     -0.386002000000      0.402650000000
$end
```

```
@@@

$comment
   ADC(2)/ptSS-PCM(EqS) solvent-field equilibration
   for the first excited state
$end

$rem
   THREADS          2
   METHOD           adc(2)
   BASIS            6-31G*
   MEM_TOTAL        6000
   MEM_STATIC       1000
   EE_SINGLETS      2 !compute 2 singlets during the equilibration
   ADC_PROP_ES      true
   SOLVENT_METHOD   pcm !activate PCM
$end

$pcm
   eqsolv      15    !maximum 15 steps, converges after 5
   eqstate     1     !Equilibrate 1st excited state
   eqs_conv    4     !Default convergence
   theory      iefpcm
   nonequilibrium true
$end

$solvent
   dielectric       78.4
   dielectric_infi   1.76
$end

$molecule
   read
$end

@@@

$comment
   Compute ADC(2) excited states in the converged solvent field
$end

$rem
   THREADS          2
   METHOD           adc(2)
   BASIS            6-31G*
   MEM_TOTAL        6000
   MEM_STATIC       1000
   EE_SINGLETS      6 !compute 6 singlets
   ADC_PROP_ES      true
   ADC_PROP_ES2ES   true !compute ES 2 ES transition moments for ESA
   SOLVENT_METHOD   pcm
$end

$pcm
   eqsolv   true !only one calculation with converged field
   eqstate  1    !Equilibrate 1st excited state
   theory   iefpcm
   nonequilibrium true
$end

$solvent
   dielectric      78.4
   dielectric_infi  1.76
$end

$molecule
   read
$end

@@@

$comment
   We can also compute ADC(3) excited states in the
   converged ADC(2) solvent field and use the self-
   ptSS term as diagnostic.
$end

$rem
   THREADS          2
   METHOD           adc(3)
   BASIS            6-31G*
   MEM_TOTAL        6000
   MEM_STATIC       1000
   EE_SINGLETS      3 !compute 3 singlets
   EE_TRIPLETS      1    !and 1 triplet
   ADC_PROP_ES      true
   SOLVENT_METHOD   pcm
$end

$pcm
   eqsolv   true !only one calculation with converged field
   eqstate  1    !Equilibrate 1st excited state
   theory   iefpcm
   nonequilibrium true
$end

$solvent
   dielectric      78.4
   dielectric_infi  1.76
$end

$molecule
   read
$end
```

**Example 6.84** Q-CHEM input for a riADC(2)/ptSS-PCM(PTED) calculation for the five lowest excited states of peroxinitrite in water. After generating a starting point in the first job, which also provides the ptSS(PTE) and ptSS(PTD) results for comparison, the solvent-field is equilibrated for the MP density in the second job. During the iterations, the calculation of excited states is disabled to speed up the calculation. In the third job, five excited states are computed at the riADC(2)/ptSS(PTED) level of theory. Although the PTD corrections for this molecule are unusually large, a comparison of the PTE, PTD and PTD* results from the first job with the PTED results from the third job will reveal a reasonable agreement between the fully consistent PTED and the perturbative PTD approaches. In the fourth job, excited states are calculated with a larger basis set. The self-ptSS term of the MP ground state will be quite small, showing that the solvent-field computed with the smaller SVP basis is a good approximation.

```
$comment
   riADC(2)/ptSS-PCM to generate starting point for
   the PTED iterations in the next Job and provide
   PTE and PTD energies for comparing with PTED
$end

$rem
   THREADS          2
   METHOD           adc(2)
   BASIS            def2-SVP
   AUX_BASIS        rimp2-VDZ
   MEM_TOTAL        6000
   MEM_STATIC       1000
   EE_SINGLETS      5
   ADC_PROP_ES      true
   SOLVENT_METHOD   pcm
$end

$pcm
   nonequilibrium true
$end

$solvent !Water
   dielectric      78.4
   dielectric_infi  1.76
$end

$molecule
   -1 1
   N    -0.068642000000     -0.600693000000     -0.723424000000
   O     0.349666000000      0.711166000000      1.187490000000
   O    -0.948593000000      0.200668000000     -0.956940000000
   O     0.659040000000     -0.386002000000      0.402650000000
$end

@@@

$comment
   riADC(2)/ptSS-PTED solvent-field equilibration for
   the MP ground state. No excited states are computed
$end

$rem
   THREADS          2
   METHOD           adc(2)
   BASIS            def2-SVP
   AUX_BASIS        rimp2-VDZ
   MEM_TOTAL        6000
   MEM_STATIC       1000
   EE_SINGLETS      0 !dont compute ES
   ADC_PROP_ES      true
   SOLVENT_METHOD   pcm !activate PCM
$end

$pcm
   eqsolv     15    !maximum 15 steps
   eqstate    0     !Equilibrate MP ground state
   eqs_conv   5     !higher convergence
   theory     iefpcm
   nonequilibrium true
$end

$solvent
   dielectric      78.4
   dielectric_infi  1.76
$end

$molecule
   read
$end

@@@

$comment
   Compute ADC(2)/ptSS-PTED excited states in the
   converged solvent field
$end

$rem
   THREADS          2
   METHOD           adc(2)
   BASIS            def2-SVP
   AUX_BASIS        rimp2-VDZ
   MEM_TOTAL        6000
   MEM_STATIC       1000
   EE_SINGLETS      5 !compute 5 singlets
   ADC_PROP_ES      true
   SOLVENT_METHOD   pcm
$end

$pcm
   eqsolv   true !only one calculation with converged field
   eqstate  0    !Equilibrate MP ground state
   theory   iefpcm
   nonequilibrium true
$end

$solvent
   dielectric 78.4
   dielectric_infi 1.76
$end

$molecule
   read
$end

@@@

$comment
   We can also compute the ES in the converged field
   with a larger basis and without RI in the stored
   solvent-field.
$end
```

```
$rem
   THREADS         2
   METHOD          adc(2)
   BASIS           def2-TZVP
   MEM_TOTAL       6000
   MEM_STATIC      1000
   EE_SINGLETS     3 !compute 3 singlets
   ADC_PROP_ES     true
   SOLVENT_METHOD  pcm
$end

$pcm
   eqsolv  true !only one calculation with converged field
   eqstate 0  !Equilibrate MP ground state
   theory iefpcm
   nonequilibrium true
$end

$solvent
   dielectric 78.4
   dielectric_infi 1.76
$end

$molecule
   read
$end
```

## 6.9 Restricted Active Space Spin-Flip (RAS-SF) and Configuration Interaction (RAS-CI)

The restricted active space spin-flip (RAS-SF) is a special form of configuration interaction that is capable of describing the ground and low-lying excited states with moderate computational cost in a single-reference formulation[119–122], including strongly correlated systems. The RAS-SF approach is essentially a much lower computational cost alternative to Complete Active Space SCF (CAS-SCF) methods. RAS-SF typically works by performing a full CI calculation within an active space that is defined by the half-occupied orbitals of a restricted open shell HF (ROHF) reference determinant. In this way the difficulties of state-specific orbital optimization in CAS-SCF are bypassed. Single excitations into (hole) and out of (particle) the active space provide state-specific relaxation instead. Unlike most CI-based methods, RAS-SF is size-consistent, as well as variational, and, the increase in computational cost with system size is modest for a fixed number of spin flips. Beware, however, for the increase in cost as a function of the number of spin-flips is exponential! RAS-SF has been shown to be capable of tackling multiple low-lying electronic states in polyradicals and reliably predicting ground state multiplicities[119–121,123–125].

RAS-SF can also be viewed as one particular case of a more general RAS-CI family of methods. For instance, instead of defining the active space via spin-flipping as above, initial orbitals of other types can be read in, and electronic excitations calculated this way may be viewed as a RAS-EE-CI method (though size-consistency will generally be lost). Similar to EOM-CC approaches (see Section 6.7), other target RAS-CI wave functions can be constructed starting from any electronic configuration as the reference and using a general excitation-type operator. For instance, one can construct an ionizing variant that removes an arbitrary number of particles that is RAS-$n$IP-CI. An electron attaching variant is RAS-$n$EA-CI[122].

Q-CHEM features two versions of RAS-CI code with different, complementary, functionality. One code (invoked by specifying CORRRELATION = RASCI) has been written by David Casanova[122]; below we will refer to this code as RASCI1. The second implementation (invoked by specifying CORRRELATION = RASCI2) is primarily by Paul Zimmerman[120]; we will refer to it as RASCI2 below.

The RASCI1 code uses an integral-driven implementation (exact integrals) and spin-adaptation of the CI configurations which results in a smaller diagonalization dimension. The current Q-CHEM implementation of RASCI1 only allows for the calculation of systems with an even number of electrons, with the multiplicity of each state being printed alongside the state energy. Shared memory parallel execution decreases compute time as all the underlying integrals routines are parallelized.

The RASCI2 code includes the ability to simulate closed and open shell systems (i.e., even and odd numbers of electrons), fast integral evaluation using the resolution of the identity (RI) approximation, shared memory parallel operation, and analysis of the $\langle S^2\rangle$ values and natural orbitals. The natural orbitals are stored in the QCSCRATCH directory in a folder called "NOs" in MOLDEN-readable format. Shared memory parallel is invoked as described in Section 2.8. A RASCI2 input requires the specification of an auxiliary basis set analogous to RI-MP2 computations (see Section 5.6.1). Otherwise, the active space as well as hole and particle excitations are specified in the same way as in RASCI1.

**Note:** Because RASCI2 uses the RI approximation, the total energies computed with the two codes will be slightly different; however, the energy differences between different states should closely match each other.

### 6.9.1 The Restricted Active Space (RAS) Scheme

In the RAS formalism, we divide the orbital space into three subspaces called RAS1, RAS2 and RAS3 (Fig. 6.2). The RAS-CI states are defined by the number of orbitals and the restrictions in each subspace.

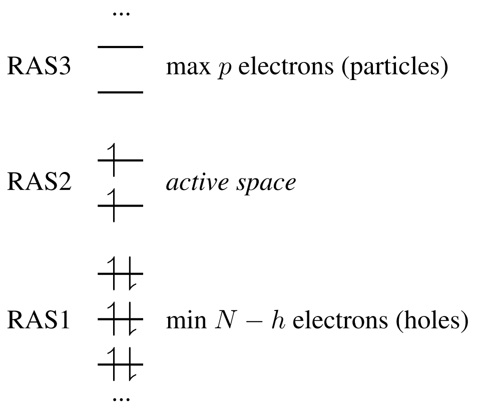

Figure 6.2: Orbital subspaces in RAS-CI employing a ROHF triplet reference.

The single reference RAS-CI electronic wave functions are obtained by applying a spin-flipping or excitation operator $\hat{R}$ on the reference determinant $\phi^{(0)}$.

$$\left|\Psi^{\text{RAS}}\right\rangle = \hat{R}\left|\phi^{(0)}\right\rangle \tag{6.83}$$

The $\hat{R}$ operator must obey the restrictions imposed in the subspaces RAS1, RAS2 and RAS3, and can be decomposed as:

$$\hat{R} = \hat{r}^{\text{RAS2}} + \hat{r}^{h} + \hat{r}^{p} + \hat{r}^{hp} + \hat{r}^{2h} + \hat{r}^{2p} + ... \tag{6.84}$$

where $\hat{r}^{\text{RAS2}}$ contains all possible electronic promotions within the RAS2 space, that is, a reduced full CI, and the rest of the terms generate configurations with different number of holes ($h$ super-index) in RAS1 and electrons in RAS3 ($p$ super-index). The current implementation truncates this series up to the inclusion of hole and particle contributions, *i.e.* the first three terms on the right hand side of Eq. (6.84).

### 6.9.2 Second-Order Perturbative Corrections to RAS-CI

In general, the RAS-CI family of methods within the $hole$ and $particle$ approximation is unable to capture the necessary amounts of dynamic correlation for the computation of relative energies with chemical accuracy. The missed correlation can be added on top of the RAS-CI wave function using multi-reference perturbation theory (MRPT).[126] The second order energy correction, *i.e.* RASCI(2), can be expressed as:

$$E^{(2)} = -\sum_k \frac{|\langle k|\hat{H}|0\rangle|^2}{E_k - E_0 + \epsilon} \tag{6.85}$$

where $0$ indicates the zero-order space and $\{|k\rangle\}$ is the complementary set of determinants. There is no natural choice for the $\{E_k\}$ excited energies in MRPT, and two different models are available within the RASCI(2) approach, that is the Davidson-Kapuy and Epstein-Nesbet partitionings. As it is common practice in many second-order MRPT corrections, the denominator energy differences in Eq. (6.85) can be level shifted with a parameter $\epsilon$.

### 6.9.3 Excitonic Analysis of the RAS-CI Wave Function

The RAS-CI wave function of multi-chromophoric systems can be decomposed in terms of local excitations (LE), charge resonances (CR) and multi-exciton configurations (ME).

$$|\Psi\rangle = |\Psi^{LE}\rangle + |\Psi^{CR}\rangle + |\Psi^{ME}\rangle \tag{6.86}$$

The wave function decomposition scheme combines the use of fragment (localized) orbitals with the computation of charge and spin cumulant indexes.[127,128] Such analysis is extremely useful in order to characterize in great detail the nature of the ground and excited states in the presence of two or more molecules or chromophoric moieties. The ME contributions can be further decomposed into different spin coupled configurations localized on each. Typically, the ME part of a singlet state in a molecular dimer can be decomposed as singlet-singlet (SS) and triplet-tripled (TT) contributions.

$$|\Psi^{ME}\rangle \approx |\Psi^{SS}\rangle + |\Psi^{TT}\rangle \tag{6.87}$$

At the moment, this analysis is only available for the decomposition of spin singlet states.

### 6.9.4 Job Control for the RASCI1 Implementation

At present the RASCI1 and RASCI2 implementations employ different keywords (which will be reconciled in a future version). This subsection applies to RASCI1 (even electron systems, spin adapted algorithm using exact integrals).

The use of the RAS-CI1 methodology is controlled by setting the *$rem* variable CORRELATION to RASCI and EXCHANGE should be set to HF. The RASCI1 implementation is only compatible with even numbers of electrons and restricted orbitals, *i.e.*, UNRESTRICTED = FALSE.

The minimum input also requires specifying the desired (non-zero) value for RAS_ROOTS, the number of electrons in the "active" RAS2 space and the number of orbitals in RAS1 and RAS2 subspaces.

**RAS_ROOTS**
Sets the number of RAS-CI roots to be computed.
TYPE:
INTEGER
DEFAULT:
None
OPTIONS:
$n$ $n > 0$ Compute $n$ RAS-CI states
RECOMMENDATION:
None. Only works with RASCI.

**RAS_ELEC**
Sets the number of electrons in RAS2 (active electrons).
TYPE:
INTEGER
DEFAULT:
None
OPTIONS:
$n$ User-defined integer, $n > 0$
RECOMMENDATION:
None. Only works with RASCI.

**RAS_ACT**
Sets the number of orbitals in RAS2 (active orbitals).
TYPE:
INTEGER
DEFAULT:
None
OPTIONS:
$n$ User-defined integer, $n > 0$
RECOMMENDATION:
None. Only works with RASCI.

**RAS_OCC**
Sets the number of orbitals in RAS1
TYPE:
INTEGER
DEFAULT:
0
OPTIONS:
$n$ User-defined integer, $n > 0$
RECOMMENDATION:
These are the initial doubly occupied orbitals (RAS1) before including $hole$ type of excitations. The RAS1 space starts from the lowest orbital up to RAS_OCC, i.e. no frozen orbitals option available yet. Only works with RASCI.

**RAS_DO_HOLE**

Controls the presence of hole excitations in the RAS-CI wave function.

TYPE:

LOGICAL

DEFAULT:

TRUE

OPTIONS:

| | |
|---|---|
| TRUE | Include hole configurations (RAS1 to RAS2 excitations) |
| FALSE | Do not include hole configurations |

RECOMMENDATION:

None. Only works with RASCI.

**RAS_DO_PART**

Controls the presence of particle excitations in the RAS-CI wave function.

TYPE:

LOGICAL

DEFAULT:

TRUE

OPTIONS:

| | |
|---|---|
| TRUE | Include particle configurations (RAS2 to RAS3 excitations) |
| FALSE | Do not include particle configurations |

RECOMMENDATION:

None. Only works with RASCI.

**RAS_AMPL_PRINT**

Defines the absolute threshold ($\times 10^2$) for the CI amplitudes to be printed.

TYPE:

INTEGER

DEFAULT:

10 0.1 minimum absolute amplitude

OPTIONS:

$n$ User-defined integer, $n \geq 0$

RECOMMENDATION:

None. Only works with RASCI.

**RAS_ACT_ORB**

Sets the user-selected active orbitals (RAS2 orbitals).

TYPE:

INTEGER ARRAY

DEFAULT:

From RAS_OCC+1 to RAS_OCC+RAS_ACT

OPTIONS:

$[i, j, k...]$ The number of orbitals must be equal to the RAS_ACT variable

RECOMMENDATION:

None. Only works with RASCI.

**RAS_NATORB**

Controls the computation of the natural orbital occupancies.

TYPE:

LOGICAL

DEFAULT:

FALSE

OPTIONS:

| | |
|---|---|
| TRUE | Compute natural orbital occupancies for all states |
| FALSE | Do not compute natural orbital occupancies |

RECOMMENDATION:

None. Only works with RASCI.

**RAS_NATORB_STATE**

Allows to save the natural orbitals of a RAS-CI computed state.

TYPE:

INTEGER

DEFAULT:

0

OPTIONS:

| | |
|---|---|
| $i$ | Saves the natural orbitals for the $i$-th state |

RECOMMENDATION:

None. Only works with RASCI.

**RAS_GUESS_CS**

Controls the number of closed shell guess configurations in RAS-CI.

TYPE:

INTEGER

DEFAULT:

0

OPTIONS:

| | |
|---|---|
| $n$ | Imposes to start with $n$ closed shell guesses |

RECOMMENDATION:

Only relevant for the computation of singlet states. Only works with RASCI.

**RAS_SPIN_MULT**

Specifies the spin multiplicity of the roots to be computed

TYPE:

INTEGER

DEFAULT:

| | |
|---|---|
| 1 | Singlet states |

OPTIONS:

| | |
|---|---|
| 0 | Compute any spin multiplicity |
| $2n + 1$ | User-defined integer, $n \geq 0$ |

RECOMMENDATION:

Only for RASCI, which at present only allows for the computation of systems with an even number of electrons. Thus, RAS_SPIN_MULT only can take odd values.

**RAS_PT2**

Perform second-order perturbative correction to RAS-CI energy

TYPE:

LOGICAL

DEFAULT:

FALSE

OPTIONS:

| | |
|---|---|
| TRUE | Compute RASCI(2) energy corrections |
| FALSE | Do not compute RASCI(2) energy corrections |

RECOMMENDATION:

None. Only works with RASCI.

**RAS_PT2_PARTITION**

Specifies the partitioning scheme in RASCI(2)

TYPE:

INTEGER

DEFAULT:

| | |
|---|---|
| 1 | Davidson-Kapuy (DK) partitioning |

OPTIONS:

| | |
|---|---|
| 2 | Epstein-Nesbet (EN) partitioning |
| 0 | Do both DK and EN partitionings |

RECOMMENDATION:

Only for RASCI if RAS_PT2 is set to true.

**RAS_PT2_VSHIFT**

Defines the energy level shift ($\times 10^3$ $au$) in RASCI(2)

TYPE:

INTEGER

DEFAULT:

0

OPTIONS:

| | |
|---|---|
| $n$ | User-defined integer |

RECOMMENDATION:

Only for RASCI if RAS_PT2 is set to true.

**RAS_NFRAG**

If $n > 0$ activates the excitation analysis in RASCI

TYPE:

INTEGER

DEFAULT:

0

OPTIONS:

| | |
|---|---|
| $n$ | Number of fragments to be considered |

RECOMMENDATION:

Only for RASCI. The printed information level is controlled by RAS_PRINT.

**RAS_NFRAG_ATOMS**

Sets the number of atoms in each fragment.

TYPE:

INTEGER ARRAY

DEFAULT:

None

OPTIONS:

$[i, j, k...]$ The sum of the numbers must be equal to the total number of atoms in the systems

RECOMMENDATION:

None. Only works with RASCI.

**RAS_FRAG_MO**

Sets the number of atoms in each fragment.

TYPE:

INTEGER ARRAY

DEFAULT:

[NOcc,NAct,NVir] Number of orbitals within RAS1, RAS2 and RAS3 spaces

OPTIONS:

$[i, j, k...]$ Defines sets of canonical MOs to be localized into $n$ fragments

RECOMMENDATION:

Setting within RAS1, RAS2 and RAS3 spaces alleviates the computational cost of the localization procedure. It might also result in improved fragment orbitals. Only works with RASCI.

### 6.9.5 Job Control Options for RASCI2

At present the RASCI1 and RASCI2 implementations employ different keywords (which will be reconciled in a future version). This subsection applies to RASCI2 (even and odd electron systems, determinant-driven algorithm using the resolution of the identity approximation).

The use of the RAS-CI2 methodology is controlled by setting the CORRELATION = RASCI2 and EXCHANGE = HF. The minimum input also requires specifying the desired (non-zero) value for RAS_N_ROOTS, and the number of active occupied and virtual orbital comprising the "active" RAS2 space. RASCI2 calculations also require specification of an auxiliary basis via AUX_BASIS.

**RAS_N_ROOTS**

Sets the number of RAS-CI roots to be computed.

TYPE:

INTEGER

DEFAULT:

None

OPTIONS:

$n$ $n > 0$ Compute $n$ RAS-CI states

RECOMMENDATION:

None. Only works with RASCI2

**RAS_ACT_OCC**
Sets the number of occupied orbitals to enter the RAS active space.
TYPE:
Integer
DEFAULT:
None
OPTIONS:
n user defined integer
RECOMMENDATION:
None. Only works with RASCI2

**RAS_ACT_VIR**
Sets the number of virtual orbitals to enter the RAS active space.
TYPE:
Integer
DEFAULT:
None
OPTIONS:
n user defined integer
RECOMMENDATION:
None. Only works with RASCI2.

**RAS_ACT_DIFF**
Sets the number of alpha vs. beta electrons
TYPE:
Integer
DEFAULT:
None
OPTIONS:
n user defined integer
RECOMMENDATION:
Set to 1 for an odd number of electrons or a cation, -1 for an anion. Only works with RASCI2.

Other *$rem* variables that can be used to control the evaluation of RASCI2 calculations are SET_ITER for the maximum number of Davidson iterations, and N_FROZEN_CORE and N_FROZEN_VIRTUAL to exclude core and/or virtual orbitals from the RASCI2 calculation.

### 6.9.6 Examples

**Example 6.85** Input for a RAS-2SF-CI calculation of three states of the DDMX tetraradical using RASCI1. The active space (RAS2) contains 4 electrons in the 4 singly occupied orbitals in the ROHF quintet reference. Natural orbital occupancies are requested.

```
$molecule
   0 5
   C      0.000000    0.000000    1.092150
   C     -1.222482    0.000000    0.303960
   C     -2.390248    0.000000    1.015958
   H     -2.344570    0.000000    2.095067
   H     -3.363161    0.000000    0.537932
   C     -1.215393    0.000000   -1.155471
   H     -2.150471    0.000000   -1.702536
   C      0.000000    0.000000   -1.769131
   C      1.215393    0.000000   -1.155471
   H      2.150471    0.000000   -1.702536
   C      1.222482    0.000000    0.303960
   C      2.390248    0.000000    1.015958
   H      2.344570    0.000000    2.095067
   H      3.363161    0.000000    0.537932
$end

$rem
   EXCHANGE         hf
   CORRELATION      rasci
   BASIS            6-31g
   UNRESTRICTED     false
   MEM_TOTAL        4000
   MEM_STATIC       100
   RAS_ROOTS        3
   RAS_ACT          4
   RAS_ELEC         4
   RAS_OCC          25
   RAS_SPIN_MULT    0
   RAS_NATORB       true
$end
```

**Example 6.86** Input for a RAS-2IP-CI calculation of triplet states of $F_2$ molecule using the dianion closed shell $F_2^{2-}$ as the reference determinant. RASCI1 code is used

```
$molecule
   -2 1
   F
   F  1  rFF

   rFF = 1.4136
$end

$rem
   EXCHANGE         hf
   CORRELATION      rasci
   BASIS            cc-pVTZ
   MEM_TOTAL        4000
   MEM_STATIC       100
   RAS_ROOTS        2
   RAS_ACT          6
   RAS_ELEC         10
   RAS_OCC          4
   RAS_SPIN_MULT    3
$end
```

**Example 6.87** Input for a FCI/6-31G calculation of water molecule expanding the RAS2 space to the entire molecular orbital set. RASCI code is used.

```
$molecule
   0 1
   O   0.000  0.000   0.120
   H  -0.762  0.000  -0.479
   H   0.762  0.000  -0.479
$end

$rem
   EXCHANGE        hf
   CORRELATION     rasci
   BASIS           6-31G
   MEM_TOTAL       4000
   MEM_STATIC      100
   RAS_ROOTS       1
   RAS_ACT         13
   RAS_ELEC        10
   RAS_OCC         0
   RAS_SPIN_MULT   1
   RAS_DO_HOLE     false
   RAS_DO_PART     false
$end
```

**Example 6.88** Methylene single spin-flip calculation using RASCI2

```
$rem
   EXCHANGE       HF
   CORRELATION    RASCI2
   BASIS          cc-pVDZ
   AUX_BASIS      rimp2-cc-pVDZ
   UNRESTRICTED   false
   RAS_ACT_OCC    1    ! # alpha electrons
   RAS_ACT_VIR    1    ! # virtuals in active space
   RAS_ACT_DIFF   0    ! # set to 1 for odd # of e-s
   RAS_N_ROOTS    4
   SET_ITER       25   ! number of iterations in RASCI
$end

$molecule
   0 3
   C     0.0000000    0.0000000    0.0000000
   H    -0.8611113    0.0000000    0.6986839
   H     0.8611113    0.0000000    0.6986839
$end
```

**Example 6.89** Two methylene separated by 10 Å; double spin-flip calculation using RASCI2. Note that the $\langle S^2 \rangle$ values for this case will not be uniquely defined at the triply-degenerate ground state.

```
$rem
   EXCHANGE       HF
   CORRELATION    RASCI2
   BASIS          cc-pVDZ
   AUX_BASIS      rimp2-cc-pVDZ
   RAS_ACT_OCC    2    ! # alpha electrons
   RAS_ACT_VIR    2    ! # virtuals in active space
   RAS_ACT_DIFF   0    ! # set to 1 for odd # of e-s
   UNRESTRICTED   false
   RAS_N_ROOTS    8
   SET_ITER       25
$end

$molecule
   0 5
   C     0.0000000     0.0000000    0.0000000
   H    -0.8611113     0.0000000    0.6986839
   H     0.8611113     0.0000000    0.6986839
   C     0.0000000    10.0000000    0.0000000
   H    -0.8611113    10.0000000    0.6986839
   H     0.8611113    10.0000000    0.6986839
$end
```

**Example 6.90** RASCI2 calculation of the nitrogen cation using double spin-flip.

```
$rem
   EXCHANGE           HF
   CORRELATION        RASCI2
   BASIS              6-31G*
   AUX_BASIS          rimp2-VDZ
   RAS_ACT_OCC        3   ! # alpha electrons
   RAS_ACT_VIR        3   ! # virtuals in active space
   RAS_ACT_DIFF       1   ! # for odd # e-s, cation
   UNRESTRICTED       false
   N_FROZEN_CORE      2
   N_FROZEN_VIRTUAL   2
   RAS_N_ROOTS        8
   SET_ITER           25
$end


$molecule
   1 6
   N    0.0000000    0.0000000    0.0000000
   N    0.0000000    0.0000000    4.5
$end
```

## 6.10 Core Ionization Energies and Core-Excited States

In experiments using high-energy radiation (such as X-ray spectroscopy) core electrons can be ionized or excited to low-lying virtual orbitals. There are two ways to compute ionization energies of core electrons in Q-CHEM. The first approach is a simple energy difference calculation in which core ionization is computed from energy differences computed for the neutral and core-ionized state. It is illustrated by this example:

**Example 6.91** Q-CHEM input for calculating chemical shift for $1s$-level of methane ($CH_4$). The first job is just an SCF calculation to obtain the orbitals and CCSD energy of the neutral. The second job solves the HF and CCSD equations for the core-ionized state.

```
$molecule
   0,1
   C      0.000000    0.000000    0.000000
   H      0.631339    0.631339    0.631339
   H     -0.631339   -0.631339    0.631339
   H     -0.631339    0.631339   -0.631339
   H      0.631339   -0.631339   -0.631339
$end

$rem
   EXCHANGE         = HF
   CORRELATION      = CCSD
   BASIS            = 6-31G*
   MAX_CIS_CYCLES   = 100
$end

@@@

$molecule
   +1,2
   C      0.000000    0.000000    0.000000
   H      0.631339    0.631339    0.631339
   H     -0.631339   -0.631339    0.631339
   H     -0.631339    0.631339   -0.631339
   H      0.631339   -0.631339   -0.631339
$end

$rem
   UNRESTRICTED     = TRUE
   EXCHANGE         = HF
   BASIS            = 6-31G*
   MAX_CIS_CYCLES   = 100
   SCF_GUESS        = read  Read MOs from previous job and use occupied as specified below
   CORRELATION      = CCSD
   MOM_START        = 1 Do not reorder orbitals in SCF procedure!
$end

$occupied
   1 2 3 4 5
   2 3 4 5
$end
```

In this job, we first compute the HF and CCSD energies of neutral $CH_4$: $E_{\rm SCF} = -40.1949062375$ and $E_{\rm CCSD} = -40.35748087$ (HF orbital energy of the neutral gives Koopmans IE, which is 11.210 hartree = 305.03 eV). In the second job, we do the same for core-ionized $CH_4$. To obtain the desired SCF solution, MOM_START option and *$occupied* keyword are used. The resulting energies are $E_{\rm SCF} = -29.4656758483$ ($\langle S^2 \rangle$ = 0.7730) and $E_{\rm CCSD} = -29.64793957$. Thus, $\Delta E_{\rm CCSD} = (40.357481 - 29.647940) = 10.709$ hartree = 291.42 eV.

This approach can be further extended to obtain multiple excited states involving core electrons by performing CIS, TDDFT, or EOM-EE calculations.

The second approach is illustrated by the following input:

**Example 6.92** Q-CHEM input for calculating chemical shift for $1s$-level of methane ($CH_4$) using EOM-IP. Here we solve SCF as usual, then reorder the MOs such that the core orbital becomes the "HOMO", then solve the CCSD and EOM-IP equations with all valence orbitals frozen and the core orbital being active.

```
$molecule
   0,1
   C      0.000000    0.000000    0.000000
   H      0.631339    0.631339    0.631339
   H     -0.631339   -0.631339    0.631339
   H     -0.631339    0.631339   -0.631339
   H      0.631339   -0.631339   -0.631339
$end

$rem
   EXCHANGE         = HF
   BASIS            = 6-31G*
   MAX_CIS_CYCLES   = 100
   CORRELATION      = CCSD
   CCMAN2           = false
   N_FROZEN_CORE    = 4 Freeze all valence orbitals
   IP_STATES        = [1,0,0,0] Find one EOM_IP state
$end

$reorder_mo
   5 2 3 4 1
   5 2 3 4 1
$end
```

Here we use EOM-IP to compute core-ionized states. Since core states are very high in energy, we use "frozen core" trick to eliminate valence ionized states from the calculation. That is, we reorder MOs such that our core is the last occupied orbital and then freeze all the rest. The so computed EOM-IP energy is 245.57 eV. From the EOM-IP amplitude, we note that this state of a Koopmans character (dominated by single core ionization); thus, canonical HF MOs provide good representation of the correlated Dyson orbital. The same strategy can be used to compute core-excited states.

The accuracy of both calculations can be improved using triples corrections, *e.g.*, CCSD(T) and EOM-IP-CCSD(dT). It is also recommend using a better basis that has more core functions.

### 6.10.1 Calculations of States Involving Core Excitation/Ionization with (TD)DFT

TDDFT is not suited to describe the extended X-ray absorption fine structure (EXAFS) region, wherein the core electron is ejected and scattered by the neighboring atoms. Core-excitation energies computed with TDDFT with standard hybrid functionals are many electron volts too low compared with experiment. Exchange-correlation functionals specifically designed to treat core excitations are available in Q-CHEM. These short-range corrected (SRC) functionals are a modification of the more familiar long-range corrected functionals (discussed in Section 4.4.6). However, in SRC-DFT the short-range component of the Coulomb operator utilizes predominantly Hartree-Fock exchange, while the mid to long-range component is primarily treated with standard DFT exchange. These functionals can be invoked by using the SRC_DFT rem. In addition, a number of parameters (OMEGA, OMEGA2, HF_LR, HF_SR) that control the shape of the short and long-range Hartree-Fock components need to be specified. Full details of these functionals and appropriate values for the parameters can be found in Refs. 129,130. An example of how to use these functionals is given below. For the $K$-shell of heavy elements (2nd row of the periodic table) relativistic effects become increasing important and a further correction for these effects is required. Also calculations for $L$-shell excitations are complicated by core-hole spin orbit coupling.

## 6.11 Real-Time SCF Methods (RT-TDDFT, RT-HF, OSCF2)

Linear response calculations are the most efficient way to predict resonant electronic response frequencies and intensities. Q-CHEM can also propagate mean-field theories (HF, DFT) in real-time with and without dissipation and finite-temperature effects. These methods time-evolve the Liouville-von Neumann equation of motion for a one-particle density operator, $\hat{\rho}(t)$:

$$(i/\hbar)\hat{\rho}(t) = \left[\hat{F}\{\rho\}, \hat{\rho}(t)\right] \tag{6.88}$$

These real-time methods are useful for simulating attosecond to picosecond timescales, density response to multiple or strong applied fields, and timescales of energy relaxation. Symmetry, non-singlet densities, Meta-GGAs and 5th-rung functionals are not supported for real-time propagation, and nuclei are fixed. The CPU cost of a single time step is comparable to that of a single SCF cycle, if the modified-midpoint unitary transformation (MMUT) propagation algorithm[131] is employed, and no more than a few times the cost of a single SCF cycle if predictor/corrector algorithms (which facilitate stable time propagation using much larger time steps) are used[132]. Memory costs are similar to those of a ground-state SCF calculation, which for large systems, or those with a large density of states, represents a dramatic reduction in the memory requirement relative to linear-reponse TDDFT. The number of required Fock-build steps can be estimated from the default electronic time-step, which is 0.02 atomic units ($4.8 \times 10^{-4}$ fs). The real-time code exploits real-time shared-memory parallelism, and the use of 8 or more cores (*–nt 8*) is suggested. The input file of a basic real-time propagation is relatively simple, but sophisticated jobs require additional input files, and generate additional output.

**Example 6.93** Q-CHEM Basic RT-TDDFT job for BH3.

```
$molecule
   0 1
   B    0.000000     0.000000     0.000000
   H    1.115609    -0.322048     0.260309
   H   -0.332368     1.137184     0.111382
   H   -0.782205    -0.814474    -0.375294
$end

$rem
   SCF_GUESS          core
   GEN_SCFMAN         true
   RTTDDFT            1
   BASIS              3-21g
   THRESH             10
   SCF_CONVERGENCE    9
   EXCHANGE           b3lyp
   SYMMETRY           false
   SYM_IGNORE         TRUE
   SCF_ALGORITHM      DIIS
   UNRESTRICTED       FALSE
   MAX_SCF_CYCLES     200
$end
```

Before executing this job, a directory (*/logs*) must be made in the output directory of the job to collect most of the results of the propagation. By default, a real-time job begins from the ground state SCF density, applies a weak, brief (0.07 atomic time units) oscillating electric field to the $y$-axis of a molecule which excites a superposition of all $y$-polarized excited states, and outputs the resulting time-dependent dipole moment, energy and other quantities to the logs directory. The parameters of the time-dependent run are printed when the propagation begins. During the propagation the state of the molecule and propagation is summarized in the Q-CHEM output file, including estimates of the elapsed and remaining simulation wall-time. Propagation stops when **MaxIter** time steps are exceeded, or will stop prematurely if the density matrix becomes nonphysical. The logs directory will be populated by several text, white space delimited tables by default. The *./logs/Pol.csv* file is a table consisting of time (in a.u.), $\mu_x$, $\mu_y$, $\mu_z$, total energy, tr$\hat{\rho}$, the gap, the electronic energy, and two unused columns. The *./logs/Fourier_x.csv* file contains Fourier transform $\mathcal{F}[\mu_x(t)]$, in the format of its total value in energy units (eV) followed by its negative imaginary part and then its real part. Analogous files *./logs/Fourier_y.csv* and *./logs/Fourier_z.csv* are also created.

By adjusting the options of the propagation with a file *TDSCF.prm*, a much larger amount of output can be generated, including the electron and hole densities at all times as sequential MOLDEN files (**.mol*) viewable with the free package GABEDIT (`gabedit.sourceforge.net`). The **.mol* files generated by the real-time code have fractional orbital occupation numbers, and do not render properly in viewers other than GABEDIT to our knowledge. So long as the applied field is weak and has short duration the positions at which peaks appear in the Fourier are the same as a linear-response TDDFT-RPA job (note: not the same as a LR-TDDFT-TDA job), as shown in the sample. In an energy-conserving job, the width of the peak is inversely proportional to the duration of the signal sample used to construct the Fourier transform. If the applied field pulse is long ($>$ 1 a.u.), or has strong intensity ($>$ 0.01 a.u.) non-linear response can be studied. Non-linear effects in real-time SCF are an area of active investigation and development.

The absorption cross-section $\sigma_{ii}(\omega)$ in the $i$ direction, $i \in \{x, y, z\}$, can be obtained from the imaginary part of the frequency-dependent polarizability $\alpha_{ii}(\omega)$:

$$\sigma_{ii}(\omega) = \left(\frac{4\pi\omega}{c}\right) \Im\big[\alpha_{ii}(\omega)\big] \ , \tag{6.89}$$

and the rotationally-averaged absorption spectrum (within the dipole approximation) is

$$A(\omega) = \tfrac{1}{3}\big[\sigma_{xx}(\omega) + \sigma_{yy}(\omega) + \sigma_{zz}(\omega)\big] \ . \tag{6.90}$$

The frequency-dependent polarizability $\alpha_{ij}(\omega)$ is obtained from the Fourier transform of $\mu_i(t)$, for a perturbing field in the $j$ direction[132]:

$$\alpha_{ij}(\omega) = \frac{\mathcal{F}\big[\mu_i(t)\big]}{\mathcal{F}\big[E_j(t)\big]} \ . \tag{6.91}$$

Thus to compute the spectrum in Eq. (6.90), three RT-TDDFT simulations are required, perturbing separately in the $x$, $y$, and $z$ directions.

Because of the large number of floating point arguments used to control a real-time job, a separate input file *TDSCF.prm* in the same directory as the Q-CHEM input file is used for parameters. The file is two columns of plain text. The first column is a string naming the parameter (which must match the case and spelling printed in the output exactly to be interpreted correctly), and the second column is a floating point number. The number must only be followed by a new line. Several inputs are interpreted as true = 1 or false = 0. The most useful parameters are discussed in this section. The code will signal if this file is not found and default values will be supplied instead.

**Example 6.94** Q-CHEM Typical TDSCF.prm for a real-time B3LYP calculation.

```
dt  0.02
Stabilize  0
TCLOn 0
MaxIter  80000
ApplyImpulse  1
ApplyCw  0
```

```
FieldFreq 0.7
Tau 0.07
FieldAmplitude 0.001
ExDir 1.0
EyDir 1.0
EzDir 1.0
Print 0
StatusEvery 10
SaveDipoles  1
DipolesEvery 2
SavePopulations  0
SaveFockEnergies  0
WriteDensities  0
SaveEvery 500
FourierEvery 5000
MMUT 1
LFLPPC 0
```

| Parameter String | Explanation |
|---|---|
| `dt` | timestep (atomic units) > 0.02 may be unstable. |
| `Stabilize` | $>0$ Forces positive occupation numbers. |
| `MaxIter` | Maximum Timesteps |
| `ApplyImpulse` | 0 = No applied gaussian impulse |
| `ApplyCw` | 0 = No Continuous Wave, 1 = Cosine applied field. |
| `FieldFreq` | Frequency of applied field (atomic units) |
| `Tau` | Time-variance of Gaussian Impulse (atomic units) |
| `FieldAmplitude` | Max. amplitude of field (atomic units) |
| `ExDir` | Field Polarization Vector (x-component) |
| `EyDir` | Field Polarization Vector (y-component) |
| `EzDir` | Field Polarization Vector (z-component) |
| `Print` | Value $>0$ makes print more debug output. |
| `StatusEvery` | Iterations between status in output file |
| `SaveDipoles` | 0 = No Pol.csv generated. |
| `DipolesEvery` | Iterations between samples of Dipole |
| `SavePopulations` | 1 = Saves diagonal of the density |
| `SaveFockEnergies` | 1 = Saves diagonal of the Fock matrix |
| `WriteDensities` | $>0$ generates .mol files readable with GABEDIT |
| `SaveEvery` | Iterations between writing of all files in /logs |
| `FourierEvery` | Iterations between Fourier Transform |
| `FourierZoom` | A zoom parameter which controls resolution of FT. |
| `MMUT` | Modified midpoint unitary transform propagator calculation (default)[131] |
| `LFLPPC` | Predictor-corrector propagator[132] |

Table 6.4: TDSCF.prm Parameters

Any undocumented options not discussed above are not officially supported at this time.

# 6.12 Visualization of Excited States

As methods for *ab initio* calculations of excited states are becoming increasingly more routine, questions arise concerning how best to extract chemical meaning from such calculations. There are several approaches for analyzing molecular excited states; they are based on reduced one-particle density matrices (OPDMs). The two objects exploited in this analysis are: (i) the difference between the ground- and excited-state OPDMs and (ii) the transition OPDM connecting the ground and excited state. In the case of CIS and TDDFT/TDA wave functions, both quantities are identical and can be directly mapped into the CIS amplitudes; however, for correlated wave functions the two objects are not the same. The most basic analysis includes calculation of attachment/detachment density[12] and natural transition orbitals[133]. These quantities allow one to arrive to a most compact description of an excited state. More detailed analysis allows one to derive additional insight about the nature of the excited state. Detailed description and illustrative examples can be found in Refs. 134,135.

This section describes the theoretical background behind attachment/detachment analysis and natural transition orbitals, while details of the input for creating data suitable for plotting these quantities is described separately in Chapter 10, which also describes additional excited-state analysis tools. For historical reasons, there are duplicate implementations of some features. For example, CIS and TDDFT wave functions can be analyzed using an original built-in code and by using a more recent module, *libwfa*.

## 6.12.1 Attachment/Detachment Density Analysis

Consider the one-particle density matrices of the initial and final states of interest, $\mathbf{P}_1$ and $\mathbf{P}_2$ respectively. Assuming that each state is represented in a finite basis of spin-orbitals, such as the molecular orbital basis, and each state is at the same geometry. Subtracting these matrices yields the difference density

$$\mathbf{\Delta} = \mathbf{P}_1 - \mathbf{P}_2 \tag{6.92}$$

Now, the eigenvectors of the one-particle density matrix $\mathbf{P}$ describing a single state are termed the natural orbitals, and provide the best orbital description that is possible for the state, in that a CI expansion using the natural orbitals as the single-particle basis is the most compact. The basis of the attachment/detachment analysis is to consider what could be termed natural orbitals of the electronic transition and their occupation numbers (associated eigenvalues). These are defined as the eigenvectors $\mathbf{U}$ defined by

$$\mathbf{U}^\dagger \mathbf{\Delta} \mathbf{U} = \delta \tag{6.93}$$

The sum of the occupation numbers $\delta_p$ of these orbitals is then

$$\mathrm{tr}(\mathbf{\Delta}) = \sum_{p=1}^{N} \delta_p = n \tag{6.94}$$

where $n$ is the net gain or loss of electrons in the transition. The net gain in an electronic transition which does not involve ionization or electron attachment will obviously be zero.

The detachment density

$$\mathbf{D} = \mathbf{U}\mathbf{d}\mathbf{U}^\dagger \tag{6.95}$$

is defined as the sum of all natural orbitals of the difference density with negative occupation numbers, weighted by the absolute value of their occupations where $\mathbf{d}$ is a diagonal matrix with elements

$$d_p = -\min(\delta_p, 0) \tag{6.96}$$

The detachment density corresponds to the electron density associated with single particle levels vacated in an electronic transition or hole density.

The attachment density

$$\mathbf{A} = \mathbf{U}\mathbf{a}\mathbf{U}^\dagger \tag{6.97}$$

is defined as the sum of all natural orbitals of the difference density with positive occupation numbers where $\mathbf{a}$ is a diagonal matrix with elements

$$a_p = \max(\delta_p, 0) \tag{6.98}$$

The attachment density corresponds to the electron density associated with the single particle levels occupied in the transition or particle density. The difference between the attachment and detachment densities yields the original difference density matrix

$$\mathbf{\Delta} = \mathbf{A} - \mathbf{D} \tag{6.99}$$

### 6.12.2 Natural Transition Orbitals

In certain situations, even the attachment/detachment densities may be difficult to analyze. An important class of examples are systems with multiple chromophores, which may support exciton states consisting of linear combinations of localized excitations. For such states, both the attachment and the detachment density are highly delocalized and occupy basically the same region of space[136]. Lack of phase information makes the attachment/detachment densities difficult to analyze, while strong mixing of the canonical MOs means that excitonic states are also difficult to characterize in terms of MOs.

Analysis of these and other excited states is greatly simplified by constructing Natural Transition Orbitals (NTOs) for the excited states. (The basic idea behind NTOs is rather old[137] and has been rediscovered several times[133,138]; these orbitals were later shown to be equivalent to CIS natural orbitals[139].) Let $\mathbf{T}$ denote the transition density matrix from an excited-state calculation. The dimension of this matrix is $O \times V$, where $O$ and $V$ denote the number of occupied and virtual MOs, respectively. The NTOs are defined by transformations $\mathbf{U}$ and $\mathbf{V}$ obtained by singular value decomposition (SVD) of the matrix $\mathbf{T}$, *i.e.*[138]

$$\mathbf{U}\mathbf{T}\mathbf{V}^\dagger = \mathbf{\Lambda} \tag{6.100}$$

The matrices $\mathbf{U}$ and $\mathbf{V}$ are unitary and $\mathbf{\Lambda}$ is diagonal, with the latter containing at most $O$ non-zero elements. The matrix $\mathbf{U}$ is a unitary transformation from the canonical occupied MOs to a set of NTOs that together represent the "hole" orbital that is left by the excited electron, while $\mathbf{V}$ transforms the canonical virtual MOs into a set of NTOs representing the excited electron. (Equivalently, the "holes" are the eigenvectors of the $O \times O$ matrix $\mathbf{T}\mathbf{T}^\dagger$ and the particles are eigenvectors of the $V \times V$ matrix $\mathbf{T}^\dagger\mathbf{T}$[133].) These "hole" and "particle" NTOs come in pairs, and their relative importance in describing the excitation is governed by the diagonal elements of $\mathbf{\Lambda}$, which are excitation amplitudes in the NTO basis. By virtue of the SVD in Eq. (6.100), any excited state may be represented using at most $O$ excitation amplitudes and corresponding hole/particle NTO pairs. (The' discussion here assumes that $V \geq O$, which is typically the case except possibly in minimal basis sets. Although it is possible to use the transpose of Eq. (6.100) to obtain NTOs when $V < O$, this has not been implemented in Q-CHEM due to its limited domain of applicability.)

The SVD generalizes the concept of matrix diagonalization to the case of rectangular matrices, and therefore reduces as much as possible the number of non-zero outer products needed for an exact representation of $\mathbf{T}$. In this sense, the NTOs represent the best possible particle/hole picture of an excited state. The detachment density is recovered as the sum of the squares of the "hole" NTOs, while the attachment density is precisely the sum of the squares of the "particle" NTOs. Unlike the attachment/detachment densities, however, NTOs preserve phase information, which can be very helpful in characterizing the diabatic character (*e.g.*, $\pi\pi^*$ or $n\pi^*$) of excited states in complex systems. Even when there is more than one significant NTO amplitude, as in systems of electronically-coupled chromophores[136], the NTOs still represent a significant compression of information, as compared to the canonical MO basis.

NTOs are available within Q-CHEM for CIS, RPA, and TDDFT excited states. For the correlated wave functions (EOM-CC and ADC), they can be computed using *libwfa* module. The simplest way to visualize the NTOs is to generate them in a format suitable for viewing with the freely-available MOLDEN or MACMOLPLT programs, as described in Chapter 10.

# References and Further Reading

[1] Ground-State Methods (Chapters 4 and 5).

[2] Basis Sets (Chapter 7) and Effective Core Potentials (Chapter 8).

[3] A. Krylov, in *Reviews in Computational Chemistry*, edited by A. L. Parrill and K. B. Lipkowitz, chapter 4, John Wiley & Sons, Inc, 2017.

[4] J. E. Del Bene, R. Ditchfield, and J. A. Pople, *J. Chem. Phys.* **55**, 2236 (1971).

[5] J. B. Foresman, M. Head-Gordon, J. A. Pople, and M. J. Frisch, *J. Phys. Chem.* **96**, 135 (1992).

[6] D. Maurice and M. Head-Gordon, *Int. J. Quantum Chem.* **29**, 361 (1995).

[7] T. D. Bouman and A. E. Hansen, *Int. J. Quantum Chem. Symp.* **23**, 381 (1989).

[8] A. E. Hansen, B. Voight, and S. Rettrup, *Int. J. Quantum Chem.* **23**, 595 (1983).

[9] J. L. McHale, Prentice Hall, New York, 1999.

[10] F. Cordova et al., *J. Chem. Phys.* **127**, 164111 (2007).

[11] D. Maurice and M. Head-Gordon, *J. Phys. Chem.* **100**, 6131 (1996).

[12] M. Head-Gordon, A. M. Graña, D. Maurice, and C. A. White, *J. Phys. Chem.* **99**, 14261 (1995).

[13] D. Casanova and M. Head-Gordon, *J. Chem. Phys.* **129**, 064104 (2008).

[14] A. I. Krylov, *Chem. Phys. Lett.* **350**, 522 (2002).

[15] X. Zhang and J. M. Herbert, *J. Chem. Phys.* **143**, 234107 (2015).

[16] J. F. Stanton, J. Gauss, N. Ishikawa, and M. Head-Gordon, *J. Chem. Phys.* **103**, 4160 (1995).

[17] S. Zilberg and Y. Haas, *J. Chem. Phys.* **103**, 20 (1995).

[18] C. M. Gittins, E. A. Rohlfing, and C. M. Rohlfing, *J. Chem. Phys.* **105**, 7323 (1996).

[19] D. Maurice and M. Head-Gordon, *Mol. Phys.* **96**, 1533 (1999).

[20] D. Maurice, *Single Electron Theories of Excited States*, PhD thesis, University of California, Berkeley, CA, 1998.

[21] S. Matsika and P. Krause, *Annu. Rev. Phys. Chem.* **62**, 621 (2011).

[22] J. M. Herbert, X. Zhang, A. F. Morrison, and J. Liu, *acr* **49**, 931 (2016).

[23] S. Fatehi, E. Alguire, Y. Shao, and J. Subotnik, *J. Chem. Phys.* **135**, 234105 (2011).

[24] X. Zhang and J. M. Herbert, *J. Chem. Phys.* **141**, 064104 (2014).

[25] X. Zhang and J. M. Herbert, *J. Chem. Phys.* **142**, 064109 (2015).

[26] Q. Ou, G. D. Bellchambers, F. Furche, and J. E. Subotnik, *J. Chem. Phys.* **142**, 064114 (2015).

[27] A. J. W. Thom, E. J. Sundstrom, and M. Head-Gordon, *Phys. Chem. Chem. Phys.* **11**, 11297 (2009).

[28] I. Mayer and P.-O. Löwdin, *Chem. Phys. Lett.* **202**, 1 (1993).

[29] M. E. Casida, in *Recent Advances in Density Functional Methods, Part I*, edited by D. P. Chong, page 155, World Scientific, Singapore, 1995.

[30] A. Dreuw and M. Head-Gordon, *Chem. Rev.* **105**, 4009 (2005).

[31] S. Hirata and M. Head-Gordon, *Chem. Phys. Lett.* **302**, 375 (1999).

[32] S. Hirata and M. Head-Gordon, *Chem. Phys. Lett.* **314**, 291 (1999).

[33] A. D. Laurent and D. Jacquemin, *Int. J. Quantum Chem.* , 2019 (2013).

[34] F. Liu et al., *Mol. Phys.* **108**, 2791 (2010).

[35] M. E. Casida, C. Jamorski, K. C. Casida, and D. R. Salahub, *J. Chem. Phys.* **108**, 4439 (1998).

[36] D. J. Tozer and N. C. Handy, *J. Chem. Phys.* **109**, 10180 (1998).

[37] A. Lange and J. M. Herbert, *J. Chem. Theory Comput.* **3**, 1680 (2007).

[38] M. J. G. Peach, P. Benfield, T. Helgaker, and D. J. Tozer, *J. Chem. Phys.* **128**, 044118 (2008).

[39] R. M. Richard and J. M. Herbert, *J. Chem. Theory Comput.* **7**, 1296 (2011).

[40] Y. Shao, M. Head-Gordon, and A. I. Krylov, *J. Chem. Phys.* **118**, 4807 (2003).

[41] Y. A. Bernard, Y. Shao, and A. I. Krylov, *J. Chem. Phys.* **136**, 204103 (2012).

[42] F. Wang and T. Ziegler, *J. Chem. Phys.* **121**, 12191 (2004).

[43] M. Seth, G. Mazur, and T. Ziegler, *Theor. Chem. Acc.* **129**, 331 (2011).

[44] N. A. Besley, *Chem. Phys. Lett.* **390**, 124 (2004).

[45] N. A. Besley, M. T. Oakley, A. J. Cowan, and J. D. Hirst, *J. Am. Chem. Soc.* **126**, 13502 (2004).

[46] N. A. Besley, *J. Chem. Phys.* **122**, 184706 (2005).

[47] D. M. Rogers, N. A. Besley, P. O'Shea, and J. D. Hirst, *J. Phys. Chem. B* **109**, 23061 (2005).

[48] J. Liu and W. Liang, *J. Chem. Phys.* **138**, 024101 (2013).

[49] J. Liu and W. Liang, *J. Chem. Phys.* **135**, 014113 (2011).

[50] J. Liu and W. Liang, *J. Chem. Phys.* **135**, 184111 (2011).

[51] A. T. B. Gilbert, N. A. Besley, and P. M. W. Gill, *J. Phys. Chem. A* **112**, 13164 (2008).

[52] N. A. Besley, A. T. B. Gilbert, and P. M. W. Gill, *J. Chem. Phys.* **130**, 124308 (2009).

[53] M. Filatov and S. Shaik, *Chem. Phys. Lett.* **304**, 429 (1999).

[54] T. Kowalczyk, T. Tsuchimochi, L. Top, P.-T. Chen, and T. Van Voorhis, *J. Chem. Phys.* **138**, 164101 (2013).

[55] M. Head-Gordon, R. J. Rico, M. Oumi, and T. J. Lee, *Chem. Phys. Lett.* **219**, 21 (1994).

[56] M. Head-Gordon, D. Maurice, and M. Oumi, *Chem. Phys. Lett.* **246**, 114 (1995).

[57] Y. M. Rhee and M. Head-Gordon, *J. Phys. Chem. A* **111**, 5314 (2007).

[58] M. Oumi, D. Maurice, T. J. Lee, and M. Head-Gordon, *Chem. Phys. Lett.* **279**, 151 (1997).

[59] M. Head-Gordon, M. Oumi, and D. Maurice, *Mol. Phys.* **96**, 593 (1999).

[60] D. Casanova, Y. M. Rhee, and M. Head-Gordon, *J. Chem. Phys.* **128**, 164106 (2008).

[61] H. Koch and P. Jørgensen, *J. Chem. Phys.* **93**, 3333 (1990).

[62] J. F. Stanton and R. J. Bartlett, *J. Chem. Phys.* **98**, 7029 (1993).

[63] A. I. Krylov, C. D. Sherrill, and M. Head-Gordon, *J. Chem. Phys.* **113**, 6509 (2000).

[64] A. I. Krylov, *Annu. Rev. Phys. Chem.* **59**, 433 (2008).

[65] H. Sekino and R. J. Bartlett, *Int. J. Quantum Chem. Symp.* **18**, 255 (1984).

[66] H. Koch, H. J. A. Jensen, P. Jørgensen, and T. Helgaker, *J. Chem. Phys.* **93**, 3345 (1990).

[67] S. V. Levchenko and A. I. Krylov, *J. Chem. Phys.* **120**, 175 (2004).

[68] A. I. Krylov, *Chem. Phys. Lett.* **338**, 375 (2001).

[69] D. Sinha, D. Mukhopadhya, R. Chaudhuri, and D. Mukherjee, *Chem. Phys. Lett.* **154**, 544 (1989).

[70] J. F. Stanton and J. Gauss, *J. Chem. Phys.* **101**, 8938 (1994).

[71] M. Nooijen and R. J. Bartlett, *J. Chem. Phys.* **102**, 3629 (1995).

[72] S. V. Levchenko, T. Wang, and A. I. Krylov, *J. Chem. Phys.* **122**, 224106 (2005).

[73] P. A. Pieniazek, S. E. Bradforth, and A. I. Krylov, *J. Chem. Phys.* **129**, 074104 (2008).

[74] A. A. Golubeva, P. A. Pieniazek, and A. I. Krylov, *J. Chem. Phys.* **130**, 124113 (2009).

[75] A. I. Krylov, *Acc. Chem. Res.* **39**, 83 (2006).

[76] D. Casanova, L. V. Slipchenko, A. I. Krylov, and M. Head-Gordon, *J. Chem. Phys.* **130**, 044103 (2009).

[77] M. Wladyslawski and M. Nooijen, in *Low-Lying Potential Energy Surfaces*, volume 828 of *ACS Symposium Series*, page 65, American Chemical Society, Washington, D. C., 2002.

[78] T. Kuś and A. I. Krylov, *J. Chem. Phys.* **135**, 084109 (2011).

[79] T. Kuś and A. I. Krylov, *J. Chem. Phys.* **136**, 244109 (2012).

[80] K. B. Bravaya, D. Zuev, E. Epifanovsky, and A. I. Krylov, *J. Chem. Phys.* **138**, 124106 (2013).

[81] T.-C. Jagau, D. Zuev, K. B. Bravaya, E. Epifanovsky, and A. I. Krylov, *J. Phys. Chem. Lett.* **5**, 310 (2014).

[82] T.-C. Jagau, K. B. Bravaya, and A. I. Krylov, *Annu. Rev. Phys. Chem.* **68**, 525 (2017).

[83] Z. Benda and T.-C. Jagau, *J. Chem. Phys.* **146**, 031101 (2017).

[84] A. Landau, K. Khistyaev, S. Dolgikh, and A. I. Krylov, *J. Chem. Phys.* **132**, 014109 (2010).

[85] J. F. Stanton and J. Gauss, *J. Chem. Phys.* **103**, 1064 (1995).

[86] A. Sadybekov and A. I. Krylov, *J. Chem. Phys.* **147**, 014107 (2017).

[87] K. Nanda and A. I. Krylov, *J. Chem. Phys.* **142**, 064118 (2015).

[88] E. Epifanovsky, K. Klein, S. Stopkowicz, J. Gauss, and A. Krylov, *J. Chem. Phys.* **143**, 064102 (2015).

[89] A. Tajti and P. G. Szalay, *J. Chem. Phys.* **131**, 124104 (2009).

[90] S. Faraji, S. Matsika, E. Epifanovsky, X. Feng, and A. I. Krylov, Calculations of non-adiabatic couplings within equation-of-motion coupled-cluster framework: Theory, implementation, and validation against multi-reference configuration interaction, (in preparation).

[91] K. Nanda and A. I. Krylov, *J. Chem. Phys.* **145**, 204116 (2016).

[92] S. Hirata, M. Nooijen, and R. J. Bartlett, *Chem. Phys. Lett.* **326**, 255 (2000).

[93] P. Piecuch and M. Włoch, *J. Chem. Phys.* **123**, 224105 (2005).

[94] P. U. Manohar and A. I. Krylov, *J. Chem. Phys.* **129**, 194105 (2008).

[95] P. U. Manohar, J. F. Stanton, and A. I. Krylov, *J. Chem. Phys.* **131**, 114112 (2009).

[96] C. M. Oana and A. I. Krylov, *J. Chem. Phys.* **127**, 234106 (2007).

[97] C. M. Oana and A. I. Krylov, *J. Chem. Phys.* **131**, 124114 (2009).

[98] M. Wormit et al., *Mol. Phys.* **112**, 774 (2014).

[99] P. H. Harbach, M. Wormit, and A. Dreuw, *J. Chem. Phys.* **141**, 064113 (2014).

[100] C. M. Krauter, M. Pernpointner, and A. Dreuw, *J. Chem. Phys.* **138**, 044107 (2013).

[101] J. Wenzel, M. Wormit, and A. Dreuw, *J. Comput. Chem.* **35**, 1900 (2014).

[102] J. Wenzel, M. Wormit, and A. Dreuw, *J. Chem. Theory Comput.* **10**, 4583 (2014).

[103] J. Wenzel, A. Holzer, M. Wormit, and A. Dreuw, *J. Chem. Phys.* **142**, 214104 (2015).

[104] J. Schirmer, *Phys. Rev. A* **26**, 2395 (1982).

[105] J. Schirmer and A. B. Trofimov, *J. Chem. Phys.* **120**, 11449 (2004).

[106] A. B. Trofimov and J. Schirmer, *J. Phys. B* **28**, 2299 (1995).

[107] A. B. Trofimov, G. Stelter, and J. Schirmer, *J. Chem. Phys.* **111**, 9982 (1999).

[108] A. B. Trofimov, G. Stelter, and J. Schirmer, *J. Chem. Phys.* **117**, 6402 (2002).

[109] A. Hellweg, S. A. Grün, and C. Hättig, *Phys. Chem. Chem. Phys.* **10**, 4119 (2008).

[110] N. O. Winter and C. Hättig, *J. Chem. Phys.* **134**, 184101 (2011).

[111] L. S. Cederbaum, W. Domcke, and J. Schirmer, *Phys. Rev. A* **22**, 206 (1980).

[112] A. Barth and L. S. Cederbaum, *Phys. Rev. A* **12223**, 1038 (1981).

[113] D. Lefrancois, M. Wormit, and A. Dreuw, *J. Chem. Phys.* **143**, 124107 (2015).

[114] J.-M. Mewes et al., *J. Phys. Chem. A* **119**, 5446 (2015).

[115] J.-M. Mewes, J. M. Herbert, and A. Dreuw, *Phys. Chem. Chem. Phys.* **19**, 1644 (2017).

[116] S. Prager, A. Zech, F. Aquilante, A. Dreuw, and T. A. Wesolowski, *J. Chem. Phys.* **144**, 204103 (2016).

[117] T. A. Wesolowski and A. Warshel, *J. Phys. Chem.* **97**, 8050 (1993).

[118] T. A. Wesolowski, *Phys. Rev. A* **77**, 012504 (2008).

[119] D. Casanova and M. Head-Gordon, *Phys. Chem. Chem. Phys.* **11**, 9779 (2009).

[120] P. M. Zimmerman, F. Bell, M. Goldey, A. T. Bell, and M. Head-Gordon, *J. Chem. Phys.* **137**, 164110 (2012).

[121] F. Bell, P. M. Zimmerman, D. Casanova, M. Goldey, and M. Head-Gordon, *Phys. Chem. Chem. Phys.* **15**, 358 (2013).

[122] D. Casanova, *J. Comput. Chem.* **34**, 720 (2013).

[123] F. Bell, D. Casanova, and M. Head-Gordon, *J. Am. Chem. Soc.* **132**, 11314 (2010).

[124] P. M. Zimmerman, F. Bell, D. Casanova, and M. Head-Gordon, *J. Am. Chem. Soc.* **133**, 19944 (2011).

[125] D. Casanova, *J. Chem. Phys.* **137**, 084105 (2012).

[126] D. Casanova, *J. Chem. Phys.* **140**, 144111 (2014).

[127] A. V. Luzanov, D. Casanova, X. Feng, and A. I. Krylov, *J. Chem. Phys.* **142**, 224104 (2015).

[128] D. Casanova and A. I. Krylov, *J. Chem. Phys.* **144** (2016).

[129] N. A. Besley, M. J. G. Peach, and D. J. Tozer, *Phys. Chem. Chem. Phys.* **11**, 10350 (2009).

[130] N. A. Besley and F. A. Asmuruf, *Phys. Chem. Chem. Phys.* **12**, 12024 (2010).

[131] X. Li et al., *Phys. Chem. Chem. Phys.* **7**, 233 (2005).

[132] Y. Zhu and J. M. Herbert, Predictor/corrector methods for efficient propagation of the time-dependent Kohn-Sham equations, (in preparation).

[133] R. L. Martin, *J. Chem. Phys.* **118**, 4775 (2003).

[134] F. Plasser, M. Wormit, and A. Dreuw, *J. Chem. Phys.* **141**, 024106 (2014).

[135] F. Plasser, S. A. Bäppler, M. Wormit, and A. Dreuw, *J. Chem. Phys.* **141**, 024107 (2014).

[136] A. W. Lange and J. M. Herbert, *J. Am. Chem. Soc.* **131**, 124115 (2009).

[137] A. V. Luzanov, A. A. Sukhorukov, and V. E. Umanskii, *Theor. Exp. Chem.* **10**, 354 (1976).

[138] I. Mayer, *Chem. Phys. Lett.* **437**, 284 (2007).

[139] P. R. Surján, *Chem. Phys. Lett.* **439**, 393 (2007).

# Chapter 7

# Basis Sets

## 7.1 Introduction

A basis set is a set of functions combined linearly to model molecular orbitals. Basis functions can be considered as representing the atomic orbitals of the atoms and are introduced in quantum chemical calculations because the equations defining the molecular orbitals are otherwise very difficult to solve.

Many standard basis sets have been carefully optimized and tested over the years. In principle, a user would employ the largest basis set available in order to model molecular orbitals as accurately as possible. In practice, the computational cost grows rapidly with the size of the basis set so a compromise must be sought between accuracy and cost. If this is systematically pursued, it leads to a "theoretical model chemistry"[3], that is, a well-defined energy procedure (*e.g.*, Hartree-Fock) in combination with a well-defined basis set.

Basis sets have been constructed from Slater, Gaussian, plane wave and delta functions. Slater functions were initially employed because they are considered "natural" and have the correct behavior at the origin and in the asymptotic regions. However, the two-electron repulsion integrals (ERIs) encountered when using Slater basis functions are expensive and difficult to evaluate. Delta functions are used in several quantum chemistry programs. However, while codes incorporating delta functions are simple, thousands of functions are required to achieve accurate results, even for small molecules. Plane waves are widely used and highly efficient for calculations on periodic systems, but are not so convenient or natural for molecular calculations.

The most important basis sets are contracted sets of atom-centered Gaussian functions. The number of basis functions used depends on the number of core and valence atomic orbitals, and whether the atom is light (H or He) or heavy (everything else). Contracted basis sets have been shown to be computationally efficient and to have the ability to yield chemical accuracy (see Appendix B). The Q-CHEM program has been optimized to exploit basis sets of the contracted Gaussian function type and has a large number of built-in standard basis sets (developed by Dunning and Pople, among others) which the user can access quickly and easily.

The selection of a basis set for quantum chemical calculations is very important. It is sometimes possible to use small basis sets to obtain good chemical accuracy, but calculations can often be significantly improved by the addition of diffuse and polarization functions. Consult the literature and review articles[3–7] to aid your selection and see the section "Further Reading" at the end of this Chapter.

## 7.2 Built-In Basis Sets

Q-CHEM is equipped with many standard basis sets[8], and allows the user to specify the required basis set by its standard symbolic representation. The available built-in basis sets include the following types:

- Pople basis sets
- Dunning basis sets
- Correlation consistent Dunning basis sets
- Ahlrichs basis sets
- Jensen polarization consistent basis sets
- Karlsruhe "def2" basis sets
- The universal Gaussian basis set (UGBS)

In addition, Q-CHEM supports the following features:

- Extra diffuse functions available for high quality excited state calculations.
- Standard polarization functions.
- Basis sets are requested by symbolic representation.
- $s$, $p$, $sp$, $d$, $f$ and $g$ angular momentum types of basis functions.
- Maximum number of shells per atom is 100.
- Pure and Cartesian basis functions.
- Mixed basis sets (see section 7.5).
- Basis set superposition error (BSSE) corrections.

The following *$rem* keyword controls the basis set:

**BASIS**
Sets the basis set to be used
TYPE:
STRING
DEFAULT:
No default basis set
OPTIONS:

| | |
|---|---|
| General, Gen | User-defined. See section below |
| Symbol | Use standard basis sets as in the table below |
| Mixed | Use a combination of different basis sets |

RECOMMENDATION:
Consult literature and reviews to aid your selection.

## 7.3 Basis Set Symbolic Representation

Examples are given in the tables below and follow the standard format generally adopted for specifying basis sets. The single exception applies to additional diffuse functions. These are best inserted in a similar manner to the polarization functions; in parentheses with the light atom designation following heavy atom designation. (*i.e.*, *heavy*, *light*). Use a period (.) as a place-holder (see examples).

| | $j$ | $k$ | $l$ | $m$ | $n$ |
|---|---|---|---|---|---|
| STO$-j(k+,l+)$G$(m,n)$ | 2,3,6 | $^a$ | $^b$ | $d$ | $p$ |
| $j-21(k+,l+)$G$(m,n)$ | 3 | $^a$ | $^b$ | $2d$ | $2p$ |
| $j-31(k+,l+)$G$(m,n)$ | 4,6 | $^a$ | $^b$ | $3d$ | $3p$ |
| $j-311(k+,l+)$G$(m,n)$ | 6 | $^a$ | $^b$ | *df*,2*df*,3*df* | *pd*,2*pd*,3*pd* |

Table 7.1: Summary of Pople type basis sets available in Q-CHEM. $m$ and $n$refer to the polarization functions on heavy and light atoms respectively. $^ak$ is the number of sets of diffuse functions on heavy $^bl$ is the number of sets of diffuse functions on light atoms.

| **Symbolic Name** | **Atoms Supported** |
|---|---|
| STO-2G | H, He, Li→Ne, Na→Ar, K, Ca, Sr |
| STO-3G | H, He, Li→Ne, Na→Ar, K→Kr, Rb→Sb |
| STO-6G | H, He, Li→Ne, Na→Ar, K→Kr |
| 3-21G | H, He, Li→Ne, Na→Ar, K→Kr, Rb→Xe, Cs |
| 4-31G | H, He, Li→Ne, P→Cl |
| 6-31G | H, He, Li→Ne, Na→Ar, K→Zn |
| 6-311G | H, He, Li→Ne, Na→Ar, Ga→Kr |
| G3LARGE | H, He, Li→Ne, Na→Ar, K→Kr |
| G3MP2LARGE | H, He, Li→Ne, Na→Ar, Ga→Kr |

Table 7.2: Atoms supported for Pople basis sets available in Q-CHEM (see the Table below for specific examples).

### 7.3.1 Customization

Q-CHEM offers a number of standard and special customization features. One of the most important is that of supplying additional diffuse functions. Diffuse functions are often important for studying anions and excited states of molecules, and for the latter several sets of additional diffuse functions may be required. These extra diffuse functions can be generated from the standard diffuse functions by applying a scaling factor to the exponent of the original diffuse function. This yields a geometric series of exponents for the diffuse functions which includes the original standard functions along with more diffuse functions.

When using very large basis sets, especially those that include many diffuse functions, or if the system being studied is very large, linear dependence in the basis set may arise. This results in an over-complete description of the space spanned by the basis functions, and can cause a loss of uniqueness in the molecular orbital coefficients. Consequently, the SCF may be slow to converge or behave erratically. Q-CHEM will automatically check for linear dependence in the basis set, and will project out the near-degeneracies, if they exist. This will result in there being slightly fewer molecular orbitals than there are basis functions.

| Symbolic Name | Atoms Supported |
|---|---|
| 3-21G | H, He, Li → Ne, Na → Ar, K →Kr, Rb → sXe, Cs |
| 3-21+G | H, He, Na → Cl, Na → Ar, K, Ca, Ga → Kr |
| 3-21G* | Na → Ar |
| 6-31G | H, He, Li → Ne, Na → Ar, K → Zn, Ga → Kr |
| 6-31+G | H, He, Li → Ne, Na → Ar, Ga → Kr |
| 6-31G* | H, He, Li → Ne, Na → Ar, K → Zn, Ga → Kr |
| 6-31G(d,p) | H, He, Li → Ne, Na → Ar, K → Zn, Ga → Kr |
| 6-31G(.,+)G | H, He, Li → Ne, Na → Ar, Ga → Kr |
| 6-31+G* | H, He, Li → Ne, Na → Ar, Ga → Kr |
| 6-311G | H, He, Li → Ne, Na → Ar, Ga → Kr |
| 6-311+G | H, He, Li → Ne, Na → Ar |
| 6-311G* | H, He, Li → Ne, Na → Ar, Ga → Kr |
| 6-311G(d,p) | H, He, Li → Ne, Na → Ar, Ga → Kr |
| G3LARGE | H, He, Li → Ne, Na → Ar, K → Kr |
| G3MP2LARGE | H, He, Li → Ne, Na → Ar, Ga → Kr |

Table 7.3: Examples of extended Pople basis sets.

| | SV$(k+, l+)(md, np)$, DZ$(k+, l+)(md, np)$, TZ$(k+, l+)(md, np)$ |
|---|---|
| $k$ | # sets of heavy atom diffuse functions |
| $l$ | # sets of light atom diffuse functions |
| $m$ | # sets of d functions on heavy atoms |
| $n$ | # sets of p functions on light atoms |

Table 7.4: Summary of Dunning-type basis sets available in Q-CHEM.

| Symbolic Name | Atoms Supported |
|---|---|
| SV | H, Li → Ne |
| DZ | H, Li → Ne, Al → Cl |
| TZ | H, Li → Ne |

Table 7.5: Atoms supported for old Dunning basis sets available in Q-CHEM.

| **Symbolic Name** | **Atoms Supported** |
|---|---|
| SV | H, Li → Ne |
| SV* | H, B → Ne |
| SV(d,p) | H, B → Ne |
| DZ | H, Li → Ne, Al→Cl |
| DZ+ | H, B → Ne |
| DZ++ | H, B → Ne |
| DZ* | H, Li → Ne |
| DZ** | H, Li → Ne |
| DZ(d,p) | H, Li → Ne |
| TZ | H, Li→Ne |
| TZ+ | H, Li→Ne |
| TZ++ | H, Li→Ne |
| TZ* | H, Li→Ne |
| TZ** | H, Li→Ne |
| TZ(d,p) | H, Li→Ne |

Table 7.6: Examples of extended Dunning basis sets.

| **Symbolic Name** | **Atoms Supported** |
|---|---|
| cc-pVDZ | H → Ar, Ca, Ga → Kr |
| cc-pVTZ | H → Ar, Ca, Ga → Kr |
| cc-pVQZ | H → Ar, Ca, Ga → Kr |
| cc-pV5Z | H → Ar, Ca, Ga → Kr |
| cc-pCVDZ | H → Ar (H and He use cc-pVDZ) |
| cc-pCVTZ | H → Ar (H and He use cc-pVTZ) |
| cc-pCVQZ | H → Ar (H and He use cc-pVQZ) |
| cc-pCV5Z | H, He, B → Ar (H and He use cc-pV5Z) |
| aug-cc-pVDZ | H → Ar, Ga → Kr |
| aug-cc-pVTZ | H → Ar, Ga → Kr |
| aug-cc-pVQZ | H → Ar, Ga → Kr |
| aug-cc-pV5Z | H, He, B → Ne, Al → Ar, Ga → Kr |
| aug-cc-pCVDZ | H → Ar (H and He use aug-cc-pVDZ) |
| aug-cc-pCVTZ | H → Ar (H and He use aug-cc-pVTZ) |
| aug-cc-pCVQZ | H → Ar (H and He use aug-cc-pVQZ) |
| aug-cc-pCV5Z | He, He, B → Ne, Al → Ar (H and He use aug-cc-pV5Z) |

Table 7.7: Atoms supported Dunning correlation-consistent basis sets available in Q-CHEM.

| **Symbolic Name** | **Atoms Supported** |
|---|---|
| TZV | Li → Kr |
| VDZ | H → Kr |
| VTZ | H → Kr |

Table 7.8: Atoms supported for Ahlrichs basis sets available in Q-CHEM.

| Symbolic Name | Atoms Supported |
|---|---|
| pc-0, pc-1, pc-2, pc-3, pc-4 | H → Ar |
| pcJ-0, pcJ-1, pcJ-2, pcJ-3, pcJ-4 | H → Ar, except Li, Be, Na, Mg |
| pcS-0, pcS-1, pcS-2, pcS-3, pcS-4 | H → Ar |

Table 7.9: Atoms supported for Jensen polarization consistent basis sets available in Q-CHEM.

| Symbolic Name | Atoms Supported |
|---|---|
| def-mSVP | H-Kr (Na-Kr are identical to def2-SV(P)) |
| def2-SV(P), def2-SVP, def2-SVPD | He-Kr, Rb-Rn (with def2-ECP) |
| def2-TZVP, def2-TZVPP, def2-TZVPD, def2-TZVPPD | He-Kr, Rb-Rn (with def2-ECP) |
| def2-QZVP, def2-QZVPP, def2-QZVPD, def2-QZVPPD | He-Kr, Rb-Rn (with def2-ECP) |
| UGBS | H-Rn |

Table 7.10: Atoms supported for Karlsruhe "def2" basis sets and the universal Gaussian basis set (UGBS) available in Q-CHEM.

Q-CHEM checks for linear-dependence by considering the eigenvalues of the overlap matrix. Very small eigenvalues are an indication that the basis set is close to being linearly dependent. The size at which the eigenvalues are considered to be too small is governed by the *$rem* variable BASIS_LIN_DEP_THRESH. By default this is set to 6, corresponding to a threshold of $10^{-6}$. This has been found to give reliable results, however, if you have a poorly behaved SCF, and you suspect there maybe linear dependence in you basis, the threshold should be increased.

**PRINT_GENERAL_BASIS**

Controls print out of built in basis sets in input format

TYPE:

LOGICAL

DEFAULT:

FALSE

OPTIONS:

TRUE Print out standard basis set information

FALSE Do not print out standard basis set information

RECOMMENDATION:

Useful for modification of standard basis sets.

**BASIS_LIN_DEP_THRESH**

Sets the threshold for determining linear dependence in the basis set

TYPE:

INTEGER

DEFAULT:

6 Corresponding to a threshold of $10^{-6}$

OPTIONS:

$n$ Sets the threshold to $10^{-n}$

RECOMMENDATION:

Set to 5 or smaller if you have a poorly behaved SCF and you suspect linear dependence in you basis set. Lower values (larger thresholds) may affect the accuracy of the calculation.

# 7.4 User-Defined Basis Sets (*$basis*)

## 7.4.1 Introduction

Users may, on occasion, prefer to use non-standard basis, and it is possible to declare user-defined basis sets in Q-CHEM input (see Chapter 3 on Q-CHEM inputs). The format for inserting a non-standard user-defined basis set is both logical and flexible, and is described in detail in the job control section below.

Note that the SAD guess is not currently supported with non-standard or user-defined basis sets. The simplest alternative is to specify the GWH or CORE options for SCF_GUESS, but these are relatively ineffective other than for small basis sets. The recommended alternative is to employ basis set projection by specifying a standard basis set for the BASIS2 keyword. See the section in Chapter 4 on initial guesses for more information.

## 7.4.2 Job Control

In order to use a user-defined basis set the BASIS *$rem* must be set to GENERAL or GEN.

When using a non-standard basis set which incorporates $d$ or higher angular momentum basis functions, the *$rem* variable PURECART needs to be initiated. This *$rem* variable indicates to the Q-CHEM program how to handle the angular form of the basis functions. As indicated above, each integer represents an angular momentum type which can be defined as either pure (1) or Cartesian (2). For example, 111 would specify all $g$, $f$ and $d$ basis functions as being in the pure form. 121 would indicate $g$- and $d$- functions are pure and $f$-functions Cartesian.

**PURECART**
    INTEGER
TYPE:
    Controls the use of pure (spherical harmonic) or Cartesian angular forms
DEFAULT:
    2111    Cartesian $h$-functions and pure $g, f, d$ functions
OPTIONS:
    $hgfd$    Use 1 for pure and 2 for Cartesian.
RECOMMENDATION:
    This is pre-defined for all standard basis sets

In standard basis sets all functions are pure, except for the $d$ functions in $n$-21G–type bases (*e.g.*, 3-21G) and $n$-31G bases (*e.g.*, 6-31G, 6-31G*,6-31+G*, ...). In particular, the 6-311G series uses pure functions for both $d$ and $f$.

## 7.4.3 Format for User-Defined Basis Sets

The format for the user-defined basis section is as follows:

```
$basis
```

$$\begin{array}{lllll}
X & 0 & & & \\
L & K & scale & & \\
\alpha_1 & C_1^{L_{min}} & C_1^{L_{min}+1} & \ldots & C_1^{L_{max}} \\
\alpha_2 & C_2^{L_{min}} & C_2^{L_{min}+1} & \ldots & C_2^{L_{max}} \\
\vdots & \vdots & \vdots & \ddots & \vdots \\
\alpha_K & C_K^{L_{min}} & C_K^{L_{min}+1} & \ldots & C_K^{L_{max}}
\end{array}$$

```
****
$end
```

where

| | |
|---|---|
| $X$ | Atomic symbol of the atom (atomic number not accepted) |
| $L$ | Angular momentum symbol (S, P, SP, D, F, G) |
| $K$ | Degree of contraction of the shell (integer) |
| $scale$ | Scaling to be applied to exponents (default is 1.00) |
| $\alpha_i$ | Gaussian primitive exponent (positive real number) |
| $C_i^L$ | Contraction coefficient for each angular momentum (non-zero real numbers). |

Atoms are terminated with $\star\star\star\star$ and the complete basis set is terminated with the *$end* keyword terminator. No blank lines can be incorporated within the general basis set input. Note that more than one contraction coefficient per line is one required for compound shells like SP. As with all Q-CHEM input deck information, all input is case-insensitive.

### 7.4.4 Example

**Example 7.1** Example of adding a user-defined non-standard basis set. Note that since $d$, $f$ and $g$ functions are incorporated, the *$rem* variable PURECART must be set. Note the use of BASIS2 for the initial guess.

```
$molecule
   0  1
   O
   H  O  oh
   H  O  oh  2  hoh

   oh  =   1.2
   hoh = 110.0
$end

$rem
   EXCHANGE   hf
   BASIS      gen      user-defined general basis
   BASIS2     sto-3g   sto-3g orbitals as initial guess
   PURECART   112      Cartesian d functions, pure f and g
$end

$basis
   H  0
   S  2  1.00
      1.30976    0.430129
      0.233136   0.678914
****
   O  0
   S  2  1.00
      49.9810    0.430129
      8.89659    0.678914
   SP 2  1.00
      1.94524    0.049472    0.511541
      0.49336    0.963782    0.612820
   D  1  1.00
      0.39000    1.000000
   F  1  1.00
      4.10000    1.000000
   G  1  1.00
      3.35000    1.000000
****
$end
```

## 7.5 Mixed Basis Sets

In addition to defining a custom basis set, it is also possible to specify different standard basis sets for different atoms. For example, in a large alkene molecule the hydrogen atoms could be modeled by the STO-3G basis, while the carbon atoms have the larger 6-31G(d) basis. This can be specified within the *$basis* block using the more familiar basis set labels.

**Note:** (1) It is not possible to augment a standard basis set in this way; the whole basis needs to be inserted as for a user-defined basis (angular momentum, exponents, contraction coefficients) and additional functions added. Standard basis set exponents and coefficients can be easily obtained by setting the PRINT_GENERAL_BASIS *$rem* variable to TRUE.
(2) The PURECART flag must be set for *all* general basis input containing $d$ angular momentum or higher functions, regardless of whether standard basis sets are entered in this non-standard manner.

The user can also specify different basis sets for atoms of the same type, but in different parts of the molecule. This allows a larger basis set to be used for the active region of a system, and a smaller basis set to be used in the less important regions. To enable this the BASIS keyword must be set to MIXED and a *$basis* section included in the input deck that gives a complete specification of the basis sets to be used. The format is exactly the same as for the user-defined basis, except that the atom number (as ordered in the *$molecule* section) must be specified in the field after the atomic symbol. A basis set must be specified for every atom in the input, even if the same basis set is to be used for all atoms of a particular element. Custom basis sets can be entered, and the shorthand labeling of basis sets is also supported.

The use of different basis sets for a particular element means the global potential energy surface is no longer unique. The user should exercise caution when using this feature of mixed basis sets, especially during geometry optimizations and transition state searches.

**Example 7.2** Example of adding a user defined non-standard basis set. The user is able to specify different standard basis sets for different atoms.

```
$molecule
   0  1
   O
   H  O  oh
   H  O  oh  2  hoh
   oh  =   1.2
   hoh = 110.0
$end

$rem
   EXCHANGE   hf
   BASIS      General   user-defined general basis
   PURECART   2         Cartesian D functions
   BASIS2     sto-3g    use STO-3G as initial guess
$end

$basis
   H 0
   6-31G
   ****
   O 0
   6-311G(d)
   ****
$end
```

**Example 7.3** Example of using a mixed basis set for methanol. The user is able to specify different standard basis sets for some atoms and supply user-defined exponents and contraction coefficients for others. This might be particularly useful in cases where the user has constructed exponents and contraction coefficients for atoms not defined in a standard basis set so that only the non-defined atoms need have the exponents and contraction coefficients entered. Note that a basis set has to be specified for every atom in the molecule, even if the same basis is to be used on an atom type. Note also that the dummy atom is not counted.

```
$molecule
   0  1
   C
   O   C  rco
   H1  C  rch1  O  h1co
   x   C  1.0   O  xcol  h1  180.0
   H2  C  rch2  x  h2cx  h1   90.0
   H3  C  rch2  x  h2cx  h1  -90.0
   H4  O  roh   C  hoc   h1  180.0

   rco   =  1.421
   rch1  =  1.094
   rch2  =  1.094
   roh   =  0.963
   h1co  =  107.2
   xco   =  129.9
   h2cx  =  54.25
   hoc   =  108.0
$end

$rem
   EXCHANGE   hf
   BASIS      mixed   user-defined mixed basis
$end

$basis
   C  1
   3-21G
   ****
   O  2
   S  3  1.00
      3.22037000E+02   5.92394000E-02
      4.84308000E+01   3.51500000E-01
      1.04206000E+01   7.07658000E-01
   SP 2 1.00
      7.40294000E+00  -4.04453000E-01   2.44586000E-01
      1.57620000E+00   1.22156000E+00   8.53955000E-01
   SP 1 1.00
      3.73684000E-01   1.00000000E+00   1.00000000E+00
   SP 1 1.00
      8.45000000E-02   1.00000000E+00   1.00000000E+00
   ****
   H  3
   6-31(+,+)G(d,p)
   ****
   H  4
   sto-3g
   ****
   H  5
   sto-3g
   ****
   H  6
   sto-3g
   ****
$end
```

## 7.6 Dual Basis Sets

There are several types of calculation that can be performed within Q-Chem using *two* atomic orbital basis sets instead of just one as we have been assuming in this chapter so far. Such calculations are said to involve *dual* basis sets. Typically iterations are performed in a smaller, primary, basis, which is specified by the *$rem* keyword BASIS2. Examples of calculations that can be performed using dual basis sets include:

- An improved initial guess for an SCF calculation in the large basis. See Section 4.5.5.
- Dual basis self-consistent field calculations (Hartree-Fock and density functional theory). See discussion in Section 4.9.
- Density functional perturbative corrections by “triple jumping”. See Section 4.10.
- Dual basis MP2 calculations. See discussion in Section 5.6.1.

**BASIS2**

Defines the (small) second basis set.

TYPE:

STRING

DEFAULT:

No default for the second basis set.

OPTIONS:

| | |
|---|---|
| Symbol | Use standard basis sets as for BASIS. |
| BASIS2_GEN | General BASIS2 |
| BASIS2_MIXED | Mixed BASIS2 |

RECOMMENDATION:

BASIS2 should be smaller than BASIS. There is little advantage to using a basis larger than a minimal basis when BASIS2 is used for initial guess purposes. Larger, standardized BASIS2 options are available for dual-basis calculations as discussed in Section 4.9 and summarized in Table 4.9.3.

In addition to built-in basis sets for BASIS2, it is also possible to enter user-defined second basis sets using an additional *$basis*2 input section, whose syntax generally follows the *$basis* input section documented above in Section 7.4.

## 7.7 Auxiliary Basis Sets for RI (Density Fitting)

While atomic orbital standard basis sets are used to expand one-electron functions such as molecular orbitals, *auxiliary basis sets* are also used in many Q-CHEM jobs to efficiently approximate products of one-electron functions, such as arise in electron correlation methods.

For a molecule of fixed size, increasing the number of basis functions *per atom*, $n$, leads to $\mathcal{O}(n^4)$ growth in the number of significant four-center two-electron integrals, since the number of non-negligible product charge distributions, $|\mu\nu\rangle$, grows as $\mathcal{O}(n^2)$. As a result, the use of large (high-quality) basis expansions is computationally costly. Perhaps the most practical way around this "basis set quality" bottleneck is the use of auxiliary basis expansions[9–11]. The ability to use auxiliary basis sets to accelerate a variety of electron correlation methods, including both energies and analytical gradients, is a major feature of Q-CHEM.

The auxiliary basis $\{|K\rangle\}$ is used to approximate products of Gaussian basis functions:

$$|\mu\nu\rangle \approx |\widetilde{\mu\nu}\rangle = \sum_K |K\rangle C_{\mu\nu}^K \tag{7.1}$$

Auxiliary basis expansions were introduced long ago, and are now widely recognized as an effective and powerful approach, which is sometimes synonymously called resolution of the identity (RI) or density fitting (DF). When using auxiliary basis expansions, the rate of growth of computational cost of large-scale electronic structure calculations with $n$ is reduced to approximately $n^3$.

If $n$ is fixed and molecule size increases, auxiliary basis expansions reduce the pre-factor associated with the computation, while not altering the scaling. The important point is that the pre-factor can be reduced by 5 or 10 times or more. Such large speedups are possible because the number of auxiliary functions required to obtain reasonable accuracy, $X$, has been shown to be only about 3 or 4 times larger than $N$.

The auxiliary basis expansion coefficients, $\mathbf{C}$, are determined by minimizing the deviation between the fitted distribution and the actual distribution, $\langle\mu\nu - \widetilde{\mu\nu}|\mu\nu - \widetilde{\mu\nu}\rangle$, which leads to the following set of linear equations:

$$\sum_L \langle K\,|L\rangle C_{\mu\nu}^{L} = \langle K\,|\mu\nu\rangle \tag{7.2}$$

Evidently solution of the fit equations requires only two- and three-center integrals, and as a result the (four-center) two-electron integrals can be approximated as the following optimal expression for a given choice of auxiliary basis set:

$$\langle\mu\nu|\lambda\sigma\rangle \approx \langle\widetilde{\mu\nu}|\widetilde{\lambda\sigma}\rangle = \sum_{K,L} C_{\mu\nu}^{L}\langle L|K\rangle C_{\lambda\sigma}^{K} \tag{7.3}$$

In the limit where the auxiliary basis is complete (*i.e.* all products of AOs are included), the fitting procedure described above will be exact. However, the auxiliary basis is invariably incomplete (as mentioned above, $X \approx 3N$) because this is essential for obtaining increased computational efficiency.

More details on Q-CHEM's use of RI methods is given in Section 5.6 on RI-MP2 and related methods, Section 5.15 on pairing methods, Section 5.8.5 on coupled cluster methods, Section 4.8.8 on DFT methods, and Section 6.9 on restricted active space methods. In the remainder of this section we focus on documenting the input associated with the auxiliary basis itself.

Q-CHEM contains a variety of built-in auxiliary basis sets, that can be specified by the *$rem* keyword AUX_BASIS.

**AUX_BASIS**

Sets the auxiliary basis set to be used

TYPE:

STRING

DEFAULT:

No default auxiliary basis set

OPTIONS:

| | |
|---|---|
| General, Gen | User-defined. As for BASIS |
| Symbol | Use standard auxiliary basis sets as in the table below |
| Mixed | Use a combination of different basis sets |

RECOMMENDATION:

Consult literature and EMSL Basis Set Exchange to aid your selection.

| **Symbolic Name** | **Atoms Supported** |
|---|---|
| RIMP2-VDZ | H, He, Li → Ne, Na → Ar, K → Br |
| RIMP2-TZVPP | H, He, Li → Ne, Na → Ar, Ga → Kr |
| RIMP2-cc-pVDZ | H, He, Li → Ne, Na → Ar, Ga → Kr |
| RIMP2-cc-pVTZ | H, He, Li → Ne, Na → Ar, Ga → Kr |
| RIMP2-cc-pVQZ | H, He, Li → Ne, Na → Ar, Ga → Kr |
| RIMP2-aug-cc-pVDZ | H, He, B → Ne, Al → Ar, Ga → Kr |
| RIMP2-aug-cc-pVTZ | H, He, B → Ne, Al → Ar, Ga → Kr |
| RIMP2-aug-cc-pVQZ | H, He, B → Ne, Al → Ar, Ga → Kr |

Table 7.11: Built-in auxiliary basis sets available in Q-CHEM for electron correlation.

In addition to built-in auxiliary basis sets, it is also possible to enter user-defined auxiliary basis sets using an *$aux_basis* input section, whose syntax generally follows the *$basis* input section documented above in Section 7.4.

## 7.8 Basis Set Superposition Error (BSSE)

When calculating binding energies, the energies of the fragments are usually higher than they should be due to the smaller effective basis set used for the individual species. This leads to an overestimate of the binding energy called the basis set superposition error. The effects of this can be corrected for by performing the calculations on the individual species in the presence of the basis set associated with the other species. This requires basis functions to be placed at arbitrary points in space, not just those defined by the nuclear centers. This can be done within Q-CHEM by using ghost atoms. These atoms have zero nuclear charge, but can support a user defined basis set. Ghost atom locations are specified in the *$molecule* section, as for any other atom, and the basis must be specified in a *$basis* section in the same manner as for a mixed basis.

**Example 7.4** A calculation on a water monomer in the presence of the full dimer basis set. The energy will be slightly lower than that without the ghost atom functions due to the greater flexibility of the basis set.

```
$molecule
   0  1
   O    1.68668  -0.00318   0.000000
   H    1.09686   0.01288  -0.741096
   H    1.09686   0.01288   0.741096
   Gh  -1.45451   0.01190   0.000000
   Gh  -2.02544  -0.04298  -0.754494
   Gh  -2.02544  -0.04298   0.754494
$end

$rem
   METHOD        mp2
   BASIS         mixed
$end

$basis
   O 1
   6-31G*
   ****
   H 2
   6-31G*
   ****
   H 3
   6-31G*
   ****
   O 4
   6-31G*
   ****
   H 5
   6-31G*
   ****
   H 6
   6-31G*
   ****
```

```
$end
```

Ghost atoms can also be specified by placing @ in front of the corresponding atomic symbol in the *$molecule* section of the input file. If @ is used to designate the ghost atoms in the system then it is not necessary to use MIXED basis set and include the *$basis* section in the input.

**Example 7.5** A calculation on ammonia in the presence of the basis set of ammonia borane.

```
$molecule
   0 1
    N     0.0000   0.0000   0.7288
    H     0.9507   0.0001   1.0947
    H    -0.4752  -0.8234   1.0947
    H    -0.4755   0.8233   1.0947
   @B     0.0000   0.0000  -0.9379
   @H     0.5859   1.0146  -1.2474
   @H     0.5857  -1.0147  -1.2474
   @H    -1.1716   0.0001  -1.2474
$end

$rem
   METHOD          B3LYP
   BASIS           6-31G(d,p)
   PURECART        1112
$end
```

Finally, there is an alternative approach to counterpoise corrections that is also available in Q-CHEM. The powerful Absolutely Localized Molecular Orbital (ALMO) methods can be very conveniently used for the fully automated evaluation of BSSE corrections with associated computational advantages also. This is described in detail, including examples, in Section 12.4.3.

## References and Further Reading

[1] Ground-State Methods (Chapters 4 and 5).

[2] Effective Core Potentials (Chapter 8).

[3] W. J. Hehre, L. Radom, P. v. R. Schleyer, and J. A. Pople, *Ab Initio Molecular Orbital Theory*, Wiley, New York, 1986.

[4] S. Huzinaga, *Comp. Phys. Rep.* **2**, 279 (1985).

[5] E. R. Davidson and D. Feller, *Chem. Rev.* **86**, 681 (1986).

[6] D. Feller and E. R. Davidson, in *Reviews in Computational Chemistry*, edited by K. B. Lipkowitz and D. B. Boyd, volume 1, page 1, Wiley-VCH, New York, 1990.

[7] F. Jensen, *Introduction to Computational Chemistry*, Wiley, New York, 1994.

[8] Basis sets were obtained from the Extensible Computational Chemistry Environment Basis Set Database, Version 1.0, as developed and distributed by the Molecular Science Computing Facility, Environmental and Molecular Sciences Laboratory which is part of the Pacific Northwest Laboratory, P.O. Box 999, Richland, Washington 99352, USA, and funded by the U.S. Department of Energy. The Pacific Northwest Laboratory is a multi-program laboratory operated by Battelle Memorial Institute for the U.S. Department of Energy under contract DE-AC06-76RLO 1830. Contact David Feller, Karen Schuchardt or Don Jones for further information.

[9] M. Feyereisen, G. Fitzgerald, and A. Komornicki, *Chem. Phys. Lett.* **208**, 359 (1993).

[10] B. I. Dunlap, *Phys. Chem. Chem. Phys.* **2**, 2113 (2000).

[11] Y. Jung, A. Sodt, P. M. W. Gill, and M. Head-Gordon, *Proc. Natl. Acad. Sci. USA* **102**, 6692 (2005).

# Chapter 8

# Effective Core Potentials

## 8.1 Introduction

The application of quantum chemical methods to elements in the lower half of the Periodic Table is more difficult than for the lighter atoms. There are two key reasons for this:

- the number of electrons in heavy atoms is large
- relativistic effects in heavy atoms are often non-negligible

Both of these problems stem from the presence of large numbers of core electrons and, given that such electrons do not play a significant *direct* role in chemical behavior, it is natural to ask whether it is possible to model their effects in some simpler way. Such enquiries led to the invention of Effective Core Potentials (ECPs) or pseudopotentials. For reviews of relativistic effects in chemistry, see for example Refs. 3–8.

If we seek to replace the core electrons around a given nucleus by a pseudopotential, while affecting the chemistry as little as possible, the pseudopotential should have the same effect on nearby valence electrons as the core electrons. The most obvious effect is the simple electrostatic repulsion between the core and valence regions but the requirement that valence orbitals must be orthogonal to core orbitals introduces additional subtler effects that cannot be neglected.

One of the key issues in the development of ECPs is the definition of the "core". So-called "large-core" ECPs include all shells except the outermost one, but "small-core" ECPs include all except the outermost *two* shells. Although the small-core ECPs are more expensive to use (because more electrons are treated explicitly), it is often found that their enhanced accuracy justifies their use.

When an ECP is constructed, it is usually based either on non-relativistic, or quasi-relativistic all-electron calculations. As one might expect, the quasi-relativistic ECPs tend to yield better results than their non-relativistic brethren, especially for atoms beyond the $3d$ block

Q-CHEM's ECP package is integrated with its electron correlation and DFT packages. Of course, no correlation or exchange-correlation energy due to the core electrons is included when using an ECP in a DFT or correlated method, respectively.

The most widely used ECPs today are of the form first proposed by Kahn *et al.*[9] in the 1970s. These model the effects of the core by a one-electron operator $U(r)$ whose matrix elements are simply added to the one-electron Hamiltonian matrix. The ECP operator is given by

$$U(r) = U_L(r) + \sum_{\ell=0}^{L-1} \sum_{m=-l}^{+l} |Y_{\ell m}\rangle \, U_l(r) \, \langle Y_{\ell m}| \tag{8.1}$$

where the radial potentials have the form

$$U_\ell(r) = \sum_{k=1}^{K_\ell} D_{\ell_k} \, r^{n_{\ell_k}} e^{-\eta_{\ell_k} r^2} \tag{8.2}$$

and $\sum_m |Y_{\ell m}\rangle \langle Y_{\ell m}|$ is the spherical harmonic projector of angular momentum $\ell$. In practice, $n_{\ell_k} = -2$, $-1$ or 0 and $L$ rarely exceeds 5. In addition, $U_L(r)$ contains a Coulombic term $N_c/r$, where $N_c$ is the number of core electrons.

## 8.2 ECP Reconstruction

The ECP matrix elements are arguably the most difficult one-electron integrals in existence. Indeed, using current methods, the time taken to compute the ECP integrals can exceed the time taken to compute the far more numerous electron repulsion integrals. Q-CHEM 5.0 implements a state-of-the-art ECP method[10] based on efficient recursion relations and upper bounds. This method relies on a restricted radial potential $U_\ell(r)$, where the radial power is only ever zero, i.e. $n = 0$. Whilst true for some ECPs, such as the Stuttgart-Bonn sets, many other ECPs have radial potentials containing $n = -2$ and $n = -1$ terms. To overcome this challenge, we reconstruct these ECP radial potentials using only $n = 0$ terms. Each $n = -2$ and $n = -1$ term is expanded as a sum of three $n = 0$ terms, each with independent contraction coefficient $D_{\ell_k}$ and Gaussian exponent $\eta_{\ell_k}$. The Gaussian exponents are given by a predetermined recipe and the contraction coefficients are computed in a least squares fitting procedure. The errors introduced by the ECP reconstruction are insignificant and of the same order as those introduced by numerical integration present in other ECP methods. This reconstruction is carried out automatically by Q-CHEM at run time.

## 8.3 Built-In ECPs

### 8.3.1 Overview

Q-CHEM is equipped with several standard ECP sets which are specified using the ECP keyword within the *$rem* block. The built-in ECPs, which are described in some detail at the end of this Chapter, fall into four families:

- The Hay-Wadt (or Los Alamos) sets (HWMB and LANL2DZ)
- The Stevens-Basch-Krauss-Jansien-Cundari set (SBKJC)
- The Christiansen-Ross-Ermler-Nash-Bursten sets (CRENBS and CRENBL)
- The Stuttgart-Bonn sets (SRLC and SRSC)

Besides the ones above, a common “def2-ECP" needs to be used with Karlsruhe basis sets for elements Rb-Rn (see section 7.3).

References and information about the definition and characteristics of most of these sets can be found at the EMSL site of the Pacific Northwest National Laboratory[11]:

```
http://www.emsl.pnl.gov/forms/basisform.html
```

Each of the built-in ECPs comes with a matching orbital basis set for the valence electrons. In general, it is advisable to use these together and, if you select a basis set other than the matching one, Q-CHEM will print a warning message in the output file. If you omit the BASIS *$rem* keyword entirely, Q-CHEM will automatically provide the matching one.

The following *$rem* variable controls which ECP is used:

**ECP**
Defines the effective core potential and associated basis set to be used
TYPE:
STRING
DEFAULT:
No ECP
OPTIONS:
General, Gen User defined. (*$ecp* keyword required)
Symbol Use standard ECPs discussed above.
RECOMMENDATION:
ECPs are recommended for first row transition metals and heavier elements. Consul the reviews for more details.

### 8.3.2 Combining ECPs

If you wish, you can use different ECP sets for different elements in the system. This is especially useful if you would like to use a particular ECP but find that it is not available for all of the elements in your molecule. To combine different ECP sets, you set the ECP and BASIS keywords to “Gen” or “General” and then add a *$ecp* block and a *$basis* block to your input file. In each of these blocks, you must name the ECP and the orbital basis set that you wish to use, separating each element by a sequence of four asterisks. There is also a built-in combination that can be invoked specifying “ECP=LACVP”. It assigns automatically 6-31G* or other suitable type basis sets for atoms H-Ar, while uses LANL2DZ for heavier atoms.

### 8.3.3 Examples

**Example 8.1** Computing the HF/LANL2DZ energy of AgCl at a bond length of 2.4 Å.

```
$molecule
   0  1
   Ag
   Cl  Ag  r

   r  =  2.4
$end

$rem
```

```
   METHOD     hf        Hartree-Fock calculation
   ECP        lanl2dz   Using the Hay-Wadt ECP
   BASIS      lanl2dz   And the matching basis set
$end
```

**Example 8.2** Computing the single point energy of HI with B3LYP/def2-SV(P) (using def2-ECP for I).

```
$molecule
   0 1
   H    0.0    0.0    0.0
   I    0.0    0.0    1.5
$end

$rem
   METHOD           b3lyp
   BASIS            def2-sv(p)
   ECP              def2-ecp
   SYMMETRY         false
   SYM_IGNORE       true
   THRESH           14
   SCF_CONVERGENCE  8
$end
```

**Example 8.3** Optimization of the structure of $Se_8$ using HF/LANL2DZ, followed by a single-point energy calculation at the MP2/LANL2DZ level.

```
$molecule
   0  1
   x1
   x2   x1  xx
   Se1  x1  sx  x2  90.
   Se2  x1  sx  x2  90.  Se1  90.
   Se3  x1  sx  x2  90.  Se2  90.
   Se4  x1  sx  x2  90.  se3  90.
   Se5  x2  sx  x1  90.  Se1  45.
   Se6  x2  sx  x1  90.  Se5  90.
   Se7  x2  sx  x1  90.  Se6  90.
   Se8  x2  sx  x1  90.  Se7  90.

   xx = 1.2
   sx = 2.8
$end

$rem
   JOBTYPE    opt
   METHOD     hf
   ECP        lanl2dz
$end

@@@

$molecule
   read
$end

$rem
   METHOD         mp2       MP2 correlation energy
   ECP           lanl2dz   Hay-Wadt ECP and basis
   SCF_GUESS     read      Read in the MOs
$end
```

**Example 8.4** Computing the HF geometry of $CdBr_2$ using the Stuttgart relativistic ECPs. The small-core ECP and basis are employed on the Cd atom and the large-core ECP and basis on the Br atoms.

```
$molecule
   0  1
   Cd
   Br1  Cd  r
   Br2  Cd  r  Br1  180

   r = 2.4
$end

$rem
   JOBTYPE    opt   Geometry optimization
   METHOD     hf    Hartree-Fock theory
   ECP        gen   Combine ECPs
   BASIS      gen   Combine basis sets
   PURECART   1     Use pure d functions
$end

$ecp
   Cd
   srsc
   ****
   Br
   srlc
   ****
$end

$basis
   Cd
   srsc
   ****
   Br
   srlc
   ****
$end
```

## 8.4 User-Defined ECPs

Many users will find that the library of built-in ECPs is adequate for their needs. However, if you need to use an ECP that is not built into Q-CHEM, you can enter it in much the same way as you can enter a user-defined orbital basis set (see Chapter 7).

### 8.4.1 Job Control for User-Defined ECPs

To apply a user-defined ECP, you must set the ECP and BASIS keywords in *$rem* to “Gen”. You then add a *$ecp* block that defines your ECP, element by element, and a *$basis* block that defines your orbital basis set, separating elements by asterisks.

The syntax within the *$basis* block is described in Chapter 7. The syntax for each record within the *$ecp* block is as follows:.

*$ecp*
For each atom that will bear an ECP
  Chemical symbol for the atom
  ECP name ; the $L$ value for the ECP ; number of core electrons removed
  For each ECP component (in the order unprojected, $\hat{P}_0$, $\hat{P}_1$, , $\hat{P}_{L-1}$
    The component name
    The number of Gaussians in the component
    For each Gaussian in the component
      The power of $r$ ; the exponent ; the contraction coefficient
A sequence of four asterisks (*i.e.*, $\star\star\star\star$)
*$end*

**Note:** (1) All of the information in the *$ecp* block is case-insensitive.
(2) The $L$ value may not exceed 4. That is, nothing beyond $G$ projectors is allowed.
(3) The power of $r$ (which includes the Jacobian $r^2$ factor) must be 0, 1 or 2.

### 8.4.2 Example

**Example 8.5** Optimizing the HF geometry of $AlH_3$ using a user-defined ECP and basis set on Al and the 3-21G basis on H.

```
$molecule
   0  1
   Al
   H1  Al  r
   H2  Al  r  H1  120
   H3  Al  r  H1  120  H2  180

   r = 1.6
$end

$rem
   JOBTYPE    opt   Geometry optimization
   METHOD     hf    Hartree-Fock theory
   ECP        gen   User-defined ECP
   BASIS      gen   User-defined basis
$end

$ecp
   Al
   Stevens_ECP  2  10
   d potential
     1
     1   1.95559  -3.03055
   s-d potential
     2
     0   7.78858   6.04650
     2   1.99025  18.87509
   p-d potential
     2
     0   2.83146   3.29465
     2   1.38479   6.87029
****
$end

$basis
   Al
   SP 3  1.00
      0.90110  -0.30377  -0.07929
      0.44950   0.13382   0.16540
      0.14050   0.76037   0.53015
   SP 1  1.00
      0.04874   0.32232   0.47724
****
   H
   3-21G
****
$end
```

## 8.5 ECPs and Density Functional Theory

Q-CHEM's ECP package and DFT package are tightly integrated and facilitate the application of advanced density functionals to molecules containing heavy elements. Any of the local, gradient-corrected and hybrid functionals discussed in Chapter 4 may be used and you may also perform ECP calculations with user-defined hybrid functionals.

In a DFT calculation with ECPs, the exchange-correlation energy is obtained entirely from the non-core electrons. This will be satisfactory if there are no chemically important core-valence effects but may introduce significant errors, particularly if you are using a "large-core" ECP.

## 8.6 ECPs and Electron Correlation

The ECP package is integrated with the electron correlation package and it is therefore possible to apply any of Q-CHEM's post-Hartree-Fock methods to systems in which some of the atoms may bear pseudopotentials. Of course, the correlation energy contribution arising from core electrons that have been replaced by an ECP is *not* included. In this sense, correlation energies with ECPs are comparable to correlation energies from frozen core calculations. However, the use of ECPs effectively removes both core electrons *and* the corresponding virtual (unoccupied) orbitals.

### 8.6.1 Example

**Example 8.6** Optimization of the structure of $Se_8$ using HF/LANL2DZ, followed by a single-point energy calculation at the MP2/LANL2DZ level.

```
$molecule
   0  1
   x1
   x2   x1  xx
   Se1  x1  sx  x2  90.
   Se2  x1  sx  x2  90.  Se1  90.
   Se3  x1  sx  x2  90.  Se2  90.
   Se4  x1  sx  x2  90.  se3  90.
   Se5  x2  sx  x1  90.  Se1  45.
   Se6  x2  sx  x1  90.  Se5  90.
   Se7  x2  sx  x1  90.  Se6  90.
   Se8  x2  sx  x1  90.  Se7  90.

   xx = 1.2
   sx = 2.8
$end

$rem
   JOBTYPE    opt
   METHOD     hf
   ECP        lanl2dz
$end

@@@

$molecule
   read
$end

$rem
   JOBTYPE      sp        Single-point energy
   METHOD       mp2       MP2 correlation energy
   ECP          lanl2dz   Hay-Wadt ECP and basis
   SCF_GUESS    read      Read in the MOs
$end
```

## 8.7 ECPs, Forces and Vibrational Frequencies

It is important to be able to optimize geometries using pseudopotentials and for this purpose Q-CHEM contains analytical first derivatives of the nuclear potential energy term for ECPs.

The ECP package is also integrated with the vibrational analysis package and it is therefore possible to compute the vibrational frequencies (and hence the infrared and Raman spectra) of systems in which some of the atoms may bear ECPs.

Q-CHEM cannot calculate analytic second derivatives of the nuclear potential-energy term when ECPs are used, and must therefore resort to finite difference methods. However, for HF and DFT calculations, it can compute analytic second derivatives for all other terms in the Hamiltonian. The program takes full advantage of this by only computing the potential-energy derivatives numerically, and adding these to the analytically calculated second derivatives of the remaining energy terms.

There is a significant speed advantage associated with this approach as, at each finite-difference step, only the potential-energy term needs to be calculated. This term requires only three-center integrals, which are far fewer in number and much cheaper to evaluate than the four-center, two-electron integrals associated with the electron-electron interaction terms. Readers are referred to Table 9.1 for a full list of the analytic derivative capabilities of Q-CHEM.

### 8.7.1 Example

**Example 8.7** Structure and vibrational frequencies of $TeO_2$ using Hartree-Fock theory and the Stuttgart relativistic large-core ECPs. Note that the vibrational frequency job reads both the optimized structure and the molecular orbitals from the geometry optimization job that precedes it. Note also that only the second derivatives of the potential energy term will be calculated by finite difference, all other terms will be calculated analytically.

```
$molecule
   0  1
   Te
   O1  Te  r
   O2  Te  r  O1  a

   r = 1.8
   a = 108
$end

$rem
   JOBTYPE    opt
   METHOD     hf
   ECP        srlc
$end

@@@

$molecule
   read
$end

$rem
   JOBTYPE     freq
   METHOD      hf
   ECP         srlc
   SCF_GUESS   read
$end
```

### 8.7.2 A Brief Guide to Q-CHEM's Built-In ECPs

The remainder of this Chapter consists of a brief reference guide to Q-CHEM's built-in ECPs. The ECPs vary in their complexity and their accuracy and the purpose of the guide is to enable the user quickly and easily to decide which ECP to use in a planned calculation.

The following information is provided for each ECP:

- The elements for which the ECP is available in Q-CHEM. This is shown on a schematic Periodic Table by shading all the elements that are *not* supported.
- The literature reference for each element for which the ECP is available in Q-CHEM.
- The matching orbital basis set that Q-CHEM will use for light (*i.e.*. non-ECP atoms). For example, if the user requests SRSC ECPs—which are defined only for atoms beyond argon—Q-CHEM will use the 6-311G* basis set for all atoms up to Ar.

- The core electrons that are replaced by the ECP. For example, in the LANL2DZ ECP for the Fe atom, the core is [Ne], indicating that the $1s$, $2s$ and $2p$ electrons are removed.

- The maximum spherical harmonic projection operator that is used for each element. This often, but not always, corresponds to the maximum orbital angular momentum of the core electrons that have been replaced by the ECP. For example, in the LANL2DZ ECP for the Fe atom, the maximum projector is of $P$-type.

- The number of valence basis functions of each angular momentum type that are present in the matching orbital basis set. For example, in the matching basis for the LANL2DZ ECP for the Fe atom, there the three $s$ shells, three $p$ shells and two $d$ shells. This basis is therefore almost of triple-split valence quality.

### 8.7.3 The HWMB ECP at a Glance

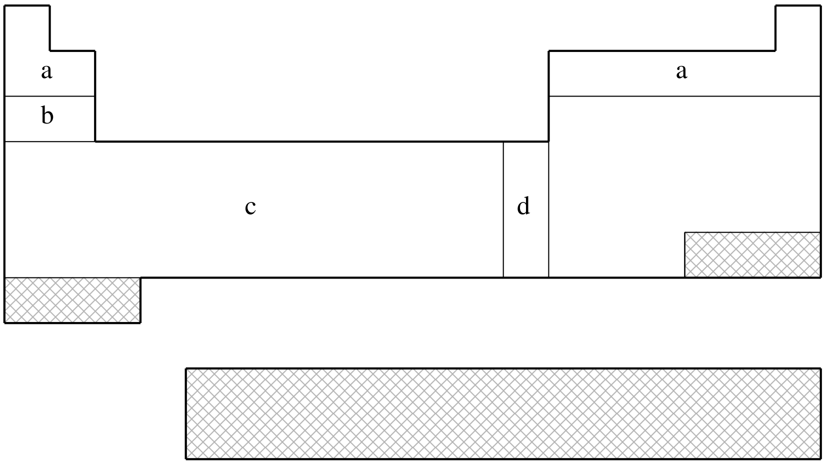

(a) No ECP ; Pople STO-3G basis used
(b) Wadt & Hay, J. Chem. Phys. 82 (1985) 285
*HWMB is* ***not*** *available for shaded elements* (c) Hay & Wadt, J. Chem. Phys. 82 (1985) 299
(d) Hay & Wadt, J. Chem. Phys. 82 (1985) 270

| Element | Core | Max Projector | Valence |
|---|---|---|---|
| H–He | *none* | *none* | (1s) |
| Li–Ne | *none* | *none* | (2s,1p) |
| Na–Ar | [Ne] | *P* | (1s,1p) |
| K–Ca | [Ne] | *P* | (2s,1p) |
| Sc–Cu | [Ne] | *P* | (2s,1p,1d) |
| Zn | [Ar] | *D* | (1s,1p,1d) |
| Ga–Kr | [Ar]+3d | *D* | (1s,1p) |
| Rb–Sr | [Ar]+3d | *D* | (2s,1p) |
| Y–Ag | [Ar]+3d | *D* | (2s,1p,1d) |
| Cd | [Kr] | *D* | (1s,1p,1d) |
| In–Xe | [Kr]+4d | *D* | (1s,1p) |
| Cs–Ba | [Kr]+4d | *D* | (2s,1p) |
| La | [Kr]+4d | *D* | (2s,1p,1d) |
| Hf–Au | [Kr]+4d+4f | *F* | (2s,1p,1d) |
| Hg | [Xe]+4f | *F* | (1s,1p,1d) |
| Tl–Bi | [Xe]+4f+5d | *F* | (1s,1p) |

### 8.7.4 The LANL2DZ ECP at a Glance

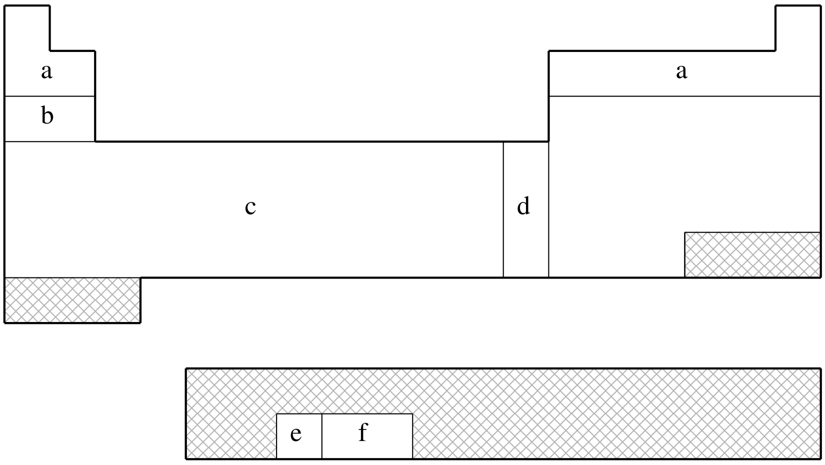

*LANL2DZ is **not** available for shaded elements*

(a) No ECP ; Pople 6-31G basis used
(b) Wadt & Hay, J. Chem. Phys. 82 (1985) 285
(c) Hay & Wadt, J. Chem. Phys. 82 (1985) 299
(d) Hay & Wadt, J. Chem. Phys. 82 (1985) 270
(e) Hay, J. Chem. Phys. 79 (1983) 5469
(f) Wadt, to be published

| **Element** | **Core** | **Max Projector** | **Valence** |
|---|---|---|---|
| H–He | *none* | *none* | (2s) |
| Li–Ne | *none* | *none* | (3s,2p) |
| Na–Ar | [Ne] | *P* | (2s,2p) |
| K–Ca | [Ne] | *P* | (3s,3p) |
| Sc–Cu | [Ne] | *P* | (3s,3p,2d) |
| Zn | [Ar] | *D* | (2s,2p,2d) |
| Ga–Kr | [Ar]+3d | *D* | (2s,2p) |
| Rb–Sr | [Ar]+3d | *D* | (3s,3p) |
| Y–Ag | [Ar]+3d | *D* | (3s,3p,2d) |
| Cd | [Kr] | *D* | (2s,2p,2d) |
| In–Xe | [Kr]+4d | *D* | (2s,2p) |
| Cs–Ba | [Kr]+4d | *D* | (3s,3p) |
| La | [Kr]+4d | *D* | (3s,3p,2d) |
| Hf–Au | [Kr]+4d+4f | *F* | (3s,3p,2d) |
| Hg | [Xe]+4f | *F* | (2s,2p,2d) |
| Tl | [Xe]+4f+5d | *F* | (2s,2p,2d) |
| Pb–Bi | [Xe]+4f+5d | *F* | (2s,2p) |
| U–Pu | [Xe]+4f+5d | *F* | (3s,3p,2d,2f) |

Note that Q-Chem 4.2.2 and later versions also support LANL2DZ-SV basis, which employs SV basis functions (instead of 6-31G) on H, Li-He elements (like some other quantum chemistry packages).

### 8.7.5 The SBKJC ECP at a Glance

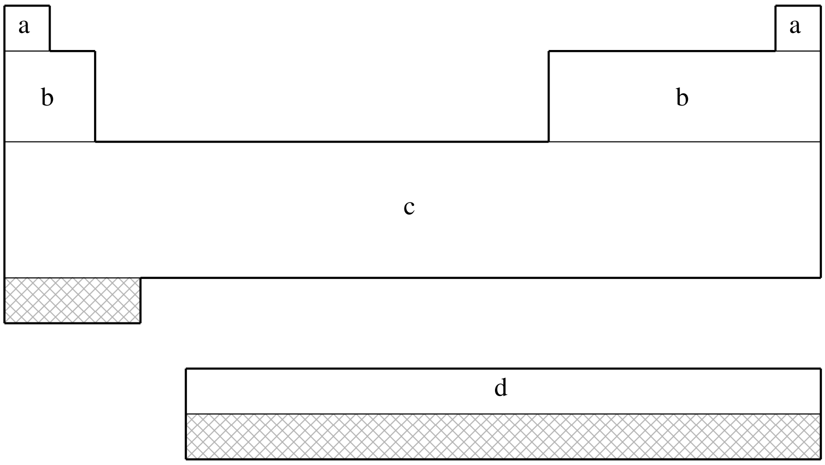

*SBKJC is **not** available for shaded elements*

(a) No ECP ; Pople 3-21G basis used

(b) W.J. Stevens, H. Basch & M. Krauss, J. Chem. Phys. 81 (1984) 6026

(c) W.J. Stevens, M. Krauss, H. Basch & P.G. Jasien, Can. J. Chem 70 (1992) 612

(d) T.R. Cundari & W.J. Stevens, J. Chem. Phys. 98 (1993) 5555

| **Element** | **Core** | **Max Projector** | **Valence** |
|---|---|---|---|
| H–He | *none* | *none* | (2s) |
| Li–Ne | [He] | *S* | (2s,2p) |
| Na–Ar | [Ne] | *P* | (2s,2p) |
| K–Ca | [Ar] | *P* | (2s,2p) |
| Sc–Ga | [Ne] | *P* | (4s,4p,3d) |
| Ge–Kr | [Ar]+3d | *D* | (2s,2p) |
| Rb–Sr | [Kr] | *D* | (2s,2p) |
| Y–In | [Ar]+3d | *D* | (4s,4p,3d) |
| Sn–Xe | [Kr]+4d | *D* | (2s,2p) |
| Cs–Ba | [Xe] | *D* | (2s,2p) |
| La | [Kr]+4d | *F* | (4s,4p,3d) |
| Ce–Lu | [Kr]+4d | *D* | (4s,4p,1d,1f) |
| Hf–Tl | [Kr]+4d+4f | *F* | (4s,4p,3d) |
| Pb–Rn | [Xe]+4f+5d | *F* | (2s,2p) |

### 8.7.6 The CRENBS ECP at a Glance

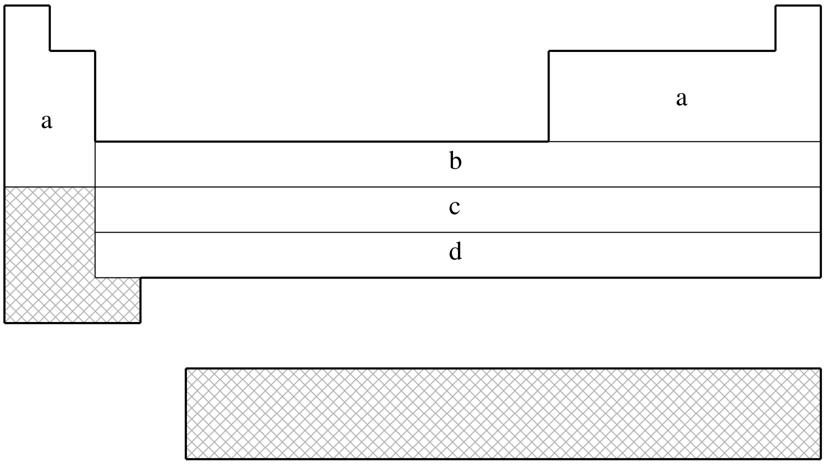

*CRENBS is **not** available for shaded elements*

(a) No ECP ; Pople STO-3G basis used

(b) Hurley, Pacios, Christiansen, Ross & Ermler, J. Chem. Phys. 84 (1986) 6840

(c) LaJohn, Christiansen, Ross, Atashroo & Ermler, J. Chem. Phys. 87 (1987) 2812

(d) Ross, Powers, Atashroo, Ermler, LaJohn & Christiansen, J. Chem. Phys. 93 (1990) 6654

| **Element** | **Core** | **Max Projector** | **Valence** |
|---|---|---|---|
| H–He | *none* | *none* | (1s) |
| Li–Ne | *none* | *none* | (2s,1p) |
| Na–Ar | *none* | *none* | (3s,2p) |
| K–Ca | *none* | *none* | (4s,3p) |
| Sc–Zn | [Ar] | $P$ | (1s,0p,1d) |
| Ga–Kr | [Ar]+3d | $D$ | (1s,1p) |
| Y–Cd | [Kr] | $D$ | (1s,1p,1d) |
| In–Xe | [Kr]+4d | $D$ | (1s,1p) |
| La | [Xe] | $D$ | (1s,1p,1d) |
| Hf–Hg | [Xe]+4f | $F$ | (1s,1p,1d) |
| Tl–Rn | [Xe]+4f+5d | $F$ | (1s,1p) |

### 8.7.7 The CRENBL ECP at a Glance

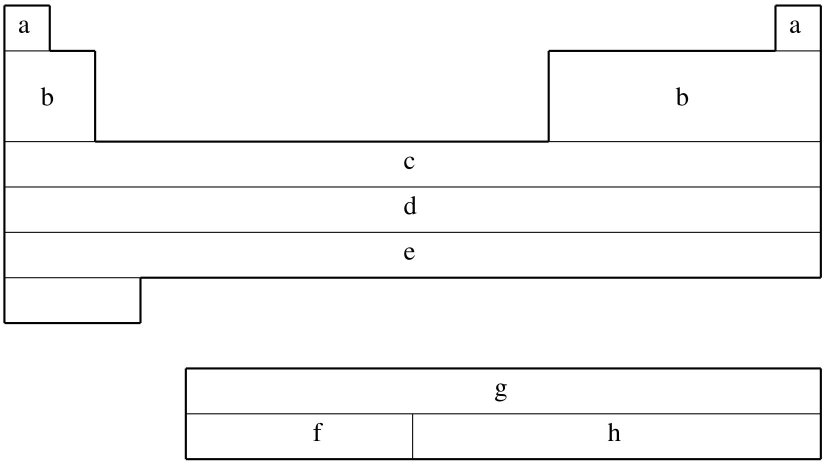

(a) No ECP ; Pople 6-311G* basis used
(b) Pacios & Christiansen, J. Chem. Phys. 82 (1985) 2664
(c) Hurley, Pacios, Christiansen, Ross & Ermler, J. Chem. Phys. 84 (1986) 6840
(d) LaJohn, Christiansen, Ross, Atashroo & Ermler, J. Chem. Phys. 87 (1987) 2812
(e) Ross, Powers, Atashroo, Ermler, LaJohn & Christiansen, J. Chem. Phys. 93 (1990) 6654
(f) Ermler, Ross & Christiansen, Int. J. Quantum Chem. 40 (1991) 829
(g) Ross, Gayen & Ermler, J. Chem. Phys. 100 (1994) 8145
(h) Nash, Bursten & Ermler, J. Chem. Phys. 106 (1997) 5133

| **Element** | **Core** | **Max Projector** | **Valence** |
|---|---|---|---|
| H–He | *none* | *none* | (3s) |
| Li–Ne | [He] | S | (4s,4p) |
| Na–Mg | [He] | S | (6s,4p) |
| Al–Ar | [Ne] | P | (4s,4p) |
| K–Ca | [Ne] | P | (5s,4p) |
| Sc–Zn | [Ne] | P | (7s,6p,6d) |
| Ga–Kr | [Ar] | P | (3s,3p,4d) |
| Rb–Sr | [Ar]+3d | D | (5s,5p) |
| Y–Cd | [Ar]+3d | D | (5s,5p,4d) |
| In–Xe | [Kr] | D | (3s,3p,4d) |
| Cs–La | [Kr]+4d | D | (5s,5p,4d) |
| Ce–Lu | [Xe] | D | (6s,6p,6d,6f) |
| Hf–Hg | [Kr]+4d+4f | F | (5s,5p,4d) |
| Tl–Rn | [Xe]+4f | F | (3s,3p,4d) |
| Fr–Ra | [Xe]+4f+5d | F | (5s,5p,4d) |
| Ac–Pu | [Xe]+4f+5d | F | (5s,5p,4d,4f) |
| Am–Lr | [Xe]+4f+5d | F | (0s,2p,6d,5f) |

### 8.7.8 The SRLC ECP at a Glance

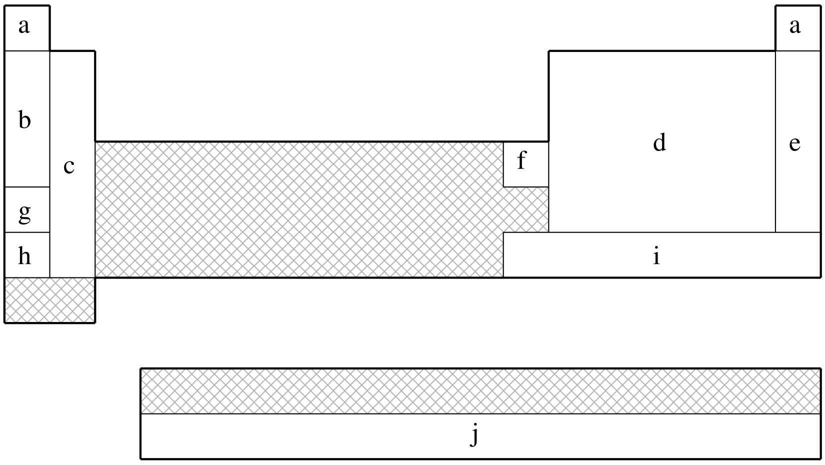

*SRLC is **not** available for shaded elements*

(a) No ECP ; Pople 6-31G basis used
(b) Fuentealba, Preuss, Stoll & Szentpaly, Chem. Phys. Lett. 89 (1982) 418
(c) Fuentealba, Szentpály, Preuss & Stoll, J. Phys. B 18 (1985) 1287
(d) Bergner, Dolg, Küchle, Stoll & Preuss, Mol. Phys. 80 (1993) 1431
(e) Nicklass, Dolg, Stoll & Preuss, J. Chem. Phys. 102 (1995) 8942
(f) Schautz, Flad & Dolg, Theor. Chem. Acc. 99 (1998) 231
(g) Fuentealba, Stoll, Szentpaly, Schwerdtfeger & Preuss, J. Phys. B 16 (1983) L323
(h) Szentpaly, Fuentealba, Preuss & Stoll, Chem. Phys. Lett. 93 (1982) 555
(i) Küchle, Dolg, Stoll & Preuss, Mol. Phys. 74 (1991) 1245
(j) Küchle, to be published

| Element | Core | Max Projector | Valence |
|---|---|---|---|
| H–He | *none* | *none* | (2s) |
| Li–Be | [He] | *P* | (2s,2p) |
| B–N | [He] | *D* | (2s,2p) |
| O–F | [He] | *D* | (2s,3p) |
| Ne | [He] | *D* | (4s,4p,3d,1f) |
| Na–P | [Ne] | *D* | (2s,2p) |
| S–Cl | [Ne] | *D* | (2s,3p) |
| Ar | [Ne] | *F* | (4s,4p,3d,1f) |
| K–Ca | [Ar] | *D* | (2s,2p) |
| Zn | [Ar]+3d | *D* | (3s,2p) |
| Ga–As | [Ar]+3d | *F* | (2s,2p) |
| Se–Br | [Ar]+3d | *F* | (2s,3p) |
| Kr | [Ar]+3d | *G* | (4s,4p,3d,1f) |
| Rb–Sr | [Kr] | *D* | (2s,2p) |
| In–Sb | [Kr]+4d | *F* | (2s,2p) |
| Te–I | [Kr]+4d | *F* | (2s,3p) |
| Xe | [Kr]+4d | *G* | (4s,4p,3d,1f) |
| Cs–Ba | [Xe] | *D* | (2s,2p) |
| Hg–Bi | [Xe]+4f+5d | *G* | (2s,2p,1d) |
| Po–At | [Xe]+4f+5d | *G* | (2s,3p,1d) |
| Rn | [Xe]+4f+5d | *G* | (2s,2p,1d) |
| Ac–Lr | [Xe]+4f+5d | *G* | (5s,5p,4d,3f,2g) |

## 8.7.9 The SRSC ECP at a Glance

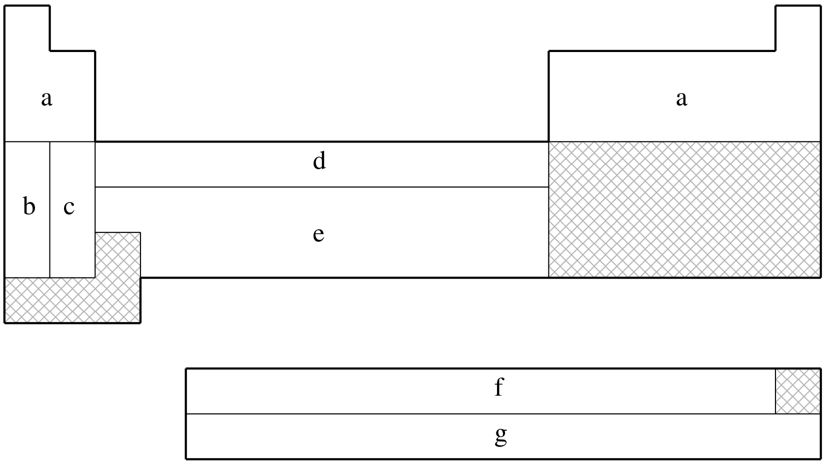

*SRSC is **not** available for shaded elements*

(a) No ECP ; Pople 6-311G* basis used
(b) Leininger, Nicklass, Küchle, Stoll, Dolg & Bergner, Chem. Phys. Lett. 255 (1996) 274
(c) Kaupp, Schleyer, Stoll & Preuss, J. Chem. Phys. 94 (1991) 1360
(d) Dolg, Wedig, Stoll & Preuss, J. Chem. Phys. 86 (1987) 866
(e) Andrae, Haeussermann, Dolg, Stoll & Preuss, Theor. Chim. Acta 77 (1990) 123
(f) Dolg, Stoll & Preuss, J. Chem. Phys. 90 (1989) 1730
(g) Küchle, Dolg, Stoll & Preuss, J. Chem. Phys. 100 (1994) 7535

| **Element** | **Core** | **Max Projector** | **Valence** |
|---|---|---|---|
| H–Ar | *none* | *none* | (3s) |
| Li–Ne | *none* | *none* | (4s,3p,1d) |
| Na–Ar | *none* | *none* | (6s,5p,1d) |
| K | [Ne] | *F* | (5s,4p) |
| Ca | [Ne] | *F* | (4s,4p,2d) |
| Sc–Zn | [Ne] | *D* | (6s,5p,3d) |
| Rb | [Ar]+3d | *F* | (5s,4p) |
| Sr | [Ar]+3d | *F* | (4s,4p,2d) |
| Y–Cd | [Ar]+3d | *F* | (6s,5p,3d) |
| Cs | [Kr]+4d | *F* | (5s,4p) |
| Ba | [Kr]+4d | *F* | (3s,3p,2d,1f) |
| Ce–Yb | [Ar]+3d | *G* | (5s,5p,4d,3f) |
| Hf–Pt | [Kr]+4d+4f | *G* | (6s,5p,3d) |
| Au | [Kr]+4d+4f | *F* | (7s,3p,4d) |
| Hg | [Kr]+4d+4f | *G* | (6s,6p,4d) |
| Ac–Lr | [Kr]+4d+4f | *G* | (8s,7p,6d,4f) |

### 8.7.10 The Karlsruhe “def2" ECP at a Glance

For elements Rb–Rn (not including the lanthanides), all the Karlsruhe “def2" basis sets are paired with a common set of ECPs.[12] It is briefly summarized in the table below (the number of valence basis functions depend on the basis set in use so it is not presented):

| **Element** | **Core** | **Max Projector** |
|---|---|---|
| H–Kr | *none* | *none* |
| Rb–Xe | [Ar]+3d | *D* |
| Cs–La | [Kr]+4d | *D* |
| Hf–Rn | [Kr]+4d+4f | *D* |

# References and Further Reading

[1] Ground-State Methods (Chapters 4 and 5).

[2] Basis Sets (Chapter 7).

[3] P. A. Christiansen, W. C. Ermler, and K. S. Pitzer, *Annu. Rev. Phys. Chem.* **36**, 407 (1985).

[4] P. Pyykko, *Chem. Rev.* **88**, 563 (1988).

[5] M. S. Gordon and T. R. Cundari, *Coord. Chem. Rev.* **147**, 87 (1996).

[6] G. Frenking et al., in *Reviews in Computational Chemistry*, edited by K. B. Lipkowitz and D. B. Boyd, volume 8, page 63, Wiley-VCH, New York, 1996.

[7] T. R. Cundari, M. T. Benson, M. L. Lutz, and S. O. Sommerer, in *Reviews in Computational Chemistry*, edited by K. B. Lipkowitz and D. B. Boyd, volume 8, page 145, Wiley-VCH, New York, 1996.

[8] J. Almlöf and O. Gropen, in *Reviews in Computational Chemistry*, edited by K. B. Lipkowitz and D. B. Boyd, volume 8, page 203, Wiley-VCH, New York, 1996.

[9] L. R. Kahn and W. A. Goddard III, *J. Chem. Phys.* **56**, 2685 (1972).

[10] S. C. McKenzie, E. Epifanovsky, A. T. B. Gilbert, and P. M. W. Gill, An efficient method for computing effective core potential integrals over Gaussian basis functions, (in preparation).

[11] Basis sets were obtained from the Extensible Computational Chemistry Environment Basis Set Database, Version 1.0, as developed and distributed by the Molecular Science Computing Facility, Environmental and Molecular Sciences Laboratory which is part of the Pacific Northwest Laboratory, P.O. Box 999, Richland, Washington 99352, USA, and funded by the U.S. Department of Energy. The Pacific Northwest Laboratory is a multi-program laboratory operated by Battelle Memorial Institute for the U.S. Department of Energy under contract DE-AC06-76RLO 1830. Contact David Feller, Karen Schuchardt or Don Jones for further information.

[12] F. Weigend and R. Ahlrichs, *Phys. Chem. Chem. Phys.* **7**, 3297 (2005).

# Chapter 9

# Exploring Potential Energy Surfaces: Searches for Critical Points and Molecular Dynamics

## 9.1 Equilibrium Geometries and Transition-State Structures

### 9.1.1 Overview

Molecular potential energy surfaces rely on the Born-Oppenheimer separation of nuclear and electronic motion. Minima on such energy surfaces correspond to the classical picture of equilibrium geometries, and transition state structures correspond to first-order saddle points. Both equilibrium and transition-state structures are stationary points for which the energy gradient vanishes. Characterization of such critical points requires consideration of the eigenvalues of the Hessian (second derivative matrix): minimum-energy, equilibrium geometries possess Hessians whose eigenvalues are all positive, whereas transition-state structures are defined by a Hessian with precisely one negative eigenvalue. (The latter is therefore a local maximum along the reaction path between minimum-energy reactant and product structures, but a minimum in all directions perpendicular to this reaction path.

The quality of a geometry optimization algorithm is of major importance; even the fastest integral code in the world will be useless if combined with an inefficient optimization algorithm that requires excessive numbers of steps to converge. Q-CHEM incorporates a geometry optimization package (OPTIMIZE—see Appendix A) developed by the late Jon Baker over more than ten years.

The key to optimizing a molecular geometry successfully is to proceed from the starting geometry to the final geometry in as few steps as possible. Four factors influence the path and number of steps:

- starting geometry
- optimization algorithm
- quality of the Hessian (and gradient)
- coordinate system

| **Level of Theory (Algorithm)** | **Analytical Gradients** | **Maximum Angular Momentum Type** | **Analytical Hessian** | **Maximum Angular Momentum Type** |
|---|---|---|---|---|
| DFT | ✓ | $h$ | ✓ | $f$ |
| HF | ✓ | $h$ | ✓ | $f$ |
| ROHF | ✓ | $h$ | ✗ | |
| MP2 | ✓ | $h$ | ✗ | |
| (V)OD | ✓ | $h$ | ✗ | |
| (V)QCCD | ✓ | $h$ | ✗ | |
| CIS (except RO) | ✓ | $h$ | ✓ | $f$ |
| CFMM | ✓ | $h$ | ✗ | |

Table 9.1: Gradients and Hessians currently available for geometry optimizations with maximum angular momentum types for analytical derivative calculations (for higher angular momentum, derivatives are computed numerically). Analytical Hessians are not yet available for meta-GGA functionals such as BMK and the M05 and M06 series.

Q-CHEM controls the last three of these, but the starting geometry is solely determined by the user, and the closer it is to the converged geometry, the fewer optimization steps will be required. Decisions regarding the optimization algorithm and the coordinate system are generally made by the OPTIMIZE package (*i.e.*, internally, within Q-CHEM) to maximize the rate of convergence. Although users may override these choices in many cases, this is not generally recommended.

Another consideration when trying to minimize the optimization time concerns the quality of the gradient and Hessian. A higher-quality Hessian (*i.e.*, analytical versus approximate) will in many cases lead to faster convergence, in the sense of requiring fewer optimization steps. However, the construction of an analytical Hessian requires significant computational effort and may outweigh the advantage of fewer optimization cycles. Currently available analytical gradients and Hessians are summarized in Table 9.1.

Features of Q-CHEM's geometry and transition-state optimization capabilities include:

- Cartesian, *Z*-matrix or internal coordinate systems
- Eigenvector Following (EF) or GDIIS algorithms
- Constrained optimizations
- Equilibrium structure searches
- Transition structure searches
- Hessian-free characterization of stationary points
- Initial Hessian and Hessian update options
- Reaction pathways using intrinsic reaction coordinates (IRC)
- Optimization of minimum-energy crossing points (MECPs) along conical seams

### 9.1.2 Job Control

Obviously a level of theory, basis set, and starting molecular geometry must be specified to begin a geometry optimization or transition-structure search. These aspects are described elsewhere in this manual, and this section describes job-control variables specific to optimizations.

**JOBTYPE**

Specifies the calculation.

TYPE:

STRING

DEFAULT:

Default is single-point, which should be changed to one of the following options.

OPTIONS:

OPT Equilibrium structure optimization.

TS Transition structure optimization.

RPATH Intrinsic reaction path following.

RECOMMENDATION:

Application-dependent.

**GEOM_OPT_HESSIAN**

Determines the initial Hessian status.

TYPE:

STRING

DEFAULT:

DIAGONAL

OPTIONS:

DIAGONAL Set up diagonal Hessian.

READ Have exact or initial Hessian. Use as is if Cartesian, or transform if internals.

RECOMMENDATION:

An accurate initial Hessian will improve the performance of the optimizer, but is expensive to compute.

**GEOM_OPT_COORDS**

Controls the type of optimization coordinates.

TYPE:

INTEGER

DEFAULT:

$-1$

OPTIONS:

0 Optimize in Cartesian coordinates.

1 Generate and optimize in internal coordinates, if this fails abort.

$-1$ Generate and optimize in internal coordinates, if this fails at any stage of the optimization, switch to Cartesian and continue.

2 Optimize in $Z$-matrix coordinates, if this fails abort.

$-2$ Optimize in $Z$-matrix coordinates, if this fails during any stage of the optimization switch to Cartesians and continue.

RECOMMENDATION:

Use the default; delocalized internals are more efficient.

**GEOM_OPT_TOL_GRADIENT**

Convergence on maximum gradient component.

TYPE:

INTEGER

DEFAULT:

300 $\equiv 300 \times 10^{-6}$ tolerance on maximum gradient component.

OPTIONS:

$n$ Integer value (tolerance = $n \times 10^{-6}$).

RECOMMENDATION:

Use the default. To converge GEOM_OPT_TOL_GRADIENT and one of GEOM_OPT_TOL_DISPLACEMENT and GEOM_OPT_TOL_ENERGY must be satisfied.

**GEOM_OPT_TOL_DISPLACEMENT**

Convergence on maximum atomic displacement.

TYPE:

INTEGER

DEFAULT:

$1200 \equiv 1200 \times 10^{-6}$ tolerance on maximum atomic displacement.

OPTIONS:

$n$ Integer value (tolerance = $n \times 10^{-6}$).

RECOMMENDATION:

Use the default. To converge GEOM_OPT_TOL_GRADIENT and one of GEOM_OPT_TOL_DISPLACEMENT and GEOM_OPT_TOL_ENERGY must be satisfied.

**GEOM_OPT_TOL_ENERGY**

Convergence on energy change of successive optimization cycles.

TYPE:

INTEGER

DEFAULT:

$100 \equiv 100 \times 10^{-8}$ tolerance on maximum (absolute) energy change.

OPTIONS:

$n$ Integer value (tolerance = value $n \times 10^{-8}$).

RECOMMENDATION:

Use the default. To converge GEOM_OPT_TOL_GRADIENT and one of GEOM_OPT_TOL_DISPLACEMENT and GEOM_OPT_TOL_ENERGY must be satisfied.

**GEOM_OPT_MAX_CYCLES**

Maximum number of optimization cycles.

TYPE:

INTEGER

DEFAULT:

50

OPTIONS:

$n$ User defined positive integer.

RECOMMENDATION:

The default should be sufficient for most cases. Increase if the initial guess geometry is poor, or for systems with shallow potential wells.

**GEOM_OPT_PRINT**

Controls the amount of OPTIMIZE print output.

TYPE:

INTEGER

DEFAULT:

3 Error messages, summary, warning, standard information and gradient print out.

OPTIONS:

0 Error messages only.
1 Level 0 plus summary and warning print out.
2 Level 1 plus standard information.
3 Level 2 plus gradient print out.
4 Level 3 plus Hessian print out.
5 Level 4 plus iterative print out.
6 Level 5 plus internal generation print out.
7 Debug print out.

RECOMMENDATION:

Use the default.

**GEOM_OPT_SYMFLAG**

Controls the use of symmetry in OPTIMIZE.

TYPE:

LOGICAL

DEFAULT:

TRUE

OPTIONS:

TRUE Make use of point group symmetry.
FALSE Do not make use of point group symmetry.

RECOMMENDATION:

Use the default.

**GEOM_OPT_MODE**

Determines Hessian mode followed during a transition state search.

TYPE:

INTEGER

DEFAULT:

0

OPTIONS:

0 Mode following off.
$n$ Maximize along mode $n$.

RECOMMENDATION:

Use the default, for geometry optimizations.

**GEOM_OPT_MAX_DIIS**

Controls maximum size of subspace for GDIIS.

TYPE:

INTEGER

DEFAULT:

0

OPTIONS:

0 Do not use GDIIS.

-1 Default size = min(NDEG, NATOMS, 4) NDEG = number of molecular degrees of freedom.

$n$ Size specified by user.

RECOMMENDATION:

Use the default or do not set $n$ too large.

**GEOM_OPT_DMAX**

Maximum allowed step size. Value supplied is multiplied by $10^{-3}$.

TYPE:

INTEGER

DEFAULT:

300 = 0.3

OPTIONS:

$n$ User-defined cutoff.

RECOMMENDATION:

Use the default.

**GEOM_OPT_UPDATE**

Controls the Hessian update algorithm.

TYPE:

INTEGER

DEFAULT:

-1

OPTIONS:

-1 Use the default update algorithm.

0 Do not update the Hessian (not recommended).

1 Murtagh-Sargent update.

2 Powell update.

3 Powell/Murtagh-Sargent update (TS default).

4 BFGS update (OPT default).

5 BFGS with safeguards to ensure retention of positive definiteness (GDISS default).

RECOMMENDATION:

Use the default.

**GEOM_OPT_LINEAR_ANGLE**

Threshold for near linear bond angles (degrees).

TYPE:

INTEGER

DEFAULT:

165 degrees.

OPTIONS:

$n$ User-defined level.

RECOMMENDATION:

Use the default.

**FDIFF_STEPSIZE**

Displacement used for calculating derivatives by finite difference.

TYPE:

INTEGER

DEFAULT:

100 Corresponding to 0.001 Å. For calculating second derivatives.

OPTIONS:

$n$ Use a step size of $n \times 10^{-5}$.

RECOMMENDATION:

Use the default except in cases where the potential surface is very flat, in which case a larger value should be used. See FDIFF_STEPSIZE_QFF for third and fourth derivatives.

**Example 9.1** As outlined, the rate of convergence of the iterative optimization process is dependent on a number of factors, one of which is the use of an initial analytic Hessian. This is easily achieved by instructing Q-CHEM to calculate an analytic Hessian and proceed then to determine the required critical point

```
$molecule
   0  1
   O
   H  1  oh
   H  1  oh 2 hoh

   oh  = 1.1
   hoh = 104
$end

$rem
   JOBTYPE    freq   Calculate an analytic Hessian
   METHOD     hf
   BASIS      6-31g(d)
$end

$comment
Now proceed with the Optimization making sure to read in the analytic
Hessian (use other available information too).
$end

@@@

$molecule
```

```
   read
$end

$rem
   JOBTYPE           opt
   METHOD            hf
   BASIS             6-31g(d)
   SCF_GUESS         read
   GEOM_OPT_HESSIAN  read   Have the initial Hessian
$end
```

### 9.1.3 Hessian-Free Characterization of Stationary Points

Q-CHEM allows the user to characterize the stationary point found by a geometry optimization or transition state search without performing a full analytical Hessian calculation, which is sometimes unavailable or computationally unaffordable. This is achieved via a finite difference Davidson procedure developed by Sharada *et al.*[2] For a geometry optimization, it solves for the lowest eigenvalue of the Hessian ($\lambda_1$) and checks if $\lambda_1 > 0$ (a negative $\lambda_1$ indicates a saddle point); for a TS search, it solves for the lowest two eigenvalues, and $\lambda_1 < 0$ and $\lambda_2 > 0$ indicate a transition state. The lowest eigenvectors of the updated P-RFO (approximate) Hessian at convergence are used as the initial guess for the Davidson solver.

The cost of this Hessian-free characterization method depends on the rate of convergence of the Davidson solver. For example, to characterize an energy minimum, it requires $2 \times N_{\text{iter}}$ total energy + gradient calculations, where $N_{\text{iter}}$ is the number of iterations that the Davidson algorithm needs to converge, and “2" is for forward and backward displacements on each iteration. According to Ref. 2, this method can be much more efficient than exact Hessian calculation for substantially large systems.

**Note:** At the moment, this method does not support QM/MM or systems with fixed atoms.

**GEOM_OPT_CHARAC**
Use the finite difference Davidson method to characterize the resulting energy minimum/transition state.
TYPE:
BOOLEAN
DEFAULT:
FALSE
OPTIONS:
FALSE do not characterize the resulting stationary point.
TRUE perform a characterization of the stationary point.
RECOMMENDATION:
Set it to TRUE when the character of a stationary point needs to be verified, especially for a transition structure.

**GEOM_OPT_CHARAC_CONV**

Overide the built-in convergence criterion for the Davidson solver.

TYPE:

INTEGER

DEFAULT:

0 (use the built-in default value $10^{-5}$)

OPTIONS:

$n$ Set the convergence criterion to $10^{-n}$.

RECOMMENDATION:

Use the default. If it fails to converge, consider loosening the criterion with caution.

**Example 9.2** Geometry optimization of a triflate anion that converges to an eclipsed conformation, which is a first order saddle point. This is verified via the finite difference Davidson method by setting GEOM_OPT_CHARAC to TRUE.

```
$molecule
   -1 1
   C  0.00000 -0.00078  0.98436
   F -1.09414 -0.63166  1.47859
   S  0.00000  0.00008 -0.94745
   O  1.25831 -0.72597 -1.28972
   O -1.25831 -0.72597 -1.28972
   O  0.00000  1.45286 -1.28958
   F  1.09414 -0.63166  1.47859
   F  0.00000  1.26313  1.47663
$end

$rem
   JOBTYPE                    opt
   METHOD                     BP86
   GEOM_OPT_DMAX              50
   BASIS                      6-311+G*
   SCF_CONVERGENCE            8
   THRESH                     14
   SYMMETRY                   FALSE
   SYM_IGNORE                 TRUE
   GEOM_OPT_TOL_DISPLACEMENT  10
   GEOM_OPT_TOL_ENERGY        10
   GEOM_OPT_TOL_GRADIENT      10
   GEOM_OPT_CHARAC            TRUE
$end
```

**Example 9.3** TS search for alanine dipeptide rearrangement reaction beginning with a guess structure converges correctly. The resulting TS structure is verified using the finite difference Davidson method.

```
$molecule
   0    1
   C          3.21659       -1.41022       -0.26053
   C          2.16708       -0.35258       -0.59607
   N          1.21359       -0.16703        0.41640
   C          0.11616        0.82394        0.50964
   C         -1.19613        0.03585        0.74226
   N         -2.18193       -0.02502       -0.18081
   C         -3.43891       -0.74663        0.01614
   O          2.19596        0.25708       -1.63440
   C          0.11486        1.96253       -0.53088
   O         -1.29658       -0.59392        1.85462
   H          3.25195       -2.14283       -1.08721
   H          3.06369       -1.95423        0.67666
   H          4.20892       -0.93714       -0.22851
   H          1.24786       -0.78278        1.21013
   H          0.25990        1.31404        1.47973
   H         -2.02230        0.38818       -1.10143
   H         -3.60706       -1.48647       -0.76756
   H         -4.29549       -0.06423        0.04327
   H         -3.36801       -1.25875        0.98106
   H         -0.68664        2.66864       -0.27269
   H          0.01029        1.65112       -1.56461
   H          1.06461        2.50818       -0.45885
$end

$rem
   JOBTYPE         freq
   EXCHANGE        B3LYP
   BASIS           6-31G
   SCF_MAX_CYCLES  250
   SYMMETRY        false
   SYM_IGNORE      true
$end

@@@

$rem
   JOBTYPE              ts
   SCF_GUESS            read
   GEOM_OPT_DMAX        100
   GEOM_OPT_MAX_CYCLES  1500
   EXCHANGE             B3LYP
   BASIS                6-31G
   MAX_SCF_CYCLES       250
   GEOM_OPT_HESSIAN     read
   SYMMETRY             false
   SYM_IGNORE           true
   GEOM_OPT_CHARAC      true
$end

$molecule
   read
$end
```

## 9.2 Improved Algorithms for Transition-Structure Optimization

Transition-structure searches tend to be more difficult (meaning, more likely to be unsuccessful) as compared to minimum-energy (equilibrium) geometry optimizations. Odds of success can be enhanced via an initial guess structure that is determined in an automated way, rather than simply “guessed” by the user. Several such automated algorithms are available in Q-CHEM, and are described in this section.

## 9.2.1 Freezing String Method

Perhaps the most significant difficulty in locating transition states is to obtain a good initial guess of the geometry to feed into a surface-walking algorithm. This difficulty becomes especially relevant for large systems, for which the dimensionality of the search space is large. Interpolation algorithms are promising for locating good guesses of the minimum-energy pathway connecting reactant and product states as well as approximate saddle-point geometries. For example, the nudged elastic band method[3,4] and the string method[5] start from a certain initial reaction pathway connecting the reactant and the product state, and then optimize in discretized path space towards the minimum-energy pathway. The highest-energy point on the approximate minimum-energy pathway becomes a good initial guess for the saddle-point configuration that can subsequently be used with any local surface-walking algorithm.

Inevitably, the performance of any interpolation method heavily relies on the choice of the initial reaction pathway, and a poorly-chosen initial pathway can cause slow convergence, or possibly convergence to an incorrect pathway. The growing-string method[6] and freezing-string method[7,8] offer solutions to this problem, in which two string fragments (one representing the reactant state and the other representing the product state) are "grown" (*i.e.*, increasingly-finely defined) until the two fragments join. The freezing-string method offers a choice between Cartesian interpolation and linear synchronous transit (LST) interpolation. It also allows the user to choose between conjugate gradient and quasi-Newton optimization techniques.

Freezing-string calculations are requested by setting JOBTYPE = FSM in the *$rem* section. Additional job-control keywords are described below, along with examples. Consult Refs. 7 and 8 for a guide to a typical use of this method.

**FSM_NNODE**
Specifies the number of nodes along the string
TYPE:
INTEGER
DEFAULT:
Undefined
OPTIONS:
$N$ number of nodes in FSM calculation
RECOMMENDATION:
$N = 15$. Use 10 to 20 nodes for a typical calculation. Reaction paths that connect multiple elementary steps should be separated into individual elementary steps, and one FSM job run for each pair of intermediates. Use a higher number when the FSM is followed by an approximate-Hessian based transition state search (Section 9.2.2).

**FSM_NGRAD**
Specifies the number of perpendicular gradient steps used to optimize each node
TYPE:
INTEGER
DEFAULT:
Undefined
OPTIONS:
$N$ Number of perpendicular gradients per node
RECOMMENDATION:
Anything between 2 and 6 should work, where increasing the number is only needed for difficult reaction paths.

**FSM_MODE**

Specifies the method of interpolation

TYPE:

INTEGER

DEFAULT:

2

OPTIONS:

1 Cartesian

2 LST

RECOMMENDATION:

In most cases, LST is superior to Cartesian interpolation.

**FSM_OPT_MODE**

Specifies the method of optimization

TYPE:

INTEGER

DEFAULT:

Undefined

OPTIONS:

1 Conjugate gradients

2 Quasi-Newton method with BFGS Hessian update

RECOMMENDATION:

The quasi-Newton method is more efficient when the number of nodes is high.

An example input appears below. Note that the *$molecule* section includes geometries for two optimized intermediates, separated by $****$. The order of the atoms is important, as Q-CHEM assumes that the $n$th atom in the reactant moves toward the $n$th atom in the product. The FSM string is printed out in the file *stringfile.txt*, which contains Cartesian coordinates of the structures that connect reactant to product. Each node along the path is labeled in this file, and its energy is provided. The geometries and energies are also printed at the end of the Q-CHEM output file, where they are labeled:

```
----------------------------------------
   STRING
----------------------------------------
```

Finally, if MOLDEN_FORMAT is set to TRUE, then geometries along the string are printed in a MOLDEN-readable format at the end of the Q-CHEM output file. The highest-energy node can be taken from this file and used to run a transition structure search as described in section 9.1. If the string returns a pathway that is unreasonable, check whether the atoms in the two input geometries are in the correct order.

**Example 9.4** Example of the freezing-string method.

```
$molecule
   0  1
   Si   1.028032  -0.131573  -0.779689
   H    0.923921  -1.301934   0.201724
   H    1.294874   0.900609   0.318888
   H   -1.713989   0.300876  -0.226231
   H   -1.532839   0.232021   0.485307
```

```
****
   Si   0.000228  -0.000484  -0.000023
   H    0.644754  -1.336958  -0.064865
   H    1.047648   1.052717   0.062991
   H   -0.837028   0.205648  -1.211126
   H   -0.855603   0.079077   1.213023
$end

$rem
   JOBTYPE        fsm
   FSM_NGRAD      3
   FSM_NNODE      12
   FSM_MODE       2
   FSM_OPT_MODE   2
   METHOD         b3lyp
   BASIS          6-31G
$end
```

### 9.2.2 Hessian-Free Transition-State Search

Once a guess structure to the transition state is obtained, standard eigenvector-following methods such as Baker's partitioned rational-function optimization (P-RFO) algorithm[9] can be employed to refine the guess to the exact transition state. The reliability of P-RFO depends on the quality of the Hessian input, which enables the method to distinguish between the reaction coordinate (characterized by a negative eigenvalue) and the remaining degrees of freedom. In routine calculations therefore, an exact Hessian is determined via frequency calculation prior to the P-RFO search. Since the cost of evaluating an exact Hessian typically scales one power of system size higher than the energy or the gradient, this step becomes impractical for systems containing large number of atoms.

The exact Hessian calculation can be avoided by constructing an approximate Hessian based on the output of FSM.[2] The tangent direction at the transition state guess on the FSM string is a good approximation to the Hessian eigenvector corresponding to the reaction coordinate. The tangent is therefore used to calculate the correct eigenvalue and corresponding eigenvector by variationally minimizing the Rayleigh-Ritz ratio[10]. The reaction coordinate information is then incorporated into a guess matrix which, in turn, is obtained by transforming a diagonal matrix in delocalized internal coordinates[11,12] to Cartesian coordinates. The resulting approximate Hessian, by design, has a single negative eigenvalue corresponding to the reaction coordinate. This matrix is then used in place of the exact Hessian as input to the P-RFO method.

An example of this one-shot, Hessian-free approach that combines the FSM and P-RFO methods in order to determine the exact transition state from reactant and product structures is shown below:

**Example 9.5**

```
$molecule
   0  1
   Si   1.028032  -0.131573  -0.779689
   H    0.923921  -1.301934   0.201724
   H    1.294874   0.900609   0.318888
   H   -1.713989   0.300876  -0.226231
   H   -1.532839   0.232021   0.485307
****
   Si   0.000228  -0.000484  -0.000023
   H    0.644754  -1.336958  -0.064865
   H    1.047648   1.052717   0.062991
   H   -0.837028   0.205648  -1.211126
   H   -0.855603   0.079077   1.213023
$end

$rem
   JOBTYPE       fsm
   FSM_NGRAD     3
   FSM_NNODE     18
   FSM_MODE      2
   FSM_OPT_MODE  2
   METHOD        b3lyp
   BASIS         6-31g
   SYMMETRY      false
   SYM_IGNORE    true
$end

@@@

$rem
   JOBTYPE              ts
   SCF_GUESS            read
   GEOM_OPT_HESSIAN     read
   MAX_SCF_CYCLES       250
   GEOM_OPT_DMAX        50
   GEOM_OPT_MAX_CYCLES  100
   METHOD               b3lyp
   BASIS                6-31g
   SYMMETRY             false
   SYM_IGNORE           true
$end

$molecule
   read
$end
```

### 9.2.3 Improved Dimer Method

Once a good approximation to the minimum energy pathway is obtained, *e.g.*, with the help of an interpolation algorithm such as the growing string method, local surface walking algorithms can be used to determine the exact location of the saddle point. Baker's P-RFO method[9], using either an approximate or an exact Hessian, has proven to be a very powerful for this purpose, but does require calculation of a full Hessian matrix.

The dimer method[13], on the other hand, is a mode-following algorithm that requires only the curvature along one direction in configuration space, rather than the full Hessian, which can be accomplished using only gradient evaluations. This method is thus especially attractive for large systems where a full Hessian calculation might be prohibitively expensive, or for saddle-point searches where the initial guess is such that the eigenvector of corresponding to the smallest Hessian eigenvalue does not correspond to the desired reaction coordinate. An improved version of the original dimer method[14,15] has been implemented in Q-CHEM, which significantly reduces the influence of numerical noise and thus significantly reduces the cost of the algorithm.

## 9.3 Constrained Optimization

Constrained optimization refers to the optimization of molecular structures (transition state or minimum-energy) in which certain parameters such as bond lengths, bond angles or dihedral angles are fixed. Jon Baker's OPTIMIZE package, implemented in Q-CHEM, makes it possible to handle constraints directly in delocalized internal coordinates using the method of Lagrange multipliers (see Appendix A). Features of constrained optimization in Q-CHEM are:

- Starting geometries need not satisfy the requested constraints.
- Constrained optimization is performed in delocalized internal coordinates, which is typically the most efficient coordinate system for optimization of large molecules.
- Q-CHEM's free-format *$opt* section allows the user to apply constraints with ease.

Constraints are imposed via the *$opt* input section, whose format is shown below, and the various parts of this input section are described below.

**Note:** As with the rest of the Q-CHEM input file, the *$opt* section is case-insensitive, but there should be no blank space at the beginning of a line.

```
$opt
CONSTRAINT
stre  atom1  atom2  value
...
bend  atom1  atom2  atom3  value
...
outp  atom1  atom2  atom3  atom4  value
...
tors  atom1  atom2  atom3  atom4  value
...
linc  atom1  atom2  atom3  atom4  value
...
linp  atom1  atom2  atom3  atom4  value
...
ENDCONSTRAINT

FIXED
atom   coordinate_reference
...
ENDFIXED

DUMMY
idum   type   list_length   defining_list
...
ENDDUMMY
```

```
CONNECT
atom   list_length   list
...
ENDCONNECT
$end
```

### 9.3.1 Geometry Optimization with General Constraints

CONSTRAINT and ENDCONSTRAINT define the beginning and end, respectively, of the constraint section of *$opt* within which users may specify up to six different types of constraints:

***interatomic distances***
Values in Ångstroms; *value* > 0:
`stre   atom1   atom2   value`

***angles***
Values in degrees, $0 \leq value \leq 180$; *atom2* is the middle atom of the bend:
`bend   atom1   atom2   atom3   value`

***out-of-plane-bends***
Values in degrees, $-180 \leq value \leq 180$ *atom2*; angle between *atom4* and the *atom1–atom2–atom3* plane:
`outp   atom1   atom2   atom3   atom4   value`

***dihedral angles***
Values in degrees, $-180 \leq value \leq 180$; angle the plane *atom1–atom2–atom3* makes with the plane *atom2–atom3–atom4*:
`tors   atom1   atom2   atom3   atom4   value`

***coplanar bends***
Values in degrees, $-180 \leq value \leq 180$; bending of *atom1–atom2–atom3* in the plane *atom2–atom3–atom4*:
`linc   atom1   atom2   atom3   atom4   value`

***perpendicular bends***
Values in degrees, $-180 \leq value \leq 180$; bending of *atom1–atom2–atom3* perpendicular to the plane *atom2–atom3–atom4*:
`linp   atom1   atom2   atom3   atom4   value`

### 9.3.2 Frozen Atoms

Absolute atom positions can be frozen with the *FIXED* section. The section starts with the *FIXED* keyword as the first line and ends with the *ENDFIXED* keyword on the last. The format to fix a coordinate or coordinates of an atom is:

```
atom   coordinate_reference
```

*coordinate_reference* can be any combination of up to three characters $X$, $Y$ and $Z$ to specify the coordinate(s) to be fixed: $X$, $Y$, $Z$, *XY*, *XZ*, *YZ*, *XYZ*. The fixing characters must be next to each other. *e.g.*,

```
    FIXED
    2 XY
    ENDFIXED
```

means the $x$-coordinate and $y$-coordinate of atom 2 are fixed, whereas

```
    FIXED
    2 X Y
    ENDFIXED
```

will yield erroneous results.

**Note:** When the *FIXED* section is specified within *$opt*, the optimization will proceed in Cartesian coordinates.

### 9.3.3 Dummy Atoms

DUMMY defines the beginning of the dummy atom section and ENDDUMMY its conclusion. Dummy atoms are used to help define constraints during constrained optimizations in Cartesian coordinates. They cannot be used with delocalized internals.

All dummy atoms are defined with reference to a list of real atoms, that is, dummy atom coordinates are generated from the coordinates of the real atoms from the dummy atoms defining list (see below). There are three types of dummy atom:

1. Positioned at the arithmetic mean of up to seven real atoms in the defining list.
2. Positioned a unit distance along the normal to a plane defined by three atoms, centered on the middle atom of the three.
3. Positioned a unit distance along the bisector of a given angle.

The format for declaring dummy atoms is:

```
DUMMY
idum    type   list_length    defining_list
ENDDUMMY
```

| | |
|---|---|
| *idum* | Center number of defining atom (must be one greater than the total number of real atoms for the first dummy atom, two greater for second *etc.*). |
| *type* | Type of dummy atom (either 1, 2 or 3; see above). |
| *list_length* | Number of atoms in the defining list. |
| *defining_list* | List of up to seven atoms defining the position of the dummy atom. |

Once defined, dummy atoms can be used to define standard internal (distance, angle) constraints as per the constraints section, above.

**Note:** The use of dummy atoms of type 1 has never progressed beyond the experimental stage.

| Internal Coordinates | Cartesian Coordinates |
|---|---|
| $opt | $opt |
| CONSTRAINT | DUMMY |
| tors I J K L 180.0 | M 2 I J K |
| ENDCONSTRAINT | ENDDUMMY |
| $end | CONSTRAINT |
| | tors I J K M 90 |
| | tors M J K L 90 |
| | ENDCONSTRAINT |
| | $end |

Table 9.2: Comparison of dihedral angle constraint method for adopted coordinates.

### 9.3.4 Dummy Atom Placement in Dihedral Constraints

Bond and dihedral angles cannot be constrained in Cartesian optimizations to exactly 0° or ±180°. This is because the corresponding constraint normals are zero vectors. Also, dihedral constraints near these two limiting values (within, say 20°) tend to oscillate and are difficult to converge.

These difficulties can be overcome by defining dummy atoms and redefining the constraints with respect to the dummy atoms. For example, a dihedral constraint of 180° can be redefined to two constraints of 90° with respect to a suitably positioned dummy atom. The same thing can be done with a 180° bond angle (long a familiar use in *Z*-matrix construction).

Typical usage is as shown in Table 9.2. Note that the order of atoms is important to obtain the correct signature on the dihedral angles. For a 0° dihedral constraint, atoms J and K should be switched in the definition of the second torsion constraint in Cartesian coordinates.

**Note:** In almost all cases the above discussion is somewhat academic, as internal coordinates are now best imposed using delocalized internal coordinates and there is no restriction on the constraint values.

### 9.3.5 Additional Atom Connectivity

Normally delocalized internal coordinates are generated automatically from the input Cartesian coordinates. This is accomplished by first determining the atomic connectivity list (*i.e.*, which atoms are formally bonded) and then constructing a set of individual primitive internal coordinates comprising all bond stretches, all planar bends and all proper torsions that can be generated based on the atomic connectivity. The delocalized internal are in turn constructed from this set of primitives.

The atomic connectivity depends simply on distance and there are default bond lengths between all pairs of atoms in the code. In order for delocalized internals to be generated successfully, all atoms in the molecule must be formally bonded so as to form a closed system. In molecular complexes with long, weak bonds or in certain transition states where parts of the molecule are rearranging or dissociating, distances between atoms may be too great for the atoms to be regarded as formally bonded, and the standard atomic connectivity will separate the system into two or more distinct parts. In this event, the generation of delocalized internal coordinates will fail. Additional atomic connectivity can be included for the system to overcome this difficulty.

CONNECT defines the beginning of the additional connectivity section and ENDCONNECT the end. The format of the CONNECT section is:

```
CONNECT
atom   list_length   list
ENDCONNECT
```

*atom* Atom for which additional connectivity is being defined.
*list_length* Number of atoms in the list of bonded atoms.
*list* List of up to 8 atoms considered as being bonded to the given atom.

**Example 9.6** Methanol geometry optimization with constraints.

```
$comment
   Methanol geom opt with constraints in bond length and bond angles.
$end

$molecule
   0  1
   C   0.14192   0.33268   0.00000
   O   0.14192  -1.08832   0.00000
   H   1.18699   0.65619   0.00000
   H  -0.34843   0.74268   0.88786
   H  -0.34843   0.74268  -0.88786
   H  -0.77395  -1.38590   0.00000
$end

$rem
   GEOM_OPT_PRINT    6
   JOBTYPE           opt
   METHOD            hf
   BASIS             3-21g
$end

$opt
CONSTRAINT
stre  1  6  1.8
bend  2  1  4  110.0
bend  2  1  5  110.0
ENDCONSTRAINT
$end
```

### 9.3.6 Application of External Forces

In 2009, three methods for optimizing the geometry of a molecule under a constant external force were introduced, which were called Force-Modified Potential Energy Surface (FMPES),[16] External Force is Explicitly Included (EFEI),[17,18] and Enforced Geometry Optimization (EGO).[19] These methods are closely related, and the interested reader is referred to ref. 20 for a detailed discussion of the similarities and differences between them. For simplicity, we will stick to the term *EFEI* in this Section. An EFEI calculation is a geometry optimization in which a constant that is equal to the external force is added to the nuclear gradient of two atoms specified by the user. The external force is applied along the vector connecting the two atoms, thus driving them apart. The geometry optimization converges when the restoring force of the molecule is equal to the external force. The EFEI method can also be used in AIMD simulations (see

Section 9.7), in which case the force is added in every time step. The basic syntax for specifying EFEI calculations is as follows.

```
$efei
atom1  atom2  force1
atom3  atom4  force2
...
$end
```

Here, *atom1* and *atom2* are the indices of the atoms to which a force is applied. *force1* is the sum of the force values that acts on *atom1* and *atom2* in nanoNewtons (nN). If this value is positive, a mechanical force of magnitude *force1*/2 acts on each of these atoms, thus driving them apart. If it is negative, an attractive force acts between the atoms. Optionally, additional pairs of atoms that are subject to a force can be specified by adding lines in the *$efei* section.

**Example 9.7** EFEI calculation of hydrogen peroxide with a constant stretching force of 2.5 nN acting on each oxygen atom

```
$molecule
   0 1
   O        -0.7059250062   -0.1776745132   -0.0698000882
   O         0.7059250062    0.1776745132   -0.0698000882
   H         1.0662092915   -0.5838921799    0.4181150580
   H        -1.0662092915    0.5838921799    0.4181150580
$end

$rem
   JOBTYPE          opt
   EXCHANGE         b3lyp
   BASIS            6-31G*
$end

$efei
   1 2 5
$end
```

## 9.4 Potential Energy Scans

It is often useful to scan the potential energy surface (PES), optimizing all other degrees of freedom for each particular value of the scanned variable(s). Such a scan may provide a rough estimate of a pathway between reactant and product—assuming the coordinate(s) for the scan has been chosen wisely—and is often used in development of classical force fields to optimize dihedral angle parameters. Ramachandran plots, for example, are key tools for studying conformational changes of peptides and proteins, and are essentially 2-dimensional torsional scans.

Q-CHEM supports one- and two-dimensional PES scans, by setting JOBTYPE equal to PES_SCAN in the *$rem* section. In addition, a *$scan* input section with the following format should be specified, in the format below but with no more than two bond-length, bond-angle, or torsional variables specified.

```
$scan
```

```
stre  atom1  atom2  value1 value2 incr
...
bend  atom1  atom2  atom3  value1 value2 incr
...
tors  atom1  atom2  atom3  atom4  value1 value2 incr
...
$end
```

The first example below demonstrates how to scan the torsional potential of butane, which is a sequence of constrained optimizations with the C1–C2–C3–C4 dihedral angle fixed at −180°, −165°, −150°, . . ., 165°, 180°.

**Example 9.8** One-dimensional torsional scan of butane

```
$molecule
   0 1
   C       1.934574    -0.128781    -0.000151
   C       0.556601     0.526657     0.000200
   C      -0.556627    -0.526735     0.000173
   C      -1.934557     0.128837    -0.000138
   H       2.720125     0.655980    -0.000236
   H       2.061880    -0.759501    -0.905731
   H       2.062283    -0.759765     0.905211
   H       0.464285     1.168064    -0.903444
   H       0.464481     1.167909     0.903924
   H      -0.464539    -1.167976     0.903964
   H      -0.464346    -1.168166    -0.903402
   H      -2.062154     0.759848     0.905185
   H      -2.720189    -0.655832    -0.000229
   H      -2.061778     0.759577    -0.905748
$end

$rem
   JOBTYPE  pes_scan
   METHOD   hf
   BASIS    sto-3g
$end

$scan
   tors 1 2 3 4 -180 180 15
$end
```

The next example is a two-dimension potential scan. The first dimension is a scan of the C1–C2–C3–C4 dihedral angle from −180° to 180° degree in 30° intervals; the second dimension is a scan of the C2–C3 bond length from 1.5 Å to 1.6 Å in 0.05 Å increments.

**Example 9.9** Two-dimensional torsional scan of butane

```
$molecule
   0 1
   C       1.934574    -0.128781    -0.000151
   C       0.556601     0.526657     0.000200
   C      -0.556627    -0.526735     0.000173
   C      -1.934557     0.128837    -0.000138
   H       2.720125     0.655980    -0.000236
   H       2.061880    -0.759501    -0.905731
   H       2.062283    -0.759765     0.905211
   H       0.464285     1.168064    -0.903444
   H       0.464481     1.167909     0.903924
   H      -0.464539    -1.167976     0.903964
   H      -0.464346    -1.168166    -0.903402
   H      -2.062154     0.759848     0.905185
   H      -2.720189    -0.655832    -0.000229
   H      -2.061778     0.759577    -0.905748
$end

$rem
   JOBTYPE  pes_scan
   METHOD   hf
   BASIS   sto-3g
$end

$scan
   tors 1 2 3 4 -180 180 30
   stre 2 3 1.5 1.6 0.05
$end
```

## 9.5 Intrinsic Reaction Coordinate

The concept of a reaction path is chemically intuitive (a pathway from reactants to products) yet somewhat theoretically ambiguous because most mathematical definitions depend upon the chosen coordinate system. Stationary points on a potential energy surface are independent of this choice, but the path connecting them is not, and there exist various mathematical definitions of a "reaction path". Q-CHEM uses the intrinsic reaction coordinate (IRC) definition, as originally defined by Fukui[21], which has come to be a fairly standard choice in quantum chemistry. The IRC is essentially sequence of small, steepest-descent paths going downhill from the transition state.

The reaction path is most unlikely to be a straight line and so by taking a finite step length along the direction of the gradient you will leave the "true" reaction path. A series of small steepest descent steps will zig-zag along the actual reaction path (a behavior known as "stitching"). Ishida *et al.*[22] developed a predictor-corrector algorithm, involving a second gradient calculation after the initial steepest-descent step, followed by a line search along the gradient bisector to get back on the path, and this algorithm was subsequently improved by Schmidt *et al.*[23]. This is the method that Q-CHEM adopts. It cannot be used for the first downhill step from the transition state, since the gradient is zero, so instead a step is taken along the Hessian mode whose frequency is imaginary.

The reaction path can be defined and followed in $Z$-matrix coordinates, Cartesian coordinates or mass-weighted Cartesian coordinates. The latter represents the "true" IRC as defined by Fukui[21]. If the rationale for following the reaction path is simply to determine which local minima are connected by a given transition state, which, is arguably the major use of IRC algorithms, then the choice of coordinates is irrelevant. In order to use the IRC code, the transition state geometry and the exact Hessian must be available. These must be computed via two prior calculations, with JOBTYPE = TS (transition structure search) and JOBTYPE = FREQ (Hessian calculation), respectively. Job control variables and examples appear below.

An IRC calculation is invoked by setting JOBTYPE = RPATH in the *$rem* section, and additional *$rem* variables are described below. IRC calculations may benefit from the methods discussed in Section 9.2 for obtaining good initial guesses for transition-state structures.

**RPATH_COORDS**

Determines which coordinate system to use in the IRC search.

TYPE:

INTEGER

DEFAULT:

0

OPTIONS:

| | |
|---|---|
| 0 | Use mass-weighted coordinates. |
| 1 | Use Cartesian coordinates. |
| 2 | Use *Z*-matrix coordinates. |

RECOMMENDATION:

Use the default.

**RPATH_DIRECTION**

Determines the direction of the eigenmode to follow. This will not usually be known prior to the Hessian diagonalization.

TYPE:

INTEGER

DEFAULT:

1

OPTIONS:

| | |
|---|---|
| 1 | Descend in the positive direction of the eigen mode. |
| -1 | Descend in the negative direction of the eigen mode. |

RECOMMENDATION:

It is usually not possible to determine in which direction to go *a priori*, and therefore both directions will need to be considered.

**RPATH_MAX_CYCLES**

Specifies the maximum number of points to find on the reaction path.

TYPE:

INTEGER

DEFAULT:

20

OPTIONS:

| | |
|---|---|
| $n$ | User-defined number of cycles. |

RECOMMENDATION:

Use more points if the minimum is desired, but not reached using the default.

**RPATH_MAX_STEPSIZE**

Specifies the maximum step size to be taken (in 0.001 a.u.).

TYPE:

INTEGER

DEFAULT:

150 corresponding to a step size of 0.15 a.u..

OPTIONS:

$n$ Step size = $n$/1000 a.u.

RECOMMENDATION:

None.

**RPATH_TOL_DISPLACEMENT**

Specifies the convergence threshold for the step. If a step size is chosen by the algorithm that is smaller than this, the path is deemed to have reached the minimum.

TYPE:

INTEGER

DEFAULT:

5000 Corresponding to 0.005 a.u.

OPTIONS:

$n$ User-defined. Tolerance = $n$/1000000 a.u.

RECOMMENDATION:

Use the default. Note that this option *only* controls the threshold for ending the RPATH job and does nothing to the intermediate steps of the calculation. A smaller value will provide reaction paths that end closer to the true minimum. Use of smaller values without adjusting RPATH_MAX_STEPSIZE, however, can lead to oscillations about the minimum.

**RPATH_PRINT**

Specifies the print output level.

TYPE:

INTEGER

DEFAULT:

2

OPTIONS:

$n$

RECOMMENDATION:

Use the default, as little additional information is printed at higher levels. Most of the output arises from the multiple single point calculations that are performed along the reaction pathway.

**Example 9.10**

```
$molecule
   0  1
   C
   H  1  1.20191
   N  1  1.22178  2  72.76337
$end

$rem
   JOBTYPE    freq
   BASIS      sto-3g
   METHOD     hf
$end

@@@

$molecule
   read
$end

$rem
   JOBTYPE            rpath
   BASIS              sto-3g
   METHOD             hf
   SCF_GUESS          read
   RPATH_MAX_CYCLES   30
$end
```

## 9.6 Nonadiabatic Couplings and Optimization of Minimum-Energy Crossing Points

### 9.6.1 Nonadiabatic Couplings

Conical intersections are degeneracies between Born-Oppenheimer potential energy surfaces that facilitate non-adiabatic transitions between excited states, *i.e.*, internal conversion and intersystem crossing processes, both of which represent a breakdown of the Born-Oppenheimer approximation[24,25]. Although simultaneous intersections between more than two electronic states are possible[24], consider for convenience the two-state case, and let

$$\mathbf{H} = \begin{pmatrix} H_{JJ}(\mathbf{R}) & H_{JK}(\mathbf{R}) \\ H_{KJ}^{*}(\mathbf{R}) & H_{KK}(\mathbf{R}) \end{pmatrix} . \tag{9.1}$$

denote the matrix representation of the vibronic (vibrational + electronic) Hamiltonian [Eq. (4.2)] in a basis of two electronic states, $J$ and $K$. (Electronic degrees of freedom have been integrated out of this expression, and $\mathbf{R}$ represents the remaining, nuclear coordinates.) By definition, the Born-Oppenheimer states are the ones that diagonalize $\mathbf{H}$ at a particular molecular geometry $\mathbf{R}$, and thus two conditions must be satisfied in order to obtain degeneracy in the Born-Oppenheimer representation: $H_{JJ} = H_{KK}$ and $H_{JK} = 0$. As such, degeneracies between two Born-Oppenheimer potential energy surfaces exist in subspaces of dimension $N_{\text{int}} - 2$, where $N_{\text{int}} = 3N_{\text{atoms}} - 6$ is the number of internal (vibrational) degrees of freedom (assuming the molecule is non-linear). This ($N_{\text{int}} - 2$)-dimensional subspace is known as the *seam space* because the two states are degenerate everywhere within this space. In the remaining two degrees of freedom, known as the *branching space*, the degeneracy between Born-Oppenheimer surfaces is lifted by an infinitesimal displacement, which in a three-dimensional plot resembles a double cone about the point of intersection, hence the name *conical intersection*.

The branching space is defined by the span of a pair of vectors $\mathbf{g}_{JK}$ and $\mathbf{h}_{JK}$. The former is simply the difference in the gradient vectors of the two states in question,

$$\mathbf{g}_{JK} = \frac{\partial E_J}{\partial \mathbf{R}} - \frac{\partial E_K}{\partial \mathbf{R}} , \tag{9.2}$$

and is readily evaluated at any level of theory for which analytic energy gradients are available (or less-readily, via finite difference, if they are not!). The definition of the *non-adiabatic coupling vector* $\mathbf{h}_{JK}$, on the other hand, is more involved and not directly amenable to finite-difference calculations:

$$\mathbf{h}_{JK} = \left\langle \Psi_J \left| \left( \partial \hat{H} / \partial \mathbf{R} \right) \right| \Psi_K \right\rangle \ . \tag{9.3}$$

This is closely related to the *derivative coupling* vector

$$\mathbf{d}_{JK} = \langle \Psi_J | (\partial / \partial \mathbf{R}) | \Psi_K \rangle = \frac{\mathbf{h}_{JK}}{E_J - E_K} \ . \tag{9.4}$$

The latter expression for $\mathbf{d}_{JK}$ demonstrates that the coupling between states becomes large in regions of the potential surface where the two states are nearly degenerate. The relative orientation and magnitudes of the vectors $\mathbf{g}_{JK}$ and $\mathbf{h}_{JK}$ determined the topography around the intersection, *i.e.*, whether the intersection is "peaked" or "sloped"; see Ref. 25 for a pedagogical overview.

Algorithms to compute the non-adiabatic couplings $\mathbf{d}_{JK}$ are not widely available in quantum chemistry codes, but thanks to the efforts of the Herbert and Subotnik groups, they are available in Q-CHEM when the wave functions $\Psi_J$ and $\Psi_K$, and corresponding electronic energies $E_J$ and $E_K$, are computed at the CIS or TDDFT level[26–29], or at the corresponding spin-flip (SF) levels of theory (SF-CIS or SF-TDDFT). The spin-flip implementation[27] is particularly significant, because only that approach—and not traditional spin-conserving CIS or TDDFT—affords correct topology around conical intersections that involve the ground state. To understand why, suppose that $J$ in Eq. (9.1) represents the ground state; call it $J = 0$ for definiteness. In linear response theory (TDDFT) or in CIS (by virtue of Brillouin's theorem), the coupling matrix elements between the reference (ground) state and all of the excited states vanish identically, hence $H_{0K}(\mathbf{R}) \equiv 0$. This means that there is only one condition to satisfy in order to obtain degeneracy, hence the branching space is one- rather than two-dimensional, for any conical intersection that involves the ground state[30]. (For intersections between two excited states, the topology should be correct.) In the spin-flip approach, however, the reference state has a different spin multiplicity than the target states; if the latter have spin quantum number $S$, then the reference state has spin $S + 1$. This has the effect that the ground state of interest (spin $S$) is treated as an excitation, and thus on a more equal footing with excited states of the same spin, and it rigorously fixes the topology problem around conical intersections[27].

Nonadiabatic (derivative) couplings are available for both CIS and TDDFT. The CIS non-adiabatic couplings can be obtained from direct differentiation of the wave functions with respect to nuclear positions[26,27]. For TDDFT, the same procedure can be carried out to calculate the approximate non-adiabatic couplings, in what has been termed the "pseudo-wave function" approach[27,31]. Formally more rigorous TDDFT non-adiabatic couplings derived from quadratic response theory are also available, although they are subject to certain undesirable, accidental singularities if for the two states $J$ and $K$ in Eq. (9.3), the energy difference $|E_J - E_K|$ is quasi-degenerate with the excitation energy $\omega_I = E_I - E_0$ for some third state, $I$[28,29]. As such, the pseudo-wave function method is the recommended approach for computing non-adiabatic couplings with TDDFT, although in the spin flip case the pseudo-wave function approach is rigorously equivalent to the pseudo-wave function approach, and is free of singularities[28].

Finally, we note that there is some evidence that SF-TDDFT calculations are most accurate when used with functionals containing ∼50% Hartree-Fock exchange[32,33], and many studies with this method (see Ref. 25 for a survey) have used the BH&HLYP functional, in which LYP correlation is combined with Becke's "half and half" (BH&H) exchange functional, consisting of 50% Hartree-Fock exchange and 50% Becke88 exchange (EXCHANGE = BHHLYP in Q-CHEM.)

### 9.6.2 Job Control and Examples

In order to perform non-adiabatic coupling calculations, the *$derivative_coupling* section must be given:

```
$derivative_coupling
one line comment
i, j, k, ...
$end
```

Nonadiabatic couplings will then be computed between all pairs of the states $i, j, k, \ldots$; use "0" to request the HF or DFT reference state, "1" for the first excited state, *etc.*

**CALC_NAC**

Determines whether we are calculating non-adiabatic couplings.

TYPE:

LOGICAL

DEFAULT:

FALSE

OPTIONS:

| | |
|---|---|
| TRUE | Calculate non-adiabatic couplings. |
| FALSE | Do not calculate non-adiabatic couplings. |

RECOMMENDATION:

None.

**CIS_DER_NUMSTATE**

Determines among how many states we calculate non-adiabatic couplings. These states must be specified in the *$derivative_coupling* section.

TYPE:

INTEGER

DEFAULT:

0

OPTIONS:

| | |
|---|---|
| 0 | Do not calculate non-adiabatic couplings. |
| $n$ | Calculate $n(n-1)/2$ pairs of non-adiabatic couplings. |

RECOMMENDATION:

None.

**SET_QUADRATIC**

Determines whether to include full quadratic response contributions for TDDFT.

TYPE:

LOGICAL

DEFAULT:

FALSE

OPTIONS:

| | |
|---|---|
| TRUE | Include full quadratic response contributions for TDDFT. |
| FALSE | Use pseudo-wave function approach. |

RECOMMENDATION:

The pseudo-wave function approach is usually accurate enough and is free of accidental singularities. Consult Refs. 28 and 29 for additional guidance.

**Example 9.11** Nonadiabatic couplings among the lowest five singlet states of ethylene, computed at the TD-B3LYP level using the pseudo-wave function approach.

```
$molecule
   0 1
   C    1.85082356   -1.78953123    0.00000000
   H    2.38603593   -2.71605577    0.00000000
   H    0.78082359   -1.78977646    0.00000000
   C    2.52815456   -0.61573833    0.00000000
   H    1.99294220    0.31078621    0.00000000
   H    3.59815453   -0.61549310    0.00000000
$end

$rem
   CIS_N_ROOTS         4
   CIS_TRIPLETS        false
   SET_ITER            50
   CIS_DER_NUMSTATE    5
   CALC_NAC            true
   EXCHANGE            b3lyp
   BASIS               6-31G*
$end

$derivative_coupling
   0 is the reference state
   0 1 2 3 4
$end
```

**Example 9.12** Nonadiabatic couplings between $S_0$ and $S_1$ states of ethylene using BH&HLYP and spin-flip TDDFT.

```
$molecule
   0 3
   C    1.85082356   -1.78953123    0.00000000
   H    2.38603593   -2.71605577    0.00000000
   H    0.78082359   -1.78977646    0.00000000
   C    2.52815456   -0.61573833    0.00000000
   H    1.99294220    0.31078621    0.00000000
   H    3.59815453   -0.61549310    0.00000000
$end

$rem
   SPIN_FLIP           true
   UNRESTRICTED        true
   CIS_N_ROOTS         4
   CIS_TRIPLETS        false
   SET_ITER            50
   CIS_DER_NUMSTATE    2
   CALC_NAC            true
   EXCHANGE            bhhlyp
   BASIS               6-31G*
$end

$derivative_coupling
   comment
   1 3
$end
```

**Example 9.13** Nonadiabatic couplings between $S_1$ and $S_2$ states of ethylene computed via quadratic response theory at the TD-B3LYP level.

```
$molecule
   0 1
   C    1.85082356   -1.78953123    0.00000000
   H    2.38603593   -2.71605577    0.00000000
   H    0.78082359   -1.78977646    0.00000000
   C    2.52815456   -0.61573833    0.00000000
   H    1.99294220    0.31078621    0.00000000
   H    3.59815453   -0.61549310    0.00000000
$end

$rem
   CIS_N_ROOTS        4
   CIS_TRIPLETS       false
   RPA                true
   SET_ITER           50
   CIS_DER_NUMSTATE   2
   CALC_NAC           true
   EXCHANGE           b3lyp
   BASIS              6-31G*
   SET_QUADRATIC      true #include full quadratic response
$end

$derivative_coupling
   comment
   1 2
$end
```

### 9.6.3 Minimum-Energy Crossing Points

The seam space of a conical intersection is really a (hyper)surface of dimension $N_{\text{int}} - 2$, and while the two electronic states in question are degenerate at every point within this space, the electronic energy varies from one point to the next. To provide a simple picture of photochemical reaction pathways, it is often convenient to locate the minimum-energy crossing point (MECP) within this $(N_{\text{int}} - 2)$-dimensional seam. Two separate minimum-energy pathway searches, one on the excited state starting from the ground-state geometry and terminating at the MECP, and the other on the ground state starting from the MECP and terminating at the ground-state geometry, then affords a photochemical mechanism. (See Ref. 34 for a simple example.) In some sense, then, the MECP is to photochemistry what the transition state is to reactions that occur on a single Born-Oppenheimer potential energy surface. One should be wary of pushing this analogy too far, because whereas a transition state reasonably be considered to be a bottleneck point on the reaction pathway, the path through a conical intersection may be downhill and perhaps therefore more likely to proceed from one surface to the other at a point “near" the intersection, and in addition there can be multiple conical intersections between the same pair of states so more than one photochemical mechanism may be at play. Such complexity could be explored, albeit at significantly increased cost, using non-adiabatic “surface hopping" *ab initio* molecular dynamics, as described in Section 9.7.6. Here we describe the computationally-simpler procedure of locating an MECP along a conical seam.

Recall that the branching space around a conical intersection between electronic states $J$ and $K$ is spanned by two vectors, $\mathbf{g}_{JK}$ [Eq. (9.2)] and $\mathbf{h}_{JK}$ [Eq. (9.3)]. While the former is readily available in analytic form for any electronic structure method that has analytic excited-state gradients, the non-adiabatic coupling vector $\mathbf{h}_{JK}$ is *not* available for most methods. For this reason, several algorithms have been developed to optimize MECPs without the need to evaluate $\mathbf{h}_{JK}$, and three such algorithms are available in Q-CHEM.

Martínez and co-workers[35] developed a penalty-constrained MECP optimization algorithm that consists of minimizing the objective function

$$F_\sigma(\mathbf{R}) = \tfrac{1}{2}\big[E_I(\mathbf{R}) + E_J(\mathbf{R})\big] + \sigma\left(\frac{\big[E_I(\mathbf{R}) - E_J(\mathbf{R})\big]^2}{E_I(\mathbf{R}) - E_J(\mathbf{R}) + \alpha}\right) , \tag{9.5}$$

where $\alpha$ is a fixed parameter to avoid singularities and $\sigma$ is a Lagrange multiplier for a penalty function meant to drive the energy gap to zero. Minimization of $F_\sigma$ is performed iteratively for increasingly large values $\sigma$.

A second MECP optimization algorithm is a simplification of the penalty-constrained approach that we call the "direct" method. Here, the gradient of the objective function is

$$\mathbf{G} = \mathbf{P}\mathbf{G}_{\text{mean}} + 2(E_K - E_J)\mathbf{G}_{\text{diff}} , \tag{9.6}$$

where

$$\mathbf{G}_{\text{mean}} = \tfrac{1}{2}(\mathbf{G}_J + \mathbf{G}_K) \tag{9.7}$$

is the mean energy gradient, with $\mathbf{G}_i = \partial E_i/\partial\mathbf{R}$ being the nuclear gradient for state $i$, and

$$\mathbf{G}_{\text{diff}} = \frac{\mathbf{G}_K - \mathbf{G}_J}{||\mathbf{G}_K - \mathbf{G}_J||} \tag{9.8}$$

is the normalized difference gradient. Finally,

$$\mathbf{P} = \mathbf{1} - \mathbf{G}_{\text{diff}}\mathbf{G}_{\text{diff}}^\top \tag{9.9}$$

projects the gradient difference direction out of the mean energy gradient in Eq. (9.6). The algorithm then consists in minimizing along the gradient $\mathbf{G}$, with for the iterative cycle over a Lagrange multiplier, which can sometimes be slow to converge.

The third and final MECP optimization algorithm that is available in Q-CHEM is the branching-plane updating method developed by Morokuma and co-workers[36] and implemented in Q-CHEM by Zhang and Herbert[34]. This algorithm uses a gradient that is similar to that in Eq. (9.6) but projects out not just $\mathbf{G}_{\text{diff}}$ in Eq. (9.9) but also a second vector that is orthogonal to it, representing an iteratively-updated approximation to the branching space.

None of these three methods requires evaluation of non-adiabatic couplings, and all three can be used to optimize MECPs at the CIS, SF-CIS, TDDFT, SF-TDDFT, and SOS-CIS(D0) levels. The direct algorithm can also be used for EOM-XX-CCSD methods (XX = EE, IP, or EA). It should be noted that since EOM-XX-CCSD is a linear response method, it suffers from the same topology problem around conical intersections involving the ground state that was described in regards to TDDFT in Section 9.6.1. With spin-flip approaches, correct topology is obtained[27].

Analytic derivative couplings are available for (SF-)CIS and (SF-)TDDFT, so for these methods one can alternatively employ an optimization algorithm that makes use of both $\mathbf{g}_{JK}$ and $\mathbf{h}_{JK}$. Such an algorithm, due to Schlegel and co-workers[37], is available in Q-CHEM and consists of optimization along the gradient in Eq. (9.6) but with a projector

$$\mathbf{P} = \mathbf{1} - \mathbf{G}_{\text{diff}}\mathbf{G}_{\text{diff}}^\top - \mathbf{y}\mathbf{y}^\top \tag{9.10}$$

where

$$\mathbf{y} = \frac{(\mathbf{1} - \mathbf{x}\mathbf{x}^\top)\mathbf{h}_{JK}}{||(\mathbf{1} - \mathbf{x}\mathbf{x}^\top)\mathbf{h}_{JK}||} , \tag{9.11}$$

in place of the projector in Eq. (9.9). Equation (9.10) has the effect of projecting the span of $\mathbf{g}_{JK}$ and $\mathbf{h}_{JK}$ (*i.e.*, the branching space) out of state-averaged gradient in Eq. (9.6). The tends to reduce the number of iterations necessary to converge the MECP, and since calculation of the (optional) $\mathbf{h}_{JK}$ vector represents only a slight amount of overhead on top of the (required) $\mathbf{g}_{JK}$ vector, this last algorithm tends to yield significant speed-ups relative to the other three[27]. As such, it is the recommended choice for (SF-)CIS and (SF-)TDDFT.

It should be noted that while the spin-flip methods cure the topology problem around conical intersections that involve the ground state, this method tends to exacerbate spin contamination relative to the corresponding spin-conserving approaches[38]. While spin contamination is certainly present in traditional, spin-conserving CIS and TDDFT, it presents the following unique challenge in spin-flip methods. Suppose, for definiteness, that one is interested in singlet excited states. Then the reference state for the spin-flip methods should be the high-spin triplet. A spin-flipping excitation will then generate $\mathrm{S}_0$, $\mathrm{S}_1$, $\mathrm{S}_2, \ldots$ but will also generate the $M_S = 0$ component of the triplet reference state, which therefore appears in what is ostensibly the singlet manifold. Q-CHEM attempts to identify this automatically, based on a threshold for $\langle \hat{S}^2 \rangle$, but severe spin contamination can sometimes defeat this algorithm[34], hampering Q-CHEM's ability to distinguish singlets from triplets (in this particular example). An alternative might be the state-tracking procedure that is described in Section 9.6.5.

### 9.6.4 Job Control and Examples

For MECP optimization, set MECP_OPT = TRUE in the *$rem* section, and note that the *$derivative_coupling* input section discussed in Section 9.6.2 is not necessary in this case.

**MECP_OPT**

Determines whether we are doing MECP optimizations.

TYPE:

LOGICAL

DEFAULT:

FALSE

OPTIONS:

| | |
|---|---|
| TRUE | Do MECP optimization. |
| FALSE | Do not do MECP optimization. |

RECOMMENDATION:

None.

**MECP_METHODS**

Determines which method to be used.

TYPE:

STRING

DEFAULT:

BRANCHING_PLANE

OPTIONS:

| | |
|---|---|
| BRANCHING_PLANE | Use the branching-plane updating method. |
| MECP_DIRECT | Use the direct method. |
| PENALTY_FUNCTION | Use the penalty-constrained method. |

RECOMMENDATION:

The direct method is stable for small molecules or molecules with high symmetry. The branching-plane updating method is more efficient for larger molecules but does not work if the two states have different symmetries. If using the branching-plane updating method, GEOM_OPT_COORDS must be set to 0 in the *$rem* section, as this algorithm is available in Cartesian coordinates only. The penalty-constrained method converges slowly and is suggested only if other methods fail.

**MECP_STATE1**

Sets the first Born-Oppenheimer state for MECP optimization.

TYPE:

INTEGER/INTEGER ARRAY

DEFAULT:

None

OPTIONS:

$[i,j]$ Find the $j$th excited state with the total spin $i$; $j = 0$ means the SCF ground state.

RECOMMENDATION:

$i$ is ignored for restricted calculations; for unrestricted calculations, $i$ can only be 0 or 1.

**MECP_STATE2**

Sets the second Born-Oppenheimer state for MECP optimization.

TYPE:

INTEGER/INTEGER ARRAY

DEFAULT:

None

OPTIONS:

$[i,j]$ Find the $j$th excited state with the total spin $i$; $j = 0$ means the SCF ground state.

RECOMMENDATION:

$i$ is ignored for restricted calculations; for unrestricted calculations, $i$ can only be 0 or 1.

**CIS_S2_THRESH**

Determines whether a state is a singlet or triplet in unrestricted calculations.

TYPE:

INTEGER

DEFAULT:

120

OPTIONS:

$n$ Sets the $\langle \hat{S}^2 \rangle$ threshold to $n/100$

RECOMMENDATION:

For the default case, states with $\langle \hat{S}^2 \rangle > 1.2$ are treated as triplet states and other states are treated as singlets.

**MECP_PROJ_HESS**

Determines whether to project out the coupling vector from the Hessian when using branching plane updating method.

TYPE:

LOGICAL

DEFAULT:

TRUE

OPTIONS:

TRUE

FALSE

RECOMMENDATION:

Use the default.

**Example 9.14** MECP optimization of an intersection between the $S_2$ and $S_3$ states of $NO_2^-$, using the direct method at the SOS-CIS(D0) level.

```
$molecule
   -1 1
   N1
   O2  N1  RNO
   O3  N1  RNO  O2  AONO

   RNO  = 1.50
   AONO = 100
$end

$rem
   JOBTYPE          = opt
   METHOD           = soscis(d0)
   BASIS            = aug-cc-pVDZ
   AUX_BASIS        = rimp2-aug-cc-pVDZ
   PURECART         = 1111
   CIS_N_ROOTS      = 4
   CIS_TRIPLETS     = false
   CIS_SINGLETS     = true
   MEM_STATIC       = 900
   MEM_TOTAL        = 1950
   MECP_OPT         = true
   MECP_STATE1      = [0,2]
   MECP_STATE2      = [0,3]
   MECP_METHODS    = mecp_direct
$end
```

**Example 9.15** Optimization of the ethylidene MECP between $S_0$ and $S_1$ in $C_2H_2$, at the SF-TDDFT level using the branching-plane updating method.

```
$molecule
   0 3
   C   0.044626  -0.2419240   0.357157
   C   0.008905   0.6727548   1.460500
   H   0.928425  -0.1459163  -0.272095
   H  -0.831032  -0.1926895  -0.288529
   H  -0.009238   0.9611331   2.479936
   H   0.068314  -1.2533580   0.778847
$end

$rem
   JOBTYPE           opt
   MECP_OPT          true
   MECP_METHODS      branching_plane
   MECP_PROJ_HESS    true ! project out y vector from the hessian
   GEOM_OPT_COORDS   0  ! currently only works for Cartesian coordinate
   METHOD            bhhlyp
   SPIN_FLIP         true
   UNRESTRICTED      true
   BASIS             6-31G(d,p)
   CIS_N_ROOTS       4
   MECP_STATE1       [0,1]
   MECP_STATE2       [0,2]
   CIS_S2_THRESH     120
$end
```

**Example 9.16** Optimization of the twisted-pyramidalized ethylene MECP between $S_0$ and $S_1$ in $C_2H_2$ using SF-TDDFT.

```
$molecule
   0 3
   C  -0.015889   0.073532  -0.059559
   C   0.012427  -0.002468   1.315694
   H   0.857876   0.147014  -0.710529
   H  -0.936470  -0.011696  -0.626761
   H   0.764557   0.663381   1.762573
   H   0.740773  -0.869764   1.328583
$end

$rem
   JOBTYPE         opt
   MECP_OPT        true
   MECP_METHODS    penalty_function
   METHOD          bhhlyp
   SPIN_FLIP       true
   UNRESTRICTED    true
   BASIS           6-31G(d,p)
   CIS_N_ROOTS     4
   MECP_STATE1     [0,1]
   MECP_STATE2     [0,2]
   CIS_S2_THRESH   120
```

```
$end
```

**Example 9.17** Optimization of the $\tilde{B}^1A_2$ and $\tilde{A}^1B_2$ states of $N_3^+$ using the direct method at the EOM-EE-CCSD level.

```
$molecule
   1 1
   N1
   N2 N1 rNN
   N3 N2 rNN N1 aNNN

   rNN  =  1.54
   aNNN = 50.0
$end

$rem
   JOBTYPE                opt
   MECP_OPT               true
   MECP_METHODS           mecp_direct
   METHOD                 eom-ccsd
   BASIS                  6-31g
   EE_SINGLETS            [0,2,0,2]
   XOPT_STATE_1           [0,2,2]
   XOPT_STATE_2           [0,4,1]
   CCMAN2                 false
   GEOM_OPT_TOL_GRADIENT  30
$end
```

**Example 9.18** Optimization of the ethylidene MECP between $S_0$ and $S_1$, using BH&HLYP spin-flip TDDFT with analytic derivative couplings.

```
$molecule
   0 3
   C   0.044626  -0.241924   0.357157
   C   0.008905   0.672754   1.460500
   H   0.928425  -0.145916  -0.272095
   H  -0.831032  -0.192689  -0.288529
   H  -0.009238   0.961133   2.479936
   H   0.068314  -1.253358   0.778847
$end

$rem
   JOBTYPE            opt
   MECP_OPT           true
   MECP_METHODS       branching_plane
   MECP_PROJ_HESS     true
   GEOM_OPT_COORDS    0
   MECP_STATE1        [0,1]
   MECP_STATE2        [0,2]
   UNRESTRICTED       true
   SPIN_FLIP          true
   CIS_N_ROOTS        4
   CALC_NAC           true
   CIS_DER_NUMSTATE   2
   SET_ITER           50
   EXCHANGE           bhhlyp
   BASIS              6-31G(d,p)
   SYMMETRY_IGNORE    true
$end
```

### 9.6.5 State-Tracking Algorithm

For optimizing excited-state geometries and other applications, it can be important to find and follow electronically excited states of a particular character as the geometry changes. Various state-tracking procedures have been proposed for such cases[38,39]. An excited-state, state-tracking algorithm available in Q-CHEM is based on the overlap of the attachment/detachment densities (Section 6.12.1) at successive steps[40]. Using the densities avoids any issues that may be introduced by sign changes in the orbitals or configuration-interaction coefficients.

Two parameters are used to influence the choice of the electronic surface. One ($\gamma_E$) controls the energy window for states included in the search, and the other ($\gamma_S$) controls how well the states must overlap in order to be considered of the same character. These can be set by the user or generated automatically based on the magnitude of the nuclear displacement. The energy window is defined relative to the estimated energy for the current step (*i.e.*, $E_{\text{est}} \pm \gamma_E$), which in turn is based on the energy, gradient and nuclear displacement of previous steps. This estimated energy is specific to the type of calculation (*e.g.*, geometry optimization).

The similarity metric for the overlap is defined as

$$\mathcal{S} = 1 - \tfrac{1}{2}\big(||\Delta\mathbf{A}|| + ||\Delta\mathbf{D}||\big) \tag{9.12}$$

where $\Delta\mathbf{A} = \mathbf{A}_{t+1} - \mathbf{A}_t$ is the difference in attachment density matrices (Eq. (6.97)) and $\Delta\mathbf{D} = \mathbf{D}_{t+1} - \mathbf{D}_t$ is the difference in detachment density matrices (Eq. (6.95)), at successive steps. Equation (9.12) uses the matrix spectral norm,

$$||\mathbf{M}|| = \big(\lambda_{\max}\mathbf{M}^\dagger\mathbf{M}\big)^{1/2} \tag{9.13}$$

where $\lambda_{\max}$ is the largest eigenvalue of $\mathbf{M}$.

The selected state always satisfies one of the following

1. It is the only state in the window defined by $\gamma_E$.
2. It is the state with the largest overlap, provided at least one state has $\mathcal{S} \geq \gamma_S$.
3. It is the nearest state energetically if all states in the window have $\mathcal{S} < \gamma_S$, or if there are no states in the energy window.

State-following can currently be used with CIS or TDDFT excited states and is initiated with the *$rem* variable STATE_FOLLOW. It can be used with geometry optimization, *ab initio* molecular dynamics[40], or with the freezing/growing-string method. The desired state is specified using SET_STATE_DERIV for optimization or dynamics, or using SET_STATE_REACTANT and SET_STATE_PRODUCT for the freezing- or growing-string methods. The results for geometry optimizations can be affected by the step size (GEOM_OPT_DMAX), and using a step size smaller than the default value can provide better results. Also, it is often challenging to converge the strings in freezing/growing-string calculations.

**STATE_FOLLOW**

Turns on state following.

TYPE:

LOGICAL

DEFAULT:

FALSE

OPTIONS:

| | |
|---|---|
| FALSE | Do not use state-following. |
| TRUE | Use state-following. |

RECOMMENDATION:

None.

**FOLLOW_ENERGY**

Adjusts the energy window for near states

TYPE:

INTEGER

DEFAULT:

0

OPTIONS:

| | |
|---|---|
| 0 | Use dynamic thresholds, based on energy difference between steps. |
| $n$ | Search over selected state $E_{\text{est}} \pm n \times 10^{-6}\ E_h$. |

RECOMMENDATION:

Use a wider energy window to follow a state diabatically, smaller window to remain on the adiabatic state most of the time.

**FOLLOW_OVERLAP**

Adjusts the threshold for states of similar character.

TYPE:

INTEGER

DEFAULT:

0

OPTIONS:

| | |
|---|---|
| 0 | Use dynamic thresholds, based on energy difference between steps. |
| $n$ | Percentage overlap for previous step and current step. |

RECOMMENDATION:

Use a higher value to require states have higher degree of similarity to be considered the same (more often selected based on energy).

## 9.7 *Ab Initio* Molecular Dynamics

Q-CHEM can propagate classical molecular dynamics trajectories on the Born-Oppenheimer potential energy surface generated by a particular theoretical model chemistry (*e.g.*, B3LYP/6-31G* or MP2/aug-cc-pVTZ). This procedure, in which the forces on the nuclei are evaluated on-the-fly, is known variously as "direct dynamics", "*ab initio* molecular dynamics" (AIMD), or "Born-Oppenheimer molecular dynamics" (BOMD). In its most straightforward form, a BOMD calculation consists of an energy + gradient calculation at each molecular dynamics time step, and thus each time step is comparable in cost to one geometry optimization step. A BOMD calculation may be requested using any SCF energy + gradient method available in Q-CHEM, including excited-state dynamics in cases where excited-state analytic gradients are available. As usual, Q-CHEM will automatically evaluate derivatives by finite-difference if the analytic versions are not available for the requested method, but in AIMD applications this is very likely to be prohibitively expensive.

While the number of time steps required in most AIMD trajectories dictates that economical (typically SCF-based) underlying electronic structure methods are required, any method with available analytic gradients can reasonably be used for BOMD, including (within Q-CHEM) HF, DFT, MP2, RI-MP2, CCSD, and CCSD(T). The RI-MP2 method, especially when combined with Fock matrix and $Z$-vector extrapolation (as described below) is particularly effective as an alternative to DFT-based dynamics.

### 9.7.1 Overview and Basic Job Control

Initial Cartesian coordinates and velocities must be specified for the nuclei. Coordinates are specified in the *$molecule* section as usual, while velocities can be specified using a *$velocity* section with the form:

```
$velocity
$v_{x,1}$ $v_{y,1}$ $v_{z,1}$
$v_{x,2}$ $v_{y,2}$ $v_{z,2}$
$v_{x,N}$ $v_{y,N}$ $v_{z,N}$
$end
```

Here $v_{x,i}$, $v_{y,i}$, and $v_{z,i}$ are the $x$, $y$, and $z$ Cartesian velocities of the $i$th nucleus, specified in atomic units (bohrs per atomic unit of time, where 1 a.u. of time is approximately 0.0242 fs). The *$velocity* section thus has the same form as the *$molecule* section, but without atomic symbols and without the line specifying charge and multiplicity. The atoms must be ordered in the same manner in both the *$velocity* and *$molecule* sections.

As an alternative to a *$velocity* section, initial nuclear velocities can be sampled from certain distributions (*e.g.*, Maxwell-Boltzmann), using the AIMD_INIT_VELOC variable described below. AIMD_INIT_VELOC can also be set to QUASICLASSICAL, which triggers the use of quasi-classical trajectory molecular dynamics (see Section 9.7.5).

Although the Q-CHEM output file dutifully records the progress of any *ab initio* molecular dynamics job, the most useful information is printed not to the main output file but rather to a directory called "AIMD" that is a subdirectory of the job's scratch directory. (All *ab initio* molecular dynamics jobs should therefore use the *–save* option described in Section 2.7.) The AIMD directory consists of a set of files that record, in ASCII format, one line of information at each time step. Each file contains a few comment lines (indicated by "#") that describe its contents and which we summarize in the list below.

- *Cost*: Records the number of SCF cycles, the total CPU time, and the total memory use at each dynamics step.
- *EComponents*: Records various components of the total energy (all in hartree).
- *Energy*: Records the total energy and fluctuations therein.
- *MulMoments*: If multipole moments are requested, they are printed here.
- *NucCarts*: Records the nuclear Cartesian coordinates $x_1$, $y_1$, $z_1$, $x_2$, $y_2$, $z_2$, …, $x_N$, $y_N$, $z_N$ at each time step, in either bohrs or Ångstroms.

- *NucForces*: Records the Cartesian forces on the nuclei at each time step (same order as the coordinates, but given in atomic units).
- *NucVeloc*: Records the Cartesian velocities of the nuclei at each time step (same order as the coordinates, but given in atomic units).
- *TandV*: Records the kinetic and potential energy, as well as fluctuations in each.
- *View.xyz*: Cartesian-formatted version of *NucCarts* for viewing trajectories in an external visualization program.

For ELMD jobs, there are other output files as well:

- *ChangeInF*: Records the matrix norm and largest magnitude element of $\Delta\mathbf{F} = \mathbf{F}(t + \delta t) - \mathbf{F}(t)$ in the basis of Cholesky-orthogonalized AOs. The files ChangeInP, ChangeInL, and ChangeInZ provide analogous information for the density matrix $\mathbf{P}$ and the Cholesky orthogonalization matrices $\mathbf{L}$ and $\mathbf{Z}$ defined in[41].
- *DeltaNorm*: Records the norm and largest magnitude element of the curvy-steps rotation angle matrix $\Delta$ defined in Ref. 41. Matrix elements of $\Delta$ are the dynamical variables representing the electronic degrees of freedom. The output file DeltaDotNorm provides the same information for the electronic velocity matrix $d\Delta/dt$.
- *ElecGradNorm*: Records the norm and largest magnitude element of the electronic gradient matrix $\mathbf{FP} - \mathbf{PF}$ in the Cholesky basis.
- *dTfict:* Records the instantaneous time derivative of the fictitious kinetic energy at each time step, in atomic units.

*Ab initio* molecular dynamics jobs are requested by specifying JOBTYPE = AIMD. Initial velocities must be specified either using a *$velocity* section or via the AIMD_INIT_VELOC keyword described below. In addition, the following *$rem* variables must be specified for any *ab initio* molecular dynamics job:

**AIMD_METHOD**

Selects an *ab initio* molecular dynamics algorithm.

TYPE:

STRING

DEFAULT:

BOMD

OPTIONS:

| | |
|---|---|
| BOMD | Born-Oppenheimer molecular dynamics. |
| CURVY | Curvy-steps Extended Lagrangian molecular dynamics. |

RECOMMENDATION:

BOMD yields exact classical molecular dynamics, provided that the energy is tolerably conserved. ELMD is an approximation to exact classical dynamics whose validity should be tested for the properties of interest.

**TIME_STEP**

Specifies the molecular dynamics time step, in atomic units (1 a.u. = 0.0242 fs).

TYPE:

INTEGER

DEFAULT:

None.

OPTIONS:

User-specified.

RECOMMENDATION:

Smaller time steps lead to better energy conservation; too large a time step may cause the job to fail entirely. Make the time step as large as possible, consistent with tolerable energy conservation.

**AIMD_TIME_STEP_CONVERSION**

Modifies the molecular dynamics time step to increase granularity.

TYPE:

INTEGER

DEFAULT:

1

OPTIONS:

$n$ The molecular dynamics time step is TIME_STEP/$n$ a.u.

RECOMMENDATION:

None

**AIMD_STEPS**

Specifies the requested number of molecular dynamics steps.

TYPE:

INTEGER

DEFAULT:

None.

OPTIONS:

User-specified.

RECOMMENDATION:

None.

*Ab initio* molecular dynamics calculations can be quite expensive, and thus Q-CHEM includes several algorithms designed to accelerate such calculations. At the self-consistent field (Hartree-Fock and DFT) level, BOMD calculations can be greatly accelerated by using information from previous time steps to construct a good initial guess for the new molecular orbitals or Fock matrix, thus hastening SCF convergence. A Fock matrix extrapolation procedure[42], based on a suggestion by Pulay and Fogarasi[43], is available for this purpose.

The Fock matrix elements $F_{\mu\nu}$ in the atomic orbital basis are oscillatory functions of the time $t$, and Q-CHEM's extrapolation procedure fits these oscillations to a power series in $t$:

$$F_{\mu\nu}(t) = \sum_{n=0}^{N} c_n\, t^n \tag{9.14}$$

The $N + 1$ extrapolation coefficients $c_n$ are determined by a fit to a set of $M$ Fock matrices retained from previous time steps. Fock matrix extrapolation can significantly reduce the number of SCF iterations required at each time step, but for low-order extrapolations, or if SCF_CONVERGENCE is set too small, a systematic drift in the total energy may be observed. Benchmark calculations testing the limits of energy conservation can be found in Ref. 42, and demonstrate that numerically exact classical dynamics (without energy drift) can be obtained at significantly reduced cost.

Fock matrix extrapolation is requested by specifying values for $N$ and $M$, as in the form of the following two *$rem* variables:

**FOCK_EXTRAP_ORDER**

Specifies the polynomial order $N$ for Fock matrix extrapolation.

TYPE:

INTEGER

DEFAULT:

0 Do not perform Fock matrix extrapolation.

OPTIONS:

$N$ Extrapolate using an $N$th-order polynomial ($N > 0$).

RECOMMENDATION:

None

**FOCK_EXTRAP_POINTS**

Specifies the number $M$ of old Fock matrices that are retained for use in extrapolation.

TYPE:

INTEGER

DEFAULT:

0 Do not perform Fock matrix extrapolation.

OPTIONS:

$M$ Save $M$ Fock matrices for use in extrapolation $(M > N)$

RECOMMENDATION:

Higher-order extrapolations with more saved Fock matrices are faster and conserve energy better than low-order extrapolations, up to a point. In many cases, the scheme ($N$ = 6, $M$ = 12), in conjunction with SCF_CONVERGENCE = 6, is found to provide about a 50% savings in computational cost while still conserving energy.

When nuclear forces are computed using underlying electronic structure methods with non-optimized orbitals (such as MP2), a set of response equations must be solved[44]. While these equations are linear, their dimensionality necessitates an iterative solution[45,46], which, in practice, looks much like the SCF equations. Extrapolation is again useful here[47], and the syntax for $Z$-vector (response) extrapolation is similar to Fock extrapolation.

**Z_EXTRAP_ORDER**

Specifies the polynomial order $N$ for Z-vector extrapolation.

TYPE:

INTEGER

DEFAULT:

0 Do not perform $Z$-vector extrapolation.

OPTIONS:

$N$ Extrapolate using an $N$th-order polynomial ($N > 0$).

RECOMMENDATION:

None

**Z_EXTRAP_POINTS**

Specifies the number $M$ of old $Z$-vectors that are retained for use in extrapolation.

TYPE:

INTEGER

DEFAULT:

0 Do not perform response equation extrapolation.

OPTIONS:

$M$ Save $M$ previous $Z$-vectors for use in extrapolation $(M > N)$

RECOMMENDATION:

Using the default $Z$-vector convergence settings, a $(M, N) = (4, 2)$ extrapolation was shown to provide the greatest speedup. At this setting, a 2–3-fold reduction in iterations was demonstrated.

Assuming decent conservation, a BOMD calculation represents exact classical dynamics on the Born-Oppenheimer potential energy surface. In contrast, so-called extended Lagrangian molecular dynamics (ELMD) methods make an approximation to exact classical dynamics in order to expedite the calculations. ELMD methods—of which the most famous is Car–Parrinello molecular dynamics—introduce a fictitious dynamics for the electronic (orbital) degrees of freedom, which are then *propagated* alongside the nuclear degrees of freedom, rather than *optimized* at each time step as they are in a BOMD calculation. The fictitious electronic dynamics is controlled by a fictitious mass parameter $\mu$, and the value of $\mu$ controls both the accuracy and the efficiency of the method. In the limit of small $\mu$ the nuclei and the orbitals propagate adiabatically, and ELMD mimics true classical dynamics. Larger values of $\mu$ slow down the electronic dynamics, allowing for larger time steps (and more computationally efficient dynamics), at the expense of an ever-greater approximation to true classical dynamics.

Q-CHEM's ELMD algorithm is based upon propagating the density matrix, expressed in a basis of atom-centered Gaussian orbitals, along shortest-distance paths (geodesics) of the manifold of allowed density matrices $\mathbf{P}$. Idempotency of $\mathbf{P}$ is maintained at every time step, by construction, and thus our algorithm requires neither density matrix purification, nor iterative solution for Lagrange multipliers (to enforce orthogonality of the molecular orbitals). We call this procedure "curvy steps" ELMD[41], and in a sense it is a time-dependent implementation of the GDM algorithm (Section 4.6) for converging SCF single-point calculations.

The extent to which ELMD constitutes a significant approximation to BOMD continues to be debated. When assessing the accuracy of ELMD, the primary consideration is whether there exists a separation of time scales between nuclear oscillations, whose time scale $\tau_{\mathrm{nuc}}$ is set by the period of the fastest vibrational frequency, and electronic oscillations, whose time scale $\tau_{\mathrm{elec}}$ may be estimated according to[41]

$$\tau_{\mathrm{elec}} \geq \left( \frac{\mu}{\varepsilon_{\mathrm{LUMO}} - \varepsilon_{\mathrm{HOMO}}} \right)^{1/2} \tag{9.15}$$

A conservative estimate, suggested in Ref. 41, is that essentially exact classical dynamics is attained when $\tau_{\mathrm{nuc}} > 10\ \tau_{\mathrm{elec}}$. In practice, we recommend careful benchmarking to insure that ELMD faithfully reproduces the BOMD observables of interest.

Due to the existence of a fast time scale $\tau_{\mathrm{elec}}$, ELMD requires smaller time steps than BOMD. When BOMD is combined with Fock matrix extrapolation to accelerate convergence, it is no longer clear that ELMD methods are substantially more efficient, at least in Gaussian basis sets[42,43].

The following *$rem* variables are required for ELMD jobs:

**AIMD_FICT_MASS**
Specifies the value of the fictitious electronic mass $\mu$, in atomic units, where $\mu$ has dimensions of (energy)$\times$(time)$^2$.
TYPE:
INTEGER
DEFAULT:
None
OPTIONS:
User-specified
RECOMMENDATION:
Values in the range of 50–200 a.u. have been employed in test calculations; consult Ref. 41 for examples and discussion.

### 9.7.2 Additional Job Control and Examples

**AIMD_INIT_VELOC**
Specifies the method for selecting initial nuclear velocities.
TYPE:
STRING
DEFAULT:
None
OPTIONS:

| | |
|---|---|
| THERMAL | Random sampling of nuclear velocities from a Maxwell-Boltzmann distribution. The user must specify the temperature in Kelvin via the *$rem* variable AIMD_TEMP. |
| ZPE | Choose velocities in order to put zero-point vibrational energy into each normal mode, with random signs. This option requires that a frequency job to be run beforehand. |
| QUASICLASSICAL | Puts vibrational energy into each normal mode. In contrast to the ZPE option, here the vibrational energies are sampled from a Boltzmann distribution at the desired simulation temperature. This also triggers several other options, as described below. |

RECOMMENDATION:
This variable need only be specified in the event that velocities are not specified explicitly in a *$velocity* section.

**AIMD_MOMENTS**

Requests that multipole moments be output at each time step.

TYPE:

INTEGER

DEFAULT:

0 Do not output multipole moments.

OPTIONS:

$n$ Output the first $n$ multipole moments.

RECOMMENDATION:

None

**AIMD_TEMP**

Specifies a temperature (in Kelvin) for Maxwell-Boltzmann velocity sampling.

TYPE:

INTEGER

DEFAULT:

None

OPTIONS:

User-specified number of Kelvin.

RECOMMENDATION:

This variable is only useful in conjunction with AIMD_INIT_VELOC = THERMAL. Note that the simulations are run at constant energy, rather than constant temperature, so the mean nuclear kinetic energy will fluctuate in the course of the simulation.

**DEUTERATE**

Requests that all hydrogen atoms be replaces with deuterium.

TYPE:

LOGICAL

DEFAULT:

FALSE Do not replace hydrogens.

OPTIONS:

TRUE Replace hydrogens with deuterium.

RECOMMENDATION:

Replacing hydrogen atoms reduces the fastest vibrational frequencies by a factor of 1.4, which allow for a larger fictitious mass and time step in ELMD calculations. There is no reason to replace hydrogens in BOMD calculations.

**Example 9.19** Simulating thermal fluctuations of the water dimer at 298 K.

```
$molecule
   0  1
   O   1.386977   0.011218   0.109098
   H   1.748442   0.720970  -0.431026
   H   1.741280  -0.793653  -0.281811
   O  -1.511955  -0.009629  -0.120521
   H  -0.558095   0.008225   0.047352
   H  -1.910308   0.077777   0.749067
$end

$rem
```

```
   JOBTYPE              aimd
   AIMD_METHOD          bomd
   METHOD               b3lyp
   BASIS                6-31g*
   TIME_STEP            20         (20 a.u. = 0.48 fs)
   AIMD_STEPS           1000
   AIMD_INIT_VELOC      thermal
   AIMD_TEMP            298
   FOCK_EXTRAP_ORDER    6          request Fock matrix extrapolation
   FOCK_EXTRAP_POINTS   12
$end
```

**Example 9.20** Propagating $F^-(H_2O)_4$ on its first excited-state potential energy surface, calculated at the CIS level.

```
$molecule
   -1   1
   O  -1.969902  -1.946636   0.714962
   H  -2.155172  -1.153127   1.216596
   H  -1.018352  -1.980061   0.682456
   O  -1.974264   0.720358   1.942703
   H  -2.153919   1.222737   1.148346
   H  -1.023012   0.684200   1.980531
   O  -1.962151   1.947857  -0.723321
   H  -2.143937   1.154349  -1.226245
   H  -1.010860   1.980414  -0.682958
   O  -1.957618  -0.718815  -1.950659
   H  -2.145835  -1.221322  -1.158379
   H  -1.005985  -0.682951  -1.978284
   F   1.431477   0.000499   0.010220
$end

$rem
   JOBTYPE            aimd
   AIMD_METHOD        bomd
   METHOD             hf
   BASIS              6-31+G*
   ECP                SRLC
   PURECART           1111
   CIS_N_ROOTS        3
   CIS_TRIPLETS       false
   CIS_STATE_DERIV    1          propagate on first excited state
   AIMD_INIT_VELOC    thermal
   AIMD_TEMP          150
   TIME_STEP          25
   AIMD_STEPS         827       (500 fs)
$end
```

**Example 9.21** Simulating vibrations of the NaCl molecule using ELMD.

```
$molecule
   0  1
   Na   0.000000   0.000000  -1.742298
   Cl   0.000000   0.000000   0.761479
$end

$rem
```

```
   JOBTYPE    freq
   METHOD     b3lyp
   ECP        sbkjc
$end

@@@

$molecule
   read
$end

$rem
   JOBTYPE           aimd
   METHOD            b3lyp
   ECP               sbkjc
   TIME_STEP         14
   AIMD_STEPS        500
   AIMD_METHOD       curvy
   AIMD_FICT_MASS    360
   AIMD_INIT_VELOC   zpe
$end
```

### 9.7.3 Thermostats: Sampling the *NVT* Ensemble

Implicit in the discussion above was an assumption of conservation of energy, which implies dynamics run in the *microcanonical* ($NVE$) ensemble. Alternatively, the AIMD code in Q-CHEM can sample the *canonical* ($NVT$) ensemble with the aid of thermostats. These mimic the thermal effects of a surrounding temperature bath, and the time average of a trajectory (or trajectories) then affords thermodynamic averages at a chosen temperature. This option is appropriate in particular when multiple minima are thermally accessible. All sampled information is once again saved in the *AIMD/* subdirectory of the *$QCSCRATCH* directory for the job. Thermodynamic averages and error analysis may be performed externally, using these data. Two commonly used thermostat options, both of which yield proper canonical distributions of the classical molecular motion, are implemented in Q-CHEM and are described in more detail below. Constant-pressure barostats (for $NPT$ simulations) are not yet implemented.

As with any canonical sampling, the trajectory evolves at the mercy of barrier heights. Short trajectories will sample only within the local minimum of the initial conditions, which may be desired for sampling the properties of a given isomer, for example. Due to the energy fluctuations induced by the thermostat, the trajectory is neither guaranteed to stay within this potential energy well nor guaranteed to overcome barriers to neighboring minima, except in the infinite-sampling limit for the latter case, which is likely never reached in practice. Importantly, the user should note that the introduction of a thermostat destroys the validity of any real-time trajectory information; thermostatted trajectories should *not* be used to assess real-time dynamical observables, but only to compute thermodynamic averages.

#### 9.7.3.1 Langevin Thermostat

A stochastic, white-noise Langevin thermostat (AIMD_THERMOSTAT = LANGEVIN) combines random "kicks" to the nuclear momenta with a dissipative, friction term. The balance of these two contributions mimics the exchange of energy with a surrounding heat bath. The resulting trajectory, in the long-time sampling limit, generates the correct canonical distribution. The implementation in Q-CHEM follows the velocity Verlet formulation of Bussi and Parrinello,[48] which remains a valid propagator for all time steps and thermostat parameters. The thermostat is coupled to each degree of freedom in the simulated system. The MD integration time step (TIME_STEP) should be chosen in the same manner as in an NVE trajectory. The only user-controllable parameter for this thermostat, therefore, is the timescale over which the implied bath influences the trajectory. The AIMD_LANGEVIN_TIMESCALE keyword determines this parameter, in units of femtoseconds. For users who are more accustomed to thinking in terms of friction strength, this parameter is proportional to the inverse friction. A small value of the timescale parameter yields a "tight" thermostat, which strongly maintains the system at the chosen temperature but does not typically allow for rapid configurational flexibility. (Qualitatively, one may think of such simulations as sampling in molasses. This analogy, however, only applies to the thermodynamic sampling properties and does not suggest any electronic role of the solvent!) These small values are generally more appropriate for small systems, where the few degrees of freedom do not rapidly exchange energy and behave may behave in a non-ergodic fashion. Alternatively, large values of the time-scale parameter allow for more flexible configurational sampling, with the tradeoff of more (short-term) deviation from the desired average temperature. These larger values are more appropriate for larger systems since the inherent, microcanonical exchange of energy within the large number of degrees of freedom already tends toward canonical properties. (Think of this regime as sampling in a light, organic solvent.) Importantly, thermodynamic averages in the infinite-sampling limit are completely independent of this time-scale parameter. Instead, the time scale merely controls the efficiency with which the ensemble is explored. If maximum efficiency is desired, the user may externally compute lifetimes from the time correlation function of the desired observable and minimize the lifetime as a function of this timescale parameter. At the end of the trajectory, the average computed temperature is compared to the requested target temperature for validation purposes.

**Example 9.22** Canonical ($NVT$) sampling using AIMD with the Langevin thermostat

```
$comment
   Short example of using the Langevin thermostat
   for canonical (NVT) sampling
$end

$molecule
   0 1
   H
   O  1  1.0
   H  2  1.0  1  104.5
$end

$rem
   JOBTYPE                  aimd
   EXCHANGE                 hf
   BASIS                    sto-3g
   AIMD_TIME_STEP           20      !in au
   AIMD_STEPS               100
   AIMD_THERMOSTAT          langevin
   AIMD_INIT_VELOC          thermal
   AIMD_TEMP                298     !in K - initial conditions AND thermostat
   AIMD_LANGEVIN_TIMESCALE  100     !in fs
$end
```

#### 9.7.3.2 Nosé-Hoover Thermostat

An alternative thermostat approach is also available, namely, the Nosé-Hoover thermostat[49] (also known as a Nosé-Hoover "chain"), which mimics the role of a surrounding thermal bath by performing a microcanonical ($NVE$) trajectory in an extended phase space. By allowing energy to be exchanged with a chain of fictitious particles that are coupled to the target system, $NVT$ sampling is properly obtained for those degrees of freedom that represent the real system. (Only the target system properties are saved in *$QCSCRATCH/AIMD* for subsequent analysis and visualization, not the fictitious Nosé-Hoover degrees of freedom.) The implementation in Q-CHEM follows that of Martyna[49], which augments the original extended-Lagrangian approach of Nosé[50,51] and Hoover[52], using a chain of auxiliary degrees of freedom to restore ergodicity in stiff systems and thus afford the correct $NVT$ ensemble. Unlike the Langevin thermostat, the collection of system and auxiliary chain particles can be propagated in a time-reversible fashion with no need for stochastic perturbations.

Rather than directly setting the masses and force constants of the auxiliary chain particles, the Q-CHEM implementation focuses instead, on the time scale of the thermostat, as was the case for the Langevin thermostat described above. The time-scale parameter is controlled by the keyword NOSE_HOOVER_TIMESCALE, given in units of femtoseconds. The only other user-controllable parameter for this function is the length of the Nosé-Hoover chain, which is typically chosen to be 3–6 fictitious particles. Importantly, the version in Q-CHEM is currently implemented as a *single* chain that is coupled to the system, as a whole. Comprehensive thermostatting in which every single degree of freedom is coupled to its own thermostat, which is sometimes used for particularly stiff systems, is not implemented and for such cases the Langevin thermostat is recommended instead. For large and/or fluxional systems, the single-chain Nosé-Hoover approach is appropriate.

**Example 9.23** Canonical ($NVT$) sampling using AIMD with the Nosé-Hoover chain thermostat

```
$molecule
   0 1
   H
   O 1 1.0
   H 2 1.0 1 104.5
$end

$rem
   JOBTYPE                aimd
   EXCHANGE               hf
   BASIS                  sto-3g
   AIMD_TIME_STEP         20      !in au
   AIMD_STEPS             100
   AIMD_THERMOSTAT        nose_hoover
   AIMD_INIT_VELOC        thermal
   AIMD_TEMP              298     !in K - initial conditions AND thermostat
   NOSE_HOOVER_LENGTH     3       !chain length
   NOSE_HOOVER_TIMESCALE  100     !in fs
$end
```

**AIMD_THERMOSTAT**

Applies thermostatting to AIMD trajectories.

TYPE:

INTEGER

DEFAULT:

none

OPTIONS:

| | |
|---|---|
| LANGEVIN | Stochastic, white-noise Langevin thermostat |
| NOSE_HOOVER | Time-reversible, Nosé-Hoovery chain thermostat |

RECOMMENDATION:

Use either thermostat for sampling the canonical (NVT) ensemble.

**AIMD_LANGEVIN_TIMESCALE**

Sets the timescale (strength) of the Langevin thermostat

TYPE:

INTEGER

DEFAULT:

none

OPTIONS:

| | |
|---|---|
| $n$ | Thermostat timescale,asn $n$ fs |

RECOMMENDATION:

Smaller values (roughly 100) equate to tighter thermostats but may inhibit rapid sampling. Larger values ($\geq$ 1000) allow for more rapid sampling but may take longer to reach thermal equilibrium.

**NOSE_HOOVER_LENGTH**

Sets the chain length for the Nosé-Hoover thermostat

TYPE:

INTEGER

DEFAULT:

none

OPTIONS:

| | |
|---|---|
| $n$ | Chain length of $n$ auxiliary variables |

RECOMMENDATION:

Typically 3-6

**NOSE_HOOVER_TIMESCALE**

Sets the timescale (strength) of the Nosé-Hoover thermostat

TYPE:

INTEGER

DEFAULT:

none

OPTIONS:

| | |
|---|---|
| $n$ | Thermostat timescale, as $n$ fs |

RECOMMENDATION:

Smaller values (roughly 100) equate to tighter thermostats but may inhibit rapid sampling. Larger values ($\geq$ 1000) allow for more rapid sampling but may take longer to reach thermal equilibrium.

### 9.7.4 Vibrational Spectra

The inherent nuclear motion of molecules is experimentally observed by the molecules' response to impinging radiation. This response is typically calculated within the mechanical and electrical harmonic approximations (second derivative calculations) at critical-point structures. Spectra, including anharmonic effects, can also be obtained from dynamics simulations. These spectra are generated from dynamical response functions, which involve the Fourier transform of auto-correlation functions. Q-CHEM can provide both the vibrational spectral density from the velocity auto-correlation function

$$D(\omega) \propto \int_{-\infty}^{\infty} dt\, e^{-i\omega t} \langle \vec{v}(0) \cdot \vec{v}(t) \rangle \tag{9.16}$$

and infrared absorption intensity from the dipole auto-correlation function

$$I(\omega) \propto \frac{\omega}{2\pi} \int_{-\infty}^{\infty} dt\, e^{-i\omega t} \langle \vec{\mu}(0) \cdot \vec{\mu}(t) \rangle \tag{9.17}$$

These two features are activated by the AIMD_NUCL_VACF_POINTS and AIMD_NUCL_DACF_POINTS keywords, respectively, where values indicate the number of data points to include in the correlation function. Furthermore, the AIMD_NUCL_SAMPLE_RATE keyword controls the frequency at which these properties are sampled (entered as number of time steps). These spectra—generated at constant energy—should be averaged over a suitable distribution of initial conditions. The averaging indicated in the expressions above, for example, should be performed over a Boltzmann distribution of initial conditions.

Note that dipole auto-correlation functions can exhibit contaminating information if the molecule is allowed to rotate/translate. While the initial conditions in Q-CHEM remove translation and rotation, numerical noise in the forces and propagation can lead to translation and rotation over time. The trans/rot correction in Q-CHEM is activated by the PROJ_TRANSROT keyword.

**AIMD_NUCL_VACF_POINTS**

Number of time points to utilize in the velocity auto-correlation function for an AIMD trajectory

TYPE:

INTEGER

DEFAULT:

0

OPTIONS:

| | |
|---|---|
| 0 | Do not compute velocity auto-correlation function. |
| $1 \leq n \leq$ AIMD_STEPS | Compute velocity auto-correlation function for last $n$ time steps of the trajectory. |

RECOMMENDATION:

If the VACF is desired, set equal to AIMD_STEPS.

**AIMD_NUCL_DACF_POINTS**

Number of time points to utilize in the dipole auto-correlation function for an AIMD trajectory

TYPE:

INTEGER

DEFAULT:

0

OPTIONS:

| | |
|---|---|
| 0 | Do not compute dipole auto-correlation function. |
| $1 \leq n \leq$ AIMD_STEPS | Compute dipole auto-correlation function for last $n$ timesteps of the trajectory. |

RECOMMENDATION:

If the DACF is desired, set equal to AIMD_STEPS.

**AIMD_NUCL_SAMPLE_RATE**

The rate at which sampling is performed for the velocity and/or dipole auto-correlation function(s). Specified as a multiple of steps; *i.e.*, sampling every step is 1.

TYPE:

INTEGER

DEFAULT:

None.

OPTIONS:

| | |
|---|---|
| $1 \leq n \leq$ AIMD_STEPS | Update the velocity/dipole auto-correlation function every $n$ steps. |

RECOMMENDATION:

Since the velocity and dipole moment are routinely calculated for *ab initio* methods, this variable should almost always be set to 1 when the VACF/DACF are desired.

**PROJ_TRANSROT**

Removes translational and rotational drift during AIMD trajectories.

TYPE:

LOGICAL

DEFAULT:

FALSE

OPTIONS:

| | |
|---|---|
| FALSE | Do not apply translation/rotation corrections. |
| TRUE | Apply translation/rotation corrections. |

RECOMMENDATION:

When computing spectra (see AIMD_NUCL_DACF_POINTS, for example), this option can be utilized to remove artificial, contaminating peaks stemming from translational and/or rotational motion. Recommend setting to TRUE for all dynamics-based spectral simulations.

### 9.7.5 Quasi-Classical Molecular Dynamics

So-called “quasi-classical” trajectories[53–55] (QCT) put vibrational energy into each mode in the initial velocity setup step, which can improve on the results of purely classical simulations, for example in the calculation of photoelectron[56] or infrared spectra[57]. Improvements include better agreement of spectral linewidths with experiment at lower temperatures and better agreement of vibrational frequencies with anharmonic calculations.

The improvements at low temperatures can be understood by recalling that even at low temperature there is nuclear motion due to zero-point motion. This is included in the quasi-classical initial velocities, thus leading to finite peak widths even at low temperatures. In contrast to that the classical simulations yield zero peak width in the low temperature limit, because the thermal kinetic energy goes to zero as temperature decreases. Likewise, even at room temperature the quantum vibrational energy for high-frequency modes is often significantly larger than the classical kinetic energy. QCT-MD therefore typically samples regions of the potential energy surface that are higher in energy and thus more anharmonic than the low-energy regions accessible to classical simulations. These two effects can lead to improved peak widths as well as a more realistic sampling of the anharmonic parts of the potential energy surface. However, the QCT-MD method also has important limitations which are described below and that the user has to monitor for carefully.

In our QCT-MD implementation the initial vibrational quantum numbers are generated as random numbers sampled from a vibrational Boltzmann distribution at the desired simulation temperature. In order to enable reproducibility of the results, each trajectory (and thus its set of vibrational quantum numbers) is denoted by a unique number using the AIMD_QCT_WHICH_TRAJECTORY variable. In order to loop over different initial conditions, run trajectories with different choices for AIMD_QCT_WHICH_TRAJECTORY. It is also possible to assign initial velocities corresponding to an average over a certain number of trajectories by choosing a negative value. Further technical details of our QCT-MD implementation are described in detail in Appendix A of Ref. 56.

**AIMD_QCT_WHICH_TRAJECTORY**
Picks a set of vibrational quantum numbers from a random distribution.
TYPE:
INTEGER
DEFAULT:
1
OPTIONS:
$n$ Picks the $n$th set of random initial velocities.
$-n$ Uses an average over $n$ random initial velocities.
RECOMMENDATION:
Pick a positive number if you want the initial velocities to correspond to a particular set of vibrational occupation numbers and choose a different number for each of your trajectories. If initial velocities are desired that corresponds to an average over $n$ trajectories, pick a negative number.

Below is a simple example input for running a QCT-MD simulation of the vibrational spectrum of water. Most input variables are the same as for classical MD as described above. The use of quasi-classical initial conditions is triggered by setting the AIMD_INIT_VELOC variable to QUASICLASSICAL.

**Example 9.24** Simulating the IR spectrum of water using QCT-MD.

```
$comment
   Don't forget to run a frequency calculation prior to this job.
$end

$molecule
   0  1
   O     0.000000    0.000000    0.520401
   H    -1.475015    0.000000   -0.557186
   H     1.475015    0.000000   -0.557186
$end


$rem
   JOBTYPE                    aimd
   INPUT_BOHR                 true
   METHOD                     hf
   BASIS                      3-21g
   SCF_CONVERGENCE            6
   TIME_STEP                  20  !  (in atomic units)
   AIMD_STEPS                 12500   6 ps total simulation time
   AIMD_TEMP                  12
   AIMD_PRINT                 2
   FOCK_EXTRAP_ORDER          6   ! Use a 6th-order extrapolation
   FOCK_EXTRAP_POINTS         12  ! of the previous 12 Fock matrices
   ! IR SPECTRAL SAMPLING
   AIMD_MOMENTS               1
   AIMD_NUCL_SAMPLE_RATE      5
   AIMD_NUCL_VACF_POINTS      1000
   ! QCT-SPECIFIC SETTINGS
   AIMD_INIT_VELOC           quasiclassical
   AIMD_QCT_WHICH_TRAJECTORY   1    ! Loop over several values to get
                                    ! the correct Boltzmann distribution.
$end
```

Other types of spectra can be calculated by calculating spectral properties along the trajectories. For example, we observed that photoelectron spectra can be approximated quite well by calculating vertical detachment energies (VDEs) along the trajectories and generating the spectrum as a histogram of the VDEs[56]. We have included several simple scripts in the *$QC/aimdman/tools* subdirectory that we hope the user will find helpful and that may serve as the basis for developing more sophisticated tools. For example, we include scripts that allow to perform calculations along a trajectory (`md_calculate_along_trajectory`) or to calculate vertical detachment energies along a trajectory (`calculate_rel_energies`).

Another application of the QCT code is to generate random geometries sampled from the vibrational wave function via a Monte Carlo algorithm. This is triggered by setting both the AIMD_QCT_INITPOS and AIMD_QCT_WHICH_TRAJECTORY variables to negative numbers, say $-m$ and $-n$, and setting AIMD_STEPS to zero. This will generate $m$ random geometries sampled from the vibrational wave function corresponding to an average over $n$ trajectories at the user-specified simulation temperature.

**AIMD_QCT_INITPOS**

Chooses the initial geometry in a QCT-MD simulation.

TYPE:

INTEGER

DEFAULT:

0

OPTIONS:

0 Use the equilibrium geometry.

$n$ Picks a random geometry according to the harmonic vibrational wave function.

$-n$ Generates $n$ random geometries sampled from the harmonic vibrational wave function.

RECOMMENDATION:

None.

For systems that are described well within the harmonic oscillator model and for properties that rely mainly on the ground-state dynamics, this simple MC approach may yield qualitatively correct spectra. In fact, one may argue that it is preferable over QCT-MD for describing vibrational effects at very low temperatures, since the geometries are sampled from a true quantum distribution (as opposed to classical and quasi-classical MD). We have included another script in the *$QC/aimdman/tools* directory to help with the calculation of vibrationally averaged properties (`monte_geom`).

**Example 9.25** MC sampling of the vibrational wave function for HCl.

```
$comment
  Generates 1000 random geometries for HCl based on the harmonic vibrational
  wave function at 1 Kelvin. The wave function is averaged over 1000
  sets of random vibrational quantum numbers (\ie{}, the ground state in
  this case due to the low temperature).
$end

$molecule
   0 1
   H    0.000000    0.000000   -1.216166
   Cl   0.000000    0.000000    0.071539
$end

$rem
   JOBTYPE                    aimd
   METHOD                     B3LYP
   BASIS                      6-311++G**
   SCF_CONVERGENCE            1
   SKIP_SCFMAN                1
   MAX_SCF_CYCLES             0
   XC_GRID                    1
   TIME_STEP                  20      (in atomic units)
   AIMD_STEPS                 0
   AIMD_INIT_VELOC            quasiclassical
   AIMD_QCT_VIBSEED           1
   AIMD_QCT_VELSEED           2
   AIMD_TEMP                  1     (in Kelvin)
   ! set aimd_qct_which_trajectory to the desired
   ! trajectory number
   AIMD_QCT_WHICH_TRAJECTORY  -1000
   AIMD_QCT_INITPOS           -1000
```

```
$end
```

It is also possible make some modes inactive, *i.e.*, to put vibrational energy into a subset of modes (all other are set to zero). The list of active modes can be specified using the *$qct_active_modes* section. Furthermore, the vibrational quantum numbers for each mode can be specified explicitly using the *$qct_vib_distribution* input section. It is also possible to set the phases using *$qct_vib_phase* (allowed values are 1 and $-1$). Below is a simple sample input:

**Example 9.26** User control over the QCT variables.

```
$comment
  Makes the 1st vibrational mode QCT-active; all other ones receive zero
  kinetic energy. We choose the vibrational ground state and a positive
  phase for the velocity.
$end

...

$qct_active_modes
  1
$end

$qct_vib_distribution
  0
$end

$qct_vib_phase
  1
$end

...
```

Finally we turn to a brief description of the limitations of QCT-MD. Perhaps the most severe limitation stems from the so-called “kinetic energy spilling” problem[58], which means that there can be an artificial transfer of kinetic energy between modes. This can happen because the initial velocities are chosen according to quantum energy levels, which are usually much higher than those of the corresponding classical systems. Furthermore, the classical equations of motion also allow for the transfer of non-integer multiples of the zero-point energy between the modes, which leads to different selection rules for the transfer of kinetic energy. Typically, energy spills from high-energy into low-energy modes, leading to spurious “hot” dynamics. A second problem is that QCT-MD is actually based on classical Newtonian dynamics, which means that the probability distribution at low temperatures can be qualitatively wrong compared to the true quantum distribution[56].

Q-CHEM implements a routine to monitor the kinetic energy within each normal mode along the trajectory and that is automatically switched on for quasi-classical simulations. It is thus possible to monitor for trajectories in which the kinetic energy in one or more modes becomes significantly larger than the initial energy. Such trajectories should be discarded. (Alternatively, see Ref. 58 for a different approach to the zero-point leakage problem.) Furthermore, this monitoring routine prints the squares of the (harmonic) vibrational wave function along the trajectory. This makes it possible to weight low-temperature results with the harmonic quantum distribution to alleviate the failure of classical dynamics for low temperatures.

### 9.7.6 Fewest-Switches Surface Hopping

As discussed in Section 9.6, optimization of minimum-energy crossing points (MECPs) along conical seams, followed by optimization of minimum-energy pathways that connect these MECPs to other points of interest on ground- and excited-state potential energy surfaces, affords an appealing one-dimensional picture of photochemical reactivity that is analogous to the "reactant → transition state → product" picture of ground-state chemistry. Just as the ground-state reaction is not obligated to proceed *exactly* through the transition-state geometry, however, an excited-state reaction need not proceed precisely through the MECP and the particulars of nuclear kinetic energy can lead to deviations. This is arguably more of an issue for excited-state reactions, where the existence of multiple conical intersections can easily lead to multiple potential reaction mechanisms. AIMD potentially offers a way to sample over the available mechanisms in order to deduce which ones are important in an automated way, but must be extended in the photochemical case to reactions that involve more than one Born-Oppenheimer potential energy surface.

The most widely-used trajectory-based method for non-adiabatic simulations is Tully's "fewest-switches" surface-hopping (FSSH) algorithm[59,60]. In this approach, classical trajectories are propagated on a single potential energy surface, but can undergo "hops" to a different potential surface in regions of near-degeneracy between surfaces. The probability of these stochastic hops is governed by the magnitude of the non-adiabatic coupling [Eq. (9.3)]. Considering the ensemble average of a swarm of trajectories then provides information about, *e.g.*, branching ratios for photochemical reactions.

The FSSH algorithm, based on the AIMD code, is available in Q-CHEM for any electronic structure method where analytic derivative couplings are available, which at present means CIS, TDDFT, and their spin-flip analogues (see Section 9.6.1). The nuclear dynamics component of the simulation is specified just as in an AIMD calculation. Artificial decoherence can be added to the calculation at additional cost according to the augmented FSSH (AFSSH) method,[61–63] which enforces stochastic wave function collapse at a rate proportional to the difference in forces between the trajectory on the active surface and position moments propagated the other surfaces. At every time step, the component of the wave function on each active surface is printed to the output file. These amplitudes, as well as the position and momentum moments (if AFSSH is requested), is also printed to a text file called *SurfaceHopper* located in the *$QC/AIMD* sub-directory of the job's scratch directory.

In order to request a FSSH calculation, only a few additional *$rem* variables must be added to those necessary for an excited-state AIMD simulation. At present, FSSH calculations can only be performed using Born-Oppenheimer molecular dynamics (BOMD) method. Furthermore, the optimized velocity Verlet (OVV) integration method is not supported for FSSH calculations.

**FSSH_LOWESTSURFACE**
Specifies the lowest-energy state considered in a surface hopping calculation.
TYPE:
INTEGER
DEFAULT:
None
OPTIONS:
$n$ Only states $n$ and above are considered in a FSSH calculation.
RECOMMENDATION:
None

**FSSH_NSURFACES**

Specifies the number of states considered in a surface hopping calculation.

TYPE:

INTEGER

DEFAULT:

None

OPTIONS:

$n$ $n$ states are considered in the surface hopping calculation.

RECOMMENDATION:

Any states which may come close in energy to the active surface should be included in the surface hopping calculation.

**FSSH_INITIALSURFACE**

Specifies the initial state in a surface hopping calculation.

TYPE:

INTEGER

DEFAULT:

None

OPTIONS:

$n$ An integer between FSSH_LOWESTSURFACE and FSSH_LOWESTSURFACE $+$ FSSH_NSURFACES $-1$.

RECOMMENDATION:

None

**AFSSH**

Adds decoherence approximation to surface hopping calculation.

TYPE:

INTEGER

DEFAULT:

0

OPTIONS:

0 Traditional surface hopping, no decoherence.

1 Use augmented fewest-switches surface hopping (AFSSH).

RECOMMENDATION:

AFSSH will increase the cost of the calculation, but may improve accuracy for some systems. See Refs. 61–63 for more detail.

**AIMD_SHORT_TIME_STEP**

Specifies a shorter electronic time step for FSSH calculations.

TYPE:

INTEGER

DEFAULT:

TIME_STEP

OPTIONS:

$n$ Specify an electronic time step duration of $n$/AIMD_TIME_STEP_CONVERSION a.u. If $n$ is less than the nuclear time step variable TIME_STEP, the electronic wave function will be integrated multiple times per nuclear time step, using a linear interpolation of nuclear quantities such as the energy gradient and derivative coupling. Note that $n$ must divide TIME_STEP evenly.

RECOMMENDATION:

Make AIMD_SHORT_TIME_STEP as large as possible while keeping the trace of the density matrix close to unity during long simulations. Note that while specifying an appropriate duration for the electronic time step is essential for maintaining accurate wave function time evolution, the electronic-only time steps employ linear interpolation to estimate important quantities. Consequently, a short electronic time step is not a substitute for a reasonable nuclear time step.

**FSSH_CONTINUE**

Restart a FSSH calculation from a previous run, using the file 396.0. When this is enabled, the initial conditions of the surface hopping calculation will be set, including the correct wave function amplitudes, initial surface, and position/momentum moments (if AFSSH) from the final step of some prior calculation.

TYPE:

INTEGER

DEFAULT:

0

OPTIONS:

0 Start fresh calculation.

1 Restart from previous run.

RECOMMENDATION:

None

**Example 9.27** FSSH simulation. Note that analytic derivative couplings must be requested via CALC_NAC, but it is unnecessary to include a *$derivative_coupling* section. The same is true for SET_STATE_DERIV, which will be set to the initial active surface automatically. Finally, one must be careful to choose a small enough time step for systems that have energetic access to a region of large derivative coupling, hence the choice for AIMD_TIME_STEP_CONVERSION and TIME_STEP.

```
$molecule
   0 1
   C   -1.620294    0.348677   -0.008838
   C   -0.399206   -0.437493   -0.012535
   C   -0.105193   -1.296810   -1.081340
   H   -0.789110   -1.374693   -1.905080
   C    1.069016   -2.045054   -1.072304
   H    1.292495   -2.701157   -1.889686
   C    1.956240   -1.940324    0.002842
   H    2.859680   -2.517019    0.008420
   C    1.666259   -1.084065    1.071007
   H    2.348104   -1.005765    1.894140
   C    0.495542   -0.335701    1.065497
   H    0.253287    0.325843    1.871866
   O   -1.931045    1.124872    0.911738
   H   -2.269528    0.227813   -0.865645
$end

$rem
   JOBTYPE                     aimd
   EXCHANGE                    hf
   BASIS                       3-21g
   CIS_N_ROOTS                 2
   SYMMETRY                    off
   SYM_IGNORE                  true
   CIS_SINGLETS                false
   CIS_TRIPLETS                true
   PROJ_TRANSROT               true
   FSSH_LOWESTSURFACE          1
   FSSH_NSURFACES              2 ! hop between T1 and T2
   FSSH_INITIALSURFACE         1 ! start on T1
   AFSSH                       0 ! no decoherence
   CALC_NAC                    true
   AIMD_STEPS                  500
   TIME_STEP                   14
   AIMD_SHORT_TIME_STEP        2
   AIMD_TIME_STEP_CONVERSION   1 ! Do not alter time_step duration
   AIMD_PRINT                  1
   AIMD_INIT_VELOC             thermal
   AIMD_TEMP                   300 # K
   AIMD_THERMOSTAT             4 # Langevin
   AIMD_INTEGRATION            vverlet
   FOCK_EXTRAP_ORDER           6
   FOCK_EXTRAP_POINTS          12
$end
```

## 9.8 *Ab initio* Path Integrals

### 9.8.1 Theory

Even in cases where the Born-Oppenheimer separation is valid, solving the electronic Schrödinger equation may only be half the battle. The remainder involves the solution of the *nuclear* Schrödinger equation for its resulting eigenvalues and eigenfunctions. This half is typically treated by the harmonic approximation at critical points, but anharmonicity, tunneling, and low-frequency ("floppy") motions can lead to extremely delocalized nuclear distributions, particularly for protons and for non-covalent interactions.

While the Born-Oppenheimer separation allows for a local solution of the electronic problem (in nuclear space), the nuclear half of the Schrödinger equation is entirely non-local and requires the computation of potential energy surfaces over large regions of configuration space. Grid-based methods, therefore, scale exponentially with the number of degrees of freedom, and are quickly rendered useless for all but very small molecules.

For equilibrium thermal distributions, the path integral (PI) formalism provides both an elegant and computationally feasible alternative. The equilibrium partition function can be written as a trace of the thermal, configuration-space density matrix,

$$Z = \mathrm{tr}\big(e^{-\beta\hat{H}}\big) = \int dx \, \langle x|e^{-\beta\hat{H}}|x\rangle = \int dx \, \rho(x,x;\beta) \; . \tag{9.18}$$

The density matrix at inverse temperature $\beta = (k_B T)^{-1}$ is defined by the last equality. Evaluating the integrals in Eq. (9.18) still requires computing eigenstates of $\hat{H}$, which is generally intractable. Inserting $N-1$ resolutions of the identity, however, one obtains

$$Z = \int dx_1 \int dx_2 \cdots \int dx_N \; \rho\left(x_1, x_2; \frac{\beta}{N}\right) \rho\left(x_2, x_3; \frac{\beta}{N}\right) \cdots \rho\left(x_N, x_1; \frac{\beta}{N}\right) \; . \tag{9.19}$$

Here, the density matrices appear at an inverse temperature $\beta/N$ that corresponds to multiplying the actual temperature $T$ by a factor of $N$.

The high-temperature form of the density matrix can be expressed as

$$\rho\left(x, x'; \frac{\beta}{N}\right) = \left(\frac{mN}{2\pi\beta\hbar^2}\right)^{1/2} \exp\left\{-\left(\frac{mN}{2\beta\hbar^2}\right)(x-x')^2 - \left(\frac{\beta}{2N}\right)\Big[V(x) + V(x')\Big]\right\} \tag{9.20}$$

which becomes exact as $T \to \infty$ (a limit in which quantum mechanics converges to classical mechanics), or in other words as $\beta \to 0$ or $N \to \infty$. Using $N$ time slices, the partition function is therefore converted into the form

$$Z = \left(\frac{mN}{2\pi\beta\hbar^2}\right)^{N/2} \int dx_1 \int dx_2 \cdots \int dx_N \; \exp\left\{-\frac{\beta}{N}\left[\frac{mN^2}{2\beta^2\hbar^2}\sum_{i=1}^{N}(x_i - x_{i+1})^2 + \sum_{i=1}^{N} V(x_i)\right]\right\} \; , \tag{9.21}$$

with the implied cyclic condition $x_{N+1} \equiv x_1$. Here, $V(x)$ is the potential function on which the "beads" move, which is the electronic potential generated by Q-CHEM.

Equation 9.21 has the form

$$Z \propto \int e^{-\beta V_{\mathrm{eff}}} \; , \tag{9.22}$$

where the form of the effective potential $V_{\mathrm{eff}}$ is evident from the integrand in Eq. (9.21). Equation (9.22) reveals that the path-integral formulation of the quantum partition function affords a *classical* configurational integral for the partition function, albeit in an extended-dimensional space The effective potential describes a classical "ring polymer" with $N$ beads, wherein neighboring beads are coupled by harmonic potentials that arise from the quantum nature of the kinetic energy. The exponentially-scaling, non-local nuclear quantum mechanics problem has therefore been mapped onto an entirely classical problem, which is amenable to standard treatments of configuration sampling. These methods typically involve molecular dynamics or Monte Carlo sampling. Importantly, the number of extended degrees of freedom, $N$, is reasonably small when the temperature is not too low: room-temperature systems involving hydrogen atoms typically are converged using roughly $N \approx 30$ beads. Therefore, fully quantum-mechanical nuclear distributions can be obtained at a cost only roughly 30 times that of a classical AIMD simulation. Path integral Monte Carlo (PIMC) is activated by setting JOBTYPE = PIMC.

The single-bead ($N = 1$) limit of the equations above is simply classical configuration sampling. When the temperature (controlled by the PIMC_TEMP keyword) is high, or where only heavy atoms are involved, the classical limit is often appropriate. The path integral machinery (with a single "bead") may be used to perform classical Boltzmann sampling. In this case, the partition function is simply

$$Z = \int dx \; e^{-\beta V(x)} \tag{9.23}$$

and this is what is ordinarily done in an AIMD simulation. Use of additional beads incorporates more quantum-mechanical delocalization, at a cost of roughly $N$ times that of the classical AIMD simulation, and this is the primary input variable in a PI simulation. It is controlled by the keyword PIMC_NBEADSPERATOM. The ratio of the inverse temperature to beads ($\beta/N$) dictates convergence with respect to the number of beads, so as the temperature is lowered, a concomitant increase in the number of beads is required.

Integration over configuration space is performed by Metropolis Monte Carlo (MC). The number of MC steps is controlled by the PIMC_MCMAX keyword and should typically be $\gtrsim 10^5$, depending on the desired level of statistical convergence. A warm-up run, in which the PI ring polymer is allowed to equilibrate without accumulating statistics, can be performed using the PIMC_WARMUP_MCMAX keyword.

As in AIMD simulations, the main results of PIMC jobs in Q-CHEM are not in the job output file but are instead output to (*$QCSCRATCH/PIMC* in the user's scratch directory, thus PIMC jobs should always be run with the *-save* option. The output files do contain some useful information, however, including a basic data analysis of the simulation. Average energies (thermodynamic estimator), bond lengths (less than 5 Å), bond length standard deviations and errors are printed at the end of the output file. The *$QCSCRATCH/PIMC* directory additionally contains the following files:

- *BondAves*: running average of bond lengths for convergence testing.
- *BondBins*: normalized distribution of significant bond lengths, binned within 5 standard deviations of the average bond length.
- *ChainCarts*: human-readable file of configuration coordinates, likely to be used for further, external statistical analysis. This file can get quite large, so be sure to provide enough scratch space!
- *ChainView.xyz*: Cartesian-formatted file for viewing the ring-polymer sampling in an external visualization program. (The sampling is performed such that the center of mass of the ring polymer system remains centered.)
- *Vcorr*: potential correlation function for the assessment of statistical correlations in the sampling.

In each of the above files, the first few lines contain a description of how the data are arranged.

One of the unfortunate rites of passage in PIMC usage is the realization of the ramifications of the stiff bead-bead interactions as convergence (with respect to $N$) is approached. Nearing convergence—where quantum mechanical results are correct—the length of statistical correlations grows enormously, and special sampling techniques are required to avoid long (or non-convergent) simulations. Cartesian displacements or normal-mode displacements of the ring polymer lead to this severe stiffening. While both of these naive sampling schemes are available in Q-CHEM, they are not recommended. Rather, the free-particle (harmonic bead-coupling) terms in the path integral action can be sampled directly. Several schemes are available for this purpose. Q-CHEM currently utilizes the simplest of these options, Levy flights. An $n$-bead segment (with $n < N$) of the ring polymer is chosen at random, with the length $n$ controlled by the PIMC_SNIP_LENGTH keyword. Between the endpoints of this segment, a free-particle path is generated by a Levy construction, which *exactly* samples the free-particle part of the action. Subsequent Metropolis testing of the resulting potential term—for which only the potential on the moved beads is required—then dictates acceptance.

Two measures of the sampling efficiency are provided in the job output file. The lifetime of the potential auto-correlation function $\langle V_0 V_\tau \rangle$ is provided in terms of the number of MC steps, $\tau$. This number indicates the number of configurations that are statically correlated. Similarly, the mean-square displacement between MC configurations is also provided. Maximizing this number and/or minimizing the statistical lifetime leads to efficient sampling. Note that the optimally efficient acceptance rate may *not* be 50% in MC simulations. In Levy flights, the only variable controlling acceptance and sampling efficiency is the length of the snippet. The statistical efficiency can be obtained from relatively short runs, during which the length of the Levy snippet should be optimized by the user.

### 9.8.2 Job Control and Examples

**PIMC_NBEADSPERATOM**

Number of path integral time slices ("beads") used on each atom of a PIMC simulation.

TYPE:

INTEGER

DEFAULT:

None.

OPTIONS:

1 Perform classical Boltzmann sampling.

$>1$ Perform quantum-mechanical path integral sampling.

RECOMMENDATION:

This variable controls the inherent convergence of the path integral simulation. The one-bead limit represents classical sampling and the infinite-bead limit represents exact quantum-mechanical sampling. Using 32 beads is reasonably converged for room-temperature simulations of molecular systems.

**PIMC_TEMP**

Temperature, in Kelvin (K), of path integral simulations.

TYPE:

INTEGER

DEFAULT:

None.

OPTIONS:

User-specified number of Kelvin for PIMC or classical MC simulations.

RECOMMENDATION:

None.

**PIMC_MCMAX**

Number of Monte Carlo steps to sample.

TYPE:

INTEGER

DEFAULT:

None.

OPTIONS:

User-specified number of steps to sample.

RECOMMENDATION:

This variable dictates the statistical convergence of MC/PIMC simulations. For converged simulations at least $10^5$ steps is recommended.

**PIMC_WARMUP_MCMAX**

Number of Monte Carlo steps to sample during an equilibration period of MC/PIMC simulations.

TYPE:

INTEGER

DEFAULT:

None.

OPTIONS:

User-specified number of steps to sample.

RECOMMENDATION:

Use this variable to equilibrate the molecule/ring polymer before collecting production statistics. Usually a short run of roughly 10% of PIMC_MCMAX is sufficient.

**PIMC_MOVETYPE**

Selects the type of displacements used in MC/PIMC simulations.

TYPE:

INTEGER

DEFAULT:

0

OPTIONS:

| | |
|---|---|
| 0 | Cartesian displacements of all beads, with occasional (1%) center-of-mass moves. |
| 1 | Normal-mode displacements of all modes, with occasional (1%) center-of-mass moves. |
| 2 | Levy flights without center-of-mass moves. |

RECOMMENDATION:

Except for classical sampling (MC) or small bead-number quantum sampling (PIMC), Levy flights should be utilized. For Cartesian and normal-mode moves, the maximum displacement is adjusted during the warm-up run to the desired acceptance rate (controlled by PIMC_ACCEPT_RATE). For Levy flights, the acceptance is solely controlled by PIMC_SNIP_LENGTH.

**PIMC_ACCEPT_RATE**

Acceptance rate for MC/PIMC simulations when Cartesian or normal-mode displacements are utilized.

TYPE:

INTEGER

DEFAULT:

None

OPTIONS:

| | |
|---|---|
| $0 < n < 100$ | User-specified rate, given as a whole-number percentage. |

RECOMMENDATION:

Choose acceptance rate to maximize sampling efficiency, which is typically signified by the mean-square displacement (printed in the job output). Note that the maximum displacement is adjusted during the warm-up run to achieve roughly this acceptance rate.

**PIMC_SNIP_LENGTH**

Number of "beads" to use in the Levy flight movement of the ring polymer.

TYPE:

INTEGER

DEFAULT:

None

OPTIONS:

$3 \leq n \leq$ PIMC_NBEADSPERATOM User-specified length of snippet.

RECOMMENDATION:

Choose the snip length to maximize sampling efficiency. The efficiency can be estimated by the mean-square displacement between configurations, printed at the end of the output file. This efficiency will typically, however, be a trade-off between the mean-square displacement (length of statistical correlations) and the number of beads moved. Only the moved beads require recomputing the potential, *i.e.*, a call to Q-CHEM for the electronic energy. (Note that the endpoints of the snippet remain fixed during a single move, so $n - 2$ beads are actually moved for a snip length of $n$. For 1 or 2 beads in the simulation, Cartesian moves should be used instead.)

**Example 9.28** Path integral Monte Carlo simulation of $H_2$ at room temperature

```
$molecule
   0  1
   H
   H 1 0.75
$end

$rem
   JOBTYPE              pimc
   METHOD               hf
   BASIS                sto-3g
   PIMC_TEMP            298
   PIMC_NBEADSPERATOM   32
   PIMC_WARMUP_MCMAX    10000     !Equilibration run
   PIMC_MCMAX           100000    !Production run
   PIMC_MOVETYPE        2         !Levy flights
   PIMC_SNIP_LENGTH     10        !Moves 8 beads per MC step (10-endpts)
$end
```

**Example 9.29** Classical Monte Carlo simulation of a water molecule at 500K

```
$molecule
   0  1
   H
   O 1 1.0
   H 2 1.0 1 104.5
$end

$rem
   JOBTYPE              pimc
   METHOD               rimp2
   BASIS                cc-pvdz
   AUX_BASIS            rimp2-cc-pvdz
   PIMC_TEMP            500
   PIMC_NBEADSPERATOM   1       !1 bead is classical sampling
   PIMC_WARMUP_MCMAX    10000   !Equilibration run
   PIMC_MCMAX           100000  !Production run
   PIMC_MOVETYPE        0       !Cartesian displacements (ok for 1 bead)
   PIMC_ACCEPT_RATE     40      !During warm-up, adjusts step size to 40% acceptance
$end
```

# References and Further Reading

[1] Geometry Optimization (Appendix A).

[2] S. M. Sharada, A. T. Bell, and M. Head-Gordon, *J. Chem. Phys.* **140**, 164115 (2014).

[3] G. Mills and H. H. Jónsson, *Phys. Rev. Lett.* **72**, 1124 (1994).

[4] G. Henkelman and H. Jónsson, *J. Chem. Phys.* **113**, 9978 (2000).

[5] E. Weinan, W. Ren, and E. Vanden-Eijnden, *Phys. Rev. B* **66**, 052301 (2002).

[6] B. Peters, A. Heyden, A. T. Bell, and A. Chakraborty, *J. Chem. Phys.* **120**, 7877 (2004).

[7] A. Behn, P. M. Zimmerman, A. T. Bell, and M. Head-Gordon, *J. Chem. Phys.* **135**, 224108 (2011).

[8] S. M. Sharada, P. M. Zimmerman, A. T. Bell, and M. Head-Gordon, *J. Chem. Theory Comput.* **8**, 5166 (2012).

[9] J. Baker, *J. Comput. Chem.* **7**, 385 (1986).

[10] Y. Kumeda, D. J. Wales, and L. J. Munro, *Chem. Phys. Lett.* **341**, 185 (2001).

[11] J. Baker, A. Kessi, and B. Delley, *J. Chem. Phys.* **105**, 192 (1996).

[12] G. Fogarasi, X. Zhou, P. W. Taylor, and P. Pulay, *J. Am. Chem. Soc.* **114**, 8191 (1992).

[13] G. Henkelman and H. Jónsson, *J. Chem. Phys.* **111**, 7010 (1999).

[14] A. Heyden, B. Peters, A. T. Bell, and F. J. Keil, *J. Phys. Chem. B* **109**, 1857 (2005).

[15] A. Heyden, A. T. Bell, and F. J. Keil, *J. Chem. Phys.* **123**, 224101 (2005).

[16] M. T. Ong, J. Leiding, H. Tao, A. M. Virshup, and T. J. Martínez, *J. Am. Chem. Soc.* **131**, 6377 (2009).

[17] J. Ribas-Arino, M. Shiga, and D. Marx, *Angew. Chem.* **121**, 4254 (2009).

[18] J. Ribas-Arino, M. Shiga, and D. Marx, *Angew. Chem. Int. Ed. Engl.* **48**, 4190 (2009).

[19] K. Wolinski and J. Baker, *Mol. Phys.* **107**, 2403 (2009).

[20] T. Stauch and A. Dreuw, *Chem. Rev.* **116**, 14137 (2016).

[21] K. Fukui, *J. Phys. Chem.* **74**, 4161 (1970).

[22] K. Ishida, K. Morokuma, and A. Komornicki, *J. Chem. Phys.* **66**, 215 (1977).

[23] M. W. Schmidt, M. S. Gordon, and M. Dupuis, *J. Am. Chem. Soc.* **107**, 2585 (1985).

[24] S. Matsika and P. Krause, *Annu. Rev. Phys. Chem.* **62**, 621 (2011).

[25] J. M. Herbert, X. Zhang, A. F. Morrison, and J. Liu, *acr* **49**, 931 (2016).

[26] S. Fatehi, E. Alguire, Y. Shao, and J. Subotnik, *J. Chem. Phys.* **135**, 234105 (2011).

[27] X. Zhang and J. M. Herbert, *J. Chem. Phys.* **141**, 064104 (2014).

[28] X. Zhang and J. M. Herbert, *J. Chem. Phys.* **142**, 064109 (2015).

[29] Q. Ou, G. D. Bellchambers, F. Furche, and J. E. Subotnik, *J. Chem. Phys.* **142**, 064114 (2015).

[30] B. G. Levine, C. Ko, J. Quenneville, and T. J. Martínez, *Mol. Phys.* **104**, 1039 (2006).

[31] Q. Ou, S. Fatehi, E. Alguire, Y. Shao, and J. Subotnik, *J. Chem. Phys.* **141**, 024114 (2014).

[32] Y. Shao, M. Head-Gordon, and A. I. Krylov, *J. Chem. Phys.* **118**, 4807 (2003).

[33] M. Huix-Rotllant et al., *Phys. Chem. Chem. Phys.* **12**, 12811 (2010).

[34] X. Zhang and J. M. Herbert, *J. Phys. Chem. B* **118**, 7806 (2014).

[35] B. G. Levine, J. D. Coe, and T. J. Martinez, *J. Phys. Chem. B* **112**, 405 (2008).

[36] S. Maeda, K. Ohno, and K. Morokuma, *J. Chem. Theory Comput.* **6**, 1538 (2010).

[37] M. J. Bearpark, M. A. Robb, and H. B. Schlegel, *Chem. Phys. Lett.* **223**, 269 (1994).

[38] X. Zhang and J. M. Herbert, *J. Chem. Phys.* **143**, 234107 (2015).

[39] Y. Harabuchi, K. Keipert, F. Zahariev, T. Taketsugu, and M. S. Gordon, *J. Phys. Chem. A* **118**, 11987 (2014).

[40] K. D. Closser, O. Gessner, and M. Head-Gordon, *J. Chem. Phys.* **140**, 134306 (2014).

[41] J. M. Herbert and M. Head-Gordon, *J. Chem. Phys.* **121**, 11542 (2004).

[42] J. M. Herbert and M. Head-Gordon, *Phys. Chem. Chem. Phys.* **7**, 3269 (2005).

[43] P. Pulay and G. Fogarasi, *Chem. Phys. Lett.* **386**, 272 (2004).

[44] C. M. Aikens et al., *Theor. Chem. Acc.* **110**, 233 (2004).

[45] J. A. Pople, R. Krishnan, H. B. Schlegel, and J. S. Binkley, *Int. J. Quantum Chem. Symp.* **13**, 225 (1979).

[46] P. P. Kombrath, J. Kong, T. R. Furlani, and M. Head-Gordon, *Mol. Phys.* **100**, 1755 (2002).

[47] R. P. Steele and J. C. Tully, *Chem. Phys. Lett.* **500**, 167 (2010).

[48] G. Bussi and M. Parrinello, *Phys. Rev. E* **75**, 056707 (2007).

[49] G. J. Martyna, M. L. Klein, and M. Tuckerman, *J. Chem. Phys.* **97**, 2635 (1992).

[50] S. Nosé, *J. Chem. Phys.* **81**, 511 (1984).

[51] S. Nosé, *Prog. Theor. Phys. Supp.* **103**, 1 (1991).

[52] W. G. Hoover, *Phys. Rev. A* **31**, 1695 (1985).

[53] M. Karplus, R. N. Porter, and R. D. Sharma, *J. Chem. Phys.* **43**, 3259 (1965).

[54] R. Porter, *Annu. Rev. Phys. Chem.* **25**, 317 (1974).

[55] R. Porter, L. Raff, and W. H. Miller, *J. Chem. Phys.* **63**, 2214 (1975).

[56] D. S. Lambrecht, G. N. I. Clark, T. Head-Gordon, and M. Head-Gordon, *J. Phys. Chem. A* **115**, 5928 (2011).

[57] E. Ramos-Cordoba, D. S. Lambrecht, and M. Head-Gordon, *Faraday Discuss.* **150**, 345 (2011).

[58] G. Czako, A. L. Kaledin, and J. M. Bowman, *J. Chem. Phys.* **132**, 164103 (2010).

[59] J. C. Tully, *J. Chem. Phys.* **93**, 1061 (1990).

[60] S. Hammes-Schiffer and J. C. Tully, *J. Chem. Phys.* **101**, 4657 (1994).

[61] J. E. Subotnik and N. Shenvi, *J. Chem. Phys.* **134**, 024105 (2011).

[62] J. E. Subotnik, *J. Phys. Chem. A* **114**, 12083 (2011).

[63] B. R. Landry and J. E. Subotnik, *J. Chem. Phys.* **137**, 22A513 (2012).

# Chapter 10

# Molecular Properties and Analysis

## 10.1 Introduction

Q-CHEM has incorporated a number of molecular properties and wave function analysis tools:

- Population analysis for ground and excited states
- Multipole moments for ground and excited states
- Extended excited-state analysis using reduced density matrices
- Calculation of molecular intracules
- Vibrational analysis (including isotopic substitution)
- Interface to the Natural Bond Orbital (NBO) package
- Molecular orbital symmetries
- Orbital localization
- Localized orbital bonding analysis
- Data generation for one- or two-dimensional plots
- Orbital visualization using the MOLDEN and MACMOLPLT programs
- Natural transition orbitals for excited states
- NMR shielding tensors and chemical shifts
- Molecular junctions

In addition, Chapter 12 describes energy decomposition analysis using the fragment-based absolutely-localized molecular orbital approach.

## 10.2 Wave Function Analysis

Q-CHEM performs a number of standard wave function analyses by default. Switching the *$rem* variable WAVEFUNCTION_ANALYSIS to FALSE will prevent the calculation of all wave function analysis features (described in this section). Alternatively, each wave function analysis feature may be controlled by its *$rem* variable. (The NBO program, which is interfaced with Q-CHEM, is capable of performing more sophisticated analyses. See Section 10.3 of this manual, along with the NBO manual, for more details.

**WAVEFUNCTION_ANALYSIS**

Controls the running of the default wave function analysis tasks.

TYPE:

LOGICAL

DEFAULT:

TRUE

OPTIONS:

TRUE Perform default wave function analysis.

FALSE Do not perform default wave function analysis.

RECOMMENDATION:

None

**Note:** WAVEFUNCTION_ANALYSIS has no effect on NBO, solvent models or vibrational analyses.

### 10.2.1 Population Analysis

The one-electron charge density, usually written as

$$\rho(\mathbf{r}) = \sum_{\mu\nu} P_{\mu\nu}\phi_\mu(\mathbf{r})\phi_\nu(\mathbf{r}) \tag{10.1}$$

represents the probability of finding an electron at the point $\mathbf{r}$, but implies little regarding the number of electrons associated with a given nucleus in a molecule. However, since the number of electrons $N$ is related to the occupied orbitals $\psi_i$ by

$$N = 2\sum_{a}^{N/N22} |\psi_a(\mathbf{r})|^2 \, d\mathbf{r} \tag{10.2}$$

We can substitute the atomic orbital (AO) basis expansion of $\psi_a$ into Eq. (10.2) to obtain

$$N = \sum_{\mu\upsilon} P_{\mu\upsilon}S_{\mu\upsilon} = \sum_{\mu} (\mathbf{PS})_{\mu\mu} = \mathrm{Tr}(\mathbf{PS}) \tag{10.3}$$

where we interpret $(\mathbf{PS})_{\mu\mu}$ as the number of electrons associated with $\phi_\mu$. If the basis functions are atom-centered, the number of electrons associated with a given atom can be obtained by summing over all the basis functions. This leads to the Mulliken formula for the net charge of the atom $A$:

$$q_A = Z_A - \sum_{\mu\in A} (\mathbf{PS})_{\mu\mu} \tag{10.4}$$

where $Z_A$ is the atom's nuclear charge. This is called a Mulliken population analysis[5]. Q-CHEM performs a Mulliken population analysis by default.

**POP_MULLIKEN**

Controls running of Mulliken population analysis.

TYPE:

LOGICAL/INTEGER

DEFAULT:

TRUE (or 1)

OPTIONS:

| | |
|---|---|
| FALSE (or 0) | Do not calculate Mulliken populations. |
| TRUE (or 1) | Calculate Mulliken populations. |
| 2 | Also calculate shell populations for each occupied orbital. |
| $-1$ | Calculate Mulliken charges for both the ground state and any CIS, RPA, or TDDFT excited states. |

RECOMMENDATION:

Leave as TRUE, unless excited-state charges are desired. Mulliken analysis is a trivial additional calculation, for ground or excited states.

**LOWDIN_POPULATION**

Run Löwdin population analysis.

TYPE:

LOGICAL

DEFAULT:

FALSE

OPTIONS:

| | |
|---|---|
| FALSE | Do not calculate Löwdin populations. |
| TRUE | Run Löwdin population analysis. |

RECOMMENDATION:

None

Although conceptually simple, Mulliken population analyses suffer from a heavy dependence on the basis set used, as well as the possibility of producing unphysical negative numbers of electrons. An alternative is that of Löwdin population analysis[6], which uses the Löwdin symmetrically orthogonalized basis set (which is still atom-tagged) to assign the electron density. This shows a reduced basis set dependence, but maintains the same essential features.

While Mulliken and Löwdin population analyses are commonly employed, and can be used to produce information about changes in electron density and also localized spin polarizations, they should not be interpreted as oxidation states of the atoms in the system. For such information we would recommend a bonding analysis technique (LOBA or NBO).

A more stable alternative to Mulliken or Löwdin charges are the so-called "CHELPG" charges ("Charges from the Electrostatic Potential on a Grid")[7]. These are the atom-centered charges that provide the best fit to the molecular electrostatic potential, evaluated on a real-space grid outside of the van der Waals region and subject to the constraint that the sum of the CHELPG charges must equal the molecular charge. Q-CHEM's implementation of the CHELPG algorithm differs slightly from the one originally algorithm described by Breneman and Wiberg[7], in that Q-CHEM weights the grid points with a smoothing function to ensure that the CHELPG charges vary continuously as the nuclei are displaced[8]. (For any particular geometry, however, numerical values of the charges are quite similar to those obtained using the original algorithm.) Note, however, that the Breneman-Wiberg approach uses a Cartesian grid and becomes expensive for large systems. (It is especially expensive when CHELPG charges are used in QM/MM-Ewald calculations[9].) For that reason, an alternative procedure based on atom-centered Lebedev grids is also available[9], which provides very similar charges using far fewer grid points. In order to use the Lebedev grid implementation the *$rem* variables CHELPG_H and CHELPG_HA must be set, which specify the number of Lebedev grid points for the hydrogen atoms and the heavy atoms, respectively.

**CHELPG**

Controls the calculation of CHELPG charges.

TYPE:

LOGICAL

DEFAULT:

FALSE

OPTIONS:

FALSE Do not calculate CHELPG charges.

TRUE Compute CHELPG charges.

RECOMMENDATION:

Set to TRUE if desired. For large molecules, there is some overhead associated with computing CHELPG charges, especially if the number of grid points is large.

**CHELPG_HEAD**

Sets the “head space”[7] (radial extent) of the CHELPG grid.

TYPE:

INTEGER

DEFAULT:

30

OPTIONS:

$N$ Corresponding to a head space of $N/10$, in Å.

RECOMMENDATION:

Use the default, which is the value recommended by Breneman and Wiberg[7].

**CHELPG_DX**

Sets the rectangular grid spacing for the traditional Cartesian CHELPG grid or the spacing between concentric Lebedev shells (when the variables CHELPG_HA and CHELPG_H are specified as well).

TYPE:

INTEGER

DEFAULT:

6

OPTIONS:

$N$ Corresponding to a grid space of $N/20$, in Å.

RECOMMENDATION:

Use the default (which corresponds to the “dense grid” of Breneman and Wiberg[7]), unless the cost is prohibitive, in which case a larger value can be selected. Note that this default value is set with the Cartesian grid in mind and not the Lebedev grid. In the Lebedev case, a larger value can typically be used.

**CHELPG_H**

Sets the Lebedev grid to use for hydrogen atoms.

TYPE:

INTEGER

DEFAULT:

NONE

OPTIONS:

$N$ Corresponding to a number of points in a Lebedev grid.

RECOMMENDATION:

CHELPG_H must always be less than or equal to CHELPG_HA. If it is greater, it will automatically be set to the value of CHELPG_HA.

**CHELPG_HA**

Sets the Lebedev grid to use for non-hydrogen atoms.

TYPE:

INTEGER

DEFAULT:

NONE

OPTIONS:

$N$ Corresponding to a number of points in a Lebedev grid (see Section 4.4.5.1.

RECOMMENDATION:

None.

Finally, Hirshfeld population analysis[10] provides yet another definition of atomic charges in molecules via a Stockholder prescription. The charge on atom $A$, $q_A$, is defined by

$$q_A = Z_A - \int d\mathbf{r} \frac{\rho_A^0(\mathbf{r})}{\sum_B \rho_B^0(\mathbf{r})} \rho(\mathbf{r}), \tag{10.5}$$

where $Z_A$ is the nuclear charge of $A$, $\rho_B^0$ is the isolated ground-state atomic density of atom $B$, and $\rho$ is the molecular density. The sum goes over all atoms in the molecule. Thus computing Hirschfeld charges requires a self-consistent calculation of the isolated atomic densities (the promolecule) as well as the total molecule. Following SCF completion, the Hirschfeld analysis proceeds by running another SCF calculation to obtain the atomic densities. Next numerical quadrature is used to evaluate the integral in Eq. (10.5). Neutral ground-state atoms are used, and the choice of appropriate reference for a charged molecule is ambiguous (such jobs will crash). As numerical integration (with default quadrature grid) is used, charges may not sum precisely to zero. A larger XC_GRID may be used to improve the accuracy of the integration.

The charges (and corresponding molecular dipole moments) obtained using Hirschfeld charges are typically underestimated as compared to other charge schemes or experimental data. To correct this, Marenich *et al.*[11] introduced "Charge Model 5" (CM5), which employs a single set of parameters to map the Hirschfeld charges onto a more reasonable representation of the electrostatic potential. CM5 charges generally lead to more accurate dipole moments as compared to the original Hirschfeld charges, at negligible additional cost. CM5 is available for molecules composed of elements H–Ca, Zn, Ge–Br, and I.

The use of neutral ground-state atoms to define the promolecular density in Hirshfeld scheme has no strict theoretical basis and there is no unique way to construct the promolecular densities. For example, $\mathrm{Li}^0\mathrm{F}^0$, $\mathrm{Li}^+\mathrm{F}^-$, or $\mathrm{Li}^-\mathrm{F}^+$ could each be used to construct the promolecular densities for LiF. Furthermore, the choice of appropriate reference for a charged molecule is ambiguous, and for this reason Hirshfeld analysis is disable in Q-CHEM for any molecule with a net charge. A solution for charged molecules is to use the iterative "Hirshfeld-I" partitioning scheme proposed by Bultinck *et al.*[12,13], in which the reference state is not predefined but rather determined self-consistently, thus eliminating the arbitrariness. The final self-consistent reference state for Hirshfeld-I partitioning usually consists of non-integer atomic populations.

In the first iteration, the Hirshfeld-I method uses neutral atomic densities (as in the original Hirshfeld scheme), $\rho_i^0(\mathbf{r})$ with electronic population $N_i^0 = \int d\mathbf{r}\,\rho_i^0(\mathbf{r}) = Z_i$. This affords charges

$$q_i^1 = Z_i - \int d\mathbf{r} \left( \frac{\rho_i^0(\mathbf{r})}{\sum_i^A \rho_i^0(\mathbf{r})} \right) \rho(\mathbf{r}) = Z_i - N_i^1 \tag{10.6}$$

on the first iteration. The new electronic population (number of electrons) for atom $i$ is $N_i^1$, and is derived from the promolecular populations $N_i^0$. One then computes new isolated atomic densities with $N_i^1 = \int d\mathbf{r}\,\rho_i^1(\mathbf{r}_1)$ and uses them to construct the promolecular densities in the next iteration. In general, the new weighting function for atom $i$ in the $k$th iteration is

$$w_{i,\mathrm{HI}}^k(\mathbf{r}) = \frac{\rho_i^{k-1}(\mathbf{r})}{\sum\limits_{i \in A} \rho_i^{k-1}(\mathbf{r})} \; . \tag{10.7}$$

The atomic densities $\rho_i^k(\mathbf{r})$ with corresponding fractional electron numbers $N_i^k$ are obtained by linear interpolation between $\rho_i^{0,\lfloor N_i^k \rfloor}(\mathbf{r})$ and $\rho_i^{0,\lceil N_i^k \rceil}(\mathbf{r})$ of the same atom[12,14]:

$$\rho_i^k(\mathbf{r}) = \left( \lceil N_i^k \rceil - N_i^k \right) \rho_i^{0,\lfloor N_i^k \rfloor}(\mathbf{r}) + \left( N_i^k - \lfloor N_i^k \rfloor \right) \rho_i^{0,\lceil N_i^k \rceil}(\mathbf{r}) \; , \tag{10.8}$$

where $\lfloor N_i^k \rfloor$ and $\lceil N_i^k \rceil$ denote the integers that bracket $N_i^k$. The two atomic densities on the right side of Eq. (10.8) are obtained from densities $\rho_i^{0,Z_A-2}, \rho_i^{0,Z_A-1}, \ldots, \rho_i^{0,Z_A+2}$ that are computed in advance. (That is, the method uses the neutral atomic density along with the densities for the singly- and doubly-charged cations and anions of the element in equation.) The Hirshfeld-I iterations are converged once the atomic populations change insignificantly between iterations, say $|N_i^k - N_i^{k-1}| < 0.0005e$[12,15].

The iterative Hirshfeld scheme generally affords more reasonable charges as compared to the original Hirshfeld scheme. In LiF, for example, the original Hirshfeld scheme predicts atomic charges of ±0.57 while the iterative scheme increases these charges to ±0.93. The integral in Eq. (10.6) is evaluated by numerical quadrature, and the cost of each iteration of Hirshfeld-I is equal to the cost of computing the original Hirshfeld charges. Within Q-CHEM, Hirshfeld-I charges are available for molecules containing only H, Li, C, N, O, F, S, and Cl. The *$rem* variable SYM_IGNORE must be set to TRUE for Hirshfeld-I analysis.

**HIRSHFELD**

Controls running of Hirshfeld population analysis.

TYPE:

LOGICAL

DEFAULT:

FALSE

OPTIONS:

TRUE Calculate Hirshfeld populations.

FALSE Do not calculate Hirshfeld populations.

RECOMMENDATION:

None

**HIRSHFELD_READ**

Switch to force reading in of isolated atomic densities.

TYPE:

LOGICAL

DEFAULT:

FALSE

OPTIONS:

| | |
|---|---|
| TRUE | Read in isolated atomic densities from previous Hirshfeld calculation from disk. |
| FALSE | Generate new isolated atomic densities. |

RECOMMENDATION:

Use the default unless system is large. Note, atoms should be in the same order with same basis set used as in the previous Hirshfeld calculation (although coordinates can change). The previous calculation should be run with the -save switch.

**HIRSHFELD_SPHAVG**

Controls whether atomic densities should be spherically averaged in pro-molecule.

TYPE:

LOGICAL

DEFAULT:

TRUE

OPTIONS:

| | |
|---|---|
| TRUE | Spherically average atomic densities. |
| FALSE | Do not spherically average. |

RECOMMENDATION:

Use the default.

**CM5**

Controls running of CM5 population analysis.

TYPE:

LOGICAL

DEFAULT:

FALSE

OPTIONS:

| | |
|---|---|
| TRUE | Calculate CM5 populations. |
| FALSE | Do not calculate CM5 populations. |

RECOMMENDATION:

None

**HIRSHITER**

Controls running of iterative Hirshfeld population analysis.

TYPE:

LOGICAL

DEFAULT:

FALSE

OPTIONS:

| | |
|---|---|
| TRUE | Calculate iterative Hirshfeld populations. |
| FALSE | Do not calculate iterative Hirshfeld populations. |

RECOMMENDATION:

None

**HIRSHITER_THRESH**

Controls the convergence criterion of iterative Hirshfeld population analysis.

TYPE:

INTEGER

DEFAULT:

5

OPTIONS:

$N$ Corresponding to the convergence criterion of $N/10000$, in $e$.

RECOMMENDATION:

Use the default, which is the value recommended in Ref. 12

### 10.2.2 Examples

**Example 10.1** The iterative Hirshfeld population analysis for $F^-(H_2O)$

```
$molecule
 -1  1
  O     1.197566    -0.108087     0.000000
  H     1.415397     0.827014     0.000000
  H     0.134830    -0.084378     0.000000
  F    -1.236389     0.012239     0.000000
$end

$rem
   SYM_IGNORE  true
   METHOD      B3LYP
   BASIS       6-31G*
   HIRSHITER   true
$end
```

### 10.2.3 Multipole Moments

This section discusses how to compute arbitrary electrostatic multipole moments for an entire molecule, including both ground- and excited-state electron densities. Occasionally, however, it is useful to decompose the electronic part of the multipole moments into contributions from individual MOs. This decomposition is especially useful for systems containing unpaired electrons[16], where the first-order moments $\langle x\rangle$, $\langle y\rangle$, and $\langle z\rangle$ characterize the centroid (mean position) of the half-filled MO, and the second-order moments determine its radius of gyration, $R_g$, which characterizes the size of the MO. Upon setting PRINT_RADII_GYRE = TRUE, Q-CHEM will print out centroids and radii of gyration for each occupied MO and for the overall electron density. If CIS or TDDFT excited states are requested, then this keyword will also print out the centroids and radii of gyration for each excited-state electron density.

**PRINT_RADII_GYRE**

Controls printing of MO centroids and radii of gyration.

TYPE:

LOGICAL/INTEGER

DEFAULT:

FALSE

OPTIONS:

| | |
|---|---|
| TRUE (or 1) | Print the centroid and radius of gyration for each occupied MO and each density. |
| 2 | Print centroids and radii of gyration for the virtual MOs as well. |
| FALSE (or 0) | Do not calculate these quantities. |

RECOMMENDATION:

None

Q-CHEM can compute Cartesian multipole moments of the charge density to arbitrary order, both for the ground state and for excited states calculated using the CIS or TDDFT methods.

**MULTIPOLE_ORDER**

Determines highest order of multipole moments to print if wave function analysis requested.

TYPE:

INTEGER

DEFAULT:

4

OPTIONS:

| | |
|---|---|
| $n$ | Calculate moments to $n$th order. |

RECOMMENDATION:

Use the default unless higher multipoles are required.

**CIS_MOMENTS**

Controls calculation of excited-state (CIS or TDDFT) multipole moments

TYPE:

LOGICAL

DEFAULT:

FALSE

OPTIONS:

| | |
|---|---|
| FALSE | Do not calculate excited-state moments. |
| TRUE | Calculate moments for each excited state. |

RECOMMENDATION:

Set to TRUE if excited-state moments are desired. (This is a trivial additional calculation.) The MULTIPOLE_ORDER controls how many multipole moments are printed.

### 10.2.4 Symmetry Decomposition

Q-CHEM's default is to write the SCF wave function molecular orbital symmetries and energies to the output file. If requested, a symmetry decomposition of the kinetic and nuclear attraction energies can also be calculated.

**SYMMETRY_DECOMPOSITION**

Determines symmetry decompositions to calculate.

TYPE:

INTEGER

DEFAULT:

1

OPTIONS:

0 No symmetry decomposition.
1 Calculate MO eigenvalues and symmetry (if available).
2 Perform symmetry decomposition of kinetic energy and nuclear attraction matrices.

RECOMMENDATION:

None

### 10.2.5 Localized Orbital Bonding Analysis

Localized Orbital Bonding Analysis (LOBA)[17] is a technique developed by Dr. Alex Thom and Eric Sundstrom at Berkeley with Prof. Martin Head-Gordon. Inspired by the work of Rhee and Head-Gordon[18], it makes use of the fact that the post-SCF localized occupied orbitals of a system provide a large amount of information about the bonding in the system.

While the canonical Molecular Orbitals can provide information about local reactivity and ionization energies, their delocalized nature makes them rather uninformative when looking at the bonding in larger molecules. Localized orbitals in contrast provide a convenient way to visualize and account for electrons. Transformations of the orbitals within the occupied subspace do not alter the resultant density; if a density can be represented as orbitals localized on individual atoms, then those orbitals can be regarded as non-bonding. If a maximally localized set of orbitals still requires some to be delocalized between atoms, these can be regarded as bonding electrons. A simple example is that of $He_2$ versus $H_2$. In the former, the delocalized $\sigma_g$ and $\sigma_u$ canonical orbitals may be transformed into 1s orbitals on each He atom, and there is no bond between them. This is not possible for the $H_2$ molecule, and so we can regard there being a bond between the atoms. In cases of multiple bonding, multiple delocalized orbitals are required.

While there are no absolute definitions of bonding and oxidation state, it has been shown that the localized orbitals match the chemically intuitive notions of core, non-bonded, single- and double-bonded electrons, *etc.* By combining these localized orbitals with population analyses, LOBA allows the nature of the bonding within a molecule to be quickly determined.

In addition, it has been found that by counting localized electrons, the oxidation states of transition metals can be easily found. Owing to polarization caused by ligands, an upper threshold is applied, populations above which are regarded as “localized” on an atom, which has been calibrated to a range of transition metals, recovering standard oxidation states ranging from $-$II to VII.

**LOBA**

Specifies the methods to use for LOBA

TYPE:

INTEGER

DEFAULT:

00

OPTIONS:

$ab$

$a$ specifies the localization method

0 Perform Boys localization.

1 Perform PM localization.

2 Perform ER localization.

$b$ specifies the population analysis method

0 Do not perform LOBA. This is the default.

1 Use Mulliken population analysis.

2 Use Löwdin population analysis.

RECOMMENDATION:

Boys Localization is the fastest. ER will require an auxiliary basis set.
LOBA 12 provides a reasonable speed/accuracy compromise.

**LOBA_THRESH**

Specifies the thresholds to use for LOBA

TYPE:

INTEGER

DEFAULT:

6015

OPTIONS:

$aabb$ $aa$ specifies the threshold to use for localization

$bb$ specifies the threshold to use for occupation

Both are given as percentages.

RECOMMENDATION:

Decrease $bb$ to see the smaller contributions to orbitals. Values of $aa$ between 40 and 75 have been shown to given meaningful results.

On a technical note, LOBA can function of both Restricted and Unrestricted SCF calculations. The figures printed in the bonding analysis count the number of electrons on each atom from that orbital (*i.e.*, up to 1 for Unrestricted or singly occupied Restricted orbitals, and up to 2 for double occupied Restricted.)

### 10.2.6 Basic Excited-State Analysis of CIS and TDDFT Wave Functions

For CIS, TDHF, and TDDFT excited-state calculations, we have already mentioned that Mulliken population analysis of the excited-state electron densities may be requested by setting POP_MULLIKEN = $-1$, and multipole moments of the excited-state densities will be generated if CIS_MOMENTS = TRUE. Another useful decomposition for excited states is to separate the excitation into "particle" and "hole" components, which can then be analyzed separately[19]. To do this, we define a density matrix for the excited electron,

$$\mathbf{D}_{ab}^{\text{elec}} = \sum_i (\mathbf{X}+\mathbf{Y})_{ai}^{\dagger} (\mathbf{X}+\mathbf{Y})_{ib} \tag{10.9}$$

and a density matrix for the hole that is left behind in the occupied space:

$$\mathbf{D}_{ij}^{\text{hole}} = \sum_a (\mathbf{X}+\mathbf{Y})_{ia}(\mathbf{X}+\mathbf{Y})_{aj}^{\dagger} \tag{10.10}$$

The quantities $\mathbf{X}$ and $\mathbf{Y}$ are the transition density matrices, *i.e.*, the components of the TDDFT eigenvector[20]. The indices $i$ and $j$ denote MOs that occupied in the ground state, whereas $a$ and $b$ index virtual MOs. Note also that $\mathbf{D}^{elec} + \mathbf{D}^{hole} = \Delta\mathbf{P}$, the difference between the ground- and excited-state density matrices.

Upon transforming $\mathbf{D}^{\text{elec}}$ and $\mathbf{D}^{\text{hole}}$ into the AO basis, one can write

$$\Delta q = \sum_\mu (\mathbf{D}^{elec}\,\mathbf{S})_{\mu\mu} = -\sum_\mu (\mathbf{D}^{hole}\,\mathbf{S})_{\mu\mu} \tag{10.11}$$

where $\Delta q$ is the total charge that is transferred from the occupied space to the virtual space. For a CIS calculation, or for TDDFT within the Tamm-Dancoff approximation[21], $\Delta q = -1$. For full TDDFT calculations, $\Delta q$ may be slightly different than $-1$.

Comparison of Eq. (10.11) to Eq. (10.3) suggests that the quantities $(\mathbf{D}^{\text{elec}}\,\mathbf{S})$ and $(\mathbf{D}^{\text{hole}}\,\mathbf{S})$ are amenable to population analyses of precisely the same sort used to analyze the ground-state density matrix. In particular, $(\mathbf{D}^{\text{elec}}\,\mathbf{S})_{\mu\mu}$ represents the $\mu$th AO's contribution to the excited electron, while $(\mathbf{D}^{\text{hole}}\,\mathbf{S})_{\mu\mu}$ is a contribution to the hole. The sum of these quantities,

$$\Delta q_\mu = (\mathbf{D}^{\text{elec}}\,\mathbf{S})_{\mu\mu} + (\mathbf{D}^{\text{hole}}\,\mathbf{S})_{\mu\mu} \tag{10.12}$$

represents the contribution to $\Delta q$ arising from the $\mu$th AO. For the particle/hole density matrices, both Mulliken and Löwdin population analyses available, and are requested by setting CIS_MULLIKEN = TRUE.

**CIS_MULLIKEN**

Controls Mulliken and Löwdin population analyses for excited-state particle and hole density matrices.

TYPE:

LOGICAL

DEFAULT:

FALSE

OPTIONS:

FALSE Do not perform particle/hole population analysis.

TRUE Perform both Mulliken and Löwdin analysis of the particle and hole density matrices for each excited state.

RECOMMENDATION:

Set to TRUE if desired. This represents a trivial additional calculation.

Although the excited-state analysis features described in this section require very little computational effort, they are turned off by default, because they can generate a large amount of output, especially if a large number of excited states are requested. They can be turned on individually, or collectively by setting CIS_AMPL_ANAL = TRUE. This collective option also requests the calculation of natural transition orbitals (NTOs), which were introduced in Section 6.12.2. (NTOs can also be requested without excited-state population analysis. Some practical aspects of calculating and visualizing NTOs are discussed below, in Section 10.5.2.)

| Descriptor | Explanation |
|---|---|
| Leading SVs | Largest NTO occupation numbers |
| Sum of SVs (Omega) | $\Omega$, Sum of NTO occupation numbers |
| PR_NTO | NTO participation ratio $\mathrm{PR}_{\mathrm{NTO}}$ |
| Entanglement entropy (S_HE) | $S_{H\|E} = -\sum_i \lambda_i \log_2 \lambda_i$ |
| Nr of entangled states (Z_HE) | $Z_{HE} = 2^{S_{H\|E}}$ |
| Renormalized S_HE/Z_HE | Replace $\lambda_i \to \lambda_i/\Omega$ |
| omega | Norm of the 1TDM $\Omega$, single-exc. character |
| <r_h> [Ang] | Mean position of hole $\langle \vec{x}_h \rangle_{\mathrm{exc}}$ |
| <r_e> [Ang] | Mean position of electron $\langle \vec{x}_e \rangle_{\mathrm{exc}}$ |
| \|<r_e - r_h>\| [Ang] | Linear e/h distance $\vec{d}_{h\to e} = \langle \vec{x}_e - \vec{x}_h \rangle_{\mathrm{exc}}$ |
| Hole size [Ang] | RMS hole size: $\sigma_h = (\langle \vec{x}_h^2 \rangle_{\mathrm{exc}} - \langle \vec{x}_h \rangle_{\mathrm{exc}}^2)^{1/2}$ |
| Electron size [Ang] | RMS elec. size: $\sigma_e = (\langle \vec{x}_e^2 \rangle_{\mathrm{exc}} - \langle \vec{x}_e \rangle_{\mathrm{exc}}^2)^{1/2}$ |
| RMS electron-hole separation [Ang] | $d_{\mathrm{exc}} = (\langle \|\vec{x}_e - \vec{x}_h\|^2 \rangle_{\mathrm{exc}})^{1/2}$ |
| Covariance(r_h, r_e) [Ang^2] | $\mathrm{COV}\,(\vec{x}_h, \vec{x}_e) = \langle \vec{x}_h \cdot \vec{x}_e \rangle_{\mathrm{exc}} - \langle \vec{x}_h \rangle_{\mathrm{exc}} \cdot \langle \vec{x}_e \rangle_{\mathrm{exc}}$ |
| Correlation coefficient | $R_{eh} = \mathrm{COV}\,(\vec{x}_h, \vec{x}_e)\,/\sigma_h \cdot \sigma_e$ |

Table 10.1: Descriptors output by Q-CHEM for transition density matrix analysis.

**CIS_AMPL_ANAL**

Perform additional analysis of CIS and TDDFT excitation amplitudes, including generation of natural transition orbitals, excited-state multipole moments, and Mulliken analysis of the excited state densities and particle/hole density matrices.

TYPE:

LOGICAL

DEFAULT:

FALSE

OPTIONS:

TRUE Perform additional amplitude analysis.

FALSE Do not perform additional analysis.

RECOMMENDATION:

None

### 10.2.7 General Excited-State Analysis

Q-Chem features a new module for extended excited-state analysis, which is interfaced to the ADC, CC/EOM-CC, CIS and TDDFT methods[22–27]. These analyses are based on the state, transition and difference density matrices of the excited states; the theoretical background for such analysis is given in Chapter 6.12.

The transition-density (1TDM) based analyses comprise the construction and export of natural transition orbitals (NTO)[28] and electron and hole densities[23], the evaluation of charge transfer numbers[22], an analysis of exciton multipole moments[25–27], and quantification of electron-hole entanglement[29]. Furthermore, the formation and export of state-averaged NTOs, and the decomposition of the excited states into transitions of state-averaged NTOs are implemented[23]. The difference and/or state densities can be exported themselves, as well as employed to construct and export natural orbitals, natural difference orbitals, and attachment and detachment densities[30]. Furthermore, two measures of unpaired electrons are computed[31]. In addition, a Mulliken or Löwdin population analysis and an exciton analysis can be performed based on the difference/

| Descriptor | Explanation |
|---|---|
| `n_u` | Number of unpaired electrons $n_u = \sum_i \min(n_i, 2 - n_i)$ |
| `n_u,nl` | Number of unpaired electrons $n_{u,nl} = \sum_i n_i^2(2 - n_i)^2$ |
| `PR_NO` | NO participation ratio $\mathrm{PR}_{\mathrm{NO}}$ |
| `p_D` and `p_A` | Promotion number $p_D$ and $p_A$ |
| `PR_D` and `PR_A` | D/A participation ratio $\mathrm{PR}_D$ and $\mathrm{PR}_A$ |
| `<r_h> [Ang]` | Mean position of detachment density $\vec{d}_D$ |
| `<r_e> [Ang]` | Mean position of attachment density $\vec{d}_A$ |
| `\|<r_e - r_h>\| [Ang]` | Linear D/A distance $\vec{d}_{D\to A} = \vec{d}_A - \vec{d}_D$ |
| `Hole size [Ang]` | RMS size of detachment density $\sigma_D$ |
| `Electron size [Ang]` | RMS size of attachment density $\sigma_A$ |

Table 10.2: Descriptors output by Q-CHEM for difference/state density matrix analysis.

state densities. The main descriptors of the various analyses that are printed for each excited state are given in Tables 10.1 and 10.2. For a detailed description with illustrative examples, see Refs. 23 and 24.

To activate any excited-state analysis STATE_ANALYSIS has to be set to TRUE. For individual analyses there is currently only a limited amount of fine grained control. The construction and export of any type of orbitals is controlled by MOLDEN_FORMAT to export the orbitals as MOLDEN files, and NTO_PAIRS which specifies the number of important orbitals to print. Setting MAKE_CUBE_FILES to TRUE triggers the construction and export of densities in "cube file" format[32] (see Section 10.5.4 for details). Activating transition densities in *$plots* will generate cube files for the transition density, the electron density, and the hole density of the respective excited states, while activating state densities or attachment/detachment densities will generate cube files for the state density, the difference density, the attachment density and the detachment density. Setting GUI = 2 will export data to the "`.fchk`" file and switches off the generation of cube files. The population analyses are controlled by POP_MULLIKEN and LOWDIN_POPULATION. Setting the latter to TRUE will enforce Löwdin population analysis to be employed, while by default the Mulliken population analysis is used.

Any MOLDEN or cube files generated by the excited state analyses can be found in the directory `plots` in the job's scratch directory. Their names always start with a unique identifier of the excited state (the exact form of this human readable identifier varies with the excited state method). The names of MOLDEN files are then followed by either `_no.mo`, `_ndo.mo`, or `_nto.mo` depending on the type of orbitals they contain. In case of cube files the state identifier is followed by `_dens`, `_diff`, `_trans`, `_attach`, `_detach`, `_elec`, or `_hole` for state, difference, transition, attachment, detachment, electron, or hole densities, respectively. All cube files have the suffice `.cube`. In unrestricted calculations an additional part is added to the file name before `.cube` which indicates $\alpha$ (`_a`) or $\beta$ (`_b`) spin. The only exception is the state density for which `_tot` or `_sd` are added indicating the total or spin-density parts of the state density.

The `_ctnum_atomic.om` files created in the main directory serve as input for a charge transfer number analysis, as explained, *e.g.*, in Refs. 22,33. These files are processed by the external `TheoDORE` program (`http://theodore-qc.sourceforge.net`) to create electron/hole correlation plots and to compute fragment based descriptors.

## 10.3 Interface to the NBO Package

Q-CHEM incorporates the Natural Bond Orbital package (v. 5.0 and 6.0) for molecular properties and wave function analysis. The NBO 5.0 package is invoked by setting the *$rem* variable NBO to TRUE and is initiated after the SCF wave function is obtained.

**Note:** If switched on for a geometry optimization, the NBO package will only be invoked at the end of the last optimization step.

Users should consult the NBO User's Manual for options and details relating to exploitation of the features offered in this package. The NBO 6.0 package[34,35] can be downloaded by the user from `nbo6.chem.wisc.edu`, and can be invoked by: (a) setting the NBOEXE environment variable, and (b) include both NBO = TRUE and RUN_NBO6 = TRUE in the Q-CHEM input file.

NBO analysis is also available for excited states calculated using CIS or TDDFT. Excited-state NBO analysis is still in its infancy, and users should be aware that the convergence of the NBO search procedure may be less well-behaved for excited states than it is for ground states, and may require specification of additional NBO parameters in the *$nbo* section that is described below. Consult Ref. 36 for details and suggestions.

**NBO**
Controls the use of the NBO package.
TYPE:
INTEGER
DEFAULT:
0
OPTIONS:
0 Do not invoke the NBO package.
1 Do invoke the NBO package, for the ground state.
2 Invoke the NBO package for the ground state, and also each CIS, RPA, or TDDFT excited state.
RECOMMENDATION:
None

The general format for passing options from Q-CHEM to the NBO program is shown below:

```
$nbo
   {NBO program keywords, parameters and options}
$end
```

**Note:** (1) *$rem* variable NBO must be set to TRUE before the *$nbo* keyword is recognized.
(2) Q-CHEM does not support facets of the NBO package which require multiple job runs

## 10.4 Orbital Localization

The concept of localized orbitals has already been visited in this manual in the context of perfect-pairing and methods. As the SCF energy is independent of the partitioning of the electron density into orbitals, there is considerable flexibility as to how this may be done. The canonical picture, where the orbitals are eigenfunctions of the Fock operator is useful in determining reactivity, for, through Koopmans' theorem, the orbital energy eigenvalues give information about the corresponding ionization energies and electron affinities. As a consequence, the HOMO and LUMO are very informative as to the reactive sites of a molecule. In addition, in small molecules, the canonical orbitals lead us to the chemical description of $\sigma$ and $\pi$ bonds.

In large molecules, however, the canonical orbitals are often very delocalized, and so information about chemical bonding is not readily available from them. Here, orbital localization techniques can be of great value in visualizing the bonding, as localized orbitals often correspond to the chemically intuitive orbitals which might be expected.

Q-CHEM has three post-SCF localization methods available. These can be performed separately over both occupied and virtual spaces. The localization scheme attributed to Boys[37,38] minimizes the radial extent of the localized orbitals, *i.e.*, $\sum_i \langle ii||\mathbf{r}_1 - \mathbf{r}_2|^2|ii\rangle$, and although is relatively fast, does not separate $\sigma$ and $\pi$ orbitals, leading to two 'banana-orbitals' in the case of a double bond[39]. Pipek-Mezey localized orbitals[39] maximize the locality of Mulliken populations, and are of a similar cost to Boys localized orbitals, but maintain $\sigma - \pi$ separation. Edmiston-Ruedenberg localized orbitals[40] maximize the self-repulsion of the orbitals, $\sum_i \langle ii|\frac{1}{r}|ii\rangle$. This is more computationally expensive to calculate as it requires a two-electron property to be evaluated, but the work of Dr. Joe Subotnik[41] and later Prof. Young-Min Rhee and Westin Kurlancheek with Prof. Martin Head-Gordon at Berkeley has, through use of the Resolution of the Identity approximation, reduced the formal cost may be asymptotically reduced to cubic scaling with the number of occupied orbitals.

**BOYSCALC**

Specifies the Boys localized orbitals are to be calculated

TYPE:

INTEGER

DEFAULT:

0

OPTIONS:

0 Do not perform localize the occupied space.
1 Allow core-valence mixing in Boys localization.
2 Localize core and valence separately.

RECOMMENDATION:

None

**ERCALC**

Specifies the Edmiston-Ruedenberg localized orbitals are to be calculated

TYPE:

INTEGER

DEFAULT:

06000

OPTIONS:

$aabcd$

$aa$ specifies the convergence threshold.
If $aa > 3$, the threshold is set to $10^{-aa}$. The default is 6.
If $aa = 1$, the calculation is aborted after the guess, allowing Pipek-Mezey orbitals to be extracted.

$b$ specifies the guess:
0 Boys localized orbitals. This is the default
1 Pipek-Mezey localized orbitals.

$c$ specifies restart options (if restarting from an ER calculation):
0 No restart. This is the default
1 Read in MOs from last ER calculation.
2 Read in MOs and RI integrals from last ER calculation.

$d$ specifies how to treat core orbitals
0 Do not perform ER localization. This is the default.
1 Localize core and valence together.
2 Do separate localizations on core and valence.
3 Localize only the valence electrons.
4 Use the *$localize* section.

RECOMMENDATION:

ERCALC 1 will usually suffice, which uses threshold $10^{-6}$.

The *$localize* section may be used to specify orbitals subject to ER localization if require. It contains a list of the orbitals to include in the localization. These may span multiple lines. If the user wishes to specify separate beta orbitals to localize, include a zero before listing the beta orbitals, which acts as a separator, *e.g.*,

```
$localize
2 3 4 0
2 3 4 5 6
$end
```

## 10.5 Visualizing and Plotting Orbitals and Densities

The free, open-source visualization program IQMOL (`www.iqmol.org`) provides a graphical user interface for Q-CHEM that can be used as a molecular structure builder, as a tool for local or remote submission of Q-CHEM jobs, and as a visualization tool for densities and molecular orbitals. Alternatively, Q-CHEM can generate orbital and density data in formats suitable for plotting with various third-party visualization programs.

### 10.5.1 Visualizing Orbitals Using MOLDEN and MACMOLPLT

Upon request, Q-CHEM will generate an input file for MOLDEN, a freely-available molecular visualization program[42,43]. MOLDEN can be used to view ball-and-stick molecular models (including stepwise visualization of a geometry optimization), molecular orbitals, vibrational normal modes, and vibrational spectra. MOLDEN also contains a powerful $Z$-matrix editor. In conjunction with Q-CHEM, orbital visualization via MOLDEN is currently supported for $s$, $p$, and $d$ functions (pure or Cartesian), as well as pure $f$ functions. Upon setting MOLDEN_FORMAT to TRUE, Q-CHEM will append a MOLDEN-formatted input file to the end of the Q-CHEM log file. As some versions of MOLDEN have difficulty parsing the Q-CHEM log file itself, we recommend that the user cut and paste the MOLDEN-formatted part of the Q-CHEM log file into a separate file to be read by MOLDEN.

**MOLDEN_FORMAT**

Requests a MOLDEN-formatted input file containing information from a Q-CHEM job.

TYPE:

LOGICAL

DEFAULT:

FALSE

OPTIONS:

TRUE Append MOLDEN input file at the end of the Q-CHEM output file.

RECOMMENDATION:

None.

MOLDEN-formatted files can also be read by MACMOLPLT, another freely-available visualization program[44,45]. MACMOLPLT generates orbital iso-contour surfaces much more rapidly than MOLDEN, however, within MACMOLPLT these surfaces are only available for Cartesian Gaussian basis functions, *i.e.*, PURECART = 2222, which may not be the default.

**Example 10.2** Generating a MOLDEN file for molecular orbital visualization.

```
$molecule
   0 1
   O
   H  1  0.95
   H  1  0.95  2  104.5
$end

$rem
   METHOD           hf
   BASIS            cc-pvtz
   PRINT_ORBITALS   true (default is to print 5 virtual orbitals)
   MOLDEN_FORMAT    true
$end
```

For geometry optimizations and vibrational frequency calculations, one need only set MOLDEN_FORMAT to TRUE, and the relevant geometry or normal mode information will automatically appear in the MOLDEN section of the Q-CHEM log file.

**Example 10.3** Generating a MOLDEN file to step through a geometry optimization.

```
$molecule
```

```
   0  1
   O
   H  1  0.95
   H  1  0.95  2  104.5
$end

$rem
   JOBTYPE         opt
   METHOD          hf
   BASIS           6-31G*
   MOLDEN_FORMAT   true
$end
```

### 10.5.2 Visualization of Natural Transition Orbitals

For excited states calculated using the CIS, RPA, or TDDFT methods, construction of Natural Transition Orbitals (NTOs), as described in Section 6.12.2, is requested using the *$rem* variable NTO_PAIRS. This variable also determines the number of hole/particle NTO pairs that are output for each excited state. Although the total number of hole/particle pairs is equal to the number of occupied MOs, typically only a very small number of these pairs (often just one pair) have significant amplitudes. (Additional large-amplitude NTOs may be encountered in cases of strong electronic coupling between multiple chromophores[46].)

**NTO_PAIRS**

Controls the writing of hole/particle NTO pairs for excited state.

TYPE:

INTEGER

DEFAULT:

0

OPTIONS:

$N$ Write $N$ NTO pairs per excited state.

RECOMMENDATION:

If activated ($N > 0$), a minimum of two NTO pairs will be printed for each state. Increase the value of $N$ if additional NTOs are desired.

When NTO_PAIRS $> 0$, Q-CHEM will generate the NTOs in MOLDEN format. The NTOs are state-specific, in the sense that each excited state has its own NTOs, and therefore a separate MOLDEN file is required for each excited state. These files are written to the job's scratch directory, in a sub-directory called *NTOs*, so to obtain the NTOs the scratch directory must be saved using the *–save* option that is described in Section 2.7. The output files in the *NTOs* directory have an obvious file-naming convention. The "hole" NTOs (which are linear combinations of the occupied MOs) are printed to the MOLDEN files in order of increasing importance, with the corresponding excitation amplitudes replacing the canonical MO eigenvalues. (This is a formatting convention only; the excitation amplitudes are unrelated to the MO eigenvalues.) Following the holes are the "particle" NTOs, which represent the excited electron and are linear combinations of the virtual MOs. These are written in order of decreasing amplitude. To aid in distinguishing the two sets within the MOLDEN files, the amplitudes of the holes are listed with negative signs, while the corresponding NTO for the excited electron has the same amplitude with a positive sign.

Due to the manner in which the NTOs are constructed (see Section 6.12.2), NTO analysis is available only when the number of virtual orbitals exceeds the number of occupied orbitals, which may not be the case for minimal basis sets.

**Example 10.4** Generating MOLDEN-formatted natural transition orbitals for several excited states of uracil.

```
$molecule
   0 1
   N    -2.181263     0.068208     0.000000
   C    -2.927088    -1.059037     0.000000
   N    -4.320029    -0.911094     0.000000
   C    -4.926706     0.301204     0.000000
   C    -4.185901     1.435062     0.000000
   C    -2.754591     1.274555     0.000000
   N    -1.954845     2.338369     0.000000
   H    -0.923072     2.224557     0.000000
   H    -2.343008     3.268581     0.000000
   H    -4.649401     2.414197     0.000000
   H    -6.012020     0.301371     0.000000
   H    -4.855603    -1.768832     0.000000
   O    -2.458932    -2.200499     0.000000
$end

$rem
   METHOD          B3LYP
   BASIS           6-31+G*
   CIS_N_ROOTS     3
   NTO_PAIRS       2
$end
```

### 10.5.3 Generation of Volumetric Data Using *$plots*

The simplest way to visualize the charge densities and molecular orbitals that Q-CHEM evaluates is via a graphical user interface, such as those described in the preceding section. An alternative procedure, which is often useful for generating high-quality images for publication, is to evaluate certain densities and orbitals on a user-specified grid of points. This is accomplished by invoking the *$plots* option, which is itself enabled by requesting IANLTY = 200.

The format of the *$plots* input is documented below. It permits plotting of molecular orbitals, the SCF ground-state density, and excited-state densities obtained from CIS, RPA or TDDFT/TDA, or TDDFT calculations. Also in connection with excited states, either transition densities, attachment/detachment densities, or natural transition orbitals (at the same levels of theory given above) can be plotted as well.

By default, the output from the *$plots* command is one (or several) ASCII files in the working directory, named *plot.mo*, *etc.*. The results then must be visualized with a third-party program capable of making 3-D plots. (Some suggestions are given in Section 10.5.4.)

An example of the use of the *$plots* option is the following input deck:

**Example 10.5** A job that evaluates the $H_2$ HOMO and LUMO on a $1 \times 1 \times 15$ grid, along the bond axis. The plotting output is in an ASCII file called *plot.mo*, which lists for each grid point, $x$, $y$, $z$, and the value of each requested MO.

```
$molecule
   0  1
   H   0.0   0.0   0.35
   H   0.0   0.0  -0.35
$end

$rem
   METHOD     hf
   BASIS      6-31g**
   IANLTY     200
$end

$plots
   Plot the HOMO and the LUMO on a line
   1   0.0   0.0
   1   0.0   0.0
  15  -3.0   3.0
   2   0   0   0
   1   2
$end
```

General format for the *$plots* section of the Q-CHEM input deck.

*$plots*

One comment line

Specification of the 3-D mesh of points on 3 lines:

$N_x \quad x_{\min} \quad x_{\max}$

$N_y \quad y_{\min} \quad y_{\max}$

$N_z \quad z_{\min} \quad z_{\max}$

A line with 4 integers indicating how many things to plot:

$N_{\rm MO} \quad N_{\rm Rho} \quad N_{\rm Trans} \quad N_{\rm DA}$

An optional line with the integer list of MO's to evaluate (only if $N_{\rm MO} > 0$)

MO(1) MO(2) . . . MO($N_{\rm MO}$)

An optional line with the integer list of densities to evaluate (only if $N_{\rm Rho} > 0$)

Rho(1) Rho(2) . . . Rho($N_{\rm Rho}$)

An optional line with the integer list of transition densities (only if $N_{\rm Trans} > 0$)

Trans(1) Trans(2) . . . Trans($N_{\rm Trans}$)

An optional line with states for detachment/attachment densities (if $N_{\rm DA} > 0$)

DA(1) DA(2) . . . DA($N_{\rm DA}$)

*$end*

Line 1 of the *$plots* keyword section is reserved for comments. Lines 2–4 list the number of one dimension points and the range of the grid (note that coordinate ranges are in Ångstroms, while all output is in atomic units). Line 5 must contain 4 non-negative integers indicating the number of: molecular orbitals ($N_{\rm MO}$), electron densities ($N_{\rm Rho}$), transition densities and attach/detach densities ($N_{\rm DA}$), to have mesh values calculated.

The final lines specify which MOs, electron densities, transition densities and CIS attach/detach states are to be plotted (the line can be left blank, or removed, if the number of items to plot is zero). Molecular orbitals are numbered $1 \ldots N_\alpha, N_\alpha + 1 \ldots N_\alpha + N_\beta$; electron densities numbered where 0= ground state, 1 = first excited state, 2 = second excited state, *etc.*; and attach/detach specified from state $1 \rightarrow N_{\rm DA}$.

By default, all output data are printed to files in the working directory, overwriting any existing file of the same name.

- Molecular orbital data is printed to a file called *plot.mo*;
- Densities are plotted to *plots.hf*;
- Restricted unrelaxed attachment/detachment analysis is sent to *plot.attach.alpha* and *plot.detach.alpha*;
- Unrestricted unrelaxed attachment/detachment analysis is sent to *plot.attach.alpha*, *plot.detach.alpha*, *plot.attach.beta* and *plot.detach.beta*;
- Restricted relaxed attachments/detachment analysis is plotted in *plot.attach.rlx.alpha* and *plot.detach.rlx.alpha*; and finally
- Unrestricted relaxed attachment/detachment analysis is sent to *plot.attach.rlx.alpha*, *plot.detach.rlx.alpha*, *plot.attach.rlx.beta* and *plot.detach.rlx.beta*.

Output is printed in atomic units, with coordinates first followed by item value, as shown below:

```
x1   y1   z1      a1   a2  ...  aN
x2   y1   z1      b1   b2  ...  bN
...
```

Instead of a standard one-, two-, or three-dimensional Cartesian grid, a user may wish to plot orbitals or densities on a set of grid points of his or her choosing. Such points are specified using a *$grid* input section whose format is simply the Cartesian coordinates of all user-specified grid points:

```
x1   y1   z1
x2   y2   z2
...
```

The *$plots* section must still be specified as described above, but if the *$grid* input section is present, then these user-specified grid points will override the ones specified in the *$plots* section.

The Q-CHEM *$plots* utility allows the user to plot transition densities and detachment/attachment densities directly from amplitudes saved from a previous calculation, without having to solve the post-SCF (CIS, RPA, TDA, or TDDFT) equations again. To take advantage of this feature, the same Q-CHEM scratch directory must be used, and the SKIP_CIS_RPA *$rem* variable must be set to TRUE. To further reduce computational time, the SCF_GUESS *$rem* can be set to READ.

**SKIP_CIS_RPA**
Skips the solution of the CIS, RPA, TDA or TDDFT equations for wave function analysis.
TYPE:
LOGICAL
DEFAULT:
FALSE
OPTIONS:
TRUE / FALSE
RECOMMENDATION:
Set to true to speed up the generation of plot data if the same calculation has been run previously with the scratch files saved.

### 10.5.4 Direct Generation of “Cube” Files

As an alternative to the output format discussed above, all of the *$plots* data may be output directly to a sub-directory named *plots* in the job's scratch directory, which must therefore be saved using the –*save* option described in Section 2.7. The plotting data in this sub-directory are not written in the *plot.** format described above, but rather in the form of so-called “cube” file, one for each orbital or density that is requested. The cube file format is a standard one for volumetric data and consists of a small header followed by the orbital or density values at each grid point, in ASCII format. (Consult Ref. 32 for the complete format specification.) Because the grid coordinates themselves are not printed (their locations are implicit from information contained in the header), each individual cube file is much smaller than the corresponding *plot.** file would be. Cube files can be read by many standard (and freely-available) graphics programs, including MacMolPlt[44,45] and VMD[47,48]. VMD, in particular, is recommended for generation of high-quality images for publication. Cube files for the MOs and densities requested in the *$plots* section are requested by setting MAKE_CUBE_FILES to TRUE, with the *$plots* section specified as described in Section 10.5.3.

**MAKE_CUBE_FILES**
Requests generation of cube files for MOs, NTOs, or NBOs.
TYPE:
LOGICAL/STRING
DEFAULT:
FALSE
OPTIONS:
FALSE Do not generate cube files.
TRUE Generate cube files for MOs and densities.
NTOS Generate cube files for NTOs.
NBOS Generate cube files for NBOs.
RECOMMENDATION:
None

**PLOT_SPIN_DENSITY**
Requests the generation of spin densities, $\rho_\alpha$ and $\rho_\beta$.
TYPE:
LOGICAL
DEFAULT:
FALSE
OPTIONS:
FALSE Do not generate spin density cube files.
TRUE Generate spin density cube files.
RECOMMENDATION:
Set to TRUE if spin densities are desired in addition to total densities. Requires that MAKE_CUBE_FILES be set to TRUE as well, and that one or more total densities is requested in the *$plots* input section. The corresponding spin densities will then be generated also.

The following example illustrates the generation of cube files for a ground and an excited-state density, including the corresponding spin densities. In this example, the *plots* sub-directory of the job's scratch directory should contain files named `dens.N.cube` (total density for state $N$, where $N = 0$ or 1 represents the ground and first excited state, respectively), `dens_alpha.N.cube` and `dens_beta.N.cube` ($\rho_\alpha$ and $\rho_\beta$ for each state), and `dens_spin.N.cube` ($\rho_\alpha - \rho_\beta$ for each state.)

**Example 10.6** Generating density and spin-density cube files for the ground and first excited state of the HOO radical.

```
$molecule
   0 2
   H     1.004123   -0.180454    0.000000
   O    -0.246002    0.596152    0.000000
   O    -1.312366   -0.230256    0.000000
$end

$rem
   PLOT_SPIN_DENSITY  true
   MAKE_CUBE_FILES    true
   SCF_CONVERGENCE    8
   METHOD             b3lyp
   BASIS              6-31+G*
   CIS_N_ROOTS        1
$end

$plots
grid information and request to plot 2 densities
   20  -5.0  5.0
   20  -5.0  5.0
   20  -5.0  5.0
   0  2  0  0
   0  1
$end
```

Cube files are also available for natural transition orbitals (Sections 6.12.2 and 10.5.2) by setting MAKE_CUBE_FILES to NTOS, although in this case the procedure is somewhat more complicated, due to the state-specific nature of these quantities. Cube files for the NTOs are generated only for a single excited state, whose identity is specified using CUBEFILE_STATE. Cube files for additional states are readily obtained using a sequence of Q-CHEM jobs, in which the second (and subsequent) jobs read in the converged ground- and excited-state information using SCF_GUESS and SKIP_CIS_RPA.

**CUBEFILE_STATE**
Determines which excited state is used to generate cube files
TYPE:
INTEGER
DEFAULT:
None
OPTIONS:
$n$ Generate cube files for the $n$th excited state
RECOMMENDATION:
None

An additional complication is the manner in which to specify which NTOs will be output as cube files. When MAKE_CUBE_FILES is set to TRUE, this is specified in the *$plots* section, in the same way that MOs would be specified for plotting. However, one must understand the order in which the NTOs are stored.

For a system with $N_\alpha$ $\alpha$-spin MOs, the occupied NTOs $1, 2, \ldots, N_\alpha$ are stored in order of increasing amplitudes, so that the $N_\alpha$'th occupied NTO is the most important. The virtual NTOs are stored next, in order of *decreasing* importance. According to this convention, the highest occupied NTO (HONTO) $\rightarrow$ lowest unoccupied NTO (LUNTO) excitation amplitude is always the most significant, for any particular excited state. Thus, orbitals $N_\alpha$ and $N_\alpha + 1$ represent the most important NTO pair, while orbitals $N_\alpha - 1$ and $N_\alpha + 2$ represent the second most important NTO pair, *etc.*.

**Example 10.7** Generating cube files for the HONTO-to-LUNTO excitation of the second singlet excited state of uracil. Note that $N_\alpha = 29$ for uracil.

```
$molecule
   0 1
   N    -2.181263     0.068208     0.000000
   C    -2.927088    -1.059037     0.000000
   N    -4.320029    -0.911094     0.000000
   C    -4.926706     0.301204     0.000000
   C    -4.185901     1.435062     0.000000
   C    -2.754591     1.274555     0.000000
   N    -1.954845     2.338369     0.000000
   H    -0.923072     2.224557     0.000000
   H    -2.343008     3.268581     0.000000
   H    -4.649401     2.414197     0.000000
   H    -6.012020     0.301371     0.000000
   H    -4.855603    -1.768832     0.000000
   O    -2.458932    -2.200499     0.000000
$end

$plots
Plot the dominant NTO pair, N --> N+1
   25  -5.0  5.0
   25  -5.0  5.0
   25  -5.0  5.0
   2  0  0  0
   29  30
$end

$rem
   METHOD           B3LYP
   BASIS            6-31+G*
   CIS_N_ROOTS      2
   CIS_TRIPLETS     FALSE
   NTO_PAIRS        TRUE    ! calculate the NTOs
   MAKE_CUBE_FILES  NTOS    ! generate NTO cube files...
   CUBEFILE_STATE   2       ! ...for the 2nd excited state
$end
```

Cube files for Natural Bond Orbitals (for either the ground state or any CIS, RPA, of TDDFT excited states) can be generated in much the same way, by setting MAKE_CUBE_FILES equal to NBOS, and using CUBEFILE_STATE to select the desired electronic state. CUBEFILE_STATE = 0 selects ground-state NBOs. The particular NBOs to be plotted are selected using the *$plots* section, recognizing that Q-CHEM stores the NBOs in order of decreasing occupancies, with all $\alpha$-spin NBOs preceding any $\beta$-spin NBOs, in the case of an unrestricted SCF calculation. (For ground states, there is typically one strongly-occupied NBO for each electron.) NBO cube files are saved to the *plots* sub-directory of the job's scratch directory. One final caveat: to get NBO cube files, the user must specify the AONBO option in the *$nbo* section, as shown in the following example.

**Example 10.8** Generating cube files for the NBOs of the first excited state of $H_2O$.

```
$rem
   METHOD           CIS
   BASIS            CC-PVTZ
   CIS_N_ROOTS      1
   CIS_TRIPLETS     FALSE
   NBO              2       ! ground- and excited-state NBO
   MAKE_CUBE_FILES  NBOS    ! generate NBO cube files...
   CUBEFILE_STATE   1       ! ...for the first excited state
$end

$nbo
  AONBO
$end

$molecule
   0 1
   O
   H  1  0.95
   H  1  0.95  2  104.5
$end

$plots
Plot the 5 high-occupancy NBOs, one for each alpha electron
   40  -8.0  8.0
   40  -8.0  8.0
   40  -8.0  8.0
   5  0  0  0
   1  2  3  4  5
$end
```

### 10.5.5 NCI Plots

We have implemented the non-covalent interaction (NCI) plots from Weitao Yang's group[49,50]. To generate these plots, one can set the PLOT_REDUCED_DENSITY_GRAD *$rem* variable to TRUE (see the nci-c8h14.in input example in *$QC/samples* directory).

## 10.6 Electrostatic Potentials

Q-CHEM can evaluate electrostatic potentials on a grid of points. Electrostatic potential evaluation is controlled by the *$rem* variable IGDESP, as documented below.

**IGDESP**

Controls evaluation of the electrostatic potential on a grid of points. If enabled, the output is in an ASCII file, *plot.esp*, in the format $x, y, z$, esp for each point.

TYPE:

INTEGER

DEFAULT:

none no electrostatic potential evaluation

OPTIONS:

| | |
|---|---|
| $-2$ | same as the option '-1', plus evaluate the ESP of $external_charges$ |
| $-1$ | read grid input via the *$plots* section of the input deck |
| 0 | Generate the ESP values at all nuclear positions |
| +$n$ | read $n$ grid points **in bohr** from the ASCII file *ESPGrid* |

RECOMMENDATION:

None

The following example illustrates the evaluation of electrostatic potentials on a grid, note that IANLTY must also be set to 200.

**Example 10.9** A job that evaluates the electrostatic potential for $H_2$ on a 1 by 1 by 15 grid, along the bond axis. The output is in an ASCII file called *plot.esp*, which lists for each grid point, $x$, $y$, $z$, and the electrostatic potential.

```
$molecule
   0  1
   H   0.0   0.0   0.35
   H   0.0   0.0  -0.35
$end

$rem
   METHOD     hf
   BASIS      6-31g**
   IANLTY     200
   IGDESP     -1
$end

$plots
   plot the HOMO and the LUMO on a line
   1   0.0   0.0
   1   0.0   0.0
  15  -3.0   3.0
   0  0  0  0
   0
$end
```

We can also compute the electrostatic potential for the transition density, which can be used, for example, to compute the Coulomb coupling in excitation energy transfer.

**ESP_TRANS**

Controls the calculation of the electrostatic potential of the transition density

TYPE:

LOGICAL

DEFAULT:

FALSE

OPTIONS:

| | |
|---|---|
| TRUE | compute the electrostatic potential of the excited state transition density |
| FALSE | compute the electrostatic potential of the excited state electronic density |

RECOMMENDATION:

NONE

The electrostatic potential is a complicated object and it is not uncommon to model it using a simplified representation based on atomic charges. For this purpose it is well known that Mulliken charges perform very poorly. Several definitions of ESP-derived atomic charges have been given in the literature, however, most of them rely on a least-squares fitting of the ESP evaluated on a selection of grid points. Although these grid points are usually chosen so that the ESP is well modeled in the "chemically important" region, it still remains that the calculated charges will change if the molecule is rotated. Recently an efficient rotationally invariant algorithm was proposed[51] that sought to model the ESP not by direct fitting, but by fitting to the multipole moments. By doing so it was found that the fit to the ESP was superior to methods that relied on direct fitting of the ESP. The calculation requires the traceless form of the multipole moments and these are also printed out during the course of the calculations. To request these multipole-derived charges the following *$rem* option should be set:

**MM_CHARGES**

Requests the calculation of multipole-derived charges (MDCs).

TYPE:

LOGICAL

DEFAULT:

FALSE

OPTIONS:

| | |
|---|---|
| TRUE | Calculates the MDCs and also the traceless form of the multipole moments |

RECOMMENDATION:

Set to TRUE if MDCs or the traceless form of the multipole moments are desired. The calculation does not take long.

## 10.7 Spin and Charge Densities at the Nuclei

Gaussian basis sets violate nuclear cusp conditions[52–54]. This may lead to large errors in wave function at nuclei, particularly for spin density calculations[55]. This problem can be alleviated by using an averaging operator that compute wave function density based on constraints that wave function must satisfy near Coulomb singularity[56,57]. The derivation of operators is based on hyper virial theorem[58] and presented in Ref. 56. Application to molecular spin densities for spin-polarized[57] and DFT[59] wave functions show considerable improvement over traditional delta function operator.

One of the simplest forms of such operators is based on the Gaussian weight function $\exp[-(Z/r_0)^2(\mathbf{r}-\mathbf{R})^2]$ that samples the vicinity of a nucleus of charge $Z$ located at $\mathbf{R}$. The parameter $r_0$ has to be small enough to neglect two-electron contributions of the order $\mathcal{O}(r_0^4)$ but large enough for meaningful averaging. The range of values between 0.15–0.3 a.u. has been shown to be adequate, with final answer being relatively insensitive to the exact choice of $r_0$[56,57]. The value of $r_0$ is chosen by RC_R0 keyword in the units of 0.001 a.u. The averaging operators are implemented for single determinant Hartree-Fock and DFT, and correlated SSG wave functions. Spin and charge densities are printed for all nuclei in a molecule, including ghost atoms.

**RC_R0**

Determines the parameter in the Gaussian weight function used to smooth the density at the nuclei.

TYPE:

INTEGER

DEFAULT:

0

OPTIONS:

0 Corresponds the traditional delta function spin and charge densities

$n$ corresponding to $n \times 10^{-3}$ a.u.

RECOMMENDATION:

We recommend value of 250 for a typical spit valence basis. For basis sets with increased flexibility in the nuclear vicinity the smaller values of $r_0$ also yield adequate spin density.

## 10.8 Atoms in Molecules

Q-CHEM can output a file suitable for analysis with the Atoms in Molecules package (AIMPAC). The source for AIMPAC can be freely downloaded from the web site:

```
http://www.chemistry.mcmaster.ca/aimpac/imagemap/imagemap.htm
```

Users should check this site for further information about installing and running AIMPAC. The AIMPAC input file is created by specifying a filename for the WRITE_WFN *$rem*.

**WRITE_WFN**

Specifies whether or not a wfn file is created, which is suitable for use with AIMPAC. Note that the output to this file is currently limited to $f$ orbitals, which is the highest angular momentum implemented in AIMPAC.

TYPE:

STRING

DEFAULT:

(NULL) No output file is created.

OPTIONS:

*filename* Specifies the output file name. The suffix *.wfn* will be appended to this name.

RECOMMENDATION:

None

## 10.9 Distributed Multipole Analysis

Distributed Multipole Analysis (DMA)[60,61] is a method to represent the electrostatic potential of a molecule in terms of a multipole expansion around a set of points. The *GDMA* code[62] by Prof. Anthony Stone can be used to perform DMA analysis after Q-CHEM calculations. The *GDMA* program works with formatted checkpoint files (.fchk) produced by Q-CHEM. For further information consult the documentation for the *GDMA* package[62].

## 10.10 Intracules

The many dimensions of electronic wave functions makes them difficult to analyze and interpret. It is often convenient to reduce this large number of dimensions, yielding simpler functions that can more readily provide chemical insight. The most familiar of these is the one-electron density $\rho(\mathbf{r})$, which gives the probability of an electron being found at the point $\mathbf{r}$. Analogously, the one-electron momentum density $\pi(\mathbf{p})$ gives the probability that an electron will have a momentum of $\mathbf{p}$. However, the wave function is reduced to the one-electron density much information is lost. In particular, it is often desirable to retain explicit two-electron information. Intracules are two-electron distribution functions and provide information about the *relative* position and momentum of electrons. A detailed account of the different type of intracules can be found in Ref. 63. Q-CHEM's intracule package was developed by Aaron Lee and Nick Besley, and can compute the following intracules for or HF wave functions:

- Position intracules, $P(u)$: describes the probability of finding two electrons separated by a distance $u$.
- Momentum intracules, $M(v)$: describes the probability of finding two electrons with relative momentum $v$.
- Wigner intracule, $W(u,v)$: describes the combined probability of finding two electrons separated by $u$ *and* with relative momentum $v$.

### 10.10.1 Position Intracules

The intracule density, $I(\mathbf{u})$, represents the probability for the inter-electronic vector $\mathbf{u} = \mathbf{u}_1 - \mathbf{u}_2$:

$$I(\mathbf{u}) = \int \rho(\mathbf{r}_1\mathbf{r}_2)\ \delta(\mathbf{r}_{12} - \mathbf{u})\ d\mathbf{r}_1\, \mathbf{dr}_2 \tag{10.13}$$

where $\rho(\mathbf{r}_1, \mathbf{r}_2)$ is the two-electron density. A simpler quantity is the spherically averaged intracule density,

$$P(u) = \int I(\mathbf{u}) \mathrm{d}\Omega_{\mathbf{u}}\ , \tag{10.14}$$

where $\Omega_{\mathbf{u}}$ is the angular part of $\mathbf{v}$, measures the probability that two electrons are separated by a scalar distance $u = |\mathbf{u}|$. This intracule is called a position intracule[63]. If the molecular orbitals are expanded within a basis set

$$\psi_a(\mathbf{r}) = \sum_{\mu} c_{\mu a} \phi_{\mu}(\mathbf{r}) \tag{10.15}$$

The quantity $P(u)$ can be expressed as

$$P(u) = \sum_{\mu\nu\lambda\sigma} \Gamma_{\mu\nu\lambda\sigma}(\mu\nu\lambda\sigma)_{\rm P} \tag{10.16}$$

where $\Gamma_{\mu\nu\lambda\sigma}$ is the two-particle density matrix and $(\mu\nu\lambda\sigma)_{\rm P}$ is the position integral

$$(\mu\nu\lambda\sigma)_{\rm P} = \int \phi_\mu^*(\mathbf{r})\ \phi_\nu(\mathbf{r})\ \phi_\lambda^*(\mathbf{r}+\mathbf{u})\phi_\sigma(\mathbf{r}+\mathbf{u})\ d\mathbf{r}\ d\Omega \tag{10.17}$$

and $\phi_\mu(\mathbf{r})$, $\phi_\nu(\mathbf{r})$, $\phi_\lambda(\mathbf{r})$ and $\phi_\sigma(\mathbf{r})$ are basis functions. For HF wave functions, the position intracule can be decomposed into a Coulomb component,

$$P_{\rm J}(u) = \frac{1}{2}\sum_{\mu\nu\lambda\sigma} D_{\mu\nu}D_{\lambda\sigma}(\mu\nu\lambda\sigma)_{\rm P} \tag{10.18}$$

and an exchange component,

$$P_{\rm K}(u) = -\frac{1}{2}\sum_{\mu\nu\lambda\sigma}\left[D^\alpha_{\mu\lambda}D^\alpha_{\nu\sigma} + D^\beta_{\mu\lambda}D^\beta_{\nu\sigma}\right](\mu\nu\lambda\sigma)_{\rm P} \tag{10.19}$$

where $D_{\mu\nu}$ *etc.* are density matrix elements. The evaluation of $P(u)$, $P_{\rm J}(u)$ and $P_{\rm K}(u)$ within Q-CHEM has been described in detail in Ref. 64.

Some of the moments of $P(u)$ are physically significant[65], for example

$$\int_0^\infty u^0 P(u)du = \frac{n(n-1)}{2} \tag{10.20}$$

$$\int_0^\infty u^0 P_{\rm J}(u)du = \frac{n^2}{2} \tag{10.21}$$

$$\int_0^\infty u^2 P_{\rm J}(u)du = nQ - \mu^2 \tag{10.22}$$

$$\int_0^\infty u^0 P_{\rm K}(u)du = -\frac{n}{2} \tag{10.23}$$

where $n$ is the number of electrons and, $\mu$ is the electronic dipole moment and $Q$ is the trace of the electronic quadrupole moment tensor. Q-CHEM can compute both moments and derivatives of position intracules.

### 10.10.2 Momentum Intracules

Analogous quantities can be defined in momentum space; $\bar{I}(\mathbf{v})$, for example, represents the probability density for the relative momentum $\mathbf{v} = \mathbf{p}_1 - \mathbf{p}_2$:

$$\bar{I}(\mathbf{v}) = \int \pi(\mathbf{p}_1, \mathbf{p}_2)\ \delta(\mathbf{p}_{12} - \mathbf{v})d\mathbf{p}_1 d\mathbf{p}_2 \tag{10.24}$$

where $\pi(\mathbf{p}_1, \mathbf{p}_2)$ momentum two-electron density. Similarly, the spherically averaged intracule

$$M(v) = \int \bar{I}(\mathbf{v})\mathrm{d}\Omega_{\mathbf{v}} \tag{10.25}$$

where $\Omega_{\mathbf{v}}$ is the angular part of $\mathbf{v}$, is a measure of relative momentum $v = |\mathbf{v}|$ and is called the momentum intracule. The quantity $M(v)$ can be written as

$$M(v) = \sum_{\mu\nu\lambda\sigma} \Gamma_{\mu\nu\lambda\sigma} \left(\mu\nu\lambda\sigma\right)_{\mathrm{M}} \tag{10.26}$$

where $\Gamma_{\mu\nu\lambda\sigma}$ is the two-particle density matrix and $(\mu\nu\lambda\sigma)_{\mathrm{M}}$ is the momentum integral[66]

$$(\mu\nu\lambda\sigma)_{\mathrm{M}} = \frac{v^2}{2\pi^2} \int \phi_\mu^*(\mathbf{r})\phi_\nu(\mathbf{r}+\mathbf{q})\phi_\lambda^*(\mathbf{u}+\mathbf{q})\phi_\sigma(\mathbf{u}) j_0(qv)\, d\mathbf{r}\, d\mathbf{q}\, d\mathbf{u} \tag{10.27}$$

The momentum integrals only possess four-fold permutational symmetry, *i.e.*,

$$(\mu\nu\lambda\sigma)_{\mathrm{M}} = (\nu\mu\lambda\sigma)_{\mathrm{M}} = (\sigma\lambda\nu\mu)_{\mathrm{M}} = (\lambda\sigma\mu\nu)_{\mathrm{M}} \tag{10.28}$$

$$(\nu\mu\lambda\sigma)_{\mathrm{M}} = (\mu\nu\sigma\lambda)_{\mathrm{M}} = (\lambda\sigma\nu\mu)_{\mathrm{M}} = (\sigma\lambda\mu\nu)_{\mathrm{M}} \tag{10.29}$$

and therefore generation of $M(v)$ is roughly twice as expensive as $P(u)$. Momentum intracules can also be decomposed into Coulomb $M_{\mathrm{J}}(v)$ and exchange $M_{\mathrm{K}}(v)$ components:

$$M_J(v) = \frac{1}{2} \sum_{\mu\nu\lambda\sigma} D_{\mu\nu} D_{\lambda\sigma} (\mu\nu\lambda\sigma)_{\mathrm{M}} \tag{10.30}$$

$$M_{\mathrm{K}}(v) = -\frac{1}{2} \sum_{\mu\nu\lambda\sigma} \left[ D_{\mu\lambda}^{\alpha} D_{\nu\sigma}^{\alpha} + D_{\mu\lambda}^{\beta} D_{\nu\sigma}^{\beta} \right] (\mu\nu\lambda\sigma)_{\mathrm{M}} \tag{10.31}$$

Again, the even-order moments are physically significant[66]:

$$\int_0^\infty v^0 M(v) dv = \frac{n(n-1)}{2} \tag{10.32}$$

$$\int_0^\infty u^0 M_{\mathrm{J}}(v) dv = \frac{n^2}{2} \tag{10.33}$$

$$\int_0^\infty v^2 P_{\mathrm{J}}(v) dv = 2nE_{\mathrm{T}} \tag{10.34}$$

$$\int_0^\infty v^0 M_{\mathrm{K}}(v) dv = -\frac{n}{2} \tag{10.35}$$

where $n$ is the number of electrons and $E_{\mathrm{T}}$ is the total electronic kinetic energy. Currently, Q-CHEM can compute $M(v)$, $M_{\mathrm{J}}(v)$ and $M_{\mathrm{K}}(v)$ using $s$ and $p$ basis functions only. Moments are generated using quadrature and consequently for accurate results $M(v)$ must be computed over a large and closely spaced $v$ range.

### 10.10.3 Wigner Intracules

The intracules $P(u)$ and $M(v)$ provide a representation of an electron distribution in either position *or* momentum space but neither alone can provide a complete description. For a combined position *and* momentum description an intracule in phase space is required. Defining such an intracule is more difficult since there is no phase space second-order reduced density. However, the second-order Wigner distribution[67],

$$W_2(\mathbf{r}_1, \mathbf{p}_1, \mathbf{r}_2, \mathbf{p}_2) = \frac{1}{\pi^6} \int \rho_2(\mathbf{r}_1 + \mathbf{q}_1, \mathbf{r}_1 - \mathbf{q}_1, \mathbf{r}_2 + \mathbf{q}_2, \mathbf{r}_2 - \mathbf{q}_2) e^{-2i(\mathbf{p}_1 \cdot \mathbf{q}_1 + \mathbf{p}_2 \cdot \mathbf{q}_2)} d\mathbf{q}_1 d\mathbf{q}_2 \tag{10.36}$$

can be interpreted as the probability of finding an electron at $\mathbf{r}_1$ with momentum $\mathbf{p}_1$ and another electron at $\mathbf{r}_2$ with momentum $\mathbf{p}_2$. [The quantity $W_2(\mathbf{r}_1, \mathbf{r}_2, \mathbf{p}_1, \mathbf{p}_2$ is often referred to as "quasi-probability distribution" since it is not positive everywhere.]

The Wigner distribution can be used in an analogous way to the second order reduced densities to define a combined position and momentum intracule. This intracule is called a Wigner intracule, and is formally defined as

$$W(u, v) = \int W_2(\mathbf{r}_1, \mathbf{p}_1, \mathbf{r}_2, \mathbf{p}_2) \delta(\mathbf{r}_{12} - \mathbf{u}) \delta(\mathbf{p}_{12} - \mathbf{v}) d\mathbf{r}_1\, d\mathbf{r}_2\, d\mathbf{p}_1\, d\mathbf{p}_2\, d\Omega_{\mathbf{u}}\, d\Omega_{\mathbf{v}} \tag{10.37}$$

If the orbitals are expanded in a basis set, then $W(u, v)$ can be written as

$$W(u, v) = \sum_{\mu\nu\lambda\sigma} \Gamma_{\mu\nu\lambda\sigma} \, (\mu\nu\lambda\sigma)_{\mathrm{W}} \tag{10.38}$$

where $(\mu\nu\lambda\sigma)_{\mathrm{W}}$ is the Wigner integral

$$(\mu\nu\lambda\sigma)_{\mathrm{W}} = \frac{v^2}{2\pi^2} \int \int \phi_\mu^*(\mathbf{r}) \phi_\nu(\mathbf{r} + \mathbf{q}) \phi_\lambda^*(\mathbf{r} + \mathbf{q} + \mathbf{u}) \phi_\sigma(\mathbf{r} + \mathbf{u}) j_0(q\, v)\; d\mathbf{r}\; dq\; d\Omega_{\mathbf{u}} \tag{10.39}$$

Wigner integrals are similar to momentum integrals and only have four-fold permutational symmetry. Evaluating Wigner integrals is considerably more difficult that their position or momentum counterparts. The fundamental $[ssss]_{\mathrm{w}}$ integral,

$$\begin{aligned}[ssss]_{\mathrm{W}} \;=\; & \frac{u^2 v^2}{2\pi^2} \int \int \exp\left[-\alpha|\mathbf{r}{-}\mathbf{A}|^2 - \beta|\mathbf{r}{+}\mathbf{q}{-}\mathbf{B}|^2 - \gamma|\mathbf{r}{+}\mathbf{q}{+}\mathbf{u}{-}\mathbf{C}|^2 - \delta|\mathbf{r}{+}\mathbf{u}{-}\mathbf{D}|^2\right] \times \\ & j_0(qv)\; d\mathbf{r}\; d\mathbf{q}\; d\Omega_{\mathbf{u}} \end{aligned} \tag{10.40}$$

can be expressed as

$$[ssss]_{\mathrm{W}} = \frac{\pi u^2 v^2 \; e^{-(R + \lambda^2 u^2 + \mu^2 v^2)}}{2(\alpha + \delta)^{3/2} (\beta + \gamma)^{3/2}} \int e^{-\mathbf{P} \cdot \mathbf{u}} j_0\left(|\mathbf{Q} + \eta \mathbf{u}| v\right)\; d\Omega_u \tag{10.41}$$

or alternatively

$$[ssss]_{\mathrm{W}} = \frac{2\pi^2 u^2 v^2 e^{-(R + \lambda^2 u^2 + \mu^2 v^2)}}{(\alpha + \delta)^{3/2} (\beta + \gamma)^{3/2}} \sum_{n=0}^{\infty} (2n + 1) i_n(P\, u) j_n(\eta u v) j_n(Qv) P_n \left(\frac{\mathbf{P} \cdot \mathbf{Q}}{P\, Q}\right) \tag{10.42}$$

Two approaches for evaluating $(\mu\nu\lambda\sigma)_{\mathrm{W}}$ have been implemented in Q-CHEM, full details can be found in Ref. 68. The first approach uses the first form of $[ssss]_{\mathrm{W}}$ and used Lebedev quadrature to perform the remaining integrations over $\Omega_{\mathbf{u}}$. For high accuracy large Lebedev grids[69–71] should be used, grids of up to 5294 points are available in Q-CHEM. Alternatively, the second form can be adopted and the integrals evaluated by summation of a series. Currently, both methods have been implemented within Q-CHEM for $s$ and $p$ basis functions only.

When computing intracules it is most efficient to locate the loop over $u$ and/or $v$ points within the loop over shell-quartets[72]. However, for $W(u,v)$ this requires a large amount of memory to store all the integrals arising from each $(u,v)$ point. Consequently, an additional scheme, in which the $u$ and $v$ points loop is outside the shell-quartet loop, is available. This scheme is less efficient, but substantially reduces the memory requirements.

### 10.10.4 Intracule Job Control

The following *$rem* variables can be used to control the calculation of intracules.

**INTRACULE**

Controls whether intracule properties are calculated (see also the *$intracule* section).

TYPE:

LOGICAL

DEFAULT:

FALSE

OPTIONS:

FALSE No intracule properties.

TRUE Evaluate intracule properties.

RECOMMENDATION:

None

**WIG_MEM**

Reduce memory required in the evaluation of $W(u,v)$.

TYPE:

LOGICAL

DEFAULT:

FALSE

OPTIONS:

FALSE Do not use low memory option.

TRUE Use low memory option.

RECOMMENDATION:

The low memory option is slower, so use the default unless memory is limited.

**WIG_LEB**

Use Lebedev quadrature to evaluate Wigner integrals.

TYPE:

LOGICAL

DEFAULT:

FALSE

OPTIONS:

FALSE Evaluate Wigner integrals through series summation.

TRUE Use quadrature for Wigner integrals.

RECOMMENDATION:

None

**WIG_GRID**

Specify angular Lebedev grid for Wigner intracule calculations.

TYPE:

INTEGER

DEFAULT:

194

OPTIONS:

Lebedev grids up to 5810 points.

RECOMMENDATION:

Larger grids if high accuracy required.

**N_WIG_SERIES**

Sets summation limit for Wigner integrals.

TYPE:

INTEGER

DEFAULT:

10

OPTIONS:

$n < 100$

RECOMMENDATION:

Increase $n$ for greater accuracy.

**N_I_SERIES**

Sets summation limit for series expansion evaluation of $i_n(x)$.

TYPE:

INTEGER

DEFAULT:

40

OPTIONS:

$n > 0$

RECOMMENDATION:

Lower values speed up the calculation, but may affect accuracy.

**N_J_SERIES**

Sets summation limit for series expansion evaluation of $j_n(x)$.

TYPE:

INTEGER

DEFAULT:

40

OPTIONS:

$n > 0$

RECOMMENDATION:

Lower values speed up the calculation, but may affect accuracy.

### 10.10.5 Format for the *$intracule* Section

| | | |
|---|---|---|
| *int_type* | 0 | Compute $P(u)$ only |
| | 1 | Compute $M(v)$ only |
| | 2 | Compute $W(u,v)$ only |
| | 3 | Compute $P(u)$, $M(v)$ and $W(u,v)$ |
| | 4 | Compute $P(u)$ and $M(v)$ |
| | 5 | Compute $P(u)$ and $W(u,v)$ |
| | 6 | Compute $M(v)$ and $W(u,v)$ |
| *u_points* | | Number of points, start, end. |
| *v_points* | | Number of points, start, end. |
| *moments* | 0–4 | Order of moments to be computed ($P(u)$ only). |
| *derivs* | 0–4 | order of derivatives to be computed ($P(u)$ only). |
| *accuracy* | $n$ | ($10^{-n}$) specify accuracy of intracule interpolation table ($P(u)$ only). |

**Example 10.10** Compute HF/STO-3G $P(u)$, $M(v)$ and $W(u,v)$ for Ne, using Lebedev quadrature with 974 point grid.

```
$molecule
   0  1
   Ne
$end

$rem
   METHOD       hf
   BASIS        sto-3g
   INTRACULE    true
   WIG_LEB      true
   WIG_GRID     974
$end

$intracule
   int_type   3
   u_points  10   0.0  10.0
   v_points   8   0.0   8.0
   moments    4
   derivs     4
   accuracy   8
$end
```

**Example 10.11** Compute HF/6-31G $W(u,v)$ intracules for $H_2O$ using series summation up to $n$=25 and 30 terms in the series evaluations of $j_n(x)$ and $i_n(x)$.

```
$molecule
   0  1
   H1
   O   H1  r
   H2  O   r  H1  theta

   r = 1.1
   theta = 106
$end

$rem
   METHOD         hf
   BASIS          6-31G
   INTRACULE      true
   WIG_MEM        true
   N_WIG_SERIES   25
   N_I_SERIES     40
   N_J_SERIES     50
$end

$intracule
   int_type    2
   u_points   30   0.0   15.0
   v_points   20   0.0   10.0
$end
```

## 10.11 Vibrational Analysis

Vibrational analysis is an extremely important tool for the quantum chemist, supplying a molecular fingerprint which is invaluable for aiding identification of molecular species in many experimental studies. Q-CHEM includes a vibrational analysis package that can calculate vibrational frequencies and their Raman[73] and infrared activities. Vibrational frequencies are calculated by either using an analytic Hessian (if available; see Table 9.1) or, numerical finite difference of the gradient. The default setting in Q-CHEM is to use the highest analytical derivative order available for the requested theoretical method.

When calculating analytic frequencies at the HF and DFT levels of theory, the coupled-perturbed SCF equations must be solved. This is the most time-consuming step in the calculation, and also consumes the most memory. The amount of memory required is $\mathcal{O}(N^2M)$ where $N$ is the number of basis functions, and $M$ the number of atoms. This is an order more memory than is required for the SCF calculation, and is often the limiting consideration when treating larger systems analytically. Q-CHEM incorporates a new approach to this problem that avoids this memory bottleneck by solving the CPSCF equations in segments[74]. Instead of solving for all the perturbations at once, they are divided into several segments, and the CPSCF is applied for one segment at a time, resulting in a memory scaling of $\mathcal{O}(N^2M/N_{\text{seg}})$, where $N_{\text{seg}}$ is the number of segments. This option is invoked automatically by the program.

Following a vibrational analysis, Q-CHEM computes useful statistical thermodynamic properties at standard temperature and pressure, including: zero-point vibration energy (ZPVE) and, translational, rotational and vibrational, entropies and enthalpies.

The performance of various *ab initio* theories in determining vibrational frequencies has been well documented; see Refs. 75–77.

### 10.11.1 Job Control

In order to carry out a frequency analysis users must *at a minimum* provide a molecule within the *$molecule* keyword and define an appropriate level of theory within the *$rem* keyword using the *$rem* variables EXCHANGE, CORRELATION (if required) (Chapter 4) and BASIS (Chapter 7). Since the default type of job (JOBTYPE) is a single point energy (SP) calculation, the JOBTYPE *$rem* variable must be set to FREQ.

It is very important to note that a vibrational frequency analysis must be performed at a stationary point on the potential surface that has been optimized at the same level of theory. Therefore a vibrational frequency analysis most naturally follows a geometry optimization in the same input deck, where the molecular geometry is obtained (see examples).

Users should also be aware that the quality of the quadrature grid used in DFT calculations is more important when calculating second derivatives. The default grid for some atoms has changed in Q-CHEM 3.0 (see Section 4.4.5) and for this reason vibrational frequencies may vary slightly form previous versions. It is recommended that a grid larger than the default grid is used when performing frequency calculations.

The standard output from a frequency analysis includes the following.

- Vibrational frequencies.
- Raman and IR activities and intensities (requires *$rem* DORAMAN).
- Atomic masses.
- Zero-point vibrational energy.
- Translational, rotational, and vibrational, entropies and enthalpies.

Several other *$rem* variables are available that control the vibrational frequency analysis. In detail, they are:

**DORAMAN**

Controls calculation of Raman intensities. Requires JOBTYPE to be set to FREQ

TYPE:

LOGICAL

DEFAULT:

FALSE

OPTIONS:

FALSE Do not calculate Raman intensities.

TRUE Do calculate Raman intensities.

RECOMMENDATION:

None

**VIBMAN_PRINT**

Controls level of extra print out for vibrational analysis.

TYPE:

INTEGER

DEFAULT:

1

OPTIONS:

1 Standard full information print out.
If VCI is TRUE, overtones and combination bands are also printed.

3 Level 1 plus vibrational frequencies in atomic units.

4 Level 3 plus mass-weighted Hessian matrix, projected mass-weighted Hessian matrix.

6 Level 4 plus vectors for translations and rotations projection matrix.

RECOMMENDATION:

Use the default.

**CPSCF_NSEG**

Controls the number of segments used to calculate the CPSCF equations.

TYPE:

INTEGER

DEFAULT:

0

OPTIONS:

0 Do not solve the CPSCF equations in segments.

$n$ User-defined. Use $n$ segments when solving the CPSCF equations.

RECOMMENDATION:

Use the default.

**Example 10.12** An EDF1/6-31+G* optimization, followed by a vibrational analysis. Doing the vibrational analysis at a stationary point is necessary for the results to be valid.

```
$molecule
   O  1
   O
   C  1  co
   F  2  fc  1  fco
   H  2  hc  1  hco  3  180.0

   co  =   1.2
   fc  =   1.4
   hc  =   1.0
   fco = 120.0
   hco = 120.0
$end

$rem
   JOBTYPE    opt
   METHOD     edf1
   BASIS      6-31+G*
$end

@@@

$molecule
   read
$end

$rem
   JOBTYPE    freq
   METHOD     edf1
   BASIS      6-31+G*
$end
```

### 10.11.2 Isotopic Substitutions

By default Q-CHEM calculates vibrational frequencies using the atomic masses of the most abundant isotopes (taken from the Handbook of Chemistry and Physics, 63rd Edition). Masses of other isotopes can be specified using the *$isotopes* section and by setting the ISOTOPES *$rem* variable to TRUE. The format of the *$isotopes* section is as follows:

```
$isotopes
   number_of_isotope_loops  tp_flag
   number_of_atoms  [temp pressure] (loop 1)
   atom_number1   mass1
   atom_number2   mass2
   ...
   number_of_atoms  [temp pressure] (loop 2)
   atom_number1   mass1
   atom_number2   mass2
   ...
$end
```

**Note:** Only the atoms whose masses are to be changed from the default values need to be specified. After each loop all masses are reset to the default values. Atoms are numbered according to the order in the *$molecule* section.

An initial loop using the default masses is always performed first. Subsequent loops use the user-specified atomic masses. Only those atoms whose masses are to be changed need to be included in the list, all other atoms will adopt the default masses. The output gives a full frequency analysis for each loop. Note that the calculation of vibrational frequencies in the additional loops only involves a rescaling of the computed Hessian, and therefore takes little additional computational time.

The first line of the *$isotopes* section specifies the number of substitution loops and also whether the temperature and pressure should be modified. The *tp_flag* setting should be set to 0 if the default temperature and pressure are to be used (298.18 K and 1 atm respectively), or else to 1 if they are to be altered. Note that the temperatures should be specified in Kelvin and pressures in atmospheres.

**ISOTOPES**
Specifies if non-default masses are to be used in the frequency calculation.
TYPE:
LOGICAL
DEFAULT:
FALSE
OPTIONS:
FALSE Use default masses only.
TRUE Read isotope masses from *$isotopes* section.
RECOMMENDATION:
None

**Example 10.13** An EDF1/6-31+G* optimization, followed by a vibrational analysis. Doing the vibrational analysis at a stationary point is necessary for the results to be valid.

```
$molecule
   0  1
   C   1.08900   0.00000   0.00000
   C  -1.08900   0.00000   0.00000
   H   2.08900   0.00000   0.00000
   H  -2.08900   0.00000   0.00000
$end

$rem
   BASIS    3-21G
   JOBTYPE  opt
   METHOD   hf
$end

@@@

$molecule
   read
$end

$rem
   BASIS       3-21G
   JOBTYPE     freq
   METHOD      hf
   SCF_GUESS   read
   ISOTOPES    1
$end

$isotopes
   2   0           ! two loops, both at std temp and pressure
   4
     1   13.00336  ! All atoms are given non-default masses
     2   13.00336
     3   2.01410
     4   2.01410
   2
     3   2.01410   ! H's replaced with D's
     4   2.01410
$end
```

### 10.11.3 Partial Hessian Vibrational Analysis

The computation of harmonic frequencies for systems with a very large number of atoms can become computationally expensive. However, in many cases only a few specific vibrational modes or vibrational modes localized in a region of the system are of interest. A typical example is the calculation of the vibrational modes of a molecule adsorbed on a surface. In such a case, only the vibrational modes of the adsorbate are useful, and the vibrational modes associated with the surface atoms are of less interest. If the vibrational modes of interest are only weakly coupled to the vibrational modes associated with the rest of the system, it can be appropriate to adopt a partial Hessian approach. In this approach[78,79], only the part of the Hessian matrix comprising the second derivatives of a subset of the atoms defined by the user is computed. These atoms are defined in the *$alist* block. This results in a significant decrease in the cost of the calculation. Physically, this approximation corresponds to assigning an infinite mass to all the atoms excluded from the Hessian and will only yield sensible results if these atoms are not involved in the vibrational modes of interest. VPT2 and TOSH anharmonic frequencies can be computed following a partial Hessian calculation.[80] It is also possible to include a subset of the harmonic vibrational modes with an anharmonic frequency calculation by invoking the ANHAR_SEL rem. This can be useful to reduce the computational cost of an anharmonic frequency calculation or to explore the coupling between specific vibrational modes.

Alternatively, vibrationally averaged interactions with the rest of the system can be folded into a partial Hessian calculation using vibrational subsystem analysis[81,82]. Based on an adiabatic approximation, this procedure reduces the cost of diagonalizing the full Hessian, while providing a local probe of fragments vibrations, and providing better than partial Hessian accuracy for the low frequency modes of large molecules[83]. Mass-effects from the rest of the system can be vibrationally averaged or excluded within this scheme.

**PHESS**

Controls whether partial Hessian calculations are performed.

TYPE:

INTEGER

DEFAULT:

0 Full Hessian calculation

OPTIONS:

1 Partial Hessian calculation.

2 Vibrational subsystem analysis (massless).

3 Vibrational subsystem analysis (weighted).

RECOMMENDATION:

None

**N_SOL**

Specifies number of atoms included in the Hessian.

TYPE:

INTEGER

DEFAULT:

No default

OPTIONS:

User defined

RECOMMENDATION:

None

**PH_FAST**

Lowers integral cutoff in partial Hessian calculation is performed.

TYPE:

LOGICAL

DEFAULT:

FALSE Use default cutoffs

OPTIONS:

TRUE Lower integral cutoffs

RECOMMENDATION:

None

**ANHAR_SEL**

Select a subset of normal modes for subsequent anharmonic frequency analysis.

TYPE:

LOGICAL

DEFAULT:

FALSE Use all normal modes

OPTIONS:

TRUE Select subset of normal modes

RECOMMENDATION:

None

**Example 10.14** This example shows a partial Hessian frequency calculation of the vibrational frequencies of acetylene on a model of the C(100) surface

```
$comment
   acetylene - C(100)
   partial Hessian calculation
$end

$molecule
0 1
   C  0.000  0.659 -2.173
   C  0.000 -0.659 -2.173
   H  0.000  1.406 -2.956
   H  0.000 -1.406 -2.956
   C  0.000  0.786 -0.647
   C  0.000 -0.786 -0.647
   C  1.253  1.192  0.164
   C -1.253  1.192  0.164
   C  1.253 -1.192  0.164
   C  1.297  0.000  1.155
   C -1.253 -1.192  0.164
   C  0.000  0.000  2.023
   C -1.297  0.000  1.155
   H -2.179  0.000  1.795
   H -1.148 -2.156  0.654
   H  0.000 -0.876  2.669
   H  2.179  0.000  1.795
   H -1.148  2.156  0.654
   H -2.153 -1.211 -0.446
   H  2.153 -1.211 -0.446
   H  1.148 -2.156  0.654
   H  1.148  2.156  0.654
   H  2.153  1.211 -0.446
   H -2.153  1.211 -0.446
   H  0.000  0.876  2.669
$end

$rem
   JOBTYPE          freq
   METHOD           hf
   BASIS            sto-3g
   PHESS            TRUE
   N_SOL            4
```

```
$end

$alist
1
2
3
4
$end
```

**Example 10.15** This example shows an anharmonic frequency calculation for ethene where only the C-H stretching modes are included in the anharmonic analysis.

```
$comment
  ethene
  restricted anharmonic frequency analysis
$end

$molecule
0 1
  C   0.6665   0.0000   0.0000
  C  -0.6665   0.0000   0.0000
  H   1.2480   0.9304   0.0000
  H  -1.2480  -0.9304   0.0000
  H  -1.2480   0.9304   0.0000
  H   1.2480  -0.9304   0.0000
$end

$rem
   JOBTYPE           freq
   METHOD            hf
   BASIS             sto-3g
   ANHAR_SEL         TRUE
   N_SOL             4
$end

$alist
9
10
11
12
$end
```

## 10.11.4 Localized Mode Vibrational Analysis

The computation of harmonic frequencies leads to molecular vibrations described by coordinates which are often highly de-localized. For larger molecules many vibrational modes can potentially contribute to a single observed spectral band, and information about the interaction between localized chemical units can become less readily available. In certain cases, localizing vibrational modes using procedures similar to the localized orbital schemes discussed previously in this manual can therefore provide a more chemically intuitive way of analysing spectral data,[84–86] interpreting two-dimensional vibrational spectra,[87] or improving calculations that go beyond the harmonic approximation.[88–90] It is also possible to include only a subset of the normal modes in the localization calculation by invoking the LOCALFREQ_SELECT rem variable. This can be useful to improve convergence in larger molecules or to explore the coupling between specific vibrational modes. These modes are defined in the *$alist* block. Alternatively it is possible to localize high and low frequency modes separately in a single calculation using LOCALFREQ_GROUPS and related inputs.

**LOCAL_FREQ**
Controls whether a vibrational mode localization calculation is performed.
TYPE:
INTEGER
DEFAULT:
0 Normal mode calculation.
OPTIONS:
1 Localized mode calculation with a Pipek-Mezey like criterion.
2 Localized mode calculation with a Boys like criterion.
RECOMMENDATION:
None

**LOCALFREQ_THRESH**
Mode localization is considered converged when the change in the localization criterion is less than $10^{-\mathrm{LOCALFREQ\_THRESH}}$.
TYPE:
INTEGER
DEFAULT:
6
OPTIONS:
$n$ User-specified integer.
RECOMMENDATION:
None

**LOCALFREQ_MAX_ITER**
Controls the maximum number of mode localization sweeps permitted.
TYPE:
INTEGER
DEFAULT:
200
OPTIONS:
$n$ User-specified integer.
RECOMMENDATION:
None

**LOCALFREQ_SELECT**
Select a subset of normal modes for subsequent anharmonic frequency analysis.
TYPE:
LOGICAL
DEFAULT:
FALSE Use all normal modes.
OPTIONS:
TRUE Select a subset of normal modes.
RECOMMENDATION:
None

**LOCALFREQ_GROUPS**

Select the number of groups of frequencies to be localized separately within a localized mode calculation. The size of the groups are then controlled using the LOCALFREQ_GROUP1, LOCALFREQ_GROUP2, and LOCALFREQ_GROUP3 keywords.

TYPE:

INTEGER

DEFAULT:

0 Localize all normal modes together.

OPTIONS:

1 Define one subset of modes to localize independently.

2 Define two subsets of modes to localize independently.

3 Define three subsets of modes to localize independently.

RECOMMENDATION:

None

**LOCALFREQ_GROUP1**

Select the number of modes to include in the first subset of modes to localize independently when the keyword LOCALFREQ_GROUPS > 0.

TYPE:

INTEGER

DEFAULT:

NONE

OPTIONS:

$n$ User-specified integer.

RECOMMENDATION:

Modes will be included starting with the lowest frequency mode and then in ascending energy order up to the defined value.

LOCALFREQ_GROUP2 and LOCALFREQ_GROUP3 are defined similarly.

## 10.12 Anharmonic Vibrational Frequencies

Computing vibrational spectra beyond the harmonic approximation has become an active area of research owing to the improved efficiency of computer techniques[91–94]. To calculate the exact vibrational spectrum within Born-Oppenheimer approximation, one has to solve the nuclear Schrödinger equation completely using numerical integration techniques, and consider the full configuration interaction of quanta in the vibrational states. This has only been carried out on di- or triatomic system[95,96]. The difficulty of this numerical integration arises because solving exact the nuclear Schrödinger equation requires a complete electronic basis set, consideration of all the nuclear vibrational configuration states, and a complete potential energy surface (PES). Simplification of the Nuclear Vibration Theory (NVT) and PES are the doorways to accelerating the anharmonic correction calculations. There are five aspects to simplifying the problem:

- Expand the potential energy surface using a Taylor series and examine the contribution from higher derivatives. Small contributions can be eliminated, which allows for the efficient calculation of the Hamiltonian.

- Investigate the effect on the number of configurations employed in a variational calculation.

- Avoid using variational theory (due to its expensive computational cost) by using other approximations, for example, perturbation theory.
- Obtain the PES indirectly by applying a self-consistent field procedure.
- Apply an *anharmonic* wave function which is more appropriate for describing the distribution of nuclear probability on an anharmonic potential energy surface.

To incorporate these simplifications, new formulae combining information from the Hessian, gradient and energy are used as a default procedure to calculate the cubic and quartic force field of a given potential energy surface.

Here, we also briefly describe various NVT methods. In the early stage of solving the nuclear Schrödinger equation (in the 1930s), second-order Vibrational Perturbation Theory (VPT2) was developed[94,97–100]. However, problems occur when resonances exist in the spectrum. This becomes more problematic for larger molecules due to the greater chance of accidental degeneracies occurring. To avoid this problem, one can do a direct integration of the secular matrix using Vibrational Configuration Interaction (VCI) theory[101]. It is the most accurate method and also the least favored due to its computational expense. In Q-CHEM 3.0, we introduce a new approach to treating the wave function, transition-optimized shifted Hermite (TOSH) theory[102], which uses first-order perturbation theory, which avoids the degeneracy problems of VPT2, but which incorporates anharmonic effects into the wave function, thus increasing the accuracy of the predicted anharmonic energies.

### 10.12.1 Vibration Configuration Interaction Theory

To solve the nuclear vibrational Schrödinger equation, one can only use direct integration procedures for diatomic molecules[95,96]. For larger systems, a truncated version of full configuration interaction is considered to be the most accurate approach. When one applies the variational principle to the vibrational problem, a basis function for the nuclear wave function of the $n$th excited state of mode $i$ is

$$\psi_i^{(n)} = \phi_i^{(n)} \prod_{j \neq i}^{m} \phi_j^{(0)} \tag{10.43}$$

where the $\phi_i^{(n)}$ represents the harmonic oscillator eigenfunctions for normal mode $q_i$. This can be expressed in terms of Hermite polynomials:

$$\phi_i^{(n)} = \left( \frac{\omega_i^{\frac{1}{2}}}{\pi^{\frac{1}{2}} 2^n n!} \right)^{\frac{1}{2}} e^{-\frac{\omega_i q_i^2}{2}} H_n(q_i \sqrt{\omega_i}) \tag{10.44}$$

With the basis function defined in Eq. (10.43), the $n$th wave function can be described as a linear combination of the Hermite polynomials:

$$\Psi^{(n)} = \sum_{i=0}^{n_1} \sum_{j=0}^{n_2} \sum_{k=0}^{n_3} \cdots \sum_{m=0}^{n_m} c_{ijk\cdots m}^{(n)} \psi_{ijk\cdots m}^{(n)} \tag{10.45}$$

where $n_i$ is the number of quanta in the $i$th mode. We propose the notation VCI($n$) where $n$ is the total number of quanta, *i.e.*:

$$n = n_1 + n_2 + n_3 + \cdots + n_m \tag{10.46}$$

To determine this expansion coefficient $c^{(n)}$, we integrate the $\hat{H}$, as in Eq. (4.1), with $\Psi^{(n)}$ to get the eigenvalues

$$c^{(n)} = E^{(n)}_{\mathrm{VCI}(n)} = \langle \Psi^{(n)} | \hat{H} | \Psi^{(n)} \rangle \tag{10.47}$$

This gives us frequencies that are corrected for anharmonicity to $n$ quanta accuracy for a $m$-mode molecule. The size of the secular matrix on the right hand of Eq. (10.47) is $((n+m)!/n!m!)^2$, and the storage of this matrix can easily surpass the memory limit of a computer. Although this method is highly accurate, we need to seek for other approximations for computing large molecules.

### 10.12.2 Vibrational Perturbation Theory

Vibrational perturbation theory has been historically popular for calculating molecular spectroscopy. Nevertheless, it is notorious for the inability of dealing with resonance cases. In addition, the non-standard formulas for various symmetries of molecules forces the users to modify inputs on a case-by-case basis[103–105], which narrows the accessibility of this method. VPT applies perturbation treatments on the same Hamiltonian as in Eq. (4.1), but divides it into an unperturbed part, $\hat{U}$,

$$\hat{U} = \sum_{i}^{m} \left( -\frac{1}{2} \frac{\partial^2}{\partial q_i^2} + \frac{{\omega_i}^2}{2} {q_i}^2 \right) \tag{10.48}$$

and a perturbed part, $\hat{V}$:

$$\hat{V} = \frac{1}{6} \sum_{ijk=1}^{m} \eta_{ijk} q_i q_j q_k + \frac{1}{24} \sum_{ijkl=1}^{m} \eta_{ijkl} q_i q_j q_k q_l \tag{10.49}$$

One can then apply second-order perturbation theory to get the $i$th excited state energy:

$$E^{(i)} = \hat{U}^{(i)} + \langle \Psi^{(i)} | \hat{V} | \Psi^{(i)} \rangle + \sum_{j \neq i} \frac{|\langle \Psi^{(i)} | \hat{V} | \Psi^{(j)} \rangle|^2}{\hat{U}^{(i)} - \hat{U}^{(j)}} \tag{10.50}$$

The denominator in Eq. (10.50) can be zero either because of symmetry or accidental degeneracy. Various solutions, which depend on the type of degeneracy that occurs, have been developed which ignore the zero-denominator elements from the Hamiltonian[103–106]. An alternative solution has been proposed by Barone[94] which can be applied to all molecules by changing the masses of one or more nuclei in degenerate cases. The disadvantage of this method is that it will break the degeneracy which results in fundamental frequencies no longer retaining their correct symmetry. He proposed

$$E_i^{\mathrm{VPT2}} = \sum_{j} \omega_j (n_j + 1/2) + \sum_{i \leq j} x_{ij} (n_i + 1/2)(n_j + 1/2) \tag{10.51}$$

where, if rotational coupling is ignored, the anharmonic constants $x_{ij}$ are given by

$$x_{ij} = \frac{1}{4\omega_i \omega_j} \left( \eta_{iijj} - \sum_{k}^{m} \frac{\eta_{iik}\eta_{jjk}}{\omega_k^2} + \sum_{k}^{m} \frac{2(\omega_i^2 + \omega_j^2 - \omega_k^2)\eta_{ijk}^2}{[(\omega_i + \omega_j)^2 - \omega_k^2]\,[(\omega_i - \omega_j)^2 - \omega_k^2]} \right) \tag{10.52}$$

### 10.12.3 Transition-Optimized Shifted Hermite Theory

So far, every aspect of solving the nuclear wave equation has been considered, except the wave function. Since Schrödinger proposed his equation, the nuclear wave function has traditionally be expressed in terms of Hermite functions, which are designed for the harmonic oscillator case. Recently[102], a modified representation has been presented. To demonstrate how this approximation works, we start with a simple example. For a diatomic molecule, the Hamiltonian with up to quartic derivatives can be written as

$$\hat{H} = -\frac{1}{2}\frac{\partial^2}{\partial q^2} + \frac{1}{2}\omega^2 q^2 + \eta_{iii} q^3 + \eta_{iiii} q^4 \tag{10.53}$$

and the wave function is expressed as in Eq. (10.44). Now, if we shift the center of the wave function by $\sigma$, which is equivalent to a translation of the normal coordinate $q$, the shape will still remain the same, but the anharmonic correction can now be incorporated into the wave function. For a ground vibrational state, the wave function is written as

$$\phi^{(0)} = \left(\frac{\omega}{\pi}\right)^{\frac{1}{4}} e^{-\frac{\omega}{2}(q-\sigma)^2} \tag{10.54}$$

Similarly, for the first excited vibrational state, we have

$$\phi^{(1)} = \left(\frac{4\omega^3}{\pi}\right)^{\frac{1}{4}} (q-\sigma)\, e^{\frac{\omega}{2}(q-\sigma)^2} \tag{10.55}$$

Therefore, the energy difference between the first vibrational excited state and the ground state is

$$\Delta E_{\text{TOSH}} = \omega + \frac{\eta_{iiii}}{8\omega^2} + \frac{\eta_{iii}\sigma}{2\omega} + \frac{\eta_{iiii}\sigma^2}{4\omega} \tag{10.56}$$

This is the fundamental vibrational frequency from first-order perturbation theory.

Meanwhile, We know from the first-order perturbation theory with an ordinary wave function within a QFF PES, the energy is

$$\Delta E_{\text{VPT1}} = \omega + \frac{\eta_{iiii}}{8\omega^2} \tag{10.57}$$

The differences between these two wave functions are the two extra terms arising from the shift in Eq. (10.56). To determine the shift, we compare the energy with that from second-order perturbation theory:

$$\Delta E_{\text{VPT2}} = \omega + \frac{\eta_{iiii}}{8\omega^2} - \frac{5{\eta_{iii}}^2}{24\omega^4} \tag{10.58}$$

Since $\sigma$ is a very small quantity compared with the other variables, we ignore the contribution of $\sigma^2$ and compare $\Delta E_{\text{TOSH}}$ with $\Delta E_{\text{VPT2}}$, which yields an initial guess for $\sigma$:

$$\sigma = -\frac{5}{12}\frac{\eta_{iii}}{\omega^3} \tag{10.59}$$

Because the only difference between this approach and the ordinary wave function is the shift in the normal coordinate, we call it "transition-optimized shifted Hermite" (TOSH) functions[102]. This approximation gives second-order accuracy at only first-order cost.

For polyatomic molecules, we consider Eq. (10.56), and propose that the energy of the $i$th mode be expressed as:

$$\Delta E_i^{\text{TOSH}} = \omega_i + \frac{1}{8\omega_i}\sum_j \frac{\eta_{iijj}}{\omega_j} + \frac{1}{2\omega_i}\sum_j \eta_{iij}\sigma_{ij} + \frac{1}{4\omega_i}\sum_{j,k} \eta_{iijk}\sigma_{ij}\sigma_{ik} \tag{10.60}$$

Following the same approach as for the diatomic case, by comparing this with the energy from second-order perturbation theory, we obtain the shift as

$$\sigma_{ij} = \frac{(\delta_{ij}-2)(\omega_i+\omega_j)\eta_{iij}}{4\omega_i\omega_j^2(2\omega_i+\omega_j)} - \sum_k \frac{\eta_{kkj}}{4\omega_k\omega_j^2} \tag{10.61}$$

### 10.12.4 Job Control

The following *$rem* variables can be used to control the calculation of anharmonic frequencies.

**ANHAR**

Performing various nuclear vibrational theory (TOSH, VPT2, VCI) calculations to obtain vibrational anharmonic frequencies.

TYPE:

LOGICAL

DEFAULT:

FALSE

OPTIONS:

| | |
|---|---|
| TRUE | Carry out the anharmonic frequency calculation. |
| FALSE | Do harmonic frequency calculation. |

RECOMMENDATION:

Since this calculation involves the third and fourth derivatives at the minimum of the potential energy surface, it is recommended that the GEOM_OPT_TOL_DISPLACEMENT, GEOM_OPT_TOL_GRADIENT and GEOM_OPT_TOL_ENERGY tolerances are set tighter. Note that VPT2 calculations may fail if the system involves accidental degenerate resonances. See the VCI *$rem* variable for more details about increasing the accuracy of anharmonic calculations.

**VCI**

Specifies the number of quanta involved in the VCI calculation.

TYPE:

INTEGER

DEFAULT:

0

OPTIONS:

User-defined. Maximum value is 10.

RECOMMENDATION:

The availability depends on the memory of the machine. Memory allocation for VCI calculation is the square of $2 * (N_{\rm Vib} + N_{\rm VCI})/N_{\rm Vib}N_{\rm VCI}$ with double precision. For example, a machine with 1.5 Gb memory and for molecules with fewer than 4 atoms, VCI(10) can be carried out, for molecule containing fewer than 5 atoms, VCI(6) can be carried out, for molecule containing fewer than 6 atoms, VCI(5) can be carried out. For molecules containing fewer than 50 atoms, VCI(2) is available. VCI(1) and VCI(3) usually overestimated the true energy while VCI(4) usually gives an answer close to the converged energy.

**FDIFF_DER**

Controls what types of information are used to compute higher derivatives. The default uses a combination of energy, gradient and Hessian information, which makes the force field calculation faster.

TYPE:

INTEGER

DEFAULT:

3 for jobs where analytical 2nd derivatives are available.

0 for jobs with ECP.

OPTIONS:

0 Use energy information only.

1 Use gradient information only.

2 Use Hessian information only.

3 Use energy, gradient, and Hessian information.

RECOMMENDATION:

When the molecule is larger than benzene with small basis set, FDIFF_DER=2 may be faster. Note that FDIFF_DER will be set lower if analytic derivatives of the requested order are not available. Please refers to IDERIV.

**MODE_COUPLING**

Number of modes coupling in the third and fourth derivatives calculation.

TYPE:

INTEGER

DEFAULT:

2 for two modes coupling.

OPTIONS:

$n$ for $n$ modes coupling, Maximum value is 4.

RECOMMENDATION:

Use the default.

**IGNORE_LOW_FREQ**

Low frequencies that should be treated as rotation can be ignored during anharmonic correction calculation.

TYPE:

INTEGER

DEFAULT:

300 Corresponding to 300 cm$^{-1}$.

OPTIONS:

$n$ Any mode with harmonic frequency less than $n$ will be ignored.

RECOMMENDATION:

Use the default.

**FDIFF_STEPSIZE_QFF**

Displacement used for calculating third and fourth derivatives by finite difference.

TYPE:

INTEGER

DEFAULT:

5291 Corresponding to 0.1 bohr. For calculating third and fourth derivatives.

OPTIONS:

$n$ Use a step size of $n \times 10^{-5}$.

RECOMMENDATION:

Use the default, unless the potential surface is very flat, in which case a larger value should be used.

**Example 10.16** A four-quanta anharmonic frequency calculation on formaldehyde at the EDF2/6-31G* optimized ground state geometry, which is obtained in the first part of the job. It is necessary to carry out the harmonic frequency first and this will print out an approximate time for the subsequent anharmonic frequency calculation. If a FREQ job has already been performed, the anharmonic calculation can be restarted using the saved scratch files from the harmonic calculation.

```
$molecule
   0 1
   C
   O, 1, CO
   H, 1, CH, 2, A
   H, 1, CH, 2, A, 3, D

   CO = 1.2
   CH = 1.0
   A  = 120.0
   D  = 180.0
$end
$rem
    JOBTYPE                     OPT
    METHOD                      EDF2
    BASIS                       6-31G*
    GEOM_OPT_TOL_DISPLACEMENT   1
    GEOM_OPT_TOL_GRADIENT       1
    GEOM_OPT_TOL_ENERGY         1
$end
@@@
$molecule
    READ
$end
$rem
    JOBTYPE                     FREQ
    METHOD                      EDF2
    BASIS                       6-31G*
    ANHAR                       TRUE
    VCI                         4
$end
```

## 10.13 NMR Shielding Tensors

NMR spectroscopy is a powerful technique to yield important information on molecular systems in chemistry and biochemistry. Since there is no direct relationship between the measured NMR signals and structural properties, the necessity for a reliable method to predict NMR chemical shifts arises. Examples for such assignments are numerous, for example, assignments of solid-state spectra[107,108]. The implementation within Q-CHEM uses gauge-including atomic orbitals (GIAOs)[109–111] to calculate the NMR chemical shielding tensors. This scheme has been proven to be reliable an accurate for many applications[112].

The shielding tensor, $\sigma$, is a second-order property depending on the external magnetic field, $B$, and the nuclear magnetic spin momentum, $m_k$, of nucleus $k$:

$$\Delta E = -m_j(1-\sigma)B \tag{10.62}$$

Using analytical derivative techniques to evaluate $\sigma$, the components of this $3 \times 3$ tensor are computed as

$$\sigma_{ij} = \sum_{\mu\nu} P_{\mu\nu} \frac{\partial^2 h_{\mu\nu}}{\partial B_i \partial m_{j,k}} + \sum_{\mu\nu} \frac{\partial P_{\mu\nu}}{\partial B_i} \frac{\partial h_{\mu\nu}}{\partial m_{j,k}} \tag{10.63}$$

where $i$ and $j$ represent are Cartesian components.

To solve for the necessary perturbed densities, $\partial P/\partial B_{x,y,z}$, a new CPSCF method based on a density matrix based formulation[113,114] is used. This formulation is related to a density matrix based CPSCF (D-CPSCF) formulation employed for the computation of vibrational frequencies[115]. Alternatively, an MO-based CPSCF calculation of shielding tensors can be chosen by the variable MOPROP. Features of the NMR package include:

- Restricted HF-GIAO and KS-DFT-GIAO NMR chemical shifts calculations
- LinK/CFMM support to evaluate Coulomb- and exchange-like matrices
- Density matrix-based coupled-perturbed SCF (D-CPSCF)
- DIIS acceleration
- Support of basis sets up to $d$ functions
- Support of LSDA/GGA/Hybrid XC functionals

### 10.13.1 Job Control

The JOBTYPE must be set to NMR to request the NMR chemical shifts.

**D_CPSCF_PERTNUM**

Specifies whether to do the perturbations one at a time, or all together.

TYPE:

INTEGER

DEFAULT:

0

OPTIONS:

0 Perturbed densities to be calculated all together.

1 Perturbed densities to be calculated one at a time.

RECOMMENDATION:

None

**D_SCF_CONV_1**

Sets the convergence criterion for the level-1 iterations. This preconditions the density for the level-2 calculation, and does not include any two-electron integrals.

TYPE:

INTEGER

DEFAULT:

4 corresponding to a threshold of $10^{-4}$.

OPTIONS:

$n < 10$ Sets convergence threshold to $10^{-n}$.

RECOMMENDATION:

The criterion for level-1 convergence must be less than or equal to the level-2 criterion, otherwise the D-CPSCF will not converge.

**D_SCF_CONV_2**

Sets the convergence criterion for the level-2 iterations.

TYPE:

INTEGER

DEFAULT:

4 Corresponding to a threshold of $10^{-4}$.

OPTIONS:

$n < 10$ Sets convergence threshold to $10^{-n}$.

RECOMMENDATION:

None

**D_SCF_MAX_1**

Sets the maximum number of level-1 iterations.

TYPE:

INTEGER

DEFAULT:

100

OPTIONS:

$n$ User defined.

RECOMMENDATION:

Use the default.

**D_SCF_MAX_2**

Sets the maximum number of level-2 iterations.

TYPE:

INTEGER

DEFAULT:

30

OPTIONS:

$n$ User defined.

RECOMMENDATION:

Use the default.

**D_SCF_DIIS**
Specifies the number of matrices to use in the DIIS extrapolation in the D-CPSCF.
TYPE:
INTEGER
DEFAULT:
11
OPTIONS:
$n$ $n$ = 0 specifies no DIIS extrapolation is to be used.
RECOMMENDATION:
Use the default.

### 10.13.2 Using NMR Shielding Constants as an Efficient Probe of Aromaticity

Unambiguous theoretical estimates of degree of aromaticity are still on high demand. The NMR chemical shift methodology offers one unique probe of aromaticity based on one defining characteristics of an aromatic system—its ability to sustain a diatropic ring current. This leads to a response to an imposed external magnetic field with a strong (negative) shielding at the center of the ring. Schleyer *et al.* have employed this phenomenon to justify a new unique probe of aromaticity [116]. They proposed the computed absolute magnetic shielding at ring centers (unweighted mean of the heavy-atoms ring coordinates) as a new aromaticity criterion, called nucleus-independent chemical shift (NICS). Aromatic rings show strong negative shielding at the ring center (negative NICS), while anti-aromatic systems reveal positive NICS at the ring center. As an example, a typical NICS value for benzene is about -11.5 ppm as estimated with Q-CHEM at Hartree-Fock/6-31G* level. The same NICS value for benzene was also reported in Ref. 116. The calculated NICS value for furan of $-13.9$ ppm with Q-CHEM is about the same as the value reported for furan in Ref. 116. Below is one input example of how to the NICS of furan with Q-CHEM, using the ghost atom option. The ghost atom is placed at the center of the furan ring, and the basis set assigned to it within the basis mix option must be the basis used for hydrogen atom.

**Example 10.17** Calculation of the NMR NICS probe of furan with Hartree-Fock/6-31G* with Q-CHEM.

```
$molecule
   0 1
   C    -0.69480       -0.62270       -0.00550
   C     0.72110       -0.63490        0.00300
   C     1.11490        0.68300        0.00750
   O     0.03140        1.50200        0.00230
   C    -1.06600        0.70180       -0.00560
   H     2.07530        1.17930        0.01410
   H     1.37470       -1.49560        0.00550
   H    -1.36310       -1.47200       -0.01090
   H    -2.01770        1.21450       -0.01040
   GH    0.02132        0.32584        0.00034 ! ghost at the ring center
$end

$rem
   JOBTYPE              NMR
   METHOD               HF
   BASIS                mixed
   SCF_ALGORITHM        DIIS
   PURCAR               111
   SEPARATE_JK          0
   LIN_K                0
   CFMM_ORDER           15
   GRAIN                1
   CFMM_PRINT           2
   CFMMSTAT             1
   PRINT_PATH_TIME      1
   LINK_MAXSHELL_NUMBER 1
   SKIP_SCFMAN          0
   IGUESS               core
   SCF_CONVERGENCE      7
   ITHRSH               10
   IPRINT               23
   D_SCF_CONVGUIDE      0
   D_SCF_METRIC         2
   D_SCF_STORAGE        50
   D_SCF_RESTART        0
   PRINT_PATH_TIME      1
   SYM_IGNORE           1
   NO_REORIENT          1
$end

$basis
C 1
6-31G*
****
C 2
6-31G*
****
C 3
6-31G*
****
O 4
6-31G*
****
C 5
6-31G*
****
H 6
6-31G*
****
H 7
6-31G*
****
H 8
6-31G*
****
H 9
6-31G*
****
H 10
6-31G*
****
```

## 10.14 Linear-Scaling NMR Chemical Shifts: GIAO-HF and GIAO-DFT

The importance of nuclear magnetic resonance (NMR) spectroscopy for modern chemistry and biochemistry cannot be overestimated. Despite tremendous progress in experimental techniques, the understanding and reliable assignment of observed experimental spectra remains often a highly difficult task, so that quantum chemical methods can be extremely useful both in the solution and the solid state (*e.g.*, Refs. 107,108,113,117,118, and references therein).

The cost for the computation of NMR chemical shifts within even the simplest quantum chemical methods such as Hartree-Fock (HF) or density functional (DFT) approximations increases conventionally with the third power of the molecular size $M$, $\mathcal{O}(M^3)$, where $\mathcal{O}(\cdot)$ stands for the scaling order. Therefore, the computation of NMR chemical shieldings has so far been limited to molecular systems in the order of 100 atoms without molecular symmetry.

For larger systems it is crucial to reduce the increase of the computational effort to linear, which has been recently achieved by Kussmann and Ochsenfeld[113,119]. In this way, the computation of NMR chemical shifts becomes possible at both HF or DFT level for molecular systems with 1000 atoms and more, while the accuracy and reliability of traditional methods is fully preserved. In our formulation we use gauge-including atomic orbitals (GIAOs)[109,110,120], which have proven to be particularly successful[121]. For example, for many molecular systems the HF (GIAO-HF) approach provides typically an accuracy of 0.2–0.4 ppm for the computation of $^1$H NMR chemical shifts (*e.g.* Refs. 107,108,113,117,118).

NMR chemical shifts are calculated as second derivatives of the energy with respect to the external magnetic field $\mathbf{B}$ and the nuclear magnetic spin $m_{Nj}$ of a nucleus $N$:

$$\sigma_{ij}^N = \frac{\partial^2 E}{\partial B_i \partial M_{Nj}} \tag{10.64}$$

where $i$, $j$ are $x$, $y$, $z$ coordinates.

For the computation of the NMR shielding tensor it is necessary to solve for the response of the one-particle density matrix with respect to the magnetic field, so that the solution of the coupled perturbed SCF (CPSCF) equations either within the HF or the DFT approach is required.

These equations can be solved within a density matrix-based formalism for the first time with only linear-scaling effort for molecular systems with a non-vanishing HOMO-LUMO gap[113]. The solution is even simpler in DFT approaches without explicit exchange, since present density functionals are not dependent on the magnetic field.

The present implementation of NMR shieldings in Q-CHEM employs the LinK (linear exchange K) method[122,123] for the formation of exchange contributions[113]. Since the derivative of the density matrix with respect to the magnetic field is skew-symmetric, its Coulomb-type contractions vanish. For the remaining Coulomb-type matrices the CFMM method[124] is adapted[113]. In addition, a multitude of different approaches for the solution of the CPSCF equations can be selected within Q-CHEM.

The so far largest molecular system for which NMR shieldings have been computed, contained 1003 atoms and 8593 basis functions (GIAO-HF/6-31G*) without molecular symmetry[113].

## 10.15 Indirect Nuclear Spin–Spin Coupling Constants

Indirect nuclear spin–spin coupling constants (also known as scalar couplings or $J$-couplings) can be evaluated in Q-CHEM at the Hartree–Fock and density functional levels of theory[125,126] (restricted wave functions only). Pure and hybrid functionals are supported. To perform a $J$-coupling calculation, set JOBTYPE to ISSC. Refer to Section 10.16.3 for more options.

The coupling tensor $\mathbf{J}^{AB}$ between atoms $A$ and $B$ is evaluated as the second derivative of the electronic energy with respect to the nuclear magnetic moments $\mathbf{m}$,

$$\mathbf{J}^{AB} = \frac{\partial^2 E}{\partial \mathbf{m}_A \partial \mathbf{m}_B}. \tag{10.65}$$

The indirect coupling tensor has five distinct contributions. The diamagnetic spin–orbit (DSO) contribution is calculated as an expectation value with the ground state wave function. The other contributions are the paramagnetic spin–orbit (PSO), spin–dipole (SD), Fermi contact (FC), and mixed SD-FC contributions. These terms require the electronic response of the systems to the perturbation due to the magnetic nuclei. Ten distinct CPSCF equations must be solved for each perturbing nucleus, which makes the calculation of $J$-coupling constants time-consuming.

Some authors have recommended[127] calculating only the Fermi contact contribution, and skipping the other contributions for $^1$H–$^1$H coupling constants. For that purpose, Q-CHEM allows you to skip the calculation of any of the four (FC, SD, PSO, DSO) contributions (the mixed SD-FC contributions is automatically calculated at no additional cost whenever both the SD and FC contributions are calculated). See section 10.16.3 for details. Note that omitting any of the contributions cannot be rationalized from a theoretical point of view. Results from such calculations should be interpreted extremely conservatively.

Specialized basis sets are highly recommended in any $J$-coupling calculation. The pcJ-$n$ basis set family[128] has been added to the basis set library.

Note that the Hartree–Fock level of theory is *not* suitable to obtain $J$-coupling constants of *any* degree of reliability. Instead, use GGA or hybrid density functionals.

**Example 10.18** An example of $J$-coupling calculation: Water molecule with B3LYP/cc-pVDZ

```
$molecule
   0 1
   O
   H1 O OH
   H2 O OH H1 HOH

   OH  = 0.947
   HOH = 105.5
$end

$rem
   JOBTYPE          ISSC
   EXCHANGE         B3LYP
   BASIS            cc-pVDZ
   LIN_K            FALSE
   SYMMETRY         TRUE
   MOPROP_CONV_1ST  6
$end
```

## 10.16 Linear–Scaling Computation of Electric Properties

The search for new optical devices is a major field of materials sciences. Here, polarizabilities and hyperpolarizabilities provide particularly important information on molecular systems. The response of the molecular systems in the presence of an external monochromatic oscillatory electric field is determined by the solution of the TDSCF equations, where the perturbation is represented as the interaction of the molecule with a single Fourier component within the dipole approximation:

$$\hat{H}^{(S)} = \frac{1}{2}\hat{\mu}\mathcal{E}\left(e^{-i\omega t} + e^{+i\omega t}\right) \tag{10.66}$$

$$\hat{\mu} = -e\sum_{i=1}^{N}\hat{r}_i \tag{10.67}$$

Here, $\mathcal{E}$ is the E-field vector, $\omega$ the corresponding frequency, $e$ the electronic charge and $\mu$ the dipole moment operator. Starting from Frenkel's variational principle the TDSCF equations can be derived by standard techniques of perturbation theory[129]. As a solution, we obtain the first-order [$\mathrm{P}^{\mathrm{x}}(\pm\omega)$] and second-order [*e.g.*, $\mathrm{P}^{\mathrm{xy}}(\pm\omega, \pm\omega)$] perturbed density matrices with which the following properties are calculated:

- Static polarizability: $\alpha_{\mathrm{xy}}(0;0) = \mathrm{tr}\left[\mathbf{H}^{\mu_{\mathrm{x}}}\mathbf{P}^{\mathrm{y}}\left(\omega = 0\right)\right]$
- Dynamic polarizability: $\alpha_{\mathrm{xy}}(\pm\omega;\mp\omega) = \mathrm{tr}\left[\mathbf{H}^{\mu_{\mathrm{x}}}\mathbf{P}^{\mathrm{y}}(\pm\omega)\right]$
- Static hyperpolarizability: $\beta_{\mathrm{xyz}}(0;0,0) = \mathrm{tr}\left[\mathbf{H}^{\mu_{\mathrm{x}}}\mathbf{P}^{\mathrm{yz}}(\omega = 0, \omega = 0)\right]$
- Second harmonic generation: $\beta_{\mathrm{xyz}}(\mp 2\omega;\pm\omega,\pm\omega) = \mathrm{tr}\left[\mathbf{H}^{\mu_{\mathrm{x}}}\mathbf{P}^{\mathrm{yz}}(\pm\omega,\pm\omega)\right]$
- Electro-optical Pockels effect: $\beta_{\mathrm{xyz}}(\mp\omega;0,\pm\omega) = \mathrm{tr}\left[\mathbf{H}^{\mu_{\mathrm{x}}}\mathbf{P}^{\mathrm{yz}}(\omega = 0,\pm\omega)\right]$
- Optical rectification: $\beta_{\mathrm{xyz}}(0;\pm\omega,\mp\omega) = \mathrm{tr}\left[\mathbf{H}^{\mu_{\mathrm{x}}}\mathbf{P}^{\mathrm{yz}}(\pm\omega,\mp\omega)\right]$

where $\mathbf{H}^{\mu_{\mathrm{x}}}$ is the matrix representation of the $x$ component of the dipole moments.

The TDSCF calculation is the most time consuming step and scales asymptotically as $\mathcal{O}(N^3)$ because of the AO/MO transformations. The scaling behavior of the two-electron integral formations, which dominate over a wide range because of a larger pre-factor, can be reduced by LinK/CFMM from quadratic to linear ($\mathcal{O}(N^2)\rightarrow\mathcal{O}(N)$).

Third-order properties can be calculated with the equations above after a second-order TDSCF calculation (MOPROP: 101/102) or by use of Wigner's $(2n+1)$ rule[130] (MOPROP: 103/104). Since the second order TDSCF depends on the first-order results, the convergence of the algorithm may be problematically. So we recommend the use of 103/104 for the calculation of first hyperpolarizabilities.

These optical properties can be computed for the first time using linear-scaling methods (LinK/CFMM) for all integral contractions[114]. Although the present implementation available in Q-CHEM still uses MO-based time-dependent SCF (TDSCF) equations both at the HF and DFT level, the pre-factor of this $\mathcal{O}(M^3)$ scaling step is rather small, so that the reduction of the scaling achieved for the integral contractions is most important. Here, all derivatives are computed analytically.

Further specifications of the dynamic properties are done in the section *$fdpfreq* in the following format:

```
$fdpfreq
   property
```

```
      frequencies
      units
   $end
```

The first line is only required for third order properties to specify the kind of first hyperpolarizability:

- `StaticHyper` Static Hyperpolarizability
- `SHG` Second harmonic generation
- `EOPockels` Electro-optical Pockels effect
- `OptRect` Optical rectification

Line number 2 contains floating-point values for the frequencies of the perturbations. Alternatively, for dynamic polarizabilities an equidistant sequence of frequencies can be specified by the keyword WALK (see example below). The last line specifies the units of the given frequencies:

- `au` Frequency (atomic units)
- `eV` Frequency (eV)
- `nm` Wavelength (nm)
- `Hz` Frequency (Hertz)
- `cmInv` Wavenumber ($\mathrm{cm}^{-1}$)

### 10.16.1 Examples for Section *$fdpfreq*

**Example 10.19** Static and Dynamic polarizabilities, atomic units:

```
$fdpfreq
   0.0 0.03 0.05
   au
$end
```

**Example 10.20** Series of dynamic polarizabilities, starting with 0.00 incremented by 0.01 up to 0.10:

```
$fdpfreq
   walk 0.00 0.10 0.01
   au
$end
```

**Example 10.21** Static first hyperpolarizability, second harmonic generation and electro-optical Pockels effect, wavelength in nm:

```
$fdpfreq
   StaticHyper SHG EOPockels
   1064
   nm
$end
```

### 10.16.2 Features of Mopropman

- Restricted/unrestricted HF and KS-DFT CPSCF/TDSCF
- LinK/CFMM support to evaluate Coulomb- and exchange-like matrices
- DIIS acceleration
- Support of LSDA/GGA/Hybrid XC functionals listed below
- Analytical derivatives

The following XC functionals are supported:

Exchange:

- Dirac
- Becke 88

Correlation:

- Wigner
- VWN (both RPA and No. 5 parameterizations)
- Perdew-Zunger 81
- Perdew 86 (both PZ81 and VWN (No. 5) kernel)
- LYP

### 10.16.3 Job Control

The following options can be used:

**MOPROP**
Specifies the job for mopropman.
TYPE:
INTEGER
DEFAULT:
0 Do not run mopropman.
OPTIONS:

| | |
|---|---|
| 1 | NMR chemical shielding tensors. |
| 2 | Static polarizability. |
| 3 | Indirect nuclear spin–spin coupling tensors. |
| 100 | Dynamic polarizability. |
| 101 | First hyperpolarizability. |
| 102 | First hyperpolarizability, reading First order results from disk. |
| 103 | First hyperpolarizability using Wigner's $(2n + 1)$ rule. |
| 104 | First hyperpolarizability using Wigner's $(2n + 1)$ rule, reading first order results from disk. |

RECOMMENDATION:
None

**MOPROP_PERTNUM**

Set the number of perturbed densities that will to be treated together.

TYPE:

INTEGER

DEFAULT:

0

OPTIONS:

0 All at once.

$n$ Treat the perturbed densities batch-wise.

RECOMMENDATION:

Use the default. For large systems, limiting this number may be required to avoid memory exhaustion.

**MOPROP_CONV_1ST**

Sets the convergence criteria for CPSCF and 1st order TDSCF.

TYPE:

INTEGER

DEFAULT:

6

OPTIONS:

$n < 10$ Convergence threshold set to $10^{-n}$.

RECOMMENDATION:

None

**MOPROP_CONV_2ND**

Sets the convergence criterion for second-order TDSCF.

TYPE:

INTEGER

DEFAULT:

6

OPTIONS:

$n < 10$ Convergence threshold set to $10^{-n}$.

RECOMMENDATION:

None

**MOPROP_MAXITER_1ST**

The maximum number of iterations for CPSCF and first-order TDSCF.

TYPE:

INTEGER

DEFAULT:

50

OPTIONS:

$n$ Set maximum number of iterations to $n$.

RECOMMENDATION:

Use the default.

**MOPROP_MAXITER_2ND**

The maximum number of iterations for second-order TDSCF.

TYPE:

INTEGER

DEFAULT:

50

OPTIONS:

$n$ Set maximum number of iterations to $n$.

RECOMMENDATION:

Use the default.

**MOPROP_ISSC_PRINT_REDUCED**

Specifies whether the isotope-independent reduced coupling tensor $\mathbf{K}$ should be printed in addition to the isotope-dependent $\mathbf{J}$-tensor when calculating indirect nuclear spin–spin couplings.

TYPE:

LOGICAL

DEFAULT:

FALSE

OPTIONS:

FALSE Do not print $\mathbf{K}$.

TRUE Print $\mathbf{K}$.

RECOMMENDATION:

None

**MOPROP_ISSC_SKIP_FC**

Specifies whether to skip the calculation of the Fermi contact contribution to the indirect nuclear spin–spin coupling tensor.

TYPE:

LOGICAL

DEFAULT:

FALSE

OPTIONS:

FALSE Calculate Fermi contact contribution.

TRUE Skip Fermi contact contribution.

RECOMMENDATION:

None

**MOPROP_ISSC_SKIP_SD**

Specifies whether to skip the calculation of the spin–dipole contribution to the indirect nuclear spin–spin coupling tensor.

TYPE:

LOGICAL

DEFAULT:

FALSE

OPTIONS:

| | |
|---|---|
| FALSE | Calculate spin–dipole contribution. |
| TRUE | Skip spin–dipole contribution. |

RECOMMENDATION:

None

**MOPROP_ISSC_SKIP_PSO**

Specifies whether to skip the calculation of the paramagnetic spin–orbit contribution to the indirect nuclear spin–spin coupling tensor.

TYPE:

LOGICAL

DEFAULT:

FALSE

OPTIONS:

| | |
|---|---|
| FALSE | Calculate paramagnetic spin–orbit contribution. |
| TRUE | Skip paramagnetic spin–orbit contribution. |

RECOMMENDATION:

None

**MOPROP_ISSC_SKIP_DSO**

Specifies whether to skip the calculation of the diamagnetic spin–orbit contribution to the indirect nuclear spin–spin coupling tensor.

TYPE:

LOGICAL

DEFAULT:

FALSE

OPTIONS:

| | |
|---|---|
| FALSE | Calculate diamagnetic spin–orbit contribution. |
| TRUE | Skip diamagnetic spin–orbit contribution. |

RECOMMENDATION:

None

**MOPROP_DIIS**

Controls the use of Pulay's DIIS in solving the CPSCF equations.

TYPE:

INTEGER

DEFAULT:

5

OPTIONS:

0 Turn off DIIS.

5 Turn on DIIS.

RECOMMENDATION:

None

**MOPROP_DIIS_DIM_SS**

Specified the DIIS subspace dimension.

TYPE:

INTEGER

DEFAULT:

20

OPTIONS:

0 No DIIS.

$n$ Use a subspace of dimension $n$.

RECOMMENDATION:

None

**SAVE_LAST_GPX**

Save last $\mathbf{G}\left[\mathbf{P}^{\mathrm{x}}\right]$ when calculating dynamic polarizabilities in order to call mopropman in a second run with MOPROP = 102.

TYPE:

INTEGER

DEFAULT:

0

OPTIONS:

0 False

1 True

RECOMMENDATION:

None

## 10.17 Electronic Couplings for Electron- and Energy Transfer

### 10.17.1 Eigenstate-Based Methods

For electron transfer (ET) and excitation energy transfer (EET) processes, the electronic coupling is one of the important parameters that determine their reaction rates. For ET, Q-CHEM provides the coupling values calculated with the generalized Mulliken-Hush (GMH)[131], fragment-charge difference (FCD)[132], Boys localization[133], and Edmiston-Ruedenbeg localization[134] schemes. For EET, options include fragment-excitation difference (FED)[135], fragment-spin difference (FSD)[136], occupied-virtual separated Boys localization[137] or Edmiston-Ruedenberg localization[134]. In all these schemes, a vertical excitation such as CIS, RPA or TDDFT is required, and the GMH, FCD, FED, FSD, Boys or ER coupling values are calculated based on the excited state results.

#### 10.17.1.1 Two-state approximation

Under the two-state approximation, the diabatic reactant and product states are assumed to be a linear combination of the eigenstates. For ET, the choice of such linear combination is determined by a zero transition dipoles (GMH) or maximum charge differences (FCD). In the latter, a $2 \times 2$ donor–acceptor charge difference matrix, $\Delta\mathbf{q}$, is defined, with elements

$$\Delta q_{mn} = q^{\mathrm{D}}_{mn} - q^{\mathrm{A}}_{mn} = \int_{\mathbf{r}\in\mathrm{D}} \rho_{mn}(\mathbf{r}) d\mathbf{r} - \int_{\mathbf{r}\in\mathrm{A}} \rho_{mn}(\mathbf{r}) d\mathbf{r}$$

where $\rho_{mn}(\mathbf{r})$ is the matrix element of the density operator between states $|m\rangle$ and $|n\rangle$.

For EET, a maximum excitation difference is assumed in the FED, in which a excitation difference matrix is similarly defined with elements

$$\Delta x_{mn} = x^{\mathrm{D}}_{mn} - x^{\mathrm{A}}_{mn} = \int_{\mathbf{r}\in\mathrm{D}} \rho^{(mn)}_{\mathrm{ex}}(\mathbf{r}) d\mathbf{r} - \int_{\mathbf{r}\in\mathrm{A}} \rho^{(mn)}_{\mathrm{ex}}(\mathbf{r}) d\mathbf{r}$$

where $\rho^{(mn)}_{\mathrm{ex}}(\mathbf{r})$ is the sum of attachment and detachment densities for transition $|m\rangle \rightarrow |n\rangle$, as they correspond to the electron and hole densities in an excitation. In the FSD, a maximum spin difference is used and the corresponding spin difference matrix is defined with its elements as,

$$\Delta s_{mn} = s^{\mathrm{D}}_{mn} - s^{\mathrm{A}}_{mn} = \int_{\mathbf{r}\in\mathrm{D}} \sigma_{(mn)}(\mathbf{r}) d\mathbf{r} - \int_{\mathbf{r}\in\mathrm{A}} \sigma_{(mn)}(\mathbf{r}) d\mathbf{r}$$

where $\sigma_{mn}(\mathbf{r})$ is the spin density, difference between $\alpha$-spin and $\beta$-spin densities, for transition from $|m\rangle \rightarrow |n\rangle$.

Since Q-CHEM uses a Mulliken population analysis for the integrations in Eqs. (10.68), (10.68), and (10.68), the matrices $\Delta\mathbf{q}$, $\Delta\mathbf{x}$ and $\Delta\mathbf{s}$ are not symmetric. To obtain a pair of orthogonal states as the diabatic reactant and product states, $\Delta\mathbf{q}$, $\Delta\mathbf{x}$ and $\Delta\mathbf{s}$ are symmetrized in Q-CHEM. Specifically,

$$\overline{\Delta q}_{mn} = (\Delta q_{mn} + \Delta q_{nm})/2 \tag{10.68a}$$

$$\overline{\Delta x}_{mn} = (\Delta x_{mn} + \Delta x_{nm})/2 \tag{10.68b}$$

$$\overline{\Delta s}_{mn} = (\Delta s_{mn} + \Delta s_{nm})/2 \tag{10.68c}$$

The final coupling values are obtained as listed below:

- For GMH,

$$V_{\mathrm{ET}} = \frac{(E_2 - E_1)\,|\vec{\mu}_{12}|}{\sqrt{(\vec{\mu}_{11} - \vec{\mu}_{22})^2 + 4\,|\vec{\mu}_{12}|^2}} \tag{10.69}$$

- For FCD,

$$V_{\mathrm{ET}} = \frac{(E_2 - E_1)\overline{\Delta q}_{12}}{\sqrt{(\Delta q_{11} - \Delta q_{22})^2 + 4\overline{\Delta q}^2_{12}}} \tag{10.70}$$

- For FED,

$$V_{\mathrm{EET}} = \frac{(E_2 - E_1)\overline{\Delta x}_{12}}{\sqrt{(\Delta x_{11} - \Delta x_{22})^2 + 4\overline{\Delta x}^2_{12}}} \tag{10.71}$$

- For FSD,

$$V_{\mathrm{EET}} = \frac{(E_2 - E_1)\overline{\Delta s}_{12}}{\sqrt{(\Delta s_{11} - \Delta s_{22})^2 + 4\overline{\Delta s}_{12}^2}} \tag{10.72}$$

Q-CHEM provides the option to control FED, FSD, FCD and GMH calculations after a single-excitation calculation, such as CIS, RPA, TDDFT/TDA and TDDFT. To obtain ET coupling values using GMH (FCD) scheme, one should set *$rem* variables STS_GMH (STS_FCD) to be TRUE. Similarly, a FED (FSD) calculation is turned on by setting the *$rem* variable STS_FED (STS_FSD) to be TRUE. In FCD, FED and FSD calculations, the donor and acceptor fragments are defined via the *$rem* variables STS_DONOR and STS_ACCEPTOR. It is necessary to arrange the atomic order in the *$molecule* section such that the atoms in the donor (acceptor) fragment is in one consecutive block. The ordering numbers of beginning and ending atoms for the donor and acceptor blocks are included in *$rem* variables STS_DONOR and STS_ACCEPTOR.

The couplings will be calculated between all choices of excited states with the same spin. In FSD, FCD and GMH calculations, the coupling value between the excited and reference (ground) states will be included, but in FED, the ground state is not included in the analysis. It is important to select excited states properly, according to the distribution of charge or excitation, among other characteristics, such that the coupling obtained can properly describe the electronic coupling of the corresponding process in the two-state approximation.

**STS_GMH**

Control the calculation of GMH for ET couplings.

TYPE:

LOGICAL

DEFAULT:

FALSE

OPTIONS:

FALSE Do not perform a GMH calculation.

TRUE Include a GMH calculation.

RECOMMENDATION:

When set to true computes Mulliken-Hush electronic couplings. It yields the generalized Mulliken-Hush couplings as well as the transition dipole moments for each pair of excited states and for each excited state with the ground state.

**STS_FCD**

Control the calculation of FCD for ET couplings.

TYPE:

LOGICAL

DEFAULT:

FALSE

OPTIONS:

FALSE Do not perform an FCD calculation.

TRUE Include an FCD calculation.

RECOMMENDATION:

None

**STS_FED**

Control the calculation of FED for EET couplings.

TYPE:

LOGICAL

DEFAULT:

FALSE

OPTIONS:

FALSE Do not perform a FED calculation.

TRUE Include a FED calculation.

RECOMMENDATION:

None

**STS_FSD**

Control the calculation of FSD for EET couplings.

TYPE:

LOGICAL

DEFAULT:

FALSE

OPTIONS:

FALSE Do not perform a FSD calculation.

TRUE Include a FSD calculation.

RECOMMENDATION:

For RCIS triplets, FSD and FED are equivalent. FSD will be automatically switched off and perform a FED calculation.

**STS_DONOR**

Define the donor fragment.

TYPE:

STRING

DEFAULT:

0 No donor fragment is defined.

OPTIONS:

*i*-*j* Donor fragment is in the $i$th atom to the $j$th atom.

RECOMMENDATION:

Note no space between the hyphen and the numbers $i$ and $j$.

**STS_ACCEPTOR**

Define the acceptor molecular fragment.

TYPE:

STRING

DEFAULT:

0 No acceptor fragment is defined.

OPTIONS:

*i*-*j* Acceptor fragment is in the $i$th atom to the $j$th atom.

RECOMMENDATION:

Note no space between the hyphen and the numbers $i$ and $j$.

**STS_MOM**

Control calculation of the transition moments between excited states in the CIS and TDDFT calculations (including SF variants).

TYPE:

LOGICAL

DEFAULT:

FALSE

OPTIONS:

FALSE Do not calculate state-to-state transition moments.

TRUE Do calculate state-to-state transition moments.

RECOMMENDATION:

When set to true requests the state-to-state dipole transition moments for all pairs of excited states and for each excited state with the ground state.

**Example 10.22** A GMH & FCD calculation to analyze electron-transfer couplings in an ethylene and a methaniminium cation.

```
$molecule
   1  1
   C     0.679952    0.000000    0.000000
   N    -0.600337    0.000000    0.000000
   H     1.210416    0.940723    0.000000
   H     1.210416   -0.940723    0.000000
   H    -1.131897   -0.866630    0.000000
   H    -1.131897    0.866630    0.000000
   C    -5.600337    0.000000    0.000000
   C    -6.937337    0.000000    0.000000
   H    -5.034682    0.927055    0.000000
   H    -5.034682   -0.927055    0.000000
   H    -7.502992   -0.927055    0.000000
   H    -7.502992    0.927055    0.000000
$end

$rem
   METHOD        CIS
   BASIS         6-31+G
   CIS_N_ROOTS   20
   CIS_SINGLETS  true
   CIS_TRIPLETS  false
   STS_GMH       true !turns on the GMH calculation
   STS_FCD       true !turns on the FCD calculation
   STS_DONOR     1-6  !define the donor fragment as atoms 1-6 for FCD calc.
   STS_ACCEPTOR  7-12 !define the acceptor fragment as atoms 7-12 for FCD calc.
   MEM_STATIC    200  !increase static memory for a CIS job with larger basis set
$end
```

**Example 10.23** An FED calculation to analyze excitation-energy transfer couplings in a pair of stacked ethylenes.

```
$molecule
   0  1
   C     0.670518    0.000000    0.000000
   H     1.241372    0.927754    0.000000
   H     1.241372   -0.927754    0.000000
   C    -0.670518    0.000000    0.000000
   H    -1.241372   -0.927754    0.000000
   H    -1.241372    0.927754    0.000000
   C     0.774635    0.000000    4.500000
   H     1.323105    0.936763    4.500000
   H     1.323105   -0.936763    4.500000
   C    -0.774635    0.000000    4.500000
   H    -1.323105   -0.936763    4.500000
   H    -1.323105    0.936763    4.500000
$end

$rem
   METHOD            CIS
   BASIS             3-21G
   CIS_N_ROOTS       20
   CIS_SINGLETS      true
   CIS_TRIPLETS      false
   STS_FED           true
   STS_DONOR         1-6
   STS_ACCEPTOR      7-12
$end
```

#### 10.17.1.2 Multi-state treatments

When dealing with multiple charge or electronic excitation centers, diabatic states can be constructed with Boys[133] or Edmiston-Ruedenberg[134] localization. In this case, we construct diabatic states $\{|\Xi_I\rangle\}$ as linear combinations of adiabatic states $\{|\Phi_I\rangle\}$ with a general rotation matrix $\mathbf{U}$ that is $N_{\text{state}} \times N_{\text{state}}$ in size:

$$|\Xi_I\rangle = \sum_{J=1}^{N_{\text{states}}} |\Phi_J\rangle \, U_{ji} \qquad\qquad I = 1 \ldots N_{\text{states}} \tag{10.73}$$

The adiabatic states can be produced with any method, in principle, but the Boys/ER-localized diabatization methods have been implemented thus far only for CIS or TDDFT methods in Q-CHEM. In analogy to orbital localization, Boys-localized diabatization corresponds to maximizing the charge separation between diabatic state centers:

$$f_{\text{Boys}}(\mathbf{U}) = f_{\text{Boys}}(\{\Xi_I\}) = \sum_{I,J=1}^{N_{\text{states}}} \left| \langle \Xi_I|\vec{\mu}|\Xi_I\rangle - \langle \Xi_J|\vec{\mu}|\Xi_J\rangle \right|^2 \tag{10.74}$$

Here, $\vec{\mu}$ represents the dipole operator. ER-localized diabatization prescribes maximizing self-interaction energy:

$$f_{ER}(\mathbf{U}) = f_{\text{ER}}(\{\Xi_I\}) = \sum_{I=1}^{N_{\text{states}}} \int d\vec{\mathcal{R}}_1 \int d\vec{\mathcal{R}}_2 \frac{\langle \Xi_I|\hat{\rho}(\vec{\mathcal{R}}_2)|\Xi_I\rangle\langle \Xi_I|\hat{\rho}(\vec{\mathcal{R}}_1)|\Xi_I\rangle}{|\vec{\mathcal{R}}_1 - \vec{\mathcal{R}}_2|} \tag{10.75}$$

where the density operator at position $\vec{\mathcal{R}}$ is

$$\hat{\rho}(\vec{\mathcal{R}}) = \sum_j \delta(\vec{\mathcal{R}} - \vec{r}^{(j)}) \tag{10.76}$$

Here, $\vec{r}^{(j)}$ represents the position of the $j$th electron.

These models reflect different assumptions about the interaction of our quantum system with some fictitious external electric field/potential: $(i)$ if we assume a fictitious field that is linear in space, we arrive at Boys localization; $(ii)$ if we assume a fictitious potential energy that responds linearly to the charge density of our system, we arrive at ER localization. Note that in the two-state limit, Boys localized diabatization reduces nearly exactly to GMH[133].

As written down in Eq. (10.74), Boys localized diabatization applies only to charge transfer, not to energy transfer. Within the context of CIS or TDDFT calculations, one can easily extend Boys localized diabatization[137] by separately localizing the occupied and virtual components of $\vec{\mu}$, $\vec{\mu}^{\,\text{occ}}$ and $\vec{\mu}^{\,\text{virt}}$:

$$\begin{aligned} f_{\text{BoysOV}}(\mathbf{U}) &= f_{\text{BoysOV}}(\{\Xi_I\}) \\ &= \sum_{I,J=1}^{N_{\text{states}}} \left( \left| \langle \Xi_I | \vec{\mu}^{\,\text{occ}} | \Xi_I \rangle - \langle \Xi_J | \vec{\mu}^{\,\text{occ}} | \Xi_J \rangle \right|^2 + \left| \langle \Xi_I | \vec{\mu}^{\,\text{virt}} | \Xi_I \rangle - \langle \Xi_J | \vec{\mu}^{\,\text{virt}} | \Xi_J \rangle \right|^2 \right) \end{aligned} \tag{10.77}$$

where

$$|\Xi_I\rangle = \sum_{ia} t_i^{Ia} |\Phi_i^a\rangle \tag{10.78}$$

and the occupied/virtual components are defined by

$$\langle \Xi_I | \, \vec{\mu} \, | \Xi_J \rangle \quad = \quad \underbrace{\delta_{IJ} \sum_i \vec{\mu}_{ii} - \sum_{aij} t_i^{Ia} t_j^{Ja} \vec{\mu}_{ij}}_{\langle \Xi_I | \, \vec{\mu}^{\,\text{occ}} \, | \Xi_J \rangle} + \underbrace{\sum_{iba} t_i^{Ia} t_i^{Jb} \vec{\mu}_{ab}}_{\langle \Xi_I | \, \vec{\mu}^{\,\text{virt}} \, | \Xi_J \rangle} \tag{10.79}$$

Note that when we maximize the Boys OV function, we are simply performing Boys-localized diabatization separately on the electron attachment and detachment densities.

Finally, for energy transfer, it can be helpful to understand the origin of the diabatic couplings. To that end, we now provide the ability to decompose the diabatic coupling between diabatic states into Coulomb (J), Exchange (K) and one-electron (O) components[138]:

$$\langle \Xi_P | \, H \, | \Xi_Q \rangle \quad = \quad \underbrace{\sum_{iab} t_i^{Pa} t_i^{Qb} F_{ab} - \sum_{ija} t_i^{Pa} t_j^{Qa} F_{ij}}_{O} + \underbrace{\sum_{ijab} t_i^{Pa} t_j^{Qb} \, (ia|jb)}_{J} - \underbrace{\sum_{ijab} t_i^{Pa} t_j^{Qb} \, (ij|ab)}_{K} \tag{10.80}$$

**BOYS_CIS_NUMSTATE**

Define how many states to mix with Boys localized diabatization. These states must be specified in the *$localized_diabatization* section.

TYPE:

INTEGER

DEFAULT:

0 Do not perform Boys localized diabatization.

OPTIONS:

2 to N where N is the number of CIS states requested (CIS_N_ROOTS)

RECOMMENDATION:

It is usually not wise to mix adiabatic states that are separated by more than a few eV or a typical reorganization energy in solvent.

**ER_CIS_NUMSTATE**
Define how many states to mix with ER localized diabatization. These states must be specified in the *$localized_diabatization* section.
TYPE:
INTEGER
DEFAULT:
0 Do not perform ER localized diabatization.
OPTIONS:
2 to N where N is the number of CIS states requested (CIS_N_ROOTS)
RECOMMENDATION:
It is usually not wise to mix adiabatic states that are separated by more than a few eV or a typical reorganization energy in solvent.

**LOC_CIS_OV_SEPARATE**
Decide whether or not to localized the "occupied" and "virtual" components of the localized diabatization function, *i.e.*, whether to localize the electron attachments and detachments separately.
TYPE:
LOGICAL
DEFAULT:
FALSE Do not separately localize electron attachments and detachments.
OPTIONS:
TRUE
RECOMMENDATION:
If one wants to use Boys localized diabatization for energy transfer (as opposed to electron transfer) , this is a necessary option. ER is more rigorous technique, and does not require this OV feature, but will be somewhat slower.

**CIS_DIABATH_DECOMPOSE**
Decide whether or not to decompose the diabatic coupling into Coulomb, exchange, and one-electron terms.
TYPE:
LOGICAL
DEFAULT:
FALSE Do not decompose the diabatic coupling.
OPTIONS:
TRUE
RECOMMENDATION:
These decompositions are most meaningful for electronic excitation transfer processes. Currently, available only for CIS, not for TDDFT diabatic states.

**Example 10.24** A calculation using ER localized diabatization to construct the diabatic Hamiltonian and couplings between a square of singly-excited Helium atoms.

```
$molecule
   0 1
   he   0  -1.0    1.0
   he   0  -1.0   -1.0
   he   0   1.0   -1.0
   he   0   1.0    1.0
$end
```

```
$rem
   method                 cis
   cis_n_roots            4
   cis_singles            false
   cis_triplets           true
   basis                  6-31g**
   scf_convergence        8
   symmetry               false
   rpa                    false
   sym_ignore             true
   sym_ignore             true
   loc_cis_ov_separate    false  ! NOT localizing attachments/detachments separately.
   er_cis_numstate        4      ! using ER to mix 4 adiabatic states.
   cis_diabatH_decompose  true   ! decompose diabatic couplings into
                                 ! Coulomb, exchange, and one-electron components.
$end

$localized_diabatization
   On the next line, list which excited adiabatic states we want to mix.
   1 2 3 4
$end
```

## 10.17.2 Diabatic-State-Based Methods

### 10.17.2.1 Electronic coupling in charge transfer

A charge transfer involves a change in the electron numbers in a pair of molecular fragments. As an example, we will use the following reaction when necessary, and a generalization to other cases is straightforward:

$$\mathrm{D^-A} \longrightarrow \mathrm{DA^-} \tag{10.81}$$

where an extra electron is localized to the donor (D) initially, and it becomes localized to the acceptor (A) in the final state. The two-state secular equation for the initial and final electronic states can be written as

$$\mathbf{H} - E\mathbf{S} = \begin{pmatrix} H_{\mathrm{ii}} - S_{\mathrm{ii}}E & H_{\mathrm{if}} - S_{\mathrm{if}}E \\ H_{\mathrm{if}} - S_{\mathrm{if}}E & H_{\mathrm{ff}} - S_{\mathrm{ff}}E \end{pmatrix} = 0 \tag{10.82}$$

This is very close to an eigenvalue problem except for the non-orthogonality between the initial and final states. A standard eigenvalue form for Eq. (10.82) can be obtained by using the Löwdin transformation:

$$\mathbf{H}_{\mathrm{eff}} = \mathbf{S}^{-1/2}\mathbf{H}\mathbf{S}^{-1/2}, \tag{10.83}$$

where the off-diagonal element of the effective Hamiltonian matrix represents the *electronic coupling* for the reaction, and it is defined by

$$V = H_{\mathrm{if}}^{\mathrm{eff}} = \frac{H_{\mathrm{if}} - S_{\mathrm{if}}(H_{\mathrm{ii}} + H_{\mathrm{ff}})/2}{1 - S_{\mathrm{if}}^2} \tag{10.84}$$

In a general case where the initial and final states are not normalized, the electronic coupling is written as

$$V = \sqrt{S_{\mathrm{ii}}S_{\mathrm{ff}}} \times \frac{H_{\mathrm{if}} - S_{\mathrm{if}}(H_{\mathrm{ii}}/S_{\mathrm{ii}} + H_{\mathrm{ff}}/S_{\mathrm{ff}})/2}{S_{\mathrm{ii}}S_{\mathrm{ff}} - S_{\mathrm{if}}^2} \tag{10.85}$$

Thus, in principle, $V$ can be obtained when the matrix elements for the Hamiltonian $H$ and the overlap matrix $S$ are calculated.

The direct coupling (DC) scheme calculates the electronic coupling values via Eq. (10.85), and it is widely used to calculate the electron transfer coupling[139–142]. In the DC scheme, the coupling matrix element is calculated directly using charge-localized determinants (the "diabatic states" in electron transfer literature). In electron transfer systems, it has been shown that such charge-localized states can be approximated by symmetry-broken unrestricted Hartree-Fock (UHF) solutions[139,140,143]. The adiabatic eigenstates are assumed to be the symmetric and anti-symmetric linear combinations of the two symmetry-broken UHF solutions in a DC calculation. Therefore, DC couplings can be viewed as a result of two-configuration solutions that may recover the non-dynamical correlation.

The core of the DC method is based on the corresponding orbital transformation[144] and a calculation for Slater's determinants in $H_{\text{if}}$ and $S_{\text{if}}$ [141,142].

#### 10.17.2.2 Corresponding orbital transformation

Let $|\Psi_a\rangle$ and $|\Psi_b\rangle$ be two single Slater-determinant wave functions for the initial and final states, and $\mathbf{a}$ and $\mathbf{b}$ be the spin-orbital sets, respectively:

$$\mathbf{a} = (a_1, a_2, \cdots, a_N) \tag{10.86}$$

$$\mathbf{b} = (b_1, b_2, \cdots, b_N) \tag{10.87}$$

Since the two sets of spin-orbitals are not orthogonal, the overlap matrix $\mathbf{S}$ can be defined as:

$$\mathbf{S} = \int \mathbf{b}^\dagger \mathbf{a}\, d\tau. \tag{10.88}$$

We note that $\mathbf{S}$ is not Hermitian in general since the molecular orbitals of the initial and final states are separately determined. To calculate the matrix elements $H_{ab}$ and $S_{ab}$, two sets of new orthogonal spin-orbitals can be used by the corresponding orbital transformation[144]. In this approach, each set of spin-orbitals $\mathbf{a}$ and $\mathbf{b}$ are linearly transformed,

$$\hat{\mathbf{a}} = \mathbf{a}\mathbf{V} \tag{10.89}$$

$$\hat{\mathbf{b}} = \mathbf{b}\mathbf{U} \tag{10.90}$$

where $\mathbf{V}$ and $\mathbf{U}$ are the left-singular and right-singular matrices, respectively, in the singular value decomposition (SVD) of $\mathbf{S}$:

$$\mathbf{S} = \mathbf{U}\hat{\mathbf{s}}\mathbf{V}^\dagger \tag{10.91}$$

The overlap matrix in the new basis is now diagonal

$$\int \hat{\mathbf{b}}^\dagger \hat{\mathbf{a}} = \mathbf{U}^\dagger \left( \int \mathbf{b}^\dagger \mathbf{a} \right) \mathbf{V} = \hat{\mathbf{s}} \tag{10.92}$$

#### 10.17.2.3 Generalized density matrix

The Hamiltonian for electrons in molecules are a sum of one-electron and two-electron operators. In the following, we derive the expressions for the one-electron operator $\Omega^{(1)}$ and two-electron operator $\Omega^{(2)}$,

$$\Omega^{(1)} = \sum_{i=1}^{N} \omega(i) \tag{10.93}$$

$$\Omega^{(2)} = \frac{1}{2} \sum_{i,j=1}^{N} \omega(i,j) \tag{10.94}$$

where $\omega(i)$ and $\omega(i,j)$, for the molecular Hamiltonian, are

$$\omega(i) = h(i) = -\frac{1}{2}\nabla_i^2 + V(i) \tag{10.95}$$

and

$$\omega(i,j) = \frac{1}{r_{ij}} \tag{10.96}$$

The evaluation of matrix elements can now proceed:

$$S_{ab} = \langle \Psi_b | \Psi_a \rangle = \det(\mathbf{U})\det(\mathbf{V}^\dagger)\prod_{i=1}^{N}\hat{s}_{ii} \tag{10.97}$$

$$\Omega_{ab}^{(1)} = \langle \Psi_b | \Omega^{(1)} | \Psi_a \rangle = \det(\mathbf{U})\det(\mathbf{V}^\dagger)\sum_{i=1}^{N}\langle \hat{b}_i | \omega(1) | \hat{a}_i \rangle \cdot \prod_{j\neq i}^{N}\hat{s}_{jj} \tag{10.98}$$

$$\Omega_{ab}^{(2)} = \langle \Psi_b | \Omega^{(2)} | \Psi_a \rangle = \frac{1}{2}\det(\mathbf{U})\det(\mathbf{V}^\dagger)\sum_{ij}^{N}\langle \hat{b}_i\hat{b}_j | \omega(1,2)(1-P_{12}) | \hat{a}_i\hat{a}_j \rangle \cdot \prod_{k\neq i,j}^{N}\hat{s}_{kk} \tag{10.99}$$

$$H_{ab} = \Omega_{ab}^{(1)} + \Omega_{ab}^{(2)} \tag{10.100}$$

In an atomic orbital basis set, $\{\chi\}$, we can expand the molecular spin orbitals $\mathbf{a}$ and $\mathbf{b}$,

$$\mathbf{a} = \chi\mathbf{A}, \qquad \hat{\mathbf{a}} = \chi\mathbf{AV} = \chi\hat{\mathbf{A}} \tag{10.101}$$

$$\mathbf{b} = \chi\mathbf{B}, \qquad \hat{\mathbf{b}} = \chi\mathbf{BU} = \chi\hat{\mathbf{B}} \tag{10.102}$$

The one-electron terms, Eq. (10.97), can be expressed as

$$\begin{aligned} \Omega_{ab}^{(1)} &= \sum_{i}^{N}\sum_{\lambda\sigma}\hat{A}_{\lambda i}T_{ii}\hat{B}_{i\sigma}^\dagger\langle\chi_\sigma|\omega(1)|\chi_\lambda\rangle \\ &= \sum_{\lambda\sigma}G_{\lambda\sigma}\omega_{\sigma\lambda} \end{aligned} \tag{10.103}$$

where $T_{ii} = S_{ab}/\hat{s}_{ii}$ and define a generalized density matrix, $\mathbf{G}$:

$$\mathbf{G} \;=\; \hat{\mathbf{A}}\mathbf{T}\hat{\mathbf{B}}^\dagger \tag{10.104}$$

Similarly, the two-electron terms, Eq. (10.99), are

$$\begin{aligned} \Omega_{ab}^{(2)} &= \frac{1}{2}\sum_{ij}\sum_{\lambda\sigma}\sum_{\mu\nu}\hat{A}_{\lambda i}\hat{A}_{\sigma j}\left(\frac{1}{\hat{s}_{ii}}\right)T_{jj}\hat{B}_{i\mu}^\dagger\hat{B}_{j\nu}^\dagger\langle\chi_\mu\chi_\nu|\omega(1,2)|\chi_\lambda\chi_\sigma\rangle \\ &= \sum_{\lambda\sigma\mu\nu}G_{\lambda\mu}^{L}G_{\sigma\nu}^{R}\langle\mu\nu||\lambda\sigma\rangle \end{aligned} \tag{10.105}$$

where $\mathbf{G}^R$ and $\mathbf{G}^L$ are generalized density matrices as defined in Eq. (10.104) except $T_{ii}$ in $\mathbf{G}^L$ is replaced by $1/(2s_{ii})$.

The $\alpha$- and $\beta$-spin orbitals are treated explicitly. In terms of the spatial orbitals, the one- and two-electron contributions can be reduced to

$$\Omega_{ab}^{(1)} = \sum_{\lambda\sigma}G_{\lambda\sigma}^{\alpha}\omega_{\sigma\lambda} + \sum_{\lambda\sigma}G_{\lambda\sigma}^{\beta}\omega_{\sigma\lambda} \tag{10.106}$$

$$\begin{aligned} \Omega_{ab}^{(2)} &= \sum_{\lambda\sigma\mu\nu}G_{\lambda\mu}^{L\alpha}G_{\sigma\nu}^{R\alpha}(\langle\mu\nu|\lambda\sigma\rangle - \langle\mu\nu|\sigma\lambda\rangle) + \sum_{\lambda\sigma\mu\nu}G_{\lambda\mu}^{L\beta}G_{\sigma\nu}^{R\alpha}\langle\mu\nu|\lambda\sigma\rangle \\ &+ \sum_{\lambda\sigma\mu\nu}G_{\lambda\mu}^{L\alpha}G_{\sigma\nu}^{R\beta}\langle\mu\nu|\lambda\sigma\rangle + \sum_{\lambda\sigma\mu\nu}G_{\lambda\mu}^{L\beta}G_{\sigma\nu}^{R\beta}(\langle\mu\nu|\lambda\sigma\rangle - \langle\mu\nu|\sigma\lambda\rangle) \end{aligned} \tag{10.107}$$

The resulting one- and two-electron contributions, Eqs. (10.106) and (10.107) can be easily computed in terms of generalized density matrices using standard one- and two-electron integral routines in Q-CHEM.

#### 10.17.2.4 Direct coupling method for electronic coupling

It is important to obtain proper charge-localized initial and final states for the DC scheme, and this step determines the quality of the coupling values. Q-CHEM provides two approaches to construct charge-localized states:

- **The "1+1" approach**
  Since the system consists of donor and acceptor molecules or fragments, with a charge being localized either donor or acceptor, it is intuitive to combine wave functions of individual donor and acceptor fragments to form a charge-localized wave function. We call this approach "1+1" since the zeroth order wave functions are composed of the HF wave functions of the two fragments.

  For example, for the case shown in Example (10.81), we can use Q-CHEM to calculate two HF wave functions: those of anionic donor and of neutral acceptor and they jointly form the initial state. For the final state, wave functions of neutral donor and anionic acceptor are used. Then the coupling value is calculated via Eq. (10.85).

  **Example 10.25** To calculate the electron-transfer coupling for a pair of stacked-ethylene with "1+1" charge-localized states

```
$molecule
  -1  2
--
  -1  2,  0  1
   C    0.662489    0.000000    0.000000
   H    1.227637    0.917083    0.000000
   H    1.227637   -0.917083    0.000000
   C   -0.662489    0.000000    0.000000
   H   -1.227637   -0.917083    0.000000
   H   -1.227637    0.917083    0.000000
--
   0  1, -1  2
   C    0.720595    0.000000    4.5
   H    1.288664    0.921368    4.5
   H    1.288664   -0.921368    4.5
   C   -0.720595    0.000000    4.5
   H   -1.288664   -0.921368    4.5
   H   -1.288664    0.921368    4.5
$end

$rem
   JOBTYPE            SP
   METHOD             HF
   BASIS              6-31G(d)
   SCF_PRINT_FRGM     FALSE
   SYM_IGNORE         TRUE
   SCF_GUESS          FRAGMO
   STS_DC             TRUE
$end
```

  In the *$molecule* subsection, the first line is for the charge and multiplicity of the whole system. The following blocks are two inputs for the two molecular fragments (donor and acceptor). In each block the first line consists of the charge and spin multiplicity in the initial state of the corresponding fragment, a comma, then the charge and multiplicity in the final state. Next lines are nuclear species and their positions of the fragment. For example, in the above example, the first block indicates that the electron donor is a doublet ethylene anion initially, and it becomes a singlet neutral species in the final state. The second block is for another ethylene going from a singlet neutral molecule to a doublet anion.

Note that the last three *$rem* variables in this example, SYM_IGNORE, SCF_GUESS and STS_DC must be set to be the values as in the example in order to perform DC calculation with "1+1" charge-localized states. An additional *$rem* variable, SCF_PRINT_FRGM is included. When it is TRUE a detailed output for the fragment HF self-consistent field calculation is given.

- **The "relaxed" approach**
  In "1+1" approach, the intermolecular interaction is neglected in the initial and final states, and so the final electronic coupling can be underestimated. As a second approach, Q-CHEM can use "1+1" wave function as an initial guess to look for the charge-localized wave function by further HF self-consistent field calculation. This approach would 'relax' the wave function constructed by "1+1" method and include the intermolecular interaction effects in the initial and final wave functions. However, this method may sometimes fail, leading to either convergence problems or a resulting HF wave function that cannot represent the desired charge-localized states. This is more likely to be a problem when calculations are performed with diffusive basis functions, or when the donor and acceptor molecules are very close to each other.

  To perform relaxed DC calculation, set STS_DC = RELAX.

## 10.18 Calculating the Population of Effectively Unpaired Electrons with DFT

In a stretched hydrogen molecule the two electrons that are paired at equilibrium forming a bond become un-paired and localized on the individual H atoms. In singlet diradicals or doublet triradicals such a weak paring exists even at equilibrium. At a single-determinant SCF level of the theory the valence electrons of a singlet system like $H_2$ remain perfectly paired, and one needs to include non-dynamical correlation to decouple the bond electron pair, giving rise to a population of effectively-unpaired ("odd", radicalized) electrons[145–147]. When the static correlation is strong, these electrons remain mostly unpaired and can be described as being localized on individual atoms.

These phenomena can be properly described within wave-function formalism. Within DFT, these effects can be described by broken-symmetry approach or by using SF-TDDFT (see Section 6.3.1). Below we describe how to derive this sort of information from pure DFT description of such low-spin open-shell systems without relying on spin-contaminated solutions.

The first-order reduced density matrix (1-RDM) corresponding to a single-determinant wave function (*e.g.*, SCF or Kohn-Sham DFT) is idempotent:

$$\int \gamma_\sigma^{\rm SCF}(1;2)\gamma_\sigma^{\rm SCF}(2;1)\,d\mathbf{r}_2 = \rho_\sigma(\mathbf{r}_1)\,,\ \gamma_\sigma^{\rm SCF}(1;2) = \sum_i^{\rm occ} \psi_{i\sigma}^{\rm ks}(1)\psi_{i\sigma}^{\rm ks}(2)\,, \tag{10.108}$$

where $\rho_\sigma(1)$ is the electron density of spin $\sigma$ at position $\mathbf{r_1}$, and $\gamma_\sigma^{\rm SCF}$ is the spin-resolved 1-RDM of a single Slater determinant. The cross product $\gamma_\sigma^{\rm SCF}(1;2)\gamma_\sigma^{\rm SCF}(2;1)$ reflects the Hartree-Fock exchange (or

Kohn-Sham exact-exchange) governed by the HF exchange hole:

$$\gamma_\sigma^{\rm SCF}(1;2)\gamma_\sigma^{\rm SCF}(2;1) = \rho_\alpha(1)h_{{\rm X}\sigma\sigma}(1,2)\,, \quad \int h_{{\rm X}\sigma\sigma}(1,2)\,d\mathbf{r}_2 = 1\;. \tag{10.109}$$

When 1-RDM includes electron correlation, it becomes non-idempotent:

$$D_\sigma(1) \equiv \rho_\sigma(1) - \int \gamma_\sigma(1;2)\gamma_\sigma(2;1)\,d\mathbf{r}_2 \geq 0\,. \tag{10.110}$$

The function $D_\sigma(1)$ measures the deviation from idempotency of the correlated 1-RDM and yields the density of effectively-unpaired (odd) electrons of spin $\sigma$ at point $\mathbf{r}_1$ [145,148]. The formation of effectively-unpaired electrons in singlet systems is therefore exclusively a correlation based phenomenon. Summing $D_\sigma(1)$ over the spin components gives the total density of odd electrons, and integrating the latter over space gives the mean total number of odd electrons $\bar{N}_u$:

$$D_u(1) = 2\sum_\sigma D_\sigma(1)d\mathbf{r}_1,\ \bar{N}_u = \int D_u(1)d\mathbf{r}_1\,. \tag{10.111}$$

The appearance of a factor of 2 in Eq. (10.111) above is required for reasons discussed in Ref. 148. In Kohn-Sham DFT, the SCF 1-RDM is always idempotent which impedes the analysis of odd electron formation at that level of the theory. Ref. 149 has proposed a remedy to this situation. It was noted that the correlated 1-RDM cross product entering Eq. (10.110) reflects an effective exchange (also known as cumulant exchange [146]). The KS exact-exchange hole is itself artificially too delocalized. However, the total exchange-correlation interaction in a finite system with strong left-right (*i.e.*, static) correlation is normally fairly localized, largely confined within a region of roughly atomic size [150]. The effective exchange described with the correlated 1-RDM cross product should be fairly localized as well. With this in mind, the following form of the correlated 1-RDM cross product was proposed [149]:

$$\gamma_\sigma(1;2)\,\gamma_\sigma(2;1) = \rho_\sigma(1)\bar{h}^{\rm eff}_{{\rm X}\sigma\sigma}(1,2)\,. \tag{10.112}$$

where the function $\bar{h}^{\rm eff}_{{\rm X}\sigma\sigma}(1;2)$ is a model DFT exchange hole of Becke-Roussel (BR) form used in Becke's B05 method [151]. The latter describes left-right static correlation effects in terms of certain effective exchange-correlation hole [151]. The extra delocalization of the HF exchange hole alone is compensated by certain physically motivated real-space corrections to it [151]:

$$\bar{h}_{{\rm XC}\alpha\alpha}(1,2) = \bar{h}^{\rm eff}_{{\rm X}\alpha\alpha}(1,2) + f_{\rm c}(1)\,\bar{h}^{\rm eff}_{{\rm X}\beta\beta}(1,2)\ , \tag{10.113}$$

where the BR exchange hole $\bar{h}^{\rm eff}_{{\rm X}\sigma\sigma}$ is used in B05 as an auxiliary function, such that the potential from the relaxed BR hole equals that of the exact-exchange hole. This results in relaxed normalization of the auxiliary BR hole less than or equal to 1:

$$\int \bar{h}^{\rm eff}_{{\rm X}\sigma\sigma}(1;2)d\mathbf{r}_2 = N^{\rm eff}_{X\sigma}(1)\ \leq 1\,. \tag{10.114}$$

The expression of the relaxed normalization $N^{\rm eff}_{{\rm X}\sigma}(\mathbf{r})$ is quite complicated, but it is possible to represent it in closed analytic form [152,153]. The smaller the relaxed normalization $N^{\rm eff}_{X\alpha}(1)$, the more delocalized the corresponding exact-exchange hole [151]. The $\alpha-\alpha$ exchange hole is further deepened by a fraction of the $\beta$–$\beta$ exchange hole, $f_{\rm c}(1)\,\bar{h}^{\rm eff}_{{\rm X}\beta\beta}(1,2)$, which gives rise to left-right static correlation. The local correlation factor $f_{\rm c}$ in Eq.(10.113) governs this deepening and hence the strength of the static correlation at each point [151]:

$$f_{\rm c}(\mathbf{r}) = \min\left(f_\alpha(\mathbf{r}),\,f_\beta(\mathbf{r}),\,1\right)\ ,\quad 0 \leq f_{\rm c}(\mathbf{r})\ \leq 1\ \ ,f_\alpha(\mathbf{r}) = \frac{1 - N^{\rm eff}_{{\rm X}\alpha}(\mathbf{r})}{N^{\rm eff}_{{\rm X}\beta}(\mathbf{r})}\,. \tag{10.115}$$

Using Eqs. (10.115), (10.111), and (10.112), the density of odd electrons becomes:

$$D_\alpha(1) = \rho_\alpha(1)(1 - N^{\rm eff}_{X\alpha}(1)) \equiv \rho_\alpha(1) f_{\rm c}(1)\, N^{\rm eff}_{X\beta}(1)\,. \tag{10.116}$$

The final formulas for the spin-summed odd electron density and the total mean number of odd electrons read:

$$D_u(1) = 4\, a^{\rm op}_{\rm nd}\, f_{\rm c}(1)\left[\rho_\alpha(1)\, N^{\rm eff}_{X\beta}(1) + \rho_\beta(1)\, N^{\rm eff}_{X\alpha}(1)\right]\ ,\ \ \bar{N}_u = \int D_u(\mathbf{r_1})\, d\mathbf{r_1}\,. \tag{10.117}$$

Here $a_{\rm c}^{\rm nd-opp} = 0.526$ is the SCF-optimized linear coefficient of the opposite-spin static correlation energy term of the B05 functional [151,153] .

It is informative to decompose the total mean number of odd electrons into atomic contributions. Partitioning in real space the mean total number of odd electrons $\bar{N}_u$ as a sum of atomic contributions, we obtain the atomic population of odd electrons ($F^{\rm r}_A$) as:

$$F^{\rm r}_A = \int_{\Omega_A} D_u(\mathbf{r_1})\, d\mathbf{r}_1\,. \tag{10.118}$$

Here $\Omega_A$ is a subregion assigned to atom $A$ in the system. To define these atomic regions in a simple way, we use the partitioning of the grid space into atomic subgroups within Becke's grid-integration scheme [154]. Since the present method does not require symmetry breaking, singlet states are calculated in restricted Kohn-Sham (RKS) manner even at strongly stretched bonds. This way one avoids the destructive effects that the spin contamination has on $F^{\rm r}_A$ and on the Kohn-Sham orbitals. The calculation of $F^{\rm r}_A$ can be done fully self-consistently only with the RI-B05 and RI-mB05 functionals. In these cases no special keywords are needed, just the corresponding EXCHANGE rem line for these functionals. Atomic population of odd electron can be estimated also with any other functional in two steps: first obtaining a converged SCF calculation with the chosen functional, then performing one single post-SCF iteration with RI-B05 or RI-mB05 functionals reading the guess from a preceding calculation, as shown on the input example below:

**Example 10.26** To calculate the odd-electron atomic population and the correlated bond order in stretched $H_2$, with B3LYP/RI-mB05, and with fully SCF RI-mB05

```
$comment
   Stretched H2: example of B3LYP calculation of
   the atomic population of odd electrons
   with post-SCF RI-BM05 extra iteration.
$end

$molecule
   0 1
   H   0.  0.   0.0
   H   0.  0.   1.5000
$end

$rem
   SCF_GUESS         CORE
   METHOD            B3LYP
   BASIS             G3LARGE
   PURECART          222
   THRESH            14
   MAX_SCF_CYCLES    80
   PRINT_INPUT       TRUE
   SCF_FINAL_PRINT   1
   INCDFT            FALSE
   XC_GRID           000128000302
   SYM_IGNORE        TRUE
   SYMMETRY          FALSE
   SCF_CONVERGENCE   9
$end

@@@

$comment
   Now one RI-B05 extra-iteration after B3LYP
   to generate the odd-electron atomic population and the
   correlated bond order.
$end

$molecule
   read
$end

$rem
   SCF_GUESS         READ
   EXCHANGE          BM05
   PURECART          22222
   BASIS             G3LARGE
   AUX_BASIS         riB05-cc-pvtz
   THRESH            14
   PRINT_INPUT       TRUE
   INCDFT            FALSE
   XC_GRID           000128000302
   SYM_IGNORE        TRUE
   SYMMETRY          FALSE
   MAX_SCF_CYCLES    0
   SCF_CONVERGENCE   9
   DFT_CUTOFFS       0
$end

@@@

$comment
   Finally, a fully SCF run RI-B05 using the previous output as a guess.
   The following input lines are obligatory here:
   PURECART     22222
   AUX_BASIS    riB05-cc-pvtz
   DFT_CUTOFFS  0
$end

$molecule
   read
$end

$rem
   SCF_GUESS        READ
   EXCHANGE         BM05
   PURECART         22222
   BASIS            G3LARGE
   AUX_BASIS        riB05-cc-pvtz
   THRESH           14
   PRINT_INPUT      TRUE
   INCDFT           FALSE
   IPRINT           3
   XC_GRID          000128000302
   SYM_IGNORE       TRUE
   SCF_FINAL_PRINT  1
   SYMMETRY         FALSE
   MAX_SCF_CYCLES   80
   SCF_CONVERGENCE  8
   DFT_CUTOFFS      0
$end
```

Once the atomic population of odd electrons is obtained, a calculation of the corresponding correlated bond order of Mayer's type follows in the code, using certain exact relationships between $F_A^{\mathrm{r}}$, $F_B^{\mathrm{r}}$, and the correlated bond order of Mayer type $B_{AB}$. Both new properties are printed at the end of the output, right after the multipoles section. It is useful to compare the correlated bond order with Mayer's SCF bond order. To print the latter, use SCF_FINAL_PRINT = 1.

## 10.19 Molecular Junctions

In molecular junctions, molecules bridge two metallic electrodes. The conductance and current-voltage relationship of molecular junctions can be calculated using either Landauer or Non-Equilibrium Green's Functions (NEGF). In both cases, the Green's function formulation is employed using a chosen level to describe the electronic structure. See Refs. 155,156 for further introduction.

In molecular junctions the current-voltage curve depends on the electron transmission function, which can be calculated using the quantum transport code developed by the Dunietz group (Kent State). The scattering-free approach, (Landauer), provides a zero-bias limit, whilst the non-equilibrium approach, (NEGF), iteratively solves for the junction under the effect of the finite-voltage biased system.

This quantum transport utility is invoked by setting the *$rem* variable TRANS_ENABLE.

**TRANS_ENABLE**
To invoke the molecular transport code.
TYPE:
INTEGER
DEFAULT:
0 Do not perform transport calculations (default).
OPTIONS:
1 Perform transport calculations.
$-1$ Print matrices needed for generating bulk model files.
RECOMMENDATION:
None

Output is provided in the Q-CHEM output file and in the following files (for closed shell system in the spin-restricted framework):

- `transmission.txt` (Transmission function in the requested energy window)
- `TDOS.txt` (Total density of states)
- `current.txt` (I-V plot only for the Landauer level)

- `FAmat.dat` (Hamiltonian matrix for follow up calculations and analysis)
- `Smat.dat` (Overlap matrix for follow up calculations and analysis)
- `IV-NEGF-all.txt` (I-V plot obtained by NEGF method)

In the case of unrestricted spin the transmission is calculated for each spin-state as indicated by the A[B] appended to the file names listed above (*e.g.* `transmissionA.txt` and `transmissionB.txt`). (The file name with the letter AB indicates output data including both spin states (*e.g.* `transmissionAB.txt`). We note that in the closed-shell spin-restricted case, the `transmission.txt` corresponds to the $\alpha$ spin, where the total transmission due to the spin symmetry is twice the values included in the file. In the NEGF calculation, the above output files are placed in the directories, `Vbias1`, `Vbias2`, $\cdots$ (the numbers in the directory names are index of bias voltage), where these output files in each directory are of data at the given voltage.

T-Chem requires setting parameters in two transport-specific sections in the input file:

- *$trans_model* (molecular model regions)
- *$trans_method* (Specifies the mode to calculated the electrode self-energies)

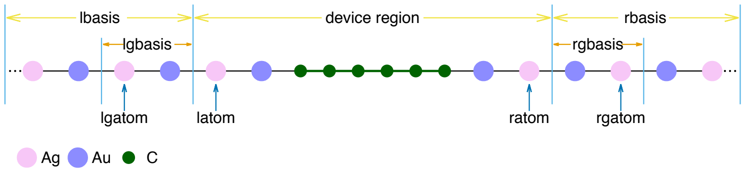

Figure 10.1: Illustration for the different regions of the molecular junction for Landauer calculation.

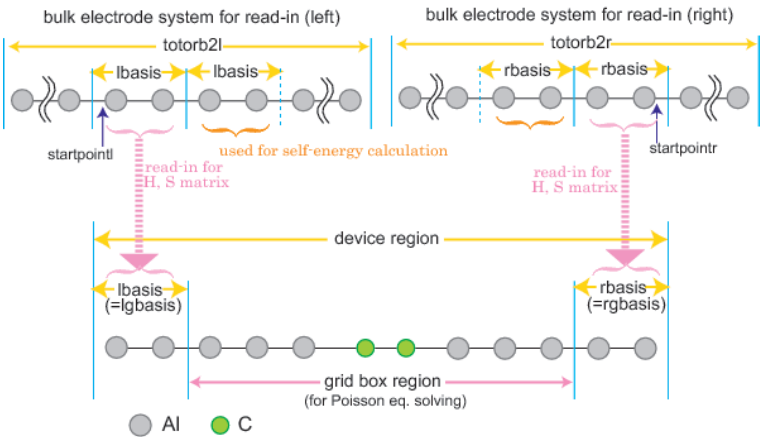

Figure 10.2: Illustration for the different regions of the molecular junction for NEGF calculation.

The *$trans_model* section provides the number of basis functions in the different regions (molecular model partitioning). There are no default values given for these parameters. The different regions are illustrated in Fig. 10.1 with a six carbon atom chain based bridge used as an example of the Landauer calculation. The partitioning as well as the scheme for the NEGF calculation is illustrated in Fig. 10.2. In these systems the electrodes are represented by a chain of Au atoms. In this example of electrode wires, each single atom represents one layer.

The necessary parameters in the *$trans_model* section are as follows:

- **trans_latom**: INTEGER, atom index in the *$molecule* section where the central/bridge region starts (the first atom in junction area).
- **trans_ratom**: INTEGER, atom index in the *$molecule* section where the central/bridge region ends (the last atom in junction area).
- **trans_lgatom**: INTEGER, atom index where the repeat unit of the left electrode starts.
- **trans_rgatom**: INTEGER, atom index where the repeat unit of the right electrode ends.

See Fig. 10.1 for illustrations of the different regions, and the way the parameters define them. Atoms within numbers **trans_lgatom**, **trans_lgatom**+1, .., **trans_latom**-1 define the repeat unit of the left electrode (similarly for right electrode).

Alternatively, the different regions can be provided with the atomic orbital (AO) index as follows:

- **trans_lbasis**: INTEGER, the number of basis functions appearing to the left of the device region (the index of the first AO within the central region).
- **trans_rbasis**: INTEGER, the number of basis functions appearing to the right of the device region right electrode (total number of basis functions minus this number equals last AO that is within the device).
- **trans_lgbasis**: INTEGER, the number of basis functions of the repeat unit of the left electrode.
- **trans_rgbasis**: INTEGER, the number of basis functions of the repeat unit of the right electrode.

For the NEGF calculation, **trans_lbasis** and **trans_lgbasis** must be the same number as shown in Fig. 10.2 (as for **trans_rbasis** and **trans_rgbasis**.

**Note:** The assignment of **trans_latom** etc. has priority. If **trans_latom** is specified, then **trans_lbasis** is ignored. Similarly for **trans_latom** and **trans_lbasis**.

For the example in Fig. 10.1, if there are a total of 18 atoms and the Au and Ag basis sets each contain 22 basis functions per atom and the repeat unit includes a pair of Au Ag atoms, then the parameters should be given as follows (only the first two columns are required, the rest are included for explanation):

| | | |
|---|---|---|
| **trans_lbasis** | 88 | No. of functions representing left electrode region (2 × 22 for Ag + 2 × 22 for Au) |
| **trans_rbasis** | 88 | No. of functions representing right electrode (2 × 22 for Ag + 2 × 22 for Au) |
| **trans_lgbasis** | 44 | Size of the repeating unit of the left electrode (22 for Ag + 22 for Au) |
| **trans_rgbasis** | 44 | Size of the repeating unit of the right electrode (22 for Ag + 22 for Au) |

Or use the atom numbers corresponding to their position in the *$molecule* section:

| | | |
|---|---|---|
| **trans_lgatom** | 3 | Third atom is used to define the repeat unit of the left electrode |
| **trans_latom** | 5 | Fifth atom is the first atom of the junction |
| **trans_ratom** | 14 | Fourteenth atom is the last atom of the junction |
| **trans_rgatom** | 16 | Sixteenth atom is used to define the repeat unit of the right electrode |

In this example, we have used for the same repeat unit for the left and right electrodes; this symmetry is not required.

**Note:** The order of atoms in the *$molecule* section is important and requires to following:

Repeating units (left) - Molecular Junction - Repeating units (right)

The atoms are provided first by the leftmost repeat unit with the left electrode then proceeds to the next repeat unit up to the surface unit. Next the bridge atoms are provided followed by the right surface unit and the right electrode region. The right electrode region starts with the surface layer and ends with the most distant layer within the bulk. The atoms order within each electrode layer (the repeat units) must be consistent. The atoms order within the bridge region (excluding the electrode repeat unit atoms) is arbitrary.

That is, the order of atoms in the molecule section has to adhere to the following:

1. atoms of the leftmost repeat unit
2. atoms of the next repeat unit
3. atoms of the left surface unit device
4. bridge atoms
5. atoms of the right surface unit
6. atoms of the next right electrode unit
7. atoms of the rightmost repeat unit

T-Chem allows for complete flexibility in determining the different regions of the electrode models. As a consequence, incorrect setting of regions is not caught by the program and may produce transmission functions that are unphysical (*e.g.* large values or even negative). Such errors can occur where the cluster model is partitioned (by mistake) within the orbital space of an atom. Regions must always be defined between atomic layers. Each repeat unit atoms should be always provided with the same internal order.

**Note:** At least a single repeat unit of the electrodes should be included in the bridge region. With the Landauer model, if **trans_readhs** == 0, then at least one layer beyond the bridge region *has* to be included, an additional layer (total of two or more) is required when **trans_method** != 0.

The necessary parameters in *$trans_method* section are listed as follows,

**trans_mode**

Mode of calculation.

INPUT SECTION: *$trans_method*

TYPE:

INTEGER

DEFAULT:

1 Landauer level.

OPTIONS:

3 A self-consistent Green's function calculation with zero bias voltage (*i.e.* NEGF with zero bias, which is used for preparation of full NEGF).

4 Full NEGF level

RECOMMENDATION:

For modes 3 and 4 SCF_ALGORITHM = NEGF must be set in in the *$rem* section.

**trans_spin**

Spin coupling scheme.

INPUT SECTION: *$trans_method*

TYPE:

INTEGER

DEFAULT:

0

OPTIONS:

0 For restricted spin calculations or closed-shell singlet states.

3 For unrestricted spin calculations or open-shell systems

RECOMMENDATION:

None

**trans_method**

Electrode surface GFs model.

INPUT SECTION: *$trans_method*

TYPE:

INTEGER

DEFAULT:

0

OPTIONS:

0 A wide band limit with a constant parameter trans_greens (default)

1 WBL using the Ke-Baranger-Yang TB at the Fermi energy.

2 WBL using the Lopez-Sancho TB at the Fermi energy.

3 Tight-binding (TB) following the procedure proposed by Ke-Baranger-Yang

4 TB following the procedure proposed by Lopez-Sancho (decimation).

RECOMMENDATION:

Only option 0 is available for the NEGF calculation at the current version.

**trans_npoint**

Number of grid points within the energy window of the transmission spectra calculation.

INPUT SECTION: *$trans_method*

TYPE:

INTEGER

DEFAULT:

300

OPTIONS:

$n$ User-specified number of points

RECOMMENDATION:

None

**trans_readhs**

Flag to read the Hamiltonian and overlap matrices for the bulk model.

INPUT SECTION: *$trans_method*

TYPE:

INTEGER

DEFAULT:

0 Use the current Hamiltonian and overlap matrices to parse the electrode integrals.

OPTIONS:

1 Use pre-calculated electrode Hamiltonian and overlap matrices.

RECOMMENDATION:

If set to 1, the following files are requred: `FAmat2l.dat` and `Smat2l.dat` (for left electrode model), `FAmat2r.dat` and `Smat2r.dat` (for right electrode model). If both electrodes are of the same type, may use symbolic links of these files to the same matrices. (For unrestricted spin model, `FBmat2l.dat` and `FBmat2r.dat` are also necessary)

**Note:** NEGF requires **trans_readhs** to be set!

**trans_htype**

Determines the TB property on the relevant coupling terms.

INPUT SECTION: *$trans_method*

TYPE:

INTEGER

DEFAULT:

0

OPTIONS:

When **trans_readhs** = 0:

0 All coupling integrals between the junction and electrode functions are allowed as determined at the cluster model level (no screening imposed).

1 Only coupling between neighboring repeating units of the electrode model are allowed – all terms of the repeating units elements that are beyond the neighboring unit are set to zero.

2 Force both the TB coupling terms and the self-energy coupling terms to the same value as determined by the electrode model. If **trans_method** != 0, the inequalities **trans_lbasis** $\geq 2\times$**trans_lgbasis** and **trans_rbasis** $\geq 2\times$**trans_rgbasis** must be satisfied.

When **trans_readhs** = 1:

2 Available using the pre-calculated electrode data.

3 The same way as 1 but using the pre-calculated electrode data. This is only for NEGF calculation.

RECOMMENDATION:

None

Further options are summarized below:

**trans_printdos** (Integer):

Controls the printout of TDOS.

0 Default, no total DOS printing.

1 A TDOS (of the junction region) will be printed to TDOS.txt (closed shell).

**trans_printiv** (Integer):

Controls printout of calculated current.

0 Default, no current calculated and printed

1 Current will be printed to `current.txt` (closed shell) or `currentA/B.txt` (unrestricted or open shell).

**trans_ipoints** (Integer):
Number of points for current calculation.

300 Default value.

**trans_adjustefermi** (Integer):
Flag to adjust the Fermi energy (FE) for **trans_mode** = 3 or 4

0 Default, no adjustment. Fixed FE specified by **trans_efermi** (and **trans_efermib**) is used.

1 FE is chosen as midpoint of HOMO and LUMO levels

2 FE is adjusted so that charge neutrality is satisfied

3 FE is adjusted by combination way of 1 and 2, *i.e.* use 2 if maximum difference of density matrix in the iteration is over $10^{-2}$ and use 3 below that.

Options 1, 2, and 3 use the same FE for $\alpha$ and $\beta$ spins. -1, -2, -3 are the same as 1, 2, 3, respectively, but allow for different FEs for $\alpha$ and $\beta$ spins.

**trans_nvbias** (Integer):
(Only for **trans_mode** = 4), number of points of bias voltage.

1 Default

The bias voltage values to be calculated are defined by dividing the range between **trans_vstart** and **trans_vmax** with this number. For example, when **trans_vstart** = 0.0, **trans_vmax** = 1.0, and **trans_nvbias** = 5, the voltages are 0.0, 0.25, 0.50, 0.75, and 1.0. For the case of **trans_nvbias** = 1, the voltage to be calculated is **trans_vmax**.

**trans_updatedmatlr** (Integer):
(Only for **trans_mode** = 3), flag to update L, R, LC, RC blocks (*i.e.* except for center block) of density matrix during SCF with zero bias. This is to prepare consistent density matrix with modified Hamiltonian matrix forced by read-in bulk electrode data. Note that it may make it difficult or slow to converge.

0 No update.

1 Update every iteration step (default).

2 Mix the new density matrix with ratio of **trans_mixing**.

The following are parameters are set to a double precision value. The allowed values are set using **trans_itodfac** as follows:

**trans_itodfac** (Integer):
Controls the accuracy for input parameters.

100 Default, the numbers can be of 0.0x precision.

1000 The input double numbers can be of 0.00x precision, *etc.*

**trans_vstart** (Double):
(Only for **trans_mode** = 4). Starting voltage bias (V). The bias voltage increases from **trans_vstart** to **trans_vmax** in the NEGF calculation.

0.0 Default

**trans_devsmear** (Double):
Imaginary smearing (in eV) added to the real Hamiltonian in central region retarded GF evaluation.

0.01 Default, cannot be smaller than 1/**trans_itodfac**

**trans_bulksmear** (Double):
Imaginary smearing (in eV) added to the real Hamiltonian in electrodes GF evaluation.
0.01 Default, cannot be smaller than 1/**trans_itodfac**

**trans_greens** (Double):
Imaginary smearing/Broadening (in eV) added to the Green's function.
0.07 Default, cannot be smaller than 1/**trans_itodfac**

**trans_efermi** (Double):
Fermi energy of the electrode (for $\alpha$ spin) (in eV) used for defining energy range in calculating current for T(E).
-5.0 Default

**trans_efermib** (Double):
Fermi energy for $\beta$ spin (in eV). If this is not given, the same value of $\alpha$ spin is used.

**trans_vmax** (Double):
Maximum voltage bias (V).
1.0 Default

**trans_gridoffset** (Double):
(Only for **trans_mode** = 4), Offset distance (in Å) to define the grid box region for bias potential energy.
5.0 Default
The box size is defined by adding the offset distance with maximum and minimum $x$, $y$ and $z$ atomic coordinates for each direction. The bias voltage $V(\mathbf{r})$ on the grid points in the box is used for calculating correction term for the Fock matrix (*i.e.* $\langle i|V|j\rangle$). Note that this box is not for correcting electrostatic potential by solving Poisson equation. The grid box region and its grid size for the Poisson equation is given by *$plots* block keyword (see also example later). The same grid size is used for both boxes.

The following are parameters for when **trans_mode** = 3, 4:

**trans_mixing** (Double):
Mixing ratio of DIIS mixing method for updating the central block of density matrix in the NEGF iteration.
1.0 Default

**trans_mixhistory** (Integer):
The number of NEGF iteration steps in which the history of density matrix is stocked for the DIIS method.
40 Default

**trans_dehcir** (Double):
Grid size, dE (in eV), for integrating the Greens function on the half circle path on imaginary plane.
1.0 Default

**trans_delpart** (Double):
Grid size, dE (in eV), for integrating the Greens function on the path of the linear part on imaginary plane.
0.01 Default

**trans_debwin** (Double):
(For **trans_mode** = 4). Grid size, dE (in eV), for integration on the non-equilibrium term.
0.01 Default

**trans_numres** (Integer):
The number of poles at Fermi energy enclosed by closed contour on the imaginary plane.

100 Default

**trans_peconv** (Integer):
The convergence criteria of the iteration of the Poisson equation. The threshold is $10^{-n}$ hartree of maximum energy difference over the all grid points.
9 Default

**trans_pemaxite** (Integer):
Maximum iteration number of the Poisson equation.
1000 Default

**trans_readesp** (Integer):
Flag of read-in electrostatic potential energy. The data is printed in "ReadInESP/" directory with option of -1 or 0, and read from the same directory name with option of 0 or 1.
-1 Print the read-in ESP data in "ReadInESP/" directory at the first step and stop calculation.
0 Print the read-in ESP data in "ReadInESP/" at the first step and continue calculation using it (default).
1 Read the pre-calculated read-in ESP data from "ReadInESP/" and continue calculation.

**trans_restart** (Integer):
Flag to restart reading the density matrix files, `DAmat.dat` (and `DBmat.dat`) from the "TransRestart/" directory.
0 No restart (default).
1 Read file of density matrix.

**Note:** The default energy window for transmission and current calculations is defined as:
**trans_emin** = **trans_efermi** - **trans_vmax**/2 and **trans_emax** = **trans_efermi** + **trans_vmax**/2
if **trans_emin** and **trans_emax** are not given.

The **trans_emin** and **trans_emax** values can be set to determine the energy window for calculating the transmission function. If specified, these values will override the window defined by **trans_efermi** and **trans_vmax** values.

If higher accuracy parameters are set, **trans_itodfac** must be increased. For example for three digits accuracy (*e.g.* **trans_efermi** = -5.341), then **trans_itodfac** = 1000 or higher must be used. (This parameter applies to all double precision parameters.)

For **trans_readhs** = 1, the following parameters to parse precalculated Hamiltonian and overlap matrices have to be provided:

- **trans_totorb2** (Integer):
  Total number of basis functions in the electrode models (if set, then same size is assumed for both electrodes) (no default value).
- **trans_totorb2l**: Integer number, total number of basis functions in left electrode model (no default value).
- **trans_totorb2r**: Integer number, total number of basis functions in right electrode model (no default value).
- **trans_startpoint**: Integer number, start point (basis number) for reading the TB integrals. Note, the basis number, that is, index number of basis function starts from 0. (if set, then same size is assumed for both electrodes) (default value 0).

- **trans_startpointl**: given as integer number, left start point (basis number) for reading the TB integrals. Note, the basis number, that is, index number of basis function starts from 0. (default value 0).
- **trans_startpointr**: given as integer number, right start point (basis number) for reading the TB integrals. Note, the basis number, that is, index number of basis function starts from 0. (no default value).

As an example of the Landauer calculation, the sample Q-CHEM input is given below.

**Example 10.27** Quantum transport Landauer calculation applied to $C_6$ between two gold electrodes.

```
$molecule
   0 1
   Ag  -11.0  0  0
   Au   -8.3  0  0
   Ag   -5.6  0  0
   Au   -2.9  0  0
   Ag   -0.2  0  0
   Au    2.5  0  0
   C     4.8  0  0
   C     6.5  0  0
   C     8.2  0  0
   C     9.9  0  0
   C    11.6  0  0
   C    13.3  0  0
   Au   15.6  0  0
   Ag   18.3  0  0
   Au   21.0  0  0
   Ag   23.7  0  0
   Au   26.4  0  0
   Ag   29.1  0  0
$end

$rem
   METHOD            B3LYP
   BASIS             lanl2dz
   ECP               lanl2dz
   GEOM_OPT_MAXCYC   200
   INCDFT            FALSE
   MEM_STATIC        8000
   MAX_SCF_CYCLES    400
   MEM_TOTAL         32000
   MOLDEN_FORMAT     TRUE
   SCF_CONVERGENCE   10
   SCF_ALGORITHM     diis
   TRANS_ENABLE      1
$end

$trans-method
   trans_spin        0
   trans_npoints     300
   trans_method      0
   trans_readhs      0
   trans_printdos    1
   trans_efermi      -6.50
   trans_vmax        4.00
```

```
$end

$trans-model
   trans_lgatom      3
   trans_latom       5
   trans_ratom       14
   trans_rgatom      16
$end
```

A sample for unrestricted spin calculation can be found in the $QC/samples/tchem directory.

For NEGF calculations, note the followings concerning input etc:

- SCF_ALGORITHM = NEGF in *$rem* is necessary for NEGF calculation.
- The same numbers for **trans_lgbasis** and **trans_lbasis**, and also for **trans_rgbasis** and **trans_rbasis** must be used.
- Only WBL method for evaluating self-energy is available for the NEGF in the current version (**trans_method** = 0)
- **trans_htype** = 3 and **trans_readhs** = 1 are required
- SYM_IGNORE = TRUE to keep the original input coordinates.
- MEM_TOTAL and MEM_STATIC may need to be set to ensure enough memory is available.
- The bias voltage of $+V/2$ is added on the left electrode, and $-V/2$ on the right electrode, where the bias potential slope is along $x$-axis, *i.e.* the system structure must be built along $x$ direction.
- In the *$plots* section (when defining a grid box for the Poisson equation solving), the grid box region must cover all atoms except for the left and right electrode parts defined in *$trans_model*. All integer index flags in *$plots* can be 0.
- For calculations on bulk electrode, the same structure with the same orientation in $xyz$-Cartesian coordinate system (but different size) must be used so as to reproduce the same overlap matrix at the used part.
- For better calculations, update of electrode relevant (non-center) blocks in the density matrix (**trans_updatedmatlr** = 1) and Fermi energy to satisfy charge neutrality (**trans_adjustefermi** = 2 or 3) are recommended at zero bias **(trans_opt** = 3) before performing a full NEGF calculation. However, these options may make it difficult or slow to reach convergence.
- The criterion for convergence in the NEGF iterations is the maximum difference in density matrix elements, and is not a energy threshold.

NEGF calculations depend on the following pre-calculated properties:

Step 1: Pre-calculations:
A: Hamiltonian and overlap matrices for the left and right bulk electrodes (required)
B: A converged junction electronic state by standard DFT (recommended)
C: Electrostatic potential of large electrode region (optional)

Step 2: Self-consistent Greens function calculation with zero bias:
Non zero bias cases should be calculated using density matrices calculated with zero bias voltage to obtain converged density matrix. It is also recommend to evaluate the Fermi energy level within the NEGF scheme.

Step 3: NEGF calculations should be obtained by increasing the bias sequentially.

Examples of these steps applied to $C_2$ between two aluminium electrodes are given below.

**Example 10.28** Step 1-A of the NEGF calculation, the pre-calculation of the bulk electrode. Flag keyword of printing matrices must be set (*i.e.* **trans_enable** != 0)

```
$molecule
   0 1
   Al    -15.04250    0.0   0.0
   Al    -12.30750    0.0   0.0
   Al    -9.572500    0.0   0.0
   Al    -6.837500    0.0   0.0
   Al    -4.102500    0.0   0.0
   Al    -1.367500    0.0   0.0
   Al     1.367500    0.0   0.0
   Al     4.102500    0.0   0.0
   Al     6.837500    0.0   0.0
   Al     9.572500    0.0   0.0
   Al     12.30750    0.0   0.0
   Al     15.04250    0.0   0.0
$end

$rem
   UNRESTRICTED        true
   SYM_IGNORE          true
   MAX_SCF_CYCLES       500
   EXCHANGE              hf
   CORRELATION         none
   ECP                 hwmb
   BASIS               hwmb
   SCF_CONVERGENCE        4
$end

@@@

$molecule
   read
$end

$rem
   UNRESTRICTED        true
   SYM_IGNORE          true
   MAX_SCF_CYCLES       500
   EXCHANGE           b3lyp
   CORRELATION         none
   ECP                 hwmb
   BASIS               hwmb
   SCF_GUESS           read
   SCF_GUESS_MIX          3
   SCF_CONVERGENCE        4
$end

@@@

$molecule
   read
$end

$rem
```

```
   UNRESTRICTED        true
   SYM_IGNORE          true
   MAX_SCF_CYCLES       500
   EXCHANGE           b3lyp
   CORRELATION         none
   ECP                 hwmb
   BASIS               hwmb
   SCF_GUESS           read
   SCF_GUESS_MIX          3
   SCF_CONVERGENCE        7
   TRANS_ENABLE          -1
$end

$trans-method
   trans_spin             2
$end
```

**Example 10.29** Step 1-B of the NEGF calculation - the pre-calculation by the standard DFT. The same molecular structure with the step 2 must be used

```
$molecule
   0 1
   Al  -13.615   0.0   0.0
   Al  -10.880   0.0   0.0
   Al   -8.145   0.0   0.0
   Al   -5.410   0.0   0.0
   Al   -2.675   0.0   0.0
   C    -0.627   0.0   0.0
   C     0.627   0.0   0.0
   Al    2.675   0.0   0.0
   Al    5.410   0.0   0.0
   Al    8.145   0.0   0.0
   Al   10.880   0.0   0.0
   Al   13.615   0.0   0.0
$end

$rem
   UNRESTRICTED          true
   SYM_IGNORE            true
   MAX_SCF_CYCLES        400
   EXCHANGE              b3lyp
   CORRELATION           none
   BASIS                 hwmb
   ECP                   hwmb
   SCF_CONVERGENCE       5
$end

@@@

$molecule
   read
$end

$rem
   UNRESTRICTED          true
   SYM_IGNORE            true
   EXCHANGE              b3lyp
   CORRELATION          none
   BASIS                hwmb
   ECP                  hwmb
   MAX_SCF_CYCLES       400
   SCF_CONVERGENCE      6
   SCF_GUESS            read
   SCF_GUESS_MIX        3
$end
```

**Example 10.30** Step 2 of the NEGF calculation. As the preparation of this step, followings are necessary:

1. `FAmat2l.dat`, `FAmat2r.dat`, `Smat2l.dat`, and `Smat2r.dat` (also `FBmat2l.dat` and `FBmat2r.dat` if the calculation is spin-unrestricted ) must be placed in the same directory of the Q-Chem input file by coping or linking the output files of the step 1-A.
2. Restart directory of the standard DFT obtained in the step 1-B must be copied to here.
3. (Optional) Read-in electrostatic potential data in "ReadInESP/" directory must be placed if this option is used (for **trans_readesp** = 1). This option can provide more bulk electrode electrostatic environment as the boundary condition of Poisson equation solving ( see the sample files in $QC/samples/tchem/) for more details).

```
$molecule
   read
$end

$rem
   JOBTYPE              sp
   UNRESTRICTED         true
   SYM_IGNORE           true
   MAXSCF               500
   EXCHANGE             b3lyp
   CORRELATION          none
   BASIS                hwmb
   ECP                  hwmb
   SCF_CONVERGENCE      4
   SCF_ALGORITHM        negf
   SCF_GUESS            read
   MEM_TOTAL            16000
   MEM_STATIC           4000
   TRANS_ENABLE         1
$end

$plots
For NEGF (for Poisson equation)
   190    -9.5     9.5
    80    -4.0     4.0
    80    -4.0     4.0
     0  0  0  0
     0
$end

$trans-method
   trans_opt           3
   trans_spin          2
   trans_npoints     500
   trans_method        0
   trans_printdos      1
   trans_printiv       1
   trans_adjustefermi  1
   trans_vmax        1.0
   trans_emin       -6.5
   trans_emax       -2.5
   trans_mixing        0.1
   trans_mixhistory   50
   trans_dehcir        1.0
   trans_delpart       0.01
   trans_numres      100
   trans_peconv        8
   trans_pemaxite   1000
   trans_updatedmatlr  0
   trans_readesp       0
   trans_htype         3
   trans_readhs        1
   trans_totorb2      48
   trans_startpointl  16
   trans_startpointr  32
$end

$trans-model
   trans_lbasis   8
   trans_rbasis   8
   trans_lgbasis  8
   trans_rgbasis  8
$end
```

**Example 10.31** Step 3 of the NEGF calculation. As the preparation of this step, followings are necessary:

1. In the same way as step 2, `FAmat2l.dat`, `FAmat2r.dat`, `Smat2l.dat`, and `Smat2r.dat` (also `FBmat2l.dat` and `FBmat2r.dat` for spin-unrestricted calculations) must be placed.
2. Restart directory for Q-Chem generated in the step 2 must be copied to here (only coordinates are used).
3. Restart directory for density matrix "TransRestart/" must be created and `DAmat.dat` (and `DBmat.dat` for spin-unrestricted) generated in the step 2 must be copied or linked in the directory.
4. Read-in electrostatic potential data in "ReadInESP/" directory used in the step 2 must be copied to here.
5. Put Fermi energy obtained in Step 2 (recommended).

```
$molecule
   read
$end

$rem
   UNRESTRICTED       true
   MAXSCF             500
   SYM_IGNORE         true
   EXCHANGE           b3lyp
   ECP                hwmb
   SCF_CONVERGENCE    4
   SCF_ALGORITHM      negf
   MEM_TOTAL          16000
   MEM_STATIC         4000
   TRANS_ENABLE       1
```

```
$end

$plots
For NEGF calculation
   190    -9.5     9.5
    80    -4.0     4.0
    80    -4.0     4.0
     0  0  0  0
     0
$end

$trans-method
   trans_opt          4
   trans_spin         2
   trans_npoints    500
   trans_method       0
   trans_printdos     1
   trans_printiv      1
   trans_adjustefermi 0
   trans_efermi      -4.421836
   trans_vmax         0.5
   trans_emin        -6.5
   trans_emax        -2.5
   trans_mixing       0.2
   trans_mixhistory   50
   trans_dehcir       1.0
   trans_delpart      0.01
   trans_debwin       0.01
   trans_numres       100
   trans_peconv       8
   trans_pemaxite     1000
   trans_gridoffset   4.0
   trans_updatedmatlr 0
   trans_nvbias       6
   trans_restart      1
   trans_readesp      1
   trans_htype        3
   trans_readhs       1
   trans_totorb2      48
   trans_startpointl  16
   trans_startpointr  32
$end

$trans-model
   trans_lbasis   8
   trans_rbasis   8
   trans_lgbasis  8
   trans_rgbasis  8
$end
```

# References and Further Reading

[1] Ground-State Methods (Chapters 4 and 5).

[2] Excited-State Calculations (Chapter 6).

[3] Basis Sets (Chapter 7).

[4] NBO 5.0 manual: www.chem.wisc.edu/∼nbo5.

[5] A. Szabo and N. S. Ostlund, *Modern Quantum Chemistry*, Dover, 1996.

[6] P.-O. Löwdin, *J. Chem. Phys.* **18**, 365 (1950).

[7] C. M. Breneman and K. B. Wiberg, *J. Comput. Chem.* **11**, 361 (1990).

[8] J. M. Herbert, L. D. Jacobson, K. U. Lao, and M. A. Rohrdanz, *Phys. Chem. Chem. Phys.* **14**, 7679 (2012).

[9] Z. C. Holden, R. M. Richard, and J. M. Herbert, *J. Chem. Phys.* **139**, 244108 (2013).

[10] F. L. Hirshfeld, *Theor. Chem. Acc.* **44**, 129 (1977).

[11] A. V. Marenich, S. V. Jerome, C. J. Cramer, and D. G. Truhlar, *J. Chem. Theory Comput.* **8**, 527 (2012).

[12] P. Bultinck, C. Van Alsenoy, P. W. Ayers, and R. Carbó-Dorca, *J. Chem. Phys.* **126**, 144111 (2007).

[13] D. E. P. Vanpoucke, P. Bultinck, and I. Van Driessche, *J. Comput. Chem.* **34**, 405 (2013).

[14] D. M. Elking, L. Perera, and L. G. Pedersen, *Comput. Phys. Commun.* **183**, 390 (2012).

[15] S. N. Steinmann and C. Corminbeoeuf, *J. Chem. Theory Comput.* **6**, 1990 (2010).

[16] C. F. Williams and J. M. Herbert, *J. Phys. Chem. A* **112**, 6171 (2008).

[17] A. J. W. Thom, E. J. Sundstrom, and M. Head-Gordon, *Phys. Chem. Chem. Phys.* **11**, 11297 (2009).

[18] Y. M. Rhee and M. Head-Gordon, *J. Am. Chem. Soc.* **130**, 3878 (2008).

[19] R. M. Richard and J. M. Herbert, *J. Chem. Theory Comput.* **7**, 1296 (2011).

[20] A. Dreuw and M. Head-Gordon, *Chem. Rev.* **105**, 4009 (2005).

[21] S. Hirata, M. Nooijen, and R. J. Bartlett, *Chem. Phys. Lett.* **326**, 255 (2000).

[22] F. Plasser and H. Lischka, *J. Chem. Theory Comput.* **8**, 2777 (2012).

[23] F. Plasser, M. Wormit, and A. Dreuw, *J. Chem. Phys.* **141**, 024106 (2014).

[24] F. Plasser, S. A. Bäppler, M. Wormit, and A. Dreuw, *J. Chem. Phys.* **141**, 024107 (2014).

[25] S. A. Bäppler, F. Plasser, M. Wormit, and A. Dreuw, *Phys. Rev. A* **90**, 052521 (2014).

[26] F. Plasser et al., *J. Comput. Chem.* **36**, 1609 (2015).

[27] S. A. Mewes, F. Plasser, and A. Dreuw, *J. Chem. Phys.* **143**, 171101 (2015).

[28] R. L. Martin, *J. Chem. Phys.* **118**, 4775 (2003).

[29] F. Plasser, *J. Chem. Phys.* **144**, 194107 (2016).

[30] M. Head-Gordon, A. M. Graña, D. Maurice, and C. A. White, *J. Phys. Chem.* **99**, 14261 (1995).

[31] M. Head-Gordon, *Chem. Phys. Lett.* **372**, 508 (2003).

[32] J. M. Herbert, The quantum chemistry of loosely-bound electrons, in *Reviews in Computational Chemistry*, edited by A. L. Parill and K. Lipkowitz, volume 28, page 391, Wiley, 2015.

[33] S. A. Mewes, J.-M. Mewes, A. Dreuw, and F. Plasser, *Phys. Chem. Chem. Phys.* **18**, 2548 (2016).

[34] E. D. Glendening, C. R. Landis, and F. Weinhold, *J. Comput. Chem.* **34**, 1429 (2013).

[35] E. D. Glendening et al., 2013.

[36] F. Weinhold, in *Computational Methods in Photochemistry*, edited by A. G. Kutateladze, volume 13 of *Molecular and Supramolecular Photochemistry*, page 393, Taylor & Francis, 2005.

[37] S. F. Boys, *Rev. Mod. Phys.* **32**, 296 (1960).

[38] S. F. Boys, in *Quantum Theory of Atoms, Molecules, and the Solid State*, edited by P.-O. Löwdin, page 253, Academic, New York, 1966.

[39] J. Pipek and P. G. Mezey, *J. Chem. Phys.* **90**, 4916 (1989).

[40] C. Edmiston and K. Ruedenberg, *Rev. Mod. Phys.* **35**, 457 (1963).

[41] J. E. Subotnik, Y. Shao, W. Liang, and M. Head-Gordon, *J. Chem. Phys.* **121**, 9220 (2004).

[42] G. Schaftenaar and J. H. Noordik, *J. Comput.-Aided Mol. Design* **14**, 123 (2000).

[43] The MOLDEN program may be freely downloaded from www.cmbi.ru.nl/molden/molden.html.

[44] B. M. Bode and M. S. Gordon, *J. Mol. Graphics Mod.* **16**, 133 (1998).

[45] MACMOLPLT may be downloaded from www.sci.ameslab.gov/∼brett/MacMolPlt.

[46] A. W. Lange and J. M. Herbert, *J. Am. Chem. Soc.* **131**, 124115 (2009).

[47] W. Humphrey, A. Dalke, and K. Schulten, *J. Molec. Graphics* **14**, 33 (1996).

[48] The VMD program may be downloaded from www.ks.uiuc.edu/Research/vmd.

[49] E. R. Johnson et al., *J. Chem. Phys.* **123**, 024101 (2005).

[50] J. Contreras-García et al., *J. Chem. Theory Comput.* **7**, 625 (2011).

[51] A. C. Simmonett, A. T. B. Gilbert, and P. M. W. Gill, *Mol. Phys.* **103**, 2789 (2005).

[52] T. Kato, *Commun. Pure Appl. Math.* **10**, 151 (1957).

[53] R. T. Pack and W. B. Brown, *J. Chem. Phys.* **45**, 556 (1966).

[54] V. A. Rassolov and D. M. Chipman, *J. Chem. Phys.* **104**, 9908 (1996).

[55] D. M. Chipman, *Theor. Chem. Acc.* **76**, 73 (1989).

[56] V. A. Rassolov and D. M. Chipman, *J. Chem. Phys.* **105**, 1470 (1996).

[57] V. A. Rassolov and D. M. Chipman, *J. Chem. Phys.* **105**, 1479 (1996).

[58] J. O. Hirschfelder, *J. Chem. Phys.* **33**, 1462 (1960).

[59] B. Wang, J. Baker, and P. Pulay, *Phys. Chem. Chem. Phys.* **2**, 2131 (2000).

[60] A. J. Stone, *Chem. Phys. Lett.* **83**, 233 (1981).

[61] A. J. Stone and M. Alderton, *Mol. Phys.* **56**, 1047 (1985).

[62] A. J. Stone, *J. Chem. Theory Comput.* **1**, 1128 (2005).

[63] P. M. W. Gill, D. P. O'Neill, and N. A. Besley, *Theor. Chem. Acc.* **109**, 241 (2003).

[64] A. M. Lee and P. M. W. Gill, *Chem. Phys. Lett.* **313**, 271 (1999).

[65] P. M. W. Gill, *Chem. Phys. Lett.* **270**, 193 (1997).

[66] N. A. Besley, A. M. Lee, and P. M. W. Gill, *Mol. Phys.* **100**, 1763 (2002).

[67] N. A. Besley, D. P. O'Neill, and P. M. W. Gill, *J. Chem. Phys.* **118**, 2033 (2003).

[68] E. Wigner, *Phys. Rev.* **40**, 749 (1932).

[69] V. I. Lebedev, *Zh. Vychisl. Mat. Mat. Fix.* **16**, 293 (1976).

[70] V. I. Lebedev, *Sibirsk. Mat. Zh.* **18**, 132 (1977).

[71] V. I. Lebedev and D. N. Laikov, *Dokl. Math.* **366**, 741 (1999).

[72] J. Cioslowski and G. Liu, *J. Chem. Phys.* **105**, 4151 (1996).

[73] B. G. Johnson and J. Florián, *Chem. Phys. Lett.* **247**, 120 (1995).

[74] P. P. Korambath, J. Kong, T. R. Furlani, and M. Head-Gordon, *Mol. Phys.* **100**, 1755 (2002).

[75] C. W. Murray, G. J. Laming, N. C. Handy, and R. D. Amos, *Chem. Phys. Lett.* **199**, 551 (1992).

[76] A. P. Scott and L. Radom, *J. Phys. Chem.* **100**, 16502 (1996).

[77] B. G. Johnson, P. M. W. Gill, and J. A. Pople, *J. Chem. Phys.* **98**, 5612 (1993).

[78] N. A. Besley and K. A. Metcalf, *J. Chem. Phys.* **126**, 035101 (2007).

[79] N. A. Besley and J. A. Bryan, *J. Phys. Chem. C* **112**, 4308 (2008).

[80] M. W. D. Hanson-Heine, M. W. George, and N. A. Besley, *J. Chem. Phys.* **136**, 224102 (2012).

[81] W. J. Zheng and B. R. Brooks, *Biophys. J.* **88**, 3109 (2005).

[82] H. L. Woodcock et al., *J. Chem. Phys.* **129**, 214109 (2008).

[83] A. Ghysels et al., *J. Comput. Chem.* **31**, 994 (2010).

[84] C. R. Jacob and M. Reiher, *J. Chem. Phys.* **130**, 084106 (2009).

[85] C. R. Jacob, S. Luber, and M. Reiher, *Chem. Eur. J* **15**, 13491 (2009).

[86] C. R. Jacob, S. Luber, and M. Reiher, *J. Phys. Chem. B* **113**, 6558 (2009).

[87] M. W. D. Hanson-Heine, F. S. Husseini, J. D. Hirst, and N. A. Besley, *J. Chem. Theory Comput.* **12**, 1905 (2016).

[88] X. Cheng and R. P. Steele, *J. Chem. Phys.* **141**, 104105 (2014).

[89] P. T. Panek and C. R. Jacob, *ChemPhysChem* **15**, 3365 (2014).

[90] M. W. D. Hanson-Heine, *J. Chem. Phys.* **143**, 164104 (2015).

[91] A. Miani, E. Cancès, P. Palmieri, A. Trombetti, and N. C. Handy, *J. Chem. Phys.* **112**, 248 (2000).

[92] R. Burcl, N. C. Handy, and S. Carter, *Spectrochim. Acta A* **59**, 1881 (2003).

[93] K. Yagi, K. Hirao, T. Taketsuga, M. W. Schmidt, and M. S. Gordon, *J. Chem. Phys.* **121**, 1383 (2004).

[94] V. Barone, *J. Chem. Phys.* **122**, 014108 (2005).

[95] S. D. Peyerimhoff, in *Encyclopedia of Computational Chemistry*, edited by P. v. R. Schleyer et al., page 2646, Wiley, Chichester, United Kingdom, 1998.

[96] T. Carrington, Jr., in *Encyclopedia of Computational Chemistry*, edited by P. v. R. Schleyer et al., page 3157, Wiley, Chichester, United Kingdom, 1998.

[97] A. Adel and D. M. Dennison, *Phys. Rev.* **43**, 716 (1933).

[98] E. B. Wilson and J. J. B. Howard, *J. Chem. Phys.* **4**, 260 (1936).

[99] H. H. Nielsen, *Phys. Rev.* **60**, 794 (1941).

[100] J. Neugebauer and B. A. Hess, *J. Chem. Phys.* **118**, 7215 (2003).

[101] R. J. Whitehead and N. C. Handy, *J. Mol. Spect.* **55**, 356 (1975).

[102] C. Y. Lin, A. T. B. Gilbert, and P. M. W. Gill, *Theor. Chem. Acc.* **120**, 23 (2008).

[103] W. D. Allen et al., *Chem. Phys.* **145**, 427 (1990).

[104] I. M. Mills, in *Molecular Spectroscopy: Modern Research*, edited by K. N. Rao and C. W. Mathews, chapter 3.2, Academic Press, New York, 1972.

[105] D. A. Clabo, W. D. Allen, R. B. Remington, Y. Yamaguchi, and H. F. Schaefer III, *Chem. Phys.* **123**, 187 (1988).

[106] H. H. Nielsen, *Rev. Mod. Phys.* **23**, 90 (1951).

[107] C. Ochsenfeld, *Phys. Chem. Chem. Phys.* **2**, 2153 (2000).

[108] C. Ochsenfeld, S. P. Brown, I. Schnell, J. Gauss, and H. W. Spiess, *J. Am. Chem. Soc.* **123**, 2597 (2001).

[109] R. Ditchfield, *Mol. Phys.* **27**, 789 (1974).

[110] K. Wolinski, J. F. Hinton, and P. Pulay, *J. Am. Chem. Soc.* **112**, 8251 (1990).

[111] M. Häser, R. Ahlrichs, H. P. Baron, P. Weiss, and H. Horn, *Theor. Chem. Acc.* **83**, 455 (1992).

[112] T. Helgaker and M. J. K. Ruud, *Chem. Rev.* **99**, 293 (1990).

[113] C. Ochsenfeld, J. Kussmann, and F. Koziol, *Angew. Chem.* **116**, 4585 (2004).

[114] J. Kussmann and C. Ochsenfeld, *J. Chem. Phys.* **127**, 204103 (2007).

[115] C. Ochsenfeld and M. Head-Gordon, *Chem. Phys. Lett.* **270**, 399 (1997).

[116] P. von Schleyer, C. Maerker, A. Dransfield, H. Jiao, and N. J. R. v. E. Hommes, *J. Am. Chem. Soc.* **118**, 6317 (1996).

[117] S. P. Brown et al., *Angew. Chem. Int. Ed. Engl.* **40**, 717 (2001).

[118] C. Ochsenfeld et al., *Solid State Nucl. Mag.* **22**, 128 (2002).

[119] J. Kussmann and C. Ochsenfeld, *J. Chem. Phys.* **127**, 054103 (2007).

[120] F. London, *J. Phys. Radium* **8**, 397 (1937).

[121] J. Gauss, *Ber. Bunsenges. Phys. Chem.* **99**, 1001 (1995).

[122] C. Ochsenfeld, C. A. White, and M. Head-Gordon, *J. Chem. Phys.* **109**, 1663 (1998).

[123] C. Ochsenfeld, *Chem. Phys. Lett.* **327**, 216 (2000).

[124] C. A. White, B. G. Johnson, P. M. W. Gill, and M. Head-Gordon, *Chem. Phys. Lett.* **230**, 8 (1994).

[125] T. Helgaker, M. Watson, and N. Handy, *J. Chem. Phys.* **113**, 9402 (2000).

[126] V. Sychrovský, J. Gräfenstein, and D. Cremer, *J. Chem. Phys.* **113**, 3530 (2000).

[127] T. Bally and P. R. Rablen, *J. Org. Chem* **76**, 4818 (2011).

[128] F. Jensen, *J. Chem. Theory Comput.* **2**, 1360 (2006).

[129] H. Sekino and R. J. Bartlett, *J. Chem. Phys.* **85**, 976 (1986).

[130] S. P. Karna and M. Dupuis, *J. Comput. Chem.* **12**, 487 (1991).

[131] R. J. Cave and M. D. Newton, *Chem. Phys. Lett.* **249**, 15 (1996).

[132] A. A. Voityuk and N. Rösch, *J. Chem. Phys.* **117**, 5607 (2002).

[133] J. E. Subotnik, S. Yeganeh, R. J. Cave, and M. A. Ratner, *J. Chem. Phys.* **129**, 244101 (2008).

[134] J. E. Subotnik, R. J. Cave, R. P. Steele, and N. Shenvi, *J. Chem. Phys.* **130**, 234102 (2009).

[135] C.-P. Hsu, Z.-Q. You, and H.-C. Chen, *J. Phys. Chem. C* **112**, 1204 (2008).

[136] Z. You and C.-P. Hsu, *J. Chem. Phys.* **133**, 074105 (2010).

[137] J. E. Subotnik, J. Vura-Weis, A. Sodt, and M. A. Ratner, *J. Phys. Chem. A* **114**, 8665 (2010).

[138] J. Vura-Weis, M. Wasielewski, M. D. Newton, and J. E. Subotnik, *J. Phys. Chem. C* **114**, 20449 (2010).

[139] K. Ohta, G. L. Closs, K. Morokuma, and N. J. Green, *J. Am. Chem. Soc.* **108**, 1319 (1986).

[140] A. Broo and S. Larsson, *Chem. Phys.* **148**, 103 (1990).

[141] A. Farazdel, M. Dupuis, E. Clementi, and A. Aviram, *J. Am. Chem. Soc.* **112**, 4206 (1990).

[142] L. Y. Zhang, R. A. Friesner, and R. B. Murphy, *J. Chem. Phys.* **107**, 450 (1997).

[143] M. D. Newton, *Chem. Rev.* **91**, 767 (1991).

[144] H. F. King, R. E. Stanton, H. Kim, R. E. Wyatt, and R. G. Parr, *J. Chem. Phys.* **47**, 1936 (1967).

[145] K. Takatsuka, T. Fueno, and K. Yamaguchi, *Theor. Chem. Acc.* **48**, 175 (1978).

[146] R. C. Bochicchio, *J. Mol. Struct. (Theochem)* **429**, 229 (1998).

[147] V. N. Staroverov and E. R. Davidson, *Chem. Phys. Lett.* **330**, 161 (2000).

[148] E. Proynov, *J. Mol. Struct. (Theochem)* **762**, 159 (2006).

[149] E. Proynov, F. Liu, and J. Kong, *Phys. Rev. A* **88**, 032510 (2013).

[150] A. D. Becke, *J. Chem. Phys.* **119**, 2972 (2003).

[151] A. D. Becke and E. R. Johnson, *J. Chem. Phys.* **122**, 154104 (2005).

[152] E. Proynov, Y. Shao, and J. Kong, *Chem. Phys. Lett.* **493**, 381 (2010).

[153] E. Proynov, F. Liu, Y. Shao, and J. Kong, *J. Chem. Phys.* **136**, 034102 (2012).

[154] A. D. Becke, *J. Chem. Phys.* **88**, 2547 (1988).

[155] S. Datta, *Quantum transport: Atom to transistor*, Cambridge University Press, Cambridge, 2005.

[156] M. Di Ventra, *Electron transport in nanoscale systems*, Cambridge University Press, Cambridge, 2008.

# Chapter 11

# Molecules in Complex Environments: Solvent Models, QM/MM and QM/EFP Features, Density Embedding

## 11.1 Introduction

Q-CHEM has incorporated a number of methods for complex systems such as molecules in solutions, proteins, polymers, molecular clusters, *etc.*, summarized as follows:

- Implicit solvation models;
- QM/MM tools;
- EFP and QM/EFP approach (polarizable electrostatic embedding); and
- Density embedding methods.

## 11.2 Chemical Solvent Models

*Ab initio* quantum chemistry makes possible the study of gas-phase molecular properties from first principles. In liquid solution, however, these properties may change significantly, especially in polar solvents. Although it is possible to model solvation effects by including explicit solvent molecules in the quantum-chemical calculation (*e.g.* a super-molecular cluster calculation, averaged over different configurations of the molecules in the first solvation shell), such calculations are very computationally demanding. Furthermore, cluster calculations typically do not afford accurate solvation energies, owing to the importance of long-range electrostatic interactions. Accurate prediction of solvation free energies is, however, crucial for modeling of chemical reactions and ligand/receptor interactions in solution.

Q-CHEM contains several different implicit solvent models, which differ greatly in their level of sophistication. These are generally known as self-consistent reaction field (SCRF) models, because the continuum solvent establishes a "reaction field" (additional terms in the solute Hamiltonian) that depends upon the solute electron density, and must therefore be updated self-consistently during the iterative convergence of the wave function. The simplest and oldest of these models that is available in Q-CHEM is the Kirkwood-Onsager model[1–3], in which the solute molecule is placed inside of a spherical cavity and its electrostatic potential is represented in terms of a single-center multipole expansion. More sophisticated models, which use a molecule-shaped cavity and the full molecular electrostatic potential, include the conductor-like screening model (COSMO)[4] and the closely related conductor-like PCM (C-PCM)[5–7], along with the "surface and simulation of volume polarization for electrostatics" [SS(V)PE] model[8]. The latter is also known as the "integral equation formalism" (IEF-PCM)[9,10].

The C-PCM and IEF-PCM/SS(V)PE are examples of what are called "apparent surface charge" SCRF models, although the term *polarizable continuum models* (PCMs), as popularized by Tomasi and co-workers[11], is now used almost universally to refer to this class of solvation models. Q-CHEM employs a Switching/ Gaussian or "SWIG" implementation of these PCMs[12–16]. This approach resolves a long-standing—though little-publicized—problem with standard PCMs, namely, that the boundary-element methods used to discretize the solute/continuum interface may lead to discontinuities in the potential energy surface for the solute molecule. These discontinuities inhibit convergence of geometry optimizations, introduce serious artifacts in vibrational frequency calculations, and make *ab initio* molecular dynamics calculations virtually impossible[12,13]. In contrast, Q-CHEM's SWIG PCMs afford potential energy surfaces that are rigorously continuous and smooth. Unlike earlier attempts to obtain smooth PCMs, the SWIG approach largely preserves the properties of the underlying integral-equation solvent models, so that solvation energies and molecular surface areas are hardly affected by the smoothing procedure.

Other solvent models available in Q-CHEM include the "Langevin dipoles" model[17,18] as well as versions 8 and 12 of the SM$x$ models and the SMD model developed at the University of Minnesota[19–21]. SM8 and SM12 are based upon the generalized Born method for electrostatics, augmented with atomic surface tensions intended to capture non-electrostatic effects (cavitation, dispersion, exchange repulsion, and changes in solvent structure). Empirical corrections of this sort are also available for the PCMs mentioned above, but within SM8 and SM12 these parameters have been optimized to reproduce experimental solvation energies. SMD (where the "D" is for "density") combines IEF-PCM with the non-electrostatic corrections, but because the electrostatics is based on the density rather than atomic point charges, it is supported for arbitrary basis sets whereas SM8 and SM12 are not.

Table 11.1 summarizes the implicit solvent models that are available in Q-CHEM. Solvent models are invoked via the SOLVENT_METHOD keyword, as shown below. Additional details about each particular solvent model can be found in the sections that follow. In general, these methods are available for any SCF level of electronic structure theory, though in the case of SM8 only certain basis sets are supported. Post-Hartree–Fock calculations can be performed by first running an SCF + PCM job, in which case the correlated wave function will employ MOs and Hartree-Fock energy levels that are polarized by the solvent.

**Note:** The job-control format for specifying implicit solvent models changed significantly starting in Q-CHEM version 4.2.1. This change was made in an attempt to simply and unify the input notation for a large number of different models.

| **Model** | **Cavity** | | **Non-Electrostatic Terms?** | **Supported Basis Sets** | **Derivatives Available?** |
|---|---|---|---|---|---|
| | Construction | Discretization | | | |
| Kirkwood-Onsager | spherical | point charges | no | all | none |
| Langevin Dipoles | atomic spheres (user-definable) | dipoles in 3-d space | no | all | none |
| C-PCM | atomic spheres (user-definable) | point charges or smooth Gaussians | user-specified | all | 1st and 2nd |
| SS(V)PE/ IEF-PCM | atomic spheres (user-definable) | point charges or smooth Gaussians | user-specified | all | 1st |
| COSMO | predefined atomic spheres | point charges | none | all | 1st and 2nd |
| Isodensity SS(V)PE | isodensity contour | point charges | none | all | none |
| SM8 | predefined atomic spheres | generalized Born | automatic | 6-31G*<br>6-31+G*<br>6-31+G** | 1st |
| SM12 | predefined atomic spheres | generalized Born | automatic | all | none |
| SMD | predefined atomic spheres | point charges | automatic | all | 1st |

Table 11.1: Summary of implicit solvation models available in Q-CHEM, indicating how the solute cavity is constructed and discretized, whether non-electrostatic terms are (or can be) included, which basis sets are available for use with each model, and whether analytic first and second derivatives are available for optimizations and frequency calculations.

**SOLVENT_METHOD**

Sets the preferred solvent method.

TYPE:

STRING

DEFAULT:

0

OPTIONS:

0 Do not use a solvation model.
ONSAGER Use the Kirkwood-Onsager model (Section 11.2.1).
PCM Use an apparent surface charge, polarizable continuum model (Section 11.2.2).
ISOSVP Use the iso-density implementation of the SS(V)PE model (Section 11.2.5).
COSMO Use COSMO (similar to C-PCM but with an outlying charge correction[22,23]; see Section 11.2.7).
SM8 Use version 8 of the Cramer-Truhlar SM$x$ model (Section 11.2.8.1).
SM12 Use version 12 of the SM$x$ model (Section 11.2.8.2).
SMD Use SMD (Section 11.2.8.3).
CHEM_SOL Use the Langevin Dipoles model (Section 11.2.9).

RECOMMENDATION:

Consult the literature. PCM is a collective name for a family of models and additional input options may be required in this case, in order to fully specify the model. (See Section 11.2.2.) Several versions of SM12 are available as well, as discussed in Section 11.2.8.2.

Before going into detail about each of these models, a few potential points of confusion warrant mention, with regards to nomenclature. First, "PCM" refers to a family of models that includes C-PCM and SS(V)PE/IEF-PCM (the latter two being completely equivalent[10]). One or the other of these models can be selected by additional job control variables in a *$pcm* input section, as described in Section 11.2.2. COSMO is very similar to C-PCM but includes a correction for that part of the solute's electron density that penetrates beyond the cavity (the so-called "outlying charge")[22,23]. This is discussed in Section 11.2.7.

Two implementations of the SS(V)PE model are also available. The PCM implementation (which is requested by setting SOLVENT_METHOD = PCM) uses a solute cavity constructed from atom-centered spheres, as with most other PCMs. On the other hand, setting SOLVENT_METHOD = ISOSVP requests an SS(V)PE calculation in which the solute cavity is defined by an isocontour of the solute's own electron density, as advocated by Chipman[8,24,25]. This is an appealing, one-parameter cavity construction, although it is unclear that this construction alone is superior in its accuracy to carefully-parameterized atomic radii[26], at least not without additional, non-electrostatic terms included[27–30] that are available in Q-CHEM's implementation of the isodensity version of SS(V)PE (Section 11.2.6). Moreover, analytic energy gradients are not available for the isodensity cavity construction, whereas they are available when the cavity is constructed from atom-centered spheres. One additional subtlety, which is discussed in detail in Ref. 14, is the fact that the PCM implementation of the equation for the SS(V)PE surface charges [Eq. (11.2)] uses an asymmetric $\mathbf{K}$ matrix. In contrast, Chipman's isodensity implementation uses a symmetrized $\mathbf{K}$ matrix. Although the symmetrized version is somewhat more computationally efficient when the number of surface charges is large, the asymmetric version is better justified, theoretically[14]. (This admittedly technical point is clarified in Section 11.2.2 and in particular in Table 11.2.)

Regarding the accuracy of these models for solvation free energies ($\Delta G_{298}$), SM8 achieves sub-kcal/mol accuracy for neutral molecules, based on comparison to a large database of experimental values, although average errors for ions are more like 4 kcal/mol[31]. To achieve comparable accuracy with IEF-PCM/SS(V)PE, non-electrostatic terms must be included[27,29,32]. The SM12 model does not improve upon SM8 in any statistical sense[20], but does lift one important restriction on the level of electronic structure that can be combined with these models. Specifically, the Generalized Born model used in SM8 is based on a variant of Mulliken-style atomic charges, and is therefore parameterized only for a few small basis sets, *e.g.*, 6-31G*. SM12, on the other hand, uses a variety of charge schemes that are stable with respect to basis-set expansion, and can therefore be combined with any level of electronic structure theory for the solute. Like IEF-PCM, the SMD model is also applicable to any basis sets, and its accuracy is comparable to SM8 and SM12[21]. Quantitative fluid-phase thermodynamics can also be obtained using Klamt's COSMO-RS approach[33,34], where RS stands for "real solvent". The COSMO-RS approach is *not* included in Q-CHEM and requires the COSMOtherm program, which is licensed separately through COSMOlogic[35], but Q-CHEM can write the input files that are need by COSMOtherm.

The following sections provide more details regarding theory and job control for the various implicit solvent models that are available in Q-CHEM. In addition, recent review articles are available for PCM methods[11], SM$x$[31], and COSMO[36]. Formal relationships between various PCMs have been discussed in Refs. 14,24.

### 11.2.1 Kirkwood-Onsager Model

The simplest implicit solvation model available in Q-CHEM is the Kirkwood-Onsager model[1–3], wherein the solute is placed inside of a spherical cavity that is surrounded by a homogeneous dielectric medium. This model is characterized by two parameters: the cavity radius, $a$, and the solvent dielectric constant, $\varepsilon$. The former is typically calculated according to

$$a = (3V_m/4\pi N_A)^{1/3} \qquad (11.1)$$

where $V_m$ is the solute's molar volume, usually obtained from experiment (molecular weight or density[37]), and $N_A$ is Avogadro's number. It is also common to add 0.5 Å to the value of $a$ in Eq. (11.1) in order to account for the first solvation shell[38]. Alternatively, $a$ is sometimes selected as the maximum distance between the solute center of mass and the solute atoms, plus the relevant van der Waals radii. A third option is to set $2a$ (the cavity diameter) equal to the largest solute–solvent internuclear distance, plus the van der Waals radii of the relevant atoms. Unfortunately, solvation energies are typically quite sensitive to the choice of $a$ (and to the construction of the solute cavity, more generally).

Unlike older versions of the Kirkwood-Onsager model, in which the solute's electron distribution was described entirely in terms of its dipole moment, Q-CHEM's version can use multipoles of arbitrarily high order, including the Born (monopole) term[39] for charged solutes, in order to describe the solute's electrostatic potential. The solute–continuum electrostatic interaction energy is then computed using analytic expressions for the interaction of the point multipoles with a dielectric continuum.

Energies and analytic gradients for the Kirkwood-Onsager solvent model are available for Hartree-Fock, DFT, and CCSD calculations. It is often advisable to perform a gas-phase calculation of the solute molecule first, which can serve as the initial guess for a subsequent Kirkwood-Onsager implicit solvent calculation.

The Kirkwood-Onsager SCRF is requested by setting SOLVENT_METHOD = ONSAGER in the *$rem* section (along with normal job control variables for an energy or gradient calculation), and furthermore specifying several additional options in a *$solvent* input section, as described below. Of these, the keyword **CavityRadius** is required. The *$rem* variable CC_SAVEAMPL may save some time for CCSD calculations using the Kirkwood-Onsager model.

**Note:** SCRF and CCSD combo works only in CCMAN (with CCMAN2 = FALSE).

**Note:** The following three job control variables belong *only* in the *$solvent* section. Do not place them in the *$rem* section. As with other parts of the Q-CHEM input file, this input section is not case-sensitive.

**CavityRadius**
Sets the radius of the spherical solute cavity.
INPUT SECTION: *$solvent*
TYPE:
FLOAT
DEFAULT:
No default.
OPTIONS:
$a$ Desired cavity radius, in Ångstroms.
RECOMMENDATION:
Use Eq. (11.1).

**Dielectric**

Sets the dielectric constant of the solvent continuum.

INPUT SECTION: *$solvent*

TYPE:

FLOAT

DEFAULT:

78.39

OPTIONS:

$\varepsilon$ Use a (dimensionless) value of $\varepsilon$.

RECOMMENDATION:

As per required solvent; the default corresponds to water at 25°C.

**MultipoleOrder**

Determines the order to which the multipole expansion of the solute charge density is carried out.

INPUT SECTION: *$solvent*

TYPE:

INTEGER

DEFAULT:

15

OPTIONS:

$\ell$ Include up to $\ell$th order multipoles.

RECOMMENDATION:

Use the default. The multipole expansion is usually converged by order $\ell = 15$.

**Example 11.1** Onsager model applied at the Hartree-Fock level to $H_2O$ in acetonitrile

```
$molecule
   0 1
   O       0.00000000     0.00000000     0.11722303
   H      -0.75908339     0.00000000    -0.46889211
   H       0.75908339     0.00000000    -0.46889211
$end

$rem
   METHOD            HF
   BASIS             6-31g**
   SOLVENT_METHOD    Onsager
$end

$solvent
   CavityRadius      1.8    !   1.8 Angstrom Solute Radius
   Dielectric        35.9   !   Acetonitrile
   MultipoleOrder    15     !   this is the default value
$end
```

**Example 11.2** CCSD/Onsager calculation applied to 1,2-dichloroethane molecule

```
$comment
   1,2-dichloroethane GAUCHE Conformation
$end
```

```
$molecule
   0 1
   C     0.654133  -0.381705   0.880884
   C    -0.654133   0.381705   0.880884
   Cl    1.732259   0.087759  -0.463055
   H     1.186245  -0.166574   1.796075
   H     0.488935  -1.444440   0.805846
   Cl   -1.732259  -0.087759  -0.463055
   H    -1.186245   0.166574   1.796075
   H    -0.488935   1.444440   0.805846
$end

$rem
   METHOD           CCSD
   BASIS            6-31g**
   N_FROZEN_CORE    FC
   CC_SAVEAMPL      1         ! Save the CC amplitudes on disk
   SOLVENT_METHOD   ONSAGER
$end

$solvent
   CavityRadius     3.65  !  in Angstroms
   Dielectric       8.93  !  methylene chloride
$end
```

**Example 11.3** Kirkwood-Onsager SCRF applied to hydrogen fluoride in water, performing a gas-phase calculation first.

```
$molecule
   0 1
   H       0.000000     0.000000    -0.862674
   F       0.000000     0.000000     0.043813
 $end

$rem
   METHOD          HF
   BASIS           6-31G*
$end

@@@

$molecule
   0 1
   H       0.000000     0.000000    -0.862674
   F       0.000000     0.000000     0.043813
$end

$rem
   JOBTYPE           FORCE
   METHOD            HF
   BASIS             6-31G*
   SOLVENT_METHOD    ONSAGER
   SCF_GUESS         READ  ! read vacuum solution as a guess
$end

$solvent
```

| Model | Literature Refs. | Matrix K | Matrix R | Scalar $f_\varepsilon$ |
|---|---|---|---|---|
| COSMO | 4 | $\mathbf{S}$ | $-f_\varepsilon \mathbf{1}$ | $(\varepsilon - 1)/(\varepsilon + 1/2)$ |
| C-PCM | 5,6 | $\mathbf{S}$ | $-f_\varepsilon \mathbf{1}$ | $(\varepsilon - 1)/\varepsilon$ |
| IEF-PCM | 8,10 | $\mathbf{S} - (f_\varepsilon/2\pi)\mathbf{DAS}$ | $-f_\varepsilon \left(\mathbf{1} - \frac{1}{2\pi}\mathbf{DA}\right)$ | $(\varepsilon - 1)/(\varepsilon + 1)$ |
| SS(V)PE | 8,25 | $\mathbf{S} - (f_\varepsilon/4\pi)\big(\mathbf{DAS} + \mathbf{SAD}^\dagger\big)$ | $-f_\varepsilon \left(\mathbf{1} - \frac{1}{2\pi}\mathbf{DA}\right)$ | $(\varepsilon - 1)/(\varepsilon + 1)$ |

Table 11.2: Definition of the matrices in Eq. (11.2) for the various PCMs that are available in Q-CHEM. The matrix $\mathbf{S}$ consists of Coulomb interactions between the cavity charges and $\mathbf{D}$ is the discretized version of the matrix that generates the outward-pointing normal electric field vector. (See Refs. 15,24,25 for detailed definitions.) The matrix $\mathbf{A}$ is diagonal and contains the surface areas of the cavity discretization elements, and $\mathbf{1}$ is a unit matrix. At the level of Eq. (11.2), COSMO and C-PCM differ only in the dielectric screening factor $f_\varepsilon$, although COSMO includes an additional outlying charge correction that goes beyond Eq. (11.2)[22,23].

```
   CavityRadius    2.5
$end
```

## 11.2.2 Polarizable Continuum Models

Clearly, the Kirkwood-Onsager model is inappropriate if the solute is very non-spherical. Nowadays, a more general class of "apparent surface charge" SCRF solvation models are much more popular, to the extent that the generic term "polarizable continuum model" (PCM) is typically used to denote these methods[11]. Apparent surface charge PCMs improve upon the Kirkwood-Onsager model in two ways. Most importantly, they provide a much more realistic description of molecular shape, typically by constructing the "solute cavity" (*i.e.*, the interface between the atomistic region and the dielectric continuum) from a union of atom-centered spheres, an aspect of the model that is discussed in Section 11.2.2.2. In addition, the exact electron density of the solute (rather than a multipole expansion) is used to polarize the continuum. Electrostatic interactions between the solute and the continuum manifest as an induced charge density on the cavity surface, which is discretized into point charges for practical calculations. The surface charges are determined based upon the solute's electrostatic potential at the cavity surface, hence the surface charges and the solute wave function must be determined self-consistently.

### 11.2.2.1 Formal Theory and Discussion of Different Models

The PCM literature has a long history[11] and there are several different models in widespread use; connections between these models have not always been appreciated[8,10,14,24]. Chipman[8,24] has shown how various PCMs can be formulated within a common theoretical framework; see Ref. 15 for a pedagogical introduction. The PCM takes the form of a set of linear equations,

$$\mathbf{Kq} = \mathbf{Rv} \ , \tag{11.2}$$

in which the induced charges $q_i$ at the cavity surface discretization points [organized into a vector $\mathbf{q}$ in Eq. (11.2)] are computed from the values $v_i$ of the solute's electrostatic potential at those same discretization points. The form of the matrices $\mathbf{K}$ and $\mathbf{R}$ depends upon the particular PCM in question. These matrices are given in Table 11.2 for the PCMs that are available in Q-CHEM.

The oldest PCM is the so-called D-PCM model of Tomasi and co-workers[40], but unlike the models listed in Table 11.2, D-PCM requires explicit evaluation of the electric field normal to the cavity surface, This is undesirable, as evaluation of the electric field is both more expensive and more prone to numerical problems as compared to evaluation of the electrostatic potential. Moreover, the dependence on the electric field can be formally eliminated at the level of the integral equation whose discretized form is given in Eq. (11.2)[8]. As such, D-PCM is essentially obsolete, and the PCMs available in Q-CHEM require only the evaluation of the electrostatic potential, not the electric field.

The simplest PCM that continues to enjoy widespread use is the Conductor-Like Screening Model (COSMO) introduced by Klamt and Schüürmann[4]. Truong and Stefanovich[5] later implemented the same model with a slightly different dielectric scaling factor ($f_\varepsilon$ in Table 11.2), and called this modification GCOSMO. The latter was implemented within the PCM formalism by Barone and Cossi *et al.*[6,7], who called the model C-PCM (for "conductor-like" PCM). In each case, the dielectric screening factor has the form

$$f_\varepsilon = \frac{\varepsilon - 1}{\varepsilon + x} \,, \tag{11.3}$$

where Klamt and Schüürmann proposed $x = 1/2$ but $x = 0$ was used in GCOSMO and C-PCM. The latter value is the correct choice for a single charge in a spherical cavity (*i.e.*, the Born ion model), although Klamt and co-workers suggest that $x = 1/2$ is a better compromise, given that the Kirkwood-Onsager analytical result is $x = \ell/(\ell + 1)$ for an $\ell$th-order multipole centered in a spherical cavity[4,23]. The distinction is irrelevant in high-dielectric solvents; the $x = 0$ and $x = 1/2$ values of $f_\varepsilon$ differ by only 0.6% for water at 25°C, for example. Truong[5] argues that $x = 0$ does a better job of preserving Gauss' Law in low-dielectric solvents, but more accurate solvation energies (at least for neutral molecules, as compared to experiment) are sometimes obtained using $x = 1/2$ (Ref. 6). This result is likely highly sensitive to cavity construction, and in any case, both versions are available in Q-CHEM.

Whereas the original COSMO model introduced by Klamt and Schüürmann[4] corresponds to Eq. (11.2) with $\mathbf{K}$ and $\mathbf{R}$ as defined in Table 11.2, Klamt and co-workers later introduced a correction for outlying charge that goes beyond Eq. (11.2)[22,23]. Klamt now consistently refers to this updated model as "COSMO"[36], and we shall adopt this nomenclature as well. COSMO, with the outlying charge correction, is available in Q-CHEM and is described in Section 11.2.7. In contrast, C-PCM consists entirely of Eq. (11.2) with matrices $\mathbf{K}$ and $\mathbf{R}$ as defined in Table 11.2, although it is possible to modify the dielectric screening factor to use the $x = 1/2$ value (as in COSMO) rather than the $x = 0$ value. Additional non-electrostatic terms can be added at the user's discretion, as discussed below, but there is no explicit outlying charge correction in C-PCM. These and other fine-tuning details for PCM jobs are controllable via the *$pcm* input section that is described in Section 11.2.3.

As compared to C-PCM, a more sophisticated treatment of continuum electrostatic interactions is afforded by the "surface and simulation of volume polarization for electrostatics" [SS(V)PE] approach[8]. Formally speaking, this model provides an exact treatment of the *surface polarization* (*i.e.*, the surface charge induced by the solute charge that is contained within the solute cavity, which induces a surface polarization owing to the discontinuous change in dielectric constant across the cavity boundary) but also an approximate treatment of the *volume polarization* (arising from the aforementioned outlying charge). The "SS(V)PE" terminology is Chipman's notation[8], but this model is formally equivalent, at the level of integral equations, to the "integral equation formalism" (IEF-PCM) that was developed originally by Cancès *et al.*[9,41]. Some difference do arise when the integral equations are discretized to form finite-dimensional matrix equations[14], and it should be noted from Table 11.2 that SS(V)PE uses a symmetrized form of the $\mathbf{K}$ matrix as compared to IEF-PCM. The *asymmetric* IEF-PCM is the recommended approach[14], although only the symmetrized version is available in the isodensity implementation of SS(V)PE that is discussed in Section 11.2.5. As with the obsolete D-PCM approach, the original version of IEF-PCM explicitly required evaluation of the

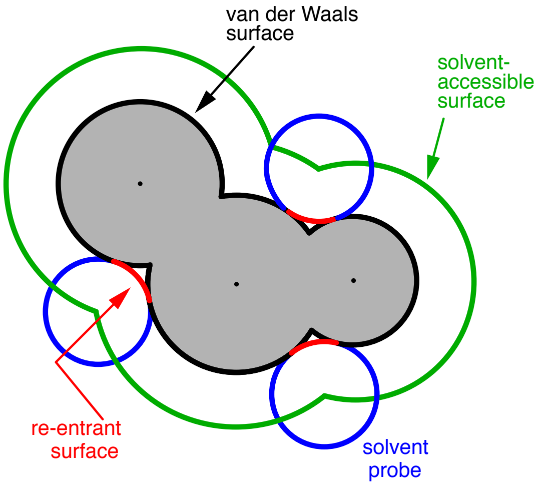

Figure 11.1: Illustration of various solute cavity surface definitions for PCMs.[16] The union of atomic van der Waals spheres (shown in gray) defines the van der Waals (vdW) surface, in black. Note that actual vdW radii from the literature are sometimes scaled in constructing the vdW surface. If a probe sphere (representing the assumed size of a solvent molecule) is rolled over the van der Waals surface, then its center point traces out the solvent accessible surface (SAS), shown in green; the SAS is equivalent to a vdW surface where the atomic radii are increases by the radius of the probe sphere. Finally, one can use the probe sphere to smooth out the sharp crevasses in the vdW surface using the re-entrant surface elements shown in red, resulting in the solvent-excluded surface (SES).

normal electric field at the cavity surface, but it was later shown that this dependence could be eliminated to afford the version described in Table 11.2[8,10]. This version requires only the electrostatic potential, and is thus preferred, and it is this version that we designate as IEF-PCM. The C-PCM model becomes equivalent to SS(V)PE in the limit $\varepsilon \to \infty$[8,14], which means that C-PCM must somehow include an *implicit* correction for volume polarization, even if this was not by design[22]. For $\varepsilon \gtrsim 50$, numerical calculations reveal that there is essentially no difference between SS(V)PE and C-PCM results[14]. Since C-PCM is less computationally involved as compared to SS(V)PE, it is the PCM of choice in high-dielectric solvents. The computational savings relative to SS(V)PE may be particularly significant for large QM/MM/PCM jobs. For a more detailed discussion of the history of these models, see the lengthy and comprehensive review by Tomasi *et al.*[11]. For a briefer discussion of the connections between these models, see Refs. 14,15,24.

#### 11.2.2.2 Cavity Construction and Discretization

Construction of the cavity surface is a crucial aspect of PCMs, as computed properties are quite sensitive to the details of the cavity construction. Most cavity constructions are based on a union of atom-centered spheres (see Fig. 11.1), but there are yet several different constructions whose nomenclature is occasionally confused in the literature. Simplest and most common is the van der Waals (vdW) surface consisting of a union of atom-centered spheres. Traditionally[42,43], and by default in Q-CHEM, the atomic radii are taken to be 1.2 times larger than vdW radii extracted from crystallographic data, originally by Bondi[44] (and thus sometimes called "Bondi radii"). This 20% augmentation is intended to mimic the fact that solvent molecules cannot approach all the way to the vdW radius of the solute atoms, though it's not altogether clear that this is an optimal value. (The default scaling factor in Q-CHEM is 1.2 but can be modified by the user.) An alternative to scaling the atomic radii is to add a certain fixed increment to each, representing the approximate size of a solvent molecule (*e.g.*, 1.4 Å for water) and leading to what is known as the *solvent accessible surface* (SAS). From another point of view, the SAS represents the surface defined by the center of a spherical solvent molecule as it rolls over the vdW surface, as suggested in Fig. 11.1. Both the vdW surface and the SAS possess cusps where the atomic spheres intersect, although these become less pronounced as the atomic radii are scaled or augmented. These cusps are eliminated in what is known as the *solvent-accessible surface* (SES), sometimes called the Connolly surface or the "molecular surface". The SES uses the surface of the probe sphere at points where it is simultaneously tangent to two or more atomic spheres to define elements of a "re-entrant surface" that smoothly connects the atomic (or "contact") surface [16].

Having chosen a model for the cavity surface, this surface is discretized using atom-centered Lebedev grids [45–47] of the same sort that are used to perform the numerical integrations in DFT. (Discretization of the re-entrant facets of the SES is somewhat more complicated but similar in spirit [16].) Surface charges $q_i$ are located at these grid points and the Lebedev quadrature weights can be used to define the surface area associated with each discretization point [12].

A long-standing (though not well-publicized) problem with the aforementioned discretization procedure is that it fails to afford continuous potential energy surfaces as the solute atoms are displaced, because certain surface grid points may emerge from, or disappear within, the solute cavity, as the atomic spheres that define the cavity are moved. This undesirable behavior can inhibit convergence of geometry optimizations and, in certain cases, lead to very large errors in vibrational frequency calculations [12]. It is also a fundamental hindrance to molecular dynamics calculations [13]. Building upon earlier work by York and Karplus [48], Lange and Herbert [12,13,16] developed a general scheme for implementing apparent surface charge PCMs in a manner that affords smooth potential energy surfaces, even for *ab initio* molecular dynamics simulations involving bond breaking [13,15]. Notably, this approach is faithful to the properties of the underlying integral equation theory on which the PCMs are based, in the sense that the smoothing procedure does not significantly perturb solvation energies or cavity surface areas [12,13]. The smooth discretization procedure combines a switching function with Gaussian blurring of the cavity surface charge density, and is thus known as the "Switching/Gaussian" (SWIG) implementation of the PCM.

Both single-point energies and analytic energy gradients are available for SWIG PCMs, when the solute is described using molecular mechanics or an SCF (Hartree-Fock or DFT) electronic structure model, except that for the SES cavity model only single-point energies are available. Analytic Hessians are available for the C-PCM model only. (As usual, vibrational frequencies for other models will be computed, if requested, by finite difference of analytic energy gradients.) Single-point energy calculations using correlated wave functions can be performed in conjunction with these solvent models, in which case the correlated wave function calculation will utilize Hartree-Fock molecular orbitals that are polarized in the presence of the continuum dielectric solvent (*i.e.*, there is no post-Hartree–Fock PCM correction).

Researchers who use these PCMs are asked to cite Refs. 13,14, which provide the details of Q-CHEM's implementation, and Ref. 16 if the SES is used. (We point the reader in particular to Ref. 13, which provides an assessment of the discretization errors that can be anticipated using various PCMs and Lebedev grids; default grid values in Q-CHEM were established based on these tests.) When publishing results based on PCM calculations, it is essential to specify both the precise model that is used (see Table 11.2) as well as how the cavity was constructed.

For example, "Bondi radii multiplied by 1.2", which is the Q-CHEM default, except for hydrogen, where the factor is reduced to 1.1 [49], as per usual. Radii for main-group elements that were not provided by Bondi are taken from Ref. 50. Absent details such as these, PCM calculations will be difficult to reproduce in other electronic structure programs.

#### 11.2.2.3 Non-Equilibrium Solvation for Vertical Excitation, Ionization and Emission

In vertical excitation or ionization, the solute undergoes a sudden change in its charge distribution. Various microscopic motions of the solvent have characteristic times to reach certain polarization response, and fast part of the solvent response (electrons) can follow such a dynamic process while the remaining degrees of freedom (nuclei) remain unchanged as in the initial state. Such splitting of the solvent response gives rise to non-equilibrium solvation. In the literature, two different approaches have been developed for describing non-equilibrium solvent effects: the linear response (LR) approach[51,52] and the state-specific (SS) approach[43,53–55]. Both are implemented in Q-CHEM[56], at the SCF level for vertical ionization and at the corresponding level (CIS, TDDFT or ADC, see Section 6.8.7) for vertical excitation. A brief introduction to these methods is given below, and users who utilize the non-equilibrium PCM features are asked to cite Refs. 56 and 57. State-specific solvent-field equilibration for long-lived excited states to compute e.g. emission energies is implemented for the ADC-suite of methods as described in section 6.8.7. Users who utilize this equilibrium-solvation PCM please cite and be referred to Ref. 58.

The LR approach considers the solvation effects as a coupling between a pair of transitions, one for solute and the other for solvent. The transition frequencies when the interaction between the solute and solvent is turned on may be determined by considering such an interaction as a perturbation. In the framework of TDDFT, the solvent/solute interaction is given by[59]

$$\begin{aligned}\omega' = &\int d\mathbf{r} \int d\mathbf{r}' \int d\mathbf{r}'' \int d\mathbf{r}''' \rho^{\mathrm{tr}*}(\mathbf{r}) \left( \frac{1}{|\mathbf{r}-\mathbf{r}'|} + g_{\mathrm{XC}}(\mathbf{r},\mathbf{r}') \right) \\ &\times \chi^*(\mathbf{r}',\mathbf{r}'',\omega) \left( \frac{1}{|\mathbf{r}''-\mathbf{r}'''|} + g_{\mathrm{XC}}(\mathbf{r}'',\mathbf{r}''') \right) \rho^{\mathrm{tr}}(\mathbf{r}''') \ ,\end{aligned} \tag{11.4}$$

where $\chi$ is the charge density response function of the solvent and $\rho^{\mathrm{tr}}(\mathbf{r})$ is the solute's transition density. This term accounts for a dynamical correction to the transition energy so that it is related to the response of the solvent to the charge density of the solute oscillating at the solute transition frequency ($\omega$). Within a PCM, only classical Coulomb interactions are taken into account, and Eq. (11.4) becomes

$$\omega'_{\mathrm{PCM}} = \int d\mathbf{r} \int d\mathbf{s} \, \frac{\rho^{\mathrm{tr}*}(\mathbf{r})}{|\mathbf{r}-\mathbf{s}|} \int d\mathbf{s}' \int d\mathbf{r}' \, \mathcal{Q}(\mathbf{s},\mathbf{s}',\varepsilon) \frac{\rho^{\mathrm{tr}}(\mathbf{r}')}{|\mathbf{s}'-\mathbf{r}'|} \ , \tag{11.5}$$

where $\mathcal{Q}$ is PCM solvent response operator for a generic dielectric constant, $\varepsilon$. The integral of $\mathcal{Q}$ and the potential of the density $\rho^{\mathrm{tr}}$ gives the surface charge density for the solvent polarization.

The state-specific (SS) approach takes into account the capability of a part of the solvent degrees of freedom to respond instantaneously to changes in the solute wave function upon excitation. Such an effect is not accounted for in the LR approach. In SS, a generic solvated-solute excited state $\Psi_i$ is obtained as a solution of a nonlinear Schrödinger equation

$$\left( \hat{H}^{\mathrm{vac}} + \hat{V}_0^{\mathrm{slow}} + \hat{V}_i^{\mathrm{fast}} \right) |\Psi_i\rangle = E_i^{\mathrm{SS}} |\Psi_i\rangle \tag{11.6}$$

that depends upon the solute's charge distribution. Here $\hat{H}^{\mathrm{vac}}$ is the usual Hamiltonian for the solute in vacuum and the reaction field operator $\hat{V}_i$ generates the electrostatic potential of the apparent surface charge density (Section 11.2.2.1), corresponding to slow and fast polarization response. The solute is polarized self-consistently with respect to the solvent's reaction field. In case of vertical ionization rather than excitation, both the ionized and non-ionized states can be treated within a ground-state formalism. For vertical excitations, self-consistent SS models[55,60] have been developed for various excited-state methods, including both CIS and TDDFT.

In a linear dielectric medium, the solvent polarization is governed by the electric susceptibility, $\chi = [\varepsilon(\omega) - 1]/4\pi$, where $\varepsilon(\omega)$ is the frequency-dependent permittivity, In case of very fast vertical transitions, the dielectric response is ruled by the optical dielectric constant, $\varepsilon_{\text{opt}} = n^2$, where $n$ is the solvent's index of refraction. In both LR and SS, the fast part of the solvent's degrees of freedom is in equilibrium with the solute density change. Within PCM, the fast solvent polarization charges for the SS excited state $i$ can be obtained by solving the following equation[54]:

$$\mathbf{K}_{\varepsilon_{\text{opt}}}\mathbf{q}_i^{\text{fast,SS}} = \mathbf{R}_{\varepsilon_{\text{opt}}}\left[\mathbf{v}_i + \mathbf{v}(\mathbf{q}_0^{\text{slow}})\right] \ . \tag{11.7}$$

Here $\mathbf{q}^{\text{fast,SS}}$ is the discretized fast surface charge. The dielectric constants in the matrices $\mathbf{K}$ and $\mathbf{R}$ (Section 11.2.2.1) are replaced with the optical dielectric constant, and $\mathbf{v}_i$ is the potential of the solute's excited state density, $\rho_i$. The quantity $\mathbf{v}(\mathbf{q}_0^{\text{slow}})$ is the potential of the slow part of the apparent surface charges in the ground state, which are given by

$$\mathbf{q}_0^{\text{slow}} = \frac{\varepsilon - \varepsilon_{\text{opt}}}{\varepsilon - 1}\mathbf{q}_0 \ . \tag{11.8}$$

For LR-PCM, the solvent polarization is subjected to the first-order changes to the electron density (TDDFT linear density response), and thus Eq. (11.7) becomes

$$\mathbf{K}_{\varepsilon_{\text{opt}}}\mathbf{q}_i^{\text{fast,LR}} = \mathbf{R}_{\varepsilon_{\text{opt}}}\mathbf{v}(\rho_i^{\text{tr}}) \ . \tag{11.9}$$

The LR approach for CIS/TDDFT excitations and the self-consistent SS method (using the ground-state SCF) for vertical ionizations are available in Q-CHEM. The self-consistent SS method for vertical excitations is *not* available, because this method is problematic in the vicinity of (near-) degeneracies between excited states, such as in the vicinity of a conical intersection. The fundamental problem in the SS approach is that each wave function $\Psi_i$ is an eigenfunction of a *different* Hamiltonian, since Eq. (11.6) depend upon the specific state of interest. To avoid the ordering and the non-orthogonality problems, we compute the vertical excitation energy using a first-order, perturbative approximation to the SS approach[61,62], in what we have termed the "ptSS" method[57]. The zeroth-order excited-state wave function can be calculated using various excited-state methods (currently available for CIS and TDDFT in Q-CHEM) with solvent-relaxed molecular orbitals obtained from a ground-state PCM calculation. As mentioned previously, LR and SS describe different solvent relaxation features in non-equilibrium solvation. In the perturbation scheme, we can calculate the LR contribution using the zeroth-order transition density, in what we have called the "ptLR" approach. The combination of ptSS and ptLR yields quantitatively good solvatochromatic shifts in combination with TDDFT but not with the correlated variants of ADC, for which the pure ptSS approach was shown to be superior.[56,57].

The LR and SS approaches can also be used in the study of photon emission processes[63]. An emission process can be treated as a vertical excitation at a stationary point on the excited-state potential surface. The basic requirement therefore is to prepare the solvent-relaxed geometry for the excited-state of interest. TDDFT/C-PCM analytic gradients and Hessian are available.

Section 6.3.5 for computational details regarding excited-state geometry optimization with PCM. An emission process is slightly more complicated than the absorption case. Two scenarios are discussed in literature, depending on the lifetime of an excited state in question. In the limiting case of ultra-fast excited state decay, when only fast solvent degrees of freedom are expected to be equilibrated with the excited-state density. In this limit, the emission energy can be computed exactly in the same way as the vertical excitation energy. In this case, excited state geometry optimization should be performed in the non-equilibrium limit. The other limit is that of long-lived excited state, *e.g.*, strongly fluorescent species and phosphorescence. In the long-lived case, excited state geometry optimization should be performed with the solvent equilibrium limit. Thus, the excited state should be computed using an equilibrium LR or SS approach, and the ground state is calculated using non-equilibrium self-consistent SS approach. The latter approach is implemented for the ADC-based methods as described in Section 6.8.7.

### 11.2.3 PCM Job Control

A PCM calculation is requested by setting SOLVENT_METHOD = PCM in the *$rem* section. As mentioned above, there are a variety of different theoretical models that fall within the PCM family, so additional fine-tuning may be required, as described below.

#### 11.2.3.1 *$pcm* section

Most PCM job control is accomplished via options specified in the *$pcm* input section, which allows the user to specify which flavor of PCM will be used, which algorithm will be used to solve the PCM equations, and other options. The format of the *$pcm* section is analogous to that of the *$rem* section:

```
$pcm
   <Keyword>  <parameter/option>
$end
```

**Note:** The following job control variables belong *only* in the *$pcm* section. Do not place them in the *$rem* section.

**Theory**
Specifies the which polarizable continuum model will be used.
INPUT SECTION: *$pcm*
TYPE:
STRING
DEFAULT:
CPCM
OPTIONS:

| | |
|---|---|
| CPCM | Conductor-like PCM with $f_\varepsilon = (\varepsilon - 1)/\varepsilon$. |
| COSMO | Original conductor-like screening model with $f_\varepsilon = (\varepsilon - 1)/(\varepsilon + 1/2)$. |
| IEFPCM | IEF-PCM with an asymmetric $\mathbf{K}$ matrix. |
| SSVPE | SS(V)PE model, equivalent to IEF-PCM with a symmetric $\mathbf{K}$ matrix. |

RECOMMENDATION:
The IEF-PCM/SS(V)PE model is more sophisticated model than either C-PCM or COSMO, and probably more appropriate for low-dielectric solvents, but it is also more computationally demanding. In high-dielectric solvents there is little difference between these models. Note that the keyword **COSMO** in this context simply affects the dielectric screening factor $f_\varepsilon$; to obtain the outlying charge correction suggested by Klamt[22,23], one should use SOLVENT_METHOD = COSMO rather than SOLVENT_METHOD = PCM. (See Section 11.2.7.)

**Method**

Specifies which surface discretization method will be used.

INPUT SECTION: *$pcm*

TYPE:

STRING

DEFAULT:

SWIG

OPTIONS:

| | |
|---|---|
| SWIG | Switching/Gaussian method |
| ISWIG | "Improved" Switching/Gaussian method with an alternative switching function |
| Spherical | Use a single, fixed sphere for the cavity surface. |
| Fixed | Use discretization point charges instead of smooth Gaussians. |

RECOMMENDATION:

Use of **SWIG** is recommended only because it is slightly more efficient than the switching function of **ISWIG**. On the other hand, **ISWIG** offers some conceptually more appealing features and may be superior in certain cases. Consult Refs. 13,14 for a discussion of these differences. The **Fixed** option uses the Variable Tesserae Number (VTN) algorithm of Li and Jensen[64], with Lebedev grid points. VTN uses point charges with no switching function or Gaussian blurring, and is therefore subject to discontinuities in geometry optimizations. It is not recommended, except to make contact with other calculations in the literature.

**SwitchThresh**

Threshold for discarding grid points on the cavity surface.

INPUT SECTION: *$pcm*

TYPE:

INTEGER

DEFAULT:

8

OPTIONS:

| | |
|---|---|
| $n$ | Discard grid points when the switching function is less than $10^{-n}$. |

RECOMMENDATION:

Use the default, which is found to avoid discontinuities within machine precision. Increasing $n$ reduces the cost of PCM calculations but can introduce discontinuities in the potential energy surface.

Construction of the solute cavity is an important part of the model and users should consult the literature in this capacity, especially with regard to the radii used for the atomic spheres. The default values provided in Q-CHEM correspond to the consensus choice that has emerged over several decades, namely, to use vdW radii scaled by a factor of 1.2. The most widely-used set of vdW radii are those determined from crystallographic data by Bondi[44], although the radius for hydrogen was later adjusted to 1.1 Å[49], and radii for those main-group elements not addressed by Bondi were provided later[50]. This extended set of vdW is used by default in Q-CHEM, and for simplicity we call these "Bondi radii" regardless of whether they come from Bondi's original paper or the later work. Alternatively, atomic radii from the Universal Force Field (UFF) are available[65]. The main appeal of UFF radii is that they are defined for all atoms of the periodic table, though the quality of these radii for PCM applications is unclear. Finally, the user may specify his or her own radii for cavity construction using a *$van_der_waals* input section, the format for which is described in Section 11.2.9. No scaling factor is applied to user-defined radii. Note that $R = 0$ is allowed for a particular atomic radius, in which case the atom in question is not used to construct the cavity surface. This feature facilitates the construction of "united atom" cavities[26], in which the hydrogen atoms do not get their own spheres and the heavy-atom radii are increased to compensate Finally, since the solvent molecules should not be able to penetrate all the way to the atomic vdW radii of the solute, it is traditional either to scale the atomic radii (vdW surface construction) or else to augment them with an assumed radius of a spherical solvent molecule (SAS construction), but not both.

**Radii**

Specifies which set of atomic van der Waals radii will be used to define the solute cavity.

INPUT SECTION: *$pcm*

TYPE:

STRING

DEFAULT:

BONDI

OPTIONS:

| | |
|---|---|
| BONDI | Use the (extended) set of Bondi radii. |
| FF | Use Lennard-Jones radii from a molecular mechanics force field. |
| UFF | Use radii form the Universal Force Field. |
| READ | Read the atomic radii from a *$van_der_waals* input section. |

RECOMMENDATION:

Bondi radii are widely used. The **FF** option requires the user to specify an MM force field using the FORCE_FIELD *$rem* variable, and also to define the atom types in the *$molecule* section (see Section 11.3). This is not required for UFF radii.

**vdwScale**

Scaling factor for the atomic van der Waals radii used to define the solute cavity.

INPUT SECTION: *$pcm*

TYPE:

FLOAT

DEFAULT:

1.2

OPTIONS:

$f$ Use a scaling factor of $f > 0$.

RECOMMENDATION:

The default value is widely used in PCM calculations, although a value of 1.0 might be appropriate if using a solvent-accessible surface.

**SASradius**

Form a "solvent accessible" surface with the given solvent probe radius.

INPUT SECTION: *$pcm*

TYPE:

FLOAT

DEFAULT:

0.0

OPTIONS:

$r$ Use a solvent probe radius of $r$, in Å.

RECOMMENDATION:

The solvent probe radius is added to the scaled van der Waals radii of the solute atoms. A common solvent probe radius for water is 1.4 Å, but the user should consult the literature regarding the use of solvent-accessible surfaces.

**SurfaceType**

Selects the solute cavity surface construction.

INPUT SECTION: *$pcm*

TYPE:

STRING

DEFAULT:

VDW_SAS

OPTIONS:

| | |
|---|---|
| VDW_SAS | van der Waals or solvent-accessible surface |
| SES | solvent-excluded surface |

RECOMMENDATION:

The vdW surface and the SAS are each comprised simply of atomic spheres and thus share a common option; the only difference is the specification of a solvent probe radius, **SASradius**. For a true vdW surface, the probe radius should be zero (which is the default), whereas for the SAS the atomic radii are traditionally not scaled, hence **vdwScale** should be set to zero (which is *not* the default). For the SES, only SWIG discretization is available, but this can be used with any set of (scaled or unscaled) atomic radii, or with radii that are augmented by **SASradius**.

Historically, discretization of the cavity surface has involved "tessellation" methods that divide the cavity surface area into finite polygonal "tesserae". (The GEPOL algorithm[66] is perhaps the most widely-used tessellation scheme.) Tessellation methods, however, suffer not only from discontinuities in the cavity surface area and solvation energy as a function of the nuclear coordinates, but in addition they lead to analytic energy gradients that are complicated to derive and implement. To avoid these problems, Q-CHEM's SWIG PCM implementation[12–14] uses Lebedev grids to discretize the atomic spheres. These are atom-centered grids with icosahedral symmetry, and may consist of anywhere from 26 to 5294 grid points per atomic sphere. The default values used by Q-CHEM were selected based on extensive numerical tests[13,14]. The default for MM atoms (in MM/PCM or QM/MM/PCM jobs) is $N = 110$ Lebedev points per atomic sphere, whereas the default for QM atoms is $N = 302$. (This represents a change relative to Q-CHEM versions earlier than 4.2.1, where the default for QM atoms was $N = 590$.) These default values exhibit good rotational invariance and absolute solvation energies that, in most cases, lie within ∼0.5–1.0 kcal/mol of the $N \to \infty$ limit[13], although exceptions (especially where charged solutes are involved) can be found[14].

**Note:** The acceptable values for the number of Lebedev points per sphere are $N$ = 26, 50, 110, 194, 302, 434, 590, 770, 974, 1202, 1454, 1730, 2030, 2354, 2702, 3074, 3470, 3890, 4334, 4802, or 5294.

**HPoints**

The number of Lebedev grid points to be placed on H atoms in the QM system.

INPUT SECTION: *$pcm*

TYPE:

INTEGER

DEFAULT:

302

OPTIONS:

Acceptable values are listed above.

RECOMMENDATION:

Use the default for geometry optimizations. For absolute solvation energies, the user may want to examine convergence with respect to $N$.

**HeavyPoints**

The number of Lebedev grid points to be placed non-hydrogen atoms in the QM system.

INPUT SECTION: *$pcm*

TYPE:

INTEGER

DEFAULT:

302

OPTIONS:

Acceptable values are listed above.

RECOMMENDATION:

Use the default for geometry optimizations. For absolute solvation energies, the user may want to examine convergence with respect to $N$.

**MMHPoints**

The number of Lebedev grid points to be placed on H atoms in the MM subsystem.

INPUT SECTION: *$pcm*

TYPE:

INTEGER

DEFAULT:

110

OPTIONS:

Acceptable values are listed above.

RECOMMENDATION:

Use the default for geometry optimizations. For absolute solvation energies, the user may want to examine convergence with respect to $N$. This option applies only to MM/PCM or QM/MM/PCM calculations.

**MMHeavyPoints**

The number of Lebedev grid points to be placed on non-hydrogen atoms in the MM subsystem.

INPUT SECTION: *$pcm*

TYPE:

INTEGER

DEFAULT:

110

OPTIONS:

Acceptable values are listed above.

RECOMMENDATION:

Use the default for geometry optimizations. For absolute solvation energies, the user may want to examine convergence with respect to $N$. This option applies only to MM/PCM or QM/MM/PCM calculations.

Especially for complicated molecules, the user may want to visualize the cavity surface. This can be accomplished by setting **PrintLevel** $\geq 2$, which will trigger the generation of several `.PQR` files that describe the cavity surface. (These are written to the Q-CHEM output file.) The `.PQR` format is similar to the common `.PDB` (Protein Data Bank) format, but also contains charge and radius information for each atom. One of the output `.PQR` files contains the charges computed in the PCM calculation and radii (in Å) that are half of the square root of the surface area represented by each surface grid point. Thus, in examining this representation of the surface, larger discretization points are associated with larger surface areas.

A second `.PQR` file contains the solute's electrostatic potential (in atomic units), in place of the charge information, and uses uniform radii for the grid points. These `.PQR` files can be visualized using various third-party software, including the freely-available Visual Molecular Dynamics (VMD) program[67,68], which is particularly useful for coloring the `.PQR` surface grid points according to their charge, and sizing them according to their contribution to the molecular surface area. (Examples of such visualizations can be found in Ref. 12.)

**PrintLevel**

Controls the printing level during PCM calculations.

INPUT SECTION: *$pcm*

TYPE:

INTEGER

DEFAULT:

0

OPTIONS:

0 Prints PCM energy and basic surface grid information. Minimal additional printing.

1 Level 0 plus PCM solute-solvent interaction energy components and Gauss' Law error.

2 Level 1 plus surface grid switching parameters and a `.PQR` file for visualization of the cavity surface apparent surface charges.

3 Level 2 plus a `.PQR` file for visualization of the electrostatic potential at the surface grid created by the converged solute.

4 Level 3 plus additional surface grid information, electrostatic potential and apparent surface charges on each SCF cycle.

5 Level 4 plus extensive debugging information.

RECOMMENDATION:

Use the default unless further information is desired.

Finally, note that setting **Method** to **Spherical** in the *$pcm* input selection requests the construction of a solute cavity consisting of a single, fixed sphere. This is generally not recommended but is occasionally useful for making contact with the results of Born models in the literature, or the Kirkwood-Onsager model discussed in Section 11.2.1. In this case, the cavity radius and its center must also be specified in the *$pcm* section. The keyword **HeavyPoints** controls the number of Lebedev grid points used to discretize the surface.

**CavityRadius**

Specifies the solute cavity radius.

INPUT SECTION: *$pcm*

TYPE:

FLOAT

DEFAULT:

None

OPTIONS:

$R$ Use a radius of $R$, in Ångstroms.

RECOMMENDATION:

None.

**CavityCenter**

Specifies the center of the spherical solute cavity.

INPUT SECTION: *$pcm*

TYPE:

FLOAT

DEFAULT:

0.0 0.0 0.0

OPTIONS:

$x$ $y$ $z$ Coordinates of the cavity center, in Ångstroms.

RECOMMENDATION:

The format is **CavityCenter** followed by three floating-point values, delineated by spaces. Uses the same coordinate system as the *$molecule* section.

#### 11.2.3.2 Examples

The following example shows a very basic PCM job. The solvent dielectric is specified in the *$solvent* section, which is described below.

**Example 11.4** A basic example of using the PCMs: optimization of trifluoroethanol in water.

```
$rem
   JOBTYPE         OPT
   BASIS           6-31G*
   METHOD          B3LYP
   SOLVENT_METHOD  PCM
$end

$pcm
   Theory          CPCM
   Method          SWIG
   Solver          Inversion
   HeavyPoints     194
   HPoints         194
   Radii           Bondi
   vdwScale        1.2
$end

$solvent
   Dielectric 78.39
$end

$molecule
   0 1
   C    -0.245826    -0.351674    -0.019873
   C     0.244003     0.376569     1.241371
   O     0.862012    -0.527016     2.143243
   F     0.776783    -0.909300    -0.666009
   F    -0.858739     0.511576    -0.827287
   F    -1.108290    -1.303001     0.339419
   H    -0.587975     0.878499     1.736246
   H     0.963047     1.147195     0.961639
   H     0.191283    -1.098089     2.489052
$end
```

The next example uses a single spherical cavity and should be compared to the Kirkwood-Onsager job, Example 11.1 on page 683.

**Example 11.5** PCM with a single spherical cavity, applied to $H_2O$ in acetonitrile

```
$molecule
   0 1
   O       0.00000000     0.00000000     0.11722303
   H      -0.75908339     0.00000000    -0.46889211
   H       0.75908339     0.00000000    -0.46889211
$end

$rem
   METHOD            HF
   BASIS             6-31g**
   SOLVENT_METHOD    pcm
$end

$pcm
   method        spherical   ! single spherical cavity with 590 discretization points
   HeavyPoints   590
   CavityRadius  1.8         ! Solute Radius, in Angstrom
   CavityCenter  0.0 0.0 0.0 ! Will be at center of Standard Nuclear Orientation
   Theory        SSVPE
$end

$solvent
   Dielectric        35.9   !   Acetonitrile
$end
```

Finally, we consider an example of a united-atom cavity. Note that a user-defined van der Waals radius is supplied only for carbon, so the hydrogen radius is taken to be zero and thus the hydrogen atoms are not used to construct the cavity surface. (As mentioned above, the format for the *$van_der_waals* input section is discussion in Section 11.2.9).

**Example 11.6** United-atom cavity construction for ethylene.

```
$comment
   Benzene (in benzene), with a united-atom cavity construction
   R = 2.28 A for carbon, R = 0 for hydrogen
$end

$molecule
   0 1
   C    1.38620    0.000000   0.000000
   C    0.69310    1.200484   0.000000
   C   -0.69310    1.200484   0.000000
   C   -1.38620    0.000000   0.000000
   C   -0.69310   -1.200484   0.000000
   C    0.69310   -1.200484   0.000000
   H    2.46180    0.000000   0.000000
   H    1.23090    2.131981   0.000000
   H   -1.23090    2.131981   0.000000
   H   -2.46180    0.000000   0.000000
   H   -1.23090   -2.131981   0.000000
   H    1.23090   -2.131981   0.000000
$end
```

```
$rem
   EXCHANGE        hf
   BASIS           6-31G*
   SOLVENT_METHOD  pcm
$end

$pcm
   theory          iefpcm   ! this is a synonym for ssvpe
   method          swig
   printlevel      1
   radii           read
$end

$solvent
   dielectric 2.27
$end

$van_der_waals
1
  6     2.28
  1     0.00
$end
```

#### 11.2.3.3 *$solvent* section

The solvent for PCM calculations is specified using the *$solvent* section, as documented below. In addition, the *$solvent* section can be used to incorporate non-electrostatic interaction terms into the solvation energy. (The **Theory** keyword in the *$pcm* section specifies only how the electrostatic interactions are handled.) The general form of the *$solvent* input section is shown below. The *$solvent* section was used above to specify parameters for the Kirkwood-Onsager SCRF model, and will be used again below to specify the solvent for SM$x$ calculations (Section 11.2.8); in each case, the particular options that can be listed in the *$solvent* section depend upon the value of the *$rem* variable SOLVENT_METHOD.

```
$solvent
   NonEls  <Option>
   NSolventAtoms <Number unique of solvent atoms>
   SolventAtom <Number1> <Number2> <Number3> <SASradius>
   SolventAtom <Number1> <Number2> <Number3> <SASradius>
   . . .
   <Keyword>  <parameter/option>
   . . .
$end
```

The keyword `SolventAtom` requires multiple parameters, whereas all other keywords require only a single parameter. In addition to any (optional) non-electrostatic parameters, the *$solvent* section is also used to specify the solvent's dielectric constant. If non-electrostatic interactions are ignored, then this is the only keyword that is necessary in the *$solvent* section. For non-equilibrium TDDFT/C-PCM calculations (Section 11.2.2.3), the optical dielectric constant should be specified in the *$solvent* section as well.

**Dielectric**

The (static) dielectric constant of the PCM solvent.

INPUT SECTION: *$solvent*

TYPE:

FLOAT

DEFAULT:

78.39

OPTIONS:

$\varepsilon$ Use a dielectric constant of $\varepsilon > 0$.

RECOMMENDATION:

The static (*i.e.*, zero-frequency) dielectric constant is what is usually called “the” dielectric constant. The default corresponds to water at 25°C.

**OpticalDielectric**

The optical dielectric constant of the PCM solvent.

INPUT SECTION: *$solvent*

TYPE:

FLOAT

DEFAULT:

1.78

OPTIONS:

$\varepsilon_\infty$ Use an optical dielectric constant of $\varepsilon_\infty > 0$.

RECOMMENDATION:

The default corresponds to water at 25°C. Note that $\varepsilon_\infty = n^2$, where $n$ is the solvent’s index of refraction.

The non-electrostatic interactions currently available in Q-CHEM are based on the work of Cossi *et al.*[69], and are computed outside of the SCF procedure used to determine the electrostatic interactions. The non-electrostatic energy is highly dependent on the input parameters and can be extremely sensitive to the radii chosen to define the solute cavity. Accordingly, the inclusion of non-electrostatic interactions is highly empirical and probably needs to be considered on a case-by-case basis. Following Ref. 69, the cavitation energy is computed using the same solute cavity that is used to compute the electrostatic energy, whereas the dispersion/repulsion energy is computed using a solvent-accessible surface.

The following keywords (in the *$solvent* section) are used to define non-electrostatic parameters for PCM calculations.

**NonEls**

Specifies what type of non-electrostatic contributions to include.

INPUT SECTION: *$solvent*

TYPE:

STRING

DEFAULT:

None

OPTIONS:

| | |
|---|---|
| Cav | Cavitation energy |
| Buck | Buckingham dispersion and repulsion energy from atomic number |
| LJ | Lennard-Jones dispersion and repulsion energy from force field |
| BuckCav | Buck + Cav |
| LJCav | LJ + Cav |

RECOMMENDATION:

A very limited set of parameters for the Buckingham potential is available at present.

**NSolventAtoms**

The number of different types of atoms.

INPUT SECTION: *$solvent*

TYPE:

INTEGER

DEFAULT:

None

OPTIONS:

$N$ Specifies that there are $N$ different types of atoms.

RECOMMENDATION:

This keyword is necessary when **NonEls** = Buck, LJ, BuckCav, or LJCav. Methanol ($CH_3OH$), for example, has three types of atoms (C, H, and O).

**SolventAtom**

Specifies a unique solvent atom.

INPUT SECTION: *$solvent*

TYPE:

Various

DEFAULT:

None.

OPTIONS:

| Input (TYPE) | Description |
|---|---|
| Number1 (INTEGER): | The atomic number of the atom |
| Number2 (INTEGER): | How many of this atom are in a solvent molecule |
| Number3 (INTEGER): | Force field atom type |
| SASradius (FLOAT): | Probe radius (in Å) for defining the solvent accessible surface |

RECOMMENDATION:

If not using LJ or LJCav, Number3 should be set to 0. The **SolventAtom** keyword is necessary when **NonEls** = Buck, LJ, BuckCav, or LJCav.

**Temperature**

Specifies the solvent temperature.

INPUT SECTION: *$solvent*

TYPE:

FLOAT

DEFAULT:

300.0

OPTIONS:

$T$ Use a temperature of $T$, in Kelvin.

RECOMMENDATION:

Used only for the cavitation energy.

**Pressure**

Specifies the solvent pressure.

INPUT SECTION: *$solvent*

TYPE:

FLOAT

DEFAULT:

1.0

OPTIONS:

$P$ Use a pressure of $P$, in bar.

RECOMMENDATION:

Used only for the cavitation energy.

**SolventRho**

Specifies the solvent number density

INPUT SECTION: *$solvent*

TYPE:

FLOAT

DEFAULT:

Determined for water, based on temperature.

OPTIONS:

$\rho$ Use a density of $\rho$, in molecules/Å$^3$.

RECOMMENDATION:

Used only for the cavitation energy.

**SolventRadius**

The radius of a solvent molecule of the PCM solvent.

INPUT SECTION: *$solvent*

TYPE:

FLOAT

DEFAULT:

None

OPTIONS:

$r$ Use a radius of $r$, in Å.

RECOMMENDATION:

Used only for the cavitation energy.

The following example illustrates the use of the non-electrostatic interactions.

**Example 11.7** Optimization of trifluoroethanol in water using both electrostatic and non-electrostatic PCM interactions. OPLSAA parameters are used in the Lennard-Jones potential for dispersion and repulsion.

```
$rem
   JOBTYPE        OPT
   BASIS          6-31G*
   METHOD         B3LYP
   SOLVENT_METHOD PCM
   FORCE_FIELD    OPLSAA
$end

$pcm
   Theory      CPCM
   Method      SWIG
   Solver      Inversion
   HeavyPoints 194
   HPoints     194
   Radii       Bondi
   vdwScale    1.2
$end

$solvent
   NonEls        LJCav
   NSolventAtoms 2
   SolventAtom   8 1 186 1.30
   SolventAtom   1 2 187 0.01
   SolventRadius 1.35
   Temperature   298.15
   Pressure      1.0
   SolventRho    0.03333
   Dielectric    78.39
$end

$molecule
   0 1
   C    -0.245826    -0.351674    -0.019873     23
   C     0.244003     0.376569     1.241371     22
   O     0.862012    -0.527016     2.143243     24
   F     0.776783    -0.909300    -0.666009     26
   F    -0.858739     0.511576    -0.827287     26
   F    -1.108290    -1.303001     0.339419     26
   H    -0.587975     0.878499     1.736246     27
   H     0.963047     1.147195     0.961639     27
   H     0.191283    -1.098089     2.489052     25
$end
```

### 11.2.3.4 Job control and Examples for Non-Equilibrium Solvation

The **OpticalDielectric** keyword in *$solvent* is always needed. The LR energy is automatically calculated while the CIS/TDDFT calculations are performed with PCM, but it is turned off while the perturbation scheme is employed.

**ChargeSeparation**

Partition fast and slow charges in solvent equilibrium state

INPUT SECTION: *$pcm*

TYPE:

STRING

DEFAULT:

No default.

OPTIONS:

| | |
|---|---|
| Marcus | Do slow-fast charge separation in the ground state. |
| Excited | Do slow-fast charge separation in an excited-state. |

RECOMMENDATION:

Charge separation is used in conjunction with the **StateSpecific** keyword in *$pcm*.

**StateSpecific**

Specifies which the state-specific method will be used.

INPUT SECTION: *$pcm*

TYPE:

Various

DEFAULT:

No default.

OPTIONS:

| | |
|---|---|
| Marcus | Run self-consistent SS method in the ground-state with a given slow polarization charges. |
| Perturb | Perform ptSS and ptLR for vertical excitations. |
| $i$ | The $i$th excited-state used for charge separation (for emission). |

RECOMMENDATION:

**NoneqGrad**

Control whether perform excited state geometry optimization in equilibrium or non-equilibrium.

INPUT SECTION: *$pcm*

TYPE:

NONE

DEFAULT:

No default.

OPTIONS:

RECOMMENDATION:

Specify it for non-equilibrium optimization otherwise equilibrium geometry optimization will be performed.

**Example 11.8** LR-TDDFT/C-PCM low-lying vertical excitation energy

```
$molecule
   0 1
   C    0  0  0.0
   O    0  0  1.21
$end
```

```
$rem
   EXCHANGE            B3LP
   CIS_N_ROOTS         10
   CIS_SINGLETS        TRUE
   CIS_TRIPLETS       TRUE
   RPA                 TRUE
   BASIS               6-31+G*
   SOLVENT_METHOD      PCM
$end

$pcm
   Theory      CPCM
   Method      SWIG
   Solver      Inversion
   Radii       Bondi
$end

$solvent
   Dielectric         78.39
   OpticalDielectric  1.777849
$end
```

**Example 11.9** PCM solvation effects on the vertical excitation energies of planar DMABN using the ptSS and ptLR methods.

```
$molecule
   0  1
   C     0.000046   -0.000398    1.904953
   C     1.210027    0.000379    1.186051
   C     1.214640   -0.000065   -0.194515
   C     0.000164   -0.000616   -0.933832
   C    -1.214349   -0.001557   -0.194687
   C    -1.209753   -0.001846    1.185775
   H     2.151949    0.001377    1.722018
   H     2.164371    0.000481   -0.709640
   H    -2.164082   -0.002008   -0.709781
   H    -2.151763   -0.002287    1.721615
   C    -0.000227    0.001061    3.325302
   N    -0.000475    0.002405    4.484321
   N     0.000053   -0.000156   -2.297372
   C    -1.258656    0.001284   -3.036994
   H    -1.041042    0.001615   -4.102376
   H    -1.860897   -0.885647   -2.811117
   H    -1.859247    0.889133   -2.810237
   C     1.258563   -0.000660   -3.037285
   H     1.860651    0.886208   -2.810755
   H     1.859362   -0.888604   -2.811461
   H     1.040664   -0.000097   -4.102609
$end

$rem
   EXCHANGE              LRC-wPBEPBE
   OMEGA                 260
   BASIS                 6-31G*
   CIS_N_ROOTS           10
   RPA                   2
   CIS_SINGLETS          1
   CIS_TRIPLETS          0
   CIS_DYNAMIC_MEM       TRUE
   CIS_RELAXED_DENSITY   TRUE
   USE_NEW_FUNCTIONAL    TRUE
   SOLVENT_METHOD        PCM
   PCM_PRINT             1
$end

$pcm
   Theory                 IEFPCM
   ChargeSeparation       Marcus
   StateSpecific          Perturb
$end

$solvent
   Dielectric             35.688000       ! Acetonitrile
   OpticalDielectric      1.806874
$end
```

**Example 11.10** Aqueous phenol ionization using state-specific non-equilibrium PCM

```
$molecule
   0  1
   C  -0.189057  -1.215927  -0.000922
   H  -0.709319  -2.157526  -0.001587
   C   1.194584  -1.155381  -0.000067
   H   1.762373  -2.070036  -0.000230
   C   1.848872   0.069673   0.000936
   H   2.923593   0.111621   0.001593
   C   1.103041   1.238842   0.001235
   H   1.595604   2.196052   0.002078
   C  -0.283047   1.185547   0.000344
   H  -0.862269   2.095160   0.000376
   C  -0.929565  -0.042566  -0.000765
   O  -2.287040  -0.159171  -0.001759
   H  -2.663814   0.725029   0.001075
$end

$rem
  EXCHANGE              wPBE
  CORRELATION           PBE
  LRC_DFT               1
  OMEGA                 300
  BASIS                 6-31+G*
  SCF_CONVERGENCE       8
  SOLVENT_METHOD        PCM
  PCM_PRINT             1
$end

$pcm
   ChargeSeparation      Marcus
$end

$solvent
   Dielectric            78.39
   OpticalDielectric     1.777849
$end
```

```
@@@

$molecule
 1  2
 read
$end

$rem
   EXCHANGE              wPBE
   CORRELATION           PBE
   LRC_DFT               1
   OMEGA                 300
   BASIS                 6-31+G*
   SCF_CONVERGENCE       8
   SOLVENT_METHOD        PCM
   PCM_PRINT             1
   SCF_GUESS             READ
$end

$pcm
   StateSpecific          Marcus
$end

$solvent
   Dielectric             78.39
   OpticalDielectric      1.777849
$end
```

**Example 11.11** PCM solvation effects on the emission energy of twisted DMABN in acetonitrile.

```
$molecule
   0  1
   C    -0.000002   -0.000003    1.894447
   C     1.230178    0.000003    1.160765
   C     1.244862    0.000001   -0.200360
   C     0.000003   -0.000013   -0.917901
   C    -1.244845   -0.000000   -0.200354
   C    -1.230160    0.000000    1.160753
   H     2.171128    0.000013    1.704064
   H     2.180670    0.000009   -0.750140
   H    -2.180657    0.000006   -0.750120
   H    -2.171112    0.000006    1.704037
   C    -0.000023   -0.000002    3.293509
   N    -0.000011   -0.000001    4.459415
   N    -0.000008   -0.000005   -2.309193
   C     0.000001    1.253881   -3.021235
   H     0.000005    1.099076   -4.098660
   H    -0.882908    1.818975   -2.705815
   H     0.882911    1.818967   -2.705805
   C    -0.000009   -1.253886   -3.021246
   H     0.882917   -1.818966   -2.705849
   H    -0.882901   -1.818992   -2.705803
   H    -0.000038   -1.099071   -4.098670
$end

$rem
   EXCHANGE              LRC-wPBEPBE
   OMEGA                 280
   BASIS                6-31G*
   CIS_N_ROOTS          10
   RPA                  2
   CIS_SINGLETS         1
   CIS_TRIPLETS         0
   CIS_DYNAMIC_MEM      TRUE
   CIS_RELAXED_DENSITY  TRUE
   USE_NEW_FUNCTIONAL   TRUE
   SOLVENT_METHOD       PCM
   PCM_PRINT            1
$end

$pcm
   ChargeSeparation       Excited
   StateSpecific          1
$end

$solvent
   Dielectric             35.688000   ! Acetonitrile
   OpticalDielectric      1.806874
$end

@@@
$molecule
   READ
$end

$rem
   EXCHANGE             LRC-wPBEPBE
   OMEGA                280
   BASIS                6-31G*
   SCF_GUESS            READ
   SCF_CONVERGENCE      8
   SOLVENT_METHOD       PCM
   PCM_PRINT            1
$end

$pcm
   StateSpecific          Marcus
$end

$solvent
   Dielectric             35.688000   ! Acetonitrile
   OpticalDielectric      1.806874
$end
```

### 11.2.4 Linear-Scaling QM/MM/PCM Calculations

Recall that PCM electrostatics calculations require the solution of the set of linear equations given in Eq. (11.2), to determine the vector $\mathbf{q}$ of apparent surface charges. The precise forms of the matrices $\mathbf{K}$ and $\mathbf{R}$ depend upon the particular PCM (Table 11.2), but in any case they have dimension $N_{\text{grid}} \times N_{\text{grid}}$, where $N_{\text{grid}}$ is the number of Lebedev grid points used to discretize the cavity surface. Construction of the matrix $\mathbf{K}^{-1}\mathbf{R}$ affords a numerically exact solution to Eq. (11.2), whose cost scales as $\mathcal{O}(N_{\text{grid}}^3)$ in CPU time and $\mathcal{O}(N_{\text{grid}}^2)$ in memory. This cost is exacerbated by smooth PCMs, which discard fewer interior grid points so that $N_{\text{grid}}$ tends to be larger, for a given solute, as compared to traditional discretization schemes.

For QM solutes, the cost of inverting $\mathbf{K}$ is usually negligible relative to the cost of the electronic structure calculation, but for the large values of $N_{\rm grid}$ that are encountered in MM/PCM or QM/MM/PCM jobs, the $\mathcal{O}(N_{\rm grid}^3)$ cost of inverting $\mathbf{K}$ is often prohibitively expensive.

To avoid this bottleneck, Lange and Herbert[15] have developed an iterative conjugate gradient (CG) solver for Eq. (11.2) whose cost scales as $\mathcal{O}(N_{\rm grid}^2)$ in CPU time and $\mathcal{O}(N_{\rm grid})$ in memory. A number of other cost-saving options are available, including efficient pre-conditioners and matrix factorizations that speed up convergence of the CG iterations, and a fast multipole algorithm for computing the electrostatic interactions[70]. Together, these features lend themselves to a solution of Eq. (11.2) whose cost scales as $\mathcal{O}(N_{\rm grid})$ in both memory and CPU time, for sufficiently large systems[15]. Currently, these options are available only for C-PCM, not for SS(V)PE/IEF-PCM.

Listed below are job control variables for the CG solver, which should be specified within the *$pcm* input section. Researchers who use this feature are asked to cite the original SWIG PCM references[13,14] as well as the reference for the CG solver[15].

**Solver**

Specifies the algorithm used to solve the PCM equations.

INPUT SECTION: *$pcm*

TYPE:

STRING

DEFAULT:

INVERSION

OPTIONS:

| | |
|---|---|
| INVERSION | Direct matrix inversion |
| CG | Iterative conjugate gradient |

RECOMMENDATION:

Matrix inversion is faster for small solutes because it needs to be performed only once in a single-point calculation. However, the CG solver (which must be applied at each SCF iteration) is recommended for large MM/PCM or QM/MM/PCM calculations.

**CGThresh**

The threshold for convergence of the conjugate gradient solver.

INPUT SECTION: *$pcm*

TYPE:

INTEGER

DEFAULT:

6

OPTIONS:

$n$ Conjugate gradient converges when the maximum residual is less than $10^{-n}$.

RECOMMENDATION:

The default typically affords PCM energies on par with the precision of matrix inversion for small systems. For systems that have difficulty with SCF convergence, one should increase $n$ or try the matrix inversion solver. For well-behaved or very large systems, a smaller $n$ might be permissible.

**DComp**

Controls decomposition of matrices to reduce the matrix norm for the CG Solver.

INPUT SECTION: *$pcm*

TYPE:

INTEGER

DEFAULT:

1

OPTIONS:

| | |
|---|---|
| 0 | Turns off matrix decomposition |
| 1 | Turns on matrix decomposition |
| 3 | Option 1 plus only stores upper half of matrix and enhances gradient evaluation |

RECOMMENDATION:

None

**PreCond**

Controls the use of the pre-conditioner for the CG solver.

INPUT SECTION: *$pcm*

TYPE:

None

DEFAULT:

Off

OPTIONS:

No options. Specify the keyword to enable pre-conditioning.

RECOMMENDATION:

A Jacobi block-diagonal pre-conditioner is applied during the conjugate gradient algorithm to improve the rate of convergence. This reduces the number of CG iterations, at the expense of some overhead. Pre-conditioning is generally recommended for large systems.

**NoMatrix**

Specifies whether PCM matrices should be explicitly constructed and stored.

INPUT SECTION: *$pcm*

TYPE:

None

DEFAULT:

Off

OPTIONS:

No options. Specify the keyword to avoid explicit construction of PCM matrices.

RECOMMENDATION:

Storing the PCM matrices requires $\mathcal{O}(N_{\rm grid}^2)$ memory. If this is prohibitive, the **NoMatrix** option forgoes explicit construction of the PCM matrices, and instead constructs the matrix elements as needed, reducing the memory requirement to $\mathcal{O}(N_{\rm grid})$ at the expense of additional computation.

**UseMultipole**

Controls the use of the adaptive fast multipole method in the CG solver.

INPUT SECTION: *$pcm*

TYPE:

None

DEFAULT:

Off

OPTIONS:

No options. Specify the keyword in order to enable the fast multipole method.

RECOMMENDATION:

The fast multipole approach formally reduces the CPU time to $\mathcal{O}(N_{\rm grid})$, but is only beneficial for spatially extended systems with several thousand cavity grid points. Requires the use of **NoMatrix**.

**MultipoleOrder**

Specifies the highest multipole order to use in the FMM.

INPUT SECTION: *$pcm*

TYPE:

INTEGER

DEFAULT:

4

OPTIONS:

$n$ The highest order multipole in the multipole expansion.

RECOMMENDATION:

Increasing the multipole order improves accuracy but also adds more computational expense. The default yields satisfactory performance in common QM/MM/PCM applications.

**Theta**

The multipole acceptance criterion.

INPUT SECTION: *$pcm*

TYPE:

FLOAT

DEFAULT:

0.6

OPTIONS:

$n$ A number between zero and one.

RECOMMENDATION:

The default is recommended for general usage. This variable determines when the use of a multipole expansion is valid. For a given grid point and box center in the FMM, a multipole expansion is accepted when $r/d \leq$ **Theta**, where $d$ is the distance from the grid point to the box center and $r$ is the radius of the box. Setting **Theta** to one will accept all multipole expansions, whereas setting it to zero will accept none. If not accepted, the grid point's interaction with each point inside the box is computed explicitly. A low **Theta** is more accurate but also more expensive than a higher **Theta**.

**NBox**

The FMM boxing threshold.

INPUT SECTION: *$pcm*

TYPE:

INTEGER

DEFAULT:

100

OPTIONS:

$n$ The maximum number of grid points for a leaf box.

RECOMMENDATION:

The default is recommended. This option is for advanced users only. The adaptive FMM boxing algorithm divides space into smaller and smaller boxes until each box has less than or equal to **NBox** grid points. Modification of the threshold can lead to speedup or slowdown depending on the molecular system and other FMM variables.

A sample input file for the linear-scaling QM/MM/PCM methodology can be found in the *$QC/samples* directory, under the name `QMMMPCM_crambin.in`. This sample involves a QM/MM description of a protein (crambin) in which a single tyrosine side chain is taken to be the QM region. The entire protein is immersed in a dielectric using C-PCM with SWIG discretization.

## 11.2.5 Iso-Density Implementation of SS(V)PE

### 11.2.5.1 Basic Job Control

As discussed above, results obtained various types of PCMs are quite sensitive to the details of the cavity construction. Q-CHEM's implementation of PCMs, using Lebedev grids, simplifies this construction somewhat, but leaves the radii of the atomic spheres as empirical parameters (albeit ones for which widely-used default values are provided). An alternative implementation of the SS(V)PE solvation model is also available[25], which attempts to further eliminate empiricism associated with cavity construction by taking the cavity surface to be a specified iso-contour of the solute's electron density. (We call this the isodensity implementation of SS(V)PE in Table 11.2, and it is based on Chipman's "symmetrized" form of the $\mathbf{K}$ matrix[14,25].) In this case, the cavity surface is discretized by projecting a single-center Lebedev grid onto the iso-contour surface. Unlike the PCM implementation discussed in Section 11.2.2, for which point-group symmetry is disabled, this implementation of SS(V)PE supports full symmetry for all Abelian point groups. The larger and/or the less spherical the solute molecule is, the more points are needed to get satisfactory precision in the results. Further experience will be required to develop detailed recommendations for this parameter. Values as small as 110 points are usually sufficient for diatomic or triatomic molecules. The default value of 1202 points is adequate to converge the energy within 0.1 kcal/mol for solutes the size of mono-substituted benzenes.

Energy gradients are also not available for this implementation of SS(V)PE, although they are available for the implementation described in Section 11.2.2 in which the cavity is constructed from atom-centered spheres. As with the PCMs discussed in that section, the solute may be described using Hartree-Fock theory or DFT; post-Hartree–Fock correlated wave functions can also take advantage of molecular orbitals that are polarized using SS(V)PE. Researchers who use the iso-density SS(V)PE feature are asked to cite Ref. 8.

In related work, Pomogaeva and Chipman[27–30] recently introduced a "composite method for implicit representation of solvent" (CMIRS) that is based on SS(V)PE electrostatics but adds non-electrostatic terms.

This model is available in Q-CHEM[71] and is discussed in Section 11.2.6. In its current implementation, CMIRS requires an iso-density SS(V)PE calculation, However, the current implementation computes the non-electrostatic interactions using the cavity and the solute's charge density generated from the iso-density SS(V)PE. To use the CMIRS model, an iso-density SS(V)PE calculation must be requested (as described below), and the **IDEFESR** must be set to 1 in the *$svp* input section (see Section 11.2.5.2).

An iso-density SS(V)PE calculation is requested by setting SOLVENT_METHOD = ISOSVP in the *$rem* section, in addition to normal job control variables for a single-point energy calculation. Whereas the other solvation models described in this chapter use specialized input sections (*e.g.*, *$pcm*) in lieu of a slew of *$rem* variables, the iso-density SS(V)PE code is an interface between Q-CHEM and a code written by Chipman[25], so some *$rem* variables are used for job control of isodensity SS(V)PE calculations. These are listed below.

**SVP_MEMORY**

Specifies the amount of memory for use by the solvation module.

TYPE:

INTEGER

DEFAULT:

125

OPTIONS:

$n$ corresponds to the amount of memory in Mb.

RECOMMENDATION:

The default should be fine for medium size molecules with the default Lebedev grid, only increase if needed.

**SVP_PATH**

Specifies whether to run a gas phase computation prior to performing the solvation procedure.

TYPE:

INTEGER

DEFAULT:

0

OPTIONS:

0 runs a gas-phase calculation and after convergence runs the SS(V)PE computation.

1 does not run a gas-phase calculation.

RECOMMENDATION:

Running the gas-phase calculation provides a good guess to start the solvation stage and provides a more complete set of solvated properties.

**SVP_CHARGE_CONV**

Determines the convergence value for the charges on the cavity. When the change in charges fall below this value, if the electron density is converged, then the calculation is considered converged.

TYPE:

INTEGER

DEFAULT:

7

OPTIONS:

$n$ Convergence threshold set to $10^{-n}$.

RECOMMENDATION:

The default value unless convergence problems arise.

**SVP_CAVITY_CONV**

Determines the convergence value of the iterative iso-density cavity procedure.

TYPE:

INTEGER

DEFAULT:

10

OPTIONS:

$n$ Convergence threshold set to $10^{-n}$.

RECOMMENDATION:

The default value unless convergence problems arise.

**SVP_GUESS**

Specifies how and if the solvation module will use a given guess for the charges and cavity points.

TYPE:

INTEGER

DEFAULT:

0

OPTIONS:

0 No guessing.

1 Read a guess from a previous Q-CHEM solvation computation.

2 Use a guess specified by the *$svpirf* section from the input

RECOMMENDATION:

It is helpful to also set SCF_GUESS to READ when using a guess from a previous Q-CHEM run.

This last *$rem* variable requires specification of a *$svpirf* input section, the format for which is the following:

```
$svpirf
   <# point> <x point>  <y point>  <z point>  <charge> <grid weight>
   <# point> <x normal> <y normal> <z normal>
$end
```

#### 11.2.5.2 The *$svp* Input Section

More refined control over SS(V)PE jobs is obtained using a *$svp* input section. These are read directly by Chipman's SS(V)PE solvation module and therefore must be specified in the context of a FORTRAN namelist. The format is as follows:

```
$svp
   <KEYWORD>=<VALUE>, <KEYWORD>=<VALUE>,...
   <KEYWORD>=<VALUE>
$end
```

For example, the section may look like this:

```
$svp
   RHOISO=0.001, DIELST=78.39, NPTLEB=110
$end
```

The following keywords are supported in the *$svp* section:

**DIELST**
The static dielectric constant.
INPUT SECTION: *$svp*
TYPE:
FLOAT
DEFAULT:
78.39
OPTIONS:
real number specifying the constant.
RECOMMENDATION:
The default value 78.39 is appropriate for water solvent.

**IDEFESR**
Specifies whether to request a CMIRS calculation.
INPUT SECTION: *$svp*
TYPE:
INTEGER
DEFAULT:
0
OPTIONS:
0 do not invoke a CMIRS calculation.
1 do invoke a CMIRS calculation.
RECOMMENDATION:

**ISHAPE**

A flag to set the shape of the cavity surface.

INPUT SECTION: *$svp*

TYPE:

INTEGER

DEFAULT:

0

OPTIONS:

0 use the electronic iso-density surface.

1 use a spherical cavity surface.

RECOMMENDATION:

Use the default surface.

**RHOISO**

Value of the electronic iso-density contour used to specify the cavity surface. (Only relevant for **ISHAPE** = 0.)

INPUT SECTION: *$svp*

TYPE:

FLOAT

DEFAULT:

0.001

OPTIONS:

Real number specifying the density in electrons/bohr$^3$.

RECOMMENDATION:

The default value is optimal for most situations. Increasing the value produces a smaller cavity which ordinarily increases the magnitude of the solvation energy.

**RADSPH**

Sphere radius used to specify the cavity surface (Only relevant for ISHAPE=1.)

INPUT SECTION: *$svp*

TYPE:

FLOAT

DEFAULT:

Half the distance between the outermost atoms plus 1.4 Ångstroms.

OPTIONS:

Real number specifying the radius in bohr (if positive) or in Ångstroms (if negative).

RECOMMENDATION:

Make sure that the cavity radius is larger than the length of the molecule.

**INTCAV**

A flag to select the surface integration method.

INPUT SECTION: *$svp*

TYPE:

INTEGER

DEFAULT:

0

OPTIONS:

0 Single center Lebedev integration.

1 Single center spherical polar integration.

RECOMMENDATION:

The Lebedev integration is by far the more efficient.

**NPTLEB**

The number of points used in the Lebedev grid for the single-center surface integration. (Only relevant if **INTCAV** = 0.)

INPUT SECTION: *$svp*

TYPE:

INTEGER

DEFAULT:

1202

OPTIONS:

Valid choices are: 6, 18, 26, 38, 50, 86, 110, 146, 170, 194, 302, 350, 434, 590, 770, 974, 1202, 1454, 1730, 2030, 2354, 2702, 3074, 3470, 3890, 4334, 4802, or 5294.

RECOMMENDATION:

The default value has been found adequate to obtain the energy to within 0.1 kcal/mol for solutes the size of mono-substituted benzenes.

**NPTTHE, NPTPHI**

The number of $(\theta,\phi)$ points used for single-centered surface integration (relevant only if **INTCAV** = 1.)

INPUT SECTION: *$svp*

TYPE:

INTEGER

DEFAULT:

8,16

OPTIONS:

$\theta,\phi$ specifying the number of points.

RECOMMENDATION:

These should be multiples of 2 and 4 respectively, to provide symmetry sufficient for all Abelian point groups. Defaults are too small for all but the tiniest and simplest solutes.

**LINEQ**

Flag to select the method for solving the linear equations that determine the apparent point charges on the cavity surface.

INPUT SECTION: *$svp*

TYPE:

INTEGER

DEFAULT:

1

OPTIONS:

0 use LU decomposition in memory if space permits, else switch to **LINEQ** = 2

1 use conjugate gradient iterations in memory if space permits, else use **LINEQ** = 2

2 use conjugate gradient iterations with the system matrix stored externally on disk.

RECOMMENDATION:

The default should be sufficient in most cases.

**CVGLIN**

Convergence criterion for solving linear equations by the conjugate gradient iterative method (relevant if **LINEQ** = 1 or 2.)

INPUT SECTION: *$svp*

TYPE:

FLOAT

DEFAULT:

1.0E-7

OPTIONS:

Real number specifying the actual criterion.

RECOMMENDATION:

The default value should be used unless convergence problems arise.

Note that the single-center surface integration approach that is used to find the iso-density surface may fail for certain very non-spherical solute molecules. The program will automatically check for this, aborting with a warning message if necessary. The single-center approach succeeds only for what is called a "star surface", meaning that an observer sitting at the center has an unobstructed view of the entire surface. Said another way, for a star surface any ray emanating out from the center will pass through the surface only once. Some cases of failure may be fixed by simply moving to a new center with the **ITRNGR** parameter described below. But some surfaces are inherently non-star surfaces and cannot be treated with this program until more sophisticated surface integration approaches are developed and implemented.

**ITRNGR**

Translation of the cavity surface integration grid.

INPUT SECTION: *$svp*

TYPE:

INTEGER

DEFAULT:

2

OPTIONS:

0 No translation (*i.e.*, center of the cavity at the origin of the atomic coordinate system)

1 Translate to the center of nuclear mass.

2 Translate to the center of nuclear charge.

3 Translate to the midpoint of the outermost atoms.

4 Translate to midpoint of the outermost non-hydrogen atoms.

5 Translate to user-specified coordinates in Bohr.

6 Translate to user-specified coordinates in Ångstroms.

RECOMMENDATION:

The default value is recommended unless the single-center integrations procedure fails.

**TRANX, TRANY, TRANZ**

$x$, $y$, and $z$ value of user-specified translation (only relevant if **ITRNGR** is set to 5 or 6).

INPUT SECTION: *$svp*

TYPE:

FLOAT

DEFAULT:

0, 0, 0

OPTIONS:

$x$, $y$, and $z$ relative to the origin in the appropriate units.

RECOMMENDATION:

None.

**IROTGR**

Rotation of the cavity surface integration grid.

INPUT SECTION: *$svp*

TYPE:

INTEGER

DEFAULT:

2

OPTIONS:

0 No rotation.

1 Rotate initial $xyz$ axes of the integration grid to coincide with principal moments of nuclear inertia (relevant if **ITRNGR** = 1)

2 Rotate initial $xyz$ axes of integration grid to coincide with principal moments of nuclear charge (relevant if **ITRNGR** = 2)

3 Rotate initial $xyz$ axes of the integration grid through user-specified Euler angles as defined by Wilson, Decius, and Cross.

RECOMMENDATION:

The default is recommended unless the knowledgeable user has good reason otherwise.

**ROTTHE ROTPHI ROTCHI**
Euler angles ($\theta$, $\phi$, $\chi$) in degrees for user-specified rotation of the cavity surface (relevant if **IROTGR** = 3).
INPUT SECTION: *$svp*
TYPE:
FLOAT
DEFAULT:
0,0,0
OPTIONS:
$\theta$, $\phi$, $\chi$ in degrees
RECOMMENDATION:
None.

**IOPPRD**
Specifies the choice of system operator form.
INPUT SECTION: *$svp*
TYPE:
INTEGER
DEFAULT:
0
OPTIONS:
0 Symmetric form.
1 Non-symmetric form.
RECOMMENDATION:
The default uses more memory but is generally more efficient, we recommend its use unless there is shortage of memory available.

By default, Q-CHEM will check the validity of the single-center expansion by searching for the iso-density surface in two different ways: first, working inwards from a large distance, and next by working outwards from the origin. If the same result is obtained (within tolerances) using both procedures, then the cavity is accepted. If the two results do not agree, then the program exits with an error message indicating that the inner iso-density surface is found to be too far from the outer iso-density surface.

Some molecules, for example $C_{60}$, can have a hole in the middle. Such molecules have two different “legal” iso-density surfaces, a small inner one inside the “hole”, and a large outer one that is the desired surface for solvation. In such cases, the cavity check described in the preceding paragraph causes the program to exit. To avoid this, one can consider turning off the cavity check that works out from the origin, leaving only the outer cavity determined by working in from large distances.

**ICVICK**

Specifies whether to perform cavity check

INPUT SECTION: *$svp*

TYPE:

INTEGER

DEFAULT:

1

OPTIONS:

0 no cavity check, use only the outer cavity

1 cavity check, generating both the inner and outer cavities and compare.

RECOMMENDATION:

Consider turning off cavity check only if the molecule has a hole and if a star (outer) surface is expected.

### 11.2.6 Composite Method for Implicit Representation of Solvent (CMIRS)

Whereas PCMs, including sophisticated ones like SS(V)PE and IEF-PCM, account for long-range solute–solvent interactions, an accurate model for free energies of solvation must also include a treatment of short-range, non-electrostatic interactions. Various models decompose these interactions in different ways, but usually the non-electrostatic terms attempt to model all or most of the following: solute–solvent dispersion (van der Waals) interactions, Pauli (exchange) repulsion between solute and solvent, the work associated with forming the solute cavity within the dielectric medium (the so-called "cavitation energy"), hydrogen-bonding and other specific interactions due to the molecular structure of the solvent, and changes in the structure (and therefore the entropy) of the neat solvent upon introduction of the solute

Pomogaeva and Chipman[27–30] have introduced an implicit solvation model that attempts to model these non-electrostatic interactions alongside a PCM-style treatment of the bulk electrostatics. They call this approach the "composite method for implicit representation of solvent" (CMIRS), and it consists first of a self-consistent treatment of solute–continuum electrostatics using the SS(V)PE model (Section 11.2.5). To this electrostatics calculation, CMIRS adds a solute–solvent dispersion term that is modeled upon the non-local VV09 van der Waals dispersion density functional[72], a Pauli repulsion contribution that depends upon the tail of the solute's electron density that extends beyond the solute cavity, and a hydrogen-bonding correction based on the maximum and minimum values of the normal component of the electric field generated by the solute at the cavity surface. The Gibbs free energy of solvation is thus modeled as

$$\Delta G_{\text{CMIRS}}(\rho_s) = \Delta G_{\text{SS(V)PE}}(\rho_s) + \Delta G_{\text{DEFESR}}(\rho_s) \ , \tag{11.10}$$

where $\Delta G_{\text{SS(V)PE}}$ is the continuum electrostatics contribution from the SS(V)PE model, which is based on a solute cavity defined as an isocontour $\rho_s$ of the solute's charge density. The second term contains the short-range dispersion, exchange, and "field-extremum short-range" (DEFESR) interactions:

$$\Delta G_{\text{DEFESR}} = \Delta G_{\text{disp}} + \Delta G_{\text{exch}} + \Delta G_{\text{FESR}} \ . \tag{11.11}$$

These terms are evaluated only once, using a converged charge density for the solute from a SS(V)PE calculation.

The CMIRS approach was implemented in Q-CHEM by Z.-Q. You and J. M. Herbert[71]. In the course of this work, a serious error was discovered in the the original implementation of $\Delta G_{\text{disp}}$ by Pomogaeva and Chipman, in the GAMESS program. Although reparameterization of a corrected version of the model leads to only small changes in the overall error statistics across a large database of experimental free energies

| Solvent | SolvRho | A | B | C | D | Gamma |
|---|---|---|---|---|---|---|
| Benzene | 0.0421 | −0.00522 | 0.01294 | | | |
| Cyclohexane | 0.0396 | −0.00938 | 0.03184 | | | |
| DMSO | 0.05279 | −0.00951 | 0.044791 | | −162.07 | 4.1 |
| $CH_3CN$ | 0.03764 | −0.008178 | 0.045278 | | −0.33914 | 1.3 |
| Water | 0.05 | −0.006736 | 0.032698 | −1249.6 | −21.405 | 3.7 |

Table 11.3: Optimized CMIRS parameters (from Ref. 71) using **RHOISO** = 0.0010 a.u. and, for ions, the proton reference $\Delta G$ value from Ref. 73.

| Solvent | SolvRho | A | B | C | D | Gamma |
|---|---|---|---|---|---|---|
| Benzene | 0.0421 | −0.00572 | 0.01116 | | | |
| Cyclohexane | 0.0396 | −0.00721 | 0.05618 | | | |
| DMSO | 0.05279 | −0.002523 | 0.011757 | | −817.93 | 4.3 |
| $CH_3CN$ | 0.03764 | −0.003805 | 0.03223 | | −0.44492 | 1.2 |
| Water | 0.05 | −0.006496 | 0.050833 | −566.7 | −30.503 | 3.2 |

Table 11.4: Optimized CMIRS parameters (from Ref. 71) using **RHOISO** = 0.0005 a.u. and, for ions, the proton reference $\Delta G$ value from Ref. 73.

of solvation, the apportionment between energy components in Eq. (11.11) changes significantly[71]. By request of Dan Chipman, the Q-CHEM implementation is termed "CMIRS v. 1.1", reserving v. 1.0 for the original GAMESS implementation of Pomogaeva and Chipman.

The CMIRS model is independently parametrized for each solvent of interest, but uses no more than five empirical parameters per solvent. It is presently available in Q-CHEM for water, acetonitrile, dimethyl sulfoxide, benzene, and cyclohexane. Error statistics for $\Delta G$ compare very favorably to those of the SM$x$ models that are described in Section 11.2.8, *e.g.*, mean unsigned errors $< 0.7$ kcal/mol in benzene and cyclohexane and $< 1.5$ kcal/mol in water. The latter statistic includes challenging ionic solutes; errors for charge-neutral aqueous solutes are smaller still[71].

The current implementation of CMIRS in Q-CHEM computes the electrostatic energy using Chipman's iso-density SS(V)PE module. The resulting iso-density cavity and the solute charge density are then employed in the calculation of the DEFESR interactions. To request a CMIRS calculation, users must set IDEFESR = 1 in an iso-density SS(V)PE calculation (see Section 11.2.5.2). The solvent-dependent empirical parameters **A**, **B**, **C**, **D**, **Gamma** in the CMIRS model need to be specified in the *$pcm_nonels* section. Three additional parameters are also required. One is the damping parameter **Delta** in the dispersion equation. We recommend the parameter fixed at $\delta = 7$ a.u. (about 3.7 Å), an optimized value that only considers dispersion at intermolecular distances larger than van der Waals contact distance. The second is solvent's average electron density **SolvRho**. The last one is the number of Gauss–Laguerre points **GauLag_N** for the integration over the solvent region in the exchange equation. We recommend 40 grid points for efficient integration with accuracy. Optimized parameters for the supported solvents are listed in Tables 11.3 and 11.4 for two different values of $\rho_s$[71].

**Example 11.12** CMIRS calculation for methane in the water solvent.

```
$rem
   EXCHANGE         = b3lyp5
   BASIS           = 6-31+g*
   SCF_CONVERGENCE = 8
   MEM_TOTAL       = 4000
   MEM_STATIC      = 400
   SYM_IGNORE      = true
   XC_GRID         = 000096001202
$end

$molecule
   0  1
   C     0.000000     0.000005     0.000000
   H     0.748558     0.801458     0.000000
   H     0.506094    -0.972902     0.000000
   H    -0.627326     0.085706     0.895425
   H    -0.627326     0.085706    -0.895425
$end

@@@

$rem
   EXCHANGE        = b3lyp5
   BASIS           = 6-31+g*
   SCF_CONVERGENCE = 8
   MAX_SCF_CYCLES  = 100
   SOLVENT_METHOD  = isosvp
   SCF_GUESS       = read
   PCM_PRINT       = 1
   MEM_TOTAL       = 4000
   MEM_STATIC      = 400
   SVP_MEMORY      = 1000
   SYM_IGNORE      = true
   XC_GRID         = 000096001202
$end

$molecule
   read
$end

$svp
   RHOISO=0.001, DIELST=78.36, NPTLEB=1202,
   ITRNGR=2, IROTGR=2, IPNRF=1, IDEFESR=1
$end

$pcm_nonels
   A         -0.006736
   B          0.032698
   C      -1249.6
   D        -21.405
   Delta    7.0
   Gamma    3.7
   SolvRho  0.05
   GauLag_N 40
$end
```

### 11.2.7 COSMO

According to Table 11.2, COSMO and C-PCM appear to differ only in the dielectric screening factor, $f_\varepsilon$ in Eq. (11.3). Indeed, surface charges in either model are computed according to

$$\mathbf{q} = -f_\varepsilon \mathbf{S}^{-1}\mathbf{v} \ , \tag{11.12}$$

and as discussed in Section 11.2.3 the user has the option to choose either the original value suggested by Klamt[4,22], $f_\varepsilon = (\varepsilon - 1)/(\varepsilon + 1/2)$, or else $f_\varepsilon = (\varepsilon - 1)/\varepsilon$ as in, *e.g.*, Refs. 5,7,14. More importantly, however, COSMO differs from C-PCM in that the former includes a correction for outlying charge that goes beyond Eq. (11.12), whereas C-PCM consists of nothing more than induced surface charges computed (self-consistently) according to Eq. (11.12)

Upon solution of Eq. (11.12), the outlying charge correction in COSMO[22,23] is obtained by first defining a larger cavity that is likely to contain essentially all of the solute's electron density; in practice, this typically means using atomic radii of 1.95 $R$, where $R$ denotes the original atomic van der Waals radius that was used to compute $\mathbf{q}$. (Note that unlike the PCMs described in Sections 11.2.2 and 11.2.3, where the atomic radii have default values but a high degree of user-controllability is allowed, the COSMO atomic radii are parameterized for this model and are fixed.) A new set of charges, $\mathbf{q}' = -f_\varepsilon(\mathbf{S}')^{-1}\mathbf{v}'$, is then computed on this larger cavity surface, and the charges on the *original* cavity surface are adjusted to new values, $\mathbf{q}'' = \mathbf{q} + \mathbf{q}'$. Finally, a corrected electrostatic potential on the original surface is computed according to $\mathbf{v}'' = -f_\varepsilon \mathbf{S}\mathbf{q}''$. It is this potential that is used to compute the solute–continuum electrostatic interaction (polarization energy), $G_{\text{pol}} = \frac{1}{2}\sum_i q_i'' v_i''$. (For comparison, when the C-PCM approach described in Section 11.2.2 is used, the electrostatic polarization energy is $G_{\text{pol}} = \frac{1}{2}\sum_i q_i v_i$, computed using the original surface charges $\mathbf{q}$ and surface electrostatic potential $\mathbf{v}$.) With this outlying charge correction, Q-CHEM's implementation of COSMO resembles the one in TURBOMOLE[74].

A COSMO calculation is requested by setting SOLVENT_METHOD = COSMO in the *$rem* section, in addition to normal job control variables. The keyword **Dielectric** in the *$solvent* section is used to set the solvent's static dielectric constant, as described above for other solvation models. COSMO calculations can also be used as a starting point for "COSMO-RS" calculations[34,75], where RS stands for "real solvent". The COSMO-RS approach is *not* included in Q-CHEM and requires the COSMOtherm program, which is licensed separately through COSMOlogic[35]. Q-CHEM users who are interested in COSMOtherm can request special versions of Q-CHEM for the generation of $\sigma$-surface files that are needed by COSMOtherm.

### 11.2.8 SM8, SM12, and SMD Models

The SM$x$ models developed by Cramer, Truhlar, and co-workers at the University of Minnesota are a class of implicit solvation models that are designed to be "universal" in the sense that they can be applied to any solvent for which a small of descriptors is known[31]. (Note that the $x$ in SM$x$ is simply a version number; SM8, SM12, and SMD are available in Q-CHEM.) In particular, the solvent descriptors are:

- dielectric constant
- refractive index
- bulk surface tension
- acidity on the Abraham scale
- basicity on the Abraham scale

- carbon aromaticity, which equals the fraction of non-hydrogenic solvent atoms that are aromatic carbon atoms
- electronegative halogenicity, which equals the fraction of non-hydrogenic solvent atoms that are F, Cl, or Br).

These models consist of a generalized Born treatment of continuum electrostatic interactions, along with non-electrostatic interactions that are parameterized in terms of atomic surface tensions. The non-electrostatic interactions include cavitation, dispersion, and changes in solvent structure, and the treatment of these non-electrostatic effects is crucial to obtaining accurate (free) energies of solvation.

#### 11.2.8.1 The SM8 Model

The SM8 model is described in detail in Ref. 19. It may be employed in conjunction with density functional theory (with any density functional available in Q-CHEM) or with Hartree-Fock theory, but is intended for use only with the 6-31G*, 6-31+G*, and 6-31+G** basis sets, for reasons discussed below.

Bulk (continuum) electrostatic interactions in SM8 are described in terms of a generalized Born (GB) SCRF, using a solute cavity constructed from atom-centered spheres. For the atoms H, C, N, O, F, Si, P, S, Cl, and Br, atomic radii have been specifically optimized for use with SM8, whereas for other atoms the Bondi radius is used[44], or else a value of 2.0 Å for atoms not included in Bondi's paper. Geometry-dependent radii are computed from these "intrinsic" Coulomb radii via a de-screening approximation[19].

In addition to GB electrostatics, there are several other contributions to the SM8 standard-state free energy of solvation. The first of these is called the electronic-nuclear-polarization (ENP) energy, or simply the electronic polarization (EP) energy if the solute geometry is assumed to be identical in the gas and solution phases. Another contribution to the free energy of solvation comes from short-range interactions with solvent molecules in the first solvation shell, and is sometimes called the cavitation/dispersion/solvent-structure (CDS) term. The CDS contribution to the solvation energy is a sum of terms that are each proportional (with geometry-dependent proportionality constants called atomic surface tensions) to the solvent-accessible surface areas (SASAs) of the individual solute atoms. The SASA of the solute molecule is the area of a surface generated by the center of a spherical effective solvent molecule rolling on the van der Waals surface of the solute molecule, as in the solvent-accessible surface that was mentioned in Section 11.2.2. The SASA is computed using the Analytic Surface Area (ASA) algorithm of Ref. 76 and Bondi's values for the van der Waals radii[44], or else a value of 2.0 Å if no Bondi radius is available. (Note that, as in the case of non-electrostatic interactions in PCMs, this means that a different molecular surface is used for the bulk electrostatics as compared to the non-electrostatic interactions.) The solvent probe radius used to generate the SASAs is set to 0.40 Å for all solvents. Note that the solvent-structure part of the CDS term includes many aspects of solvent structure that are not described by bulk electrostatics, for example, hydrogen bonding, exchange repulsion, and the variation of the effective dielectric constant in the first solvation shell, relative to its bulk value. The semi-empirical nature of the CDS term also makes up for errors due to $(i)$ assuming fixed and model-dependent values of the intrinsic Coulomb radii, and $(ii)$ any systematic errors in the description of the solute–solvent electrostatic interactions using the GB approximation.

The final component of the SM8 solvation free energy is the concentration component. This is zero if the standard-state concentration of the solute is the same in the gas and solution phases (*e.g.*, if it is 1 mole/liter in the gas phase as well as in the solution). Otherwise, this correction can be computed using ideal gas formulas, as discussed below.

SM8 does not require the user to assign molecular mechanics atom types to atoms or groups; all atomic surface tensions in the theory are unique and continuous functions of the solute geometry, defined by the model and calculated internally within Q-CHEM. In principle, SM8 can be used with any level of electronic structure theory so long as accurate partial charges can be computed, but Q-CHEM's implementation of SM8 specifically uses self-consistently polarized Charge Model 4 (CM4) class IV charges[77] CM4 charges are obtained from Löwdin population analysis charges, via a mapping whose parameters depend on the basis set (and only on the basis set, not on the density functional or anything else). Basis sets supported for SM8 calculations in Q-CHEM are:

- 6-31G*
- 6-31+G*
- 6-31+G**

The charge mapping parameters are given in Ref. 77. Other basis sets should not be used in SM8 calculations.

The SM8 solvation free energy is output at $T = 298$ K for a standard-state concentration of 1 M in both the gas and solution phase. However, solvation free energies in the literature are often tabulated using a standard state of $P = 1$ atm for the gase. To convert 1 M-to1 M solvation free energies at 298 K to a standard state consisting of $P = 1$ atm for the gas and a 1 M concentration in solution, add $+1.89$ kcal/mol to the computed solvation free energy.

Solution-phase geometry optimizations can be carried out, but basis sets that use spherical harmonic $d$ functions, or angular momentum higher than $d$ ($f$, $g$, *etc.*) are not supported. Since, by definition, the 6-31G*, 6-31+G*, and 6-31+G** basis sets have Cartesian $d$ shells, they are examples of basis sets that may be used for geometry optimization with SM8. Solution-phase Hessian calculations can be carried out by numerical differentiation of analytical energy gradients or by double differentiation of energies, although the former procedure is both more stable and more economical. The analytic gradients of SM8 are based on the analytical derivatives of the polarization free energy and the analytical derivatives of the CDS terms derived in Ref. 78.

An SM8 calculation is requested by setting SOLVENT_METHOD = SM8 in the *$rem* section, along with other job-control variables appropriate for a Hartree-Fock or DFT calculation. Additional variables for SM$x$ calculations should be listed in a *$smx* input section; for SM8, the only additional variable that is required is the name of the solvent:

**Solvent**
Sets the SM$x$ solvent
INPUT SECTION: *$smx*
TYPE:
STRING
DEFAULT:
water
OPTIONS:
Any name from the list of solvents given below.
RECOMMENDATION:
NONE

1,1,1-trichloroethane
1,1,2-trichloroethane
1,1-dichloroethane
1,2,4-trimethylbenzene
1,4-dioxane
1-bromo-2-methylpropane
1-bromopentane
1-bromopropane
1-butanol
1-chloropentane
1-chloropropane
1-decanol
1-fluorooctane
1-heptanol
1-hexanol
1-hexene
1-hexyne
1-iodobutane
1-iodopentene
1-iodopropane
1-nitropropane
1-nonanol
1-octanol
1-pentanol
1-pentene
1-pentyne
1-propanol
2,2,20trifluoroethanol
2,2,4-trimethylpentane
2,4-dimethylpentane
2,4-dimethylpyridine
2,6-dimethylpyridine
2-bromopropane
2-chlorobutane
2-heptanone
2-hexanone
2-methylpentane
2-methylpyridine
2-nitropropane
2-octanone
2-pentanone
2-propanol
2-propen-1-ol
3-methylpyridine
3-pentanone
4-heptanone
4-methyl-2-pentanone
4-methylpyridine
bromoethane
bromooctane
butanal
butanoicacid
butanone
butanonitrile
butylethanoate
butylamine
butylbenzene
carbon disulfide
carbon tetrachloride
chlorobenzene
chlorotoluene
*cis*-1,2-dimethylcyclohexane
decalin
cyclohexane
cyclohexanone
cyclopentane
cyclopentanol
cyclopentanone
decane
dibromomethane
dibutyl ether
dichloromethane
diethyl ether
diethylsulfide
diethylamine
diiodomethane
dimethyldisulfide
dimethylacetamide
dimethylformamide
dimethylpyridine
dimethyl sulfoxide
dipropylamine
dodecane
*E*-1,2-dichloroethene
*E*-2-pentene
ethanethiol
ethanol
ethylethanoate
ethylmethanoate
ethylphenyl ether
ethylbenzene
ethylene glycol
fluorobenzene
formamide
formic acid
hexadecyliodide
*m*-ethylbenzoate
*m*-ethylethanoate
*m*-ethylmethanoate
*m*-ethylphenylketone
*m*-ethylpropanoate
*m*-ethylbutanoate
*m*-ethylcyclohexane
*m*-ethylformamide
*m*-xylene
heptane
hexadecane
hexane
nitrobenzene
nitroethane
nitromethane
methylaniline
nonane
octane
pentane
*o*-chlorotoluene
*o*-cresol
*o*-dichlorobenzene
*o*-nitrotoluene
*o*-xylene
pentadecane
pentanal
pentanoic acid
pentylethanoate
pentylamine
perfluorobenzene
phenyl ether
propanal
propanoic acid
propanonitrile
propylethanoate
propylamine
*p*-xylene
pyridine
pyrrolidine
*sec*-butanol
*t*-butanol
*t*-butylbenzene
tetrachloroethene
tetrahydrofuran
tetrahyrothiophenedioxide
tetralin
thiophene
thiophenol

5-nonanone
acetic acid
acetone
acetonitrile
aniline
anisole
benzaldehyde
benzene
benzonitrile
benzyl alcohol
bromobenzene
hexanoic acid
iodobenzene
iodoethane
iodomethane
isobutanol
isopropyl ether
isopropylbenzene
isopropyltoluene
$m$-cresol
mesitylene
methanol
toluene
$trans$-decalin
tribromomethane
tributylphosphate
trichloroethene
trichloromethane
triethylamine
undecane
water
$Z$-1,2-dichloroethene
other

The final choice, **Solvent** = "other", requires an additional free-format file called "solvent_data" that should contain the float-point values of the following solvent descriptors:

| | |
|---|---|
| Dielec | dielectric constant, $\epsilon$, of the solvent |
| SolN | index of refraction at optical frequencies at 293 K, $n_{20}^{D}$ |
| SolA | Abraham's hydrogen bond acidity, $\sum \alpha_2^H$ |
| SolB | Abraham's hydrogen bond basicity, $\sum \beta_2^H$ |
| SolG | $\gamma = \gamma_m/\gamma^0$ (default is 0.0), where $\gamma_m$ is the macroscopic surface tension at air/solvent interface at 298 K, and $\gamma^0$ is 1 cal mol$^{-1}$ Å$^{-2}$ (1 dyne/cm = 1.43932 cal mol$^{-1}$ Å$^{-2}$) |
| SolC | aromaticity, $\phi$ : the fraction of non-hydrogenic solvent atoms that are aromatic carbon atoms |
| SolH | electronegative "halogenicity", $\psi$ : the fraction of non-hydrogenic solvent atoms that are F, Cl or Br |

For a desired solvent, these values can be derived from experiment or from interpolation or extrapolation of data available for other solvents. Solvent parameters for common organic solvents are tabulated in the Minnesota Solvent Descriptor Database. The latest version of this database is available at:

`http://comp.chem.umn.edu/solvation/mnsddb.pdf`

The SM8 test suite contains the following representative examples:

- single-point solvation energy and analytical gradient calculation for 2,2-dichloroethenyl dimethyl phosphate in water at the M06-2X/6-31G* level;
- single-point solvation energy calculation for 2,2-dichloroethenyl dimethyl phosphate in benzene at the M06-2X/6-31G* level;
- single-point solvation energy calculation for 2,2-dichloroethenyl dimethyl phosphate in ethanol at the M06-2X/6-31G* level;
- single-point solvation energy calculation for 5-fluorouracil in water at the M06/6-31+G* level;
- single-point solvation energy calculation for 5-fluorouracil in octanol at the M06-L/6-31+G* level;
- single-point solvation energy and analytical gradient calculation for 5-fluorouracil in fluorobenzene at the M06-HF/6-31+G** level;
- geometry optimization for protonated methanol $\mathrm{CH_3OH_2^+}$ in water at the B3LYP/6-31G* level;

- finite-difference frequency (with analytical gradient) calculation for protonated methanol $CH_3OH_2^+$ in water at the B3LYP/6-31G* level.

Users who wish to calculate solubilities can calculate them from the free energies of solvation by the method described in Ref. 79. The present model can also be used with confidence to calculate partition coefficients (*e.g.*, Henry's Law constants, octanol/water partition coefficients, *etc.*) by the method described in Ref. 80.

The user should note that the free energies of solvation calculated by the SM8 model in the current version of Q-CHEM are all what may be called equilibrium free energies of solvation. The non-equilibrium algorithm required for vertical excitation energies[81] is not yet available in Q-CHEM.

#### 11.2.8.2 The SM12 Model

The SM12 model[20] is also available in Q-CHEM. Similar to SM8, it employs (a) the generalized Born approximation for the bulk electrostatic contribution to the free energy of solvation, and (b) the same formulas (with re-optimized parameters) for CDS contributions. SM12 holds several advantages over SM8, and perhaps foremost among these is that it uses CM5 charges[82], which are based on Hirshfeld population analysis, or else charges derived from the electrostatic potential[83,84], for the bulk electrostatics term. These charges are stable with respect to extension of the basis set, and thus SM12 can be used with larger basis sets whereas SM8 is limited to 6-31G*, 6-31+G*, and 6-31+G**, due to instabilities in the Löwdin charges in larger basis sets. In addition, SM12 is parameterized using a more diverse training set as compared to SM8, and is defined for the entire periodic table. However, the SM12 analytic gradient is not available in Q-CHEM at present.

An SM12 calculation is requested by setting SOLVENT_METHOD = SM12 in the *$rem* section. The manner in which the electrostatic term is computed is controlled by the **Charges** keyword in the *$smx* input section.

**Charges**
Sets the type of atomic charges for the SM12 electrostatic term.
INPUT SECTION: *$smx*
TYPE:
STRING
DEFAULT:
CM5
OPTIONS:

| | |
|---|---|
| CM5 | Charge Model 5 charges[82] |
| MK | Merz-Singh-Kollman charges[83] |
| CHELPG | ChElPG charges[84] |

RECOMMENDATION:
None. Merz-Singh-Kollman and ChElPG charges are fit to reproduce the molecular electrostatic potential on the van der Waals surface or on a cubic grid, respectively, whereas CM5 is an empirical model based on Hirshfeld population analysis.

**Example 11.13** SM12CM5 calculation of the solvation free energy of water in the 1-octanol solvent.

```
$molecule
   0 1
   O   0.000000  0.125787   0.000000
   H   0.758502  -0.503148  0.000000
   H  -0.758502  -0.503148  0.000000
$end

$rem
   SCF_GUESS         core
   METHOD            b3lyp
   BASIS             6-31G*
   SYM_IGNORE        true
   SOLVENT_METHOD    sm12
$end

$smx
   solvent 1octanol
   charges chelpg
$end
```

#### 11.2.8.3 The SMD Model

The SMD model[21] is also available in Q-CHEM. Within this model, the electrostatic contribution to the free energy solvation is described via the IEF-PCM model, where the CDS contributions follow the formulas as SM8 and SM12 with the parameters re-optimized to be compatible with the IEF-PCM electrostatics. Relative to SM8 or SM12, where the electrostatic interactions are defined in terms of atomic point charges that are sensitive to the choice of basis set (and therefore only certain basis sets are supported for use with these models), SMD can be used with any basis set.

An SMD energy or gradient calculation is requested by setting SOLVENT_METHOD = SMD in the *$rem* section. While Q-CHEM users can vary the parameters for the IEF-PCM part of the SMD calculation, this should be done with caution because a modified IEF-PCM electrostatics might be less compatible with CDS parameters and thus lead to less accurate results.

**Example 11.14** SMD force calculation for tetrahydrofuran (THF) in the pentane solvent.

```
$molecule
   0 1
   C    -0.361658    -0.986967     0.222366
   C    -1.331098     0.144597    -0.108363
   O    -0.592574     1.354183     0.036738
   C     0.798089     1.070899     0.136509
   C     0.964682    -0.396154    -0.256319
   H    -0.625676    -1.925862    -0.267011
   H    -0.333229    -1.158101     1.302753
   H    -1.697529     0.068518    -1.140448
   H    -2.193412     0.181620     0.562129
   H     1.130199     1.238399     1.169839
   H     1.348524     1.754318    -0.514697
   H     1.050613    -0.489646    -1.343151
   H     1.843065    -0.855802     0.199659
$end

$rem
   JOBTYPE           force
   METHOD            b3lyp
   BASIS             6-31G*
   SOLVENT_METHOD    smd
$end
```

```
$smx
   solvent pentane
$end
```

### 11.2.9 Langevin Dipoles Model

Q-CHEM provides the option to calculate molecular properties in aqueous solution and the magnitudes of the hydration free energies by the Langevin dipoles (LD) solvation model developed by Jan Florián and Arieh Warshel [17,18] at the University of Southern California. In this model, a solute molecule is surrounded by a sphere of point dipoles, with centers on a cubic lattice. Each of these "Langevin" dipoles changes its size and orientation in the electrostatic field of the solute and the other Langevin dipoles. The electrostatic field from the solute is determined rigorously by the integration of its charge density, whereas for dipole–dipole interactions, a 12 Å cutoff is used. The Q-CHEM/CHEMSOL 1.0 implementation of the LD model is fully self-consistent in that the molecular quantum mechanical calculation takes into account solute–solvent interactions. Further details on the implementation and parameterization of this model can be found in the original literature [17,18].

The results of CHEMSOL calculations are printed in the standard output file. Below is a part of the output for a calculation on the methoxide anion (corresponding to the sample input given later on, and the sample file in the *$QC/samples* directory).

| Energy Component | Value / kcal mol$^{-1}$ |
|---|---:|
| LD Electrostatic energy | $-86.14$ |
| Hydrophobic energy | $0.28$ |
| van der Waals energy | $-1.95$ |
| Bulk correction | $-10.07$ |
| Solvation free energy, $\Delta G$(ILD) | $-97.87$ |

Table 11.6: Results of the iterative Langevin Dipoles (ILD) solvation model, for aqueous methoxide.

The total hydration free energy, $\Delta G$(ILD) is calculated as a sum of several contributions. Note that the electrostatic part of $\Delta G$ is calculated by using the linear-response approximation [17] and contains contributions from the *polarization* of the solute charge distribution due to its interaction with the solvent. This results from the self-consistent implementation of the Langevin dipoles model within Q-CHEM.

To perform an LD calculation in Q-CHEM, specify normal job-control variables for a Hartree-Fock or DFT calculation, and set SOLVENT_METHOD = CHEM_SOL in the *$rem* section. Additional fine-tuning is accomplished using a set of keywords in a *$chem_sol* input section. The remainder of this section summarizes these keywords.

**EField**

Determines how the solute charge distribution is approximated in evaluating the electrostatic field of the solute.

INPUT SECTION: *$chemsol*

TYPE:

INTEGER

DEFAULT:

1

OPTIONS:

1 Exact solute charge distribution is used.

0 Solute charge distribution is approximated by Mulliken atomic charges.

RECOMMENDATION:

None. The Mulliken-based procedure is faster but less rigorous.

**NGrids**

Sets the number of grids used to calculate the average hydration free energy.

INPUT SECTION: *$chemsol*

TYPE:

INTEGER

DEFAULT:

5 $\Delta G_{\mathrm{hydr}}$ will be averaged over 5 different grids.

OPTIONS:

$n$ Use $n$ different grids.

RECOMMENDATION:

None. The maximum allowed value of $n$ is 20.

**Print**

Controls printing in the CHEMSOL part of the Q-CHEM output file.

INPUT SECTION: *$chemsol*

TYPE:

INTEGER

DEFAULT:

0

OPTIONS:

0 Limited printout

1 Full printout

RECOMMENDATION:

None.

Accurate calculations of hydration free energies require a judicious choice of the solute–solvent boundary in terms of atom-type dependent parameters. The default atomic van der Waals radii available in Q-CHEM were chosen to provide reasonable hydration free energies for most solutes and basis sets. These parameters basically coincide with the CHEMSOL 2.0 radii given in Ref. 18. The only difference between the Q-CHEM and CHEMSOL 2.0 atomic radii stems from the fact that Q-CHEM parameter set uses radii for carbon and oxygen that are independent of the atom's hybridization state. User-defined atomic radii can be specified by declaring the option **ReadRadii** in the *$chem_sol* input section, and then placing the radii in the *$van_der_waals* section. Two different (and mutually exclusive) formats can be used, as shown below.

```
$van_der_waals
1
atomic_number   vdW_radius
...
$end

$van_der_waals
2
sequential_atom_number   vdW_radius
...
$end
```

The purpose of the second format is to permit the user to customize the radius of specific atoms, in the order that they appear in the *$molecule* section, rather than simply by atomic numbers as in format 1. The radii of atoms that are not listed in the *$van_der_waals* input will be assigned default values. The atomic radii that were used in the calculation are printed in the CHEMSOL part of the output file in the column denoted *rp*. All radii should be given in Ångstroms.

**Example 11.15** A Langevin dipoles calculation on the methoxide anion. A customized value is specified for the radius of the C atom.

```
$molecule
  -1  1
   C   0.0000   0.0000  -0.5274
   O   0.0000   0.0000   0.7831
   H   0.0000   1.0140  -1.0335
   H   0.8782  -0.5070  -1.0335
   H  -0.8782  -0.5070  -1.0335
$end

$rem
   METHOD            hf
   BASIS             6-31G
   SCF_CONVERGENCE   6
   SOLVENT_METHOD    Chem_Sol
$end

$chemsol
ReadRadii
$end

$van_der_waals
2
1 2.5
$end
```

## 11.2.10 Poisson Equation Boundary Conditions

### 11.2.10.1 Theory

Each of the implicit solvation model described above is designed for isotropic, bulk solvation, which can be qualitatively described by a scalar dielectric constant, $\epsilon$. For an *anisotropic* environment, such as a liquid/vapor interface, a more general approach is to employ a spatially-varying dielectric function $\epsilon(\mathbf{r})$, and to then solve Poisson's equation for the total electrostatic potential, $\varphi_{\text{tot}}(\mathbf{r})$ in three-dimensional space:

$$\hat{\boldsymbol{\nabla}} \cdot \left[\epsilon(\mathbf{r}) \hat{\boldsymbol{\nabla}} \varphi_{\text{tot}}(\mathbf{r})\right] = -4\pi \rho_{\text{sol}}(\mathbf{r}) \ . \tag{11.13}$$

The quantity $\rho_{\text{sol}}(\mathbf{r})$ on the right is the solute's charge density arising from its electronic and nuclear components,

$$\rho_{\text{sol}}(\mathbf{r}) = \rho_{\text{elec}}(\mathbf{r}) + \rho_{\text{nuc}}(\mathbf{r}) \ . \tag{11.14}$$

The total electrostatic potential on the left side of Eq. (11.13) is comprised of the solute potential as well as the induced polarization potential:

$$\varphi_{\text{tot}}(\mathbf{r}) = \varphi_{\text{elec}}(\mathbf{r}) + \varphi_{\text{nuc}}(\mathbf{r}) + \varphi_{\text{pol}}(\mathbf{r}) \ . \tag{11.15}$$

To compute $\rho_{\text{elec}}(\mathbf{r})$, the electronic electrostatic potential in vacuum is first evaluated on a Cartesian grid via

$$\varphi_{\text{elec}}(\mathbf{r}) = \sum_{\mu\nu}^{N_{\text{basis}}} P_{\mu\nu} \left\langle g_\mu(\mathbf{r}_{\text{grid}}) \middle| \frac{1}{|\mathbf{r} - \mathbf{r}_{\text{grid}}|} \middle| g_\nu(\mathbf{r}_{\text{grid}}) \right\rangle_{\mathbf{r}_{\text{grid}}} \ , \tag{11.16}$$

where $\mathbf{P}$ is the one-electron density matrix, $g_\mu$ is an atom-centered Gaussian basis function, and the subscript $\mathbf{r}_{\text{grid}}$ signifies that the integral is performed over the Cartesian grid coordinates. $\rho_{\text{elec}}(\mathbf{r})$ is then computed as

$$\rho_{\text{elec}}(\mathbf{r}) = -\frac{1}{4\pi} \nabla^2 \varphi_{\text{elec}}(\mathbf{r}) \ , \tag{11.17}$$

where the Laplacian operator is discretized using an order eight finite difference scheme. $\rho_{\text{nuc}}(\mathbf{r})$ is constructed classically: for nucleus $A$, $Z_A/dV$ is added to the nearest Cartesian grid point, where $Z_A$ is the nuclear charge of $A$ and $dV$ is the volume element of the Cartesian grid. This is equivalent to smearing the nuclear charge over one voxel of the Cartesian grid. Formally,

$$\rho_{\text{nuc}}(\mathbf{r}) = -\sum_{A}^{N_{\text{atoms}}} Z_A \, \delta\left(\mathbf{r} - \mathbf{R}_A\right) \ , \tag{11.18}$$

where $\mathbf{R}_A$ is the position vector of the Cartesian grid point nearest nucleus $A$. The exact nuclear electrostatic potential in vacuum is computed as

$$\varphi_{\text{nuc}}(\mathbf{r}) = -\frac{1}{4\pi} \sum_{A}^{N_{\text{atoms}}} \frac{Z_A}{|\mathbf{r} - \mathbf{R}_A|} \ . \tag{11.19}$$

The Dirac delta function in Eq. (11.18) has dimensions of volume$^{-1}$ and incorporates the factor of $dV^{-1}$.

Having computed the electronic and nuclear charge densities and electrostatic potentials in vacuum, which exactly solves Eq. (11.13) for $\epsilon(\mathbf{r}) = 1$, the induced polarization charge density and potential are iteratively solved following closely the procedure outlined in Refs. 85 and 86 . Eq. (11.13) is rewritten to appear as Poisson's equation in vacuum with an additional source charge density:

$$\begin{aligned} \hat{\nabla}^2 \varphi_{\text{tot}}(\mathbf{r}) &= -4\pi \left[\frac{\rho_{\text{sol}}(\mathbf{r})}{\epsilon(\mathbf{r})} + \frac{\hat{\boldsymbol{\nabla}} \ln \epsilon(\mathbf{r}) \cdot \hat{\boldsymbol{\nabla}} \varphi_{\text{tot}}(\mathbf{r})}{4\pi}\right] \\ &= -4\pi \left[\rho_{\text{sol}}(\mathbf{r}) + \rho_{\text{pol}}(\mathbf{r})\right] \ , \end{aligned} \tag{11.20}$$

where the polarization charge density is

$$\rho_{\mathrm{pol}}(\mathbf{r}) = \rho_{\mathrm{iter}}(\mathbf{r}) + \left(\frac{1-\epsilon(\mathbf{r})}{\epsilon(\mathbf{r})}\right)\rho_{\mathrm{sol}}(\mathbf{r}) \ . \tag{11.21}$$

The iterative charge density $\rho_{\mathrm{iter}}(\mathbf{r})$ takes the form

$$\rho_{\mathrm{iter}}^{(k+1)}(\mathbf{r}) = \frac{\hat{\boldsymbol{\nabla}}\ln\epsilon(\mathbf{r})\cdot\hat{\boldsymbol{\nabla}}\varphi_{\mathrm{tot}}^{(k)}(\mathbf{r})}{4\pi} \ , \tag{11.22}$$

and is nonzero only in regions where the dielectric function is inhomogenous. The second term on the right side of Eq. (11.21) is a scaled solute charge density that is exactly zero in regions of vacuum. $\rho_{\mathrm{iter}}(\mathbf{r})$ is iterated to convergence by performing updates $\rho_{\mathrm{iter}}^{(k)}(\mathbf{r}) \to \rho_{\mathrm{iter}}^{(k+1)}(\mathbf{r})$ using Eq. (11.22). Note that for iteration $k = 0$, $\varphi_{\mathrm{tot}}^{(0)}(\mathbf{r})$ in Eq. (11.22) is the solute electrostatic potential. Each time $\rho_{\mathrm{iter}}(\mathbf{r})$ is updated, a new polarization charge density is generated and Eq. (11.20) is solved to obtain a new total electrostatic potential. The updates are continued until the Euclidean norm of the residual vector falls below a threshold, taken to be $10^{-5}$ a.u. by default. To stabilize the updates of $\rho_{\mathrm{iter}}(\mathbf{r})$, a damping procedure is performed as follows:

$$\begin{aligned}\rho_{\mathrm{iter}}^{(k+1)}(\mathbf{r}) &= \frac{\eta}{4\pi}\left[\hat{\boldsymbol{\nabla}}\ln\epsilon(\mathbf{r})\cdot\hat{\boldsymbol{\nabla}}\varphi_{\mathrm{tot}}^{(k)}(\mathbf{r})\right] + (1-\eta)\,\rho_{\mathrm{iter}}^{(k)}(\mathbf{r}) \\ &= \eta\rho_{\mathrm{iter}}^{(k+1)} + (1-\eta)\,\rho_{\mathrm{iter}}^{(k)}(\mathbf{r}) \ ,\end{aligned} \tag{11.23}$$

where $\eta = 0.6$ as in Refs. 85 and 86 .

Once the total charge density and electrostatic potential are iterated to self-consistently, the free energy of solvation is computed as

$$G_{\mathrm{pol}} = \frac{1}{2}\int d\mathbf{r}\ \varphi_{\mathrm{pol}}(\mathbf{r})\ \rho_{\mathrm{sol}}(\mathbf{r}) \ , \tag{11.24}$$

where

$$\varphi_{\mathrm{pol}}(\mathbf{r}) = \varphi_{\mathrm{tot}}(\mathbf{r}) - \varphi_{\mathrm{sol}}(\mathbf{r}) \ . \tag{11.25}$$

Since $\varphi_{\mathrm{tot}}(\mathbf{r})$ and $\rho_{\mathrm{tot}}(\mathbf{r})$ are computed self-consistently at each SCF iteration, the polarization effects must be incorporated into the Kohn-Sham Hamiltonian. This is accomplished by adding the correction term $\delta G_{\mathrm{pol}}/\delta\rho_{\mathrm{elec}}$ to the Fock matrix, equivalent to

$$\Delta F_{\mu\nu} = \int d\mathbf{r}\ \varphi_{\mathrm{pol}}(\mathbf{r})\ g_{\mu}(\mathbf{r})\ g_{\nu}(\mathbf{r}) \ . \tag{11.26}$$

in matrix form. For additional details and a full description of the algorithm, consult Ref. 87 or the Supporting Information of Ref. 88.

### 11.2.10.2 Non-Equilibrium Solvation for Vertical Ionization

Non-equilibrium solvation within the framework of PCMs is discussed in Section 11.2.2.3 and references therein, and that methodology has been adapted for vertical ionization processes in conjunction with Poisson equation boundary conditions. A state-specific approach has been implemented, which requires the solution of a nonlinear Schrödinger equation given by Eq. (11.6). For the reference state, corresponding to $i = 0$ in Eq. (11.6), this is equivalent to solving Eq. (11.13) for the induced polarization potential and computing the solvation free energy and Fock matrix correction according to Eqs. (11.24) and (11.26), respectively. For the ionized state, $i$, the solvent polarization must be partitioned into fast and slow components. Within the Marcus partitioning scheme, Eq. (11.20) becomes[87]:

$$\hat{\nabla}^2\varphi_{\mathrm{tot},i}(\mathbf{r}) = -4\pi\left[\rho_{\mathrm{sol},i}(\mathbf{r}) + \rho_{\mathrm{pol},0}^{\mathrm{slow}}(\mathbf{r}) + \rho_{\mathrm{pol},i}^{\mathrm{fast}}(\mathbf{r})\right] \ , \tag{11.27}$$

where the fast polarization charge density, $\rho^{\text{fast}}_{\text{pol},i}(\mathbf{r})$, of the ionized state is given by

$$\rho^{\text{fast}}_{\text{pol},i}(\mathbf{r}) = \rho_{\text{iter},i}(\mathbf{r}) + \left(\frac{1-\epsilon_{\text{opt}}(\mathbf{r})}{\epsilon_{\text{opt}}(\mathbf{r})}\right)\left(\rho_{\text{sol},i}(\mathbf{r}) + \rho^{\text{slow}}_{\text{pol},0}(\mathbf{r})\right) \,, \tag{11.28}$$

and the fast polarization potential, $\varphi^{\text{fast}}_{\text{pol},i}(\mathbf{r})$, is

$$\varphi^{\text{fast}}_{\text{pol},i}(\mathbf{r}) = \varphi_{\text{tot},i}(\mathbf{r}) - \varphi_{\text{sol},i}(\mathbf{r}) - \varphi^{\text{slow}}_{\text{pol},0}(\mathbf{r}) \,. \tag{11.29}$$

The superscript notation indicates the component of solvent polarization, and the additional subscript index indicates from which state (reference or ionized) the quantity derives. In Eq. (11.28), $\epsilon_{\text{opt}}$ is the optical dielectric of the solvent, and $\rho_{\text{iter},i}$ is computed using Eq. (11.23) with $\epsilon_{\text{opt}}(\mathbf{r})$ and $\varphi^{\text{fast}}_{\text{tot},i}(\mathbf{r})$. For the Marcus partitioning scheme, the slow component of the induced solvent polarization charge density is computed as the three-dimensional analog of Eq. (11.8), which utilizes the two-dimensional apparent surface charges.

#### 11.2.10.3 Poisson Equation Job Control

A calculation utilizing the Poisson equation boundary conditions is initialized by setting SOLVE_PEQ = TRUE in the *$rem* section. For computational efficiency, solvent effects from the Poisson equation solver are not computed until the error of the vacuum SCF calculation falls below a certain threshold, taken to be $10^{-3}$ a.u. This is controlled by the user through the PEQ_SWITCH keyword, which is also set in the *$rem* section.

**Note:** When SOLVE_PEQ = TRUE, the keywords SYM_IGNORE and NO_REORIENT are also set to TRUE.

**SOLVE_PEQ**
Perform a solvation free energy calculation on a Cartesian grid utilizing Poisson equation boundary conditions.
TYPE:
STRING
DEFAULT:
False
OPTIONS:
TRUE/FALSE
RECOMMENDATION:
None.

**PEQ_SWITCH**
Inclusion of solvent effects begins when the SCF error falls below $10^{-\text{PEQ\_SWITCH}}$.
TYPE:
INTEGER
DEFAULT:
3
OPTIONS:
$n$ Corresponding to $10^{-n}$
RECOMMENDATION:
Use the default unless solvent effects need to be incorporated at earlier SCF cycles.

#### 11.2.10.4 *$peqs_grid* and *$peqs* sections

Job control for the Poisson equation solver routines is set up in two sections: *$peqs_grid* and *$peqs*. The *$peqs_grid* section is where the user will specify the Cartesian grid utilized in the Poisson equation routines as follows:

```
$peqs_grid
   DimX <Nx> <Xmin> <Xmax>
   DimY <Ny> <Ymin> <Ymax>
   DimZ <Nz> <Zmin> <Zmax>
$end
```

The Cartesian grid must be orthorhombic and Nx, Ny, and Nz refer to the number of grid points for the $x-$, $y-$, and $z-$axes, respectively.

**Note:** An order four multi-grid is implemented to speed up convergence of the conjugate gradient algorithm employed to solve Eq. (11.20). Therefore an odd number of grid points must be used with the additional constraint that the quantities Nx-1, Ny-1, and Nz-1 must all be divisible by 8.

The values in the last two columns, specifying the minimum and maximum values of the Cartesian grid for each coordinate, are assumed to be in Ångstroms. The length of the grid along each axis is computed as, for example, $Lx\ =$ Xmax - Xmin, and the grid spacings are defined as $\Delta x\ =\ Lx/(Nx-1)$. The volume element of the Cartesian grid, $dV$, surrounding the discussion of Eq. (11.18), is $dV=\Delta x\Delta y\Delta z$.

The *$peqs* section controls features such as the type of cavity construction of the solute and other required parameters for interfacial or non-equilibrium solvation. The format of the *$peqs* section follows that of the *$rem* section:

```
$peqs
   <Keyword>  <parameter/option>
$end
```

**PEQMaxIter**

Sets the maximum number of iterations used in the conjugate gradient solver.

INPUT SECTION: *$peqs*

TYPE:

INTEGER

DEFAULT:

50

OPTIONS:

User-defined.

RECOMMENDATION:

Use the default unless the system is slowly converging.

**PEQSolverThresh**

The electrostatic potential is considered converged when the error falls below $10^{-\mathrm{PEQSolverThresh}}$.

INPUT SECTION: *$peqs*

TYPE:

INTEGER

DEFAULT:

5

OPTIONS:

$n$ Corresponding to $10^{-n}$

RECOMMENDATION:

Use the default unless a tighter convergence criterion is desired at a higher computational cost.

**PolarIterScale**

A mixing parameter used to stabilize the iterative method when computing the polarization charge density.

INPUT SECTION: *$peqs*

TYPE:

FLOAT

DEFAULT:

0.6

OPTIONS:

$\eta$ Desired value of the mixing parameter (unit-less).

RECOMMENDATION:

Use the default, which was tested and used in Refs. 85 and 86, unless the system is difficult to converge.

**BatchSize**

Improves the efficiency of obtaining the electronic electrostatic potential on the grid by computing atomic orbital integrals in batches (i.e. performing the necessary integrals on small parts of the Cartesian grid instead of in its entirety).

INPUT SECTION: *$peqs*

TYPE:

INTEGER

DEFAULT:

5000

OPTIONS:

$n$ Corresponding to a batch size of $n$ grid points.

RECOMMENDATION:

For large grids ($\geq 10^6$ grid points), a batch size $n \approx \frac{1}{3}NxNyNz$ is recommended.

**SolventDielectric**

Sets the dielectric value of the solvent.

INPUT SECTION: *$peqs*

TYPE:

FLOAT

DEFAULT:

78.39

OPTIONS:

$\varepsilon$ Desired value of $\epsilon$ (unit-less).

RECOMMENDATION:

Consult the literature to determine the value corresponding to the desired solvent and temperature. The default value corresponds to water at 25°C.

**OpticalDielectric**

Sets the optical dielectric value of the solvent.

INPUT SECTION: *$peqs*

TYPE:

FLOAT

DEFAULT:

1.7778

OPTIONS:

$\varepsilon_{\mathrm{opt}}$ Desired value of $\varepsilon_{\mathrm{opt}}$ (unit-less).

RECOMMENDATION:

Consult the literature to determine the value corresponding to the desired solvent and temperature. Note that $\varepsilon_{\mathrm{opt}} = n^2$ where $n$ is the solvent index of refraction. The default value corresponds to water at 25°C.

**SoluteCavity**

Specifies the type of solute cavity, which determines the form of $\epsilon(\mathbf{r})$.

INPUT SECTION: *$peqs*

TYPE:

STRING

DEFAULT:

Vacuum

OPTIONS:

| | |
|---|---|
| Vacuum | Perform calculation in vacuum ($\epsilon(\mathbf{r}) = 1$). |
| RigidVDW | Create a cavity using spherically symmetric error functions. |
| Spherical | Create a spherical cavity around the solute. |

RECOMMENDATION:

None.

In conventional PCMs, the solute cavity is a rigid, two-dimensional surface constructed from atomic spheres, which are generally taken to be the van der Waals radius ($r_{vdW}$) scaled by a factor of 1.2 (see discussion in Section 11.2.3). The cavity is rigid in the sense that once the atomic coordinates are specified, it remains unchanged during the SCF cycles. Furthermore, there is an abrupt and discontinuous change in the dielectric at the solute/solvent boundary. A three-dimensional analog of this cavity, using continuous and differentiable spherically symmetric error functions, has been implemented for the Poisson equation solver, and follows the procedure in Ref. 85:

$$\epsilon(\mathbf{r};\{\mathbf{R}_A\}) = (\epsilon_{\text{solvent}} - 1)\left\{\prod_{A}^{N_{\text{atoms}}} h(d_A, \Delta; |\mathbf{r} - \mathbf{R}_A|)\right\}, \tag{11.30}$$

where

$$h(d_A, \Delta; |\mathbf{r} - \mathbf{R}_A|)\} = \frac{1}{2}\left[1 + \text{erf}\left(\frac{|\mathbf{r} - \mathbf{R}_A| - d_A}{\Delta}\right)\right] . \tag{11.31}$$

Eq. (11.30) smoothly interpolates the dielectric from vacuum to solvent ($\epsilon_{\text{solvent}}$) over a length scale of $\approx 4\Delta$, which is controlled with the **RigidScale** keyword. In Eqs. (11.30) and (11.31), $\mathbf{r}$ is the vector of Cartesian grid coordinates, $\mathbf{R}_A$ specifies the atomic coordinates of the solute, and $d_A$ sets the center of the error function for atom $A$. By default, $d_A$ is set to be $r_{vdW}$ scaled by a factor of 1.2, but this can be controlled by the user with the **VDWType**, **VDWScale**, and **VDWShift** keywords described below.

**RigidScale**

Sets the length scale on which the error function employed in the RigidVDW solute cavity construction transitions the dielectric from vacuum to solvent.

INPUT SECTION: *$peqs*

TYPE:

FLOAT

DEFAULT:

0.265 Ångstroms

OPTIONS:

$\Delta$ Specifies the desired scaling factor in Ångstroms for the error functions.

RECOMMENDATION:

Use the default value, which was tuned in Ref. 85 and yielded $\approx$ 1.0 kcal/mol error for a variety of polar and non-polar molecules, or consult the literature.

**VDWType**

Specifies details for the RigidVDW cavity construction.

INPUT SECTION: *$peqs*

TYPE:

STRING

DEFAULT:

Scaled

OPTIONS:

| | |
|---|---|
| Unscaled | $d_A = r_{\text{vdW}}$ |
| Scaled | $d_A = r_{\text{vdW}} \cdot scale$ |
| Shifted | $d_A = (r_{\text{vdW}} + shift) \cdot scale$ |

RECOMMENDATION:

None. The values of $scale$ and $shift$ are set with the **VDWScale** and **VDWShift** keywords.

**VDWScale**

Sets the empirical scale factor applied to the atomic van der Waals radius.

INPUT SECTION: *$peqs*

TYPE:

FLOAT

DEFAULT:

1.2

OPTIONS:

$scale$ Specifies the desired scaling factor (unit-less) of the atomic van der Waals radius.

RECOMMENDATION:

Use the default value.

**VDWShift**

Adjusts the center of the spherically symmetric error functions when constructing the **RigidVDW** cavity.

INPUT SECTION: *$peqs*

TYPE:

FLOAT

DEFAULT:

0.0 Ångstroms

OPTIONS:

$shift$ Specifies the desired shift in Ångstroms.

RECOMMENDATION:

None. If **VDWType** is set to Shifted, the van der Waals scale factor is set to 1.0 by default. This can be adjusted by the user with the **VDWScale** keyword.

Setting the **SoluteCavity** keyword to **Spherical** requests the construction of a spherical cavity around the solute, and the dielectric is smoothly interpolated from vacuum to solvent using a hyperbolic tangent function as in Ref 88:

$$\epsilon(r) = \frac{1}{2}\Big\{(\epsilon_{\text{solvent}} + 1) + (\epsilon_{\text{solvent}} - 1)\,\tanh\big[\alpha(r - r_{\text{mid}})\big]\Big\}\ . \tag{11.32}$$

$r_{\text{mid}}$ is where the dielectric assumes the value $\epsilon(r_{\text{mid}}) = (\epsilon_{\text{solvent}} + 1)/2$. The value of $r_{\text{mid}}$ is taken to be the sum of the sphere radius, $R$, and half of the interpolation length, $L$: $r_{\text{mid}} = R + L/2$. The sphere radius and interpolation length are controlled with the **SphereRadius** and **InterpolLength** keywords described below. The parameter $\alpha$ controls the sharpness of the switching process and is approximated as $4/L$.

**SphereRadius**

Sets the radius of the spherical solute cavity.

INPUT SECTION: *$peqs*

TYPE:

FLOAT

DEFAULT:

No default.

OPTIONS:

$R$ Desired spherical cavity radius in Ångstroms.

RECOMMENDATION:

None. See the Supporting Information of Ref. 88 for more information.

**InterpolLength**

Sets the length scale on which the dielectric is smoothly interpolated from vacuum to solvent.

INPUT SECTION: *$peqs*

TYPE:

FLOAT

DEFAULT:

No default.

OPTIONS:

$L$ Desired interpolation length in Ångstroms.

RECOMMENDATION:

None.

**InterpolScale**

For a given interpolation length ($L$), **InterpolScale** ($\alpha$) sets the sharpness of the dielectric transition from vacuum to solvent.

INPUT SECTION: *$peqs*

TYPE:

FLOAT

DEFAULT:

$\alpha = 4.0 / L$

OPTIONS:

$\alpha$ Desired interpolation scale factor in Ångstroms$^{-1}$.

RECOMMENDATION:

Use the default unless a broader (smaller $\alpha$) or narrower (larger $\alpha$) transition is desired.

**Interface**

Perform a solvation calculation at a solvent/vacuum interface.

INPUT SECTION: *$peqs*

TYPE:

STRING

DEFAULT:

False

OPTIONS:

True Modify the dielectric function to simulate an interface between solvent and vacuum.

False Perform a solvation calculation in bulk solvent.

RECOMMENDATION:

The user will also need to specify the length scale on which the dielectric is smoothly interpolated from the bulk solvent value to vacuum, and the location of the Gibbs dividing surface (see below).

By setting **Interface** = True, the dielectric function on the Cartesian grid is further modified to mimic a solvent/vacuum interface. First, the solute cavity is constructed as specified by the **SoluteCavity** keyword as discussed above. Then, the dielectric is smoothly interpolated in the $z-$direction across the Gibbs dividing surface ($z_{\text{GDS}}$) using the following hyperbolic tangent switching function:

$$\epsilon(z) = \frac{1}{2}\Big\{(\epsilon_{\text{solvent}} + 1) + (1 - \epsilon_{\text{solvent}})\,\tanh\big[\beta(z - z_{\text{GDS}})\big]\Big\}\ . \tag{11.33}$$

Eq. (11.33) will interpolate the dielectric function over the interface length, $I$, centered at the Gibbs dividing surface, $z_{\mathrm{GDS}}$. Both of these values are controlled by the keywords **InterfaceLength** and **GibbsDS**, respectively. Similar to $\alpha$ used in the spherical cavity construction, the parameter $\beta$ controls the sharpness of the interpolation across the Gibbs dividing surface and is approximated as $4/I$.

**InterfaceLength**

Sets the length scale over which the dielectric function is smoothly transitioned from bulk solvent to vacuum in the $z$-direction

INPUT SECTION: *$peqs*

TYPE:

FLOAT

DEFAULT:

None

OPTIONS:

$I$ Desired interface length in Ångstroms.

RECOMMENDATION:

See the Supporting Information of Ref. 88 for a full description of the solvent/vacuum interface construction.

**GibbsDS**

Sets the location of the Gibbs dividing surface in the $z-$direction for an interface.

INPUT SECTION: *$peqs*

TYPE:

FLOAT

DEFAULT:

None

OPTIONS:

$z_{\mathrm{GDS}}$ Desired location of the Gibbs dividing surface in Ångstroms.

RECOMMENDATION:

Consult the literature. One such way to determine this value is to compute a density profile of the solvent as a function of $z$ and set this location to be where the solvent density has decreased to 50% of the bulk value. Usually, $z_{\mathrm{GDS}} \approx I/2.0$, where $I$ is the interface length described above.

**NonequilJob**

Obtain the non-equilibrium free energy of solvation for a vertical ionization process.

INPUT SECTION: *$peqs*

TYPE:

STRING

DEFAULT:

False

OPTIONS:

True Compute the non-equilibrium free energy for a vertical ionization process.

False Compute the equilibrium solvation free energy.

RECOMMENDATION:

None.

**NonequilPartition**

Specifies the scheme used to partition the fast and slow charges of the solvent.

INPUT SECTION: *$peqs*

TYPE:

STRING

DEFAULT:

Marcus

OPTIONS:

| | |
|---|---|
| Marcus | Employ the Marcus partitioning scheme. |
| Pekar | Employ the Pekar partitioning scheme. |

RECOMMENDATION:

Use the default. The non-equilibrium free energies are partition independent[56] and the Pekar scheme is computationally more expensive than the Marcus scheme.

**NonequilState**

Specifies the state of interest for a non-equilibrium vertical ionization.

INPUT SECTION: *$peqs*

TYPE:

STRING

DEFAULT:

Reference

OPTIONS:

| | |
|---|---|
| Reference | The reference state from which to vertically remove an electron. |
| Ionized | The vertically ionized state. |

RECOMMENDATION:

None.

#### 11.2.10.5 Examples

The following example illustrates a free energy solvation calculation of a water molecule immersed in water. The Cartesian grid is cubic with a side length of 20.0 Ångstroms and 153 grid points along each axis. The solute cavity is chosen to be **RigidVDW** centered on the scaled van der Waals radii. The dielectric is not set here, but takes the default value of 78.39.

**Example 11.16** Free energy of solvation of water in water.

```
$rem
   SCF_CONVERGENCE   5
   THRESH            14
   EXCHANGE          omegab97x-v
   BASIS             6-311G*
   SOLVE_PEQ         true
   PEQ_SWITCH        3
   MEM_TOTAL         75000
   MEM_STATIC        8000
$end

$molecule
   0 1
   O     0.053004    -0.020947    -0.034784
   H     0.003424     0.185855     0.910594
   H    -0.844842     0.146674    -0.358413
$end

$peqs
   SoluteCavity  RigidVDW
   VDWType       Scaled
   VDWScale      1.2
   BatchSize     1193859
$end

$peqs_grid
   DimX 153 -10.00 10.00
   DimY 153 -10.00 10.00
   DimZ 153 -10.00 10.00
$end
```

The next example illustrates a free energy solvation calculation of a water molecule at a water/vacuum interface with the Gibbs dividing surface placed at 0.85 Ångstroms, and the length of the interface is set to be 1.5 Ångstroms. The Cartesian grid, solute cavity, and solvent dielectric are the same as in the previous example.

**Example 11.17** Free energy of solvation of water at a water/vacuum interface.

```
$rem
   SCF_CONVERGENCE   5
   THRESH            14
   EXCHANGE          omegab97x-v
   BASIS             6-311G*
   SOLVE_PEQ         true
   PEQ_SWITCH        3
   MEM_TOTAL         75000
   MEM_STATIC        8000
$end

$molecule
   0 1
   O     0.053004    -0.020947    -0.034784
   H     0.003424     0.185855     0.910594
   H    -0.844842     0.146674    -0.358413
$end

$peqs
   SoluteCavity      RigidVDW
   VDWType           Scaled
   VDWScale          1.2
   Interface         true
   InterfaceLength   1.5
   GibbsDS           0.85
   BatchSize         1193859
$end

$peqs_grid
   DimX 153 -10.00 10.00
   DimY 153 -10.00 10.00
   DimZ 153 -10.00 10.00
$end
```

The final example illustrates a non-equilibrium (NONEQUILJOB = TRUE) solvation calculation for the vertical ionization of $H_2O^-$ in bulk water. This is a compound job that will first calculate the equilibrium solvation free energy of the anionic state (NONEQUILSTATE = REFERENCE), and then compute the non-equilibrium correction for the ionized state (NONEQUILSTATE = IONIZED). The two jobs are separated by ”@@@". The Cartesian grid and solvent dielectric are the same as the previous examples, but the solute cavity is chosen to be Spherical with a radius of 1.884503499 Å. The Marcus scheme (NONEQUILPARTITION = MARCUS) is employed to partition the fast and slow charges of the solvent.

**Example 11.18** Non-equilibrium free energy of solvation for the vertical ionization of $H_2O^-$.

```
$rem
   SCF_CONVERGENCE   5
   THRESH            14
   EXCHANGE          omegab97x-v
   BASIS             6-311G*
   SOLVE_PEQ         true
   PEQ_SWITCH        3
   MEM_TOTAL         75000
   MEM_STATIC        8000
$end

$molecule
   -1 2
   O     0.053004    -0.020947    -0.034784
   H     0.003424     0.185855     0.910594
   H    -0.844842     0.146674    -0.358413
$end

$peqs
   SoluteCavity        Spherical
   SphereRadius        1.884503499
   InterpolLength      1.0
   NonequilJob         true
   NonequilState       Reference
   NonequilPartition   Marcus
   BatchSize           1193859
$end

$peqs_grid
   DimX 153 -10.00 10.00
   DimY 153 -10.00 10.00
   DimZ 153 -10.00 10.00
$end

@@@

$rem
   scf_convergence   5
   thresh            14
   exchange          omegab97x-v
   basis             6-311G*
   solve_peq         true
   peq_switch        3
   mem_total         75000
   mem_static        8000
$end
```

```
$molecule
   0 1
   O     0.053004    -0.020947    -0.034784
   H     0.003424     0.185855     0.910594
   H    -0.844842     0.146674    -0.358413
$end

$peqs
   SoluteCavity        Spherical
   SphereRadius        1.884503499
   InterpolLength      1.0
   NonequilJob         true
   NonequilState       Ionized
   NonequilPartition   Marcus
   BatchSize           1193859
$end

$peqs_grid
   DimX 153 -10.00 10.00
   DimY 153 -10.00 10.00
   DimZ 153 -10.00 10.00
$end
```

## 11.3 Stand-Alone QM/MM Calculations

Q-CHEM can perform hybrid quantum mechanics/molecular mechanics (QM/MM) calculations either as a stand-alone program (which is described in this Section) or in conjunction with the CHARMM package[89] (see Section 11.4).

### 11.3.1 Available QM/MM Methods and Features

Three modes of operation are available:

- MM calculations only (no QM)
- QM/MM calculations using a two-layer ONIOM model with mechanical embedding
- QM/MM calculations using the Janus model for electronic embedding

Q-CHEM can carry out purely MM calculations, wherein the entire molecular system is described by a MM force field and no electronic structure calculation is performed. The MM force fields available are present are AMBER[90], CHARMM[91], and OPLSAA[92].

As implemented in Q-CHEM, the ONIOM model[93] is a mechanical embedding scheme that partitions a molecular system into two subsystems (layers): an MM subsystem and a QM subsystem. The total energy of an ONIOM system is given by

$$E_{\rm total} = E_{\rm total}^{\rm MM} - E_{\rm QM}^{\rm MM} + E_{\rm QM}^{\rm QM} \tag{11.34}$$

where $E_{\rm total}^{\rm MM}$ is the MM energy of the total system (*i.e.*, QM + MM subsystems), $E_{\rm QM}^{\rm MM}$ is the MM energy of the QM subsystem, and $E_{\rm QM}^{\rm QM}$ is the QM energy of the QM subsystem. MM energies are computed via a specified MM force field, and QM energies are computed via a specified electronic structure calculation.

The advantage of the ONIOM model is its simplicity, which allows for straightforward application to a wide variety of systems. A disadvantage of this approach, however, is that QM subsystem does not interact directly with the MM subsystem. Instead, such interactions are incorporated indirectly, in the $E_{total}^{MM}$ contribution to the total energy. As a result, the QM electron density is not polarized by the electrostatic charges of the MM subsystem.

If the QM/MM interface partitions the two subsystems across a chemical bond, a link atom (hydrogen) must be introduced to act as a cap for the QM subsystem. Currently, Q-CHEM supports only carbon link atoms, of atom type 26, 35, and 47 in the CHARMM27 force field.

The Janus model[94] is an electronic embedding scheme that also partitions the system into MM and QM subsystems, but is more versatile than the ONIOM model. The Janus model in Q-CHEM is based upon the "YinYang atom" model of Shao and Kong [95]. In this approach, the total energy of the system is simply the sum of the subsystem energies,

$$E_{\text{total}} = E_{\text{MM}} + E_{\text{QM}} \tag{11.35}$$

The MM subsystem energy, $E_{\text{MM}}$, includes van der Waals interactions between QM and MM atoms but not QM/MM Coulomb interactions. Rather, $E_{\text{QM}}$ includes the direct Coulomb potential between QM atoms and MM atoms as external charges during the QM calculation, thus allowing the QM electron density to be polarized by the MM atoms. Because of this, Janus is particularly well suited (as compared to ONIOM) for carrying out excited-state QM/MM calculations, for excited states of a QM model system embedded within the electrostatic environment of the MM system. Within a Janus calculation, Q-CHEM first computes $E_{\text{MM}}$ with the specified force field and then computes $E_{\text{QM}}$ with the specified electronic structure theory.

When the Janus QM/MM partition cuts across a chemical bond, a YinYang atom[95] is automatically introduced by Q-CHEM. This atom acts as a hydrogen cap in the QM calculation, yet also participates in MM interactions. To retain charge neutrality of the total system, the YinYang atom has a single electron and a modified nuclear charge in the QM calculation, equal to $q_{nuclear} = 1 + q_{\text{MM}}$ (*i.e.*, the charge of a proton plus the charge on the YinYang atom in the MM subsystem).

Because this modified charge will affect the bond containing the YinYang atom, an additional repulsive Coulomb potential is applied between the YinYang atom and its connecting QM atom to maintain a desirable bond length. The additional repulsive Coulomb energy is added to $E_{\text{MM}}$. The YinYang atom can be an atom of any kind, but it is highly recommended to use carbon atoms as YinYang atoms.

Q-CHEM's stand-alone QM/MM capabilities also include the following features:

- Analytic QM/MM gradients are available for QM subsystems described with density functional theory (DFT) or Hartree-Fock (HF) electronic structure theory, allowing for geometry optimizations and QM/MM molecular dynamics.
- Single-point QM/MM energy evaluations are available for QM subsystems described with most post-HF correlated wave functions.
- Single-point QM/MM calculations are available for excited states of the QM subsystem, where the latter may be described using CIS, TDDFT, or correlated wave function models. Analytic gradients for excited states are available for QM/MM calculations if the QM subsystem is described using CIS.
- Single-point MM or QM/MM energy evaluations and analytic gradients are available using periodic boundary conditions with Ewald summation.
- Implicit solvation for both Janus QM/MM calculations as well as MM-only calculations is available using the Polarizable Continuum Models (PCMs) discussed in Section 11.2.2.

- Gaussian blurring of MM external charges is available for Janus QM/MM calculations.
- User-defined MM atoms types, MM parameters, and force fields.

## 11.3.2 Using the Stand-Alone QM/MM Features

### 11.3.2.1 *$molecule* section

To perform QM/MM calculations, the user must assign MM atom types for each atom in the *$molecule* section. The format for this specification is modeled upon that used by the TINKER molecular modeling package[96], although the TINKER program is *not* required to perform QM/MM calculations using Q-CHEM. Force field parameters and MM atom type numbers used within Q-CHEM are identical to those used TINKER for the AMBER99, CHARMM27, and OPLSAA force fields, and the format of the force field parameters files is also the same.

The *$molecule* section must use Cartesian coordinates to define the molecular geometry for internal QM/MM calculations; the Z-matrix format is not valid. MM atom types are specified in the *$molecule* section immediately after the Cartesian coordinates on a line so that the general format for the *$molecule* section is

```
$molecule
  <Charge> <Multiplicity>
  <Atom> <X> <Y> <Z> <MM atom type>
  . . .
$end
```

For example, one can define a TIP3P water molecule using AMBER99 atom types, as follows:

```
$molecule
   0 1
   O        -0.790909    1.149780    0.907453  2001
   H        -1.628044    1.245320    1.376372  2002
   H        -0.669346    1.913705    0.331002  2002
$end
```

When the input is specified as above, Q-CHEM will determine the MM bond connectivity based on the distances between atoms; if two atoms are sufficiently close, they are considered to be bonded. Occasionally this approach can lead to problems when non-bonded atoms are in close proximity of one another, in which case Q-CHEM might classify them as bonded regardless of whether the appropriate MM bond parameters are available. To avoid such a scenario, the user can specify the bonds explicitly by setting the *$rem* variable USER_CONNECT = TRUE, in which case the *$molecule* section must have the following format

```
$molecule
  <Charge> <Multiplicity>
  <Atom> <X> <Y> <Z> <MM atom type> <Bond 1> <Bond 2> <Bond 3> <Bond 4>
  . . .
$end
```

Each `<Bond #>` is the index of an atom to which `<Atom>` is bonded. Four bonds must be specified for each atom, even if that atom is connected to fewer than four other atoms. (For non-existent bonds, use zero as a placeholder.) Currently, Q-CHEM supports no more than four MM bonds per atom.

After setting USER_CONNECT = TRUE, a TIP3P water molecule in the AMBER99 force field could be specified as follows:

```
$molecule
   0 1
   O      -0.790909    1.149780    0.907453  2001  2 3 0 0
   H      -1.628044    1.245320    1.376372  2002  1 0 0 0
   H      -0.669346    1.913705    0.331002  2002  1 0 0 0
$end
```

Explicitly defining the bonds in this way is highly recommended.

#### 11.3.2.2 *$force_field_params* section

In many cases, all atoms types (within both the QM and MM subsystems) will be defined by a given force field. In certain cases, however, a particular atom type may not be defined in a given force field. For example, a QM/MM calculation on the propoxide anion might consist of a QM subsystem containing an alkoxide functional group, for which MM parameters do not exist. Even though the alkoxide moiety is described using quantum mechanics, van der Waals parameters are nominally required for atoms within the QM subsystem, which interact with the MM atoms via Lennard-Jones-type interactions.

In such cases, there are four possible options, the choice of which is left to the user's discretion:

1. Use a similar MM atom type as a substitute for the missing atom type.
2. Ignore the interactions associated with the missing atom type.
3. Define a new MM atom type and associated parameters.
4. Define a new force field.

These options should be applied with care. Option 1 involves selecting an atom type that closely resembles the undefined MM atom. For example, the oxygen atom of an alkoxide moiety could perhaps use the MM atom type corresponding to the oxygen atom of a neutral hydroxyl group. Alternatively, the atom type could be ignored altogether (option 2) by specifying MM atom type 0 (zero). Setting the atom type to zero should be accompanied with setting all four explicit bond connections to placeholders if USER_CONNECT = TRUE. An atom type of zero will cause all MM energies involving that atom to be zero.

The third option in the list above requires the user to specify a *$force_field_params* section in the Q-CHEM input file. This input section can be used to add new MM atom type definitions to one of Q-CHEM's built-in force fields. At a minimum, the user must specify the atomic charge and two Lennard-Jones parameters (radius and well depth, $\epsilon$), for each new MM atom type. Bond, angle, and torsion parameters for stretches, bends, and torsions involving the new atom type may also be specified, if desired. The format for the *$force_field_params* input section is

```
$force_field_params
NumAtomTypes <n>
AtomType -1 <Charge> <LJ Radius> <LJ Epsilon>
AtomType -2 <Charge> <LJ Radius> <LJ Epsilon>
. . .
AtomType -n <Charge> <LJ Radius> <LJ Epsilon>
Bond <a> <b> <Force constant> <Equilibrium Distance>
. . .
Angle <a> <b> <c> <Force constant> <Equilibrium Angle>
. . .
Torsion <a> <b> <c> <d> <Force constant> <Phase Angle> <Multiplicity>
. . .
$end
```

The first line in this input section specifies how many new MM atom types appear in this section (<n>). These are specified on the following lines labeled with the AtomType tag. The atom type numbers are required to be negative and to appear in the order $-1, -2, -3, \ldots, -n$. The *$molecule* section for a water molecule, with user-defined MM parameters for both oxygen and hydrogen, might appear as follows:

```
$molecule
   0 1
   O        -0.790909    1.149780    0.907453        -1   2 3 0 0
   H        -1.628044    1.245320    1.376372        -2   1 0 0 0
   H        -0.669346    1.913705    0.331002        -2   1 0 0 0
$end
```

The remainder of each AtomType line in the *$force_field_params* section consists of a charge (in elementary charge units), a Lennard-Jones radius (in Å), and a Lennard-Jones well depth ($\epsilon$, in kcal/mol).

Each (optional) Bond line in the *$force_field_params* section defines bond-stretching parameters for a bond that contains a new MM atom type. The bond may consist of both atoms <a> and <b> defined an AtomType line, or else <a> may be defined with an AtomType line and <b> defined as a regular atom type for the force field. In the latter case, the label for <b> should be the number of its general van der Waals type. For example, the atom type for a TIP3P oxygen in AMBER99 is 2001, but its van der Waals type is 21, so the latter would be specified in the Bond line. The remaining entries of each Bond line are the harmonic force constant, in kcal/mol/Å$^2$, and the equilibrium distance, in Å.

Similar to the Bond lines, each (optional) Angle line consists of one or more new atom types along with existing van der Waals types. The central atom of the angle is <b>. The harmonic force constant (in units of kcal/mol/degree) and equilibrium bond angle (in degrees) are the final entries in each Bond line.

Each (optional) Torsion line consists of one or more new MM atom types along with regular van der Waals types. The connectivity of the four atoms that constitute the dihedral angle is <a>–<b>–<c>–<d>, and the torsional potential energy function is

$$E_{\text{torsion}}(\theta) = k_{\text{torsion}}[1 + \cos(m\theta - \phi)] \tag{11.36}$$

The force constant ($k_{\text{torsion}}$) is specified in kcal/mol and the phase angle ($\phi$) in degrees. The multiplicity ($m$) is an integer.

#### 11.3.2.3 User-Defined Force Fields

Option 4 in the list on page 750 is the most versatile, and allows the user to define a completely new force field. This option is selected by setting FORCE_FIELD = READ, which tells Q-CHEM to read force field parameters from a text file whose name is specified in the *$force_field_params* section as follows:

```
$force_field_params
    Filename <path/filename>
$end
```

Here, `<path/filename>` is the full (absolute) path and name of the file that Q-CHEM will attempt to read for the MM force field. For example, if the user has a file named `MyForceField.prm` that resides in the path `/Users/me/parameters/`, then this would be specified as

```
$force_field_params
   Filename /Users/me/parameters/MyForceField.prm
$end
```

Within the force field file, the user should first declare various rules that the force field will use, including how van der Waals interactions will be treated, scaling of certain interactions, and the type of improper torsion potential. The rules are declared in the file as follows:

```
RadiusRule <option>
EpsilonRule <option>
RadiusSize <option>
ImptorType <option>
vdw-14-scale <x>
chg-14-scale <x>
torsion-scale <x>
```

Currently, only a Lennard-Jones potential is available for van der Waals interactions. `RadiusRule` and `EpsilonRule` control how to average $\sigma$ and $\epsilon$, respectively, between atoms A and B in their Lennard-Jones potential. The options available for both of these rules are `Arithmetic` [*e.g.*, $\sigma_{AB} = (\sigma_A + \sigma_B)/2$] or `Geometric` [*e.g.*, $\sigma_{AB} = (\sigma_A \sigma_B)^{1/2}$]. `RadiusSize` has options `Radius` or `Diameter`, which specify whether the parameter $\sigma$ is the van der Waals radius or diameter in the Lennard-Jones potential.

`ImptorType` controls the type of potential to be used for improper torsion (out-of-plane bending) energies, and has two options: `Trigonometric` or `Harmonic`. These options are described in more detail below.

The scaling rules takes a floating point argument `<x>`. The `vdw-14-scale` and `chg-14-scale` rules only affect van der Waals and Coulomb interactions, respectively, between atoms that are separated by three consecutive bonds (atoms 1 and 4 in the chain of bonds). These interaction energies will be scaled by `<x>`. Similarly, `torsion-scale` scales dihedral angle torsion energies.

After declaring the force field rules, the number of MM atom types and van der Waals types in the force field must be specified using:

```
NAtom <n>
Nvdw <n>
```

where <n> is a positive integer.

Next, the atom types, van der Waals types, bonds, angles, dihedral angle torsion, improper torsions, and Urey-Bradley parameters can be declared in the following format:

```
Atom 1 <Charge> <vdw Type index> <Optional description>
Atom 2 <Charge> <vdw Type index> <Optional description>
. . .
Atom <NAtom> <Charge> <vdw Type index> <Optional description>
. . .
vdw 1 <Sigma> <Epsilon> <Optional description>
vdw 2 <Sigma> <Epsilon> <Optional description>
. . .
vdw <Nvdw> <Sigma> <Epsilon> <Optional description>
. . .
Bond <a> <b> <Force constant> <Equilibrium Distance>
. . .
Angle <a> <b> <c> <Force constant> <Equilibrium Angle>
. . .
Torsion <a> <b> <c> <d> <Force constant 1> <Phase Angle 1> <Multiplicity 1>
. . .
Improper <a> <b> <c> <d> <Force constant> <Equilibrium Angle> <Multiplicity>
. . .
UreyBrad <a> <b> <c>  <Force constant> <Equilibrium Distance>
```

The parameters provided in the force field parameter file correspond to a basic MM energy functional of the form

$$E_{\rm MM} = E_{\rm Coul} + E_{\rm vdW} + E_{\rm bond} + E_{\rm angle} + E_{\rm torsion} + E_{\rm imptor} + E_{\rm UreyBrad} \tag{11.37}$$

Coulomb and van der Waals interactions are computed for all non-bonded pairs of atoms that are at least three consecutive bonds apart (*i.e.*, 1–4 pairs and more distant pairs). The Coulomb energy between atom types 1 and 2 is simply

$$E_{\rm Coul} = f_{\rm scale}\frac{q_1 q_2}{r_{12}} \tag{11.38}$$

where $q_1$ and $q_2$ are the respective charges on the atoms (specified with <Charge> in elementary charge units) and $r_{12}$ is the distance between the two atoms. For 1–4 pairs, $f_{scale}$ is defined with chg-14-scale but is unity for all other valid pairs. The van der Waals energy between two atoms with van der Waals types a and b, and separated by distance $r_{ab}$, is given by a "6-12" Lennard-Jones potential:

$$E_{\rm vdW}(r_{ab}) = f_{\rm scale}\,\epsilon_{ab}\left[\left(\frac{\sigma_{ab}}{r_{ab}}\right)^{12} - 2\left(\frac{\sigma_{ab}}{r_{ab}}\right)^{6}\right] \tag{11.39}$$

Here, $f_{\rm scale}$ is the scaling factor for 1–4 interactions defined with vdw-14-scale and is unity for other valid interactions. The quantities $\epsilon_{ab}$ and $\sigma_{ab}$ are the averages of the parameters of atoms a and b as defined with `EpsilonRule` and `RadiusRule`, respectively (see above). The units of `<Sigma>` are Å , and the units of `<Epsilon>` are kcal/mol. Hereafter, we refer to atoms' van der Waals types with `a, b, c, ...` and atoms' charges with `1,2, 3, ....`

The bond energy is a harmonic potential,

$$E_{\text{bond}}(r_{ab}) = k_{\text{bond}}(r_{ab} - r_{eq})^2 \tag{11.40}$$

where $k_{\text{bond}}$ is provided by `<Force Constant>` in kcal/mol/Å$^2$ and $r_{eq}$ by `<Equilibrium Distance>` in Å. Note that `<a>` and `<b>` in the `Bond` definition correspond to the van der Waals type indices from the `vdw` definitions, *not* the `Atom` indices.

The bending potential between two adjacent bonds connecting three different atoms (`<a>-<b>-<c>`) is also taken to be harmonic,

$$E_{\text{angle}}(\theta_{abc}) = k_{\text{angle}}(\theta_{abc} - \theta_{eq})^2 \tag{11.41}$$

Here, $k_{\text{angle}}$ is provided by `<Force Constant>` in kcal/mol/degrees and $\theta_{eq}$ by `<Equilibrium Angle>` in degrees. Again, `<a>`, `<b>`, and `<c>` correspond to van der Waals types defined with `vdw`.

The energy dependence of the `<a>-<b>-<c>-<d>` dihedral torsion angle, where `<a>`, `<b>`, `<c>`, and `<d>` are van der Waals types, is defined by

$$E_{\text{torsion}}(\theta_{abcd}) = f_{\text{scale}} \sum_m k_{abcd}[1 + \cos(m\theta_{abcd} - \phi)] \tag{11.42}$$

Here, $f_{scale}$ is the scaling factor defined by `torsion-scale`. The force constant $k_{abcd}$ is defined with `<Force constant>` in kcal/mol, and the phase angle $\phi$ is defined with `<Phase Angle>` in degrees. The summation is over multiplicities, $m$, and Q-CHEM supports up to three different values of $m$ per dihedral angle. The force constants and phase angles may depend on $m$, so if more than one multiplicity is used, then `<Force constant> <Phase Angle> <Multiplicity>` should be specified for each multiplicity. For example, to specify a dihedral torsion between van der Waals types 2–1–1–2, with multiplicities $m = 2$ and $m = 3$, we might have:

```
Torsion  2  1  1  2  2.500  180.0  2 1.500 60.0 3
```

*Improper* torsion angle energies for four atoms `<a>-<b>-<c>-<d>`, where `<c>` is the central atom, can be computed in one of two ways, as controlled by the `ImptorType` rule. If `ImptorType` is set to `Trigonometric`, then the improper torsion energy has a functional form similar to that used for dihedral angle torsions:

$$E_{\text{imptor}}(\theta_{abcd}) = \frac{k_{abcd}}{N_{\text{equiv}}}[1 + \cos(m\,\theta_{abcd} - \phi)] \tag{11.43}$$

Here, $\theta_{abcd}$ is the out-of-plane angle of atom `<c>`, in degrees, and $k_{abcd}$ is the force constant defined with `<Force Constant>`, in kcal/mol. The phase $\phi$ and multiplicity $m$ need to be specified in the `Improper` declaration, although the definition of an improper torsion suggests that these values should be set to $\phi = 0$ and $m = 2$. The quantity $N_{equiv}$ accounts for the number of equivalent permutations of atoms `<a>`, `<b>`, and `<d>`, so that the improper torsion angle is only computed once. If `ImptorType` is set to `Harmonic`, then in place of Eq. (11.43), the following energy function is used:

$$E_{\text{imptor}}(\theta_{abcd}) = \frac{k_{abcd}}{N_{\text{equiv}}}\theta_{abcd}^2 \tag{11.44}$$

The Urey-Bradley energy, which accounts for a non-bonded interaction between atoms `<a>` and `<c>` that are separated by two bonds (*i.e.*, a 1-3 interaction through `<a>-<b>-<c>`), is given by

$$E_{\text{UreyBrad}}(r_{ac}) = k_{abc}(r_{ac} - r_{eq})^2 \tag{11.45}$$

The distance in Å between atoms `<a>` and `<c>` is $r_{ac}$, the equilibrium distance $r_{eq}$ is provided by `<Equilibrium Distance>` in Å, and the force constant $k_{abc}$ is provided by `<Force Constant>` in kcal/mol/Å$^2$.

A short example of a valid text-only file defining a force field for a flexible TIP3P water could be as follows:

```
//-- Force Field Example --//

// -- Rules -- //
RadiusRule Geometric
RadiusSize Radius
EpsilonRule Geometric
ImptorType Trigonometric
vdw-14-scale 1.0
chg-14-scale 0.8
torsion-scale 0.5

// -- Number of atoms and vdw to expect -- //
NAtom 2
Nvdw 2

// -- Atoms -- //
Atom 1 -0.8340  2  TIP3P Oxygen
Atom 2  0.4170  1  TIP3P Hydrogen

// -- vdw -- //
vdw 1  0.0000  0.0000 H parameters
vdw 2  1.7682  0.1521 O parameters

// -- Bond -- //
Bond 1 2  553.0  0.9572

// -- Angle -- //
Angle 1 2 1  100.0  104.52
```

Lines that do not begin with one of the keywords will be ignored, and have been used here as comments.

#### 11.3.2.4 *$qm_atoms* and *$forceman* sections

For QM/MM calculations (but not for purely MM calculations) the user must specify the QM subsystem using a *$qm_atoms* input section, which assumes the following format:

```
$qm_atoms
   <QM atom 1 index> <QM atom 2 index> . . .
   . . .
   <QM atom n index>
$end
```

Multiple indices can appear on a single line and the input can be split across multiple lines. Each index is an integer corresponding to one of the atoms in the *$molecule* section, beginning at 1 for the first atom in the *$molecule* section. Link atoms for the ONIOM model and YinYang atoms for the Janus model are not specified in the *$qm_atoms* section, as these are inserted automatically whenever a bond connects a QM atom and an MM atom.

Q-Chem 4.2.2 and later versions also support, for example

```
$qm_atoms
   18:31 35
$end
```

which specifies 15 QM atoms (atoms 18 through 31; atom 35).

For Janus QM/MM calculations, there are several ways of dealing with van der Waals interactions between the QM and MM atoms. By default, van der Waals interactions are computed for all QM–MM and MM–MM atom pairs but not for QM–QM atom pairs. In some cases, the user may prefer not to neglect the van der Waals interactions between QM–QM atoms, or the user may prefer to neglect any van der Waals interaction that involves a QM atom. Q-CHEM allows the user this control via two options in the *$forceman* section. To turn on QM–QM atom van der Waals interactions, the user should include the following in their input:

```
$forceman
   QM-QMvdw
$end
```

Similarly, to turn off all van der Waals interactions with QM atoms, the following should be included:

```
$forceman
   NoQM-QMorQM-MMvdw
$end
```

#### 11.3.2.5 Periodic Boundary Conditions

Periodic boundary conditions (using Ewald summation for the long-range Coulomb interactions) can be used in conjunction with both MM-only calculations and QM/MM calculations. The approach is based off of the work of Nam *et al.*[97] and (independently) Riccardi *et al.*[98], as implemented in both the AMBER[99] and CHARMM[98,100] programs. These approaches use Mulliken charges to represent the periodic images of the wave function, and while suitable for semi-empirical calculations with minimal basis sets, instabilities in the Mulliken charges for extended basis sets lead to SCF convergence failure in the QM/MM-Ewald calculations[101]. The implementation in Q-CHEM thus allows for the use of CHELPG charges to represent the image wave functions, affording an algorithm that is stable in extended basis sets[101,102].

The efficiency of the Ewald summation is governed by the parameter, $\alpha$, that controls the partition of the Coulomb potential into short- and long-range components, and in the QM/MM-Ewald method there are separate values of $\alpha$ for the QM and MM portions of the calculations. Improper selection of $\alpha_{\rm MM}$ and/ or $\alpha_{\rm QM}$ can greatly increase the computational time, and the choices that are optimal for MM calculations need not be optimal for QM/MM calculations[101]. The cost of the MM Ewald summation scales as $\mathcal{O}(N_{\rm recip}N_{\rm atoms})$, where $N_{\rm recip}$ is the number of reciprocal-space lattice vectors that is used for the $k$-space sum. The QM portion of the calculation scales as $\mathcal{O}(N_{\rm recip}N_{\rm QM}N_{\rm atoms})$, where $N_{\rm QM}$ is the number of QM atoms (whereas $N_{\rm atoms} = N_{\rm QM} + N_{\rm MM}$ is the total number of atoms). The MM Ewald parameter is thus selected to minimize the amount of work that is done in real space. The optimal value, which is typically $\alpha_{\rm MM} \approx 0.5$ Å$^{-1}$, can be found by solving the equation[101]

$$\alpha_{\rm MM} = 2C/L \tag{11.46}$$

where

$$C = \left[-\ln\left(10^{-\text{SCF\_CONVERGENCE}}\right)\right]^{1/2} \tag{11.47}$$

and $L$ is the length of the simulation cell. (Only cubic simulation cells are available at present.) In contrast, the parameter $\alpha_{\rm QM}$ should be selected to minimize the total number of vectors in both real and reciprocal space. The optimal value, which is often $\alpha_{\rm QM} \approx 0.1$ Å$^{-1}$, is determined by solving the equation[101]

$$\frac{2CL^3\alpha_{\rm QM}^3}{\pi^{3/2}} + \frac{\alpha_{\rm QM}^2 L^2}{\pi^{1/2}} - \alpha_{\rm QM}L - 2C = 0\ . \tag{11.48}$$

To perform an MM- or QM/MM-Ewald job, one must set MM_SUBTRACTIVE = TRUE in the *$rem* section, but otherwise job control is largely done through the *$forceman* section. The following variables must be set for every type of Ewald calculation.

- The keyword **Ewald** will turn on Ewald summation.
- The keyword **alpha** should be followed by a value for the MM Ewald parameter and then the QM Ewald parameter. (The latter must be set even for MM-only jobs.)
- **Box_length** specifies the side length of the cubic simulation cell, in Å.

The following parameters are optional for further job control.

- **Dielectric** specifies a dielectric constant for the surrounding medium, which appears in the "dipole term" of Ewald summation ($E_{\rm dipole}$ in Ref. 101). If no value is set, the dielectric constant is set to infinity, corresponding to "tin foil" boundary conditions.
- The keyword **Ewald_SCF_thresh_on**, followed by a real number, causes Q-CHEM to wait until the DIIS error falls below the specified value before adding the Ewald correction to the Fock matrix, thus obviating the sometimes-costly Ewald correction in early SCF cycles. (The default value is 1.0, which turns on Ewald summation immediately in most cases)

A short example of a *$forceman* section using Ewald summation could be as follows:

```
$forceman
   ewald
   alpha                  0.35   0.1
   box_length             15.00
   dielectric             88.0
   mm_read_scratch
   ewald_scf_thresh_on    0.0001
$end
```

### 11.3.3 Additional Job Control Variables

A QM/MM job is requested by setting the *$rem* variables QM_MM_INTERFACE and FORCE_FIELD. Also required are a *$qm_atoms* input section and appropriate modifications to the *$molecule* section, as described above. Additional job control variables are detailed here.

**QM_MM_INTERFACE**

Enables internal QM/MM calculations.

TYPE:

STRING

DEFAULT:

NONE

OPTIONS:

| | |
|---|---|
| MM | Molecular mechanics calculation (*i.e.*, no QM region) |
| ONIOM | QM/MM calculation using two-layer mechanical embedding |
| JANUS | QM/MM calculation using electronic embedding |

RECOMMENDATION:

The ONIOM model and Janus models are described above. Choosing MM leads to no electronic structure calculation. However, when using MM, one still needs to define the *$rem* variables BASIS and EXCHANGE in order for Q-CHEM to proceed smoothly.

**FORCE_FIELD**

Specifies the force field for MM energies in QM/MM calculations.

TYPE:

STRING

DEFAULT:

NONE

OPTIONS:

| | |
|---|---|
| AMBER99 | AMBER99 force field |
| CHARMM27 | CHARMM27 force field |
| OPLSAA | OPLSAA force field |

RECOMMENDATION:

None.

**CHARGE_CHARGE_REPULSION**

The repulsive Coulomb interaction parameter for YinYang atoms.

TYPE:

INTEGER

DEFAULT:

550

OPTIONS:

$n$ Use Q = $n \times 10^{-3}$

RECOMMENDATION:

The repulsive Coulomb potential maintains bond lengths involving YinYang atoms with the potential $V(r) = Q/r$. The default is parameterized for carbon atoms.

**GAUSSIAN_BLUR**

Enables the use of Gaussian-delocalized external charges in a QM/MM calculation.

TYPE:

LOGICAL

DEFAULT:

FALSE

OPTIONS:

TRUE Delocalizes external charges with Gaussian functions.

FALSE Point charges

RECOMMENDATION:

None

**GAUSS_BLUR_WIDTH**

Delocalization width for external MM Gaussian charges in a Janus calculations.

TYPE:

INTEGER

DEFAULT:

NONE

OPTIONS:

$n$ Use a width of $n \times 10^{-4}$ Å.

RECOMMENDATION:

Blur all MM external charges in a QM/MM calculation with the specified width. Gaussian blurring is currently incompatible with PCM calculations. Values of 1.0–2.0 Å are recommended in Ref. 103.

**MODEL_SYSTEM_CHARGE**

Specifies the QM subsystem charge if different from the *$molecule* section.

TYPE:

INTEGER

DEFAULT:

NONE

OPTIONS:

$n$ The charge of the QM subsystem.

RECOMMENDATION:

This option only needs to be used if the QM subsystem (model system) has a charge that is different from the total system charge.

**MODEL_SYSTEM_MULT**

Specifies the QM subsystem multiplicity if different from the *$molecule* section.

TYPE:

INTEGER

DEFAULT:

NONE

OPTIONS:

$n$ The multiplicity of the QM subsystem.

RECOMMENDATION:

This option only needs to be used if the QM subsystem (model system) has a multiplicity that is different from the total system multiplicity. ONIOM calculations must be closed shell.

**USER_CONNECT**

Enables explicitly defined bonds.

TYPE:

STRING

DEFAULT:

FALSE

OPTIONS:

TRUE Bond connectivity is read from the *$molecule* section

FALSE Bond connectivity is determined by atom proximity

RECOMMENDATION:

Set to TRUE if bond connectivity is known, in which case this connectivity must be specified in the *$molecule* section. This greatly accelerates MM calculations.

**MM_SUBTRACTIVE**

Specifies whether a subtractive scheme is used in the $E_{\mathrm{Coul}}$, Eq. (11.38), portion of the calculation.

TYPE:

LOGICAL

DEFAULT:

FALSE

OPTIONS:

FALSE Only pairs that are not 1-2, 1-3, or 1-4 pairs are used.

TRUE All pairs are calculated, and then the pairs that are double counted (1-2, 1-3, and 1-4) are subtracted out.

RECOMMENDATION:

When running QM/MM or MM calculations there is not recommendation. When running a QM/MM Ewald calculation the value must be set to TRUE.

### 11.3.4 QM/MM Examples

- QM/MM Example 1

  Features of this job:

  - Geometry optimization using ONIOM mechanical embedding.
  - MM region (water 1) described using OPLSAA.
  - QM region (water 2) described using PBE0/6-31G*.
  - *$molecule* input section contains user-defined MM bonds. A zero is used as a placeholder if there are no more connections.

**Example 11.19** ONIOM optimization of water dimer.

```
$rem
   METHOD            pbe0
   BASIS             6-31G*
   QM_MM_INTERFACE   oniom
   FORCE_FIELD       oplsaa
   USER_CONNECT      true
   JOBTYPE           opt
   MOLDEN_FORMAT     true
$end
```

```
$qm_atoms
   4 5 6
$end

$molecule
   0 1
   O   -0.790909    1.149780    0.907453  186  2  3  0  0
   H   -1.628044    1.245320    1.376372  187  1  0  0  0
   H   -0.669346    1.913705    0.331002  187  1  0  0  0
   O    1.178001   -0.686227    0.841306  186  5  6  0  0
   H    0.870001   -1.337091    1.468215  187  4  0  0  0
   H    0.472696   -0.008397    0.851892  187  4  0  0  0
$end
```

- QM/MM Example 2

  Features of this job:

  - Janus electronic embedding with a YingYang link atom (the glycosidic carbon at the C1′ position of the deoxyribose).
  - MM region (deoxyribose) is described using AMBER99.
  - QM region (adenine) is described using HF/6-31G*.
  - The first 5 electronically excited states are computed with CIS. MM energy interactions between a QM atom and an MM atom (*e.g.*, van der Waals interactions, as well as angles involving a single QM atom) are assumed to be the same in the excited states as in the ground state.
  - *$molecule* input section contains user-defined MM bonds.
  - Gaussian-blurred charges are used on all MM atoms, with a width set to 1.5 Å.

**Example 11.20** Excited-state single-point QM/MM calculation on deoxyadenosine.

```
$rem
   METHOD            cis
   BASIS             6-31G*
   QM_MM_INTERFACE   janus
   USER_CONNECT      true
   FORCE_FIELD       amber99
   GAUSSIAN_BLUR     true
   GAUSS_BLUR_WIDTH  15000
   CIS_N_ROOTS       5
   CIS_TRIPLETS      false
   MOLDEN_FORMAT     true
   PRINT_ORBITALS    true
$end

$qm_atoms
   18 19 20 21 22 23 24 25 26 27 28 29 30 31
$end

$molecule
   0 1
   O     0.000000     0.000000     0.000000   1244      2      9      0      0
   C     0.000000     0.000000     1.440000   1118      1      3     10     11
   C     1.427423     0.000000     1.962363   1121      2      4      6     12
   O     1.924453    -1.372676     1.980293   1123      3      5      0      0
   C     2.866758   -1.556753    0.934073   1124      4      7     13     18
   C     2.435730    0.816736    1.151710   1126      3      7      8     14
   C     2.832568   -0.159062    0.042099   1128      5      6     15     16
   O     3.554295    1.211441    1.932365   1249      6     17      0      0
   H    -0.918053    0.000000   -0.280677   1245      1      0      0      0
   H    -0.520597   -0.885828    1.803849   1119      2      0      0      0
   H    -0.520597    0.885828    1.803849   1120      2      0      0      0
   H     1.435560    0.337148    2.998879   1122      3      0      0      0
   H     3.838325   -1.808062    1.359516   1125      5      0      0      0
   H     1.936098    1.681209    0.714498   1127      6      0      0      0
   H     2.031585   -0.217259   -0.694882   1129      7      0      0      0
   H     3.838626    0.075227   -0.305832   1130      7      0      0      0
   H     4.214443    1.727289    1.463640   1250      8      0      0      0
   N     2.474231   -2.760890    0.168322   1132      5     19     27      0
   C     1.538394   -2.869204   -0.826353   1136     18     20     28      0
   N     1.421481   -4.070993   -1.308051   1135     19     21      0      0
   C     2.344666   -4.815233   -0.582836   1134     20     22     27      0
   C     2.704630   -6.167666   -0.619591   1140     21     23     24      0
   N     2.152150   -7.057611   -1.455273   1142     22     29     30      0
   N     3.660941   -6.579606    0.239638   1139     22     25      0      0
   C     4.205243   -5.691308    1.066416   1138     24     26     31      0
   N     3.949915   -4.402308    1.191662   1137     25     27      0      0
   C     2.991769   -4.014545    0.323275   1133     18     21     26      0
   H     0.951862   -2.033257   -1.177884   1145     19      0      0      0
   H     2.449361   -8.012246   -1.436882   1143     23      0      0      0
   H     1.442640   -6.767115   -2.097307   1144     23      0      0      0
   H     4.963977   -6.079842    1.729564   1141     25      0      0      0
$end
```

- QM/MM Example 3

  Features of this job:

  - An MM-only calculation. BASIS and EXCHANGE need to be defined, in order to prevent a crash, but no electronic structure calculation is actually performed.
  - All atom types and MM interactions are defined in *$force_field_params* using the CHARMM27 force field. Atomic charges, equilibrium bond distances, and equilibrium angles have been extracted from a HF/6-31G* calculation, but the force constants and van der Waals parameters are fictitious values invented for this example.
  - Molecular dynamics is propagated for 10 steps within a microcanonical ensemble (NVE), which is the only ensemble available at present. Initial velocities are sampled from a Boltzmann distribution at 400 K.

**Example 11.21** MM molecular dynamics with user-defined MM parameters.

```
$rem
   BASIS             sto-3g
   METHOD            hf
   QM_MM_INTERFACE   MM
   FORCE_FIELD       charmm27
   USER_CONNECT      true
   JOBTYPE           aimd
   TIME_STEP         42
   AIMD_STEPS        10
   AIMD_INIT_VELOC   thermal
   AIMD_TEMP         400
```

```
$end

$molecule
  -2 1
   C    0.803090    0.000000    0.000000  -1  2  3  6  0
   C   -0.803090    0.000000    0.000000  -1  1  4  5  0
   H    1.386121    0.930755    0.000000  -2  1  0  0  0
   H   -1.386121   -0.930755    0.000000  -2  2  0  0  0
   H   -1.386121    0.930755    0.000000  -2  2  0  0  0
   H    1.386121   -0.930755    0.000000  -2  1  0  0  0
$end

$force_field_params
   NumAtomTypes 2
   AtomType -1  -0.687157  2.0000  0.1100
   AtomType -2  -0.156422  1.3200  0.0220
   Bond     -1  -1  250.00  1.606180
   Bond     -1  -2  300.00  1.098286
   Angle    -2  -1  -2  50.00  115.870
   Angle    -2  -1  -1  80.00  122.065
   Torsion  -2  -1  -1  -2  2.500  180.0  2
$end
```

Further examples of QM/MM calculations can be found in the *$QC/samples* directory, including a QM/MM/PCM example, `QMMMPCM_crambin.in`. This calculation consists of a protein molecule (crambin) described using a force field, but with one tyrosine side chain described using electronic structure theory. The entire QM/MM system is placed within an implicit solvent model, of the sort described in Section 11.2.2.

## 11.4 Q-CHEM/CHARMM Interface

Q-CHEM can be used a QM back-end for QM/MM calculations using CHARMM package[89]. In this case, both software packages are required to perform the calculations, but all the code required for communication between the programs is incorporated in the released versions. Stand-alone QM/MM calculations are described in Section 11.3.

QM/MM jobs that utilize the CHARMM interface are controlled using the following *$rem* keywords:

**QM_MM**

Turns on the Q-CHEM/CHARMM interface.

TYPE:

LOGICAL

DEFAULT:

FALSE

OPTIONS:

TRUE Do QM/MM calculation through the Q-CHEM/CHARMM interface.

FALSE Turn this feature off.

RECOMMENDATION:

Use the default unless running calculations with CHARMM.

**QMMM_PRINT**

Controls the amount of output printed from a QM/MM job.

TYPE:

LOGICAL

DEFAULT:

FALSE

OPTIONS:

TRUE Limit molecule, point charge, and analysis printing.

FALSE Normal printing.

RECOMMENDATION:

Use the default unless running calculations with CHARMM.

**QMMM_CHARGES**

Controls the printing of QM charges to file.

TYPE:

LOGICAL

DEFAULT:

FALSE

OPTIONS:

TRUE Writes a charges.dat file with the Mulliken charges from the QM region.

FALSE No file written.

RECOMMENDATION:

Use the default unless running calculations with CHARMM where charges on the QM region need to be saved.

**IGDEFIELD**

Triggers the calculation of the electrostatic potential and/or the electric field at the positions of the MM charges.

TYPE:

INTEGER

DEFAULT:

UNDEFINED

OPTIONS:

O Computes ESP.

1 Computes ESP and EFIELD.

2 Computes EFIELD.

RECOMMENDATION:

Must use this *$rem* when IGDESP is specified.

**GEOM_PRINT**

Controls the amount of geometric information printed at each step.

TYPE:

LOGICAL

DEFAULT:

FALSE

OPTIONS:

TRUE Prints out all geometric information; bond distances, angles, torsions.

FALSE Normal printing of distance matrix.

RECOMMENDATION:

Use if you want to be able to quickly examine geometric parameters at the beginning and end of optimizations. Only prints in the beginning of single point energy calculations.

**QMMM_FULL_HESSIAN**

Trigger the evaluation of the full QM/MM Hessian.

TYPE:

LOGICAL

DEFAULT:

FALSE

OPTIONS:

TRUE Evaluates full Hessian.

FALSE Hessian for QM-QM block only.

RECOMMENDATION:

None

**LINK_ATOM_PROJECTION**

Controls whether to perform a link-atom projection

TYPE:

LOGICAL

DEFAULT:

TRUE

OPTIONS:

TRUE Performs the projection

FALSE No projection

RECOMMENDATION:

Necessary in a full QM/MM Hessian evaluation on a system with link atoms

**HESS_AND_GRAD**

Enables the evaluation of both analytical gradient and Hessian in a single job

TYPE:

LOGICAL

DEFAULT:

FALSE

OPTIONS:

TRUE Evaluates both gradient and Hessian.

FALSE Evaluates Hessian only.

RECOMMENDATION:

Use only in a frequency (and thus Hessian) evaluation.

**GAUSSIAN_BLUR**

Enables the use of Gaussian-delocalized external charges in a QM/MM calculation.

TYPE:

LOGICAL

DEFAULT:

FALSE

OPTIONS:

TRUE Delocalizes external charges with Gaussian functions.

FALSE Point charges

RECOMMENDATION:

None

**SKIP_CHARGE_SELF_INTERACT**

Ignores the electrostatic interactions among external charges in a QM/MM calculation.

TYPE:

LOGICAL

DEFAULT:

FALSE

OPTIONS:

TRUE No electrostatic interactions among external charges.

FALSE Computes the electrostatic interactions among external charges.

RECOMMENDATION:

None

**Example 11.22** Do a basic QM/MM optimization of the water dimer. You need CHARMM to do this but this is the Q-CHEM file that is needed to test the QM/MM functionality. These are the bare necessities for a Q-CHEM/CHARMM QM/MM calculation.

```
$molecule
   0 1
   O    -0.91126   1.09227   1.02007
   H    -1.75684   1.51867   1.28260
   H    -0.55929   1.74495   0.36940
$end


$rem
   METHOD        hf        ! HF Exchange
   BASIS         cc-pvdz   ! Correlation Consistent Basis
   QM_MM         true      ! Turn on QM/MM calculation
   JOBTYPE       force     ! Need this for QM/MM optimizations
$end

$external_charges
   1.20426      -0.64330   0.79922  -0.83400
   1.01723      -1.36906   1.39217   0.41700
   0.43830      -0.06644   0.91277   0.41700
$end
```

The Q-CHEM/CHARMM interface is unique in that:

- The external point charges can be replaced with Gaussian-delocalized charges with a finite width[103]. This is an empirical way to include the delocalized character of the electron density of atoms in the MM region. This can be important for the electrostatic interaction of the QM region with nearby atoms in the MM region.
- We allow the evaluation of the full QM/MM Hessian[104]. When link atoms are inserted to saturate the QM region, all Hessian elements associated with link atoms are automatically projected onto their QM and MM host atoms.
- For systems with a large number of MM atoms, one can define blocks consisting of multiple MM atoms (*i.e.*, mobile blocks) and efficiently evaluate the corresponding mobile-block Hessian (MBH) for normal mode analysis.

## 11.5 Effective Fragment Potential Method

The Effective Fragment Potential (EFP) method is a computationally inexpensive way of modeling intermolecular interactions in non-covalently bound systems. The EFP approach can be viewed as a QM/MM scheme with no empirical parameters. Originally EFP was developed by Gordon's group[105,106], and was implemented in GAMESS[107]. A review of the EFP theory and applications can be found in Ref. 108,109. A related approach, also based on distributed multipoles, is called XPol; it is described in Section 12.9.

A new implementation of the EFP method based on the libefp library (see `http://www.libefp.org`) has been added to Q-Chem.[110] The new EFP module is called EFPMAN2. EFPMAN2 can run calculations in parallel on a shared memory multi-core computer and is much faster than the previous EFP implementation in Q-Chem. EFPMAN2 is interfaced with CCMAN and CCMAN2 modules to allow coupled cluster and EOM-CC calculations with EFP. CIS and TDDFT calculations with EFP are also available.

### 11.5.1 Theoretical Background

The total energy of the system consists of the interaction energy of the effective fragments ($E^{\text{ef}-\text{ef}}$) and the energy of the *ab initio* (*i.e.*, QM) region in the field of the fragments. The former includes electrostatics, polarization, dispersion and exchange-repulsion contributions (the charge-transfer term, which might be important for description of the ionic and highly polar species, is omitted in the current implementation):

$$E^{\text{ef-ef}} = E_{\text{elec}} + E_{\text{pol}} + E_{\text{disp}} + E_{\text{ex-rep}}. \tag{11.49}$$

The QM-EF interactions are computed as follows. The electrostatics and polarization parts of the EFP potential contribute to the quantum Hamiltonian via one-electron terms,

$$H'_{pq} = H_{pq} + \langle p|\hat{V}^{\text{elec}} + \hat{V}^{\text{pol}}|q\rangle \tag{11.50}$$

whereas dispersion and exchange-repulsion QM-EF interactions are treated as additive corrections to the total energy.

The electrostatic component of the EFP energy accounts for Coulomb interactions. In molecular systems with hydrogen bonds or polar molecules, this is the leading contribution to the total inter-molecular interaction energy[111]. An accurate representation of the electrostatic potential is achieved by using multipole expansion (obtained from the Stone's distributed multipole analysis) around atomic centers and bond midpoints (*i.e.*, the points with high electronic density) and truncating this expansion at octupoles[105,106,112,113].

The fragment-fragment electrostatic interactions consist of charge-charge, charge-dipole, charge-quadrupole, charge-octupole, dipole-dipole, dipole-quadrupole, and quadrupole-quadrupole terms, as well as terms describing interactions of electronic multipoles with the nuclei and nuclear repulsion energy.

Electrostatic interaction between an effective fragment and the QM part is described by perturbation $\hat{V}^{\text{elec}}$ of the *ab initio* Hamiltonian (see Eq. (11.50)). The perturbation enters the one-electron part of the Hamiltonian as a sum of contributions from the expansion points of the effective fragments. Contribution from each expansion point consists of four terms originating from the electrostatic potential of the corresponding multipole (charge, dipole, quadrupole, and octupole).

The multipole representation of the electrostatic density of a fragment breaks down when the fragments are too close. The multipole interactions become too repulsive due to significant overlap of the electronic densities and the charge-penetration effect. The magnitude of the charge-penetration effect is usually around 15% of the total electrostatic energy in polar systems, however, it can be as large as 200% in systems with weak electrostatic interactions[114]. To account for the charge-penetration effect, the simple exponential damping of the charge-charge term is used[114,115]. The charge-charge screened energy between the expansion points $k$ and $l$ is given by the following expression, where $\alpha_k$ and $\alpha_l$ are the damping parameters associated with the corresponding expansion points:

$$\begin{aligned} E_{kl}^{\text{ch-ch}} &= \left[1-(1+\alpha_k R_{kl}/2)e^{-\alpha_k R_{kl}}\right] q^k q^l / R_{kl} \quad , \text{ if } \alpha_k = \alpha_l \\ \text{or} \quad &= \left(1 - \frac{\alpha_l^2}{\alpha_l^2-\alpha_k^2} e^{-\alpha_k R_{kl}} - \frac{\alpha_k^2}{\alpha_k^2-\alpha_l^2} e^{-\alpha_l R_{kl}}\right) q^k q^l / R_{kl} \quad , \text{ if } \alpha_k \neq \alpha_l \end{aligned} \tag{11.51}$$

Damping parameters are included in the potential of each fragment, but QM-EFP electrostatic interactions are currently calculated without damping corrections.

Alternatively, one can obtain the short-range charge-penetration energy using the spherical Gaussian overlap (SGO) approximation[116]:

$$E_{kl}^{\text{pen}} = -2\left(\frac{1}{-2ln|S_{kl}|}\right)^{\frac{1}{2}} \frac{S_{kl}^2}{R_{kl}} \tag{11.52}$$

where $S_{kl}$ is the overlap integral between localized MOs $k$ and $l$ (calculated for the exchange-repulsion term, Eq. (11.62)). This charge-penetration energy is calculated and printed separately from the rest of the electrostatic energy. Using overlap-based damping generally results in a more balanced description of intermolecular interactions and is recommended.

Polarization accounts for the intramolecular charge redistribution in response to external electric field. It is the major component of many-body interactions responsible for cooperative molecular behavior. EFP employs distributed polarizabilities placed at the centers of valence LMOs. Unlike the isotropic total molecular polarizability tensor, the distributed polarizability tensors are anisotropic.

The polarization energy of a system consisting of an *ab initio* and effective fragment regions is computed as[105]

$$E^{\text{pol}} = -\frac{1}{2}\sum_k \mu^k (F^{\text{mult},k} + F^{\text{ai,nuc},k}) + \frac{1}{2}\sum_k \bar{\mu}^k F^{\text{ai,elec},k} \tag{11.53}$$

where $\mu^k$ and $\bar{\mu}^k$ are the induced dipole and the conjugated induced dipole at the distributed point $k$; $F^{\text{mult},k}$ is the external field due to static multipoles and nuclei of other fragments, and $F^{\text{ai,elec},k}$ and $F^{\text{ai,nuc},k}$ are the fields due to the electronic density and nuclei of the *ab initio* part, respectively.

The induced dipoles at each polarizability point $k$ are computed as

$$\mu^k = \alpha^k F^{\text{total},k} \tag{11.54}$$

where $\alpha^k$ is the distributed polarizability tensor at $k$. The total field $F^{\text{total},k}$ comprises from the static field and the field due to other induced dipoles, $F_k^{\text{ind}}$, as well as the field due to nuclei and electronic density of the *ab initio* region:

$$F^{\text{ai,total},k} = F^{\text{mult},k} + F^{\text{ind},k} + F^{\text{ai,elec},k} + F^{\text{ai,nuc},k} \tag{11.55}$$

As follows from the above equation, the induced dipoles on a particular fragment depend on the values of the induced dipoles of all other fragments. Moreover, the induced dipoles on the effective fragments depend on the *ab initio* electronic density, which, in turn, is affected by the field created by these induced dipoles through a one electron contribution to the Hamiltonian:

$$\hat{V}^{\text{pol}} = -\frac{1}{2}\sum_k \sum_a^{x,y,z} \frac{(\mu_a^k + \bar{\mu}_a^k)a}{R^3} \tag{11.56}$$

where $R$ and $a$ are the distance and its Cartesian components between an electron and the polarizability point $k$. In sum, the total polarization energy is computed self-consistently using a two level iterative procedure. The objectives of the higher and lower levels are to converge the wave function and induced dipoles for a given fixed wave function, respectively. In the absence of the *ab initio* region, the induced dipoles of the EF system are iterated until self-consistent with each other.

Self-consistent treatment of polarization accounts for many-body interaction effects. Polarization energy between EFP fragments is augmented by gaussian-like damping functions with default parameter $\alpha = \beta = 0.6$, applied to electric field $F$[116]:

$$F = F_0 f^{\text{damp}} \tag{11.57}$$

$$f^{\text{damp}} = 1.0 - exp(-\sqrt{\alpha\beta}r^2)(1 + \sqrt{\alpha\beta}r^2) \tag{11.58}$$

Dispersion provides a leading contribution to van der Waals and $\pi$-stacking interactions. The dispersion interaction is expressed as the inverse $R$ dependence:

$$E^{\text{disp}} = \sum_n C_6 R^{-6} \tag{11.59}$$

where coefficients $C_6$ are derived from the frequency-dependent distributed polarizabilities with expansion points located at the LMO centroids, *i.e.*, at the same centers as the polarization expansion points. The higher-order dispersion terms (induced dipole-induced quadrupole, induced quadrupole/induced quadrupole, *etc.*) are approximated as $1/3$ of the $C_6$ term[117].

For small distances between effective fragments dispersion interactions are corrected for charge penetration and electronic density overlap effect either with the Tang-Toennies damping formula[118] with parameter $b = 1.5$:

$$C_6^{kl} \to \left(1 - e^{-bR}\sum_{k=0}^{6}\frac{(bR)^k}{k!}\right) C_6^{kl} \tag{11.60}$$

or using interfragment overlap (so called overlap-based damping)[116]:

$$C_6^{kl} \to \left(1 - S_{kl}^2\left(1 - 2\log|S_{kl}| + 2\log^2|S_{kl}|\right)\right) C_6^{kl} \tag{11.61}$$

QM-EFP dispersion interactions are currently disabled.

Exchange-repulsion originates from the Pauli exclusion principle, which states that the wave function of two identical fermions must be anti-symmetric. In traditional classical force fields, exchange-repulsion is introduced as a positive (repulsive) term, *e.g.*, $R^{-12}$ in the Lennard-Jones potential. In contrast, EFP uses a wave function-based formalism to account for this inherently quantum effect. Exchange-repulsion is the only non-classical component of EFP and the only one that is repulsive.

The exchange-repulsion interaction is derived as an expansion in the intermolecular overlap, truncated at the quadratic term[119,120], which requires that each effective fragment carries a basis set that is used to calculate overlap and kinetic one-electron integrals for each interacting pair of fragments. The exchange-repulsion contribution from each pair of localized orbitals $i$ and $j$ belonging to fragments $A$ and $B$, respectively, is:

$$\begin{aligned} E_{ij}^{\mathrm{exch}} &= -4\sqrt{\frac{-2\ln|S_{ij}|}{\pi}}\,\frac{S_{ij}^2}{R_{ij}} \\ &\quad -2S_{ij}\left(\sum_{k\in A}F_{ik}^{A}S_{kj}+\sum_{l\in B}F_{jl}^{B}S_{il}-2T_{ij}\right) \\ &\quad +2S_{ij}^2\left(\sum_{J\in B}-Z_J R_{iJ}^{-1}+2\sum_{l\in B}R_{il}^{-1}+\sum_{I\in A}-Z_I R_{Ij}^{-1}+2\sum_{k\in A}R_{kj}^{-1}-R_{ij}^{-1}\right) \end{aligned} \tag{11.62}$$

where $i$, $j$, $k$ and $l$ are the LMOs, $I$ and $J$ are the nuclei, $S$ and $T$ are the intermolecular overlap and kinetic energy integrals, and $F$ is the Fock matrix element.

The expression for the $E_{ij}^{\mathrm{exch}}$ involves overlap and kinetic energy integrals between pairs of localized orbitals. In addition, since Eq. (11.62) is derived within an infinite basis set approximation, it requires a reasonably large basis set to be accurate [6-31+G* is considered to be the smallest acceptable basis set, 6-311++G(3df,2p) is recommended]. These factors make exchange-repulsion the most computationally expensive part of the EFP energy calculations of moderately sized systems.

Large systems require additional considerations. Since total exchange-repulsion energy is given by a sum of terms in Eq. (11.62) over all the fragment pairs, its computational cost formally scales as $\mathcal{O}(N^2)$ with the number of effective fragments $N$. However, exchange-repulsion is a short-range interaction; the overlap and kinetic energy integrals decay exponentially with the inter-fragment distance. Therefore, by employing a distance-based screening, the number of overlap and kinetic energy integrals scales as $\mathcal{O}(N)$. Consequently, for large systems exchange-repulsion may become less computationally expensive than the long-range components of EFP (such as Coulomb interactions).

The QM-EFP exchange-repulsion energy is currently disabled.

### 11.5.2 Excited-State Calculations with EFP

Interface of EFP with EOM-CCSD (both via CCMAN and CCMAN2), CIS, CIS(D), and TDDFT has been developed[121,122]. In the EOM-CCSD/EFP calculations, the reference-state CCSD equations for the $T$ cluster amplitudes are solved with the HF Hamiltonian modified by the electrostatic and polarization contributions due to the effective fragments, Eq. (11.50). In the coupled-cluster calculation, the induced dipoles of the fragments are frozen at their HF values.

The transformed Hamiltonian $\bar{H}$ effectively includes Coulomb and polarization contributions from the EFP part. As $\bar{H}$ is diagonalized in an EOM calculation, the induced dipoles of the effective fragments are frozen at their reference state value, *i.e.*, the EOM equations are solved with a constant response of the EFP environment. To account for solvent response to electron rearrangement in the EOM target states (*i.e.*, excitation or ionization), a perturbative non-iterative correction is computed for each EOM root as follows. The one-electron density of the target EOM state (excited or ionized) is calculated and used to re-polarize the environment, *i.e.*, to recalculate the induced dipoles of the EFP part in the field of an EOM state. These dipoles are used to compute the polarization energy corresponding to this state.

The total energy of the excited state with inclusion of the perturbative response of the EFP polarization is:

$$E_{\rm IP}^{\rm EOM/EFP} = E_{\rm EOM} + \Delta E_{\rm pol} \tag{11.63}$$

where $E_{\rm EOM}$ is the energy found from EOM-CCSD procedure and $\Delta E_{\rm pol}$ has the following form:

$$\begin{aligned}\Delta E_{\rm pol} \quad = \quad & \frac{1}{2}\sum_{k}\sum_{a}^{x,y,z}\Big[-(\mu_{{\rm ex},a}^{k}-\mu_{{\rm gr},a}^{k})(F_a^{{\rm mult},k}+F_a^{{\rm nuc},k}) \\ & +(\tilde{\mu}_{{\rm ex},a}^{k}F_{{\rm ex},a}^{{\rm ai},k}-\tilde{\mu}_{{\rm gr},a}^{k}F_{{\rm gr},a}^{{\rm ai},k})-(\mu_{{\rm ex},a}^{k}-\mu_{{\rm gr},a}^{k}+\tilde{\mu}_{{\rm ex},a}^{k}-\tilde{\mu}_{{\rm gr},a}^{k})F_{{\rm ex},a}^{{\rm ai},k}\Big]\end{aligned} \tag{11.64}$$

where $F_{\rm gr}^{\rm ai}$ and $F_{\rm ex}^{\rm ai}$ are the fields due to the reference (HF) state and excited-state electronic densities, respectively. $\mu_{\rm gr}^{k}$ and $\tilde{\mu}_{\rm gr}^{k}$ are the induced dipole and conjugated induced dipole at the distributed polarizability point $k$ consistent with the reference-state density, while $\mu_{\rm ex}^{k}$ and $\tilde{\mu}_{\rm ex}^{k}$ are the induced dipoles corresponding to the excited state density.

The first two terms in Eq. (11.64) provide a difference of the polarization energy of the QM/EFP system in the excited and ground electronic states; the last term is the leading correction to the interaction of the ground-state-optimized induced dipoles with the wave function of the excited state.

The EOM states have both direct and indirect polarization contributions. The indirect term comes from the orbital relaxation of the solute in the field due to induced dipoles of the solvent. The direct term given by Eq. (11.64) is the response of the polarizable environment to the change in solute's electronic density upon excitation. Note that the direct polarization contribution can be very large (tenths of eV) in EOM-IP/EFP since the electronic densities of the neutral and the ionized species are very different.

An important advantage of the perturbative EOM/EFP scheme is that it does not compromise multi-state nature of EOM and that the electronic wave functions of the target states remain orthogonal to each other since they are obtained with the same (reference-state) field of the polarizable environment. For example, transition properties between these states can be calculated.

EOM-CC/EFP scheme works with any type of the EOM excitation operator $R_k$ currently supported in Q-CHEM, *i.e.*, spin-flipping (SF), excitation energies (EE), ionization potential (IP), electron affinity (EA) (see Section 6.7.12 for details). However, direct polarization correction requires calculation of one-electron density of the excited state, and will be computed only for the methods with implemented one-electron properties.

Implementation of CIS/EFP, CIS(D)/EFP, and TDDFT/EFP methods is similar to the implementation of EOM/EFP. Polarization correction as in Eq. 11.64 is calculated and added to the CIS or TDDFT excitation energies.

### 11.5.3 Extension to Macromolecules: Fragmented EFP Scheme

Macromolecules such as proteins or DNA present a large number of electronic structure problems (photochemistry, redox chemistry, reactivity) that can be described within QM/EFP framework. EFP has been extended to deal with such complex systems via the so-called fragmented EFP scheme (fEFP). The current Q-CHEM implementation allows one to (i) compute interaction energy between a ligand and a macromolecule (both represented by EFP) and (ii) to calculate the excitation energies, ionization potentials, electronic affinities of a QM moiety interacting with a fEFP macromolecule using QM/EFP scheme (see Section 11.5.2). In the present implementation, the ligand cannot be covalently bound to the macromolecule.

There are multiple ways to cut a large molecule into units depending on the position of the cut between two covalently bound residues. An obvious way to cut a protein is to cut through peptide bonds such that each fragment represents one amino acid. Alternatively, one can cut bonds between two atoms of the same nature (carbonyl and carbon-$\alpha$ or carbon-$\alpha$ and the first carbon of the side chain). The user can choose the most appropriate way to cut.

Consider a protein ($P$) consisting of $N$ amino acids, $A_1A_2\ldots A_N$, and is split into $N$ fragments ($A_i$). The fragments can be saturated by either Hydrogen Link Atom[83] (HLA) or by mono-valent groups of atoms from the neighboring fragment(s) called hereafter Cap Link Atom (CLA). If fragments are capped using the HLA scheme, the hydrogen is located along the peptide bond axis and at the distance corresponding to the equilibrium bond length of a CH bond:

$$P = A_1H + \sum_{i=2}^{N-1} HA_iH + HA_N \tag{11.65}$$

In the CLA scheme, the cap has exactly the same geometry as the respective neighboring group. If the cuts are made through peptide bonds (one fragment is one amino acid), the caps ($C^i$) are either an aldehyde to saturate the -N(H) end of the fragment, or an amine to saturate the -C(=O) extremity of the fragment.

$$P = A_1C^2 + \sum_{i=2}^{N-1} C^{i-1}A_iC^{i+1} + C^{N-1}A_N \tag{11.66}$$

Q-CHEM provides a two-step script, `prefefp.pl`, located in *$QC/bin* which takes a PDB file and breaks it into capped fragments in the GAMESS format, such that the EFP parameters for these capped fragments can be generated, as explained in Section 11.5.7. As the EFP parameters are generated for each capped fragment, the neighboring fragments have duplicated parameter points (overlapping areas) in both the HLA and CLA schemes due to the overlapping caps. Since multipole expansion points and polarizability expansion points are computed on each capped residue by the standard procedure, the multipole (and damping terms) and polarizabilities need to be removed ($C^{\emptyset}$) from the overlapping areas.

Equations (11.65) and (11.66) become:

$$P = A_1C^{\emptyset} + \sum_{i=2}^{N-1} C^{\emptyset}A_iC^{\emptyset} + C^{\emptyset}A_N \tag{11.67}$$

The details concerning this removing procedure are presented in Section 11.5.7.

Once these duplicate parameters are removed from the EFP parameters of the capped fragments, the EFP-EFP and QM-EFP calculations can be conducted as usual.

Currently, fEFP includes electrostatic and polarization contributions, which appear in EFP(ligand)/fEFP(macromolecule) and in QM/fEFP calculations (note that the QM part is not covalently bound to the macromolecule). Consequently, the total interaction energy ($E^{\text{tot}}$) between a ligand ($L$) and a protein ($P$) divided into fragments is:

$$E^{\text{tot}}(P-L) = E^{\text{elec}}(P-L) + E^{\text{pol}}(P-L) \tag{11.68}$$

The electrostatics is an additive term; its contribution to fragment-fragment and ligand-fragment interaction is computed as follows:

$$E^{\text{elec}}(P-L) = \sum_{i}^{N} E^{\text{elec}}\left(C^{\emptyset}A_{i=1}C^{\emptyset} - L\right) \tag{11.69}$$

The polarization contribution in an EFP system (no QM) is:

$$E^{\text{pol}}(P-L) = -\frac{1}{2}\sum_{k\in P,L} \mu^k F^{\text{mult},k} + \frac{1}{2}\sum_{k\in P} \mu^k F^{\text{mult},k} \tag{11.70}$$

The first term is the polarization energy obtained upon convergence of the induced dipoles of the ligand ($\mu^k_{\text{efp}}(L)$) and all fragments ($\mu^k_{\text{fefp}}(A_i)$). The system is thus fully polarized, all fragments (A$_i$ or L) are polarizing each other until self-consistency.

$$\begin{aligned} \mu^k_{\text{efp}}(L) &= \sum_{k\in A_i} \alpha^k (F^{\text{mult},k} + F^{\text{ind},k}) \\ \mu^k_{fefp}(A_i) &= \sum_{j\neq i}\sum_{k\in L,A_j} \alpha^k (F^{\text{mult},k} + F^{\text{ind},k}) \end{aligned} \tag{11.71}$$

The second term of Eq. (11.70) is the polarization of the protein by itself; this value has to be subtracted once the induced dipoles (Eq. 11.71) converged.

The LA scheme is available to perform QM/fEFP job. In this situation the fEFP has to include a macromolecule (covalent bond between fragments). This scheme is not able yet to perform QM/fEFP/EFP in which a macromolecule and solvent molecules would be described at the EFP level of theory.

In addition to the HLA and CLA schemes, Q-CHEM also features Molecular Fragmentation with Conjugated Caps approach (MFCC) which avoids the issue of overlapping of saturated fragments and was developed in 2003 by Zhang[123,124]. MFCC procedure consists of a summation over the interactions between a ligand and capped residues (CLA scheme) and a subtraction over the interactions of merged caps ($C^{i+1}C^{i-1}$), the so-called "concaps", with the ligand. $N-1$ concap fragments are actually used to subtract the overlapping effect.

$$P = A_1C^2 + \sum_{i=2}^{N-1} C^{i-1}A_iC^{i+1} + C^{N-1}A_N - \sum_{i}^{N-1} C^{i+1}C^{i-1} \tag{11.72}$$

In this scheme the contributions due to overlapping caps simply cancel out and the EFP parameters do not need any modifications, in contrast to the HLA or CLA procedures. However, the number of parameters that need to be generated is larger ($N$ capped fragments + $N-1$ concaps).

The MFCC electrostatic interaction energy is given as the sum of the interaction energy between each capped fragment ($C^{i-1}A_iC^{i+1}$) and the ligand minus the interaction energy between each concap ($C^{i-1}C^{i+1}$) and the ligand:

$$E^{\text{elec}}(P-L) = \sum_{i}^{N} E^{\text{elec}}\left(C^{i-1}A_iC^{i+1} - L\right) - \sum_{i}^{N-1} E^{\text{elec}}\left(C^{i-1}C^{i+1} - L\right) \tag{11.73}$$

The main advantage of MFCC is that the multipole expansion obtained on each capped residue or concap are kept during the $E^{\text{elec}}(P-L)$ calculation. In the present implementation, there are no polarization contributions. The MFCC scheme is not yet available for QM/fEFP.

## 11.5.4 Running EFP Jobs

The current version supports single point calculations in systems consisting of ($i$) *ab initio* and EFP regions (QM/MM); or ($ii$) EFP region only. The *ab initio* region can be described by conventional quantum methods like HF, DFT, or correlated methods including methods for the excited states [CIS, CIS(D), TDDFT, EOM-CCSD methods]. Theoretical details on the interface of EFP with EOM-CCSD and CIS(D) can be found in Refs. 121,122.

**Note:** EFP provides both implicit (through orbital response) and explicit (as instantaneous response of the polarizable EFP fragments) corrections to the electronic excited states. EFP-modified excitation energies are printed in the property section of the output.

Electrostatic, polarization, exchange-repulsion, and dispersion contributions are calculated between EFs; only electrostatic and polarization terms are evaluated between *ab initio* and EF regions.

The *ab initio* region is specified by regular Q-CHEM input using *$molecule* and *$rem* sections. In calculations with no QM part, the *$molecule* section should contain a dummy atom (for example, helium).

Positions of EFs are specified in the *$efp_fragments* section. Two geometry formats are available for fragments, Euler angle format and XYZ format. In Euler angle format, each line in this section contains the information on an individual fragment: fragment's name and position, specified by center-of-mass coordinates ($x$, $y$, $z$) and the Euler rotation angles ($\alpha$, $\beta$, $\gamma$) relative to the fragment frame, *i.e.*, the coordinates of the standard fragment provided in the fragment library. The XYZ format is identical to the coordinate format used in GAMESS; i.e., the name of the fragment is provided on the first line followed by three lines specifying names and x,y,z coordinates of first three atoms of the fragment.

When using EFPMAN2 you can also specify positions and orientations of the fragments using ($x$, $y$, $z$) coordinates of the first three atoms of the fragment. To enable this feature use EFP_COORD_XYZ keyword. The format of input goes as follows: for each fragment the first line should contain the name of the fragment and the following three lines should specify coordinates of the three first atoms belonging to a fragment. The sample input can be found in the examples section below.

### 11.5.5 Library of Fragments

The effective fragments are rigid and their potentials are generated from a set of *ab initio* calculations on each unique isolated fragment. The EFP includes: ($i$) multipoles (produced by the Stone's Distributed Multipolar Analysis) for Coulomb and polarization terms; ($ii$) static polarizability tensors centered at localized molecular orbital (LMO) centroids (obtained from coupled-perturbed Hartree-Fock calculations), which are used for calculations of polarization; ($iii$) dynamic polarizability tensors centered on the LMOs that are generated by time-dependent HF calculations and used for calculations of dispersion; and ($iv$) the Fock matrix, basis set, and localized orbitals needed for the exchange-repulsion term. Additionally, the EF potential contains coordinates of atoms, coordinates of the points of multi-polar expansion (typically, atoms and bond mid-points), coordinates of the LMO centroids, electrostatic and polarization screening parameters, and atomic labels of the EF atoms.

Q-CHEM provides a library of standard fragments with precomputed effective fragment potentials. Currently the library includes common organic solvents, nucleobases, and molecules from S22 and S66 datasets for non-covalent interactions; see Table 11.7. EFP potentials in GAMESS format are supported by new EFPMAN2 module. They are stored in *$QCAUX/fraglib* directory.

**Note:** The fragments from Q-CHEM fragment library have _L added to their names to distinguish them from user-defined fragments.

The parameters for the standard fragments were computed as follows. The geometries of the solvent molecules were optimized by MP2/cc-pVTZ; geometries of nucleobases were optimized with RI-MP2/cc-pVTZ. Geometries of molecules from S22 and S66 datasets are discussed in Ref.125. The EFP parameters were obtained in GAMESS. To generate the electrostatic multipoles and electrostatic screening parameters, analytic DMA procedure was used, with 6-31+G* basis for non-aromatic compounds and 6-31G* for aromatic compounds and nucleobases. The rest of the potential, *i.e.*, static and dynamic polarizability tensors, wave function, Fock matrix, *etc.*, were obtained using 6-311++G(3df,2p) basis set.

Table 11.7: Standard fragments available in Q-CHEM

| | |
|---|---|
| acetone | ACETONE_L |
| acetonitrile | ACETONITRILE_L |
| adenine | ADENINE_L |
| ammonia | AMMONIA_L |
| benzene | BENZENE_L |
| carbon tetrachloride | CCL4_L |
| cytosine C1 | CYTOSINE_C1_L |
| cytosine C2a | CYTOSINE_C2A_L |
| cytosine C2b | CYTOSINE_C2B_L |
| cytosine C3a | CYTOSINE_C3A_L |
| cytosine C3b | CYTOSINE_C3B_L |
| dichloromethane | DCM_L |
| dimethyl sulfoxide | DMSO_L |
| guanine enol N7 | GUANINE_EN7_L |
| guanine enol N9 | GUANINE_EN9_L |
| guanine enol N9RN7 | GUANINE_EN9RN7_L |
| guanine keton N7 | GUANINE_KN7_L |
| guanine keton N9 | GUANINE_KN9_L |
| methane | METHANE_L |
| methanol | METHANOL_L |
| phenol | PHENOL_L |
| thymine | THYMINE_L |
| toluene | TOLUENE_L |
| water | WATER_L |
| acetamide, S66, gas phase | ACETAMIDE_L |
| acetamide, S66, H-bonded dimer | ACETAMIDE_HB_L |
| acetic acid, S66, gas phase | ACETICAC_L |
| acetic acid, S66, H-bonded dimer | ACETICAC_HB_L |
| adenine, S22 stack dimer | ADENINE_L |
| adenine, S22 WC dimer | ADENINE_WC_L |
| 2-aminopyridine, S22 | AMINOPYRIDINE_L |
| cyclopentane, S66 | CPENTANE_L |
| ethylene | ETHENE_L |
| acetylene | ETHYNE_L |
| formic acid, S22 H-bonded dimer | FORMICAC_HB_L |
| formamide, S22 dimer | FORMID_L |
| hydrogen cyanide | HCN_L |
| indole, S22 | INDOLE_L |
| methylamine, S66 | MENH2_L |
| neopentane, S66 | NEOPENTANE_L |
| $O_2$ | O2_L |
| pentane, S66 | PENTANE_L |
| peptide, S66 | PEPTIDE_L |
| pyrazine | PYRAZINE_L |
| pyridine, S66 | PYRIDINE_L |
| 2-pyridoxine, S22 | PYRIDOXINE_L |
| thymine, S22 stack dimer | THYMINE_L |
| thymine, S22 WC dimer | THYMINE_WC_L |
| uracil, S66, gas phase | URACIL_L |
| uracil, S66, H-bonded dimer | URACIL_HB_L |

### 11.5.6 Calculation of User-Defined EFP Potentials

User-defined EFP parameters can be generated in MAKEFP job in GAMESS (see the GAMESS manual for details).

The EFP potential generation begins by determining an accurate structure for the fragment (EFP is the frozen-geometry potential, so the fragment geometry will remain the same in all subsequent calculations). We recommend MP2/cc-PVTZ level of theory.

#### 11.5.6.1 Generating EFP Parameters in GAMESS

EFP parameters can be generated in GAMESS using MAKEFP job (RUNTYP=MAKEFP). For EFP parameters calculations, 6-311++G(3df,2p) basis set is recommended. Original Stone's distributed multipole analysis (bigexp=0 in the group $stone is recommended for non-aromatic compound; optionally, one may decrease the basis set to 6-31G* or 6-31+G* for generation of electrostatic multipoles and screening parameters. (To prepare such a "mixed" potential, one has to run two separate MAKEFP calculations in larger and smaller bases, and combine the corresponding parts of the potential). In aromatic compounds, one must either use numerical grid for generation of multipoles (bigexp=4.0) or use 6-31G* basis with standard analytic DMA, which is recommended. The MAKEFP job produces (usually in the scratch directory) the .efp file containing all the necessary EFP parameters. See GAMESS manual for further details. Below are examples of the RUNTYP=MAKEFP GAMESS input file for water and benzene.

```
GAMESS input example for water.

 $contrl units=angs local=boys runtyp=makefp coord=cart icut=11 $end
 $system timlim=99999 mwords=200 $end
 $scf soscf=.f. diis=.t. conv=1.0d-06 $end
 $basis gbasis=n311 ngauss=6 npfunc=2 ndfunc=3 nffunc=1
   diffs=.t. diffsp=.t. $end
 $stone
   bigexp=0.0
 $end
 $damp ifttyp(1)=3,2 iftfix(1)=1,1 thrsh=500.0 $end
 $dampgs
h3=h2
bo31=bo21
 $end
 $data
 water h2o (geometry: mp2/cc-pvtz)
 c1
o1 8.0  0.0000  0.0000  0.1187
h2 1.0 0.0000  0.7532 -0.4749
h3 1.0 0.0000 -0.7532 -0.4749
 $end

GAMESS input example for benzene.

 $contrl units=bohr local=boys runtyp=makefp coord=cart icut=11 $end
 $system timlim=99999 mwords=200 $end
 $scf soscf=.f. diis=.t. conv=1.0d-06  $end
 $basis gbasis=n311 ngauss=6 npfunc=2 ndfunc=3 nffunc=1
   diffs=.t. diffsp=.t. $end
 $stone
   bigexp=4.0
 $end
 $damp ifttyp(1)=3,2 iftfix(1)=1,1 thrsh=500.0 $end
 $dampgs
c6=c5
c2=c1
c3=c1
c4=c1
c5=c1
c6=c1
h8=h7
h9=h7
h10=h7
h11=h7
h12=h7
bo32=bo21
bo43=bo21
bo54=bo21
bo61=bo21
bo65=bo21
bo82=bo71
bo93=bo71
bo104=bo71
bo115=bo71
bo126=bo71
 $end
 $data
benzene c6h6 (geometry: mp2/cc-pvtz)
c1
c1     6.0    1.3168      -2.2807       0.0000
c2     6.0    2.6336       0.0000       0.0000
c3     6.0    1.3168       2.2807       0.0000
c4     6.0   -1.3168       2.2807       0.0000
c5     6.0   -2.6336      -0.0000       0.0000
c6     6.0   -1.3168      -2.2807       0.0000
h7     1.0    2.3386      -4.0506       0.0000
h8     1.0    4.6772       0.0000       0.0000
h9     1.0    2.3386       4.0506       0.0000
h10    1.0   -2.3386       4.0506       0.0000
h11    1.0   -4.6772       0.0000       0.0000
h12    1.0   -2.3386      -4.0506       0.0000
 $end
```

### 11.5.7 fEFP Input Structure

A two-step script, `prefefp.pl` located in *$QC/bin*, allows users to break molecular structures from a PDB file into the capped fragments in the GAMESS format, such that parameters for fEFP calculations can be generated.

To use the `prefefp.pl` scripts you need a PDB file, a MAP file, and a directory with all your .efp parameter files. Run the following commands to: (1) obtain the $N$ input file generating the $N$ EFP parameters for the $N$ capped fragments, and (2) create the EFP input file in XYZ format.

```
perl prefp.pl 1 <PDB file> <MAP file>
perl prefp.pl 2 <PDB file> <.efp path> <MAP file> <GMS input file name>
```

At the first step the script splits the biomolecule (PDB format) into $N$ fragments generating $N$ GAMESS MAKEFP input files with the help of a MAP file.

At the second step the .efp file from GAMESS MAKEFP is analyzed and is auto-edited using the same MAP file to create the final EFP input (XYZ format).

The MAP file is required as an input for the script. It defines groups of atoms belonging to each EFP fragment both for the MAKEFP calculation and for the consequent EFP jobs. Here is a description of the MAP file: Each fragment described using section $RESIDUE followed by closing $end In this example the Lys2 is extracted cutting through the peptidic bond, the cut bond is saturated with hydrogen atom. The explanation of each variable is given below.

```
$Residue
Name = lys2
PreAtoms = 14-35
NH = 14,12
CH = 34,36
PostAtoms = 14-35
Rescharge = +1
USEFP = lys2
$end
```

The four first lines are required for the first step of the script (GAMESS MAKEFP job); the next ones are necessary for the actual EFP job.
`Name`: Residue name
`PreAtoms`: Atoms which belongs to the residue for GAMESS MAKEFP calculation.
`CH, NH, or OH`: In the case of broken bonds a hydrogen atom is added so that in X-Y bond (X belongs to the Lys2 residue and Y belongs to the previous or next residue) the Y atom is replaced by H along the X-Y axis. The default equilibrium distance for the X-H bond is set to 1.08 Å for a C-H bond, to 1.00 Å for a N-H bond, and to 0.94 Å for a O-H bond. It required to specify the atom number of the X and Y atoms.
`PostAtoms`: Atoms which belong to the residue after removing the overlapping fragment atoms or caps when the HLA or the CLA scheme is used. This important step removes multipoles and polarizability expansion points of those atoms according to the cutoff procedure (set by default to 1.3 Å and 1.2 Å for multipoles and polarizability expansion points, respectively). Multipole expansion at duplicated points are eliminated but to maintain the net integer charge on each amino acid the monopole expansion of the caps is redistributed on the natural fragment. This method is called Expand-Remove-Redistribute. Concerning the

polarizability expansion points, only one polarizability expansion point is removed when a hydrogen atom saturates the dangling bond, whereas 6 or 5 polarizability points are removed when the cap is an amine or an aldehyde, respectively.
`ResCharge`: The net charge of the residue after removing the overlapping fragment atoms (cfr. LA scheme).
`USEFP`: Name of the EFP fragment (and .efp file) to use with this fragment in the actual EFP calculation.

**Note:** In the MFCC scheme, the two first letters of the concap fragment have to be ’CC’.

**Note:** If the *PostAtoms* keyword is not present, the second script will generate an EFP job file without any modification of the parameters, which is useful for the MFCC scheme.

### 11.5.8 Input keywords

**EFP_COORD_XYZ**
Use coordinates of three atoms instead of Euler angles to specify position and orientation of the fragments
TYPE:
LOGICAL
DEFAULT:
FALSE
OPTIONS:
TRUE FALSE
RECOMMENDATION:
None

**EFP_DIRECT_POLARIZATION_DRIVER**
Use direct solver for EFP polarization
TYPE:
LOGICAL
DEFAULT:
FALSE
OPTIONS:
TRUE FALSE
RECOMMENDATION:
Direct polarization solver provides stable convergence of induced dipoles which may otherwise become problematic in case of closely lying or highly polar or charged fragments. The computational cost of direct polarization versus iterative polarization becomes higher for systems containing more than  10000 polarizable points.

**EFP_ENABLE_LINKS**
Enable fragment links in EFP region
TYPE:
LOGICAL
DEFAULT:
FALSE
OPTIONS:
TRUE FALSE
RECOMMENDATION:
None

**EFP**
Specifies that EFP calculation is requested
TYPE:
LOGICAL
DEFAULT:
FALSE
OPTIONS:
TRUE FALSE
RECOMMENDATION:
The keyword should be present if excited state calculation is requested

**EFP_FRAGMENTS_ONLY**
Specifies whether there is a QM part
TYPE:
LOGICAL
DEFAULT:

| | |
|---|---|
| FALSE | QM part is present |

OPTIONS:

| | |
|---|---|
| TRUE | Only MM part is present: all fragments are treated by EFP |
| FALSE | QM part is present: do QM/MM EFP calculation |

RECOMMENDATION:
None

**EFP_INPUT**
Specifies the format of EFP input
TYPE:
LOGICAL
DEFAULT:

| | |
|---|---|
| FALSE | Dummy atom (*e.g.*, He) in *$molecule* section should be present |

OPTIONS:

| | |
|---|---|
| TRUE | A format without dummy atom in *$molecule* section |
| FALSE | A format with dummy atom in *$molecule* section |

RECOMMENDATION:
None

**FEFP_EFP**

Specifies that fEFP_EFP calculation is requested to compute the total interaction energies between a ligand (the last fragment in the $efp_fragments section) and the protein (represented by fEFP)

TYPE:

STRING

DEFAULT:

OFF

OPTIONS:

| | |
|---|---|
| OFF | disables fEFP |
| LA | enables fEFP with the Link Atom (HLA or CLA) scheme (only electrostatics and polarization) |
| MFCC | enables fEFP with MFCC (only electrostatics) |

RECOMMENDATION:

The keyword should be invoked if EFP/fEFP is requested (interaction energy calculations). This keyword has to be employed with EFP_FRAGMENT_ONLY = TRUE. To switch on/off electrostatics or polarzation interactions, the usual EFP controls are employed.

**FEFP_QM**

Specifies that fEFP_QM calculation is requested to perform a QM/fEFPcompute computation. The fEFP part is a fractionated macromolecule.

TYPE:

STRING

DEFAULT:

OFF

OPTIONS:

| | |
|---|---|
| OFF | disables fEFP_QM and performs a QM/EFP calculation |
| LA | enables fEFP_QM with the Link Atom scheme |

RECOMMENDATION:

The keyword should be invoked if QM/fEFP is requested. This keyword has to be employed with efp_fragment_only false. Only electrostatics is available.

**EFP_ELEC**

Controls fragment-fragment electrostatics in EFP

TYPE:

LOGICAL

DEFAULT:

TRUE

OPTIONS:

| | |
|---|---|
| TRUE | switch on electrostatics |
| FALSE | switch off electrostatics |

RECOMMENDATION:

None

**EFP_POL**

Controls fragment-fragment polarization in EFP

TYPE:

LOGICAL

DEFAULT:

TRUE

OPTIONS:

| | |
|---|---|
| TRUE | switch on polarization |
| FALSE | switch off polarization |

RECOMMENDATION:

None

**EFP_DISP**

Controls fragment-fragment dispersion in EFP

TYPE:

LOGICAL

DEFAULT:

TRUE

OPTIONS:

| | |
|---|---|
| TRUE | switch on dispersion |
| FALSE | switch off dispersion |

RECOMMENDATION:

None

**EFP_EXREP**

Controls fragment-fragment exchange repulsion in EFP

TYPE:

LOGICAL

DEFAULT:

TRUE

OPTIONS:

| | |
|---|---|
| TRUE | switch on exchange repulsion |
| FALSE | switch off exchange repulsion |

RECOMMENDATION:

None

**EFP_QM_ELEC**

Controls QM-EFP electrostatics

TYPE:

LOGICAL

DEFAULT:

TRUE

OPTIONS:

| | |
|---|---|
| TRUE | switch on QM-EFP electrostatics |
| FALSE | switch off QM-EFP electrostatics |

RECOMMENDATION:

None

**EFP_QM_POL**

Controls QM-EFP polarization

TYPE:

LOGICAL

DEFAULT:

TRUE

OPTIONS:

TRUE switch on QM-EFP polarization

FALSE switch off QM-EFP polarization

RECOMMENDATION:

None

**EFP_QM_DISP**

Controls QM-EFP dispersion

TYPE:

LOGICAL

DEFAULT:

FALSE

OPTIONS:

TRUE switch on QM-EFP dispersion

FALSE switch off QM-EFP dispersion

RECOMMENDATION:

None

**EFP_QM_EXREP**

Controls QM-EFP exchange-repulsion

TYPE:

LOGICAL

DEFAULT:

FALSE

OPTIONS:

TRUE switch on QM-EFP exchange-repulsion

FALSE switch off QM-EFP exchange-repulsion

RECOMMENDATION:

None

**EFP_ELEC_DAMP**

Controls fragment-fragment electrostatic screening in EFP

TYPE:

INTEGER

DEFAULT:

2

OPTIONS:

0 switch off electrostatic screening

1 use overlap-based damping correction

2 use exponential damping correction if screening parameters are provided in the EFP potential

RECOMMENDATION:

Overlap-based damping is recommended

**EFP_DISP_DAMP**

Controls fragment-fragment dispersion screening in EFP

TYPE:

INTEGER

DEFAULT:

2

OPTIONS:

0 switch off dispersion screening

1 use Tang-Toennies screening, with fixed parameter $b = 1.5$

2 use overlap-based damping

RECOMMENDATION:

None

**EFP_POL_DAMP**

Controls fragment-fragment polarization screening in EFP

TYPE:

INTEGER

DEFAULT:

1

OPTIONS:

0 switch off polarization screening

1 use Tang-Toennies screening

RECOMMENDATION:

None

**EFP_QM_ELEC_DAMP**

Controls QM-EFP electrostatics screening in EFP

TYPE:

INTEGER

DEFAULT:

0

OPTIONS:

0 switch off electrostatic screening

1 use overlap based damping correction

RECOMMENDATION:

None

### 11.5.9 Examples

**Example 11.23** Basic EFP-only calculation of benzene dimer in XYZ input format with new EFPMAN2 module. EFP parameters are read from the fragment library (*$QCAUX/fraglib*).

```
$comment
   Pure EFP energy computation on benzene dimer
$end

$molecule
   0 1
   He       5.0    5.0    5.0
$end

$rem
   METHOD               hf
   BASIS                6-31G(d)
   JOBTYPE              sp
   PURECART             2222
   EFP_FRAGMENTS_ONLY   true
   EFP_DISP_DAMP        1
   EFP_COORD_XYZ        1
$end

$efp_fragments
BENZENE_L
   A01C   -0.07088   -2.35729    1.06421
   A02C    0.75298   -3.00688    0.16337
   A03C    0.51391   -2.89905   -1.19436
BENZENE_L
   A01C   -1.72945    1.38131   -0.01219
   A02C   -0.47330    1.37787   -0.59037
   A03C    0.65547    1.37017    0.20840
$end
```

**Example 11.24** Basic EFP-only calculation of benzene dimer in Euler angle input format with new EFP-MAN2 module. EFP parameters are read from the fragment library (*$QCAUX/fraglib*).

```
$molecule
   0 1
   He       5.0    5.0    5.0
$end

$rem
   METHOD               hf
   BASIS                6-31G(d)
   JOBTYPE              sp
   PURECART             2222
   EFP_FRAGMENTS_ONLY   true
   EFP_DISP_DAMP        1
$end

$efp_fragments
   BENZENE_L -0.30448173 -2.24210052 -0.29383131 -0.642499 1.534222 -0.568147
   BENZENE_L -0.60075437  1.36443336  0.78647823  3.137879 1.557344 -2.568550
$end
```

**Example 11.25** QM/MM computation of one water molecule in QM part and one water + two ammonia molecules in EFP part. EFP parameters are read from the fragment library (*$QCAUX/fraglib*).

```
$molecule
   0 1
   O   0.0000      0.0000      0.2243
   H  -1.4233      0.0000     -0.8973
   H   1.4233      0.0000     -0.8973
$end

$rem
```

```
   METHOD          hf
   BASIS           6-31G(d)
   JOBTYPE         sp
   PURECART        2222
   EFP_DISP_DAMP   1
$end

$efp_fragments
   WATER_L   -2.12417561  1.22597097 -0.95332054 -2.902133 1.734999 -1.953647
   AMMONIA_L  1.04358758  1.90477190  2.88279926 -1.105309 2.033306 -1.488582
   AMMONIA_L -4.16795656 -0.98129149 -1.27785935  2.526442 1.658262 -2.742084
$end
```

**Example 11.26** EOM-IP-CCSD/EFP calculation; CN radical hydrated by 6 waters.

```
$comment
   EOM-IP/EFP; CN radical hydrated by 6 waters
   all active orbitals and frozen core are tested
$end

$molecule
   -1 1
    C   1.004122   2.504092  -0.325463
    N   0.816221   2.319773   0.780625
$end

$rem
   BASIS                6-31+G*
   METHOD               eom-ccsd
   EFP_FRAGMENTS_ONLY   false
   PURECART             2222
   SCF_CONVERGENCE      8
   IP_STATES            4
   EFP                  1
   EOM_FAKE_IPEA        true
   CCMAN2               false
   EFP_EXREP            0
$end

$efp_fragments
   WATER_L 1.12736608 -1.43556954 -0.73517708 -1.45590530  2.99520330  0.11722720
   WATER_L 1.25577919  0.62068648 -2.69876653  2.56168924  1.26470722  0.33910203
   WATER_L 3.76006184 -1.03358049  0.45980636 -1.53852111  2.58787281 -1.98107746
   WATER_L 4.81593067  2.87535152 -0.24524178 -1.86802100  0.73283467 -2.17837806
   WATER_L 4.07402278  0.74020006 -1.92695949  2.21177738  1.69303397 -2.30505848
   WATER_L 3.60104027  1.35547341  1.88776964  0.43895304  1.25442317  1.07742578
$end
```

**Example 11.27** QM/MM computation of one water molecule in the QM part and one water + two ammonia molecules in the MM part. The EFP parameters will be taken from the EFP library (*$QCAUX/fraglib*).

```
$molecule
   0    1
   O1   0.47586     0.56326     0.53843
   H2   0.77272     1.00240     1.33762
   H3   0.04955    -0.23147     0.86452
$end
```

```
$rem
   METHOD     hf
   BASIS      6-31G(d)
   JOBTYPE    sp
   PURECART   2222
$end

$efp_fragments
   WATER_L   -2.12417561  1.22597097 -0.95332054 -2.902133 1.734999 -1.953647
   AMMONIA_L  1.04358758  1.90477190  2.88279926 -1.105309 2.033306 -1.488582
   AMMONIA_L -4.16795656 -0.98129149 -1.27785935  2.526442 1.658262 -2.742084
$end
```

**Example 11.28** Excited states of formaldehyde with 6 EFP water molecules by CIS(D).

```
$molecule
   0 1
   C1    1.063245   2.026797   0.433887
   O2    1.115445   1.079872   1.154242
   H3    1.094466   3.039490   0.836046
   H4    0.983660   1.924177  -0.645223
$end

$rem
   BASIS                6-31+G*
   EFP_FRAGMENTS_ONLY   false
   PURECART             2222
   SCF_CONVERGENCE      8
   METHOD               cis(d)
   EE_SINGLETS          2
   EE_TRIPLETS          2
   EFP                  1
$end

$efp_fragments
   WATER_L 1.45117729 -1.31271387 -0.39790305 -1.075756  2.378141  1.029199
   WATER_L 1.38370965  0.22282733 -2.74327999  2.787663  1.446660  0.168420
   WATER_L 4.35992117 -1.31285676  0.15919381 -1.674869  2.547933 -2.254831
   WATER_L 4.06184149  2.79536141  0.05055916 -1.444143  0.750463 -2.291224
   WATER_L 4.09898096  0.83731430 -1.93049301  2.518412  1.592607 -2.199818
   WATER_L 3.96160175  0.71581837  2.05653146  0.825946  1.414384  0.966187
$end
```

## 11.6 Projector-based Density Embedding

The exact density embedding method adapted from the method of Manby, Miller, and co-workers [126] allows embedding calculations to extend beyond electrostatic embedding. This embedding scheme allows for the fragmentation of a system into two interacting subsystems, which can be treated at two different levels of quantum mechanics (QM/QM), for example coupled cluster embedded in DFT. This type of embedding fully accounts for polarization as well as quantum mechanical exchange, as calculated from the supermolecular embedding density and the exchange correlation functional used. The goal of this embedding theory is to perform, say, a DFT calculation on fragment 1 in the presence of fragment 2.

### 11.6.1 Theory

Conventional super-molecular KS-DFT calculations contain several non-additive terms consisting of kinetic energies and exchange-correlation effects. These non-additive terms are eliminated by applying a level-shift projection operator to maintain orthogonality between fragments when performing a 1-in-2 energy calculation.

The process begins by performing a KS-DFT calculation on the full system, or super-molecule. The KS-DFT calculation is then repeated for fragment 1-in-2, which is fragment 1 in the presence of the localized MOs of fragment 2 taken from the super-molecular full calculation. The Fock Matrix for this calculation is constructed as follows,

$$\mathbf{f}^{(1)} = \mathbf{h} + \mathbf{J}[\gamma^{(1)} + \gamma^{(2)}] - \nu_{xc}[\gamma^{(1)} + \gamma^{(2)}] + \mu\mathbf{P}^{(2)} \tag{11.74}$$

where P is the level-shift projection operator constructed as:

$$\mathbf{P}^{(2)}_{\alpha\beta} = [\mathbf{S}\gamma^{(2)}\mathbf{S}]_{\alpha\beta} \tag{11.75}$$

where $\gamma^{(2)}$ is the localized density of fragment 2, and S is the AO overlap matrix. Upon convergence, an energy correction term is added to the final energy to account for the level-shift projection operator contribution to the Fock Matrix energy. The correction term is calculated as the following:

$$E_{\text{correction}} = \mu * tr(\gamma^{(1)}\mathbf{P}^{(2)}) \tag{11.76}$$

Once the KS-DFT energy of fragment 1-in-2 is computed, a post KS method can be applied to this converged density to obtain the high-level QM additive energy of fragment 1. The same procedure can be repeated for fragment 2-in-1, without continuing to a post-DFT method to yield the low-level QM additive energy of the fragment 2. These energies are then summed to yield the total energy.

### 11.6.2 Job Control for Density Embedding Calculations

To use density embedding on a system, one must split the super-molecular system into two fragments indexed 1 and 2, and set EMBEDMAN to 1. This is done through the standard Q-CHEM fragment input syntax. Two separate jobs must be run to find the total energy of fragment 1-in-2 at a high level QM theory, and fragment 2-in-1 at a low level QM theory. The order of the fragments in the *$molecule* section determines which fragment will undergo the high level QM. The user must submit a separate job for the 2-in-1 low-level QM calculation, with the order of the fragments reversed and EMBED_THEORY set to 0, which is the default value. The user must then add the final energies of the calculations to determine the total QM/QM embedded energy.

For the current Q-CHEM implementation of density embedding, it is necessary to specify the basis as MIXED, which requires to define the basis for each individual atom. When using CCSD(T), one should specify CCMAN2 as TRUE, for Q-CHEM's most updated coupled-cluster code. The current implementation of density embedding only works in combination with the following settings: SCF_ALGORITHM = DIIS, INCFOCK = 0, and PURECART = 222. It is also recommended that users disable symmetry for calculations with SYMMETRY = FALSE, and SYM_IGNORE = TRUE. Refer to the sample input for correct job settings.

**EMBEDMAN**

Turns density embedding on.

TYPE:

INTEGER

DEFAULT:

0

OPTIONS:

0 Do not use density embedding.

1 Turn on density embedding.

RECOMMENDATION:

Use EMBEDMAN for QM/QM density embedded calculations.

**EMBED_THEORY**

Specifies post-DFT method performed on fragment one.

TYPE:

INTEGER

DEFAULT:

0

OPTIONS:

0 No post HF method, only DFT on fragment one.

1 Perform CCSD(T) calculation on fragment one.

2 Perform MP2 calculation on fragment one.

RECOMMENDATION:

This should be 1 or 2 for the high-level QM calculation of fragment 1-in-2, and 0 for fragment 2-in-1 low-level QM calculation.

**EMBED_MU**

Specifies exponent value of projection operator scaling factor, $\mu$ [Eq. (11.74) and (11.76)].

TYPE:

INTEGER

DEFAULT:

7

OPTIONS:

n $\mu = 10^n$.

RECOMMENDATION:

Values of 2 - 7 are recommended. A higher value of $\mu$ leads to better orthogonality of the fragment MOs but $\mu > 10^7$ introduces numerical noise. $\mu < 10^2$ results in non-additive terms becoming too large. Energy corrections are fairly insensitive to changes in $\mu$ within the range of $10^2 - 10^7$.

**EMBED_THRESH**

Specifies threshold cutoff for AO contribution used to determine which MOs belong to which fragments

TYPE:

INTEGER

DEFAULT:

500

OPTIONS:

n Threshold = $n/1000$

RECOMMENDATION:

Acceptable values range from 0 to 1000. Should only need to be tuned for non-highly localized MOs

**Example 11.29** Input for a CCSD(T)/PBE density embedding calculation of He-in-HF. The sum of the final energies for these two jobs will yield the total QM/QM energy.

```
$molecule
   0 1
--
   0 1
   He      -4.63032        2.10289       -1.62399
--
   0 1
   F       -8.00612        1.74605       -1.25581
   H       -7.40964        1.84462       -0.47756
$end

$rem
   JOBTYPE          SP
   EXCHANGE         PBE
   CORRELATION      PBE
   BASIS            mixed  ! Must specify basis sets per atom in $basis section below
   PURECART         222
   MAX_SCF_CYCLES   100
   SCF_ALGORITHM    DIIS
   INCFOCK          0
   SYMMETRY         false
   SYM_IGNORE       true
   CC_SYMMETRY      false
   CCMAN2           true
   EMBEDMAN         1      ! Turning density embedding on
   EMBED_THEORY     1      ! Running CCSD(T) on fragment 1 in 2, or He in FH
   EMBED_MU         7      ! Default value
   EMBED_THRESH     500    ! Default value for assigning MOs to fragments
$end

$basis
  he 1
  6-31G
  ****
  f 2
  6-31G
  ****
  h 3
  6-31G
```

```
    ****
  $end

  @@@

  $molecule
  0 1
  --
  0 1
     F       -8.00612        1.74605       -1.25581
     H       -7.40964        1.84462       -0.47756
  --
  0 1
     He      -4.63032        2.10289       -1.62399
  $end

  $rem
    JOBTYPE          SP
    EXCHANGE         PBE
    CORRELATION      PBE
    BASIS            mixed
    PURECART         222
    MAXSCF           100
    SCF_ALGORITHM    DIIS
    INCFOCK          0
    SYMMETRY         false
    SYM_IGNORE       true
    EMBEDMAN         1
    EMBED_THEORY     0       ! There will be no post-DFT calculations for HF-in-He
  $end

  $basis
    f 1
    6-31G
    ****
    h 2
    6-31G
    ****
    he 3
    6-31G
    ****
  $end
```

## 11.7 Frozen-Density Embedding Theory based methods

Frozen-Density Embedding Theory (FDET) [127,128] provides a formal framework in which the whole system is described by means of two independent quantities: the embedded wave function (interacting or not) and the density associated with the environment. The total energy equation in frozen density embedding theory for a wave function in state $I$ embedded in a environment density $\rho_B$ reads (for definitions see Table 11.8):

$$E_{AB}^{\text{tot}}[\Psi_A^I, \rho_B] = \langle \Psi_A^I | \hat{H}_A | \Psi_A^I \rangle + V_B^{\text{nuc}}[\rho_A^I] + J_{\text{int}}[\rho_A^I, \rho_B] + E_{xc}^{\text{nad}}[\rho_A^I, \rho_B] \\ + T_s^{\text{nad}}[\rho_A^I, \rho_B] + E_{v_B}^{\text{HK}}[\rho_B] + V_A^{\text{nuc}}[\rho_B] \tag{11.77}$$

The embedding operator $\hat{v}_{\text{emb}}$, which is added to the Hamiltonian of subsystem A $\left(\hat{H}_A\right)$, is given in the form of a potential:

$$v_{\mathrm{emb}}[\rho_A^I, \rho_B, v_B](\mathbf{r}) = v_B(\mathbf{r}) + \int \frac{\rho_B(\mathbf{r}')}{|\mathbf{r}-\mathbf{r}'|}\mathrm{d}\mathbf{r} + \frac{\delta E_{xc,T}^{\mathrm{nad}}[\rho_A^I, \rho_B]}{\delta \rho_A^I(\mathbf{r})} \tag{11.78}$$

The last term (non-electrostatic component) in equation 11.78 causes the embedding potential to be $\rho_A$-dependent, which in return induces an inconsistency between the potential and the energy. In the canonical form of FDET (*conventional* FDET) this inconsistency is addressed by performing macrocycles in which the embedding potential is repeatedly constructed using the current (embedded) density $\rho_A^{\mathrm{curr}}(\mathbf{r})$ after each cycle until self-consistency is reached.

In *linearized FDET* the non-additive energy functionals (for abbreviation denoted as $E_{xc,T}^{\mathrm{nad}}[\rho_A^I, \rho_B]$) are each approximated by a functional which is linear in $\rho_A(\mathbf{r})$. The approximation is constructed as a Taylor expansion of the non-additive energy functional at a reference density $\rho_A^{\mathrm{ref}}(\mathbf{r})$ with the series being truncated after the linear term.

$$E_{xc,T}^{\mathrm{nad}}[\rho_A^I, \rho_B] \approx E_{xc,T}^{\mathrm{nad}}[\rho_A^{\mathrm{ref}}, \rho_B] + \int \left(\rho_A^I(\mathbf{r}) - \rho_A^{\mathrm{ref}}(\mathbf{r})\right) \frac{\delta E_{xc,T}^{nad}[\rho_A^{\mathrm{ref}}, \rho_B]}{\delta \rho_A^{\mathrm{ref}}(\mathbf{r})}\mathrm{d}\mathbf{r} \tag{11.79}$$

In contrast to conventional FDET, the embedding potential then becomes $\rho_A$-independent and macrocycles are no longer necessary. Another consequence of the linearization is that orthogonality between states is maintained since the same potential is used for all states.

## 11.7.1 FDE-ADC

FDE-ADC[129] is a density embedding method based on the combination of the Algebraic Diagrammatic Construction scheme for the polarization propagator (ADC, Section 6.8) and Frozen-Density Embedding Theory (FDET). In this particular variant the subsystem A is represented by a wave function whereas subsystem B is described by a density. The FDE-ADC method uses the linearized FDET approximation[130].

### 11.7.1.1 FDE-ADC Job Control

The FDE-ADC job control is accomplished in two sections, *$rem* and *$fde*. Enabling FDE-ADC, specification of the ADC method and other ADC job control parameters (thresholds, max. iterations etc) should be set in the *$rem* section. FDE-ADC also supports the excited state analysis (STATE_ANALYSIS) carried out by the *libwfa* module.

The fragments are specified via the fragment descriptors (see Section 12) in the *$molecule* section, whereas the first fragment corresponds to the embedded species (A) while the second fragment represents the environment (B).

**Note:** The current implementation allows only for closed shell fragments.

**FDE**

Turns density embedding on.

TYPE:

BOOLEAN

DEFAULT:

False

OPTIONS:

| | |
|---|---|
| True | Perform an FDE-ADC calculation. |
| False | Don't perform FDE-ADC calculation. |

RECOMMENDATION:

Set the *$rem* variable FDE to TRUE to start a FDE-ADC calculation.

**METHOD**

Determines which FDE-ADC method should be used if FDE = True.

TYPE:

STRING

DEFAULT:

None

OPTIONS:

| | |
|---|---|
| adc(2) | Perform an FDE-ADC(2)-s calculation. |
| adc(2)-x | Perform an FDE-ADC(2)-x calculation. |
| adc(3) | Perform an FDE-ADC(3) calculation (potential constructed with MP(2) density). |
| cvs-adc(2) | Perform an FDE-ADC(2)-s calculation of core excitations. |
| cvs-adc(2)-x | Perform an FDE-ADC(2)-x calculation of core excitations. |
| cvs-adc(3) | Perform an FDE-ADC(3) calculation of core excitations. |

RECOMMENDATION:

None

The FDE-ADC job control with respect to embedding parameters is accomplished via options in the *$fde* input section. The format of the *$fde* section requires key and value pairs separated by a space character:

```
$fde
   <Keyword>  <parameter>
$end
```

**Note:** The following job control variables belong *only* in the *$fde* section. Do not place them in the *$rem* section.

The super-molecular expansion (SE) uses the full basis set of the super-system for calculations on each fragment. Because of the computational cost this option should only be used for small to medium sized super-systems. Note that for visualization of orbitals or densities SE only supports the generation of volumetric data via MAKE_CUBE_FILES (MOLDEN files are not supported, *i.e.* MOLDEN_FORMAT should be avoided).

The reassembling of density matrix (RADM)[129] option allows for calculations on larger systems by only including the basis functions of the embedded species for the ADC calculation. RADM introduces an approximation for the construction of the embedding potential by using an artificially (but cheaply) constructed density matrix for subsystem A. With RADM, all regular options for visualization are supported

(MAKE_CUBE_FILES *and* MOLDEN_FORMAT). The RADM option is the recommended choice for an FDE-ADC calculation.

Analogous to a regular DFT calculation in Q-CHEM(by using METHOD) the exchange-correlation functional combination can either be selected with one keyword **XC_Func**,or by defining **X_Func** and **C_Func** (similar to EXCHANGE and CORRELATION).

**T_Func**
Kinetic energy functional used for the construction of the embedding potential.
INPUT SECTION: *$fde*
TYPE:
STRING
DEFAULT:
None
OPTIONS:
TF Use Thomas-Fermi kinetic energy functional.
RECOMMENDATION:
None

**XC_Func**
Exchange-Correlation functional used for the construction of the embedding potential.
INPUT SECTION: *$fde*
TYPE:
STRING
DEFAULT:
None
OPTIONS:
All LDA/GGA exchange-correlation functionals available in Q-CHEM.
RECOMMENDATION:
Only use LDA or GGA-type functionals.

**X_Func**
Exchange functional used for the construction of the embedding potential.
INPUT SECTION: *$fde*
TYPE:
STRING
DEFAULT:
None
OPTIONS:
All LDA/GGA exchange functionals available in Q-CHEM.
RECOMMENDATION:
Only use LDA or GGA-type functionals. **XC_Func** and **X_Func** are mutually exclusive.

**C_Func**

Exchange-Correlation functional used for the construction of the embedding potential.

INPUT SECTION: *$fde*

TYPE:

STRING

DEFAULT:

None

OPTIONS:

All LDA/GGA correlation functionals available in Q-CHEM.

RECOMMENDATION:

Only use LDA or GGA-type functionals. **XC_Func** and **C_Func** are mutually exclusive.

**Expansion**

Specifies which basis set expansion should be used.

INPUT SECTION: *$fde*

TYPE:

STRING

DEFAULT:

None

OPTIONS:

| | |
|---|---|
| SE/super/supermolecular | Supermolecular basis is used for both System A and B. |
| RADM | Use RADM approximation (see above). |

RECOMMENDATION:

SE should be used for testing purposes only since it is very expensive for large systems. Use the RADM approximation for larger systems.

**rhoB_method**

Method to calculate the environment density (B).

INPUT SECTION: *$fde*

TYPE:

STRING

DEFAULT:

None

OPTIONS:

| | |
|---|---|
| HF | Use Hartree-Fock method. |
| DFT | Use Density Functional Theory. |

RECOMMENDATION:

If DFT is specified, the respective exchange-correlation functional has to defined using the keyword **XC_FUNC_B** or **X_FUNC_B** and **C_FUNC_B**.

**XC_Func_B**

Exchange-Correlation functional used for the environment DFT calculation.

INPUT SECTION: *$fde*

TYPE:

STRING

DEFAULT:

None

OPTIONS:

All LDA/GGA/global-hybrid-GGA exchange-correlation functionals available in Q-CHEM.

RECOMMENDATION:

None

**X_Func_B**

Exchange functional used for the environment DFT calculation.

INPUT SECTION: *$fde*

TYPE:

STRING

DEFAULT:

None

OPTIONS:

All LDA/GGA exchange functionals available in Q-CHEM.

RECOMMENDATION:

**XC_Func_B** and **X_Func_B** are mutually exclusive.

**C_Func_B**

Correlation functional used for the environment DFT calculation.

INPUT SECTION: *$fde*

TYPE:

STRING

DEFAULT:

None

OPTIONS:

All LDA/GGA correlation functionals available in Q-CHEM.

RECOMMENDATION:

**XC_Func_B** and **C_Func_B** are mutually exclusive.

**PrintLevel**

Print level for FDE-ADC output.

INPUT SECTION: *$fde*

TYPE:

INTEGER

DEFAULT:

0

OPTIONS:

0 minimum print level

1 extended print level

2 maximum print level

3 max. print level and additional text files (densities, etc.)

RECOMMENDATION:

None

#### 11.7.1.2 Examples

**Example 11.30** Input for a FDE-ADC(2)/cc-pVDZ calculation in supermolecular expansion on CO embedded in one water molecule.

```
$rem
   SYM_IGNORE           = true
   METHOD               = adc(2)
   EE_STATES            = 2
   BASIS                = cc-pvdz
   FDE                  = true
   MEM_STATIC           = 1024
   MEM_TOTAL            = 16000
   ADC_DAVIDSON_MAXITER = 100
   ADC_DAVIDSON_CONV    = 5
$end

$molecule
   0 1
--
   0 1
   C    -3.618090    1.376803   -0.020795
   O    -4.735683    1.525556    0.115023
--
   0 1
   O    -7.956372    1.485406    0.116792
   H    -6.992316    1.421133    0.177470
   H    -8.105846    2.442220    0.111599
$end

$fde
   T_Func       TF
   XC_Func      PBE
   expansion    super
   rhoB_method  HF
$end
```

#### 11.7.1.3 FDE-ADC output

In general the FDE-ADC output indicates all important stages of the FDE-ADC calculation, which are:

1. Generation of $\rho_A^{\text{ref}}$,
2. Generation of $\rho_B$,
3. Construction of the embedding potential,
4. Start of FDE-ADC calculation and
5. Final FDE-ADC summary.

In the following table definitions of the terms printed to the output are collected. These quantities are printed for every state, *i.e.* for every $\rho_A^I(\mathbf{r})$. In addition, the non-electrostatic interactions with respect to the reference density $\rho_A^{\text{ref}}(\mathbf{r})$ are printed at the top of the FDE-ADC summary.

| | |
|---|---|
| *Subsystem Energies* | |
| `Embedded system (A)` | $\langle\Psi_A^I\|\hat{H}_A + v_{\text{emb}}^{\text{lin}}\|\Psi_A^I\rangle$ |
| `Environment (B)` | $E_B = E_{v_B}^{\text{HK}}[\rho_B]$ or $E_{\text{HF}}$ |
| *Electrostatic Interactions* | |
| `rho_A <-> rho_B` | $J_{\text{int}}[\rho_A, \rho_B] = \int\int \frac{\rho_A(\mathbf{r})\rho_B(\mathbf{r}')}{\|\mathbf{r}-\mathbf{r}'\|}\text{d}\mathbf{r}\text{d}\mathbf{r}'$ |
| `rho_A <-> Nuc_B` | $V_B^{\text{nuc}}[\rho_A] = \int \rho_A(\mathbf{r})v_B(\mathbf{r})\text{d}\mathbf{r}$ |
| `rho_B <-> Nuc_A` | $V_A^{\text{nuc}}[\rho_B] = \int \rho_B(\mathbf{r})v_A(\mathbf{r})\text{d}\mathbf{r}$ |
| `Nuc_A <-> Nuc_B` | $V_{N_A N_B} = \sum_i \sum_j \frac{Z_i Z_j}{\|R_i - R_j\|}$ |
| *Non-Electrostatic Interactions* | |
| `non-additive E_xc` | $E_{xc}^{\text{nad}}[\rho_A^I, \rho_B]$ |
| `non-additive T_s` | $T_s^{\text{nad}}[\rho_A^I, \rho_B]$ |
| `integrated v_xc nad` | $\int \rho_A^I(\mathbf{r})v_{xc}^{\text{nad}}(\mathbf{r})\text{d}\mathbf{r}$ |
| `integrated v_T nad` | $\int \rho_A^I(\mathbf{r})v_T^{\text{nad}}(\mathbf{r})\text{d}\mathbf{r}$ |
| *Final FDE-ADC energies* | |
| `Delta_Lin` | $\int(\rho_A^I(\mathbf{r}) - \rho_A^{\text{ref}}(\mathbf{r}))v_{xc,T}^{\text{nad}}(\mathbf{r})\text{d}\mathbf{r}$ |
| `Final Energy (A)` | $E_A^{\text{emb}}[\Psi_A^I, \rho_B] = \langle\Psi_A^I\|\hat{H}_A\|\Psi_A^I\rangle + J_{\text{int}}[\rho_A^I, \rho_B] + V_B^{\text{nuc}}[\rho_A^I]$<br>$+E_{xc,T}^{\text{nad}}[\rho_A^{\text{ref}}, \rho_B] + \Delta^{\text{lin}}[\rho_A^I, \rho_A^{\text{ref}}, \rho_B] + V_A^{\text{nuc}}[\rho_B] + V_{N_A N_B}$ |
| `Final Energy (A+B)` | $E_A^{\text{emb}}[\Psi_A^I, \rho_B] + E_B$ |

Table 11.8: Definition of output terms.

# References and Further Reading

[1] J. G. Kirkwood, *J. Chem. Phys.* **2**, 767 (1934).

[2] L. Onsager, *J. Am. Chem. Soc.* **58**, 1486 (1936).

[3] J. G. Kirkwood, *J. Chem. Phys.* **7**, 911 (1939).

[4] A. Klamt and G. Schüürmann, *J. Chem. Soc. Perkin Trans. 2* , 799 (1993).

[5] T. N. Truong and E. V. Stefanovich, *Chem. Phys. Lett.* **240**, 253 (1995).

[6] V. Barone and M. Cossi, *J. Phys. Chem. A* **102**, 1995 (1998).

[7] M. Cossi, N. Rega, G. Scalmani, and V. Barone, *J. Comput. Chem.* **24**, 669 (2003).

[8] D. M. Chipman, *J. Chem. Phys.* **112**, 5558 (2000).

[9] E. Cancès, *J. Chem. Phys.* **107**, 3032 (1997).

[10] E. Cancès and B. Mennucci, *J. Chem. Phys.* **114**, 4744 (2001).

[11] J. Tomasi, B. Mennucci, and R. Cammi, *Chem. Rev.* **106**, 2999 (2005).

[12] A. W. Lange and J. M. Herbert, *J. Phys. Chem. Lett.* **1**, 556 (2010).

[13] A. W. Lange and J. M. Herbert, *J. Chem. Phys.* **133**, 244111 (2010).

[14] A. W. Lange and J. M. Herbert, *Chem. Phys. Lett.* **509**, 77 (2011).

[15] J. M. Herbert and A. W. Lange, The polarizable continuum model for (bio)molecular electrostatics: Basic theory and recent advances for macromolecules and simulations, in *Many-Body Effects and Electrostatics in Multi-Scale Computations of Biomolecules*, edited by Q. Cui, P. Ren, and M. Meuwly, chapter 11, pages 363–416, Pan Stanford, 2016.

[16] A. W. Lange, J. M. Herbert, B. J. Albrecht, and J. M. Herbert, Intrinsically smooth discretization of Connolly's solvent-excluded molecular surface, (submitted).

[17] J. Florián and A. Warshel, *J. Phys. Chem. B* **101**, 5583 (1997).

[18] J. Florián and A. Warshel, *J. Phys. Chem. B* **103**, 10282 (1999).

[19] A. V. Marenich, R. M. Olson, C. P. Kelly, C. J. Cramer, and D. G. Truhlar, *J. Chem. Theory Comput.* **3**, 2011 (2007).

[20] A. V. Marenich, C. J. Cramer, and D. G. Truhlar, *J. Chem. Theory Comput.* **9**, 609 (2013).

[21] A. V. Marenich, R. M. Olson, C. P. Kelly, C. J. Cramer, and D. G. Truhlar, *J. Phys. Chem. B* **113**, 2009 (6378).

[22] A. Klamt and V. Jonas, *J. Chem. Phys.* **105**, 9972 (1996).

[23] K. Baldridge and A. Klamt, *J. Chem. Phys.* **106**, 6622 (1997).

[24] D. M. Chipman, *Theor. Chem. Acc.* **107**, 80 (2002).

[25] D. M. Chipman and M. Dupuis, *Theor. Chem. Acc.* **107**, 90 (2002).

[26] V. Barone, M. Cossi, and J. Tomasi, *J. Chem. Phys.* **107**, 3210 (1997).

[27] A. Pomogaeva and D. M. Chipman, *J. Chem. Theory Comput.* **7**, 3952 (2011).

[28] A. Pomogaeva and D. M. Chipman, *J. Phys. Chem. A* **117**, 5812 (2013).

[29] A. Pomogaeva and D. M. Chipman, *J. Chem. Theory Comput.* **10**, 211 (2014).

[30] A. Pomogaeva and D. M. Chipman, *J. Phys. Chem. A* **119**, 5173 (2015).

[31] C. J. Cramer and D. G. Truhlar, *Acc. Chem. Res.* **41**, 760 (2008).

[32] A. Klamt et al., *Acc. Chem. Res.* **42**, 489 (2009).

[33] A. Klamt, *J. Phys. Chem.* **99**, 2225 (1995).

[34] A. Klamt, F. Eckert, and W. Arlt, *Annu. Rev. Chem. Biomol. Eng.* **1**, 101 (2010).

[35] http://www.cosmologic.de/index.php.

[36] A. Klamt, *Wiley Interdiscip. Rev.: Comput. Mol. Sci.* **1**, 699 (2011).

[37] R. C. Weast, editor, *CRC Handbook of Chemistry and Physics*, Chemical Rubber Company, Boca Rotan, 70th edition, 1989.

[38] M. W. Wong, M. J. Frisch, and K. B. Wiberg, *J. Am. Chem. Soc.* **113**, 4776 (1991).

[39] M. Born, *Z. Phys.* **1**, 45 (1920).

[40] S. Miertuš, E. Scrocco, and J. Tomasi, *Chem. Phys.* **55**, 117 (1981).

[41] J. Tomasi, B. Mennucci, and E. Cancès, *J. Mol. Struct. (Theochem)* **464**, 211 (1999).

[42] R. Bonaccorsi, P. Palla, and J. Tomasi, *J. Am. Chem. Soc.* **106**, 1945 (1984).

[43] J. Tomasi and M. Persico, *Chem. Rev.* **94**, 2027 (1994).

[44] A. Bondi, *J. Phys. Chem.* **68**, 441 (1964).

[45] V. I. Lebedev, *Zh. Vychisl. Mat. Mat. Fix.* **16**, 293 (1976).

[46] V. I. Lebedev, *Sibirsk. Mat. Zh.* **18**, 132 (1977).

[47] V. I. Lebedev and D. N. Laikov, *Dokl. Math.* **366**, 741 (1999).

[48] D. M. York and M. Karplus, *J. Phys. Chem. A* **103**, 11060 (1999).

[49] R. S. Rowland and R. Taylor, *J. Phys. Chem.* **100**, 7384 (1996).

[50] M. Mantina, A. C. Chamberlin, R. Valero, C. J. Cramer, and D. G. Truhlar, *J. Phys. Chem. A* **113**, 5806 (2009).

[51] R. Cammi and B. Mennucci, *J. Chem. Phys.* **110**, 9877 (1999).

[52] M. Cossi and V. Barone, *J. Chem. Phys.* **115**, 4708 (2001).

[53] R. Cammi and J. Tomasi, *Int. J. Quantum Chem. Symp.* **29**, 465 (1995).

[54] M. Cossi and V. Barone, *J. Phys. Chem. A* **104**, 10614 (2000).

[55] R. Improta, V. Barone, G. Scalmani, and M. J. Frisch, *J. Chem. Phys.* **125**, 054103 (2006).

[56] Z. You, J.-M. Mewes, A. Dreuw, and J. M. Herbert, *J. Chem. Phys.* **143**, 204104 (2015).

[57] J.-M. Mewes et al., *J. Phys. Chem. A* **119**, 5446 (2015).

[58] J.-M. Mewes, J. M. Herbert, and A. Dreuw, *Phys. Chem. Chem. Phys.* **19**, 1644 (2017).

[59] C.-P. Hsu, G. R. Fleming, M. Head-Gordon, and T. Head-Gordon, *J. Chem. Phys.* **114**, 3065 (2001).

[60] A. V. Marenich et al., *Chem. Sci.* **2**, 2143 (2011).

[61] R. Cammi, S. Corni, B. Mennucci, and J. Tomasi, *J. Chem. Phys.* **122**, 104513 (2005).

[62] M. Caricato et al., *J. Chem. Phys.* **124**, 124520 (2006).

[63] R. Improta, G. Scalmani, M. J. Frisch, and V. Barone, *J. Chem. Phys.* **127**, 074504 (2007).

[64] H. Li and J. H. Jensen, *J. Comput. Chem.* **25**, 1449 (2004).

[65] A. K. Rappé, C. J. Casewit, K. S. Colwell, W. A. Goddard III, and W. M. Skiff, *J. Am. Chem. Soc.* **114**, 10024 (1992).

[66] J. L. Pascual-Ahuir, E. Silla, and I. T. non, *J. Comput. Chem.* **15**, 1127 (1994).

[67] W. Humphrey, A. Dalke, and K. Schulten, *J. Molec. Graphics* **14**, 33 (1996).

[68] The VMD program may be downloaded from www.ks.uiuc.edu/Research/vmd.

[69] M. Cossi, B. Mennucci, and R. Cammi, *J. Comput. Chem.* **17**, 57 (1996).

[70] P. Li, H. Johnston, and R. Krasny, *J. Comput. Phys.* **228**, 3858 (2009).

[71] Z. You and J. M. Herbert, *J. Chem. Theory Comput.* **12**, 4338 (2016).

[72] O. A. Vydrov and T. Van Voorhis, *Phys. Rev. Lett.* **103**, 063004 (2009).

[73] C. P. Kelly, C. J. Cramer, and D. G. Truhlar, *J. Phys. Chem. B* **111**, 408 (2007).

[74] A. Schäfer, A. Klamt, D. Sattle, J. C. W. Lohrenz, and F. Eckert, *Phys. Chem. Chem. Phys.* **2**, 2187 (2000).

[75] A. Klamt, F. Eckert, and M. Hornig, *J. Comput.-Aided Mol. Design* **15**, 355 (2001).

[76] D. A. Liotard, G. D. Hawkins, G. C. Lynch, C. J. Cramer, and D. G. Truhlar, *J. Comput. Chem.* **16**, 422 (1995).

[77] C. P. Kelly, C. J. Cramer, and D. G. Truhlar, *J. Chem. Theory Comput.* **1**, 1133 (2005).

[78] T. Zhu, J. Li, D. A. Liotard, C. J. Cramer, and D. G. Truhlar, *J. Chem. Phys.* **110**, 5503 (1999).

[79] J. D. Thompson, C. J. Cramer, and D. G. Truhlar, *J. Chem. Phys.* **119**, 1661 (2003).

[80] C. J. Cramer and D. G. Truhlar, in *Free Energy Calculations and Rational Drug Design*, edited by M. R. Reddy and M. D. Erion, page 63, Kluwer/Plenum, New York, 2001.

[81] J. Li, C. J. Cramer, and D. G. Truhlar, *Int. J. Quantum Chem.* **77**, 264 (2000).

[82] A. V. Marenich, S. V. Jerome, C. J. Cramer, and D. G. Truhlar, *J. Chem. Theory Comput.* **8**, 527 (2012).

[83] U. C. Singh and P. A. Kollman, *J. Comput. Chem.* **7**, 718 (1986).

[84] C. M. Breneman and K. B. Wiberg, *J. Comput. Chem.* **11**, 361 (1990).

[85] G. Fisicaro, L. Genovese, O. Andreussi, N. Marzari, and S. Goedecker, *J. Chem. Phys.* **144**, 014103 (2016).

[86] O. Andreussi, I. Dabo, and N. Marzari, *J. Chem. Phys.* **136**, 064102 (2012).

[87] M. P. Coons and J. M. Herbert, Non-equilibrium, anisotropic continuum boundary conditions for electronic structure calculations: Theory, implementation, and applications to compute vertical ionization energies of aqueous ions at the air/water interface, (in preparation).

[88] M. P. Coons, Z. You, and J. M. Herbert, *J. Am. Chem. Soc.* **138**, 10879 (2016).

[89] H. L. Woodcock et al., *J. Comput. Chem.* **28**, 1485 (2007).

[90] J. Wang, P. Cieplak, and P. A. Kollman, *J. Comput. Chem.* **21**, 1049 (2000).

[91] N. Foloppe and A. D. MacKerell, *J. Comput. Chem.* **21**, 86 (2000).

[92] W. L. Jorgensen, D. S. Maxwell, and J. Tirado-Rives, *J. Am. Chem. Soc.* **117**, 11225 (1996).

[93] T. Vreven and K. Morokuma, *Annu. Rep. Comp. Chem.* **2**, 35 (2006).

[94] H. M. Senn and W. Thiel, *Topics Curr. Chem.* **268**, 173 (2007).

[95] Y. Shao and J. Kong, *J. Phys. Chem. A* **111**, 3661 (2007).

[96] P. Ren and J. W. Ponder, *J. Phys. Chem. B* **107**, 5933 (2003).

[97] K. Nam, J. Gao, and D. M. York, *J. Chem. Theory Comput.* **1**, 2 (2005).

[98] D. Riccardi, P. Schaefer, and Q. Cui, *J. Phys. Chem. B* **109**, 17715 (2005).

[99] R. C. Walker, M. F. Crowley, and D. A. Case, *J. Comput. Chem.* **29**, 1019 (2008).

[100] B. R. Brooks et al., *J. Comput. Chem.* **30**, 1545 (2009).

[101] Z. C. Holden, R. M. Richard, and J. M. Herbert, *J. Chem. Phys.* **139**, 244108 (2013).

[102] Z. C. Holden, M. P. Coons, and J. M. Herbert, Analytic gradients for periodic image charges derived from the electrostatic potential and application to Ewald summation in QM/MM calculations, (in preparation).

[103] D. Das et al., *J. Chem. Phys.* **117**, 10534 (2002).

[104] H. L. Woodcock et al., *J. Chem. Phys.* **129**, 214109 (2008).

[105] P. N. Day et al., *J. Chem. Phys.* **105**, 1968 (1996).

[106] M. S. Gordon et al., *J. Phys. Chem. A* **105**, 293 (2001).

[107] M. W. Schmidt et al., *J. Comput. Chem.* **14**, 1347 (1983).

[108] D. Ghosh et al., *J. Phys. Chem. A* **114**, 12739 (2010).

[109] M. S. Gordon, D. G. Fedorov, S. R. Pruitt, and L. V. Slipchenko, *Chem. Rev.* **112**, 632 (2012).

[110] I. A. Kaliman and L. V. Slipchenko, *J. Comput. Chem.* **34**, 2284 (2013).

[111] A. D. Buckingham, *Q. Rev. Chem. Soc.* **13**, 183 (1959).

[112] A. J. Stone, *Chem. Phys. Lett.* **83**, 233 (1981).

[113] A. J. Stone and M. Alderton, *Mol. Phys.* **56**, 1047 (1985).

[114] L. V. Slipchenko and M. S. Gordon, *J. Comput. Chem.* **28**, 276 (2007).

[115] M. A. Freitag, M. S. Gordon, J. H. Jensen, and W. J. Stevens, *J. Chem. Phys.* **112**, 7300 (2000).

[116] L. V. Slipchenko and M. S. Gordon, *Mol. Phys.* **107**, 999 (2009).

[117] I. Adamovic and M. S. Gordon, *Mol. Phys.* **103**, 379 (2005).

[118] K. T. Tang and J. P. Toennies, *J. Chem. Phys.* **80**, 3726 (1984).

[119] J. H. Jensen and M. S. Gordon, *Mol. Phys.* **89**, 1313 (1996).

[120] J. H. Jensen and M. S. Gordon, *J. Chem. Phys.* **108**, 4772 (1998).

[121] L. V. Slipchenko, *J. Phys. Chem. A* **114**, 8824 (2010).

[122] D. Kosenkov and L. V. Slipchenko, *J. Phys. Chem. A* **115**, 392 (2011).

[123] D. W. Zhang and J. Z. H. Zhang, *J. Chem. Phys.* **119**, 3599 (2003).

[124] D. W. Zhang, X. H. Chen, and J. Z. H. Zhang, *J. Comput. Chem.* **24**, 1846 (2003).

[125] J. C. Flick, D. Kosenkov, E. G. Hohenstein, C. D. Sherrill, and L. V. Slipchenko, *J. Chem. Theory Comput.* **8**, 2835 (2012).

[126] F. R. Manby, M. Stella, J. D. Goodpaster, and T. F. Miller III, *J. Chem. Theory Comput.* **8**, 2564 (2012).

[127] T. A. Wesolowski and A. Warshel, *J. Phys. Chem.* **97**, 8050 (1993).

[128] T. A. Wesolowski, *Phys. Rev. A* **77**, 012504 (2008).

[129] S. Prager, A. Zech, F. Aquilante, A. Dreuw, and T. A. Wesolowski, *J. Chem. Phys.* **144**, 204103 (2016).

[130] A. Zech, F. Aquilante, and T. A. Wesolowski, *J. Chem. Phys.* **143**, 164106 (2015).

# Chapter 12

# Fragment-Based Methods

## 12.1 Introduction

Molecular complexes and molecular clusters represent a broad class of systems with interesting chemical and physical properties. Such systems can be naturally partitioned into fragments each representing a molecule or several molecules. Q-CHEM contains a set of methods designed to use such partitioning either for physical or computational advantage. Some of these methods (*e.g.* the ALMO-EDA method and its most recent updates/extensions) were developed and implemented by Dr. Rustam Z. Khaliullin, Dr. Paul R. Horn, Yuezhi Mao, Dr. Daniel S. Levine, and Qinghui Ge working with Prof. Martin Head-Gordon at the University of California–Berkeley. Other methods (*e.g.* the XSAPT family of methods, TDDFT(MI)) were developed by Drs. Leif D. Jacobson, Ka Un Lao, and Jie Liu working with Prof. John M. Herbert at Ohio State University.

The list of methods that use partitioning includes:

- Initial guess at the MOs as a superposition of the converged MOs on the isolated fragments (FRAGMO guess) [1].
- Constrained (locally-projected) SCF methods for molecular interactions (SCF MI methods) between closed shell fragments [1], and also open shell fragments [2].
- Single Roothaan-step (RS) correction methods that improve FRAGMO and SCF MI description of molecular systems [1,2].
- Automated calculation of the BSSE with counterpoise correction method (full SCF and RS implementation).
- The original version the ALMO-EDA method (energy decomposition analysis based on absolutely localized molecular orbitals), including the associated charge transfer analysis [2–4] and the analysis of intermolecular bonding in terms of complementary occupied-virtual pairs (COVPs) [2,4,5].
- An improved version (“second generation") of the ALMO-EDA method [6–9], including its extension to single-bond interactions [10].
- The adiabatic ALMO-EDA method that bridges intermolecular interactions and molecular properties [11].

- The variational explicit polarization (XPol) method, a self-consistent, charge-embedded, monomer-based SCF calculation[12–14]
- Symmetry-adapted perturbation theory (SAPT), a monomer-based method for computing intermolecular interaction energies and decomposing them into physically-meaningful components[15,16].
- XPol+SAPT (XSAPT), which extends the SAPT methodology to systems consisting of more than two monomers[13,14,17].
- Closed- and open-shell AO-XSAPT(KS)+D, a dispersion-corrected version of XSAPT in atomic orbital basis that affords accurate intermolecular interaction energies at very low cost[18–20].
- A stable and physically-motivated energy decomposition approach, SAPT/cDFT, in which cDFT is used to define the charge-transfer component of the interaction energy and SAPT defines the electrostatic, polarization, Pauli repulsion, and van der Waals contributions[21].
- The electrostatically embedded many-body expansion[22] and the fragment molecular orbital method[23,24], for decomposing large clusters into small numbers of monomers, facilitating larger calculations.
- The Ab Initio Frenkel Davydov Model[25,26], a low-order scaling, highly parallelizable approach to computing excited state properties of liquids, crystals, and aggregates.
- TDDFT for molecular interactions [TDDFT(MI)], an excited-state extension of SCF(MI) that offers a reduced-cost way to compute excited states in molecular clusters, crystals, and aggregates[27–29].

Another fragment-based approach, the Effective Fragment Potential (EFP) method[30], was developed by Prof. Lyudmila V. Slipchenko at Purdue University and Prof. Anna I. Krylov at USC; this method is described in Section 11.5.

## 12.2 Specifying Fragments in the *$molecule* Section

To request any of the methods mentioned above one must specify how system is partitioned into fragments. All atoms and all electrons in the systems should be assigned to a fragment. Each fragment must contain an integer number of electrons. In the current implementation, both open and closed-shell fragments are allowed. In order to specify fragments, the fragment descriptors must be inserted into the *$molecule* section of the Q-CHEM input file. A fragment descriptor consists of two lines: the first line must start with two hyphens followed by optional comments, the second line must contain the charge and the multiplicity of the fragment. At least two fragments must be specified. Fragment descriptors in the *$molecule* section does not affect jobs that are not designed to use fragmentation.

**Example 12.1** Fragment descriptors in the *$molecule* section.

```
$molecule
   0 1
-- water molecule - proton donor
   0 1
   O1
   H2 O1 0.96
   H3 O1 0.96 H2 105.4
-- water molecule - proton acceptor
   0 1
   O4 O1 ROO  H2 105.4 H3   0.0
```

```
      X5 O4 2.00 O1 120.0 H2 180.0
      H6 O4 0.96 X5  55.6 O1  90.0
      H7 O4 0.96 X5  55.6 01 -90.0

      ROO = 2.4
   $end
```

Open shell systems must have a number of alpha electrons greater than the number of beta electrons. However, individual fragments in the system can be made to contain excess beta electrons by specifying a negative multiplicity. For instance, a multiplicity of $-2$ indicates one excess beta electron, as in the second fragment of the following example.

**Example 12.2** Open shell fragment descriptors in the *$molecule* section. The second fraghment is made with a negative multiplicity, so that overall the number of alpha and beta electrons match, yielding an approximate singlet state.

```
$molecule
   0 1
--  An alpha spin H atom
   0 2
   H1
--  A beta spin H atom
   0 -2
   H2 H1  1.50
$end
```

## 12.3 FRAGMO Initial Guess for SCF Methods

An accurate initial guess can be generated for molecular systems by superimposing converged molecular orbitals on isolated fragments. This initial guess is requested by specifying FRAGMO option for SCF_GUESS keyword and can be used for both the conventional SCF methods and the locally-projected SCF methods. The number of SCF iterations can be greatly reduced when FRAGMO is used instead of SAD. This can lead to significant time savings for jobs on multi-fragment systems with large basis sets[3]. Unlike the SAD guess, the FRAGMO guess is idempotent.

To converge molecular orbitals on isolated fragments, a child Q-CHEM job is executed for each fragment. *$rem* variables of the child jobs are inherited from the *$rem* section of the parent job. If SCF_PRINT_FRGM is set to TRUE the output of the child jobs is redirected to the output file of the parent job. Otherwise, the output is suppressed.

Additional keywords that control child Q-CHEM processes can be set in the *$rem_frgm* section of the parent input file. This section has the same structure as the *$rem* section. Options in the *$rem_frgm* section override options of the parent job. *$rem_frgm* is intended to specify keywords that control the SCF routine on isolated fragments. Please be careful with the keywords in *$rem_frgm* section. *$rem* variables FRGM_METHOD, FRGM_LPCORR, JOBTYPE, BASIS, PURECART, ECP are not allowed in *$rem_frgm* and will be ignored. *$rem* variables FRGM_METHOD, FRGM_LPCORR, JOBTYPE, and SCF_GUESS are not inherited from the parent job.

**Example 12.3** FRAGMO guess can be used with the conventional SCF calculations. *$rem_frgm* keywords in this example specify that the SCF on isolated fragments does not have to be converged tightly. See also Example 11.2 for an open-shell fragment example.

```
$molecule
0 1
--
0 1
O          -0.106357    0.087598    0.127176
H           0.851108    0.072355    0.136719
H          -0.337031    1.005310    0.106947
--
0 1
O           2.701100   -0.077292   -0.273980
H           3.278147   -0.563291    0.297560
H           2.693451   -0.568936   -1.095771
--
0 1
O           2.271787   -1.668771   -2.587410
H           1.328156   -1.800266   -2.490761
H           2.384794   -1.339543   -3.467573
--
0 1
O          -0.518887   -1.685783   -2.053795
H          -0.969013   -2.442055   -1.705471
H          -0.524180   -1.044938   -1.342263
$end

$rem
   METHOD          EDF1
   BASIS           6-31(2+,2+)g(df,pd)
   SCF_GUESS       FRAGMO
   SCF_PRINT_FRGM  FALSE
$end

$rem_frgm
   SCF_CONVERGENCE 2
   THRESH          5
$end
```

The use of FRAGMO guess is also supported when GEN_SCFMAN = TRUE. It is extended to support more SCF orbital types (R/U/RO/G). Meanwhile, users are allowed to read in the previously generated FRAGMO guess instead of recalculating them if there is no difference between these jobs on the fragment level. This can be particularly useful for scenarios such as scanning a potential energy curve for an intermolecular complex, or for restarting an EDA job. This is controlled by the *$rem* variable FRAGMO_GUESS_MODE.

**FRAGMO_GUESS_MODE**

Decide what to do regarding to the FRAGMO guess in the present job.

TYPE:

INTEGER

DEFAULT:

0

OPTIONS:

0 Spawn fragment jobs sequentially and collect the results as the FRAGMO guess at the end.

1 Generate fragment inputs in folders “FrgX" under the scratch directory of the present job and then terminate. Users can then take advantage of a queuing system to run these jobs simultaneously using “FrgX" as their scratch folders (should be handled with scripting).

2 Read in the available fragment data.

RECOMMENDATION:

Consider using “1" if the fragment calculations are evenly expensive. Use “2" when FRAGMO guess is pre-computed.

**Example 12.4** FRAGMO guess for ROSCF calculation in GEN_SCFMAN. The first fragment is RO and the second fragment is close-shell, while the super-system is computed with RO as well. The complex in the second job has a modified interfragment distance so it can make use of the FRAGMO guess generated by the first job. Note that ROSCF = TRUE is needed to treat the fragments and the super-system consistently.

```
$molecule
1 2
--
0 2
C1
H1 C1 1.09267
H2 C1 1.09267 H1 107.60335
H3 C1 1.09267 H2 107.60335 H1 115.692
--
1 1
Na C1 scan    H3 111.28008 H2 -122.154

scan = 2.0
$end

$rem
   METHOD           b3lyp
   BASIS            6-31g
   GEN_SCFMAN       true
   UNRESTRICTED     false
   SCF_CONVERGENCE  8
   ROSCF            true
   SCF_GUESS        fragmo
   THRESH           14
   SYMMETRY         false
   SYM_IGNORE       true
$end

@@@

$molecule
1 2
--
```

```
0 2
C1
H1 C1 1.09267
H2 C1 1.09267 H1 107.60335
H3 C1 1.09267 H2 107.60335 H1 115.692
--
1 1
Na C1 scan    H3 111.28008 H2 -122.154

scan = 3.0
$end

$rem
   METHOD             b3lyp
   BASIS              6-31g
   GEN_SCFMAN         true
   UNRESTRICTED       false
   SCF_CONVERGENCE    8
   ROSCF              true
   SCF_GUESS          fragmo
   FRAGMO_GUESS_MODE  2 !read in the available fragment data
   THRESH             14
   SYMMETRY           false
   SYM_IGNORE         true
$end
```

## 12.4 Locally-Projected SCF Methods

Constrained locally-projected SCF is an efficient method for removing the SCF diagonalization bottleneck in calculations for systems of weakly interacting components such as molecular clusters and molecular complexes[1,2]. The method is based on the equations of the locally-projected SCF for molecular interactions (SCF MI)[1,2,31–33]. In the SCF MI method, the occupied molecular orbitals on a fragment can be expanded only in terms of the atomic orbitals of the same fragment. Such constraints produce non-orthogonal MOs that are localized on fragments and are called absolutely-localized molecular orbitals (ALMOs). The ALMO approximation excludes charge-transfer from one fragment to another. It also prevents electrons on one fragment from borrowing the atomic orbitals of other fragments to compensate for incompleteness of their own AOs and, therefore, removes the BSSE from the interfragment binding energies. The locally-projected SCF methods perform an iterative minimization of the SCF energy with respect to the ALMOs coefficients. The convergence of the algorithm is accelerated with the locally-projected modification of the DIIS extrapolation method[1].

The ALMO approximation significantly reduces the number of variational degrees of freedom of the wave function. The computational advantage of the locally-projected SCF methods over the conventional SCF method grows with both basis set size and number of fragments. Although still cubic scaling, SCF MI effectively removes the diagonalization step as a bottleneck in these calculations, because it contains such a small prefactor. In the current implementation, the SCF MI methods do not speed up the evaluation of the Fock matrix and, therefore, do not perform significantly better than the conventional SCF in the calculations dominated by the Fock build.

Two locally-projected schemes are implemented. One is based on the locally-projected equations of Stoll *et al.*[31], the other utilizes the locally-projected equations of Gianinetti *et al.*[32] These methods have comparable performance. The Stoll iteration is only slightly faster than the Gianinetti iteration but the Stoll equations might be a little bit harder to converge. The Stoll equations also produce ALMOs that are orthogonal within a fragment. The type of the locally-projected SCF calculations is requested by specifying either STOLL or GIA for the FRGM_METHOD keyword.

**Example 12.5** Locally-projected SCF method of Stoll

```
$molecule
0 1
--
-1 1
B          0.068635    0.164710    0.123580
F         -1.197609    0.568437   -0.412655
F          0.139421   -1.260255   -0.022586
F          1.118151    0.800969   -0.486494
F          0.017532    0.431309    1.531508
--
+1 1
N         -2.132381   -1.230625    1.436633
H         -1.523820   -1.918931    0.977471
H         -2.381590   -0.543695    0.713005
H         -1.541511   -0.726505    2.109346
H         -2.948798   -1.657993    1.873482
$end

$rem
   METHOD          BP86
   BASIS           6-31(+,+)G(d,p)
   FRGM_METHOD     STOLL
$end

$rem_frgm
   SCF_CONVERGENCE 2
   THRESH          5
$end
```

### 12.4.1 Locally-Projected SCF Methods with Single Roothaan-Step Correction

Locally-projected SCF cannot quantitatively reproduce the full SCF intermolecular interaction energies for systems with significant charge-transfer between the fragments (*e.g.*, hydrogen bonding energies in water clusters). Good accuracy in the intermolecular binding energies can be achieved if the locally-projected SCF MI iteration scheme is combined with a charge-transfer perturbative correction[1]. To account for charge-transfer, one diagonalization of the full Fock matrix is performed after the locally-projected SCF equations are converged and the final energy is calculated as infinite-order perturbative correction to the locally-projected SCF energy. This procedure is known as single Roothaan-step (RS) correction[1,34,35]. It is performed if FRGM_LPCORR is set to RS. To speed up evaluation of the charge-transfer correction, second-order perturbative correction to the energy can be evaluated by solving the linearized single-excitation amplitude equations. This algorithm is called the approximate Roothaan-step correction and can be requested by setting FRGM_LPCORR to ARS.

Both ARS and RS corrected energies are very close to the full SCF energy for systems of weakly interacting fragments but are less computationally expensive than the full SCF calculations. To test the accuracy of the ARS and RS methods, the full SCF calculation can be done in the same job with the perturbative correction by setting FRGM_LPCORR to RS_EXACT_SCF or to ARS_EXACT_SCF. It is also possible to evaluate only the full SCF correction by setting FRGM_LPCORR to EXACT_SCF.

The iterative solution of the linear single-excitation amplitude equations in the ARS method is controlled by a set of NVO keywords described below.

*Restrictions.* Only single point HF and DFT energies can be evaluated with the locally-projected methods. Geometry optimization can be performed using numerical gradients. Wave function correlation methods (MP2, CC, *etc.*.) are not implemented for the absolutely-localized molecular orbitals. SCF_ALGORITHM cannot be set to anything but DIIS, however, all SCF convergence algorithms can be used on isolated fragments (set SCF_ALGORITHM in the *$rem_frgm* section).

**Example 12.6** Comparison between the RS corrected energies and the conventional SCF energies can be made by calculating both energies in a single run.

```
$molecule
0 1
--
0 1
O      -1.56875     0.11876     0.00000
H      -1.90909    -0.78106     0.00000
H      -0.60363     0.02937     0.00000
--
0 1
O       1.33393    -0.05433     0.00000
H       1.77383     0.32710    -0.76814
H       1.77383     0.32710     0.76814
$end

$rem
   METHOD          HF
   BASIS           AUG-CC-PVTZ
   FRGM_METHOD     GIA
   FRGM_LPCORR     RS_EXACT_SCF
$end

$rem_frgm
   SCF_CONVERGENCE 2
   THRESH          5
$end
```

### 12.4.2 Roothaan-Step Corrections to the FRAGMO Initial Guess

For some systems good accuracy for the intermolecular interaction energies can be achieved without converging SCF MI calculations and applying either the RS or ARS charge-transfer correction directly to the FRAGMO initial guess. Set FRGM_METHOD to NOSCF_RS or NOSCF_ARS to request the single Roothaan correction or approximate Roothaan correction, respectively. To get a somewhat better energy estimate set FRGM_METHOD to NOSCF_DRS and NOSCF_RS_FOCK. In the case of NOSCF_RS_FOCK, the same steps as in the NOSCF_RS method are performed followed by one more Fock build and calculation of the proper SCF energy. In the case of the double Roothaan-step correction, NOSCF_DRS, the same steps as in NOSCF_RS_FOCK are performed followed by one more diagonalization. The final energy in the NOSCF_DRS method is evaluated as a perturbative correction, similar to the single Roothaan-step correction.

Charge-transfer corrections applied directly to the FRAGMO guess are included in Q-CHEM to test accuracy and performance of the locally-projected SCF methods. However, for some systems they give a reasonable estimate of the binding energies at a cost of one (or two) SCF step(s).

### 12.4.3 Automated Evaluation of the Basis-Set Superposition Error

Evaluation of the basis-set superposition error (BSSE) is automated in Q-CHEM. To calculate BSSE-corrected binding energies, specify fragments in the *$molecule* section and set JOBTYPE to BSSE. The BSSE jobs are not limited to the SCF energies and can be evaluated for multi-fragment systems at any level of theory. Q-CHEM separates the system into fragments as specified in the *$molecule* section and performs a series of jobs on (a) each fragment, (b) each fragment with the remaining atoms in the system replaced by the ghost atoms, and (c) on the entire system. Q-CHEM saves all calculated energies and prints out the uncorrected and the BSSE corrected binding energies. The *$rem_frgm* section can be used to control calculations on fragments, however, make sure that the fragments and the entire system are treated equally. It means that all numerical methods and convergence thresholds that affect the final energies (such as SCF_CONVERGENCE, THRESH, PURECART, XC_GRID) should be the same for the fragments and for the entire system. Avoid using *$rem_frgm* in the BSSE jobs unless absolutely necessary.

*Important*. It is recommended to include PURECART keyword in all BSSE jobs. GENERAL basis cannot be used for the BSSE calculations in the current implementation. Use MIXED basis instead.

**Example 12.7** Evaluation of the BSSE corrected intermolecular interaction energy

```
$molecule
0 1
--
0 1
O         -0.089523    0.063946    0.086866
H          0.864783    0.058339    0.103755
H         -0.329829    0.979459    0.078369
--
0 1
O          2.632273   -0.313504   -0.750376
H          3.268182   -0.937310   -0.431464
H          2.184198   -0.753305   -1.469059
--
0 1
O          0.475471   -1.428200   -2.307836
H         -0.011373   -0.970411   -1.626285
H          0.151826   -2.317118   -2.289289
$end

$rem
   JOBTYPE         BSSE
   METHOD          MP2
   BASIS           6-31(+,+)G(d,p)
$end
```

## 12.5 The First-Generation ALMO-EDA and Charge-Transfer Analysis (CTA)

### 12.5.1 Energy Decomposition Analysis Based on Absolutely Localized Molecular Orbitals

The strength of intermolecular binding is inextricably connected to the fundamental nature of interactions between the molecules. Intermolecular complexes can be stabilized through weak dispersive forces, electrostatic effects (*e.g.*, charge–charge, charge–dipole, and charge–induced dipole interactions) and donor-acceptor type orbital interactions such as forward and back-donation of electron density between the molecules. Depending on the extent of these interactions, the intermolecular binding could vary in strength from just several kJ/mol (van der Waals complexes) to several hundred kJ/mol (metal–ligand bonds in metal complexes). Understanding the contributions of various interaction modes enables one to tune the strength of the intermolecular binding to the ideal range by designing materials that promote desirable effects. One of the most powerful techniques that modern first principles electronic structure methods provide to study and analyze the nature of intermolecular interactions is the decomposition of the total molecular binding energy into the physically meaningful components such as dispersion, electrostatic, polarization, charge transfer, and geometry relaxation terms.

Energy decomposition analysis based on absolutely-localized molecular orbitals (ALMO EDA) is implemented in Q-CHEM[3], including the open shell generalization[2]. In ALMO EDA, the total intermolecular binding energy is decomposed into the "frozen density" component (FRZ), the polarization (POL) term, and the charge-transfer (CT) term. The "frozen density" term is defined as the energy change that corresponds to bringing infinitely separated fragments together without *any* relaxation of their MOs. The FRZ term is calculated as a difference between the FRAGMO guess energy and the sum of the converged SCF energies on isolated fragments. The polarization (POL) energy term is defined as the energy lowering due to the *intrafragment* relaxation of the frozen occupied MOs on the fragments. The POL term is calculated as a difference between the converged SCF MI energy and the FRAGMO guess energy. Finally, the charge-transfer (CT) energy term is due to further *interfragment* relaxation of the MOs. It is calculated as a difference between the fully converged SCF energy and the converged SCF MI energy.

The total charge-transfer term includes the energy lowering due to electron transfer from the occupied orbitals on one molecule (more precisely, occupied in the converged SCF MI state) to the virtual orbitals of another molecule as well as the further energy change caused by induction that accompanies such an occupied/virtual mixing. The energy lowering of the occupied-virtual electron transfer can be described with a single non-iterative Roothaan-step correction starting from the converged SCF MI solution. Most importantly, the mathematical form of the SCF MI(RS) energy expression allows one to decompose the occupied-virtual mixing term into bonding and back-bonding components for each pair of molecules in the complex. The remaining charge-transfer energy term (*i.e.*, the difference between SCF MI(RS) energy and the full SCF energy) includes all induction effects that accompany occupied-virtual charge transfer and is generally small. This last term is called higher order (HO) relaxation. Unlike the RS contribution, the higher order term cannot be divided naturally into forward and back-donation terms. The BSSE associated with each charge-transfer term (forward donation, back-bonding, and higher order effects) can be corrected individually.

To perform energy decomposition analysis, specify fragments in the *$molecule* section and set JOBTYPE to EDA. For a complete EDA job, Q-CHEM

- performs the SCF on isolated fragments (use the *$rem_frgm* section if convergence issues arise but make sure that keywords in this section do not affect the final energies of the fragments),

- generates the FRAGMO guess to obtain the FRZ term,
- converges the SCF MI equations to evaluate the POL term,
- performs evaluation of the perturbative (RS or ARS) variational correction to calculate the forward donation and back-bonding components of the CT term for each pair of molecules in the system,
- converges the full SCF procedure to evaluate the higher order relaxation component of the CT term.

The FRGM_LPCORR keyword controls evaluation of the CT term in an EDA job. To evaluate all of the CT components mentioned above set this keyword to RS_EXACT_SCF or ARS_EXACT_SCF. If the HO term in not important then the final step (*i.e.*, the SCF calculation) can be skipped by setting FRGM_LPCORR to RS or ARS. If only the total CT term is required then set FRGM_LPCORR to EXACT_SCF.

ALMO charge transfer analysis (ALMO CTA) is performed together with ALMO EDA[4]. The ALMO charge transfer scale, $DeltaQ$, provides a measure of the distortion of the electronic clouds upon formation of an intermolecular bond and is such that all CT terms (*i.e.*, forward-donation, back-donation, and higher order relaxation) have well defined energetic effects (*i.e.*, ALMO CTA is consistent with ALMO EDA).

To remove the BSSE from the CT term (both on the energy and charge scales), set EDA_BSSE to TRUE. Q-CHEM generates an input file for each fragment with MIXED basis set to perform the BSSE correction. As with all jobs with MIXED basis set and d or higher angular momentum basis functions on atoms, the PURECART keyword needs to be initiated. If EDA_BSSE=TRUE GENERAL basis sets cannot be used in the current implementation.

Please note that the energy of the geometric distortion of the fragments is not included into the total binding energy calculated in an EDA job. The geometry optimization of isolated fragments must be performed to account for this term.

**Example 12.8** Energy decomposition analysis of the binding energy between the water molecules in a tetramer. ALMO CTA results are also printed out.

```
$molecule
0 1
--
0 1
O          -0.106357    0.087598    0.127176
H           0.851108    0.072355    0.136719
H          -0.337031    1.005310    0.106947
--
0 1
O           2.701100   -0.077292   -0.273980
H           3.278147   -0.563291    0.297560
H           2.693451   -0.568936   -1.095771
--
0 1
O           2.271787   -1.668771   -2.587410
H           1.328156   -1.800266   -2.490761
H           2.384794   -1.339543   -3.467573
--
0 1
O          -0.518887   -1.685783   -2.053795
H          -0.969013   -2.442055   -1.705471
H          -0.524180   -1.044938   -1.342263
```

```
$end

$rem
   JOBTYPE          EDA
   METHOD           EDF1
   BASIS            6-31(+,+)g(d,p)
   PURECART         1112
   FRGM_METHOD      GIA
   FRGM_LPCORR      RS_EXACT_SCF
   EDA_BSSE         TRUE
$end
```

**Example 12.9** An open shell EDA example of Na$^+$ interacting with the methyl radical.

```
$molecule
   1 2
--
   0 2
   C       -1.447596  -0.000023   0.000019
   H       -1.562749   0.330361  -1.023835
   H       -1.561982   0.721445   0.798205
   H       -1.561187  -1.052067   0.225866
--
   1 1
   Na       1.215591   0.000036  -0.000032
$end

$rem
   JOBTYPE               EDA
   METHOD                B3LYP
   BASIS                 6-31G*
   UNRESTRICTED          TRUE
   SCF_GUESS             FRAGMO
   FRGM_METHOD           STOLL
   FRGM_LPCORR           RS_EXACT_SCF
   EDA_BSSE              TRUE
   DIIS_SEPARATE_ERRVEC 1
$end
```

### 12.5.2 Analysis of Charge-Transfer Based on Complementary Occupied/Virtual Pairs

In addition to quantifying the amount and energetics of intermolecular charge transfer, it is often useful to have a simple description of orbital interactions in intermolecular complexes. The polarized ALMOs obtained from the SCF MI procedure and used as a reference basis set in the decomposition analysis do not directly show which occupied-virtual orbital pairs are of most importance in forming intermolecular bonds. By performing rotations of the polarized ALMOs within a molecule, it is possible to find a “chemist’s basis set” that represents bonding between molecules in terms of just a few localized orbitals called complementary occupied-virtual pairs (COVPs). This orbital interaction model validates existing conceptual descriptions of intermolecular bonding. For example, in the modified ALMO basis, hydrogen bonding in water dimer is represented as an electron pair localized on an oxygen atom donating electrons to the O–H $\sigma$-antibonding orbital on the other molecule[5], and the description of synergic bonding in metal complexes agrees well with simple Dewar-Chatt-Duncanson model[4,36,37].

Set EDA_COVP to TRUE to perform the COVP analysis of the CT term in an EDA job. COVP analysis is currently implemented only for systems of two fragments. Set EDA_PRINT_COVP to TRUE to print out localized orbitals that form occupied-virtual pairs. In this case, MOs obtained in the end of the run (SCF MI orbitals, SCF MI(RA) orbitals, converged SCF orbitals) are replaced by the orbitals of COVPs. Each orbital is printed with the corresponding CT energy term in kJ/mol (instead of the energy eigenvalues in hartrees). These energy labels make it easy to find correspondence between an occupied orbital on one molecule and the virtual orbital on the other molecule. The examples below show how to print COVP orbitals. One way is to set *$rem* variable PRINT_ORBITALS, the other is to set IANLTY to 200 and use the *$plots* section in the Q-CHEM input. In the first case the orbitals can be visualized using MOLDEN (set MOLDEN_FORMAT to TRUE), in the second case use VMD or a similar third party program capable of making 3D plots.

**Example 12.10** COVP analysis of the CT term. The COVP orbitals are printed in the Q-CHEM and MOLDEN formats.

```
$molecule
0 1
--
0 1
O          -1.521720    0.129941    0.000000
H          -1.924536   -0.737533    0.000000
H          -0.571766   -0.039961    0.000000
--
0 1
O           1.362840   -0.099704    0.000000
H           1.727645    0.357101   -0.759281
H           1.727645    0.357101    0.759281
$end

$rem
   JOBTYPE         EDA
   BASIS           6-31G
   PURECART        1112
   METHOD          B3LYP
   FRGM_METHOD     GIA
   FRGM_LPCORR     RS_EXACT_SCF
   EDA_COVP        TRUE
   EDA_PRINT_COVP  TRUE
   PRINT_ORBITALS  16
   MOLDEN_FORMAT   TRUE
$end
```

**Example 12.11** COVP analysis of the CT term. Note that it is not necessary to run a full EDA job. It is suffice to set FRGM_LPCORR to RS or ARS and EDA_COVP to TRUE to perform the COVP analysis. The orbitals of the most significant occupied-virtual pair are printed into an ASCII file called *plot.mo* which can be converted into a cube file and visualized in VMD.

```
$molecule
0 1
--
0 1
O          -1.521720    0.129941    0.000000
H          -1.924536   -0.737533    0.000000
H          -0.571766   -0.039961    0.000000
--
```

```
0 1
O          1.362840   -0.099704    0.000000
H          1.727645    0.357101   -0.759281
H          1.727645    0.357101    0.759281
$end

$rem
   BASIS            6-31G
   PURECART         1112
   METHOD           B3LYP
   FRGM_METHOD      GIA
   FRGM_LPCORR      RS
   IANLTY           200
   EDA_COVP         TRUE
   EDA_PRINT_COVP   TRUE
$end

$plots
MOs
   80  -4.0  4.0
   60  -3.0  3.0
   60  -3.0  3.0
   2   0  0  0
   6  11
$end
```

## 12.6 Job Control for Locally-Projected SCF Methods

**FRGM_METHOD**

Specifies a locally-projected method.

TYPE:

STRING

DEFAULT:

NONE

OPTIONS:

| | |
|---|---|
| STOLL | Locally-projected SCF equations of Stoll are solved. |
| GIA | Locally-projected SCF equations of Gianinetti are solved. |
| NOSCF_RS | Single Roothaan-step correction to the FRAGMO initial guess. |
| NOSCF_ARS | Approximate single Roothaan-step correction to the FRAGMO initial guess. |
| NOSCF_DRS | Double Roothaan-step correction to the FRAGMO initial guess. |
| NOSCF_RS_FOCK | Non-converged SCF energy of the single Roothaan-step MOs. |

RECOMMENDATION:

STOLL and GIA are for variational optimization of the ALMOs. NOSCF options are for computationally fast corrections of the FRAGMO initial guess.

**FRGM_LPCORR**

Specifies a correction method performed after the locally-projected equations are converged.

TYPE:

STRING

DEFAULT:

NONE

OPTIONS:

| | |
|---|---|
| ARS | Approximate Roothaan-step perturbative correction. |
| RS | Single Roothaan-step perturbative correction. |
| EXACT_SCF | Full SCF variational correction. |
| ARS_EXACT_SCF | Both ARS and EXACT_SCF in a single job. |
| RS_EXACT_SCF | Both RS and EXACT_SCF in a single job. |

RECOMMENDATION:

For large basis sets use ARS, use RS if ARS fails.

**SCF_PRINT_FRGM**

Controls the output of Q-CHEM jobs on isolated fragments.

TYPE:

LOGICAL

DEFAULT:

FALSE

OPTIONS:

| | |
|---|---|
| TRUE | The output is printed to the parent job output file. |
| FALSE | The output is not printed. |

RECOMMENDATION:

Use TRUE if details about isolated fragments are important.

**EDA_BSSE**

Calculates the BSSE correction when performing the energy decomposition analysis.

TYPE:

LOGICAL

DEFAULT:

FALSE

OPTIONS:

TRUE/FALSE

RECOMMENDATION:

Set to TRUE unless a very large basis set is used.

**EDA_COVP**

Perform COVP analysis when evaluating the RS or ARS charge-transfer correction. COVP analysis is currently implemented only for systems of two fragments.

TYPE:

LOGICAL

DEFAULT:

FALSE

OPTIONS:

TRUE/FALSE

RECOMMENDATION:

Set to TRUE to perform COVP analysis in an EDA or SCF MI(RS) job.

**EDA_PRINT_COVP**

Replace the final MOs with the CVOP orbitals in the end of the run.

TYPE:

LOGICAL

DEFAULT:

FALSE

OPTIONS:

TRUE/FALSE

RECOMMENDATION:

Set to TRUE to print COVP orbitals instead of conventional MOs.

**NVO_LIN_MAX_ITE**

Maximum number of iterations in the preconditioned conjugate gradient solver of the single-excitation amplitude equations.

TYPE:

INTEGER

DEFAULT:

30

OPTIONS:

$n$ User–defined number of iterations.

RECOMMENDATION:

None.

**NVO_LIN_CONVERGENCE**

Target error factor in the preconditioned conjugate gradient solver of the single-excitation amplitude equations.

TYPE:

INTEGER

DEFAULT:

3

OPTIONS:

$n$ User–defined number.

RECOMMENDATION:

Solution of the single-excitation amplitude equations is considered converged if the maximum residual is less than $10^{-n}$ multiplied by the current DIIS error. For the ARS correction, $n$ is automatically set to 1 since the locally-projected DIIS error is normally several orders of magnitude smaller than the full DIIS error.

**NVO_METHOD**

Sets method to be used to converge solution of the single-excitation amplitude equations.

TYPE:

INTEGER

DEFAULT:

9

OPTIONS:

$n$ User–defined number.

RECOMMENDATION:

This is an experimental option. Use the default.

**NVO_UVV_PRECISION**

Controls convergence of the Taylor series when calculating the $U_{vv}$ block from the single-excitation amplitudes. Series is considered converged when the maximum element of the term is less than $10^{-n}$.

TYPE:

INTEGER

DEFAULT:

11

OPTIONS:

$n$ User–defined number.

RECOMMENDATION:

NVO_UVV_PRECISION must be the same as or larger than THRESH.

**NVO_UVV_MAXPWR**

Controls convergence of the Taylor series when calculating the $U_{vv}$ block from the single-excitation amplitudes. If the series is not converged at the $n$th term, more expensive direct inversion is used to calculate the $U_{vv}$ block.

TYPE:

INTEGER

DEFAULT:

10

OPTIONS:

$n$ User–defined number.

RECOMMENDATION:

None.

**NVO_TRUNCATE_DIST**

Specifies which atomic blocks of the Fock matrix are used to construct the preconditioner.

TYPE:

INTEGER

DEFAULT:

-1

OPTIONS:

| | |
|---|---|
| $n > 0$ | If distance between a pair of atoms is more than $n$ Ångstroms do not include the atomic block. |
| -2 | Do not use distance threshold, use NVO_TRUNCATE_PRECOND instead. |
| -1 | Include all blocks. |
| 0 | Include diagonal blocks only. |

RECOMMENDATION:

This option does not affect the final result. However, it affects the rate of the PCG algorithm convergence. For small systems, use the default.

**NVO_TRUNCATE_PRECOND**

Specifies which atomic blocks of the Fock matrix are used to construct the preconditioner. This variable is used only if NVO_TRUNCATE_DIST is set to $-2$.

TYPE:

INTEGER

DEFAULT:

2

OPTIONS:

$n$ If the maximum element in an atomic block is less than $10^{-n}$ do not include the block.

RECOMMENDATION:

Use the default. Increasing $n$ improves convergence of the PCG algorithm but overall may slow down calculations.

## 12.7 The Second-Generation ALMO-EDA Method

The ALMO-EDA method introduced in Section 12.5 is a very useful tool for unraveling the nature of intermolecular interactions. Nevertheless, it has two major shortcomings: (i) Although the polarization (POL) energy is variationally evaluated, it does not have a meaningful basis set limit. As the employed basis set becomes larger, the POL term starts to be contaminated by charge transfer (CT) and loses its intended meaning. (ii) The frozen (FRZ) interaction is a monolithic term in the original ALMO-EDA scheme. In practice, further decomposition of the FRZ term is often desired. For example, if one wants to use ALMO-EDA as a tool for the development of empirical force fields, the separation of the FRZ term into contributions from permanent electrostatics, Pauli repulsion and dispersion will be helpful since they are usually modeled by distinct functional forms in classical force fields. These drawbacks have been addressed recently, defining the second generation of the ALMO-EDA method (also referred to as "EDA2" in the text below)[6,8,9].

### 12.7.1 Generalized SCFMI Calculations and Additional Features

The original definition of the ALMOs used in SCFMI calculations is based on the fragment-blocking structure of the AO-to-MO transformation matrix, *i.e.*, for a given fragment, the associated MOs can only be expanded by the AO basis functions centered on the atoms that belong to the same fragment. Here we propose a generalized definition for SCFMI calculations: given a set of basis vectors ($\mathbf{G}$) in which each of them is tagged to a fragment but is allowed to be spanned by any AO basis function, it defines the working basis of the SCFMI problem. Then, within this basis, the locally projected SCF equations can be solved in a similar way, with the constraint that the MO coefficient matrix in the working basis ($\mathbf{G}$) is fragment-block-diagonal, while the MO coefficient matrix in the AO basis does not necessarily retain the blocking structure. The basis vectors in $\mathbf{G}$ can be either non-orthogonal or orthogonal between fragments. More details on the generalized SCFMI equations are available in ref. 6.

This generalized SCFMI scheme is implemented in GEN_SCFMAN (the original AO-block based scheme is available in GEN_SCFMAN as well). It is utilized for the variational optimization of the polarized (but CT-forbidden) intermediate state in "EDA2" (see Section 12.7.2). Another preferable feature of this generalized scheme is that the interfragment linear dependency in $\mathbf{G}$ can be properly handled. Therefore, this scheme can be used to replace the original AO-block based SCFMI without becoming ill-defined when interfragment linear dependency occurs. In contrast, the original ALMO-EDA method that employs the AO-block based approach fails when the sum of the number of orbitals on each fragment is not equal to the number of orbitals for the super-system (the latter is determined by the total number of AO basis functions and BASIS_LIN_DEP_THRESH), which often happens when substantially large basis sets are used or when the super-system comprises a large number of fragments.

SCFMI calculations based on the GEN_SCFMAN implementation are triggered by setting GEN_SCFMAN = TRUE and FRGM_METHOD = STOLL or GIA (the other options of FRGM_METHOD are not allowed). A subset of supported algorithms in GEN_SCFMAN are available for restricted (R) and unrestricted (U) SCFMI, including DIIS, GDM_LS, and NEWTON_CG. While the DIIS algorithm iteratively solves for the locally-projected SCF equations, the latter two methods use the energy derivatives with respect to the on-fragment orbital rotations to minimize the energy until the gradient reaches zero. As for standard calculations using GEN_SCFMAN, internal stability analysis is also available for R- and U-SCFMI, and one can set FD_MAT_VEC_PROD to TRUE if the analytical Hessian is not available for the employed density functional.

As in the original implementation, perturbative corrections can be applied on top of the SCFMI solution to approach the full SCF result, and this is still controlled by FRGM_LPCORR. Note that among the options introduced in Section 12.6, only ARS and RS are allowed here since the exact SCF calculation is actually beyond the scope of SCFMI.

In addition, with this more general implementation users are allowed to specify some fragments to be frozen during the SCFMI calculation, *i.e.*, intrafragment relaxation does not occur on these fragments.

This is achieved by specifying the *$rem* variable SCFMI_FREEZE_SS. Such a calculation can be interpreted as an active fragment being embedded in a frozen environment where the interaction between them is treated quantum mechanically.

**SCFMI_MODE**

Determine whether generalized SCFMI is used and also the property of the working basis.

TYPE:

INTEGER

DEFAULT:

0 AO-block based SCFMI (the original definition of ALMOs).

1 Generalized SCFMI with basis vectors that are non-orthogonal between fragments.

2 Generalized SCFMI with basis vectors that are orthogonal between fragments.

OPTIONS:

0 (“1" is used by basic “EDA2" calculations).

RECOMMENDATION:

None

**SCFMI_FREEZE_SS**

Keep the first several fragments unrelaxed in an SCFMI calculation.

TYPE:

INTEGER

DEFAULT:

$n$ Freeze the first $n$ fragments.

OPTIONS:

0 (all fragments are active)

RECOMMENDATION:

None

**Example 12.12** Generalized SCFMI calculation for the water dimer with single Roothaan-step perturbative correction. For this specific case, the result is identical to that given by AO-block based SCFMI (SCFMI_MODE = 0).

```
$molecule
0 1
--
0 1
O  -1.551007  -0.114520   0.000000
H  -1.934259   0.762503   0.000000
H  -0.599677   0.040712   0.000000
--
0 1
O   1.350625   0.111469   0.000000
H   1.680398  -0.373741  -0.758561
H   1.680398  -0.373741   0.758561
$end

$rem
   JOBTYPE          sp
   METHOD           b3lyp
   GEN_SCFMAN       true
   BASIS            6-31+G(d)
   GEN_SCFMAN        true
   SCF_CONVERGENCE   8
   THRESH            14
   SYMMETRY          false
   SYM_IGNORE        true
   FRGM_METHOD       stoll
   FRGM_LPCORR       rs
   SCFMI_MODE        1 !gen scfmi (non-orthogonal)
$end
```

### 12.7.2 Polarization Energy with a Well-defined Basis Set Limit

The definition of polarization energy lowering in the original ALMO-EDA utilizes the full AO space of each fragment as the variational degrees of freedom. This is based on the assumption that the AO basis functions are fragment-ascribable based on their atomic centers. However, this assumption becomes inappropriate when very large basis sets are used, especially those with diffuse functions (*e.g.* def2-QZVPPD). In such scenarios, basis functions on a given fragment tend to describe other fragments so that the "absolute localization" constraint becomes weaker and finally gets effectively removed. This is why the original ALMO-EDA scheme does not have a well-defined basis set limit for its polarization energy.

To overcome this problem, Horn and Head-Gordon proposed a new definition for the POL term in the ALMO-EDA method based on fragment electrical response functions (FERFs)[6]. FERFs on a given fragment are prepared by solving CPSCF equations after its SCF solution is found:

$$H_{ai,bj}(\Delta_\mu)_{bj} = (M_\mu)_{ai}, \tag{12.1}$$

where $\mathbf{H}$ is SCF orbital Hessian and $\mathbf{M}_\mu$ is a component ($\mu$) of a multipole matrix with a certain order. The resulting fragment response matrices ($\{\Delta_\mu\}$) are a set of $n_\text{v} \times n_\text{o}$ matrices. Then, a singular value decomposition (SVD) is performed on $\Delta_\mu$:

$$(\Delta_\mu)_{ai} = (L_\mu)_{ab}(d_\mu)_{bj}(R_\mu^T)_{ji}, \tag{12.2}$$

and the left vectors (not including the null vectors) will be used to construct a truncated virtual space, which is used to define the variational degrees of freedom for the SCFMI problem:

$$\mathbf{V}_\mu = \mathbf{C}_\text{vir}\mathbf{L}_\mu, \tag{12.3}$$

where $\mathbf{C}_\text{vir}$ denotes the original virtual orbitals of the given fragment.

The basic spirit of using FERFs is to obtain a subset of virtuals that is most pertinent to the electrical polarization of a given fragment, while the redundant variational degrees of freedom (which might be CT-like) are excluded. This scheme is shown to give a well-defined basis set limit for the polarization energy that relies on the SCFMI calculation. The multipole orders (dipole (D), quadrupole (Q), and octopole (O)) included on the RHS of eq. 12.2 decide the span of FERFs on each fragment. Numerical experiments suggest that the inclusion of dipole- and quadrupole-type responses is able to long-range induced electrostatics correctly and also gives a well-defined basis set limit, which is thus recommended as the working basis of the SCFMI problem. The full span of the polarization subspace of fragment $A$ is thus:

$$\mathbf{O}_A \oplus \text{span}\{\mathbf{V}_{\mu x}, \mathbf{V}_{\mu y}, \mathbf{V}_{\mu z}\} \oplus \text{span}\{\mathbf{V}_{Q2,-2}, \mathbf{V}_{Q2,-1}, \mathbf{V}_{Q2,0}, \mathbf{V}_{Q2,1}, \mathbf{V}_{Q2,2}\}. \tag{12.4}$$

Therefore, each occupied orbital will be paired with eight virtual orbitals (if the employed AO basis is large enough).

The polarization subspaces constructed as in eq. 12.4 are non-orthogonal between fragments. Therefore, it is named as the “nDQ" model for polarization. There is another version of this method which enforces interfragment orthogonality between the polarization subspaces and it is correspondingly termed as “oDQ" (or with other multipole orders). The preparation of orthogonal FERFs is more complicated (see ref. 6 for the details) and usually gives less favorable polarization energies. For most general cases, we recommend the use of the “nDQ" model. Calculations using FERFs are performed using the generalized SCFMI procedure introduced in Section 12.7.1.

**CHILD_MP**

Compute FERFs for fragments and use them as the basis for SCFMI calculations.

TYPE:

BOOLEAN

DEFAULT:

FALSE

OPTIONS:

| | |
|---|---|
| FALSE | Do not compute FERFs (use the full AO span of each fragment). |
| TRUE | Compute fragment FERFs. |

RECOMMENDATION:

Use FERFs to compute polarization energy when large basis sets are used. In an “EDA2" calculation, this *$rem* variable is set based on the given option automatically.

**CHILD_MP_ORDERS**

The multipole orders included in the prepared FERFs. The last digit specifies how many multipoles to compute, and the digits in the front specify the multipole orders: 1: dipole (D); 2: quadrupole (Q); 3: octopole (O).

TYPE:

INTEGER

DEFAULT:

0

OPTIONS:

| | |
|---|---|
| 11 | D |
| 122 | DQ |
| 1233 | DQO |

RECOMMENDATION:

Use 122 (DQ) when FERF is needed.

**Example 12.13** Generalized SCFMI calculation for the water dimer using nDQ FERFs.

```
$molecule
0 1
--
0 1
O  -1.551007  -0.114520   0.000000
H  -1.934259   0.762503   0.000000
H  -0.599677   0.040712   0.000000
--
0 1
O   1.350625   0.111469   0.000000
H   1.680398  -0.373741  -0.758561
H   1.680398  -0.373741   0.758561
$end
```

```
$rem
   JOBTYPE            sp
   METHOD             wb97x-v
   GEN_SCFMAN         true
   BASIS              6-31+G(d)
   GEN_SCFMAN         true
   SCF_ALGORITHM      diis
   SCF_CONVERGENCE    8
   THRESH             14
   SYMMETRY           false
   SYM_IGNORE         true
   SCF_FINAL_PRINT    1
   FRGM_METHOD        stoll
   SCFMI_MODE         1 !nonortho gen scfmi
   CHILD_MP           true
   CHILD_MP_ORDERS    122 !DQ
   FD_MAT_VEC_PROD    false
$end
```

### 12.7.3 Further Decomposition of the Frozen Interaction Energy

The frozen interaction energy in ALMO-EDA is defined as the energy difference between the unrelaxed frozen (Heitler-London) wave function and the isolated fragments. In other literature (*e.g.* Ref. 38), this interaction is often decomposed in a classical fashion:

$$\Delta E_{\mathrm{frz}} = \Delta E_{\mathrm{elec}}^{\mathrm{cls}} + \Delta E_{\mathrm{pauli}}^{\mathrm{cls}}, \tag{12.5}$$

where the contribution from permanent electrostatics is defined as the Coulomb interaction between isolated fragment charge distributions:

$$\Delta E_{\mathrm{elec}}^{\mathrm{cls}} = \sum_{A<B} \int_{r_1} \int_{r_2} \rho_A^{\mathrm{tot}}(\mathbf{r}_1) \frac{1}{\mathbf{r}_{12}} \rho_B^{\mathrm{tot}}(\mathbf{r}_2) \mathrm{d}\mathbf{r}_1 \mathrm{d}\mathbf{r}_2 \tag{12.6}$$

and the remainder constitutes the Pauli (or exchange) term. Such a decomposition (referred to as the classical decomposition below) is associated with two issues: (i) the evaluation of permanent electrostatics makes use of the “promolecule" state (whose density is the simple sum of monomer densities) rather than a properly anti-symmetrized wave function; (ii) when dispersion-corrected density functionals are utilized, the Pauli term contains dispersion interaction and thus loses its original meaning.

Horn *et al.* proposed a new scheme to further decompose the frozen term into contributions from permanent electrostatics (ELEC), Pauli repulsion (PAULI) and dispersion (DISP)[8]:

$$\Delta E_{\mathrm{frz}} = \Delta E_{\mathrm{elec}} + \Delta E_{\mathrm{pauli}} + \Delta E_{\mathrm{disp}} \tag{12.7}$$

This approach is compatible with the use of all kinds of density functionals except double-hybrids, and all three components of the FRZ term are computed with the antisymmetrized frozen wave function. The key step of this method is the orthogonal decomposition of the 1PDM associated with the frozen wave function into contributions from individual fragments: $\mathbf{P}_{\mathrm{frz}} = \sum_A \tilde{\mathbf{P}}_A$. This is achieved by minimizing an objective function as follows:

$$\Omega = \sum_A E_A[\tilde{\mathbf{P}}_A] - E_A[\mathbf{P}_A] \tag{12.8}$$

while interfragment orthogonality is enforced between $\tilde{\mathbf{P}}_A$'s. The readers are referred to Ref. 8 for more details about the orthogonal decomposition.

The ELEC term is then defined as the Coulomb interaction between distorted fragment densities ($\tilde{\rho}_A(\mathbf{r})$):

$$\Delta E_{\text{elec}} = \sum_{A<B} \int_{r_1} \int_{r_2} \tilde{\rho}_A^{\text{tot}}(\mathbf{r}_1) \frac{1}{\mathbf{r}_{12}} \tilde{\rho}_B^{\text{tot}}(\mathbf{r}_2) \mathrm{d}\mathbf{r}_1 \mathrm{d}\mathbf{r}_2. \tag{12.9}$$

The DISP term is evaluated by subtracting the dispersion-free part of the total exchange-correlation (XC) interaction, where an auxiliary "dispersion-free" (DF) XC functional is used in company with the primary XC functional:

$$\Delta E_{\text{disp}} = \left( E_{\text{xc}}[\mathbf{P}_{\text{frz}}] - \sum_A E_{\text{xc}}[\tilde{\mathbf{P}}_A] \right) - \left( E_{\text{xc}}^{\text{DF}}[\mathbf{P}_{\text{frz}}] - \sum_A E_{\text{xc}}^{\text{DF}}[\tilde{\mathbf{P}}_A] \right). \tag{12.10}$$

It is suggested that HF is an appropriate DFXC to be used for dispersion-corrected hybrid functionals (*e.g.* $\omega$B97M-V, B3LYP-D3), while revPBE is appropriate for semi-local functionals (*e.g.* B97M-V).

The remainder of the frozen interaction goes into the PAULI term, which includes the net repulsive interaction given by eq. 12.8 and the "dispersion-free" part of the XC interaction:

$$\Delta E_{\text{pauli}} = \sum_A (E_A[\tilde{\mathbf{P}}_A] - E_A[\mathbf{P}_A]) + \left( E_{\text{xc}}^{\text{DF}}[\mathbf{P}_{\text{frz}}] - \sum_A E_{\text{xc}}^{\text{DF}}[\tilde{\mathbf{P}}_A] \right). \tag{12.11}$$

The PAULI term and the ELEC term can also be combined together and reported as the dispersion-free frozen (DFFRZ) term if desired.

In Q-CHEM's implementation of "EDA2", the classical frozen decomposition and the new scheme defined by eqs. 12.9–12.11 are both calculated by default. The classical ELEC term only depends on monomer properties and the distances between fragments, therefore, it can be particularly useful for scenarios such as force field development (as the reference for permanent electrostatics). When the DISP term calculated by the new scheme is available, a modified classical Pauli term[39] is also reported, which is simply defined as

$$\Delta E_{\text{pauli}}^{\text{mod}} = \Delta E_{\text{pauli}}^{\text{cls}} - \Delta E_{\text{disp}}, \tag{12.12}$$

*i.e.*, the dispersion contribution is removed from the classical Pauli term computed using its original definition. Alternatively, this can also be achieved without performing the orthogonal decomposition, by setting CLS_DISP to TRUE. This also evaluates the DISP term via eq. 12.10 except that undistorted monomer densities ($\mathbf{P}_A$'s) are used instead of their distorted counterparts ($\tilde{\mathbf{P}}_A$'s).

**FRZ_ORTHO_DECOMP**

Perform the decomposition of frozen interaction energy based on the orthogonal decomposition of the 1PDM associated with the frozen wave function.

TYPE:

BOOLEAN

DEFAULT:

FALSE (automatically set to TRUE by EDA2 options 1–5)

OPTIONS:

FALSE Do not perform the orthogonal decomposition.

TRUE Perform the frozen energy decomposition using orthogonal fragment densities.

RECOMMENDATION:

Use default value automatically set by "EDA2".

**Note:** Users are allowed to turn off the orthogonal decomposition by setting FRZ_ORTHO_DECOMP to -1. Also, for calculations that involve ECPs, it is automatically set to FALSE since unreasonable results will be produced otherwise.

**FRZ_ORTHO_DECOMP_CONV**
Convergence criterion for the minimization problem that gives the orthogonal fragment densities.
TYPE:
INTEGER
DEFAULT:
6
OPTIONS:
$n$ $10^{-n}$
RECOMMENDATION:
Use the default unless tighter convergence is preferred.

**EDA_CLS_ELEC**
Perform the classical decomposition of the frozen term.
TYPE:
BOOLEAN
DEFAULT:
FALSE (automatically set to TRUE by EDA2 options 1–5)
OPTIONS:
FALSE Do not compute the classical ELEC and PAULI terms.
TRUE Perform the classical decomposition.
RECOMMENDATION:
TRUE

**EDA_CLS_DISP**
Compute the DISP contribution without performing the orthogonal decomposition, which will then be subtracted from the classical PAULI term.
TYPE:
BOOLEAN
DEFAULT:
FALSE
OPTIONS:
FALSE Use the DISP term computed with orthogonal decomposition (if available).
TRUE Use the DISP term computed using undistorted monomer densities.
RECOMMENDATION:
Set it to TRUE when orthogonal decomposition is not performed.

**DISP_FREE_X**

Specify the employed “dispersion-free" exchange functional.

TYPE:

STRING

DEFAULT:

HF

OPTIONS:

Exchange functionals (*e.g.* revPBE) or exchange-correlation functionals (*e.g.* B3LYP) supported by Q-CHEM.

RECOMMENDATION:

HF is recommended for hybrid (primary) functionals (*e.g.*$\omega$B97X-V) and revPBE for semi-local ones (*e.g.*B97M-V). Other reasonable options (*e.g.* B3LYP for B3LYP-D3) can also be applied.

**DISP_FREE_C**

Specify the employed “dispersion-free" correlation functional.

TYPE:

STRING

DEFAULT:

NONE

OPTIONS:

Correlation functionals supported by Q-CHEM.

RECOMMENDATION:

Put the appropriate correlation functional paired with the chosen exchange functional (*e.g.* put PBE if DISP_FREE_X is revPBE); put NONE if DISP_FREE_X is set to an exchange-correlation functional.

### 12.7.4 Job Control for EDA2

The use of the FERF model for the evaluation of polarization energy and the further decomposition of the frozen term define the second generation of the ALMO-EDA method. Meanwhile, under the same code structure, the original AO-block based ALMO model and other related methods (such as the constrained relaxation of the frozen wave function[7] which renders the frozen energy variationally computed, and the polMO model[40] that arguably gives a lower limit to the polarization contribution) are also available. This entire set of methods implemented in Q-CHEM based on GEN_SCFMAN (see Section 4.7) is termed as “EDA2". Up till today, it has covered most of the functionality of the original ALMO-EDA implementation in Q-CHEM except the features related to CTA and COVP analysis. We look forward to switching to “EDA2" entirely in the near future.

The job control for EDA2 is largely simplified by a series of preset options provided by the developers. The option number is set through the EDA2 *$rem* variable (introduced below). Besides that, for the sake of flexibility, users are allowed to overwrite the values of part of the preset *$rem* variables:

- Related to the isolated fragment calculations:
  - EDA_CHILD_SUPER_BASIS: use the super-system basis for fragment calculations (default: FALSE).
  - FRAGMO_GUESS_MODE: as introduced in Section 12.3 (default: 0).
- Related to the decomposition of the FRZ term:

  - FRZ_ORTHO_DECOMP: it can be turned off by setting its value to -1 in the *$rem* section (default: TRUE).
  - FRZ_ORTHO_DECOMP_CONV: as introduced in Section 12.7.3 (default: 6).
  - EDA_CLS_DISP: as introduced in Section 12.7.3 (default: FALSE).
  - DISP_FREE_X: as introduced in Section 12.7.3 (default: HF).
  - DISP_FREE_C: as introduced in Section 12.7.3 (default: NONE).

- Related to the evaluation of POL:
  - CHILD_MP_ORDERS: as introduced in Section 12.7.2 (default: 122 (DQ)).
  - SCFMI_FREEZE_SS: as introduced in Section 12.7.1 (default: 0).

- Related to the evaluation of CT and BSSE:
  - EDA_NO_CT: skip the evaluation of the CT term in the EDA procedure (default: FALSE (automatically turned on when SCFMI_FREEZE_SS = TRUE)).
  - EDA_BSSE: use counterpoise-corrected monomer calculations to evaluate the BSSE (default: FALSE).

**EDA2**

Switch on EDA2 and specify the option set number.

TYPE:

INTEGER

DEFAULT:

0

OPTIONS:

0 Do not run through EDA2.
1 Frozen energy decomposition + nDQ-FERF polarization
(the standard EDA2 option)
2 Frozen energy decomposition + (AO-block-based) ALMO polarization
(old scheme with the addition of frozen decomposition)
3 Frozen energy decomposition + oDQ-FERF polarization
(NOT commonly used)
4 Frozen wave function relaxation + Frozen energy decomposition + nDQ-FERF polarization
(NOT commonly used)
5 Frozen energy decomposition + polMO polarization
(NOT commonly used).
10 No preset. Completely controlled by user's *$rem* input
(for developers only)

RECOMMENDATION:

Turn on EDA2 for Q-CHEM's ALMO-EDA jobs unless CTA with the old scheme is desired. Option 1 is recommended in general, especially when substantially large basis sets are employed. The original ALMO scheme (option 2) can be used when the employed basis set is of small or medium size (arguably no larger than augmented triple-$\zeta$). The other options are rarely used for routine applications.

**Example 12.14** Energy decomposition analysis for the ammonia-borane complex. The FERF-nDQ model is used for the POL term (as very large basis set is employed here), and decomposition of the frozen interaction energy is performed (Hartree-Fock is employed as the DFXC functional by default).

```
$molecule
0 1
--
0 1
N         0.000000    0.000000   -0.727325
H         0.947371    0.000000   -1.091577
H        -0.473685   -0.820448   -1.091577
H        -0.473685    0.820448   -1.091577
--
0 1
B         0.000000    0.000000    0.930725
H        -1.165774    0.000000    1.243063
H         0.582887   -1.009590    1.243063
H         0.582887    1.009590    1.243063
$end

$rem
   JOBTYPE           eda
   EDA2              1
   METHOD            wB97M-V
   BASIS             def2-QZVPPD
   SYMMETRY          false
   MEM_TOTAL         4000
   MEM_STATIC        1000
   THRESH            14
   SCF_CONVERGENCE   8
   XC_GRID           000099000590
   NL_GRID           1
   FD_MAT_VEC_PROD   false
$end
```

**Example 12.15** Energy decomposition analysis of the water dimer with a low-cost model chemistry. The original ALMO model is used for the evaluation of polarization energy, and revPBE is chosen as the DFXC functional. Counterpoise correction for the BSSE is applied.

```
$molecule
0 1
--
0 1
H1
O1 H1 0.95641
H2 O1 0.96500  H1 104.77306
--
0 1
O2 H2 dist     O1 171.85474 H1 180.000
H3 O2 0.95822  H2 111.79807 O1 -58.587
H4 O2 0.95822  H2 111.79807 O1 58.587

dist = 2.0
$end

$rem
   JOBTYPE           eda
   EDA2              2
   METHOD            b97m-v
   BASIS             def2-svpd
   SCF_CONVERGENCE   8
   THRESH          14
   SYMMETRY        false
   DISP_FREE_X     revPBE
   DISP_FREE_C     PBE
   EDA_BSSE        true
$end
```

## 12.8 The Adiabatic ALMO-EDA Method

Despite the huge success and usefulness of today's most popular EDA methods, they still face some limitations in their capabilities. For instance, EDAs are usually performed at complex geometries that are obtained from unconstrained electronic structure calculations (*e.g.* optimized equilibrium geometries). For strongly interacting systems, close intermolecular contacts driven by POL and particularly CT often result in largely unfavorable FRZ interaction, which offers little physical insights besides indicating obviously substantial intermolecular overlap. Another limitation is that the conventional EDA methods often partitions a "single-point" interaction energy evaluated at a given geometry. Therefore, the influence of FRZ, POL and CT on the structural and vibrational properties of an intermolecular complex cannot be directly characterized.

Recently Mao *et al.* reformulated the original ALMO-EDA method in an "adiabatic" picture[11]. The term "adiabatic" is borrowed from spectroscopy, which indicates that the energy differences are evaluated at relaxed geometry on each potential energy surface (PES). In this scheme, the total binding energy (including monomer geometry distortions) is repartitioned into adiabatic FRZ, POL and CT terms:

$$\Delta E_{\mathrm{bind}} = \Delta E_{\mathrm{frz}}^{(\mathrm{ad})} + \Delta E_{\mathrm{pol}}^{(\mathrm{ad})} + \Delta E_{\mathrm{ct}}^{(\mathrm{ad})}. \tag{12.13}$$

The adiabatic frozen interaction energy is given by the difference between the energy minimum of the frozen PES (on which the energy of each point is computed using the corresponding frozen wave function) and the sum of fully relaxed, non-interacting fragment energies:

$$\Delta E_{\mathrm{frz}}^{(\mathrm{ad})} = E[\mathbf{P}_{\mathrm{frz}}^{(\mathrm{frz})}] - \sum_A E_A^{(0)}. \tag{12.14}$$

Similarly, the adiabatic POL and CT terms can be obtained by performing geometry optimizations on the polarized (SCFMI) and fully relaxed (unconstrained SCF) PESs:

$$\Delta E_{\mathrm{pol}}^{(\mathrm{ad})} = E[\mathbf{P}_{\mathrm{pol}}^{(\mathrm{pol})}] - E[\mathbf{P}_{\mathrm{frz}}^{(\mathrm{frz})}], \tag{12.15}$$

$$\Delta E_{\mathrm{ct}}^{(\mathrm{ad})} = E[\mathbf{P}_{\mathrm{full}}^{(\mathrm{full})}] - E[\mathbf{P}_{\mathrm{pol}}^{(\mathrm{pol})}]. \tag{12.16}$$

With this method, the changes in monomer structures and intermolecular coordinates due to FRZ, POL and CT and the accompanied energetics are provided. Moreover, at the energy minimum (or other stationary points) on each PES, the other properties such as multipole points, vibrational frequencies and intensities can also be computed, therefore the effect of different intermolecular interaction components on them can also be characterized.

The geometry optimization on the frozen PES is facilitated by the analytical gradient of the frozen wave function energy implemented in Q-CHEM. As for the geometry optimization on the polarized PES, the nuclear gradient of the SCFMI energy has the same form as that of the full SCF energy if the original ALMO model is utilized. These analytical gradients can also be used for finite difference calculations of harmonic frequencies by setting IDERIV = 1. We note that the analytical gradients of SCFMI calculations that use

FERFs are not available yet, and SCFMI_MODE = 0 is required for computing the forces on the frozen and polarized PESs. Also, the current implementation of this method requires users to perform geometry optimization on the three PESs separately (see the example below) and evaluate the energy components by taking several Q-CHEM outputs (including geometry optimizations for the monomers) together, which is probably not so convenient. We look forward to extending the functionality of this method and improving its implementation in the near future.

**FRZ_GEOM**

Compute forces on the frozen PES.

TYPE:

BOOLEAN

DEFAULT:

FALSE

OPTIONS:

| | |
|---|---|
| FALSE | Do not compute forces on the frozen PES. |
| TRUE | Compute forces on the frozen PES. |

RECOMMENDATION:

Set it to TRUE when optimized geometry or vibrational frequencies on the frozen PES are desired.

**POL_GEOM**

Compute forces on the polarized (converged SCFMI) PES.

TYPE:

BOOLEAN

DEFAULT:

FALSE

OPTIONS:

| | |
|---|---|
| FALSE | Do not compute forces on the polarized PES. |
| TRUE | Compute forces on the polarized PES. |

RECOMMENDATION:

Set it to TRUE when optimized geometry or vibrational frequencies on the polarized PES are desired.

**Example 12.16** Geometry optimization of the ammonia-borane complex on the fully relaxed, polarized, and frozen potential energy surfaces successively.

```
$molecule
0 1
--
0 1
H       0.000000     0.000000     0.000000
H       0.000000     0.000000     1.629090
H       1.417687     0.000000     0.814543
N       0.473683    -0.370067     0.814542
--
0 1
N       3.494032    -1.531250     0.814538
H       3.967715    -1.901317    -0.000008
H       2.550028    -1.901319     0.814537
H       3.967715    -1.901317     1.629083
$end
```

```
$rem
   JOBTYPE           opt  !optimization on the fully relaxed PES
   GEN_SCFMAN        true
   METHOD            wb97x-d
   BASIS             6-31+g*
   XC_GRID           1
   THRESH            14
   SCF_CONVERGENCE   9
   SCF_GUESS         fragmo
   SYMMETRY          false
   SYM_IGNORE        true
$end

@@@

$molecule
   read
$end

$rem
   JOBTYPE           opt
   POL_GEOM          true !optimization on the polarized PES
   GEN_SCFMAN        true
   METHOD            wb97x-d
   BASIS             6-31+g*
   XC_GRID           1
   THRESH            14
   SCF_CONVERGENCE   9
   SYMMETRY          false
   SYM_IGNORE        true
   SCFMI_MODE        0
$end

@@@

$molecule
   read
$end

$rem
   JOBTYPE           opt
   FRZ_GEOM          true !optimization on the frozen PES
   GEN_SCFMAN        true
   METHOD            wb97x-d
   BASIS             6-31+g*
   XC_GRID           1
   THRESH            14
   SCF_CONVERGENCE   9
   SYMMETRY          false
   SYM_IGNORE        true
   SCFMI_MODE        0
$end
```

**Example 12.17** Geometry optimization of the $CF_3H\cdots Cl^-$ complex on the frozen PES followed by a calculation for harmonic frequencies at the equilibrium geometry.

```
$molecule
```

```
-1 1
--
0 1
C         0.000000    0.000000    0.905509
H         0.000000    0.000000   -0.179815
F         1.250779    0.000000    1.406437
F        -0.625389   -1.083207    1.406437
F        -0.625389    1.083207    1.406437
--
-1 1
Cl        0.000000    0.000000   -2.664391
$end

$rem
   JOBTYPE                       opt
   FRZ_GEOM                      true
   GEN_SCFMAN                    true
   METHOD                        wb97X-V
   BASIS                         def2-svpd
   XC_GRID                       000075000302
   THRESH                        14
   SCF_CONVERGENCE               9
   SYMMETRY                      false
   SYM_IGNORE                    false
   SCFMI_MODE                    0
   GEOM_OPT_TOL_GRADIENT         100
   GEOM_OPT_TOL_DISPLACEMENT     100
   GEOM_OPT_TOL_ENERGY           10
   FD_MAT_VEC_PROD               false
$end

@@@

$molecule
   read
$end

$rem
   JOBTYPE           freq
   FRZ_GEOM          true
   GEN_SCFMAN        true
   METHOD            wb97X-V
   BASIS             def2-svpd
   XC_GRID           000075000302
   THRESH            14
   SCF_CONVERGENCE   9
   SYMMETRY          false
   SYM_IGNORE        false
   IDERIV            1
   SCFMI_MODE        0
   FD_MAT_VEC_PROD   false
$end
```

## 12.9 The Explicit Polarization (XPol) Method

### 12.9.1 Theory

XPol is an approximate, fragment-based molecular orbital method that was developed as a "next-generation" force field[12,41–43]. The basic idea of the method is to treat a molecular liquid, solid, or cluster as a collection of fragments, where each fragment is a molecule. Intra-molecular interactions are treated with a self-consistent field method (Hartree-Fock or DFT), but each fragment is embedded in a field of point charges that represent electrostatic interactions with the other fragments. These charges are updated self-consistently by collapsing each fragment's electron density onto a set of atom-centered point charges, using charge analysis procedures (Mulliken, Löwdin, or CHELPG, for example; see Section 10.2.1). This approach incorporates many-body polarization, at a cost that scales linearly with the number of fragments, but neglects the anti-symmetry requirement of the total electronic wave function. As a result, intermolecular exchange-repulsion is neglected, as is dispersion since the latter is an electron correlation effect. As such, the XPol treatment of polarization must be augmented with empirical, Lennard–Jones-type intermolecular potentials in order to obtain meaningful optimized geometries, vibrational frequencies or dynamics.

The XPol method is based upon an *ansatz* in which the super-system wave function is written as a direct product of fragment wave functions,

$$|\Psi\rangle = \prod_{A}^{N_{\text{frag}}} |\Psi_A\rangle, \tag{12.17}$$

where $N_{\text{frag}}$ is the number of fragments. We assume here that the fragments are molecules and that covalent bonds remain intact. The fragment wave functions are anti-symmetric with respect to exchange of electrons within a fragment, but not to exchange between fragments. For closed-shell fragments described by Hartree-Fock theory, the XPol total energy is[12,13]

$$E_{\text{XPol}} = \sum_A \left[ 2 \sum_a \mathbf{c}_a^\dagger \left( \mathbf{h}^A + \mathbf{J}^A - \tfrac{1}{2}\mathbf{K}^A \right) \mathbf{c}_a + E_{\text{nuc}}^A \right] + E_{\text{embed}}. \tag{12.18}$$

The term in square brackets is the ordinary Hartree-Fock energy expression for fragment $A$. Thus, $\mathbf{c}_a$ is a vector of occupied MO expansion coefficients (in the AO basis) for the occupied MO $a \in A$; $\mathbf{h}^A$ consists of the one-electron integrals; and $\mathbf{J}^A$ and $\mathbf{K}^A$ are the Coulomb and exchange matrices, respectively, constructed from the density matrix for fragment $A$. The additional terms in Eq. (12.18),

$$E_{\text{embed}} = \tfrac{1}{2} \sum_A \sum_{B \neq A} \sum_{J \in B} \left( -2 \sum_a \mathbf{c}_a^\dagger \mathbf{I}_J \mathbf{c}_a + \sum_{I \in A} L_{IJ} \right) q_J, \tag{12.19}$$

arise from the electrostatic embedding. The matrix $\mathbf{I}_J$ is defined by its AO matrix elements,

$$(\mathbf{I}_J)_{\mu\nu} = \left\langle \mu \left| \frac{1}{|\vec{r} - \vec{R}_J|} \right| \nu \right\rangle, \tag{12.20}$$

and $L_{IJ}$ is given by

$$L_{IJ} = \frac{Z_I}{|\vec{R}_I - \vec{R}_J|}. \tag{12.21}$$

According to Eqs. (12.18) and (12.19), each fragment is embedded in the electrostatic potential arising from a set of point charges, $\{q_J\}$, on all of the other fragments; the factor of $1/2$ in Eq. (12.19) avoids double-counting. Exchange interactions between fragments are ignored, and the electrostatic interactions between fragments are approximated by interactions between the charge density of one fragment and point charges on the other fragments.

Crucially, the vectors $\mathbf{c}_a$ are constructed within the ALMO *ansatz*[1], so that MOs for each fragment are represented in terms of only those AOs that are centered on atoms in the same fragment. This choice affords a method whose cost grows linearly with respect to $N_{\text{frag}}$, and where basis set superposition error is excluded by construction. In compact basis sets, the ALMO *ansatz* excludes inter- fragment charge transfer as well.

The original XPol method of Xie *et al.*[12,42,43] uses Mulliken charges for the embedding charges $q_J$ in Eq. (12.19), though other charge schemes could be envisaged. In non-minimal basis sets, the use of Mulliken charges is beset by severe convergence problems[13], and Q-CHEM's implementation of XPol offers the alternative of using either Löwdin charges or CHELPG charges[44], the latter being derived from the electrostatic potential as discussed in Section 10.2.1. The CHELPG charges are found to be stable and robust, albeit with a somewhat larger computational cost as compared to Mulliken or Löwdin charges[13,14]. An algorithm to compute CHELPG charges using atom-centered Lebedev grids rather than traditional Cartesian grids is available[45] (see Section 10.2.1), which uses far fewer grid points and thus can significantly improve the performance for the XPol/CHELPG method, where these charges must be iteratively updated.

Researchers who use Q-CHEM's XPol code are asked to cite Refs. 13, and 14.

### 12.9.2 Supplementing XPol with Empirical Potentials

In order to obtain physical results, one must either supplement the XPol energy expression with either empirical intermolecular potentials or else with an *ab initio* treatment of intermolecular interactions. The latter approach is described in Section 12.11. Here, we describe how to add Lennard-Jones or Buckingham potentials to the XPol energy, using the *$xpol_mm* and *$xpol_params* sections described below.

The Lennard-Jones potential is

$$V_{\text{LJ}}(R_{ij}) = 4\epsilon_{ij}\left[\left(\frac{\sigma_{ij}}{R_{ij}}\right)^{12} - \left(\frac{\sigma_{ij}}{R_{ij}}\right)^{6}\right] , \tag{12.22}$$

where $R_{ij}$ represents the distance between atoms $i$ and $j$. This potential is characterized by two parameters, a well depth $\epsilon_{ij}$ and a length scale $\sigma_{ij}$. Although quite common, the $R^{-12}$ repulsion is unrealistically steep. The Buckingham potential replaces this with an exponential function,

$$V_{\text{Buck}}(R_{ij}) = \epsilon_{ij}\left[Ae^{-B\frac{R_{ij}}{\sigma_{ij}}} - C\left(\frac{\sigma_{ij}}{R_{ij}}\right)^{6}\right] , \tag{12.23}$$

Here, $A$, $B$, and $C$ are additional (dimensionless) constants, independent of atom type. In both Eq. (12.22) and Eq. (12.23), the parameters $\epsilon_{ij}$ and $\sigma_{ij}$ are determined using the geometric mean of atomic well-depth and length-scale parameters. For example,

$$\sigma_{ij} = \sqrt{\sigma_i\sigma_j} \; . \tag{12.24}$$

The atomic parameters $\sigma_i$ and $\epsilon_i$ must be specified using a *$xpol_mm* section in the Q-CHEM input file. The format is a molecular mechanics-like specification of atom types and connectivities. All atoms specified in the *$molecule* section must also be specified in the *$xpol_mm* section. Each line must contain an atom number, atomic symbol, Cartesian coordinates, integer atom type, and any connectivity data. The *$xpol_params* section specifies, for each atom type, a value for $\epsilon$ in kcal/mol and a value for $\sigma$ in

Ångstroms. A Lennard-Jones potential is used by default; if a Buckingham potential is desired, then the first line of the *$xpol_params* section should contain the string BUCKINGHAM followed by values for the $A$, $B$, and $C$ parameters.

### 12.9.3 Job Control Variables for XPol

XPol calculations are enabled by setting the *$rem* variable XPOL to TRUE. These calculations can be used in combination with Hartree-Fock theory and with most density functionals, a notable exception being that XPol is not yet implemented for meta-GGA functionals (Section 4.4.3). Combining XPol with solvation models (Section 11.2) or external charges (*$external_charges*) is also not available. Analytic gradients are available when Mulliken or Löwdin embedding charges are used, but not yet available for CHELPG embedding charges.

**XPOL**
Perform a self-consistent XPol calculation.
TYPE:
BOOLEAN
DEFAULT:
FALSE
OPTIONS:

| | |
|---|---|
| TRUE | Perform an XPol calculation. |
| FALSE | Do not perform an XPol calculation. |

RECOMMENDATION:
NONE

**XPOL_CHARGE_TYPE**
Controls the type of atom-centered embedding charges for XPol calculations.
TYPE:
STRING
DEFAULT:
QLOWDIN
OPTIONS:

| | |
|---|---|
| QLOWDIN | Löwdin charges. |
| QMULLIKEN | Mulliken charges. |
| QCHELPG | CHELPG charges. |

RECOMMENDATION:
Problems with Mulliken charges in extended basis sets can lead to XPol convergence failure. Löwdin charges tend to be more stable, and CHELPG charges are both robust and provide an accurate electrostatic embedding. However, CHELPG charges are more expensive to compute, and analytic energy gradients are not yet available for this choice.

**XPOL_MPOL_ORDER**

Controls the order of multipole expansion that describes electrostatic interactions.

TYPE:

STRING

DEFAULT:

CHARGES

OPTIONS:

GAS No electrostatic embedding; monomers are in the gas phase.

CHARGES Charge embedding.

DENSITY Density embedding.

RECOMMENDATION:

Should be set to GAS to do a dimer SAPT calculation (see Section 12.10).

**XPOL_PRINT**

Print level for XPol calculations.

TYPE:

INTEGER

DEFAULT:

1

OPTIONS:

$N$ Integer print level

RECOMMENDATION:

Higher values prints more information

**XPOL_OMEGA**

Controls the range-separation parameter, $\omega$, that is used in long-range-corrected DFT.

TYPE:

BOOLEAN

DEFAULT:

FALSE

OPTIONS:

TRUE Use different $\omega$ values for different fragments.

FALSE Use a single value of $\omega$ for all fragments.

RECOMMENDATION:

If FALSE, the *$rem* variable OMEGA should be used to specify the single value of $\omega$. If TRUE, separate values for each fragment should be specified in an *$lrc_omega* input section. Values in the *$lrc_omega* section have the same units as the *$rem* variable OMEGA, namely, $\omega =$ OMEGA/1000, in atomic units.

### 12.9.4 Examples

XPol on its own is not a useful method (as it neglects all intermolecular interactions except for polarization), so the two examples below demonstrate the use of XPol in conjunction with a Lennard-Jones and a Buckingham potential, respectively.

**Example 12.18** An XPol single point calculation on the water dimer using a Lennard-Jones potential.

```
$molecule
```

```
0 1
-- water 1
0 1
O          -1.364553     .041159     .045709
H          -1.822645     .429753    -.713256
H          -1.841519    -.786474     .202107
-- water 2
0 1
O           1.540999     .024567     .107209
H            .566343     .040845     .096235
H           1.761811    -.542709    -.641786
$end

$rem
   METHOD           HF
   BASIS            3-21G
   XPOL             TRUE
   XPOL_CHARGE_TYPE QLOWDIN
$end

$xpol_mm
   1 O          -1.364553     .041159     .045709 1 2 3
   2 H          -1.822645     .429753    -.713256 2 1
   3 H          -1.841519    -.786474     .202107 2 1
   4 O           1.540999     .024567     .107209 1 5 6
   5 H            .566343     .040845     .096235 2 4
   6 H           1.761811    -.542709    -.641786 2 4
$end

$xpol_params
   1            0.16     3.16
   2            0.00     0.00
$end
```

**Example 12.19** An XPol single point calculation on the water dimer using a Buckingham potential.

```
$molecule
0 1
-- water 1
0 1
O          -1.364553     .041159     .045709
H          -1.822645     .429753    -.713256
H          -1.841519    -.786474     .202107
-- water 2
0 1
O           1.540999     .024567     .107209
H            .566343     .040845     .096235
H           1.761811    -.542709    -.641786
$end

$rem
   METHOD           HF
   BASIS            3-21G
   XPOL             TRUE
   XPOL_CHARGE_TYPE QLOWDIN
$end

$xpol_mm
```

```
   1 O         -1.364553     .041159     .045709 1 2 3
   2 H         -1.822645     .429753    -.713256 2 1
   3 H         -1.841519    -.786474     .202107 2 1
   4 O          1.540999     .024567     .107209 1 5 6
   5 H           .566343     .040845     .096235 2 4
   6 H          1.761811    -.542709    -.641786 2 4
$end

$xpol_params
   BUCKINGHAM   500000.0 12.5 2.25
   1            0.16     3.16
   2            0.00     0.00
$end
```

## 12.10 Symmetry-Adapted Perturbation Theory (SAPT)

### 12.10.1 Theory

Symmetry-adapted perturbation theory (SAPT) is a theory of intermolecular interactions. When computing intermolecular interaction energies one typically computes the energy of two molecules infinitely separated and in contact, then computes the interaction energy by subtraction. SAPT, in contrast, is a perturbative expression for the interaction energy itself. The various terms in the perturbation series are physically meaningful, and this decomposition of the interaction energy can aid in the interpretation of the results. A brief overview of the theory is given below; for additional technical details, the reader is referred to Jeziorski *et al.* [15,46]. Additional context can be found in a pair of more recent review articles [16,47].

In SAPT, the Hamiltonian for the A $\cdots$ B dimer is written as

$$\hat{H} = \hat{F}^A + \hat{F}^B + \xi\hat{W}^A + \eta\hat{W}^B + \zeta\hat{V} \ , \tag{12.25}$$

where $\hat{W}^A$ and $\hat{W}^B$ are Møller-Plesset fluctuation operators for fragments $A$ and $B$, whereas $\hat{V}$ consists of the intermolecular Coulomb operators. This part of the perturbation is conveniently expressed as

$$\hat{V} = \sum_{i\in A}\sum_{j\in B} \hat{v}(ij) \tag{12.26}$$

with

$$\hat{v}(ij) = \frac{1}{|\vec{r}_i - \vec{r}_j|} + \frac{\hat{v}_A(j)}{N_A} + \frac{\hat{v}_B(i)}{N_B} + \frac{V_0}{N_A N_B} \ . \tag{12.27}$$

The quantity $V_0$ is the nuclear interaction energy between the two fragments and

$$\hat{v}_A(j) = -\sum_{I\in A} \frac{Z_I}{|\vec{r}_j - \vec{R}_I|} \tag{12.28}$$

describes the interaction of electron $j \in B$ with nucleus $I \in A$.

Starting from a zeroth-order Hamiltonian $\hat{H}_0 = \hat{F}^A + \hat{F}^B$ and zeroth-order wave functions that are direct products of monomer wave functions, $|\Psi_0\rangle = |\Psi_A\rangle|\Psi_B\rangle$, the SAPT approach is based on a symmetrized Rayleigh-Schrödinger perturbation expansion [15,46] with respect to the perturbation parameters $\xi$, $\eta$, and $\zeta$ in Eq. (12.25). The resulting interaction energy can be expressed as [15,46]

$$E_{\text{int}} = \sum_{i=1}^{\infty}\sum_{j=0}^{\infty} \left(E^{(ij)}_{\text{pol}} + E^{(ij)}_{\text{exch}}\right) \ . \tag{12.29}$$

Because it makes no sense to treat $\hat{W}^A$ and $\hat{W}^B$ at different orders of perturbation theory, there are only two indices in this expansion: $j$ for the monomer fluctuations potentials and $i$ for the intermolecular perturbation. The terms $E_{\text{pol}}^{(ij)}$ are known collectively as the *polarization expansion*, and these are precisely the same terms that would appear in ordinary Rayleigh-Schrödinger perturbation theory, which is valid when the monomers are well-separated. The polarization expansion contains electrostatic, induction and dispersion interactions, but in the *symmetrized* Rayleigh-Schrödinger expansion, each term $E_{\text{pol}}^{(ij)}$ has a corresponding exchange term, $E_{\text{exch}}^{(ij)}$, that arises from an anti-symmetrizer $\hat{\mathcal{A}}_{AB}$ that is introduced in order to project away the Pauli-forbidden components of the interaction energy that would otherwise appear[15].

The version of SAPT that is implemented in Q-CHEM assumes that $\xi = \eta = 0$, an approach that is usually called SAPT0[47]. Within the SAPT0 formalism, the interaction energy is formally expressed by the following symmetrized Rayleigh-Schrödinger expansion[15,46]:

$$E_{\text{int}}(\zeta) = \frac{\langle \Psi_0 | \zeta \hat{V} \hat{\mathcal{A}}_{AB} | \Psi(\zeta) \rangle}{\langle \Psi_0 | \hat{\mathcal{A}}_{AB} | \Psi(\zeta) \rangle} \ , \tag{12.30}$$

The anti-symmetrizer $\hat{\mathcal{A}}_{AB}$ in this expression can be written as

$$\hat{\mathcal{A}}_{AB} = \frac{N_A! N_B!}{(N_A + N_B)!} \, \hat{\mathcal{A}}_A \hat{\mathcal{A}}_B \big( \hat{1} + \hat{\mathcal{P}}^{AB} + \hat{\mathcal{P}}' \big) \ , \tag{12.31}$$

where $\hat{\mathcal{A}}_A$ and $\hat{\mathcal{A}}_B$ are anti-symmetrizers for the two monomers and $\hat{\mathcal{P}}^{AB}$ is a sum of all one-electron exchange operators between the two monomers. The operator $\hat{\mathcal{P}}'$ in Eq. (12.31) denotes all of the three-electron and higher-order exchanges. This operator is neglected in what is known as the "single-exchange" approximation[15,46], which is expected to be quite accurate at typical van der Waals and larger intermolecular separations, but sometimes breaks down at smaller intermolecular separations[48].

Only terms up to $\zeta = 2$ in Eq. (12.30)—that is, second order in the intermolecular interaction—have been implemented in Q-CHEM. It is common to relabel these low-order terms in the following way [*cf.* Eq. (12.29)]:

$$E_{\text{int}}^{\text{SAPT0}} = E_{\text{elst}}^{(1)} + E_{\text{exch}}^{(1)} + E_{\text{pol}}^{(2)} + E_{\text{exch}}^{(2)} \ . \tag{12.32}$$

The electrostatic part of the first-order energy correction is denoted $E_{\text{elst}}^{(1)}$ and represents the Coulomb interaction between the two monomer electron densities[15]. The quantity $E_{\text{exch}}^{(1)}$ is the corresponding first-order (*i.e.*, Hartree-Fock) exchange correction. Explicit formulas for these corrections can be found in Ref. 46. The second-order term from the polarization expansion, denoted $E_{\text{pol}}^{(2)}$ in Eq. (12.32), consists of a dispersion contribution (which arises for the first time at second order) as well as a second-order correction for induction. The latter can be written

$$E_{\text{ind}}^{(2)} = E_{\text{ind}}^{(2)}(A \leftarrow B) + E_{\text{ind}}^{(2)}(B \leftarrow A) \ , \tag{12.33}$$

where the notation $A \leftarrow B$, for example, indicates that the frozen charge density of $B$ polarizes the density of $A$. In detail,

$$E_{\text{ind}}^{(2)}(A \leftarrow B) = 2 \sum_{ar} t_{ar} (w_B)_{ra} \tag{12.34}$$

where

$$(w_B)_{ar} = (\hat{v}_B)_{ar} + \sum_{b} (ar|bb) \tag{12.35}$$

and $t_{ar} = (w_B)_{ar} / (\epsilon_a - \epsilon_r)$. The second term in Eq. (12.33), in which $A$ polarizes $B$, is obtained by interchanging labels[13]. The second-order dispersion correction has a form reminiscent of the MP2 correlation energy:

$$E_{\text{disp}}^{(2)} = 4 \sum_{abrs} \frac{(ar|bs)(ra|sb)}{\epsilon_a + \epsilon_b - \epsilon_r - \epsilon_s} \ . \tag{12.36}$$

The induction and dispersion corrections both have accompanying exchange corrections (exchange-induction and exchange-dispersion) [15,46].

The similarity between Eq. (12.36) and the MP2 correlation energy means that SAPT jobs, like MP2 calculations, can be greatly accelerated using resolution-of-identity (RI) techniques, and an RI version of SAPT is available in Q-CHEM. To use it, one must specify an auxiliary basis set. The same ones used for RI-MP2 work equally well for RI-SAPT, but one should always select the auxiliary basis set that is tailored for use with the primary basis of interest, as in the RI-MP2 examples in Section 5.6.1.

It is common to replace $E^{(2)}_{\rm ind}$ and $E^{(2)}_{\rm exch-ind}$ in Eq. (12.32) with their "response" ($resp$) analogues, which are the infinite-order correction for polarization arising from a frozen partner density [15,46]. Operationally, this substitution involves replacing the second-order induction amplitudes, $t_{ar}$ in Eq. (12.34), with amplitudes obtained from solution of the coupled-perturbed Hartree-Fock equations [49]. (The perturbation is simply the electrostatic potential of the other monomer.) In addition, it is common to correct the SAPT0 binding energy for higher-order polarization effects by adding a correction term of the form [15,47]

$$\delta E^{\rm HF}_{\rm int} = E^{\rm HF}_{\rm int} - \left(E^{(1)}_{\rm elst} + E^{(1)}_{\rm exch} + E^{(2)}_{\rm ind,resp} + E^{(2)}_{\rm exch-ind,resp}\right) \tag{12.37}$$

to the interaction energy. Here, $E^{\rm HF}_{int}$ is the counterpoise-corrected Hartree-Fock binding energy for $\rm A \cdots B$. Both the response corrections and the $\delta E^{\rm HF}_{\rm int}$ correction are optionally available in Q-CHEM's implementation of SAPT.

It is tempting to replace Hartree-Fock MOs and eigenvalues in the SAPT0 formulas with their Kohn-Sham counterparts, as a low-cost means of introducing monomer electron correlation. The resulting procedure is known as SAPT(KS) [50], and does offer an improvement on SAPT0 for some strongly hydrogen-bonded systems [14]. Unfortunately, SAPT(KS) results are generally in poor agreement with benchmark dispersion energies [14], owing to incorrect asymptotic behavior of approximate exchange-correlation potentials [51]. The dispersion energies can be greatly improved through the use of long-range corrected (LRC) functionals in which the range-separation parameter, $\omega$, is "tuned" so as to satisfy the condition $\epsilon_{\rm HOMO} = -{\rm IP}$, where $\epsilon_{\rm HOMO}$ is the HOMO energy and "IP" represents the ionization potential [52]. Monomer-specific values of $\omega$, tuned using the individual monomer IPs, substantially improve SAPT(KS) dispersion energies, though the results are still not of benchmark quality [52]. Other components of the interaction energy, however, can be described quite accurately SAPT(KS) in conjunction with a tuned version of LRC-$\omega$PBE [52]. Use of monomer-specific $\omega$ values is controlled by the variable XPOL_OMEGA in the *$rem* section, and individual values are entered via an *$lrc_omega* input section. The omega values of monomers at geometries optimized at RIMP2/aug-cc-pVDZ using LRC-$\omega$PBE functional based on $\epsilon_{\rm HOMO} = -{\rm IP}$ condition are listed in Table 12.1.

Finally, some discussion of basis sets is warranted. Typically, SAPT calculations are performed in the so-called dimer-centered basis set (DCBS) [53], which means that the combined $A + B$ basis set is used to calculate the zeroth-order wave functions for both $A$ and $B$. This leads to the unusual situation that there are more MOs than basis functions: one set of occupied and virtual MOs for each monomer, both expanded in the same (dimer) AO basis. As an alternative to the DCBS, one might calculate $|\Psi_A\rangle$ using only $A$'s basis functions (similarly for $B$), in which case the SAPT calculation is said to employ the monomer-centered basis set (MCBS) [53]. However, MCBS results are generally of poorer quality. As an efficient alternative to the DCBS, Jacobson and Herbert [13] introduced a projected ("proj") basis set, borrowing an idea from dual-basis MP2 calculations [54]. In this approach, the SCF iterations are performed in the MCBS but then Fock matrices for fragments $A$ and $B$ are constructed in the dimer ($A+B$) basis set and "pseudo-canonicalized", meaning that the occupied-occupied and virtual-virtual blocks of these matrices are diagonalized. This procedure does not mix occupied and virtual orbitals, and thus leaves the fragment densities and zeroth-order fragment energies unchanged. However, it does provide a larger set of virtual orbitals that extend over the partner fragment. This larger virtual space is then used to evaluate the perturbative corrections. All three of these basis options (MCBS, DCBS, and projected basis) are available in Q-CHEM.

### 12.10.2 Job Control for SAPT Calculations

Q-CHEM's implementation of SAPT0 was designed from the start as a correction for XPol calculations, a functionality that is described in Section 12.11. As such, a SAPT calculation is requested by setting both of the *$rem* variable SAPT and XPOL to TRUE. (Alternatively, one may set RISAPT=TRUE to use the RI version of SAPT.) If one wishes to perform a traditional SAPT calculation based on gas-phase SCF monomer wave functions rather than XPol monomer wave functions, then the *$rem* variable XPOL_MPOL_ORDER should be set to GAS.

SAPT energy components are printed separately at the end of a SAPT job. If EXCHANGE = HF, then the calculation corresponds to SAPT0, whereas a SAPT(KS) calculation is requested by specifying the desired density functional.

**Note:** Meta-GGAs are not yet available for SAPT(KS) calculations in Q-CHEM.] At present, only single-point energies for closed-shell (restricted) calculations are possible. Frozen orbitals are also unavailable.

Researchers who use Q-CHEM's SAPT code are asked to cite Refs. 13 and 14.

**SAPT**

Requests a SAPT calculation.

TYPE:

BOOLEAN

DEFAULT:

FALSE

OPTIONS:

| | |
|---|---|
| TRUE | Run a SAPT calculation. |
| FALSE | Do not run SAPT. |

RECOMMENDATION:

If SAPT is set to TRUE, one should also specify XPOL = TRUE and XPOL_MPOL_ORDER = GAS.

**RISAPT**

Requests an RI-SAPT calculation

TYPE:

BOOLEAN

DEFAULT:

FALSE

OPTIONS:

| | |
|---|---|
| TRUE | Compute four-index integrals using the RI approximation. |
| FALSE | Do not use RI. |

RECOMMENDATION:

Set to TRUE if an appropriate auxiliary basis set is available, as RI-SAPT is much faster and affords negligible errors (as compared to ordinary SAPT) if the auxiliary basis set is matched to the primary basis set. (The former must be specified using AUX_BASIS.)

**SAPT_ORDER**

Selects the order in perturbation theory for a SAPT calculation.

TYPE:

STRING

DEFAULT:

SAPT2

OPTIONS:

| | |
|---|---|
| SAPT1 | First order SAPT. |
| SAPT2 | Second order SAPT. |
| ELST | First-order Rayleigh-Schrödinger perturbation theory. |
| RSPT | Second-order Rayleigh-Schrödinger perturbation theory. |

RECOMMENDATION:

SAPT2 is the most meaningful.

**SAPT_EXCHANGE**

Selects the type of first-order exchange that is used in a SAPT calculation.

TYPE:

STRING

DEFAULT:

S_SQUARED

OPTIONS:

| | |
|---|---|
| S_SQUARED | Compute first order exchange in the single-exchange ("$S^2$") approximation. |
| S_INVERSE | Compute the exact first order exchange. |

RECOMMENDATION:

The single-exchange approximation is expected to be adequate except possibly at very short intermolecular distances, and is somewhat faster to compute.

**SAPT_BASIS**

Controls the MO basis used for SAPT corrections.

TYPE:

STRING

DEFAULT:

MONOMER

OPTIONS:

| | |
|---|---|
| MONOMER | Monomer-centered basis set (MCBS). |
| DIMER | Dimer-centered basis set (DCBS). |
| PROJECTED | Projected basis set. |

RECOMMENDATION:

The DCBS is more costly than the MCBS and can only be used with XPOL_MPOL_ORDER = GAS (*i.e.*, it is not available for use with XPol). The PROJECTED choice is an efficient compromise that is available for use with XPol.

**SAPT_CPHF**

Requests that the second-order corrections $E^{(2)}_{\rm ind}$ and $E^{(2)}_{\rm exch-ind}$ be replaced by their infinite-order "response" analogues, $E^{(2)}_{\rm ind,resp}$ and $E^{(2)}_{\rm exch-ind,resp}$.

TYPE:

BOOLEAN

DEFAULT:

FALSE

OPTIONS:

TRUE Evaluate the response corrections and use $E^{(2)}_{\rm ind,resp}$ and $E^{(2)}_{\rm exch-ind,resp}$

FALSE Omit these corrections and use $E^{(2)}_{\rm ind}$ and $E^{(2)}_{\rm exch-ind}$.

RECOMMENDATION:

Computing the response corrections requires solving CPHF equations for pair of monomers, which is somewhat expensive but may improve the accuracy when the monomers are polar.

**SAPT_DSCF**

Request the $\delta E^{\rm HF}_{\rm int}$ correction

TYPE:

BOOLEAN

DEFAULT:

FALSE

OPTIONS:

TRUE Evaluate this correction.

FALSE Omit this correction.

RECOMMENDATION:

Evaluating the $\delta E^{\rm HF}_{\rm int}$ correction requires an SCF calculation on the entire (super)system. This corrections effectively yields a "Hartree-Fock plus dispersion" estimate of the interaction energy.

**SAPT_PRINT**

Controls level of printing in SAPT.

TYPE:

INTEGER

DEFAULT:

1

OPTIONS:

$N$ Integer print level

RECOMMENDATION:

Larger values generate additional output.

**Example 12.20** Example showing a SAPT0 calculation using the RI approximation in a DCBS.

```
$rem
   BASIS            AUG-CC-PVDZ
   AUX_BASIS        RIMP2-AUG-CC-PVDZ
   METHOD           HF
   RISAPT           TRUE
   XPOL             TRUE
   XPOL_MPOL_ORDER  GAS   ! gas-phase monomer wave functions
   SAPT_BASIS       DIMER
   SYM_IGNORE       TRUE
$end

$molecule
0 1
-- formamide
   0 1
   C -2.018649  0.052883  0.000000
   O -1.452200  1.143634  0.000000
   N -1.407770 -1.142484  0.000000
   H -1.964596 -1.977036  0.000000
   H -0.387244 -1.207782  0.000000
   H -3.117061 -0.013701  0.000000
-- formamide
   0 1
   C  2.018649 -0.052883  0.000000
   O  1.452200 -1.143634  0.000000
   N  1.407770  1.142484  0.000000
   H  1.964596  1.977036  0.000000
   H  0.387244  1.207782  0.000000
   H  3.117061  0.013701  0.000000
$end
```

## 12.11 The XPol+SAPT (XSAPT) Method

### 12.11.1 Theory

XPol+SAPT, or "XSAPT", was introduced by Jacobson and Herbert[13,14] as a low-order-scaling, systematically-improvable method applicable to large systems. The idea is simply to replace the need for empirical parameters in the XPol method with on-the-fly evaluation of exchange-repulsion and dispersion interactions via pairwise-additive SAPT. (This basic idea has spawned several related approaches; see Ref. 20 for an overview of XSAPT-based methods.) Stated differently, XSAPT uses XPol to evaluate many-body (non-pairwise-additive) polarization effects, but then assumes that dispersion and exchange-repulsion interactions *are* pairwise additive, and evaluates them via pairwise SAPT0 or SAPT(KS) calculations.

In particular, the zeroth-order Hamiltonian for XSAPT is taken by the sum of fragment Fock operators defined by the XPol procedure, and the perturbation is the usual SAPT intermolecular perturbation [Eq. (12.27)] less the intermolecular interactions contained in the XPol fragment Fock operators. A standard SAPT0 correction is then computed for each pair of monomers, using Eq. (12.32) in conjunction with the modified perturbation, to obtain dimer interaction energy $E_{\text{int}}^{AB}$. The total XSAPT energy is then

$$E_{\text{XSAPT}} = \sum_A \left( \sum_a \left[ 2\,\epsilon_a^A - \mathbf{c}_a^\dagger (\mathbf{J}^A - \tfrac{1}{2}\mathbf{K}^A)\mathbf{c}_a \right] + E_{\text{nuc}}^A + \sum_{B>A} E_{\text{int}}^{AB} \right) . \qquad (12.38)$$

In this expression, we have removed the over-counting of two-electron interactions present in Hartree-Fock theory, effectively taking the *intra*fragment perturbation to first order. The generalization to a Kohn-Sham description of the monomers is straightforward, and is available in Q-CHEM.

The inclusion of many-body polarization within the zeroth-order Hamiltonian makes the subsequent SAPT corrections less meaningful in terms of energy decomposition analysis. For instance, the first-order electrostatic correction in XSAPT is *not* the total electrostatic energy, since the former corrects for errors in the approximate electrostatic treatment at zeroth order (*i.e.*, the electrostatic embedding). The dispersion correction may be less contaminated, since all of the XSAPT modifications to the traditional SAPT perturbation are one-electron operators and therefore the pairwise dispersion correction differs from its traditional SAPT analogue only insofar as the MOs are perturbed by the electrostatic embedding. This should be kept in mind when interpreting the output of an XSAPT calculation, although Lao and Herbert[19,20] later proposed a many-body energy decomposition scheme for XSAPT that extends traditional SAPT energy decomposition to systems containing more than two monomers. (The aforementioned contamination problems are avoid through pairwise $\delta_{\mathrm{int}}^{\mathrm{HF}}$ corrections, comparing XSAPT results to traditional SAPT based on gas-phase monomers.) An XSAPT calculation is requested by setting the *$rem* variables XPOL and SAPT equal to TRUE and also setting XPOL_MPOL_ORDER = CHARGES.

Researchers who use Q-CHEM's XPol+SAPT code are asked to cite Refs. 13 and 14. The latter contains a thorough discussion of the theory; a briefer summary can be found in Ref. 17.

**Example 12.21** Example showing an XPol+SAPT0 calculation using CHELPG charges and CPHF.

```
$rem
   BASIS             CC-PVDZ
   METHOD            HF
   XPOL              TRUE
   XPOL_MPOL_ORDER   CHARGES
   XPOL_CHARGE_TYPE  QCHELPG
   SAPT              TRUE
   SAPT_CPHF         TRUE
   SYM_IGNORE        TRUE
$end

$molecule
0 1
-- formic acid
   0 1
   C  -1.888896 -0.179692  0.000000
   O  -1.493280  1.073689  0.000000
   O  -1.170435 -1.166590  0.000000
   H  -2.979488 -0.258829  0.000000
   H  -0.498833  1.107195  0.000000
-- formic acid
   0  1
   C  1.888896  0.179692  0.000000
   O  1.493280 -1.073689  0.000000
   O  1.170435  1.166590  0.000000
   H  2.979488  0.258829  0.000000
   H  0.498833 -1.107195  0.000000
$end
```

### 12.11.2 AO-XSAPT(KS)+D

As mentioned above, the dispersion components of the (X)SAPT(KS) interaction energy are not of benchmark quality, even when tuned LRC functionals are employed[52]. The dispersion and exchange-dispersion terms are also the most expensive part of a SAPT0 or SAPT(KS) calculation, scaling as the fourth and fifth powers, respectively, of monomer size, whereas other terms are cubic scaling at worst. Both the efficiency and the accuracy of XSAPT(KS) calculations are thus improved if $E^{(2)}_{\mathrm{disp}} + E^{(2)}_{\mathrm{exch-disp}}$ is replaced by an empirical atom–atom dispersion potential and those non-dispersion components are reformulated in the atomic orbital (AO) basis to avoid the four-index integral transformation that is required in the original, molecular orbital version of the method. The resulting method is called AO-XSAPT(KS)+D[18–20]; consult Ref. 20 for an overview.

An AO-XSAPT(KS)+D calculation is requested by setting SAPT_AO and SAPT_DISP_CORR equal to TRUE. There are three versions of the dispersion potential, a "first generation" (+D1) version[18], second-generation (+D2) version[19], and third-generation (+D3) version[20]; the user can select amongst these using SAPT_DISP_VERSION. Although all three versions exhibit similar performance for total binding energies[20], the +D2 and +D3 potentials were fit directly to *ab initio* dispersion potentials and do a much better job of reproducing individual energy components, as compared to +D1[19,20]. Furthermore, the training set was expanded in the third generation to eliminate the largest errors in +D2 calculations, which tend to be $\pi$-stacked systems, and +D3 is the recommended dispersion correction.

As with XPol, the XSAPT and XSAPT(KS)+D methods do not function with a solvation model or with external changes. Currently, only single-point energies are available with no frozen orbitals.

Researchers who use XSAPT(KS)+D are asked to cite Ref. 18 for +D1, Ref. 19 for +D2, or Ref. 20 for +D3. The AO implementation of XSAPT is described in Ref. 55.

**SAPT_AO**

Request an atomic-orbital version of SAPT

TYPE:

BOOLEAN

DEFAULT:

FALSE

OPTIONS:

TRUE Use an AO version of SAPT.

FALSE Use a MO version of SAPT.

RECOMMENDATION:

Non-dispersion terms are calculated by AO-SAPT with $O(N^3)$ scaling.

**SAPT_DISP_CORR**

Request an empirical dispersion potential instead of calculating $E^{(2)}_{\text{disp}}$ and $E^{(2)}_{\text{exch-disp}}$ directly

TYPE:

BOOLEAN

DEFAULT:

FALSE

OPTIONS:

TRUE Use a dispersion force field.

FALSE calculate $E^{(2)}_{\rm disp}$ and $E^{(2)}_{\rm exch-disp}$.

RECOMMENDATION:

Using dispersion potentials combined with AO version of SAPT reduces the scaling from $O(N^5)$ to $O(N^3)$ with respect to monomer size.

**SAPT_DISP_VERSION**

Controls which dispersion potential is used for SAPT

TYPE:

INTEGER

DEFAULT:

3

OPTIONS:

1 Use the "first generation" (+D1) dispersion potentials from Hesselmann[18,56].

2 Use the "second generation" (+D2) dispersion potentials from Podeszwa.[19,57].

3 Use the "third generation" (+D3) dispersion potentials from Lao[20].

RECOMMENDATION:

Use +D3. Whereas +D1 was fit to reproduce binding energies, the +D2 and +D3 potentials were fit directly to dispersion energies $E^{(2)}_{\mathrm{disp}} + E^{(2)}_{\mathrm{exch-disp}}$ computed at the SAPT(DFT) and SAPT2+(3) levels, and performs well for both total binding energies as well as individual energy components[19,20]. In developing +D3, the training set was expanded to eliminate outliers involving $\pi$ stacking[20].

**Example 12.22** AO-XSAPT(KS)+D3 calculation of water-water interaction.

```
$rem
   SYM_IGNORE         true
   EXCHANGE           gen
   BASIS              aug-cc-pVTZ
   XPOL               true ! must be set to true for sapt jobs too
   XPOL_MPOL_ORDER    charges
   XPOL_CHARGE_TYPE   qchelpg
   XPOL_OMEGA         true
   XPOL_PRINT         3
   SAPT_PRINT         3
   SAPT               true
   SAPT_AO            true
   SAPT_ORDER         2          ! can be set to 1, ELST or RSPT
   SAPT_BASIS         projected ! monomer, dimer (if only 2 monomers), or projected
   SAPT_DISP_CORR     true
   SAPT_DISP_VERSION  3
   MEM_TOTAL          46000
   MEM_STATIC         4000
   AO2MO_DISK         35000
   THRESH             12
   SCF_CONVERGENCE    7
   LRC_DFT            true
   CHELPG             true
   CHELPG_DX          5
   CHELPG_HEAD        30
   CHELPG_H           110
   CHELPG_HA          590
$end

$xc_functional
   x   wPBE   1.0
   c   PBE   1.0
$end

$lrc_omega
   502
   502
$end

$molecule
0 1
--
   0 1
   O  -1.551007  -0.114520   0.000000
   H  -1.934259   0.762503   0.000000
   H  -0.599677   0.040712   0.000000
--
   0 1
   O   1.350625   0.111469   0.000000
   H   1.680398  -0.373741  -0.758561
   H   1.680398  -0.373741   0.758561
$end
```

For energy decomposition analysis using, *e.g.*, AO-XSAPT(KS)+D3, three individual calculations must be performed: AO-XSAPT(KS)+D3, AO-SAPT(KS)+D3, and AO-SAPT0, as demonstrated in the example below. The electrostatic, exchange, and dispersion energies can be obtained in the AO-SAPT(KS)+D3 calculation by searching the keywords "E1_elst", "E1_exch", and "Empirical E2_disp + E2_exch-disp", respectively. The induction energy includes three parts. First, there is $E^{(2)}_{\text{ind}} + E^{(2)}_{\text{exch-ind}}$ ("E2_ind" and "E2_exch-ind"), obtained from the AO-SAPT(KS)+D3 calculation. The second part is the total energy difference between AO-XSAPT(KS)+D3 and AO-SAPT(KS)+D3, and the total energy can be obtained by searching for "SAPT corrected total energy" in both calculations. This second part provides the many-body polarization and approximate infinite-order response correction. The final part of the energy decomposition accounts for higher-order polarization effects that can be approximated by searching the AO-SAPT0 calculation for the keyword "dSCF" ($\delta E^{\text{HF}}_{\text{int}}$ correction). The total binding energy is the sum of electrostatic, exchange, induction, and dispersion components obtained above.

**Example 12.23** The AO-XSAPT(KS)+D3 energy-decomposition analysis for water dimer, which requires three individual calculations.

```
$comment
   (1) AO-XSAPT(KS)+D3
$end

$rem
   SYM_IGNORE         true
   EXCHANGE           gen
   BASIS              cc-pVDZ
   XPOL               true ! must be set to true for sapt jobs too
   XPOL_MPOL_ORDER    charges ! gas or charges
   XPOL_CHARGE_TYPE   qchelpg  ! qlowdin,qmulliken,qchelpg
   XPOL_OMEGA         true
   XPOL_PRINT         3
   SAPT_PRINT         3
   SAPT               true
   SAPT_AO            true
   SAPT_ORDER         2          ! can be set to 1, ELST or RSPT
   SAPT_BASIS         projected ! monomer, dimer (if only 2 monomers), or projected
   SAPT_DISP_CORR     true
   SAPT_DISP_VERSION  3
   MEM_TOTAL          46000
   MEM_STATIC         4000
   AO2MO_DISK         35000
   THRESH             12
   SCF_CONVERGENCE    7
   LRC_DFT            true
   CHELPG             true
   CHELPG_DX          5
   CHELPG_HEAD        30
   CHELPG_H           110
   CHELPG_HA          590
$end

$xc_functional
   x   wPBE   1.0
   c    PBE   1.0
$end

$lrc_omega
   502
   502
$end

$molecule
0 1
--
   0 1
   O  -1.551007  -0.114520   0.000000
   H  -1.934259   0.762503   0.000000
   H  -0.599677   0.040712   0.000000
--
   0 1
   O   1.350625   0.111469   0.000000
   H   1.680398  -0.373741  -0.758561
   H   1.680398  -0.373741   0.758561
$end

@@@

$comment
   (2) AO-SAPT(KS)+D3
$end

$rem
   SYM_IGNORE         true
   EXCHANGE           gen
   BASIS              cc-pVDZ
   XPOL               true ! must be set to true for sapt jobs too
   XPOL_MPOL_ORDER    gas ! gas or charges
   XPOL_OMEGA         true
   XPOL_PRINT         3
   SAPT_PRINT         3
   SAPT               true
   SAPT_AO            true
   SAPT_ORDER         2           ! can be set to 1, ELST or RSPT
   SAPT_BASIS         projected ! monomer, dimer (if only 2 monomers), or projected
   SAPT_DISP_CORR     true
   SAPT_DISP_VERSION  3
   MEM_TOTAL          46000
   MEM_STATIC         4000
   AO2MO_DISK          35000
   THRESH              12
   SCF_CONVERGENCE     7
   LRC_DFT             true
$end

$xc_functional
   x   wPBE   1.0
   c    PBE   1.0
$end

$lrc_omega
   502
   502
$end

$molecule
0 1
--
   0 1
   O  -1.551007  -0.114520   0.000000
   H  -1.934259   0.762503   0.000000
   H  -0.599677   0.040712   0.000000
--
   0 1
   O   1.350625   0.111469   0.000000
   H   1.680398  -0.373741  -0.758561
   H   1.680398  -0.373741   0.758561
$end

@@@

$comment
   (3) AO-SAPT0
$end

$rem
   SYM_IGNORE         true
   EXCHANGE           hf
   BASIS              cc-pVDZ
   XPOL               true ! must be set to true for sapt jobs too
   XPOL_MPOL_ORDER    gas ! gas or charges
   XPOL_PRINT         3
   SAPT_PRINT         3
   SAPT               true
   SAPT_AO            true
   SAPT_ORDER         2          ! can be set to 1, ELST or RSPT
   SAPT_BASIS         dimer ! monomer, dimer (if only 2 monomers), or projected
   SAPT_CPHF          true
   SAPT_DSCF          true
   MEM_TOTAL          46000
   MEM_STATIC         4000
   AO2MO_DISK         35000
   THRESH             12
   SCF_CONVERGENCE    7
$end

$molecule
```

```
0 1
--
   0 1
   O  -1.551007  -0.114520   0.000000
   H  -1.934259   0.762503   0.000000
   H  -0.599677   0.040712   0.000000
--
   0 1
   O   1.350625   0.111469   0.000000
   H   1.680398  -0.373741  -0.758561
   H   1.680398  -0.373741   0.758561
$end
```

## 12.12 Energy Decomposition Analysis based on SAPT/cDFT

Many schemes for decomposing quantum chemical calculations of intermolecular interaction energies into physically meaningful components can be found in the literature, but the definition of the charge-transfer (CT) contribution has proven particularly vexing to define in a satisfactory way and typically depends strongly on the choice of basis set,[21,58,59] because as virtual orbitals on monomer $A$ start to extend significantly over monomer $B$ as the basis set approaches completeness, the distinction between polarization (excitations localized on $A$, introduced by the perturbing influence of $B$) and CT (excitations from $A$ to $B$) becomes blurred[21]. This ambiguity renders orbital-dependent definitions of CT highly dependent on the choice of atomic orbital basis set. On the other hand, constrained density functional theory (cDFT, Section 4.11), where a CT-free reference state can be defined based on “promolecule” densities, affords a definition of CT that is scarcely dependent on the basis set and is in accord with chemical intuition in simple cases.[21]

For intermolecular interactions, the cDFT definition of CT can be combined with a definition of the remaining components of the interaction energy (electrostatics, induction, Pauli repulsion, and van der Waals interactions) based on symmetry-adapted perturbation theory (SAPT, Section 12.10). In traditional SAPT, the CT interaction energy resides within the induction energy (also known as the polarization energy), which is therefore itself highly dependent upon the basis set. However, using cDFT to define the CT component and subtracting this out of the SAPT induction energy, both the CT and the remaining induction energies are largely independent of basis set[21]. SAPT/cDFT therefore provides a stable and physically-motivated energy decomposition, which can be invoked by setting the *$rem* variable SAPT_CDFT_EDA = TRUE in a SAPT calculation. A *$cdft* section must be set to specify the monomer charges and spins for the cDFT calculation. Researchers who use Q-CHEM's SAPT/cDFT code are asked to cite Ref. 21.

**SAPT_CDFT_EDA**
Request a SAPT/cDFT energy decomposition analysis
TYPE:
BOOLEAN
DEFAULT:
FALSE
OPTIONS:
TRUE Run a SAPT/cDFT calculation.
FALSE Do not run SAPT/cDFT.
RECOMMENDATION:
None

**Example 12.24** Energy decomposition analysis for the water dimer using AO-SAPT+D3/cDFT.

```
$comment
   a $cdft section must be set to specify the monomer charges and spins
   for the cDFT calculation.
$end

$rem
   SYM_IGNORE         true
   EXCHANGE           gen
   BASIS              aug-cc-pvdz
   XPOL               true ! must be set to true for sapt jobs too
   XPOL_MPOL_ORDER    gas ! gas or charges
   XPOL_OMEGA         true
   XPOL_PRINT         3
   SAPT_PRINT         3
   SAPT               true
   SAPT_AO            true
   SAPT_ORDER         2          ! can be set to 1, ELST or RSPT
   SAPT_BASIS         dimer ! monomer, dimer (if only 2 monomers), or projected
   SAPT_DISP_CORR     true
   SAPT_DISP_VERSION  3
   LRC_DFT            true
   SAPT_CDFT_EDA      true
$end

$xc_functional
   x   wPBE   1.0
   c    PBE   1.0
$end

$lrc_omega
   500
   500
$end

$cdft
   0
   1 1 3
   0
   1 1 3 s
$end

$molecule
0 1
--
   0 1
   O   -0.702196054  -0.056060256   0.009942262
   H   -1.022193224   0.846775782  -0.011488714
   H    0.257521062   0.042121496   0.005218999
--
0 1
   O    2.220871067   0.026716792   0.000620476
   H    2.597492682  -0.411663274   0.766744858
   H    2.593135384  -0.449496183  -0.744782026
$end
```

## 12.13 The Many-Body Expansion Method

### 12.13.1 Theory and Implementation Details

The many-body expansion (MBE) for a system of $N$ monomers is given by

$$E = \sum_{I=1}^{N} E_I + \sum_{I}^{N} \sum_{J>I}^{N} \Delta E_{IJ} + \sum_{I}^{N} \sum_{J>I}^{N} \sum_{K>J}^{N} \Delta E_{IJK} + \cdots , \tag{12.39}$$

in which $E_I$ represents the energy of monomer $I$, $\Delta E_{IJ}$ = $E_{IJ} - E_I - E_J$ is a two-body correction for dimer $IJ$, and $\Delta E_{IJK}$ = $E_{IJK} - \Delta E_{IJ} - \Delta E_{IK} - \Delta E_{JK} - E_I - E_J - E_k$ is a three-body correction for trimer $IJK$, etc. In a large system and/or a large basis set, truncation of this expression at the two- or three-body level may dramatically reduce the amount of computer time that is required to compute the energy. Convergence of the MBE can be accelerated by embedding the monomer ($E_I$), dimer ($E_{IJ}$), trimer ($E_{IJK}$), . . . calculations in some representation of the electrostatic potential of the rest of the system. A simple means to do this is via atom-centered point charges that could be obtained when the $E_I$ terms are calculated; this is the so-called electrostatically-embedded many-body expansion (EE-MBE)[22]. Alternatively, since the monomer electron densities are available from the $E_I$ terms as well, one could use these densities to compute the actual monomer–monomer Coulomb interactions, and this forms the basis of the fragment molecular orbital (FMO) method[23,24]. In particular, the "bodies" (fragments) cannot be covalently bonded to one another, and therefore this is a method appropriate for non-covalent clusters of molecules. Moreover, individual subsystem calculations have been parallelized across processors using MPI, hence the present implementation is using the real power of the MBE. Analytic gradients are also available for MBE and EE-MBE, but not FMO.

It is well known that the interaction energies of non-covalent clusters are usually overestimated (often substantially) owing to basis-set superposition error (BSSE), which disappears only very slowly as the basis sets approach completeness. The widely used Boys–Bernardi counterpoise (CP) procedure corrects for this by computing all energies (including cluster and monomers) using the cluster basis set. (Note, however, that basis-set extrapolation is still necessary for high-quality binding energies; in $(\mathrm{H_2O})_6$, for example, a CP-corrected MP2/aug-cc-pVQZ calculation is still $\approx$ 1 kcal/mol from the MP2 basis-set limit[60]. Fortunately, the MBE allows for use of large basis sets in order to perform basis-set extrapolations in sizable clusters[60,61].) Two low-cost CP corrections that are consistent with an $n$-body expansion have been proposed: the many-body CP correction, MBCP($n$)[60,61], and the $n$-body Valiron-Mayer function counterpoise correction, VMFC($n$)[62]. The two approaches are equivalent for $n = 2$ but the MBCP($n$) method requires far fewer subsystem calculations starting at $n = 3$ and is thus significantly cheaper, while affording very similar results as compared to VMFC($n$)[60,61].

Q-CHEM's implementation of the EE-MBE($n$) approach (electrostatically-embedded $n$-body expansion) is designed to use *$mbe_charges* section to specify embedding charges. As such, a MBE calculation is requested by setting MANY_BODY_INT = TRUE. The variable MBE_EMBEDDING = CHARGES/GAS sets the MBE calculations with or without using embedding charges. The variable MBE_ORDER sets the truncation order, $n$. As an alternative to point charges, density embedding is also available, in which Coulomb interactions are computed between proper monomer electron densities. The MBE with density embedding is equivalent to the original version of the fragment molecular orbital (FMO)[23]. (Many subsequent modifications to the FMO algorithm have been introduced[24,63] but are not yet available in Q-CHEM. These include, in particular, the option to use point charges or approximate electron repulsion integrals to compute the Coulomb interactions between distant monomers[64,65], which actually makes FMO more like EE-MBE at long range.) This density-embedded version of FMO is available in Q-CHEM by setting XPOL = TRUE, XPOL_MPOL_ORDER = DENSITY, and FRAG_MOL_ORB = TRUE. The variable FMO_ORDER sets the truncation order, $n$. The MBE version of BSSE is requested by setting MANY_BODY_BSSE = MBCP or VMFC. The variable MBE_BSSE_ORDER sets the truncation order, $n$.

Researchers who use Q-CHEM's MBE code are asked to cite Ref. 66,67 and—if the MBCP($n$) method is used—to cite Ref. 60 as well.

### 12.13.2 Job Control and Examples for Many-Body Calculations

The following *$rem* variables control MBE jobs.

**MANY_BODY_INT**
Perform a MBE calculation.
TYPE:
BOOLEAN
DEFAULT:
FALSE
OPTIONS:

| | |
|---|---|
| TRUE | Perform a MBE calculation. |
| FALSE | Do not perform a MBE calculation. |

RECOMMENDATION:
NONE

**MBE_ORDER**
Controls the truncation order $n$ for MBE.
TYPE:
INTEGER
DEFAULT:
2
OPTIONS:

| | |
|---|---|
| $N$ | Order of MBE |

RECOMMENDATION:
MBE can be performed up to fifth order.

**MBE_EMBEDDING**
Controls the type of MBE calculations.
TYPE:
STRING
DEFAULT:
GAS
OPTIONS:

| | |
|---|---|
| GAS | MBE without charge embedding. |
| CHARGES | MBE with charge embedding. |

RECOMMENDATION:
NONE.

**MANY_BODY_BSSE**

Controls the type of many-body BSSE corrections.

TYPE:

STRING

DEFAULT:

MBCP

OPTIONS:

| | |
|---|---|
| MBCP | Use many-body counterpoise correction. |
| VMFC | Use Valiron-Mayer function counterpoise correction. |

RECOMMENDATION:

NONE.

**MBE_BSSE_ORDER**

Controls the order of many-body BSSE corrections.

TYPE:

INTEGER

DEFAULT:

2

OPTIONS:

$n$ Order of many-body BSSE corrections

RECOMMENDATION:

MBCP and VMFC can be performed up to fourth order.

**FRAG_MOL_ORB**

Perform a FMO calculation.

TYPE:

BOOLEAN

DEFAULT:

FALSE

OPTIONS:

| | |
|---|---|
| TRUE | Perform a FMO calculation. |
| FALSE | Do not perform a FMO calculation. |

RECOMMENDATION:

NONE

**FMO_ORDER**

Controls the truncation order $n$ for FMO.

TYPE:

INTEGER

DEFAULT:

NONE

OPTIONS:

$N$ Order of FMO

RECOMMENDATION:

FMO can be performed up to third order.

**Example 12.25** Example showing a 3-body EE-MBE calculation using TIP3P charges.

```
$rem
   SYM_IGNORE        true
   METHOD            B3LYP
   BASIS             cc-pVDZ
   MANY_BODY_INT     true
   MBE_ORDER         3
   MBE_EMBEDDING     charges
   THRESH            14
   SCF_CONVERGENCE   7
$end

$molecule
0 1
--
   0 1
   O -1.126149 -1.748387 -0.423240
   H -0.234788 -1.493897 -0.661862
   H -1.062789 -2.681331 -0.218819
--
   0 1
   O -0.254210 1.611495 -1.293845
   H -1.001520 1.163510 -1.690129
   H -0.153399 2.411746 -1.809248
--
   0 1
   O 1.694541 -0.226287 1.705739
   H 0.785920 0.073487 1.677909
   H 2.047134 0.150917 2.511706
--
   0 1
   O -0.864533 0.522472 1.218817
   H -0.694120 1.093542 0.469789
   H -1.131418 -0.310426 0.829702
$end

$mbe_charges
  -0.834
   0.417
   0.417
  -0.834
   0.417
   0.417
  -0.834
   0.417
   0.417
  -0.834
   0.417
   0.417
$end
```

**Example 12.26** Example showing a 3-body MBCP calculation.

```
$rem
   SYM_IGNORE        true
   METHOD            B3LYP
   BASIS             cc-pVDZ
   MANY_BODY_BSSE    mbcp
   MBE_BSSE_ORDER    3
   THRESH            14
   SCF_CONVERGENCE   7
$end

$molecule
0 1
--
   0 1
   O -1.126149 -1.748387 -0.423240
   H -0.234788 -1.493897 -0.661862
   H -1.062789 -2.681331 -0.218819
--
   0 1
   O -0.254210 1.611495 -1.293845
   H -1.001520 1.163510 -1.690129
   H -0.153399 2.411746 -1.809248
--
   0 1
   O 1.694541 -0.226287 1.705739
   H 0.785920 0.073487 1.677909
   H 2.047134 0.150917 2.511706
--
   0 1
   O -0.864533 0.522472 1.218817
   H -0.694120 1.093542 0.469789
   H -1.131418 -0.310426 0.829702
$end
```

**Example 12.27** Example showing a 3-body FMO calculation.

```
$rem
   SYM_IGNORE        true
   METHOD            B3LYP
   BASIS             cc-pVDZ
   XPOL              true
   XPOL_MPOL_ORDER   density
   FRAG_MOL_ORB      true
   FMO_ORDER         3
   THRESH            14
   SCF_CONVERGENCE   7
$end

$molecule
0 1
--
   0 1
   O -1.126149 -1.748387 -0.423240
   H -0.234788 -1.493897 -0.661862
   H -1.062789 -2.681331 -0.218819
--
   0 1
   O -0.254210 1.611495 -1.293845
   H -1.001520 1.163510 -1.690129
   H -0.153399 2.411746 -1.809248
--
   0 1
   O 1.694541 -0.226287 1.705739
   H 0.785920 0.073487 1.677909
   H 2.047134 0.150917 2.511706
--
   0 1
   O -0.864533 0.522472 1.218817
   H -0.694120 1.093542 0.469789
   H -1.131418 -0.310426 0.829702
$end
```

## 12.14 Ab-Initio Frenkel Davydov Exciton Model (AIFDEM)

### 12.14.1 Theory

A fairly old idea for treating the excited states of a broad and highly relevant class of weakly interacting molecular aggregates is the so called Frankel-Davydov Exciton model. In such a model the excited states of the total aggregate is treated as a linear combination of excitations that are localized on molecular sites; the $I$th excited state, $|\Xi_I\rangle$, can be written,

$$|\Xi_I\rangle = \sum_n^{\text{sites}} \sum_i^{\text{states}} K_n^{Ii} |\Psi_n^i\rangle \prod_{m\neq n} |\Psi_m\rangle, \tag{12.40}$$

where $|\Psi_n^i\rangle$ is the $i$th excited state of the $n$th molecular fragment and when un-superscripted corresponds to the ground state of the same. Eigenstates and energies are found by computing the electronic Hamiltonian matrix in this direct product, exciton-site basis and diagonalizing it. The AIFDEM[25] approach is an *ab-initio* realization of this *ansatz* whereby the exciton-site basis is compromised of direct products of *ab-initio* wave functions that are computed for the isolated fragments. Fragment ground states are described by single SCF determinants, $\Phi_A$, and fragment excited states are linear combinations of singly-excited determinants,

$$|\Psi_A^*\rangle = \sum_{ia} C^{ia} |\Phi_A^{ia}\rangle. \tag{12.41}$$

The AIFDEM approach computes elements of the Hamiltonian,

$$\langle\Psi_A^*\Psi_B\Psi_C\ldots|\hat{H}|\Psi_A\Psi_B^*\Psi_C\ldots\rangle = \sum_{ia\sigma}\sum_{kb\tau} C_\sigma^{ia} C_\tau^{kb} \langle\Phi_A^{ia}\Phi_B\Phi_C\ldots|\hat{H}|\Phi_A\Phi_B^{kb}\Phi_C\ldots\rangle\ , \tag{12.42}$$

and overlap matrices,

$$\langle\Psi_A^*\Psi_B\Psi_C\ldots|\Psi_A\Psi_B^*\Psi_C\ldots\rangle = \sum_{ia\sigma}\sum_{kb\tau} C_\sigma^{ia} C_\tau^{kb} \langle\Phi_A^{ia}\Phi_B\Phi_C\ldots|\Phi_A\Phi_B^{kb}\Phi_C\ldots\rangle\ . \tag{12.43}$$

The fragment excited states are transformed into the NTO basis, see section 6.12.2, to minimize the number of terms in the expansions and the corresponding orbitals transformation, see section 10.17.2.2, is utilized to compute the matrix elements of the non-orthogonal orbitals for each term in the RHS of equations (12.42) and (12.43). The eigenstates and eigenenergies of the exciton Hamiltonian are printed and saved to a scratch file; transition dipole moments between the ground and first ten exciton eigenstates are also computed.

The cost to compute each matrix element scales as the size of the super-system, approximately $\mathcal{O}\left(N^{2-4}\right)$, since all fragments must be included in the direct products in equations (12.42) and (12.43). To reduce this scaling a physically motivated charge embedding scheme was recently introduced[26] that only treats the excited fragments, and neighbors within a user specified distance threshold, with full QM while the other ground state fragment interactions are approximated by point charges. Point charge type is specified using the XPOL_CHARGE_TYPE keyword. In general, the inclusion of neighboring fragments in the QM part of the matrix element evaluation does not seem to significantly improve the accuracy and diminishes the cost savings of the charge embedding procedure. Therefore, the minimal " 0 Å " threshold, where only the excited fragments are treated with QM, can be considered optimal. Charge embedding with the minimal threshold affords and algorithm that scales as $F^2 \times \mathcal{O}\left(n_{\text{pair}}^{2-4}\right)$, where $F$ is the number of fragments and $n_{\text{pair}}$ is the size of a pair of fragments.

The exciton-site basis can be expanded to include higher lying fragment excited states which gives the wave function variational flexibility and can significantly improve accuracy for polar systems and delocalized excited states. The number of fragment excited states to include in the basis is specified by the CIS_N_ROOTS keyword (should be equal to 1 at minimum). A cost effective means of including polarization effects is to utilize the XPol method to compute fragment ground states, see section 12.9 and associated job controls, fragment excited states are then computed using the XPol polarized MOs. Charge transfer-like states of the form, $|\Phi_A^+\Phi_B^-\Phi_C\ldots\rangle$, where $\Phi_A^{+(-)}$ represent cation (anion) determinants from unrestricted SCF calculations on the isolated fragments, can also be included in the basis.

The exciton-site basis states are spin adapted, their multiplicity determines that of the target excited state and this must be specified by setting CIS_SINGLETS or CIS_TRIPLETS to TRUE. The number of terms that are included in equations (12.42) and (12.43) can be rationally truncated at some fraction of the norm of the fragment NTO amplitudes to reduce computational cost at the expense of some accuracy. Computation time scales approximately quadratically with the number of these terms and a threshold of about 85% has been found to maintain acceptable accuracy for organic molecules with reasonable cost. The fragment orbitals and excited states may be computed with any level of SCF and single excitation theory, including DFT and TDDFT, however the coupling matrix elements are always computed with a CIS-like Hamiltonian with no DFT exchange-correlation. Both OpenMP, and MPI parallel implementations are available; the former distributes two-electron integral computation across cores in a node as in a traditional excited state calculation, the latter can distribute matrix element evaluations across hundreds of cores with minimal overhead.

## 12.14.2 Job Control for AIFDEM

**AIFDEM**

Perform an AIFDEM calculation.

TYPE:

LOGICAL

DEFAULT:

FALSE

OPTIONS:

| | |
|---|---|
| FALSE | Do not perform an AIFDEM calculation. |
| TRUE | Perform an AIFDEM calculation. |

RECOMMENDATION:

False

**AIFDEM_NTOTHRESH**

Controls the number of NTOs that are retained in the exciton-site basis states.

TYPE:

INTEGER

DEFAULT:

99

OPTIONS:

$n$ Threshold percentage of the norm of fragment NTO amplitudes.

RECOMMENDATION:

A threshold of $85\%$ gives a good trade-off of computational time and accuracy for organic molecules.

**AIFDEM_EMBED_RANGE**

Specifies the size of the QM region for charge embedding

TYPE:

INTEGER

DEFAULT:

FULL_QM

OPTIONS:

| | |
|---|---|
| FULL_QM | No charge embedding. |
| 0 | Treat only excited fragments with QM. |
| $n$ | Range (Å) from excited fragments within which to treat other fragments with QM. |

RECOMMENDATION:

Minimal, 0 Å, threshold maintains accuracy while significantly reducing computational time.

**AIFDEM_CTSTATES**

Include charge-transfer-like cation/anion pair states in the AIFDEM basis.

TYPE:

LOGICAL

DEFAULT:

FALSE

OPTIONS:

| | |
|---|---|
| TRUE | Include CT states. |
| FALSE | Do not include CT states. |

RECOMMENDATION:

None

**Example 12.28** Example showing singlet excited state calculation, on $(H_2O)_4$. XPol is used to generate monomer wave functions with ChElPG charges. Minimal QM charge embedding is used for the exciton model with three excited states per fragment.

```
$rem
   BASIS                aug-cc-pvdz
   EXCHANGE             HF
   CIS_N_ROOTS          3
   CIS_TRIPLETS         FALSE
   XPOL                 TRUE
   XPOL_CHARGE_TYPE     QCHELPG
   AIFDEM               TRUE
   AIFDEM_EMBED_RANGE   0
   AIFDEM_NTOTHRESH     90
   NTO_PAIRS            1
$end

$molecule
0 1
--H2O 0
   0 1
   O          1.74078        1.59716       -1.49814
   H          2.22908        2.18316       -2.08914
   H          0.88038        2.04726       -1.32684
--H2O 1
   0 1
   O          1.31998       -1.18934       -1.91734
   H          1.49988       -0.22974       -1.89044
   H          1.69058       -1.52594       -1.07704
--H2O 2
   0 1
   O         -0.68982        2.59476       -0.72224
   H         -1.14372        3.37086       -1.07364
   H         -1.35592        1.84986       -0.78334
--H2O 3
   0 1
   O         -1.27512       -1.77394       -1.69524
   H         -0.32252       -1.52884       -1.85604
   H         -1.53992       -2.30454       -2.45644
$end
```

### 12.14.3 AIFDEM Derivatives

The non-adiabatic coupling vector codifies the coupling of electronic states caused by motion of the nuclei and this quantity may be computed within the framework of the AIFDEM. For two AIFDEM eigenstates, $I$ and $J$, the non-adiabatic coupling vector can be computed as,

$$\mathbf{h}^{IJ} = \mathbf{K}_I \mathbf{H}^{[x]} \mathbf{K}_J. \tag{12.44}$$

Here, $\mathbf{H}^{[x]}$ is the derivative of the AIFDEM Hamiltonian with respect to nuclear coordinate $x$. Related quantities that are important in the context of carrier mobility in organic semiconductors are the, Local, "Holstein", and Non-Local, "Peierls", electron/phonon coupling constants. These can be computed by transforming $\mathbf{H}^{[x]}$ to dimensionless normal modes coordinates. Analytic evaluation of $\mathbf{H}^{[x]}$ and the analogous quantity for the AIFDEM overlap matrix, $\mathbf{S}^{[x]}$, have been implemented[68] in Q-CHEM. To compute AIFDEM derivatives, simply request a standard AIFDEM job and set CIS_STATE_DERIV= 1. Note that, at this time, AIFDEM derivatives only support a single excited state in the exciton-site basis and do not support charge embedding.

## 12.15 TDDFT for Molecular Interactions

### 12.15.1 Theory

There exist a broad class of weakly interacting molecular complexes which give rise to interesting excited-state properties that are potentially very different from those of a single chromophore. The “TDDFT for molecular interactions" or TDDFT(MI) method is designed for efficient excited-state calculations in such cases in (potentially large) systems composed of weakly-interacting but electronically-coupled monomers[27,29]. Such systems include molecular aggregates, chromophores in explicit solvent, and even proteins, for which the traditional TDDFT method become prohibitively expensive. TDDFT(MI) starts from a ground-state SCF(MI) calculation, and the use of ALMOs is central to its efficiency. In addition, the excitations are confined within monomer units and the explicit charge-transfer excitations are ignored, significantly reduced the two-electron integrals cost. The method works by coupling together excitations computed individually on different molecular fragments, and the number of excited states per fragment can be increased (at very low cost) in order to increase the variational flexibility of this exciton-type basis. Thus, despite the localized nature of the basis states, TDDFT(MI) is capable of describing collective excitations that are delocalized over multiple monomer units, as for example in the case of organic semiconductors. In general, TDDFT(MI) reproduces full super-system TDDFT excitation energies to within $\sim$0.2 eV, but with an order or magnitude reduction in total CPU time[27]. Formally, the cost of the method scales as $\mathcal{O}(N_{\text{fragment}}^2 N_{\text{roots}}^2 N_{\text{sub-AO}}^x)$ where $N_{\text{fragment}}$ is the number of monomers, $N_{\text{roots}}$ is the number of excited states per monomer, and $N_{\text{sub-AO}}$ is the number of AOs on a dimer subsystem. The exponent $x$ (with $2 \leq x \leq 4$) reflects the cost of forming the Fock-like matrices of a traditional TDDFT calculation.

An especially promising application of the TDDFT(MI) method is to study excitation energies of a single chromophore in solution using a large number of explicit, quantum-mechanical solvent molecules. In such cases, the excitations are localized on the single chromophore and we can introduce a local excitation approximation (LEA) to TDDFT(MI) in which all of the Coulomb and exchange couplings between the solvent molecules and the chromophore are neglected[28]. Following the ground-state SCF(MI) calculation, the cost of the TDDFT part of the calculation becomes essentially the same as the cost of a TDDFT calculation on the gas-phase chromophore. In addition, this approach avoids the appearance of, and mixing with, spurious charge-transfer-to-solvent states[28,29], of the sort that are known to arise in TDDFT calculations with explicit solvent[69,70]. Three versions of LEA-TDDFT(MI), named LEA0, LEA-Q and LEAc, have been implemented in Q-CHEM[28]. In the LEA0 method, ALMOs from the ground state SCF(MI) calculation are used to perform the TDDFT calculation. In LEAc, a sub-block of the TDDFT(MI) working equation localized on chromophore is extracted to calculate the excitation energies. Finally, LEA-Q is almost the same as LEAc except for some transformations to eliminate the overlap matrices. These approaches have been applied to converge solvatochromatic shifts for several aqueous chromophores[28].

## 12.15.2 Job Control for TDDFT(MI)

In addition to the normal TDDFT job controls variables described in Section 6.3.3, there are several others to request TDDFT(MI). Note that only single-point energies (not gradients) are available for this method.

**TDDFT_MI**
Perform an TDDFT(MI) calculation
TYPE:
LOGICAL
DEFAULT:
FALSE
OPTIONS:
FALSE Do not perform an TDDFT(MI) calculation
TRUE Perform an TDDFT(MI) calculation
RECOMMENDATION:
False

**MI_ACTIVE_FRAGMENT**
Sets the active fragment
TYPE:
INTEGER
DEFAULT:
NO DEFAULT
OPTIONS:
$n$ Specify the fragment on which the TDDFT calculation is to be performed, for LEA-TDDFT(MI).
RECOMMENDATION:
None

**MI_LEA**
Controls the LEA-TDDFT(MI) methods
TYPE:
INTEGER
DEFAULT:
NO DEFAULT
OPTIONS:
0 The LEA0 method
1 The LEA-Q method
2 The LEAc method
RECOMMENDATION:
1

## 12.16 The ALMO-CIS and ALMO-CIS+CT methods

### 12.16.1 Theory

The ALMO-CIS[71] and ALMO-CIS+CT[72] methods are local variants of configuration interaction singles (CIS), and are formulated through the use of absolutely localized molecular orbitals (ALMOs). They share the same spirit with the TDDFT(MI) method (see Section 12.15), but were originally designed to target large numbers of excited states in atomic/molecular clusters, such as the entire $n = 2$ band in helium clusters that contain hundreds of atoms.

In ALMO-CIS and ALMO-CIS+CT, we solve a truncated non-orthogonal CIS eigen-equation:

$$A_{ia,jb}t^{jb} = \omega S_{ia,jb}t^{jb} \tag{12.45}$$

The use of ALMOs allows associating each MO index ($i$, $a$, $j$ or $b$) to a fragment. In ALMO-CIS, approximation is made such that only the amplitudes corresponding to intrafragment transitions are non-zero, i.e., $t^{jb} = 0$ if the occupied orbital $j$ and the virtual orbital $b$ reside on two different fragments. The Hamiltonian and overlap matrix are also truncated, with $i$ ($j$) and $a$ ($b$) belonging to the same fragment. This approximation excludes interfragment charge transfer (CT) excitations entirely and sometimes may lead to insufficient accuracy. In ALMO-CIS+CT, the CT effect is reintroduced by setting a distance cutoff $r_{\text{cut}}$, so that transitions between neighboring fragments within a distance smaller than $r_{\text{cut}}$ are allowed ($i$ ($j$) and $a$ ($b$) belonging to such a pair of fragments are also included in the eigen-equation). In both ALMO-CIS and ALMO-CIS+CT, dimension of the eigenvalue problem scales linearly with respect to system size, instead of having a quadratic scaling as in standard CIS. Because of the reduction of matrix size, it is computationally feasible to explicitly build the Hamiltonian and diagonalize it to get a full band of eigenstates for relatively large systems, and the overall scaling of ALMO-CIS/ALMO-CIS+CT is cubic, in contrast with the sixth order scaling of standard CIS for a full-spectrum calculation.

Besides the full-spectrum calculations described above, use of the Davidson algorithm is also available for ALMO-CIS and ALMO-CIS+CT, which targets a few lowest excited states. This implementation, unlike the original full-spectrum version, also supports the local variants of TDDFT/TDA calculations that share the same working equation (eq. 12.45).

### 12.16.2 Job Control for ALMO-CIS/ALMO-CIS+CT

In addition to the standard CIS job controls variables described in Section 6.2.8, there are several additional *$rem* variables to specify for an ALMO-CIS/ALMO-CIS+CT calculation.

**LOCAL_CIS**
Invoke ALMO-CIS/ALMO-CIS+CT.
TYPE:
INTEGER
DEFAULT:
0
OPTIONS:
0 Regular CIS
1 ALMO-CIS/ALMO-CIS+CT without RI(slow)
2 ALMO-CIS/ALMO-CIS+CT with RI
RECOMMENDATION:
2 if ALMO-CIS is desired.

**NN_THRESH**
The distance cutoff for neighboring fragments (between which CT is enabled).
TYPE:
INTEGER
DEFAULT:
0
OPTIONS:
0 Do not include interfragment transitions (ALMO-CIS).
$n$ Include interfragment excitations between pairs of fragments the distances between whom are smaller than $n$ Bohr (ALMO-CIS+CT).
RECOMMENDATION:
None

**EIGSLV_METH**

Control the method for solving the ALMO-CIS eigen-equation

TYPE:

INTEGER

DEFAULT:

0

OPTIONS:

0 Explicitly build the Hamiltonian then diagonalize (full-spectrum).

1 Use the Davidson method (currently only available for restricted cases).

RECOMMENDATION:

None

**Example 12.29** ALMO-CIS+CT calculation ($r_{\text{cut}} = 10$ $a_0$) for all the $n = 2$ states of a helium dimer.

```
$molecule
0 1
--
   0 1
   He      2.8    0.     0.
--
   0 1
   He      0.     0.     0.
$end

$rem
   basis          gen
   aux_basis      rimp2-cc-pvdz
   purecart       1111
   method         hf
   sym_ignore     true
   symmetry       false
   frgm_method    stoll
   cis_n_roots    8
   cis_triplets   false
   local_cis      2 ! use RI for ALMO-CIS
   nn_thresh      10
$end

$rem_frgm
   cis_n_roots 0
$end

$basis
****
HE   0
S    3    1.000000
3.84216340D+01    2.37660000D-02
5.77803000D+00    1.54679000D-01
1.24177400D+00    4.69630000D-01
S    1    1.000000
2.97964000D-01    1.00000000D+00
SP   1    1.000000
4.80000000D-02    1.00000000D+00   1.00000000D+00
****
$end
```

# References and Further Reading

[1] R. Z. Khaliullin, M. Head-Gordon, and A. T. Bell, *J. Chem. Phys.* **124**, 204105 (2006).

[2] P. R. Horn, E. J. Sundstrom, T. A. Baker, and M. Head-Gordon, *J. Chem. Phys.* **138**, 134119 (2013).

[3] R. Z. Khaliullin, E. A. Cobar, R. C. Lochan, A. T. Bell, and M. Head-Gordon, *J. Phys. Chem. A* **111**, 8753 (2007).

[4] R. Z. Khaliullin, A. T. Bell, and M. Head-Gordon, *J. Chem. Phys.* **128**, 184112 (2008).

[5] R. Z. Khaliullin, A. T. Bell, and M. Head-Gordon, *Chem. Eur. J* **15**, 851 (2009).

[6] P. R. Horn and M. Head-Gordon, *J. Chem. Phys.* **143**, 114111 (2015).

[7] P. R. Horn and M. Head-Gordon, *J. Chem. Phys.* **144**, 084118 (2016).

[8] P. R. Horn, Y. Mao, and M. Head-Gordon, *J. Chem. Phys.* **144**, 114107 (2016).

[9] P. R. Horn, Y. Mao, and M. Head-Gordon, *Phys. Chem. Chem. Phys.* **18**, 23067 (2016).

[10] D. S. Levine, P. R. Horn, Y. Mao, and M. Head-Gordon, *J. Chem. Theory Comput.* **12**, 4812 (2016).

[11] Y. Mao, P. R. Horn, and M. Head-Gordon, *Phys. Chem. Chem. Phys.* **19**, 5944 (2017).

[12] W. Xie, L. Song, D. G. Truhlar, and J. Gao, *J. Chem. Phys.* **128**, 234108 (2008).

[13] L. D. Jacobson and J. M. Herbert, *J. Chem. Phys.* **134**, 094118 (2011).

[14] J. M. Herbert, L. D. Jacobson, K. U. Lao, and M. A. Rohrdanz, *Phys. Chem. Chem. Phys.* **14**, 7679 (2012).

[15] B. Jeziorski, R. Moszynski, and K. Szalewicz, *Chem. Rev.* **94**, 1887 (1994).

[16] K. Szalewicz, *Wiley Interdiscip. Rev.: Comput. Mol. Sci.* **2**, 254 (2012).

[17] L. D. Jacobson, R. M. Richard, K. U. Lao, and J. M. Herbert, *Annu. Rep. Comp. Chem.* **9**, 25 (2013).

[18] K. U. Lao and J. M. Herbert, *J. Phys. Chem. Lett.* **3**, 3241 (2012).

[19] K. U. Lao and J. M. Herbert, *J. Chem. Phys.* **139**, 034107 (2013).

[20] K. U. Lao and J. M. Herbert, *J. Phys. Chem. A* **119**, 235 (2015).

[21] K. U. Lao and J. M. Herbert, *J. Chem. Theory Comput.* **12**, 2569 (2016).

[22] E. E. Dahlke and D. G. Truhlar, *J. Chem. Theory Comput.* **3**, 46 (2007).

[23] K. Kitaura, E. Ikeo, T. Asada, T. Nakano, and M. Uebayasi, *Chem. Phys. Lett.* **313**, 701 (1999).

[24] D. G. Fedorov and K. Kitaura, *J. Phys. Chem. A* **111**, 6904 (2007).

[25] A. F. Morrison, Z.-Q. You, and J. M. Herbert, *J. Chem. Theory Comput.* **10**, 5366 (2014).

[26] A. F. Morrison and J. M. Herbert, *J. Phys. Chem. Lett.* **6**, 4390 (2015).

[27] J. Liu and J. M. Herbert, *J. Chem. Phys.* **143**, 034106 (2015).

[28] J. Liu and J. M. Herbert, *J. Chem. Theory Comput.* **12**, 157 (2016).

[29] J. M. Herbert, X. Zhang, A. F. Morrison, and J. Liu, *acr* **49**, 931 (2016).

[30] D. Ghosh et al., *J. Phys. Chem. A* **114**, 12739 (2010).

[31] H. Stoll, G. Wagenblast, and H. Preuss, *Theor. Chem. Acc.* **57**, 169 (1980).

[32] E. Gianinetti, M. Raimondi, and E. Tornaghi, *Int. J. Quantum Chem.* **60**, 157 (1996).

[33] T. Nagata, O. Takahashi, K. Saito, and S. Iwata, *J. Chem. Phys.* **115**, 3553 (2001).

[34] W. Z. Liang and M. Head-Gordon, *J. Phys. Chem. A* **108**, 3206 (2004).

[35] W. Z. Liang and M. Head-Gordon, *J. Chem. Phys.* **120**, 10379 (2004).

[36] E. A. Cobar, R. Z. Khaliullin, R. G. Bergman, and M. Head-Gordon, *Proc. Natl. Acad. Sci. USA* **104**, 6963 (2007).

[37] R. C. Lochan, R. Z. Khaliullin, and M. Head-Gordon, *Inorg. Chem.* **47**, 4032 (2008).

[38] M. Hopffgarten and G. Frenking, *Wiley Interdiscip. Rev.: Comput. Mol. Sci.* **2**, 43 (2012).

[39] Y. Mao, O. Demerdash, M. Head-Gordon, and T. Head-Gordon, *J. Chem. Theory Comput.* **12**, 5422 (2016).

[40] R. J. Azar, P. R. Horn, E. J. Sundstrom, and M. Head-Gordon, *J. Chem. Phys.* **138**, 084102 (2013).

[41] J. Gao, *J. Chem. Phys.* **109**, 2346 (1998).

[42] W. Xie and J. Gao, *J. Chem. Theory Comput.* **3**, 1890 (2007).

[43] W. Xie, M. Orozco, D. G. Truhlar, and J. Gao, *J. Chem. Theory Comput.* **5**, 459 (2009).

[44] C. M. Breneman and K. B. Wiberg, *J. Comput. Chem.* **11**, 361 (1990).

[45] Z. C. Holden, R. M. Richard, and J. M. Herbert, *J. Chem. Phys.* **139**, 244108 (2013).

[46] B. Jeziorski et al., SAPT: A program for many-body symmetry-adapted perturbation theory calculations of intermolecular interaction energies, in *Methods and Techniques in Computational Chemistry: METECC-94*, edited by E. Clementi, volume B, chapter 3, page 79, STEF, Cagliari, 1993.

[47] E. G. Hohenstein and C. D. Sherrill, *Wiley Interdiscip. Rev.: Comput. Mol. Sci.* **2**, 304 (2012).

[48] K. U. Lao and J. M. Herbert, *J. Phys. Chem. A* **116**, 3042 (2012).

[49] J. A. Pople, R. Krishnan, H. B. Schlegel, and J. S. Binkley, *Int. J. Quantum Chem. Symp.* **13**, 225 (1979).

[50] H. L. Williams and C. F. Chabalowski, *J. Phys. Chem. A* , 646 (2001).

[51] A. J. Misquitta and K. Szalewicz, *Chem. Phys. Lett.* **357**, 301 (2002).

[52] K. U. Lao and J. M. Herbert, *J. Chem. Phys.* **140**, 044108 (2014).

[53] H. L. Williams, E. M. Mas, and K. Szalewicz, *J. Chem. Phys.* **103**, 7374 (1995).

[54] R. P. Steele, R. A. DiStasio, Jr., Y. Shao, J. Kong, and M. Head-Gordon, *J. Chem. Phys.* **125**, 074108 (2006).

[55] K. U. Lao and J. M. Herbert, Implementation of restricted and unrestricted versions of extended symmetry-adapted perturbation theory (XSAPT) in the atomic orbital basis, and benchmark calculations for large supramolecular complexes, (in preparation).

[56] A. Hesselmann, *J. Phys. Chem. A* **115**, 11321 (2011).

[57] R. Podeszwa, K. Pernal, K. Patkowski, and K. Szalewicz, *J. Phys. Chem. Lett.* **1**, 550 (2010).

[58] E. Ronca, L. Belpassi, and F. Tarantelli, *ChemPhysChem* **15**, 2682 (2014).

[59] J. Řezáč and A. de la Lande, *J. Chem. Theory Comput.* **11**, 528 (2015).

[60] R. M. Richard, K. U. Lao, and J. M. Herbert, *J. Phys. Chem. Lett.* **4**, 2674 (2013).

[61] R. M. Richard, K. U. Lao, and J. M. Herbert, *J. Chem. Phys.* **139**, 224102 (2013).

[62] M. Kamiya, S. Hirata, and M. Valiev, *J. Chem. Phys.* **128**, 074103 (2008).

[63] D. G. Fedorov and K. Kitaura, in *The Fragment Molecular Orbital Method: Practical Applications to Large Molecular Systems*, edited by D. G. Fedorov and K. Kitaura, chapter 2, page 5, CRC Press, Boca Rotan, FL, 2009.

[64] T. Nakano et al., *Chem. Phys. Lett.* **351**, 475 (2002).

[65] D. G. Fedorov, L. V. Slipchenko, and K. Kitaura, *J. Phys. Chem. A* **114**, 8742 (2010).

[66] R. M. Richard, K. U. Lao, and J. M. Herbert, *J. Chem. Phys.* **141**, 014108 (2014).

[67] K. U. Lao, K.-Y. Liu, R. M. Richard, and J. M. Herbert, *J. Chem. Phys.* **144**, 164105:1 (2016).

[68] A. Morrison and J. M. Herbert, *J. Chem. Phys.* **146**, 224110 (2017).

[69] A. Lange and J. M. Herbert, *J. Chem. Theory Comput.* **3**, 1680 (2007).

[70] C. M. Isborn, B. D. Mar, B. F. E. Curchod, I. Tavernelli, and T. J. Martínex, *J. Phys. Chem. B* **117**, 12189 (2013).

[71] K. D. Closser, Q. Ge, Y. Mao, Y. Shao, and M. Head-Gordon, *J. Chem. Theory Comput.* **11**, 5791 (2015).

[72] Q. Ge et al., *J. Chem. Phys.* **146**, 044111 (2017).

| Monomer | $\omega_{\mathrm{IP}}$ / $a_0^{-1}$ |
|---|---|
| adenine | 0.271 |
| 2-aminopyridine | 0.293 |
| benzene | 0.280 |
| ethyne | 0.397 |
| ethene | 0.359 |
| methane | 0.454 |
| formamide | 0.460 |
| formic acid | 0.412 |
| water | 0.502 |
| HCN | 0.452 |
| indole | 0.267 |
| ammonia | 0.440 |
| phenol | 0.292 |
| pyrazine | 0.367 |
| 2-pyridoxine | 0.294 |
| thymine | 0.284 |
| uracil | 0.295 |
| $\mathrm{MeNH_2}$ | 0.397 |
| $\mathrm{MeOH}$ | 0.438 |
| $\mathrm{AcNH_2}$ | 0.453 |
| $\mathrm{AcOH}$ | 0.381 |
| cyclopentane | 0.420 |
| neopentane | 0.287 |
| pentane | 0.365 |
| peptide | 0.341 |
| pyridine | 0.316 |
| $\mathrm{F^-}$ | 0.480 |
| $\mathrm{Cl^-}$ | 0.372 |
| $\mathrm{SO_4^{2-}}$ | 0.344 |
| $\mathrm{Li^+}$ | 2.006 |
| $\mathrm{Na^+}$ | 1.049 |
| $\mathrm{K^+}$ | 0.755 |

Table 12.1: Tuned values of the range separation parameter, $\omega$.

# Appendix A

# Geometry Optimization with Q-Chem

## A.1 Introduction

Geometry optimization refers to the determination of stationary points, principally minima and transition states, on molecular potential energy surfaces. It is an iterative process, requiring the repeated calculation of energies, gradients and (possibly) Hessians at each optimization cycle until convergence is attained. The optimization step involves modifying the current geometry, utilizing current and previous energy, gradient and Hessian information to produce a revised geometry which is closer to the target stationary point than its predecessor was. The art of geometry optimization lies in calculating the step $\mathbf{h}$, the displacement from the starting geometry on that cycle, so as to converge in as few cycles as possible.

There are four main factors that influence the rate of convergence. These are:

- Initial starting geometry.
- Algorithm used to determine the step $\mathbf{h}$.
- Quality of the Hessian (second derivative) matrix.
- Coordinate system chosen.

The first of these factors is obvious: the closer the initial geometry is to the final converged geometry the fewer optimization cycles it will take to reach it. The second factor is again obvious: if a poor step $\mathbf{h}$ is predicted, this will obviously slow down the rate of convergence. The third factor is related to the second: the best algorithms make use of second derivative (curvature) information in calculating $\mathbf{h}$, and the better this information is, the better will be the predicted step. The importance of the fourth factor (the coordinate system) has been generally appreciated later on: a good choice of coordinates can enhance the convergence rate by an order of magnitude (a factor of 10) or more, depending on the molecule being optimized.

Q-Chem includes a powerful suite of algorithms for geometry optimization written by Jon Baker and known collectively as Optimize. These algorithms have been developed and perfected over the past ten years and the code is robust and has been well tested. Optimize is a general geometry optimization package for locating both minima and transition states. It can optimize using Cartesian, *Z*-matrix coordinates or delocalized internal coordinates. The last of these are generated automatically from the Cartesian coordinates and are often found to be particularly effective. It also handles fixed constraints on distances, angles, torsions and out-of-plane bends, between any atoms in the molecule, whether or not the desired constraint is satisfied in the starting geometry. Finally it can freeze atomic positions, or any $x$, $y$, $z$ Cartesian atomic coordinates.

OPTIMIZE is designed to operate with minimal user input. All that is required is the initial guess geometry, either in Cartesian coordinates (*e.g.*, from a suitable model builder such as HyperChem) or as a *Z*-matrix, the type of stationary point being sought (minimum or transition state) and details of any imposed constraints. All decisions as to the optimization strategy (what algorithm to use, what coordinate system to choose, how to handle the constraints) are made by OPTIMIZE.

Note particularly, that although the starting geometry is input in a particular coordinate system (as a *Z*-matrix, for example) these coordinates are not necessarily used during the actual optimization. The best coordinates for the majority of geometry optimizations are delocalized internals, and these will be tried first. Only if delocalized internals fail for some reason, or if conditions prevent them being used (*e.g.*, frozen atoms) will other coordinate systems be tried. If all else fails the default is to switch to Cartesian coordinates. Similar defaults hold for the optimization algorithm, maximum step size, convergence criteria, *etc.* You may of course override the default choices and force a particular optimization strategy, but it is not normally necessary to provide OPTIMIZE with anything other than the minimal information outlined above.

The heart of the OPTIMIZE package (for both minima and transition states) is Baker's eigenvector-following (EF) algorithm[1]. This was developed following the work of Cerjan and Miller[2] and Simons and co-workers[3,4]. The Hessian mode-following option incorporated into this algorithm is capable of locating transition states by walking uphill from the associated minima. By following the lowest Hessian mode, the EF algorithm can locate transition states starting from any reasonable input geometry and Hessian.

An additional option available for minimization is Pulay's GDIIS algorithm[5], which is based on the well known DIIS technique for accelerating SCF convergence[6]. GDIIS must be specifically requested, as the EF algorithm is the default.

Although optimizations can be carried out in Cartesian or *Z*-matrix coordinates, the best choice, as noted above, is usually delocalized internal coordinates. These coordinates were developed by Baker *et al.*[7], and can be considered as a further extension of the natural internal coordinates developed by Pulay *et al.*[8,9] and the redundant optimization method of Pulay and Fogarasi[10].

OPTIMIZE incorporates a very accurate and efficient Lagrange multiplier algorithm for constrained optimization. This was originally developed for use with Cartesian coordinates[11,12] and can handle constraints that are not satisfied in the starting geometry. The Lagrange multiplier approach has been modified for use with delocalized internals[13]; this is much more efficient and is now the default. The Lagrange multiplier code can locate constrained transition states as well as minima.

## A.2 Theoretical Background

Consider the energy, $E(\mathbf{x}_0)$ at some point $\mathbf{x}_0$ on a potential energy surface. We can express the energy at a nearby point $\mathbf{x} = \mathbf{x}_0 + \mathbf{h}$ by means of the Taylor series

$$E(\mathbf{x}_0 + \mathbf{h}) = E(\mathbf{x}_0) + \mathbf{h}^t \frac{dE(\mathbf{x}_0)}{d\mathbf{x}} + \frac{1}{2}\mathbf{h}^t \frac{d^2E(\mathbf{x}_0)}{d\mathbf{x}_1 d\mathbf{x}_2}\mathbf{h} + \cdots \tag{A.1}$$

If we knew the exact form of the energy functional $E(\mathbf{x})$ and all its derivatives, we could move from the current point $\mathbf{x}_0$ directly to a stationary point, (*i.e.*, we would know exactly what the step $\mathbf{h}$ ought to be).

Since we typically know only the lower derivatives of $E(\mathbf{x})$ at best, then we can estimate the step $\mathbf{h}$ by differentiating the Taylor series with respect to $\mathbf{h}$, keeping only the first few terms on the right hand side, and setting the left hand side, $dE(\mathbf{x}_0 + \mathbf{h})/d\mathbf{h}$, to zero, which is the value it would have at a genuine stationary point. Thus

$$\frac{dE(\mathbf{x}_0 + \mathbf{h})}{d\mathbf{h}} = \frac{dE(\mathbf{x}_0)}{d\mathbf{x}} + \frac{d^2E(\mathbf{x}_0)}{d\mathbf{x}_1 d\mathbf{x}_2}\mathbf{h} + \text{higher terms (ignored)} \tag{A.2}$$

from which

$$\mathbf{h} = -\mathbf{H}^{-1}\mathbf{g} \tag{A.3}$$

where

$$\frac{dE}{d\mathbf{x}} \equiv \mathbf{g} \text{ (gradient vector)}, \qquad \frac{d^2E}{d\mathbf{x_1}d\mathbf{x_2}} \equiv \mathbf{H} \text{ (Hessian matrix)} \tag{A.4}$$

Equation (A.3) is known as the Newton-Raphson step. It is the major component of almost all geometry optimization algorithms in quantum chemistry.

The above derivation assumed exact first (gradient) and second (Hessian) derivative information. Analytical gradients are available for all methodologies supported in Q-CHEM; however analytical second derivatives are not. Furthermore, even if they were, it would not necessarily be advantageous to use them as their evaluation is usually computationally demanding, and, efficient optimizations can in fact be performed without an exact Hessian. An excellent compromise in practice is to begin with an approximate Hessian matrix, and update this using gradient and displacement information generated as the optimization progresses. In this way the starting Hessian can be "improved" at essentially no cost. Using Eq. (A.3) with an approximate Hessian is called the quasi Newton-Raphson step.

The nature of the Hessian matrix (in particular its eigenvalue structure) plays a crucial role in a successful optimization. All stationary points on a potential energy surface have a zero gradient vector; however the character of the stationary point (*i.e.*, what type of structure it corresponds to) is determined by the Hessian. Diagonalization of the Hessian matrix can be considered to define a set of mutually orthogonal directions on the energy surface (the eigenvectors) together with the curvature along those directions (the eigenvalues). At a local minimum (corresponding to a well in the potential energy surface) the curvature along all of these directions must be positive, reflecting the fact that a small displacement along any of these directions causes the energy to rise. At a transition state, the curvature is negative (*i.e.*, the energy is a maximum) along one direction, but positive along all the others. Thus, for a stationary point to be a transition state the Hessian matrix at that point must have one and only one negative eigenvalue, while for a minimum the Hessian must have all positive eigenvalues. In the latter case the Hessian is called *positive definite*. If searching for a minimum it is important that the Hessian matrix be positive definite; in fact, unless the Hessian is positive definite there is no guarantee that the step predicted by Eq. (A.3) is even a descent step (*i.e.*, a direction that will actually lower the energy). Similarly, for a transition state search, the Hessian must have one negative eigenvalue. Maintaining the Hessian eigenvalue structure is not difficult for minimization, but it can be a difficulty when trying to find a transition state.

In a diagonal Hessian representation the Newton-Raphson step can be written

$$\mathbf{h} = \sum \frac{-F_i}{b_i}\mathbf{u}_i \tag{A.5}$$

where $\mathbf{u}_i$ and $b_i$ are the eigenvectors and eigenvalues of the Hessian matrix $\mathbf{H}$ and $F_i = \mathbf{u}_i^t\mathbf{g}$ is the component of $\mathbf{g}$ along the local direction (eigenmode)$\mathbf{u}_i$. As discussed by Simons *et al.* [3], the Newton-Raphson step can be considered as minimizing along directions $\mathbf{u}_i$ which have positive eigenvalues and maximizing along directions with negative eigenvalues. Thus, if the user is searching for a minimum and the Hessian matrix is positive definite, then the Newton-Raphson step is appropriate since it is attempting to minimize along all directions simultaneously. However, if the Hessian has one or more negative eigenvalues, then the basic Newton-Raphson step is not appropriate for a minimum search, since it will be maximizing and not minimizing along one or more directions. Exactly the same arguments apply during a transition state search except that the Hessian must have one negative eigenvalue, because the user has to maximize along one direction. However, there must be *only* one negative eigenvalue. A positive definite Hessian is a disaster for a transition state search because the Newton-Raphson step will then lead towards a minimum.

If firmly in a region of the potential energy surface with the right Hessian character, then a careful search (based on the Newton-Raphson step) will almost always lead to a stationary point of the correct type. However, this is only true if the Hessian is exact. If an approximate Hessian is being improved by updating, then there is no guarantee that the Hessian eigenvalue structure will be retained from one cycle to the next unless one is very careful during the update. Updating procedures that "guarantee" conservation of a positive definite Hessian do exist (or at least warn the user if the update is likely to introduce negative eigenvalues). This can be very useful during a minimum search; but there are no such guarantees for preserving the Hessian character (one and only one negative eigenvalue) required for a transition state.

In addition to the difficulties in retaining the correct Hessian character, there is the matter of obtaining a "correct" Hessian in the first instance. This is particularly acute for a transition state search. For a minimum search it is possible to "guess" a reasonable, positive-definite starting Hessian (for example, by carrying out a molecular mechanics minimization initially and using the mechanics Hessian to begin the *ab initio* optimization) but this option is usually not available for transition states. Even if the user calculates the Hessian exactly at the starting geometry, the guess for the structure may not be sufficiently accurate, and the expensive, exact Hessian may not have the desired eigenvalue structure.

Consequently, particularly for a transition state search, an alternative to the basic Newton-Raphson step is clearly needed, especially when the Hessian matrix is inappropriate for the stationary point being sought.

One of the first algorithms that was capable of taking corrective action during a transition state search if the Hessian had the wrong eigenvalue structure, was developed by Poppinger[14], who suggested that, instead of taking the Newton-Raphson step, if the Hessian had all positive eigenvalues, the lowest Hessian mode be followed uphill; whereas, if there were two or more negative eigenvalues, the mode corresponding to the least negative eigenvalue be followed downhill. While this step should lead the user back into the right region of the energy surface, it has the disadvantage that the user is maximizing or minimizing along one mode only, unlike the Newton-Raphson step which maximizes/minimizes along all modes simultaneously. Another drawback is that successive such steps tend to become linearly dependent, which degrades most of the commonly used Hessian updates.

## A.3 Eigenvector-Following (EF) Algorithm

The work of Cerjan and Miller[2], and later Simons and co-workers[3,4], showed that there was a better step than simply directly following one of the Hessian eigenvectors. A simple modification to the Newton-Raphson step is capable of guiding the search away from the current region towards a stationary point with the required characteristics. This is

$$\mathbf{h} = \sum_i \frac{-F_i}{(b_i - \lambda)} \mathbf{u}_i \tag{A.6}$$

in which $\lambda$ can be regarded as a shift parameter on the Hessian eigenvalue $b_i$. Scaling the Newton-Raphson step in this manner effectively directs the step to lie primarily, but not exclusively (unlike Poppinger's algorithm[14]), along one of the local eigenmodes, depending on the value chosen for $\lambda$. References 2–4 all utilize the same basic approach of Eq. (A.6) but differ in the means of determining the value of $\lambda$.

The EF algorithm[1] utilizes the rational function approach presented in Refs. 4, yielding an eigenvalue equation of the form

$$\begin{pmatrix} \mathbf{H} & \mathbf{g} \\ \mathbf{g}^t & 0 \end{pmatrix} \begin{pmatrix} \mathbf{h} \\ 1 \end{pmatrix} = \lambda \begin{pmatrix} \mathbf{h} \\ 1 \end{pmatrix} \tag{A.7}$$

from which a suitable $\lambda$ can be obtained. Expanding Eq. (A.7) yields

$$(\mathbf{H} - \lambda)\mathbf{h} + \mathbf{g} = 0 \tag{A.8}$$

and

$$\mathbf{g}^t\mathbf{h} = \lambda \tag{A.9}$$

In terms of a diagonal Hessian representation, Eq. (A.8) rearranges to Eq. (A.6), and substitution of Eq. (A.6) into the diagonal form of Eq. (A.9) gives

$$\sum_i \frac{-F_i^2}{(b_i - \lambda)} = \lambda \tag{A.10}$$

which can be used to evaluate $\lambda$ iteratively.

The eigenvalues, $\lambda$, of the RFO equation Eq. (A.7) have the following important properties[4]:

- The $(n + 1)$ values of $\lambda$ bracket the $n$ eigenvalues of the Hessian matrix $\lambda_i < b_i < \lambda_{i+1}$.
- At a stationary point, one of the eigenvalues, $\lambda$, of Eq. (A.7) is zero and the other $n$ eigenvalues are those of the Hessian at the stationary point.
- For a saddle point of order $m$, the zero eigenvalue separates the $m$ negative and the $(n - m)$ positive Hessian eigenvalues.

This last property, the separability of the positive and negative Hessian eigenvalues, enables two shift parameters to be used, one for modes along which the energy is to be maximized and the other for which it is minimized. For a transition state (a first-order saddle point), in terms of the Hessian eigenmodes, we have the two matrix equations

$$\begin{pmatrix} b_1 & F_1 \\ F_1 & 0 \end{pmatrix} \begin{pmatrix} h_1 \\ 1 \end{pmatrix} = \lambda_p \begin{pmatrix} h_1 \\ 1 \end{pmatrix} \tag{A.11}$$

$$\begin{pmatrix} b_2 & & & F_2 \\ & \ddots & \mathbf{0} & \vdots \\ & \mathbf{0} & b_n & F_n \\ F_2 & \cdots & F_n & 0 \end{pmatrix} \begin{pmatrix} h_2 \\ \vdots \\ h_n \\ 1 \end{pmatrix} = \lambda_n \begin{pmatrix} h_2 \\ \vdots \\ h_n \\ 1 \end{pmatrix} \tag{A.12}$$

where it is assumed that we are maximizing along the lowest Hessian mode $\mathbf{u}_1$. Note that $\lambda_p$ is the highest eigenvalue of Eq. (A.11), which is always positive and approaches zero at convergence, and $\lambda_n$ is the lowest eigenvalue of Eq. (A.12), which it is always negative and again approaches zero at convergence.

Choosing these values of $\lambda$ gives a step that attempts to maximize along the lowest Hessian mode, while at the same time minimizing along all the other modes. It does this regardless of the Hessian eigenvalue structure (unlike the Newton-Raphson step). The two shift parameters are then used in Eq. (A.6) to give the final step

$$\mathbf{h} = \frac{-F_1}{(b_1 - \lambda_p)}\mathbf{u}_1 - \sum_{i=2}^{n} \frac{-F_i}{(b_i - \lambda_n)}\mathbf{u}_i \tag{A.13}$$

If this step is greater than the maximum allowed, it is scaled down. For minimization only one shift parameter, $\lambda_n$, would be used which would act on all modes.

In Eq. (A.11) and Eq. (A.12) it was assumed that the step would maximize along the lowest Hessian mode, $b_1$, and minimize along all the higher modes. However, it is possible to maximize along modes other than the lowest, and in this way perhaps locate transition states for alternative rearrangements/dissociations from the same initial starting point. For maximization along the $k$th mode (instead of the lowest mode), Eq. (A.11) is replaced by

$$\begin{pmatrix} b_k & F_k \\ F_k & 0 \end{pmatrix} \begin{pmatrix} h_k \\ 1 \end{pmatrix} = \lambda_p \begin{pmatrix} h_k \\ 1 \end{pmatrix} \tag{A.14}$$

and Eq. (A.12) would now exclude the $k$th mode but include the lowest. Since what was originally the $k$th mode is the mode along which the negative eigenvalue is required, then this mode will eventually become the lowest mode at some stage of the optimization. To ensure that the original mode is being followed smoothly from one cycle to the next, the mode that is actually followed is the one with the greatest overlap with the mode followed on the previous cycle. This procedure is known as *mode following*. For more details and some examples, see Ref. 1.

## A.4 Delocalized Internal Coordinates

The choice of coordinate system can have a major influence on the rate of convergence during a geometry optimization. For complex potential energy surfaces with many stationary points, a different choice of coordinates can result in convergence to a different final structure.

The key attribute of a good set of coordinates for geometry optimization is the degree of coupling between the individual coordinates. In general, the less coupling the better, as variation of one particular coordinate will then have minimal impact on the other coordinates. Coupling manifests itself primarily as relatively large partial derivative terms between different coordinates. For example, a strong harmonic coupling between two different coordinates, $i$ and $j$, results in a large off-diagonal element, $H_{ij}$, in the Hessian (second derivative) matrix. Normally this is the only type of coupling that can be directly "observed" during an optimization, as third and higher derivatives are ignored in almost all optimization algorithms.

In the early days of computational quantum chemistry geometry optimizations were carried out in Cartesian coordinates. Cartesians are an obvious choice as they can be defined for all systems and gradients and second derivatives are calculated directly in Cartesian coordinates. Unfortunately, Cartesians normally make a poor coordinate set for optimization as they are heavily coupled. Cartesians have been returning to favor later on because of their very general nature, and because it has been clearly demonstrated that if reliable second derivative information is available (*i.e.*, a good starting Hessian) and the initial geometry is reasonable, then Cartesians can be as efficient as any other coordinate set for small to medium-sized molecules[12,15]. Without good Hessian data, however, Cartesians are inefficient, especially for long chain acyclic systems.

In the 1970s Cartesians were replaced by Z-matrix coordinates. Initially the Z-matrix was utilized simply as a means of geometry input; it is far easier to describe a molecule in terms of bond lengths, bond angles and dihedral angles (the natural way a chemist thinks of molecular structure) than to develop a suitable set of Cartesian coordinates. It was subsequently found that optimization was generally more efficient in Z-matrix coordinates than in Cartesians, especially for acyclic systems. This is not always the case, and care must be taken in constructing a suitable Z-matrix. A good general rule is ensure that each variable is defined in such a way that changing its value will not change the values of any of the other variables. A brief discussion concerning good Z-matrix construction strategy is given by Schlegel[16].

In 1979 Pulay *et al.* published a key paper, introducing what were termed natural internal coordinates into geometry optimization[8]. These coordinates involve the use of individual bond displacements as stretching coordinates, but linear combinations of bond angles and torsions as deformational coordinates. Suitable linear combinations of bends and torsions (the two are considered separately) are selected using group theoretical arguments based on local pseudo symmetry. For example, bond angles around an $sp^3$ hybridized carbon atom are all approximately tetrahedral, regardless of the groups attached, and idealized tetrahedral symmetry can be used to generate deformational coordinates around the central carbon atom.

The major advantage of natural internal coordinates in geometry optimization is their ability to significantly reduce the coupling, both harmonic and anharmonic, between the various coordinates. Compared to natural internals, *Z*-matrix coordinates arbitrarily omit some angles and torsions (to prevent redundancy), and this can induce strong anharmonic coupling between the coordinates, especially with a poorly constructed *Z*-matrix. Another advantage of the reduced coupling is that successful minimizations can be carried out in natural internals with only an approximate (*e.g.*, diagonal) Hessian provided at the starting geometry. A good starting Hessian is still needed for a transition state search.

Despite their clear advantages, natural internals have only become used widely at a later stage. This is because, when used in the early programs, it was necessary for the user to define them. This situation changed in 1992 with the development of computational algorithms capable of automatically generating natural internals from input Cartesians[9]. For minimization, natural internals have become the coordinates of first choice[9,12].

There are some disadvantages to natural internal coordinates as they are commonly constructed and used:

- Algorithms for the automatic construction of natural internals are complicated. There are a large number of structural possibilities, and to adequately handle even the most common of them can take several thousand lines of code.
- For the more complex molecular topologies, most assigning algorithms generate more natural internal coordinates than are required to characterize all possible motions of the system (*i.e.*, the generated coordinate set contains redundancies).
- In cases with a very complex molecular topology (*e.g.*, multiply fused rings and cage compounds) the assigning algorithm may be unable to generate a suitable set of coordinates.

The redundancy problem has been addressed in an excellent paper by Pulay and Fogarasi[10], who have developed a scheme for carrying out geometry optimization directly in the redundant coordinate space.

Baker *et al.* have developed a set of delocalized internal coordinates[7] which eliminate all of the above-mentioned difficulties. Building on some of the ideas in the redundant optimization scheme of Pulay and Fogarasi[10], delocalized internals form a complete, non-redundant set of coordinates which are as good as, if not superior to, natural internals, and which can be generated in a simple and straightforward manner for essentially any molecular topology, no matter how complex.

Consider a set of $n$ internal coordinates $\mathbf{q} = (q_1, q_2, \ldots q_n)^t$ Displacements $\Delta\mathbf{q}$ in $\mathbf{q}$ are related to the corresponding Cartesian displacements $\Delta\mathbf{X}$ by means of the usual $\mathbf{B}$-matrix[17],

$$\Delta\mathbf{q} = \mathbf{B}\Delta\mathbf{X} \tag{A.15}$$

If any of the internal coordinates $\mathbf{q}$ are redundant, then the rows of the $\mathbf{B}$-matrix will be linearly dependent.

Delocalized internal coordinates are obtained simply by constructing and diagonalizing the matrix $\mathbf{G} = \mathbf{BB}^t$. Diagonalization of $\mathbf{G}$ results in two sets of eigenvectors; a set of $m$ (typically $3N - 6$, where $N$ is the number of atoms) eigenvectors with eigenvalues $\lambda > 0$, and a set of $nm$ eigenvectors with eigenvalues $\lambda = 0$ (to numerical precision). In this way, any redundancies present in the original coordinate set $\mathbf{q}$ are isolated (they correspond to those eigenvectors with zero eigenvalues). The eigenvalue equation of $\mathbf{G}$ can thus be written

$$\mathbf{G}(\mathbf{UR}) = (\mathbf{UR}) \begin{pmatrix} \Lambda & 0 \\ 0 & 0 \end{pmatrix} \tag{A.16}$$

where $\mathbf{U}$ is the set of non-redundant eigenvectors of $\mathbf{G}$ (those with $\lambda > 0$) and $\mathbf{R}$ is the corresponding redundant set.

The nature of the original set of coordinates $\mathbf{q}$ is unimportant, as long as it spans all the degrees of freedom of the system under consideration. We include in $\mathbf{q}$, all bond stretches, all planar bends and all proper torsions that can be generated based on the atomic connectivity. These individual internal coordinates are termed *primitives*. This blanket approach generates far more primitives than are necessary, and the set $\mathbf{q}$ contains much redundancy. This is of little concern, as solution of Eq. (A.16) takes care of all redundancies.

Note that eigenvectors in both $\mathbf{U}$ and $\mathbf{R}$ will each be linear combinations of potentially all the original primitives. Despite this apparent complexity, we take the set of non-redundant vectors $\mathbf{U}$ as our working coordinate set. Internal coordinates so defined are much more delocalized than natural internal coordinates (which are combinations of a relatively small number of bends or torsions) hence, the term delocalized internal coordinates.

It may appear that because delocalized internals are such a complicated mixing of the original primitive internals, they are a poor choice for use in an actual optimization. On the contrary, arguments can be made that delocalized internals are, in fact, the "best" possible choice, certainly at the starting geometry. The interested reader is referred to the original literature for more details[7].

The situation for geometry optimization, comparing Cartesian, *Z*-matrix and delocalized internal coordinates, and assuming a "reasonable" starting geometry, is as follows:

- For small or very rigid medium-sized systems (up to about 15 atoms), optimizations in Cartesian and internal coordinates ("good" *Z*-matrix or delocalized internals) should perform similarly.
- For medium-sized systems (say 15–30 atoms) optimizations in Cartesians should perform as well as optimizations in internal coordinates, provided a reliable starting Hessian is available.
- For large systems (30+ atoms), unless these are very rigid, neither Cartesian nor *Z*-matrix coordinates can compete with delocalized internals, even with good quality Hessian information. As the system increases, and with less reliable starting geometries, the advantage of delocalized internals can only increase.

There is one particular situation in which Cartesian coordinates may be the best choice. Natural internal coordinates (and by extension delocalized internals) show a tendency to converge to low energy structures[12]. This is because steps taken in internal coordinate space tend to be much larger when translated into Cartesian space, and, as a result, higher energy local minima tend to be "jumped over", especially if there is no reliable Hessian information available (which is generally not needed for a successful optimization). Consequently, if the user is looking for a local minimum (*i.e.*, a meta-stable structure) and has both a good starting geometry and a decent Hessian, the user should carry out the optimization in Cartesian coordinates.

## A.5 Constrained Optimization

Constrained optimization refers to the optimization of molecular structures in which certain parameters (*e.g.*, bond lengths, bond angles or dihedral angles) are fixed. In quantum chemistry calculations, this has traditionally been accomplished using *Z*-matrix coordinates, with the desired parameter set in the *Z*-matrix and simply omitted from the optimization space. In 1992, Baker presented an algorithm for constrained optimization directly in Cartesian coordinates [11]. Baker's algorithm used both penalty functions and the classical method of Lagrange multipliers [18], and was developed in order to impose constraints on a molecule obtained from a graphical model builder as a set of Cartesian coordinates. Some improvements widening the range of constraints that could be handled were made in 1993 [12]. Q-CHEM includes the latest version of this algorithm, which has been modified to handle constraints directly in delocalized internal coordinates [13].

The essential problem in constrained optimization is to minimize a function of, for example, $n$ variables $F(\mathbf{x})$ subject to a series of m constraints of the form $C_i(\mathbf{x}) = 0$, $i = l.\ m$. Assuming $m < n$, then perhaps the best way to proceed (if this were possible in practice) would be to use the $m$ constraint equations to eliminate $m$ of the variables, and then solve the resulting unconstrained problem in terms of the $((n - m)$ independent variables. This is exactly what occurs in a *Z*-matrix optimization. Such an approach cannot be used in Cartesian coordinates as standard distance and angle constraints are non-linear functions of the appropriate coordinates. For example a distance constraint (between atoms $i$ and $j$ in a molecule) is given in Cartesians by $(R_{ij} - R_0) = 0$, with

$$R_{ij} = \sqrt{(x_i - x_j)^2 + (y_i - y_j)^2 + (z_i - z_j)^2} \tag{A.17}$$

and $R_0$ the constrained distance. This obviously cannot be satisfied by elimination. What can be eliminated in Cartesians are the individual $x$, $y$ and $z$ coordinates themselves and in this way individual atoms can be totally or partially frozen.

Internal constraints can be handled in Cartesian coordinates by introducing the Lagrangian function

$$L(\mathbf{x}, \lambda) = F(\mathbf{x}) - \sum_{i=1}^{m} \lambda_i C_i(\mathbf{x}) \tag{A.18}$$

which replaces the function $F(\mathbf{x})$ in the unconstrained case. Here, the $\lambda_i$ are the so-called Lagrange multipliers, one for each constraint $C_i(\mathbf{x})$. Differentiating Eq. (A.18) with respect to $\mathbf{x}$ and $\lambda$ affords

$$\frac{dL(\mathbf{x}, \lambda)}{dx_j} = \frac{dF(\mathbf{x})}{dx_j} - \sum_{i=1}^{m} \lambda_i \frac{dC_i(\mathbf{x})}{dx_j} \tag{A.19}$$

$$\frac{dL(\mathbf{x}, \lambda)}{d\lambda_i} = -C_i(\mathbf{x}) \tag{A.20}$$

At a stationary point of the Lagrangian we have $\nabla\mathbf{L} = 0$, *i.e.*, all $dL/dx_j = 0$ and all $dL/d\lambda_i = 0$. This latter condition means that all $C_i(\mathbf{x}) = 0$ and thus all constraints are satisfied. Hence, finding a set of values ($\mathbf{x}$, $\lambda$) for which $\nabla\mathbf{L} = 0$ will give a possible solution to the constrained optimization problem in exactly the same way as finding an $\mathbf{x}$ for which $\mathbf{g} = \nabla\mathbf{F} = 0$ gives a solution to the corresponding unconstrained problem.

The Lagrangian second derivative matrix, which is the analogue of the Hessian matrix in an unconstrained optimization, is given by

$$\nabla^2\mathbf{L} = \begin{pmatrix} \frac{d^2L(\mathbf{x},\lambda)}{dx_j dx_k} & \frac{d^2L(\mathbf{x},\lambda)}{dx_j d\lambda_i} \\ \frac{d^2L(\mathbf{x},\lambda)}{dx_j d\lambda_i} & \frac{d^2L(\mathbf{x},\lambda)}{d\lambda_j d\lambda_i} \end{pmatrix} \tag{A.21}$$

where

$$\frac{d^2L(\mathbf{x},\lambda)}{dx_j dx_k} = \frac{d^2F(\mathbf{x})}{dx_j dx_k} - \sum_{i=1}^{m} \lambda_i \frac{d^2C_i(\mathbf{x})}{dx_j dx_k} \tag{A.22}$$

$$\frac{d^2L(\mathbf{x},\lambda)}{dx_j d\lambda_i} = \frac{-dC_i(\mathbf{x})}{dx_j} \tag{A.23}$$

$$\frac{d^2L(\mathbf{x},\lambda)}{d\lambda_j d\lambda_i} = 0 \tag{A.24}$$

Thus, in addition to the standard gradient vector and Hessian matrix for the unconstrained function $F(\mathbf{x})$, we need both the first and second derivatives (with respect to coordinate displacement) of the constraint functions. Once these quantities are available, the corresponding Lagrangian gradient, given by Eq. (A.19), and Lagrangian second derivative matrix, given by Eq. (A.21), can be formed, and the optimization step calculated in a similar manner to that for a standard unconstrained optimization[11].

In the Lagrange multiplier method, the unknown multipliers, $\lambda_i$, are an integral part of the parameter set. This means that the optimization space consists of all $n$ variables $\mathbf{x}$ plus all $m$ Lagrange multipliers $\lambda$, one for each constraint. The total dimension of the constrained optimization problem, $nm$, has thus increased by $m$ compared to the corresponding unconstrained case. The Lagrangian Hessian matrix, $\nabla^2\mathbf{L}$, has $m$ extra modes compared to the standard (unconstrained) Hessian matrix, $\nabla^2\mathbf{F}$. What normally happens is that these additional modes are dominated by the constraints (*i.e.*, their largest components correspond to the constraint Lagrange multipliers) and they have negative curvature (a negative Hessian eigenvalue). This is perhaps not surprising when one realizes that any motion in the parameter space that breaks the constraints is likely to lower the energy.

Compared to a standard unconstrained minimization, where a stationary point is sought at which the Hessian matrix has all positive eigenvalues, in the constrained problem we are looking for a stationary point of the Lagrangian function at which the Lagrangian Hessian matrix has as many negative eigenvalues as there are constraints (*i.e.*, we are looking for an $m$th-order saddle point). For further details and practical applications of constrained optimization using Lagrange multipliers in Cartesian coordinates, see[11].

Eigenvector following can be implemented in a constrained optimization in a similar way to the unconstrained case. Considering a constrained minimization with $m$ constraints, then Eq. (A.11) is replaced by

$$\begin{pmatrix} b_1 & & & F_1 \\ & \ddots & \mathbf{0} & \vdots \\ & \mathbf{0} & b_m & F_m \\ F_1 & \cdots & F_m & 0 \end{pmatrix} \begin{pmatrix} h_1 \\ \vdots \\ h_m \\ 1 \end{pmatrix} = \lambda_p \begin{pmatrix} h_1 \\ \vdots \\ h_m \\ 1 \end{pmatrix} \tag{A.25}$$

and Eq. (A.12) by

$$\begin{pmatrix} b_{m+1} & & & F_{m+1} \\ & \ddots & \mathbf{0} & \vdots \\ & \mathbf{0} & b_{m+n} & F_{m+n} \\ F_{m+1} & \cdots & F_{m+n} & 0 \end{pmatrix} \begin{pmatrix} h_{m+1} \\ \vdots \\ h_{m+n} \\ 1 \end{pmatrix} = \lambda_n \begin{pmatrix} h_{m+1} \\ \vdots \\ h_{m+n} \\ 1 \end{pmatrix} \tag{A.26}$$

where now the $b_i$ are the eigenvalues of $\nabla^2\mathbf{L}$, with corresponding eigenvectors $\mathbf{u}_i$, and $F_i = \mathbf{u}_i^t\nabla\mathbf{L}$. Here Eq. (A.25) includes the $m$ constraint modes along which a negative Lagrangian Hessian eigenvalue is required, and Eq. (A.26) includes all the other modes.

Equations (A.25) and (A.26) implement eigenvector following for a constrained minimization. Constrained transition state searches can be carried out by selecting one extra mode to be maximized in addition to the $m$ constraint modes, *i.e.*, by searching for a saddle point of the Lagrangian function of order $m + l$.

It should be realized that, in the Lagrange multiplier method, the desired constraints are only satisfied at convergence, and not necessarily at intermediate geometries. The Lagrange multipliers are part of the optimization space; they vary just as any other geometrical parameter and, consequently the degree to which the constraints are satisfied changes from cycle to cycle, approaching 100% satisfied near convergence. One advantage this brings is that, unlike in a standard *Z*-matrix approach, constraints do not have to be satisfied in the starting geometry.

Imposed constraints can normally be satisfied to very high accuracy, $10^{-6}$ or better. However, problems can arise for both bond and dihedral angle constraints near 0° and 180° and, instead of attempting to impose a single constraint, it is better to split angle constraints near these limiting values into two by using a dummy atom Baker:1993b, exactly analogous to splitting a 180° bond angle into two 90° angles in a *Z*-matrix.

**Note:** Exact 0° and 180° single angle constraints cannot be imposed, as the corresponding constraint normals, $\nabla\mathbf{C}_i$, are zero, and would result in rows and columns of zeros in the Lagrangian Hessian matrix.

## A.6 Delocalized Internal Coordinates

We do not give further details of the optimization algorithms available in Q-CHEM for imposing constraints in Cartesian coordinates, as it is far simpler and easier to do this directly in delocalized internal coordinates.

At first sight it does not seem particularly straightforward to impose any constraints at all in delocalized internals, given that each coordinate is potentially a linear combination of all possible primitives. However, this is deceptive, and in fact all standard constraints can be imposed by a relatively simple Schmidt orthogonalization procedure. In this instance consider a unit vector with unit component corresponding to the primitive internal (stretch, bend or torsion) that one wishes to keep constant. This vector is then projected on to the full set, $\mathbf{U}$, of active delocalized coordinates, normalized, and then all $n$, for example, delocalized internals are Schmidt orthogonalized in turn to this normalized, projected constraint vector. The last coordinate taken in the active space should drop out (since it will be linearly dependent on the other vectors and the constraint vector) leaving $(n - 1)$ active vectors and one constraint vector.

In more detail, the procedure is as follows (taken directly from Ref. 7). The initial (usually unit) constraint vector $\mathbf{C}$ is projected on to the set $\mathbf{U}$ of delocalized internal coordinates according to

$$\mathbf{C}^{\text{proj}} = \sum \left\langle \mathbf{C} | \mathbf{C}\mathbf{U}_k \mathbf{U}_k \right\rangle \mathbf{U}_k \tag{A.27}$$

where the summation is over all $n$ active coordinates $\mathbf{U}_k$. The projected vector $\mathbf{C}^{\text{proj}}$ is then normalized and an $(n + l)$ dimensional vector space $\mathbf{V}$ is formed, comprising the normalized, projected constraint vector together with all active delocalized coordinates

$$\mathbf{V} = \left\{ \mathbf{C}^{\text{proj}}, \mathbf{U}_k \; k = 1.n \right\} \tag{A.28}$$

This set of vectors is Schmidt orthogonalized according to the standard procedure,

$$\tilde{\mathbf{V}}_k = \alpha_k \left( \mathbf{V}_k - \sum_{l=1}^{k-1} \left\langle \mathbf{V}_k \middle| \mathbf{V}_k \tilde{\mathbf{V}}_l \tilde{\mathbf{V}}_l \right\rangle \tilde{\mathbf{V}}_l \right) \tag{A.29}$$

where the first vector taken, $\mathbf{V}_1$, is $\mathbf{C}^{\rm proj}$. The $\alpha_k$ in Eq. (A.29) is a normalization factor. As noted above, the last vector taken, $\mathbf{V}_{n+1} = \mathbf{U}_k$, will drop out, leaving a fully orthonormal set of $(n-1)$ active vectors and one constraint vector.

After the Schmidt orthogonalization the constraint vector will contain all the weight in the active space of the primitive to be fixed, which will have a zero component in all of the other $(n-1)$ vectors. The fixed primitive has thus been isolated entirely in the constraint vector which can now be removed from the active subspace for the geometry optimization step.

Extension of the above procedure to multiple constraints is straightforward. In addition to constraints on individual primitives, it is also possible to impose combinatorial constraints. For example, if, instead of a unit vector, one started the constraint procedure with a vector in which two components were set to unity, then this would impose a constraint in which the sum of the two relevant primitives were always constant. In theory any desired linear combination of any primitives could be constrained.

Note further that imposed constraints are not confined to those primitive internals generated from the initial atomic connectivity. If we wish to constrain a distance, angle or torsion between atoms that are not formally connected, then all we need to do is add that particular coordinate to our primitive set. It can then be isolated and constrained in exactly the same way as a formal connectivity constraint.

Everything discussed thus far regarding the imposition of constraints in delocalized internal coordinates has involved isolating each constraint in one vector which is then eliminated from the optimization space. This is very similar in effect to a *Z*-matrix optimization, in which constraints are imposed by elimination. This, of course, can only be done if the desired constraint is satisfied in the starting geometry. We have already seen that the Lagrange multiplier algorithm, used to impose distance, angle and torsion constraints in Cartesian coordinates, can be used even when the constraint is not satisfied initially. The Lagrange multiplier method can also be used with delocalized internals, and its implementation with internal coordinates brings several simplifications and advantages.

In Cartesians, as already noted, standard internal constraints (bond distances, angles and torsions) are somewhat complicated non-linear functions of the $x$, $y$ and $z$ coordinates of the atoms involved. A torsion, for example, which involves four atoms, is a function of twelve different coordinates. In internals, on the other hand, each constraint is a coordinate in its own right and is therefore a simple linear function of just one coordinate (itself).

If we denote a general internal coordinate by $R$, then the constraint function $C_i(\mathbf{R})$ is a function of one coordinate, $R_i$, and it and its derivatives can be written

$$C_i(R_i) = R_i - R_0 \tag{A.30}$$

$$dC_i(R_i)/dR_i = 1; \quad dC_i(R_i)/dR_j = 0 \tag{A.31}$$

$$d^2C_i(R_i)/dR_i dR_j = 0 \tag{A.32}$$

where $R_0$ is the desired value of the constrained coordinate, and $R_i$ is its current value. From Eq. (A.31) we see that the constraint normals, $dC_i(\mathbf{R})/dR_i$, are simply unit vectors and the Lagrangian Hessian matrix, Eq. (A.21), can be obtained from the normal Hessian matrix by adding $m$ columns (and $m$ rows) of, again, unit vectors.

A further advantage, in addition to the considerable simplification, is the handling of $0^\circ$ and $180^\circ$ dihedral angle constraints. In Cartesian coordinates it is not possible to formally constrain bond angles and torsions to exactly $0^\circ$ or $180^\circ$ because the corresponding constraint normal is a zero vector. Similar difficulties do not arise in internal coordinates, at least for torsions, because the constraint normals are unit vectors regardless of the value of the constraint; thus $0^\circ$ and $180^\circ$ dihedral angle constraints can be imposed just as easily as any other value. $180^\circ$ bond angles still cause difficulties, but near-linear arrangements of atoms require special treatment even in unconstrained optimizations; a typical solution involves replacing a near $180^\circ$ bond angle by two special linear co-planar and perpendicular bends[19], and modifying the torsions where necessary. A linear arrangement can be enforced by constraining the co-planar and perpendicular bends.

One other advantage over Cartesians is that in internals the constraint coordinate can be eliminated once the constraint is satisfied to the desired accuracy (the default tolerance is $10^{-6}$ in atomic units: Bohrs and radians). This is not possible in Cartesians due to the functional form of the constraint. In Cartesians, therefore, the Lagrange multiplier algorithm must be used throughout the entire optimization, whereas in delocalized internal coordinates it need only be used until all desired constraints are satisfied; as constraints become satisfied they can simply be eliminated from the optimization space and once all constraint coordinates have been eliminated standard algorithms can be used in the space of the remaining unconstrained coordinates. Normally, unless the starting geometry is particularly poor in this regard, constraints are satisfied fairly early on in the optimization (and at more or less the same time for multiple constraints), and Lagrange multipliers only need to be used in the first half-dozen or so cycles of a constrained optimization in internal coordinates.

## A.7 GDIIS

Direct inversion in the iterative subspace (DIIS) was originally developed by Pulay for accelerating SCF convergence[6]. Subsequently, Csaszar and Pulay used a similar scheme for geometry optimization, which they termed GDIIS[5]. The method is somewhat different from the usual quasi-Newton type approach and is included in OPTIMIZE as an alternative to the EF algorithm. Tests indicate that its performance is similar to EF, at least for small systems; however there is rarely an advantage in using GDIIS in preference to EF.

In GDIIS, geometries $\mathbf{x}_i$ generated in previous optimization cycles are linearly combined to find the "best" geometry on the current cycle

$$\mathbf{x}_n = \sum_{i=1}^{m} c_i \mathbf{x}_i \tag{A.33}$$

where the problem is to find the best values for the coefficients $c_i$.

If we express each geometry, $\mathbf{x}_i$, by its deviation from the sought-after final geometry, $\mathbf{x}_f$, *i.e.*, $\mathbf{x}_f = \mathbf{x}_i + \mathbf{e}_i$, where $\mathbf{e}_i$ is an error vector, then it is obvious that if the conditions

$$\mathbf{r} = \sum c_i \mathbf{e}_i \tag{A.34}$$

and

$$\sum c_i = 1 \tag{A.35}$$

are satisfied, then the relation

$$\sum c_i \mathbf{x}_i = \mathbf{x}_f \tag{A.36}$$

also holds.

The true error vectors $\mathbf{e}_i$ are, of course, unknown. However, in the case of a nearly quadratic energy function they can be approximated by

$$\mathbf{e}_i = -\mathbf{H}^{-1}\mathbf{g}_i \tag{A.37}$$

where $\mathbf{g}_i$ is the gradient vector corresponding to the geometry $\mathbf{x}_i$ and $\mathbf{H}$ is an approximation to the Hessian matrix. Minimization of the norm of the residuum vector $\mathbf{r}$, Eq. (A.34), together with the constraint equation, Eq. (A.35), leads to a system of $(m+l)$ linear equations

$$\begin{pmatrix} B_{11} & \cdots & B_{1m} & 1 \\ \vdots & \ddots & \vdots & \vdots \\ B_{m1} & \cdots & B_{mm} & 1 \\ 1 & \cdots & 1 & 0 \end{pmatrix} \begin{pmatrix} c_1 \\ \vdots \\ c_m \\ -\lambda \end{pmatrix} = \begin{pmatrix} 0 \\ \vdots \\ 0 \\ 1 \end{pmatrix} \tag{A.38}$$

where $B_{ij} = \langle \mathbf{e}_i | \mathbf{e}_j \rangle$ is the scalar product of the error vectors $\mathbf{e}_i$ and $\mathbf{e}_j$, and $\lambda$ is a Lagrange multiplier.

The coefficients $c_i$ determined from Eq. (A.38) are used to calculate an intermediate interpolated geometry

$$\mathbf{x}'_{m+1} = \sum c_i \mathbf{x}_i \tag{A.39}$$

and its corresponding interpolated gradient

$$\mathbf{g}'_{m+1} = \sum c_i \mathbf{g}_i \tag{A.40}$$

A new, independent geometry is generated from the interpolated geometry and gradient according to

$$\mathbf{x}_{m+1} = \mathbf{x}'_{m+1} - \mathbf{H}^{-1}\mathbf{g}'_{m+1} \tag{A.41}$$

**Note:** Convergence is theoretically guaranteed regardless of the quality of the Hessian matrix (as long as it is positive definite), and the original GDIIS algorithm used a static Hessian (*i.e.*, the original starting Hessian, often a simple unit matrix, remained unchanged during the entire optimization). However, updating the Hessian at each cycle generally results in more rapid convergence, and this is the default in OPTIMIZE.

Other modifications to the original method include limiting the number of previous geometries used in Eq. (A.33) and, subsequently, by neglecting earlier geometries, and eliminating any geometries more than a certain distance from the current geometry (default = 0.3 a.u.).

# References and Further Reading

[1] J. Baker, *J. Comput. Chem.* **7**, 385 (1986).

[2] C. J. Cerjan and W. H. Miller, *J. Chem. Phys.* **75**, 2800 (1981).

[3] J. Simons, P. Jørgensen, H. Taylor, and J. Ozment, *J. Phys. Chem.* **87**, 2745 (1983).

[4] A. Banerjee, N. Adams, J. Simons, and R. Shepard, *J. Phys. Chem.* **89**, 52 (1985).

[5] P. Csaszar and P. Pulay, *J. Mol. Struct. (Theochem)* **114**, 31 (1984).

[6] P. Pulay, *J. Comput. Chem.* **3**, 556 (1982).

[7] J. Baker, A. Kessi, and B. Delley, *J. Chem. Phys.* **105**, 192 (1996).

[8] P. Pulay, G. Fogarasi, F. Pang, and J. E. Boggs, *J. Am. Chem. Soc.* **101**, 2550 (1979).

[9] G. Fogarasi, X. Zhou, P. W. Taylor, and P. Pulay, *J. Am. Chem. Soc.* **114**, 8191 (1992).

[10] P. Pulay and G. Fogarasi, *J. Chem. Phys.* **96**, 2856 (1992).

[11] J. Baker, *J. Comput. Chem.* **13**, 240 (1992).

[12] J. Baker and D. Bergeron, *J. Comput. Chem.* **14**, 1339 (1993).

[13] J. Baker, *J. Comput. Chem.* **18**, 1079 (1997).

[14] D. Poppinger, *Chem. Phys. Lett.* **35**, 550 (1975).

[15] J. Baker and W. J. Hehre, *J. Comput. Chem.* **12**, 606 (1991).

[16] H. B. Schlegel, *Theor. Chem. Acc.* **66**, 333 (1984).

[17] E. B. Wilson, J. C. Decius, and P. C. Cross, *Molecular Vibrations*, McGraw-Hill, New York, 1955.

[18] R. Fletcher, *Practial Methods of Optimization*, volume 2, Wiley, New York, 1981.

[19] S. Califano, *Vibrational States*, Wiley, London, 1976.

# Appendix B

# AOInts

## B.1 Introduction

Within the Q-Chem program, an Atomic Orbital integrals (AOInts) package has been developed which, while relatively invisible to the user, is one of the keys to the overall speed and efficiency of the Q-Chem program.

"Ever since Boys' introduction of Gaussian basis sets to quantum chemistry in 1950, the calculation and handling of the notorious two-electron repulsion integrals (ERIs) over Gaussian functions has been an important avenue of research for practicing computational chemists. Indeed, the emergence of practically useful computer programs has been fueled in no small part by the development of sophisticated algorithms to compute the very large number of ERIs that are involved in calculations on molecular systems of even modest size"[1].

The ERI engine of any competitive quantum chemistry software package will be one of the most complicated aspects of the package as whole. Coupled with the importance of such an engine's efficiency, a useful yardstick of a program's anticipated performance can be quickly measured by considering the components of its ERI engine. In recent times, developers at Q-Chem, Inc. have made significant contributions to the advancement of ERI algorithm technology (for example, see Refs. 1–10), and it is not surprising that Q-Chem's AOInts package is considered the most advanced of its kind.

## B.2 Historical Perspective

Prior to the 1950s, the most difficult step in the systematic application of Schrödinger wave mechanics to chemistry was the calculation of the notorious two-electron integrals that measure the repulsion between electrons. Boys[11] showed that this step can be made easier (although still time consuming) if Gaussian, rather than Slater, orbitals are used in the basis set. Following the landmark paper of computational chemistry[12] (again due to Boys) programs were constructed that could calculate all the ERIs that arise in the treatment of a general polyatomic molecule with $s$ and $p$ orbitals. However, the programs were painfully slow and could only be applied to the smallest of molecular systems.

In 1969, Pople constructed a breakthrough ERI algorithm, a hundred time faster than its predecessors. The algorithm remains the fastest available for its associated integral classes and is now referred to as the

Pople-Hehre axis-switch method[13].

Over the two decades following Pople's initial development, an enormous amount of research effort into the construction of ERIs was documented, which built on Pople's original success. Essentially, the advances of the newer algorithms could be identified as either better coping with angular momentum ($L$) or, contraction ($K$); each new method increasing the speed and application of quantum mechanics to solving real chemical problems.

By 1990, another barrier had been reached. The contemporary programs had become sophisticated and both academia and industry had begun to recognize and use the power of *ab initio* quantum chemistry, but the software was struggling with "dusty deck syndrome" and it had become increasingly difficult for it to keep up with the rapid advances in hardware development. Vector processors, parallel architectures and the advent of the graphical user interface were all demanding radically different approaches to programming and it had become clear that a fresh start, with a clean slate, was both inevitable and desirable. Furthermore, the integral bottleneck had re-emerged in a new guise and the standard programs were now hitting the $N^2$ wall. Irrespective of the speed at which ERIs could be computed, the unforgiving fact remained that the number of ERIs required scaled quadratically with the size of the system.

The Q-CHEM project was established to tackle this problem and to seek new methods that circumvent the $N^2$ wall. Fundamentally new approaches to integral theory were sought and the ongoing advances that have resulted[14–18] have now placed Q-CHEM firmly at the vanguard of the field. It should be emphasized, however, that the $\mathcal{O}(N)$ methods that we have developed still require short-range ERIs to treat interactions between nearby electrons, thus the importance of contemporary ERI code remains.

The chronological development and evolution of integral methods can be summarized by considering a time line showing the years in which important new algorithms were first introduced. These are best discussed in terms of the type of ERI or matrix elements that the algorithm can compute efficiently.

| | | | |
|---|---|---|---|
| 1950 | Boys | 11 | ERIs with low $L$ and low $K$ |
| 1969 | Pople | 13 | ERIs with low $L$ and high $K$ |
| 1976 | Dupuis | 19 | Integrals with any $L$ and low $K$ |
| 1978 | McMurchie | 20 | Integrals with any $L$ and low $K$ |
| 1982 | Almlöf | 21 | Introduction of the direct SCF approach |
| 1986 | Obara | 22 | Integrals with any $L$ and low $K$ |
| 1988 | Head-Gordon | 8 | Integrals with any $L$ and low $K$ |
| 1991 | Gill | 1,6 | Integrals with any $L$ and any $K$ |
| 1994 | White | 14 | J matrix in linear work |
| 1996 | Schwegler | 18,23 | HF exchange matrix in linear work |
| 1997 | Challacombe | 17 | Fock matrix in linear work |

## B.3 AOINTS: Calculating ERIs with Q-CHEM

The area of molecular integrals with respect to Gaussian basis functions has recently been reviewed[2] and the user is referred to this review for deeper discussions and further references to the general area. The purpose of this short account is to present the basic approach, and in particular, the implementation of ERI algorithms and aspects of interest to the user in the AOINTS package which underlies the Q-CHEM program.

We begin by observing that all of the integrals encountered in an *ab initio* calculation, of which overlap, kinetic energy, multipole moment, internuclear repulsion, nuclear-electron attraction and inter electron repulsion are the best known, can be written in the general form

$$(\mathbf{ab}|\mathbf{cd}) = \int \phi_{\mathbf{a}}(\mathbf{r_1})\phi_{\mathbf{b}}(\mathbf{r_1})\theta(r_{12})\phi_{\mathbf{c}}(\mathbf{r_2})\phi_{\mathbf{d}}(\mathbf{r_2})d\mathbf{r_1}d\mathbf{r_2} \tag{B.1}$$

where the basis functions are contracted Gaussians (CGTF)

$$\phi_{\mathbf{a}}(\mathbf{r}) = (x - A_x)^{a_x}(y - A_y)^{a_y}(z - A_z)^{a_z}\sum_{i=1}^{K_a} D_{ai}e^{-\alpha_i|\mathbf{r}-\mathbf{A}|^2} \tag{B.2}$$

and the operator $\theta$ is a two-electron operator. Of the two-electron operators (Coulomb, CASE, anti-Coulomb and delta-function) used in the Q-CHEM program, the most significant is the Coulomb, which leads us to the ERIs.

An ERI is the classical Coulomb interaction ($\theta(x) = 1/x$ in B.1) between two charge distributions referred to as bras $(\mathbf{ab}|$ and kets $|\mathbf{cd})$.

## B.4 Shell-Pair Data

It is common to characterize a bra, a ket and a bra-ket by their degree of contraction and angular momentum. In general, it is more convenient to compile data for shell-pairs rather than basis-function pairs. A shell is defined as that sharing common exponents and centers. For example, in the case of a number of Pople derived basis sets, four basis functions, encompassing a range of angular momentum types (*i.e.*, $s$, $p_x$, $p_y$, $p_z$ on the same atomic center sharing the same exponents constitute a single shell.

The shell-pair data set is central to the success of any modern integral program for three main reasons. First, in the formation of shell-pairs, all pairs of shells in the basis set are considered and categorized as either significant or negligible. A shell-pair is considered negligible if the shells involved are so far apart, relative to their diffuseness, that their overlap is negligible. Given the rate of decay of Gaussian basis functions, it is not surprising that most of the shell-pairs in a large molecule are negligible, that is, the number of significant shell-pairs increases linearly with the size of the molecule. Second, a number of useful intermediates which are frequently required within ERI algorithms should be computed once in shell-pair formation and stored as part of the shell-pair information, particularly those which require costly divisions. This prevents re-evaluating simple quantities. Third, it is useful to sort the shell-pair information by type (*i.e.*, angular momentum and degree of contraction). The reasons for this are discussed below.

Q-CHEM's shell-pair formation offers the option of two basic integral shell-pair cutoff criteria; one based on the integral threshold (*$rem* variable THRESH) and the other relative to machine precision.

Intelligent construction of shell-pair data scales linearly with the size of the basis set, requires a relative amount of CPU time which is almost entirely negligible for large direct SCF calculations, and for small jobs, constitutes approximately 10% of the job time.

## B.5 Shell-Quartets and Integral Classes

Given a sorted list of shell-pair data, it is possible to construct all potentially important shell-quartets by pairing of the shell-pairs with one another. Because the shell-pairs have been sorted, it is possible to deal with batches of integrals of the same type or class (*e.g.*, $(ss|ss)$, $(sp|sp)$, $(dd|dd)$, *etc.*) where an integral class is characterized by both angular momentum ($L$) and degree of contraction ($K$). Such an approach is advantageous for vector processors and for semi-direct integral algorithms where the most expensive (high $K$ or $L$ integral classes can be computed once, stored in memory (or disk) and only less expensive classes rebuilt on each iteration.

While the shell-pairs may have been carefully screened, it is possible for a pair of significant shell-pairs to form a shell-quartet which need not be computed directly. Three cases are:

- The quartet is equivalent, by point group symmetry, to another quartet already treated.
- The quartet can be ignored on the basis of cheaply computed ERI bounds[7] on the largest quartet bra-ket.
- On the basis of an incremental Fock matrix build, the largest density matrix element which will multiply any of the bra-kets associated with the quartet may be negligibly small.

**Note:** Significance and negligibility is always based on the level of integral threshold set by the *$rem* variable THRESH.

## B.6 Fundamental ERI

The fundamental ERI[2] and the basis of all ERI algorithms is usually represented

$$\begin{aligned}[\mathbf{0}]^{(0)} &= [ss|ss]^{(0)} \\ &= D_A D_B D_C D_D \int e^{-\alpha|\mathbf{r_1}-\mathbf{A}|^2} e^{-\beta|\mathbf{r_1}-\mathbf{B}|^2} \left[\frac{1}{r_{12}}\right] e^{-\gamma|\mathbf{r_2}-\mathbf{C}|^2} e^{-\delta|\mathbf{r_2}-\mathbf{D}|^2} d\mathbf{r_1} d\mathbf{r_2} \end{aligned} \tag{B.3}$$

which can be reduced to a one-dimensional integral of the form

$$[\mathbf{0}]^{(0)} = U(2\vartheta^2)^{1/2} \left(\frac{2}{\pi}\right)^{1/2} \int\limits_0^1 e^{-Tu^2} du \tag{B.4}$$

and can be efficiently computed using a modified Chebyshev interpolation scheme[5]. Equation (B.4) can also be adapted for the general case $[\mathbf{0}]^{(m)}$ integrals required for most calculations. Following the fundamental ERI, building up to the full bra-ket ERI (or intermediary matrix elements, see later) are the problems of angular momentum and contraction.

**Note:** Square brackets denote primitive integrals and parentheses denote fully-contracted integrals.

## B.7 Angular Momentum Problem

The fundamental integral is essentially an integral without angular momentum (*i.e.*, it is an integral of the type $[ss|ss]$). Angular momentum, usually depicted by $L$, has been problematic for efficient ERI formation, evident in the above time line. Initially, angular momentum was calculated by taking derivatives of the fundamental ERI with respect to one of the Cartesian coordinates of the nuclear center. This is an extremely inefficient route, but it works and was appropriate in the early development of ERI methods. Recursion relations[22,24] and the newly developed tensor equations[3] are the basis for the modern approaches.

## B.8 Contraction Problem

The contraction problem may be described by considering a general contracted ERI of $s$-type functions derived from the STO-3G basis set. Each basis function has degree of contraction $K$ = 3. Thus, the ERI may be written

$$\begin{aligned}(ss|ss) &= \sum_{i=1}^{3}\sum_{j=1}^{3}\sum_{k=1}^{3}\sum_{l=1}^{3} D_{Ai}D_{Bj}D_{Ck}D_{Dl} \\ &\quad\times \int e^{-\alpha_i|\mathbf{r_1}-\mathbf{A}|^2} e^{-\beta_j|\mathbf{r_1}-\mathbf{B}|^2}\left[\frac{1}{r_{12}}\right] e^{-\gamma_k|\mathbf{r_2}-\mathbf{C}|^2} e^{-\delta_l|\mathbf{r}_2-\mathbf{D}|^2} d\mathbf{r_1}d\mathbf{r_2} \\ &= \sum_{i=1}^{3}\sum_{j=1}^{3}\sum_{k=1}^{3}\sum_{l=1}^{3}[s_is_j|s_ks_l] \end{aligned} \qquad \text{(B.5)}$$

and requires 81 primitive integrals for the single ERI. The problem escalates dramatically for more highly contracted sets (STO-6G, 6-311G) and has been the motivation for the development of techniques for shell-pair modeling[25], in which a second shell-pair is constructed with fewer primitives that the first, but introduces no extra error relative to the integral threshold sought.

The Pople-Hehre axis-switch method[13] is excellent for high contraction low angular momentum integral classes.

## B.9 Quadratic Scaling

The success of quantitative modern quantum chemistry, relative to its primitive, qualitative beginnings, can be traced to two sources: better algorithms and better computers. While the two technologies continue to improve rapidly, efforts are heavily thwarted by the fact that the total number of ERIs increases quadratically with the size of the molecular system. Even large increases in ERI algorithm efficiency yield only moderate increases in applicability, hindering the more widespread application of *ab initio* methods to areas of, perhaps, biochemical significance where semi-empirical techniques[26,27] have already proven so valuable.

Thus, the elimination of quadratic scaling algorithms has been the theme of many research efforts in quantum chemistry throughout the 1990s and has seen the construction of many alternative algorithms to alleviate the problem. Johnson was the first to implement DFT exchange/correlation functionals whose computational cost scaled linearly with system size[28]. This paved the way for the most significant breakthrough in the area with the linear scaling CFMM algorithm[14] leading to linear scaling DFT calculations[29]. Further breakthroughs have been made with traditional theory in the form of the QCTC[17,30,31] and ONX[18,23] algorithms, while more radical approaches[15,16] may lead to entirely new approaches to *ab initio* calculations. Investigations into the quadratic Coulomb problem has not only yielded linear scaling algorithms, but is also providing large insights into the significance of many molecular energy components.

Linear scaling Coulomb and SCF exchange/correlation algorithms are not the end of the story as the $\mathcal{O}(N^3)$ diagonalization step has been rate limiting in semi-empirical techniques and, been predicted[32] to become rate limiting in *ab initio* approaches in the medium term. However, divide-and-conquer techniques[33–36] and the recently developed quadratically convergent SCF algorithm[37] show great promise for reducing this problem.

## B.10 Algorithm Selection

No single ERI algorithm is available to efficiently handle all integral classes; rather, each tends to have specific integral classes where the specific algorithm outperforms the alternatives. The PRISM algorithm[6] is an intricate collection of pathways and steps in which the path chosen is that which is the most efficient for a given class. It appears that the most appropriate path for a given integral class depends on the relative position of the contraction step (lowly contracted bra-kets prefer late contraction, highly contracted bra-kets are most efficient with early contraction steps).

Careful studies have provided FLOP counts which are the current basis of integral algorithm selection, although care must be taken to ensure that algorithms are not rate limited by MOPs[4]. Future algorithm selection criteria will take greater account of memory, disk, chip architecture, cache size, vectorization and parallelization characteristics of the hardware, many of which are already exist within Q-CHEM.

## B.11 More Efficient Hartree–Fock Gradient and Hessian Evaluations

Q-CHEM combines the Head-Gordon–Pople (HGP) method[8] and the COLD prism method[3] for Hartree-Fock gradient and Hessian evaluations. All two-electron four-center integrals are classified according to their angular momentum types and degrees of contraction. For each type of integrals, the program chooses one with a lower cost. In practice, the HGP method is chosen for most integral classes in a gradient or Hessian calculation, and thus it dominates the total CPU time.

Recently the HGP codes within Q-CHEM were completely rewritten for the evaluation of the P II$^x$ P term in the gradient evaluation, and the P II$^{xy}$ P term in the Hessian evaluation. Our emphasis is to improve code efficiency by reducing cache misses rather than by reducing FLOP counts. Some timing results from a Hartree-Fock calculation on azt are shown below.

## B.12 User-Controllable Variables

AOINTS has been optimally constructed so that the fastest integral algorithm for ERI calculation is chosen for the given integral class and batch. Thus, the user has not been provided with the necessary variables for overriding the program's selection process. The user is, however, able to control the accuracy of the cutoff used during shell-pair formation (METECO) and the integral threshold (THRESH). In addition, the user

| **Basis Set** | **AIX** | | | **Linux** | | |
|---|---|---|---|---|---|---|
| | Gradient Evaluation: P II$^x$ P Term | | | | | |
| | Old | New | New/Old | Old | New | New/Old |
| 3-21G | 34 s | 20 s | 0.58 | 25 s | 14 s | 0.56 |
| 6-31G** | 259 s | 147 s | 0.57 | 212 s | 120 s | 0.57 |
| DZ | 128 s | 118 s | 0.92 | 72 s | 62 s | 0.86 |
| cc-pVDZ | 398 s | 274 s | 0.69 | 308 s | 185 s | 0.60 |
| | Hessian Evaluation: P II$^{xy}$ P term | | | | | |
| | Old | New | New/Old | Old | New | New/Old |
| 3-21G | 294 s | 136 s | 0.46 | 238 s | 100 s | 0.42 |
| 6-31G** | 2520 s | 976 s | 0.39 | 2065 s | 828 s | 0.40 |
| DZ | 631 s | 332 s | 0.53 | 600 s | 230 s | 0.38 |
| cc-pVDZ | 3202 s | 1192 s | 0.37 | 2715 s | 866 s | 0.32 |

Table B.1: AIX timings were obtained on an IBM RS/6000 workstation with AIX4 operating system, and Linux timings on an Opteron cluster where the Q-CHEM executable was compiled with an Intel 32-bit compiler.

can force the use of the direct SCF algorithm (DIRECT_SCF) and increase the default size of the integrals storage buffer (INCORE_INTS_BUFFER).

Currently, some of Q-CHEM's linear scaling algorithms, such as QCTC and ONX algorithms, require the user to specify their use. It is anticipated that further research developments will lead to the identification of situations in which these, or combinations of these and other algorithms, will be selected automatically by Q-CHEM in much the same way that PRISM algorithms choose the most efficient pathway for given integral classes.

## References and Further Reading

[1] P. M. W. Gill, M. Head-Gordon, and J. A. Pople, *J. Phys. Chem.* **94**, 5564 (1990).

[2] P. M. W. Gill, *Adv. Quantum Chem.* **25**, 142 (1994).

[3] T. R. Adams, R. D. Adamson, and P. M. W. Gill, *J. Chem. Phys.* **107**, 124 (1997).

[4] M. J. Frisch, B. G. Johnson, P. M. W. Gill, D. J. Fox, and R. H. Nobes, *Chem. Phys. Lett.* **206**, 225 (1993).

[5] P. M. W. Gill, B. G. Johnson, and J. A. Pople, *Int. J. Quantum Chem.* **40**, 745 (1991).

[6] P. M. W. Gill and J. A. Pople, *Int. J. Quantum Chem.* **40**, 753 (1991).

[7] P. M. W. Gill, B. G. Johnson, and J. A. Pople, *Chem. Phys. Lett.* **217**, 65 (1994).

[8] M. Head-Gordon and J. A. Pople, *J. Chem. Phys.* **89**, 5777 (1988).

[9] B. G. Johnson, P. M. W. Gill, and J. A. Pople, *Chem. Phys. Lett.* **206**, 229 (1993).

[10] B. G. Johnson, P. M. W. Gill, and J. A. Pople, *Chem. Phys. Lett.* **206**, 239 (1993).

[11] S. F. Boys, *Proc. Roy. Soc. Ser. A* **200**, 542 (1950).

[12] S. F. Boys, G. B. Cook, C. M. Reeves, and I. Shavitt, *Nature* **178**, 1207 (1956).

[13] J. A. Pople and W. J. Hehre, *J. Comput. Phys.* **27**, 161 (1978).

[14] C. A. White, B. G. Johnson, P. M. W. Gill, and M. Head-Gordon, *Chem. Phys. Lett.* **230**, 8 (1994).

[15] R. D. Adamson, J. P. Dombroski, and P. M. W. Gill, *Chem. Phys. Lett.* **254**, 329 (1996).

[16] J. P. Dombroski, S. W. Taylor, and P. M. W. Gill, *J. Phys. Chem.* **100**, 6272 (1996).

[17] M. Challacombe and E. Schwegler, *J. Chem. Phys.* **106**, 5526 (1997).

[18] E. Schwegler and M. Challacombe, *J. Chem. Phys.* **105**, 2726 (1996).

[19] M. Dupuis, J. Rys, and H. F. King, *J. Chem. Phys.* **65**, 111 (1976).

[20] L. E. McMurchie and E. R. Davidson, *J. Comput. Phys.* **26**, 218 (1978).

[21] J. Almlöf, K. Faegri, and K. Korsell, *J. Comput. Chem.* **3**, 385 (1982).

[22] S. Obara and A. Saika, *J. Chem. Phys.* **84**, 3963 (1986).

[23] E. Schwegler and M. Challacombe, *J. Chem. Phys.* **106**, 9708 (1996).

[24] S. Obara and A. Saika, *J. Chem. Phys.* **89**, 1540 (1988).

[25] R. D. Adamson, Shell-pair economisation, Master's thesis, Massey University, Palmerston North, New Zealand, 1995.

[26] M. J. S. Dewar, *Org. Mass. Spect.* **28**, 305 (1993).

[27] M. J. S. Dewar, *The Molecular Orbital Theory of Organic Chemistry*, McGraw-Hill, New York, 1969.

[28] B. G. Johnson, *Development, Implementation, and Performance of Efficient Methodologies for Density Functional Calculations*, PhD thesis, Carnegie Mellon University, Pittsburgh, PA, 1993.

[29] C. A. White, B. G. Johnson, P. M. W. Gill, and M. Head-Gordon, *Chem. Phys. Lett.* **253**, 268 (1996).

[30] M. Challacombe, E. Schwegler, and J. Almlöf, *J. Chem. Phys.* **104**, 4685 (1996).

[31] M. Challacombe, E. Schwegler, and J. Almlöf, Modern developments in Hartree-Fock theory: Fast methods for computing the Coulomb matrix, Technical report, University of Minnesota and Minnesota Supercomputer Institute, Minneapolis, MN, 1995.

[32] D. L. Strout and G. E. Scuseria, *J. Chem. Phys.* **102**, 8448 (1995).

[33] W. Yang, *Phys. Rev. A* **44**, 7823 (1991).

[34] W. Yang, *Phys. Rev. Lett.* **66**, 1438 (1991).

[35] W. Yang and T.-S. Lee, *J. Chem. Phys.* **103**, 5674 (1995).

[36] T.-S. Lee, D. M. York, and W. Yang, *J. Chem. Phys.* **105**, 2744 (1996).

[37] C. Ochsenfeld and M. Head-Gordon, *Chem. Phys. Lett.* **270**, 399 (1997).

# Appendix C

# Q-CHEM Quick Reference

## C.1 Q-CHEM Text Input Summary

- Users are able to enter input sections in any order; see Table 3.1 for a complete list of input sections.
- Each input section must be terminated with *$end*.
- Not all input sections are required, but *$rem* and *$molecule* are compulsory.
- The entire Q-CHEM input is case-insensitive.
- Multiple jobs are separated by the string `@@@` on a single line.

### C.1.1 Keyword: *$molecule*

Four methods are available for inputing geometry information:

- *Z*-matrix (Ångstroms and degrees):

```
$molecule
   {Z-matrix}
   {blank line, if parameters are being used}
   {Z-matrix parameters, if used}
$end
```

- Cartesian Coordinates (Ångstroms):

```
$molecule
   {Cartesian coordinates}
   {blank line, if parameter are being used}
   {Coordinate parameters, if used}
$end
```

- Read from a previous calculation:

```
$molecule
```

```
   read
$end
```

- Read from a file:

```
$molecule
   read filename
$end
```

### C.1.2 Keyword: *$rem*

See also the list of *$rem* variables at the end of this Appendix. The general format is:

```
$rem
   REM_VARIABLE   VALUE   [optional comment]
$end
```

### C.1.3 Keyword: *$basis*

The format for the user–defined basis section is as follows:

$$
\begin{array}{lllllll}
\multicolumn{7}{l}{\texttt{\$basis}} \\
 & X & 0 & & & & \\
 & L & K & scale & & & \\
 & \alpha_1 & C_1^{L_{min}} & C_1^{L_{min}+1} & \ldots & C_1^{L_{max}} \\
 & \alpha_2 & C_2^{L_{min}} & C_2^{L_{min}+1} & \ldots & C_2^{L_{max}} \\
 & \vdots & \vdots & \vdots & \ddots & \vdots \\
 & \alpha_K & C_K^{L_{min}} & C_K^{L_{min}+1} & \ldots & C_K^{L_{max}} \\
\multicolumn{7}{l}{\star\star\star\star} \\
\multicolumn{7}{l}{\texttt{\$end}}
\end{array}
$$

| | | |
|---|---|---|
| where | $X$ | Atomic symbol of the atom (atomic number not accepted) |
| | $L$ | Angular momentum symbol (S, P, SP, D, F, G) |
| | $K$ | Degree of contraction of the shell (integer) |
| | $scale$ | Scaling to be applied to exponents (default is 1.00) |
| | $a_i$ | Gaussian primitive exponent (positive real number) |
| | $C_i^L$ | Contraction coefficient for each angular momentum (non–zero real numbers). |

Atoms are terminated with $\star\star\star\star$ and the complete basis set is terminated with the *$end* keyword terminator. No blank lines can be incorporated within the general basis set input. Note that more than one contraction coefficient per line is one required for compound shells like SP. As with all Q-CHEM input deck information, all input is case–insensitive.

### C.1.4 Keyword: *$comment*

Note that the entire input deck is echoed to the output file, thus making the *$comment* keyword largely redundant.

```
    $comment
       User comments - copied to output file
    $end
```

### C.1.5 Keyword: *$ecp*

```
$ecp
```

For each atom that will bear an ECP
    Chemical symbol for the atom
    ECP name; the $L$ value for the ECP; number of core electrons removed
    For each ECP component (in the order unprojected, $\hat{P}_0$, $\hat{P}_1$, , $\hat{P}_{L-1}$
        The component name
        The number of Gaussians in the component
        For each Gaussian in the component
            The power of $r$; the exponent; the contraction coefficient

```
****
$end
```

**Note:** (1) All of the information in the *$ecp* block is case–insensitive.
(2) The $L$ value may not exceed 4. That is, nothing beyond $G$ projectors is allowed.
(3) The power of $r$ (which includes the Jacobian $r^2$ factor) must be 0, 1 or 2.

### C.1.6 Keyword: *$empirical_dispersion*

```
    $empirical_dispersion
    S6 S6_value
    D D_value
    C6 element_1 C6_value_for_element_1 element_2 C6_value_for_element_2
    VDW_RADII element_1 radii_for_element_1 element_2 radii_for_element_2
    $end
```

**Note:** This section is only for values that the user wants to change from the default values recommended by Grimme.

### C.1.7 Keyword: *$external_charges*

All input should be given in atomic units.

Update: While charges should indeed be listed in atomic units, the units for distances depend on the user input. If the structure is specified in Ångstroms (the default), the coordinates for external charges should also be in Ångstroms. If the structure is specified in atomic units, the coordinates for external charges should also be in atomic units. (See INPUT_BOHR.)

```
$external_charges
   x-coord1   y-coord1   z-coord1   charge1
   x-coord2   y-coord2   z-coord2   charge2
$end
```

### C.1.8 Keyword: *$intracule*

```
$intracule
```

| | | |
|---|---|---|
| *int_type* | 0 | Compute $P(u)$ only |
| | 1 | Compute $M(v)$ only |
| | 2 | Compute $W(u,v)$ only |
| | 3 | Compute $P(u)$, $M(v)$ and $W(u,v)$ |
| | 4 | Compute $P(u)$ and $M(v)$ |
| | 5 | Compute $P(u)$ and $W(u,v)$ |
| | 6 | Compute $M(v)$ and $W(u,v)$ |
| *u_points* | | Number of points, start, end. |
| *v_points* | | Number of points, start, end. |
| *moments* | 0–4 | Order of moments to be computed ($P(u)$ only). |
| *derivs* | 0–4 | order of derivatives to be computed ($P(u)$ only). |
| *accuracy* | $n$ | ($10^{-n}$) specify accuracy of intracule interpolation table ($P(u)$ only). |

```
$end
```

### C.1.9 Keyword: *$isotopes*

Note that masses should be given in atomic units.

```
$isotopes
   number_extra_loops  tp_flag
      number_of_atoms  [temp pressure]
      atom_number1 mass1
      atom_number2 mass2
   ...
$end
```

### C.1.10 Keyword: *$multipole_field*

Multipole fields are all in atomic units.

```
$multipole_field
   field_component1   value1
   field_component2   value2
   ...
$end
```

### C.1.11 Keyword: *$nbo*

Refer to Chapter 10 and the NBO manual for further information. Note that the NBO *$rem* variable must be set to ON to initiate the NBO package.

```
$nbo
   [ NBO options ]
$end
```

### C.1.12 Keyword: *$occupied*

```
$occupied
   1  2  3  4 ...  nalpha
   1  2  3  4 ...  nbeta
$end
```

### C.1.13 Keyword: *$opt*

Note that units are in Ångstroms and degrees. Also see the summary in the next section of this Appendix.

```
$opt
CONSTRAINT
stre  atom1  atom2  value
...
bend  atom1  atom2  atom3  value
...
outp  atom1  atom2  atom3  atom4  value
...
tors  atom1  atom2  atom3  atom4  value
...
linc  atom1  atom2  atom3  atom4  value
...
linp  atom1  atom2  atom3  atom4  value
...
ENDCONSTRAINT

FIXED
atom   coordinate_reference
...
ENDFIXED

DUMMY
idum   type   list_length   defining_list
...
ENDDUMMY

CONNECT
```

```
    atom   list_length   list
    ...
    ENDCONNECT
    $end
```

## C.1.14 Keyword: *$svp*

```
$svp
<KEYWORD>=<VALUE>, <KEYWORD>=<VALUE>,...
<KEYWORD>=<VALUE>
$end
```

For example, the section may look like this:

```
$svp
    RHOISO=0.001, DIELST=78.39, NPTLEB=110
$end
```

## C.1.15 Keyword: *$svpirf*

```
$svpirf
    <# point> <x point> <y point> <z point> <charge> <grid weight>
    <# point> <x normal> <y normal> <z normal>
$end
```

## C.1.16 Keyword: *$plots*

`$plots`

One comment line

Specification of the 3–D mesh of points on 3 lines:

$N_x \quad x_{\min} \quad x_{\max}$

$N_y \quad y_{\min} \quad y_{\max}$

$N_z \quad z_{\min} \quad z_{\max}$

A line with 4 integers indicating how many things to plot:

$N_{\rm MO} \quad N_{\rm Rho} \quad N_{\rm Trans} \quad N_{\rm DA}$

An optional line with the integer list of MO's to evaluate (only if $N_{\rm MO} > 0$)

MO(1) MO(2) . . . MO($N_{\rm MO}$)

An optional line with the integer list of densities to evaluate (only if $N_{\rm Rho} > 0$)

Rho(1) Rho(2) . . . Rho($N_{\rm Rho}$)

An optional line with the integer list of transition densities (only if $N_{\rm Trans} > 0$)

Trans(1) Trans(2) . . . Trans($N_{\rm Trans}$)

An optional line with states for detachment/attachment densities (if $N_{\rm DA} > 0$)

DA(1) DA(2) . . . DA($N_{\rm DA}$)

`$end`

### C.1.17 Keyword: *$localized_diabatization*

```
$plots
```

One comment line.

One line with an an array of adiabatic states to mix together.

$< adiabat1 >$ $< adiabat2 >$ $< adiabat3 > \ldots$

```
$end
```

**Note:** We count adiabatic states such that the first excited state is $< adiabat >= 1$, the fifth is $< adiabat >= 5$, and so forth.

### C.1.18 Keyword *$van_der_waals*

**Note:** All radii are given in Ångstroms.

```
    $van_der_waals
       1
       atomic_number   VdW_radius
    $end
```

(alternative format)

```
    $van_der_waals
       2
       sequential_atom_number   VdW_radius
    $end
```

### C.1.19 Keyword: *$xc_functional*

```
    $xc_functional
       X  exchange_symbol  coefficient
       X  exchange_symbol  coefficient
       ...
       C  correlation_symbol  coefficient
       C  correlation_symbol  coefficient
       ...
       K  coefficient
    $end
```

## C.2 Geometry Optimization with General Constraints

CONSTRAINT and ENDCONSTRAINT define the beginning and end, respectively, of the constraint section of *$opt* within which users may specify up to six different types of constraints:

***interatomic distances***
Values in Ångstroms; *value* $> 0$:

```
stre   atom1   atom2   value
```

***angles***
Values in degrees, $0 \leq value \leq 180$; *atom2* is the middle atom of the bend:

```
bend   atom1   atom2   atom3   value
```

***out–of–plane–bends***
Values in degrees, $-180 \leq value \leq 180$ *atom2*; angle between *atom4* and the *atom1–atom2–atom3* plane:

```
outp   atom1   atom2   atom3   atom4   value
```

***dihedral angles***
Values in degrees, $-180 \leq value \leq 180$; angle the plane *atom1–atom2–atom3* makes with the plane *atom2–atom3–atom4*:

```
tors   atom1   atom2   atom3   atom4   value
```

***coplanar bends***
Values in degrees, $-180 \leq value \leq 180$; bending of *atom1–atom2–atom3* in the plane *atom2–atom3–atom4*:

```
linc   atom1   atom2   atom3   atom4   value
```

***perpendicular bends***
Values in degrees, $-180 \leq value \leq 180$; bending of *atom1–atom2–atom3* perpendicular to the plane *atom2–atom3–atom4*:

```
linp   atom1   atom2   atom3   atom4   value
```

Absolute atom positions can be frozen with the *FIXED* section. The section starts with the *FIXED* keyword as the first line and ends with the *ENDFIXED* keyword on the last. The format to fix a coordinate or coordinates of an atom is:

```
atom   coordinate_reference
```

*coordinate_reference* can be any combination of up to three characters $X$, $Y$ and $Z$ to specify the coordinate(s) to be fixed: $X$, $Y$, $Z$, *XY*, *XZ*, *YZ*, *XYZ*. The fixing characters must be next to each other. *e.g.*,

```
FIXED
2 XY
ENDFIXED
```

## C.3 *$rem* Variable List

The general format of the *$rem* input for Q-CHEM text input files is simply as follows:

```
    $rem
       rem_variable   rem_option   [comment]
       rem_variable   rem_option   [comment]
    $end
```

This input is not case sensitive. The following sections contain the names and options of available *$rem* variables for users. The format for describing each *$rem* variable is as follows:

**REM_VARIABLE**
A short description of what the variable controls
TYPE:
Defines the variable as either INTEGER, LOGICAL or STRING.
DEFAULT:
Describes Q-CHEM's internal default, if any exists.
OPTIONS:
Lists options available for the user
RECOMMENDATION:
Gives a quick recommendation.

### C.3.1 General

BASIS
BASIS_LIN_DEP_THRESH
EXCHANGE
CORRELATION
ECP
JOBTYPE
METHOD
PURECART

### C.3.2 SCF Control

BASIS2
BASISPROJTYPE
DIIS_PRINT
DIIS_SUBSPACE_SIZE
DIRECT_SCF
INCFOCK
MAX_DIIS_CYCLES
MAX_SCF_CYCLES
PSEUDO_CANONICAL
SCF_ALGORITHM
SCF_CONVERGENCE
SCF_FINAL_PRINT
SCF_GUESS
SCF_GUESS_MIX
SCF_GUESS_PRINT
SCF_PRINT
THRESH
THRESH_DIIS_SWITCH
UNRESTRICTED
VARTHRESH

### C.3.3 DFT Options

CORRELATION
EXCHANGE
FAST_XC
INC_DFT
INCDFT_DENDIFF_THRESH
INCDFT_GRIDDIFF_THRESH
INCDFT_DENDIFF_VARTHRESH
INCDFT_GRIDDIFF_VARTHRESH
XC_GRID
XC_SMART_GRID

### C.3.4 Large Molecules

CFMM_ORDER
DIRECT_SCF
EPAO_ITERATE
EPAO_WEIGHTS
GRAIN
INCFOCK
INTEGRAL_2E_OPR
INTEGRALS_BUFFER
LIN_K
MEM_STATIC
MEM_TOTAL
METECO
OMEGA
PAO_ALGORITHM
PAO_METHOD
THRESH
VARTHRESH
RI_J
RI_K
ARI
ARI_R0
ARI_R1

### C.3.5 Correlated Methods

AO2MO_DISK
CD_ALGORITHM
CORE_CHARACTER
CORRELATION
MEM_STATIC
MEM_TOTAL
N_FROZEN_CORE
N_FROZEN_VIRTUAL
PRINT_CORE_CHARACTER

### C.3.6 Correlated Methods Handled by CCMAN and CCMAN2

Most of these *$rem* variables that start CC_.

These are relevant for CCSD and other CC methods (OD, VOD, CCD, QCCD, CCVB-SD, etc).

CC_CANONIZE
CC_RESTART_NO_SCF
CC_T_CONV
CC_DIIS_SIZE
CC_DIIS_FREQ
CC_DIIS_START
CC_DIIS_MAX_OVERLAP
CC_DIIS_MIN_OVERLAP
CC_RESTART
CC_SAVEAMPL

These options are only relevant to methods involving orbital optimization (OOCD, VOD, QCCD, VQCCD):

CC_MP2NO_GUESS
CC_MP2NO_GRAD
CC_DIIS
CC_DIIS12_SWITCH
CC_THETA_CONV
CC_THETA_GRAD_CONV
CC_THETA_STEPSIZE
CC_RESET_THETA
CC_THETA_GRAD_THRESH
CC_HESS_THRESH
CC_ED_CCD
CC_QCCD_THETA_SWITCH
CC_PRECONV_T2Z
CC_PRECONV_T2Z_EACH
CC_PRECONV_FZ
CC_ITERATE_OV
CC_CANONIZE_FREQ
CC_CANONIZE_FINAL

Properties and optimization:

CC_REF_PROP
CC_FULLRESPONSE
CC_REF_PROP_TE

### C.3.7 Perfect pairing, Coupled cluster valence bond, and related methods

CCVB_METHOD
GVB_N_PAIRS
GVB_ORB_MAX_ITER
GVB_ORB_CONV
GVB_AMP_SCALE
GVB_PRINT
CCVB_GUESS
GVB_LOCAL
GVB_RESTART
GVB_ORB_SCALE
GVB_DO_SANO

### C.3.8 Excited States: CIS, TDDFT, SF-XCIS and SOS-CIS(D)

CIS_CONVERGENCE
CIS_GUESS_DISK_TYPE
CIS_RELAXED_DENSITY
CIS_STATE_DERIV
MAX_CIS_CYCLES
XCIS
CIS_GUESS_DISK
CIS_N_ROOTS
CIS_SINGLETS
CIS_TRIPLETS
RPA
SPIN_FLIP_XCIS

### C.3.9 Excited States: EOM-CC and CI Methods

Those are keywords relevant to EOM-CC and CI methods handled by CCMAN/CCMAN2. Most of these *$rem* variables that start CC_ and EOM_.

EOM_DAVIDSON_CONVERGENCE
EOM_DAVIDSON_THRESHOLD
EOM_NGUESS_DOUBLES
EOM_DOEXDIAG
EOM_PRECONV_SINGLES
EOM_IPEA_FILTER
CC_REST_AMPL
CC_EOM_PROP
CC_STATE_TO_OPT
CC_EOM_PROP_TE
EOM_DAVIDSON_MAXVECTORS
EOM_DAVIDSON_MAX_ITER
EOM_NGUESS_SINGLES
EOM_PRECONV_DOUBLES
EOM_PRECONV_SD
EOM_FAKE_IPEA
CC_REST_TRIPLES
CC_TRANS_PROP
CC_EOM_PROP
CC_FULLRESPONSE

## C.3.10 Geometry Optimizations

CIS_STATE_DERIV
FDIFF_STEPSIZE
GEOM_OPT_COORDS
GEOM_OPT_DMAX
GEOM_OPTHESSIAN
GEOM_OPT_LINEAR_ANGLE
GEOM_OPT_MAX_CYCLES
GEOM_OPT_MAX_DIIS
GEOM_OPT_MODE
GEOM_OPT_PRINT
GEOM_OPTSYMFLAG
GEOM_OPT_PRINT
GEOM_OPTTOL_ENERGY
GEOM_OPT_TOL_DISPLACEMENT
GEOM_OPT_TOL_ENERGY
GEOM_OPT_TOL_GRADIENT
GEOMP_OPT_UPDATE
IDERIV
JOBTYPE
SCF_GUESS_ALWAYS
CC_STATE_TO_OPT

## C.3.11 Vibrational Analysis

DORAMAN
CPSCF_NSEG
FDIFF_STEPSIZE
IDERIV
ISOTOPES
JOBTYPE
VIBMAN_PRINT
ANHAR
VCI
FDIFF_DER
MODE_COUPLING
IGNORE_LOW_FREQ
FDIFF_STEPSIZE_QFF

## C.3.12 Reaction Coordinate Following

JOBTYPE
RPATH_COORDS
RPATH_DIRECTION
RPATH_MAX_CYCLES
RPATH_MAX_STEPSIZE
RPATH_PRINT
RPATH_TOL_DISPLACEMENT

## C.3.13 NMR Calculations

D_CPSCF_PERTNUM
D_SCF_CONV_1
D_SCF_CONV_2
D_SCF_DIIS
D_SCF_MAX_1
D_SCF_MAX_2
JOBTYPE

### C.3.14 Wave function Analysis and Molecular Properties

CHEMSOL
CHEMSOL_EFIELD
CHEMSOL_NN
CHEM_SOL_PRINT
CIS_RELAXED_DENSITY
IGDESP
INTRACULE
MULTIPOLE_ORDER
NBO
POP_MULLIKEN
PRINT_DIST_MATRIX
PRINT_ORBITALS
READ_VDW
SOLUTE_RADIUS
SOLVENT_DIELECTRIC
STABILITY_ANALYSIS
WAVEFUNCTION_ANALYSIS
WRITE_WFN

### C.3.15 Symmetry

CC_SYMMETRY
SYM_IGNORE
SYMMETRY
SYMMETRY_DECOMPOSITION
SYM_TOL

### C.3.16 Printing Options

CC_PRINT
CHEMSOL_PRINT
DIIS_PRINT
GEOM_OPT_PRINT
MOM_PRINT
PRINT_CORE_CHARACTER
PRINT_DIST_MATRIX
PRINT_GENERAL_BASIS
PRINT_ORBITALS
RPATH_PRINT
SCF_FINAL_PRINT
SCF_GUESS_PRINT
SCF_PRINT
VIBMAN_PRINT
WRITE_WFN

### C.3.17 Resource Control

MEM_TOTAL
MEM_STATIC
AO2MO_DISK
CC_MEMORY
INTEGRALS_BUFFER
MAX_SUB_FILE_NUM
DIRECT_SCF

## C.4 Alphabetical Listing of *$rem* Variables

**EIGSLV_METH**

Control the method for solving the ALMO-CIS eigen-equation

TYPE:

INTEGER

DEFAULT:

0

OPTIONS:

0 Explicitly build the Hamiltonian then diagonalize (full-spectrum).

1 Use the Davidson method (currently only available for restricted cases).

RECOMMENDATION:

None

**LOCAL_CIS**

Invoke ALMO-CIS/ALMO-CIS+CT.

TYPE:

INTEGER

DEFAULT:

0

OPTIONS:

0 Regular CIS

1 ALMO-CIS/ALMO-CIS+CT without RI(slow)

2 ALMO-CIS/ALMO-CIS+CT with RI

RECOMMENDATION:

2 if ALMO-CIS is desired.

**NN_THRESH**

The distance cutoff for neighboring fragments (between which CT is enabled).

TYPE:

INTEGER

DEFAULT:

0

OPTIONS:

0 Do not include interfragment transitions (ALMO-CIS).

$n$ Include interfragment excitations between pairs of fragments the distances between whom are smaller than $n$ Bohr (ALMO-CIS+CT).

RECOMMENDATION:

None

**ADC_CVS**

Activates the use of the CVS approximation for the calculation of CVS-ADC core-excited states.

TYPE:

LOGICAL

DEFAULT:

FALSE

OPTIONS:

| | |
|---|---|
| TRUE | Activates the CVS approximation. |
| FALSE | Do not compute core-excited states using the CVS approximation. |

RECOMMENDATION:

Set to TRUE, if to obtain core-excited states for the simulation of X-ray absorption spectra. In the case of TRUE, the *$rem* variable CC_REST_OCC has to be defined as well.

**ADC_C_C**

Set the spin-opposite scaling parameter $c_c$ for the ADC(2) calculation. The parameter value is obtained by multiplying the given integer by $10^{-3}$.

TYPE:

INTEGER

DEFAULT:

| | |
|---|---|
| 1170 | Optimized value $c_c = 1.17$ for ADC(2)-s or |
| 1000 | $c_c = 1.0$ for ADC(2)-x |

OPTIONS:

| | |
|---|---|
| $n$ | Corresponding to $n \cdot 10^{-3}$ |

RECOMMENDATION:

Use the default.

**ADC_C_T**

Set the spin-opposite scaling parameter $c_T$ for an SOS-ADC(2) calculation. The parameter value is obtained by multiplying the given integer by $10^{-3}$.

TYPE:

INTEGER

DEFAULT:

| | |
|---|---|
| 1300 | Optimized value $c_T = 1.3$. |

OPTIONS:

| | |
|---|---|
| $n$ | Corresponding to $n \cdot 10^{-3}$ |

RECOMMENDATION:

Use the default.

**ADC_C_X**

Set the spin-opposite scaling parameter $c_x$ for the ADC(2)-x calculation. The parameter value is obtained by multiplying the given integer by $10^{-3}$.

TYPE:

INTEGER

DEFAULT:

1300 Optimized value $c_x = 0.9$ for ADC(2)-x.

OPTIONS:

$n$ Corresponding to $n \cdot 10^{-3}$

RECOMMENDATION:

Use the default.

**ADC_DAVIDSON_CONV**

Controls the convergence criterion of the Davidson procedure.

TYPE:

INTEGER

DEFAULT:

6 Corresponding to $10^{-6}$

OPTIONS:

$n \leq 12$ Corresponding to $10^{-n}$.

RECOMMENDATION:

Use the default unless higher accuracy is required or convergence problems are encountered.

**ADC_DAVIDSON_MAXITER**

Controls the maximum number of iterations of the Davidson procedure.

TYPE:

INTEGER

DEFAULT:

60

OPTIONS:

$n$ Number of iterations

RECOMMENDATION:

Use the default unless convergence problems are encountered.

**ADC_DAVIDSON_MAXSUBSPACE**

Controls the maximum subspace size for the Davidson procedure.

TYPE:

INTEGER

DEFAULT:

$5\times$ the number of excited states to be calculated.

OPTIONS:

$n$ User-defined integer.

RECOMMENDATION:

Should be at least $2 - 4\times$ the number of excited states to calculate. The larger the value the more disk space is required.

**ADC_DAVIDSON_THRESH**

Controls the threshold for the norm of expansion vectors to be added during the Davidson procedure.

TYPE:

INTEGER

DEFAULT:

Twice the value of ADC_DAVIDSON_CONV, but at maximum $10^{-14}$.

OPTIONS:

$n \leq 14$ Corresponding to $10^{-n}$

RECOMMENDATION:

Use the default unless convergence problems are encountered. The threshold value $10^{-n}$ should always be smaller than the convergence criterion ADC_DAVIDSON_CONV.

**ADC_DIIS_ECONV**

Controls the convergence criterion for the excited state energy during DIIS.

TYPE:

INTEGER

DEFAULT:

6 Corresponding to $10^{-6}$

OPTIONS:

$n$ Corresponding to $10^{-n}$

RECOMMENDATION:

None

**ADC_DIIS_MAXITER**

Controls the maximum number of DIIS iterations.

TYPE:

INTEGER

DEFAULT:

50

OPTIONS:

$n$ User-defined integer.

RECOMMENDATION:

Increase in case of slow convergence.

**ADC_DIIS_RCONV**

Convergence criterion for the residual vector norm of the excited state during DIIS.

TYPE:

INTEGER

DEFAULT:

6 Corresponding to $10^{-6}$

OPTIONS:

$n$ Corresponding to $10^{-n}$

RECOMMENDATION:

None

**ADC_DIIS_SIZE**

Controls the size of the DIIS subspace.

TYPE:

INTEGER

DEFAULT:

7

OPTIONS:

$n$ User-defined integer

RECOMMENDATION:

None

**ADC_DIIS_START**

Controls the iteration step at which DIIS is turned on.

TYPE:

INTEGER

DEFAULT:

1

OPTIONS:

$n$ User-defined integer.

RECOMMENDATION:

Set to a large number to switch off DIIS steps.

**ADC_DO_DIIS**

Activates the use of the DIIS algorithm for the calculation of ADC(2) excited states.

TYPE:

LOGICAL

DEFAULT:

FALSE

OPTIONS:

| | |
|---|---|
| TRUE | Use DIIS algorithm. |
| FALSE | Do diagonalization using Davidson algorithm. |

RECOMMENDATION:

None.

**ADC_NGUESS_DOUBLES**

Controls the number of excited state guess vectors which are double excitations.

TYPE:

INTEGER

DEFAULT:

0

OPTIONS:

$n$ User-defined integer.

RECOMMENDATION:

**ADC_NGUESS_SINGLES**

Controls the number of excited state guess vectors which are single excitations. If the number of requested excited states exceeds the total number of guess vectors (singles and doubles), this parameter is automatically adjusted, so that the number of guess vectors matches the number of requested excited states.

TYPE:

INTEGER

DEFAULT:

Equals to the number of excited states requested.

OPTIONS:

$n$ User-defined integer.

RECOMMENDATION:

**ADC_PRINT**

Controls the amount of printing during an ADC calculation.

TYPE:

INTEGER

DEFAULT:

1 Basic status information and results are printed.

OPTIONS:

0 Quiet: almost only results are printed.

1 Normal: basic status information and results are printed.

2 Debug: more status information, extended information on timings.

...

RECOMMENDATION:

Use the default.

**ADC_PROP_ES2ES**

Controls the calculation of transition properties between excited states (currently only transition dipole moments and oscillator strengths), as well as the computation of two-photon absorption cross-sections of excited states using the sum-over-states expression.

TYPE:

LOGICAL

DEFAULT:

FALSE

OPTIONS:

TRUE Calculate state-to-state transition properties.

FALSE Do not compute transition properties between excited states.

RECOMMENDATION:

Set to TRUE, if state-to-state properties or sum-over-states two-photon absorption cross-sections are required.

**ADC_PROP_ES**

Controls the calculation of excited state properties (currently only dipole moments).

TYPE:

LOGICAL

DEFAULT:

FALSE

OPTIONS:

TRUE Calculate excited state properties.

FALSE Do not compute state properties.

RECOMMENDATION:

Set to TRUE, if properties are required.

**ADC_PROP_TPA**

Controls the calculation of two-photon absorption cross-sections of excited states using matrix inversion techniques.

TYPE:

LOGICAL

DEFAULT:

FALSE

OPTIONS:

TRUE Calculate two-photon absorption cross-sections.

FALSE Do not compute two-photon absorption cross-sections.

RECOMMENDATION:

Set to TRUE, if to obtain two-photon absorption cross-sections.

**ADD_CHARGED_CAGE**

Add a point charge cage of a given radius and total charge.

TYPE:

INTEGER

DEFAULT:

0 No cage.

OPTIONS:

0 No cage.

1 Dodecahedral cage.

2 Spherical cage.

RECOMMENDATION:

Spherical cage is expected to yield more accurate results, especially for small radii.

**AFSSH**

Adds decoherence approximation to surface hopping calculation.

TYPE:

INTEGER

DEFAULT:

0

OPTIONS:

0 Traditional surface hopping, no decoherence.

1 Use augmented fewest-switches surface hopping (AFSSH).

RECOMMENDATION:

AFSSH will increase the cost of the calculation, but may improve accuracy for some systems. See Refs. 1–3 for more detail.

**AIFDEM_CTSTATES**

Include charge-transfer-like cation/anion pair states in the AIFDEM basis.

TYPE:

LOGICAL

DEFAULT:

FALSE

OPTIONS:

TRUE Include CT states.

FALSE Do not include CT states.

RECOMMENDATION:

None

**AIFDEM_EMBED_RANGE**

Specifies the size of the QM region for charge embedding

TYPE:

INTEGER

DEFAULT:

FULL_QM

OPTIONS:

FULL_QM No charge embedding.

0 Treat only excited fragments with QM.

$n$ Range (Å) from excited fragments within which to treat other fragments with QM.

RECOMMENDATION:

Minimal, 0 Å, threshold maintains accuracy while significantly reducing computational time.

**AIFDEM_NTOTHRESH**

Controls the number of NTOs that are retained in the exciton-site basis states.

TYPE:

INTEGER

DEFAULT:

99

OPTIONS:

$n$ Threshold percentage of the norm of fragment NTO amplitudes.

RECOMMENDATION:

A threshold of $85\%$ gives a good trade-off of computational time and accuracy for organic molecules.

**AIFDEM**

Perform an AIFDEM calculation.

TYPE:

LOGICAL

DEFAULT:

FALSE

OPTIONS:

| | |
|---|---|
| FALSE | Do not perform an AIFDEM calculation. |
| TRUE | Perform an AIFDEM calculation. |

RECOMMENDATION:

False

**AIMD_FICT_MASS**

Specifies the value of the fictitious electronic mass $\mu$, in atomic units, where $\mu$ has dimensions of (energy)$\times$(time)$^2$.

TYPE:

INTEGER

DEFAULT:

None

OPTIONS:

User-specified

RECOMMENDATION:

Values in the range of 50–200 a.u. have been employed in test calculations; consult Ref. 4 for examples and discussion.

**AIMD_INIT_VELOC**

Specifies the method for selecting initial nuclear velocities.

TYPE:

STRING

DEFAULT:

None

OPTIONS:

| | |
|---|---|
| THERMAL | Random sampling of nuclear velocities from a Maxwell-Boltzmann distribution. The user must specify the temperature in Kelvin via the *$rem* variable AIMD_TEMP. |
| ZPE | Choose velocities in order to put zero-point vibrational energy into each normal mode, with random signs. This option requires that a frequency job to be run beforehand. |
| QUASICLASSICAL | Puts vibrational energy into each normal mode. In contrast to the ZPE option, here the vibrational energies are sampled from a Boltzmann distribution at the desired simulation temperature. This also triggers several other options, as described below. |

RECOMMENDATION:

This variable need only be specified in the event that velocities are not specified explicitly in a *$velocity* section.

**AIMD_LANGEVIN_TIMESCALE**

Sets the timescale (strength) of the Langevin thermostat

TYPE:

INTEGER

DEFAULT:

none

OPTIONS:

$n$ Thermostat timescale,asn $n$ fs

RECOMMENDATION:

Smaller values (roughly 100) equate to tighter thermostats but may inhibit rapid sampling. Larger values ($\geq$ 1000) allow for more rapid sampling but may take longer to reach thermal equilibrium.

**AIMD_METHOD**

Selects an *ab initio* molecular dynamics algorithm.

TYPE:

STRING

DEFAULT:

BOMD

OPTIONS:

BOMD Born-Oppenheimer molecular dynamics.

CURVY Curvy-steps Extended Lagrangian molecular dynamics.

RECOMMENDATION:

BOMD yields exact classical molecular dynamics, provided that the energy is tolerably conserved. ELMD is an approximation to exact classical dynamics whose validity should be tested for the properties of interest.

**AIMD_MOMENTS**

Requests that multipole moments be output at each time step.

TYPE:

INTEGER

DEFAULT:

0 Do not output multipole moments.

OPTIONS:

$n$ Output the first $n$ multipole moments.

RECOMMENDATION:

None

**AIMD_NUCL_DACF_POINTS**

Number of time points to utilize in the dipole auto-correlation function for an AIMD trajectory

TYPE:

INTEGER

DEFAULT:

0

OPTIONS:

| | |
|---|---|
| 0 | Do not compute dipole auto-correlation function. |
| $1 \leq n \leq$ AIMD_STEPS | Compute dipole auto-correlation function for last $n$ timesteps of the trajectory. |

RECOMMENDATION:

If the DACF is desired, set equal to AIMD_STEPS.

**AIMD_NUCL_SAMPLE_RATE**

The rate at which sampling is performed for the velocity and/or dipole auto-correlation function(s). Specified as a multiple of steps; *i.e.*, sampling every step is 1.

TYPE:

INTEGER

DEFAULT:

None.

OPTIONS:

| | |
|---|---|
| $1 \leq n \leq$ AIMD_STEPS | Update the velocity/dipole auto-correlation function every $n$ steps. |

RECOMMENDATION:

Since the velocity and dipole moment are routinely calculated for *ab initio* methods, this variable should almost always be set to 1 when the VACF/DACF are desired.

**AIMD_NUCL_VACF_POINTS**

Number of time points to utilize in the velocity auto-correlation function for an AIMD trajectory

TYPE:

INTEGER

DEFAULT:

0

OPTIONS:

| | |
|---|---|
| 0 | Do not compute velocity auto-correlation function. |
| $1 \leq n \leq$ AIMD_STEPS | Compute velocity auto-correlation function for last $n$ time steps of the trajectory. |

RECOMMENDATION:

If the VACF is desired, set equal to AIMD_STEPS.

**AIMD_QCT_INITPOS**

Chooses the initial geometry in a QCT-MD simulation.

TYPE:

INTEGER

DEFAULT:

0

OPTIONS:

| | |
|---|---|
| 0 | Use the equilibrium geometry. |
| $n$ | Picks a random geometry according to the harmonic vibrational wave function. |
| $-n$ | Generates $n$ random geometries sampled from<br>the harmonic vibrational wave function. |

RECOMMENDATION:

None.

**AIMD_QCT_WHICH_TRAJECTORY**

Picks a set of vibrational quantum numbers from a random distribution.

TYPE:

INTEGER

DEFAULT:

1

OPTIONS:

| | |
|---|---|
| $n$ | Picks the $n$th set of random initial velocities. |
| $-n$ | Uses an average over $n$ random initial velocities. |

RECOMMENDATION:

Pick a positive number if you want the initial velocities to correspond to a particular set of vibrational occupation numbers and choose a different number for each of your trajectories. If initial velocities are desired that corresponds to an average over $n$ trajectories, pick a negative number.

**AIMD_SHORT_TIME_STEP**

Specifies a shorter electronic time step for FSSH calculations.

TYPE:

INTEGER

DEFAULT:

TIME_STEP

OPTIONS:

| | |
|---|---|
| $n$ | Specify an electronic time step duration of $n$/AIMD_TIME_STEP_CONVERSION a.u. If $n$ is less than the nuclear time step variable TIME_STEP, the electronic wave function will be integrated multiple times per nuclear time step, using a linear interpolation of nuclear quantities such as the energy gradient and derivative coupling. Note that $n$ must divide TIME_STEP evenly. |

RECOMMENDATION:

Make AIMD_SHORT_TIME_STEP as large as possible while keeping the trace of the density matrix close to unity during long simulations. Note that while specifying an appropriate duration for the electronic time step is essential for maintaining accurate wave function time evolution, the electronic-only time steps employ linear interpolation to estimate important quantities. Consequently, a short electronic time step is not a substitute for a reasonable nuclear time step.

**AIMD_STEPS**

Specifies the requested number of molecular dynamics steps.

TYPE:

INTEGER

DEFAULT:

None.

OPTIONS:

User-specified.

RECOMMENDATION:

None.

**AIMD_TEMP**

Specifies a temperature (in Kelvin) for Maxwell-Boltzmann velocity sampling.

TYPE:

INTEGER

DEFAULT:

None

OPTIONS:

User-specified number of Kelvin.

RECOMMENDATION:

This variable is only useful in conjunction with AIMD_INIT_VELOC = THERMAL. Note that the simulations are run at constant energy, rather than constant temperature, so the mean nuclear kinetic energy will fluctuate in the course of the simulation.

**AIMD_THERMOSTAT**

Applies thermostatting to AIMD trajectories.

TYPE:

INTEGER

DEFAULT:

none

OPTIONS:

| | |
|---|---|
| LANGEVIN | Stochastic, white-noise Langevin thermostat |
| NOSE_HOOVER | Time-reversible, Nosé-Hoovery chain thermostat |

RECOMMENDATION:

Use either thermostat for sampling the canonical (NVT) ensemble.

**AIMD_TIME_STEP_CONVERSION**

Modifies the molecular dynamics time step to increase granularity.

TYPE:

INTEGER

DEFAULT:

1

OPTIONS:

| | |
|---|---|
| $n$ | The molecular dynamics time step is TIME_STEP/$n$ a.u. |

RECOMMENDATION:

None

**ANHAR_SEL**

Select a subset of normal modes for subsequent anharmonic frequency analysis.

TYPE:

LOGICAL

DEFAULT:

FALSE Use all normal modes

OPTIONS:

TRUE Select subset of normal modes

RECOMMENDATION:

None

**ANHAR**

Performing various nuclear vibrational theory (TOSH, VPT2, VCI) calculations to obtain vibrational anharmonic frequencies.

TYPE:

LOGICAL

DEFAULT:

FALSE

OPTIONS:

TRUE Carry out the anharmonic frequency calculation.

FALSE Do harmonic frequency calculation.

RECOMMENDATION:

Since this calculation involves the third and fourth derivatives at the minimum of the potential energy surface, it is recommended that the GEOM_OPT_TOL_DISPLACEMENT, GEOM_OPT_TOL_GRADIENT and GEOM_OPT_TOL_ENERGY tolerances are set tighter. Note that VPT2 calculations may fail if the system involves accidental degenerate resonances. See the VCI *$rem* variable for more details about increasing the accuracy of anharmonic calculations.

**AO2MO_DISK**

Sets the amount of disk space (in megabytes) available for MP2 calculations.

TYPE:

INTEGER

DEFAULT:

2000 Corresponding to 2000 Mb.

OPTIONS:

$n$ User-defined number of megabytes.

RECOMMENDATION:

Should be set as large as possible, discussed in Section 5.4.1.

**ARI_R0**

Determines the value of the inner fitting radius (in Ångstroms)

TYPE:

INTEGER

DEFAULT:

4 A value of 4 Å will be added to the atomic van der Waals radius.

OPTIONS:

$n$ User defined radius.

RECOMMENDATION:

For some systems the default value may be too small and the calculation will become unstable.

**ARI_R1**

Determines the value of the outer fitting radius (in Ångstroms)

TYPE:

INTEGER

DEFAULT:

5 A value of 5 Å will be added to the atomic van der Waals radius.

OPTIONS:

$n$ User defined radius.

RECOMMENDATION:

For some systems the default value may be too small and the calculation will become unstable. This value also determines, in part, the smoothness of the potential energy surface.

**ARI**

Toggles the use of the atomic resolution-of-the-identity (ARI) approximation.

TYPE:

LOGICAL

DEFAULT:

FALSE ARI will not be used by default for an RI-JK calculation.

OPTIONS:

TRUE Turn on ARI.

RECOMMENDATION:

For large (especially 1D and 2D) molecules the approximation may yield significant improvements in Fock evaluation time.

**AUX_BASIS**

Specifies the type of auxiliary basis to be used in a method that involves RI-fitting procedures.

TYPE:

STRING

DEFAULT:

No default is assigned. Must be defined in the input

OPTIONS:

Symbol. Choose among the auxiliary basis sets collected in the qchem qcaux basis library

RECOMMENDATION:

Try a few different types of aux bases first

**BASIS2**

Sets the small basis set to use in basis set projection.

TYPE:

STRING

DEFAULT:

No second basis set default.

OPTIONS:

Symbol. Use standard basis sets as per Chapter 7.

| | |
|---|---|
| BASIS2_GEN | General BASIS2 |
| BASIS2_MIXED | Mixed BASIS2 |

RECOMMENDATION:

BASIS2 should be smaller than BASIS. There is little advantage to using a basis larger than a minimal basis when BASIS2 is used for initial guess purposes. Larger, standardized BASIS2 options are available for dual-basis calculations (see Section 4.9).

**BASISPROJTYPE**

Determines which method to use when projecting the density matrix of BASIS2

TYPE:

STRING

DEFAULT:

FOPPROJECTION (when DUAL_BASIS_ENERGY=false)
OVPROJECTION (when DUAL_BASIS_ENERGY=true)

OPTIONS:

| | |
|---|---|
| FOPPROJECTION | Construct the Fock matrix in the second basis |
| OVPROJECTION | Projects MOs from BASIS2 to BASIS. |

RECOMMENDATION:

None

**BASIS_LIN_DEP_THRESH**

Sets the threshold for determining linear dependence in the basis set

TYPE:

INTEGER

DEFAULT:

6 Corresponding to a threshold of $10^{-6}$

OPTIONS:

$n$ Sets the threshold to $10^{-n}$

RECOMMENDATION:

Set to 5 or smaller if you have a poorly behaved SCF and you suspect linear dependence in you basis set. Lower values (larger thresholds) may affect the accuracy of the calculation.

**BASIS**

Specifies the basis sets to be used.

TYPE:

STRING

DEFAULT:

No default basis set

OPTIONS:

| | |
|---|---|
| General, Gen | User defined (*$basis* keyword required). |
| Symbol | Use standard basis sets as per Chapter 7. |
| Mixed | Use a mixture of basis sets (see Chapter 7). |

RECOMMENDATION:

Consult literature and reviews to aid your selection.

**BOYSCALC**

Specifies the Boys localized orbitals are to be calculated

TYPE:

INTEGER

DEFAULT:

0

OPTIONS:

| | |
|---|---|
| 0 | Do not perform localize the occupied space. |
| 1 | Allow core-valence mixing in Boys localization. |
| 2 | Localize core and valence separately. |

RECOMMENDATION:

None

**BOYS_CIS_NUMSTATE**

Define how many states to mix with Boys localized diabatization. These states must be specified in the *$localized_diabatization* section.

TYPE:

INTEGER

DEFAULT:

0 Do not perform Boys localized diabatization.

OPTIONS:

2 to N where N is the number of CIS states requested (CIS_N_ROOTS)

RECOMMENDATION:

It is usually not wise to mix adiabatic states that are separated by more than a few eV or a typical reorganization energy in solvent.

**CAGE_CHARGE**

Defines the total charge of the cage.

TYPE:

INTEGER

DEFAULT:

400 Add a cage charged +4e.

OPTIONS:

$n$ Total charge of the cage is $n$/100 a.u.

RECOMMENDATION:

None

**CAGE_POINTS**

Defines number of point charges for the spherical cage.

TYPE:

INTEGER

DEFAULT:

100

OPTIONS:

$n$ Number of point charges to use.

RECOMMENDATION:

None

**CAGE_RADIUS**

Defines radius of the charged cage.

TYPE:

INTEGER

DEFAULT:

225

OPTIONS:

$n$ radius is $n$/100 Å.

RECOMMENDATION:

None

**CALC_NAC**

Whether or not non-adiabatic couplings will be calculated for the EOM-CC, CIS, and TDDFT wave functions.

TYPE:

INTEGER

DEFAULT:

0 (do not compute NAC)

OPTIONS:

1 NYI for EOM-CC

2 Compute NACs using Szalay's approach (this what needs to be specified for EOM-CC).

RECOMMENDATION:

Additional response equations will be solved and gradients for all EOM states and for summed states will be computed, which increases the cost of calculations. Request only when needed and do not ask for too many EOM states.

**CALC_SOC**

Whether or not the spin-orbit couplings between CC/EOM/ADC/CIS/TDDFT electronic states will be calculated. In the CC/EOM-CC suite, by default the couplings are calculated between the CCSD reference and the EOM-CCSD target states. In order to calculate couplings between EOM states, CC_STATE_TO_OPT must specify the initial EOM state.

TYPE:

LOGICAL

DEFAULT:

FALSE (no spin-orbit couplings will be calculated)

OPTIONS:

FALSE, TRUE

RECOMMENDATION:

One-electron and mean-field two-electron SOCs will be computed by default. To enable full two-electron SOCs, two-particle EOM properties must be turned on (see CC_EOM_PROP_TE).

**CALC_SOC**

Controls whether to calculate the SOC constants for EOM-CC, ADC, and TDDFT within the TDA.

TYPE:

LOGICAL

DEFAULT:

FALSE

OPTIONS:

| | |
|---|---|
| FALSE | Do not perform the SOC calculation. |
| TRUE | Perform the SOC calculation. |

RECOMMENDATION:

None

**CCVB_GUESS**

Specifies the initial guess for CCVB calculations

TYPE:

INTEGER

DEFAULT:

NONE

OPTIONS:

| | |
|---|---|
| 1 | Standard GVBMAN guess (orbital localization via GVB_LOCAL + Sano procedure). |
| 2 | Use orbitals from previous GVBMAN calculation, along with SCF_GUESS = read. |
| 3 | Convert UHF orbitals into pairing VB form. |

RECOMMENDATION:

Option 1 is the most useful overall. The success of GVBMAN methods is often dependent on localized orbitals, and this guess shoots for these. Option 2 is useful for comparing results to other GVBMAN methods, or if other GVBMAN methods are able to obtain a desired result more efficiently. Option 3 can be useful for bond-breaking situations when a pertinent UHF solution has been found. It works best for small systems, or if the unrestriction is a local phenomenon within a larger molecule. If the unrestriction is non-local and the system is large, this guess will often produce a solution that is not the global minimum. Any UHF solution has a certain number of pairs that are unrestricted, and this will be output by the program. If GVB_N_PAIRS exceeds this number, the standard GVBMAN initial-guess procedure will be used to obtain a guess for the excess pairs

**CCVB_METHOD**

Optionally modifies the basic CCVB method

TYPE:

INTEGER

DEFAULT:

1

OPTIONS:

| | |
|---|---|
| 1 | Standard CCVB model |
| 3 | Independent electron pair approximation (IEPA) to CCVB |
| 4 | Variational PP (the CCVB reference energy) |

RECOMMENDATION:

Option 1 is generally recommended. Option 4 is useful for preconditioning, and for obtaining localized-orbital solutions, which may be used in subsequent calculations. It is also useful for cases in which the regular GVBMAN PP code becomes variationally unstable. Option 3 is a simple independent-amplitude approximation to CCVB. It avoids the cubic-scaling amplitude equations of CCVB, and also is able to reach the correct dissociation energy for any molecular system (unlike regular CCVB which does so only for cases in which UHF can reach a correct dissociate limit). However the IEPA approximation to CCVB is sometimes variationally unstable, which we have yet to observe in regular CCVB.

**CC_BACKEND**

Used to specify the computational back-end of CCMAN2.

TYPE:

STRING

DEFAULT:

VM Default shared-memory disk-based back-end

OPTIONS:

| | |
|---|---|
| XM | *libxm* shared-memory disk-based back-end |
| CTF | Distributed-memory back-end for MPI jobs |

RECOMMENDATION:

Use XM for large jobs with limited memory or when the performance of the default disk-based back-end is not satisfactory, CTF for MPI jobs

**CC_CANONIZE_FINAL**

Whether to semi-canonicalize orbitals at the end of the ground state calculation.

TYPE:

LOGICAL

DEFAULT:

FALSE unless required

OPTIONS:

TRUE/FALSE

RECOMMENDATION:

Should not normally have to be altered.

**CC_CANONIZE_FREQ**

The orbitals will be semi-canonicalized every $n$ theta resets. The thetas (orbital rotation angles) are reset every CC_RESET_THETA iterations. The counting of iterations differs for active space (VOD, VQCCD) calculations, where the orbitals are always canonicalized at the first theta-reset.

TYPE:

INTEGER

DEFAULT:

50

OPTIONS:

$n$ User-defined integer

RECOMMENDATION:

Smaller values can be tried in cases that do not converge.

**CC_CANONIZE**

Whether to semi-canonicalize orbitals at the start of the calculation (*i.e.* Fock matrix is diagonalized in each orbital subspace)

TYPE:

LOGICAL

DEFAULT:

TRUE

OPTIONS:

TRUE/FALSE

RECOMMENDATION:

Should not normally have to be altered.

**CC_CONVERGENCE**

Overall convergence criterion for the coupled-cluster codes. This is designed to ensure at least $n$ significant digits in the calculated energy, and automatically sets the other convergence-related variables (CC_E_CONV, CC_T_CONV, CC_THETA_CONV, CC_THETA_GRAD_CONV) $[10^{-n}]$.

TYPE:

INTEGER

DEFAULT:

6 Energies.

7 Gradients.

OPTIONS:

$n$ Corresponding to $10^{-n}$ convergence criterion. Amplitude convergence is set automatically to match energy convergence.

RECOMMENDATION:

Use the default

**CC_DIIS12_SWITCH**

When to switch from DIIS2 to DIIS1 procedure, or when DIIS2 procedure is required to generate DIIS guesses less frequently. Total value of DIIS error vector must be less than $10^{-n}$, where $n$ is the value of this option.

TYPE:

INTEGER

DEFAULT:

5

OPTIONS:

$n$ User-defined integer

RECOMMENDATION:

None

**CC_DIIS_FREQ**

DIIS extrapolation will be attempted every n iterations. However, DIIS2 will be attempted every iteration while total error vector exceeds CC_DIIS12_SWITCH. DIIS1 cannot generate guesses more frequently than every 2 iterations.

TYPE:

INTEGER

DEFAULT:

2

OPTIONS:

$N$ User-defined integer

RECOMMENDATION:

None

**CC_DIIS_MAX_OVERLAP**

DIIS extrapolations will not begin until square root of the maximum element of the error overlap matrix drops below this value.

TYPE:

DOUBLE

DEFAULT:

100 Corresponding to 1.0

OPTIONS:

$abcde$ Integer code is mapped to $abc \times 10^{-de}$

RECOMMENDATION:

None

**CC_DIIS_MIN_OVERLAP**

The DIIS procedure will be halted when the square root of smallest element of the error overlap matrix is less than $10^{-n}$, where $n$ is the value of this option. Small values of the B matrix mean it will become near-singular, making the DIIS equations difficult to solve.

TYPE:

INTEGER

DEFAULT:

11

OPTIONS:

$n$ User-defined integer

RECOMMENDATION:

None

**CC_DIIS_SIZE**

Specifies the maximum size of the DIIS space.

TYPE:

INTEGER

DEFAULT:

7

OPTIONS:

$n$ User-defined integer

RECOMMENDATION:

Larger values involve larger amounts of disk storage.

**CC_DIIS_START**

Iteration number when DIIS is turned on. Set to a large number to disable DIIS.

TYPE:

INTEGER

DEFAULT:

3

OPTIONS:

$n$ User-defined

RECOMMENDATION:

Occasionally DIIS can cause optimized orbital coupled-cluster calculations to diverge through large orbital changes. If this is seen, DIIS should be disabled.

**CC_DIIS**

Specify the version of Pulay's Direct Inversion of the Iterative Subspace (DIIS) convergence accelerator to be used in the coupled-cluster code.

TYPE:

INTEGER

DEFAULT:

0

OPTIONS:

0 Activates procedure 2 initially, and procedure 1 when gradients are smaller than DIIS12_SWITCH.

1 Uses error vectors defined as differences between parameter vectors from successive iterations. Most efficient near convergence.

2 Error vectors are defined as gradients scaled by square root of the approximate diagonal Hessian. Most efficient far from convergence.

RECOMMENDATION:

DIIS1 can be more stable. If DIIS problems are encountered in the early stages of a calculation (when gradients are large) try DIIS1.

**CC_DIRECT_RI**

Controls use of RI and Cholesky integrals in conventional (undecomposed) form

TYPE:

LOGICAL

DEFAULT:

FALSE

OPTIONS:

FALSE use all integrals in decomposed format

TRUE transform all RI or Cholesky integral back to conventional format

RECOMMENDATION:

By default all integrals are used in decomposed format allowing significant reduction of memory use. If all integrals are transformed back (TRUE option) no memory reduction is achieved and decomposition error is introduced, however, the integral transformation is performed significantly faster and conventional CC/EOM algorithms are used.

**CC_DOV_THRESH**

Specifies the minimum allowed values for the coupled-cluster energy denominators. Smaller values are replaced by this constant during early iterations only, so the final results are unaffected, but initial convergence is improved when the guess is poor.

TYPE:

DOUBLE

DEFAULT:

2502 Corresponding to 0.25

OPTIONS:

$abcde$ Integer code is mapped to $abc \times 10^{-de}$

RECOMMENDATION:

Increase to 0.5 or 0.75 for non-convergent coupled-cluster calculations.

**CC_DO_DYSON_EE**

Whether excited state Dyson orbitals will be calculated for EOM-IP/EA-CCSD calculations.

TYPE:

LOGICAL

DEFAULT:

FALSE (the option must be specified to run this calculation)

OPTIONS:

TRUE/FALSE

RECOMMENDATION:

none

**CC_DO_DYSON**

Whether ground state Dyson orbitals will be calculated for EOM-IP/EA-CCSD calculations.

TYPE:

LOGICAL

DEFAULT:

FALSE (the option must be specified to run this calculation)

OPTIONS:

TRUE/FALSE

RECOMMENDATION:

none

**CC_EOM_2PA**

Whether or not the transition moments and cross-sections for two-photon absorption will be calculated. By default, the transition moments are calculated between the CCSD reference and the EOM-CCSD target states. In order to calculate transition moments between a set of EOM-CCSD states and another EOM-CCSD state, the CC_STATE_TO_OPT must be specified for this state.

TYPE:

INTEGER

DEFAULT:

0 (do not compute 2PA transition moments)

OPTIONS:

1 Compute 2PA using the fastest algorithm (use $\tilde{\sigma}$-intermediates for canonical and $\sigma$-intermediates for RI/CD response calculations).

2 Use $\sigma$-intermediates for 2PA response equation calculations.

3 Use $\tilde{\sigma}$-intermediates for 2PA response equation calculations.

RECOMMENDATION:

Additional response equations (6 for each target state) will be solved, which increases the cost of calculations. The cost of 2PA moments is about 10 times that of energy calculation. Use the default algorithm. Setting CC_EOM_2PA $> 0$ turns on CC_TRANS_PROP.

**CC_EOM_PROP**

Whether or not the non-relaxed (expectation value) one-particle EOM-CCSD target state properties will be calculated. The properties currently include permanent dipole moment, the second moments $\langle X^2 \rangle$, $\langle Y^2 \rangle$, and $\langle Z^2 \rangle$ of electron density, and the total $\langle R^2 \rangle = \langle X^2 \rangle + \langle Y^2 \rangle + \langle Z^2 \rangle$ (in atomic units). Incompatible with JOBTYPE=FORCE, OPT, FREQ.

TYPE:

LOGICAL

DEFAULT:

FALSE (no one-particle properties will be calculated)

OPTIONS:

FALSE, TRUE

RECOMMENDATION:

Additional equations (EOM-CCSD equations for the left eigenvectors) need to be solved for properties, approximately doubling the cost of calculation for each irrep. The cost of the one-particle properties calculation itself is low. The one-particle density of an EOM-CCSD target state can be analyzed with NBO or libwfa packages by specifying the state with CC_STATE_TO_OPT and requesting NBO = TRUE and CC_EOM_PROP = TRUE.

**CC_E_CONV**

Convergence desired on the change in total energy, between iterations.

TYPE:

INTEGER

DEFAULT:

10

OPTIONS:

$n$ $10^{-n}$ convergence criterion.

RECOMMENDATION:

None

**CC_FNO_THRESH**

Initialize the FNO truncation and sets the threshold to be used for both cutoffs (OCCT and POVO)

TYPE:

INTEGER

DEFAULT:

None

OPTIONS:

| | |
|---|---|
| range | 0000-10000 |
| $abcd$ | Corresponding to $ab.cd\%$ |

RECOMMENDATION:

None

**CC_FNO_USEPOP**

Selection of the truncation scheme

TYPE:

INTEGER

DEFAULT:

1 OCCT

OPTIONS:

0 POVO

RECOMMENDATION:

None

**CC_FULLRESPONSE**

Fully relaxed properties (including orbital relaxation terms) will be computed. The variable CC_REF_PROP must be also set to TRUE.

TYPE:

LOGICAL

DEFAULT:

FALSE (no orbital response will be calculated)

OPTIONS:

FALSE, TRUE

RECOMMENDATION:

Not available for non UHF/RHF references and for the methods that do not have analytic gradients (*e.g.*, QCISD).

**CC_HESS_THRESH**

Minimum allowed value for the orbital Hessian. Smaller values are replaced by this constant.

TYPE:

DOUBLE

DEFAULT:

102 Corresponding to 0.01

OPTIONS:

$abcde$ Integer code is mapped to $abc \times 10^{-de}$

RECOMMENDATION:

None

**CC_INCL_CORE_CORR**

Whether to include the correlation contribution from frozen core orbitals in non iterative (2) corrections, such as OD(2) and CCSD(2).

TYPE:

LOGICAL

DEFAULT:

TRUE

OPTIONS:

TRUE FALSE

RECOMMENDATION:

Use the default unless no core-valence or core correlation is desired (*e.g.*, for comparison with other methods or because the basis used cannot describe core correlation).

**CC_ITERATE_ON**

In active space calculations, use a “mixed” iteration procedure if the value is greater than 0. Then if the RMS orbital gradient is larger than the value of CC_THETA_GRAD_THRESH, micro-iterations will be performed to converge the occupied-virtual mixing angles for the current active space. The maximum number of space iterations is given by this option.

TYPE:

INTEGER

DEFAULT:

0

OPTIONS:

$n$ Up to $n$ occupied-virtual iterations per overall cycle

RECOMMENDATION:

Can be useful for non-convergent active space calculations

**CC_ITERATE_OV**

In active space calculations, use a “mixed” iteration procedure if the value is greater than 0. Then, if the RMS orbital gradient is larger than the value of CC_THETA_GRAD_THRESH, micro-iterations will be performed to converge the occupied-virtual mixing angles for the current active space. The maximum number of such iterations is given by this option.

TYPE:

INTEGER

DEFAULT:

0 No “mixed” iterations

OPTIONS:

$n$ Up to $n$ occupied-virtual iterations per overall cycle

RECOMMENDATION:

Can be useful for non-convergent active space calculations.

**CC_MAX_ITER**

Maximum number of iterations to optimize the coupled-cluster energy.

TYPE:

INTEGER

DEFAULT:

200

OPTIONS:

$n$ up to $n$ iterations to achieve convergence.

RECOMMENDATION:

None

**CC_MEMORY**

Specifies the maximum size, in Mb, of the buffers for in-core storage of block-tensors in CCMAN and CCMAN2.

TYPE:

INTEGER

DEFAULT:

50% of MEM_TOTAL. If MEM_TOTAL is not set, use 1.5 Gb. A minimum of 192 Mb is hard-coded.

OPTIONS:

$n$ Integer number of Mb

RECOMMENDATION:

Larger values can give better I/O performance and are recommended for systems with large memory (add to your *.qchemrc* file. When running CCMAN2 exclusively on a node, CC_MEMORY should be set to 75–80% of the total available RAM. )

**CC_MP2NO_GRAD**

If CC_MP2NO_GUESS is TRUE, what kind of one-particle density matrix is used to make the guess orbitals?

TYPE:

LOGICAL

DEFAULT:

FALSE

OPTIONS:

TRUE 1 PDM from MP2 gradient theory.

FALSE 1 PDM expanded to $2^{\mathrm{nd}}$ order in perturbation theory.

RECOMMENDATION:

The two definitions give generally similar performance.

**CC_MP2NO_GUESS**

Will guess orbitals be natural orbitals of the MP2 wave function? Alternatively, it is possible to use an effective one-particle density matrix to define the natural orbitals.

TYPE:

LOGICAL

DEFAULT:

FALSE

OPTIONS:

TRUE Use natural orbitals from an MP2 one-particle density matrix (see *CC_MP2NO_GRAD*).

FALSE Use current molecular orbitals from SCF.

RECOMMENDATION:

None

**CC_ORBS_PER_BLOCK**

Specifies target (and maximum) size of blocks in orbital space.

TYPE:

INTEGER

DEFAULT:

16

OPTIONS:

$n$ Orbital block size of $n$ orbitals.

RECOMMENDATION:

None

**CC_POL**

Whether or not the static polarizability for the CCSD wave function will be calculated.

TYPE:

LOGICAL

DEFAULT:

FALSE (CCSD static polarizability will not be calculated)

OPTIONS:

FALSE, TRUE

RECOMMENDATION:

Static polarizabilities are expensive since they require solving three additional response equations. Do no request this property unless you need it.

**CC_PRECONV_FZ**

In active space methods, whether to pre-converge other wave function variables for fixed initial guess of active space.

TYPE:

INTEGER

DEFAULT:

0

OPTIONS:

0 No pre-iterations before active space optimization begins.

$n$ Maximum number of pre-iterations via this procedure.

RECOMMENDATION:

None

**CC_PRECONV_T2Z_EACH**

Whether to pre-converge the cluster amplitudes before each change of the orbitals in optimized orbital coupled-cluster methods. The maximum number of iterations in this preconvergence procedure is given by the value of this parameter.

TYPE:

INTEGER

DEFAULT:

0 (FALSE)

OPTIONS:

0 No pre-convergence before orbital optimization.

$n$ Up to $n$ iterations in this pre-convergence procedure.

RECOMMENDATION:

A very slow last resort option for jobs that do not converge.

**CC_PRECONV_T2Z**

Whether to pre-converge the cluster amplitudes before beginning orbital optimization in optimized orbital cluster methods.

TYPE:

INTEGER

DEFAULT:

0 (FALSE)

10 If CC_RESTART, CC_RESTART_NO_SCF or CC_MP2NO_GUESS are TRUE

OPTIONS:

0 No pre-convergence before orbital optimization.

$n$ Up to $n$ iterations in this pre-convergence procedure.

RECOMMENDATION:

Experiment with this option in cases of convergence failure.

**CC_PRINT**

Controls the output from post-MP2 coupled-cluster module of Q-CHEM

TYPE:

INTEGER

DEFAULT:

1

OPTIONS:

$0-7$ higher values can lead to deforestation…

RECOMMENDATION:

Increase if you need more output and don’t like trees

**CC_QCCD_THETA_SWITCH**

QCCD calculations switch from OD to QCCD when the rotation gradient is below this threshold [$10^{-n}$]

TYPE:

INTEGER

DEFAULT:

2 $10^{-2}$ switchover

OPTIONS:

$n$ $10^{-n}$ switchover

RECOMMENDATION:

None

**CC_REF_PROP_TE**

Request for calculation of non-relaxed two-particle CCSD properties. The two-particle properties currently include $\langle S^2 \rangle$. The one-particle properties also will be calculated, since the additional cost of the one-particle properties calculation is inferior compared to the cost of $\langle S^2 \rangle$. The variable CC_REF_PROP must be also set to TRUE.

TYPE:

LOGICAL

DEFAULT:

FALSE (no two-particle properties will be calculated)

OPTIONS:

FALSE, TRUE

RECOMMENDATION:

The two-particle properties are computationally expensive, since they require calculation and use of the two-particle density matrix (the cost is approximately the same as the cost of an analytic gradient calculation). Do not request the two-particle properties unless you really need them.

**CC_REF_PROP**

Whether or not the non-relaxed (expectation value) or full response (including orbital relaxation terms) one-particle CCSD properties will be calculated. The properties currently include permanent dipole moment, the second moments $\langle X^2 \rangle$, $\langle Y^2 \rangle$, and $\langle Z^2 \rangle$ of electron density, and the total $\langle R^2 \rangle = \langle X^2 \rangle + \langle Y^2 \rangle + \langle Z^2 \rangle$ (in atomic units). Incompatible with JOBTYPE=FORCE, OPT, FREQ.

TYPE:

LOGICAL

DEFAULT:

FALSE (no one-particle properties will be calculated)

OPTIONS:

FALSE, TRUE

RECOMMENDATION:

Additional equations need to be solved (lambda CCSD equations) for properties with the cost approximately the same as CCSD equations. Use the default if you do not need properties. The cost of the properties calculation itself is low. The CCSD one-particle density can be analyzed with NBO package by specifying NBO=TRUE, CC_REF_PROP=TRUE and JOBTYPE=FORCE.

**CC_RESET_THETA**

The reference MO coefficient matrix is reset every n iterations to help overcome problems associated with the theta metric as theta becomes large.

TYPE:

INTEGER

DEFAULT:

15

OPTIONS:

$n$ $n$ iterations between resetting orbital rotations to zero.

RECOMMENDATION:

None

**CC_RESTART_NO_SCF**

Should an optimized orbital coupled cluster calculation begin with optimized orbitals from a previous calculation? When TRUE, molecular orbitals are initially orthogonalized, and CC_PRECONV_T2Z and CC_CANONIZE are set to TRUE while other guess options are set to FALSE

TYPE:

LOGICAL

DEFAULT:

FALSE

OPTIONS:

TRUE/FALSE

RECOMMENDATION:

None

**CC_RESTART**

Allows an optimized orbital coupled cluster calculation to begin with an initial guess for the orbital transformation matrix U other than the unit vector. The scratch file from a previous run must be available for the U matrix to be read successfully.

TYPE:

LOGICAL

DEFAULT:

FALSE

OPTIONS:

| | |
|---|---|
| FALSE | Use unit initial guess. |
| TRUE | Activates CC_PRECONV_T2Z, CC_CANONIZE, and<br>turns off CC_MP2NO_GUESS |

RECOMMENDATION:

Useful for restarting a job that did not converge, if files were saved.

**CC_RESTR_AMPL**

Controls the restriction on amplitudes is there are restricted orbitals

TYPE:

INTEGER

DEFAULT:

1

OPTIONS:

| | |
|---|---|
| 0 | All amplitudes are in the full space |
| 1 | Amplitudes are restricted, if there are restricted orbitals |

RECOMMENDATION:

None

**CC_RESTR_TRIPLES**

Controls which space the triples correction is computed in

TYPE:

INTEGER

DEFAULT:

0

OPTIONS:

| | |
|---|---|
| 0 | Triples are computed in the full space |
| 1 | Triples are restricted to the active space |

RECOMMENDATION:

None

**CC_REST_AMPL**

Forces the integrals, $T$, and $R$ amplitudes to be determined in the full space even though the CC_REST_OCC and CC_REST_VIR keywords are used.

TYPE:

LOGICAL

DEFAULT:

TRUE

OPTIONS:

| | |
|---|---|
| FALSE | Do apply restrictions |
| TRUE | Do not apply restrictions |

RECOMMENDATION:

None

**CC_REST_OCC**

Sets the number of restricted occupied orbitals including frozen occupied orbitals.

TYPE:

INTEGER

DEFAULT:

0

OPTIONS:

| | |
|---|---|
| $n$ | Restrict $n$ occupied orbitals. |

RECOMMENDATION:

None

**CC_REST_TRIPLES**

Restricts $R_3$ amplitudes to the active space, *i.e.*, one electron should be removed from the active occupied orbital and one electron should be added to the active virtual orbital.

TYPE:

INTEGER

DEFAULT:

1

OPTIONS:

| | |
|---|---|
| 1 | Applies the restrictions |

RECOMMENDATION:

None

**CC_REST_VIR**

Sets the number of restricted virtual orbitals including frozen virtual orbitals.

TYPE:

INTEGER

DEFAULT:

0

OPTIONS:

$n$ Restrict $n$ virtual orbitals.

RECOMMENDATION:

None

**CC_SCALE_AMP**

If not 0, scales down the step for updating coupled-cluster amplitudes in cases of problematic convergence.

TYPE:

INTEGER

DEFAULT:

0 no scaling

OPTIONS:

$abcd$ Integer code is mapped to $abcd \times 10^{-2}$, *e.g.*, 90 corresponds to 0.9

RECOMMENDATION:

Use 0.9 or 0.8 for non convergent coupled-cluster calculations.

**CC_STATE_TO_OPT**

Specifies which state to optimize.

TYPE:

INTEGER ARRAY

DEFAULT:

None

OPTIONS:

$[i,j]$ optimize the $j$th state of the $i$th irrep.

RECOMMENDATION:

None

**CC_SYMMETRY**

Controls the use of symmetry in coupled-cluster calculations

TYPE:

LOGICAL

DEFAULT:

TRUE

OPTIONS:

TRUE Use the point group symmetry of the molecule

FALSE Do not use point group symmetry (all states will be of $A$ symmetry).

RECOMMENDATION:

It is automatically turned off for any finite difference calculations, *e.g.* second derivatives.

**CC_THETA_CONV**

Convergence criterion on the RMS difference between successive sets of orbital rotation angles [$10^{-n}$].

TYPE:

INTEGER

DEFAULT:

5 Energies

6 Gradients

OPTIONS:

$n$ $10^{-n}$ convergence criterion.

RECOMMENDATION:

Use default

**CC_THETA_GRAD_CONV**

Convergence desired on the RMS gradient of the energy with respect to orbital rotation angles [$10^{-n}$].

TYPE:

INTEGER

DEFAULT:

7 Energies

8 Gradients

OPTIONS:

$n$ $10^{-n}$ convergence criterion.

RECOMMENDATION:

Use default

**CC_THETA_GRAD_THRESH**

RMS orbital gradient threshold [$10^{-n}$] above which “mixed iterations” are performed in active space calculations if CC_ITERATE_OV is TRUE.

TYPE:

INTEGER

DEFAULT:

2

OPTIONS:

$n$ $10^{-n}$ threshold.

RECOMMENDATION:

Can be made smaller if convergence difficulties are encountered.

**CC_THETA_STEPSIZE**

Scale factor for the orbital rotation step size. The optimal rotation steps should be approximately equal to the gradient vector.

TYPE:

INTEGER

DEFAULT:

| | |
|---|---|
| 100 | Corresponding to 1.0 |

OPTIONS:

| | |
|---|---|
| $abcde$ | Integer code is mapped to $abc \times 10^{-de}$<br>If the initial step is smaller than 0.5, the program will increase step<br>when gradients are smaller than the value of THETA_GRAD_THRESH,<br>up to a limit of 0.5. |

RECOMMENDATION:

Try a smaller value in cases of poor convergence and very large orbital gradients. For example, a value of 01001 translates to 0.1

**CC_TRANS_PROP**

Whether or not the transition dipole moment (in atomic units) and oscillator strength for the EOM-CCSD target states will be calculated. By default, the transition dipole moment is calculated between the CCSD reference and the EOM-CCSD target states. In order to calculate transition dipole moment between a set of EOM-CCSD states and another EOM-CCSD state, the CC_STATE_TO_OPT must be specified for this state.

TYPE:

LOGICAL

DEFAULT:

FALSE (no transition dipole and oscillator strength will be calculated)

OPTIONS:

FALSE, TRUE

RECOMMENDATION:

Additional equations (for the left EOM-CCSD eigenvectors plus lambda CCSD equations in case if transition properties between the CCSD reference and EOM-CCSD target states are requested) need to be solved for transition properties, approximately doubling the computational cost. The cost of the transition properties calculation itself is low.

**CC_T_CONV**

Convergence criterion on the RMS difference between successive sets of coupled-cluster doubles amplitudes [$10^{-n}$]

TYPE:

INTEGER

DEFAULT:

| | |
|---|---|
| 8 | energies |
| 10 | gradients |

OPTIONS:

| | |
|---|---|
| $n$ | $10^{-n}$ convergence criterion. |

RECOMMENDATION:

Use default

**CC_Z_CONV**

Convergence criterion on the RMS difference between successive doubles $Z$-vector amplitudes $[10^{-n}]$.

TYPE:

INTEGER

DEFAULT:

| | |
|---|---|
| 8 | Energies |
| 10 | Gradients |

OPTIONS:

$n$ $10^{-n}$ convergence criterion.

RECOMMENDATION:

Use Default

**CDFTCI_PRINT**

Controls level of output from CDFT-CI procedure to Q-CHEM output file.

TYPE:

INTEGER

DEFAULT:

0

OPTIONS:

| | |
|---|---|
| 0 | Only print energies and coefficients of CDFT-CI final states |
| 1 | Level 0 plus CDFT-CI overlap, Hamiltonian, and population matrices |
| 2 | Level 1 plus eigenvectors and eigenvalues of the CDFT-CI population matrix |
| 3 | Level 2 plus promolecule orbital coefficients and energies |

RECOMMENDATION:

Level 3 is primarily for program debugging; levels 1 and 2 may be useful for analyzing the coupling elements

**CDFTCI_RESTART**

To be used in conjunction with CDFTCI_STOP, this variable causes CDFT-CI to read already-converged states from disk and begin SCF convergence on later states. Note that the same *$cdft* section must be used for the stopped calculation and the restarted calculation.

TYPE:

INTEGER

DEFAULT:

0

OPTIONS:

$n$ Start calculations on state $n+1$

RECOMMENDATION:

Use this setting in conjunction with CDFTCI_STOP.

**CDFTCI_SKIP_PROMOLECULES**

Skips promolecule calculations and allows fractional charge and spin constraints to be specified directly.

TYPE:

BOOLEAN

DEFAULT:

FALSE

OPTIONS:

FALSE Standard CDFT-CI calculation is performed.

TRUE Use the given charge/spin constraints directly, with no promolecule calculations.

RECOMMENDATION:

Setting to TRUE can be useful for scanning over constraint values.

**CDFTCI_STOP**

The CDFT-CI procedure involves performing independent SCF calculations on distinct constrained states. It sometimes occurs that the same convergence parameters are not successful for all of the states of interest, so that a CDFT-CI calculation might converge one of these diabatic states but not the next. This variable allows a user to stop a CDFT-CI calculation after a certain number of states have been converged, with the ability to restart later on the next state, with different convergence options.

TYPE:

INTEGER

DEFAULT:

0

OPTIONS:

$n$ Stop after converging state $n$ (the first state is state $1$)

$0$ Do not stop early

RECOMMENDATION:

Use this setting if some diabatic states converge but others do not.

**CDFTCI_SVD_THRESH**

By default, a symmetric orthogonalization is performed on the CDFT-CI matrix before diagonalization. If the CDFT-CI overlap matrix is nearly singular (*i.e.*, some of the diabatic states are nearly degenerate), then this orthogonalization can lead to numerical instability. When computing $\mathbf{S}^{-1/2}$, eigenvalues smaller than $10^{-\mathrm{CDFTCI\_SVD\_THRESH}}$ are discarded.

TYPE:

INTEGER

DEFAULT:

4

OPTIONS:

$n$ for a threshold of $10^{-n}$.

RECOMMENDATION:

Can be decreased if numerical instabilities are encountered in the final diagonalization.

**CDFTCI**

Initiates a constrained DFT-configuration interaction calculation

TYPE:

LOGICAL

DEFAULT:

FALSE

OPTIONS:

| | |
|---|---|
| TRUE | Perform a CDFT-CI Calculation |
| FALSE | No CDFT-CI |

RECOMMENDATION:

Set to TRUE if a CDFT-CI calculation is desired.

**CDFT_BECKE_POP**

Whether the calculation should print the Becke atomic charges at convergence

TYPE:

LOGICAL

DEFAULT:

TRUE

OPTIONS:

| | |
|---|---|
| TRUE | Print Populations |
| FALSE | Do not print them |

RECOMMENDATION:

Use the default. Note that the Mulliken populations printed at the end of an SCF run will not typically add up to the prescribed constraint value. Only the Becke populations are guaranteed to satisfy the user-specified constraints.

**CDFT_CRASHONFAIL**

Whether the calculation should crash or not if the constraint iterations do not converge.

TYPE:

LOGICAL

DEFAULT:

TRUE

OPTIONS:

| | |
|---|---|
| TRUE | Crash if constraint iterations do not converge. |
| FALSE | Do not crash. |

RECOMMENDATION:

Use the default.

**CDFT_LAMBDA_MODE**

Allows CDFT potentials to be specified directly, instead of being determined as Lagrange multipliers.

TYPE:

BOOLEAN

DEFAULT:

FALSE

OPTIONS:

FALSE Standard CDFT calculations are used.

TRUE Instead of specifying target charge and spin constraints, use the values from the input deck as the value of the Becke weight potential

RECOMMENDATION:

Should usually be set to FALSE. Setting to TRUE can be useful to scan over different strengths of charge or spin localization, as convergence properties are improved compared to regular CDFT(-CI) calculations.

**CDFT_POSTDIIS**

Controls whether the constraint is enforced after DIIS extrapolation.

TYPE:

LOGICAL

DEFAULT:

TRUE

OPTIONS:

TRUE Enforce constraint after DIIS

FALSE Do not enforce constraint after DIIS

RECOMMENDATION:

Use the default unless convergence problems arise, in which case it may be beneficial to experiment with setting CDFT_POSTDIIS to FALSE. With this option set to TRUE, energies should be variational after the first iteration.

**CDFT_PREDIIS**

Controls whether the constraint is enforced before DIIS extrapolation.

TYPE:

LOGICAL

DEFAULT:

FALSE

OPTIONS:

TRUE Enforce constraint before DIIS

FALSE Do not enforce constraint before DIIS

RECOMMENDATION:

Use the default unless convergence problems arise, in which case it may be beneficial to experiment with setting CDFT_PREDIIS to TRUE. Note that it is possible to enforce the constraint both before and after DIIS by setting both CDFT_PREDIIS and CDFT_POSTDIIS to TRUE.

**CDFT_THRESH**

Threshold that determines how tightly the constraint must be satisfied.

TYPE:

INTEGER

DEFAULT:

5

OPTIONS:

N Constraint is satisfied to within $10^{-N}$.

RECOMMENDATION:

Use the default unless problems occur.

**CDFT**

Initiates a constrained DFT calculation

TYPE:

LOGICAL

DEFAULT:

FALSE

OPTIONS:

| | |
|---|---|
| TRUE | Perform a Constrained DFT Calculation |
| FALSE | No Density Constraint |

RECOMMENDATION:

Set to TRUE if a Constrained DFT calculation is desired.

**CD_ALGORITHM**

Determines the algorithm for MP2 integral transformations.

TYPE:

STRING

DEFAULT:

Program determined.

OPTIONS:

| | |
|---|---|
| DIRECT | Uses fully direct algorithm (energies only). |
| SEMI_DIRECT | Uses disk-based semi-direct algorithm. |
| LOCAL_OCCUPIED | Alternative energy algorithm (see 5.4.1). |

RECOMMENDATION:

Semi-direct is usually most efficient, and will normally be chosen by default.

**CFMM_ORDER**

Controls the order of the multipole expansions in CFMM calculation.

TYPE:

INTEGER

DEFAULT:

| | |
|---|---|
| 15 | For single point SCF accuracy |
| 25 | For tighter convergence (optimizations) |

OPTIONS:

$n$ Use multipole expansions of order $n$

RECOMMENDATION:

Use the default.

**CHARGE_CHARGE_REPULSION**

The repulsive Coulomb interaction parameter for YinYang atoms.

TYPE:

INTEGER

DEFAULT:

550

OPTIONS:

$n$ Use Q = $n \times 10^{-3}$

RECOMMENDATION:

The repulsive Coulomb potential maintains bond lengths involving YinYang atoms with the potential $V(r) = Q/r$. The default is parameterized for carbon atoms.

**CHELPG_DX**

Sets the rectangular grid spacing for the traditional Cartesian CHELPG grid or the spacing between concentric Lebedev shells (when the variables CHELPG_HA and CHELPG_H are specified as well).

TYPE:

INTEGER

DEFAULT:

6

OPTIONS:

$N$ Corresponding to a grid space of $N/20$, in Å.

RECOMMENDATION:

Use the default (which corresponds to the "dense grid" of Breneman and Wiberg[5]), unless the cost is prohibitive, in which case a larger value can be selected. Note that this default value is set with the Cartesian grid in mind and not the Lebedev grid. In the Lebedev case, a larger value can typically be used.

**CHELPG_HA**

Sets the Lebedev grid to use for non-hydrogen atoms.

TYPE:

INTEGER

DEFAULT:

NONE

OPTIONS:

$N$ Corresponding to a number of points in a Lebedev grid (see Section 4.4.5.1.

RECOMMENDATION:

None.

**CHELPG_HEAD**

Sets the "head space"[5] (radial extent) of the CHELPG grid.

TYPE:

INTEGER

DEFAULT:

30

OPTIONS:

$N$ Corresponding to a head space of $N/10$, in Å.

RECOMMENDATION:

Use the default, which is the value recommended by Breneman and Wiberg[5].

**CHELPG_H**

Sets the Lebedev grid to use for hydrogen atoms.

TYPE:

INTEGER

DEFAULT:

NONE

OPTIONS:

| | |
|---|---|
| $N$ | Corresponding to a number of points in a Lebedev grid. |

RECOMMENDATION:

CHELPG_H must always be less than or equal to CHELPG_HA. If it is greater, it will automatically be set to the value of CHELPG_HA.

**CHELPG**

Controls the calculation of CHELPG charges.

TYPE:

LOGICAL

DEFAULT:

FALSE

OPTIONS:

| | |
|---|---|
| FALSE | Do not calculate CHELPG charges. |
| TRUE | Compute CHELPG charges. |

RECOMMENDATION:

Set to TRUE if desired. For large molecules, there is some overhead associated with computing CHELPG charges, especially if the number of grid points is large.

**CHILD_MP_ORDERS**

The multipole orders included in the prepared FERFs. The last digit specifies how many multipoles to compute, and the digits in the front specify the multipole orders: 1: dipole (D); 2: quadrupole (Q); 3: octopole (O).

TYPE:

INTEGER

DEFAULT:

0

OPTIONS:

| | |
|---|---|
| 11 | D |
| 122 | DQ |
| 1233 | DQO |

RECOMMENDATION:

Use 122 (DQ) when FERF is needed.

**CHILD_MP**

Compute FERFs for fragments and use them as the basis for SCFMI calculations.

TYPE:

BOOLEAN

DEFAULT:

FALSE

OPTIONS:

FALSE Do not compute FERFs (use the full AO span of each fragment).

TRUE Compute fragment FERFs.

RECOMMENDATION:

Use FERFs to compute polarization energy when large basis sets are used. In an “EDA2" calculation, this *$rem* variable is set based on the given option automatically.

**CHOLESKY_TOL**

Tolerance of Cholesky decomposition of two-electron integrals

TYPE:

INTEGER

DEFAULT:

3

OPTIONS:

$n$ Corresponds to a tolerance of $10^{-n}$

RECOMMENDATION:

2 - qualitative calculations, 3 - appropriate for most cases, 4 - quantitative (error in total energy typically less than 1 $\mu$hartree)

**CISTR_PRINT**

Controls level of output.

TYPE:

LOGICAL

DEFAULT:

FALSE Minimal output.

OPTIONS:

TRUE Increase output level.

RECOMMENDATION:

None

**CIS_AMPL_ANAL**

Perform additional analysis of CIS and TDDFT excitation amplitudes, including generation of natural transition orbitals, excited-state multipole moments, and Mulliken analysis of the excited state densities and particle/hole density matrices.

TYPE:

LOGICAL

DEFAULT:

FALSE

OPTIONS:

TRUE Perform additional amplitude analysis.

FALSE Do not perform additional analysis.

RECOMMENDATION:

None

**CIS_CONVERGENCE**

CIS is considered converged when error is less than $10^{-\mathrm{CIS\_CONVERGENCE}}$

TYPE:

INTEGER

DEFAULT:

6 CIS convergence threshold $10^{-6}$

OPTIONS:

$n$ Corresponding to $10^{-n}$

RECOMMENDATION:

None

**CIS_DER_NUMSTATE**

Determines among how many states we calculate non-adiabatic couplings. These states must be specified in the *$derivative_coupling* section.

TYPE:

INTEGER

DEFAULT:

0

OPTIONS:

0 Do not calculate non-adiabatic couplings.

$n$ Calculate $n(n-1)/2$ pairs of non-adiabatic couplings.

RECOMMENDATION:

None.

**CIS_DIABATH_DECOMPOSE**

Decide whether or not to decompose the diabatic coupling into Coulomb, exchange, and one-electron terms.

TYPE:

LOGICAL

DEFAULT:

FALSE Do not decompose the diabatic coupling.

OPTIONS:

TRUE

RECOMMENDATION:

These decompositions are most meaningful for electronic excitation transfer processes. Currently, available only for CIS, not for TDDFT diabatic states.

**CIS_DYNAMIC_MEM**

Controls whether to use static or dynamic memory in CIS and TDDFT calculations.

TYPE:

LOGICAL

DEFAULT:

FALSE

OPTIONS:

| | |
|---|---|
| FALSE | Partly use static memory |
| TRUE | Fully use dynamic memory |

RECOMMENDATION:

The default control requires static memory (MEM_STATIC) to hold a temporary array whose minimum size is $OV$ × CIS_N_ROOTS. For a large calculation, one has to specify a large value for MEM_STATIC, which is not recommended (see Chapter 2). Therefore, it is recommended to use dynamic memory for large calculations.

**CIS_GUESS_DISK_TYPE**

Determines the type of guesses to be read from disk

TYPE:

INTEGER

DEFAULT:

Nil

OPTIONS:

| | |
|---|---|
| 0 | Read triplets only |
| 1 | Read triplets and singlets |
| 2 | Read singlets only |

RECOMMENDATION:

Must be specified if CIS_GUESS_DISK is TRUE.

**CIS_GUESS_DISK**

Read the CIS guess from disk (previous calculation).

TYPE:

LOGICAL

DEFAULT:

FALSE

OPTIONS:

| | |
|---|---|
| FALSE | Create a new guess. |
| TRUE | Read the guess from disk. |

RECOMMENDATION:

Requires a guess from previous calculation.

**CIS_MOMENTS**

Controls calculation of excited-state (CIS or TDDFT) multipole moments

TYPE:

LOGICAL

DEFAULT:

FALSE

OPTIONS:

| | |
|---|---|
| FALSE | Do not calculate excited-state moments. |
| TRUE | Calculate moments for each excited state. |

RECOMMENDATION:

Set to TRUE if excited-state moments are desired. (This is a trivial additional calculation.) The MULTIPOLE_ORDER controls how many multipole moments are printed.

**CIS_MULLIKEN**

Controls Mulliken and Löwdin population analyses for excited-state particle and hole density matrices.

TYPE:

LOGICAL

DEFAULT:

FALSE

OPTIONS:

| | |
|---|---|
| FALSE | Do not perform particle/hole population analysis. |
| TRUE | Perform both Mulliken and Löwdin analysis of the particle and hole density matrices for each excited state. |

RECOMMENDATION:

Set to TRUE if desired. This represents a trivial additional calculation.

**CIS_N_ROOTS**

Sets the number of CI-Singles (CIS) excited state roots to find.

TYPE:

INTEGER

DEFAULT:

0 Do not look for any excited states.

OPTIONS:

$n$ $n > 0$ Looks for $n$ CIS excited states.

RECOMMENDATION:

None

**CIS_RELAXED_DENSITY**

Use the relaxed CIS density for attachment/detachment density analysis.

TYPE:

LOGICAL

DEFAULT:

FALSE

OPTIONS:

| | |
|---|---|
| FALSE | Do not use the relaxed CIS density in analysis. |
| TRUE | Use the relaxed CIS density in analysis. |

RECOMMENDATION:

None

**CIS_S2_THRESH**

Determines whether a state is a singlet or triplet in unrestricted calculations.

TYPE:

INTEGER

DEFAULT:

120

OPTIONS:

$n$ Sets the $\langle \hat{S}^2 \rangle$ threshold to $n/100$

RECOMMENDATION:

For the default case, states with $\langle \hat{S}^2 \rangle > 1.2$ are treated as triplet states and other states are treated as singlets.

**CIS_SINGLETS**

Solve for singlet excited states in RCIS calculations (ignored for UCIS).

TYPE:

LOGICAL

DEFAULT:

TRUE

OPTIONS:

| | |
|---|---|
| TRUE | Solve for singlet states. |
| FALSE | Do not solve for singlet states. |

RECOMMENDATION:

None

**CIS_STATE_DERIV**

Sets CIS state for excited state optimizations and vibrational analysis.

TYPE:

INTEGER

DEFAULT:

0 Does not select any of the excited states.

OPTIONS:

$n$ Select the $n$th state.

RECOMMENDATION:

Check to see that the states do not change order during an optimization, due to state crossings.

**CIS_TRIPLETS**

Solve for triplet excited states in RCIS calculations (ignored for UCIS).

TYPE:

LOGICAL

DEFAULT:

TRUE

OPTIONS:

| | |
|---|---|
| TRUE | Solve for triplet states. |
| FALSE | Do not solve for triplet states. |

RECOMMENDATION:

None

**CM5**

Controls running of CM5 population analysis.

TYPE:

LOGICAL

DEFAULT:

FALSE

OPTIONS:

TRUE Calculate CM5 populations.

FALSE Do not calculate CM5 populations.

RECOMMENDATION:

None

**COMBINE_K**

Controls separate or combined builds for short-range and long-range K

TYPE:

LOGICAL

DEFAULT:

FALSE

OPTIONS:

FALSE (or 0) Build short-range and long-range K separately (twice as expensive as a global hybrid)

TRUE (or 1) Build short-range and long-range K together ($\approx$ as expensive as a global hybrid)

RECOMMENDATION:

Most pre-defined range-separated hybrid functionals in Q-CHEM use this feature by default. However, if a user-specified RSH is desired, it is necessary to manually turn this feature on.

**COMPLEX_CCMAN**

Requests complex-scaled or CAP-augmented CC/EOM calculations.

TYPE:

LOGICAL

DEFAULT:

FALSE

OPTIONS:

TRUE Engage complex CC/EOM code.

RECOMMENDATION:

Not available in CCMAN. Need to specify CAP strength or complex-scaling parameter in *$complex_ccman* section.

**COMPLEX_MIX**

Mix a certain percentage of the real part of the HOMO to the imaginary part of the LUMO.

TYPE:

INTEGER

DEFAULT:

0

OPTIONS:

0–100 The mix angle = $\pi$·COMPLEX_MIX/100.

RECOMMENDATION:

It may help find the stable complex solution (similar idea as SCF_GUESS_MIX).

**COMPLEX**

Run an SCF calculation with complex MOs using GEN_SCFMAN.

TYPE:

BOOLEAN

DEFAULT:

FALSE

OPTIONS:

| | |
|---|---|
| TRUE | Use complex orbitals. |
| FALSE | Use real orbitals. |

RECOMMENDATION:

Set to TRUE if desired.

**CORE_CHARACTER**

Selects how the core orbitals are determined in the frozen-core approximation.

TYPE:

INTEGER

DEFAULT:

0

OPTIONS:

| | |
|---|---|
| 0 | Use energy-based definition. |
| 1-4 | Use Mulliken-based definition (see Table 5.2 for details). |

RECOMMENDATION:

Use the default, unless performing calculations on molecules with heavy elements.

**CORE_IONIZE**

Indicates how orbitals are specified for reduced excitation spaces.

TYPE:

INTEGER

DEFAULT:

1

OPTIONS:

| | |
|---|---|
| 1 | all valence orbitals are listed in *$solute* section |
| 2 | only hole(s) are specified all other occupations same as ground state |

RECOMMENDATION:

For MOM + TDDFT this specifies the input form of the *$solute* section. If set to 1 all occupied orbitals must be specified, 2 only the empty orbitals to ignore must be specified.

**CORRELATION**

Specifies the correlation level of theory, either DFT or wave function-based.

TYPE:

STRING

DEFAULT:

None No Correlation

OPTIONS:

| | |
|---|---|
| None | No Correlation. |
| VWN | Vosko-Wilk-Nusair parameterization #5 |
| LYP | Lee-Yang-Parr |
| PW91, PW | GGA91 (Perdew) |
| PW92 | LSDA 92 (Perdew and Wang)[6] |
| PK09 | LSDA (Proynov-Kong)[7] |
| LYP(EDF1) | LYP(EDF1) parameterization |
| Perdew86, P86 | Perdew 1986 |
| PZ81, PZ | Perdew-Zunger 1981 |
| PBE | Perdew-Burke-Ernzerhof 1996 |
| TPSS | The correlation component of the TPSS functional |
| B94 | Becke 1994 correlation in fully analytic form |
| B94hyb | Becke 1994 correlation as above, but readjusted for use only within the hybrid scheme BR89B94hyb |
| PK06 | Proynov-Kong 2006 correlation (known also as “tLap” |
| (B88)OP | OP correlation[8], optimized for use with B88 exchange |
| (PBE)OP | OP correlation[8], optimized for use with PBE exchange |
| Wigner | Wigner |
| MP2 | |
| Local_MP2 | Local MP2 calculations (TRIM and DIM models) |
| CIS(D) | MP2-level correction to CIS for excited states |
| MP3 | |
| MP4SDQ | |
| MP4 | |
| CCD | |
| CCD(2) | |
| CCSD | |
| CCSD(T) | |
| CCSD(2) | |
| QCISD | |
| QCISD(T) | |
| OD | |
| OD(T) | |
| OD(2) | |
| VOD | |
| VOD(2) | |
| QCCD | |
| VQCCD | |

RECOMMENDATION:

Consult the literature and reviews for guidance.

**CPSCF_NSEG**

Controls the number of segments used to calculate the CPSCF equations.

TYPE:

INTEGER

DEFAULT:

0

OPTIONS:

| | |
|---|---|
| 0 | Do not solve the CPSCF equations in segments. |
| $n$ | User-defined. Use $n$ segments when solving the CPSCF equations. |

RECOMMENDATION:

Use the default.

**CUBEFILE_STATE**

Determines which excited state is used to generate cube files

TYPE:

INTEGER

DEFAULT:

None

OPTIONS:

| | |
|---|---|
| $n$ | Generate cube files for the $n$th excited state |

RECOMMENDATION:

None

**CUDA_RI-MP2**

Enables GPU implementation of RI-MP2

TYPE:

LOGICAL

DEFAULT:

FALSE

OPTIONS:

| | |
|---|---|
| FALSE | GPU-enabled MGEMM off |
| TRUE | GPU-enabled MGEMM on |

RECOMMENDATION:

Necessary to set to 1 in order to run GPU-enabled RI-MP2

**CUTOCC**

Specifies occupied orbital cutoff.

TYPE:

INTEGER

DEFAULT:

50

OPTIONS:

| | |
|---|---|
| 0-200 | CUTOFF = CUTOCC/100 |

RECOMMENDATION:

None

**CUTVIR**

Specifies virtual orbital cutoff.

TYPE:

INTEGER

DEFAULT:

0 No truncation

OPTIONS:

0-100 CUTOFF = CUTVIR/100

RECOMMENDATION:

None

**DEUTERATE**

Requests that all hydrogen atoms be replaces with deuterium.

TYPE:

LOGICAL

DEFAULT:

FALSE Do not replace hydrogens.

OPTIONS:

TRUE Replace hydrogens with deuterium.

RECOMMENDATION:

Replacing hydrogen atoms reduces the fastest vibrational frequencies by a factor of 1.4, which allow for a larger fictitious mass and time step in ELMD calculations. There is no reason to replace hydrogens in BOMD calculations.

**DFPT_EXCHANGE**

Specifies the secondary functional in a HFPC/DFPC calculation.

TYPE:

STRING

DEFAULT:

None

OPTIONS:

None

RECOMMENDATION:

See reference for recommended basis set, functional, and grid pairings.

**DFPT_XC_GRID**

Specifies the secondary grid in a HFPC/DFPC calculation.

TYPE:

STRING

DEFAULT:

None

OPTIONS:

None

RECOMMENDATION:

See reference for recommended basis set, functional, and grid pairings.

**DFTVDW_ALPHA1**

Parameter in XDM calculation with higher-order terms

TYPE:

INTEGER

DEFAULT:

83

OPTIONS:

10-1000

RECOMMENDATION:

None

**DFTVDW_ALPHA2**

Parameter in XDM calculation with higher-order terms.

TYPE:

INTEGER

DEFAULT:

155

OPTIONS:

10-1000

RECOMMENDATION:

None

**DFTVDW_JOBNUMBER**

Basic vdW job control

TYPE:

INTEGER

DEFAULT:

0

OPTIONS:

0 Do not apply the XDM scheme.

1 Add vdW as energy/gradient correction to SCF.

2 Add vDW as a DFT functional and do full SCF (this option only works with XDM6).

RECOMMENDATION:

None

**DFTVDW_KAI**

Damping factor $k$ for $C_6$-only damping function

TYPE:

INTEGER

DEFAULT:

800

OPTIONS:

10–1000

RECOMMENDATION:

None

**DFTVDW_METHOD**

Choose the damping function used in XDM

TYPE:

INTEGER

DEFAULT:

1

OPTIONS:

1 Use Becke's damping function including $C_6$ term only.

2 Use Becke's damping function with higher-order ($C_8$ and $C_{10}$) terms.

RECOMMENDATION:

None

**DFTVDW_MOL1NATOMS**

The number of atoms in the first monomer in dimer calculation

TYPE:

INTEGER

DEFAULT:

0

OPTIONS:

0–$N_{\rm atoms}$

RECOMMENDATION:

None

**DFTVDW_PRINT**

Printing control for VDW code

TYPE:

INTEGER

DEFAULT:

1

OPTIONS:

0 No printing.

1 Minimum printing (default)

2 Debug printing

RECOMMENDATION:

None

**DFTVDW_USE_ELE_DRV**

Specify whether to add the gradient correction to the XDM energy. only valid with Becke's $C_6$ damping function using the interpolated BR89 model.

TYPE:

LOGICAL

DEFAULT:

1

OPTIONS:

1 Use density correction when applicable.

0 Do not use this correction (for debugging purposes).

RECOMMENDATION:

None

**DFT_C**

Controls whether the DFT-C empirical BSSE correction should be added.

TYPE:

LOGICAL

DEFAULT:

FALSE

OPTIONS:

| | |
|---|---|
| FALSE | (or 0) Do not apply the DFT-C correction |
| TRUE | (or 1) Apply the DFT-C correction |

RECOMMENDATION:

NONE

**DFT_D3_3BODY**

Controls whether the three-body interaction in Grimme's DFT-D3 method should be applied (see Eq. (14) in Ref. 9).

TYPE:

LOGICAL

DEFAULT:

FALSE

OPTIONS:

| | |
|---|---|
| FALSE (or 0) | Do not apply the three-body interaction term |
| TRUE | Apply the three-body interaction term |

RECOMMENDATION:

NONE

**DFT_D3_A1**

The nonlinear parameter $\alpha_1$ in eqs. (4.55), (4.56), (4.57), and (4.58). Utilized in DFT-D3(BJ), DFT-D3(CSO), DFT-D3M(0), DFT-D3M(BJ), and DFT-D3(op).

TYPE:

INTEGER

DEFAULT:

100000

OPTIONS:

| | |
|---|---|
| $n$ | Corresponding to $\alpha_1 = n/100000$. |

RECOMMENDATION:

NONE

**DFT_D3_A2**

The nonlinear parameter $\alpha_2$ in eqs. (4.55) and (4.58). Utilized in DFT-D3(BJ), DFT-D3M(BJ), and DFT-D3(op).

TYPE:

INTEGER

DEFAULT:

100000

OPTIONS:

| | |
|---|---|
| $n$ | Corresponding to $\alpha_2 = n/100000$. |

RECOMMENDATION:

NONE

**DFT_D3_POWER**

The nonlinear parameter $\beta_6$ in eq. (4.58). Utilized in DFT-D3(op). Must be greater than or equal to 6 to avoid divergence.

TYPE:

INTEGER

DEFAULT:

600000

OPTIONS:

$n$ Corresponding to $\beta_6 = n/100000$.

RECOMMENDATION:

NONE

**DFT_D3_RS6**

The nonlinear parameter $s_{r,6}$ in eqs. (4.54) and (4.57). Utilized in DFT-D3(0) and DFT-D3M(0).

TYPE:

INTEGER

DEFAULT:

100000

OPTIONS:

$n$ Corresponding to $s_{r,6} = n/100000$.

RECOMMENDATION:

NONE

**DFT_D3_RS8**

The nonlinear parameter $s_{r,8}$ in eqs. (4.54) and (4.57). Utilized in DFT-D3(0) and DFT-D3M(0).

TYPE:

INTEGER

DEFAULT:

100000

OPTIONS:

$n$ Corresponding to $s_{r,8} = n/100000$.

RECOMMENDATION:

NONE

**DFT_D3_S6**

The linear parameter $s_6$ in eq. (4.53). Utilized in all forms of DFT-D3.

TYPE:

INTEGER

DEFAULT:

100000

OPTIONS:

$n$ Corresponding to $s_6 = n/100000$.

RECOMMENDATION:

NONE

**DFT_D3_S8**

The linear parameter $s_8$ in eq. (4.53). Utilized in DFT-D3(0), DFT-D3(BJ), DFT-D3M(0), DFT-D3M(BJ), and DFT-D3(op).

TYPE:

INTEGER

DEFAULT:

100000

OPTIONS:

$n$ Corresponding to $s_8 = n/100000$.

RECOMMENDATION:

NONE

**DFT_D_A**

Controls the strength of dispersion corrections in the Chai–Head-Gordon DFT-D scheme, Eq. (4.52).

TYPE:

INTEGER

DEFAULT:

600

OPTIONS:

$n$ Corresponding to $a = n/100$.

RECOMMENDATION:

Use the default.

**DFT_D**

Controls the empirical dispersion correction to be added to a DFT calculation.

TYPE:

LOGICAL

DEFAULT:

None

OPTIONS:

| | |
|---|---|
| FALSE | (or 0) Do not apply the DFT-D2, DFT-CHG, or DFT-D3 scheme |
| EMPIRICAL_GRIMME | DFT-D2 dispersion correction from Grimme |
| EMPIRICAL_CHG | DFT-CHG dispersion correction from Chai and Head-Gordon |
| EMPIRICAL_GRIMME3 | DFT-D3(0) dispersion correction from Grimme (deprecated as of Q-CHEM 5.0) |
| D3_ZERO | DFT-D3(0) dispersion correction from Grimme *et al.* |
| D3_BJ | DFT-D3(BJ) dispersion correction from Grimme *et al.* |
| D3_CSO | DFT-D3(CSO) dispersion correction from Schröder *et al.* |
| D3_ZEROM | DFT-D3M(0) dispersion correction from Smith *et al.* |
| D3_BJM | DFT-D3M(BJ) dispersion correction from Smith *et al.* |
| D3_OP | DFT-D3(op) dispersion correction from Witte *et al.* |
| D3 | Recommended; chooses the "best" available D3 dispersion correction |

RECOMMENDATION:

NONE

**DH**

Controls the application of DH-DFT scheme.

TYPE:

LOGICAL

DEFAULT:

FALSE

OPTIONS:

| | |
|---|---|
| FALSE (or 0) | Do not apply the DH-DFT scheme |
| TRUE (or 1) | Apply DH-DFT scheme |

RECOMMENDATION:

NONE

**DIIS_ERR_RMS**

Changes the DIIS convergence metric from the maximum to the RMS error.

TYPE:

LOGICAL

DEFAULT:

FALSE

OPTIONS:

TRUE, FALSE

RECOMMENDATION:

Use the default, the maximum error provides a more reliable criterion.

**DIIS_PRINT**

Controls the output from DIIS SCF optimization.

TYPE:

INTEGER

DEFAULT:

0

OPTIONS:

| | |
|---|---|
| 0 | Minimal print out. |
| 1 | Chosen method and DIIS coefficients and solutions. |
| 2 | Level 1 plus changes in multipole moments. |
| 3 | Level 2 plus Multipole moments. |
| 4 | Level 3 plus extrapolated Fock matrices. |

RECOMMENDATION:

Use the default

**DIIS_SEPARATE_ERRVEC**

Control optimization of DIIS error vector in unrestricted calculations.

TYPE:

LOGICAL

DEFAULT:

FALSE Use a combined $\alpha$ and $\beta$ error vector.

OPTIONS:

FALSE Use a combined $\alpha$ and $\beta$ error vector.

TRUE Use separate error vectors for the $\alpha$ and $\beta$ spaces.

RECOMMENDATION:

When using DIIS in Q-CHEM a convenient optimization for unrestricted calculations is to sum the $\alpha$ and $\beta$ error vectors into a single vector which is used for extrapolation. This is often extremely effective, but in some pathological systems with symmetry breaking, can lead to false solutions being detected, where the $\alpha$ and $\beta$ components of the error vector cancel exactly giving a zero DIIS error. While an extremely uncommon occurrence, if it is suspected, set DIIS_SEPARATE_ERRVEC = TRUE to check.

**DIIS_SUBSPACE_SIZE**

Controls the size of the DIIS and/or RCA subspace during the SCF.

TYPE:

INTEGER

DEFAULT:

15

OPTIONS:

User-defined

RECOMMENDATION:

None

**DIP_SINGLETS**

Sets the number of singlet DIP roots to find. Valid only for closed-shell references.

TYPE:

INTEGER/INTEGER ARRAY

DEFAULT:

0 Do not look for any singlet DIP states.

OPTIONS:

$[i, j, k \ldots]$ Find $i$ DIP singlet states in the first irrep, $j$ states in the second irrep *etc.*

RECOMMENDATION:

None

**DIP_STATES**

Sets the number of DIP roots to find. For closed-shell reference, defaults into DIP_SINGLETS. For open-shell references, specifies all low-lying states.

TYPE:

INTEGER/INTEGER ARRAY

DEFAULT:

0 Do not look for any DIP states.

OPTIONS:

$[i, j, k \ldots]$ Find $i$ DIP states in the first irrep, $j$ states in the second irrep *etc.*

RECOMMENDATION:

None

**DIP_TRIPLETS**

Sets the number of triplet DIP roots to find. Valid only for closed-shell references.

TYPE:

INTEGER/INTEGER ARRAY

DEFAULT:

0 Do not look for any DIP triplet states.

OPTIONS:

$[i, j, k \ldots]$ Find $i$ DIP triplet states in the first irrep, $j$ states in the second irrep *etc.*

RECOMMENDATION:

None

**DIRECT_SCF**

Controls direct SCF.

TYPE:

LOGICAL

DEFAULT:

Determined by program.

OPTIONS:

TRUE Forces direct SCF.

FALSE Do not use direct SCF.

RECOMMENDATION:

Use the default; direct SCF switches off in-core integrals.

**DISP_FREE_C**

Specify the employed “dispersion-free" correlation functional.

TYPE:

STRING

DEFAULT:

NONE

OPTIONS:

Correlation functionals supported by Q-CHEM.

RECOMMENDATION:

Put the appropriate correlation functional paired with the chosen exchange functional (*e.g.* put PBE if DISP_FREE_X is revPBE); put NONE if DISP_FREE_X is set to an exchange-correlation functional.

**DISP_FREE_X**

Specify the employed “dispersion-free" exchange functional.

TYPE:

STRING

DEFAULT:

HF

OPTIONS:

Exchange functionals (*e.g.* revPBE) or exchange-correlation functionals (*e.g.* B3LYP) supported by Q-CHEM.

RECOMMENDATION:

HF is recommended for hybrid (primary) functionals (*e.g.*$\omega$B97X-V) and revPBE for semi-local ones (*e.g.*B97M-V). Other reasonable options (*e.g.* B3LYP for B3LYP-D3) can also be applied.

**DORAMAN**

Controls calculation of Raman intensities. Requires JOBTYPE to be set to FREQ

TYPE:

LOGICAL

DEFAULT:

FALSE

OPTIONS:

FALSE Do not calculate Raman intensities.

TRUE Do calculate Raman intensities.

RECOMMENDATION:

None

**DSF_STATES**

Sets the number of doubly spin-flipped target states roots to find.

TYPE:

INTEGER/INTEGER ARRAY

DEFAULT:

0 Do not look for any DSF states.

OPTIONS:

$[i, j, k \ldots]$ Find $i$ doubly spin-flipped states in the first irrep, $j$ states in the second irrep *etc.*

RECOMMENDATION:

None

**DUAL_BASIS_ENERGY**

Activates dual-basis SCF (HF or DFT) energy correction.

TYPE:

LOGICAL

DEFAULT:

FALSE

OPTIONS:

Analytic first derivative available for HF and DFT (see JOBTYPE)

Can be used in conjunction with MP2 or RI-MP2

See BASIS, BASIS2, BASISPROJTYPE

RECOMMENDATION:

Use Dual-Basis to capture large-basis effects at smaller basis cost. Particularly useful with RI-MP2, in which HF often dominates. Use only proper subsets for small-basis calculation.

**D_CPSCF_PERTNUM**

Specifies whether to do the perturbations one at a time, or all together.

TYPE:

INTEGER

DEFAULT:

0

OPTIONS:

0 Perturbed densities to be calculated all together.

1 Perturbed densities to be calculated one at a time.

RECOMMENDATION:

None

**D_SCF_CONV_1**

Sets the convergence criterion for the level-1 iterations. This preconditions the density for the level-2 calculation, and does not include any two-electron integrals.

TYPE:

INTEGER

DEFAULT:

4 corresponding to a threshold of $10^{-4}$.

OPTIONS:

$n < 10$ Sets convergence threshold to $10^{-n}$.

RECOMMENDATION:

The criterion for level-1 convergence must be less than or equal to the level-2 criterion, otherwise the D-CPSCF will not converge.

**D_SCF_CONV_2**

Sets the convergence criterion for the level-2 iterations.

TYPE:

INTEGER

DEFAULT:

4 Corresponding to a threshold of $10^{-4}$.

OPTIONS:

$n < 10$ Sets convergence threshold to $10^{-n}$.

RECOMMENDATION:

None

**D_SCF_DIIS**

Specifies the number of matrices to use in the DIIS extrapolation in the D-CPSCF.

TYPE:

INTEGER

DEFAULT:

11

OPTIONS:

$n$ $n$ = 0 specifies no DIIS extrapolation is to be used.

RECOMMENDATION:

Use the default.

**D_SCF_MAX_1**

Sets the maximum number of level-1 iterations.

TYPE:

INTEGER

DEFAULT:

100

OPTIONS:

$n$ User defined.

RECOMMENDATION:

Use the default.

**D_SCF_MAX_2**

Sets the maximum number of level-2 iterations.

TYPE:

INTEGER

DEFAULT:

30

OPTIONS:

$n$ User defined.

RECOMMENDATION:

Use the default.

**EA_STATES**

Sets the number of attached target states roots to find. By default, $\alpha$ electron will be attached (see EOM_EA_ALPHA).

TYPE:

INTEGER/INTEGER ARRAY

DEFAULT:

| | |
|---|---|
| 0 | Do not look for any EA states. |

OPTIONS:

| | |
|---|---|
| $[i, j, k \ldots]$ | Find $i$ EA states in the first irrep, $j$ states in the second irrep *etc.* |

RECOMMENDATION:

None

**ECP**

Defines the effective core potential and associated basis set to be used

TYPE:

STRING

DEFAULT:

No ECP

OPTIONS:

| | |
|---|---|
| General, Gen | User defined. (*$ecp* keyword required) |
| Symbol | Use standard ECPs discussed above. |

RECOMMENDATION:

ECPs are recommended for first row transition metals and heavier elements. Consul the reviews for more details.

**EDA2**

Switch on EDA2 and specify the option set number.

TYPE:

INTEGER

DEFAULT:

0

OPTIONS:

| | |
|---|---|
| 0 | Do not run through EDA2. |
| 1 | Frozen energy decomposition + nDQ-FERF polarization<br>(the standard EDA2 option) |
| 2 | Frozen energy decomposition + (AO-block-based) ALMO polarization<br>(old scheme with the addition of frozen decomposition) |
| 3 | Frozen energy decomposition + oDQ-FERF polarization<br>(NOT commonly used) |
| 4 | Frozen wave function relaxation + Frozen energy decomposition + nDQ-FERF polarization<br>(NOT commonly used) |
| 5 | Frozen energy decomposition + polMO polarization<br>(NOT commonly used). |
| 10 | No preset. Completely controlled by user's *$rem* input<br>(for developers only) |

RECOMMENDATION:

Turn on EDA2 for Q-CHEM's ALMO-EDA jobs unless CTA with the old scheme is desired. Option 1 is recommended in general, especially when substantially large basis sets are employed. The original ALMO scheme (option 2) can be used when the employed basis set is of small or medium size (arguably no larger than augmented triple-$\zeta$). The other options are rarely used for routine applications.

**EDA_BSSE**

Calculates the BSSE correction when performing the energy decomposition analysis.

TYPE:

LOGICAL

DEFAULT:

FALSE

OPTIONS:

TRUE/FALSE

RECOMMENDATION:

Set to TRUE unless a very large basis set is used.

**EDA_CLS_DISP**

Compute the DISP contribution without performing the orthogonal decomposition, which will then be subtracted from the classical PAULI term.

TYPE:

BOOLEAN

DEFAULT:

FALSE

OPTIONS:

FALSE Use the DISP term computed with orthogonal decomposition (if available).

TRUE Use the DISP term computed using undistorted monomer densities.

RECOMMENDATION:

Set it to TRUE when orthogonal decomposition is not performed.

**EDA_CLS_ELEC**

Perform the classical decomposition of the frozen term.

TYPE:

BOOLEAN

DEFAULT:

FALSE (automatically set to TRUE by EDA2 options 1–5)

OPTIONS:

FALSE Do not compute the classical ELEC and PAULI terms.

TRUE Perform the classical decomposition.

RECOMMENDATION:

TRUE

**EDA_COVP**

Perform COVP analysis when evaluating the RS or ARS charge-transfer correction. COVP analysis is currently implemented only for systems of two fragments.

TYPE:

LOGICAL

DEFAULT:

FALSE

OPTIONS:

TRUE/FALSE

RECOMMENDATION:

Set to TRUE to perform COVP analysis in an EDA or SCF MI(RS) job.

**EDA_PRINT_COVP**

Replace the final MOs with the CVOP orbitals in the end of the run.

TYPE:

LOGICAL

DEFAULT:

FALSE

OPTIONS:

TRUE/FALSE

RECOMMENDATION:

Set to TRUE to print COVP orbitals instead of conventional MOs.

**EE_SINGLETS**

Sets the number of singlet excited state roots to find. Valid only for closed-shell references.

TYPE:

INTEGER/INTEGER ARRAY

DEFAULT:

0 Do not look for any excited states.

OPTIONS:

$[i, j, k \ldots]$ Find $i$ excited states in the first irrep, $j$ states in the second irrep *etc.*

RECOMMENDATION:

None

**EE_STATES**

Sets the number of excited state roots to find. For closed-shell reference, defaults into EE_SINGLETS. For open-shell references, specifies all low-lying states.

TYPE:

INTEGER/INTEGER ARRAY

DEFAULT:

0 Do not look for any excited states.

OPTIONS:

$[i, j, k \ldots]$ Find $i$ excited states in the first irrep, $j$ states in the second irrep *etc.*

RECOMMENDATION:

None

**EE_TRIPLETS**

Sets the number of triplet excited state roots to find. Valid only for closed-shell references.

TYPE:

INTEGER/INTEGER ARRAY

DEFAULT:

0 Do not look for any excited states.

OPTIONS:

$[i, j, k \ldots]$ Find $i$ excited states in the first irrep, $j$ states in the second irrep *etc.*

RECOMMENDATION:

None

**EFP_COORD_XYZ**

Use coordinates of three atoms instead of Euler angles to specify position and orientation of the fragments

TYPE:

LOGICAL

DEFAULT:

FALSE

OPTIONS:

TRUE FALSE

RECOMMENDATION:

None

**EFP_DIRECT_POLARIZATION_DRIVER**

Use direct solver for EFP polarization

TYPE:

LOGICAL

DEFAULT:

FALSE

OPTIONS:

TRUE FALSE

RECOMMENDATION:

Direct polarization solver provides stable convergence of induced dipoles which may otherwise become problematic in case of closely lying or highly polar or charged fragments. The computational cost of direct polarization versus iterative polarization becomes higher for systems containing more than 10000 polarizable points.

**EFP_DISP_DAMP**

Controls fragment-fragment dispersion screening in EFP

TYPE:

INTEGER

DEFAULT:

2

OPTIONS:

| | |
|---|---|
| 0 | switch off dispersion screening |
| 1 | use Tang-Toennies screening, with fixed parameter $b = 1.5$ |
| 2 | use overlap-based damping |

RECOMMENDATION:

None

**EFP_DISP**

Controls fragment-fragment dispersion in EFP

TYPE:

LOGICAL

DEFAULT:

TRUE

OPTIONS:

| | |
|---|---|
| TRUE | switch on dispersion |
| FALSE | switch off dispersion |

RECOMMENDATION:

None

**EFP_ELEC_DAMP**

Controls fragment-fragment electrostatic screening in EFP

TYPE:

INTEGER

DEFAULT:

2

OPTIONS:

| | |
|---|---|
| 0 | switch off electrostatic screening |
| 1 | use overlap-based damping correction |
| 2 | use exponential damping correction if screening parameters are provided in the EFP potential |

RECOMMENDATION:

Overlap-based damping is recommended

**EFP_ELEC**

Controls fragment-fragment electrostatics in EFP

TYPE:

LOGICAL

DEFAULT:

TRUE

OPTIONS:

| | |
|---|---|
| TRUE | switch on electrostatics |
| FALSE | switch off electrostatics |

RECOMMENDATION:

None

**EFP_ENABLE_LINKS**

Enable fragment links in EFP region

TYPE:

LOGICAL

DEFAULT:

FALSE

OPTIONS:

TRUE FALSE

RECOMMENDATION:

None

**EFP_EXREP**

Controls fragment-fragment exchange repulsion in EFP

TYPE:

LOGICAL

DEFAULT:

TRUE

OPTIONS:

| | |
|---|---|
| TRUE | switch on exchange repulsion |
| FALSE | switch off exchange repulsion |

RECOMMENDATION:

None

**EFP_FRAGMENTS_ONLY**

Specifies whether there is a QM part

TYPE:

LOGICAL

DEFAULT:

FALSE QM part is present

OPTIONS:

TRUE Only MM part is present: all fragments are treated by EFP

FALSE QM part is present: do QM/MM EFP calculation

RECOMMENDATION:

None

**EFP_INPUT**

Specifies the format of EFP input

TYPE:

LOGICAL

DEFAULT:

FALSE Dummy atom (*e.g.*, He) in *$molecule* section should be present

OPTIONS:

TRUE A format without dummy atom in *$molecule* section

FALSE A format with dummy atom in *$molecule* section

RECOMMENDATION:

None

**EFP_POL_DAMP**

Controls fragment-fragment polarization screening in EFP

TYPE:

INTEGER

DEFAULT:

1

OPTIONS:

0 switch off polarization screening

1 use Tang-Toennies screening

RECOMMENDATION:

None

**EFP_POL**

Controls fragment-fragment polarization in EFP

TYPE:

LOGICAL

DEFAULT:

TRUE

OPTIONS:

TRUE switch on polarization

FALSE switch off polarization

RECOMMENDATION:

None

**EFP_QM_DISP**

Controls QM-EFP dispersion

TYPE:

LOGICAL

DEFAULT:

FALSE

OPTIONS:

| | |
|---|---|
| TRUE | switch on QM-EFP dispersion |
| FALSE | switch off QM-EFP dispersion |

RECOMMENDATION:

None

**EFP_QM_ELEC_DAMP**

Controls QM-EFP electrostatics screening in EFP

TYPE:

INTEGER

DEFAULT:

0

OPTIONS:

| | |
|---|---|
| 0 | switch off electrostatic screening |
| 1 | use overlap based damping correction |

RECOMMENDATION:

None

**EFP_QM_ELEC**

Controls QM-EFP electrostatics

TYPE:

LOGICAL

DEFAULT:

TRUE

OPTIONS:

| | |
|---|---|
| TRUE | switch on QM-EFP electrostatics |
| FALSE | switch off QM-EFP electrostatics |

RECOMMENDATION:

None

**EFP_QM_EXREP**

Controls QM-EFP exchange-repulsion

TYPE:

LOGICAL

DEFAULT:

FALSE

OPTIONS:

| | |
|---|---|
| TRUE | switch on QM-EFP exchange-repulsion |
| FALSE | switch off QM-EFP exchange-repulsion |

RECOMMENDATION:

None

**EFP_QM_POL**

Controls QM-EFP polarization

TYPE:

LOGICAL

DEFAULT:

TRUE

OPTIONS:

| | |
|---|---|
| TRUE | switch on QM-EFP polarization |
| FALSE | switch off QM-EFP polarization |

RECOMMENDATION:

None

**EFP**

Specifies that EFP calculation is requested

TYPE:

LOGICAL

DEFAULT:

FALSE

OPTIONS:

TRUE FALSE

RECOMMENDATION:

The keyword should be present if excited state calculation is requested

**EMBEDMAN**

Turns density embedding on.

TYPE:

INTEGER

DEFAULT:

0

OPTIONS:

| | |
|---|---|
| 0 | Do not use density embedding. |
| 1 | Turn on density embedding. |

RECOMMENDATION:

Use EMBEDMAN for QM/QM density embedded calculations.

**EMBED_MU**

Specifies exponent value of projection operator scaling factor, $\mu$ [Eq. (11.74) and (11.76)].

TYPE:

INTEGER

DEFAULT:

7

OPTIONS:

| | |
|---|---|
| n | $\mu = 10^n$. |

RECOMMENDATION:

Values of 2 - 7 are recommended. A higher value of $\mu$ leads to better orthogonality of the fragment MOs but $\mu > 10^7$ introduces numerical noise. $\mu < 10^2$ results in non-additive terms becoming too large. Energy corrections are fairly insensitive to changes in $\mu$ within the range of $10^2 - 10^7$.

**EMBED_THEORY**

Specifies post-DFT method performed on fragment one.

TYPE:

INTEGER

DEFAULT:

0

OPTIONS:

0 No post HF method, only DFT on fragment one.

1 Perform CCSD(T) calculation on fragment one.

2 Perform MP2 calculation on fragment one.

RECOMMENDATION:

This should be 1 or 2 for the high-level QM calculation of fragment 1-in-2, and 0 for fragment 2-in-1 low-level QM calculation.

**EMBED_THRESH**

Specifies threshold cutoff for AO contribution used to determine which MOs belong to which fragments

TYPE:

INTEGER

DEFAULT:

500

OPTIONS:

n Threshold $= n/1000$

RECOMMENDATION:

Acceptable values range from 0 to 1000. Should only need to be tuned for non-highly localized MOs

**EOM_CORR**

Specifies the correlation level.

TYPE:

STRING

DEFAULT:

None No correction will be computed

OPTIONS:

SD(DT) EOM-CCSD(dT), available for EE, SF, and IP

SD(FT) EOM-CCSD(fT), available for EE, SF, IP, and EA

SD(ST) EOM-CCSD(sT), available for IP

RECOMMENDATION:

None

**EOM_DAVIDSON_CONVERGENCE**

Convergence criterion for the RMS residuals of excited state vectors.

TYPE:

INTEGER

DEFAULT:

5 Corresponding to $10^{-5}$

OPTIONS:

$n$ Corresponding to $10^{-n}$ convergence criterion

RECOMMENDATION:

Use the default. Normally this value be the same as EOM_DAVIDSON_THRESHOLD.

**EOM_DAVIDSON_MAXVECTORS**

Specifies maximum number of vectors in the subspace for the Davidson diagonalization.

TYPE:

INTEGER

DEFAULT:

60

OPTIONS:

$n$ Up to $n$ vectors per root before the subspace is reset

RECOMMENDATION:

Larger values increase disk storage but accelerate and stabilize convergence.

**EOM_DAVIDSON_MAX_ITER**

Maximum number of iteration allowed for Davidson diagonalization procedure.

TYPE:

INTEGER

DEFAULT:

30

OPTIONS:

$n$ User-defined number of iterations

RECOMMENDATION:

Default is usually sufficient

**EOM_DAVIDSON_THRESHOLD**

Specifies threshold for including a new expansion vector in the iterative Davidson diagonalization. Their norm must be above this threshold.

TYPE:

INTEGER

DEFAULT:

00103 Corresponding to 0.00001

OPTIONS:

$abcde$ Integer code is mapped to $abc \times 10^{-(de+2)}$, i.e., 02505->$2.5{\times}10^{-6}$

RECOMMENDATION:

Use the default unless converge problems are encountered. Should normally be set to the same values as EOM_DAVIDSON_CONVERGENCE, if convergence problems arise try setting to a value slightly larger than EOM_DAVIDSON_CONVERGENCE.

**EOM_EA_ALPHA**

Sets the number of attached target states derived by attaching $\alpha$ electron (M$_s$=$\frac{1}{2}$, default in EOM-EA).

TYPE:

INTEGER/INTEGER ARRAY

DEFAULT:

0 Do not look for any EA states.

OPTIONS:

$[i, j, k \ldots]$ Find $i$ EA states in the first irrep, $j$ states in the second irrep *etc.*

RECOMMENDATION:

None

**EOM_EA_BETA**

Sets the number of attached target states derived by attaching $\beta$ electron (M$_s$=$-\frac{1}{2}$, EA-SF).

TYPE:

INTEGER/INTEGER ARRAY

DEFAULT:

0 Do not look for any EA states.

OPTIONS:

$[i, j, k \ldots]$ Find $i$ EA states in the first irrep, $j$ states in the second irrep *etc.*

RECOMMENDATION:

None

**EOM_FAKE_IPEA**

If TRUE, calculates fake EOM-IP or EOM-EA energies and properties using the diffuse orbital trick. Default for EOM-EA and Dyson orbital calculations in CCMAN.

TYPE:

LOGICAL

DEFAULT:

FALSE (use proper EOM-IP code)

OPTIONS:

FALSE, TRUE

RECOMMENDATION:

None. This feature only works for CCMAN.

**EOM_IPEA_FILTER**

If TRUE, filters the EOM-IP/EA amplitudes obtained using the diffuse orbital implementation (see EOM_FAKE_IPEA). Helps with convergence.

TYPE:

LOGICAL

DEFAULT:

FALSE (EOM-IP or EOM-EA amplitudes will not be filtered)

OPTIONS:

FALSE, TRUE

RECOMMENDATION:

None

**EOM_IP_ALPHA**

Sets the number of ionized target states derived by removing $\alpha$ electron (M$_s = -\frac{1}{2}$).

TYPE:

INTEGER/INTEGER ARRAY

DEFAULT:

0 Do not look for any IP/$\alpha$ states.

OPTIONS:

$[i, j, k \ldots]$ Find $i$ ionized states in the first irrep, $j$ states in the second irrep *etc.*

RECOMMENDATION:

None

**EOM_IP_BETA**

Sets the number of ionized target states derived by removing $\beta$ electron (M$_s$=$\frac{1}{2}$, default for EOM-IP).

TYPE:

INTEGER/INTEGER ARRAY

DEFAULT:

0 Do not look for any IP/$\beta$ states.

OPTIONS:

$[i, j, k \ldots]$ Find $i$ ionized states in the first irrep, $j$ states in the second irrep *etc.*

RECOMMENDATION:

None

**EOM_NGUESS_DOUBLES**

Specifies number of excited state guess vectors which are double excitations.

TYPE:

INTEGER

DEFAULT:

0

OPTIONS:

$n$ Include $n$ guess vectors that are double excitations

RECOMMENDATION:

This should be set to the expected number of doubly excited states, otherwise they may not be found.

**EOM_NGUESS_SINGLES**

Specifies number of excited state guess vectors that are single excitations.

TYPE:

INTEGER

DEFAULT:

Equal to the number of excited states requested

OPTIONS:

$n$ Include $n$ guess vectors that are single excitations

RECOMMENDATION:

Should be greater or equal than the number of excited states requested, unless .

**EOM_POL**

Whether or not the static polarizability for the EOM-CCSD wave function will be calculated.

TYPE:

LOGICAL

DEFAULT:

FALSE (EOM polarizability will not be calculated)

OPTIONS:

FALSE, TRUE

RECOMMENDATION:

Static polarizabilities are expensive since they require solving three additional response equations. Do no request this property unless you need it.

**EOM_PRECONV_DOUBLES**

When not zero, doubly excited vectors are converged prior to a full excited states calculation. Sets the maximum number of iterations for pre-converging procedure

TYPE:

INTEGER

DEFAULT:

0

OPTIONS:

| | |
|---|---|
| 0 | Do not pre-converge |
| N | Perform N Davidson iterations pre-converging doubles. |

RECOMMENDATION:

Occasionally necessary to ensure a doubly excited state is found. Also used in DSF calculations instead of EOM_PRECONV_SINGLES

**EOM_PRECONV_SD**

When not zero, EOM vectors are pre-converged prior to a full excited states calculation. Sets the maximum number of iterations for pre-converging procedure.

TYPE:

INTEGER

DEFAULT:

0

OPTIONS:

| | |
|---|---|
| 0 | do not pre-converge |
| N | perform N Davidson iterations pre-converging singles and doubles. |

RECOMMENDATION:

Occasionally necessary to ensure that all low-lying states are found. Also, very useful in EOM(2,3) calculations.

None

**EOM_PRECONV_SINGLES**

When not zero, singly excited vectors are converged prior to a full excited states calculation. Sets the maximum number of iterations for pre-converging procedure.

TYPE:

INTEGER

DEFAULT:

0

OPTIONS:

0 do not pre-converge

1 pre-converge singles

RECOMMENDATION:

Sometimes helps with problematic convergence.

**EOM_REF_PROP_TE**

Request for calculation of non-relaxed two-particle EOM-CC properties. The two-particle properties currently include $\langle S^2 \rangle$. The one-particle properties also will be calculated, since the additional cost of the one-particle properties calculation is inferior compared to the cost of $\langle S^2 \rangle$. The variable CC_EOM_PROP must be also set to TRUE. Alternatively, CC_CALC_SSQ can be used to request $\langle S^2 \rangle$ calculation.

TYPE:

LOGICAL

DEFAULT:

FALSE (no two-particle properties will be calculated)

OPTIONS:

FALSE, TRUE

RECOMMENDATION:

The two-particle properties are computationally expensive since they require calculation and use of the two-particle density matrix (the cost is approximately the same as the cost of an analytic gradient calculation). Do not request the two-particle properties unless you really need them.

**EOM_SHIFT**

Specifies energy shift in EOM calculations.

TYPE:

INTEGER

DEFAULT:

0

OPTIONS:

$n$ corresponds to $n \cdot 10^{-3}$ hartree shift (i.e., 11000 = 11 hartree); solve for eigenstates around this value.

RECOMMENDATION:

Not available in CCMAN.

**EOM_USER_GUESS**

Specifies if user-defined guess will be used in EOM calculations.

TYPE:

LOGICAL

DEFAULT:

FALSE

OPTIONS:

TRUE Solve for a state that has maximum overlap with a trans-n specified in *$eom_user_guess*.

RECOMMENDATION:

The orbitals are ordered by energy, as printed in the beginning of the CCMAN2 output. Not available in CCMAN.

**EPAO_ITERATE**

Controls iterations for EPAO calculations (see PAO_METHOD).

TYPE:

INTEGER

DEFAULT:

0 Use non-iterated EPAOs based on atomic blocks of SPS.

OPTIONS:

$n$ Optimize the EPAOs for up to $n$ iterations.

RECOMMENDATION:

Use the default. For molecules that are not too large, one can test the sensitivity of the results to the type of minimal functions by the use of optimized EPAOs in which case a value of $n = 500$ is reasonable.

**EPAO_WEIGHTS**

Controls algorithm and weights for EPAO calculations (see PAO_METHOD).

TYPE:

INTEGER

DEFAULT:

115 Standard weights, use $1^{\text{st}}$ and $2^{\text{nd}}$ order optimization

OPTIONS:

15 Standard weights, with $1^{\text{st}}$ order optimization only.

RECOMMENDATION:

Use the default, unless convergence failure is encountered.

**ERCALC**

Specifies the Edmiston-Ruedenberg localized orbitals are to be calculated

TYPE:

INTEGER

DEFAULT:

06000

OPTIONS:

$aabcd$

$aa$ specifies the convergence threshold.
If $aa > 3$, the threshold is set to $10^{-aa}$. The default is 6.
If $aa = 1$, the calculation is aborted after the guess, allowing Pipek-Mezey orbitals to be extracted.

$b$ specifies the guess:
0 Boys localized orbitals. This is the default
1 Pipek-Mezey localized orbitals.

$c$ specifies restart options (if restarting from an ER calculation):
0 No restart. This is the default
1 Read in MOs from last ER calculation.
2 Read in MOs and RI integrals from last ER calculation.

$d$ specifies how to treat core orbitals
0 Do not perform ER localization. This is the default.
1 Localize core and valence together.
2 Do separate localizations on core and valence.
3 Localize only the valence electrons.
4 Use the *$localize* section.

RECOMMENDATION:

ERCALC 1 will usually suffice, which uses threshold $10^{-6}$.

**ER_CIS_NUMSTATE**

Define how many states to mix with ER localized diabatization. These states must be specified in the *$localized_diabatization* section.

TYPE:

INTEGER

DEFAULT:

0 Do not perform ER localized diabatization.

OPTIONS:

2 to N where N is the number of CIS states requested (CIS_N_ROOTS)

RECOMMENDATION:

It is usually not wise to mix adiabatic states that are separated by more than a few eV or a typical reorganization energy in solvent.

**ESP_TRANS**

Controls the calculation of the electrostatic potential of the transition density

TYPE:

LOGICAL

DEFAULT:

FALSE

OPTIONS:

| | |
|---|---|
| TRUE | compute the electrostatic potential of the excited state transition density |
| FALSE | compute the electrostatic potential of the excited state electronic density |

RECOMMENDATION:

NONE

**EXCHANGE**

Specifies the exchange functional or exchange-correlation functional for hybrid.

TYPE:

STRING

DEFAULT:

No default exchange functional

OPTIONS:

| | |
|---|---|
| HF | Fock exchange |
| Slater, S | Slater (Dirac 1930) |
| ETheta_LDA, ETheta_LSDA | TAO-DFT local density approximation for $E_\theta$ [10]<br>(use in conjunction with another exchange functional) |
| Becke86, B86 | Becke 1986 |
| Becke, B, B88 | Becke 1988 |
| muB88 | Short-range Becke exchange, as formulated by Song *et al.* [11] |
| Gill96, Gill | Gill 1996 |
| GG99 | Gilbert and Gill, 1999 |
| Becke(EDF1), B(EDF1) | Becke (uses EDF1 parameters) |
| PW86, | Perdew-Wang 1986 |
| rPW86, | Refitted PW86 for use in vdW-DF-10 and VV10 |
| PW91, PW | Perdew-Wang 1991 |
| PBE | Perdew-Burke-Ernzerhof 1996 |
| AK13 | Armiento and Kümmel, 2013 [12] |
| TPSS | The nonempirical exchange-correlation scheme of Tao, Perdew, Staroverov, and Scuseria (requires also that the user specify "TPSS" for correlation) |
| TPSSH | The hybrid version of TPSS (with no input line for correlation) |
| PBE0, PBE1PBE | PBE hybrid with 25% HF exchange |
| PBEOP | PBE exchange + one-parameter progressive correlation |
| wPBE | Short-range $\omega$PBE exchange, as formulated by Henderson *et al.* [13] |
| muPBE | Short-range $\mu$PBE exchange, due to Song *et al.* [11] |
| B97 | Becke97 XC hybrid |
| B97-1 | Becke97 re-optimized by Hamprecht *et al.* |
| B97-2 | Becke97-1 optimized further by Wilson *et al.* |
| B3PW91, Becke3PW91, B3P | B3PW91 hybrid |
| B3LYP, Becke3LYP | B3LYP hybrid |
| B3LYP5 | B3LYP based on correlation functional #5 of |
| HCTH | HCTH hybrid |
| HCTH-120 | HCTH-120 hybrid |
| HCTH-147 | HCTH-147 hybrid |
| HCTH-407 | HCTH-407 hybrid |
| | Vosko, Wilk, and Nusair rather than their functional #3 |
| BOP | B88 exchange + one-parameter progressive correlation |
| EDF1 | EDF1 |
| EDF2 | EDF2 |
| VSXC | VSXC meta-GGA, not a hybrid |
| BMK | BMK hybrid |
| M05 | M05 hybrid |
| M052X | M05-2X hybrid |
| M06L | M06-L hybrid |
| M06HF | M06-HF hybrid |
| M06 | M06 hybrid |
| M062X | M06-2X hybrid |
| M08HX | M08-HX hybrid |
| M08SO | M08-SO hybrid |
| M11L | M11-L hybrid |
| M11 | M11 long-range corrected hybrid |
| SOGGA | SOGGA hybrid |

**FAST_XC**

Controls direct variable thresholds to accelerate exchange-correlation (XC) in DFT.

TYPE:

LOGICAL

DEFAULT:

FALSE

OPTIONS:

| | |
|---|---|
| TRUE | Turn FAST_XC on. |
| FALSE | Do not use FAST_XC. |

RECOMMENDATION:

Caution: FAST_XC improves the speed of a DFT calculation, but may occasionally cause the SCF calculation to diverge.

**FDE**

Turns density embedding on.

TYPE:

BOOLEAN

DEFAULT:

False

OPTIONS:

| | |
|---|---|
| True | Perform an FDE-ADC calculation. |
| False | Don’t perform FDE-ADC calculation. |

RECOMMENDATION:

Set the *$rem* variable FDE to TRUE to start a FDE-ADC calculation.

**FDIFF_DER**

Controls what types of information are used to compute higher derivatives. The default uses a combination of energy, gradient and Hessian information, which makes the force field calculation faster.

TYPE:

INTEGER

DEFAULT:

| | |
|---|---|
| 3 | for jobs where analytical 2nd derivatives are available. |
| 0 | for jobs with ECP. |

OPTIONS:

| | |
|---|---|
| 0 | Use energy information only. |
| 1 | Use gradient information only. |
| 2 | Use Hessian information only. |
| 3 | Use energy, gradient, and Hessian information. |

RECOMMENDATION:

When the molecule is larger than benzene with small basis set, FDIFF_DER=2 may be faster. Note that FDIFF_DER will be set lower if analytic derivatives of the requested order are not available. Please refers to IDERIV.

**FDIFF_STEPSIZE_QFF**

Displacement used for calculating third and fourth derivatives by finite difference.

TYPE:

INTEGER

DEFAULT:

5291 Corresponding to 0.1 bohr. For calculating third and fourth derivatives.

OPTIONS:

$n$ Use a step size of $n \times 10^{-5}$.

RECOMMENDATION:

Use the default, unless the potential surface is very flat, in which case a larger value should be used.

**FDIFF_STEPSIZE**

Displacement used for calculating derivatives by finite difference.

TYPE:

INTEGER

DEFAULT:

100 Corresponding to 0.001 Å. For calculating second derivatives.

OPTIONS:

$n$ Use a step size of $n \times 10^{-5}$.

RECOMMENDATION:

Use the default except in cases where the potential surface is very flat, in which case a larger value should be used. See FDIFF_STEPSIZE_QFF for third and fourth derivatives.

**FD_MAT_VEC_PROD**

Compute Hessian-vector product using the finite difference technique.

TYPE:

BOOLEAN

DEFAULT:

FALSE (TRUE when the employed functional contains NLC)

OPTIONS:

FALSE Compute Hessian-vector product analytically.

TRUE Use finite difference to compute Hessian-vector product.

RECOMMENDATION:

Set it to TRUE when analytical Hessian is not available.

**Note:** For simple R and U calculations, it can always be set to FALSE, which indicates that only the NLC part will be computed with finite difference.

**FEFP_EFP**

Specifies that fEFP_EFP calculation is requested to compute the total interaction energies between a ligand (the last fragment in the $efp_fragments section) and the protein (represented by fEFP)

TYPE:

STRING

DEFAULT:

OFF

OPTIONS:

| | |
|---|---|
| OFF | disables fEFP |
| LA | enables fEFP with the Link Atom (HLA or CLA) scheme (only electrostatics and polarization) |
| MFCC | enables fEFP with MFCC (only electrostatics) |

RECOMMENDATION:

The keyword should be invoked if EFP/fEFP is requested (interaction energy calculations). This keyword has to be employed with EFP_FRAGMENT_ONLY = TRUE. To switch on/off electrostatics or polarzation interactions, the usual EFP controls are employed.

**FEFP_QM**

Specifies that fEFP_QM calculation is requested to perform a QM/fEFPcompute computation. The fEFP part is a fractionated macromolecule.

TYPE:

STRING

DEFAULT:

OFF

OPTIONS:

| | |
|---|---|
| OFF | disables fEFP_QM and performs a QM/EFP calculation |
| LA | enables fEFP_QM with the Link Atom scheme |

RECOMMENDATION:

The keyword should be invoked if QM/fEFP is requested. This keyword has to be employed with efp_fragment_only false. Only electrostatics is available.

**FMO_ORDER**

Controls the truncation order $n$ for FMO.

TYPE:

INTEGER

DEFAULT:

NONE

OPTIONS:

| | |
|---|---|
| $N$ | Order of FMO |

RECOMMENDATION:

FMO can be performed up to third order.

**FOA_FUNDGAP**

Compute the frozen-orbital approximation of the fundamental gap.

TYPE:

Boolean

DEFAULT:

FALSE

OPTIONS:

FALSE Do not compute FOA derivative discontinuity and fundamental gap.

TRUE Compute and print FOA fundamental gap information. Implies KS_GAP_PRINT.

RECOMMENDATION:

Use in conjunction with KS_GAP_UNIT if true.

**FOCK_EXTRAP_ORDER**

Specifies the polynomial order $N$ for Fock matrix extrapolation.

TYPE:

INTEGER

DEFAULT:

0 Do not perform Fock matrix extrapolation.

OPTIONS:

$N$ Extrapolate using an $N$th-order polynomial ($N > 0$).

RECOMMENDATION:

None

**FOCK_EXTRAP_POINTS**

Specifies the number $M$ of old Fock matrices that are retained for use in extrapolation.

TYPE:

INTEGER

DEFAULT:

0 Do not perform Fock matrix extrapolation.

OPTIONS:

$M$ Save $M$ Fock matrices for use in extrapolation $(M > N)$

RECOMMENDATION:

Higher-order extrapolations with more saved Fock matrices are faster and conserve energy better than low-order extrapolations, up to a point. In many cases, the scheme ($N$ = 6, $M$ = 12), in conjunction with SCF_CONVERGENCE = 6, is found to provide about a 50% savings in computational cost while still conserving energy.

**FOLLOW_ENERGY**

Adjusts the energy window for near states

TYPE:

INTEGER

DEFAULT:

0

OPTIONS:

0 Use dynamic thresholds, based on energy difference between steps.

$n$ Search over selected state $E_{\text{est}} \pm n \times 10^{-6}\ E_h$.

RECOMMENDATION:

Use a wider energy window to follow a state diabatically, smaller window to remain on the adiabatic state most of the time.

**FOLLOW_OVERLAP**

Adjusts the threshold for states of similar character.

TYPE:

INTEGER

DEFAULT:

0

OPTIONS:

| | |
|---|---|
| 0 | Use dynamic thresholds, based on energy difference between steps. |
| $n$ | Percentage overlap for previous step and current step. |

RECOMMENDATION:

Use a higher value to require states have higher degree of similarity to be considered the same (more often selected based on energy).

**FON_E_THRESH**

DIIS error below which occupations will be kept constant.

TYPE:

INTEGER

DEFAULT:

4

OPTIONS:

n freeze occupations below DIIS error of $10^{-n}$

RECOMMENDATION:

This should be one or two numbers bigger than the desired SCF convergence threshold.

**FON_NORB**

Number of orbitals above and below the Fermi level that are allowed to have fractional occupancies.

TYPE:

INTEGER

DEFAULT:

4

OPTIONS:

n number of active orbitals

RECOMMENDATION:

The number of valence orbitals is a reasonable choice.

**FON_T_END**

Final electronic temperature for FON calculation.

TYPE:

INTEGER

DEFAULT:

0

OPTIONS:

Any desired final temperature.

RECOMMENDATION:

Pick the temperature to either reproduce experimental conditions (*e.g.* room temperature) or as low as possible to approach zero-temperature.

**FON_T_METHOD**

Selects cooling algorithm.

TYPE:

INTEGER

DEFAULT:

1

OPTIONS:

1 temperature is scaled by a factor in each cycle

2 temperature is decreased by a constant number in each cycle

RECOMMENDATION:

We have made slightly better experience with a constant cooling rate. However, choose constant temperature when in doubt.

**FON_T_SCALE**

Determines the step size for the cooling.

TYPE:

INTEGER

DEFAULT:

90

OPTIONS:

n temperature is scaled by $0.01 \cdot n$ in each cycle (cooling method 1)

n temperature is decreased by n K in each cycle (cooling method 2)

RECOMMENDATION:

The cooling rate should be neither too slow nor too fast. Too slow may lead to final energies that are at undesirably high temperatures. Too fast may lead to convergence issues. Reasonable choices for methods 1 and 2 are 98 and 50, respectively. When in doubt, use constant temperature.

**FON_T_START**

Initial electronic temperature (in K) for FON calculation.

TYPE:

INTEGER

DEFAULT:

1000

OPTIONS:

Any desired initial temperature.

RECOMMENDATION:

Pick the temperature to either reproduce experimental conditions (*e.g.* room temperature) or as low as possible to approach zero-temperature.

**FORCE_FIELD**

Specifies the force field for MM energies in QM/MM calculations.

TYPE:

STRING

DEFAULT:

NONE

OPTIONS:

| | |
|---|---|
| AMBER99 | AMBER99 force field |
| CHARMM27 | CHARMM27 force field |
| OPLSAA | OPLSAA force field |

RECOMMENDATION:

None.

**FRAGMO_GUESS_MODE**

Decide what to do regarding to the FRAGMO guess in the present job.

TYPE:

INTEGER

DEFAULT:

0

OPTIONS:

| | |
|---|---|
| 0 | Spawn fragment jobs sequentially and collect the results as the FRAGMO guess at the end. |
| 1 | Generate fragment inputs in folders “FrgX" under the scratch directory of the present job and then terminate. Users can then take advantage of a queuing system to run these jobs simultaneously using “FrgX" as their scratch folders (should be handled with scripting). |
| 2 | Read in the available fragment data. |

RECOMMENDATION:

Consider using “1" if the fragment calculations are evenly expensive. Use “2" when FRAGMO guess is pre-computed.

**FRAG_MOL_ORB**

Perform a FMO calculation.

TYPE:

BOOLEAN

DEFAULT:

FALSE

OPTIONS:

| | |
|---|---|
| TRUE | Perform a FMO calculation. |
| FALSE | Do not perform a FMO calculation. |

RECOMMENDATION:

NONE

**FRGM_LPCORR**

Specifies a correction method performed after the locally-projected equations are converged.

TYPE:

STRING

DEFAULT:

NONE

OPTIONS:

| | |
|---|---|
| ARS | Approximate Roothaan-step perturbative correction. |
| RS | Single Roothaan-step perturbative correction. |
| EXACT_SCF | Full SCF variational correction. |
| ARS_EXACT_SCF | Both ARS and EXACT_SCF in a single job. |
| RS_EXACT_SCF | Both RS and EXACT_SCF in a single job. |

RECOMMENDATION:

For large basis sets use ARS, use RS if ARS fails.

**FRGM_METHOD**

Specifies a locally-projected method.

TYPE:

STRING

DEFAULT:

NONE

OPTIONS:

| | |
|---|---|
| STOLL | Locally-projected SCF equations of Stoll are solved. |
| GIA | Locally-projected SCF equations of Gianinetti are solved. |
| NOSCF_RS | Single Roothaan-step correction to the FRAGMO initial guess. |
| NOSCF_ARS | Approximate single Roothaan-step correction to the FRAGMO initial guess. |
| NOSCF_DRS | Double Roothaan-step correction to the FRAGMO initial guess. |
| NOSCF_RS_FOCK | Non-converged SCF energy of the single Roothaan-step MOs. |

RECOMMENDATION:

STOLL and GIA are for variational optimization of the ALMOs. NOSCF options are for computationally fast corrections of the FRAGMO initial guess.

**FRZ_GEOM**

Compute forces on the frozen PES.

TYPE:

BOOLEAN

DEFAULT:

FALSE

OPTIONS:

| | |
|---|---|
| FALSE | Do not compute forces on the frozen PES. |
| TRUE | Compute forces on the frozen PES. |

RECOMMENDATION:

Set it to TRUE when optimized geometry or vibrational frequencies on the frozen PES are desired.

**FRZ_ORTHO_DECOMP_CONV**

Convergence criterion for the minimization problem that gives the orthogonal fragment densities.

TYPE:

INTEGER

DEFAULT:

6

OPTIONS:

$n$ $10^{-n}$

RECOMMENDATION:

Use the default unless tighter convergence is preferred.

**FRZ_ORTHO_DECOMP**

Perform the decomposition of frozen interaction energy based on the orthogonal decomposition of the 1PDM associated with the frozen wave function.

TYPE:

BOOLEAN

DEFAULT:

FALSE (automatically set to TRUE by EDA2 options 1–5)

OPTIONS:

| | |
|---|---|
| FALSE | Do not perform the orthogonal decomposition. |
| TRUE | Perform the frozen energy decomposition using orthogonal fragment densities. |

RECOMMENDATION:

Use default value automatically set by “EDA2".

**FSM_MODE**

Specifies the method of interpolation

TYPE:

INTEGER

DEFAULT:

2

OPTIONS:

| | |
|---|---|
| 1 | Cartesian |
| 2 | LST |

RECOMMENDATION:

In most cases, LST is superior to Cartesian interpolation.

**FSM_NGRAD**

Specifies the number of perpendicular gradient steps used to optimize each node

TYPE:

INTEGER

DEFAULT:

Undefined

OPTIONS:

$N$ Number of perpendicular gradients per node

RECOMMENDATION:

Anything between 2 and 6 should work, where increasing the number is only needed for difficult reaction paths.

**FSM_NNODE**

Specifies the number of nodes along the string

TYPE:

INTEGER

DEFAULT:

Undefined

OPTIONS:

$N$ number of nodes in FSM calculation

RECOMMENDATION:

$N = 15$. Use 10 to 20 nodes for a typical calculation. Reaction paths that connect multiple elementary steps should be separated into individual elementary steps, and one FSM job run for each pair of intermediates. Use a higher number when the FSM is followed by an approximate-Hessian based transition state search (Section 9.2.2).

**FSM_OPT_MODE**

Specifies the method of optimization

TYPE:

INTEGER

DEFAULT:

Undefined

OPTIONS:

| | |
|---|---|
| 1 | Conjugate gradients |
| 2 | Quasi-Newton method with BFGS Hessian update |

RECOMMENDATION:

The quasi-Newton method is more efficient when the number of nodes is high.

**FSSH_CONTINUE**

Restart a FSSH calculation from a previous run, using the file 396.0. When this is enabled, the initial conditions of the surface hopping calculation will be set, including the correct wave function amplitudes, initial surface, and position/momentum moments (if AFSSH) from the final step of some prior calculation.

TYPE:

INTEGER

DEFAULT:

0

OPTIONS:

| | |
|---|---|
| 0 | Start fresh calculation. |
| 1 | Restart from previous run. |

RECOMMENDATION:

None

**FSSH_INITIALSURFACE**

Specifies the initial state in a surface hopping calculation.

TYPE:

INTEGER

DEFAULT:

None

OPTIONS:

$n$ An integer between FSSH_LOWESTSURFACE and FSSH_LOWESTSURFACE $+$ FSSH_NSURFACES $-1$.

RECOMMENDATION:

None

**FSSH_LOWESTSURFACE**

Specifies the lowest-energy state considered in a surface hopping calculation.

TYPE:

INTEGER

DEFAULT:

None

OPTIONS:

$n$ Only states $n$ and above are considered in a FSSH calculation.

RECOMMENDATION:

None

**FSSH_NSURFACES**

Specifies the number of states considered in a surface hopping calculation.

TYPE:

INTEGER

DEFAULT:

None

OPTIONS:

$n$ $n$ states are considered in the surface hopping calculation.

RECOMMENDATION:

Any states which may come close in energy to the active surface should be included in the surface hopping calculation.

**FTC_CLASS_THRESH_MULT**

Together with FTC_CLASS_THRESH_ORDER, determines the cutoff threshold for included a shell-pair in the $dd$ class, *i.e.*, the class that is expanded in terms of plane waves.

TYPE:

INTEGER

DEFAULT:

5 Multiplicative part of the FTC classification threshold. Together with the default value of the FTC_CLASS_THRESH_ORDER this leads to the $5 \times 10^{-5}$ threshold value.

OPTIONS:

$n$ User specified.

RECOMMENDATION:

Use the default. If diffuse basis sets are used and the molecule is relatively big then tighter FTC classification threshold has to be used. According to our experiments using Pople-type diffuse basis sets, the default $5 \times 10^{-5}$ value provides accurate result for an alanine5 molecule while $1 \times 10^{-5}$ threshold value for alanine10 and $5 \times 10^{-6}$ value for alanine15 has to be used.

**FTC_CLASS_THRESH_ORDER**

Together with FTC_CLASS_THRESH_MULT, determines the cutoff threshold for included a shell-pair in the $dd$ class, *i.e.*, the class that is expanded in terms of plane waves.

TYPE:

INTEGER

DEFAULT:

5 Logarithmic part of the FTC classification threshold. Corresponds to $10^{-5}$

OPTIONS:

$n$ User specified

RECOMMENDATION:

Use the default.

**FTC_SMALLMOL**

Controls whether or not the operator is evaluated on a large grid and stored in memory to speed up the calculation.

TYPE:

INTEGER

DEFAULT:

1

OPTIONS:

1 Use a big pre-calculated array to speed up the FTC calculations

0 Use this option to save some memory

RECOMMENDATION:

Use the default if possible and use 0 (or buy some more memory) when needed.

**FTC**

Controls the overall use of the FTC.

TYPE:

INTEGER

DEFAULT:

0

OPTIONS:

0 Do not use FTC in the Coulomb part

1 Use FTC in the Coulomb part

RECOMMENDATION:

Use FTC when bigger and/or diffuse basis sets are used.

**GAUSSIAN_BLUR**

Enables the use of Gaussian-delocalized external charges in a QM/MM calculation.

TYPE:

LOGICAL

DEFAULT:

FALSE

OPTIONS:

TRUE Delocalizes external charges with Gaussian functions.

FALSE Point charges

RECOMMENDATION:

None

**GAUSS_BLUR_WIDTH**

Delocalization width for external MM Gaussian charges in a Janus calculations.

TYPE:

INTEGER

DEFAULT:

NONE

OPTIONS:

$n$ Use a width of $n \times 10^{-4}$ Å.

RECOMMENDATION:

Blur all MM external charges in a QM/MM calculation with the specified width. Gaussian blurring is currently incompatible with PCM calculations. Values of 1.0–2.0 Å are recommended in Ref. 14.

**GEN_SCFMAN_ALGO_1**

The first algorithm to be used in a hybrid-algorithm calculation.

TYPE:

STRING

DEFAULT:

0

OPTIONS:

All the available SCF_ALGORITHM options, including the GEN_SCFMAN additions (Section 4.7.1).

RECOMMENDATION:

None

**GEN_SCFMAN_CONV_1**

The convergence criterion given to the first algorithm. If reached, switch to the next algorithm.

TYPE:

INTEGER

DEFAULT:

0

OPTIONS:

$n$ $10^{-n}$

RECOMMENDATION:

None

**GEN_SCFMAN_HYBRID_ALGO**

Use multiple algorithms in an SCF calculation based on GEN_SCFMAN.

TYPE:

BOOLEAN

DEFAULT:

FALSE

OPTIONS:

| | |
|---|---|
| FALSE | Use a single SCF algorithm (given by SCF_ALGORITHM). |
| TRUE | Use multiple SCF algorithms (to be specified). |

RECOMMENDATION:

Set it to TRUE when the use of more than one algorithm is desired.

**GEN_SCFMAN_ITER_1**

Maximum number of iterations given to the first algorithm. If used up, switch to the next algorithm.

TYPE:

INTEGER

DEFAULT:

50

OPTIONS:

User-defined

RECOMMENDATION:

None

**GEOM_OPT_CHARAC_CONV**

Overide the built-in convergence criterion for the Davidson solver.

TYPE:

INTEGER

DEFAULT:

0 (use the built-in default value $10^{-5}$)

OPTIONS:

$n$ Set the convergence criterion to $10^{-n}$.

RECOMMENDATION:

Use the default. If it fails to converge, consider loosening the criterion with caution.

**GEOM_OPT_CHARAC**

Use the finite difference Davidson method to characterize the resulting energy minimum/transition state.

TYPE:

BOOLEAN

DEFAULT:

FALSE

OPTIONS:

| | |
|---|---|
| FALSE | do not characterize the resulting stationary point. |
| TRUE | perform a characterization of the stationary point. |

RECOMMENDATION:

Set it to TRUE when the character of a stationary point needs to be verified, especially for a transition structure.

**GEOM_OPT_COORDS**

Controls the type of optimization coordinates.

TYPE:

INTEGER

DEFAULT:

$-1$

OPTIONS:

| | |
|---|---|
| 0 | Optimize in Cartesian coordinates. |
| 1 | Generate and optimize in internal coordinates, if this fails abort. |
| $-1$ | Generate and optimize in internal coordinates, if this fails at any stage of the optimization, switch to Cartesian and continue. |
| 2 | Optimize in $Z$-matrix coordinates, if this fails abort. |
| $-2$ | Optimize in $Z$-matrix coordinates, if this fails during any stage of the optimization switch to Cartesians and continue. |

RECOMMENDATION:

Use the default; delocalized internals are more efficient.

**GEOM_OPT_DMAX**

Maximum allowed step size. Value supplied is multiplied by $10^{-3}$.

TYPE:

INTEGER

DEFAULT:

300 = 0.3

OPTIONS:

| | |
|---|---|
| $n$ | User-defined cutoff. |

RECOMMENDATION:

Use the default.

**GEOM_OPT_HESSIAN**

Determines the initial Hessian status.

TYPE:

STRING

DEFAULT:

DIAGONAL

OPTIONS:

| | |
|---|---|
| DIAGONAL | Set up diagonal Hessian. |
| READ | Have exact or initial Hessian. Use as is if Cartesian, or transform if internals. |

RECOMMENDATION:

An accurate initial Hessian will improve the performance of the optimizer, but is expensive to compute.

**GEOM_OPT_LINEAR_ANGLE**

Threshold for near linear bond angles (degrees).

TYPE:

INTEGER

DEFAULT:

165 degrees.

OPTIONS:

$n$ User-defined level.

RECOMMENDATION:

Use the default.

**GEOM_OPT_MAX_CYCLES**

Maximum number of optimization cycles.

TYPE:

INTEGER

DEFAULT:

50

OPTIONS:

$n$ User defined positive integer.

RECOMMENDATION:

The default should be sufficient for most cases. Increase if the initial guess geometry is poor, or for systems with shallow potential wells.

**GEOM_OPT_MAX_DIIS**

Controls maximum size of subspace for GDIIS.

TYPE:

INTEGER

DEFAULT:

0

OPTIONS:

0 Do not use GDIIS.

-1 Default size = min(NDEG, NATOMS, 4) NDEG = number of molecular degrees of freedom.

$n$ Size specified by user.

RECOMMENDATION:

Use the default or do not set $n$ too large.

**GEOM_OPT_MODE**

Determines Hessian mode followed during a transition state search.

TYPE:

INTEGER

DEFAULT:

0

OPTIONS:

0 Mode following off.

$n$ Maximize along mode $n$.

RECOMMENDATION:

Use the default, for geometry optimizations.

**GEOM_OPT_PRINT**

Controls the amount of OPTIMIZE print output.

TYPE:

INTEGER

DEFAULT:

3 Error messages, summary, warning, standard information and gradient print out.

OPTIONS:

0 Error messages only.

1 Level 0 plus summary and warning print out.

2 Level 1 plus standard information.

3 Level 2 plus gradient print out.

4 Level 3 plus Hessian print out.

5 Level 4 plus iterative print out.

6 Level 5 plus internal generation print out.

7 Debug print out.

RECOMMENDATION:

Use the default.

**GEOM_OPT_SYMFLAG**

Controls the use of symmetry in OPTIMIZE.

TYPE:

LOGICAL

DEFAULT:

TRUE

OPTIONS:

| | |
|---|---|
| TRUE | Make use of point group symmetry. |
| FALSE | Do not make use of point group symmetry. |

RECOMMENDATION:

Use the default.

**GEOM_OPT_TOL_DISPLACEMENT**

Convergence on maximum atomic displacement.

TYPE:

INTEGER

DEFAULT:

$1200 \equiv 1200 \times 10^{-6}$ tolerance on maximum atomic displacement.

OPTIONS:

$n$ Integer value (tolerance = $n \times 10^{-6}$).

RECOMMENDATION:

Use the default. To converge GEOM_OPT_TOL_GRADIENT and one of GEOM_OPT_TOL_DISPLACEMENT and GEOM_OPT_TOL_ENERGY must be satisfied.

**GEOM_OPT_TOL_ENERGY**

Convergence on energy change of successive optimization cycles.

TYPE:

INTEGER

DEFAULT:

$100 \equiv 100 \times 10^{-8}$ tolerance on maximum (absolute) energy change.

OPTIONS:

$n$ Integer value (tolerance = value $n \times 10^{-8}$).

RECOMMENDATION:

Use the default. To converge GEOM_OPT_TOL_GRADIENT and one of GEOM_OPT_TOL_DISPLACEMENT and GEOM_OPT_TOL_ENERGY must be satisfied.

**GEOM_OPT_TOL_GRADIENT**

Convergence on maximum gradient component.

TYPE:

INTEGER

DEFAULT:

300 $\equiv 300 \times 10^{-6}$ tolerance on maximum gradient component.

OPTIONS:

$n$ Integer value (tolerance = $n \times 10^{-6}$).

RECOMMENDATION:

Use the default. To converge GEOM_OPT_TOL_GRADIENT and one of GEOM_OPT_TOL_DISPLACEMENT and GEOM_OPT_TOL_ENERGY must be satisfied.

**GEOM_OPT_UPDATE**

Controls the Hessian update algorithm.

TYPE:

INTEGER

DEFAULT:

-1

OPTIONS:

| | |
|---|---|
| -1 | Use the default update algorithm. |
| 0 | Do not update the Hessian (not recommended). |
| 1 | Murtagh-Sargent update. |
| 2 | Powell update. |
| 3 | Powell/Murtagh-Sargent update (TS default). |
| 4 | BFGS update (OPT default). |
| 5 | BFGS with safeguards to ensure retention of positive definiteness (GDISS default). |

RECOMMENDATION:

Use the default.

**GEOM_PRINT**

Controls the amount of geometric information printed at each step.

TYPE:

LOGICAL

DEFAULT:

FALSE

OPTIONS:

| | |
|---|---|
| TRUE | Prints out all geometric information; bond distances, angles, torsions. |
| FALSE | Normal printing of distance matrix. |

RECOMMENDATION:

Use if you want to be able to quickly examine geometric parameters at the beginning and end of optimizations. Only prints in the beginning of single point energy calculations.

**GHF**

Run a generalized Hartree-Fock calculation with GEN_SCFMAN.

TYPE:

BOOLEAN

DEFAULT:

FALSE

OPTIONS:

| | |
|---|---|
| TRUE | Run a GHF calculation. |
| FALSE | Do not use GHF. |

RECOMMENDATION:

Set to TRUE if desired.

**GRAIN**

Controls the number of lowest-level boxes in one dimension for CFMM.

TYPE:

INTEGER

DEFAULT:

-1 Program decides best value, turning on CFMM when useful

OPTIONS:

| | |
|---|---|
| -1 | Program decides best value, turning on CFMM when useful |
| 1 | Do not use CFMM |
| $n \geq 8$ | Use CFMM with $n$ lowest-level boxes in one dimension |

RECOMMENDATION:

This is an expert option; either use the default, or use a value of 1 if CFMM is not desired.

**GVB_AMP_SCALE**

Scales the default orbital amplitude iteration step size by $n$/1000 for IP/RCC. PP amplitude equations are solved analytically, so this parameter does not affect PP.

TYPE:

INTEGER

DEFAULT:

1000 Corresponding to 100%

OPTIONS:

$n$ User-defined, 0–1000

RECOMMENDATION:

Default is usually fine, but in some highly-correlated systems it can help with convergence to use smaller values.

**GVB_DO_ROHF**

Sets the number of Unrestricted-in-Active Pairs to be kept restricted.

TYPE:

INTEGER

DEFAULT:

0

OPTIONS:

$n$ User-Defined

RECOMMENDATION:

If $n$ is the same value as GVB_N_PAIRS returns the ROHF solution for GVB, only works with the UNRESTRICTED = TRUE implementation of GVB with GVB_OLD_UPP = 0 (its default value)

**GVB_DO_SANO**

Sets the scheme used in determining the active virtual orbitals in a Unrestricted-in-Active Pairs GVB calculation.

TYPE:

INTEGER

DEFAULT:

2

OPTIONS:

0 No localization or Sano procedure

1 Only localizes the active virtual orbitals

2 Uses the Sano procedure

RECOMMENDATION:

Different initial guesses can sometimes lead to different solutions. Disabling sometimes can aid in finding more non-local solutions for the orbitals.

**GVB_GUESS_MIX**

Similar to SCF_GUESS_MIX, it breaks alpha/beta symmetry for UPP by mixing the alpha HOMO and LUMO orbitals according to the user-defined fraction of LUMO to add the HOMO. 100 corresponds to a 1:1 ratio of HOMO and LUMO in the mixed orbitals.

TYPE:

INTEGER

DEFAULT:

0

OPTIONS:

$n$ User-defined, $0 \leq n \leq 100$

RECOMMENDATION:

25 often works well to break symmetry without overly impeding convergence.

**GVB_LOCAL**

Sets the localization scheme used in the initial guess wave function.

TYPE:

INTEGER

DEFAULT:

2 Pipek-Mezey orbitals

OPTIONS:

0 No Localization

1 Boys localized orbitals

2 Pipek-Mezey orbitals

RECOMMENDATION:

Different initial guesses can sometimes lead to different solutions. It can be helpful to try both to ensure the global minimum has been found.

**GVB_N_PAIRS**

Alternative to CC_REST_OCC and CC_REST_VIR for setting active space size in GVB and valence coupled cluster methods.

TYPE:

INTEGER

DEFAULT:

PP active space (1 occ and 1 virt for each valence electron pair)

OPTIONS:

$n$ user-defined

RECOMMENDATION:

Use the default unless one wants to study a special active space. When using small active spaces, it is important to ensure that the proper orbitals are incorporated in the active space. If not, use the *$reorder_mo* feature to adjust the SCF orbitals appropriately.

**GVB_OLD_UPP**

Which unrestricted algorithm to use for GVB.

TYPE:

INTEGER

DEFAULT:

0

OPTIONS:

0 Use Unrestricted-in-Active Pairs described in Ref. 15

1 Use Unrestricted Implementation described in Ref. 16

RECOMMENDATION:

Only works for Unrestricted PP and no other GVB model.

**GVB_ORB_CONV**

The GVB-CC wave function is considered converged when the root-mean-square orbital gradient and orbital step sizes are less than $10^{-\text{GVB\_ORB\_CONV}}$. Adjust THRESH simultaneously.

TYPE:

INTEGER

DEFAULT:

5

OPTIONS:

$n$ User-defined

RECOMMENDATION:

Use 6 for PP(2) jobs or geometry optimizations. Tighter convergence (*i.e.* 7 or higher) cannot always be reliably achieved.

**GVB_ORB_MAX_ITER**

Controls the number of orbital iterations allowed in GVB-CC calculations. Some jobs, particularly unrestricted PP jobs can require 500–1000 iterations.

TYPE:

INTEGER

DEFAULT:

256

OPTIONS:

User-defined number of iterations.

RECOMMENDATION:

Default is typically adequate, but some jobs, particularly UPP jobs, can require 500–1000 iterations if converged tightly.

**GVB_ORB_SCALE**

Scales the default orbital step size by $n$/1000.

TYPE:

INTEGER

DEFAULT:

1000 Corresponding to 100%

OPTIONS:

$n$ User-defined, 0–1000

RECOMMENDATION:

Default is usually fine, but for some stretched geometries it can help with convergence to use smaller values.

**GVB_POWER**

Coefficient for GVB_IP exchange type amplitude regularization to improve the convergence of the amplitude equations especially for spin-unrestricted amplitudes near dissociation. This is the leading coefficient for an amplitude dampening term included in the energy denominator: -($c$/10000)$(e^{t^p_{ij}} - 1)/(e^1 - 1)$

TYPE:

INTEGER

DEFAULT:

6

OPTIONS:

$p$ User-defined

RECOMMENDATION:

Should be decreased if unrestricted amplitudes do not converge or converge slowly at dissociation, and should be kept even valued.

**GVB_PRINT**

Controls the amount of information printed during a GVB-CC job.

TYPE:

INTEGER

DEFAULT:

0

OPTIONS:

$n$ User-defined

RECOMMENDATION:

Should never need to go above 0 or 1.

**GVB_REGULARIZE**

Coefficient for GVB_IP exchange type amplitude regularization to improve the convergence of the amplitude equations especially for spin-unrestricted amplitudes near dissociation. This is the leading coefficient for an amplitude dampening term $-(c/10000)(e^{t^p_{ij}}-1)/(e^1-1)$

TYPE:

INTEGER

DEFAULT:

0 For restricted

1 For unrestricted

OPTIONS:

$c$ User-defined

RECOMMENDATION:

Should be increased if unrestricted amplitudes do not converge or converge slowly at dissociation. Set this to zero to remove all dynamically-valued amplitude regularization.

**GVB_REORDER_1**

Tells the code which two pairs to swap first.

TYPE:

INTEGER

DEFAULT:

0

OPTIONS:

$n$ User-defined XXXYYY

RECOMMENDATION:

This is in the format of two 3-digit pair indices that tell the code to swap pair XXX with YYY, for example swapping pair 1 and 2 would get the input 001002. Must be specified in GVB_REORDER_PAIRS $\geq 1$.

**GVB_REORDER_2**

Tells the code which two pairs to swap second.

TYPE:

INTEGER

DEFAULT:

0

OPTIONS:

$n$ User-defined XXXYYY

RECOMMENDATION:

This is in the format of two 3-digit pair indices that tell the code to swap pair XXX with YYY, for example swapping pair 1 and 2 would get the input 001002. Must be specified in GVB_REORDER_PAIRS $\geq$ 2.

**GVB_REORDER_3**

Tells the code which two pairs to swap third.

TYPE:

INTEGER

DEFAULT:

0

OPTIONS:

$n$ User-defined XXXYYY

RECOMMENDATION:

This is in the format of two 3-digit pair indices that tell the code to swap pair XXX with YYY, for example swapping pair 1 and 2 would get the input 001002. Must be specified in GVB_REORDER_PAIRS $\geq$ 3.

**GVB_REORDER_4**

Tells the code which two pairs to swap fourth.

TYPE:

INTEGER

DEFAULT:

0

OPTIONS:

$n$ User-defined XXXYYY

RECOMMENDATION:

This is in the format of two 3-digit pair indices that tell the code to swap pair XXX with YYY, for example swapping pair 1 and 2 would get the input 001002. Must be specified in GVB_REORDER_PAIRS $\geq$ 4.

**GVB_REORDER_5**

Tells the code which two pairs to swap fifth.

TYPE:

INTEGER

DEFAULT:

0

OPTIONS:

$n$ User-defined XXXYYY

RECOMMENDATION:

This is in the format of two 3-digit pair indices that tell the code to swap pair XXX with YYY, for example swapping pair 1 and 2 would get the input 001002. Must be specified in GVB_REORDER_PAIRS $\geq$ 5.

**GVB_REORDER_PAIRS**

Tells the code how many GVB pairs to switch around.

TYPE:

INTEGER

DEFAULT:

0

OPTIONS:

$n$ $0 \leq n \leq 5$

RECOMMENDATION:

This allows for the user to change the order the active pairs are placed in after the orbitals are read in or are guessed using localization and the Sano procedure. Up to 5 sequential pair swaps can be made, but it is best to leave this alone.

**GVB_RESTART**

Restart a job from previously-converged GVB-CC orbitals.

TYPE:

LOGICAL

DEFAULT:

FALSE

OPTIONS:

TRUE/FALSE

RECOMMENDATION:

Useful when trying to converge to the same GVB solution at slightly different geometries, for example.

**GVB_SHIFT**

Value for a statically valued energy shift in the energy denominator used to solve the coupled cluster amplitude equations, $n$/10000.

TYPE:

INTEGER

DEFAULT:

0

OPTIONS:

$n$ User-defined

RECOMMENDATION:

Default is fine, can be used in lieu of the dynamically valued amplitude regularization if it does not aid convergence.

**GVB_SYMFIX**

Should GVB use a symmetry breaking fix.

TYPE:

INTEGER

DEFAULT:

0

OPTIONS:

| | |
|---|---|
| 0 | no symmetry breaking fix |
| 1 | symmetry breaking fix with virtual orbitals spanning the active space |
| 2 | symmetry breaking fix with virtual orbitals spanning the whole virtual space |

RECOMMENDATION:

It is best to stick with type 1 to get a symmetry breaking correction with the best results coming from CORRELATION=NP and GVB_SYMFIX = 1.

**GVB_SYMPEN**

Sets the pre-factor for the amplitude regularization term for the SB amplitudes.

TYPE:

INTEGER

DEFAULT:

160

OPTIONS:

$\gamma$ User-defined

RECOMMENDATION:

Sets the pre-factor for the amplitude regularization term for the SB amplitudes: $-(\gamma/1000)(e^{(c*100)*t^2}-1)$.

**GVB_SYMSCA**

Sets the weight for the amplitude regularization term for the SB amplitudes.

TYPE:

INTEGER

DEFAULT:

125

OPTIONS:

$c$ User-defined

RECOMMENDATION:

Sets the weight for the amplitude regularization term for the SB amplitudes: $-(\gamma/1000)(e^{(c*100)*t^2}-1)$.

**GVB_TRUNC_OCC**

Controls how many pairs' occupied orbitals are truncated from the GVB active space.

TYPE:

INTEGER

DEFAULT:

0

OPTIONS:

$n$ User-defined

RECOMMENDATION:

This allows for asymmetric GVB active spaces removing the $n$ lowest energy occupied orbitals from the GVB active space while leaving their paired virtual orbitals in the active space. Only the models including the SIP and DIP amplitudes (ie NP and 2P) benefit from this all other models this equivalent to just reducing the total number of pairs.

**GVB_TRUNC_VIR**

Controls how many pairs' virtual orbitals are truncated from the GVB active space.

TYPE:

INTEGER

DEFAULT:

0

OPTIONS:

$n$ User-defined

RECOMMENDATION:

This allows for asymmetric GVB active spaces removing the $n$ highest energy occupied orbitals from the GVB active space while leaving their paired virtual orbitals in the active space. Only the models including the SIP and DIP amplitudes (ie NP and 2P) benefit from this all other models this equivalent to just reducing the total number of pairs.

**GVB_UNRESTRICTED**

Controls restricted versus unrestricted PP jobs. Usually handled automatically.

TYPE:

LOGICAL

DEFAULT:

same value as UNRESTRICTED

OPTIONS:

TRUE/FALSE

RECOMMENDATION:

Set this variable explicitly only to do a UPP job from an RHF or ROHF initial guess. Leave this variable alone and specify UNRESTRICTED = TRUE to access the new Unrestricted-in-Active-Pairs GVB code which can return an RHF or ROHF solution if used with GVB_DO_ROHF

**HESS_AND_GRAD**

Enables the evaluation of both analytical gradient and Hessian in a single job

TYPE:

LOGICAL

DEFAULT:

FALSE

OPTIONS:

| | |
|---|---|
| TRUE | Evaluates both gradient and Hessian. |
| FALSE | Evaluates Hessian only. |

RECOMMENDATION:

Use only in a frequency (and thus Hessian) evaluation.

**HFPT_BASIS**

Specifies the secondary basis in a HFPC/DFPC calculation.

TYPE:

STRING

DEFAULT:

None

OPTIONS:

None

RECOMMENDATION:

See reference for recommended basis set, functional, and grid pairings.

**HFPT**

Activates HFPC/DFPC calculation.

TYPE:

LOGICAL

DEFAULT:

FALSE

OPTIONS:

Single-point energy only

RECOMMENDATION:

Use Dual-Basis to capture large-basis effects at smaller basis cost. See reference for recommended basis set, functional, and grid pairings.

**HF_LR**

Sets the fraction of Hartree-Fock exchange at $r_{12} = \infty$.

TYPE:

INTEGER

DEFAULT:

No default

OPTIONS:

| | |
|---|---|
| $n$ | Corresponding to HF_LR = $n/1000$ |

RECOMMENDATION:

None

**HF_SR**

Sets the fraction of Hartree-Fock exchange at $r_{12} = 0$.

TYPE:

INTEGER

DEFAULT:

No default

OPTIONS:

$n$ Corresponding to HF_SR = $n/1000$

RECOMMENDATION:

None

**HIRSHFELD_READ**

Switch to force reading in of isolated atomic densities.

TYPE:

LOGICAL

DEFAULT:

FALSE

OPTIONS:

| | |
|---|---|
| TRUE | Read in isolated atomic densities from previous Hirshfeld calculation from disk. |
| FALSE | Generate new isolated atomic densities. |

RECOMMENDATION:

Use the default unless system is large. Note, atoms should be in the same order with same basis set used as in the previous Hirshfeld calculation (although coordinates can change). The previous calculation should be run with the -save switch.

**HIRSHFELD_SPHAVG**

Controls whether atomic densities should be spherically averaged in pro-molecule.

TYPE:

LOGICAL

DEFAULT:

TRUE

OPTIONS:

| | |
|---|---|
| TRUE | Spherically average atomic densities. |
| FALSE | Do not spherically average. |

RECOMMENDATION:

Use the default.

**HIRSHFELD**

Controls running of Hirshfeld population analysis.

TYPE:

LOGICAL

DEFAULT:

FALSE

OPTIONS:

| | |
|---|---|
| TRUE | Calculate Hirshfeld populations. |
| FALSE | Do not calculate Hirshfeld populations. |

RECOMMENDATION:

None

**HIRSHITER_THRESH**

Controls the convergence criterion of iterative Hirshfeld population analysis.

TYPE:

INTEGER

DEFAULT:

5

OPTIONS:

$N$ Corresponding to the convergence criterion of $N/10000$, in $e$.

RECOMMENDATION:

Use the default, which is the value recommended in Ref. 17

**HIRSHITER**

Controls running of iterative Hirshfeld population analysis.

TYPE:

LOGICAL

DEFAULT:

FALSE

OPTIONS:

| | |
|---|---|
| TRUE | Calculate iterative Hirshfeld populations. |
| FALSE | Do not calculate iterative Hirshfeld populations. |

RECOMMENDATION:

None

**IDERIV**

Controls the order of derivatives that are evaluated analytically. The user is not normally required to specify a value, unless numerical derivatives are desired. The derivatives will be evaluated numerically if IDERIV is set lower than JOBTYPE requires.

TYPE:

INTEGER

DEFAULT:

Set to the order of derivative that JOBTYPE requires

OPTIONS:

| | |
|---|---|
| 2 | Analytic second derivatives of the energy (Hessian) |
| 1 | Analytic first derivatives of the energy. |
| 0 | Analytic energies only. |

RECOMMENDATION:

Usually set to the maximum possible for efficiency. Note that IDERIV will be set lower if analytic derivatives of the requested order are not available.

**IGDEFIELD**

Triggers the calculation of the electrostatic potential and/or the electric field at the positions of the MM charges.

TYPE:

INTEGER

DEFAULT:

UNDEFINED

OPTIONS:

O Computes ESP.

1 Computes ESP and EFIELD.

2 Computes EFIELD.

RECOMMENDATION:

Must use this *$rem* when IGDESP is specified.

**IGDESP**

Controls evaluation of the electrostatic potential on a grid of points. If enabled, the output is in an ASCII file, *plot.esp*, in the format $x, y, z$, esp for each point.

TYPE:

INTEGER

DEFAULT:

none no electrostatic potential evaluation

OPTIONS:

$-2$ same as the option '-1', plus evaluate the ESP of $external_charges$

$-1$ read grid input via the *$plots* section of the input deck

0 Generate the ESP values at all nuclear positions

+$n$ read $n$ grid points **in bohr** from the ASCII file *ESPGrid*

RECOMMENDATION:

None

**IGNORE_LOW_FREQ**

Low frequencies that should be treated as rotation can be ignored during
anharmonic correction calculation.

TYPE:

INTEGER

DEFAULT:

300 Corresponding to 300 cm$^{-1}$.

OPTIONS:

$n$ Any mode with harmonic frequency less than $n$ will be ignored.

RECOMMENDATION:

Use the default.

**INCDFT_DENDIFF_THRESH**

Sets the threshold for screening density matrix values in the IncDFT procedure.

TYPE:

INTEGER

DEFAULT:

SCF_CONVERGENCE + 3

OPTIONS:

$n$ Corresponding to a threshold of $10^{-n}$.

RECOMMENDATION:

If the default value causes convergence problems, set this value higher to tighten the threshold.

**INCDFT_DENDIFF_VARTHRESH**

Sets the lower bound for the variable threshold for screening density matrix values in the IncDFT procedure. The threshold will begin at this value and then vary depending on the error in the current SCF iteration until the value specified by INCDFT_DENDIFF_THRESH is reached. This means this value must be set lower than INCDFT_DENDIFF_THRESH.

TYPE:

INTEGER

DEFAULT:

0 Variable threshold is not used.

OPTIONS:

$n$ Corresponding to a threshold of $10^{-n}$.

RECOMMENDATION:

If the default value causes convergence problems, set this value higher to tighten accuracy. If this fails, set to 0 and use a static threshold.

**INCDFT_GRIDDIFF_THRESH**

Sets the threshold for screening functional values in the IncDFT procedure

TYPE:

INTEGER

DEFAULT:

SCF_CONVERGENCE + 3

OPTIONS:

$n$ Corresponding to a threshold of $10^{-n}$.

RECOMMENDATION:

If the default value causes convergence problems, set this value higher to tighten the threshold.

**INCDFT_GRIDDIFF_VARTHRESH**

Sets the lower bound for the variable threshold for screening the functional values in the IncDFT procedure. The threshold will begin at this value and then vary depending on the error in the current SCF iteration until the value specified by INCDFT_GRIDDIFF_THRESH is reached. This means that this value must be set lower than INCDFT_GRIDDIFF_THRESH.

TYPE:

INTEGER

DEFAULT:

0 Variable threshold is not used.

OPTIONS:

$n$ Corresponding to a threshold of $10^{-n}$.

RECOMMENDATION:

If the default value causes convergence problems, set this value higher to tighten accuracy. If this fails, set to 0 and use a static threshold.

**INCDFT**

Toggles the use of the IncDFT procedure for DFT energy calculations.

TYPE:

LOGICAL

DEFAULT:

TRUE

OPTIONS:

| | |
|---|---|
| FALSE | Do not use IncDFT |
| TRUE | Use IncDFT |

RECOMMENDATION:

Turning this option on can lead to faster SCF calculations, particularly towards the end of the SCF. Please note that for some systems use of this option may lead to convergence problems.

**INCFOCK**

Iteration number after which the incremental Fock matrix algorithm is initiated

TYPE:

INTEGER

DEFAULT:

1 Start INCFOCK after iteration number 1

OPTIONS:

User-defined (0 switches INCFOCK off)

RECOMMENDATION:

May be necessary to allow several iterations before switching on INCFOCK.

**INTEGRALS_BUFFER**

Controls the size of in-core integral storage buffer.

TYPE:

INTEGER

DEFAULT:

15 15 Megabytes.

OPTIONS:

User defined size.

RECOMMENDATION:

Use the default, or consult your systems administrator for hardware limits.

**INTEGRAL_2E_OPR**

Determines the two-electron operator.

TYPE:

INTEGER

DEFAULT:

-2 Coulomb Operator.

OPTIONS:

-1 Apply the CASE approximation.

-2 Coulomb Operator.

RECOMMENDATION:

Use the default unless the CASE operator is desired.

**INTERNAL_STABILITY_CONV**

Convergence criterion for the Davidson solver (for the lowest eigenvalues).

TYPE:

INTEGER

DEFAULT:

4 (3 when FD_MAT_ON_VECS = TRUE)

OPTIONS:

$n$ Terminate Davidson iterations when the norm of the residual vector is below $10^{-n}$.

RECOMMENDATION:

Use the default.

**INTERNAL_STABILITY_DAVIDSON_ITER**

Maximum number of Davidson iterations allowed in one stability analysis.

TYPE:

INTEGER

DEFAULT:

50

OPTIONS:

$n$ Perform up to $n$ Davidson iterations.

RECOMMENDATION:

Use the default.

**INTERNAL_STABILITY_ITER**

Maximum number of new SCF calculations permitted after the first stability analysis is performed.

TYPE:

INTEGER

DEFAULT:

0 (automatically set to 1 if INTERNAL_STABILITY = TRUE)

OPTIONS:

| | |
|---|---|
| $n$ | $n$ new SCF calculations permitted. |

RECOMMENDATION:

Give a larger number if 1 is not enough (still unstable).

**INTERNAL_STABILITY_ROOTS**

Number of lowest Hessian eigenvalues to solve for.

TYPE:

INTEGER

DEFAULT:

2

OPTIONS:

| | |
|---|---|
| $n$ | Solve for $n$ lowest eigenvalues. |

RECOMMENDATION:

Use the default.

**INTERNAL_STABILITY**

Perform internal stability analysis in GEN_SCFMAN.

TYPE:

BOOLEAN

DEFAULT:

FALSE

OPTIONS:

| | |
|---|---|
| FALSE | Do not perform internal stability analysis after convergence. |
| TRUE | Perform internal stability analysis and generate the corrected MOs. |

RECOMMENDATION:

Turn it on when the SCF solution is prone to unstable solutions, especially for open-shell species.

**INTRACULE**

Controls whether intracule properties are calculated (see also the *$intracule* section).

TYPE:

LOGICAL

DEFAULT:

FALSE

OPTIONS:

| | |
|---|---|
| FALSE | No intracule properties. |
| TRUE | Evaluate intracule properties. |

RECOMMENDATION:

None

**IP_STATES**

Sets the number of ionized target states roots to find. By default, $\beta$ electron will be removed (see EOM_IP_BETA).

TYPE:

INTEGER/INTEGER ARRAY

DEFAULT:

0 Do not look for any IP states.

OPTIONS:

$[i, j, k \ldots]$ Find $i$ ionized states in the first irrep, $j$ states in the second irrep *etc.*

RECOMMENDATION:

None

**ISOTOPES**

Specifies if non-default masses are to be used in the frequency calculation.

TYPE:

LOGICAL

DEFAULT:

FALSE

OPTIONS:

| | |
|---|---|
| FALSE | Use default masses only. |
| TRUE | Read isotope masses from *$isotopes* section. |

RECOMMENDATION:

None

**JOBTYPE**

Specifies the type of calculation.

TYPE:

STRING

DEFAULT:

SP

OPTIONS:

| | |
|---|---|
| SP | Single point energy. |
| OPT | Geometry minimization. |
| TS | Transition structure search. |
| FREQ | Frequency calculation. |
| FORCE | Analytical force calculation. |
| RPATH | Intrinsic reaction coordinate calculation. |
| NMR | NMR chemical shift calculation. |
| ISSC | Indirect nuclear spin-spin coupling calculation. |
| BSSE | Basis-set superposition error (counterpoise) correction. |
| EDA | Energy decomposition analysis. |

RECOMMENDATION:

None

**KS_GAP_PRINT**

Control printing of (generalized Kohn-Sham) HOMO-LUMO gap information.

TYPE:

Boolean

DEFAULT:

false

OPTIONS:

| | |
|---|---|
| false | (default) do not print gap information |
| true | print gap information |

RECOMMENDATION:

Use in conjunction with KS_GAP_UNIT if true.

**KS_GAP_UNIT**

Unit for KS_GAP_PRINT and FOA_FUNDGAP (see Section 4.4.11)

TYPE:

INTEGER

DEFAULT:

0

OPTIONS:

| | |
|---|---|
| 0 | (default) hartrees |
| 1 | eV |

RECOMMENDATION:

none

**LB94_BETA**

Sets the $\beta$ parameter for the LB94 XC potential

TYPE:

INTEGER

DEFAULT:

500

OPTIONS:

| | |
|---|---|
| $n$ | Corresponding to $\beta = n/10000$. |

RECOMMENDATION:

Use the default.

**LINK_ATOM_PROJECTION**

Controls whether to perform a link-atom projection

TYPE:

LOGICAL

DEFAULT:

TRUE

OPTIONS:

| | |
|---|---|
| TRUE | Performs the projection |
| FALSE | No projection |

RECOMMENDATION:

Necessary in a full QM/MM Hessian evaluation on a system with link atoms

**LIN_K**

Controls whether linear scaling evaluation of exact exchange (LinK) is used.

TYPE:

LOGICAL

DEFAULT:

Program chooses, switching on LinK whenever CFMM is used.

OPTIONS:

| | |
|---|---|
| TRUE | Use LinK |
| FALSE | Do not use LinK |

RECOMMENDATION:

Use for HF and hybrid DFT calculations with large numbers of atoms.

**LOBA_THRESH**

Specifies the thresholds to use for LOBA

TYPE:

INTEGER

DEFAULT:

6015

OPTIONS:

$aabb$ $aa$ specifies the threshold to use for localization

$bb$ specifies the threshold to use for occupation

Both are given as percentages.

RECOMMENDATION:

Decrease $bb$ to see the smaller contributions to orbitals. Values of $aa$ between 40 and 75 have been shown to given meaningful results.

**LOBA**

Specifies the methods to use for LOBA

TYPE:

INTEGER

DEFAULT:

00

OPTIONS:

$ab$

$a$ specifies the localization method

0 Perform Boys localization.

1 Perform PM localization.

2 Perform ER localization.

$b$ specifies the population analysis method

0 Do not perform LOBA. This is the default.

1 Use Mulliken population analysis.

2 Use Löwdin population analysis.

RECOMMENDATION:

Boys Localization is the fastest. ER will require an auxiliary basis set.

LOBA 12 provides a reasonable speed/accuracy compromise.

**LOCALFREQ_GROUP1**

Select the number of modes to include in the first subset of modes to localize independently when the keyword LOCALFREQ_GROUPS > 0.

TYPE:

INTEGER

DEFAULT:

NONE

OPTIONS:

$n$ User-specified integer.

RECOMMENDATION:

Modes will be included starting with the lowest frequency mode and then in ascending energy order up to the defined value.

**LOCALFREQ_GROUPS**

Select the number of groups of frequencies to be localized separately within a localized mode calculation. The size of the groups are then controlled using the LOCALFREQ_GROUP1, LOCALFREQ_GROUP2, and LOCALFREQ_GROUP3 keywords.

TYPE:

INTEGER

DEFAULT:

0 Localize all normal modes together.

OPTIONS:

1 Define one subset of modes to localize independently.
2 Define two subsets of modes to localize independently.
3 Define three subsets of modes to localize independently.

RECOMMENDATION:

None

**LOCALFREQ_MAX_ITER**

Controls the maximum number of mode localization sweeps permitted.

TYPE:

INTEGER

DEFAULT:

200

OPTIONS:

$n$ User-specified integer.

RECOMMENDATION:

None

**LOCALFREQ_SELECT**

Select a subset of normal modes for subsequent anharmonic frequency analysis.

TYPE:

LOGICAL

DEFAULT:

FALSE Use all normal modes.

OPTIONS:

TRUE Select a subset of normal modes.

RECOMMENDATION:

None

**LOCALFREQ_THRESH**

Mode localization is considered converged when the change in the localization criterion is less than $10^{-\mathrm{LOCALFREQ\_THRESH}}$.

TYPE:

INTEGER

DEFAULT:

6

OPTIONS:

$n$ User-specified integer.

RECOMMENDATION:

None

**LOCAL_FREQ**

Controls whether a vibrational mode localization calculation is performed.

TYPE:

INTEGER

DEFAULT:

0 Normal mode calculation.

OPTIONS:

1 Localized mode calculation with a Pipek-Mezey like criterion.

2 Localized mode calculation with a Boys like criterion.

RECOMMENDATION:

None

**LOCAL_INTERP_ORDER**

Controls the order of the B-spline

TYPE:

INTEGER

DEFAULT:

6

OPTIONS:

$n$ An integer

RECOMMENDATION:

The default value is sufficiently accurate

**LOC_CIS_OV_SEPARATE**

Decide whether or not to localized the "occupied" and "virtual" components of the localized diabatization function, *i.e.*, whether to localize the electron attachments and detachments separately.

TYPE:

LOGICAL

DEFAULT:

FALSE Do not separately localize electron attachments and detachments.

OPTIONS:

TRUE

RECOMMENDATION:

If one wants to use Boys localized diabatization for energy transfer (as opposed to electron transfer) , this is a necessary option. ER is more rigorous technique, and does not require this OV feature, but will be somewhat slower.

**LOWDIN_POPULATION**

Run Löwdin population analysis.

TYPE:

LOGICAL

DEFAULT:

FALSE

OPTIONS:

| | |
|---|---|
| FALSE | Do not calculate Löwdin populations. |
| TRUE | Run Löwdin population analysis. |

RECOMMENDATION:

None

**LRC_DFT**

Controls the application of long-range-corrected DFT

TYPE:

LOGICAL

DEFAULT:

FALSE

OPTIONS:

| | |
|---|---|
| FALSE (or 0) | Do not apply long-range correction. |
| TRUE (or 1) | Add 100% long-range Hartree-Fock exchange to the requested functional. |

RECOMMENDATION:

The *$rem* variable OMEGA must also be specified, in order to set the range-separation parameter.

**MANY_BODY_BSSE**

Controls the type of many-body BSSE corrections.

TYPE:

STRING

DEFAULT:

MBCP

OPTIONS:

| | |
|---|---|
| MBCP | Use many-body counterpoise correction. |
| VMFC | Use Valiron-Mayer function counterpoise correction. |

RECOMMENDATION:

NONE.

**MANY_BODY_INT**

Perform a MBE calculation.

TYPE:

BOOLEAN

DEFAULT:

FALSE

OPTIONS:

| | |
|---|---|
| TRUE | Perform a MBE calculation. |
| FALSE | Do not perform a MBE calculation. |

RECOMMENDATION:

NONE

**MAX_CIS_CYCLES**

Maximum number of CIS iterative cycles allowed.

TYPE:

INTEGER

DEFAULT:

30

OPTIONS:

| | |
|---|---|
| $n$ | User-defined number of cycles. |

RECOMMENDATION:

Default is usually sufficient.

**MAX_CIS_SUBSPACE**

Maximum number of subspace vectors allowed in the CIS iterations

TYPE:

INTEGER

DEFAULT:

As many as required to converge all roots

OPTIONS:

$n$ User-defined number of subspace vectors

RECOMMENDATION:

The default is usually appropriate, unless a large number of states are requested for a large molecule. The total memory required to store the subspace vectors is bounded above by $2nOV$, where $O$ and $V$ represent the number of occupied and virtual orbitals, respectively. $n$ can be reduced to save memory, at the cost of a larger number of CIS iterations. Convergence may be impaired if $n$ is not much larger than CIS_N_ROOTS.

**MAX_DIIS_CYCLES**

The maximum number of DIIS iterations before switching to (geometric) direct minimization when SCF_ALGORITHM is DIIS_GDM or DIIS_DM. See also THRESH_DIIS_SWITCH.

TYPE:

INTEGER

DEFAULT:

50

OPTIONS:

1 Only a single Roothaan step before switching to (G)DM

$n$ $n$ DIIS iterations before switching to (G)DM.

RECOMMENDATION:

None

**MAX_RCA_CYCLES**

The maximum number of RCA iterations before switching to DIIS when SCF_ALGORITHM is RCA_DIIS.

TYPE:

INTEGER

DEFAULT:

50

OPTIONS:

N N RCA iterations before switching to DIIS

RECOMMENDATION:

None

**MAX_SCF_CYCLES**

Controls the maximum number of SCF iterations permitted.

TYPE:

INTEGER

DEFAULT:

50

OPTIONS:

$n$ $n > 0$ User-selected.

RECOMMENDATION:

Increase for slowly converging systems such as those containing transition metals.

**MBE_BSSE_ORDER**

Controls the order of many-body BSSE corrections.

TYPE:

INTEGER

DEFAULT:

2

OPTIONS:

$n$ Order of many-body BSSE corrections

RECOMMENDATION:

MBCP and VMFC can be performed up to fourth order.

**MBE_EMBEDDING**

Controls the type of MBE calculations.

TYPE:

STRING

DEFAULT:

GAS

OPTIONS:

| | |
|---|---|
| GAS | MBE without charge embedding. |
| CHARGES | MBE with charge embedding. |

RECOMMENDATION:

NONE.

**MBE_ORDER**

Controls the truncation order $n$ for MBE.

TYPE:

INTEGER

DEFAULT:

2

OPTIONS:

$N$ Order of MBE

RECOMMENDATION:

MBE can be performed up to fifth order.

**MECP_METHODS**

Determines which method to be used.

TYPE:

STRING

DEFAULT:

BRANCHING_PLANE

OPTIONS:

| | |
|---|---|
| BRANCHING_PLANE | Use the branching-plane updating method. |
| MECP_DIRECT | Use the direct method. |
| PENALTY_FUNCTION | Use the penalty-constrained method. |

RECOMMENDATION:

The direct method is stable for small molecules or molecules with high symmetry. The branching-plane updating method is more efficient for larger molecules but does not work if the two states have different symmetries. If using the branching-plane updating method, GEOM_OPT_COORDS must be set to 0 in the *$rem* section, as this algorithm is available in Cartesian coordinates only. The penalty-constrained method converges slowly and is suggested only if other methods fail.

**MECP_OPT**

Determines whether we are doing MECP optimizations.

TYPE:

LOGICAL

DEFAULT:

FALSE

OPTIONS:

| | |
|---|---|
| TRUE | Do MECP optimization. |
| FALSE | Do not do MECP optimization. |

RECOMMENDATION:

None.

**MECP_PROJ_HESS**

Determines whether to project out the coupling vector from the Hessian when using branching plane updating method.

TYPE:

LOGICAL

DEFAULT:

TRUE

OPTIONS:

TRUE

FALSE

RECOMMENDATION:

Use the default.

**MECP_STATE1**

Sets the first Born-Oppenheimer state for MECP optimization.

TYPE:

INTEGER/INTEGER ARRAY

DEFAULT:

None

OPTIONS:

$[i,j]$ Find the $j$th excited state with the total spin $i$; $j = 0$ means the SCF ground state.

RECOMMENDATION:

$i$ is ignored for restricted calculations; for unrestricted calculations, $i$ can only be 0 or 1.

**MECP_STATE2**

Sets the second Born-Oppenheimer state for MECP optimization.

TYPE:

INTEGER/INTEGER ARRAY

DEFAULT:

None

OPTIONS:

$[i,j]$ Find the $j$th excited state with the total spin $i$; $j = 0$ means the SCF ground state.

RECOMMENDATION:

$i$ is ignored for restricted calculations; for unrestricted calculations, $i$ can only be 0 or 1.

**MEM_STATIC**

Sets the memory for Fortran AO integral calculation and transformation modules.

TYPE:

INTEGER

DEFAULT:

64 corresponding to 64 Mb.

OPTIONS:

$n$ User-defined number of megabytes.

RECOMMENDATION:

For direct and semi-direct MP2 calculations, this must exceed OVN + requirements for AO integral evaluation (32–160 Mb), as discussed above.

**MEM_TOTAL**

Sets the total memory available to Q-CHEM, in megabytes.

TYPE:

INTEGER

DEFAULT:

2000 Corresponding to 2000 Mb.

OPTIONS:

$n$ User-defined number of megabytes.

RECOMMENDATION:

Use the default, or set equal to the physical memory of your machine. Note that if the memory allocation total more than 1 Gb for a CCMAN job, the memory is allocated as follows

| | |
|---|---|
| 12% | MEM_STATIC |
| 50% | CC_MEMORY |
| 35% | Other memory requirements: |

**METECO**

Sets the threshold criteria for discarding shell-pairs.

TYPE:

INTEGER

DEFAULT:

2 Discard shell-pairs below $10^{-\mathrm{THRESH}}$.

OPTIONS:

1 Discard shell-pairs four orders of magnitude below machine precision.

2 Discard shell-pairs below $10^{-\mathrm{THRESH}}$.

RECOMMENDATION:

Use the default.

**METHOD**

Specifies the exchange-correlation functional.

TYPE:

STRING

DEFAULT:

No default

OPTIONS:

*NAME* Use METHOD = *NAME*, where *NAME* is either HF for Hartree-Fock theory or else one of the DFT methods listed in Section 4.4.3.4.

RECOMMENDATION:

In general, consult the literature to guide your selection. Our recommendations for DFT are indicated in bold in Section 4.4.3.4.

**MGC_AMODEL**

Choice of approximate cluster model.

TYPE:

INTEGER

DEFAULT:

Determines how the CC equations are approximated:

OPTIONS:

0 Local Active-Space Amplitude iterations (pre-calculate GVB orbitals with your method of choice (RPP is good)).

7 Optimize-Orbitals using the VOD 2-step solver.
(Experimental-only use with MGC_AMPS = 2, 24 ,246)

8 Traditional Coupled Cluster up to CCSDTQPH.

9 MR-CC version of the Pair-Models. (Experimental)

RECOMMENDATION:

None

**MGC_AMPS**

Choice of Amplitude Truncation

TYPE:

INTEGER

DEFAULT:

None

OPTIONS:

2$\leq$ n $\leq$ 123456, a sorted list of integers for every amplitude
which will be iterated. Choose 1234 for PQ and 123456 for PH

RECOMMENDATION:

None

**MGC_LOCALINTER**

Pair filter on an intermediate.

TYPE:

LOGICAL

DEFAULT:

FALSE

OPTIONS:

Any nonzero value enforces the pair constraint on intermediates,
significantly reducing computational cost. Not recommended for $\leq$ 2 pair locality

RECOMMENDATION:

None

**MGC_LOCALINTS**

Pair filter on an integrals.

TYPE:

LOGICAL

DEFAULT:

FALSE

OPTIONS:

Enforces a pair filter on the 2-electron integrals, significantly

reducing computational cost. Generally useful. for more than 1 pair locality.

RECOMMENDATION:

None

**MGC_NLPAIRS**

Number of local pairs on an amplitude.

TYPE:

INTEGER

DEFAULT:

None

OPTIONS:

Must be greater than 1, which corresponds to the PP model. 2 for PQ, and 3 for PH.

RECOMMENDATION:

None

**MGEMM_THRESH**

Sets MGEMM threshold to determine the separation between "large" and "small" matrix elements. A larger threshold value will result in a value closer to the single-precision result. Note that the desired factor should be multiplied by 10000 to ensure an integer value.

TYPE:

INTEGER

DEFAULT:

10000 (corresponds to 1)

OPTIONS:

$n$ User-specified threshold

RECOMMENDATION:

For small molecules and basis sets up to triple-$\zeta$, the default value suffices to not deviate too much from the double-precision values. Care should be taken to reduce this number for larger molecules and also larger basis-sets.

**MI_ACTIVE_FRAGMENT**

Sets the active fragment

TYPE:

INTEGER

DEFAULT:

NO DEFAULT

OPTIONS:

$n$ Specify the fragment on which the TDDFT calculation is to be performed, for LEA-TDDFT(MI).

RECOMMENDATION:

None

**MI_LEA**

Controls the LEA-TDDFT(MI) methods

TYPE:

INTEGER

DEFAULT:

NO DEFAULT

OPTIONS:

0 The LEA0 method

1 The LEA-Q method

2 The LEAc method

RECOMMENDATION:

1

**MM_CHARGES**

Requests the calculation of multipole-derived charges (MDCs).

TYPE:

LOGICAL

DEFAULT:

FALSE

OPTIONS:

TRUE Calculates the MDCs and also the traceless form of the multipole moments

RECOMMENDATION:

Set to TRUE if MDCs or the traceless form of the multipole moments are desired. The calculation does not take long.

**MM_SUBTRACTIVE**

Specifies whether a subtractive scheme is used in the $E_{\text{Coul}}$, Eq. (11.38), portion of the calculation.

TYPE:

LOGICAL

DEFAULT:

FALSE

OPTIONS:

FALSE Only pairs that are not 1-2, 1-3, or 1-4 pairs are used.

TRUE All pairs are calculated, and then the pairs that are double counted (1-2, 1-3, and 1-4) are subtracted out.

RECOMMENDATION:

When running QM/MM or MM calculations there is not recommendation. When running a QM/MM Ewald calculation the value must be set to TRUE.

**MODEL_SYSTEM_CHARGE**

Specifies the QM subsystem charge if different from the *$molecule* section.

TYPE:

INTEGER

DEFAULT:

NONE

OPTIONS:

$n$ The charge of the QM subsystem.

RECOMMENDATION:

This option only needs to be used if the QM subsystem (model system) has a charge that is different from the total system charge.

**MODEL_SYSTEM_MULT**

Specifies the QM subsystem multiplicity if different from the *$molecule* section.

TYPE:

INTEGER

DEFAULT:

NONE

OPTIONS:

$n$ The multiplicity of the QM subsystem.

RECOMMENDATION:

This option only needs to be used if the QM subsystem (model system) has a multiplicity that is different from the total system multiplicity. ONIOM calculations must be closed shell.

**MODE_COUPLING**

Number of modes coupling in the third and fourth derivatives calculation.

TYPE:

INTEGER

DEFAULT:

2 for two modes coupling.

OPTIONS:

$n$ for $n$ modes coupling, Maximum value is 4.

RECOMMENDATION:

Use the default.

**MOLDEN_FORMAT**

Requests a MOLDEN-formatted input file containing information from a Q-CHEM job.

TYPE:

LOGICAL

DEFAULT:

FALSE

OPTIONS:

TRUE Append MOLDEN input file at the end of the Q-CHEM output file.

RECOMMENDATION:

None.

**MOM_METHOD**

Determines the target orbitals with which to maximize the overlap on each SCF cycle.

TYPE:

INTEGER

DEFAULT:

3

OPTIONS:

| | |
|---|---|
| 3 | Maximize overlap with the orbitals from the previous SCF cycle. |
| 13 | Maximize overlap with the initial guess orbitals. |

RECOMMENDATION:

If appropriate guess orbitals can be obtained, then MOM_METHOD = 13 can provide more reliable convergence to the desired solution.

**MOM_PRINT**

Switches printing on within the MOM procedure.

TYPE:

LOGICAL

DEFAULT:

FALSE

OPTIONS:

| | |
|---|---|
| FALSE | Printing is turned off |
| TRUE | Printing is turned on. |

RECOMMENDATION:

None

**MOM_START**

Determines when MOM is switched on to stabilize DIIS iterations.

TYPE:

INTEGER

DEFAULT:

0 (FALSE)

OPTIONS:

| | |
|---|---|
| 0 (FALSE) | MOM is not used |
| $n$ | MOM begins on cycle $n$. |

RECOMMENDATION:

Set to 1 if preservation of initial orbitals is desired. If MOM is to be used to aid convergence, an SCF without MOM should be run to determine when the SCF starts oscillating. MOM should be set to start just before the oscillations.

**MOPROP_CONV_1ST**

Sets the convergence criteria for CPSCF and 1st order TDSCF.

TYPE:

INTEGER

DEFAULT:

6

OPTIONS:

| | |
|---|---|
| $n < 10$ | Convergence threshold set to $10^{-n}$. |

RECOMMENDATION:

None

**MOPROP_CONV_2ND**

Sets the convergence criterion for second-order TDSCF.

TYPE:

INTEGER

DEFAULT:

6

OPTIONS:

$n < 10$ Convergence threshold set to $10^{-n}$.

RECOMMENDATION:

None

**MOPROP_DIIS_DIM_SS**

Specified the DIIS subspace dimension.

TYPE:

INTEGER

DEFAULT:

20

OPTIONS:

0 No DIIS.

$n$ Use a subspace of dimension $n$.

RECOMMENDATION:

None

**MOPROP_DIIS**

Controls the use of Pulay's DIIS in solving the CPSCF equations.

TYPE:

INTEGER

DEFAULT:

5

OPTIONS:

0 Turn off DIIS.

5 Turn on DIIS.

RECOMMENDATION:

None

**MOPROP_ISSC_PRINT_REDUCED**

Specifies whether the isotope-independent reduced coupling tensor $\mathbf{K}$ should be printed in addition to the isotope-dependent $\mathbf{J}$-tensor when calculating indirect nuclear spin–spin couplings.

TYPE:

LOGICAL

DEFAULT:

FALSE

OPTIONS:

FALSE Do not print $\mathbf{K}$.

TRUE Print $\mathbf{K}$.

RECOMMENDATION:

None

**MOPROP_ISSC_SKIP_DSO**

Specifies whether to skip the calculation of the diamagnetic spin–orbit contribution to the indirect nuclear spin–spin coupling tensor.

TYPE:

LOGICAL

DEFAULT:

FALSE

OPTIONS:

| | |
|---|---|
| FALSE | Calculate diamagnetic spin–orbit contribution. |
| TRUE | Skip diamagnetic spin–orbit contribution. |

RECOMMENDATION:

None

**MOPROP_ISSC_SKIP_FC**

Specifies whether to skip the calculation of the Fermi contact contribution to the indirect nuclear spin–spin coupling tensor.

TYPE:

LOGICAL

DEFAULT:

FALSE

OPTIONS:

| | |
|---|---|
| FALSE | Calculate Fermi contact contribution. |
| TRUE | Skip Fermi contact contribution. |

RECOMMENDATION:

None

**MOPROP_ISSC_SKIP_PSO**

Specifies whether to skip the calculation of the paramagnetic spin–orbit contribution to the indirect nuclear spin–spin coupling tensor.

TYPE:

LOGICAL

DEFAULT:

FALSE

OPTIONS:

| | |
|---|---|
| FALSE | Calculate paramagnetic spin–orbit contribution. |
| TRUE | Skip paramagnetic spin–orbit contribution. |

RECOMMENDATION:

None

**MOPROP_ISSC_SKIP_SD**

Specifies whether to skip the calculation of the spin–dipole contribution to the indirect nuclear spin–spin coupling tensor.

TYPE:

LOGICAL

DEFAULT:

FALSE

OPTIONS:

| | |
|---|---|
| FALSE | Calculate spin–dipole contribution. |
| TRUE | Skip spin–dipole contribution. |

RECOMMENDATION:

None

**MOPROP_MAXITER_1ST**

The maximum number of iterations for CPSCF and first-order TDSCF.

TYPE:

INTEGER

DEFAULT:

50

OPTIONS:

$n$ Set maximum number of iterations to $n$.

RECOMMENDATION:

Use the default.

**MOPROP_MAXITER_2ND**

The maximum number of iterations for second-order TDSCF.

TYPE:

INTEGER

DEFAULT:

50

OPTIONS:

$n$ Set maximum number of iterations to $n$.

RECOMMENDATION:

Use the default.

**MOPROP_PERTNUM**

Set the number of perturbed densities that will to be treated together.

TYPE:

INTEGER

DEFAULT:

0

OPTIONS:

| | |
|---|---|
| 0 | All at once. |
| $n$ | Treat the perturbed densities batch-wise. |

RECOMMENDATION:

Use the default. For large systems, limiting this number may be required to avoid memory exhaustion.

**MOPROP**

Specifies the job for mopropman.

TYPE:

INTEGER

DEFAULT:

0 Do not run mopropman.

OPTIONS:

| | |
|---|---|
| 1 | NMR chemical shielding tensors. |
| 2 | Static polarizability. |
| 3 | Indirect nuclear spin–spin coupling tensors. |
| 100 | Dynamic polarizability. |
| 101 | First hyperpolarizability. |
| 102 | First hyperpolarizability, reading First order results from disk. |
| 103 | First hyperpolarizability using Wigner's $(2n + 1)$ rule. |
| 104 | First hyperpolarizability using Wigner's $(2n + 1)$ rule, reading first order results from disk. |

RECOMMENDATION:

None

**MRXC_CLASS_THRESH_MULT**

Controls the of smoothness precision

TYPE:

INTEGER

DEFAULT:

1

OPTIONS:

$im$ An integer

RECOMMENDATION:

A prefactor in the threshold for MRXC error control: $im \times 10^{-io}$

**MRXC_CLASS_THRESH_ORDER**

Controls the of smoothness precision

TYPE:

INTEGER

DEFAULT:

6

OPTIONS:

$io$ An integer

RECOMMENDATION:

The exponent in the threshold of the MRXC error control: $im \times 10^{-io}$

**MRXC**

Controls the use of MRXC.

TYPE:

INTEGER

DEFAULT:

0

OPTIONS:

0 Do not use MRXC

1 Use MRXC in the evaluation of the XC part

RECOMMENDATION:

MRXC is very efficient for medium and large molecules, especially when medium and large basis sets are used.

**MULTIPOLE_ORDER**

Determines highest order of multipole moments to print if wave function analysis requested.

TYPE:

INTEGER

DEFAULT:

4

OPTIONS:

$n$ Calculate moments to $n$th order.

RECOMMENDATION:

Use the default unless higher multipoles are required.

**NBO**

Controls the use of the NBO package.

TYPE:

INTEGER

DEFAULT:

0

OPTIONS:

0 Do not invoke the NBO package.

1 Do invoke the NBO package, for the ground state.

2 Invoke the NBO package for the ground state, and also each CIS, RPA, or TDDFT excited state.

RECOMMENDATION:

None

**NL_CORRELATION**

Specifies a non-local correlation functional that includes non-empirical dispersion.

TYPE:

STRING

DEFAULT:

None No non-local correlation.

OPTIONS:

| | |
|---|---|
| None | No non-local correlation |
| vdW-DF-04 | the non-local part of vdW-DF-04 |
| vdW-DF-10 | the non-local part of vdW-DF-10 (also known as vdW-DF2) |
| VV09 | the non-local part of VV09 |
| VV10 | the non-local part of VV10 |

RECOMMENDATION:

Do not forget to add the LSDA correlation (PW92 is recommended) when using vdW-DF-04, vdW-DF-10, or VV09. VV10 should be used with PBE correlation. Choose exchange functionals carefully: HF, rPW86, revPBE, and some of the LRC exchange functionals are among the recommended choices.

**NL_GRID**

Specifies the grid to use for non-local correlation.

TYPE:

INTEGER

DEFAULT:

1

OPTIONS:

Same as for XC_GRID

RECOMMENDATION:

Use the default unless computational cost becomes prohibitive, in which case SG-0 may be used. XC_GRID should generally be finer than NL_GRID.

**NL_VV_B**

Sets the parameter $b$ in VV10. This parameter controls the short range behavior of the non-local correlation energy.

TYPE:

INTEGER

DEFAULT:

No default

OPTIONS:

$n$ Corresponding to $b = n/100$

RECOMMENDATION:

The optimal value depends strongly on the exchange functional used. $b = 5.9$ is recommended for rPW86. For further details see Ref. 18.

**NL_VV_C**

Sets the parameter $C$ in VV09 and VV10. This parameter is fitted to asymptotic van der Waals $C_6$ coefficients.

TYPE:

INTEGER

DEFAULT:

| | |
|---|---|
| 89 | for VV09 |
| No default | for VV10 |

OPTIONS:

| | |
|---|---|
| $n$ | Corresponding to $C = n/10000$ |

RECOMMENDATION:

$C = 0.0093$ is recommended when a semi-local exchange functional is used. $C = 0.0089$ is recommended when a long-range corrected (LRC) hybrid functional is used. For further details see Ref. 18.

**NOCI_PRINT**

Specify the debug print level of NOCI.

TYPE:

INTEGER

DEFAULT:

1

OPTIONS:

| | |
|---|---|
| $n$ | Positive integer |

RECOMMENDATION:

Increase this for additional debug information.

**NOSE_HOOVER_LENGTH**

Sets the chain length for the Nosé-Hoover thermostat

TYPE:

INTEGER

DEFAULT:

none

OPTIONS:

| | |
|---|---|
| $n$ | Chain length of $n$ auxiliary variables |

RECOMMENDATION:

Typically 3-6

**NOSE_HOOVER_TIMESCALE**

Sets the timescale (strength) of the Nosé-Hoover thermostat

TYPE:

INTEGER

DEFAULT:

none

OPTIONS:

| | |
|---|---|
| $n$ | Thermostat timescale, as $n$ fs |

RECOMMENDATION:

Smaller values (roughly 100) equate to tighter thermostats but may inhibit rapid sampling. Larger values ($\geq$ 1000) allow for more rapid sampling but may take longer to reach thermal equilibrium.

**NTO_PAIRS**

Controls the writing of hole/particle NTO pairs for excited state.

TYPE:

INTEGER

DEFAULT:

0

OPTIONS:

$N$ Write $N$ NTO pairs per excited state.

RECOMMENDATION:

If activated ($N > 0$), a minimum of two NTO pairs will be printed for each state. Increase the value of $N$ if additional NTOs are desired.

**NVO_LIN_CONVERGENCE**

Target error factor in the preconditioned conjugate gradient solver of the single-excitation amplitude equations.

TYPE:

INTEGER

DEFAULT:

3

OPTIONS:

$n$ User–defined number.

RECOMMENDATION:

Solution of the single-excitation amplitude equations is considered converged if the maximum residual is less than $10^{-n}$ multiplied by the current DIIS error. For the ARS correction, $n$ is automatically set to 1 since the locally-projected DIIS error is normally several orders of magnitude smaller than the full DIIS error.

**NVO_LIN_MAX_ITE**

Maximum number of iterations in the preconditioned conjugate gradient solver of the single-excitation amplitude equations.

TYPE:

INTEGER

DEFAULT:

30

OPTIONS:

$n$ User–defined number of iterations.

RECOMMENDATION:

None.

**NVO_METHOD**

Sets method to be used to converge solution of the single-excitation amplitude equations.

TYPE:

INTEGER

DEFAULT:

9

OPTIONS:

$n$ User–defined number.

RECOMMENDATION:

This is an experimental option. Use the default.

**NVO_TRUNCATE_DIST**

Specifies which atomic blocks of the Fock matrix are used to construct the preconditioner.

TYPE:

INTEGER

DEFAULT:

-1

OPTIONS:

| | |
|---|---|
| $n > 0$ | If distance between a pair of atoms is more than $n$ Ångstroms<br>do not include the atomic block. |
| -2 | Do not use distance threshold, use NVO_TRUNCATE_PRECOND instead. |
| -1 | Include all blocks. |
| 0 | Include diagonal blocks only. |

RECOMMENDATION:

This option does not affect the final result. However, it affects the rate of the PCG algorithm convergence. For small systems, use the default.

**NVO_TRUNCATE_PRECOND**

Specifies which atomic blocks of the Fock matrix are used to construct the preconditioner. This variable is used only if NVO_TRUNCATE_DIST is set to $-2$.

TYPE:

INTEGER

DEFAULT:

2

OPTIONS:

| | |
|---|---|
| $n$ | If the maximum element in an atomic block is less than $10^{-n}$ do not include<br>the block. |

RECOMMENDATION:

Use the default. Increasing $n$ improves convergence of the PCG algorithm but overall may slow down calculations.

**NVO_UVV_MAXPWR**

Controls convergence of the Taylor series when calculating the $U_{vv}$ block from the single-excitation amplitudes. If the series is not converged at the $n$th term, more expensive direct inversion is used to calculate the $U_{vv}$ block.

TYPE:

INTEGER

DEFAULT:

10

OPTIONS:

| | |
|---|---|
| $n$ | User–defined number. |

RECOMMENDATION:

None.

**NVO_UVV_PRECISION**

Controls convergence of the Taylor series when calculating the $U_{vv}$ block from the single-excitation amplitudes. Series is considered converged when the maximum element of the term is less than $10^{-n}$.

TYPE:

INTEGER

DEFAULT:

11

OPTIONS:

$n$ User–defined number.

RECOMMENDATION:

NVO_UVV_PRECISION must be the same as or larger than THRESH.

**N_FROZEN_CORE**

Sets the number of frozen core orbitals in a post-Hartree–Fock calculation.

TYPE:

INTEGER

DEFAULT:

FC

OPTIONS:

FC Frozen Core approximation (all core orbitals frozen).

$n$ Freeze $n$ core orbitals (if set to 0, all electrons will be active).

RECOMMENDATION:

Correlated calculations calculations are more efficient with frozen core orbitals. Use default if possible.

**N_FROZEN_VIRTUAL**

Sets the number of frozen virtual orbitals in a post-Hartree–Fock calculation.

TYPE:

INTEGER

DEFAULT:

0

OPTIONS:

$n$ Freeze $n$ virtual orbitals.

RECOMMENDATION:

None

**N_I_SERIES**

Sets summation limit for series expansion evaluation of $i_n(x)$.

TYPE:

INTEGER

DEFAULT:

40

OPTIONS:

$n > 0$

RECOMMENDATION:

Lower values speed up the calculation, but may affect accuracy.

**N_J_SERIES**

Sets summation limit for series expansion evaluation of $j_n(x)$.

TYPE:

INTEGER

DEFAULT:

40

OPTIONS:

$n > 0$

RECOMMENDATION:

Lower values speed up the calculation, but may affect accuracy.

**N_SOL**

Specifies number of atoms included in the Hessian.

TYPE:

INTEGER

DEFAULT:

No default

OPTIONS:

User defined

RECOMMENDATION:

None

**N_WIG_SERIES**

Sets summation limit for Wigner integrals.

TYPE:

INTEGER

DEFAULT:

10

OPTIONS:

$n < 100$

RECOMMENDATION:

Increase $n$ for greater accuracy.

**OCCUPATIONS**

Activates pFON calculation.

TYPE:

INTEGER

DEFAULT:

0

OPTIONS:

| | |
|---|---|
| 0 | Integer occupation numbers |
| 1 | Not yet implemented |
| 2 | Pseudo-fractional occupation numbers (pFON) |

RECOMMENDATION:

Use pFON to improve convergence for small-gap systems.

**OCC_RI_K**

Controls the use of the occ-RI-K approximation for constructing the exchange matrix

TYPE:

LOGICAL

DEFAULT:

False Do not use occ-RI-K.

OPTIONS:

True Use occ-RI-K.

RECOMMENDATION:

Larger the system, better the performance

**OMEGA2**

Sets the Coulomb attenuation parameter for the long-range component.

TYPE:

INTEGER

DEFAULT:

No default

OPTIONS:

$n$ Corresponding to $\omega 2 = n/1000$, in units of bohr$^{-1}$

RECOMMENDATION:

None

**OMEGA_GDD_SCALING**

Sets the empirical constant $C$ in $\omega_{\text{GDD}}$ tuning procedure.

TYPE:

INTEGER

DEFAULT:

885

OPTIONS:

$n$ Corresponding to $C = n/1000$.

RECOMMENDATION:

The quantity $n$ = 885 was determined by Lao and Herbert in Ref. 19 using LRC-$\omega$PBE and def2-TZVPP augmented with diffuse functions on non-hydrogen atoms that are taken from Dunning's aug-cc-pVTZ basis set.

**OMEGA_GDD**

Controls the application of $\omega_{\text{GDD}}$ tuning for long-range-corrected DFT

TYPE:

LOGICAL

DEFAULT:

FALSE

OPTIONS:

FALSE (or 0) Do not apply $\omega_{\text{GDD}}$ tuning.

TRUE (or 1) Use $\omega_{\text{GDD}}$ tuning.

RECOMMENDATION:

The *$rem* variable OMEGA must also be specified, in order to set the initial range-separation parameter.

**OMEGA**

Sets the range-separation parameter, $\omega$, also known as $\mu$, in functionals based on Hirao's RSH scheme.

TYPE:

INTEGER

DEFAULT:

No default

OPTIONS:

$n$ Corresponding to $\omega = n/1000$, in units of bohr$^{-1}$

RECOMMENDATION:

None

**OMEGA**

Sets the Coulomb attenuation parameter for the short-range component.

TYPE:

INTEGER

DEFAULT:

No default

OPTIONS:

$n$ Corresponding to $\omega = n/1000$, in units of bohr$^{-1}$

RECOMMENDATION:

None

**OS_ROSCF**

Run an open-shell singlet ROSCF calculation with GEN_SCFMAN.

TYPE:

BOOLEAN

DEFAULT:

FALSE

OPTIONS:

TRUE OS_ROSCF calculation is performed.

FALSE Do not run OS_ROSCF (it will run a close-shell RSCF calculation instead).

RECOMMENDATION:

Set to TRUE if desired.

**PAO_ALGORITHM**

Algorithm used to optimize polarized atomic orbitals (see PAO_METHOD)

TYPE:

INTEGER

DEFAULT:

0

OPTIONS:

0 Use efficient (and riskier) strategy to converge PAOs.

1 Use conservative (and slower) strategy to converge PAOs.

RECOMMENDATION:

None

**PAO_METHOD**

Controls evaluation of polarized atomic orbitals (PAOs).

TYPE:

STRING

DEFAULT:

EPAO For local MP2 calculations Otherwise no default.

OPTIONS:

PAO Perform PAO-SCF instead of conventional SCF.

EPAO Obtain EPAOs after a conventional SCF.

RECOMMENDATION:

None

**PARI_K**

Controls the use of the PARI-K approximation in the construction of the exchange matrix

TYPE:

LOGICAL

DEFAULT:

FALSE Do not use PARI-K.

OPTIONS:

TRUE Use PARI-K.

RECOMMENDATION:

Use for basis sets aug-cc-pVTZ and larger.

**PBHT_ANALYSIS**

Controls whether overlap analysis of electronic excitations is performed.

TYPE:

LOGICAL

DEFAULT:

FALSE

OPTIONS:

FALSE Do not perform overlap analysis.

TRUE Perform overlap analysis.

RECOMMENDATION:

None

**PBHT_FINE**

Increases accuracy of overlap analysis.

TYPE:

LOGICAL

DEFAULT:

FALSE

OPTIONS:

FALSE

TRUE Increase accuracy of overlap analysis.

RECOMMENDATION:

None

**PEQ_SWITCH**

Inclusion of solvent effects begins when the SCF error falls below $10^{-\text{PEQ\_SWITCH}}$.

TYPE:

INTEGER

DEFAULT:

3

OPTIONS:

$n$ Corresponding to $10^{-n}$

RECOMMENDATION:

Use the default unless solvent effects need to be incorporated at earlier SCF cycles.

**PHESS**

Controls whether partial Hessian calculations are performed.

TYPE:

INTEGER

DEFAULT:

0 Full Hessian calculation

OPTIONS:

1 Partial Hessian calculation.

2 Vibrational subsystem analysis (massless).

3 Vibrational subsystem analysis (weighted).

RECOMMENDATION:

None

**PH_FAST**

Lowers integral cutoff in partial Hessian calculation is performed.

TYPE:

LOGICAL

DEFAULT:

FALSE Use default cutoffs

OPTIONS:

TRUE Lower integral cutoffs

RECOMMENDATION:

None

**PIMC_ACCEPT_RATE**

Acceptance rate for MC/PIMC simulations when Cartesian or normal-mode displacements are utilized.

TYPE:

INTEGER

DEFAULT:

None

OPTIONS:

$0 < n < 100$ User-specified rate, given as a whole-number percentage.

RECOMMENDATION:

Choose acceptance rate to maximize sampling efficiency, which is typically signified by the mean-square displacement (printed in the job output). Note that the maximum displacement is adjusted during the warm-up run to achieve roughly this acceptance rate.

**PIMC_MCMAX**

Number of Monte Carlo steps to sample.

TYPE:

INTEGER

DEFAULT:

None.

OPTIONS:

User-specified number of steps to sample.

RECOMMENDATION:

This variable dictates the statistical convergence of MC/PIMC simulations. For converged simulations at least $10^5$ steps is recommended.

**PIMC_MOVETYPE**

Selects the type of displacements used in MC/PIMC simulations.

TYPE:

INTEGER

DEFAULT:

0

OPTIONS:

| | |
|---|---|
| 0 | Cartesian displacements of all beads, with occasional (1%) center-of-mass moves. |
| 1 | Normal-mode displacements of all modes, with occasional (1%) center-of-mass moves. |
| 2 | Levy flights without center-of-mass moves. |

RECOMMENDATION:

Except for classical sampling (MC) or small bead-number quantum sampling (PIMC), Levy flights should be utilized. For Cartesian and normal-mode moves, the maximum displacement is adjusted during the warm-up run to the desired acceptance rate (controlled by PIMC_ACCEPT_RATE). For Levy flights, the acceptance is solely controlled by PIMC_SNIP_LENGTH.

**PIMC_NBEADSPERATOM**

Number of path integral time slices (“beads”) used on each atom of a PIMC simulation.

TYPE:

INTEGER

DEFAULT:

None.

OPTIONS:

| | |
|---|---|
| 1 | Perform classical Boltzmann sampling. |
| $>1$ | Perform quantum-mechanical path integral sampling. |

RECOMMENDATION:

This variable controls the inherent convergence of the path integral simulation. The one-bead limit represents classical sampling and the infinite-bead limit represents exact quantum-mechanical sampling. Using 32 beads is reasonably converged for room-temperature simulations of molecular systems.

**PIMC_SNIP_LENGTH**

Number of "beads" to use in the Levy flight movement of the ring polymer.

TYPE:

INTEGER

DEFAULT:

None

OPTIONS:

$3 \leq n \leq$ PIMC_NBEADSPERATOM User-specified length of snippet.

RECOMMENDATION:

Choose the snip length to maximize sampling efficiency. The efficiency can be estimated by the mean-square displacement between configurations, printed at the end of the output file. This efficiency will typically, however, be a trade-off between the mean-square displacement (length of statistical correlations) and the number of beads moved. Only the moved beads require recomputing the potential, *i.e.*, a call to Q-CHEM for the electronic energy. (Note that the endpoints of the snippet remain fixed during a single move, so $n-2$ beads are actually moved for a snip length of $n$. For 1 or 2 beads in the simulation, Cartesian moves should be used instead.)

**PIMC_TEMP**

Temperature, in Kelvin (K), of path integral simulations.

TYPE:

INTEGER

DEFAULT:

None.

OPTIONS:

User-specified number of Kelvin for PIMC or classical MC simulations.

RECOMMENDATION:

None.

**PIMC_WARMUP_MCMAX**

Number of Monte Carlo steps to sample during an equilibration period of MC/PIMC simulations.

TYPE:

INTEGER

DEFAULT:

None.

OPTIONS:

User-specified number of steps to sample.

RECOMMENDATION:

Use this variable to equilibrate the molecule/ring polymer before collecting production statistics. Usually a short run of roughly 10% of PIMC_MCMAX is sufficient.

**PLOT_SPIN_DENSITY**

Requests the generation of spin densities, $\rho_\alpha$ and $\rho_\beta$.

TYPE:

LOGICAL

DEFAULT:

FALSE

OPTIONS:

| | |
|---|---|
| FALSE | Do not generate spin density cube files. |
| TRUE | Generate spin density cube files. |

RECOMMENDATION:

Set to TRUE if spin densities are desired in addition to total densities. Requires that MAKE_CUBE_FILES be set to TRUE as well, and that one or more total densities is requested in the *$plots* input section. The corresponding spin densities will then be generated also.

**POL_GEOM**

Compute forces on the polarized (converged SCFMI) PES.

TYPE:

BOOLEAN

DEFAULT:

FALSE

OPTIONS:

| | |
|---|---|
| FALSE | Do not compute forces on the polarized PES. |
| TRUE | Compute forces on the polarized PES. |

RECOMMENDATION:

Set it to TRUE when optimized geometry or vibrational frequencies on the polarized PES are desired.

**POP_MULLIKEN**

Controls running of Mulliken population analysis.

TYPE:

LOGICAL/INTEGER

DEFAULT:

TRUE (or 1)

OPTIONS:

| | |
|---|---|
| FALSE (or 0) | Do not calculate Mulliken populations. |
| TRUE (or 1) | Calculate Mulliken populations. |
| 2 | Also calculate shell populations for each occupied orbital. |
| $-1$ | Calculate Mulliken charges for both the ground state and any CIS, RPA, or TDDFT excited states. |

RECOMMENDATION:

Leave as TRUE, unless excited-state charges are desired. Mulliken analysis is a trivial additional calculation, for ground or excited states.

**PRINT_CORE_CHARACTER**

Determines the print level for the CORE_CHARACTER option.

TYPE:

INTEGER

DEFAULT:

0

OPTIONS:

0 No additional output is printed.

1 Prints core characters of occupied MOs.

2 Print level 1, plus prints the core character of AOs.

RECOMMENDATION:

Use the default, unless you are uncertain about what the core character is.

**PRINT_DIST_MATRIX**

Controls the printing of the inter-atomic distance matrix

TYPE:

INTEGER

DEFAULT:

15

OPTIONS:

0 Turns off the printing of the distance matrix

$n$ Prints the distance matrix if the number of atoms in the molecule is less than or equal to $n$.

RECOMMENDATION:

Use default unless distances are required for large systems

**PRINT_GENERAL_BASIS**

Controls print out of built in basis sets in input format

TYPE:

LOGICAL

DEFAULT:

FALSE

OPTIONS:

TRUE Print out standard basis set information

FALSE Do not print out standard basis set information

RECOMMENDATION:

Useful for modification of standard basis sets.

**PRINT_ORBITALS**

Prints orbital coefficients with atom labels in analysis part of output.

TYPE:

INTEGER/LOGICAL

DEFAULT:

FALSE

OPTIONS:

| | |
|---|---|
| FALSE | Do not print any orbitals. |
| TRUE | Prints occupied orbitals plus 5 virtual orbitals. |
| NVIRT | Number of virtual orbitals to print. |

RECOMMENDATION:

Use true unless more virtual orbitals are desired.

**PRINT_RADII_GYRE**

Controls printing of MO centroids and radii of gyration.

TYPE:

LOGICAL/INTEGER

DEFAULT:

FALSE

OPTIONS:

| | |
|---|---|
| TRUE (or 1) | Print the centroid and radius of gyration for each occupied MO and each density. |
| 2 | Print centroids and radii of gyration for the virtual MOs as well. |
| FALSE (or 0) | Do not calculate these quantities. |

RECOMMENDATION:

None

**PROJ_TRANSROT**

Removes translational and rotational drift during AIMD trajectories.

TYPE:

LOGICAL

DEFAULT:

FALSE

OPTIONS:

| | |
|---|---|
| FALSE | Do not apply translation/rotation corrections. |
| TRUE | Apply translation/rotation corrections. |

RECOMMENDATION:

When computing spectra (see AIMD_NUCL_DACF_POINTS, for example), this option can be utilized to remove artificial, contaminating peaks stemming from translational and/or rotational motion. Recommend setting to TRUE for all dynamics-based spectral simulations.

**PSEUDO_CANONICAL**

When SCF_ALGORITHM = DM, this controls the way the initial step, and steps after subspace resets are taken.

TYPE:

LOGICAL

DEFAULT:

FALSE

OPTIONS:

| | |
|---|---|
| FALSE | Use Roothaan steps when (re)initializing |
| TRUE | Use a steepest descent step when (re)initializing |

RECOMMENDATION:

The default is usually more efficient, but choosing TRUE sometimes avoids problems with orbital reordering.

**PURECART**

INTEGER

TYPE:

Controls the use of pure (spherical harmonic) or Cartesian angular forms

DEFAULT:

| | |
|---|---|
| 2111 | Cartesian $h$-functions and pure $g, f, d$ functions |

OPTIONS:

| | |
|---|---|
| $hgfd$ | Use 1 for pure and 2 for Cartesian. |

RECOMMENDATION:

This is pre-defined for all standard basis sets

**QMMM_CHARGES**

Controls the printing of QM charges to file.

TYPE:

LOGICAL

DEFAULT:

FALSE

OPTIONS:

| | |
|---|---|
| TRUE | Writes a charges.dat file with the Mulliken charges from the QM region. |
| FALSE | No file written. |

RECOMMENDATION:

Use the default unless running calculations with CHARMM where charges on the QM region need to be saved.

**QMMM_FULL_HESSIAN**

Trigger the evaluation of the full QM/MM Hessian.

TYPE:

LOGICAL

DEFAULT:

FALSE

OPTIONS:

| | |
|---|---|
| TRUE | Evaluates full Hessian. |
| FALSE | Hessian for QM-QM block only. |

RECOMMENDATION:

None

**QMMM_PRINT**

Controls the amount of output printed from a QM/MM job.

TYPE:

LOGICAL

DEFAULT:

FALSE

OPTIONS:

| | |
|---|---|
| TRUE | Limit molecule, point charge, and analysis printing. |
| FALSE | Normal printing. |

RECOMMENDATION:

Use the default unless running calculations with CHARMM.

**QM_MM_INTERFACE**

Enables internal QM/MM calculations.

TYPE:

STRING

DEFAULT:

NONE

OPTIONS:

| | |
|---|---|
| MM | Molecular mechanics calculation (*i.e.*, no QM region) |
| ONIOM | QM/MM calculation using two-layer mechanical embedding |
| JANUS | QM/MM calculation using electronic embedding |

RECOMMENDATION:

The ONIOM model and Janus models are described above. Choosing MM leads to no electronic structure calculation. However, when using MM, one still needs to define the *$rem* variables BASIS and EXCHANGE in order for Q-CHEM to proceed smoothly.

**QM_MM**

Turns on the Q-CHEM/CHARMM interface.

TYPE:

LOGICAL

DEFAULT:

FALSE

OPTIONS:

| | |
|---|---|
| TRUE | Do QM/MM calculation through the Q-CHEM/CHARMM interface. |
| FALSE | Turn this feature off. |

RECOMMENDATION:

Use the default unless running calculations with CHARMM.

**RAS_ACT_DIFF**

Sets the number of alpha vs. beta electrons

TYPE:

Integer

DEFAULT:

None

OPTIONS:

n user defined integer

RECOMMENDATION:

Set to 1 for an odd number of electrons or a cation, -1 for an anion. Only works with RASCI2.

**RAS_ACT_OCC**

Sets the number of occupied orbitals to enter the RAS active space.

TYPE:

Integer

DEFAULT:

None

OPTIONS:

n user defined integer

RECOMMENDATION:

None. Only works with RASCI2

**RAS_ACT_ORB**

Sets the user-selected active orbitals (RAS2 orbitals).

TYPE:

INTEGER ARRAY

DEFAULT:

From RAS_OCC+1 to RAS_OCC+RAS_ACT

OPTIONS:

$[i, j, k...]$ The number of orbitals must be equal to the RAS_ACT variable

RECOMMENDATION:

None. Only works with RASCI.

**RAS_ACT_VIR**

Sets the number of virtual orbitals to enter the RAS active space.

TYPE:

Integer

DEFAULT:

None

OPTIONS:

n user defined integer

RECOMMENDATION:

None. Only works with RASCI2.

**RAS_ACT**

Sets the number of orbitals in RAS2 (active orbitals).

TYPE:

INTEGER

DEFAULT:

None

OPTIONS:

$n$ User-defined integer, $n > 0$

RECOMMENDATION:

None. Only works with RASCI.

**RAS_AMPL_PRINT**

Defines the absolute threshold ($\times 10^2$) for the CI amplitudes to be printed.

TYPE:

INTEGER

DEFAULT:

10 0.1 minimum absolute amplitude

OPTIONS:

$n$ User-defined integer, $n \geq 0$

RECOMMENDATION:

None. Only works with RASCI.

**RAS_DO_HOLE**

Controls the presence of hole excitations in the RAS-CI wave function.

TYPE:

LOGICAL

DEFAULT:

TRUE

OPTIONS:

| | |
|---|---|
| TRUE | Include hole configurations (RAS1 to RAS2 excitations) |
| FALSE | Do not include hole configurations |

RECOMMENDATION:

None. Only works with RASCI.

**RAS_DO_PART**

Controls the presence of particle excitations in the RAS-CI wave function.

TYPE:

LOGICAL

DEFAULT:

TRUE

OPTIONS:

| | |
|---|---|
| TRUE | Include particle configurations (RAS2 to RAS3 excitations) |
| FALSE | Do not include particle configurations |

RECOMMENDATION:

None. Only works with RASCI.

**RAS_ELEC**

Sets the number of electrons in RAS2 (active electrons).

TYPE:

INTEGER

DEFAULT:

None

OPTIONS:

$n$ User-defined integer, $n > 0$

RECOMMENDATION:

None. Only works with RASCI.

**RAS_FRAG_MO**

Sets the number of atoms in each fragment.

TYPE:

INTEGER ARRAY

DEFAULT:

[NOcc,NAct,NVir] Number of orbitals within RAS1, RAS2 and RAS3 spaces

OPTIONS:

$[i, j, k...]$ Defines sets of canonical MOs to be localized into $n$ fragments

RECOMMENDATION:

Setting within RAS1, RAS2 and RAS3 spaces alleviates the computational cost of the localization procedure. It might also result in improved fragment orbitals. Only works with RASCI.

**RAS_GUESS_CS**

Controls the number of closed shell guess configurations in RAS-CI.

TYPE:

INTEGER

DEFAULT:

0

OPTIONS:

$n$ Imposes to start with $n$ closed shell guesses

RECOMMENDATION:

Only relevant for the computation of singlet states. Only works with RASCI.

**RAS_NATORB_STATE**

Allows to save the natural orbitals of a RAS-CI computed state.

TYPE:

INTEGER

DEFAULT:

0

OPTIONS:

$i$ Saves the natural orbitals for the $i$-th state

RECOMMENDATION:

None. Only works with RASCI.

**RAS_NATORB**

Controls the computation of the natural orbital occupancies.

TYPE:

LOGICAL

DEFAULT:

FALSE

OPTIONS:

| | |
|---|---|
| TRUE | Compute natural orbital occupancies for all states |
| FALSE | Do not compute natural orbital occupancies |

RECOMMENDATION:

None. Only works with RASCI.

**RAS_NFRAG_ATOMS**

Sets the number of atoms in each fragment.

TYPE:

INTEGER ARRAY

DEFAULT:

None

OPTIONS:

| | |
|---|---|
| $[i, j, k...]$ | The sum of the numbers must be equal to the total number of atoms in the systems |

RECOMMENDATION:

None. Only works with RASCI.

**RAS_NFRAG**

If $n > 0$ activates the excitation analysis in RASCI

TYPE:

INTEGER

DEFAULT:

0

OPTIONS:

| | |
|---|---|
| $n$ | Number of fragments to be considered |

RECOMMENDATION:

Only for RASCI. The printed information level is controlled by RAS_PRINT.

**RAS_N_ROOTS**

Sets the number of RAS-CI roots to be computed.

TYPE:

INTEGER

DEFAULT:

None

OPTIONS:

| | |
|---|---|
| $n$ | $n > 0$ Compute $n$ RAS-CI states |

RECOMMENDATION:

None. Only works with RASCI2

**RAS_OCC**

Sets the number of orbitals in RAS1

TYPE:

INTEGER

DEFAULT:

0

OPTIONS:

$n$ User-defined integer, $n > 0$

RECOMMENDATION:

These are the initial doubly occupied orbitals (RAS1) before including $hole$ type of excitations. The RAS1 space starts from the lowest orbital up to RAS_OCC, i.e. no frozen orbitals option available yet. Only works with RASCI.

**RAS_PT2_PARTITION**

Specifies the partitioning scheme in RASCI(2)

TYPE:

INTEGER

DEFAULT:

1 Davidson-Kapuy (DK) partitioning

OPTIONS:

2 Epstein-Nesbet (EN) partitioning

0 Do both DK and EN partitionings

RECOMMENDATION:

Only for RASCI if RAS_PT2 is set to true.

**RAS_PT2_VSHIFT**

Defines the energy level shift ($\times 10^3$ $au$) in RASCI(2)

TYPE:

INTEGER

DEFAULT:

0

OPTIONS:

$n$ User-defined integer

RECOMMENDATION:

Only for RASCI if RAS_PT2 is set to true.

**RAS_PT2**

Perform second-order perturbative correction to RAS-CI energy

TYPE:

LOGICAL

DEFAULT:

FALSE

OPTIONS:

TRUE Compute RASCI(2) energy corrections

FALSE Do not compute RASCI(2) energy corrections

RECOMMENDATION:

None. Only works with RASCI.

**RAS_ROOTS**

Sets the number of RAS-CI roots to be computed.

TYPE:

INTEGER

DEFAULT:

None

OPTIONS:

$n$ $n > 0$ Compute $n$ RAS-CI states

RECOMMENDATION:

None. Only works with RASCI.

**RAS_SPIN_MULT**

Specifies the spin multiplicity of the roots to be computed

TYPE:

INTEGER

DEFAULT:

1 Singlet states

OPTIONS:

| | |
|---|---|
| 0 | Compute any spin multiplicity |
| $2n + 1$ | User-defined integer, $n \geq 0$ |

RECOMMENDATION:

Only for RASCI, which at present only allows for the computation of systems with an even number of electrons. Thus, RAS_SPIN_MULT only can take odd values.

**RCA_PRINT**

Controls the output from RCA SCF optimizations.

TYPE:

INTEGER

DEFAULT:

0

OPTIONS:

| | |
|---|---|
| 0 | No print out |
| 1 | RCA summary information |
| 2 | Level 1 plus RCA coefficients |
| 3 | Level 2 plus RCA iteration details |

RECOMMENDATION:

None

**RC_R0**

Determines the parameter in the Gaussian weight function used to smooth the density at the nuclei.

TYPE:

INTEGER

DEFAULT:

0

OPTIONS:

0 Corresponds the traditional delta function spin and charge densities

$n$ corresponding to $n \times 10^{-3}$ a.u.

RECOMMENDATION:

We recommend value of 250 for a typical spit valence basis. For basis sets with increased flexibility in the nuclear vicinity the smaller values of $r_0$ also yield adequate spin density.

**RISAPT**

Requests an RI-SAPT calculation

TYPE:

BOOLEAN

DEFAULT:

FALSE

OPTIONS:

TRUE Compute four-index integrals using the RI approximation.

FALSE Do not use RI.

RECOMMENDATION:

Set to TRUE if an appropriate auxiliary basis set is available, as RI-SAPT is much faster and affords negligible errors (as compared to ordinary SAPT) if the auxiliary basis set is matched to the primary basis set. (The former must be specified using AUX_BASIS.)

**RI_J**

Toggles the use of the RI algorithm to compute J.

TYPE:

LOGICAL

DEFAULT:

FALSE RI will not be used to compute J.

OPTIONS:

TRUE Turn on RI for J.

RECOMMENDATION:

For large (especially 1D and 2D) molecules the approximation may yield significant improvements in Fock evaluation time when used with ARI.

**RI_K_GRAD**

Turn on the nuclear gradient calculations

TYPE:

LOGICAL

DEFAULT:

FALSE Do not invoke occ-RI-K based gradient

OPTIONS:

TRUE Use occ-RI-K based gradient

RECOMMENDATION:

Use "RI_J false"

**RI_K**

Toggles the use of the RI algorithm to compute K.

TYPE:

LOGICAL

DEFAULT:

FALSE RI will not be used to compute K.

OPTIONS:

TRUE Turn on RI for K.

RECOMMENDATION:

For large (especially 1D and 2D) molecules the approximation may yield significant improvements in Fock evaluation time when used with ARI.

**ROKS_LEVEL_SHIFT**

Introduce a level shift of N/100 hartree to aid convergence.

TYPE:

INTEGER

DEFAULT:

0

OPTIONS:

0 No shift

N level shift of N/100 hartree.

RECOMMENDATION:

Use in cases of problematic convergence.

**ROKS**

Controls whether ROKS calculation will be performed.

TYPE:

LOGICAL

DEFAULT:

FALSE

OPTIONS:

FALSE ROKS is not performed.

TRUE ROKS will be performed.

RECOMMENDATION:

Set to TRUE if ROKS calculation is desired. You should also set UNRESTRICTED = FALSE

**ROSCF**

Run an ROSCF calculation with GEN_SCFMAN.

TYPE:

BOOLEAN

DEFAULT:

FALSE

OPTIONS:

FALSE Let Q-CHEM automatically decide if RO is needed.

TRUE Run an ROSCF calculation forcefully.

RECOMMENDATION:

No need to set this rem for standard calculations.

**RPATH_COORDS**

Determines which coordinate system to use in the IRC search.

TYPE:

INTEGER

DEFAULT:

0

OPTIONS:

0 Use mass-weighted coordinates.

1 Use Cartesian coordinates.

2 Use *Z*-matrix coordinates.

RECOMMENDATION:

Use the default.

**RPATH_DIRECTION**

Determines the direction of the eigenmode to follow. This will not usually be known prior to the Hessian diagonalization.

TYPE:

INTEGER

DEFAULT:

1

OPTIONS:

1 Descend in the positive direction of the eigen mode.

-1 Descend in the negative direction of the eigen mode.

RECOMMENDATION:

It is usually not possible to determine in which direction to go *a priori*, and therefore both directions will need to be considered.

**RPATH_MAX_CYCLES**

Specifies the maximum number of points to find on the reaction path.

TYPE:

INTEGER

DEFAULT:

20

OPTIONS:

$n$ User-defined number of cycles.

RECOMMENDATION:

Use more points if the minimum is desired, but not reached using the default.

**RPATH_MAX_STEPSIZE**

Specifies the maximum step size to be taken (in 0.001 a.u.).

TYPE:

INTEGER

DEFAULT:

150 corresponding to a step size of 0.15 a.u..

OPTIONS:

$n$ Step size = $n$/1000 a.u.

RECOMMENDATION:

None.

**RPATH_PRINT**

Specifies the print output level.

TYPE:

INTEGER

DEFAULT:

2

OPTIONS:

$n$

RECOMMENDATION:

Use the default, as little additional information is printed at higher levels. Most of the output arises from the multiple single point calculations that are performed along the reaction pathway.

**RPATH_TOL_DISPLACEMENT**

Specifies the convergence threshold for the step. If a step size is chosen by the algorithm that is smaller than this, the path is deemed to have reached the minimum.

TYPE:

INTEGER

DEFAULT:

5000 Corresponding to 0.005 a.u.

OPTIONS:

$n$ User-defined. Tolerance = $n$/1000000 a.u.

RECOMMENDATION:

Use the default. Note that this option *only* controls the threshold for ending the RPATH job and does nothing to the intermediate steps of the calculation. A smaller value will provide reaction paths that end closer to the true minimum. Use of smaller values without adjusting RPATH_MAX_STEPSIZE, however, can lead to oscillations about the minimum.

**RPA**

Do an RPA calculation in addition to a CIS or TDDFT/TDA calculation.

TYPE:

LOGICAL/INTEGER

DEFAULT:

FALSE

OPTIONS:

FALSE Do not do an RPA calculation.<br>
TRUE Do an RPA calculation.<br>
2 Do an RPA calculation without running CIS or TDDFT/TDA first.

RECOMMENDATION:

None

**MAKE_CUBE_FILES**

Requests generation of cube files for MOs, NTOs, or NBOs.

TYPE:

LOGICAL/STRING

DEFAULT:

FALSE

OPTIONS:

| | |
|---|---|
| FALSE | Do not generate cube files. |
| TRUE | Generate cube files for MOs and densities. |
| NTOS | Generate cube files for NTOs. |
| NBOS | Generate cube files for NBOs. |

RECOMMENDATION:

None

**SAPT_AO**

Request an atomic-orbital version of SAPT

TYPE:

BOOLEAN

DEFAULT:

FALSE

OPTIONS:

| | |
|---|---|
| TRUE | Use an AO version of SAPT. |
| FALSE | Use a MO version of SAPT. |

RECOMMENDATION:

Non-dispersion terms are calculated by AO-SAPT with $O(N^3)$ scaling.

**SAPT_BASIS**

Controls the MO basis used for SAPT corrections.

TYPE:

STRING

DEFAULT:

MONOMER

OPTIONS:

| | |
|---|---|
| MONOMER | Monomer-centered basis set (MCBS). |
| DIMER | Dimer-centered basis set (DCBS). |
| PROJECTED | Projected basis set. |

RECOMMENDATION:

The DCBS is more costly than the MCBS and can only be used with XPOL_MPOL_ORDER = GAS (*i.e.*, it is not available for use with XPol). The PROJECTED choice is an efficient compromise that is available for use with XPol.

**SAPT_CDFT_EDA**

Request a SAPT/cDFT energy decomposition analysis

TYPE:

BOOLEAN

DEFAULT:

FALSE

OPTIONS:

TRUE Run a SAPT/cDFT calculation.

FALSE Do not run SAPT/cDFT.

RECOMMENDATION:

None

**SAPT_CPHF**

Requests that the second-order corrections $E_{\mathrm{ind}}^{(2)}$ and $E_{\mathrm{exch-ind}}^{(2)}$ be replaced by their infinite-order "response" analogues, $E_{\mathrm{ind,resp}}^{(2)}$ and $E_{\mathrm{exch-ind,resp}}^{(2)}$.

TYPE:

BOOLEAN

DEFAULT:

FALSE

OPTIONS:

TRUE Evaluate the response corrections and use $E_{\mathrm{ind,resp}}^{(2)}$ and $E_{\mathrm{exch-ind,resp}}^{(2)}$

FALSE Omit these corrections and use $E_{\mathrm{ind}}^{(2)}$ and $E_{\mathrm{exch-ind}}^{(2)}$.

RECOMMENDATION:

Computing the response corrections requires solving CPHF equations for pair of monomers, which is somewhat expensive but may improve the accuracy when the monomers are polar.

**SAPT_DISP_CORR**

Request an empirical dispersion potential instead of calculating $E_{\text{disp}}^{(2)}$ and $E_{\text{exch-disp}}^{(2)}$ directly

TYPE:

BOOLEAN

DEFAULT:

FALSE

OPTIONS:

TRUE Use a dispersion force field.

FALSE calculate $E_{\mathrm{disp}}^{(2)}$ and $E_{\mathrm{exch-disp}}^{(2)}$.

RECOMMENDATION:

Using dispersion potentials combined with AO version of SAPT reduces the scaling from $O(N^5)$ to $O(N^3)$ with respect to monomer size.

**SAPT_DISP_VERSION**

Controls which dispersion potential is used for SAPT

TYPE:

INTEGER

DEFAULT:

3

OPTIONS:

1 Use the "first generation" (+D1) dispersion potentials from Hesselmann[20,21].

2 Use the "second generation" (+D2) dispersion potentials from Podeszwa.[22,23].

3 Use the "third generation" (+D3) dispersion potentials from Lao[24].

RECOMMENDATION:

Use +D3. Whereas +D1 was fit to reproduce binding energies, the +D2 and +D3 potentials were fit directly to dispersion energies $E^{(2)}_{\rm disp} + E^{(2)}_{\rm exch-disp}$ computed at the SAPT(DFT) and SAPT2+(3) levels, and performs well for both total binding energies as well as individual energy components[23,24]. In developing +D3, the training set was expanded to eliminate outliers involving $\pi$ stacking[24].

**SAPT_DSCF**

Request the $\delta E^{\rm HF}_{\rm int}$ correction

TYPE:

BOOLEAN

DEFAULT:

FALSE

OPTIONS:

TRUE Evaluate this correction.

FALSE Omit this correction.

RECOMMENDATION:

Evaluating the $\delta E^{\rm HF}_{\rm int}$ correction requires an SCF calculation on the entire (super)system. This corrections effectively yields a "Hartree-Fock plus dispersion" estimate of the interaction energy.

**SAPT_EXCHANGE**

Selects the type of first-order exchange that is used in a SAPT calculation.

TYPE:

STRING

DEFAULT:

S_SQUARED

OPTIONS:

S_SQUARED Compute first order exchange in the single-exchange ("$S^2$") approximation.

S_INVERSE Compute the exact first order exchange.

RECOMMENDATION:

The single-exchange approximation is expected to be adequate except possibly at very short intermolecular distances, and is somewhat faster to compute.

**SAPT_ORDER**

Selects the order in perturbation theory for a SAPT calculation.

TYPE:

STRING

DEFAULT:

SAPT2

OPTIONS:

| | |
|---|---|
| SAPT1 | First order SAPT. |
| SAPT2 | Second order SAPT. |
| ELST | First-order Rayleigh-Schrödinger perturbation theory. |
| RSPT | Second-order Rayleigh-Schrödinger perturbation theory. |

RECOMMENDATION:

SAPT2 is the most meaningful.

**SAPT_PRINT**

Controls level of printing in SAPT.

TYPE:

INTEGER

DEFAULT:

1

OPTIONS:

| | |
|---|---|
| $N$ | Integer print level |

RECOMMENDATION:

Larger values generate additional output.

**SAPT**

Requests a SAPT calculation.

TYPE:

BOOLEAN

DEFAULT:

FALSE

OPTIONS:

| | |
|---|---|
| TRUE | Run a SAPT calculation. |
| FALSE | Do not run SAPT. |

RECOMMENDATION:

If SAPT is set to TRUE, one should also specify XPOL = TRUE and XPOL_MPOL_ORDER = GAS.

**SASF_RPA**

Do an SA-SF-CIS/DFT calculation.

TYPE:

LOGICAL

DEFAULT:

FALSE

OPTIONS:

| | |
|---|---|
| FALSE | Do not do an SA-SF-CIS/DFT calculation. |
| TRUE | Do an SA-SF-CIS/DFT calculation (requires ROHF ground state). |

RECOMMENDATION:

None

**SAVE_LAST_GPX**

Save last $\mathbf{G}\left[\mathbf{P}^{\mathrm{x}}\right]$ when calculating dynamic polarizabilities in order to call mopropman in a second run with MOPROP = 102.

TYPE:

INTEGER

DEFAULT:

0

OPTIONS:

0 False

1 True

RECOMMENDATION:

None

**SCALE_NUCLEAR_CHARGE**

Scales charge of each nuclei by a certain value. The nuclear repulsion energy is calculated for the unscaled nuclear charges.

TYPE:

INTEGER

DEFAULT:

0 No scaling.

OPTIONS:

$n$ A total positive charge of (1+$n$/100)e is added to the molecule.

RECOMMENDATION:

NONE

**SCFMI_FREEZE_SS**

Keep the first several fragments unrelaxed in an SCFMI calculation.

TYPE:

INTEGER

DEFAULT:

$n$ Freeze the first $n$ fragments.

OPTIONS:

0 (all fragments are active)

RECOMMENDATION:

None

**SCFMI_MODE**

Determine whether generalized SCFMI is used and also the property of the working basis.

TYPE:

INTEGER

DEFAULT:

0 AO-block based SCFMI (the original definition of ALMOs).

1 Generalized SCFMI with basis vectors that are non-orthogonal between fragments.

2 Generalized SCFMI with basis vectors that are orthogonal between fragments.

OPTIONS:

0 (“1" is used by basic “EDA2" calculations).

RECOMMENDATION:

None

**SCF_ALGORITHM**

Algorithm used for converging the SCF.

TYPE:

STRING

DEFAULT:

DIIS Pulay DIIS.

OPTIONS:

| | |
|---|---|
| DIIS | Pulay DIIS. |
| DM | Direct minimizer. |
| DIIS_DM | Uses DIIS initially, switching to direct minimizer for later iterations (See THRESH_DIIS_SWITCH, MAX_DIIS_CYCLES). |
| DIIS_GDM | Use DIIS and then later switch to geometric direct minimization (See THRESH_DIIS_SWITCH, MAX_DIIS_CYCLES). |
| GDM | Geometric Direct Minimization. |
| RCA | Relaxed constraint algorithm |
| RCA_DIIS | Use RCA initially, switching to DIIS for later iterations (see THRESH_RCA_SWITCH and MAX_RCA_CYCLES described later in this chapter) |
| ROOTHAAN | Roothaan repeated diagonalization. |

RECOMMENDATION:

Use DIIS unless performing a restricted open-shell calculation, in which case GDM is recommended. If DIIS fails to find a reasonable approximate solution in the initial iterations, RCA_DIIS is the recommended fallback option. If DIIS approaches the correct solution but fails to finally converge, DIIS_GDM is the recommended fallback.

**SCF_CONVERGENCE**

SCF is considered converged when the wave function error is less that $10^{-\mathrm{SCF\_CONVERGENCE}}$. Adjust the value of THRESH at the same time. (Starting with Q-CHEM 3.0, the DIIS error is measured by the maximum error rather than the RMS error as in earlier versions.)

TYPE:

INTEGER

DEFAULT:

| | |
|---|---|
| 5 | For single point energy calculations. |
| 8 | For geometry optimizations and vibrational analysis. |
| 8 | For SSG calculations, see Chapter 5. |

OPTIONS:

User-defined

RECOMMENDATION:

Tighter criteria for geometry optimization and vibration analysis. Larger values provide more significant figures, at greater computational cost.

**SCF_FINAL_PRINT**

Controls level of output from SCF procedure to Q-CHEM output file at the end of the SCF.

TYPE:

INTEGER

DEFAULT:

| | |
|---|---|
| 0 | No extra print out. |

OPTIONS:

| | |
|---|---|
| 0 | No extra print out. |
| 1 | Orbital energies and break-down of SCF energy. |
| 2 | Level 1 plus MOs and density matrices. |
| 3 | Level 2 plus Fock and density matrices. |

RECOMMENDATION:

The break-down of energies is often useful (level 1).

**SCF_GUESS_ALWAYS**

Switch to force the regeneration of a new initial guess for each series of SCF iterations (for use in geometry optimization).

TYPE:

LOGICAL

DEFAULT:

False

OPTIONS:

| | |
|---|---|
| False | Do not generate a new guess for each series of SCF iterations in an optimization; use MOs from the previous SCF calculation for the guess, if available. |
| True | Generate a new guess for each series of SCF iterations in a geometry optimization. |

RECOMMENDATION:

Use the default unless SCF convergence issues arise

**SCF_GUESS_MIX**

Controls mixing of LUMO and HOMO to break symmetry in the initial guess. For unrestricted jobs, the mixing is performed only for the alpha orbitals.

TYPE:

INTEGER

DEFAULT:

| | |
|---|---|
| 0 (FALSE) | Do not mix HOMO and LUMO in SCF guess. |

OPTIONS:

| | |
|---|---|
| 0 (FALSE) | Do not mix HOMO and LUMO in SCF guess. |
| 1 (TRUE) | Add 10% of LUMO to HOMO to break symmetry. |
| $n$ | Add $n \times 10\%$ of LUMO to HOMO ($0 < n < 10$). |

RECOMMENDATION:

When performing unrestricted calculations on molecules with an even number of electrons, it is often necessary to break alpha/beta symmetry in the initial guess with this option, or by specifying input for *$occupied*.

**SCF_GUESS_PRINT**

Controls printing of guess MOs, Fock and density matrices.

TYPE:

INTEGER

DEFAULT:

0

OPTIONS:

| | |
|---|---|
| 0 | Do not print guesses. |
| SAD | |
| 1 | Atomic density matrices and molecular matrix. |
| 2 | Level 1 plus density matrices. |
| CORE and GWH | |
| 1 | No extra output. |
| 2 | Level 1 plus Fock and density matrices and, MO coefficients and eigenvalues. |
| READ | |
| 1 | No extra output |
| 2 | Level 1 plus density matrices, MO coefficients and eigenvalues. |

RECOMMENDATION:

None

**SCF_GUESS**

Specifies the initial guess procedure to use for the SCF.

TYPE:

STRING

DEFAULT:

| | |
|---|---|
| SAD | Superposition of atomic densities (available only with standard basis sets) |
| GWH | For ROHF where a set of orbitals are required. |
| FRAGMO | For a fragment MO calculation |

OPTIONS:

| | |
|---|---|
| CORE | Diagonalize core Hamiltonian |
| SAD | Superposition of atomic density |
| SADMO | Purified superposition of atomic densities (available only with standard basis sets) |
| GWH | Apply generalized Wolfsberg-Helmholtz approximation |
| READ | Read previous MOs from disk |
| FRAGMO | Superimposing converged fragment MOs |

RECOMMENDATION:

SAD or SADMO guess for standard basis sets. For general basis sets, it is best to use the BASIS2 *$rem*. Alternatively, try the GWH or core Hamiltonian guess. For ROHF it can be useful to READ guesses from an SCF calculation on the corresponding cation or anion. Note that because the density is made spherical, this may favor an undesired state for atomic systems, especially transition metals. Use FRAGMO in a fragment MO calculation.

**SCF_MINFIND_INCREASEFACTOR**

Controls how the height of the penalty function changes when repeatedly trapped at the same solution

TYPE:

INTEGER

DEFAULT:

10100 meaning 1.01

OPTIONS:

$abcde$ corresponding to $a.bcde$

RECOMMENDATION:

If the algorithm converges to a solution which corresponds to a previously located solution, increase both the normalization N and the width lambda of the penalty function there. Then do a restart.

**SCF_MINFIND_INITLAMBDA**

Control the initial width of the penalty function.

TYPE:

INTEGER

DEFAULT:

02000 meaning 2.000

OPTIONS:

$abcde$ corresponding to $ab.cde$

RECOMMENDATION:

The initial inverse-width (*i.e.*, the inverse-variance) of the Gaussian to place to fill solution's well. Measured in electrons$^{(} - 1)$. Increasing this will repeatedly converging on the same solution.

**SCF_MINFIND_INITNORM**

Control the initial height of the penalty function.

TYPE:

INTEGER

DEFAULT:

01000 meaning 1.000

OPTIONS:

$abcde$ corresponding to $ab.cde$

RECOMMENDATION:

The initial normalization of the Gaussian to place to fill a well. Measured in hartrees.

**SCF_MINFIND_MIXENERGY**

Specify the active energy range when doing Active mixing

TYPE:

INTEGER

DEFAULT:

00200 meaning 00.200

OPTIONS:

$abcde$ corresponding to $ab.cde$

RECOMMENDATION:

The standard deviation of the Gaussian distribution used to select the orbitals for mixing (centered on the Fermi level). Measured in Hartree. To find less-excited solutions, decrease this value

**SCF_MINFIND_MIXMETHOD**

Specify how to select orbitals for random mixing

TYPE:

INTEGER

DEFAULT:

0

OPTIONS:

0 Random mixing: select from any orbital to any orbital.

1 Active mixing: select based on energy, decaying with distance from the Fermi level.

2 Active Alpha space mixing: select based on energy, decaying with distance from the Fermi level only in the alpha space.

RECOMMENDATION:

Random mixing will often find very high energy solutions. If lower energy solutions are desired, use 1 or 2.

**SCF_MINFIND_NRANDOMMIXES**

Control how many random mixes to do to generate new orbitals

TYPE:

INTEGER

DEFAULT:

10

OPTIONS:

$n$ Perform $n$ random mixes.

RECOMMENDATION:

This is the number of occupied/virtual pairs to attempt to mix, per separate density (*i.e.*, for unrestricted calculations both alpha and beta space will get this many rotations). If this is negative then only mix the highest 25% occupied and lowest 25% virtuals.

**SCF_MINFIND_RANDOMMIXING**

Control how to choose new orbitals after locating a solution

TYPE:

INTEGER

DEFAULT:

00200 meaning .02 radians

OPTIONS:

$abcde$ corresponding to $a.bcde$ radians

RECOMMENDATION:

After locating an SCF solution, the orbitals are mixed randomly to move to a new position in orbital space. For each occupied and virtual orbital pair picked at random and rotate between them by a random angle between 0 and this. If this is negative then use exactly this number, *e.g.*, $-15708$ will almost exactly swap orbitals. Any number$< -15708$ will cause the orbitals to be swapped exactly.

**SCF_MINFIND_READDISTTHRESH**

The distance threshold at which to consider two solutions the same

TYPE:

INTEGER

DEFAULT:

00100 meaning 0.1

OPTIONS:

$abcde$ corresponding to $ab.cde$

RECOMMENDATION:

The threshold to regard a minimum as the same as a read in minimum. Measured in electrons. If two minima are closer together than this, reduce the threshold to distinguish them.

**SCF_MINFIND_RESTARTSTEPS**

Restart with new orbitals if no minima have been found within this many steps

TYPE:

INTEGER

DEFAULT:

300

OPTIONS:

$n$ Restart after $n$ steps.

RECOMMENDATION:

If the SCF calculation spends many steps not finding a solution, lowering this number may speed up solution-finding. If the system converges to solutions very slowly, then this number may need to be raised.

**SCF_MINFIND_RUNCORR**

Run post-SCF correlated methods on multiple SCF solutions

TYPE:

INTEGER

DEFAULT:

0

OPTIONS:

If this is set $> 0$, then run correlation methods for all found SCF solutions.

RECOMMENDATION:

Post-HF correlation methods should function correctly with excited SCF solutions, but their convergence is often much more difficult owing to intruder states.

**SCF_MINFIND_WELLTHRESH**

Specify what SCF_MINFIND believes is the basin of a solution

TYPE:

INTEGER

DEFAULT:

5

OPTIONS:

$n$ for a threshold of $10^{-n}$

RECOMMENDATION:

When the DIIS error is less than $10^{-n}$, penalties are switched off to see whether it has converged to a new solution.

**SCF_PRINT_FRGM**

Controls the output of Q-CHEM jobs on isolated fragments.

TYPE:

LOGICAL

DEFAULT:

FALSE

OPTIONS:

TRUE The output is printed to the parent job output file.

FALSE The output is not printed.

RECOMMENDATION:

Use TRUE if details about isolated fragments are important.

**SCF_PRINT**

Controls level of output from SCF procedure to Q-CHEM output file.

TYPE:

INTEGER

DEFAULT:

0 Minimal, concise, useful and necessary output.

OPTIONS:

0 Minimal, concise, useful and necessary output.

1 Level 0 plus component breakdown of SCF electronic energy.

2 Level 1 plus density, Fock and MO matrices on each cycle.

3 Level 2 plus two-electron Fock matrix components (Coulomb, HF exchange and DFT exchange-correlation matrices) on each cycle.

RECOMMENDATION:

Proceed with care; can result in *extremely* large output files at level 2 or higher. These levels are primarily for program debugging.

**SCF_READMINIMA**

Read in solutions from a previous SCF meta-dynamics calculation

TYPE:

INTEGER

DEFAULT:

0

OPTIONS:

$n$ Read in $n$ previous solutions and attempt to locate them all.

$-n$ Read in $n$ previous solutions, but only attempt to locate solution $n$.

RECOMMENDATION:

This may not actually locate all solutions required and will probably locate others too. The SCF will also stop when the number of solutions specified in SCF_SAVEMINIMA are found. Solutions from other geometries may also be read in and used as starting orbitals. If a solution is found and matches one that is read in within SCF_MINFIND_READDISTTHRESH, its orbitals are saved in that position for any future calculations. The algorithm works by restarting from the orbitals and density of a the minimum it is attempting to find. After 10 failed restarts (defined by SCF_MINFIND_RESTARTSTEPS), it moves to another previous minimum and attempts to locate that instead. If there are no minima to find, the restart does random mixing (with 10 times the normal random mixing parameter).

**SCF_SAVEMINIMA**

Turn on SCF meta-dynamics and specify how many solutions to locate.

TYPE:

INTEGER

DEFAULT:

0

OPTIONS:

0 Do not use SCF meta-dynamics

$n$ Attempt to find $n$ distinct SCF solutions.

RECOMMENDATION:

Perform SCF Orbital meta-dynamics and attempt to locate $n$ different SCF solutions. Note that these may not all be minima. Many saddle points are often located. The last one located will be the one used in any post-SCF treatments. In systems where there are infinite point groups, this procedure cannot currently distinguish between spatial rotations of different densities, so will likely converge on these multiply.

**SET_QUADRATIC**

Determines whether to include full quadratic response contributions for TDDFT.

TYPE:

LOGICAL

DEFAULT:

FALSE

OPTIONS:

TRUE Include full quadratic response contributions for TDDFT.

FALSE Use pseudo-wave function approach.

RECOMMENDATION:

The pseudo-wave function approach is usually accurate enough and is free of accidental singularities. Consult Refs. 25 and 26 for additional guidance.

**SET_STATE_DERIV**

Sets the excited state index for analytical gradient calculation for geometry optimizations and vibrational analysis with SOS-CIS($D_0$)

TYPE:

INTEGER

DEFAULT:

0

OPTIONS:

$n$ Select the $n$th state.

RECOMMENDATION:

Check to see that the states do no change order during an optimization. For closed-shell systems, either CIS_SINGLETS or CIS_TRIPLETS must be set to false.

**SFX_AMP_OCC_A**

Defines a customer amplitude guess vector in SF-XCIS method.

TYPE:

INTEGER

DEFAULT:

0

OPTIONS:

$n$ builds a guess amplitude with an $\alpha$-hole in the $n$th orbital (requires SFX_AMP_VIR_B).

RECOMMENDATION:

Only use when default guess is not satisfactory.

**SFX_AMP_VIR_B**

Defines a user-specified amplitude guess vector in SF-XCIS method.

TYPE:

INTEGER

DEFAULT:

0

OPTIONS:

$n$ builds a guess amplitude with a $\beta$-particle in the $n$th orbital (requires SFX_AMP_OCC_A).

RECOMMENDATION:

Only use when default guess is not satisfactory.

**SF_STATES**

Sets the number of spin-flip target states roots to find.

TYPE:

INTEGER/INTEGER ARRAY

DEFAULT:

0 Do not look for any spin-flip states.

OPTIONS:

$[i, j, k \ldots]$ Find $i$ SF states in the first irrep, $j$ states in the second irrep *etc.*

RECOMMENDATION:

None

**SKIP_CHARGE_SELF_INTERACT**

Ignores the electrostatic interactions among external charges in a QM/MM calculation.

TYPE:

LOGICAL

DEFAULT:

FALSE

OPTIONS:

| | |
|---|---|
| TRUE | No electrostatic interactions among external charges. |
| FALSE | Computes the electrostatic interactions among external charges. |

RECOMMENDATION:

None

**SKIP_CIS_RPA**

Skips the solution of the CIS, RPA, TDA or TDDFT equations for wave function analysis.

TYPE:

LOGICAL

DEFAULT:

FALSE

OPTIONS:

TRUE / FALSE

RECOMMENDATION:

Set to true to speed up the generation of plot data if the same calculation has been run previously with the scratch files saved.

**SOLVENT_METHOD**

Sets the preferred solvent method.

TYPE:

STRING

DEFAULT:

0

OPTIONS:

| | |
|---|---|
| 0 | Do not use a solvation model. |
| ONSAGER | Use the Kirkwood-Onsager model (Section 11.2.1). |
| PCM | Use an apparent surface charge, polarizable continuum model (Section 11.2.2). |
| ISOSVP | Use the iso-density implementation of the SS(V)PE model (Section 11.2.5). |
| COSMO | Use COSMO (similar to C-PCM but with an outlying charge correction[27,28]; see Section 11.2.7). |
| SM8 | Use version 8 of the Cramer-Truhlar SM$x$ model (Section 11.2.8.1). |
| SM12 | Use version 12 of the SM$x$ model (Section 11.2.8.2). |
| SMD | Use SMD (Section 11.2.8.3). |
| CHEM_SOL | Use the Langevin Dipoles model (Section 11.2.9). |

RECOMMENDATION:

Consult the literature. PCM is a collective name for a family of models and additional input options may be required in this case, in order to fully specify the model. (See Section 11.2.2.) Several versions of SM12 are available as well, as discussed in Section 11.2.8.2.

**SOLVE_PEQ**

Perform a solvation free energy calculation on a Cartesian grid utilizing Poisson equation boundary conditions.

TYPE:

STRING

DEFAULT:

False

OPTIONS:

TRUE/FALSE

RECOMMENDATION:

None.

**SOS_FACTOR**

Controls the strength of the opposite-spin component of PT2 correlation energy.

TYPE:

INTEGER

DEFAULT:

0

OPTIONS:

$n$ Corresponding to $c_{\text{os}} = n/10^6$ in Eq. (4.71).

RECOMMENDATION:

NONE

**SOS_UFACTOR**

Sets the scaling parameter $c_U$

TYPE:

INTEGER

DEFAULT:

| | |
|---|---|
| 151 | For SOS-CIS(D), corresponding to 1.51 |
| 140 | For SOS-CIS($D_0$), corresponding to 1.40 |

OPTIONS:

$n$ $c_U = n/100$

RECOMMENDATION:

Use the default

**SPIN_FLIP_XCIS**

Do a SF-XCIS calculation.

TYPE:

LOGICAL

DEFAULT:

FALSE

OPTIONS:

| | |
|---|---|
| FALSE | Do not do an SF-XCIS calculation. |
| TRUE | Do an SF-XCIS calculation (requires ROHF triplet ground state). |

RECOMMENDATION:

None

**SPIN_FLIP**

Selects whether to perform a standard excited state calculation, or a spin-flip calculation. Spin multiplicity should be set to 3 for systems with an even number of electrons, and 4 for systems with an odd number of electrons.

TYPE:

LOGICAL

DEFAULT:

FALSE

OPTIONS:

TRUE/FALSE

RECOMMENDATION:

None

**SRC_DFT**

Selects form of the short-range corrected functional.

TYPE:

INTEGER

DEFAULT:

No default

OPTIONS:

1 SRC1 functional.

2 SRC2 functional.

RECOMMENDATION:

None

**SSG**

Controls the calculation of the SSG wave function.

TYPE:

INTEGER

DEFAULT:

0

OPTIONS:

0 Do not compute the SSG wave function

1 Do compute the SSG wave function

RECOMMENDATION:

See also the UNRESTRICTED and DIIS_SUBSPACE_SIZE *$rem* variables.

**SSS_FACTOR**

Controls the strength of the same-spin component of PT2 correlation energy.

TYPE:

INTEGER

DEFAULT:

0

OPTIONS:

$n$ Corresponding to $c_{\rm ss} = n/10^6$ in Eq. (4.71).

RECOMMENDATION:

NONE

**STABILITY_ANALYSIS**

Performs stability analysis for a HF or DFT solution.

TYPE:

LOGICAL

DEFAULT:

FALSE

OPTIONS:

TRUE Perform stability analysis.

FALSE Do not perform stability analysis.

RECOMMENDATION:

Set to TRUE when a HF or DFT solution is suspected to be unstable.

**STATE_ANALYSIS**

Activates excited state analyses using libwfa.

TYPE:

LOGICAL

DEFAULT:

FALSE (no excited state analyses)

OPTIONS:

TRUE, FALSE

RECOMMENDATION:

Set to TRUE if excited state analysis is required, but also if plots of densities or orbitals are needed. For details see section 10.2.7.

**STATE_FOLLOW**

Turns on state following.

TYPE:

LOGICAL

DEFAULT:

FALSE

OPTIONS:

| | |
|---|---|
| FALSE | Do not use state-following. |
| TRUE | Use state-following. |

RECOMMENDATION:

None.

**STS_ACCEPTOR**

Define the acceptor molecular fragment.

TYPE:

STRING

DEFAULT:

0 No acceptor fragment is defined.

OPTIONS:

$i$-$j$ Acceptor fragment is in the $i$th atom to the $j$th atom.

RECOMMENDATION:

Note no space between the hyphen and the numbers $i$ and $j$.

**STS_DONOR**

Define the donor fragment.

TYPE:

STRING

DEFAULT:

0 No donor fragment is defined.

OPTIONS:

$i$-$j$ Donor fragment is in the $i$th atom to the $j$th atom.

RECOMMENDATION:

Note no space between the hyphen and the numbers $i$ and $j$.

**STS_FCD**

Control the calculation of FCD for ET couplings.

TYPE:

LOGICAL

DEFAULT:

FALSE

OPTIONS:

| | |
|---|---|
| FALSE | Do not perform an FCD calculation. |
| TRUE | Include an FCD calculation. |

RECOMMENDATION:

None

**STS_FED**

Control the calculation of FED for EET couplings.

TYPE:

LOGICAL

DEFAULT:

FALSE

OPTIONS:

| | |
|---|---|
| FALSE | Do not perform a FED calculation. |
| TRUE | Include a FED calculation. |

RECOMMENDATION:

None

**STS_FSD**

Control the calculation of FSD for EET couplings.

TYPE:

LOGICAL

DEFAULT:

FALSE

OPTIONS:

| | |
|---|---|
| FALSE | Do not perform a FSD calculation. |
| TRUE | Include a FSD calculation. |

RECOMMENDATION:

For RCIS triplets, FSD and FED are equivalent. FSD will be automatically switched off and perform a FED calculation.

**STS_GMH**

Control the calculation of GMH for ET couplings.

TYPE:

LOGICAL

DEFAULT:

FALSE

OPTIONS:

| | |
|---|---|
| FALSE | Do not perform a GMH calculation. |
| TRUE | Include a GMH calculation. |

RECOMMENDATION:

When set to true computes Mulliken-Hush electronic couplings. It yields the generalized Mulliken-Hush couplings as well as the transition dipole moments for each pair of excited states and for each excited state with the ground state.

**STS_MOM**

Control calculation of the transition moments between excited states in the CIS and TDDFT calculations (including SF variants).

TYPE:

LOGICAL

DEFAULT:

FALSE

OPTIONS:

| | |
|---|---|
| FALSE | Do not calculate state-to-state transition moments. |
| TRUE | Do calculate state-to-state transition moments. |

RECOMMENDATION:

When set to true requests the state-to-state dipole transition moments for all pairs of excited states and for each excited state with the ground state.

**SVP_CAVITY_CONV**

Determines the convergence value of the iterative iso-density cavity procedure.

TYPE:

INTEGER

DEFAULT:

10

OPTIONS:

$n$ Convergence threshold set to $10^{-n}$.

RECOMMENDATION:

The default value unless convergence problems arise.

**SVP_CHARGE_CONV**

Determines the convergence value for the charges on the cavity. When the change in charges fall below this value, if the electron density is converged, then the calculation is considered converged.

TYPE:

INTEGER

DEFAULT:

7

OPTIONS:

$n$ Convergence threshold set to $10^{-n}$.

RECOMMENDATION:

The default value unless convergence problems arise.

**SVP_GUESS**

Specifies how and if the solvation module will use a given guess for the charges and cavity points.

TYPE:

INTEGER

DEFAULT:

0

OPTIONS:

0 No guessing.

1 Read a guess from a previous Q-CHEM solvation computation.

2 Use a guess specified by the *$svpirf* section from the input

RECOMMENDATION:

It is helpful to also set SCF_GUESS to READ when using a guess from a previous Q-CHEM run.

**SVP_MEMORY**

Specifies the amount of memory for use by the solvation module.

TYPE:

INTEGER

DEFAULT:

125

OPTIONS:

$n$ corresponds to the amount of memory in Mb.

RECOMMENDATION:

The default should be fine for medium size molecules with the default Lebedev grid, only increase if needed.

**SVP_PATH**

Specifies whether to run a gas phase computation prior to performing the solvation procedure.

TYPE:

INTEGER

DEFAULT:

0

OPTIONS:

0 runs a gas-phase calculation and after
convergence runs the SS(V)PE computation.

1 does not run a gas-phase calculation.

RECOMMENDATION:

Running the gas-phase calculation provides a good guess to start the solvation stage and provides a more complete set of solvated properties.

**SYMMETRY_DECOMPOSITION**

Determines symmetry decompositions to calculate.

TYPE:

INTEGER

DEFAULT:

1

OPTIONS:

0 No symmetry decomposition.

1 Calculate MO eigenvalues and symmetry (if available).

2 Perform symmetry decomposition of kinetic energy and nuclear attraction matrices.

RECOMMENDATION:

None

**SYMMETRY**

Controls the efficiency through the use of point group symmetry for calculating integrals.

TYPE:

LOGICAL

DEFAULT:

TRUE Use symmetry for computing integrals.

OPTIONS:

TRUE Use symmetry when available.

FALSE Do not use symmetry. This is always the case for RIMP2 jobs

RECOMMENDATION:

Use the default unless benchmarking. Note that symmetry usage is disabled for RIMP2, FFT, and QM/MM jobs.

**SYM_IGNORE**

Controls whether or not Q-CHEM determines the point group of the molecule and reorients the molecule to the standard orientation.

TYPE:

LOGICAL

DEFAULT:

FALSE Do determine the point group (disabled for RIMP2 jobs).

OPTIONS:

TRUE/FALSE

RECOMMENDATION:

Use the default unless you do not want the molecule to be reoriented. Note that symmetry usage is disabled for RIMP2 jobs.

**SYM_TOL**

Controls the tolerance for determining point group symmetry. Differences in atom locations less than $10^{-\mathrm{SYM\_TOL}}$ are treated as zero.

TYPE:

INTEGER

DEFAULT:

5 Corresponding to $10^{-5}$.

OPTIONS:

User defined.

RECOMMENDATION:

Use the default unless the molecule has high symmetry which is not being correctly identified. Note that relaxing this tolerance too much may introduce errors into the calculation.

**TAO_DFT_THETA_NDP**

Controls the value of the fictitious temperature $\theta$ in TAO-DFT.

TYPE:

INTEGER

DEFAULT:

3

OPTIONS:

$n$ $\theta = m \times 10^{-n}$ (hartrees), where $m$ is the value of TAO_DFT_THETA

RECOMMENDATION:

NONE

**TAO_DFT_THETA**

Controls the value of the fictitious temperature $\theta$ in TAO-DFT.

TYPE:

INTEGER

DEFAULT:

7

OPTIONS:

$m$ $\theta = m \times 10^{-n}$ (hartrees), where $n$ is the value of TAO_DFT_THETA_NDP

RECOMMENDATION:

NONE

**TAO_DFT**

Controls whether to use TAO-DFT.

TYPE:

Boolean

DEFAULT:

false

OPTIONS:

false Do not use TAO-DFT

true Use TAO-DFT

RECOMMENDATION:

NONE

**TDDFT_MI**

Perform an TDDFT(MI) calculation

TYPE:

LOGICAL

DEFAULT:

FALSE

OPTIONS:

| | |
|---|---|
| FALSE | Do not perform an TDDFT(MI) calculation |
| TRUE | Perform an TDDFT(MI) calculation |

RECOMMENDATION:

False

**THRESH_DIIS_SWITCH**

The threshold for switching between DIIS extrapolation and direct minimization of the SCF energy is $10^{-\text{THRESH\_DIIS\_SWITCH}}$ when SCF_ALGORITHM is DIIS_GDM or DIIS_DM. See also MAX_DIIS_CYCLES

TYPE:

INTEGER

DEFAULT:

2

OPTIONS:

User-defined.

RECOMMENDATION:

None

**THRESH_RCA_SWITCH**

The threshold for switching between RCA and DIIS when SCF_ALGORITHM is RCA_DIIS.

TYPE:

INTEGER

DEFAULT:

3

OPTIONS:

| | |
|---|---|
| N | Algorithm changes from RCA to DIIS when Error is less than $10^{-N}$. |

RECOMMENDATION:

None

**THRESH**

Cutoff for neglect of two electron integrals. $10^{-\text{THRESH}}$ (THRESH $\leq 14$).

TYPE:

INTEGER

DEFAULT:

8 For single point energies.

10 For optimizations and frequency calculations.

14 For coupled-cluster calculations.

OPTIONS:

$n$ for a threshold of $10^{-n}$.

RECOMMENDATION:

Should be at least three greater than SCF_CONVERGENCE. Increase for more significant figures, at greater computational cost.

**TIME_STEP**

Specifies the molecular dynamics time step, in atomic units (1 a.u. = 0.0242 fs).

TYPE:

INTEGER

DEFAULT:

None.

OPTIONS:

User-specified.

RECOMMENDATION:

Smaller time steps lead to better energy conservation; too large a time step may cause the job to fail entirely. Make the time step as large as possible, consistent with tolerable energy conservation.

**TRANS_ENABLE**

To invoke the molecular transport code.

TYPE:

INTEGER

DEFAULT:

0 Do not perform transport calculations (default).

OPTIONS:

1 Perform transport calculations.

$-1$ Print matrices needed for generating bulk model files.

RECOMMENDATION:

None

**TRNSS**

Controls whether reduced single excitation space is used.

TYPE:

LOGICAL

DEFAULT:

FALSE Use full excitation space.

OPTIONS:

TRUE Use reduced excitation space.

RECOMMENDATION:

None

**TRTYPE**

Controls how reduced subspace is specified.

TYPE:

INTEGER

DEFAULT:

1

OPTIONS:

| | |
|---|---|
| 1 | Select orbitals localized on a set of atoms. |
| 2 | Specify a set of orbitals. |
| 3 | Specify a set of occupied orbitals, include excitations to all virtual orbitals. |

RECOMMENDATION:

None

**UNRESTRICTED**

Controls the use of restricted or unrestricted orbitals.

TYPE:

LOGICAL

DEFAULT:

| | |
|---|---|
| FALSE | Closed-shell systems. |
| TRUE | Open-shell systems. |

OPTIONS:

| | |
|---|---|
| FALSE | Constrain the spatial part of the alpha and beta orbitals to be the same. |
| TRUE | Do not Constrain the spatial part of the alpha and beta orbitals. |

RECOMMENDATION:

Use the default unless ROHF is desired. Note that for unrestricted calculations on systems with an even number of electrons it is usually necessary to break $\alpha/\beta$ symmetry in the initial guess, by using SCF_GUESS_MIX or providing *$occupied* information (see Section 4.5 on initial guesses).

**USECUBLAS_THRESH**

Sets threshold of matrix size sent to GPU (smaller size not worth sending to GPU).

TYPE:

INTEGER

DEFAULT:

250

OPTIONS:

| | |
|---|---|
| n | user-defined threshold |

RECOMMENDATION:

Use the default value. Anything less can seriously hinder the GPU acceleration

**USER_CONNECT**

Enables explicitly defined bonds.

TYPE:

STRING

DEFAULT:

FALSE

OPTIONS:

| | |
|---|---|
| TRUE | Bond connectivity is read from the *$molecule* section |
| FALSE | Bond connectivity is determined by atom proximity |

RECOMMENDATION:

Set to TRUE if bond connectivity is known, in which case this connectivity must be specified in the *$molecule* section. This greatly accelerates MM calculations.

**USE_LIBPT**

Enable libpt for CCSD(T) calculations in CCMAN2.

TYPE:

LOGICAL

DEFAULT:

FALSE

OPTIONS:

TRUE FALSE

RECOMMENDATION:

**USE_MGEMM**

Use the mixed-precision matrix scheme (MGEMM) if you want to make calculations in your card in single-precision (or if you have a single-precision-only GPU), but leave some parts of the RI-MP2 calculation in double precision)

TYPE:

LOGICAL

DEFAULT:

FALSE

OPTIONS:

| | |
|---|---|
| FALSE | MGEMM disabled |
| TRUE | MGEMM enabled |

RECOMMENDATION:

Use when having single-precision cards

**USE_RVV10**

Used to turn on the rVV10 NLC functional

TYPE:

LOGICAL

DEFAULT:

FALSE

OPTIONS:

| | |
|---|---|
| FALSE | VV10 NLC is utilized (the default for NL_CORRELATION) |
| TRUE | rVV10 NLC is utilized |

RECOMMENDATION:

Set to TRUE if the rVV10 NLC is desired.

**VARTHRESH**

Controls the temporary integral cut-off threshold. $tmp\_thresh = 10^{-\text{VARTHRESH}} \times DIIS\_error$

TYPE:

INTEGER

DEFAULT:

0 Turns VARTHRESH off

OPTIONS:

$n$ User-defined threshold

RECOMMENDATION:

3 has been found to be a practical level, and can slightly speed up SCF evaluation.

**VCI**

Specifies the number of quanta involved in the VCI calculation.

TYPE:

INTEGER

DEFAULT:

0

OPTIONS:

User-defined. Maximum value is 10.

RECOMMENDATION:

The availability depends on the memory of the machine. Memory allocation for VCI calculation is the square of $2 * (N_{\text{Vib}} + N_{\text{VCI}})/N_{\text{Vib}}N_{\text{VCI}}$ with double precision. For example, a machine with 1.5 Gb memory and for molecules with fewer than 4 atoms, VCI(10) can be carried out, for molecule containing fewer than 5 atoms, VCI(6) can be carried out, for molecule containing fewer than 6 atoms, VCI(5) can be carried out. For molecules containing fewer than 50 atoms, VCI(2) is available. VCI(1) and VCI(3) usually overestimated the true energy while VCI(4) usually gives an answer close to the converged energy.

**VIBMAN_PRINT**

Controls level of extra print out for vibrational analysis.

TYPE:

INTEGER

DEFAULT:

1

OPTIONS:

1 Standard full information print out.
If VCI is TRUE, overtones and combination bands are also printed.
3 Level 1 plus vibrational frequencies in atomic units.
4 Level 3 plus mass-weighted Hessian matrix, projected mass-weighted Hessian matrix.
6 Level 4 plus vectors for translations and rotations projection matrix.

RECOMMENDATION:

Use the default.

**WANG_ZIEGLER_KERNEL**

Controls whether to use the Wang-Ziegler non-collinear exchange-correlation kernel in a SF-DFT calculation.

TYPE:

LOGICAL

DEFAULT:

FALSE

OPTIONS:

| | |
|---|---|
| FALSE | Do not use non-collinear kernel. |
| TRUE | Use non-collinear kernel. |

RECOMMENDATION:

None

**WAVEFUNCTION_ANALYSIS**

Controls the running of the default wave function analysis tasks.

TYPE:

LOGICAL

DEFAULT:

TRUE

OPTIONS:

| | |
|---|---|
| TRUE | Perform default wave function analysis. |
| FALSE | Do not perform default wave function analysis. |

RECOMMENDATION:

None

**WIG_GRID**

Specify angular Lebedev grid for Wigner intracule calculations.

TYPE:

INTEGER

DEFAULT:

194

OPTIONS:

Lebedev grids up to 5810 points.

RECOMMENDATION:

Larger grids if high accuracy required.

**WIG_LEB**

Use Lebedev quadrature to evaluate Wigner integrals.

TYPE:

LOGICAL

DEFAULT:

FALSE

OPTIONS:

| | |
|---|---|
| FALSE | Evaluate Wigner integrals through series summation. |
| TRUE | Use quadrature for Wigner integrals. |

RECOMMENDATION:

None

**WIG_MEM**

Reduce memory required in the evaluation of $W(u, v)$.

TYPE:

LOGICAL

DEFAULT:

FALSE

OPTIONS:

| | |
|---|---|
| FALSE | Do not use low memory option. |
| TRUE | Use low memory option. |

RECOMMENDATION:

The low memory option is slower, so use the default unless memory is limited.

**WRITE_WFN**

Specifies whether or not a wfn file is created, which is suitable for use with AIMPAC. Note that the output to this file is currently limited to $f$ orbitals, which is the highest angular momentum implemented in AIMPAC.

TYPE:

STRING

DEFAULT:

| | |
|---|---|
| (NULL) | No output file is created. |

OPTIONS:

| | |
|---|---|
| *filename* | Specifies the output file name. The suffix *.wfn* will be appended to this name. |

RECOMMENDATION:

None

**XCIS**

Do an XCIS calculation in addition to a CIS calculation.

TYPE:

LOGICAL

DEFAULT:

FALSE

OPTIONS:

| | |
|---|---|
| FALSE | Do not do an XCIS calculation. |
| TRUE | Do an XCIS calculation (requires ROHF ground state). |

RECOMMENDATION:

None

**XC_GRID**

Specifies the type of grid to use for DFT calculations.

TYPE:

INTEGER

DEFAULT:

Functional-dependent; see Table 4.4.

OPTIONS:

| | |
|---|---|
| 0 | Use SG-0 for H, C, N, and O; SG-1 for all other atoms. |
| $n$ | Use SG-$n$ for all atoms, $n = 1, 2,$ or 3 |
| $XY$ | A string of two six-digit integers $X$ and $Y$, where $X$ is the number of radial points and $Y$ is the number of angular points where possible numbers of Lebedev angular points, which must be an allowed value from Table 4.3 in Section 4.4.5. |
| $-XY$ | Similar format for Gauss-Legendre grids, with the six-digit integer $X$ corresponding to the number of radial points and the six-digit integer $Y$ providing the number of Gauss-Legendre angular points, $Y = 2N^2$. |

RECOMMENDATION:

Use the default unless numerical integration problems arise. Larger grids may be required for optimization and frequency calculations.

**XC_SMART_GRID**

Uses SG-0 (where available) for early SCF cycles, and switches to the (larger) target grid specified by XC_GRID for final cycles of the SCF.

TYPE:

LOGICAL

DEFAULT:

FALSE

OPTIONS:

| | |
|---|---|
| TRUE (or 1) | Use the smaller grid for the initial cycles. |
| FALSE (or 0) | Use the target grid for all SCF cycles. |

RECOMMENDATION:

The use of the smart grid can save some time on initial SCF cycles.

**XOPT_SEAM_ONLY**

Orders an intersection seam search only, no minimization is to perform.

TYPE:

LOGICAL

DEFAULT:

FALSE

OPTIONS:

| | |
|---|---|
| TRUE | Find a point on the intersection seam and stop. |
| FALSE | Perform a minimization of the intersection seam. |

RECOMMENDATION:

In systems with a large number of degrees of freedom it might be useful to locate the seam first setting this option to TRUE and use that geometry as a starting point for the minimization.

**XOPT_STATE_1, XOPT_STATE_2**

Specify two electronic states the intersection of which will be searched.

TYPE:

[INTEGER, INTEGER, INTEGER]

DEFAULT:

No default value (the option must be specified to run this calculation)

OPTIONS:

[spin, irrep, state]

| | |
|---|---|
| spin = 0 | Addresses states with low spin,<br>see also CC_NLOWSPIN. |
| spin = 1 | Addresses states with high spin,<br>see also CC_NHIGHSPIN. |
| irrep | Specifies the irreducible representation to which the state belongs, for $C_{2v}$ point group symmetry irrep = 1 for $A_1$, irrep = 2 for $A_2$,<br>irrep = 3 for $B_1$, irrep = 4 for $B_2$. |
| state | Specifies the state number within the irreducible representation, state = 1 means the lowest excited state, state = 2 is the second excited state, etc. |
| 0, 0, -1 | Ground state. |

RECOMMENDATION:

Only intersections of states with different spin or symmetry can be calculated at this time.

**XPOL_CHARGE_TYPE**

Controls the type of atom-centered embedding charges for XPol calculations.

TYPE:

STRING

DEFAULT:

QLOWDIN

OPTIONS:

| | |
|---|---|
| QLOWDIN | Löwdin charges. |
| QMULLIKEN | Mulliken charges. |
| QCHELPG | CHELPG charges. |

RECOMMENDATION:

Problems with Mulliken charges in extended basis sets can lead to XPol convergence failure. Löwdin charges tend to be more stable, and CHELPG charges are both robust and provide an accurate electrostatic embedding. However, CHELPG charges are more expensive to compute, and analytic energy gradients are not yet available for this choice.

**XPOL_MPOL_ORDER**

Controls the order of multipole expansion that describes electrostatic interactions.

TYPE:

STRING

DEFAULT:

CHARGES

OPTIONS:

| | |
|---|---|
| GAS | No electrostatic embedding; monomers are in the gas phase. |
| CHARGES | Charge embedding. |
| DENSITY | Density embedding. |

RECOMMENDATION:

Should be set to GAS to do a dimer SAPT calculation (see Section 12.10).

**XPOL_OMEGA**

Controls the range-separation parameter, $\omega$, that is used in long-range-corrected DFT.

TYPE:

BOOLEAN

DEFAULT:

FALSE

OPTIONS:

| | |
|---|---|
| TRUE | Use different $\omega$ values for different fragments. |
| FALSE | Use a single value of $\omega$ for all fragments. |

RECOMMENDATION:

If FALSE, the *$rem* variable OMEGA should be used to specify the single value of $\omega$. If TRUE, separate values for each fragment should be specified in an *$lrc_omega* input section. Values in the *$lrc_omega* section have the same units as the *$rem* variable OMEGA, namely, $\omega$ = OMEGA/1000, in atomic units.

**XPOL_PRINT**

Print level for XPol calculations.

TYPE:

INTEGER

DEFAULT:

1

OPTIONS:

| | |
|---|---|
| $N$ | Integer print level |

RECOMMENDATION:

Higher values prints more information

**XPOL**

Perform a self-consistent XPol calculation.

TYPE:

BOOLEAN

DEFAULT:

FALSE

OPTIONS:

| | |
|---|---|
| TRUE | Perform an XPol calculation. |
| FALSE | Do not perform an XPol calculation. |

RECOMMENDATION:

NONE

**Z_EXTRAP_ORDER**

Specifies the polynomial order $N$ for Z-vector extrapolation.

TYPE:

INTEGER

DEFAULT:

0 Do not perform $Z$-vector extrapolation.

OPTIONS:

$N$ Extrapolate using an $N$th-order polynomial ($N > 0$).

RECOMMENDATION:

None

**Z_EXTRAP_POINTS**

Specifies the number $M$ of old $Z$-vectors that are retained for use in extrapolation.

TYPE:

INTEGER

DEFAULT:

0 Do not perform response equation extrapolation.

OPTIONS:

$M$ Save $M$ previous $Z$-vectors for use in extrapolation $(M > N)$

RECOMMENDATION:

Using the default $Z$-vector convergence settings, a $(M, N) = (4, 2)$ extrapolation was shown to provide the greatest speedup. At this setting, a 2–3-fold reduction in iterations was demonstrated.

**GEN_SCFMAN**

Use GEN_SCFMAN for the present SCF calculation.

TYPE:

BOOLEAN

DEFAULT:

FALSE

OPTIONS:

| | |
|---|---|
| FALSE | Use the old SCF code. |
| TRUE | Use GEN_SCFMAN. |

RECOMMENDATION:

Setting to TRUE when features in GEN_SCFMAN are needed.

# References and Further Reading

[1] J. E. Subotnik and N. Shenvi, *J. Chem. Phys.* **134**, 024105 (2011).

[2] J. E. Subotnik, *J. Phys. Chem. A* **114**, 12083 (2011).

[3] B. R. Landry and J. E. Subotnik, *J. Chem. Phys.* **137**, 22A513 (2012).

[4] J. M. Herbert and M. Head-Gordon, *J. Chem. Phys.* **121**, 11542 (2004).

[5] C. M. Breneman and K. B. Wiberg, *J. Comput. Chem.* **11**, 361 (1990).

[6] J. P. Perdew and Y. Wang, *Phys. Rev. B* **45**, 13244 (1992).

[7] E. Proynov and J. Kong, *Phys. Rev. A* **79**, 014103 (2009).

[8] T. Tsuneda, T. Suzumura, and K. Hirao, *J. Chem. Phys.* **110**, 10664 (1999).

[9] S. Grimme, J. Antony, S. Ehrlich, and H. Krieg, *J. Chem. Phys.* **132**, 154104 (2010).

[10] J.-D. Chai, *J. Chem. Phys.* **136**, 154104 (2012).

[11] J. W. Song, T. Hirosawa, T. Tsuneda, and K. Hirao, *J. Chem. Phys.* **126**, 154105 (2007).

[12] R. Armiento and S. Kümmel, *Phys. Rev. Lett.* **111**, 036402 (2013).

[13] T. M. Henderson, B. G. Janesko, and G. E. Scuseria, *J. Chem. Phys.* **128**, 194105 (2008).

[14] D. Das et al., *J. Chem. Phys.* **117**, 10534 (2002).

[15] K. V. Lawler, D. W. Small, and M. Head-Gordon, *J. Phys. Chem. A* **114**, 2930 (2010).

[16] G. J. O. Beran, B. Austin, A. Sodt, and M. Head-Gordon, *J. Phys. Chem. A* **109**, 9183 (2005).

[17] P. Bultinck, C. Van Alsenoy, P. W. Ayers, and R. Carbó-Dorca, *J. Chem. Phys.* **126**, 144111 (2007).

[18] O. A. Vydrov and T. Van Voorhis, *J. Chem. Phys.* **133**, 244103 (2010).

[19] K. U. Lao and J. M. Herbert, Implementation of restricted and unrestricted versions of extended symmetry-adapted perturbation theory (XSAPT) in the atomic orbital basis, and benchmark calculations for large supramolecular complexes, (in preparation).

[20] A. Hesselmann, *J. Phys. Chem. A* **115**, 11321 (2011).

[21] K. U. Lao and J. M. Herbert, *J. Phys. Chem. Lett.* **3**, 3241 (2012).

[22] R. Podeszwa, K. Pernal, K. Patkowski, and K. Szalewicz, *J. Phys. Chem. Lett.* **1**, 550 (2010).

[23] K. U. Lao and J. M. Herbert, *J. Chem. Phys.* **139**, 034107 (2013).

[24] K. U. Lao and J. M. Herbert, *J. Phys. Chem. A* **119**, 235 (2015).

[25] X. Zhang and J. M. Herbert, *J. Chem. Phys.* **142**, 064109 (2015).

[26] Q. Ou, G. D. Bellchambers, F. Furche, and J. E. Subotnik, *J. Chem. Phys.* **142**, 064114 (2015).

[27] A. Klamt and V. Jonas, *J. Chem. Phys.* **105**, 9972 (1996).

[28] K. Baldridge and A. Klamt, *J. Chem. Phys.* **106**, 6622 (1997).